

Controlled/Living Radical Polymerization

August 11, 2012 | <http://pubs.acs.org>
Publication Date: September 7, 2006 | doi: 10.1021/bk-2006-0944.fw001

ACS SYMPOSIUM SERIES 944

Controlled/Living Radical Polymerization

From Synthesis to Materials

Krzysztof Matyjaszewski, EDITOR
Carnegie Mellon University

**Sponsored by the
ACS Division of Polymer Chemistry, Inc.**



American Chemical Society, Washington, DC

In Controlled/Living Radical Polymerization; Matyjaszewski, K.;
ACS Symposium Series; American Chemical Society: Washington, DC, 2006.



Library of Congress Cataloging-in-Publication Data

Controlled/living polymerization : from synthesis to materials / Krzysztof Matyjaszewski, editor.

p. cm.—(ACS symposium series ISSN 0097-6156 ; 944)

Includes bibliographical references and index.

ISBN 13: 978-0-8412-3991-3 (alk. paper)

ISBN 10: 0-8412-3991-6 (alk. paper)

1. Polymerization—Congresses. 2. Free radical reactions—Congresses.

I. Matyjaszewski, K. (Krzysztof) II. Series.

QD281.P64.C655 2006
547'.28—dc22

2006045178

The paper used in this publication meets the minimum requirements of American National Standard for Information Sciences—Permanence of Paper for Printed Library Materials, ANSI Z39.48-1984.

Copyright © 2006 American Chemical Society

Distributed by Oxford University Press

All Rights Reserved. Reprographic copying beyond that permitted by Sections 107 or 108 of the U.S. Copyright Act is allowed for internal use only, provided that a per-chapter fee of \$33.00 plus \$0.75 per page is paid to the Copyright Clearance Center, Inc., 222 Rosewood Drive, Danvers, MA 01923, USA. Republication or reproduction for sale of pages in this book is permitted only under license from ACS. Direct these and other permission requests to ACS Copyright Office, Publications Division, 1155 16th Street, N.W., Washington, DC 20036.

The citation of trade names and/or names of manufacturers in this publication is not to be construed as an endorsement or as approval by ACS of the commercial products or services referenced herein; nor should the mere reference herein to any drawing, specification, chemical process, or other data be regarded as a license or as a conveyance of any right or permission to the holder, reader, or any other person or corporation, to manufacture, reproduce, use, or sell any patented invention or copyrighted work that may in any way be related thereto. Registered names, trademarks, etc., used in this publication, even without specific indication thereof, are not to be considered unprotected by law.

PRINTED IN THE UNITED STATES OF AMERICA

Foreword

The ACS Symposium Series was first published in 1974 to provide a mechanism for publishing symposia quickly in book form. The purpose of the series is to publish timely, comprehensive books developed from ACS sponsored symposia based on current scientific research. Occasionally, books are developed from symposia sponsored by other organizations when the topic is of keen interest to the chemistry audience.

Before agreeing to publish a book, the proposed table of contents is reviewed for appropriate and comprehensive coverage and for interest to the audience. Some papers may be excluded to better focus the book; others may be added to provide comprehensiveness. When appropriate, overview or introductory chapters are added. Drafts of chapters are peer-reviewed prior to final acceptance or rejection, and manuscripts are prepared in camera-ready format.

As a rule, only original research papers and original review papers are included in the volumes. Verbatim reproductions of previously published papers are not accepted.

ACS Books Department

Preface

This book is addressed to chemists who are interested in radical processes and especially in controlled/living radical polymerization. It summarizes the most recent accomplishments in the field.

This volume comprises the topical reviews and specialists' contributions presented at the American Chemical Society (ACS) Symposium entitled *Advances in Controlled/Living Radical Polymerization* that was held in Washington, D.C., August 28–September 1, 2005. The Washington, D.C. Meeting was a sequel to the previous ACS Symposia held in San Francisco, California, in 1997, in New Orleans, Louisiana in 1999, and in Boston, Massachusetts, in 2002. They were summarized in the ACS Symposium Series Volume 685, *Controlled Radical Polymerization*, Volume 768, *Controlled/Living Radical Polymerization: Progress in ATRP, NMP and RAFT* and Volume 854 *Advances in Controlled/Living Radical Polymerization*. The Washington, D.C. Meeting was very successful with 77 lectures and 119 posters presented, which illustrates a continuous growth in comparison with the San Francisco Meeting (32 lectures and 35 posters), with the New Orleans (50 lectures and 50 posters), and with the Boston Meeting (80 lectures and 79 posters).

The first chapter provides an overview of the current status of controlled/living radical polymerization (CRP) systems. Twenty chapters in this book cover atom transfer radical polymerization (ATRP) and include mechanistic features and materials made by ATRP. Chemistry and materials made by nitroxide and other stable free radical polymerizations (SFRP) are presented in six chapters. Systems based on degenerative transfer such as reversible-addition fragmentation transfer (RAFT) are summarized in fourteen chapters.

Chapters published in this book show that controlled/living radical polymerization has made a significant progress within the last decade. New systems have been discovered; substantial progress has been achieved in understanding the reactions involved in ATRP, SFRP, and RAFT. The rate and equilibrium constants as well as concentrations of the involved species were quantitatively measured for some systems but a more detailed structure-reactivity relationship for all CRP systems

is needed. Some effects of structural variation on properties were reported but a comprehensive and precise relationship between molecular structure and macroscopic properties is not yet available. It will be also important to understand the effect of polydispersities and other imperfections on materials properties in order to optimize a cost-performance ratio. Several new commercial applications of CRP were already announced at the Washington, D.C. Meeting and it is anticipated that many new products will be soon on the market.

The financial support for the symposium from the following organizations is acknowledged: ACS Division of Polymer Chemistry, Inc., ACS Petroleum Research Foundation, Arkema, Atofina, Bayer, Bausch & Lomb, Boston Scientific, BYK, Cabot, Ciba Vision, Dionex, EFKA, Firmenich, Kaneka, Mitsubishi Chemicals, Mitsui Chemicals, Rohmax, and Rohm & Haas. The editorial assistance from Joyce Von Vreckin is gratefully acknowledged.

Krzysztof Matyjaszewski

Department of Chemistry
Carnegie Mellon University
4400 Fifth Avenue
Pittsburgh, PA 15213

Controlled/Living Radical Polymerization

August 11, 2012 | <http://pubs.acs.org>
Publication Date: September 7, 2006 | doi: 10.1021/bk-2006-0944.pr001

Chapter 1

Controlled/Living Radical Polymerization: State of the Art in 2005

Krzysztof Matyjaszewski

**Center for Macromolecular Engineering, Department of Chemistry,
Carnegie Mellon University, 4400 Fifth Avenue, Pittsburgh, PA 15213**

Recent progress and future challenges in Controlled/Living Radical Polymerization (CRP) are discussed. Stable free radical polymerization (SFRP), atom transfer radical polymerization (ATRP), and degenerate transfer processes, including reversible addition fragmentation transfer (RAFT) are the most successful CRP techniques. They enable preparation of new materials from readily available monomers under undemanding conditions. Future developments require better understanding structure-reactivity relationship and deeper insight into the reactive intermediates by spectroscopic and computational techniques. The precise relationship between the structure and properties of materials prepared by CRP is also needed. This study should include the effect of higher polydispersities and other imperfections to optimize cost-performance ratio. Fast growth of areas related to hybrids and bioconjugate materials is anticipated.

Controlled/living radical polymerization (CRP) is among the most rapidly developing areas of chemistry and polymer science.¹⁻⁴ During the last decade, many novel previously inaccessible materials have been prepared using CRP.⁵ They include macromolecules with precisely controlled composition and architecture but also many new hybrids in which well-defined organic polymers are covalently attached to inorganic materials or to natural products.⁶⁻¹²

The last decade has witnessed an explosive increase in the number of publications on CRP, a dramatic increase in the number of patent applications and several symposia devoted partially, or entirely, to CRP.

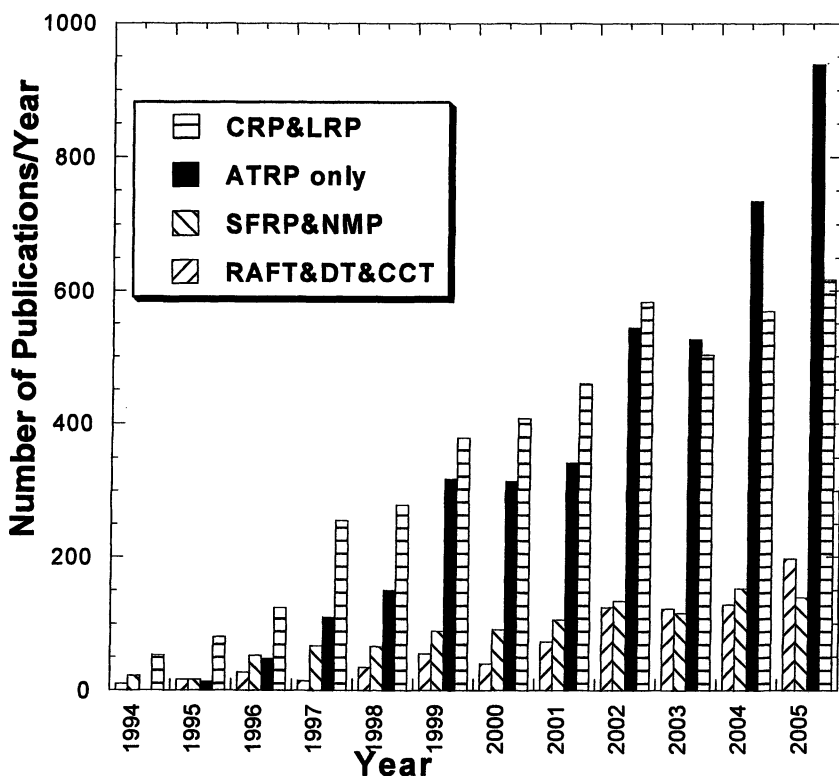


Figure 1. Results of SciFinder Search on various CRP systems as of February 5, 2006. Detailed explanation of terms is provided in the text.

Figure 1 illustrates results of a recent SciFinder Scholar search using the following terms: *controlled radical polymn* or *living radical polymn* ("CRP&LRP" in Figure 1), *ATRP* or *atom transfer (radical) polymn* ("ATRP

only”, this search does not include terms such as metal mediated or metal catalyzed radical polymerization), *SFRP* or *NMP* or *stable free polymn* or *nitroxide mediated polymn* (“*SFRP&NMP*”) and *RAFT* or *reversible addition transfer* or *degenerative transfer* or *catalytic chain transfer* (“*RAFT&DT&CT*”). The latter two terms were refined with a term *radical polymn* since they coincide with other common chemical names such as *N-methylpyrrolidone* or *raft-associated proteins*. In summary, since 1995 over 8,000 papers have been published on various CRP systems, more than half on ATRP. Currently, nearly 3 papers per day are published on ATRP. There is also another trend which can be deduced from Figure 1. Progressively more papers are published on specific techniques of CRP rather than referring to a generic CRP or LRP terms.

All CRP methods rely on formation of a dynamic equilibrium between tiny amounts of propagating radicals and various types of dormant species.^{4,13,14} Radicals always terminate and therefore CRP is never “living” in the purest sense of the living polymerization definition.¹⁵⁻¹⁷ If the polymerization rate is the same (in the conventional process or in a CRP), the same radical concentration is present and essentially the same number (concentration) of chains terminate. However, in the conventional process, all chains are terminated (e.g., 10^{-3} M), whereas in a CRP, as a result of the large total concentration of chains (e.g., 10^{-1} M of dormant and active/terminated chains), the % of terminated chains (10^{-3} M) constitute only small fraction of all chains (~1 %, typically between 1 and 10%). The remaining are dormant species, capable of reactivation, allowing functionalization or chain extension to form block copolymers, etc. Since the proportion of terminated chains is small, they may not affect the physical properties of the targeted materials.

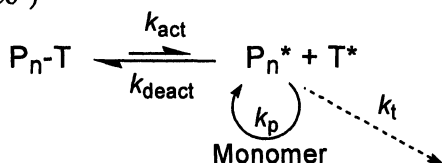
A very important difference between conventional and CRP processes is the approach to the steady state. In the conventional radical polymerization, steady state is achieved by balancing the rate of initiation and termination. In order to prepare polymers with high molecular weights ($M_n \sim 100,000$, i.e. with $DP \sim 1000$), the rate of propagation must be 1000 times higher than the termination rate. Consequently initiation must be also 1000 times slower than propagation. This prerequisite prevents synthesis of well defined polymers. In order to prepare polymers with controlled molecular weights ($DP_n = \Delta[M]/[I]_0$) and narrow molecular weight distribution, initiation should be relatively fast, at least comparable to propagation. In systems controlled by the persistent radical effect, such as ATRP and SFRP, steady state is achieved by balancing rates of activation and deactivation rather than initiation and termination. For the first time in radical polymerization this allows decoupling of the rates of initiation and termination. The latter must still be thousands times slower than propagation, but the former can now be as fast as propagation.

The key that controls CRP is the dynamics of exchange between active radicals and various types of dormant species. This exchange must be fast,

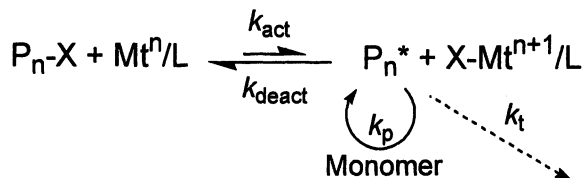
generally as fast as propagation. The fast exchange provides all chains a similar probability of growth and consequently narrow molecular weight distribution. It must be noted, that one may prepare polymers with preserved chain end functionalities, capable of cross-propagation and block copolymer formation, even if exchange is slow. Under these conditions, polydispersities will be higher, but chains will be still “living”, and capable of growth. In fact, fine tuning the exchange rate offers a possibility of designing molecular weight distribution and thereby influencing polymer properties.

As shown in Figure 2, there are three approaches to the exchange process. Two of them employ the persistent radical effect, (PRE).¹⁷

- 1) SFRP: Spontaneous reversible activation of the dormant species (T^* = nitroxide or Co^{II})



- 2) ATRP: Catalyzed reversible activation of the dormant species ($\text{Mt}^n = \text{Cu}^{\text{I}}, \text{Fe}^{\text{II}}, \text{Ru}^{\text{II}}$)



- 3) DT: Dominating fraction of a dormant species participates in degenerative transfer with a tiny amount of radicals ($X = \text{iodide or dithioester}$)

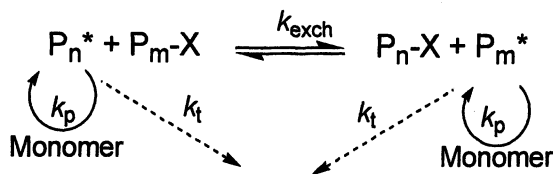


Figure 2. The three main CRP methods: SFRP, ATRP and DT

In a CRP controlled by PRE, the exchange can be either spontaneous (stable free radical polymerization, SFRP, exemplified typically by nitroxide mediated polymerization, NMP, and cobalt mediated polymerization)¹⁸⁻²¹ or catalyzed (atom transfer radical polymerization, ATRP).²²⁻²⁵ Both are based on the

principle of a reversible activation/deactivation. The alternative approach utilizes a degenerative transfer (DT) mechanism with either alkyl iodides²⁶ or dithioesters/xanthates (reversible addition fragmentation transfer, RAFT²⁷ or MADIX)²⁸⁻³⁰ as transfer agents. There are several other mediators for SFRP, such as boronyloxy, other stable organic radicals, or other metals and there are other transfer agents, most notably tellurium or antimony derivatives.^{31,32} In some cases, control can be accomplished by several mechanisms participating together. For example, Mo or Os complexes can simultaneously participate in ATRP and SFRP processes.^{33,34} Use of alkyl iodides in ATRP opens up a pathway to the DT exchange process, in addition to the ATRP mechanism.^{17,35} Some tellurium derivatives can participate via SFRP and DT process as well. Dithiocarbamates, can be activated by light and contribute to the SFRP mechanism, as originally shown by Otsu.³⁶

The three techniques have been constantly improved and applied to the preparation of well-defined polymers from new monomers. For example, in SFRP, recently developed nitroxides have been used to successfully polymerize acrylates, acrylamides, and most recently also methacrylates in the presence of small amounts of styrene.³⁷ Cobalt porphyrines were originally used for CRP of acrylates but more recently for vinyl acetate.³⁸⁻⁴¹ Both systems were successfully applied to aqueous dispersed media. These recent discoveries are discussed in subsequent chapters of these proceedings.

In ATRP, the range of monomers have been extended to vinyl acetate, dienes and vinyl chloride.^{23,42} Also, new metals (Mo, Os, Ti)^{33,43,44} and new ligands were successfully introduced, as discussed in several chapters in this volume. ATRP was successfully carried out in miniemulsion and microemulsion^{45,46} as well as in CO₂ or ionic liquids.⁴⁷ New initiating systems have been developed for ATRP. In addition to "normal" and "reverse" ATRP, simultaneous reverse and normal initiation (SR&NI),⁴⁸ activators generated by electron transfer (AGET)^{49,50} and activators re-generated by electron transfer (ARGET)⁵¹ can be used. They start from oxidatively stable transition metal complexes (Cu^{II}) and are activated in the presence of reducing agents. AGET employs reducing agents which do not generate initiating radicals, such as Sn^{II} (2-ethylhexanoate)₂ or ascorbic acid. ARGET is carried out in the presence of ppm of Cu catalyst and ~ 100 ppm of reducing agent to compensate for bimolecular termination. An alternative approach to reduce the amount of transition metal in the product is to immobilize the catalyst and recycle it. Interesting concepts involve temporary immobilization or use of magnetic particles, as discussed in the following chapters.

RAFT and MADIX are the two most successful degenerative transfer processes but significant progress has been also accomplished in iodine DT and in the use of Te, As and other organometallic mediators. The thioesters end

group has been successfully removed from polymers in the presence of large amounts of organic radical initiators, as shown in chapters in this volume.

As mentioned before, one of the main driving forces for the rapid expansion of CRP is preparation of (co)polymers with precisely controlled architectures which form new materials for targeted applications.

Several chapters in this book demonstrate synthesis of new block copolymers, stars, grafts, brushes. There are new approaches for the preparation of functional polymers and their subsequent modification using e.g. "click" chemistry.⁵²⁻⁵⁵ New bioconjugates were prepared by either ATRP or RAFT.^{9,56,57} Similarly, new organic-inorganic hybrids were synthesized.⁵⁸⁻⁶⁰

However, perhaps most exciting is the progress in commercialization of products made by CRP. Several corporations started commercial production of tailored materials using SFRP, ATRP and also DT processes to benefit our society.

Outlook

In an introductory chapter, opening the proceedings volume from the last ACS Symposium on CRP in Boston (ACS Symp., Vol. 854), I referred to three major challenges for CRP:

1. Affecting stereo- and chemoselectivities in CRP
2. Enhancing livingness of CRP systems by increasing k_p/k_t ratio
3. Improving copolymerization of polar and non-polar monomers.

It gives me real satisfaction that significant progress has been accomplished in all three areas:

1. Lewis acids and other complexing agents used to alter reactivity ratios and polymer tacticity in conventional radical processes were successfully applied to CRP systems.^{61 62} This led to the synthesis of the first stereo-block copolymers prepared by radical means, using dimethylacrylamide as the only monomer. In a similar way, block copolymers with alternating and random copolymer segments were prepared.⁶³ Further progress in this area requires development of new more selective and more efficient complexation agents.

2. Complexation agents may not only affect stereochemistry but also influence k_p/k_t ratios. Application of high pressure to CRP systems noticeably increased k_p/k_t ratio due to the differences in activation volumes.^{64,65} It will be interesting to explore the possibility of using compartmentalization to prevent macroscopic gelation and crosslinking during CRP with multifunctional initiators.

3. Olefins and non-conjugated vinyl monomers were successfully copolymerized with acrylates to provide statistical copolymers with composition

similar to those in conventional process and predetermined by intrinsic reactivity ratios.⁶⁶⁻⁶⁸ However, polydispersities in these CRP processes were significantly lower. Unfortunately, molecular weights were also quite low. It will be interesting to prepare polymers with higher molecular weights, and explore the affect of complexation agents and prepare some segmented copolymers which can phase separate on the nanoscale.

It seems that we have currently reached a basic understanding of various CRP systems but further progress is still needed in the following areas:

A. Mechanisms and structure-reactivity correlation

We should also further develop the fundamental understanding of reaction mechanisms and we also need to correlate the structure of involved reagents with their reactivities. Here, computational chemistry will start playing a progressively more important role.⁶⁹⁻⁷¹ A deeper insight into the reaction intermediates and energetic pathways will be very helpful. However, it requires quite a large basis set, since many reaction pathways maybe dramatically affected by tiny changes in the structure of the substituents, as already demonstrated in RAFT. Thus, continued studies on model reactions and their correlation with macromolecular systems are very much needed to better understand and optimize the existing processes. Furthermore, the generated knowledge will help to develop new processes and new mediating agents.

B. Structure- property relationship, imperfections and cost-performance balance

An equally important issue is the correlation of macromolecular structure of well-defined polymers with their macroscopic properties.⁷²⁻⁷⁵ Here, theory combined with computational / simulation approaches will be very helpful.^{76,77} Regardless, a phenomenological relationship between structure and properties will be needed. A very important issue is the influence of imperfections (higher polydispersities, loss of functionality, or a loss of an arm in star-like systems) on the properties. Also how does sequence distribution in copolymers affects properties? How do block, graft copolymers compare with statistical copolymers or with multisegmented or gradient copolymers? How does one design the best gradient structure and how is it verified experimentally? Termination and some side reactions cannot be totally avoided and will be always present in CRP but it may be less expensive to prepare polymers faster but with higher contribution of chain breaking reactions. How do these inherent imperfections affect properties? Would they allow a more flexible processing regime? Would they lead to new morphologies with enhanced curvature and sponge-like systems? Regardless, a cost-performance balance will be a key issue for many commercial products.

C. Hybrids and bioconjugates

As mentioned before, inorganic-organic hybrids and bioconjugates are two of the most rapidly developing applications of CRP. Dense grafting from flat, cylindrical and spherical surfaces (both convex and concave) not only prevents aggregation of particles but leads to a new class nano-composites with totally new electronic and mechanical properties. Development of new biomaterials and bioconjugates based on water soluble components and especially stimuli responsive organic polymers will accelerate in the near future. Synthesis of polymers which can respond not only to temperature but also, light, pH, ionic affect and pressure or magnetic field will yield new “intelligent” biomaterials.

We anticipate that these and many other issues will be studied during the next few years and will be presented at the next ACS Symposium on CRP, especially as commercial importance of CRP rapidly and continuously increases.

Acknowledgments. Support from the National Science Foundation (CHE 04-05627) and DMR (05-49353) is gratefully acknowledged.

References

1. Matyjaszewski, K. *ACS Symp. Ser.* **1998**, *685*, 2-30.
2. Matyjaszewski, K. *ACS Symp. Ser.* **2000**, *768*, 2-26.
3. Matyjaszewski, K. *ACS Symp. Ser.* **2003**, *854*, 2-9.
4. Matyjaszewski, K.; Davis, T. P. *Handbook of Radical Polymerization*; Wiley-Interscience: Hoboken, 2002.
5. Matyjaszewski, K.; Spanswick, J. *Materials Today (Oxford, United Kingdom)* **2005**, *8*, 26-33.
6. Matyjaszewski, K. *Prog. Polym. Sci.* **2005**, *30*, 858-875.
7. Lehn, J.-M. *Prog. Polym. Sci.* **2005**, *30*, 814-831.
8. Frechet, J. M. J. *Prog. Polym. Sci.* **2005**, *30*, 844-857.
9. Klok, H.-A. *J. Polym. Sci., Part A: Polym. Chem.* **2005**, *43*, 1-17.
10. Hawker, C. J.; Wooley, K. L. *Science* **2005**, *309*, 1200-1205.
11. Malkoch, M.; Thibault, R. J.; Drockenmuller, E.; Messerschmidt, M.; Voit, B.; Russell, T. P.; Hawker, C. J. *J. Am. Chem. Soc.* **2005**, *127*, 14942-14949.
12. Luzinov, I.; Minko, S.; Tsukruk, V. V. *Prog. Polym. Sci.* **2004**, *29*, 635-698.
13. Matyjaszewski, K.; Gaynor, S.; Greszta, D.; Mardare, D.; Shigemoto, T. *J. Phys. Org. Chem.* **1995**, *8*, 306-315.
14. Matyjaszewski, K. *J. Macromol. Sci., Pure Appl. Chem.* **1997**, *A34*, 1785-1801.

15. Szwarc, M.; Levy, M.; Milkovich, R. *J. Am. Chem. Soc.* **1956**, *78*, 2657.
16. Szwarc, M. *Nature* **1956**, *178*, 1168.
17. Goto, A.; Fukuda, T. *Prog. Polym. Sci.* **2004**, *29*, 329-385.
18. Wayland, B. B.; Poszmik, G.; Mukerjee, S. L.; Fryd, M. *J. Am. Chem. Soc.* **1994**, *116*, 7943-7944.
19. Hawker, C. J.; Bosman, A. W.; Harth, E. *Chem. Rev.* **2001**, *101*, 3661-3688.
20. Georges, M. K.; Veregin, R. P. N.; Kazmaier, P. M.; Hamer, G. K. *Macromolecules* **1993**, *26*, 2987.
21. Benoit, D.; Grimaldi, S.; Robin, S.; Finet, J.-P.; Tordo, P.; Gnanou, Y. *J. Am. Chem. Soc.* **2000**, *122*, 5929-5939.
22. Wang, J. S.; Matyjaszewski, K. *J. Am. Chem. Soc.* **1995**, *117*, 5614-5615.
23. Kamigaito, M.; Ando, T.; Sawamoto, M. *Chem. Rev.* **2001**, *101*, 3689-3745.
24. Wang, J.-S.; Matyjaszewski, K. *J. Am. Chem. Soc.* **1995**, *117*, 5614-5615.
25. Matyjaszewski, K.; Xia, J. *Chem. Rev.* **2001**, *101*, 2921-2990.
26. Matyjaszewski, K.; Gaynor, S.; Wang, J.-S. *Macromolecules* **1995**, *28*, 2093-2095.
27. Chiefari, J.; Rizzardo, E. In *Handbook of Radical Polymerization*; Matyjaszewski, K., Davis, T. P., Eds.; Wiley-Interscience: Hoboken, 2002, pp 629-690.
28. Chiefari, J.; Chong, Y. K. B.; Ercole, F.; Krstina, J.; Jeffery, J.; Le, T. P. T.; Mayadunne, R. T. A.; Meijs, G. F.; Moad, C. L.; Moad, G.; Rizzardo, E.; Thang, S. H. *Macromolecules* **1998**, *31*, 5559.
29. Destarac, M.; Charmot, D.; Franck, X.; S. Z, Z. *Macromol. Rapid Comm.* **2000**, *21*, 1035-1039.
30. Adamy, M.; van Herk, A. M.; Destarac, M.; Monteiro, M. J. *Macromolecules* **2003**, *36*, 2293-2301.
31. Goto, A.; Kwak, Y.; Fukuda, T.; Yamago, S.; Iida, K.; Nakajima, M.; Yoshida, J.-I. *J. Am. Chem. Soc.* **2003**, *125*, 8720-8721.
32. Yamago, S.; Ray, B.; Iida, K.; Yoshida, J.; Tada, T.; Yoshizawa, K.; Kwak, Y.; Goto, A.; Fukuda, T. *J. Am. Chem. Soc.* **2004**, *126*, 13908-13909.
33. Poli, R.; Stoffelbach, F.; Maria, S.; Mata, J. *Chemistry--A European Journal* **2005**, *11*, 2537-2548.
34. Maria, S.; Stoffelbach, F.; Mata, J.; Daran, J.-C.; Richard, P.; Poli, R. *J. Am. Chem. Soc.* **2005**, *127*, 5946-5956.
35. Kamigaito, M.; Onishi, I.; Kimura, S.; Kotani, Y.; Sawamoto, M. *Chem. Commun.* **2002**, 2694-2695.
36. Otsu, T. *J. Polym. Sci., Part A: Polym. Chem.* **2000**, *38*, 2121-2136.
37. Charleux, B.; Nicolas, J.; Guerret, O. *Macromolecules* **2005**, *38*, 5485-5492.
38. Kaneyoshi, H.; Matyjaszewski, K. *Macromolecules* **2005**, *38*, 8163-8169.
39. Lu, Z.; Fryd, M.; Wayland, B. B. *Macromolecules* **2004**, *37*, 2686-2687.
40. Debuigne, A.; Caille, J.-R.; Willet, N.; Jerome, R. *Macromolecules* **2005**, *38*, 9488-9496.

41. Debuigne, A.; Caille, J.-R.; Jerome, R. *Angewandte Chemie, International Edition* **2005**, *44*, 1101-1104, S1101/1101-S1101/1103.
42. Percec, V.; Popov, A. V.; Ramirez-Castillo, E.; Weichold, O. *J. Polym. Sci., Part A: Polym. Chem.* **2003**, *41*, 3283-3299.
43. Braunecker, W. A.; Itami, Y.; Matyjaszewski, K. *Macromolecules* **2005**, *38*, 9402-9404.
44. Asandei, A. D.; Moran, I. W. *J. Polym. Sci., Part A: Polym. Chem.* **2005**, *43*, 6028-6038.
45. Li, M.; Jahed, N. M.; Min, K.; Matyjaszewski, K. *Macromolecules* **2004**, *37*, 2434-2441.
46. Min, K.; Matyjaszewski, K. *Macromolecules* **2005**, *38*, 8131-8134.
47. Kubisa, P. *Prog. Polym. Sci.* **2004**, *29*, 3-12.
48. Li, M.; Min, K.; Matyjaszewski, K. *Macromolecules* **2004**, *37*, 2106-2112.
49. Min, K.; Gao, H.; Matyjaszewski, K. *J. Am. Chem. Soc.* **2005**, *127*, 3825-3830.
50. Jakubowski, W.; Matyjaszewski, K. *Macromolecules* **2005**, *38*, 4139-4146.
51. Jakubowski, W.; Min, K.; Matyjaszewski, K. *Macromolecules* **2006**, *39*, 39-45.
52. Wu, P.; Feldman, A. K.; Nugent, A. K.; Hawker, C. J.; Scheel, A.; Voit, B.; Pyun, J.; Frechet, J. M. J.; Sharpless, K. B.; Fokin, V. V. *Angewandte Chemie, International Edition* **2004**, *43*, 3928-3932.
53. Tsarevsky, N. V.; Sumerlin, B. S.; Matyjaszewski, K. *Macromolecules* **2005**, *38*, 3558-3561.
54. Tsarevsky, N. V.; Bernaerts, K. V.; Dufour, B.; Du Prez, F. E.; Matyjaszewski, K. *Macromolecules* **2004**, *37*, 9308-9313.
55. Lutz, J.-F.; Boerner, H. G.; Weichenhan, K. *Macromol. Rapid Commun.* **2005**, *26*, 514-518.
56. Lele, B. S.; Murata, H.; Matyjaszewski, K.; Russell, A. J. *Biomacromolecules* **2005**, *6*, 3380-3387.
57. Gil, E. S.; Hudson, S. M. *Prog. Polym. Sci.* **2004**, *29*, 1173-1222.
58. Pyun, J.; Kowalewski, T.; Matyjaszewski, K. *Macromol. Rapid Commun.* **2003**, *24*, 1043-1059.
59. Pyun, J.; Matyjaszewski, K. *Chem. Mater.* **2001**, *13*, 3436-3448.
60. Kruk, M.; Dufour, B.; Celer, E. B.; Kowalewski, T.; Jaroniec, M.; Matyjaszewski, K. *J. Phys. Chem. A* **2005**, *in press*.
61. Ray, B.; Isobe, Y.; Matsumoto, K.; Habae, S.; Okamoto, Y.; Kamigaito, M.; Sawamoto, M. *Macromolecules* **2004**, *37*, 1702-1710.
62. Lutz, J.-F.; Neugebauer, D.; Matyjaszewski, K. *J. Am. Chem. Soc.* **2003**, *125*, 6986-6993.
63. Lutz, J.-F.; Kirci, B.; Matyjaszewski, K. *Macromolecules* **2003**, *36*, 3136-3145.
64. Arita, T.; Buback, M.; Janssen, O.; Vana, P. *Macromol. Rapid Commun.* **2004**, *25*, 1376-1381.

65. Barner-Kowollik, C.; Buback, M.; Egorov, M.; Fukuda, T.; Goto, A.; Olaj, O. F.; Russell, G. T.; Vana, P.; Yamada, B.; Zetterlund, P. B. *Prog. Polym. Sci.* **2005**, *30*, 605-643.
66. Nagel, M.; Poli, D.; Sen, A. *Macromolecules* **2005**, *38*, 7262-7265.
67. Liu, S.; Sen, A. *Macromolecules* **2001**, *34*, 1529-1532.
68. Venkatesh, R.; Vergouwen, F.; Klumperman, B. *Macromol. Chem. Phys.* **2005**, *206*, 547-552.
69. Feldermann, A.; Coote, M. L.; Stenzel, M. H.; Davis, T. P.; Barner-Kowollik, C. *J. Am. Chem. Soc.* **2004**, *126*, 15915-15923.
70. Gillies, M. B.; Matyjaszewski, K.; Norrby, P.-O.; Pintauer, T.; Poli, R.; Richard, P. *Macromolecules* **2003**, *36*, 8551-8559.
71. Matyjaszewski, K.; Poli, R. *Macromolecules* **2005**, *38*, 8093-8100.
72. Sukhorukov, G.; Fery, A.; Moehwald, H. *Prog. Polym. Sci.* **2005**, *30*, 885-897.
73. Macosko, C. W.; Jeon, H. K.; Hoye, T. R. *Prog. Polym. Sci.* **2005**, *30*, 939-947.
74. Meijer, H. E. H.; Govaert, L. E. *Prog. Polym. Sci.* **2005**, *30*, 915-938.
75. Leibler, L. *Prog. Polym. Sci.* **2005**, *30*, 898-914.
76. Matyjaszewski, K.; Ziegler, M. J.; Arehart, S. V.; Greszta, D.; Pakula, T. *J. Phys. Org. Chem.* **2000**, *13*, 775-786.
77. Matyjaszewski, K.; Miller, P. J.; Shukla, N.; Immaraporn, B.; Gelman, A.; Luokala, B. B.; Siclovan, T. M.; Kickelbick, G.; Vallant, T.; Hoffmann, H.; Pakula, T. *Macromolecules* **1999**, *32*, 8716-8724.

Chapter 2

Living Radical Polymerization Catalyzed with Hydrophilic and Thermosensitive Ruthenium(II) Complexes in Aqueous Media

Toshihide Yoshitani¹, Yasuhiro Watanabe¹, Tsuyoshi Ando¹,
Masami Kamigaito², and Mitsuo Sawamoto^{1,*}

¹Department of Polymer Chemistry, Graduate School of Engineering,
Kyoto University, Kyoto 615-8510, Japan

²Department of Applied Chemistry, Graduate School of Engineering,
Nagoya University, Nagoya 464-8603, Japan

Ruthenium(II) complexes with thermosensitive phosphine ligands carrying a poly(ethylene glycol) (PEG) chain, e.g., Ru(II)Cp*Cl[PPh₂C₆H₄(PEG)] actively catalyzed homogeneous and dispersion living radical polymerization of methyl methacrylate in toluene and in its mixture with water. Because of the PEG ligands, the catalysts are highly soluble in water at temperature below 80 °C (cloud point), while lipophilic at higher temperature, and thereby are reversibly transferred from an aqueous phase to an organic phase, allowing their efficient removal (> 97%) from the as-polymerized polymer solution by simply lowering the temperature below the cloud point.

Water has recently attracted attention as promising solvents and media for organic reactions and polymerizations, because it is abundant, nontoxic, and environmentally friendly, in addition to its high heat capacity for temperature regulation.¹ In sharp contrast to ionic reactions, free radical polymerization is often performed in aqueous media mostly under heterogeneous conditions such as suspension, dispersion, or emulsion in industrial process to solve thermal and/or viscosity problems.² Under most of such conditions, the polymers are usually obtained with uncontrolled molecular weights and architectures, because of complex heterogeneous reactions. Not very often but sometimes, in addition, water harms the active species or catalysts.

Controlled or living polymerizations in aqueous media are thus challenging subjects and have been investigated in many systems: metathesis, cationic, ring-opening anionic, and radical polymerizations. Transition metal-catalyzed living radical polymerization is one of the hopeful candidates for controlled polymerization in water to which the growing radical is stable, while due care should be taken to ensure the stability of the catalysts that are, in general, potentially susceptible to deactivation and decomposition by water.³⁻⁸

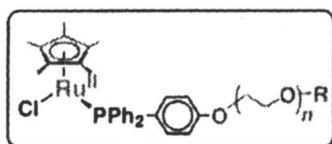
Recently, we have been investigating the metal-catalyzed living radical polymerization in organic and/or aqueous media. For example, finely controlled or living dispersion polymerizations of methacrylates, styrene, and related monomers are in fact feasible when coupled with selected ruthenium or iron catalysts.⁹ In these suspension aqueous media, the polymerizations proceed in the organic phase dispersed in water, and in some cases the reactions are faster than in homogeneous organic media.

Despite such fine polymerization control and effectiveness in the aqueous-phase systems, however, the metal catalysts remain in the organic phase containing polymers, and thus the difficulty to separate the catalyst from the reaction mixture remains unsolved, as with the corresponding homogeneous systems in organic solvents.

A solution for this problem may be to introduce thermally dictated phase-transfer catalysis into these living polymerizations, where the metal catalysts can change their solubility in water (and organic solvent) as a function of temperature. Most typical examples of such catalysis involve poly(ethylene oxide) [or poly(ethylene glycol) (PEG)] ligands, which are soluble in water at temperature lower than a certain threshold (cloud point), while turning insoluble and thus soluble in organic solvents above this point (see Scheme 1). In this work, a thermosensitive (PEG) was introduced into the phosphine ligand (PEG-phosphine) of a ruthenium catalyst, which will change its hydrophilicity and solubility in water, reversibly in response to temperature (Scheme 1). Such a thermosensitive catalyst is supposed to be not only easy to remove from organic solution containing polymers but also recyclable for further polymerization. Similar investigations have recently been reported by some groups but with fluorinated ligands/fluorinated¹⁰ solvents or in ionic liquids.¹¹

In this paper we report a living radical polymerization with the thermosensitive Ru(II) catalyst with a PEG ligand both in homogeneous organic solutions and in heterogeneous suspension systems in water, in the latter thermally regulated phase-transfer catalysis allowed ready separation of the catalysts residues from polymers and potential recycling of the catalyst.

Thermosensitive Ru(II) Complex

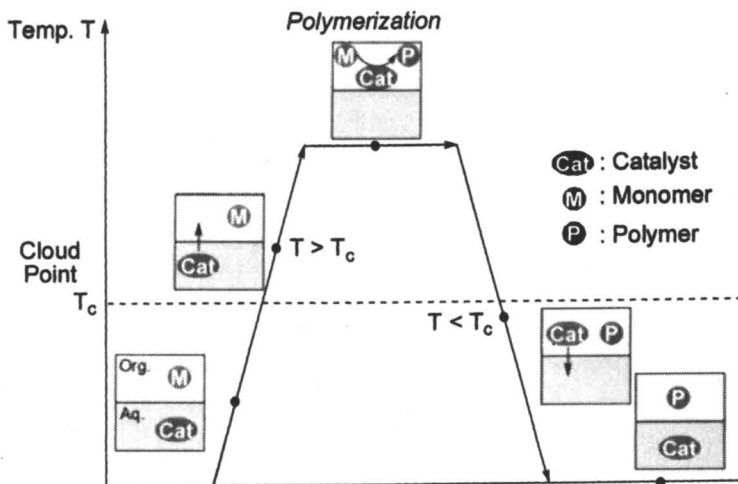
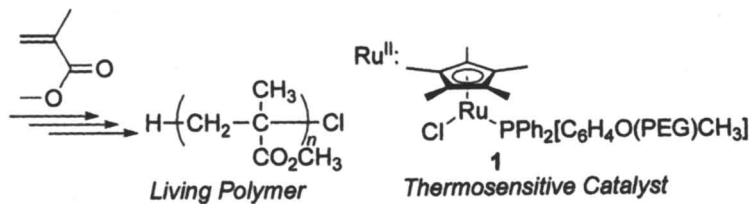
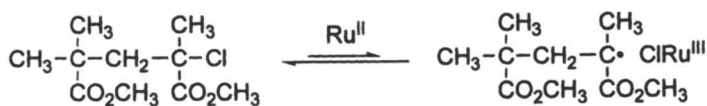
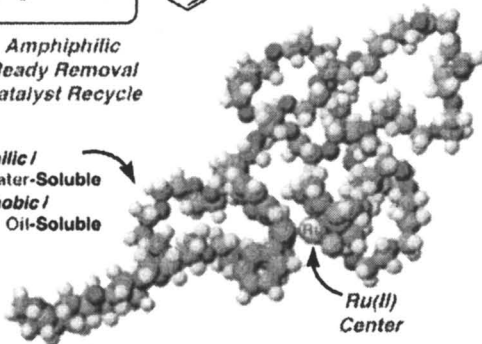


Thermosensitive
Active in Water

Amphiphilic
Ready Removal
Catalyst Recycle

- Thermosensitive
- Low Temp: **Hydrophilic / Water-Soluble**
- High Temp: **Hydrophobic / Oil-Soluble**

(Chem3D/ MMD)



Scheme 1. Living radical polymerization with thermosensitive Ru(II) catalyst.

MMA Polymerization with Ru(Cp*)Cl(PEG-phosphine) in Toluene

MMA polymerization was first examined with H-(MMA)₂-Cl (an MMA dimer capped with a chlorine; initiator), Ru(Cp*)Cl(PEG-phosphine) (**1**) (catalyst), which was prepared in situ by mixing [Ru(Cp*)Cl]₄ [a cyclic tetramer of Ru(Cp*)Cl] and 8 eq. of PEG-phosphine ([Ru]/[phosphine] = 1/2), in toluene at 80 °C (Figure 1). By NMR analysis the catalyst **1** is considered to carry only one PEG-phosphine ligand, in contrast to RuCl₂(PPh₃)₂ and RuCl(Ind)(PPh₃)₂ (Ph: phenyl; Ind: indenyl), which have multiple phosphines to fulfill the 18-electron structures.

The polymerization proceeded smoothly to reach 90% conversion in 170 h, and gave the polymers with controlled molecular weights ($M_n = 11600$) and very narrow molecular weight distributions (MWD) ($M_w/M_n = 1.12$), by size-exclusion chromatography (SEC). It is noteworthy that the PEG-phosphine system induced much faster polymerization than that of PPh₃ counterpart (336 h, 60%). On the other hand, the addition of PEG to Ru(Cp*)Cl(PPh₃)₂ or [Ru(Cp*)Cl]₄ resulted in much slower polymerizations. Thus, PEG-phosphine works not only as the ligand to induce living radical polymerization but also as an additive which enhances the catalytic activity.¹²

Equally important, the catalyst was readily removed by washing the reaction mixture with cold water after polymerization, thereby 93% of the catalyst was removed (determined by ICP-AES).

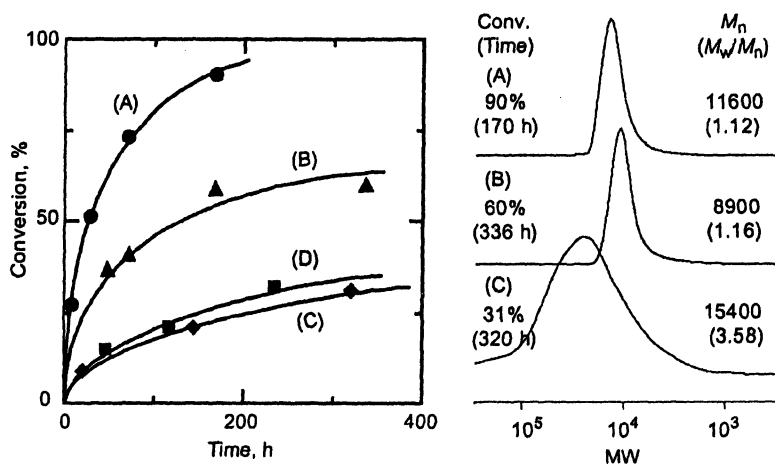


Figure 1. Polymerization of MMA catalyzed with Ru complex **1** in toluene at 80 °C: $[MMA]_0/[H-(MMA)_2-Cl]_0/[Ru]_0 = 2000/20/2.0$ mM. (A) **1** (●); (B) Ru(Cp*)Cl(PPh₃)₂/PEG (▲); (C) [Ru(Cp*)Cl]₄/PPh₃/PEG (◆) (D) [Ru(Cp*)Cl]₄.

Suspension Polymerization with **1** in Water: Thermally Regulated Phase Transfer Catalysis

As mentioned above, Ru(II) catalyst **1** is thermosensitive to change in nature from hydrophilic to hydrophobic upon responding raising temperature across the cloud point (e.g., ca. 80 °C for **1** with a PEG chain of average DP = 45). The polymerization of MMA in aqueous media was then examined. The mixture of MMA and the initiator in toluene was added into a perfectly homogeneous solution of **1** in water (Figure 2A). At first, the mixture separated into two distinct phases at ambient temperature around 25 °C (Figure 2B), and stirring this mixture led to an emulsion, due to the amphiphilic nature of the PEG ligand (Figure 2C). When the emulsion was heated to 80 °C, during which process the catalyst turned hydrophobic, aqueous and organic phases separated again, but the catalyst was now transferred into the organic phase (Figure 2D). With the catalyst exposed to the monomer/initiator mixture in the organic phase, a polymerization proceeded in suspension under vigorous stirring at this temperature. The stirred suspension was then cooled down to 0 °C to terminate the polymerization, and the reaction media became an emulsion once again, with the catalyst now returning to the amphiphilic and more hydrophilic state at this low temperature (Figure 2E). A portion of toluene was added into the mixture to decrease the viscosity, and thereby the solution separated into two phases slowly (Figure 2F).

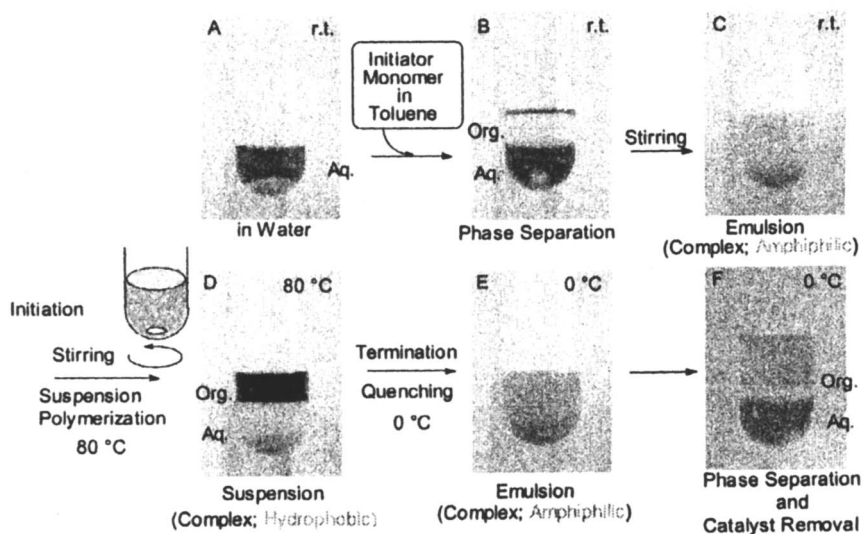


Figure 2. Procedure of the suspension polymerization of MMA with **1**.

Figure 3 shows the results of the suspension polymerizations catalyzed with **1**. The polymerization turned out to proceed much faster than in the corresponding homogeneous system in toluene: Aqueous system; 33 h, 94% (Figure 3B); toluene system; 124 h, 92% (Figure 3C). Such acceleration effects are also observed in other aqueous systems.^{9a} Addition of tributylamine, an additive, gave faster polymerization and polymers with controlled M_n and narrow MWD (Figure 3A).

The molecular weights of the obtained polymer (by size-exclusion chromatography with PMMA standards) agreed well with the calculated values assuming that one initiator produced one polymer chain, and the molecular weight distribution remains very narrow ($M_w/M_n = 1.12$).

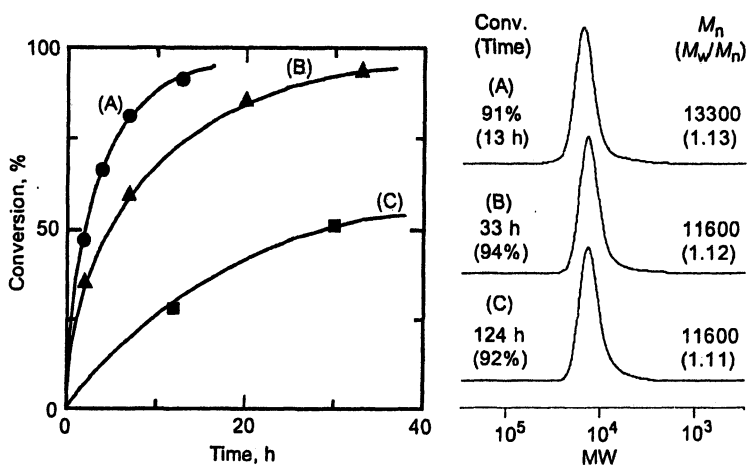


Figure 3. Suspension polymerization of MMA catalyzed with **1** in the presence (A, ●) or absence (B, ▲) of tributylamine in toluene/water (organic/water = 1/1 v/v), and solution polymerization in toluene (C, ■) at 80 °C. $[MMA]_0/[H-(MMA)_2-Cl]_0/[Ru(Cp^*)Cl]_0/[PEG-Ligand]_0 = 4000/40/1.0/8.0$ mM.

Catalyst Removal by Phase Transfer Catalysis and Catalyst Recycling

Catalyst Removal from Products

Catalyst removal and recycle was then examined. Taking advantage of the thermosensitivity of the PEG-phosphine ligand, a simple temperature cycle enabled an efficient removal of the catalyst (and possibly its residues) from the product polymers. In the suspension polymerization describe above, for

example, the product polymers were isolated from the final two-phase mixture (Figure 2F). The visually colorless and white solid indicated an efficient removal of the Ru residue, which should be dark brown. According to the metal-residue analysis by inductively coupled plasma atomic emission spectroscopy (ICP-EMS), the Ru content in the isolated polymers was 28 ppm, indicating ca. 97-% removal of the catalyst relative to the original content (1000 ppm) calculated from the initial catalyst concentration.

In the solution polymerization in toluene, also described above, the as-polymerized polymer solution in toluene, intensely colored dark brown due the catalyst, was washed three times with cold water, giving a nearly colorless transparent liquid from which the polymers were isolated by evaporation. ICP-EMS analysis of the isolated polymer showed a 93-% catalyst removal (from 1000 ppm to 72 ppm). A similar attempt for the polymers obtained with Ru(Cp*)Cl(PPh₃)₂ (a lipophilic catalyst), in contrast, resulted in just a 50-% removal (to 503 ppm).

Catalyst Recycle

After the first-phase polymerization in aqueous suspension at 80 °C had been completed (Figure 2F), the reaction mixture was cooled to below room temperature to induce phase separation and the solubility change in catalyst 1 into a hydrophilic state. The organic phase was removed, and a fresh mixture of MMA and the initiator [H-(MMA)₂-Cl] in toluene was then injected into the reaction tube followed by heating to 80 °C for radical polymerization; no amine additive was employed.

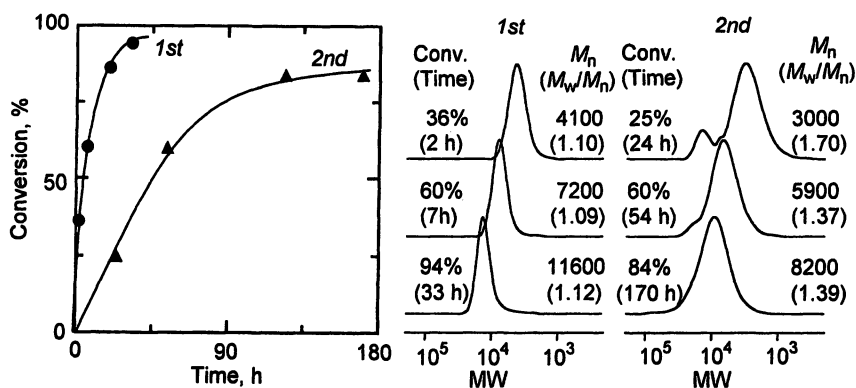


Figure 4. Catalyst recycle for living radical suspension polymerization of MMA with H-(MMA)₂-Cl/1 in toluene/water at 80 °C (organic/water = 1/1 v/v): [MMA]₀/[H-(MMA)₂-Cl]₀/[[Ru(Cp*)Cl]₀]/[PEG-Ligand]₀ = 4000/40/1.0/8.0 mM.

Though the second polymerization was slower than the first, it gave polymers with controlled M_n and relatively narrow MWDs ($M_w/M_n \sim 1.3$) (Figure 4), indicating that the recovered catalyst, though handled in air upon phase separation, remains active for living radical polymerization.

The slower polymerization with the recovered and recycled catalyst, however, suggests a partial loss of the complex **1** and/or its decomposition, which was not clarified further and should be a subject of future study. For the same reason, a repeated recovery and recycling of the catalyst was not attempted. Nevertheless, the results indicate that the thermosensitive catalyst with the PEG-phosphine ligand is promising for efficient removal of the Ru residue from the products as well as possible recycling of the precious catalyst by simple phase transfer catalysis.

Conclusions

In conclusion, the new ruthenium complex **1** bearing PEG chain exhibited the higher catalytic activity as well as thermosensitivity that enables catalyst removal and possibly catalyst recycle.

Experimental

Materials

Methyl methacrylate (Tokyo Kasei, >99%) was dried overnight over calcium chloride, and purified by double distillation from calcium hydride before use. $H-(MMA)_2-Cl$ ¹³ and PEG-phosphine¹⁴ and $[Ru(Cp^*)Cl]$ ₄¹⁵ were prepared according to the literatures. The ligand and Ru complex were handled in a glovebox (M. Braun Labmaster 130) under a moisture- and oxygen-free argon atmosphere ($H_2O < 1$ ppm, $O_2 < 1$ ppm). Toluene and THF were dried overnight over calcium chloride and distilled from sodium/benzophenone ketyl. *n*-Octane (internal standard for gas chromatography for MMA) was dried overnight over calcium chloride and was distilled twice from calcium hydride. Poly(ethylene glycol) methyl ether (Aldrich; $M_n \sim 2,000$; DP ~ 45), thionyl chloride (Wako, >95%), 4-iodophenol (Aldrich, 99%), sodium hydride (Wako, ca. 65% dispersion in mineral oil), potassium acetate (Aldrich, 99.98%), transdi(μ -acetato)bis[*o*-(*di*-*o*-tolyl-phosphino)benzyl]dipalladium(II) (STREM, 98%), diphenylphosphine (Tokyo Kasei, 90%), and potassium carbonate (Wako, 99.5%) were used as received.

Synthesis of End-Chlorinated PEG

Poly(ethylene glycol) methyl ether (8.0 g, 4.0 mmol) was refluxed in 10.0 mL of thionyl chloride at 90 °C for 17 h. Volatile substances were removed by evaporation to obtain end-chlorinated PEG [Cl-(CH₂CH₂O)_n-CH₃] (8.07 g). ¹H NMR (500.16 MHz, CDCl₃): δ 3.76 (t, 2H, ClCH₂), 3.48–3.80 (br, 180H, OCH₂), 3.38 (s, 3H, OCH₃).

Synthesis of Sodium 4-Iodophenoxide

A solution of 4-iodophenol (7.68 g, 34.9 mmol) in 10 mL of THF was added into slurry of sodium hydride (2.60 g, 71.5 mmol) in 10 mL of THF at room temperature and stirred for 1 h. The reaction solution was filtered and evaporated to obtain sodium 4-iodophenoxide (8.45 g).

Synthesis of Poly(ethylene Glycol) Methyl Ether 4-Iodophenyl Ether

In a two-necked round bottom flask, end-chlorinated PEG (6.12 g, 3.06 mmol) and sodium 4-iodophenoxide (1.20 g, 4.62 mmol) were reacted in 25 mL of DMA at 90 °C for 5 h. The solvent was removed by evaporation and the product was extracted with toluene (6.29 g, yield = 95.5%). ¹H NMR (500.16 MHz, CDCl₃): δ 7.54 (d, 2H, *ortho* to I), 6.69 (d, 2H, *meta* to I), 3.48–3.86 (br, 180H, OCH₂), 3.38 (s, 3H, OCH₃).

Synthesis of PEG-Phosphine¹⁴

In a two-necked round bottom flask, poly(ethylene glycol) methyl ether 4-iodophenyl ether (6.29 g, 2.89 mmol), potassium acetate (0.670 g, 6.83 mmol), and trans-di(μ-acetato)bis[*o*-(di-*o*-tolyl-phosphino)benzyl]dipalladium(II) (10.7 mg, 0.0114 mmol) were combined under an inert atmosphere. A 30 mL aliquot of dimethylacetamide was added, and the mixture was degassed. After addition of 1.00 mL of diphenylphosphine (1.08 g, 5.80 mmol), the reaction mixture was heated at 110 °C for 17 h. After removal of the solvent the residue was dissolved in 40.0 mL of chloroform, 1.30 g of potassium carbonate was added, and the mixture was stirred overnight. After filtration, the phosphine-ligand was obtained by evaporation (3.95 g, yield = 61%). ¹H NMR (500.16 MHz, CDCl₃): δ 6.85–7.40 (br, 14H, aromatic), 3.48–3.90 (br, 180H, OCH₂), 3.38 (s, 3H, OCH₃).

Solution Polymerization

The solution polymerization of MMA with catalyst **1** was carried out by the syringe technique under argon in baked glass tubes equipped with a three-way stopcock. Typical procedures are as follows (see Figure 1): In a 50 mL round-bottomed flask was placed $[\text{Ru}(\text{Cp}^*)\text{Cl}]_4$ (0.0035 mmol, 3.8 mg). To this, toluene (4.74 mL), PEG-phosphine (0.028 mmol, 0.28 mL, 100 mM in toluene), *n*-octane (0.32 mL; internal standard for gas chromatography), MMA (14 mmol, 1.50 mL), and a solution of initiator $\text{H}-(\text{MMA})_2-\text{Cl}$ (0.14 mmol, 0.156 mL, 900 mM in toluene) were added sequentially in this order at 25 °C under argon. The total volume of the reaction mixture was thus 7.0 mL. Five aliquots (1.0 mL each) of the solution were distributed into the baked glass tubes with a three-way stopcock and placed in an oil bath at 80 °C. In predetermined intervals, the reaction was terminated by cooling the mixture to -78 °C. Conversion of MMA was determined by gas chromatography with *n*-octane as an internal standard. The quenched reaction solutions were diluted with toluene (ca. 15 mL), washed with cold water, and evaporated to dryness to give the polymers.

Suspension Polymerization

Ru complex **1** was prepared by mixing $[\text{Ru}(\text{Cp}^*)\text{Cl}]_4$ (0.069 mmol, 74.3 mg) and PEG-phosphine (0.55 mmol, 1.20 g) under dry nitrogen at 80 °C in toluene for 1 h, and the solvent was removed by evaporation; no further purification was

The isolated complex **1** (0.024 mmol, 112 mg) was dissolved in 6.0 mL of water, and the solution was distributed into glass tubes equipped with a three-way stopcock (1.0 mL each). A mixture of toluene (2.54 mL), *n*-octane (0.56 mL), MMA (24 mmol, 2.58 mL), and $\text{H}-(\text{MMA})_2-\text{Cl}$ (0.24 mmol, 0.32 mL, 734 mM in toluene) was added into the glass tubes; thus the total volume of the solution was 6.0 mL. The polymerization was initiated by placing the tubes in an oil bath at 80 °C. During the reaction period, the reaction media was stirred by a magnetic stirrer.

Polymer Characterization

The M_n , M_w/M_n , and MWD curves of the polymers were determined by size-exclusion chromatography in chloroform at 40 °C on the three polystyrene gel columns (Shodex K-805L × 3) that were connected to Jasco PU-980 precision pump and a Jasco RI-930 refractive index detector. The columns were calibrated against eleven standard poly(MMA) samples (Polymer Laboratories;

$M_n = 630\text{--}1,200,000$; $M_w/M_n = 1.04\text{--}1.22$) as well as the monomer. The metal residue content in polymers was analyzed by inductively coupled plasma atomic emission spectroscopy (ICP-EMS) on a Jarrell-Ash IRIS AP instrument.

Acknowledgments

This work was supported by a Grant-in-aid for Scientific Research on Priority Area (No. 13128201) from Ministry of Education, Culture, Sports, Science and Technology, Japan. We thank Mr. H. Sasaki and Mr. T. Ono (Kuraray Co. Ltd.) for ICP-AES analysis.

References

1. Li, C.-J.; Chan, T.-H. *Organic Reactions in Aqueous Media*; Jown Wiley & Sons: New York, 1997.
2. Moad, G.; Solomon, D. H. *The Chemistry of Free Radical Polymerization*; Elsevier Science: Oxford, U. K., 1995.
3. (a) Kamigaito, M.; Ando, T.; Sawamoto, M. *Chem. Rev.* **2001**, *101*, 3689. (b) Matyjaszewski, K.; Xia, J. *Chem. Rev.* **2001**, *101*, 2921. (c) Hawker, C. J.; Bosma, A. W.; Harth, E. *Chem. Rev.* **2001**, *101*, 3661. (d) Matyjaszewski, K., Ed.; *ACS Symposium Series 768*; American Chemical Society: Washington, DC, 2000. (e) Sawamoto, M.; Kamigaito, M. In *Synthesis of Polymers*; Schlüter, A.-D., Ed.; Materials Science and Technology Series; Wiley-VCH: Weinheim, Germany, 1999, Chapter 6; pp 163–194.
4. Kato, M.; Kamigaito, M.; Sawamoto, M.; Higashimura, T. *Macromolecules* **1995**, *28*, 1721.
5. Wang, J.-S.; Matyjaszewski, K. *J. Am. Chem. Soc.* **1995**, *117*, 5614.
6. Percec, V.; Barboiu, B. *Macromolecules* **1995**, *28*, 7970.
7. Granel, C.; Dubois, Ph.; Jérôme, R.; Teyssié, Ph. *Macromolecules* **1996**, *29*, 8576.
8. Haddleton, D. M.; Jasieczek, C. B.; Hannon, M. J.; Shooter, A. J. *Macromolecules* **1997**, *30*, 2190.
9. (a) Nishikawa, T.; Kamigaito, M.; Sawamoto, M. *Macromolecules* **1999**, *32*, 2204. (b) Fuji, Y.; Ando, T.; Kamigaito, M.; Sawamoto, M. *Macromolecules* **2002**, *35*, 2949. (c) Sawamoto, M.; Kamigaito, M. *Macromol. Symp.* **2002**, *177*, 17.
10. Haddleton, D. M.; Jackson, S. G.; Bon, S. A. F. *J. Am. Chem. Soc.* **2000**, *122*, 1542.
11. Carmichael, A. J.; Haddleton, D. M.; Bon, S. A. F.; Seddon, K. R. *Chem. Commun.* **2000**, 1237.

12. (a) Ando, T.; Kato, M.; Kamigaito, M.; Sawamoto, M. *Macromolecules* **1996**, *29*, 1070. (b) Hamasaki, S.; Sawauchi, C.; Kamigaito, M.; Sawamoto, M. *J. Polym. Sci., Part A, Polym. Chem.* **2002**, *40*, 617. (c) Hamasaki, S.; Kamigaito, M.; Sawamoto, M. *Macromolecules* **2002**, *35*, 2934.
13. Ando, T.; Kamigaito, M.; Sawamoto, M. *Macromolecules* **2000**, *33*, 2819.
14. Persigehl, P.; Jordan, R.; Nuyken, O. *Macromolecules* **2000**, *33*, 6977.
15. Fagan, P. J.; Ward, M. D.; Calabrese, J. C. *J. Am. Chem. Soc.* **1989**, *111*, 1698.

Chapter 3

Stereospecific Living Radical Polymerization

Masami Kamigaito¹, Kotaro Satoh¹, Decheng Wan¹,
Yuya Sugiyama¹, Kazuhiko Koumura¹, Takuya Shibata¹,
and Yoshio Okamoto²

¹Department of Applied Chemistry, Graduate School of Engineering, and
²Eco Topia Science Institute, Nagoya University, Nagoya 464–8603, Japan

The simultaneous control of the molecular weights and tacticity was attained by several appropriate combinations of a controlled/living radical polymerization and a stereospecific radical polymerization. They included the ruthenium- and iron-catalyzed living radical polymerizations of methacrylates and acrylamides in polar solvents and in the presence of metal triflates, respectively, the iodine-transfer radical polymerization of vinyl acetate in fluoroalcohols, and the radical polymerization of *N*-vinylpyrrolidone with RAFT/MADIX agents in fluoroalcohols. In each case, the combined system can give polymers with controlled molecular weights and a high iso- or syndiotacticity.

Introduction

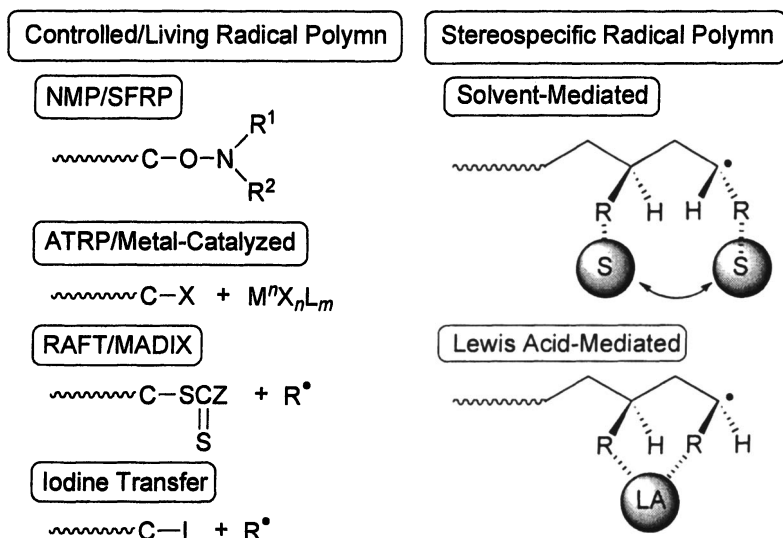
The simultaneous control of the molecular weights and stereochemistry of a polymer chain is one of the most challenging targets in radical polymerization although either is now achievable by many methods (Scheme 1).

Specifically for controlling the molecular weights, there have been significant developments over the past 10 years, which can produce polymers with the molecular weights controlled by the monomer to initiator ratio and narrow molecular weight distributions (MWDs) (1). Some of the systems are

versatile and available for various vinyl monomers. The representative polymerizations are the nitroxide-mediated polymerization (NMP) (2,3), metal-catalyzed living radical polymerization or atom transfer radical polymerization (ATRP) (4–8), and polymerization controlled by reversible addition fragmentation chain transfer (RAFT) (9) or macromolecular design via the interchange of xanthates (MADIX) (10). The concept or the strategy for controlling the molecular weights is common, namely, to introduce the dormant species that can rapidly interchange with the growing radical species with the aid of some stimulus such as heat, catalyst, or radical generator.

In comparison to a large number of examples concerning the molecular weight control, there are not very many for controlling the tacticity of the polymers. However, in more recent years, general methods for controlling the tacticity in radical polymerization of various polar monomers have been developed (11). They rely on the use of polar solvents or Lewis acid additives that can interact with the substituents of the monomer or the growing terminal via hydrogen-bonding or coordination.

For example, a bulky and protic fluoroalcohol affords syndiotactic polymers from vinyl acetate (12) and methyl methacrylate (13) while a metal triflate or MgBr_2 gives isotactic polymers in (meth)acrylamide (14) and methacrylate (15, 16) polymerizations.



Scheme 1. Several systems for controlled/living radical polymerization and stereospecific radical polymerization.

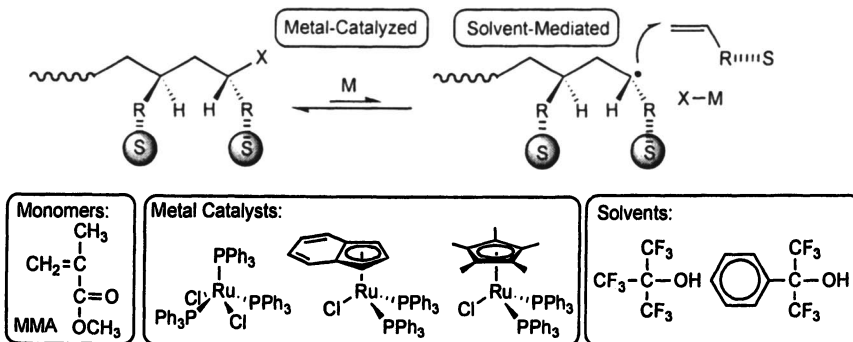
These developments more or less suggest one to examine the simultaneous control of the molecular weights and tacticity by effectively combining the living and stereospecific radical polymerizations. The key to the success is to find

appropriate combinations where one of the controls should not be lost by the other component. Although several effective combinations have already been reported for a few monomers, it is still unclear which combination is desirable and applicable for certain types of monomers (17–20). This article is an overview of our quite recent results on stereospecific living radical polymerizations that can simultaneously control the molecular weights and tacticity. They include (1) the ruthenium-catalyzed living radical polymerizations of methacrylates in fluoroalcohols, (2) the iron-catalyzed living radical polymerizations of acrylamides in the presence of metal triflates, (3) the iodine-transfer radical polymerizations of vinyl acetate in fluoroalcohols, and (4) the xanthate-mediated radical polymerizations of *N*-vinylpyrrolidone in fluoroalcohols.

Results and Discussion

Ruthenium-Catalyzed Systems in Fluoroalcohols for Methyl Methacrylate

As we have shown that $\text{RuCl}_2(\text{PPh}_3)_3$ is tolerant to various polar solvents like methanol and water and can induce the living radical polymerization of methyl methacrylate (MMA) even in such solvents (21), we first examined the ruthenium complex in a protic and bulky fluoroalcohol $[(\text{CF}_3)_3\text{COH}]$ for the possible syndiospecific living radical polymerization of MMA (Scheme 2).



Scheme 2. Ruthenium-catalyzed living radical polymerization in fluoroalcohols.

As shown in Figure 1, $\text{RuCl}_2(\text{PPh}_3)_3$ induced a faster polymerization in the fluoroalcohol at 60 °C than in toluene at 80 °C. Under the same conditions, the indenyl complex $[\text{Ru}(\text{Ind})\text{Cl}(\text{PPh}_3)_2]$ led to a much faster polymerization. The number-average molecular weights (M_n) of the obtained polymers were close to the calculated values assuming that one molecule of the initiator $[\text{Me}_2\text{C}(\text{CO}_2\text{Me})\text{CH}_2\text{C}(\text{CO}_2\text{Me})(\text{Me})\text{Cl}]$ generates one living polymer chain. The

MWDs of the polymers were relatively narrow. Therefore, these ruthenium catalysts show higher activities in the fluoroalcohol and still maintain their control of the polymer molecular weights. Furthermore, the polymers obtained using $\text{RuCl}_2(\text{PPh}_3)_3$ in $(\text{CF}_3)_3\text{COH}$ had a higher syndiotacticity ($rr = 68\%$) than with the same catalyst in toluene ($rr = 63\%$). Thus $(\text{CF}_3)_3\text{COH}$ generated the syndiotactic PMMA even with the ruthenium-catalyzed system, where the rr was almost the same as that with the AIBN-induced system (13).

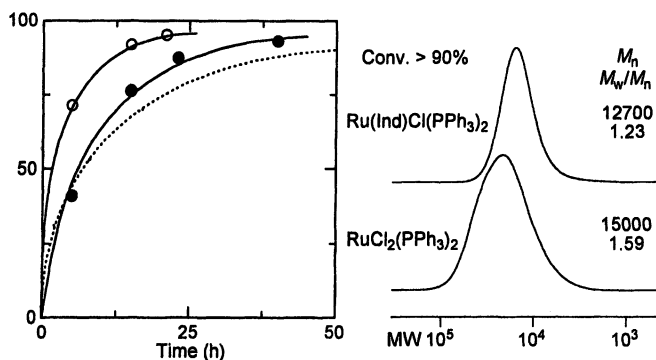


Figure 1. Polymerization of MMA with $\text{RuCl}_2(\text{PPh}_3)_3$ (J) and $\text{Ru}(\text{Ind})\text{Cl}(\text{PPh}_3)_2$ (E) in $(\text{CF}_3)_3\text{COH}$ at $60\text{ }^\circ\text{C}$: $[M]_0 = 2.0\text{ M}$; $[(\text{MMA})_2\text{-Cl}]_0 = 20\text{ mM}$; $[\text{Ru}^{\text{II}}]_0 = 10\text{ mM}$; $[\text{n-Bu}_3\text{N}]_0 = 40\text{ mM}$. The dashed line is for the polymerization with $\text{RuCl}_2(\text{PPh}_3)_3$ in toluene at $80\text{ }^\circ\text{C}$ with the same reagent concentrations.

A further improvement was accomplished using $\text{RuCp}^*\text{Cl}(\text{PPh}_3)_2$ (22) in another bulky fluoroalcohol $[(\text{CF}_3)_2\text{C}(\text{Ph})\text{OH}]$ at a lower temperature (Figure 2).

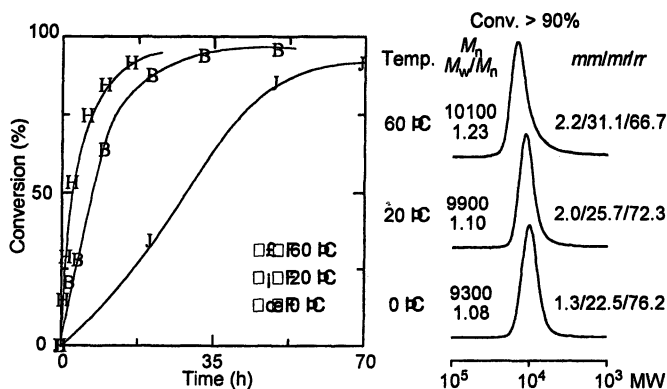


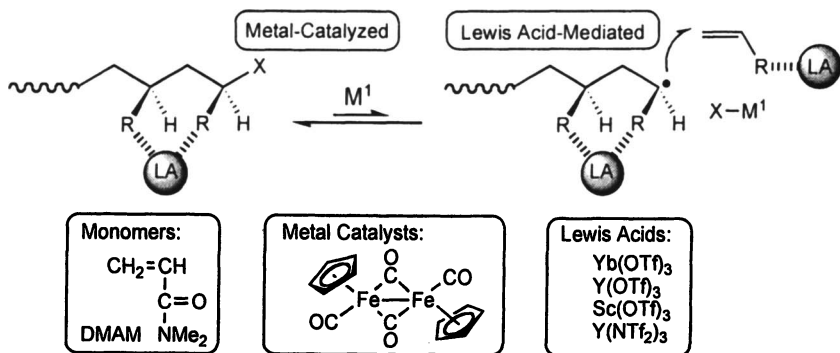
Figure 2. Polymerization of MMA with $\text{RuCp}^*\text{Cl}(\text{PPh}_3)_2$ in $(\text{CF}_3)_2\text{C}(\text{Ph})\text{OH}$: $[M]_0 = 2.0\text{ M}$; $[(\text{MMA})_2\text{-Cl}]_0 = 20\text{ mM}$; $[\text{Ru}^{\text{II}}]_0 = 4.0\text{ mM}$; $[\text{n-Bu}_3\text{N}]_0 = 40\text{ mM}$.

The Cp*-complex led to efficient polymerizations even at 0 °C to give polymers with controlled molecular weights in agreement with the calculated values and very narrow MWDs ($M_w/M_n < 1.1$). The triad racemo content (rr) increased with the decreasing temperature and reached 76% at 0 °C.

These results indicate that the ruthenium-catalyzed living radical polymerization proceeds via a syndiospecific chain growth to afford polymers with controlled molecular weights and high syndiotacticity.

Iron-Catalyzed Systems with Metal Triflates for Acrylamides

Among the variety of iron catalysts effective for the living radical polymerizations, an iron(I) complex, $[\text{FeCp}(\text{CO})_2]_2$, is one of the most active and versatile and is especially effective for the fast living radical polymerization of acrylates and acrylamides (23). The Cp-based iron carbonyl complexes are exclusively tolerant to water unlike the other iron catalysts such as $\text{FeBr}_2(\text{PPh}_3)_2$ for the living radical polymerization (24). On the other hand, the isospecific radical polymerization of (meth)acrylamides was reported with the use of metal triflates such as $\text{Y}(\text{OTf})_3$ and $\text{Yb}(\text{OTf})_3$, especially in MeOH, where the highly isotactic polymer was obtained ($m = 90\%$) (14). The added Lewis acid most probably coordinates to the carbonyl groups of the growing polymer chain end and/or monomer to restrict the free rotation of the sp^2 -like growing carbon radical species and results in isospecific chain growth (25). Thus we employed $[\text{FeCp}(\text{CO})_2]_2$ in the presence of $\text{Y}(\text{OTf})_3$ for the possible isospecific living radical polymerization of *N,N*-dimethylacrylamide (DMAM) (Scheme 3) (26).



Scheme 3. Iron-catalyzed living radical polymerization with Lewis acid.

Upon the addition of $\text{Y}(\text{OTf})_3$ into the iron-based living radical system ($\text{Me}_2\text{C}(\text{CO}_2\text{Et})\text{I}/[\text{FeCp}(\text{CO})_2]_2/\text{I}_2$) in toluene/methanol (1/1 v/v), the polymerization was drastically accelerated and reached a 96% conversion within 1 h. A similar acceleration was observed in the AIBN-initiated conventional

radical polymerization using the same monomer due to the coordination of the Lewis acid to the growing polymer terminal and monomer. The iron(I) complex thus survives even in the presence of the metal triflate in MeOH and possesses the ability of efficiently forming the polymers. The M_n of the polymers increased in direct proportion to monomer conversion and agreed well with the calculated values (Figure 3). The MWDs were broader in the presence of $Y(OTf)_3$ probably due to the fast propagation of the radical species originating from the coordination of the Lewis acid.

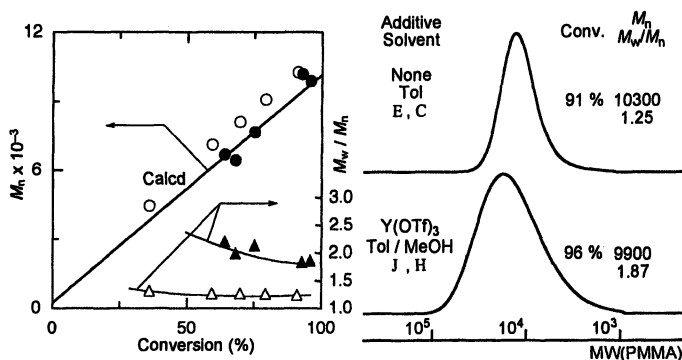


Figure 3. Polymerization of DMAM with $[FeCp(CO)_2]_2$ at 60 °C: $[M]_0 = 4.0$ M; $[Me_2C(CO_2Et)I]_0 = 40$ mM; $[Fe^I]_0 = 40$ mM; $[I_2]_0 = 20$ mM; $[Y(OTf)_3]_0 = 0$ or 200 mM.

The meso-dyad content (m) of the polymers obtained with $[FeCp(CO)_2]_2$ and $Y(OTf)_3$ was 82%, being as high as that obtained in AIBN and $Y(OTf)_3$ under similar conditions (Figure 4).

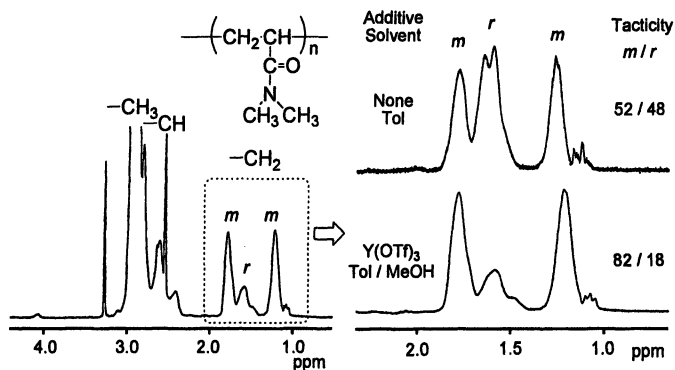
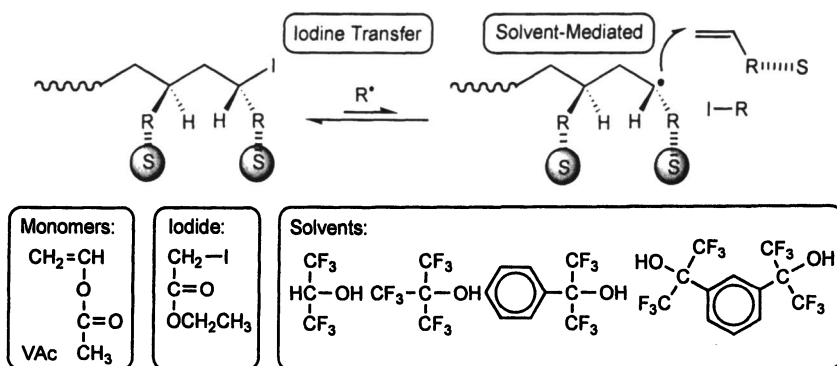


Figure 4. 1H NMR Spectra (in $DMSO-d_6$, at 170 °C) of poly(DMAM) obtained with the Fe^I -based system in the absence and presence of $Y(OTf)_3$ at 60 °C.

These results indicate that both the iron and the yttrium catalysts fulfill their roles to result in polymers with controlled molecular weights and high isotacticity. A similar system was also reported for the combination of CuBr and Y(OTf)₃ while the polymerization seemed to stop around 50% conversion probably due to the loss of the activity of the copper catalyst (18). Therefore, the iron(I) catalyst shows a relatively high activity although the polymerization may also proceed via an iodine-transfer mechanism.

Iodine-Transfer Radical Polymerization in Fluoroalcohols for Vinyl Acetate

Vinyl acetate (VAc) is a unique vinyl monomer that can be polymerized only via a radical mechanism into high molecular weight polymers while the polymer is familiar as the precursor of poly(vinyl alcohol). Since the molecular weights and the tacticity of poly(vinyl alcohol) significantly affect the polymer property, the control of the radical polymerization of VAc is valued from the viewpoint of not only fundamental but also industrial chemistry. However, the unconjugated vinyl group renders the control very difficult in comparison to conjugated monomers because the resulting radical species is highly reactive resulting in rapid propagation and some inherent side reactions. Irrespective of such tough situations, there have been several effective systems for controlling the molecular weights and tacticity. Among those for controlling the molecular weights, which now include iodine-transfer (27), iron-catalyzed (23c), RAFT/MADIX (29–34), organotellurium (35), and cobalt-mediated (36,37) radical polymerizations, the iodine-transfer radical polymerization is one of the simplest due to the easily accessible initiating species consisting of an alkyl iodide and a radical generator. For controlling the steric structure, some bulky and protic fluoroalcohols are highly effective in leading to the syndiospecific radical polymerization of VAc (12). Herein, we investigated the iodine-transfer radical polymerization in several fluoroalcohols (Scheme 4) (38).



Scheme 4. Iodine-transfer radical polymerization of VAc in fluoroalcohols.

The iodine-transfer radical polymerization of VAc was investigated in $(\text{CF}_3)_3\text{COH}$, $(\text{CF}_3)_2\text{CHOH}$, $(\text{CF}_3)_2\text{C}(\text{Ph})\text{OH}$, and $m\text{-C}_6\text{H}_4[\text{C}(\text{CF}_3)_2\text{OH}]_2$ at 20 °C with V-70 $[\text{MeOCMe}_2\text{CH}_2\text{CMe}(\text{CN})\text{N}=\text{NCMe}(\text{CN})\text{CH}_2\text{CMe}_2\text{OMe}]$ as the azo-based low-temperature radical initiator. In all the solvents, the polymerization smoothly occurred (Figure 5). The initial rate in the three fluoroalcohols except for hexafluoroisopropanol was greater than in the bulk while the final conversions were lower. The MWDs of the polymers depend on the fluoroalcohols and became broader in the following order: $m\text{-C}_6\text{H}_4[\text{C}(\text{CF}_3)_2\text{OH}]_2$ ($M_w/M_n = 1.20$) < $(\text{CF}_3)_2\text{C}(\text{Ph})\text{OH}$ (1.46) \sim $(\text{CF}_3)_3\text{COH}$ (1.46) < bulk (1.73) < $(\text{CF}_3)_2\text{CHOH}$ (2.67). In most of the fluoroalcohols, the molecular weight control was better than in the bulk, where the best molecular weight control was achieved with the fluorodiols ($M_w/M_n = 1.20$). The polymerization in $(\text{CF}_3)_2\text{CHOH}$ apparently suffers from some side reactions.

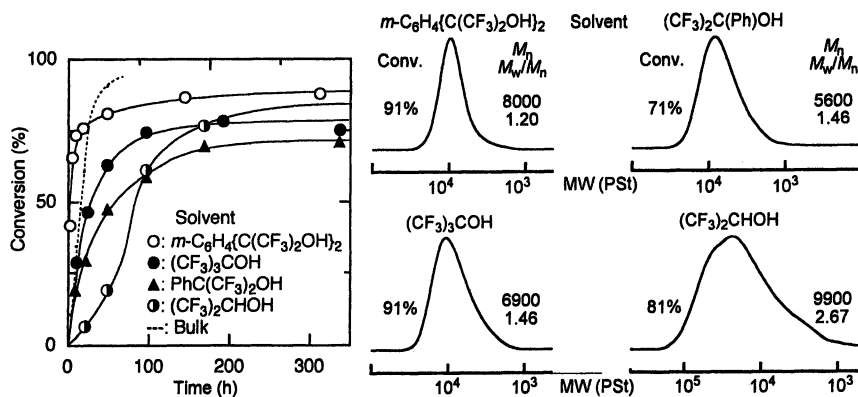


Figure 5. Iodine-transfer radical polymerization of VAc in fluoroalcohols at 20 °C: $[M]_0 = 2.0 \text{ M}$; $[\text{CH}_2(\text{CO}_2\text{Et})\text{I}]_0 = 20 \text{ mM}$; $[\text{V-70}]_0 = 40 \text{ mM}$; $\text{VAc}/\text{fluoroalcohol} = 1/4$ (v/v).

Figure 6 shows the typical ^1H NMR spectra of poly(VAc) and poly(vinyl alcohol) obtained by saponification. The tacticity of poly(vinyl alcohol) can be calculated from the hydroxyl protons at 4–5 ppm. As summarized in the inset table in Figure 6, all the fluoroalcohols gave a high syndiotacticity in comparison with that in the bulk. The fluorodiols also proved effective for the syndiotactic polymerization similar to $(\text{CF}_3)_3\text{COH}$. Specifically, in $m\text{-C}_6\text{H}_4[\text{C}(\text{CF}_3)_2\text{OH}]_2$, the simultaneous control of the molecular weight and tacticity was most efficiently attained.

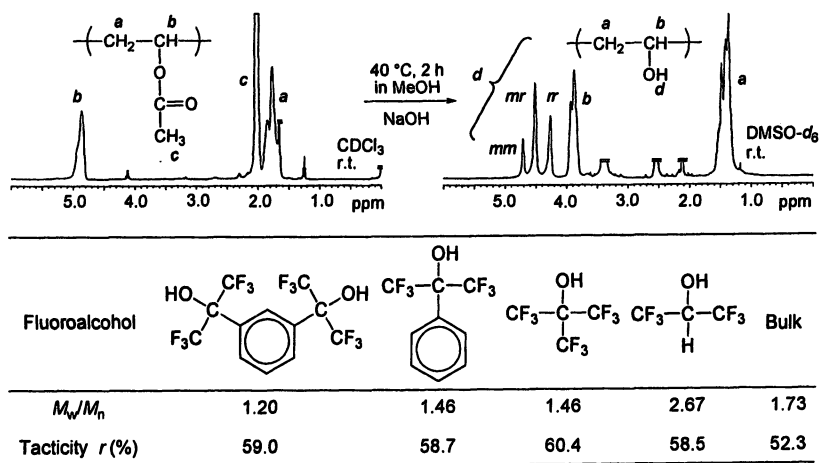
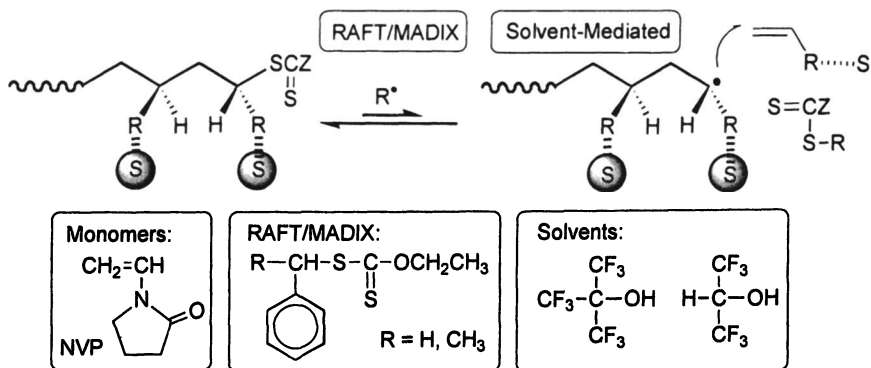


Figure 6. ^1H NMR Spectra of poly(VAc) and poly(vinyl alcohol) obtained with iodine-transfer radical polymerization in fluoroalcohols at 20 °C and the control of molecular weight and tacticity.

RAFT/MADIX Polymerization in Fluoroalcohols for *N*-Vinylpyrrolidone

N-Vinylpyrrolidone (NVP) is another unconjugated vinyl monomer, from which high molecular weight polymers are obtained only by radical polymerization. In contrast to the wide applicability of the polymers as non-toxic polymers, only a few examples of the controlled polymerizations have been reported for this monomer (11e,39) due to the highly reactive radical species and the polar substituents. Thus we investigated the control of the molecular weight and tacticity using xanthates and fluoroalcohols, respectively, and then combined them together for the simultaneous control (Scheme 5) (40).



Scheme 5. RAFT/MADIX polymerization of NVP in fluoroalcohols.

The AIBN-initiated bulk radical polymerization of NVP was first investigated in the absence and the presence of xanthates at 60 °C. The use of xanthates slightly retarded the radical polymerization as usually observed in the RAFT polymerization of other monomers (Figure 7). The molecular weights of the polymers obtained with these xanthates increased as the polymerization proceeded. Especially, with the xanthate possessing the 1-phenylethyl fragment, the M_n increased in direct proportion to polymer yield and agreed well with the calculated values assuming that one molecule of the polymer chain is generated from one molecule of xanthate.

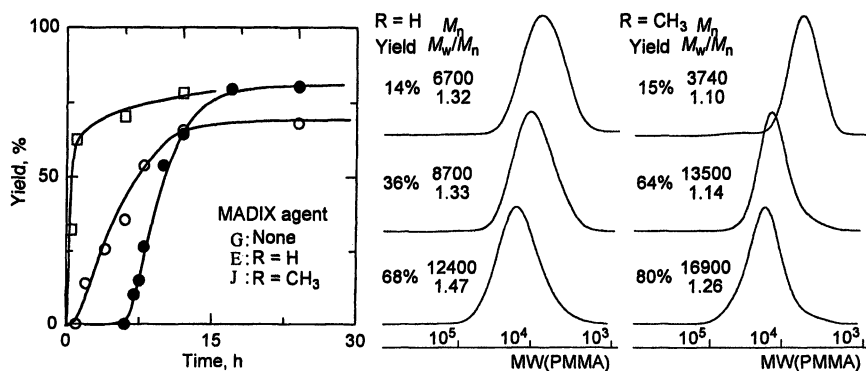


Figure 7. Xanthate-mediated polymerization of NVP in bulk at 60 °C: $[M]_0 = 9.5 \text{ M}$; $[\text{xanthate}]_0 = 63 \text{ mM}$; $[\text{AIBN}]_0 = 13 \text{ mM}$.

Table I. Free Radical Polymerization of NVP in Fluoroalcohols^a

| Temp., °C | Solvent | Yield, % | M_n^b | M_w/M_n^b | r_1 , % ^c |
|-----------|--------------------------------------|----------|---------|-------------|------------------------|
| 60 | Bulk | 58 | 135 200 | 3.11 | 53.5 |
| 60 | CF ₃ CH ₂ OH | 59 | 116 200 | 2.96 | 54.5 |
| 60 | (CF ₃) ₂ CHOH | 57 | 149 500 | 3.05 | 55.6 |
| 60 | (CF ₃) ₃ COH | 36 | 121 200 | 2.89 | 58.0 |
| 20 | Bulk | 58 | 126 900 | 4.79 | 53.5 |
| 20 | CF ₃ CH ₂ OH | 65 | 130 000 | 3.11 | 54.6 |
| 20 | (CF ₃) ₂ CHOH | 73 | 164 000 | 2.30 | 55.8 |
| 20 | (CF ₃) ₃ COH | 83 | 92 400 | 3.36 | 59.0 |

^a Polymerization conditions: fluoroalcohol/NVP = 1.65/1 v/v, in the presence of 1% (based on monomer) AIBN, reaction time: 12 h (60 °C), 36 h (20 °C), reaction at 20 °C was under UV irradiation. (400-W high-pressure mercury lamp).

^b Determined by SEC in DMF containing 0.1 M LiCl.

^c Determined by ¹³C NMR in D₂O at 84 °C.

As for the tacticity control, three fluoroalcohols [$\text{CF}_3\text{CH}_2\text{OH}$, $(\text{CF}_3)_2\text{CHOH}$, $(\text{CF}_3)_3\text{COH}$] were employed for possible stereoregulation. An increase in the number of CF_3 -groups, bulkiness, and acidity increased the syndiotacticity of the resulting poly(NVP) (Table I). Specifically, in $(\text{CF}_3)_3\text{COH}$ at a low temperature (20°C), the highest racemo content was attained ($r = 59.0\%$).

The simultaneous control of the molecular weight and tacticity was then examined using the phenylethyl-type xanthate in $(\text{CF}_3)_3\text{COH}$ at 20°C . The obtained polymer had controlled molecular weights ($M_n = 12600$), narrow MWDs ($M_w/M_n = 1.28$), and a high syndiotacticity ($r = 59.8\%$).

Conclusions

The simultaneous control of the molecular weights and tacticity was attained by various combinations of the living and stereospecific radical polymerization of several monomers (Table II). The simultaneous control for each monomer has now been achieved by a specific combination of the systems indicated by a gray-colored cell in the table. Although the judicious choice of the reagents and reaction conditions is necessary for the precise control of both, the stereospecific living radical polymerization would provide fruitful developments in precision polymer synthesis and functional materials.

Table II. Status Quo of Living and Stereospecific Radical Polymerization

| Radical Polymn Monomers | | Controlled/Living | | | | Stereospecific | |
|----------------------------|---|-------------------|----------------|----------------|--------|---|---|
| | | NMP/ SFRP | ATRP/ Metal | RAFT/ MADIX | Iodine | Solvent | Lewis Acid |
| Conjugated | $\begin{array}{c} \text{CH}_3 \\ \\ \text{CH}_2=\text{C} \\ \\ \text{C}=\text{O} \\ \\ \text{OR} \end{array}$ | — | ○ | ○ | — | Syndio-Fluoroalcohol ($\text{R} = \text{CH}_3$) Aprotic Solvent ($\text{R} = \text{CH}_2\text{CH}_2\text{OH}$) | Iso-Metal Triflate MgBr_2 ($\text{R} = \text{CH}_3$) |
| | $\begin{array}{c} \text{CH}_2=\text{CH} \\ \\ \text{C}=\text{O} \\ \\ \text{NMe}_2 \end{array}$ | ○ | ○ | ○ | — | — | Iso-Metal Triflate |
| Unconjugated | $\begin{array}{c} \text{CH}_2=\text{CH} \\ \\ \text{OCCH}_3 \\ \\ \text{O} \end{array}$ | — | ○ | ○ | ○ | Syndio-Fluoroalcohol | (Decomposition) |
| | $\begin{array}{c} \text{CH}_2=\text{CH} \\ \\ \text{N} \\ \\ \text{O} \end{array}$ | — | — | ○ | — | Syndio-Fluoroalcohol | (Decomposition) |

— : Not Attained or Not Studied

Acknowledgment

This work was supported in part by the 21st Century Program "Nature-Guided Materials Processing" and a Grant-in-Aid for Scientific Research (B) No. 16350062 and Priority Areas "Advanced Molecular Transformations of Carbon Resources" from the Ministry of Education, Culture, Sports, Science and Technology, Japan, the Mitsubishi Foundation, and Tokuyama Science Foundation.

References

1. (a) *Controlled Radical Polymerization*; Matyjaszewski, K., Ed.; ACS Symposium Series 685; American Chemical Society: Washington, DC, 1998. (b) *Controlled/Living Radical Polymerization*; Matyjaszewski, K., Ed.; ACS Symposium Series 768; American Chemical Society: Washington, DC, 2000. (c) *Advances in Controlled/Living Radical Polymerization*; Matyjaszewski, K., Ed.; ACS Symposium Series 854; American Chemical Society: Washington, DC, 2003.
2. (a) Georges, M. K.; Veregin, R. P. N.; Kazmaier, P. M.; Hamer, G. K. *Macromolecules* **1993**, *26*, 2987. (b) Georges, M. K.; Veregin, R. P. N.; Kazmaier, P. M.; Hamer, G. K. *Trends Polym. Sci.* **1994**, *2*, 66.
3. (a) Hawker, C. J. *J. Am. Chem. Soc.* **1994**, *116*, 11185. (b) Hawker, C. J.; Bosman, A. W.; Harth, E. *Chem. Rev.* **2001**, *101*, 3661.
4. (a) Kato, M.; Kamigaito, M.; Sawamoto, M.; Higashimura, T. *Macromolecules* **1995**, *28*, 1721. (b) Kamigaito, M.; Ando, T.; Sawamoto, M. *Chem. Rev.* **2001**, *101*, 3689. (c) Kamigaito, M.; Ando, T.; Sawamoto, M. *Chem. Rec.* **2004**, *4*, 159.
5. (a) Wang, J.-S.; Matyjaszewski, K. *J. Am. Chem. Soc.* **1995**, *117*, 5614. (b) Matyjaszewski, K.; Xia, J. *Chem. Rev.* **2001**, *101*, 2921.
6. Percec, V.; Barboiu, B. *Macromolecules* **1995**, *28*, 7970.
7. Granel, C.; Dubois, P.; Jérôme, R.; Teyssié, P. *Macromolecules* **1996**, *29*, 8576.
8. Haddleton, D. M.; Jasieczek, C. B.; Hannon, M. J.; Shooter, A. J. *Macromolecules* **1997**, *30*, 2190.
9. (a) Chiefari, J.; Chong, Y. K.; Ercole, F.; Krstina, J. Jeffery, K.; Tam, P. T. Le.; Mayadunne, R. T. A.; Meijs, G. F.; Moad, C. L.; Moad, G.; Rizzardo, E.; Thang, S. H. *Macromolecules* **1998**, *31*, 5559. (b) Chong, Y. K.; Kristina, J.; Tam, P. T. Le.; Moad, G.; Postma, A.; Rizzardo, E.; Thang, S. H. *Macromolecules* **2003**, *36*, 2256. (c) Chiefari, J.; Mayadunne, R. T. A.; Moad, C. L.; Moad, G.; Rizzardo, E.; Postma, A.; Skidmoe, M. A.; Thang,

- S. H. *Macromolecules* **2003**, *36*, 2273. (d) Le, T. P.; Moad, G.; Rizzardo, E.; Thang, S. H. PCT Int. Appl. WO 98/01478.
10. (a) Destarac, M.; Bzducha, W.; Taton, D.; Gauthier-Gillaizeau, I.; Zard, S. *Macromol. Rapid Commun.* **2002**, *23*, 1049. (b) Charmot, D.; Corpart, P.; Michelet, D.; Zard, S.; Biadatti, T. PCT Int. Appl. WO 98/58974. (c) Destarac, M.; Charmot, D.; Zard, S.; Franck, X. PCT Int. Appl. WO 00/75207.
 11. Habaue, S.; Okamoto, Y. *Chem. Rec.* **2001**, *1*, 46.
 12. (a) Yamada, K.; Nakano, T.; Okamoto, Y. *Macromolecules* **1998**, *31*, 7598. (b) Yamada, K.; Nakano, T.; Okamoto, Y. *J. Polym. Sci., Part A: Polym. Chem.* **1999**, *37*, 2677. (c) Yamada, K.; Nakano, T.; Okamoto, Y. *J. Polym. Sci., Part A: Polym. Chem.* **2000**, *38*, 220. (d) Yamada, K.; Nakano, T.; Okamoto, Y. *Polym. J.* **2000**, *32*, 707.
 13. (a) Isobe, Y.; Yamada, K.; Nakano, T.; Okamoto, Y. *Macromolecules* **1999**, *32*, 5979. (b) Isobe, Y.; Yamada, K.; Nakano, T.; Okamoto, Y. *J. Polym. Sci., Part A: Polym. Chem.* **2000**, *38*, 4693.
 14. (a) Isobe, Y.; Fujioka, D.; Habaue, S.; Okamoto, Y. *J. Am. Chem. Soc.* **2001**, *123*, 7180. (b) Habaue, S.; Isobe, Y.; Okamoto, Y. *Tetrahedron* **2002**, *58*, 8205. (c) Suito, Y.; Isobe, Y.; Habaue, S.; Okamoto, Y. *J. Polym. Sci., Part A: Polym. Chem.* **2002**, *40*, 2496. (d) Isobe, Y.; Suito, Y.; Habaue, S.; Okamoto, Y. *J. Polym. Sci., Part A: Polym. Chem.* **2003**, *41*, 1027. (e) Ray, B.; Isobe, Y.; Habaue, S.; Kamigaito, M.; Okamoto, Y. *Polym. J.* **2004**, *36*, 728.
 15. Isobe, Y.; Nakano, T.; Okamoto, Y. *J. Polym. Sci., Part A: Polym. Chem.* **2001**, *39*, 1463.
 16. Matsumoto, A.; Nakamura, S. *J. Appl. Polym. Sci.* **1999**, *74*, 290.
 17. (a) Ray, B.; Isobe, Y.; Morioka, K.; Habaue, S.; Okamoto, Y.; Kamigaito, M.; Sawamoto, M. *Macromolecules* **2003**, *36*, 543. (b) Ray, B.; Isobe, Y.; Matsumoto, K.; Habaue, S.; Okamoto, Y.; Kamigaito, M.; Sawamoto, M. *Macromolecules* **2004**, *37*, 1702. (c) Ray, B.; Okamoto, Y.; Kamigaito, M.; Sawamoto, M.; Seno, K.; Kanaoka, S.; Aoshima, S. *Polym. J.* **2005**, *37*, 234.
 18. (a) Lutz, J.-F.; Neugebauer, D.; Matyjaszewski, K. *J. Am. Chem. Soc.* **2003**, *125*, 6986. (b) Lutz, J.-F.; Jakubowski, W.; Matyjaszewski, K. *Macromol. Rapid Commun.* **2004**, *25*, 486.
 19. Miura, Y.; Satoh, T.; Narumi, A.; Nishizawa, O.; Okamoto, Y.; Kakuchi, T. *Macromolecules* **2005**, *38*, 1041.
 20. Mori, H.; Sutoh, K.; Endo, T. *Macromolecules* **2005**, *38*, 9055.
 21. (a) Nishikawa, T.; Ando, T.; Kamigaito, M.; Sawamoto, M. *Macromolecules* **1997**, *30*, 2244. (b) Nishikawa, T.; Kamigaito, M.; Sawamoto, M. *Macromolecules* **1999**, *32*, 2204.
 22. Watanabe, Y.; Ando, T.; Kamigaito, M.; Sawamoto, M. *Macromolecules* **2001**, *34*, 4370.

23. (a) Kotani, Y.; Kamigaito, M.; Sawamoto, M. *Macromolecules* **2000**, *33*, 3543. (b) Kamigaito, M.; Onishi, I.; Kimura, S.; Kotani, Y.; Sawamoto, M. *Chem. Commun.* **2002**, 2694. (c) Wakioka, M.; Baek, K.-Y.; Ando, T.; Kamigaito, M.; Sawamoto, M. *Macromolecules* **2002**, *35*, 330.
24. Fuji, Y.; Ando, T.; Kamigaito, M.; Sawamoto, M. *Macromolecules* **2002**, *35*, 2949.
25. Okamoto, Y.; Habaue, S.; Isobe, Y. *ACS Symposium Series* **2003**, *854*, 59.
26. (a) Sugiyama, Y.; Kamigaito, M.; Okamoto, Y. *Polym. Prepr. Jpn.* **2004**, *53*, 430. (b) Sugiyama, Y.; Satoh, K.; Kamigaito, M.; Okamoto, Y. *J. Polym. Sci., Part A: Polym. Chem.*, in press.
27. (a) Ueda, N.; Kamigaito, M.; Sawamoto, M. *Polym. Prepr. Jpn.* **1996**, *45*, 1267; **1997**, *46*, 149; **1998**, *47*, 134. (b) Ueda, N.; Kamigaito, M.; Sawamoto, M. The 37th IUPAC International Symposium on Macromolecules, Preprints, Gold Coast, Australia, 1998, p. 237. (c) Ueda, N. JP Patents 10,060,021 (Aug. 13, 1996); 11,147,914 (Nov. 17, 1997); 11,171,926 (Dec. 11, 1997).
28. Iovu, M. C.; Matyjaszewski, K. *Macromolecules* **2003**, *36*, 9346.
29. Rizzardo, E.; Chiefari, J.; Mayadunne, R. T. A.; Moad, G.; Thang, S. H. *ACS Symp. Ser.* **2000**, *786*, 278.
30. Charmot, D.; Corpart, P.; Adam, H.; Zard, S. Z.; Biadatti, T.; Bouhadir, G. *Macromol. Symp.* **2000**, *150*, 23.
31. Destarac, M.; Charmot, D.; Franck, X.; Zard, S. Z. *Macromol. Rapid Commun.* **2000**, *21*, 1035.
32. Stenzel, M. H.; Cummins, L.; Roberts, G. E.; Davis, T. P.; Vana, P.; Barner-Kowollik, C. *Macromol. Chem. Phys.* **2003**, *204*, 1160.
33. Coote, M. L.; Radom, L. *Macromolecules* **2004**, *37*, 590.
34. Favier, A.; Barner-Kowollik, C.; Davis, T.; Stenzel, M. H. *Macromol. Chem. Phys.* **2004**, *205*, 925.
35. (a) Yamago, S.; Iida, K.; Yoshida, J. *J. Am. Chem. Soc.* **2002**, *124*, 2874. (b) Yamago, S.; Iida, K.; Yoshida, J. *J. Am. Chem. Soc.* **2002**, *124*, 13666.
36. (a) Debuigne, A.; Caille, J.-R.; Jérôme, R. *Angew. Chem. Int. Ed.* **2005**, *44*, 1101. (b) Debuigne, A.; Caille, J.-R.; Jérôme, R. *Macromolecules* **2005**, *38*, 5452.
37. Kaneyoshi, H.; Matyjaszewski, K. *Macromolecules* **2005**, *38*, 8163.
38. Koumura, K.; Satoh, K.; Kamigaito, M.; Okamoto, Y. *Polym. Prepr. Jpn.* **2005**, *54*, 2482.
39. Yamago, S.; Ray, B.; Iida, K.; Yoshida, J.; Tada, T.; Yoshizawa, K.; Kwak, Y.; Goto, A.; Fukuda, T. *J. Am. Chem. Soc.* **2004**, *126*, 13908.
40. Wan, D.; Satoh, K.; Kamigaito, M.; Okamoto, Y. *Macromolecules* **2005**, *38*, 10397.

Chapter 4

Controlled Radical Polymerization of Vinyl Monomers Catalyzed by Ruthenium *N*-Heterocyclic Carbene Complexes

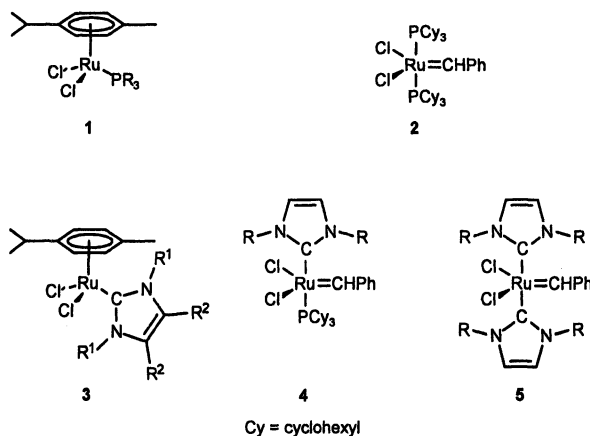
Sébastien Delfosse, Aurore Richel, Lionel Delaude,
Albert Demonceau*, and Alfred F. Noels

Laboratory of Macromolecular Chemistry and Organic Catalysis,
University of Liège, Sart-Tilman (B.6a), B-4000 Liège, Belgium

The relative catalytic activities of a series of ruthenium-based complexes of the general formula $[\text{RuCl}_2(p\text{-cymene})(\text{NHC})]$, $[\text{RuCl}_2(=\text{CHPh})(\text{PR}_3)(\text{NHC})]$, and $[\text{RuCl}_2(=\text{CHPh})(\text{NHC})_2]$ (NHC is a *N*-heterocyclic carbene ligand) were determined by investigating the atom transfer radical polymerization (ATRP) of methyl methacrylate and styrene. The catalytic activity of a variety of related $[\text{RuCl}(\text{O}^{\wedge}\text{N})(=\text{CHR})(\text{NHC})]$ complexes and of their cationic counterparts, $[\text{Ru}(\text{O}^{\wedge}\text{N})(=\text{CHR})(\text{NHC})]^+ \text{BF}_4^-$ ($\text{R} = \text{Ph}$ or OEt , $\text{O}^{\wedge}\text{N}$ is a Schiff base ligand), is also reported. The results clearly demonstrate that, with both methyl methacrylate and styrene, subtle modifications of the substituents of the NHC ligand lead to dramatic changes in the ability of the resulting ruthenium complexes to favor the occurrence of a well-behaved ATRP.

The ability to control molecular architecture constitutes a major challenge for synthetic polymer chemists. Controlled radical polymerization has in recent years revitalized the rather mature field of radical olefin polymerization in an unprecedented way, and has provided access to well-defined polymers and copolymers. Stable free radicals, such as nitroxides, have been introduced for control of radical polymerization. In 1995, Sawamoto (1) and Matyjaszewski (2) have replaced the stable nitroxide free radical with transition metal species to obtain, respectively, a variety of ruthenium- and copper-mediated controlled radical polymerization systems, a methodology which goes by the name of atom transfer radical polymerization (ATRP).

Back in 1999, we found that the 18-electron complexes $[\text{RuCl}_2(p\text{-cymene})(\text{PR}_3)]$ ($p\text{-cymene} = 4\text{-isopropyltoluene}$) (1) were highly efficient catalytic systems for promotion of the controlled radical polymerization of vinyl monomers, such as methyl methacrylate (Table 1) and styrene (Table 2) (3).



Scheme 1. Ruthenium-*p*-cymene and ruthenium-benzylidene complexes bearing either phosphine or NHC ligands

Table 1. Polymerization of Methyl Methacrylate Initiated by Ethyl 2-Bromo-2-methylpropionate and Catalyzed by Ruthenium Complexes 1 and 2

| Complex | Polymer yield (%) | M_n | M_w/M_n | f |
|--------------------------------|-------------------|--------|-----------|------|
| 1a ($PR_3 = PPh_3$) | 20 | 25 000 | 1.6 | 0.3 |
| 1b ($PR_3 = PPh_2Cy$) | 58 | 41 000 | 1.25 | 0.55 |
| 1c ($PR_3 = PPhCy_2$) | 90 | 60 500 | 1.10 | 0.6 |
| 1d ($PR_3 = PCy_3$) | 100 | 41 500 | 1.12 | 0.95 |
| 1e ($PR_3 = PiPr_3$) | 80 | 40 500 | 1.10 | 0.8 |
| 2 | 95 | 66 000 | 1.28 | 0.6 |

It appeared that only basic and bulky phosphines, such as dicyclohexylphenylphosphine (**1c**), tricyclohexylphosphine (**1d**), and triisopropylphosphine (**1e**) presented both high catalytic activity and high control of the polymerization process (high initiation efficiency, f , and low molecular weight distribution, $M_w/M_n = 1.1$). Under these experimental conditions, all the criteria of living polymerization were fulfilled. Indeed, the plots of $\ln([M]_0/[M])$ vs. time and of M_n vs. monomer conversion were linear. Furthermore, the control of the polymerizations was confirmed by the addition of a second equivalent of monomer feed to the completely polymerized system. This second polymerization reaction was also quantitative, and only a slight increase in polydispersity was observed.

Surprisingly, the best catalyst systems for ATRP have been shown to be also the most active ones for the ring-opening metathesis polymerization (ROMP) of strained and low-strain cycloolefins (**4**). In both reactions, the same stereoelectronic requirements for the phosphine ligand of the ruthenium complex have been demonstrated. This observation prompted us to test $[RuCl_2(=CHPh)(PCy_3)_2]$, **2**, the Grubbs ruthenium-carbene complex commonly used for olefin metathesis (**5**), as a catalyst for the radical polymerization of methyl methacrylate (Table 1) and styrene (Table 2).

Table 2. Polymerization of Styrene Initiated by (1-Bromoethyl)benzene and Catalyzed by Ruthenium Complexes 1 and 2

| Complex | Polymer yield (%) | M_n | M_w/M_n | f |
|---|-------------------|--------|-----------|------|
| 1a (PR ₃ = PPh ₃) | 39 | 26 000 | 1.8 | 0.6 |
| 1b (PR ₃ = PPh ₂ Cy) | 45 | 20 000 | 1.7 | 0.85 |
| 1c (PR ₃ = PPhCy ₂) | 48 | 19 500 | 1.45 | 0.95 |
| 1d (PR ₃ = PCy ₃) | 64 | 28 500 | 1.3 | 0.85 |
| 1e (PR ₃ = P <i>i</i> Pr ₃) | 40 | 15 500 | 1.2 | 1.0 |
| 2 | 61 | 29 000 | 1.38 | 0.8 |

The same protocol was followed for all the polymerization tests. Polymerization of methyl methacrylate: Ruthenium complex (0.0117 mmol) was placed in a glass tube containing a bar magnet and capped by a three-way stopcock. The reactor was purged of air (three vacuum–nitrogen cycles) before methyl methacrylate (1 mL, 9.35 mmol) and the initiator (ethyl 2-bromo-2-methylpropionate 0.1 M in toluene, 0.232 mL) were added ([MMA]₀:[initiator]₀:[Ru]₀ = 800:2:1). The mixture was heated in a thermostated oil bath for 16 h at 85 °C and, after cooling, dissolved in THF and the product precipitated in heptane. The polymer was filtered off and dried overnight under vacuum. The same procedure was used for the polymerization of styrene ([styrene]₀:[initiator]₀: [Ru]₀ = 750:2:1), except that the initiator was (1-bromoethyl)benzene, the temperature of the oil bath was 110 °C, and the solvent used for precipitation of the polymer was technical methanol.

M_n and M_w/M_n were determined by size-exclusion chromatography with PMMA and polystyrene calibrations.

Initiation efficiency, $f = M_{n, \text{theor.}}/M_{n, \text{exp.}}$ with $M_{n, \text{theor.}} = ([\text{monomer}]_0/[\text{initiator}]_0) \times M_w(\text{monomer}) \times \text{conversion}$.

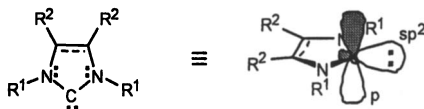
Gratifyingly, the Grubbs complex was found to be also active in ATRP, and even more active than [RuCl₂(*p*-cymene)(PCy₃)], **1d**, but to the detriment of polymer control (3).

Since ATRP is based on a dynamic equilibration between active propagating radicals and dormant species, it is anticipated that catalytic engineering at the metal center should shift this equilibrium to the most suitable position, so as to maintain a low concentration of propagating radicals while keeping a useful rate of polymerization for polymers to be obtained on a sensible time-scale. To further improve the catalyst efficiency in the ATRP process, we have launched an investigation on the role of the ligands associated to ruthenium.

In recent years, *N*-heterocyclic carbenes (NHCs) (**6**) have frequently been used as phosphine-substitutes for late transition metal catalysts and in many cases, an improved catalytic performance of the NHC-complexes was observed, such as in olefin metathesis (7) or in various palladium-catalyzed C–C coupling reactions, in particular the Heck, Suzuki, and Kumada reactions. The present contribution is aiming at illustrating how replacement of the phosphine(s) in complexes **1** and **2** by *N*-heterocyclic carbene ligands (¶ 3–5, Scheme 1) influences ATRP of vinyl monomers.

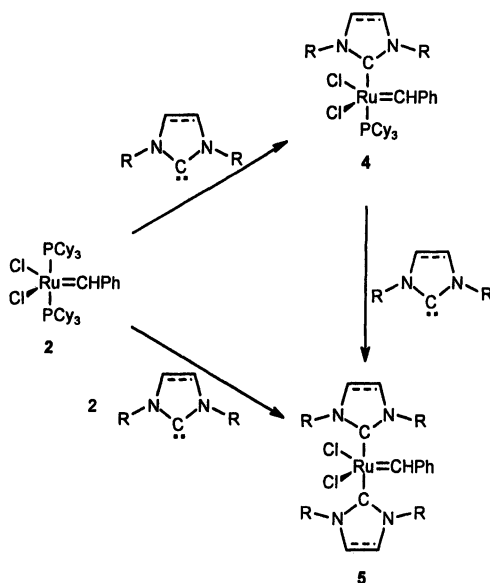
N-Heterocyclic Carbenes vs. Phosphines

The electronic structure of the carbene center of a *N*-heterocyclic carbene can be seen as a strongly bent singlet carbene in which the carbene carbon is approximately sp^2 hybridized (Scheme 2) (8).



Scheme 2. Structure of a *N*-heterocyclic carbene

The two substituents and a lone pair of electrons occupy the three sp^2 -hybrid orbitals and a formally vacant *p*-orbital remains at carbon. The lone pair of electrons on carbon behaves chemically similar to the lone pair of electrons on phosphorus in phosphines. Guided by this simple analogy, organometallic chemists have successfully replaced the ubiquitous phosphine ligand with a NHC in a large number of organometallic complexes. However, the real strength and versatility of the new NHC ligands rest not in their similarity with phosphines, but rather in how they differ from the more conventional phosphines and in the new structural and electronic features they can introduce. In this latter respect, NHCs have their own special features to offer over phosphines. The coordinating lone pair of electrons in a NHC is harder and more basic than a phosphine lone pair. Thus, the reaction of traditional Grubbs complexes **2** and **4** with NHCs leads ultimately to the related bis(NHC) complex **5**, demonstrating experimentally the strong σ -donor properties of NHCs over phosphines (Scheme 3).



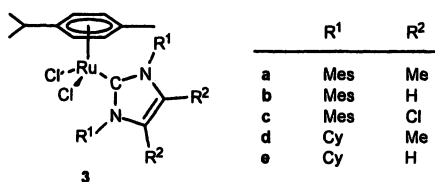
Scheme 3. Synthesis and reactivity of ruthenium–NHC complexes **4** and **5**

On the other hand, the formally vacant p-orbital at the carbene center has the potential to function as a weak π -acceptor, but has different directional character than P–X σ^* -bonds (or d-orbitals) on a phosphine. The planar NHCs also present a steric profile that is greatly different from that of phosphines.

Within the last decade, numerous variations of the basic NHC structure have appeared and have found application in modern catalysis as carbene–metal complexes. However, in contrast to phosphine-based transition metal catalysts, NHC-based catalysts exhibit longer lifetimes in catalytic cycles, which may be due to better retention of the NHC ligands over their phosphine analogues on the metal center. Furthermore, NHC complexes generally possess better stability against air and moisture than their phosphine analogues.

Ruthenium–*p*-Cymene Complexes Bearing a NHC Ligand

Polymerization of methyl methacrylate initiated by ethyl 2-bromo-2-methylpropionate and ruthenium–NHC complexes **3a–f** was investigated at 85 °C under inert atmosphere.

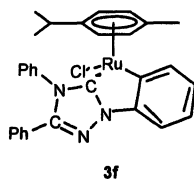


Mes = 2,4,6-trimethylphenyl (mesityl), Cy = cyclohexyl

Scheme 4. Ruthenium–*p*-cymene complexes bearing a NHC ligand

Complexes **3b** and **3c** with R¹ = mesityl and R² = H or Cl, respectively, were the most efficient catalysts for this reaction (Table 3). The semilogarithmic plots of $\ln([M]_0/[M])$ vs. time were linear in both cases with a pseudo-first order rate constant (k_{app}) of $10.6 \times 10^{-6} \text{ s}^{-1}$ for **3b** and $3.85 \times 10^{-6} \text{ s}^{-1}$ for **3c**, indicating that the radical concentration remained constant throughout the polymerization run (Figure 1b). With these two complexes, the molecular weights increased linearly with conversion, indicative of a good control over M_n (Figure 1c). Polydispersities (M_w/M_n) were quite low (typically *ca.* 1.3) and decreased with monomer conversion (Figure 1d). By contrast, complex **3a** displayed an induction period after which the semilogarithmic plot was almost linear ($k_{app} = 16.4 \times 10^{-6} \text{ s}^{-1}$) (Figure 1a). Furthermore, M_n did not increase linearly with conversion and did not agree with theoretical values (Figure 1c) (9).

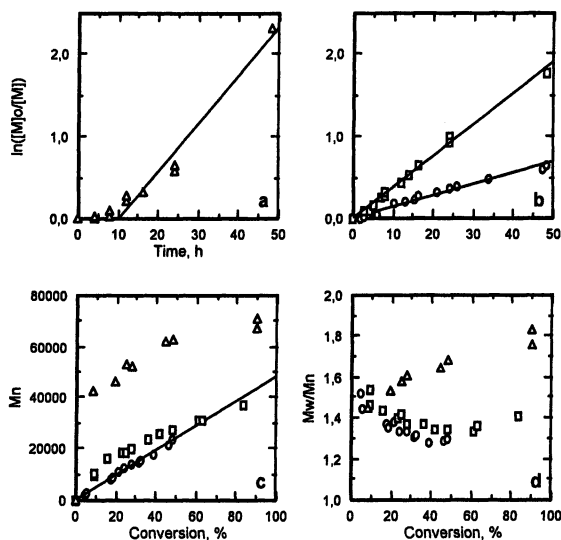
When styrene was subjected to ATRP, complex **3e** proved to be the most efficient catalyst (Table 4). The polymerization was well controlled as indicated by the linearity of the plots of $\ln([M]_0/[M])$ vs. time (Figure 2a) and of M_n vs. conversion (Figure 2b). Accordingly, M_w/M_n decreased steadily with time and reached a low of 1.25 upon completion of the reaction (Figure 2c). All the other R¹–R² combinations tested resulted in poorly or uncontrolled polymerizations. Indeed, replacement of hydrogen atoms by methyl groups on both olefinic carbons of the NHC ligand dramatically altered the course of the reaction.



Scheme 5. Ruthenium-*p*-cymene complex bearing an ortho-metallated NHC ligand (11)

Table 3. Polymerization of Methyl Methacrylate Initiated by Ethyl 2-Bromo-2-methylpropionate and Catalyzed by Ruthenium Complexes 3

| Complex | Polymer yield (%) | M_n | M_w/M_n | f |
|-----------|-------------------|---------|-----------|------|
| 3a | 28 | 52 000 | 1.6 | 0.2 |
| 3b | 49 | 28 000 | 1.35 | 0.7 |
| 3c | 24 | 12 900 | 1.33 | 0.75 |
| 3d | 94 | 160 000 | 2.45 | 0.25 |
| 3e | 51 | 36 000 | 1.75 | 0.55 |
| 3f | 100 | 52 000 | 2.0 | 0.75 |



Figures 1, a and b. Time dependence of $\ln([M]_0/[M])$ for the polymerization of MMA catalyzed by complexes **3a** (Δ), **3b** (\square), and **3c** (\circ). **Figures 1, c and d.** Dependence of the PMMA molecular weight M_n and molecular weight distribution M_w/M_n on monomer conversion for the polymerization of MMA catalyzed by complexes **3a** (Δ), **3b** (\square), and **3c** (\circ) (see Table 3).

Table 4. Polymerization of Styrene Initiated by (1-Bromoethyl)benzene and Catalyzed by Ruthenium Complexes 3

| Complex | Polymer yield (%) | M_n | M_w/M_n | f |
|---------|-------------------|--------|-----------|------|
| 3a | 66 | 53 000 | 1.75 | 0.5 |
| 3b | 51 | 28 000 | 1.8 | 0.7 |
| 3c | 10 | 10 200 | 1.9 | 0.4 |
| 3d | 77 | 53 000 | 1.9 | 0.55 |
| 3e | 86 | 47 000 | 1.25 | 0.7 |

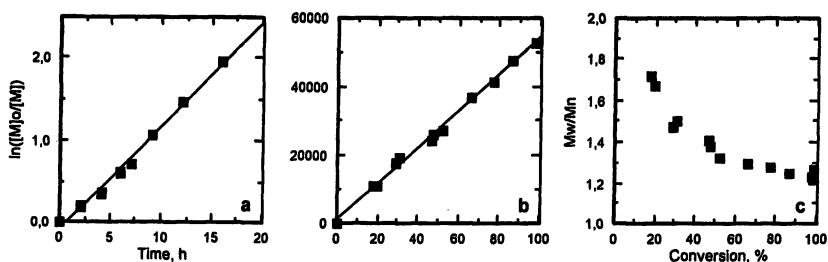


Figure 2. (a) Time dependence of $\ln([M]_0/[M])$ for the polymerization of styrene catalyzed by complex 3e. (b) Dependence of the polystyrene molecular weight M_n and (c) molecular weight distribution M_w/M_n on monomer conversion for the polymerization of styrene catalyzed by complex 3e (see Table 4).

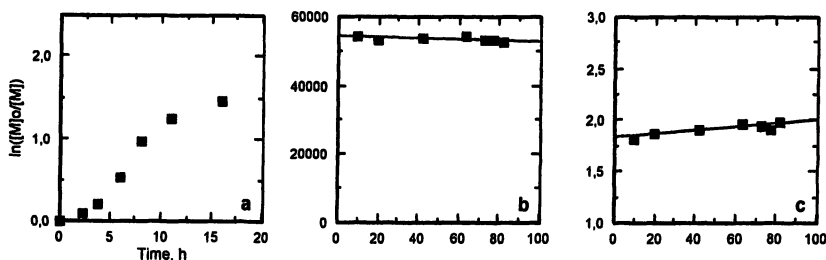
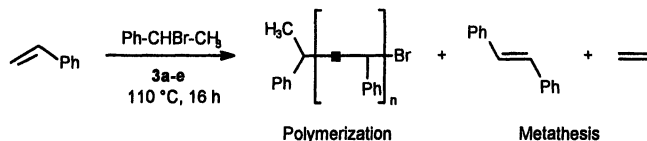


Figure 3. (a) Time dependence of $\ln([M]_0/[M])$ for the polymerization of styrene catalyzed by complex 3d. (b) Dependence of the polystyrene molecular weight M_n and (c) molecular weight distribution M_w/M_n on monomer conversion for the polymerization of styrene catalyzed by complex 3d (see Table 4).

With complex 3d, the semilogarithmic plot of $\ln([M]_0/[M])$ vs. time was no longer linear (Figure 3a), and M_n as well as M_w/M_n remained constant ($\approx 55\ 000$ and 1.9, respectively) throughout the run (Figure 3, b and c). A similar trend was observed for the polymerization of MMA using 3e ($M_n \approx 35\ 000$ and $M_w/M_n \approx 1.75$, cf. Table 3), indicating that both reactions were most likely taking place through a redox-initiated free radical process (9).

Table 5. Polymerization vs. Metathesis of Styrene in the Presence of (1-Bromoethyl)benzene and Ruthenium Complexes 3



| Complex | Polymer yield (%) | Metathesis (%) |
|---------|-------------------|----------------|
| 3a | 66 | 25 |
| 3b | 51 | 5 |
| 3c | 10 | 70 |
| 3d | 77 | 0 |
| 3e | 86 | 0 |

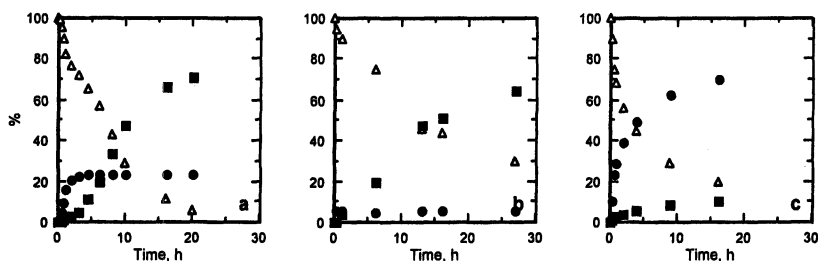


Figure 4. Time dependence of styrene (Δ), polystyrene (\blacksquare), and stilbene (\bullet) in the presence of catalysts **3a** (a), **3b** (b), and **3c** (c) (see Table 5).

An important result in the frame of this discussion was that styrene underwent metathesis in addition to radical polymerization when ruthenium–NHC catalyst precursors bearing R^1 mesityl groups were present in the reaction medium (Table 5). Thus, *cis*- and *trans*-stilbene (the latter isomer being largely predominant) were obtained in varying proportions according to the R^2 substituents (Table 5). With complexes **3a** ($R^2 = \text{Me}$) and **3b** ($R^2 = \text{H}$), stilbene formation accounted for 25 and 5 % of the monomer conversion, respectively, whereas ATRP gave rise to polystyrene in 66 and 51 % yields, respectively. With complex **3c** ($R^2 = \text{Cl}$), olefin metathesis took the precedence over polymerization and afforded a 70 % yield of stilbene after 16 h at 110 °C. Within the same period, a mere 10 % polymer yield was obtained. Furthermore, examination of the evolution of the reaction products, polystyrene and stilbene, vs. time (Figure 4) indicated that in all cases, in the early stages of the reaction, metathesis of styrene was much faster than polymerization. However, the metathetic activity of catalyst **3b** dropped rapidly to the benefit of the polymerization, whereas with **3c**, a high metathetic activity was maintained throughout the reaction. Under the same conditions, catalyst **3a** displayed a borderline reactivity profile.

Interestingly, complexes **3d** and **3e** bearing *N*-cyclohexyl-substituted NHC ligands were devoid of any significant activity for the metathesis of styrene and initiated only the radical polymerization process, with a very good control in the case of **3e**. Therefore,

Thus, mixed ligand complex **4** exhibited the lowest activity, whereas little difference was observed between bis(NHC) complexes **5a** (R = Cy) and **5b** (R = *i*Pr); both of them afforded PMMA possessing essentially the same features (M_n and M_w/M_n). Complex **2** bearing two PCy₃ ligands gave the narrowest molecular weight distribution ($M_w/M_n = 1.28$), although the molecular weight was higher than the calculated value ($f = 0.6$). Broader M_w/M_n values resulted from substitution of one or both PCy₃ by a *N*-heterocyclic carbene. With complexes **5**, M_n were fairly well controlled by the monomer to the initiator ratio ($f \approx 0.9$).

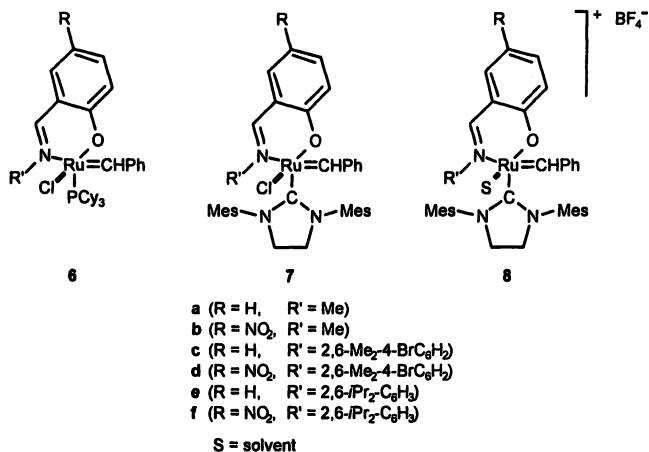
Complexes **2**, **4**, and **5** also polymerized styrene (Table 7). With complex **2**, a smooth polymerization took place. The conversion reached 61 % in 16 h, with a molecular weight distribution near 1.4. M_w/M_n were however broader for polystyrenes obtained using ruthenium–NHC complexes **4** and **5** ($M_w/M_n = 1.55$ – 1.8).

A mechanistic investigation revealed that ATRP was mediated by ruthenium species bereft of the benzylidene moiety (12). Indeed, as monitored by ¹H-NMR at 85 °C, under conditions mimicking polymerization of MMA, complete disappearance of the benzylidene fragment of complex **4** was observed within 20 min., whereas complexes **2** and **5b** showed 55 and 88 % decomposition, respectively, over the same period of time.

Ruthenium–Benzylidene Complexes Bearing Schiff Base and NHC Ligands

In recent years, Schiff base ligands have been used extensively in homogeneous catalysis due to their very attractive properties. Indeed, Schiff bases are easily accessible through one-step procedures *via* almost quantitative condensation of an aldehyde with an amine. These O,N-bidentate ligands are also more resistant to oxidation than phosphines. Furthermore, the steric and electronic properties of Schiff base ligands can be easily modulated by varying the nature, the number and the position of the substituents in the compound, offering therefore ample possibilities for catalyst engineering and fine tuning. The two donor atoms (N and O) of the chelated Schiff base exhibit opposite features: the phenolate oxygen atom is a hard donor and will stabilize a higher oxidation state of the metal whereas the imine nitrogen is a softer one and, accordingly, will rather stabilize the lower oxidation state of the metal.

Quite recently, Verpoort extended our approach to Schiff base–ruthenium complexes bearing either tricyclohexylphosphine (**6**) or NHC (imidazolinyldene) ligands (**7** and **8**) (13). On performing ATRP reactions on a set of common vinyl monomers with catalyst precursors **6** and **7**, yields and polymer characteristics (M_n and M_w/M_n) were found to depend substantially both on the precatalyst and type of the monomer. Indeed, as shown in Table 8, only complexes **6d**, **7c**, and **7d** could conveniently catalyze the polymerization of methyl methacrylate. By contrast, all precatalysts were able to convert styrene, although significant differences in their performance were observed (Table 9). With the systems exhibiting the lowest activity (**6a** and **b**, and **7a** and **b**), only 8–10 % conversion was reached, whereas the most active systems, **6d** and **7d**, efficiently converted styrene in 88 and 75 % yields, respectively. Moreover, with catalyst systems **6d** and **7d**, both PMMA (Table 8) and polystyrene (Table 9) displayed the lowest polydispersity. Furthermore, the corresponding cationic complexes **8** have also been investigated. Comparative studies on ATRP of MMA and styrene, using both toluene and water/toluene mixtures as the solvent, demonstrated that the solvent was crucial for the activity and controllability of the process. Moreover, in aqueous/organic biphasic conditions, the ruthenium cationic complexes **8** were highly active and polymers with controlled molecular weights and narrow molecular weight distributions were formed.



Scheme 7. Ruthenium-benzylidene complexes bearing Schiff base and NHC ligands

Table 8. Polymerization of Methyl Methacrylate Initiated by Ethyl 2-Bromo-2-methylpropionate and Catalyzed by Ruthenium Complexes 6 and 7

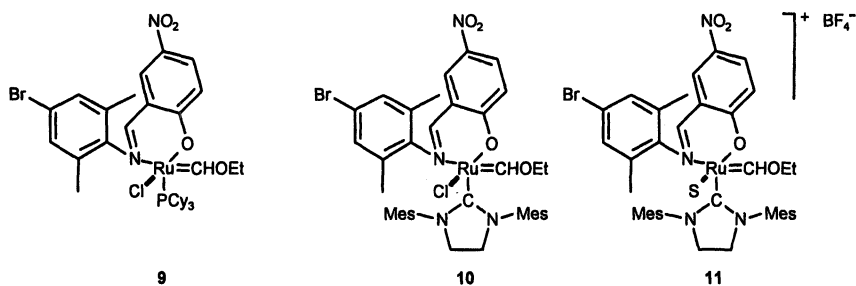
| Complex | Polymer yield (%) | M_n | M_w/M_n | f |
|-----------|-------------------|--------|-----------|------|
| 6a | <5 | | | |
| 6b | <5 | | | |
| 6c | 11 | 6 300 | 1.25 | 0.70 |
| 6d | 28 | 13 000 | 1.22 | 0.87 |
| 6e | 7 | 4 800 | 1.56 | 0.51 |
| 6f | 10 | 6 600 | 1.51 | 0.61 |
| 7a | <5 | | | |
| 7b | 6 | | | |
| 7c | 24 | 14 800 | 1.23 | 0.65 |
| 7d | 27 | 13 300 | 1.18 | 0.81 |
| 7e | 11 | 8 600 | 1.34 | 0.51 |
| 7f | 15 | 11 600 | 1.31 | 0.52 |

Of note is the behavior of the Fischer-type Schiff base-ruthenium alkylidene complexes **9** and **10** (14). When tested for ATRP of MMA, catalyst **10** manifested itself as one of the most active Ru-carbene systems known to date, leading to almost quantitative conversion of the monomer. Significantly, catalyst **10** gave a polymer with a polydispersity index of 1.30 and an initiation efficiency of 0.97.

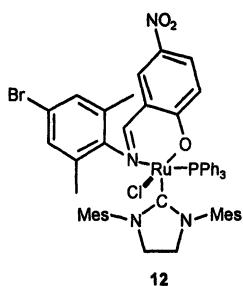
Furthermore, the cationic congener, **11**, was also very active (100 % conversion) in pure toluene and water/toluene mixtures. In both cases, the observed M_w/M_n remained relatively narrow (1.28 and 1.40, respectively). The exact mode of action of the carbene entity is not clear yet. It is presently assumed that the active ATRP species derive from

Table 9. Polymerization of Styrene Initiated by (1-Bromoethyl)benzene and Catalyzed by Ruthenium Complexes 6 and 7

| Complex | Polymer yield (%) | M_n | M_w/M_n | f |
|-----------|-------------------|--------|-----------|------|
| 6a | 10 | | | |
| 6b | 10 | | | |
| 6c | 74 | 38 000 | 1.65 | 0.81 |
| 6d | 88 | 41 000 | 1.44 | 0.89 |
| 6e | 56 | 29 000 | 1.75 | 0.67 |
| 6f | 65 | 32 000 | 1.71 | 0.85 |
| 7a | 8 | | | |
| 7b | 10 | | | |
| 7c | 67 | 37 000 | 1.33 | 0.75 |
| 7d | 75 | 37 000 | 1.25 | 0.84 |
| 7e | 43 | 27 000 | 1.44 | 0.67 |
| 7f | 51 | 33 000 | 1.48 | 0.64 |



Scheme 8. Fischer-type ruthenium-alkylidene complex bearing Schiff base and NHC ligands



Scheme 9. Ruthenium-triphenylphosphine complex bearing Schiff base and NHC ligands

the carbene fragment. This assumption is strongly supported by the observation that the phosphine-containing system, **12**, is inactive in ATRP (14, 15).

Phosphines vs. *N*-Heterocyclic Carbene Ligands in ATRP: Cyclic Voltammetry Investigations

[RuCl₂(*p*-cymene)(L)] complexes, L = PR₃ or NHC

In order to rationalize the effect of the ligand L in [RuCl₂(*p*-cymene)(L)] complexes (L = PR₃ (**1**) or NHC (**3**)), we investigated these complexes by means of electrochemistry (16). As indicated in Table 10, all of the [RuCl₂(*p*-cymene)(PR₃)] complexes (**1**) were reversibly oxidized at a potential, E° , ranging from +0.570 to +0.690 V referenced to the ferrocene/ferrocenium couple. Noteworthy, a qualitative correlation could be deduced between E° and [RuCl₂(*p*-cymene)(PR₃)]'s activities for the polymerization of MMA (Table 1). Indeed, the complexes with a lower redox potential, [RuCl₂(*p*-cymene)(PR₃)] with PR₃ = PPhCy₂ (**1c**), PCy₃ (**1d**), and PiPr₃ (**1e**), induced a faster polymerization. For the polymerization of styrene (Table 2), a correlation was found with complexes **1a–d**, but not with [RuCl₂(*p*-cymene)(PiPr₃)] (**1e**).

Table 10. Cyclic Voltammetry Data for Ruthenium Complexes 1 and 3 ^a

| Complex | E° (V) | ΔE (V) | Complex | E° (V) | ΔE (V) |
|---|---------------|--------------------|-----------|--------------------|--------------------|
| 1a (PR ₃ = PPh ₃) | 0.680 | 0.075 ^b | 3a | 0.325 | 0.090 ^b |
| 1b (PR ₃ = PPh ₂ Cy) | 0.690 | 0.069 ^b | 3b | 0.450 ^c | – ^{b,d} |
| 1c (PR ₃ = PPhCy ₂) | 0.630 | 0.066 ^b | 3c | 0.555 | 0.110 ^b |
| 1d (PR ₃ = PCy ₃) | 0.575 | 0.060 ^b | 3d | 0.470 ^c | – ^{b,d} |
| 1e (PR ₃ = PiPr ₃) | 0.600 | 0.060 ^b | 3e | 0.590 | 0.080 ^b |

^a Sample, 2 mM; *n*Bu₄NPF₆ (0.1 M) in dry and degassed CH₂Cl₂, under nitrogen at room temperature; scan rate, 50 mV s^{–1}; potentials are reported in volt vs. ferrocene as an internal standard.

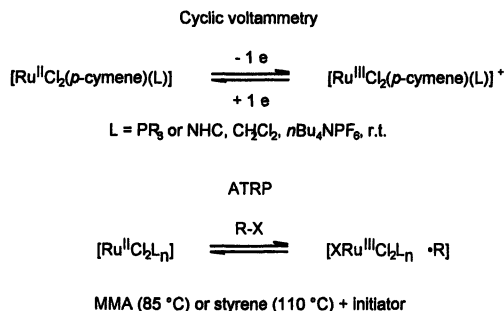
^b Under our conditions (Ag/AgCl/saturated KCl reference electrode), the E_p^{ox} and E_p^{red} peak separation (ΔE) of the ferrocene/ferrocenium couple was 0.060 V for complexes **1**, and 0.080 V for complexes **3**, depending on the set of electrodes used, whereas the theoretical value for a reversible one-electron transfer process is 0.059 V.

^c Oxidation potential, E_p^{ox} .

^d Irreversible redox couple.

[RuCl₂(*p*-cymene)(NHC)] complexes **3a**, **3c**, and **3e** gave rise to accessible and reversible one-electron redox couples. Complexes **3b** and **3d**, on the other hand, displayed irreversible redox couples, in apparent contradiction with the polymerization results. Indeed, complex **3b** catalyzed a well-controlled ATRP of MMA, whereas **3d** and **3e** promoted the redox-initiated free-radical polymerization of styrene and MMA. Comparison of the redox potentials, E° , of complexes **3c** and **3e** posed an additional problem. Although the E° values (0.555 and 0.590 V, respectively) were quite similar, complexes **3c** and **3e** displayed different abilities to control ATRP, suggesting that E° is not necessarily predictive of the catalyst's efficiency for ATRP with this particular series of ruthenium–NHC complexes.

Steric and/or conformational constraints around the ruthenium atom may explain this discrepancy. We may also argue that, although they seem to be related, cyclic voltammetry and ATRP are basically different processes (Scheme 10). Cyclic voltammetry experiments are indeed performed on well-defined [Ru^{II}Cl₂(*p*-cymene)(L)] complexes, which are –formally– oxidized to the corresponding radical cations [Ru^{III}Cl₂(*p*-cymene)(L)]⁺ (unless the oxidized species undergo further reactions) through a one-electron transfer.

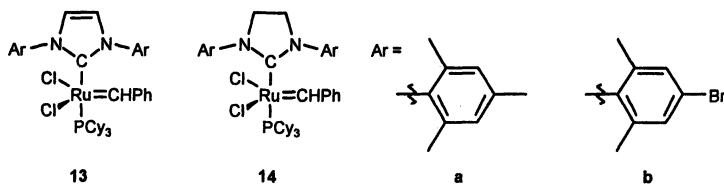


Scheme 10. Cyclic voltammetry vs. ATRP

In ATRP, the ruthenium(II) species is oxidized through halogen transfer from the covalent R–X bond of the initiator or the polymer chain ends. Therefore, a more plausible explanation for the discrepancies between cyclic voltammetry data and catalytic activities is that the well-defined [RuCl₂(*p*-cymene)(L)] complexes used for the polymerization of MMA and styrene are precatalysts. The actual catalytic active species are indeed likely devoid of the *p*-cymene ligand, as indicated by ¹H-NMR spectroscopy, under conditions mimicking polymerization of MMA and styrene (16).

[RuCl₂(=CHPh)(PCy₃)(L)] complexes, L = PCy₃ or NHC

Several studies in the literature have been devoted to studying the donor properties of saturated and unsaturated NHC vs. phosphine ligands. As illustrated above (Scheme 3) there can be no doubt that NHC ligands are significantly more electron-donating than phosphines. This has been confirmed recently (17) on comparing the Ru(II)/Ru(III) redox potential of the Grubbs complex [RuCl₂(=CHPh)(PCy₃)₂] (**2**) (*E*^o = +0.585 V) with that of the parent Ru–NHC complexes **13a** (*E*^o = +0.455 V) and **14a** (*E*^o = +0.447 V).



Scheme 11. Representative Grubbs complexes

Table 11. Cyclic Voltammetry Data for Representative Grubbs Complexes

| Complex | <i>E</i> ^o (V) | Δ <i>E</i> (V) |
|------------|---------------------------|----------------|
| 2 | 0.585 | 0.087 |
| 13a | 0.455 | 0.082 |
| 13b | 0.536 | 0.075 |
| 14a | 0.447 | 0.077 |
| 14b | 0.537 | 0.074 |

Thus, replacing a single tricyclohexylphosphine ligand by a NHC ligand resulted in a cathodic shift of the redox potential by *ca.* 130 mV, while the redox potentials of the unsaturated NHC–Ru complex **13a** and the saturated NHC–Ru complex **14a** were almost identical. On the other hand, the two bromine substituted complexes **13b** and **14b** were anodically shifted by *ca.* +85 mV with respect to **13a** and **14a**, indicating that variation of the group at the *para* position of the aryl substituents of the NHC ligand has a profound influence on the redox potential Ru(II)/Ru(III).

A more systematic investigation of the influence of the remote *para*-substituents revealed significant shifts of the Ru(II)/Ru(III) redox potentials, in agreement with the electron donating ability of the remote substituents. The fact that the aryl rings are electronically decoupled from the *N*-heterocycle provides strong evidence of the π -face coordination of the aryl groups on the ruthenium center, so that the donor properties of aryl substituted NHCs are not only characterized by lone pair donation from the carbene carbon, but also by donation of electron density of the aromatic π -face of the NHC aryl groups towards the metal. It is also worth noting that in olefin metathesis, no correlation could be found between the redox potential Ru(II)/Ru(III) and the catalytic activity. A similar investigation is needed in ATRP catalyzed by ruthenium–benzylidene complexes to gain information on the electronic situation at the metal center in complexes **2** and **4–11**.

Conclusions

In exploring the reactivity of a series of ruthenium-based complexes of the general formula $[\text{RuCl}_2(p\text{-cymene})\text{L}]$ and $[\text{RuCl}_2(=\text{CHPh})\text{LL}']$ (L and L' are either a bulky and basic phosphine, such as PCy_3 , or a *N*-heterocyclic carbene ligand), it was found that ruthenium– PCy_3 complexes were more efficient than their ruthenium–NHC analogues. By contrast, within the family of $[\text{RuCl}(\text{O}^-\text{N})(=\text{CHPh})\text{L}]$ complexes (O^-N is a Schiff base ligand), the polymer yields and the molecular weights were not significantly affected by the ligand, L (PCy_3 or NHC), although ruthenium–NHC complexes **7** were generally superior to the ruthenium– PCy_3 derivatives, **6**, when the polymer distributions were compared.

The ruthenium–*p*-cymene complexes **3**, $[\text{RuCl}_2(p\text{-cymene})(\text{NHC})]$, described in this study are of special interest since, depending on the substituents of the carbene ligand, they can be tuned to promote ATRP or olefin metathesis of carbon–carbon double bonds. Complexes **3b** and **3c** with $\text{R}^1 = \text{mesityl}$ and $\text{R}^2 = \text{H}$ or Cl , respectively, were most suitable for promoting the ATRP of methyl methacrylate. Their use resulted in well-behaved polymerizations and afforded polymers with narrow molecular weight distributions and high initiation efficiencies. In the case of styrene, complex **3e** ($\text{R}^1 = \text{Cy}$, $\text{R}^2 = \text{H}$) was the most efficient catalyst precursor for initiating a controlled radical polymerization. A switch in the reaction pathway could be induced, however, by replacing the cyclohexyl group with a mesityl substituent on the nitrogen atoms. Thus, complexes **3a–c** displayed a dual activity and afforded both the ATRP and the cross-metathesis products. Among the three species tested, the chloro derivative **3c** led to the highest proportion of stilbene compared to polystyrene.

At the present time, it remains difficult to put forward general guidelines to rationalize the choice of a specific ruthenium–NHC catalyst precursor for a given reaction. Depending on the monomer and the experimental conditions adopted (presence of an initiator, solvent, temperature, ...), the coordination sphere around the metal center

must be specifically tailored to afford the most efficient catalytic system. Fine tuning of the electronic, steric, and solubility parameters of the carbene ligand undoubtedly contributes to these adjustments, but any correlation between well-defined ruthenium–NHC complexes and the active coordinatively unsaturated species generated *in situ* is blurred by the elusive nature of the actual catalytic system.

Acknowledgments

We are grateful to the ‘Fonds National de la Recherche Scientifique’ (F.N.R.S.), Brussels, for the purchase of major instrumentation, and the ‘Région wallonne’ (Programme FIRST Europe) for a fellowship to A.R.

References

1. Kamigaito, M.; Ando, T.; Sawamoto, M. *Chem. Rev.* **2001**, *101*, 3689.
2. Matyjaszewski, K.; Xia, J. *Chem. Rev.* **2001**, *101*, 2921.
3. (a) Simal, F.; Demonceau, A.; Noels, A. F. *Angew. Chem. Int. Ed.* **1999**, *38*, 538. (b) Simal, F.; Demonceau, A.; Noels, A. F. *Tetrahedron Lett.* **1999**, *40*, 5689. (c) Simal, F.; Sebillé, S.; Hallet, L.; Demonceau, A.; Noels, A. F. *Macromol. Symp.* **2000**, *161*, 73.
4. Demonceau, A.; Stumpf, A. W.; Saive, E.; Noels, A. F. *Macromolecules* **1997**, *30*, 3127.
5. (a) Schwab, P.; France, M. B.; Ziller, J. W.; Grubbs, R. H. *Angew. Chem., Int. Ed. Engl.* **1995**, *34*, 2039. (b) Schwab, P.; Grubbs, R. H.; Ziller, J. W. *J. Am. Chem. Soc.* **1996**, *118*, 100.
6. (a) Bourissou, D.; Guerret, O.; Gabbaï, F. P.; Bertrand, G. *Chem. Rev.* **2000**, *100*, 91. (b) Herrmann, W. A. *Angew. Chem. Int. Ed.* **2002**, *41*, 1290.
7. Scholl, M.; Trnka, T. M.; Morgan, J. P.; Grubbs, R. H. *Tetrahedron Lett.* **1999**, *40*, 2247.
8. Arduengo, A. J.; Bannenberg, T. *The Strem Chemiker*, Vol. XIV No. 1, 2002, 2.
9. Delaude, L.; Delfosse, S.; Richel, A.; Demonceau, A.; Noels, A. F. *Chem. Commun.* **2003**, 1526.
10. Richel, A.; Delfosse, S.; Cremasco, C.; Delaude, L.; Demonceau, A.; Noels, A. F. *Tetrahedron Lett.* **2003**, *44*, 6011.
11. Simal, F.; Delaude, L.; Jan, D.; Demonceau, A.; Noels, A. F. *Polym. Prepr. (Am. Chem. Soc., Div. Polym. Chem.)* **1999**, *40(2)*, 336.
12. Simal, F.; Delfosse, S.; Demonceau, A.; Noels, A. F.; Denk, K.; Kohl, F. J.; Weskamp, T.; Herrmann, W. A. *Chem. Eur. J.* **2002**, *8*, 3047.
13. (a) De Clercq, B.; Verpoort, F. *Macromolecules* **2002**, *35*, 8943. (b) De Clercq, B.; Verpoort, F. *Polym. Bull.* **2003**, *50*, 153.
14. Opstal, T.; Verpoort, F. *Angew. Chem. Int. Ed.* **2003**, *42*, 2876.
15. (a) Drozdak, R.; Allaert, B.; Ledoux, N.; Dragutan, I.; Dragutan, V.; Verpoort, F. *Adv. Synth. Catal.* **2005**, *347*, 1721. (b) Drozdak, R.; Allaert, B.; Ledoux, N.; Dragutan, I.; Dragutan, V.; Verpoort, F. *Coord. Chem. Rev.* **2005**, *249*, 3055.
16. Richel, A.; Tutusaus, O.; Viñas, C.; Teixidor, F.; Demonceau, A.; Noels, A. F. *Polym. Prepr. (Am. Chem. Soc., Div. Polym. Chem.)* **2005**, *46(2)*, 227.
17. Stübner, M.; Plenio, H. *Chem. Commun.* **2005**, 5417.

Chapter 5

Factors Determining the Performance of Copper-Based Atom Transfer Radical Polymerization Catalysts and Criteria for Rational Catalyst Selection

Nicolay V. Tsarevsky, Wei Tang, Samuel J. Brooks,
and Krzysztof Matyjaszewski

Department of Chemistry, Carnegie Mellon University, 4400 Fifth Avenue,
Pittsburgh, PA 15213

The performance of copper-based ATRP catalysts can be predicted based on the stability constants of the Cu^{II} and Cu^{I} complexes with the ligand L (β^{II} and β^{I} , respectively). Both β^{II} and β^{I} should be large in order to prevent catalyst deactivation through competitive coordination of monomer and/or polymer. A high $\beta^{\text{II}}/\beta^{\text{I}}$ ratio is required for high catalytic activity. Catalysts for which the Cu^{II} complex is more halogenophilic are more active, and provide better polymerization control due to the less pronounced deactivator dissociation. If ATRP is carried out in aqueous media, in addition to the above requirements, the ratio $\beta^{\text{II}}/(\beta^{\text{I}})^2[\text{L}]$ should be low to prevent disproportionation of the Cu^{I} complex. Acidic monomers may be polymerized if the ligands meet all outlined requirements and are also as weakly basic as possible.

Introduction

In the past decade, atom transfer radical polymerization (ATRP)(1-3) has surfaced as one of the most powerful synthetic techniques in polymer science. It allows for the synthesis of well-defined polymeric materials with predetermined molecular weight and composition, and narrow molecular weight distribution derived from substituted styrenes, (meth)acrylates, acrylonitrile, or acrylamides. The use of multifunctional initiators and inimers makes it possible to control the molecular architecture of the polymers and many examples of star, brush, and hyperbranched copolymers prepared by ATRP have been reported.(2,4) The polymers synthesized by ATRP are halide-terminated and can participate in numerous reactions with nucleophiles. In addition, the use of functional initiators allows for the controlled synthesis of homo- or heterotelechelic macromolecules.(5) Post-polymerization modifications of either the end group(s) or the monomer units is another strategy to prepare functional polymers.

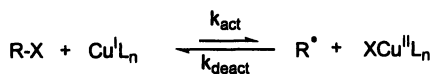
The development of ATRP catalysts that can be used in ppm quantities while maintaining a satisfactory control over polymerization and sufficiently high reaction rates is a challenge that needs to be addressed since it is of major importance for making ATRP an environmentally benign process.(6) ATRP is a metal complex-catalyzed process, and understanding the role the catalyst plays and describing the side reactions in which it can participate, are crucially important for improving the control over the polymerization of “difficult” monomers such as unsaturated acids, amides, and vinyl esters. In addition, carrying out well-controlled polymerizations in environmentally friendly reaction media such as water, alcohols, or supercritical carbon dioxide is highly desirable. To accomplish this, the interaction of the metal complex with various solvents that can alter its activity should be understood.

A recent extensive review deals with the structural characterization of ATRP catalysts.(7) Successful attempts to correlate the activity of various ATRP catalysts with the nature of both the central metal and the ligands have been made.(8) Herein, the basic criteria for rational selection of appropriate ligands for copper-based ATRP catalysts are outlined.

Evaluation of ATRP Catalyst Performance

The ATRP Equilibrium and its Components

The copper-mediated atom transfer process is presented schematically in Figure 1; the equilibrium constant $K_{\text{ATRP}} = k_{\text{act}}/k_{\text{deact}}$ is a product of four simpler equilibrium constants.(8)



Contributing Reactions

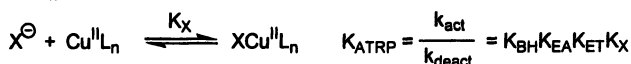
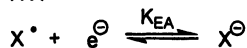


Figure 1. Representation of atom transfer as a combination of a C-X bond homolysis of alkyl halide (RX), two redox processes, and a heterolytic cleavage of Cu^{II}-X bond. L represents a ligand. (8)

The value of K_{ATRP} is mainly responsible for the observed rate of polymerization R_p as shown by eq (1).(2,9)

$$R_p = k_p K_{\text{ATRP}} \frac{[\text{RX}][\text{Cu}^{\text{I}}\text{L}_n]}{[\text{XCu}^{\text{II}}\text{L}_n]} [\text{M}] \quad (1)$$

In the above dependence, k_p is the propagation rate constant of the monomer M.

The polymerization control is reflected by a low value of M_w/M_n or polydispersity index (PDI). In systems with fast exchange between dormant and active species, it decreases as the polymerization proceeds. The value of PDI depends on the rate of deactivation, and is lower for ATRP deactivators $\text{XCu}^{\text{II}}\text{L}_n$ reacting rapidly with radicals (high value of k_{deact}), according to eq (2).(10,11)

$$\text{PDI} = \frac{M_w}{M_n} = 1 + \left(\frac{k_p [\text{RX}]_0}{k_{\text{deact}} [\text{XCu}^{\text{II}}\text{L}_n]} \right) \left(\frac{2}{\text{conv}} - 1 \right) \quad (2)$$

The nature of the ATRP catalyst has an impact on three of the equilibrium constants shown in Figure 1: K_{ET} and K_{X} depend upon the nature of the ligand L, while K_{EA} , and K_{X} depend upon the halide. The concentration of deactivator $\text{XCu}^{\text{II}}\text{L}_n$ present in the system depends upon the value of K_{X} (*vide infra*). Therefore, both the ATRP rate (eq (1)) and polymerization control (eq (2)) are catalyst-dependent and it is necessary to understand the correlation between structure and catalytic activity. This should ultimately make possible the rational design of highly active catalysts applicable to a variety of monomers.

With the exception of K_{BH} all the equilibrium constants shown in Figure 1 change dramatically with the polarity, ability to form hydrogen bonds, and donor

properties of the reaction medium. For instance, in protic solvents the stability of the deactivator $\text{XCu}^{\text{II}}\text{L}_n$ (i.e., K_X) can be several orders of magnitude lower than in non-protic solvents, leading to inefficient deactivation and poor control (eq (2)).(12) This paper presents some recent results illustrating the importance of ligand, halide, and solvent selection in the optimization of ATRP catalysts.

Measurement of ATRP Equilibrium Constants and Rate Constants

As briefly outlined above, the values of the rate constants k_{act} and k_{deact} as well as their ratio K_{ATRP} should be high in order to achieve fast polymerization rates and good polymerization control. To evaluate an ATRP catalyst requires the knowledge of all these reaction parameters. The rate constant k_{act} can be determined by reacting an alkyl halide with an excess of the Cu^{I} complex, and trapping the formed radicals by agents such as nitroxides. The consumption of alkyl halide (monitored by spectroscopic or chromatographic techniques) under these conditions is directly related to k_{act} : $\ln([\text{RX}]_0/[\text{RX}]) = k_{\text{act}}[\text{Cu}^{\text{I}}\text{L}_n]_0 t$.(13,14) It is possible to determine k_{act} and K_{ATRP} independently, and to calculate the values of k_{deact} from the ratio $k_{\text{act}}/K_{\text{ATRP}}$. Alternative experimental methods for determination of k_{deact} include the clock reaction in which the radicals are simultaneously trapped by TEMPO and the deactivator $\text{XCu}^{\text{II}}\text{L}_n$,(15) and analysis of the initial degrees of polymerization with no reactivation, end groups, and molecular weight distributions.(16-18)

Experimentally, the values of K_{ATRP} can be determined from polymerization kinetics data. In this case, an apparent value, $K_{\text{ATRP}}/[\text{XCu}^{\text{II}}\text{L}_n]$, is obtained from the slope of the dependence of $\ln([M]_0/[M])/(k_p[\text{Cu}^{\text{I}}\text{L}_n]_0[\text{RX}]_0)$ on time.(19) Alternatively, the classical equation describing the time dependence of accumulation of deactivator due to the persistent radical effect is used:(9,20,21)

$$[\text{XCu}^{\text{II}}\text{L}_n] = \left(3K_{\text{ATRP}}^2 k_t [\text{RX}]_0^2 [\text{Cu}^{\text{I}}\text{L}_n]_0^2 \right)^{1/3} t^{1/3} \quad (3)$$

To determine K_{ATRP} , a Cu^{I} complex is reacted with an alkyl halide, and the deactivator concentration (experimentally accessible through ESR or electronic spectroscopy) is monitored as a function of time. Then, a plot of $[\text{XCu}^{\text{II}}\text{L}_n]$ vs. $t^{1/3}$ is constructed, and K_{ATRP} is determined from the slope provided that the termination rate constant k_t is known.(8) This method is useful only for reactions that reach equilibrium rapidly, and then only for relatively low conversions of activator, $\text{Cu}^{\text{I}}\text{L}_n$, and alkyl halide. If these conditions are not met, the linear dependence (eq (3)) is not observed. The reason is that eq (3) was originally

derived with the assumption that $k_{\text{act}}[\text{Cu}^{\text{I}}\text{L}_n]_0[\text{RX}]_0 = k_{\text{deact}}[\text{R}^*][\text{XCu}^{\text{II}}\text{L}_n]$, i.e., that the concentrations of the activator and initiator do not change significantly during the experiment. This approach is valid only for time regimes in which the product $[\text{R}^*][\text{XCu}^{\text{II}}\text{L}_n]$ remains constant. This is a severe limitation when the values of K_{ATRP} for active catalysts should be determined.

Recently, the equations describing the persistent radical effect were modified taking into account that the concentrations of both the activator and initiator change during the experiment.(22) If the activator and initiator are mixed in a 1:1 molar ratio, the reaction stoichiometry requires that $[\text{RX}]_0 - [\text{RX}] = [\text{Cu}^{\text{I}}\text{L}_n]_0 - [\text{Cu}^{\text{I}}\text{L}_n] = [\text{XCu}^{\text{II}}\text{L}_n]$. Using the assumption (justified by simulations) that the rate of generation of deactivator exceeds significantly the rate of consumption of radicals, new equations describing the time-dependence of $[\text{XCu}^{\text{II}}\text{L}_n]$ were obtained. For the simple 1:1 stoichiometry ($[\text{Cu}^{\text{I}}\text{L}_n]_0 = [\text{RX}]_0$), a function $F([\text{XCu}^{\text{II}}\text{L}_n])$ is defined whose values are plotted against time, and K_{ATRP} is obtained from the slope of the linear dependence:

$$F([\text{XCu}^{\text{II}}\text{L}_n]) = \frac{[\text{Cu}^{\text{I}}\text{L}_n]_0^2}{3([\text{Cu}^{\text{I}}\text{L}_n]_0 - [\text{XCu}^{\text{II}}\text{L}_n])^3} - \frac{[\text{Cu}^{\text{I}}\text{L}_n]_0}{([\text{Cu}^{\text{I}}\text{L}_n]_0 - [\text{XCu}^{\text{II}}\text{L}_n])^2} + \frac{1}{[\text{Cu}^{\text{I}}\text{L}_n]_0 - [\text{XCu}^{\text{II}}\text{L}_n]} \quad (4)$$

$$= 2k_1K_{\text{ATRP}}^2t + \frac{1}{3[\text{Cu}^{\text{I}}\text{L}_n]_0}$$

The case when $[\text{Cu}^{\text{I}}\text{L}_n]_0 \neq [\text{RX}]_0$ has also been described and has been successfully utilized for the determination of K_{ATRP} .(22)

Ligand selection

Catalyst Activity

Some typical ligands used to form copper complexes with application in ATRP are listed in Figure 2. In the early stage of development of copper-mediated ATRP, bpy and its alkyl derivatives, possessing better solubility in nonpolar media, were used as the ligands.(1,23-25) Other similar ligands such as 1,10-phen and its derivatives were also employed in the ATRP of Sty.(26) The ATRP of Sty was slower with the CuCl complex of a substituted 1,10-phen, namely 4,7-diphenyl-1,10-phenanthroline, than with dNbpy.(26) It was soon realized (27) that linear aliphatic amines such as PMDETA and HMTETA formed more active Cu^{I} complexes that could be successfully used to control the polymerization of Sty, MA, and MMA. A branched tetradentate ligand, Me_6TREN , formed an exceptionally active Cu^{I} complex that could be used at ambient temperature and at low concentration (10 % relative to the initiator) to

control the polymerization of MA, still at sufficiently high rate.(28) The activity of several successful ATRP catalysts was found to decrease in the order $\text{CuBr}/\text{Me}_6\text{TREN} > \text{CuBr}/\text{PMDETA} > \text{CuBr}/\text{dNbpy}$.(28) It was found that Me_4cyclam formed very active Cu^{I} complex,(29) which was even more active than that of Me_6TREN .(30) Unfortunately, although the ATRP reactions catalyzed by $\text{Cu}^{\text{I}}(\text{Me}_4\text{cyclam})$ were very fast, the degree of control was not satisfactory due to inefficient radical deactivation by the $\text{XCu}^{\text{II}}(\text{Me}_4\text{cyclam})$ complex. Picolyamine derivatives such as BPMOA and TPMA were also studied as ligands for the copper-mediated ATRP of Sty, MA, and MMA and it was demonstrated that the TPMA complex possessed considerable activity (however, lower than the Me_6TREN complex).(31) Pyridinecarbaldehyde imine (PyIm-R) ligands have been successfully used in the ATRP of various methacrylates.(32) The effect of the alkyl substituent at the nitrogen atom of these and glyoxal diimine-type (GIm-R) ligands on the activity of the Cu^{I} -based ATRP catalysts derived therefrom was studied and it was shown that in general branching in the alkyl group led to slower polymerizations.(33)

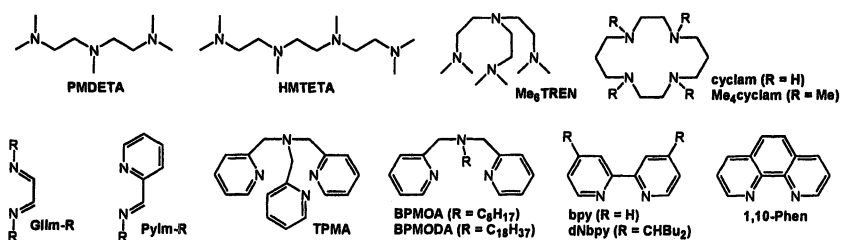


Figure 2. Examples of nitrogen-containing ligands used to form copper-based ATRP catalysts.

ATRP is fundamentally a redox process, and it is natural to correlate the catalytic activity of copper-based complexes with their redox properties.(34) In a detailed study, CuCl and CuBr complexes of bpy, dNbpy, BPMOA, BPMODA, TPMA, PMDETA, and Me_6TREN were all characterized by cyclic voltammetry and the measured redox potentials were correlated with the activity of the complexes in the ATRP of MA.(19) The logarithm of the apparent ATRP equilibrium constant, $K_{\text{ATRP}}/[\text{XCu}^{\text{II}}\text{L}_n]$, was a linearly decreasing function of the measured $E_{1/2}$ values. The values of either k_{act} or K_{ATRP} and the redox potential of a series of copper complexes with tridentate N-based ligands (where the nitrogen atom was amine-, imine-, or pyridine-type) were also correlated.(15) The low reducing power of Cu^{I} complexes of tetradentate bis(pyridinecarbaldehyde imine) ligands was used to explain the comparatively slow MMA ATRP catalyzed by these complexes.(35) 1,8-Diazabicyclo[5.4.0]undec-7-ene (DBU) was used as a ligand for the copper-mediated ATRP of Sty, MA, and MMA, and it was shown that the

polymerizations were relatively slow. This was due to the relatively high redox potential of the copper complex (more positive by 110 mV than that of the bpy complex, and by 220 mV than of the PMDETA complex).(36) The substituents at the ligands also affect the redox properties of the complexes. In general, the addition of more electron-donating groups stabilizes the Cu^I oxidation state leading to lower ATRP catalytic activity. This has been observed, for instance, when hydrogen atoms from an N-H group in the ligand are replaced by alkyl,(37,38) or allyl groups.(38) When a C-N fragment in a ligand molecule is substituted by C=N, usually a pronounced relative stabilization of the Cu^I compared to the Cu^{II} complex is observed.(39,40)

So far, only N-based ligands were discussed. The nature of the donor atoms in a ligand has a profound effect on the redox properties of its complexes. For instance, the very low reducing power of Cu^I complexes with thioether ligands makes these ligands inappropriate for ATRP catalysts. This is the result of the marked stabilization of the Cu^I relative to the Cu^{II} state. The redox potentials for the Cu^{II}L/Cu^IL couple for several thioethers (both open-chain and macrocycles) were in the range of 500 – 800 mV vs. NHE.(41) Mixed donor ligands such as the analogues of TPMA shown in Figure 3 were studied and it was shown that the increase of the number of sulfur atoms led to formation of less reducing Cu^I complexes.(42) These observations lead to the conclusion that although sulfur-only-containing ligands are not appropriate as components of active ATRP catalysts, “heterodonor” ligands could perform better. Such complexes are of interest because they may be sufficiently stable in the presence of acids and therefore may be used to mediate the ATRP of acidic monomers.

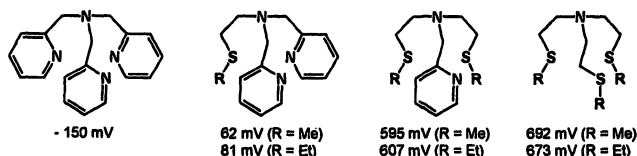


Figure 3. Ligands with similar structural features and redox potentials of their copper complexes vs. NHE.(42) Note the gradual increase of the redox potential as the number of sulfur atoms is increased.

In summary, the activity of the ATRP catalyst is directly related to its reducing power, i.e. to the value of K_{ET} or the redox potential of the couple Cu^{II}L_n / Cu^IL_n. The redox potential is in turn related to the relative stabilization of the Cu^{II} vs. the Cu^I state upon complexation with the ligand L. For ligands forming 1:1 complexes with copper ions, the following relation holds:(43)

$$E = E^0 + \frac{RT}{F} \left(\ln \frac{[Cu^{II}]_{tot}}{[Cu^I]_{tot}} - \ln \frac{1 + \beta^II [L]}{1 + \beta^I [L]} \right) \approx E^0 + \frac{RT}{F} \left(\ln \frac{[Cu^{II}]_{tot}}{[Cu^I]_{tot}} - \ln \frac{\beta^II}{\beta^I} \right) \quad (5)$$

where β^I is the stability constant of the Cu^IL complex. Thus, the knowledge of the readily measurable stability constants of Cu^{II}L_n and Cu^IL_n is sufficient to predict the catalytic activity of a given complex. Ideally, the value of K_X should be known as well, for it also contributes to the value of K_{ATRP} . Table 1 lists experimental values of β^{II}/β^I (in aqueous media) for copper complexes often used as ATRP catalysts along with the measured values of K_{ATRP} in the reaction with ethyl 2-bromoisobutyrate in acetonitrile. Although the two sets of numbers were determined in two different solvents, the trend that higher values of β^{II}/β^I correspond to higher values of K_{ATRP} is clearly seen.

Table 1. Correlation between the ratio β^{II}/β^I and K_{ATRP} for various Cu^I complexes used as ATRP catalysts

| <i>Catalyst</i> | β^{II} / β^I ^a | K_{ATRP} ^b |
|-----------------|-------------------------------------|------------------------------------|
| CuBr / bpy | 2.95 (44) | 3.93×10^{-9} (22) |
| CuBr / HMTETA | 39.8 (38) | 8.38×10^{-9} ^c |
| CuBr / PMDETA | 14500 (38) | 7.46×10^{-8} (22) |
| CuBr / TPMA | 49000 (42) | 9.65×10^{-6} (22) |

^a Measured in aqueous solution.

^b Reaction with ethyl 2-bromoisobutyrate in CH_3CN at 22 ± 2 °C.

^c This work.

Aqueous ATRP Systems. Disproportionation of the Catalyst

The complexes of Cu^I are generally unstable in aqueous media and tend to disproportionate. For instance, the disproportionation of non-complexed Cu^I in water is characterized by an equilibrium constant as large as $K_{\text{disp}} = 10^6$.⁽⁴⁵⁾ Addition of a ligand L can significantly affect the equilibrium and K_{disp} changes to a new value, K_{disp}^* , determined by the stabilization of Cu^{II} relative to Cu^I upon coordination with L:

$$K_{\text{disp}}^* = \frac{1 + \sum_{j=1}^n \beta_j^{II} [\text{L}]^j}{\left(1 + \sum_{j=1}^n \beta_j^I [\text{L}]^j\right)^2}; \quad \text{for 1:1 complex: } K_{\text{disp}}^* = \frac{1 + \beta^{II} [\text{L}]}{(1 + \beta^I [\text{L}])^2} K_{\text{disp}} \approx \frac{\beta^{II}}{(\beta^I)^2 [\text{L}]} K_{\text{disp}} \quad (6)$$

Examination of eqs (5) and (6) shows that for ligands forming 1:1 complexes with copper ions, the activity of the catalyst is proportional to β^{II}/β^I whereas the tendency of the Cu^I complex to disproportionate in aqueous solution (which should be minimized) depends on the ratio $\beta^{II}/(\beta^I)^2 [\text{L}]$.⁽⁴⁶⁾ Thus, a map

can be constructed (Figure 4) that can be used to select a ligand for aqueous ATRP that forms an active complex, yet stable towards disproportionation.

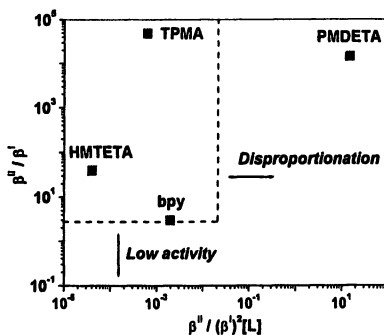


Figure 4. Map for selection of catalysts for ATRP in aqueous media ($[L] = 0.01$ mM). (Reproduced from reference 47. Copyright American Chemical Society.)

The complex $\text{Cu}^{\text{I}}/\text{PMDETA}$ is not suitable for aqueous ATRP due to very fast disproportionation. On the other hand, ligands such as bpy, HMTETA, and TPMA can all be used in aqueous media. The catalysts containing these ligands will have, according to Figure 4, rather different activities. If necessary, the catalyst disproportionation in water can be suppressed by using an appropriate cosolvent, stabilizing Cu^{I} vs Cu^{II} such as pyridine. It was demonstrated that the use of pyridine as a cosolvent for aqueous ATRP of ionic monomers such as sodium 4-styrenesulfonate and 2-(N,N,N-trialkylammonio)ethyl methacrylate salts completely suppressed the catalyst disproportionation and well-defined polyelectrolytes were obtained.⁽⁴⁶⁾

Acidic and Coordinating Monomers

Attempts to directly polymerize acidic monomers (such as acrylic or methacrylic acid) by ATRP have failed due to interactions of acids with the catalyst leading to complete loss of activity. The concept of conditional stability constants^(48,49) allows for calculation of the stability of an ATRP catalyst in acidic solutions. Generally, the complexes of very basic ligands are rather sensitive to pH of the medium, although in the case when the ligand forms particularly kinetically stable copper complexes, the complex protonation can become negligible. Eq (7) gives the dependence of the conditional stability constant β^* of a complex as a function of acid concentration.

$$\beta^* = \frac{\beta}{\alpha_L} \left(\alpha_L = 1 + \frac{[\text{H}^+]}{K_{a,r}} + \frac{[\text{H}^+]^2}{K_{a,r}K_{a,r-1}} + \dots + \frac{[\text{H}^+]^r}{K_{a,r}K_{a,r-1}\dots K_{a,1}} \right) \quad (7)$$

In the above equation, $K_{a,1}, \dots, K_{a,r}$ are the acidity constants of the protonated ligand. Figure 5 is a graphical representation of eq (7) for the Cu^{II} complexes of ligands for which the protonation constants and the formation constants of Cu^{II} complexes are known: PMDETA,(38) HMTETA,(50) Me_6TREN ,(50) cyclam,(50) Me_4cyclam ,(50) and TPMA.(42) As seen, the complexes of basic ligands, especially when their stability constants even in the absence of protonation are relatively low (e.g., the Cu^{II} complexes of PMDETA and HMTETA) are very much destabilized in acidic media. The appropriate ligand for ATRP of acidic monomers should form complexes of Cu^{I} and Cu^{II} that are both sufficiently stable in acidic media, but also the ratio of $\beta^{\text{II}}/\beta^{\text{I}}$ should be large enough to ensure sufficient catalytic activity. Moreover, if the ATRP reaction is to be performed in aqueous media, the possibility of catalyst disproportionation should be considered as well. From this point of view, TPMA is a promising candidate as a ligand for the aqueous ATRP of acidic monomers.

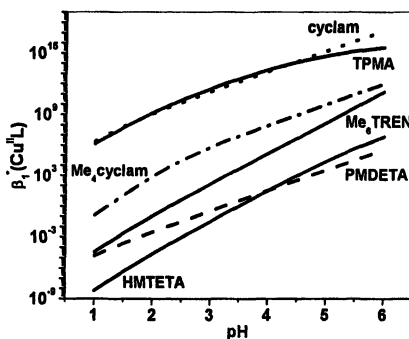


Figure 5. Dependence of the conditional stability constant of $\text{Cu}^{\text{II}}\text{L}$ complexes used as ATRP catalysts upon pH of the medium.(51)

The coordination of various monomers such as styrene, methyl acrylate, and methyl methacrylate to the $\text{Cu}^{\text{I}}/\text{PMDETA}$ complex with non-coordinating anions was recently reported.(52,53) This coordination is relatively weak and does not affect the performance of the ATRP catalyst. In the special case when the monomer or the polymer derived therefrom can strongly complex to the copper center of the ATRP catalyst, the catalyst activity can only be preserved if ligands forming very stable Cu^{I} and Cu^{II} complexes are used. Knowledge of equilibrium constants of the side reactions is essential for evaluation of the conditional stability of ATRP catalysts, as illustrated above for the case of ligand protonation by acidic monomers and polymers.

The Role of the Halide Ligand

Halogenophilicity of the $\text{Cu}^{\text{II}}\text{L}_n$ Complex

According to eq (2), the polymerization control should be unsatisfactory in systems, in which the deactivating $\text{XCu}^{\text{II}}\text{L}_n$ complex is unstable. The concentration of deactivator actually present in the reaction mixture depends upon the value of the stability constant K_X as well as upon the total concentrations of Cu^{II} complexes and halide ions present.(12)

$$[\text{XCu}^{\text{II}}\text{L}_n] = \frac{F - \sqrt{F^2 - 4K_X^2 [\text{Cu}^{\text{II}}\text{L}_n]_{\text{tot}} [\text{X}]_{\text{tot}}}}{2K_X} \quad (F = 1 + K_X [\text{Cu}^{\text{II}}\text{L}_n]_{\text{tot}} + K_X [\text{X}]_{\text{tot}}) \quad (8)$$

The values of K_X for $X = \text{Br}$ or Cl have been determined in various mixed water-containing solvents. The halogenophilicity decreases dramatically as the water content in the mixed solvent increases leading to inefficient deactivation. This in turn causes the fast and poorly controlled polymerizations, often observed in ATRP in aqueous or protic media. However, the use of large initial amounts of deactivator $\text{XCu}^{\text{II}}\text{L}_n$ as well as the addition of halide salts to the reaction mixture that can regenerate the dissociated deactivator proved a successful strategy for conducting well-controlled ATRP in protic solvents.(12)

Deactivation Rate Constant and Stability of the Polymeric Dormant State

It is intuitive that the deactivation reaction, i.e. the transfer of the halogen atom from the Cu^{II} halide complex to the radical (either low molecular weight or polymeric), depends on the nature of the halogen atom. The rate constants of deactivation of 1-phenylethyl radicals (which mimic the polystyrene propagating radical) with $[\text{Cu}^{\text{II}}(\text{dNbpy})_2\text{X}]$ complexes at 75 °C are $k_{\text{deact}} = 2.5 \times 10^7 \text{ M}^{-1}\text{s}^{-1}$ ($X = \text{Br}$) and $4.3 \times 10^6 \text{ M}^{-1}\text{s}^{-1}$ ($X = \text{Cl}$). (14) Based on these values, it is expected that the level of control over polymerization will be better (more efficient deactivation) with bromine- rather than with chlorine-based catalysts if specific side reactions (*vide infra*) are absent. Indeed, this has been experimentally observed, for example in the controlled polymerization of HEMA in protic medium catalyzed by copper-bpy complexes.(12) Similar results were reported by Jewrajka et al.(54)

The polymerization control (eq (2)) can be improved by employing a catalyst containing initially $\text{XCu}^{\text{II}}\text{L}_n$ or by selecting a solvent for which K_X is relatively large. This guarantees that insignificant part of deactivator will be lost (eq (8)). However, the choice of the halide in the catalyst should also be based upon considerations of the deactivation rate constant. In the case when the alkyl halide initiator or polymeric dormant state can easily participate in nucleophilic

substitution reactions (e.g., 1-phenylethyl halide and halide-terminated polystyrene or the similar compounds with pyridine units), the use of chloride-based catalyst is advantageous since S_N reactions of alkyl chlorides are significantly slower than for alkyl bromides.

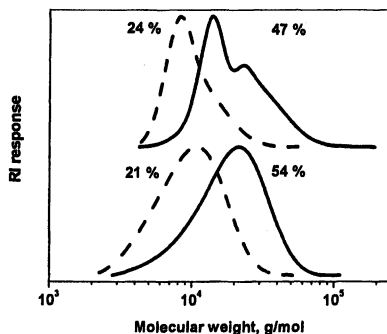


Figure 6. SEC traces of poly4VP prepared by ATRP at 30 °C in H_2O -MeOH (1:1) with CuBr/HMTETA (top) or CuCl/HMTETA (bottom) catalyst (monomer conversions indicated at each curve). $[4VP]_0:[RBr]_0:[Cu]_{tot} = 100:1:1$ and $4VP:solvent = 1:1$.

Figure 6 shows that the ATRP of 4-vinylpyridine (4VP) using 2-bromoisobutyrate ester as the initiator and CuBr/HMTETA as the catalyst yielded a polymer with polymodal molecular weight distribution. The polymodality was the result of reaction of the bromine-terminated poly4VP with either the monomer or polymer yielding pyridinium salts and therefore leading to branching. This reaction was suppressed when CuCl/HMTETA was employed as the catalyst, and a polymer of narrower and monomodal molecular weight distribution was produced.⁽⁵¹⁾

Conclusions

Knowledge of the stability constants of copper complexes in both the high and low oxidation states is important for the design of active ATRP catalysts that provide good polymerization control. The catalyst activity depends on the relative stability of the Cu^{II} and Cu^I complexes (β^{II} and β^I , respectively). In aqueous media, the ATRP catalyst may disproportionate but this reaction can be completely suppressed by the use of ligand or cosolvent stabilizing the lower oxidation state. For ligands L forming 1:1 complexes with copper ions, the best

ATRP catalyst should be selected in such a way that the ratio $\beta^{\text{II}}/\beta^{\text{I}}$ is as high as possible while the ratio $\beta^{\text{II}}/(\beta^{\text{I}})^2[\text{L}]$ is as low as possible. A map for selection of appropriate ATRP catalysts for aqueous media was constructed taking into account both requirements. The easy to calculate conditional stability of the ATRP catalyst should be considered in the design of catalysts for the ATRP of special (acidic or coordinating) monomers. Ligands of low basicity should be used for the ATRP of acidic monomers. In order to avoid side reactions such as competitive complexation by monomer and/or polymer to the copper center, both β^{I} and β^{II} should be large. The control over polymerization also largely depends upon the halogenophilicity of the higher oxidation state complex. For solvents in which it is low, the deactivation can be enhanced and control improved by addition of halide salts to the reaction mixture. Generally, copper bromide-based catalysts give better control (due to larger deactivation rate constant) and faster reactions (due to larger ATRP equilibrium constant) than chloride-based catalysts. However, when nucleophilic or basic monomers are polymerized, the use of chloride-based catalyst is essential to achieve good control. Quantitative criteria are outlined for the rational selection of ATRP catalysts.

Acknowledgments. The authors thank NSF (grant CHE-04-05627) and EPA (grant R82958001) for funding.

References

1. Wang, J.-S.; Matyjaszewski, K. *J. Am. Chem. Soc.* **1995**, *117*, 5614.
2. Matyjaszewski, K.; Xia, J. *Chem. Rev.* **2001**, *101*, 2921.
3. Kamigaito, M.; Ando, T.; Sawamoto, M. *Chem. Rev.* **2001**, *101*, 3689.
4. Matyjaszewski, K. *Prog. Polym. Sci.* **2005**, *30*, 858.
5. Coessens, V.; Pintauer, T.; Matyjaszewski, K. *Prog. Polym. Sci.* **2001**, *26*, 337.
6. Tsarevsky, N. V.; Matyjaszewski, K. *J. Polym. Sci.: Part A: Polym. Chem.* **2006**, *in press*.
7. Pintauer, T.; Matyjaszewski, K. *Coord. Chem. Rev.* **2005**, *249*, 1155.
8. Pintauer, T.; McKenzie, B.; Matyjaszewski, K. *ACS Symp. Ser.* **2003**, *854*, 130.
9. Goto, A.; Fukuda, T. *Prog. Polym. Sci.* **2004**, *29*, 329.
10. Matyjaszewski, K. *Macromol. Symp.* **1996**, *111*, 47.
11. Litvinenko, G.; Mueller, A. H. E. *Macromolecules* **1997**, *30*, 1253.
12. Tsarevsky, N. V.; Pintauer, T.; Matyjaszewski, K. *Macromolecules* **2004**, *37*, 9768.
13. Goto, A.; Fukuda, T. *Macromol. Rapid Commun.* **1999**, *20*, 633.

14. Matyjaszewski, K.; Paik, H.-j.; Zhou, P.; Diamanti, S. J. *Macromolecules* **2001**, *34*, 5125.
15. Matyjaszewski, K.; Goebelt, B.; Paik, H.-j.; Horwitz, C. P. *Macromolecules* **2001**, *34*, 430.
16. Greszta, D.; Matyjaszewski, K. *Macromolecules* **1996**, *29*, 7661.
17. Gromada, J.; Matyjaszewski, K. *Macromolecules* **2002**, *35*, 6167.
18. Chambard, G.; Klumperman, B.; German, A. L. *Macromolecules* **2002**, *35*, 3420.
19. Qiu, J.; Matyjaszewski, K.; Thouin, L.; Amatore, C. *Macromol. Chem. Phys.* **2000**, *201*, 1625.
20. Fischer, H. *J. Polym. Sci., Part A: Polym. Chem.* **1999**, *37*, 1885.
21. Fischer, H. *Chem. Rev.* **2001**, *101*, 3581.
22. Tang, W.; Tsarevsky, N. V.; Matyjaszewski, K. *J. Am. Chem. Soc.* **2006**, *128*, 1598.
23. Wang, J. S.; Matyjaszewski, K. *Macromolecules* **1995**, *28*, 7901.
24. Patten, T. E.; Xia, J.; Abernathy, T.; Matyjaszewski, K. *Science* **1996**, *272*, 866.
25. Matyjaszewski, K.; Patten, T. E.; Xia, J. *J. Am. Chem. Soc.* **1997**, *119*, 674.
26. Destarac, M.; Bessiere, J. M.; Boutevin, B. *Macromol. Rapid Commun.* **1997**, *18*, 967.
27. Xia, J.; Matyjaszewski, K. *Macromolecules* **1997**, *30*, 7697.
28. Xia, J.; Gaynor, S. G.; Matyjaszewski, K. *Macromolecules* **1998**, *31*, 5958.
29. Teodorescu, M.; Matyjaszewski, K. *Macromolecules* **1999**, *32*, 4826.
30. Rademacher, J. T.; Baum, M.; Pallack, M. E.; Brittain, W. J.; Simonsick, W. J., Jr. *Macromolecules* **2000**, *33*, 284.
31. Xia, J.; Matyjaszewski, K. *Macromolecules* **1999**, *32*, 2434.
32. Haddleton, D. M.; Jasieczek, C. B.; Hannon, M. J.; Shooter, A. J. *Macromolecules* **1997**, *30*, 2190.
33. Haddleton, D. M.; Crossman, M. C.; Dana, B. H.; Duncalf, D. J.; Heming, A. M.; Kukulj, D.; Shooter, A. J. *Macromolecules* **1999**, *32*, 2110.
34. Matyjaszewski, K. *Macromolecules* **1998**, *31*, 4710.
35. Iovu, M. C.; Maithufi, N. G.; Mapolie, S. F. *Polym. Int.* **2003**, *52*, 899.
36. Fournier, D.; Romagne, M.-L.; Pascual, S.; Montembault, V.; Fontaine, L. *Eur. Polym. J.* **2005**, *41*, 1576.
37. Golub, G.; Cohen, H.; Paoletti, P.; Bencini, A.; Messori, L.; Bertini, I.; Meyerstein, D. *J. Am. Chem. Soc.* **1995**, *117*, 8353.
38. Navon, N.; Golub, G.; Cohen, H.; Paoletti, P.; Valtancoli, B.; Bencini, A.; Meyerstein, D. *Inorg. Chem.* **1999**, *38*, 3484.
39. Olson, D. C.; Vasilevskis, J. *Inorg. Chem.* **1971**, *10*, 463.
40. Fabbrizzi, L.; Lari, A.; Poggi, A.; Seghi, B. *Inorg. Chem.* **1982**, *21*, 2083.
41. Rorabacher, D. B.; Bernardo, M. M.; Vande Linde, A. M. Q.; Leggett, G. H.; Westerby, B. C.; Martin, M. J.; Ochrymowycz, L. A. *Pure Appl. Chem.* **1988**, *60*, 501.

42. Ambundo, E. A.; Deydier, M.-V.; Grall, A. J.; Aguera-Vega, N.; Dressel, L. T.; Cooper, T. H.; Heeg, M. J.; Ochrymowycz, L. A.; Rorabacher, D. B. *Inorg. Chem.* **1999**, *38*, 4233.
43. Lingane, J. J. *Chem. Rev.* **1941**, *29*, 1.
44. *Stability Constants of Metal-Ion Complexes. Supplement No 1. Special Publication No 25*; The Chemical Society: London, 1971.
45. Datta, D. *Ind. J. Chem.* **1987**, *26A*, 605.
46. Tsarevsky, N. V.; Pintauer, T.; Matyjaszewski, K. *Polym. Prepr.* **2002**, *43(2)*, 203.
47. Tsarevsky, N. V.; Matyjaszewski, K. *ACS Symp. Ser.* **2006**, *937*, in press.
48. Schwarzenbach, G. *Die Komplextometrische Titration*; 2nd ed.; Enke: Stuttgart, 1956.
49. Ringbom, A. *Complexation in Analytical Chemistry*; Interscience: New York, 1963.
50. Golub, G.; Lashaz, A.; Cohen, H.; Paoletti, P.; Bencini, A.; Valtancoli, B.; Meyerstein, D. *Inorg. Chim. Acta* **1997**, *255*, 111.
51. Tsarevsky, N. V.; McKenzie, B.; Tang, W.; Matyjaszewski, K. *Polym. Prepr.* **2005**, *46(2)*, 482.
52. Braunecker, W. A.; Pintauer, T.; Tsarevsky, N. V.; Kickelbick, G.; Matyjaszewski, K. *J. Organometal. Chem.* **2005**, *690*, 916.
53. Braunecker, W. A.; Tsarevsky, N. V.; Pintauer, T.; Gil, R. G.; Matyjaszewski, K. *Macromolecules* **2005**, *38*, 4081.
54. Jewrajka, S. K.; Chatterjee, U.; Mandal, B. M. *Macromolecules* **2004**, *37*, 4325.

Chapter 6

Magnetic Nanoparticle Supported Catalyst for Atom Transfer Radical Polymerization of Methyl Methacrylate

Shijie Ding, Maciej Radosz, and Youqing Shen*

Department of Chemical and Petroleum Engineering,
University of Wyoming, 1000 East University Avenue, Laramie, WY 82071

Magnetic nanoparticles were used to support a CuBr/MNP-TEDETA catalyst used for an ATRP of methyl methacrylate (MMA). The supported catalyst mediated a living/controlled radical polymerization of MMA as effectively as unsupported catalysts. With the addition of 22 mol% of Cu(II)Br₂, the polymer molecular weights were well-controlled with initiator efficiency of 0.85 and polydispersity lower than 1.2. The supported catalysts could be easily separated/isolated using a magnetic field. The catalyst could be reused with slightly decreased activity but much improved control. The activity of the recycled catalyst could be regenerated by copper metal. A PEG-block-PMMA was synthesized with 92.2% conversion and low polydispersity by this supported catalyst. It was concluded that nano-sized supports had reduced adverse effects on catalysis.

Introduction

Atom transfer radical polymerization (ATRP) has been successfully used in living polymerizations of various vinyl monomers (1-3) and functional monomers (4-8), producing polymers with well-controlled molecular weights. ATRP is also a versatile synthetic tool to prepare well-defined (co)polymer architectures including block (9-10), star (11-13), brush (14-16), comb (17), dendrimer-like (11,18-19) and hyperbranched (co)polymers (20-21). A remaining challenge for ATRP is the difficulty of separating the homogenous ATRP catalysts from their products. The residues of the transition metal complex catalysts color the products and may also make the products toxic. Therefore, the concentration of the catalyst residue in the products must be reduced to a low level for safe applications (22).

Post-polymerization purification methods such as catalyst extraction with catalyst-soluble solvents (8), catalyst adsorption with ion-exchange resins (23) and filtration of polymer solutions through columns of alumina or silica gel, have been developed for removal of catalysts from polymers prepared by ATRP (22). The disadvantages of these methods include cost, loss of polymer, difficulty in scale-up, and difficulties in separating the catalyst from functional polymers that interact with the catalysts (22).

Immiscible liquid-liquid biphasic polymerization, in which the transition metal complex catalysts were modified to preferentially locate in one phase and the polymer in the other, has also been extended from organic synthesis to ATRP. Fluorous solvent (24), supercritical CO₂ (25) and ionic liquids (26-27) were explored for the removal of catalyst from polymers. Recently, we reported the development of an ionic liquid catalyst, which during the polymerization, this ionic liquid catalyst can be dispersed as small droplets in organic solvents to catalyze liquid-liquid biphasic ATRP; after polymerization, the phase separation of the catalyst from the polymerization solution leads to catalyst separation and recycling. In this way, the amount of ionic liquid used in the reaction is greatly reduced, only 5 wt% of the organic solvent (28).

Immobilization of catalysts on solids also provides an efficient method for catalyst separation with a possibility to reuse the catalysts for cost saving. This concept was successfully used in batch (29-31) and continuous ATRP (32-33). Catalysts tethered on solid surfaces such as silica gel, polystyrene beads and Janda Jel resins can be easily recovered (34-40). However, the level of control over the polymerization by these covalently solid-supported catalysts was lower than that of unsupported catalysts. The deterioration of control over the polymerization was caused by the slower deactivation of the growing radicals. The deactivation rate constant for the solid-immobilized catalyst was reduced to the diffusion limit, ca. $10^5 \text{ L}\cdot\text{mol}^{-1}\cdot\text{s}^{-1}$, which is much less than the diffusion limit of homogenous catalysts, ca. $10^9 \text{ L}\cdot\text{mol}^{-1}\cdot\text{s}^{-1}$. Because the activation rate constant

remains unchanged, the overall effect of catalyst immobilization on solids is slower deactivation of the generated radicals, resulting in a higher radical concentration and uncontrolled chain growth (22, 41). Another effect of the catalyst immobilization on solids is that the catalyst on the solid surface may not be able to reach inside the polymer coil to catalyze the reactions, especially when the solids are porous (22, 39-40). The addition of soluble deactivators or free ligand to the solid-supported catalysts (41-43), and use of a soluble supports (44-47) or "catalyst sponge" (48-50) that releases free catalyst for homogeneous catalysis, could significantly improve the level of control over the polymerization (22).

Generally, the solid supports used for immobilization were in micrometer sizes, and some had porous structure. This causes a significant decrease in catalyst diffusivity. Inspired by the development of a supported catalysis for small molecular reactions (51), we used magnetic nanoparticles to support a catalyst for ATRP. It is envisioned that a smaller (nanometer sized) support with a regular shape may have reduced adverse effects on the diffusivity of the immobilized catalyst. The separation of nanosized magnetic supports can be easily achieved by applying a magnetic field.

Experimental

Materials

Acryloyl chloride (Lancaster, 96%), methyl α -bromophenylacetate (Aldrich, 97%, MBP), 3-aminopropyltrimethoxysilane (Aldrich, 97%), *N,N,N',N'*-tetraethyldiethylenetriamine (Aldrich, tech.90%, TEDETA), *N,N,N',N'*-pentamethyldiethylenetriamine (Aldrich, 99%, PMDETA), nitric acid (EM, A.C.S.), Fe_3O_4 powder (Nanostructured & Amorphous Materials Inc., APS 20-30 nm) were used directly without further purification. Toluene (Baker) and methyl methacrylate (Aldrich, 99%, MMA) were distilled before use. Copper(I) bromide (Aldrich, 98%) was stirred with glacial acetic acid, filtered, washed with ethanol and dried.

Grafting TEDETA ligand onto Fe_3O_4 magnetic nanoparticles (MNP-TEDETA)

As shown in Scheme 1, Fe_3O_4 magnetic nanoparticles (5.0 g, 20-30 nm) were refluxed with 3-aminopropyltrimethoxysilane (20 ml, 0.113 mol) in dry

toluene (30.0 ml) for 4 days. The solids were separated by applying an external magnetic field, and washed with 4×100 mL dry toluene and then 2×100 mL dry acetone. The resulted product was dried under vacuum for 12 h. Elemental analysis: N, 0.61 %.

The resulting solids were dispersed in 50 ml of dry dichloromethane and the flask was cooled in an ice-water bath. Triethylamine (16.0 ml, 0.113 mol) was added and stirred for 30 min. Then acryloyl chloride (4.0 ml, 49.2 mmol) was added dropwise over 30 min. The mixture was stirred at room temperature for 48 h. It was successively washed with acetone (3×100 ml), DI H₂O (3×100 ml), and again acetone (2×100 ml). The resulting product was dried under vacuum for 5 h, then dispersed in methanol (30.0 ml) and stirred with TEDETA (5.0 ml, 19.4 mmol) at room temperature for one week. The solids were separated by magnetic field and washed with acetone 5×100 mL. The resulting product was dried under vacuum for 12 h. Elemental analysis: N, 1.87 %.

Preparation of poly(ethylene glycol) macroinitiator(Ini-PEG)

PEG₄₅-OH (20.0 g, 0.010 mol) was dissolved in 300 mL of toluene in a 500 ml three-neck flask then triethylamine (2.78mL, 0.020 mol) was added and the solution was cooled to 0 °C. 2-Bromoisobutyryl bromide (2.47 mL, 0.020 mol) was added dropwise via a syringe over 1 h. The reaction mixture was stirred overnight at room temperature. The solution was filtered and the solvent was removed in vacuo. The crude polymer was dried under vacuum overnight, then dissolved in water at pH 8.5, and extracted with dichloromethane. The organic layer was collected, dried over CaCl₂, and purified under vacuum to remove the residual solvent. A 10-fold excess of diethyl ether was added to precipitate the PEG initiator (Ini-PEG). The product was dried under high vacuum overnight. Yield = 15.8 g.

Polymerization by CuBr/MNP-TEDETA catalyst

Reaction conditions for a typical polymerization are as follows: CuBr (0.0135g, 0.0941 mmol), MNP-TEDETA (0.2818g, TEDETA 0.0941 mmol) and a stirring bar were put into a reaction tube. The tube was tightly sealed and degassed by ten vacuum/nitrogen cycles. Degassed toluene (3.0 ml) was added via a degassed syringe. The mixture was stirred and bubbled with nitrogen for 5 minutes. The sealed tube was sonicated at room temperature for 10 min. Degassed MMA (0.943 g, 9.41 mmol) was added and then the mixture was degassed again for 2 minutes and stirred at 25 °C for 1 h. The tube was

immersed in an oil bath preset at the polymerization temperature. Finally, the initiator (MBP, 15.0 μ l, 0.0955 mmol) was added to the mixture with stirring. Samples (0.050 ml) were withdrawn at timed intervals from the tube using nitrogen-purged syringes, and dissolved in CDCl_3 . The conversions were measured by $^1\text{H-NMR}$ spectroscopy and the molecular weight and polydispersity of the polymers were measured by GPC.

Recycle of CuBr/MNP-TEDETA catalyst

After the polymerization was complete, the reactor tube was cooled to room temperature and placed on a magnetic bar. The catalyst was attracted to the bottom of the reactor. The polymer solution was decanted and the residual solid was washed by 3×3.0 ml degassed toluene under nitrogen. Degassed MMA, toluene and initiator were charged to the tube and the second polymerization run was conducted following the same procedure as the first polymerization run.

Regeneration of CuBr/MNP-TEDETA catalyst

The recovered solid was washed with 3×3.0 ml degassed toluene under nitrogen. About 1 g of copper metal beads (~ 1 mm diameter) and 3.0 ml of toluene were added and stirred with the catalyst at 40°C overnight. The resulting reactivated catalyst was separated from the copper beads and transferred into a degassed, tightly sealed tube. Then degassed MMA, toluene and initiator were added, and the polymerization was performed following the same procedure as the first polymerization run.

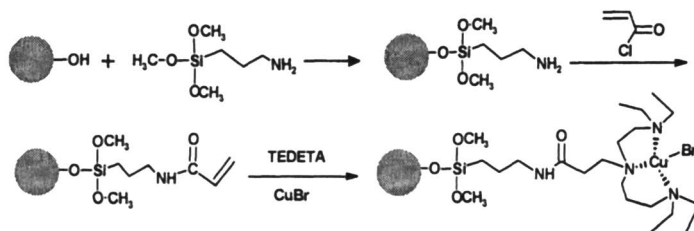
Characterization.

Gel permeation chromatography (GPC) was used to determine polymer molecular weights and molecular weight distributions (PDI) using polystyrene standards (Polysciences Corporation) to generate a universal calibration curve. The measurements were operated on a Waters SEC equipped with a Waters 2414 refractive index detector and two 300 mm Solvent-Saving GPC Columns (molecular weight ranges: 1×10^2 - 5×10^3 , 5×10^3 - 5×10^5) at a flow rate of 0.30 mL/min using THF as solvent at 30°C . Data were recorded and processed using Waters software package. ^1H NMR spectra were recorded on a Bruker Avance DRX-400 spectrometer using CDCl_3 as solvent. Chemical shifts were reported downfield from 0.00 ppm using TMS as internal reference. Elemental analysis was conducted by Midwest Microlab, LLC, Indianapolis, IN.

The residue copper concentration in crude polymer products was measured by ICP-MS at the Department of Geology of the University of Wyoming. The polymer solution was dried under vacuum and then the polymer powder (50.0 mg) was dissolved in nitric acid with heating. The solution was then diluted to 25.0 ml for ICP-MS analysis.

Results and Discussion

The TEDETA ligand was immobilized onto magnetic nanoparticles via two steps (Scheme 1): Fe_3O_4 magnetic nanoparticles (20-30 nm) were refluxed with 3-aminopropylsilane in dry toluene to introduce the amine groups onto the surface of the nanoparticles (52) and then they were end-capped with acryloxyl groups by the reaction of the amine groups with acryloyl chloride. A Michael reaction of the acryloxyl group with tetraethyldiethylenetriamine (TEDETA) attached the ligand onto the support. Elemental analysis showed that the nitrogen content was 1.87 wt %. Accordingly the calculated loading of TEDETA was 7.19 wt%, and the TEDETA density on the nanoparticle surface was about 3 molecules/ nm^2 . The unmodified magnetic nanoparticles strongly aggregated together to form large lumps in toluene; whereas after TEDETA was immobilized on the surface the modified magnetic nanoparticles could be dispersed in toluene.



Scheme 1. Grafting TEDETA ligand onto Fe_3O_4 magnetic nanoparticles (MNP-TEDETA)

ATRP of MMA with magnetic nanoparticles supported catalyst $\text{CuBr}/\text{MNP-TEDETA}$

The ATRP of methyl methacrylate (MMA) was carried out in toluene at 70°C using methyl α -bromophenylacetate (MBP) as initiator and $\text{CuBr}/\text{MNP-TEDETA}$ as the catalyst. A polymerization catalyzed by unsupported catalyst $\text{CuBr}/\text{PMDETA}$ was conducted under identical conditions for comparison.

Figure 1 shows that both polymerizations exhibited first-order kinetics; the polymerization rate of MMA with supported CuBr/MNP-TEDETA catalyst was very close to that catalyzed by the unsupported CuBr/PMDETA catalyst, indicating similar activity. Figure 2 shows that the molecular weights of PMMA from the polymerization with the supported CuBr/MNP-TEDETA catalyst increased linearly with increase of conversion, and was close to the theoretical molecular weights with polydispersity less than 1.3. However, the molecular weights of PMMA produced by the unsupported CuBr/PMDETA catalyst were much higher than the theoretical values, indicating a low initiator efficiency due to early the consumption of the initiators by radical terminations, as observed the precipitation of Cu(II) complex. Therefore, the magnetic nanoparticle supported CuBr/MNP-TEDETA catalyst can effectively mediate the polymerization with similar activity but improved control over polymerization compared to the unsupported catalyst.

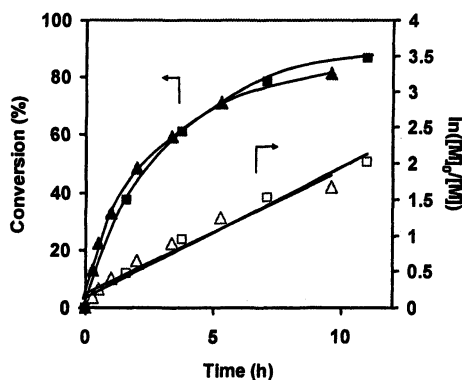


Figure 1. MMA polymerization with magnetic nanoparticle supported catalyst CuBr/MNP-TEDETA (■, □) and unsupported catalyst CuBr/PMDETA (▲, △) in toluene. 70 °C, [MMA] = 2.35 mol/L, [CuBr] = [Ligand] = [MBP] = 0.0235 mol/L.

Improving the initiator efficiency

In order to further improve the initiator efficiency, 22 mol% Cu(II)Br₂, relative to the total catalyst, was added to the polymerization. Figure 3 shows that the addition of 22 mol% of Cu(II)Br₂ (i.e. 22 mol% CuBr₂ and 78% mol% CuBr, and therefore an absolute decrease in CuBr), only suppressed the initial jump in activity, whereas the overall catalyst activity was only slightly decreased. Conversion reached a similar level (80%) in 10 h. Figure 4 shows that with the addition of 22 mol% of Cu(II), initiator efficiency was substantially increased, from 0.5 to 0.85, and polydispersity was decreased to less than 1.2. This is different from the results obtained with catalysts immobilized on the

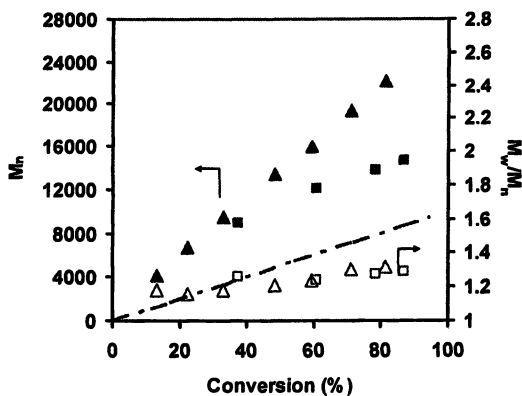


Figure 2. PMMA molecular weights and molecular weight distribution as a function of conversion in the polymerization of MMA with magnetic nanoparticle supported catalyst CuBr/MNP-TEDETA (■, □) and unsupported catalyst CuBr/PMDETA (▲, △) in toluene. See Figure 1 for experimental conditions.

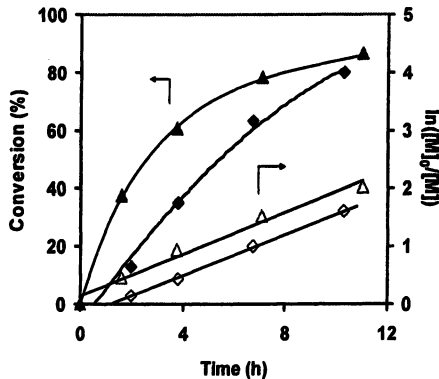


Figure 3. MMA polymerization catalyzed by magnetic nanoparticles supported catalyst CuBr/MNP-TEDETA in toluene with the addition of Cu(II)Br₂. 70 °C, [MMA] = 2.35 mol/L, [CuBr+CuBr₂] = [Ligand] = [MBP] = 0.0235 mol/L. Cu(II)Br₂ relatively to the total catalyst: 0 mol% (▲, △), 22 mol% (◆, ◇).

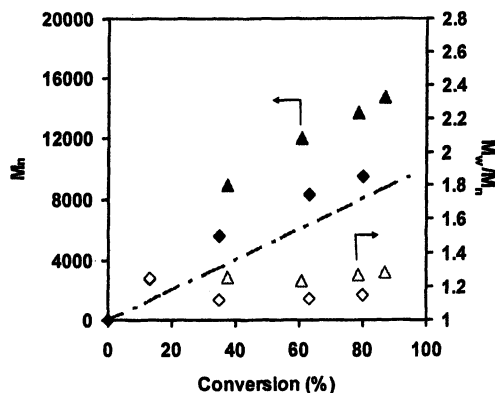


Figure 4. PMMA molecular weight and polydispersity as a function of conversion in the polymerizations catalyzed by CuBr/MNP-TEDETA in toluene with the addition of Cu(II)Br₂ relatively to the total catalyst : 0 mol% (▲, △), 22 mol% (◆, ◇). See Figure 3 for experiment condition.

micrometer-sized supports, when the addition of Cu(II) had little effect on the degree of control over polymerization (34).

Catalyst recycling and regeneration

After the polymerization was completed, the solution was cooled down to room temperature. The tube was placed on a magnetic bar and the supported catalyst was attracted on the bottom of the reactor. The upper layer was carefully removed using a degassed syringe. The polymer solution had no color. ICP-MS analysis showed that the concentration of copper bromide in solution was less than 6 ppm. The solid left in the reactor was washed with toluene under nitrogen three times, and then degassed MMA, toluene and initiator were added and a second run (first re-used) polymerization was performed following the same procedure as the first polymerization run. A third run (second catalyst reused) polymerization was performed similarly. The first reused catalyst had lower activity than the fresh catalyst, but had similar control over polymerization (Figures 5 & 6). The second reused catalyst retained similar activity to the first reused catalyst, but the molecular weights were much closer to the theoretical molecular weights. The polydispersity of the polymers from these three polymerization runs were similar, all less than 1.2. These results suggest that the reduction in activity of the recycled catalyst was not due to loss of catalyst but

the presence of more Cu(II) species produced by radical termination reactions in the first polymerization run. In order to verify this conclusion, we tested whether the polymerization could be conducted by the catalyst that had leached into the solution. A sample of the degassed catalyst was stirred in a MMA-toluene polymerization solution at 70 °C for 30 min. The supported catalyst was removed by a magnetic bar and then MBP (initiator) was added to the clear solution and a polymerization was conducted under the same conditions. After stirring at 70°C for 18 h, no polymerization was detected by either NMR or GPC. This indicates that the small amount of catalyst that may have leached into the solution was not sufficient to catalyze the polymerization, and the polymerizations were indeed catalyzed by the supported catalyst.

The activity of the recycled catalyst could be regenerated by simply stirring with copper metal. After the second polymerization run the catalyst was washed with toluene and then stirred with about 1 g of copper beads under nitrogen at 40 °C in toluene for 12 h. The regenerated catalyst was used for a new polymerization run. Figures 5 & 6 show that after the regeneration, the activity of catalyst and the degree of control over polymerization was similar to that of the fresh catalyst. This also reconfirms that the decrease in activity of the recycled catalyst was due to the presence of an increased level of Cu(II) species. The mechanism of the reactivation, that is, how the reaction between Cu(0) and tethered Cu(II) occurred, is still not clear.

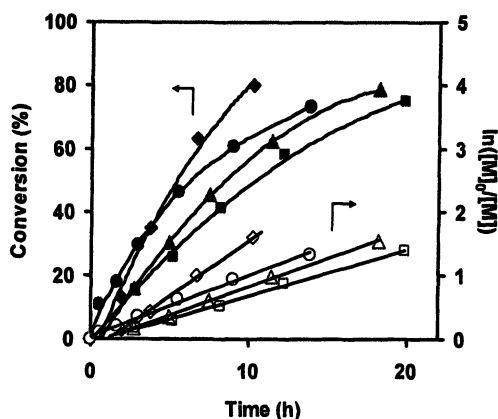


Figure 5. MMA polymerizations catalyzed by fresh, recycled and regenerated magnetic nanoparticles supported catalyst CuBr/MNP-TEDETA in toluene with the addition of 22 mol% Cu(II)Br₂. Experimental conditions: 70 °C, [MMA] = 2.35 mol/L, [22mol% CuBr₂+ 78mol% CuBr] = [Ligand] = [MBP] = 0.0235 mol/L; Fresh catalyst (◆, ◇); first-reused catalyst (▲, △), second-reused catalyst (■, □); regenerated catalyst with copper metal (●, ○)

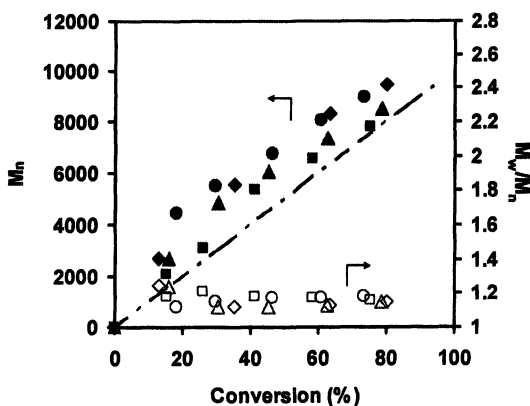


Figure 6. PMMA molecular weight and polydispersity as a function of conversion in the polymerizations catalyzed by fresh (\blacklozenge , \diamond), first re-used (\blacktriangle , \triangle), second-reused (\blacksquare , \square), and regenerated (\bullet , \circ) catalyst of CuBr/MNP-TEDETA. See Figure 5 for experimental conditions.

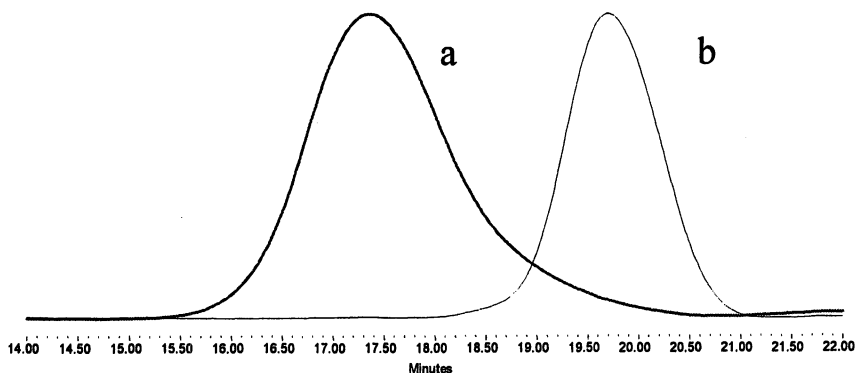


Figure 7. GPC traces of (a) PEG-*b*-PMMA block copolymer and (b) PEG macroinitiator. 70 °C, [MMA] = 2.35 mol/L, [Cu(I)Br] = 0.0183 mol/L, [Cu(II)Br₂] = 0.00520 mol/L, [Ligand] = [Ini-PEG] = 0.0235 mol/L.

Block copolymerization

The ability of the magnetic supported CuBr/MNP-TEDETA catalyst to mediate a block copolymerization was examined by conducting a block copolymerization of MMA using a PEG macroinitiator (Ini-PEG) under similar conditions to the homopolymerization reactions. A block copolymer of PEG-b-PMMA was isolated with 92.2% MMA conversion after 18 h polymerization. The resulting polymer had M_n of 16000 and polydispersity of 1.44 (Figure 7). This demonstrates that the magnetic nanoparticle supported catalyst is also good for block copolymerization.

Conclusions

We have demonstrated that a magnetic nanoparticle supported CuBr/MNP-TEDETA catalyst can effectively mediate a living polymerization of MMA forming polymers with a polydispersity less than 1.3. In the presence of 22 mol% of Cu(II)Br₂, the initiator efficiency could be increased to 0.85 and the polydispersity could be decreased to less than 1.2. The supported catalyst could be recycled and reused to conduct a second-run and a third-run with improved control over the polymerization but decreased activity. The activity of recycled catalyst could be regained by regenerating the supported catalyst with copper metal. The supported catalyst was also good for block copolymerization forming a PEG-b-PMMA. This work demonstrates that nanometer sized supports have minor effects on catalysis in terms of activity and control of polymerization.

Acknowledgement

We thank the University of Wyoming and the Government of State of Wyoming (EORI) for financial support. We also appreciate Dr. Steven Boese of University of Wyoming, Geology and Geophysics Department for ICP-MS analysis.

References

1. Matyjaszewski, K and Xia, J. *Chem. Rev.* **2001**, *101*, 2921-2990.
2. Kamigaito, M.; Ando, T.; Sawamoto, M. *Chem. Rev.* **2001**, *101*, 3689-3746.
3. Percec, V.; Popov, A. V.; Ramirez-Castillo, E.; Monteriro, M.; Barboiu, B.; Weichold, O.; Asandei, A. D.; Mitchell, C. M. *J. Am. Chem. Soc.* **2002**, *124*, 4940-4941.

4. Robinson, K. L.; Khan, M. A.; de Paz Banez, M. V.; Wang, X. S.; Armes, S. P. *Macromolecules* **2001**, *34*, 3155-3158.
5. Wang, X.-S.; Jackson, R. A.; Armes, S.P. *Macromolecules* **2000**, *33*, 255-257.
6. Save, M.; Weaver, J. V. M.; Armes, S. P.; MacKenna, P. *Macromolecules* **2002**, *35*, 1152-1159.
7. Zhang, X.; Matyjaszewski, K. *Macromolecules* **1999**, *32*, 1763-1766.
8. Kasko, A. M.; Heintz, A. M.; Pugh, C. *Macromolecules* **1998**, *31*, 256-271.
9. Boyes, S. G.; Brittain, W. J.; Wend, X. and Cheng, S. Z. D. *Macromolecules* **2002**, *35*, 4960-4967.
10. Tsarevsky, N. V.; Sarbu, T.; Gobelt, B.; Matyjaszeski, K. *Macromolecules* **2002**, *35*, 6142-6148.
11. Glauser, T.; Stancik, C. M.; Moller, M.; Voytek, S.; Gast, A. P.; Hedrick, J. L. *Macromolecules* **2002**, *35*, 5774-5781.
12. Costa, R. O. R.; Vasconcelos, W. L.; Tamaki, R.; Laine, R. M. *Macromolecules* **2001**, *34*, 5398-5407.
13. Wu, X.; Fraser, C. L. *Macromolecules* **2000**, *33*, 4053-4060.
14. Kim, J-B.; Huang, W.; Bruening, M. L.; Baker, G. L. *Macromolecules* **2002**, *35*, 5410-5416.
15. Borner, H. G.; Beers, K.; Matyjaszewski, K.; Sheiko, S. S.; Moller, M. *Macromolecules* **2001**, *34*, 4375-4383.
16. Zhao, B. *Polymer* **2003**, *44*, 4079-4083.
17. Chang, C.; Pugh, C. *Macromolecules* **2001**, *34*, 2027-2039.
18. Hedrick, J. L.; Trollsas, M.; Hawker, C. J.; Atthoff, B.; Claesson, H.; Heise, A.; Miller, R. D.; Mecerreys, D.; Jerome, R.; Dubois, P. *Macromolecules* **1998**, *31*, 8691-8705.
19. Heise, A.; Diamanti, S.; Hedrick, J. L.; Frank, C. W.; Miller, R. D. *Macromolecules* **2001**, *34*, 3798-3801.
20. Matyjaszewski, K.; Gaynor, S. G. *Macromolecules* **1997**, *30*, 7042-7049.
21. Matyjaszewski, K.; Gaynor, S. G.; Kulfan, A.; Podwika, M. *Macromolecules* **1997**, *30*, 5192-5194.
22. Shen, Y.; Tang, H.; Ding, S. *Prog. Polym. Sci.* **2004**, *29*, 1053-1078.
23. Matyjaszewski, K.; Pintauer, T.; Gaynor, S. *Macromolecules* **2000**, *33*, 1476-1478.
24. Heddleton, D. M.; Jackson, S. G.; Bon, S. A. F. *J. Am. Chem. Soc.* **2000**, *122*, 1542-1543.
25. Xia, J.; Johnson, T.; Gaynor, S. G.; Matyjaszewski, K.; DeSimone, J. *Macromolecules* **1999**, *32*, 4802-4805.
26. Carmichael, A. J.; Haddleton, D. M.; Bon, S. A. F.; Seddon, K. R. *Chem. Commun.* **2000**, 1237-1238.
27. Sarbu, T.; Matyjaszewski, K. *Macromol. Chem. Phys.* **2001**, *202*, 3379-3391.

28. Ding, S.; Radosz, M. and Shen, Y. *Macromolecules* **2005**, *38*, 5921-5928.
29. Haddleton, D. M.; Duncalf, D. J.; Kukulj, D.; Radigue, A. P. *Macromolecules* **1999**, *32*, 4769-4775.
30. Shen, Y.; Zhu, S.; Zeng, F. and Pelton, R. *Macromolecules* **2000**, *33*, 5427-5431.
31. Shen, Y.; Zhu, S.; Zeng, F. and Pelton, R. *Macromolecular Chemistry Physics* **2000**, *201*, 1387-1394.
32. Shen, Y.; Zhu, S. and Pelton, R. *Macromol. Rapid Commun.* **2000**, *21*, 956-959.
33. Shen, Y.; Zhu, S. and Pelton, R. *AICHE J.* **2002**, *48*, 2609-2619.
34. Kickelbick, G.; Paik, H.-j.; Matyjaszewski, K. *Macromolecules* **1999**, *32*, 2941-2947.
35. Haddleton, D. M.; Kukulj, D.; Radigue, A. P. *Chem. Commun.* **1999**, 99.
36. Shen, Y.; Zhu, S.; Zeng, F. and Pelton, R. *J. Polym. Sci. Part A: Polym. Chem.* **2001**, *39*, 1051-1059.
37. Shen, Y.; Zhu, S. and Pelton, R. *Macromolecules* **2001**, *34*, 5812-5818.
38. Honigfort, M. E.; Brittain, W. J. *Macromolecules* **2003**, *36*, 3111-3114.
39. Nguyen, J. V.; Jones, C. W. *Macromolecules* **2004**, *37*, 1190-1203.
40. Nguyen, J. V.; Jones, C. W. *J. Catalysis* **2005**, *232*, 276-294.
41. Hong, S. C. and Matyjaszewski, K. *Macromolecules* **2002**, *35*, 7592-7605.
42. Hong, S.C.; Neugebauer, D.; Inoue, Y.; Lutz, J.-F.; Matyjaszewski, K. *Macromolecules* **2003**, *36*, 27-35.
43. Duquesne, E.; Degee, Ph.; Habimana, J.; Dubois, Ph. *Chem. Commun.* **2004**, *6*, 640-641.
44. Liou, S.; Rademacher, J. T.; Malaba, D.; Pallack, M. E.; Brittain, W. J. *Macromolecules* **2000**, *33*, 4295-4296.
45. Shen, Y.; Zhu, S.; Pelton, R. *Macromolecules* **2001**, *34*, 3182-3185.
46. Shen, Y.; Zhu, S. *Macromolecules* **2001**, *34*, 8603-8609.
47. Barre, G.; Taton, D.; Lastecoueres, D.; Vincent, J.-M. *J. Am. Chem. Soc.* **2004**, *126*, 7764-7765.
48. Shen, Y.; Yang, J.; Ding, S.; Radosz, M. *Polym. Mater. Sci. Eng.* **2003**, *89*, 784-785.
49. Yang, J.; Ding, S.; Radosz, M.; Shen, Y. *Macromolecules* **2004**, *37*, 1728-1734.
50. Ding, S.; Yang, J.; Radosz, M.; Shen, Y. *J. Polym. Sci. Part A: Polym. Chem.* **2004**, *42*, 22-30.
51. Yoon, T.; Kim, J.; Lee, J. *Inorg. Chim. Acta* **2003**, *345*, 228-234.
52. Pan, B.; Gao, F.; Gu, H. *J. Colloid and Inter. Sci.* **2005**, *284*, 1-6.

Chapter 7

Loss in Activity and Catalyst Recyclability in Batch and Continuous Supported Atom Transfer Radical Polymerization

Santiago Faucher, Shiping Zhu*

Department of Chemical Engineering, McMaster University,
1280 Main Street West, Hamilton, Ontario, Canada L8S 4L7, Canada

Cu^IBr/HMTETA physically adsorbed to silica-gel is used in batch and continuous ATRP processes to study the loss in catalyst activity with catalyst reuse. The loss in catalyst activity cannot be attributed to an oxidation of the catalyst as the catalyst is found to be fully regenerated by an addition of fresh ligand. The primary location for catalytic activity is found to be in solution and it is the loss of these soluble species that account for the loss in activity. A partitioning equilibrium of the active catalyst species between the support's surface and the solution accounts for the recyclability of the catalyst and the differences in process performance.

Introduction

Atom transfer radical polymerization (ATRP) is one of the many recently discovered living free radical polymerization mechanisms that allows for the tailoring of macromolecules (1,2). The process is catalytic using a complexed metal salt, usually copper halides, to mediate the polymerization. Generally, high loadings of this catalyst are necessary to mediate the polymerization since the catalysts have low activities, as compared to olefin polymerizations. These high catalyst loadings contaminate the polymer product making purification necessary. While this is manageable in the laboratory, purification on a larger industrial scale makes this process less attractive.

Two approaches are taken to overcome this challenge. The first is to improve the catalyst's activity thereby allowing lower catalyst concentrations to

be used; ideally to a level at which post-purification becomes unnecessary. While some advances have been made in this area, further developments in catalyst systems are required to achieve high conversions, fast rates and good control of the polymerizations at even lower catalyst loadings (3,4). The second approach is to support the catalyst making it easily recoverable and recyclable. Soluble/recoverable, by-phasic and solid supported catalysts have been successful towards these ends but further reductions of residual catalyst concentrations in polymer are sought (5-23).

In this group of supported systems the solid supported catalysts are found to lose a large fraction of their activity with recycling (5-12). Two hypotheses are generally presented to account for this loss in activity. The most common being the oxidation of the metal center to its deactivating state (Cu^{II}), which causes a slowing of the polymerization (5-12). However where attempted, regeneration of the catalyst to its active form (Cu^{I}) has not yielded complete recovery of the catalyst's activity (8-10). The second and seldom proposed hypothesis is that the catalyst complex is lost with recycling (5-7). This is on account of the low residual metal concentrations in polymer, which are in the order of 1 to 10% of the initial metal loading (7-9,11-14,23). These catalyst losses are lower than the observed losses in catalyst activity (7-9,11,12). Thus neither hypothesis has yielded a satisfactory explanation for the loss in catalyst activity with recycling and most importantly no method of avoiding or mitigating the loss in catalyst activity has been devised.

In this work we study the loss in catalyst activity in one of the physically adsorbed yet highly recyclable catalyst systems that has been developed by our group ($\text{CuBr}/1,1,4,7,10,10\text{-Hexamethyltriethylenetetramine}$ physically adsorbed to silica gel) (6,15).

Experimental Section

Materials

MMA (Aldrich, 99.9%) is distilled under vacuum and stored at 4 °C before use. 1,1,4,7,10,10-Hexamethyltriethylenetetramine (HMTETA, 99%), $\text{Cu}^{\text{I}}\text{Br}$ (98%), and methyl α -bromophenylacetate (MBP, 97%, initiator) are used as received from Aldrich. Toluene is distilled from CaH_2 . Silica gel (100–200 mesh), chromatographic grade, Sargent-Welch Scientific Co. is boiled in deionized water for 5 hours, air-dried and then vacuum-dried.

Measurements

Conversions, number- and weight-average molecular weights (M_n and M_w , respectively), and copper concentrations are measured by ^1H NMR, gel permeation chromatography relative to narrow polystyrene standard and

inductively coupled plasma atomic emission spectroscopy (ICP-AES), respectively, as described elsewhere (23).

Batch Supported ATRP with Catalyst Recycling and Regeneration

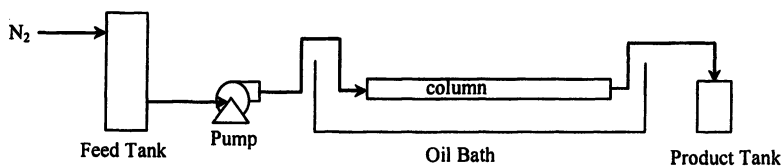
Polymerization: $\text{Cu}^{\text{I}}\text{Br}$ (64.5 mg, 0.45 mmol), and silica-gel (645 mg) are added to a Schlenk flask. The flask is degassed by five vacuum-nitrogen cycles. MMA (4.5 g, 45 mmol) and toluene (8.86 g) are added to the flask. The mixture is bubbled with nitrogen for 40 minutes with stirring. HMTETA (122.3 μL , 0.45 mmol) is added dropwise to the flask and bubbled with nitrogen for an additional 20 minutes. Degassed initiator, MBP (70.8 μL , 0.45 mmol), is then added dropwise to the flask. The flask is placed in an oil bath at 90°C and stirred by a magnetic bar. Kinetic samples, 0.3 ml, are withdrawn from the flask with a nitrogen-purged syringe. The samples are stored in hermetic vials and placed in a freezer for future assay.

Catalyst Recovery and Recycling: The catalyst is recovered for use in a second and later third polymerization using the following procedure. At the end of the polymerization the flask's contents are left to settle overnight. The supernatant is removed via syringe. The remaining catalyst solids are washed twice with 20 mL of toluene. Pre-purged toluene, MMA and MBP, in the quantities outlined above, are added to the flask containing the supported catalyst recovered. The flask is then placed in an oil bath preset at 90°C to run a subsequent polymerization. All described operations are completed under N_2 atmosphere.

Catalyst Regeneration: To the used and recovered catalyst, HMTETA (122.3 μL , 0.45 mmol) and toluene (8.86 g) are added. This mixture is left to stir for 15 minutes prior to the addition of MMA and initiator in the same quantities as outlined above for a subsequent polymerization.

Continuous Supported ATRP with Catalyst Regeneration

Process Description (see Scheme 1): A feed reservoir, blanketed by N_2 and cooled by dry ice, holds the monomer, initiator and solvent to be conveyed continuously by the pump to the column reactor via 1 mm stainless steel tubing. The column reactor is immersed in an oil bath preset at 90°C. The feed is activated by the supported catalyst in the column to undergo ATRP. The product polymer is collected at the column outlet. **Catalyst Preparation:** Silica gel (12 g) is weighted into a Schlenk flask and degassed by five vacuum-nitrogen cycles. Toluene (50 ml), $\text{Cu}^{\text{I}}\text{Br}$ (0.6 g) and HMTETA (0.958 g) are added to the flask under N_2 . The mixture is bubbled with N_2 for 10 min with stirring and then stirred for 3 hours. This catalyst is used to pack the column under N_2 ; approximately 7.1 g (dry) of the catalyst fills a stainless steel column 900 mm in length with an inner diameter of 4.5 mm.



Scheme 1

Polymerization: A typical polymerization is as follows: 100 ml Degassed MMA/MBP/toluene solution (MMA/toluene = 1/3 (w/w), [MMA]:[MBP] = 100:1) is added to the feed reservoir. The pump flow rate is set to 1.2 ml/hr. The feed reservoir is refilled as required. Kinetic samples of the polymerized solution are collected from the column product stream.

Catalyst Regeneration: HMTETA (1 ml, 1.5 molar equivalent of the fresh ligand in the column) is loaded into a nitrogen purged syringe and injected into the column feed line via a built-in injection loop.

Results

Copper Losses with Catalyst Recycling in Batch ATRPs

A batch polymerization using the catalyst $\text{Cu}^{\text{I}}\text{Br}/\text{HMTETA}$ physically adsorbed to silica gel is run. At the end of the polymerization stirring is stopped and the catalyst settles out of solution. The batch reactor is then removed from the oil bath and the supernatant solution siphoned off by a N_2 purged syringe. The solution is split into three N_2 purged vials (4 ml). The first vial is submitted directly for copper assay. The supernatant solutions in the second and third vials are submitted for copper assay following 24 and 90 hours respectively. Thus in these delayed assays, the catalyst has more time to settle out of the solution and is not detected in the supernatant solution. The catalyst remaining in the reaction flask is washed twice with 20 ml of toluene at room temperature and the washes are assayed for copper.

As seen in Table 1, the copper concentration decreases with increasing settling time. After 24 and 90 hours of settling, the supernatant solution contains 14% and 5%, respectively, of the total copper originally loaded. Washing the residual catalyst twice removes 2% of the total copper loaded. Thus under typical recycling conditions copper losses are in the range of 7 to 16%.

Loss and Regeneration of Catalyst Activity in Batch Supported ATRP

Three batch polymerizations are run. In the first polymerization fresh catalyst is used. At the end of the polymerization the catalyst is left to settle out

Table 1: Copper Lost with the Supernatant Solution as a Function of Settling Time and Catalyst Washes

| <i>Description</i> | <i>Copper in Solution</i> | | |
|-------------------------------------|-------------------------------------|--|--------------------------|
| | <i>Actual</i> [‡] (ppm) | <i>Theoretical</i> [‡] (ppm) | <i>% of Total Loaded</i> |
| Solution – end of pol. [*] | 469 | 2137 | 21.9 |
| Solution – 24 hours [*] | 298 | 2137 | 13.9 |
| Solution – 90 hours [†] | 109 | 2137 | 5.1 |
| 1st Catalyst Wash | 21 | NA | 1.2 |
| 2nd Catalyst Wash | 16 | NA | 1.1 |
| Total Cu Lost/Cycle | | | 7 to 16 |

Notes; ^{*}Allowed solids to settle briefly prior to siphoning off solution. ^{*}, [†] Left solution to settle 24 and 90 hours, respectively, under N₂ at room temperature prior to supernatant copper assay. [‡]Measured by ICP-AES. [‡]Assuming all Cu reports to solution.

of the solution overnight. The clear supernatant is then siphoned off. The remaining catalyst is washed twice with toluene and then re-used in a second polymerization. MMA, toluene and initiator (as in the first polymerization) are loaded to the flask along with the used catalyst and the flask placed in the oil bath to polymerize. At the end of this second polymerization, the catalyst is recovered, washed and recycled again as described above. In this third polymerization, however, fresh ligand is added to the flask. Figure 1 shows the conversion and molecular weight development profiles for the three runs.

A loss in catalyst activity occurs between the first and second polymerization (Figure 1). A comparison of the slopes of the first order rate plots ($\ln[M]_0/[M]$ vs. time) shows that the apparent rate constant (propagation rate constant \times radical concentration) for the recycled catalyst is 30% lower than that for the fresh catalyst. Thus given the similar reaction conditions, 30% of the catalyst's activity has been lost following the first recycle. Polymer molecular weights and distributions are well controlled and narrow in both polymerizations. Polydispersities range between 1.1 and 1.3. Molecular weights increase linearly with conversion as expected for this living polymerization.

The catalyst in the third polymerization (recovered from the second run + fresh ligand) shows the same activity as the fresh catalyst used, see Figure 1. The conversion profiles of the first and third run are practically identical with conversions reaching 94% in both runs. The development of the molecular weight and polydispersity are also similar as evidenced in Figure 1.

Loss and Regeneration of Catalyst Activity in Continuous ATRP

A column packed with Cu^IBr/HMTETA physically adsorbed to silica gel is placed in a bath at 90°C and continuously fed a solution containing MMA,

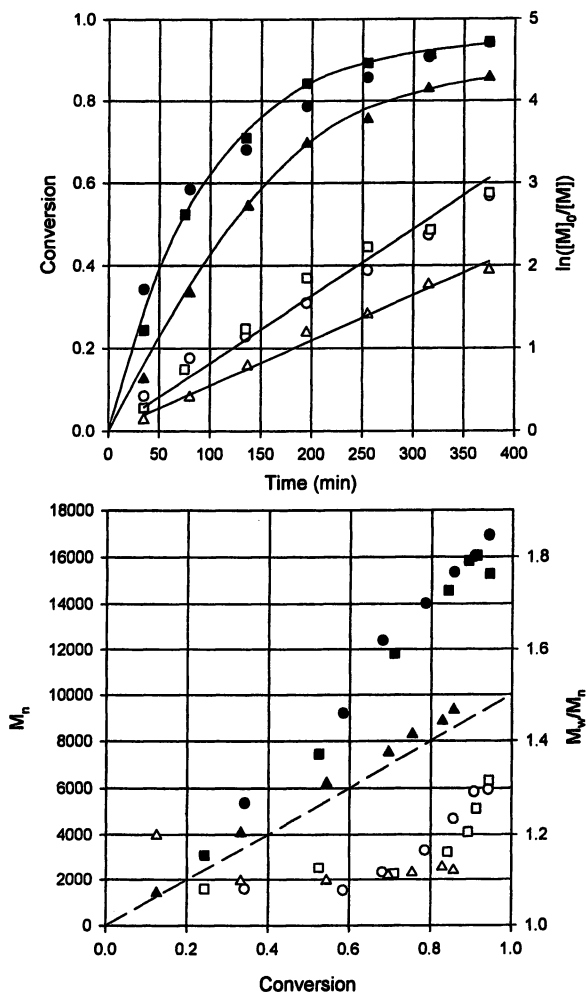


Figure 1: Monomer conversion, polymer molecular weights and distributions for three batch supported ATRPs: 90°C, [MMA]/[MBP]/[CuBr]/[HMTETA] = 100:1:1:1 (molar), toluene/MMA = 2 (w/w), and silica gel/CuBr = 10 (w/w). First run - fresh catalyst (●, ○), second run - catalyst from run 1 (▲, △), third run - catalyst from run 2 plus fresh ligand added (1 equiv to run 1) (■, □).

Toluene and MBP as shown in Scheme 1. This continuous reactor is operated over 3 weeks (500 hours). At the exit to the column, samples of the polymer containing solution are collected to follow the systems performance (Figure 2). Upon depletion of the catalyst's activity, following 240 hours, a single injection of fresh ligand is made to the column's feed line. No new Cu^IBr is added.

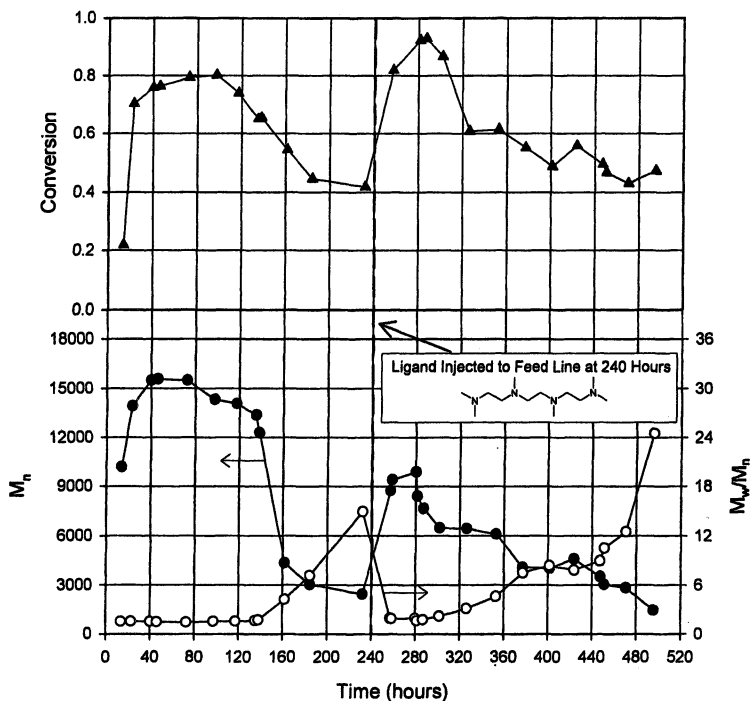


Figure 2: Monomer conversion, polymer molecular weight and molecular weight distribution of the continuous reactor product stream.

Monomer conversions reach 80% over the first 100 hours and then drop, as the catalyst loses activity, to plateau at 40%. Similarly, polymer molecular weights increase to 15,000 g/mol but later (140 hours) drop abruptly to 2500 g/mol. The trend in the polymer molecular weight distribution (M_w/M_n) has similar inflection points. For the first 120 hours of operation polydispersities range between 1.42 and 1.55. However, at 140 hours of operation they begin to rise sharply, eventually reaching values of 15 at 230 hours. The polymer produced in the first 140 hours displays the characteristics of a controlled living polymerization ($M_n \propto$ conversion, low M_w/M_n). In contrast, the polymer produced after 140 hours appears poorly controlled. The catalyst in the column is therefore no longer sufficiently active to mediate the ATRP equilibrium and an uncontrolled free radical polymerization ensues.

Following 240 hours of operation, the feed line to the spent catalyst column is injected with a single shot of fresh ligand through a built-in injection loop. Subsequently, monomer conversions, polymer molecular weights and distributions return to levels comparable to those prior to the depletion of the catalyst in the column ($t < 140$ hours). Conversions increase from 40% to 93%,

molecular weights increase from 2500 to 9900 g/mol and polydispersities decrease from 15 to 1.63. The catalyst is rejuvenated for a period of approximately 50 hours as compared to the column residence time of 8 hours. Following this, conversions, molecular weights and polydispersities return to levels observed under the spent catalyst conditions (40%, 1500 g/mol and 25 respectively). Thus an injection of fresh ligand reactivates the depleted catalyst in the column.

Performance Comparison of Catalyst in Continuous and Batch Reactors

Insight into the cause of the loss in catalyst activity can be gained by comparing the performance of the catalyst in the continuous and batch processes. Table 2 summarizes the key data. The catalyst in the continuous reactor is capable of producing 163 g of poly(methyl methacrylate) for every gram of copper used prior to becoming inactive. In contrast the catalyst used in the batch reactor produces (when recycled once) 284 g of poly(methyl methacrylate) for every gram of copper. In the batch case, the catalyst remains active and could be used to produce additional polymer.

Table 2: Catalyst Performance Comparison in Continuous and Batch Atom Transfer Radical Polymerizations

| Parameters | Reactor Type [†] | | | |
|--------------------------------------|---------------------------|---------------------|---------------------|--------------------|
| | Continuous [†] | Batch | | |
| | | 1 st Use | 2 nd Use | Total [‡] |
| Operating Time (hrs) | 136 | 6 | 6 | 12 |
| Polymer Produced (g) | 25.6 | 4.2 | 3.9 | 8.1 |
| Copper Used (g) | 0.157 [‡] | 0.0286 | From first. | 0.0286 |
| Polymer/Cu (wgt/wgt) [‡] | 163 | 147 | 137 | 284 |
| Used Catalyst Condition [‡] | Not Active | Active | Active | Active |

Notes: [‡]Data from Figures 1 and 2. [†]While polymerization is controlled. [‡]Polymer produced to copper used (weight ratio). [‡]Used catalyst in continuous process no longer mediates ATRP, catalyst in batch process does and could be reused further.

Split Filter Test

Batch supported ATRPs are undertaken. Partway through the polymerization the solution is filtered away from the supported catalyst and the filtrate placed in a second reaction flask (case 1) to polymerize further in order to gauge its catalytic activity. Similarly, in a second experiment (case 2) the filtrate is placed in a flask loaded with Cu^IBr. The filtered solutions' catalytic activities are compared to that of an unfiltered supported ATRP. Table 3 summarizes the results.

Conversion in the filtered solution (case 1) increased from 22 to 78% as compared to 26 to 94% for the control experiment (unfiltered). The apparent rate constants ($k_p \times [R\cdot]$) for the filtered solution is 50% of its unfiltered counterpart. Thus a large fraction of the catalytic activity is attributable to unsupported catalytic species. When the filtered solution is placed in contact with fresh $\text{Cu}^{\text{I}}\text{Br}$ (case 2), the catalyst activity of the filtrate increases and is comparable to that of the control experiment. Thus the presence of $\text{Cu}^{\text{I}}\text{Br}$ has an accelerating effect on the polymerization. Since $\text{Cu}^{\text{I}}\text{Br}$ does not promote polymerization of MMA in the absence of ligand, it must accelerate the system via a reduction of the soluble $\text{Cu}^{\text{II}}\text{Br}_2/\text{L}$ to $\text{Cu}^{\text{I}}\text{Br}/\text{L}$ (the activating catalyst).

Table 3: Kinetic Data for Solutions Filtered Away from the Supported Catalyst 30 minutes into the Polymerization and an Unfiltered Polymerization

| Rxn. Time (s) | Control Not Filtered ^{††} | | | Case 1 Filtered ^{††‡} | | | Case 2 Filt. ^{†‡} + CuBr^{F} |
|---------------|------------------------------------|-------|-----------|--------------------------------|-------|-----------|---|
| | Conv. | M_n | M_w/M_n | Conv. | M_n | M_w/M_n | Conv. |
| 30 | 26 | 3180 | 1.08 | 22 | 3250 | 1.10 | 19 |
| 60 | 43 | 4800 | 1.07 | 27 | 4110 | 1.07 | 49 |
| 90 | 59 | 6400 | 1.08 | 35 | 5020 | 1.06 | 57 |
| 135 | 73 | 8170 | 1.11 | 47 | 6440 | 1.07 | 64 |
| 195 | 85 | 9890 | 1.16 | 61 | 7960 | 1.08 | 71 |
| 255 | 90 | 10850 | 1.22 | 70 | 9200 | 1.09 | 71 |
| 315 | 94 | 11220 | 1.27 | 74 | 10200 | 1.11 | |
| 375 | 93 | 11530 | 1.29 | 78 | 11030 | 1.11 | |

Notes: [†]Data from reference 24. [‡]Reaction conditions: toluene/methyl methacrylate = 2 (w/w), [MMA]:[Initiator]:[$\text{Cu}^{\text{I}}\text{Br}$]:[HMTETA] = 100:1:1:1 (molar), silica gel/ $\text{Cu}^{\text{I}}\text{Br}$ = 5 (w/w), 90°C. [§]Filtered at 30 minutes of polymerization time through a 0.2 μm PTFE filter into another schlenk flask under N_2 atmosphere immersed in a 90°C oil bath. [¶]In the new reaction flask 0.45 mmol of $\text{Cu}^{\text{I}}\text{Br}$ was added (1 equivalent to $\text{Cu}^{\text{I}}\text{Br}$ prior to filtration).

Effect of Silica Gel Loading

ATRP of MMA are run with varying silica gel concentrations while all other reaction parameters are kept constant (Figure 3). At or below silica gel concentrations of 60 g/L the polymerization kinetics are comparable. At higher loadings the polymerization rates decrease. At concentrations of 130 and 170 g/L, polymerization rates are 50% and 35%, respectively, of those at the lower

concentrations. Molecular weight developments as a function of conversion for the varying silica gel loadings (not shown) are comparable indicating similar initiator efficiencies. Molecular weight distributions are generally below 1.4.

Discussion

In the literature, the main causes to which the loss in surface supported catalyst activity are attributed are the catalyst's oxidation and a loss of catalyst (5-12). For the catalyst studied here, however, the data does not support the oxidation hypothesis since the catalyst can be regenerated with an addition of fresh ligand (Figures 1 and 2). Further evidence of this lack of oxidation is found through visual observation of the spent catalyst in the continuous process which retains its blue un-oxidized colour. We therefore focus on the second hypothesis, a loss of catalyst, to explain the loss in activity.

The measured copper losses (7 to 16%, Table 1) are significantly lower than the activity lost with recycling (30%, Figure 1). This is a first indication that the lost catalyst species contribute disproportionately more to the system's activity than the catalyst retained by the silica gel. This is demonstrated more directly by the split-filter tests and the deteriorated performance of the continuous

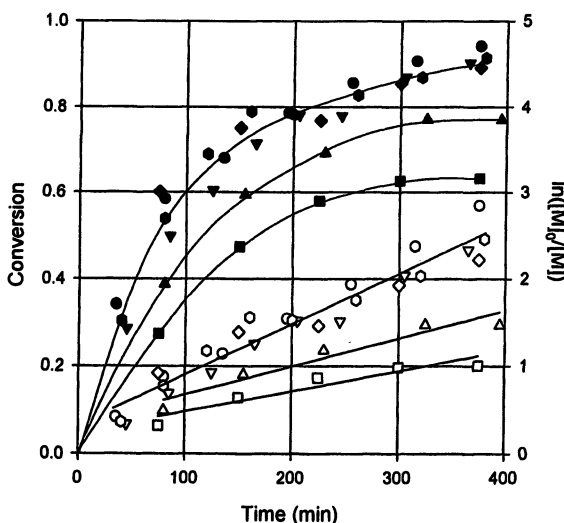


Figure 3: Effect of silica-gel loading on the kinetics of batch supported ATRPs of MMA using Si-gel/CuBr/HMTETA as catalyst. Conversion (filled in symbols) and first order rate plot (clear symbols) are shown. Silica gel concentrations (g/L): 0 (▼, ▽), 22 (●, ○), 40 (●, ○), 60 (◆, ◇), 130 (▲, △), and 170 (■, □). All other reaction conditions as per Figure 1.

reactor following 140 hours. The split-filter tests show that a small amount of *soluble* (in contrast to *adsorbed*) catalyst species account for more than 50% of the total catalytic activity (Table 3) (24). Similarly, in the continuous process the higher conversions achieved prior to 140 hours show that the catalyst species lost have high activity (Figure 2). The simultaneous loss in the control of polydispersity at 140 hours also demonstrates that the lost catalyst species are necessary to mediate the ATRP equilibrium and that the retained catalyst is incapable of accomplishing this. The ability of the supported catalyst species to mediate the faster deactivation mechanism is questionable given diffusion constraints (9). Thus the loss of catalyst activity and control of polydispersity results from a loss of the *soluble* catalyst species.

The regeneration of the system's activity with ligand addition (Figures 1 and 2) shows that $\text{Cu}^{\text{I}}\text{Br}$ is not the limiting reagent (lost or oxidized) but rather that the ligand is. It is not clear why this occurs. An adsorption of uncomplexed ligand and/or ill defined metal-ligand complexes to the support's surface (25) may account for this. Once fresh ligand is added, however, new *soluble* complexes form from non or partly complexed $\text{Cu}^{\text{I}}\text{Br}$ on the silica gel surface thereby completely regenerating the catalytic activity (Figures 1 and 2).

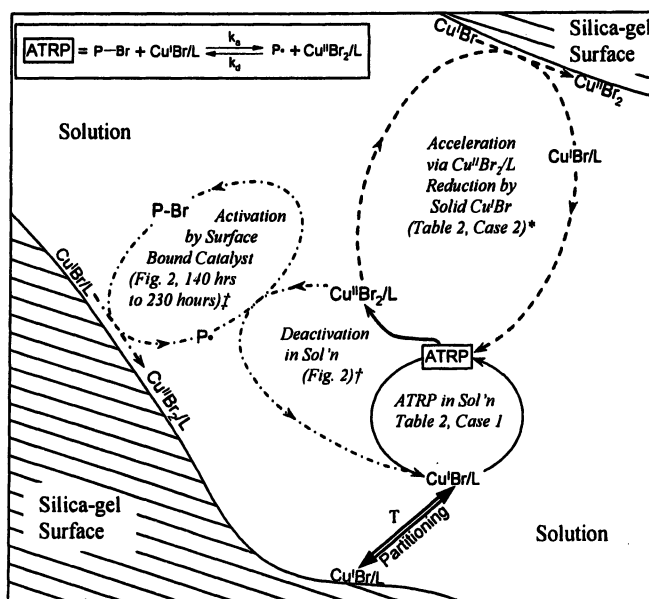
The recyclability of the catalyst is explained by a reversible partitioning equilibrium between the silica gel and solution that is temperature dependent. Thus in batch reactions when the system is heated the catalyst desorbs into solution where it mediates the process. At the end of the polymerization a fraction of this catalyst readsorbs to the support's surface, the rest is lost with the product accounting for the loss in catalyst activity upon recycling.

This explains the lower catalyst activity retention in the continuous process. Here, the desorbed catalyst remains in solution and exits the reactor with the product as a result of the constant reaction temperatures (90°C). In the batch reactor, the cooler (25°C) catalyst recovery temperatures allow a larger fraction of the desorbed catalyst to be readsorbed by the support. More direct evidence of a partitioning equilibrium is presented in Figure 3. Here reaction rates are found to decrease with increasing silica gel concentration. This indicates that the surface area has an impact on the concentration of *soluble* catalyst species, which is consistent with the partitioning theory.

Scheme 2 summarizes the demonstrated ATRP mechanisms for the system studied here. This mechanism is inspired by the work of Matyjaszewski who developed a shuttle bus system to overcome diffusion limited deactivation in supported ATRPs (9). There are some key differences, however, between the shuttle bus system and that which we present here for $\text{Cu}^{\text{I}}\text{Br}/\text{HMTETA}/\text{Si-gel}$. First, the *soluble* catalyst species result from desorption of catalyst from the surface. Second, the *soluble* catalyst accounts for the majority of the catalysis and activation by the surface is a minor component. Third, an acceleration mechanism via reduction of *soluble* $\text{Cu}^{\text{II}}\text{Br}_2/\text{L}$ to $\text{Cu}^{\text{I}}\text{Br}/\text{L}$ by solid $\text{Cu}^{\text{I}}\text{Br}$ is demonstrated.

Conclusions

The loss in catalyst activity with recycling using $\text{Cu}^{\text{I}}\text{Br}/\text{HMTETA}$ physically adsorbed to silica gel does not result from oxidation of the catalyst. The catalyst is found to retain its rich blue unoxidized colour in the continuous process and the catalyst's activity can be regenerated by an addition of fresh ligand. Rather, the loss in catalyst activity results from the loss of a small quantity of *soluble* catalyst species that partition between the support's surface and the solution where they are active. The *soluble* catalyst accounts for a large fraction of the system's catalytic activity (+50%) and is essential for mediating the ATRP equilibrium. The catalyst adsorbed to the surface is incapable of mediating this equilibrium. A mechanism, depicted in Scheme 2, is presented to summarize the observed phenomena.



Scheme 2: Demonstrated Mechanism of ATRP using $\text{Cu}^{\text{I}}\text{Br}/\text{HMTETA}$ Adsorbed to Silica-gel as Catalyst. Notes: Abbreviations are ligand (L), temperature sensitive (T), dormant polymer chain (P-Br), activation and deactivation rate constants (k_a , k_d); ‡spent catalyst activates but does not mediate ATRP; †deactivation via soluble catalyst; *uncomplexed $\text{Cu}^{\text{I}}\text{Br}$ does not on its own promote ATRP; propagation not shown for clarity.

References

1. Wang, J-S.; Matyjaszewski, K. *J. Am. Chem. Soc.* **1995**, *117* (20), 5614.
2. Kato, M.; Kamigaito, M.; Sawamoto, M.; Higashimura, T. *Macromolecules* **1995**, *28* (5), 1721.
3. Queffelec, J.; Gaynor, S.G.; Matyjaszewski, K. *Macromolecules* **2000**, *33*, 8629.
4. Faucher, S.; Zhu, S. *Ind. Eng. Chem. Res.* **2005**, *44*, 677.
5. Haddleton, D.M.; Kukulj, D.; Radigue, A.P. *Chem. Commun.* **1999**, 99.
6. Shen, Y.; Zhu, S.; Zeng, F.; Pelton, R.H. *Macromolecules* **2000**, *33*, 5427.
7. Haddleton, D.M.; Duncalf, D.J.; Kukulj, D.; Radigue, A.P. *Macromolecules* **1999**, *32*, 4769.
8. Nguyen, J.V.; Jones, C.W. *J. Cat.* **2005**, *232*, 276.
9. Hong, S.C.; Matyjaszewski, K. *Macromolecules* **2002**, *35*, 7592
10. Shen, Y.; Zhu, S.; Zeng, F.; Pelton, R. *J. of Polymer Science: Part A: Polym. Chem.* **2001**, *39*, 1051.
11. Ding, S.; Yang, J.; Radosz, M.; Shen, Y. *J. Pol. Sci. Part A: Pol. Chem.* **2004**, *42*, 22.
12. Honigfort, M.E.; Brittain, W.J. *Macromolecules* **2003**, *36*, 3111-3114.
13. Kickelbick, G.; Paik, H-J.; Matyjaszewski, K. *Macromolecules* **1999**, *32*, 2941.
14. Duquesne, E.; Degée, Ph.; Habimana, J.; Dubois, Ph. *Chem. Commun.* **2004**, 640.
15. Shen, Y.; Zhu, S.; Pelton, R. *Macromol. Rapid Commun.* **2000**, *21*, 956.
16. Haddleton, D.M.; Jackson, S.G.; Bon, S.A.F. *J. Am. Chem. Soc.* **2000**, *122*, 1542.
17. Barré, G.; Taton, D.; Lastécouères, D.; Vincent, J-M. *J. Am. Chem. Soc.* **2004**, *126*, 7764.
18. Shen, Y.; Zhu, S. *Macromolecules*, **2001**, *34*, 8603.
19. Liou, S.; Rademacher, J.T.; Malaba, D.; Pallack, M.E.; Brittain, W.J. *Macromolecules* **2000**, *33*, 4295.
20. Kumar, K.R.; Kizhakkedathu, J.N.; Brooks, D.E. *Macromol. Chem. Phys.* **2004**, *205*, 567.
21. Kotre, T.; Nuyken, O.; Weberskirch, R. *Macromol. Chem. Phys.* **2004**, *205*, 1187.
22. Honigfort, M.E.; Brittain, W.J.; Bosanac, T.; Wilcox, C.S. *Macromolecules* **2002**, *35*, 4849.
23. Faucher, S.; Zhu, S. *Macromolecules* **2006**, *39*, 3.
24. Faucher, S.; Zhu, S. *Macromol. Rapid. Com.* **2004**, *25*, 991.
25. Nguyen, J.V.; Jones, C.W. *J. of Polymer Science: Part A: Polym. Chem.* **2004**, *42*, 1367.

Chapter 8

Alkylated Linear Amine Ligands for Homogeneous Atom Transfer Radical Polymerization

Metin H. Acar, C. Remzi Becer, H. Alper Ondur,
and Şebnem İnceoğlu

Chemistry Department, Istanbul Technical University, Maslak,
34469 Istanbul, Turkey

The ligand has an important role in atom transfer radical polymerization (ATRP) due to its complexation with the metal salt. The structure of the ligand strongly affects the catalyst activity and the control of the polymerization. Solubility of the ligand and its metal complexes in organic media is of particular importance to attain homogeneous polymerization conditions in ATRP. The rate of polymerization is also affected by the relative solubilities of the activating and the deactivating species of the catalyst. A series of alkylated linear amine ligands were synthesized in a simple and versatile reaction and their effect was investigated in copper-mediated ATRP. They show a homogeneous and relatively fast polymerization reaction compared to most other ATRP ligands

Introduction

In the past decade, controlled radical polymerization has rapidly developed. Since it was first reported by independent groups in 1995 (1-4), metal-mediated radical polymerization, more generally known as atom transfer radical polymerization (ATRP) has been one of the most efficient and versatile controlled/living radical polymerization methods to control the structure, chain length, distribution and chain end functionality of polymers. This technique can also be used to obtain linear polymers and copolymers with different topologies (5-10) as well as low polydispersities.

Transition metal catalysts are the key to ATRP since they determine the position of the atom transfer equilibrium and the dynamics of exchange between the dormant and active species. The main effect of the ligand is to solubilize the transition-metal salt in organic media and to regulate the proper reactivity and dynamic halogen exchange between the metal center and the dormant species or persistent radical. Ligands, typically amines or phosphines, are used to increase the solubility of the complex transition metal salts in the solution and to tune the reactivity of the metal towards halogen abstraction. So far, a range of multidentate neutral nitrogen ligands have been developed as active and efficient complexing agents for copper-mediated ATRP (10). Tridentate (11-15) and tetradentate (16-22) aliphatic amine ligands generally provide faster polymerizations than bidentate ligands, while monodentate nitrogen ligands yield redox-initiated free radical polymerization. In addition, ligands with an ethylene linkage between the nitrogens are more efficient than those with a propylene or butylene linkage (23). The nitrogen ligands that have been used in Cu-based ATRP are summarized in Table I.

Linear amines with ethylene linkage such as tetramethylethylenediamine (TMEDA), 1,1,4,7,7-pentamethyldiethylenetriamine (PMDETA), and 1,1,4,7,10,10-hexamethyltriethylenetetramine (HMTETA) were synthesized and first examined for ATRP as ligands in Matyjaszewski's group (11). They stated the reasons for examining these types of ligands; *i*) they are less expensive, *ii*) due to the absence of the extensive π -bonding in the simple amines, the subsequent copper complexes are less colored, and *iii*) since the coordination complexes between copper and simple amines tend to have lower redox potentials than the copper-bipy complex, the employment of simple amines as the ligand in ATRP may lead to faster polymerization rates.

Solubility of the ligand and its metal complexes in organic media is of particular importance to attain homogeneous polymerization conditions. The rate of polymerization is also affected by the relative solubilities of the activating and the deactivating species of the catalyst. In heterogeneous systems, a low stationary concentration of the catalyst species allows for a controlled polymerization, but the polymerization is much slower than in homogeneous systems (23). A ligand with a long aliphatic chain on the nitrogen atoms forms metal complexes of greater solubility in organic solvents. The increasing length of the alkyl substituents, on the other hand, induces steric effects and can alter the redox potential of the metal center. Any shift in the redox potential affects the electron transfer and the activation-deactivation equilibrium (12). The most common amine ligands used in Cu-based ATRP are summarized in Table I.

In this study, in order to demonstrate the effect of homogeneity, we continued (21) to synthesize a series of ligands by the Hoffmann reaction of diethylenetriamine, triethylenetetramine and poly(ethylene imine) with linear alkylbromides of different chain lengths (C_2H_5- , C_4H_9- , $C_6H_{13}-$). Alkylated

Table I. Commonly Used Amine Ligands for Cu-Based ATRP

| <i>Amine Structure</i> | <i>Alkyl lenght</i> | <i>Condition</i> | <i>Ref</i> |
|------------------------------------|---------------------|------------------|------------------|
| Aliphatic Linear | Short | heterogeneous | 11-12,22 |
| | Long | homogeneous | 13-15, 21, 26-27 |
| Aliphatic Branched | Short | homogeneous | 16, 28-30 |
| | Long | homogeneous | 31-34 |
| Diazabutadiene derivatives | Short | heterogeneous | 35 |
| | Long | heterogeneous | 35 |
| Substituted Bipyridine | Short | heterogeneous | 1, 4, 36-39 |
| | Long | homogeneous | 40-41 |
| Substituted Terpyridine | Short | heterogeneous | 42 |
| | Long | homogeneous | 42 |
| Substituted pyridylmethanimine | Short | heterogeneous | 43-44 |
| | Long | homogeneous | 45-47 |
| Subs. & Unsubs. phenantroline | Short | heterogeneous | 48 |
| | Long | - | - |
| Substituted pyridine carboximidate | Short | heterogeneous | 49 |
| | Long | homogeneous | 49 |

linear amine ligands (ALALs) were selected because of low cost and robust and versatile synthetic methods. After the synthesis, the alkylated tri-, tetra- and multidentate nitrogen ligands were used in the ATRP of methyl methacrylate (MMA) and styrene (S) in the presence of CuBr co-catalyst and suitable initiators. All of these ligands provide well defined polymeric structures of low polydispersities due to the homogeneity of the reaction media.

Experimental

Materials

Diethylenetriamine (DETA, 99 %), triethylenetetramine (TETA, 60 %), Polyimine ($M_n=423$ g/mol), 1-bromobutane (99%), 1-bromohexane (98 %), Copper(I) bromide (CuBr, 99.99 %), potassium carbonate (99+ %), 1,1,4,7,7-pentamethyl diethylenetriamine (PMDETA, 99 %), bipyridine (BPy), and dinonyl bipyridine (dNBpy, 97 %) were purchased from Aldrich Chemical Co.

Methyl methacrylate (MMA, Across 99 %), styrene (S, 99 %), bromoethane (98 %), ethyl-2-bromo isobutyrate (EBiB, used for MMA, 98 %), ethyl-2-bromo propionate (EBP, used for S, 99 %) were purchased from Acros Organics Co. Ethanol (99.5 %) and anhydrous sodium sulphate (99 %) were purchased from J. T. Baker Co. All reagents were used without further purification. Tris(2-(dimethylamino)ethyl)amine (Me₆TREN) was synthesized according to the literature (28-30).

Instrumentation

¹H NMR spectra of the ligands were collected with a Bruker 200 MHz NMR instrument using CDCl₃ as the solvent. Monomer conversion was determined using an ATI Unicam gas chromatograph equipped with a FID detector and a J&W scientific 15 m DB WAX widebore capillary column. Molecular weights and molecular weight distributions of the polymers were measured on a GPC system consisting of a Agilent 1100 series pump, four Waters Styragel HR columns (5E, 4E, 3, 2) and a Agilent 1100 RI detector, with a THF flow rate of 0.3 mL/min; poly(methyl methacrylate) and polystyrene were used as standards.

Synthesis of Alkylated Linear Amine Ligands, (ALALs)

ALALs that are derivatives of tridentate, tetradentate and multidentate linear amines: 1,1,4,7,7-pentaethyldiethylene (PEDETA), 1,1,4,7,7-pentabutyl diethylenetriamine (PBDETA), 1,1,4,7,7-pentahexyldiethylenetriamine (PHDETA), 1,1,4,7,10,10-hexaethyltriethylenetetramine (HETETA), 1,1,4,7,10,10-hexabutyltriethylenetetramine (HBTETA), 1,1,4,7,10,10-hexahexyltriethylenetetramine (HHTETA), and ethyl substituted polyimine (EPI) were synthesized according to a procedure in our previous report (21).

The synthesis of PEDETA is given as a representative procedure: Ethyl bromide (0.255 mol) solution in ethanol (100 ml) was added dropwise to DETA (0.05 mol). The mixture was stirred for two hours at 15 °C, followed by the addition of potassium carbonate (0.4 mol). The mixture was stirred for 3 days and after replenishing the potassium carbonate (0.4 mol), stirring was continued for 3 more days. The organic phase, separated by adding ~300 ml of distilled water and 100 ml of ethyl acetate, was dried over sodium sulphate overnight. After the filtration, the ethyl acetate was evaporated on a rotary evaporator. Dry THF (80 ml) was added and the solution was passed through a column filled with neutral alumina. Evaporation of the solvent and distillation yielded a yellowish oily product, yield 9.6 g (78.8 %). ¹H NMR (200 MHz, CDCl₃): δ 0.9-1.0 (m. 18 H), 2.44 (t. 15 H).

Polymerization

A typical ATRP procedure was performed as follows. The catalyst, CuBr was placed in a 48-ml flask which contained a side arm with a Teflon valve sealed with a Teflon stopper. The flask was deoxygenated by vacuum-thaw-nitrogen cycles. MMA (6.09 mol.l^{-1}) or S (7.91 mol.l^{-1}), anisole, and ligand were added to the flask. Finally, an appropriate initiator was added and the flask was placed in a thermostatically controlled oil bath. All liquid components were sparged with nitrogen prior to transferring them into the flask. A monomer/initiator/catalyst/ligands ratio of 200/1/1/1 was used for both MMA and S polymerizations. Samples were taken periodically via a syringe to follow the kinetics of the polymerization process. The samples were diluted with THF and methanol was added. Gas chromatography (GC) and gel permeation chromatography (GPC) measurements were carried out.

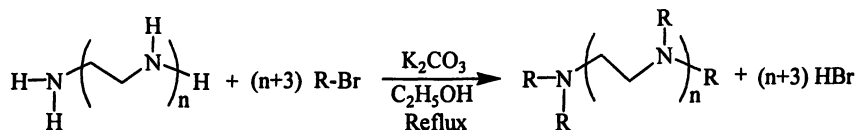
Results and Discussion

Ligand Synthesis

The synthesis of the ligands is depicted in Scheme 1. The yields and structures were shown in Table II. The ^1H NMR spectrum of PEDETA as a representative ligand is shown in Figure 1. PEDETA has two different types of hydrogen atoms, which are attached to the terminal carbon atom of the alkyl substituents (marked as "a") and the others are attached to the carbon atom adjacent to the nitrogen (marked as "b"). The ratio of the integral values of these hydrogen atoms was found identical to the theoretical ratio (15/18, a/b). Gas chromatographic analysis showed no trace of 1-bromohexane residues in the product. The purity of the product can also be verified by the absence of a residual NH signal at 3.45 ppm in the ^1H NMR spectrum.

After investigation of conditions such as ligand and catalyst ratio, the $[\text{Monomer}]_0/[\text{Initiator}]_0/[\text{Catalyst}]_0/[\text{Ligand}]_0=200/1/1/1$ ratio was applied in the ATRP of MMA and S. All the ALALs that were used in the ATRP of MMA and S gave homogeneous polymerization media.

Representative semi-logarithmic kinetic plots of MMA and S polymerizations using PEDETA as a ligand show linear relationships (Figure 2).



n: 2, 3, 9

R: C_2H_5 -, C_4H_9 -, C_6H_{13} -

Scheme 1. Synthesis of alkylated linear amine ligands

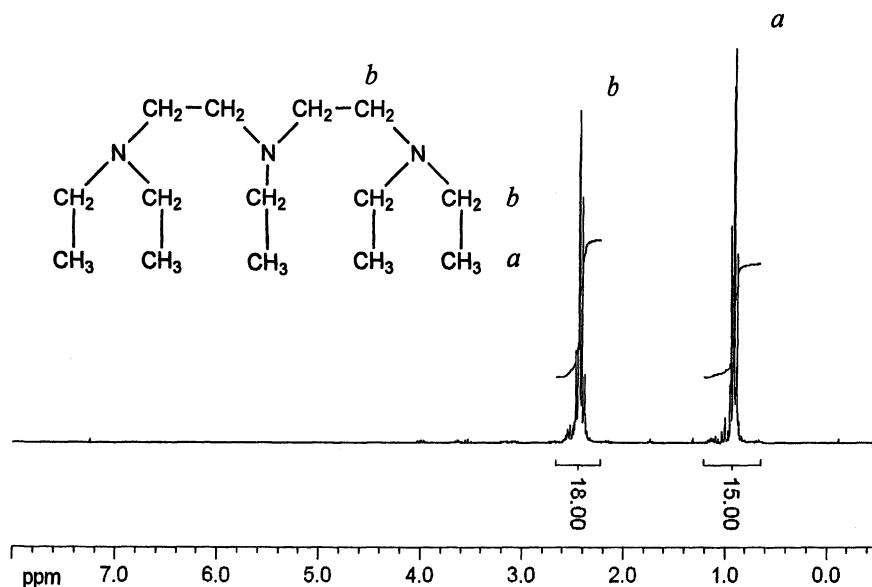


Figure 1. ^1H NMR spectrum of PEDETA in CDCl_3

This indicates that the kinetics are first order with respect to the monomer concentration in the polymerization and that the concentration of the active centers is constant during the polymerization. It also shows that termination is absent or negligible. The linearity of the molecular weight versus conversion plots suggests that chain transfer is also absent or negligible (Figure 3). The low M_w/M_n values support the observed controlled radical polymerization behavior.

In order to compare the effect of ALALs with well known ATRP ligands, two sets of ATRPs of MMA and S were carried out under the same experimental conditions and the results are shown in Table III and Table IV, respectively. All of the kinetic curves of these ligands show linearity, except some deviation for dNbpy and $M_6\text{Tren}$. The initiator efficiency (calculated from last kinetic data) is low in MMA polymerization, which is a commonly observed. The polydispersities of PMMA and PS are relatively narrow, as low as 1.05. The k_p^{app} is as high as $3.3 \times 10^{-4} \text{ s}^{-1}$ for PMMA and $8.7 \times 10^{-3} \text{ s}^{-1}$ for S in the presence of PEDETA as ligand.

In these ATRP reactions of MMA and S, homogeneity was achieved by using PEDETA, PBDETA, PHDETA, HETETA, HBTETA, HHTETA, EPI, $\text{ME}_6\text{-Tren}$ and dNbpy ligands. PEDETA has the highest k_p^{app} for MMA and HETETA has the highest k_p^{app} for S among the examined ligands. The apparent rate constant, k_p^{app} , decreases by increasing the alkyl chain length of the monomer or both the linear tridentate and tetradentate amine ligands.

Table II: Structure of the alkylated linear amine ligands

| <i>Entry</i> | <i>Ligands</i> | <i>Structure</i> |
|--------------|----------------|------------------|
| 1 | PEDETA | |
| 2 | PBDETA | |
| 3 | PHDETA | |
| 4 | HETETA | |
| 5 | HBTETA | |
| 6 | HHTETA | |
| 7 | EPI | |

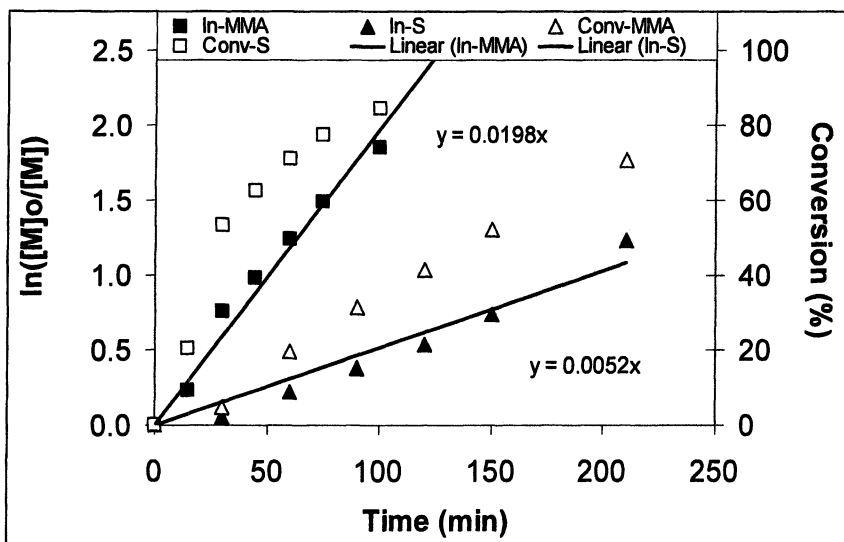


Figure 2. Kinetic plots of MMA and S polymerizations using PEDETA as a ligand. [MMA]: 6.09 mol.l^{-1} in anisole at 80°C ; [S]: 7.91 mol.l^{-1} in anisole at 110°C ; $[\text{Monomer}]_0/[\text{Initiator}]_0/[\text{CuBr}]_0/[\text{PEDETA}]_0 = 200/1/1/1$

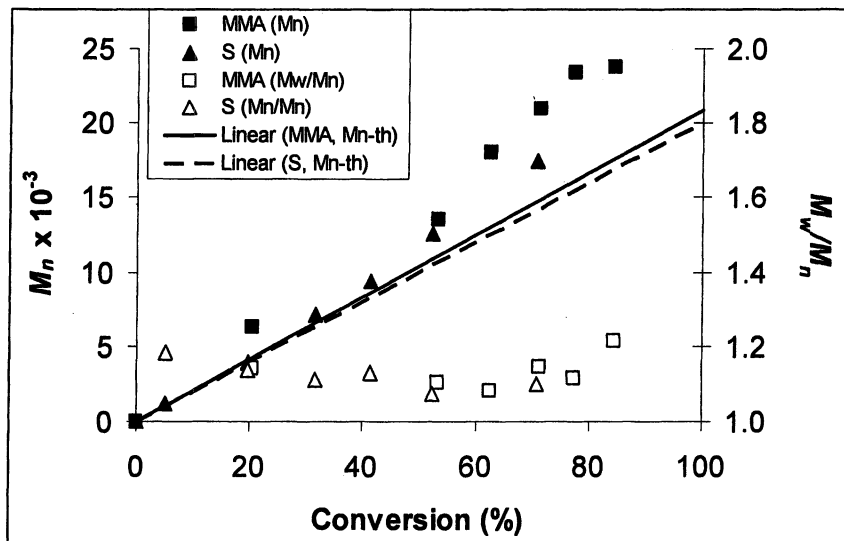


Figure 3. M_n versus conversion plots of MMA and S polymerizations using PEDETA as a ligand. [MMA]: 6.09 mol.l^{-1} in anisole at 80°C ; [S]: 7.91 mol.l^{-1} in anisole at 110°C ; $[\text{Monomer}]_0/[\text{Initiator}]_0/[\text{CuBr}]_0/[\text{PETETA}]_0 = 200/1/1/1$

Table III: ATRP of MMA Using Different Amine Ligands

| Entry | Ligand | Time (min) | Conversion ^c (%) | M_n , th ^c | M_n , ^c | M_w/M_n | k_p ^{app} ($10^{-4} \cdot s^{-1}$) | Ini eff. (β) |
|-------|------------------------------------|------------|-----------------------------|-------------------------|----------------------|-----------|---|----------------------|
| 1 | PEDETA ^a | 100 | 84 | 16800 | 23700 | 1.21 | 3.30 | 0.71 |
| 2 | PBDETA ^a | 100 | 82 | 16400 | 21400 | 1.15 | 2.85 | 0.72 |
| 3 | PHDETA ^a | 100 | 85 | 17000 | 23600 | 1.11 | 2.75 | 0.74 |
| 4 | HETETA ^a | 100 | 82 | 16400 | 22100 | 1.19 | 2.63 | 0.74 |
| 5 | HBTEA ^a | 100 | 79 | 16800 | 22500 | 1.24 | 2.42 | 0.75 |
| 6 | HHTETA ^a | 100 | 76 | 16200 | 23800 | 1.10 | 2.17 | 0.68 |
| 7 | HHTETA ^b | 120 | 65 | 19500 | 23000 | 1.15 | 1.10 | 0.85 |
| 8 | DiNBpy ^a | 360 | 51 | 10200 | 9900 | 1.20 | 0.42 | 1.00 |
| 9 | ME ₆ -Tren ^a | 150 | 67 | 13400 | 27000 | 1.59 | 1.27 | 0.49 |
| 10 | PMDETA ^a | 100 | 71 | 14200 | 24000 | 1.11 | 2.30 | 0.60 |
| 11 | BPy ^a | 150 | 73 | 14600 | 16800 | 1.33 | 1.88 | 0.87 |
| 12 | EPI ^a | 120 | 68 | 13600 | 24400 | 1.28 | 1.60 | 0.56 |

a) [MMA]: 6.09 mol.l⁻¹ in anisole at 80 °C; [MMA]₀/[EBiB]₀/[CuBr]₀/[Ligand]₀ = 200/1/1/1.

b) [MMA]: 9.36 mol.l⁻¹ 75 °C; [MMA]₀/[EiBr]₀/[CuBr]₀/[Ligand]₀ = 300/1/1/1, Ref. 21.

c) Last point of the kinetic data.

Table IV: ATRP of S Using Different Amine Ligands

| Entry | Ligand | Time (min) | Conversion ^c (%) | $M_{n,th}^c$ | M_n^c | M_w/M_n | k_p^{app} ($10^4 \cdot s^{-1}$) | Ini eff. (θ) |
|-------|-----------------------------------|------------|-----------------------------|--------------|---------|-----------|-------------------------------------|-----------------------|
| 1 | PEDETA ^a | 210 | 71 | 14800 | 17500 | 1.10 | 0.87 | 0.81 |
| 2 | PBDETA ^a | 210 | 53 | 11050 | 11500 | 1.20 | 0.58 | 0.96 |
| 3 | PHDETA ^a | 210 | 50 | 10400 | 14300 | 1.07 | 0.52 | 0.73 |
| 4 | HETEТА ^a | 210 | 83 | 17300 | 19300 | 1.17 | 1.15 | 0.90 |
| 5 | HBTEТА ^a | 210 | 73 | 15200 | 16500 | 1.19 | 0.87 | 0.92 |
| 6 | HHTETA ^a | 210 | 71 | 14800 | 14300 | 1.23 | 0.80 | 1.00 |
| 7 | HHTETA ^b | 120 | 74 | 15400 | 13000 | 1.15 | 1.10 | >1.00 |
| 8 | DiNBpy ^a | 420 | 20 | 4150 | 2800 | 1.10 | 0.12 | >1.00 |
| 9 | ME ₆ Tren ^a | 210 | 54 | 13400 | 27000 | 1.03 | 0.78 | 0.49 |
| 10 | PMDETA ^a | 210 | 63 | 13100 | 12600 | 1.05 | 0.78 | 1.00 |
| 11 | BPy ^a | 300 | 24 | 5000 | 3200 | 1.21 | 0.15 | >1.00 |

a) [S]: 7.91 mol.l⁻¹ in anisole at 110 °C; [S]₀/[EBP]₀/[CuBr]₀/[Ligand]₀ = 200/1/1/1.

b) [S]: 8.70 mol.l⁻¹ at 110 °C; [S]₀/[1-PEBr]₀/[CuBr]₀/[HHTETA]₀ = 200/1/1/1, Ref. 21.

c) Last point of the kinetic data.

Conclusions

A series of alkylated linear amine ligands were synthesized in a simple and versatile reaction. They show homogeneous and relatively fast polymerization reactions compared to most other ATRP ligands. Apparently, increasing the alkyl chain length by only one methylene unit, i.e. ethyl substitution, is sufficient to give homogeneous ATRP of MMA and S, which was not achieved with methyl substituted ligands (e.g., PMDETA).

Acknowledgements

Financial support for this work was provided by the Research Foundation of Istanbul Technical University.

References

1. Wang, J. S.; Matyjaszewski, K. *Macromolecules* **1995**, *28*, 7901–7910.
2. Wang, J. S.; Matyjaszewski, K. *J. Am. Chem. Soc.* **1995**, *117*, 5614–5615.
3. Kato, M.; Kamigaito, M.; Sawamoto, M.; Higashimura, T. *Macromolecules* **1995**, *28*, 1721–1723.
4. Percec, V.; Barboiu, B. *Macromolecules* **1995**, *28*, 7970–7972.
5. Matyjaszewski, K., Ed. *Controlled Radical Polymerization*; Am. Chem. Soc., Washington, D.C., 1998; ACS Symp Ser 685.
6. Matyjaszewski, K., Ed. *Controlled/Living Radical Polymerization. Progress in ATRP, NMP, and RAFT*; Am Chem Soc, Washington D.C., 2000; ACS Symp Ser 768.
7. Patten, T. E.; Matyjaszewski, K. *Acc. Chem. Res.* **1999**, *32*, 895–903.
8. Kamigaito, M.; Ando, T.; Sawamoto, M. *Chem. Rev.* **2001**, *101*, 3689–3746.
9. Matyjaszewski, K.; Xia, J. *Chem. Rev.* **2001**, *101*, 2921–2990.
10. Matyjaszewski, K.; Xia, J. In *Handbook of Radical Polymerization*; Matyjaszewski, K.; Davis, T. P., Eds.; Wiley: New York, 2002; Chapter, pp 602.
11. Xia, J.; Matyjaszewski, K. *Macromolecules* **1997**, *30*, 7697–7700.
12. Matyjaszewski, K.; Goebelt, B.; Paik, H.-J.; Horwitz, C. P. *Macromolecules* **2001**, *34*, 430–440.
13. Shen, Y.; Zhu, S.; Zeng, F.; Pelton, R. H. *Macromol. Chem. Phys.* **2000**, *201*, 1169–1175.
14. Shen, Y.; Zhu, S.; Pelton, R. H. *Macromolecules* **2001**, *34*, 3182–3185.
15. Shen, Y.; Zhu, S. *Macromolecules* **2001**, *34*, 8603–8609.
16. Xia, J.; Gaynor, S. G.; Matyjaszewski, K. *Macromolecules* **1998**, *31*, 5958–5959.

17. Gromada, J.; Matyjaszewski, K. *Polym. Prepr.* **2002**, 43(2), 195–196.
18. Shen, Y.; Zhu, S. *AIChEJ* **2002**, 48, 2609–2619.
19. Zeng, F.; Shen, Y.; Zhu, S.; Pelton, R. *Macromolecules* **2000**, 33, 1628–1635.
20. Faucher, S.; Zhu, S. *Ind. Eng. Chem. Res.* **2005**, 44, 677–685.
21. Acar, M. H.; Bicak N. *J. Polym. Sci.-A-Polym. Chem.* **2003**, 41, 1677–1680.
22. Davis, K. A.; Matyjaszewski, K. *Chinese J. Polym. Sci.* **2004**, 22, 195–204.
23. Xia, J.; Zhang, X.; Matyjaszewski, K. *In Transition Metal Macromolecular Design*; Boffa, L. S.; Novak, B. M., Eds.; ACS Symposium Series 760; American Chemical Society: Washington, DC, 2000; Chapter, pp 207.
24. Pintauer, T.; Matyjaszewski, K. *Coord. Chem. Rev.* **2005**, 249, 1155–1184.
25. Faucher, S.; Okrutny, P.; Zhu, S. *Macromolecules* **2006**, 39, 3–5
26. Acar, M. H.; Becer, C. R.; Ondur, H. A.; Inceoglu, S. *Polym. Prepr.* **2005** 46(2), 433–434.
27. Chu, J.; Chen, J.; Zhang, K. *J. Polym. Sci. Part A: Polym. Chem.* **2004**, 42, 1963–1969.
28. Ciampolini, M., and N. Nardi, N., *Inorg. Chem.* **1966**, 5, 41.
29. Queffelec, J.; Gaynor, S. G.; Matyjaszewski, K. *Macromolecules* **2000**, 33, 8629–8639.
30. Inceoglu, S.; Olugebefola, S. C.; Acar, M. H.; Mayes, A. M. *Des. Monomers Polym.* **2004**, 7, 181–189.
31. Barre, G.; Taton, D.; Lastecoueres, D.; Vincent, J-M. *J. Am. Chem. Soc.* **2004**, 126, 7764–7765.
32. Gromada, J.; Spanswick, J.; Matyjaszewski, K. *Macromol. Chem. Phys.* **2004**, 205, 551–566.
33. Inoue, Y.; Matyjaszewski, K. *Macromolecules* **2003**, 36, 7432–7438.
34. Inoue, Y.; Matyjaszewski, K. *Macromolecules* **2004**, 37, 4014–4021.
35. Haddleton, D.; Crossman, M. C.; Dana, B. H.; Duncalf, D. J.; Heming, A. M.; Kukulj, D.; Shooter, A. *Macromolecules* **1999**, 32, 2110–2119.
36. Schubert, U. S.; Spindler, C. E.; Eschbaumer, C.; Nuyken, O. *Polym. Prepr.* **1999**, 40(2), 416.
37. Schubert, U. S.; Hochwimmer, G.; Spindler, C. E.; Nuyken, O. *Macromol. Rapid. Commun.* **1999**, 20, 351.
38. Matyjaszewski, K.; Patten, T. E.; Xia, J. *J. Am. Chem. Soc.* **1997**, 119, 674
39. Paik, H. –J.; Matyjaszewski, K. *Polym. Prepr.* **1996**, 37(2), 274.
40. Patten, T. E.; Xia, J.; Abernathy, T.; Matyjaszewski, K. *Science* **1996**, 272, 866
41. Percec, V.; Barboiu, B.; Neuman, A.; Ronda, J. C.; Zhao, M. *Macromolecules* **1996**, 29, 3665.
42. Kickelbick, G.; Matyjaszewski, K. *Macromol. Rapid Commun.* **1999**, 20, 341.

43. D. Haddleton, A. J. Clark, M. C. Crossman, D. J. Duncalf, A. M. Heming, S. R. Morsley, A. Shooter, *Chem. Commun.* **1997**, 1173.
44. Iovu, M.; Maithufi, N.; Mapolie, S. *Macromol. Symp.* **2003**, 193, 209-226.
45. Xia, J.; Gaynor, S. G. Matyjaszewski, K. *Macromolecules* **1999**, 32, 2434.
46. Qui, J.; Shipp, D.; Gaynor, S.; Matyjaszewski, K. *Polym. Prep.* **1999**, 40(2), 418.
47. Liou, S.; Rademacher, J. T.; Malaba, D.; Pallack, M. E.; Brittain, W. J. *Macromolecules* **2000**, 33, 4295-4296.
48. Desterac, M.; Bessiere, J.-M.; Boutevin, B. *Macromol. Rapid Commun.* **1997**, 18, 967.
49. Lee, D. W.; Seo, E. Y.; Cho, S. I.; Yi, C. S. *J. Polym. Sci: Part A: Polym. Chem.* **2004**, 42, 2747-2755.

Chapter 9

Electron Spin Resonance Study of Methacrylate Radicals Generated from Purified Oligomers Prepared by Atom Transfer Radical Polymerization

Atsushi Kajiwara

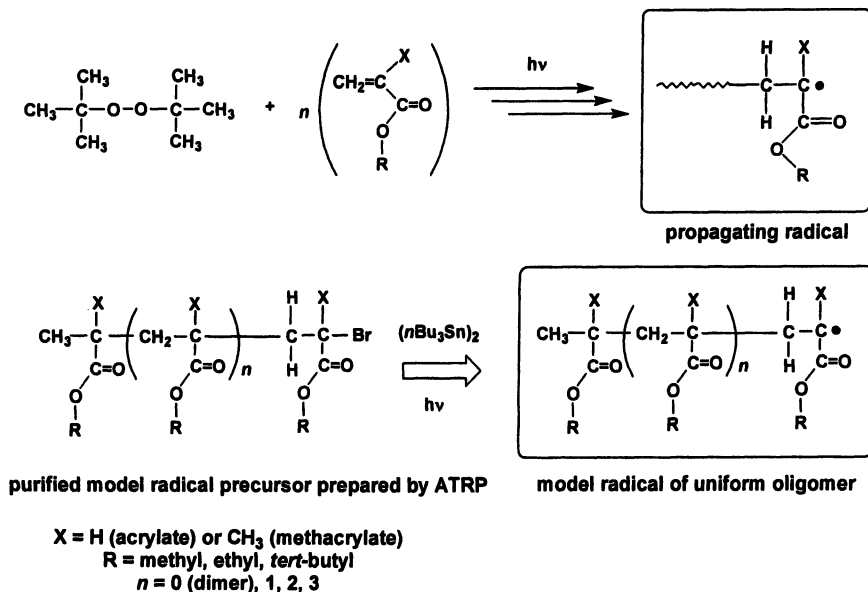
Department of Materials Science, Nara University of Education,
Takabatake-cho, Nara 630-8528, Japan

Abstract: Radical precursors of oligo(meth)acrylates with uniform structures were prepared by atom transfer radical polymerization (ATRP) and purified. Model radicals with given chain lengths were generated by reaction with an organotin compound. The radicals were observed by electron spin resonance (ESR) spectroscopy. Each ESR spectrum of dimeric, trimeric, tetrameric, and pentameric *tert*-butyl acrylate model radicals observed at various temperatures provided clear experimental evidence of the 1,5-hydrogen shift. Uniform MMA oligomeric radicals, from dimer to pentamer, were also investigated systematically by ESR. This combination of ESR and ATRP gave significant information on the properties of radicals in radical polymerizations.

Introduction

Propagating radicals in radical polymerizations can be observed by ESR (Electron Spin Resonance) spectroscopy. The well-resolved spectra obtained from ESR provide information not only on the structure, properties, and concentration of radicals but also on the initiating and propagating (oligomeric and polymeric) radicals in radical polymerizations (1-4).

Atom transfer radical polymerization (ATRP) is one of the most widely applied polymerization techniques in the field of controlled/living radical polymerization. The polymers formed in ATRP contain terminal carbon-halogen bonds. Giese *et al.* (Figure 1) (5) has reported that these bonds can be homolytically cleaved by reaction with organotin compounds. Accordingly, various radicals that model the end groups in an ATRP can be formed from the corresponding precursors prepared by atom transfer radical addition (ATRA) and ATRP and the generated radicals can be studied by ESR spectroscopy. Variation of the chain length and composition of polymeric radical precursors elucidates the affect of chain length and penultimate units on the ESR spectra of the formed radicals (6). It was previously reported (7), that the ESR spectra of propagating *tert*-butyl methacrylate radicals show chain length dependency.



Scheme 1 Generation of propagating radicals (a) and oligomeric model radicals (b). ESR spectra of methacrylate showed chain length dependence. ESR spectra of acrylate radicals show clear proof of a 1,5-hydrogen shift.

In another case, large amounts of mid-chain radicals in acrylate polymerizations were detected by ESR spectroscopy. It was suggested that the terminal propagating radicals had readily rearranged to form a mid-chain radical.³ ESR study of model radicals generated from radical precursors prepared by ATRP provided significant information on the rearrangement. Accordingly, ESR spectroscopy in combination with ATRP has given an unambiguous proof of several reactions that are involved in radical polymerization.

Previous research was mainly conducted for the cases of polymeric radicals. Although the model polymeric radicals, generated from radical precursors prepared by ATRP, had narrow polydispersity, they were mixtures of polymers with various chain lengths. In this research work, uniform oligomeric radicals, with various chain lengths, were generated as models of propagating radicals. The model radicals were generated from oligomers that were prepared by ATRP and purified by column chromatography. Each uniform oligomer was a pure compound with an exact molecular weight. A systematic study using uniform oligomers with various chain lengths would provide a clearer perspective in the study of the radicals.

In the conventional radical polymerization of acrylates, it is clear that a large amount of mid-chain radicals are readily formed by intermolecular chain transfer reactions or intramolecular backbiting reactions. It has been reported (8-11), and our previous study also suggested (3), that the reaction occurred via a 1,5-hydrogen shift. However, a detailed mechanism for the transfer reaction is not clear. There is no clear experimental evidence for the "1,5-" reaction and possibilities of a 1,7-, a 1,9-hydrogen shift or some other reaction e.g. intermolecular chain transfer remain. The uniform oligomers studied are models for the initial stage of propagation. An ESR study, using uniform oligomers would clarify any ambiguity and a systematic study will provide a clearer perspective on the minimum chain lengths required for a radical to participate in a chain transfer reaction.

In the case of methacrylates, chain lengths of the propagating radicals observed by *in situ* ESR were estimated for the case of *tert*-butyl methacrylate. The findings are based on the distorted conformation of the propagating chain end radicals caused by the presence of the attached long chain. However, the origin of the distortion was not clear. ESR spectroscopy of uniform oligomethacrylates would provide important information on the molecular dynamics of the radicals.

In this article, preparation of uniform oligomers by ATRP and ESR study of these uniform radicals generated from the oligomers will be shown.

Results and Discussion

tert-Butyl Acrylate (*t*BA)

GPC elution diagrams of model radical precursors of dimer, trimer, and tetramer are shown in Figure 1 along with that of mixture. As shown in the figure, separation and purification were successful. The pentamer was also isolated and purified. Model radicals with clearly defined structures were generated by the reaction of the corresponding alkyl bromides (H-ethyl acrylate (EA)-*t*BA-Br, H-EA-*t*BA-*t*BA-Br, H-EA-*t*BA-*t*BA-*t*BA-Br, H-EA-*t*BA-*t*BA-*t*BA-*t*BA-Br) with an organotin compound under irradiation. The resulting radicals had structures of hydrogenated radicals, i.e., H-EA-*t*BA•, H-EA-*t*BA-*t*BA•, H-EA-*t*BA-*t*BA-*t*BA•, and H-EA-*t*BA-*t*BA-*t*BA-*t*BA• respectively. Each of these radicals was investigated by ESR spectroscopy at various temperatures. Clear well-resolved spectra were observed and precise values for hyperfine coupling constants (hfc) can be determined from the spectra.

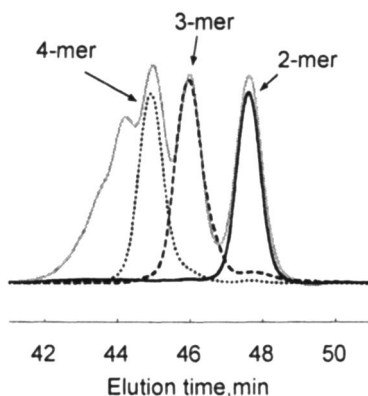


Figure 1 GPC elution diagram of purified dimer, trimer, and tetramer of *t*BA as uniform radical precursor along with that of mixture of oligomers.

The ESR spectrum of the dimeric radical (H-EA-*t*BA•) showed a doublet of triplets in each spectrum at various temperatures within the range of -30 to +150 °C. The doublet and triplet were reasonably considered to be due to the splitting from the α -proton and two equivalent β -methylene protons, respectively. Nothing happened to the dimeric radical even at higher temperatures. On the other hand, model trimeric and tetrameric radicals showed a clear temperature dependent irreversible change, as shown below.

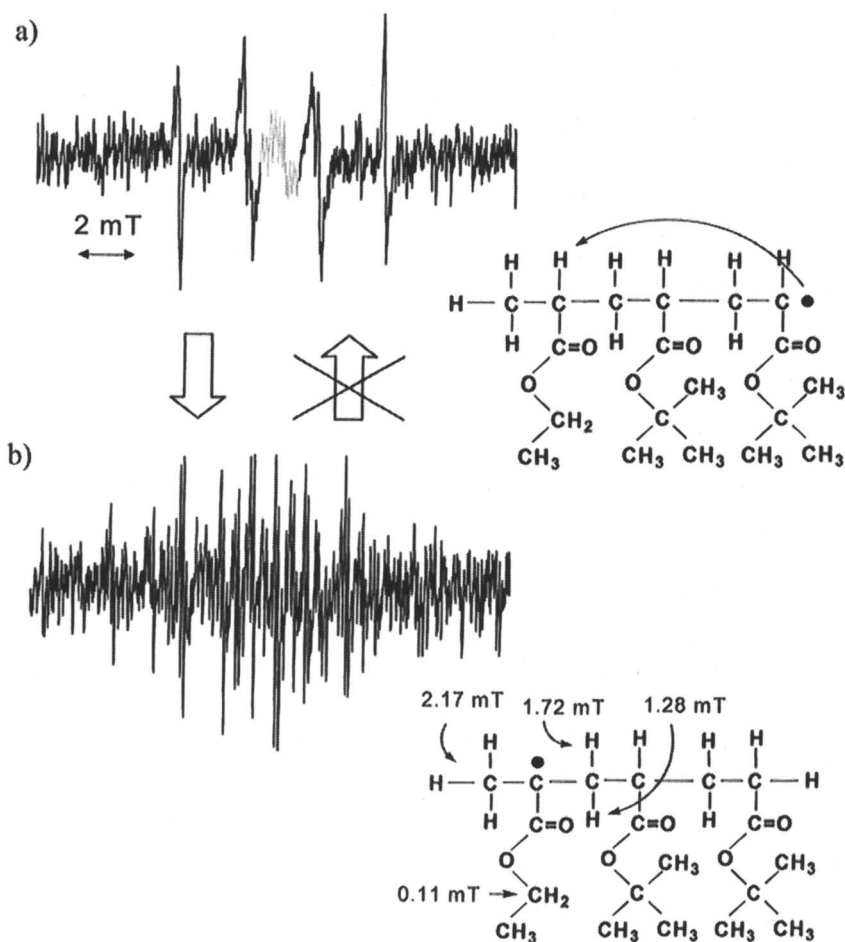


Figure 2 ESR spectra of trimeric model radical (*H-EA-tBA-tBA*•) at $-30\text{ }^{\circ}\text{C}$ (a) and at $+120\text{ }^{\circ}\text{C}$ (b) with their estimated structures. Upon heating, an irreversible spectroscopic change occurred due to hydrogen abstraction.

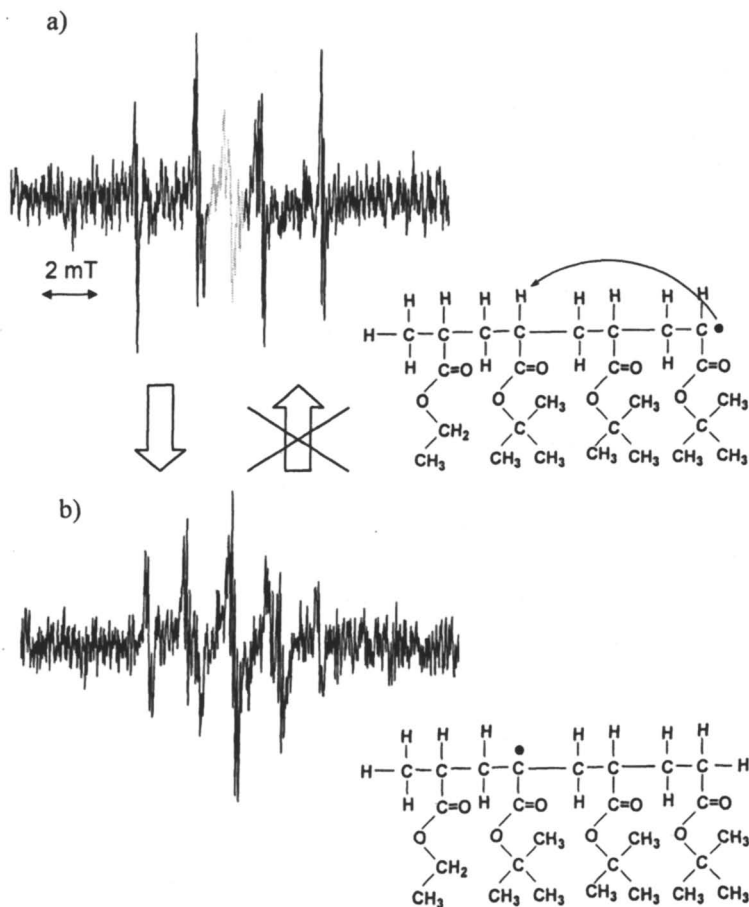


Figure 3 ESR spectra of tetrameric model radical ($H-EA-tBA-tBA-tBA\bullet$) at $-30\text{ }^{\circ}\text{C}$ (a) and at $+120\text{ }^{\circ}\text{C}$ (b) with their estimated structures. Upon heating, irreversible spectroscopic change occurred due to hydrogen abstraction.

In the case of the model trimeric radical (H-EA-*t*BA-*t*BA \cdot), the spectrum observed at -30 °C (Fig. 2a) was very similar to that of the dimeric radical. This spectrum is ascribed to a chain end radical as shown in the figure. ESR spectra were measured every 30 degree as the temperature was increased from -30 °C to 120 °C. As the temperature was raised, the spectrum gradually changed and irreversibly to a different one. From 0 °C to 60 °C, two kinds of overlapping spectra were observed. The change was complete at 120 °C. The resulting spectrum, observed at higher temperatures, was totally different from that at lower temperatures (Fig. 2b). When a 1,5-hydrogen shift occurs, the radical should migrate from one end to the other end of the trimeric model radical as shown in Figure 2. The spectrum can be simulated using hyperfine splitting constants shown in the figure. The most important feature of this simulation is a small triplet that appeared in each spectroscopic line. When this trimer was prepared by ATRP, ethyl 2-bromo propionate was used as the initiator and the initiator fragment was counted as first monomer unit. So, we only had an ethyl ester group at the other chain end. The presence of a small triplet clearly indicates that the radical is located on the first ethyl acrylate unit. Consequently, we can say that the radical migrated from one end to the other end of the trimer.

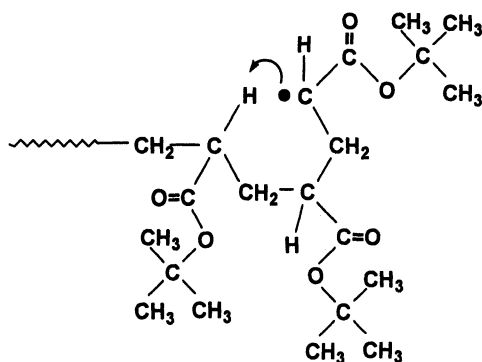


Figure 4 1,5-Hydrogen shift of propagating radical of *t*BA.

A similar ESR study was done for the tetrameric model radical (H-EA-*t*BA-*t*BA-*t*BA \cdot). The ESR spectra at -30 °C and 120 °C are shown in Figure 3. The low temperature spectrum, observed at -30 °C, was very similar to those from the dimeric and trimeric model radicals. A similar irreversible spectroscopic change took place, as in the case of the trimeric model radical, at higher temperatures. However the final spectrum was different from that of trimeric model radical. In the case of a tetrameric model radical, a 1,5-hydrogen shift would cause transfer of a radical from the chain end to the first *t*BA unit, which is located two units

before the other end unit, through a six-membered ring structure (Figure 3). The transferred radical should have mid-chain type structure with methylene groups at both sides (H-EA-*t*BA(•)-*t*BA-*t*BA-H). The spectrum of the radical shown in Fig. 3b is ascribable to a mid-chain radical. These findings provide clear experimental evidence of a 1,5-hydrogen shift at the propagating chain end of acrylate radical polymerizations.

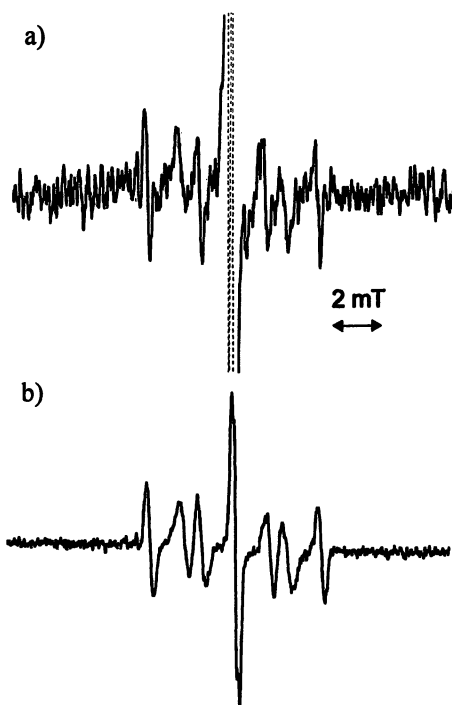


Figure 5 ESR spectra observed at 150 °C for pentameric model radical (a) and polymerization in situ of tBA initiated with tBPO under irradiation (b).

A pentameric model radical was also generated and observed by ESR and a similar temperature dependent spectroscopic change to those seen in the case of the trimer and tetramer was observed. The resulting high temperature spectrum is shown in Figure 5a. This less resolved spectrum is very similar to those observed in polymeric acrylate radicals, as shown in the spectrum below (Fig. 5b).

These findings strongly suggested that the mechanism of the chain transfer reaction in an acrylate radical polymerization is a 1,5-hydrogen shift that occurs

through a six-membered ring structure. Formation of a six-membered ring is a kinetically favorable process and the transfer occurred from a secondary radical to form a thermodynamically more stable tertiary radical. One further piece of information can be obtained from the result of the pentamer radical. Actually, the pentamer has one more chance to migrate from a mid-chain radical to the other chain end. However, this migration was not observed. The reason for this is unresolved.

Although we still have a slight possibility for intermolecular chain transfer, these systematic studies have provided a clearer perspective of the mechanism of the chain transfer reaction of propagating acrylate radicals. Further investigation will provide decisive proof of the mechanism.

Table 1. *M_w* and *T_g* for poly/BA polymerized by ATRP and thermal radical polymerization

| | <i>M_w</i> | <i>T_g</i> , °C |
|------------------------|----------------------|---------------------------|
| ATRP | 33300 | 47.3 |
| Thermal polymerization | 27700 | 42.2 |
| ATRP | 95000 | 49.5 |
| Thermal polymerization | 101000 | 45.0 |

Let us leave the mechanism of the chain transfer reaction and turn to the properties of resulting polyacrylates made by conventional and controlled radical polymerizations. The presence of large amounts of mid-chain radicals would cause branching in the resulting polymers and large amounts of mid-chain radicals were observed in thermal initiated radical polymerizations. On the other hand, radicals generated from precursors prepared by ATRP only showed chain end radical even for the case of DP = 100. This means that ATRP gave relatively linear polyacrylates in comparison with the conventional polymerization. These findings suggest two kinds of polyacrylates can be prepared by conventional radical polymerization and ATRP. Although investigation of the branching structures by spectroscopic methods has been attempted, it is extremely difficult. Therefore ¹³C NMR experiments were carried out to count the number of quaternary carbon atoms present in poly(2-ethylhexyl acrylate) and poly(butyl acrylate), to measure the number of branching points (12, 13). From these experiments, 3-8 % of branching was reported. However, this method did not show how long the branches were. Therefore thermal properties of polyacrylates prepared by conventional radical polymerization were measured and compared with the results of polyacrylates prepared by ATRP. The results are shown in Table 1. A total of four different kinds of polyacrylates, with *M_w* ~ 30000 and ~ 100000 prepared by conventional radical polymerizations and ATRP, were measured. In both cases, the polyacrylates prepared by ATRP had a 4-5 degree higher *T_g* than those prepared by conventional radical polymerization. These are

meaningful differences and the results indicate that the length of the branches in polyacrylates prepared by conventional radical polymerizations are long enough to affect the thermal properties of the polymer. This provides indirect proof of the formation of a mid-chain radical and potential initiation activity of the radicals.

Methyl methacrylate (MMA)

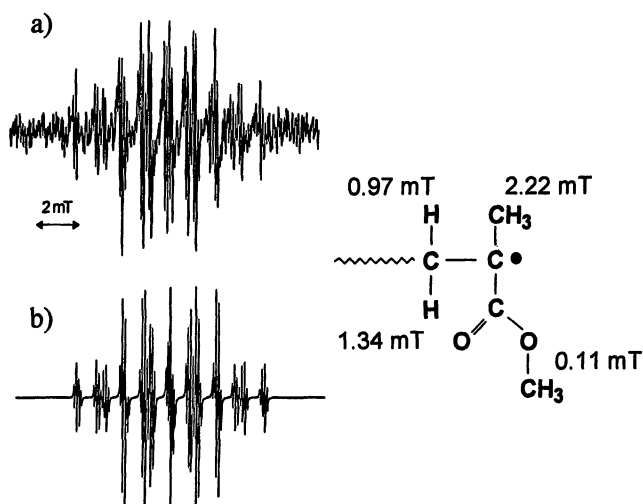


Figure 6 Observed ESR spectrum of propagating radical of MMA in radical polymerizations at 150 °C (a) along with its simulation (b). Values of hyperfine splitting constants are shown in the Figure.

The ESR spectra observed in the polymerization of MMA also show a clear temperature dependent change, indicating that there are two exchangeable conformations whose existence has been shown in the elucidation of ESR spectra of methacrylates so far. ESR spectrum of propagating radicals of MMA in polymerization systems at 150 °C is shown in Figure 6 along with its simulation.

The experimental spectrum was reasonably simulated with the values of hfc as shown in Figure 6. The characteristic feature of the spectrum is in difference in the values of hfc on two β -methylene protons.

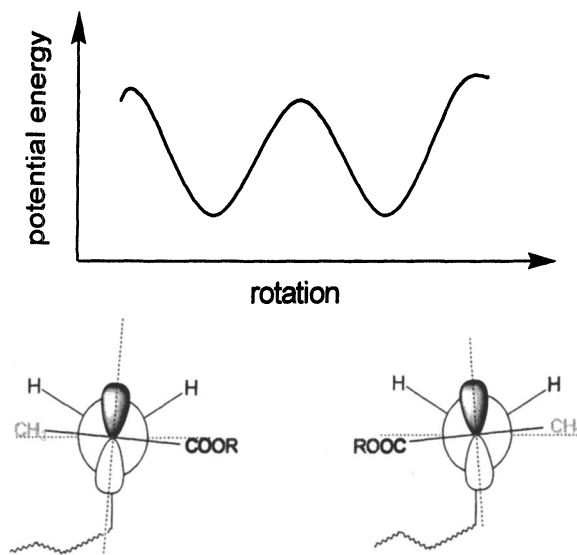


Figure 7 Schematic energy diagram of rotation around C_{α} - C_{β} bond of the propagating radical of methacrylate. Newman projections of structures of stable two conformers are shown below the diagram.

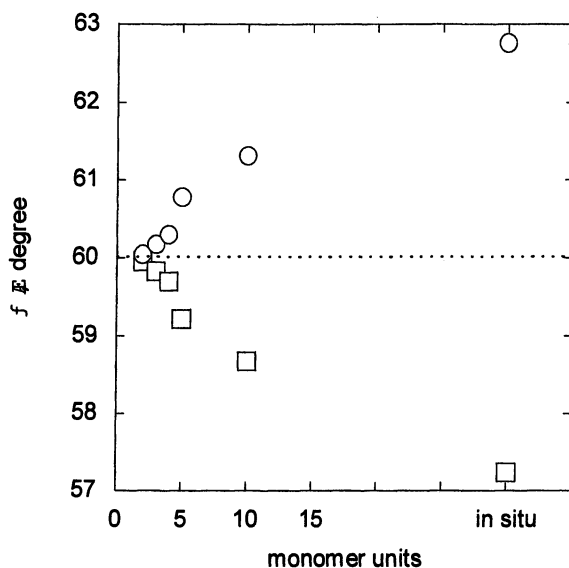


Figure 8 Chain length dependent change of angle between C_{β} -H bond and $p\pi$ -orbital.

There are two stable conformers for the chain end radicals. The schematic energy diagram of this terminal rotation and suggested distorted structures by Newman projection are shown in Figure 7. The difference in hfc of the two β -methylene protons means that the structures of the terminal radicals are somehow distorted. The distortion may be caused by the presence of a long attached propagated chain. A systematic chain length dependent change in the magnitude of the difference between the two coupling constants had been observed for 30, 50, and 100-mers of model *tert*-butyl methacrylate radicals.

Dimeric, trimeric, tetrameric, and pentameric MMA oligomers were prepared by ATRP and purified by column chromatography. Purification was successful and each uniform dimeric, trimeric, tetrameric, and pentameric model MMA propagating radical was generated from the corresponding purified bromide and observed by ESR spectroscopy. In the case of the MMA oligomers, clear and well-resolved spectra were also observed. ESR spectra of these oligomeric model radicals observed at 150 °C can be simulated with isotropic simulation program, indicating smooth rotation around C_{α} - C_{β} bonds. The ESR spectrum of the dimeric model radical (H-EMA-MMA \cdot) can be simulated with almost equivalent values for hfc of two β -methylene protons. This means that in the dimer the rotation around C_{α} - C_{β} bond is very smooth. Apparently, the coupling constant of two β -methylene protons changed from equivalent to inequivalent as the chain length increased. Even at 150 °C, the trimeric, tetrameric, and pentameric model radicals showed inequivalent values of hfc for the β -methylene protons. The differences between the two β -methylene protons increased with increasing chain length and values of hfc, angles between $p\pi$ -orbital and C_{β} -H bonds in the Newman projections can be estimated, as shown in Figure 8. The dimer showed almost equivalent β -protons, however the trimer already showed a conformation that deviated from a symmetrical structure. The presence of two monomer units may cause asymmetry. This distortion may be related to the origin of stereoregularity in polymethacrylates.

Experimental

Oligomeric (meth)acrylates were synthesized by ATRP using a molar excess of initiator compared to monomer, in presence of a Cu^I/Cu^{II} PMDETA complex (δ). The oligomers obtained were a mixture of dimer, trimer, tetramer, pentamer and higher oligomers. Each oligomer, from dimers to pentamers, were separated and purified from the mixtures by repeated column chromatography. Molecular weights and molecular weight distributions were measured using a TOSOH CCP&8020 series GPC system with TSK-gel columns using THF as an eluent. The purity and molecular weight of the purified materials were confirmed using

electron spray ionization mass spectroscopy (ESI-MS). Uniform oligomeric radicals were generated by reaction of the oligomer with organotin compounds under irradiation.

The generated radicals were observed by ESR spectroscopy by means of JEOL JES RE-2X ESR spectrometer equipped with universal cavity and temperature control accessory. Spectroscopic simulation was carried out by JEOL IPRIT data analysis system.

Conclusions

The developments of ATRP has provided a tool to develop a deeper understanding of conventional radical polymerizations. A combination of ATRP and ESR spectroscopy has provided additional information on the basic chemistry of radical polymerizations of (meth)acrylates. Comparison of the temperature dependent behavior of the ESR spectra of dimeric, trimeric, and tetrameric *t*BA model radicals at various temperatures clearly show that an intramolecular 1,5-hydrogen shift of propagating radicals occurs during the polymerization of acrylates. Analysis of the ESR spectra of MMA oligomers show a chain length dependent conformational change of propagating radicals especially in the initial stage of polymerization. These findings provide useful information on both kinetic analysis of polymerizations and investigation of stereospecific polymerization of methacrylates.

Acknowledgements

The author is grateful to Professor Krzysztof Matyjaszewski, Carnegie Mellon University, for his kind advice and help for preparation of radical precursors by ATRP. The author wishes to thank Professor Mikiharu Kamachi, Fukui University of Technology for valuable advice. Thanks are due to Professor Norikazu Ueyama and Dr. Taka-aki Okamura, Graduate School of Science, Osaka University for measurements of ESI-mass spectra of radical precursors. The author would like to thank Professor Tatsuki Kitayama, Graduate School of Engineering, Osaka University for measurements of DSC of polyacrylates. Special thanks are due to Professor Robert G. Gilbert, University of Sydney for helpful comments on the mechanism of transfer reactions of acrylates. This research work was supported in part by a Grant-in-Aid (No. 15550107) from the Ministry of Education, Culture, Sports, Science, and Technology of Japan. Financial support from the Japan Society for the Promotion of Science (JSPS) for Japan-U.S. Cooperative Science Program is gratefully acknowledged.

References

1. Kamachi, M. In *Controlled Radical Polymerization*, ACS Symposium Series 685; Matyjaszewski, K. ed., American Chemical Society: Washington, DC., 1998; Chapter 9, pp. 145-168.
2. Kajiwara, A.; Matyjaszewski, K.; Kamachi, M. In *Controlled/Living Radical Polymerization*, ACS Symposium Series 768; Matyjaszewski, K. ed., American Chemical Society, Washington, DC., 2000; Chapter 5, pp. 68-81.
3. Kajiwara, A.; Kamachi, M. In *Advances in Controlled/Living Radical Polymerization*, ACS Symposium Series 854; Matyjaszewski, K. ed., American Chemical Society, Washington, DC., 2003; Chapter 7, pp. 86-100.
4. Kamachi, M. *J. Polym. Sci., Part A: Polym. Chem.*, **2002**, *40*, 269.
5. Giese, B.; Damm, W.; Wetterich, F.; Zeitz, H.-G. *Tetrahedron Lett.*, **1992**, *33*, 1863.
6. Kajiwara, A.; Nanda, A. K.; Matyjaszewski, K. *Macromolecules*, **2004**, *37*, 1378.
7. Kajiwara, A.; Maeda, K.; Kubo, N.; Kamachi, M. *Macromolecules*, **2003**, *36*, 526.
8. Willemse, R. X. E.; van Heck, A. M.; Panchenko, E.; Junkers, T.; Buback, M. *Macromolecules*, **2005**, *38*, 5098.
9. Britton, D.; Heatley, F.; Lovell, P. A. *Macromolecules*, **2001**, *34*, 817.
10. Plessis, C.; Arzamendi, G.; Alberdi, J. M.; Agnely, M.; Leiza, J. R.; Asua, J. M. *Macromolecules*, **2001**, *34*, 6138.
11. Plessis, C.; Arzamendi, G.; Leiza, J. R.; Schoonbrood, H. A. S.; Charmot, D.; Asua, J. M. *Macromolecules*, **2000**, *33*, 4.
12. Heatley, F.; P. A. Lovell, P. A.; Yamashita, T. *Macromolecules*, **2001**, *34*, 7636.
13. Ahmad, N. M.; F. Heatley, F.; Lovell, P. A. *Macromolecules*, **1998**, *31*, 2822.

Chapter 10

Ti-Catalyzed Living Radical Polymerization of Styrene Initiated by Epoxide Radical Ring Opening

Alexandru D. Asandei, Isaac W. Moran, Gobinda Saha,
and Yanhui Chen

Department of Chemistry and Institute of Materials Science,
Polymer Program, University of Connecticut, 97 North Eagleville Road,
Storrs, CT 06269-3136

The steric and electronic ligand effects in the Ti-catalyzed living radical polymerization (LRP) of styrene initiated by epoxide radical ring opening (RRO) was investigated in a series of Ti(III) complexes (L_nTiX_m) derived in situ from Zn reduction of commercially available Ti(IV) precursors. Based on the ability to perform initiation by epoxide RRO and mediate LRP *via* reversible C-Ti bond formation, these catalysts ranked: L = metallocene (η^5 -RCp: R = H ~ Et ~ ^tPr ~ ^tBu > Ind >> Cp*) >> O-ligands (alkoxides > bisketonates) >> N ligands (Tp > Pc), while X = Cl > Br >> F ~ Me and $L_nTiCl_m > L_{n-1}TiCl_{m+1}$. The inexpensive Cp₂TiCl₂ was one of the most active species.

Introduction

Over the last decade, convenient molecular weight (M_n) and polydispersity (M_w/M_n) control and relative robustness vs. ionic procedures have enabled living radical polymerization (LRP) to become a fundamental tool in modern polymer chemistry. Consequently, the wide applications of LRP to complex macromolecular synthesis have prompted extensive efforts in the development of novel initiators and catalytic systems. Detailed investigations have demonstrated that M_n and M_w/M_n can be controlled by reversible termination of growing chains with persistent radicals or degenerative transfer (DT) agents (1). Mechanistically, LRP occurs by atom transfer (ATRP), dissociation-combination (DC) or degenerative transfer (DT) (1). ATRP is catalyzed by late transition metal (Cu, Ru, Ni, Fe, Mo etc) (1,2) halides in conjunction with ligands and additives. DC is mediated by organic (nitroxides) (3) or organometallic (Co, Mo) (4) persistent radicals, while DT employs sulfur-based reversible addition-fragmentation (RAFT) (1) agents as well as iodine (5), Te or Sb derivatives (6).

Living radical polymerizations are typically initiated from activated halides or thermal systems (1a,b). However, the restricted selection of initiator types may limit the direct use of polymer chains as macromolecular building blocks. Therefore, the polymer synthesis toolbox would be greatly enhanced by the availability of a wider initiator assortment that provide access to new functional chain ends, while the development of new catalysts for simultaneous one-pot living polymerizations of dissimilar monomers would be highly desirable in the synthesis of complex monodisperse polymeric architectures.

Recently, apart from their applications in α -olefin coordination polymerizations and organometallic reactions (7), *early* transition metal complexes have become increasingly employed in radical organic chemistry (8). One of the most successful examples, the soluble paramagnetic $Cp_2Ti(III)Cl$ complex (9), is inexpensively synthesized in situ by the Zn reduction of $Cp_2Ti(IV)Cl_2$ (10). The lime-green Cp_2TiCl (10b) is a very mild one electron transfer agent and catalyzes a variety of radical reactions (11) including the radical ring opening (RRO) of epoxides (12).

We have recently introduced the Cp_2TiCl -catalyzed LRP of styrene initiated by epoxide RRO as a novel initiation and respectively catalysis methodology for LRP (13). Furthermore, we have also demonstrated that Ti alkoxides generated in-situ by epoxide RRO are efficient catalysts for the living ring opening polymerization of cyclic esters (14). Therefore, epoxides and titanium complexes represent potent new classes of initiators and respectively catalysts for both radical and ring opening polymerizations. In addition, as fundamental motifs in organic and polymer chemistry, they have the advantage of inexpensive commercial availability with wide structural diversity.

As the Ti complex is involved in both initiation and reversible termination steps, the catalyst ability to efficiently perform both epoxide RRO and reversible chain endcapping determines the polymerization livingness. Accordingly, the Ti reactivity can be fine-tuned by manipulation of steric and electronic ligand effects. However, while Ti complexes were thoroughly studied in Ziegler-Natta and metallocene polymerizations (15), understanding of ligand effects in Ti-catalyzed radical reactions is limited (8,16,17). Thus, towards the rational design of multifunctional catalytic systems for living radical, ring opening and coordination polymerizations, we have started to investigate the effect of Ti ligands and reaction conditions in the LRP of styrene initiated by epoxide RRO and catalyzed by Ti(III) complexes derived from Zn reduction of structurally diverse, commercially available Ti(IV) precursors (18). Herein we present investigations of a series of 19 Ti complexes (Chart 1) with nitrogen (PcTiCl₂, TpTiCl₃) and oxygen ligands ((dpm)₃Ti, (dpm)₂TiCl₂, (iPrO)₂TiCl₂, (iPrO)₃TiCl) as well as η⁵-cyclopentadienyl (Cp) half-sandwich (LTiCl₃, L = Cp, Cp*, Ind) and sandwich metallocenes (L₂TiCl₂, L = Cp, EtCp, iPrCp, tBuCp, Cp*, Ind; Cp₂TiX₂, X = F, Cl, Br, CO and tBuCp₂TiMe₂). Some of these complexes were successful in stereospecific styrene coordination polymerization using MAO but were not investigated for either epoxide RRO or LRP.

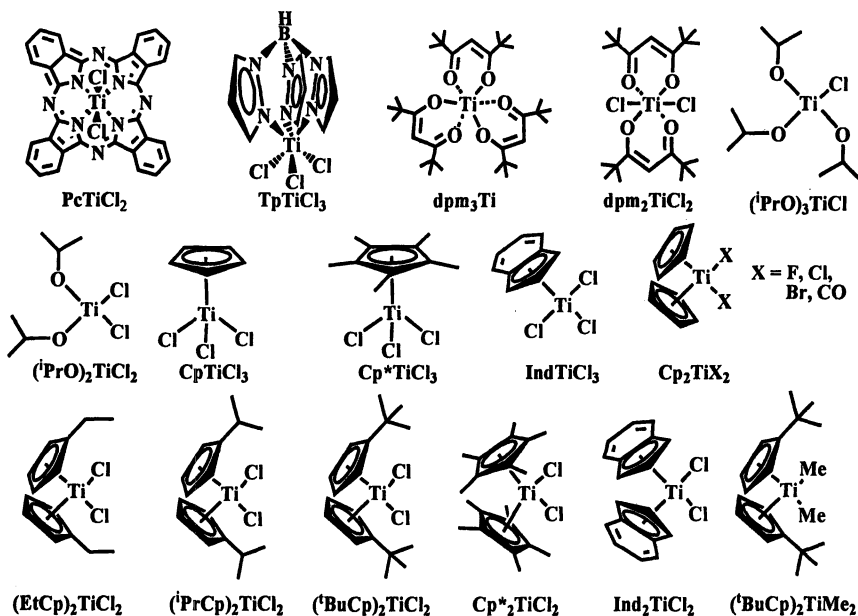


Chart 1. Structures of the L_nTiX_m precursors.

Experimental

Materials. Bis(cyclopentadienyl)titanium dichloride (Cp_2TiCl_2 , 97 %, recrystallized from CH_2Cl_2), cyclopentadienyltitanium trichloride (CpTiCl_3 , 99%), chlorotitanium triisopropoxide ($(^i\text{PrO})_3\text{TiCl}$, 98%), bis(^tbutylcyclopentadienyl)titanium dichloride ($^t\text{BuCp}_2\text{TiCl}_2$) (all from Acros); bis(cyclopentadienyl) titanium dibromide (Cp_2TiBr_2 , Pfaltz & Bauer); dichlorotitanium diisopropoxide ($(^i\text{PrO})_2\text{TiCl}_2$, 95+%, TCI) bis(ethylcyclopentadienyl)titanium (IV) dichloride ($\text{EtCp}_2\text{TiCl}_2$, 98%), bis(^lpropylcyclopentadienyl)titanium dichloride ($^l\text{PrCp}_2\text{TiCl}_2$, 98%), dimethylbis(^tbutylcyclopentadienyl)titanium (IV) ($^t\text{BuCp}_2\text{TiMe}_2$, 98%), bis(pentamethylcyclopentadienyl)titanium dichloride (Cp^*TiCl_2 , 99%), trichloro(pentamethylcyclopentadienyl)titanium(IV) (Cp^*TiCl_3 , 98%), indenyltitanium trichloride (IndTiCl_3 , 99%), tris(2,2,6,6-tetramethyl-3,5-heptanedionato)titanium (III) ($(\text{dpm})_3\text{Ti}$, 99%), hydrotris(pyrazol-1-ylborato)trichlorotitanium (IV) (TpTiCl_3 , 95%), bis(cyclopentadienyl) dicarbonyl titanium (II) ($\text{Cp}_2\text{Ti}(\text{CO})_2$, 98%) (all from Strem); dichlorobis(2,2,6,6-tetramethyl-3,5-heptanedionato)titanium(IV) ($(\text{dpm})_2\text{TiCl}_2$, 97%), dichlorobis(indenyl)titanium(IV) ($\text{Ind}_2\text{TiCl}_2$), titanium(IV) phthalocyanine dichloride (PcTiCl_2 , 95%), Zn (nanosize, $d_{\text{aver}} = 35$ nm) 99+ %, glycidyl 4-methoxyphenyl ether (GME, 99%), and 1,4-butanediol diglycidyl ether (BDGE, 95%), (all from Aldrich) were used as received. Bis(cyclopentadienyl)titanium difluoride was prepared (19). 1,4-dioxane (99.7 %, Fisher) was distilled from a blue solution of Na/benzophenone. Styrene (99+ %, Fluka), was dried over CaH_2 (93%, Acros), filtered, and passed through an acidic Al_2O_3 column.

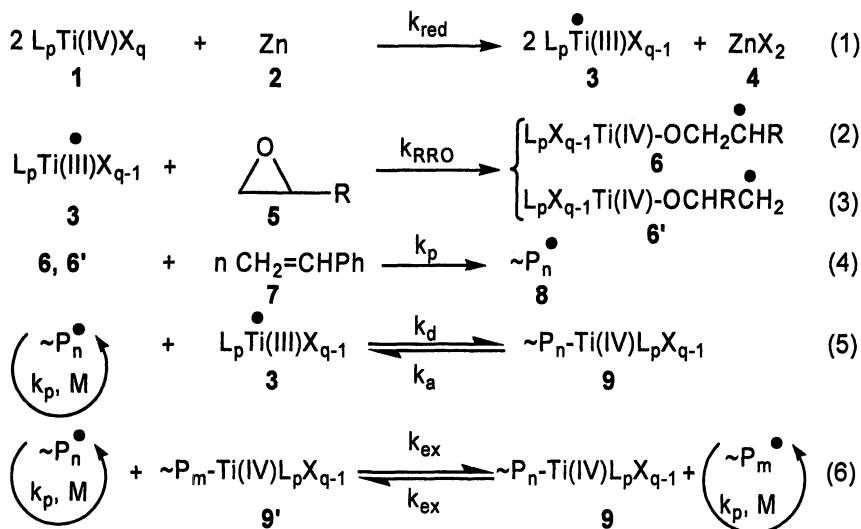
Techniques. $^1\text{H-NMR}$ (500 MHz) spectra were recorded on a Bruker DRX-500 at 24 °C in CDCl_3 (Aldrich; 0.03% v/v TMS as internal standard). GPC analyses were performed on a Waters 150-C Plus gel permeation chromatograph equipped with a Waters 410 differential refractometer, a Waters 2487 dual wavelength absorbance UV-VIS detector set at 254 nm, a Polymer Laboratories PL-ELS 1000 evaporative light scattering (ELS) detector and with a Jordi Flash Gel (1×10^5 Å, 2×10^4 Å, 1×10^3 Å) column setup with THF as eluent at 3 mL/min at 34 °C. Number-average (M_n) and weight-average molecular weights (M_w) were determined from polystyrene calibration plots.

Polymerizations. Catalyst (Cp_2TiCl_2 , 86.9 mg, 0.35 mmol), Zn (45.6 mg, 0.70 mmol) and dioxane (0.5 mL containing ~10 mg CaH_2 , as trace water scavenger) were added to a 25-mL Schlenk tube. The tube was degassed by several freeze pump thaw cycles, filled with Ar, and the reduction was carried out at rt. The characteristic lime-green $\text{Cp}_2\text{Ti(III)Cl}$ color was observed in under 5 min. The tube was then cooled to -78 °C and a mixture of styrene (0.5 mL,

4.36 mmol) and BDGE (16.8 μL , 0.087 mmol) was injected and the tube was re-degassed and heated at 90 $^{\circ}\text{C}$. Samples taken under Ar were used for conversion and molecular weight determination by NMR and respectively by GPC.

Results and Discussion

The proposed mechanism of the Ti-catalyzed LRP of styrene initiated by epoxide RRO is outlined in Scheme 2. The Ti(III) species were generated in situ by Zn reduction (Ar, dioxane, rt) of the Ti(IV) precursor (eq. 1). As Zn is a heterogeneous component, a Zn/Ti = 2/1 ratio was typically employed. The occurrence of the reduction was easily recognized by the characteristic green/blue color of the Ti(III) complexes. With very few exceptions (20), the reduction potentials in this Ti series are not available, but it is likely that Zn was not reductive enough for $\text{Cp}_2^*\text{TiCl}_2$, Cp_2TiF_2 , Cp_2TiCO_2 and $^t\text{BuCp}_2\text{TiMe}_2$ which did not undergo a color change even in more polar solvents at higher temperatures and led to very little polymer formation. In all other cases, injection of excess epoxide into Ti(III) solutions rapidly recovered of the original Ti(IV) color indicating the occurrence of epoxide RRO.



Scheme 1. Ti-catalyzed styrene LRP initiated by epoxide RRO (L = ligand, X = halide).

Epoxides are unique initiators as their Ti-catalyzed RRO occurs with the formation of a pair of very reactive primary and secondary constitutionally β -titanoxo radicals derived from RRO regioselectivity (17) (eqs. 2,3). Interestingly, these species possess the same thermodynamic stabilization as the corresponding alkyl radicals (21). In this study, the polymerizations were initiated from 1,4-butanediol diglycidyl ether (BDGE) a diepoxide that provided the best results in our earlier experiments with Cp_2TiCl_2 (13). Addition of the epoxide derived radicals to styrene initiates the polymerization (eq. 4) which proceeds in a living fashion, mediated by the reversible end-capping of the propagating chain end with a second equivalent of Ti(III). The reversible C-Ti bond homolysis most likely occurs *via* a combination of the DC and DT mechanisms (eqs. 5, 6) (13). Thus, one Ti equivalent is required for the epoxide RRO and another one for the polymerization control.

The conversion dependence of M_n and M_w/M_n for these Ti-catalyzed styrene polymerizations is presented in Figures 1-4 while a comparison of the results at similar conversions is summarized in Table I. In the case of N-ligands (exp. 1, 2) no polymerization was observed for the poorly soluble PcTiCl_2 (22) while the TpTiCl_3 scorpionate derivative (23) formed an insoluble purple precipitate typically associated with over-reduction (23*b,c*), and thus provided a broad, poorly controlled polymerization (*vide infra*).

Four different complexes with O-ligands were subsequently studied (exp 3-7). Ti alkoxides were previously used as additives for Ru (2*b*) and Mo (24) catalyzed radical polymerizations as well as in various organic reactions (7). Such compounds are relatively inexpensive and moreover, while other transition metal catalyzed processes are strongly colored, they are typically colorless and expected to generate white polymer. However, due to the limited steric accessibility of the metal centers (25), both Ti bis(ketonates) performed rather poorly. Thus, no polymer was obtained from $(\text{dpm})_3\text{Ti}$ while an uncontrolled free radical polymerization (FRP) was observed for $(\text{dpm})_2\text{TiCl}_2$. However, a clear improvement was observed (Figure 1) for both $(^i\text{PrO})_2\text{TiCl}_2$ and $(^i\text{PrO})_3\text{TiCl}$ which were the first catalysts in this series to display a linear dependence of M_n on conversion.

The broad M_w/M_n values and low initiator efficiencies (IE) are a consequence of the slow RRO initiation due to the strong lone pair donation of the alkoxide ligands. This effect reduces the Ti oxophilicity (7*b*), thus decreasing the rate and yield of the epoxide-RRO. The better control afforded by $(^i\text{PrO})_3\text{TiCl}$ vs. $(^i\text{PrO})_2\text{TiCl}_2$ is related to the increased steric demand of the three ^iPrO ligands which may weaken the C-Ti bond enough to allow for a more efficient reversible termination.

Interestingly, the BDGE-initiated polymerizations slowly gelled at higher conversions but the polymer dissolved immediately upon addition of a drop of dilute HCl. In addition, polymerizations initiated from monofunctional epoxides

Table I. Styrene Polymerizations Catalyzed by Ti Complexes.

| Exp. | [St]/[BDGE]/ [L _n TiX _m]/[Zn] | L _n TiX _m | T °C | M _n × 10 ⁻³ ^a | M _w /M _n ^a | k _p ^{app b} 10 ⁴ × min ⁻¹ | Init. Effic. ^c |
|------|---|--|---------|--|---|--|------------------------------|
| 1 | 50/1/4/8 | PcTiCl ₂ | 90 | NA | NA | NA | NA |
| 2 | 50/1/4/8 | TpTiCl ₃ | 90 | 49.8 | 2.83 | 3.50 | 0.12 |
| 3 | 50/1/4/8 | (dpm) ₃ Ti | 90 | NA | NA | NA | NA |
| 4 | 50/1/4/8 | (dpm) ₂ TiCl ₂ | 90 | 6.4 | 1.53 | 5.50 | NA |
| 5 | 50/1/4/8 | (ⁱ PrO) ₂ TiCl ₂ | 90 | 180 | 1.54 | 33.1 | 0.02 |
| 6 | 50/1/4/8 | (ⁱ PrO) ₃ TiCl | 90 | 18.3 | 1.66 | 61.1 | 0.14 |
| 7 | 50/1/4/3 ^d | (ⁱ PrO) ₃ TiCl | 90 | 25.6 | 1.42 | 48.3 | 0.12 |
| 8 | 50/1/4/8 | Cp*TiCl ₃ | 90 | 10.2 | 1.65 | 3.00 | N/A |
| 9 | 50/1/4/8 | Cp*TiCl ₃ | 110 | 18.8 | 1.66 | 39.0 | 0.16 |
| 10 | 50/1/4/8 | IndTiCl ₃ | 90 | 14.3 | 1.26 | 28.6 | 0.22 |
| 11 | 50/1/4/8 | CpTiCl ₃ | 90 | 14.5 | 1.23 | 29.1 | 0.24 |
| 12 | 50/1/2/4 | CpTiCl ₃ | 90 | 47 | 1.91 | 33.3 | 0.06 |
| 13 | 50/1/1/2 | CpTiCl ₃ | 90 | 21.7 | 1.51 | 79.3 | 0.46 |
| 14 | 50/1/4/8 | Cp* ₂ TiCl ₂ | 90 | 4.9 | 1.54 | 1.30 | N/A |
| 15 | 50/1/4/8 | Ind ₂ TiCl ₂ | 90 | 6.8 | 1.23 | 17.6 | 0.38 |
| 16 | 50/1/4/8 | Ind ₂ TiCl ₂ | 70 | 4.8 | 1.12 | 11.8 | 0.57 |
| 17 | 50/1/4/8 | EtCp ₂ TiCl ₂ | 90 | 4.7 | 1.13 | 72.5 | 0.56 |
| 18 | 50/1/4/8 | ⁱ PrCp ₂ TiCl ₂ | 90 | 2.4 | 1.10 | 91.1 | 0.64 |
| 19 | 50/1/4/8 | ^t BuCp ₂ TiCl ₂ | 90 | 9.9 | 1.10 | 54.6 | 0.34 |
| 20 | 50/1/4/8 | Cp ₂ TiBr ₂ | 90 | 10.2 | 1.21 | 18.0 | 0.27 |
| 21 | 50/1/4/8 | Cp ₂ TiCl ₂ | 90 | 4.5 | 1.17 | 68.6 | 0.63 |
| 22 | 50/1/4/2 | Cp ₂ TiCl ₂ | 90 | 7.1 | 2.11 | 9.60 | 0.39 |
| 23 | 50/1/4/4 | Cp ₂ TiCl ₂ | 90 | 2.9 | 1.63 | 30.5 | 0.83 |
| 24 | 50/1/4/8 | Cp ₂ TiCl ₂ | 130 | 10.9 | 1.58 | 128.0 | 0.28 |
| 25 | 50/1/4/8 | Cp ₂ TiCl ₂ | 110 | 7.4 | 1.22 | 120.0 | 0.30 |
| 26 | 50/1/4/8 | Cp ₂ TiF ₂ | 90 | N/A | N/A | N/A | N/A |
| 27 | 50/1/4/8 | ^t BuCp ₂ TiMe ₂ | 90 | N/A | N/A | N/A | N/A |
| 28 | 50/1/4/8 | Cp ₂ Ti(CO) ₂ | 90 | N/A | N/A | N/A | N/A |

^aAt 50% Conv.^bCalculated as the slope of the kinetic plots.^cIE = M_n^{theor}/M_n^{GPC} with M_n^{theor} = MW_{Initiator} + [St]₀/[Initiator]₀*MW_{St}*conv.^dGME as initiator.

(GME) did not form gels and provided $M_w/M_n = 1.4$, the narrowest in the alkoxide series. However, further optimization efforts met with limited success. We attribute this behavior to the facile ligand exchange process of Ti alkoxides (7,26). This is consistent with the slow O-Ti-O inorganic crosslinking from BDGE but also indicates an underlying limitation of Ti alkoxides in LRP.

A comparison of four piano-stool trichloro half-sandwich metallocene and scorpionate Ti complexes ($LTiCl_3$, L = Cp, Cp*, Ind and Tp, exp 2, 8-13), is provided in Figure 2. As described above, potential over-reduction of $TpTiCl_3$ leads to a poor polymerization performance. By contrast, the strong electron releasing effect of Cp* (20,27,28) increases the reduction potential, stabilizes the higher oxidation state and renders the Zn reduction difficult. Consequently, after epoxide RRO, Cp*Ti(III)Cl₂ traps the growing chain with a relatively strong Ti-C bond. Thus, at 90 °C, the dissociation equilibrium is strongly shifted towards the dormant species and a very slow, poorly controlled process is observed.

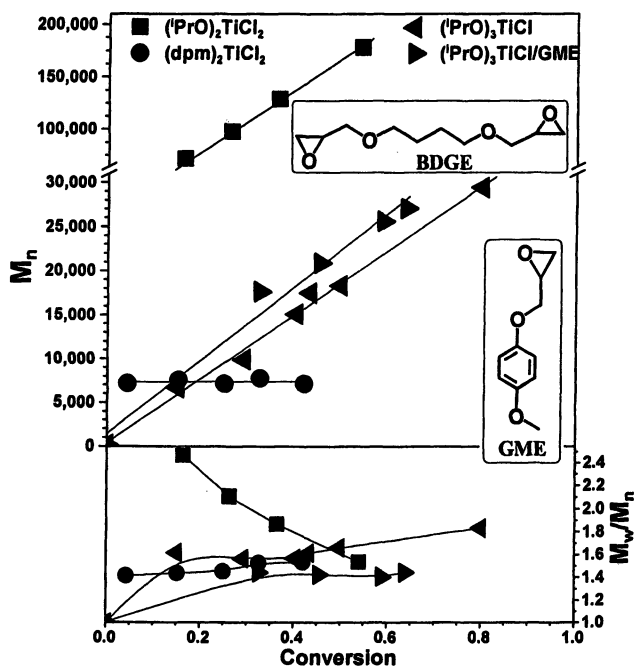


Figure 1. Ligand and initiator effect in Ti-alkoxide catalyzed styrene polymerizations initiated by epoxides: conversion dependence of M_n and M_w/M_n $[St]/[BDGE]/[L_nTiX_m]/[Zn] = 50/1/4/8$, 90 °C. $(iPrO)_2TiCl_2$ (■), $(dpm)_2TiCl_2$ (●), $(iPrO)_3TiCl$ (◄); $[St]/[GME]/[(iPrO)_3TiCl]/[Zn] = 50/1/4/3$, (►).

However, increasing the temperature to 110 °C increases the dissociation rate, and consequently, a linear dependence of M_n on conversion emerges, with a PDI of about 1.6. By contrast, both Ind and Cp which are very close in electronic effects (29) and have identical reduction potentials (20c) are readily reduced by Zn and catalyze the LRP of styrene with very similar values of the rates ($k_p^{app} \sim 3 \times 10^3 \text{ min}^{-1}$), IE (0.2) and M_w/M_n (1.25). Most likely, in the dormant species, the Ind ring points away from the polystyrene chain end, thus providing a steric effect comparable to Cp. Thus, a comparison of these catalysts (Figure 2) reveals a $\text{Cp} \sim \text{Ind} \gg \text{Cp}^* \gg \text{Tp}$ ligand trend and indicates that electronic effects may be more important than steric considerations in the LTiCl_3 group. As described above, two Ti equivalents are required per epoxide group: one opens the epoxide, while the second mediates reversible termination. This is further demonstrated (Figure 2, exp 11-13) by the effect of the $\text{BDGE}/\text{CpTi(III)Cl}_2$ ratio.

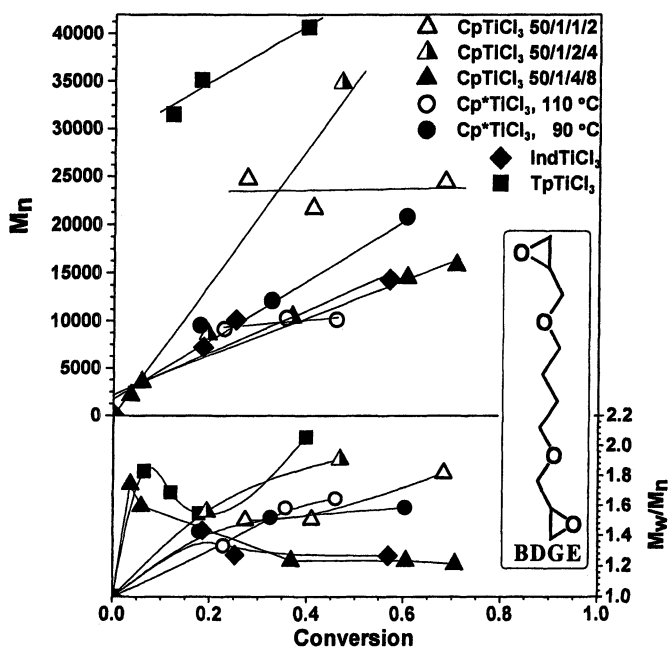


Figure 2. Effect of ligand, epoxide/Ti(III) ratio, and temperature in the LTiCl_3 -catalyzed styrene polymerization initiated from epoxides: dependence of M_n and M_w/M_n on conversion. $[\text{St}]/[\text{BDGE}]/[\text{LTiCl}_3]/[\text{Zn}] = 50/1/4/8$; $T = 90 \text{ }^\circ\text{C}$ for CpTiCl_3 (∇), Cp^*TiCl_3 (\circ), IndTiCl_3 (\blacktriangle), TpTiCl_3 (\blacksquare), and $T = 110 \text{ }^\circ\text{C}$ for Cp^*TiCl_3 (\bullet). $[\text{St}]/[\text{BDGE}]/[\text{CpTiCl}_3]/[\text{Zn}] = 50/1/1/2$ (\triangle), $50/1/2/4$ (Δ), $T = 90 \text{ }^\circ\text{C}$.

As BDGE is a difunctional initiator, a BDGE/Ti = 1/4 ratio is theoretically necessary for a living process. Thus, a BDGE/Ti = 1/1 ratio is insufficient for LRP and leads to the irreversible consumption of all available Ti(III) by excess epoxide. Consequently, only a free radical polymerization is observed. Upon increasing the available Ti(III) to BDGE/Ti = 1/2, partial living features such as linear dependence of M_n on conversion are observed. However, the M_w/M_n is quite broad. Nonetheless, the correct stoichiometric ratio provides a clear LRP with a linear dependence of M_n on conversion and low polydispersity ($M_w/M_n < 1.2$). These results support the proposed requirement of 2 Ti(III) equivalents/epoxide.

The results from the polymerizations mediated by L_2TiX_2 -derived catalysts using an optimum (13) BDGE/Ti/Zn = 1/4/8 ratio are presented in Table 1 (exp 14-28) and in Figures 3, 4. No Zn reduction was observed for Cp_2TiF_2 (29), tBuCp_2TiMe_2 , $Cp_2Ti(CO)_2$ and $Cp^*_2TiCl_2$, which with two Cp^* strong electron donating groups is considered to already be a one electron reduced species (29). With these exceptions, the other RCp_2TiX_2 metallocenes (exp 15-21) were the most successful of the series and provided a clean LRP of styrene with linear M_n vs. conversion plots, low M_w/M_n values (~ 1.15) and relatively similar kinetics.

The observed ligand effects are the cumulative result of the ligand influence on both the epoxide RRO and on the chain end dissociation equilibrium. Inspection of the data in Figure 3 and Table 1 reveals that in the RCp_2TiCl_2 series, these effects are subtle and not very large. Thus, although the bulkier tBuCp (17) or Ind may lower the yield in the epoxide RRO (8,12,17) and reduce IE, the Cp monosubstitution pattern does not have an appreciable consequence on the polymerization. Indeed, RCp_2TiCl_2 (R = H, Et, iPr , tBu) have very similar polydispersity ($M_w/M_n < 1.2$), IE (0.5-0.6) and rate ($k_p^{app} = 0.4-0.5 h^{-1}$) values. Apparently, there is insufficient difference in the stereoelectronic ligand effect (7,29) to strongly affect the Ti-C dissociation equilibrium. The low sensitivity to the ligand nature is most likely a consequence of the radical mechanism and of the constant balance between the electronic and steric effects in this series. Thus, while the C-Ti bond homolysis tendency decreases with increasing ligand electron donation on going from Cp to tBuCp , this trend is counterbalanced by the corresponding increase in the steric bulk of the ligand. Preliminary molecular modeling experiments indicate that in the dormant species, the Cp substituents are oriented away from the polystyrene chain, thus supporting a weaker steric influence. By contrast, much stronger steric effects are observed with similar species in MAO-coordination polymerization (15). This observation, in conjunction with the atactic nature of the polystyrene (13), lends additional support to the radical mechanism of these polymerizations.

In the case of Ind_2TiCl_2 , the stronger steric effect of the two Ind ligands (7) weakens the C-Ti bond and shifts the dissociation equilibrium towards the active species, causing broader M_w/M_n and a larger M_n intercept at lower conversions.

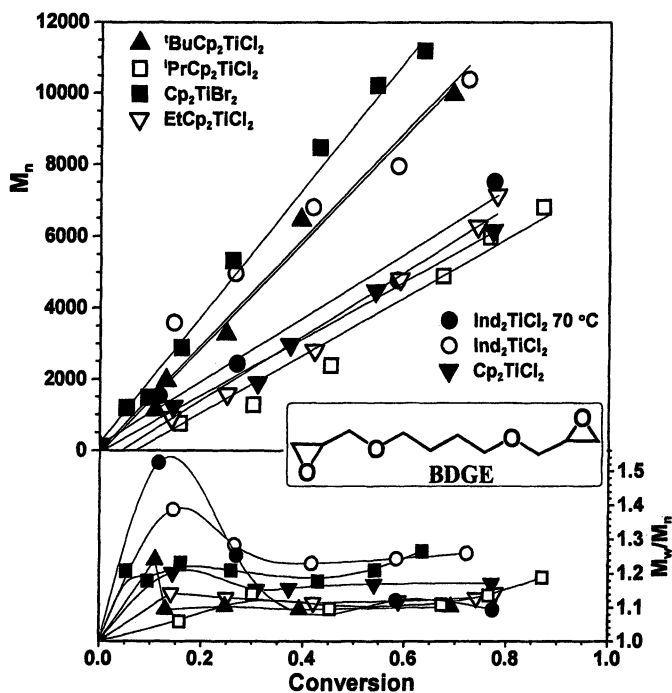


Figure 3. Effect of ligand structure in the RCp_2TiCl_2 -catalyzed polymerization of styrene initiated by epoxide radical ring opening: dependence of M_n and M_w/M_n on conversion. $[St]/[BDGE]/[RCp_2TiCl_2]/[Zn] = 50/1/4/8$. iBu_2TiCl_2 (\blacktriangle), Ind_2TiCl_2 (\circ), Cp_2TiBr_2 (\blacksquare), iPrCp_2TiCl_2 (∇), Cp_2TiCl_2 (\blacktriangledown) and $EtCp_2TiCl_2$ (\triangledown), all at $T = 90^\circ C$. Ind_2TiCl_2 (\bullet) at $70^\circ C$.

Thus, as expected, lowering the temperature (exp. 15, 16) from $90^\circ C$ to $70^\circ C$ results in a simultaneous increase in IE from 0.33 to about 0.56, a decrease in M_w/M_n from 1.23 to 1.12 and a very low M_n intercept. In addition, indenyl ring slippage (7,30) may also affect the catalyst reactivity at higher temperatures.

The effect of the halide or methyl substituents in Cp_2TiX_2 is also presented in exp. 20, 21, 26-28 and Figure 3. While complexes with $X = F, Me$ and CO ligands could not be reduced by Zn and did not yield polymerization, both Br and Cl performed reasonably well, with better IE and M_w/M_n values for Cp_2TiCl_2 . This is due to the weaker C-Ti chain end bond with Cp_2TiBr and the formation of a mixture a products from the Zn reduction of Cp_2TiBr_2 (20e).

The effect of temperature and Zn was further explored (Figure 4 and exp 22-27) for Cp_2TiCl_2 . A linear dependence of M_n on conversion occurs at all temperatures in the 90 - $130^\circ C$ range.

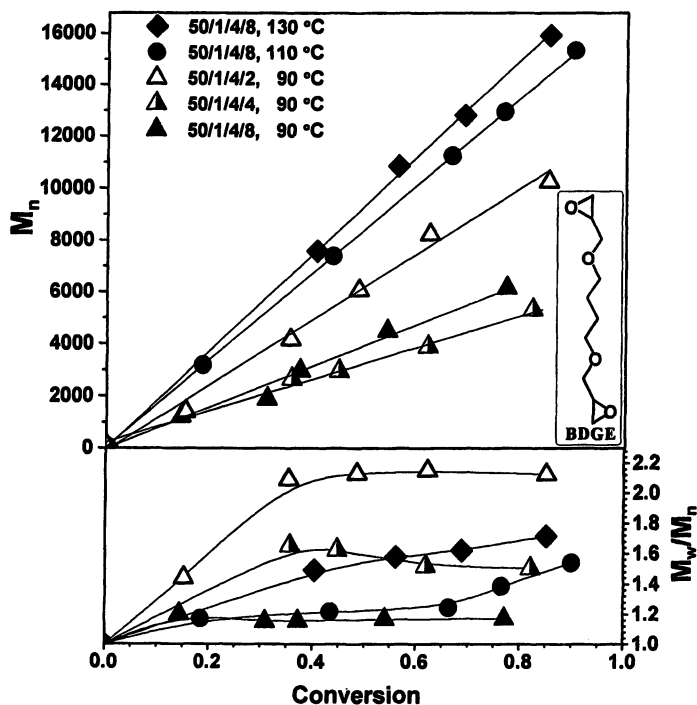


Figure 4. Effect of temperature and Ti(IV)/Zn ratio in the Cp_2TiCl_2 -catalyzed styrene polymerization initiated by epoxide radical ring opening: dependence of M_n and M_w/M_n on conversion. $[St]/[BDGE]/[Cp_2TiCl_2]/[Zn] = 50/1/4/8$ at 130 °C (◆), 110 °C (●), 90 °C (▲) and $[St]/[BDGE]/[Cp_2TiCl_2]/[Zn] = 50/1/4/2$ (△) and 50/1/4/4 (▲) at 90 °C.

However, larger polydispersity ($M_w/M_n = 1.8$) is observed at 130 °C. Upon decreasing temperature from 130 °C to 110 °C and finally to 90 °C, an increase in IE from 0.3 to 0.6 is observed. This is likely due to the thermal suppression of competing side reactions including termination, transfer and epoxide deoxygenation (12). Lower temperatures still provide living polymerizations but with lower rates. Consequently, an optimum in polydispersity and IE occurs at 90 °C. The effect of the amount of Zn is also described in Figure 4 and exp 22-24. A Ti/Zn = 1/0.5 ratio (*i.e.* Ti/Zn = 4/2 for the difunctional BDGE epoxide) should theoretically suffice. Indeed, a linear dependence of M_n on conversion is already observed at this ratio. However, the polydispersity is large ($M_w/M_n = 2.1$) most likely due to slow initiation. Thus, the metallic nature of Zn demands its use in a slight excess. Indeed, increasing the amount of Zn from Ti/Zn = 4/2 to 4/4 and 4/8 leads to a continuous decrease in polydispersity from 2.1 to 1.5

and finally to below 1.2. This reflects the heterogeneous nature of Zn as well as its possible involvement (*via* fast Ti reduction) (31) in both the initiation and reversible termination. Consequently, the presence of excess Zn is critical for the quality of this polymerization.

Conclusions

The present investigation of the ligand effect in the living radical polymerization of styrene initiated by epoxide radical ring opening and catalyzed by Ti(III) complexes reveal several trends which reflect the combined catalyst ability to perform both epoxide RRO and reversible Ti-C bond formation: First, $\eta^5\text{-RCp} > \text{O-ligands} \gg \text{N ligands}$. Thus, cyclopentadienyls ($\eta^5\text{-RCp}$) are vastly superior to both oxygen and nitrogen homoleptic ligands and provide living radical polymerization of styrene with reasonably low M_w/M_n values. The N-ligand complexes were either insoluble or with a mismatched reduction potential and thus performed very poorly ($T_p > P_c$). O-ligands (alkoxides $>$ bisketonates) did provide a linear dependence of M_n on conversion but the fast ligand exchange and low yield in the radical ring opening initiation led to relatively broad polydispersity. The strong steric effect of the bisketonates ligands limited their use in the polymerization. Second, in the metallocene series, by contrast to the corresponding MAO-activated coordination processes, a relatively weak dependence of the polymerization on the nature of the Cp substituent was observed. Thus, for RCp , $\text{R} = \text{H} \sim \text{Et} \sim \text{}^i\text{Pr} \sim \text{}^t\text{Bu} > \text{Ind} \gg \text{Cp}^*$. This can be provisionally rationalized as the result of the Cp ligand substituents pointing away from the dormant polystyrene chain and of the balance between their electronic and steric effects. Third, sandwich titanocenes provided better living features than the half-sandwich derivatives ($\text{L}_2\text{TiCl}_2 > \text{LTiCl}_3$, $\text{L} = \text{Cp, Ind}$) and similarly, $(\text{}^i\text{PrO})_3\text{TiCl} > (\text{}^i\text{PrO})_2\text{TiCl}_2$. Thus, $\text{L}_n\text{TiCl}_m > \text{L}_{n-1}\text{TiCl}_{m+1}$. In addition to the steric contribution, this trend qualitatively parallels the decrease in the Lewis acidity with decreasing the number of Cl ligands⁷ and increasing the number of electron donating substituents. However, strong donors (Cp^*) are also less performant. In addition, chlorine ligands allowed for better control than the bromine derivatives ($\text{Cl} > \text{Br} \gg \text{F} \sim \text{Me}$).

It is rewarding that the most promising catalysts are also the least expensive ones for both metallocenes (Cp_2TiCl_2) and alkoxides ($(\text{O}^i\text{Pr})_3\text{TiCl}$). Furthermore, we anticipate that most Ti structures currently used in coordination polymerization may also be successful in living radical polymerization in conjunction with Zn, epoxides or other initiators. Investigations of epoxides and Ti complexes as multifunctional initiators and catalysts for LRP and ROP, as well as studies on bridging LRP and coordination polymerizations are currently in progress in our laboratory.

Acknowledgements

The the National Science Foundation (CHEM-0518247) and the Donors of the Petroleum Research Fund (PRF-G) administered by the American Chemical Society are gratefully acknowledged for financial support.

References

1. (a) *Handbook of Radical Polymerization*; Matyjaszewski, K., Davis, T. P., Eds.; Wiley-Interscience: New York, 2002. (b) Matyjaszewski, K.; Xia, J. *Chem. Rev.* **2001**, *101*, 2921-2990. (c) Goto, A.; Fukuda, T. *Progr. Polym. Sci.* **2004**, *29*, 329-385.
2. (a) Coessens, V.; Pintauer, T.; Matyjaszewski, K. *Progr. Polym. Sci.* **2001**, *26*, 337-377. (b) Kamigaito, M.; Ando, T.; Sawamoto, M. *Chem. Rev.* **2001**, *101*, 3689-3745.
3. Hawker, C.J.; Bosman, A.W.; Harth, E. *Chem. Rev.* **2001**, *101*, 3661-3688.
4. (a) Wayland, B.; Mukerjee, S.; Poszmik, G.; Woska, D.; Basicckes, L.; Gridnev, A.; Fryd, M.; Ittel, S. *ACS Symp. Ser.* **1998**, *685*, 305-315. (b) Le Grogneq, E.; Claverie, J.; Poli, R. *J. Am. Chem. Soc.* **2001**, *123*, 9513-9514.
5. (a) Gaynor, S.G.; Wang, J.S.; Matyjaszewski, K. *Macromolecules* **1995**, *28*, 8051-8056. (b) Percec, V.; Popov, A. V.; Castillo, E. R.; Monteiro, M.; Barboiu, B.; Weichold, O.; Asandei, A. D.; Mitchell, C. M. *J. Am. Chem. Soc.* **2002**, *124*, 4940-4941. (c) Asandei, A. D.; Percec, V. *J. Polym. Sci.: Part A: Polym. Chem.* **2001**, *39*, 3392.
6. (a) Yamago, S.; Iida, K.; Yoshida, J. I. *J. Am. Chem. Soc.* **2002**, *124*, 2874. (b) Yamago, S.; Ray, B.; Iida, K.; Yoshida, J.; Tada, T.; Yoshizawa, K.; Kwak, Y.; Goto, A.; Fukuda, T. *J. Am. Chem. Soc.* **2004**, *126*, 13908.
7. (a) Reetz, M. T. In *Organotitanium Reagents in Organic Synthesis*; Hafner, K., Lehn, J. M., Rees, C.W., Schleyer, P. R., Trost, B. M., Eds.; Springer-Verlag: Berlin, 1986. (b) Crabtree, R. H. *The Organometallic Chemistry of the Transition Metals*, 3rd ed.; John Wiley & Sons: New York, 2001.
8. Gansauer, A.; Rinker, B. In *Titanium and Zirconium in Organic Synthesis*; Marek, I. Ed.; Wiley-VCH: Weinheim, 2002; Chapter 12, p 435-449.
9. (a) Spencer, R. P.; Schwartz, J. *Tetrahedron* **2000**, *56*, 2103-2112. (b) Coutts, R. S. P.; Wailes, P. C.; Martin, R. L. *J. Organomet. Chem.* **1973**, *47*, 375-382. (c) Reid, A. F.; Wailes, P. C. *Aust. J. Chem.* **1965**, *18*, 9-13.
10. (a) Green, M. L. H.; Lucas, C. R. *J. Chem. Soc. Dalton Trans.* **1972**, *8*, 1000-1003. (b) Jungst, R.; Sekutowski, D.; Davis, J.; Luly, M.; Stucky, J. *Inorg. Chem.* **1977**, *16*, 1645-1655.

11. Barden, M. C.; Schwartz, J. *J. Am. Chem. Soc.* **1996**, *118*, 5484-5485.
12. (a) Rajanbabu, T. V.; Nugent, W. A. *J. Am. Chem. Soc.* **1994**, *116*, 986. (b) Gansauer, A.; Blhum, H.; Lauterbach, T. *Adv. Synth. Catal.* **2001**, *343*, 785.
13. Asandei, A. D.; Moran, I. W. *J. Am. Chem. Soc.* **2004**, *126*, 15932-15933.
14. Asandei, A. D.; Saha, G. *Macromol. Rapid Commun.* **2005**, *26*, 626-631.
15. *Metallocenes*; Togni, A.; Halterman, R. Ed. Wiley-VCH: Weinheim, 1998.
16. Dunlap, M. S.; Nicholas, K. M. *J. Organomet. Chem.* **2001**, *630*, 125-131.
17. (a) Gansäuer, A.; Rinker, B.; Barchuk, A.; Nieger, M. *Organometallics* **2004**, *23*, 1168-1171. (b) Gansäuer, A.; Lauterbach, T.; Narayan, S. *Angew. Chem. Int. Ed.* **2003**, *42*, 5556-5573.
18. (a) Asandei, A. D.; Moran, I. W. *J. Polym. Sci.: Part A: Polym. Chem.* **2005**, *43*, 6028-6038. (b) Asandei, A. D.; Moran, I. W. *J. Polym. Sci.: Part A: Polym. Chem.* **2005**, *43*, 6039-6047. (c) Asandei, A. D.; Moran, I. W. *J. Polym. Sci.: Part A: Polym. Chem.* **2006**, *44*, 1060. (d) Asandei, A. D.; Saha, G. *J. Polym. Sci.: Part A: Polym. Chem.* **2006**, *44*, 1106.
19. Wilkinson, G.; Birmingham, J. *J. Am. Chem. Soc.* **1954**, *76*, 4281-4284.
20. (a) Gassman, P. G.; Macomber, D.; Hershberger, J. W. *Organometallics* **1983**, *2*, 1470. (b) Pattiasina, J.; Heeres, H.; van Bolhuis, F.; Meetsma, A.; Teuben, J. H.; Spek, A. *Organometallics* **1987**, *6*, 1004-1010. (c) Wei, T.; Natarajan, K.; Lang, H.; Holze, R.; *J. Electroanal. Chem.* **2002**, *533*, 127-133. (d) Latesky, S.; Keddington, J.; McMullen, A.; Rothwell, I.; Huffman, J. *Inorg. Chem.* **1985**, *24*, 995-1001. (e) Enemærke, R.; Larsen, J.; Hjollund, G. H.; Skrydstrup, T.; Daasbjerg, K. *Organometallics* **2005**, *24*, 1252-1262.
21. Friedrich, J.; Dolg, M.; Gansauer, A.; Geich-Gimbel, D.; Lauterbach, T. *J. Am. Chem. Soc.* **2005**, *127*, 7071-7077.
22. Taube, R. *Z. Chem.*, **1963**, *3*, 194.
23. Trofimenko, S. *Chem. Rev.* **1993**, *93*, 943-980.
24. Stoffelbach, F.; Poli, R. *Chem. Commun.* **2004**, 2666-2667.
25. Lindmark, A.; Fay, R. *Inorg. Chem.* **1975**, *14*, 282-287.
26. Fay, R. C.; Lindmark, A. F. *J. Am. Chem. Soc.* **1983**, *105*, 2118-2127.
27. Finch, W.; Anslyn, E.; Grubbs, R. *J. Am. Chem. Soc.* **1988**, *110*, 2406-2413.
28. Langmaier, J.; Samec, Z.; Varga V.; Horacek, M.; Mach, K. *J. Organomet. Chem.* **1999**, *579*, 348-355.
29. (a) Gassman, P.; Winter, C. *J. Am. Chem. Soc.* **1988**, *110*, 613. (b) Howie, R.; McQuillan, G.; Thompson, D. *J. Organomet. Chem.* **1984**, *268*, 149.
30. O'Connor, J. M.; Casey, C. P. *Chem. Rev.* **1987**, *87*, 307-318.
31. Jensen, T. R.; Yoon, S. C.; Dash, A. K.; Luo, L. B.; Marks, T. J. *J. Am. Chem. Soc.* **2003**, *125*, 14482-11494.

Chapter 11

Click Functionalization of Well-Defined Copolymers Prepared by Atom Transfer Radical Polymerization

**Brent S. Sumerlin¹, Nicolay V. Tsarevsky², Haifeng Gao²,
Patricia Golas², Guillaume Louche², Robert Y. Lee²,
and Krzysztof Matyjaszewski²**

¹Department of Chemistry, Southern Methodist University,
P.O. Box 750314, Dallas, TX 75275

²Department of Chemistry, Carnegie Mellon University, 4400 Fifth Avenue,
Pittsburgh, PA 15213

Copper(I)-catalyzed 1,3-dipolar cycloaddition of azides and alkynes has proven to be a promising method to functionalize well-defined polymers prepared by atom transfer radical polymerization (ATRP). Due to high efficiency and fidelity under moderate reaction conditions, this “click chemistry” method allows the modification of polymer end groups to give functional telechelic polymers. Additionally, ATRP of azide-containing monomers results in polymer with azido groups in each monomer unit. These polymers demonstrate enhanced reactivity for click reactions, as compared to the monomer with comparable structure. This review will describe the progress made in the combination of ATRP and click chemistry to prepare functional materials by highly efficient post-polymerization modification.

Introduction

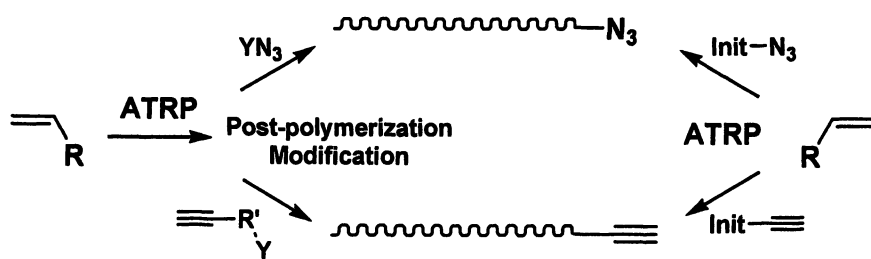
Controlled/living radical polymerization (CRP) techniques facilitate the preparation of a broad variety of polymeric materials with predetermined molecular weights, narrow molecular weight distributions, and high degrees of chain end functionalization (1). When compared to their ionic counterparts, CRP methods provide comparable control while having the advantage of enhanced functional group tolerance and the ability to be conducted under less stringent conditions. Atom transfer radical polymerization (ATRP) (2-5) has emerged as one of the most widely used CRP methods due to facile experimental setup and the use of readily accessible and inexpensive initiators and catalysts.

Post-polymerization modification remains a viable means to incorporate functionality potentially incompatible with polymerization, characterization, or processing conditions (6,7). A potential drawback of such a method of functionalization is the possibility of relatively low yields and side reactions with other groups within the polymer. Therefore, efficient and specific reactions are desirable in order for post-polymerization modification to be successful. Two independent groups recently reported that with the use of a Cu(I) catalyst, azide (8)-terminal alkyne coupling reactions result in the highly specific and efficient preparation of 1,4-disubstituted 1,2,3-triazole products under moderate reaction conditions (9,10). These particular reactions can be conducted in aqueous or organic media and little or no side reactions are observed. The practicality and versatility of the Cu(I)-catalyzed coupling reaction led to its inclusion in the class of efficient and specific organic reactions, commonly termed "click chemistry", as coined by Sharpless et al (11).

Due to its utility for the preparation of functional polymers, ATRP, combined with the efficiency of click chemistry, is an interesting and promising strategy to synthesize various end-functionalized polymers. Recently, several groups have reported the synthesis of (co)polymers via CRP and subsequent click reactions (12-18). Herein, we review the progress in the synthesis and characterization of well-defined (co)polymers via ATRP and the subsequent functionalization of monomer unit or chain end functionality by click chemistry. Particular focus is given to our own contributions, but the work of others is highlighted as well in order to more fully describe the current state-of-the-art in the field. Due to the near-quantitative yields and high fidelity associated with the copper(I)-catalyzed Huisgen 1,3-dipolar cycloadditions, these reactions offer potential in the functionalization of polymeric materials. Two approaches of post-polymerization modification can be envisioned: (i) end group and (ii) monomer unit functionalization. In each case, efficient and specific reactivity is desirable.

End Group Functionalization

With the advent of click chemistry and, in particular, the azide-alkyne coupling reactions mentioned above, a new strategy has been realized for the functionalization of end groups for polymers prepared by ATRP. Two approaches for the end group functionalization of polymers prepared by ATRP are possible (Scheme 1). First, the polymers produced by ATRP preserve the terminal halogen atom(s) and can be successfully converted into various end groups through appropriate transformation, especially nucleophilic substitutions. For instance, the transformation of a terminal halogen atom to an azide anion is very efficient (6,19-22). The second approach consists of employing a functional initiator to prepare polymers by ATRP. Including the functional moiety in the initiator structure assures that each chain contains the functional group, and post-polymerization modification may not be necessary. Regardless of the method used, the obtained organic azido group can be employed for a variety of chemical transformations to produce numerous types of end functional groups, such as amino, hydroxy, carboxy moieties.

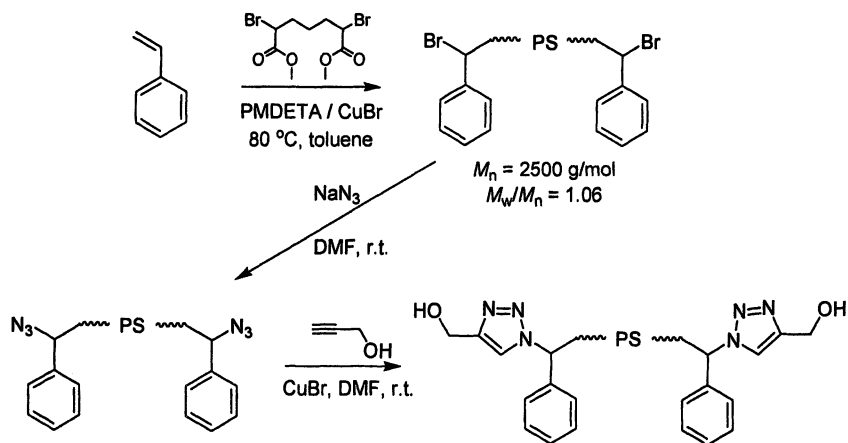


Scheme 1. Methods for the ATRP synthesis of azide- or alkyne-terminal polymers to be subsequently employed in click reactions.

Polymer-Small Molecule Click Reactions

Reacting azide- or alkyne-terminal polymers with a complimentary small molecule containing additional functionality is a viable means to prepare telechelic chains with particularly interesting end groups. For instance, Lutz et al. reported the polymerization of styrene via ATRP and terminal substitution with the azide anion resulted in polymers that were subsequently reacted with various functional alkynes in order to obtain telechelic functional polymers (12).

We employed a similar approach to prepare α,ω -telechelic polystyrene (23). As outlined in Scheme 2, a difunctional initiator was used in the polymerization of styrene to yield homopolymer contained α,ω -bromo end groups. After reacting with NaN_3 , α,ω -diazido polystyrene (PS) was obtained, and ^1NMR spectroscopy indicated that nearly all of the bromo end groups were substituted by the azide (Figure 2). The resulting homotelechelic polystyrene was reacted with propargyl alcohol (PgOH) in DMF with CuBr as a catalyst. CuBr is sufficiently soluble in DMF, and no additional ligand was employed during the click process. Under these moderate conditions, the click process was essentially complete after 4 h at room temperature, as determined by ^1H NMR spectroscopy.



Scheme 2. Synthesis of difunctional PS via ATRP and subsequent azidation and click functionalization with propargyl alcohol. (Adapted with permission from reference 19. Copyright 2005 American Chemical Society.)

While the average number of hydroxyls per PS chain end was determined to be greater than 0.96, the results from NMR spectra were not able to provide complete information about the success of the click reaction. Therefore, gradient polymer elution chromatography (GPEC) (24,25) was employed to evaluate the distribution of the hydroxyl groups along the PS chains. GPEC is a method of affinity chromatography that separates polymers according to their interaction with a stationary column. A mobile phase is gradually changed from a poor solvent to a good solvent, and the polymer chains with weaker column interaction elute first. In this case, a normal phase bare-silica column was used as the stationary phase. When the eluent composition changed from hexanes (poor

solvent) to THF (good solvent), the linear PS chains containing less hydroxyl end-groups elute earlier.

The GPEC traces corroborated the results obtained from NMR by indicating that nearly all of the terminal azide groups were converted to hydroxyls within 8.5 h at room temperature (Figure 1) (23). Due to separation based on chemical functionality, the unreacted starting material (N_3 -PS- N_3 , I) was resolved from both the mono- (N_3 -PS-OH, II) and difunctional (HO-PS-OH, III) products. Integration of the appropriate peaks allowed the concentration of each species (I-III) to be followed with time. This facilitated the determination of rate constants for the reaction of both the first and second groups with PgOH as $k_1 = (3.2 \pm 0.2) \times 10^{-4} \text{ s}^{-1}$ and $k_2 = (1.1 \pm 0.1) \times 10^{-4} \text{ s}^{-1}$, respectively.

Terminal functionality capable of derivatization by click chemistry can also be achieved by employing functional initiators. Mantovani et al. prepared azido-terminated polymers by ATRP (15) of methyl methacrylate with an azide-containing initiator. Depending on the length of the aliphatic spacer between the azido group and the initiating halogen, this approach could be accompanied by side reactions that resulted in loss of the terminal azide. Nonetheless, due to the

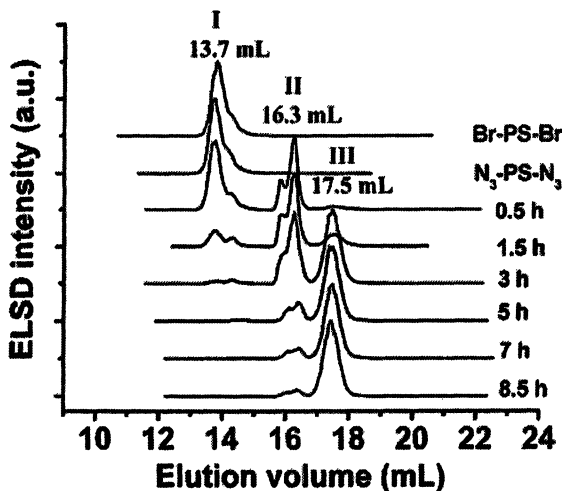


Figure 1. GPEC elution chromatograms of α,ω -dibromo- (I), α,ω -diazo- (II), and α,ω -dihydroxy-terminated(III) PS at different times during the reaction of N_3 -PS- N_3 with PgOH. (Adapted with permission from reference 19. Copyright 2005 American Chemical Society.)

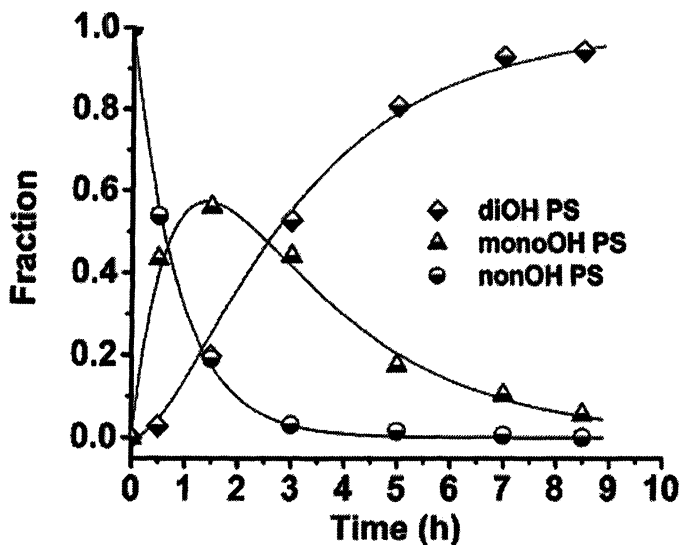


Figure 2. Fraction of dihydroxy-, monohydroxy-, and nonhydroxy-PS as a function of reaction time of N_3 -PS- N_3 and PgOH. (Adapted with permission from reference 19. Copyright 2005 American Chemical Society.)

lower rates of substitution associated with the functionalization of the tertiary halogens of methacrylates, this approach is an attractive alternative for preparing azide-terminated polymethacrylates. The resulting poly(methyl methacrylate) (PMMA) was then UV or fluorescently labeled by reaction with alkyne-functionalized dyes.

Polymer-Polymer Click Reactions

Post-polymerization coupling reactions between two polymers with functional groups present in only a low concentration are generally associated with low yields and reduced rates of reactions. Employing a highly-efficient reaction pathway may facilitate higher coupling efficiencies (26), which makes azide-alkyne coupling reactions a particularly attractive candidate mechanism. Post-polymerization modification by nucleophilic substitution of terminal halogens allowed Opsteen and van Hest to prepare azide-terminated polymers that were subsequently reacted with other polymers containing alkyne end

groups (13). Due to the high efficiency and rates of reactions associated with the click coupling mechanism, this method proved a reliable means to prepare block copolymers in a modular format. This could be particularly attractive when it is desirable to obtain block copolymers from two homopolymers that cannot be easily prepared with a common polymerization mechanism.

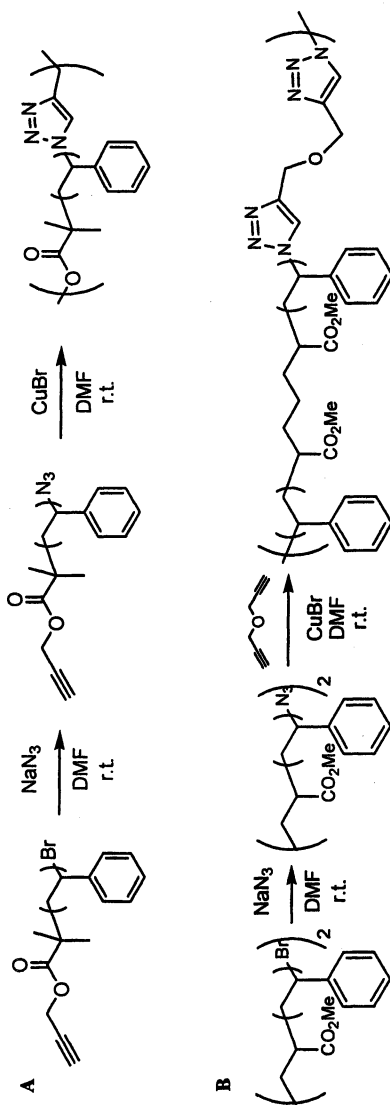
Along similar lines, we employed azide-alkyne coupling of difunctional homo- or hetero-telechelic polymers as a step-growth polymerization mechanism to make higher molecular weight materials from polymeric "monomers" (14) (Scheme 3). Propargyl 2-bromoisobutyrate (P*g*BiB) was used to initiate the polymerization of styrene, and the bromine end group of the resulting polymer was reacted with sodium azide to give α -alkyne- ω -azido-terminated PS (Scheme 3, A). After isolation and purification, this polymer was self-coupled in the presence of CuBr and an increase in molecular weight from $M_n = 2,590$ to 21,500 g/mol was observed. The increased chain length was due to a step-growth polymerization via azide-alkyne coupling of the end groups. In addition to the high molecular weight polymer prepared, there was evidence of an intramolecular reaction to yield macrocycles.

A second approach involved a click reaction being performed using a 1:1 mixture of diazido-terminated polystyrene and propargyl ether (Scheme 3, B). Thus, homo-telechelic polymer chains were coupled via reaction with a complimentary difunctional small molecule. The M_n of the original diazido-terminated PS was 2,020 g/mol, and after step-growth coupling with propargyl ether in the presence of CuBr, an M_n of 16 700 g/mol was obtained.

As indicated from the studies mentioned above, azide-alkyne coupling of polymers is a viable means to prepare block copolymers by a modular method or higher molecular weight materials by coupling of homopolymers. While polymer-polymer reactions specifically between end groups can often be associated with low yields due to steric hindrance, click chemistry is an attractive alternative that facilitates increased efficiency under relatively moderate conditions.

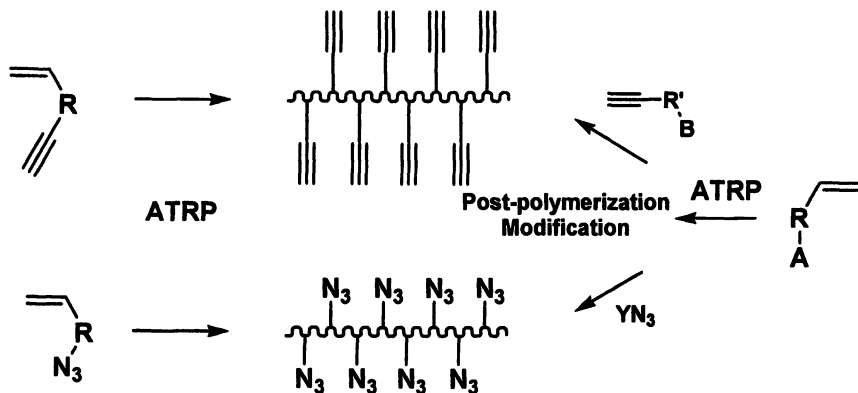
Monomer Unit Functionalization

Incorporating a desirable functionality throughout a polymer chain can be accomplished by direct polymerization of functional monomers or by post-polymerization modification on reactive monomer units (Scheme 4). Subsequent functionalization should be highly efficient due to the large number of monomer units to be derivatized, and specificity is important due to the possibility of side reactions with other moieties along the chain. These requirements make click chemistry an attractive method of modifying polymers to increase their pendant functionality.



Scheme 3. (A) Synthesis of α -acetylene- ω -azido-terminated PS and its subsequent homocoupling and (B) Synthesis of diazido-terminated PS and its coupling with propargyl ether.

(Adapted with permission from reference 14. Copyright 2005 American Chemical Society.)

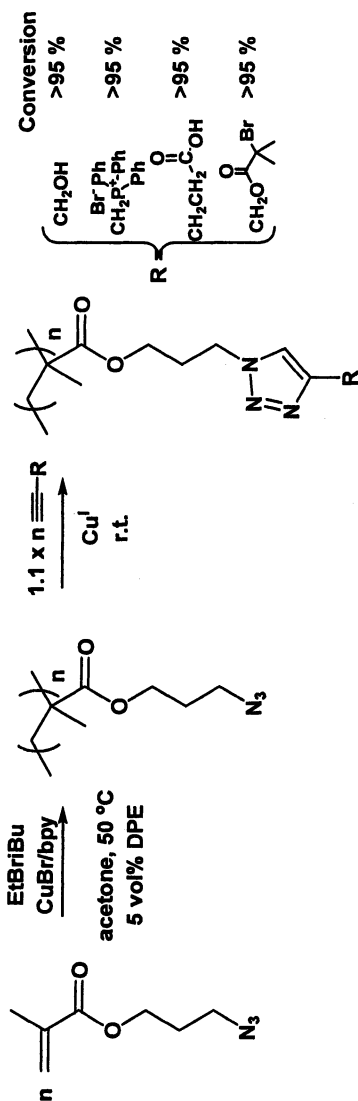


Scheme 4. Methods for introducing pendant azido or alkyne functionality into polymers prepared by ATRP.

These two approaches have been employed to introduce azido and alkyne groups into polymers. Helms and coworkers polymerized trimethylsilyl-protected vinyl acetylene, and subsequent deprotection permitted coupling with benzyl ether dendritic azides to yield dendronized linear polymers (27). However, because the polymerization was by a conventional radical mechanism, the resulting backbone was rather ill-defined.

Previously, Tsarevsky et al. reported the preparation of well-defined homo- and copolymers of acrylonitrile by ATRP. Another form of click chemistry was employed to derivatize the acrylonitrile structural units to yield 5-vinyl tetrazole units by reacting with NaN_3 (28). We extended this approach by polymerizing the azide functional monomer 3-azidopropyl methacrylate (AzPMA) by ATRP (Scheme 5) (29). Good control was observed, as indicated by the semilogarithmic kinetic plot and the linear increase in M_n with conversion for two polymerizations with varying $[M]_0$: $[I]_0$ ratios. The controlled nature of the polymerization was further denoted by the successful synthesis of block copolymers using poly(AzPMA) as a macroinitiator for a block copolymerization with *N,N*-dimethylaminoethyl methacrylate. High blocking efficiency with the second monomer confirmed chain end retention.

Post-polymerization-modification of polyAzPMA ($M_n = 18,400$ g/mol, $M_w/M_n = 1.33$), with PgOH in the presence of CuBr led to near-quantitative functionalization in less than 2 h at room temperature in DMF, as evidenced by ^1H NMR spectroscopy. Other functional propargyl species were reacted with similar high yields, including propargyl triphenylphosphonium bromide, propargyl 2-bromoisobutyrate, and 4-pentynoic acid. The success observed for the latter example establishes coupling of acid-containing alkynes to polymeric azides as an additional alternative for introducing carboxylic acid groups that are incompatible with the conditions typically employed for ATRP.



Scheme 5. Synthesis of AzPMA and the subsequent ATRP and post-polymerization modification with various functional alkynes.

Because of steric constraints and inaccessibility of functional groups along polymer chains, post-polymerization modification reactions are often slower and less efficient than the analogous reaction between two low molecular weight species. However, the rate of azide-alkyne coupling of polyAzPMA was observed to be significantly *higher* than that for AzPMA monomer (Figure 3) (29). Vinyl monomers are known to coordinate to Cu(I) (30), which could potentially affect the activity of the catalyst, but taking into account that methacrylate coordination is relatively weak, it is unlikely that this is the reason for the discrepancy in rates between monomer and polymer. Moreover, the reaction of PgOH with 3-azidopropanol resulted in similar kinetic profiles as those observed for the monomer. The accelerated rate of reaction with the polymer was somewhat unexpected but can potentially be explained by anchimeric assistance. Previous reports have shown that polytriazoles can sufficiently solubilize Cu(I) (31). This phenomenon was particularly important for the case of poly(AzPMA) since the click reaction was conducted in DMF without an additionally added ligand. Thus, as the click reaction proceeded, triazoles formed along the backbone complexed Cu(I), leading to an effective higher local catalyst concentration in the immediate vicinity of neighboring unreacted azido groups. Similar autocatalytic results were reported by Rodionov et al. (32) during the coupling of alkynes to diazido compounds.

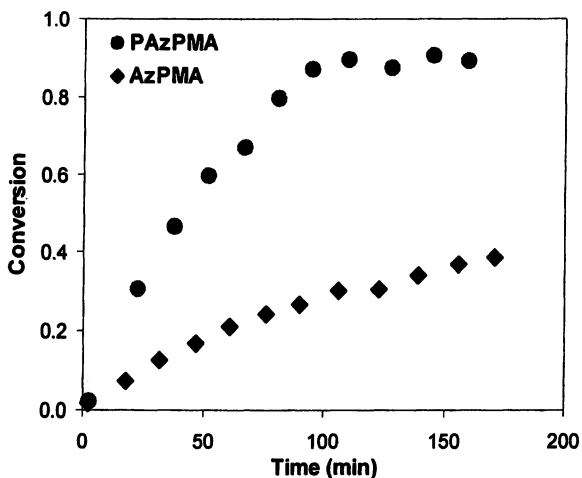


Figure 3. Conversion vs. time for the reaction of PgOH with polyAzPMA. (Adapted with permission from reference 23. Copyright 2005 American Chemical Society.)

Summary

Click chemistry via Cu(I)-catalyzed 1,3-dipolar cycloaddition of azides and alkynes is a promising method to functionalize (co)polymers of various structures. Combining the high efficiency and fidelity of click chemistry with the control of molecular weight and chain end retention facilitated by ATRP allows the modification of well-defined (co)polymers to give terminal or pendant functional macromolecules. Accordingly, block copolymers and chain extended homopolymers have been prepared by coupling end-functional polymers, and enhanced functionality has been introduced along the backbone of polymers that contained azido groups in the monomer units. Due to the multiplicity of functionality and the propensity of Cu(I)-facilitated azide-alkyne coupling to be autocatalytic, reactions on polymers may often be even more efficient than the reaction of low molecular weight analogs. These findings, along with the reports of others, indicate the combination of click chemistry and precise polymer synthesis is an attractive means to prepare novel functional polymeric materials.

References

1. *Handbook of Radical Polymerization*; Matyjaszewski, K.; Davis, T. P., Eds.; Wiley: New York, 2002.
2. Kamigaito, M.; Ando, T.; Sawamoto, M. *Chem. Rev.* **2001**, *101*, 3689-3745.
3. Kato, M.; Kamigaito, M.; Sawamoto, M.; Higashimura, T. *Macromolecules* **1995**, *28*, 1721-3.
4. Matyjaszewski, K.; Xia, J. *Chem. Rev.* **2001**, *101*, 2921-2990.
5. Wang, J.-S.; Matyjaszewski, K. *J. Am. Chem. Soc.* **1995**, *117*, 5614-5615.
6. Coessens, V.; Pintauer, T.; Matyjaszewski, K. *Prog. Polym. Sci.* **2001**, *26*, 337-377.
7. Schulz, D. N.; Patil, A. O. *ACS Symp. Ser.* **1998**, *704*, 1-14.
8. Bräse, S.; Gil, C.; Knepper, K.; Zimmermann, V. *Angew. Chem. Int. Ed.* **2005**, *44*, 5188-5240.
9. Rostovtsev, V. V.; Green, L. G.; Fokin, V. V.; Sharpless, K. B. *Angew. Chem. Int. Ed.* **2002**, *41*, 2596-2599.
10. Tornøe, C. W.; Christensen, C.; Meldal, M. *J. Org. Chem.* **2002**, *67*, 3057-3064.
11. Kolb, H. C.; Finn, M. G.; Sharpless, K. B. *Angew. Chem. Int. Ed.* **2001**, *40*, 2004-2021.
12. Lutz, J. F.; Börner, H. G.; Weichenhan, K. *Macromol. Rapid Commun.* **2005**, *26*, 514-518.
13. Opsteen, J. A.; van Hest, J. C. M. *Chem. Commun.* **2005**, 57-59.

14. Tsarevsky, N. V.; Sumerlin, B. S.; Matyjaszewski, K. *Macromolecules* **2005**, *38*, 3558-3561.
15. Mantovani, G.; Admiral, V.; Tao, L.; Haddleton, D. M. *Chem. Commun.* **2005**, 2089-2091.
16. Joralemon, M. J.; O'Reilly, R. K.; Hawker, C. J.; Wooley, K. L. *J. Am. Chem. Soc.* **2005**, *127*, 16892-16899.
17. O'Reilly, R. K.; Joralemon, M. J.; Wooley, K. L.; Hawker, C. J. *Chem. Mat.* **2005**, *17*, 5976-5988.
18. Wu, P.; Malkoch, M.; Hunt, J. N.; Vestberg, R.; Kaltgrad, E.; Finn, M. G.; Fokin, V. V.; Sharpless, K. B.; Hawker, C. J. *Chem. Commun.* **2005**, 5775-5777.
19. Coessens, V.; Matyjaszewski, K. *J. Macromol. Sci., Pure Appl. Chem.* **1999**, *A36*, 667-679.
20. Coessens, V.; Nakagawa, Y.; Matyjaszewski, K. *Polym. Bull.* **1998**, *40*, 135-142.
21. Matyjaszewski, K.; Nakagawa, Y.; Gaynor, S. G. *Macromol. Rapid Commun.* **1997**, *18*, 1057-1066.
22. Nakagawa, Y.; Matyjaszewski, K. *Polym. J.* **1998**, *30*, 138-141.
23. Gao, H.; Louche, G.; Sumerlin, B. S.; Jahed, N.; Golas, P.; Matyjaszewski, K. *Macromolecules* **2005**, *38*, 8979-8982.
24. Glockner, G. *Gradient HPLC and Chromatographic Cross-Fractionation*; Springer: Heidelberg, 1991.
25. Philipsen, H. J. A.; Klumperman, B.; German, A. L. *J. Chromatogr., A* **1996**, *746*, 211.
26. Sarbu, T.; Lin, K.-Y.; Spanswick, J.; Gil, R. R.; Siegwart, D. J.; Matyjaszewski, K. *Macromolecules* **2004**, *37*, 9694-9700.
27. Helms, B.; Mynar, J. L.; Hawker, C. J.; Frechet, J. M. J. *J. Am. Chem. Soc.* **2004**, *126*, 15020-15021.
28. Tsarevsky, N. V.; Bernaerts, K. V.; Dufour, B.; Du Prez, F. E.; Matyjaszewski, K. *Macromolecules* **2004**, *37*, 9308-9313.
29. Sumerlin, B. S.; Tsarevsky, N. V.; Louche, G.; Lee, R. Y.; Matyjaszewski, K. *Macromolecules* **2005**, *38*, 7540-7545.
30. Braunecker, W. A.; Pintauer, T.; Tsarevsky, N. V.; Kickelbick, G.; Matyjaszewski, K. *J. Organomet. Chem.* **2005**, *690*, 916-924.
31. Chan, T. R.; Hilgraf, R.; Sharpless, K. B.; Fokin, V. V. *Org. Lett.* **2004**, *6*, 2853-2855.
32. Rodionov, V. O.; Fokin, V. V.; Finn, M. G. *Angew. Chem. Int. Ed.* **2005**, *44*, 2-6.

Chapter 12

Polymers with Pendant Allyl Ester Groups Prepared via Atom Transfer Radical Polymerization: Synthesis, Characterization, and Microstructuring of Thin Films

**René Nagelsdiek¹, Petra Mela², Martina Mennicken¹, Helmut Keul¹,
and Martin Möller^{1,2,*}**

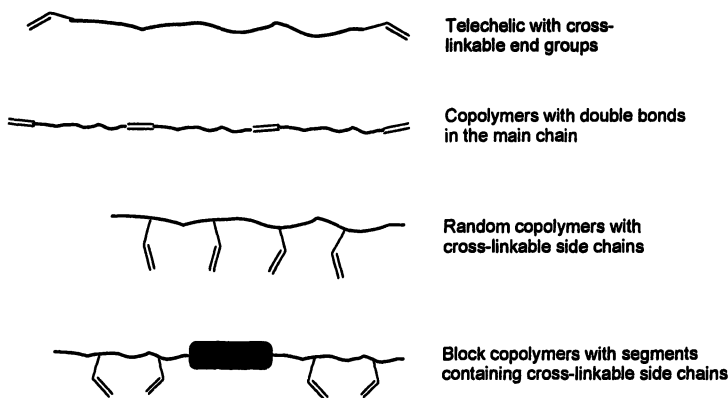
¹Lehrstuhl für Textilchemie und Makromolekulare Chemie der RWTH,
Aachen, Germany

²DWI an der RWTH Aachen e.V. Pauwelsstrasse 8, D-52056 Aachen,
Germany

Random copolymers of styrene (St) and allyl methacrylate (AMA) as well as of methyl methacrylate (MMA), butyl methacrylate (BMA) and AMA were prepared by copolymerization of the mixture of monomers via atom transfer radical polymerization (ATRP). The control of the reaction depends on the monomer conversion, the monomer to initiator ratio and the concentration of AMA in the feed. Block copolymers with a poly(carbonate) - or a poly(phenylene oxide) block and PAMA end blocks were obtained by ATRP of AMA using the macroinitiator technique. All these copolymers with allyl ester side chains are soluble; films were prepared and cross-linking was achieved by irradiation in the presence of suitable photoinitiators. Moreover, microstructuring of polymer layers on solid substrates was achieved by laterally resolved photochemical cross-linking.

Introduction

The prepolymer concept is a widely used concept for the preparation of cross-linked materials. It is characterized by three attributes: (i) Polymerization and cross-linking are independent processing steps; (ii) the prepolymer does not contain toxic monomers and can therefore be handled under less stringent conditions; (iii) properties of the prepolymers such as solubility, glass transition, and viscosity, can be tailored offering potential for applications like coatings, microstructuring, and 3D-lithography (“rapid prototyping”). Cross-linking of prepolymers is frequently achieved by radical addition reactions on double bonds (e.g., alkyd resins or unsaturated polyesters). These double bonds can be terminal double bonds in the prepolymer (telechelic polymer, cf. Scheme 1). However, this approach suffers from the low concentration of double bonds. Alternatively, double bonds can be located in the main chain or in side groups of a polymer chain. These in-chain groups or side groups can either be distributed in the whole polymer chain at random or in distinct sequences (cf. Scheme 1).



Scheme 1: Suitable polymer architectures for prepolymers which can be cross-linked via a radical process.

Allyl ester side groups offer the potential of cross-linking for a variety of polymers. Soluble polymers containing these side groups can be achieved by controlled radical (co)polymerization of allyl methacrylate (AMA) by means of ATRP. In this process, radical polymerization preferentially occurs at the methacrylic double bond whereas the allylic double bond is less reactive (1). Due to the activation/deactivation equilibrium, premature cross-linking processes are prevented up to high conversion if the polymerization is carried out as an ATRP (note that the *free* radical polymerization leads to cross-linking at low conversion) (1). In two recent papers, we reported on the homo- and

copolymerization of AMA (1,2). Although available, the homopolymer of AMA is of minor interest for application since it tends to auto-cross-link in air at room temperature (1,3). "Dilution" of the cross-linkable side groups was achieved by means of copolymerization. These random copolymers of AMA with styrene (St) (1) or methacrylates (2), respectively, can be stored in air without the occurrence of cross-linking. Moreover, copolymerization leads to a variety of copolymers featuring different properties (e.g., glass transition temperature); enclosure of a few mole percent of AMA repeating units into the polymer assures a potential cross-linking at a later stage. However, the atom transfer radical copolymerization of AMA is limited to vinyl comonomers such as acrylates, methacrylates, and styrenes. We considered it to be desirable to extend the "toolbox" of cross-linkable materials to further classes of polymers, in particular high performance polymers (e.g., polycarbonates or poly(phenylene oxides)). These polymers are mainly prepared by polycondensation reactions. Hence, two different polymerization processes are required: (i) polycondensation and (ii) radical polymerization via ATRP. Consequently the macroinitiator approach appeared to be most suitable for this purpose. In this concept, the following steps are performed: (i) Synthesis of a telechelic high performance polymer by polycondensation; (ii) preparation of a bifunctional ATRP macroinitiator by chain analogous reaction of the telechelic polycondensation product (e.g., by esterification); (iii) ATRP of AMA using the bifunctional macroinitiator leading to a triblock copolymer P(AMA)-[polycondensate]-P(AMA). Note that in the latter step, a low monomer/initiator ratio is expected to be sufficient to assure cross-linking on demand.

Experimental Section

Materials and Methods

All chemicals were commercially available and purified according to (1,2). Analytical measurements were performed as described in (1,2).

Procedures

Spin coating: Thin polymer films were created on silicon and TiNi substrates by spin coating a 5 or 10 wt.% solution of the polymer in THF (Convac 1001S/ST 147 spin coater). The polymer solution already contained a certain amount of photoinitiator (P(St-co-AMA): 20 wt.% Irgacure 819, referring to the mass of the polymer; PMMA: 0,2 wt.% DMPAP and addition of 10 wt.% DegDMA). The solution was passed through a syringe filter (Schleicher & Schuell MicroScience, Spartan 13/0.2 RC58, pore diameter 0.2

μm , regenerated cellulose). Spin coating was carried out at a constant rotation speed [5000 rpm for P(St-co-AMA) and 2000 rpm for P(MMA-co-BMA-co-AMA)] for 30-60 s. Coated substrates were stored in the dark.

Microstructuring: Copper Transmission Electron Microscopy (TEM) grids were used as shadow mask for photolithography (Agar Scientific, 400 mesh hexagon, diameter 3.05 mm). Irradiation was done with an Osram Ultra Vitalux 300 W UV lamp. The distance between the sample and the lamp was 10 cm and the exposure time was 3h for P(St-co-AMA) and 2h for P(MMA-co-BMA-co-AMA). After irradiation, the P(St-co-AMA) layers were developed by dissolving the unexposed polymer in cyclohexane for 90 min at room temperature (r.T). The P(MMA-co-BMA-co-AMA) layers were developed in acetonitrile for 24 h at r.T.

Substrates: Silicon wafers (375 μm thick, CrysTek GmbH, Berlin, Germany) were cut into 15x15 mm square pieces. The pieces were cleaned in an ultrasonic bath in acetone, deionized water, and isopropanol, each solvent for two minutes. The TiNi substrates were prepared by sputter deposition (Caesar Research Center, Bonn, Germany) of 1 μm thick $\text{Ti}_{39}\text{Ni}_{43}\text{Hf}_{18}$ layers on single-side polished 500 μm thick silicon wafers. The cleaning was as described for the plain silicon pieces.

Syntheses

Poly(St-co-AMA): (1-Bromoethyl)benzene (0.93 g, 5 mmol), CuBr (0.72 g, 5 mmol), Bpy (1.95 g, 12.5 mmol), St (20.83 g, 200 mmol), and AMA (6.31 g, 50 mmol) were stirred in BuAc (25 mL). The reaction was started by immersion into an oil bath (130 °C). After 5 h the mixture was rapidly cooled to room temperature and quenched by addition of CH_2Cl_2 (20 mL) followed by stirring in air until the copper complex was completely oxidized. The copper complex was removed by filtration and subsequent extraction with 5 % HCl. The polymer was precipitated into methanol. Yield: 14.67 g (52 %), $M_{n,GPC} = 6500$, $M_w/M_n = 1.55$, molar ratio of repeating units: 78:22 (St/AMA).

Poly(MMA-co-BMA-co-AMA): MMA (22.00 g, 220.0 mmol), BMA (13.39 g, 94.3 mmol), and AMA (3.96 g, 31.4 mmol) were dissolved in BuAc (20 mL). FPSC (0.07 g, 0.35 mmol), CuCl (0.07 g, 0.7 mmol), and PMDETA (0.14 g, 0.8 mmol) were added and the reaction medium was stirred for 6 h at 60 °C. The workup procedure was carried out analogously to the styrene copolymer (precipitation in pentane). Yield: 16.16 g (41 %), $M_n = 85100$, $M_w/M_n = 2.10$, molar ratio of repeating units: 62:28:10 (MMA/BMA/AMA).

End-group functionalized PC and PPO: The macroinitiators were prepared according to the literature (4,5). Polymerization of AMA using PC and PPO macroinitiators was carried out in anisole according to the procedure described for random copolymers. Polymerization conditions are listed in Table 1.

Table 1: ATRP of AMA using bifunctional ATRP macroinitiators.

| No | Macroinit. type ($M_{n,NMR}$) in g (mmol) | CuX | Bpy in g (mmol) | AMA | Anisole in mL | T — °C | t — h |
|----|---|---------------|--------------------|---------------|------------------|--------------|-------------|
| 1 | BPA-PC (3000) 1.00 (0.3) | 0.19 (1.3) | 0.52 (3.3) | 0.25 (2.0) | 3 | 90 | 16 |
| 2 | TMC-BP-PC (4300) 2.00 (0.5) | 0.27 (1.9) | 0.73 (4.7) | 0.50 (4.0) | 6 | 90 | 2 |
| 3 | PPO (6000) 1.00 (0.2) | 0.10 (0.7) | 0.26 (1.7) | 0.25 (2.0) | 3 | 90 | 0.8 |
| 4 | PPO (6000) 1.00 (0.2) | 0.10 (0.7) | 0.26 (1.7) | 0.25 (2.0) | 3 | 90 | 0.5 |
| 5 | PPO (6000) 1.00 (0.2) | 0.10 (0.7) | 0.26 (1.7) | 0.25 (2.0) | 3 | 70 | 1.5 |

The polymerization was quenched by addition of CH_2Cl_2 for PC or toluene for PPO. Precipitation was carried out in methanol in all cases. The analytical data are found in table 2.

NMR data: *modified bisphenol A PC*, carbonate repeating unit: $\delta = 1.68$ (s, 6H, CH_3), 7.16 (m, 4H, CHC-O), 7.25 (m, 4H, $\text{CHCC}(\text{CH}_3)_2$) ppm; AMA repeating unit: $\delta = 0.8 - 2.8$ (br, 5H, CH_2 and CH_3 , backbone), 4.3 - 4.7 (br s, 2H, OCH_2), 5.0 - 5.5 (br m, 2H, $\text{OCH}_2\text{CHCH}_2$), 5.7 - 6.1 (br m, 1H, OCH_2CH) ppm.

modified TMC bisphenol PC, carbonate repeating unit: $\delta = 0.34/0.98$ (s, 3H / s, 6H, CH_3), 0.87/1.37 (d, $^3J \approx 12$ Hz, 2H, CH_2CHCH_3 ax and eq), 1.16 (m, 1H, CHCH_3), 1.8 - 2.1 (complex, 2H, $\text{CH}_2\text{C}(\text{CH}_3)_2$), 2.44/2.66 (d, $^3J = 13.2$ Hz, 1H / d, $^3J = 13.2$ Hz, 1H, $\text{CH}(\text{CH}_3)\text{CH}_2\text{C}(\text{CH}_3)_2$ ax and eq), 6.6 - 7.5 (complex, 8H, H_{aromatic}) ppm; AMA repeating unit: $\delta = 0.8 - 2.8$ (br, 5H, CH_2 and CH_3 , backbone), 4.3 - 4.7 (br s, 2H, OCH_2), 5.1 - 5.5 (br m, 2H, $\text{OCH}_2\text{CHCH}_2$), 5.7 - 6.1 (br m, 1H, OCH_2CH) ppm.

modified PPO, phenylene oxide repeating unit: $\delta = 2.09$ (s, 6H, CH₃), 6.47 (s, 2H, CH) ppm; AMA repeating unit: $\delta = 0.7 - 2.4$ (br, 5H, CH₂ and CH₃, backbone), 4.3 – 4.7 (br s, 2H, OCH₂), 5.1 – 5.5 (br m, 2H, OCH₂CHCH₂), 5.8 – 6.1 (br m, 1H, OCH₂CH) ppm.

Table 2: Results of the polymerization reactions presented in Table 1.

| No. | Macroinit. $M_{n,GPC}$ (M_w/M_n) | Product $M_{n,GPC}$ (M_w/M_n) | Yield in g | Mol ratio of RU of initial block and AMA | Average number of AMA-RU per chain end |
|-----|--|---|---------------|--|--|
| 1 | 4400 (1.60) | 5400 (1.15) | 0.56 | 72 : 28 | 2.4 |
| 2 | 4500 (1.31) | 5000 (1.69) | 1.68 | 66 : 34 | 3.0 |
| 3 | 7800 (1.62) | cross- linked | -- | -- | -- |
| 4 | 7800 (1.62) | 16500 (4.22) | 0.83 | 87 : 13 | 3.4 |
| 5 | 7800 (1.62) | 12500 (2.11) | 0.83 | 89 : 11 | 2.7 |

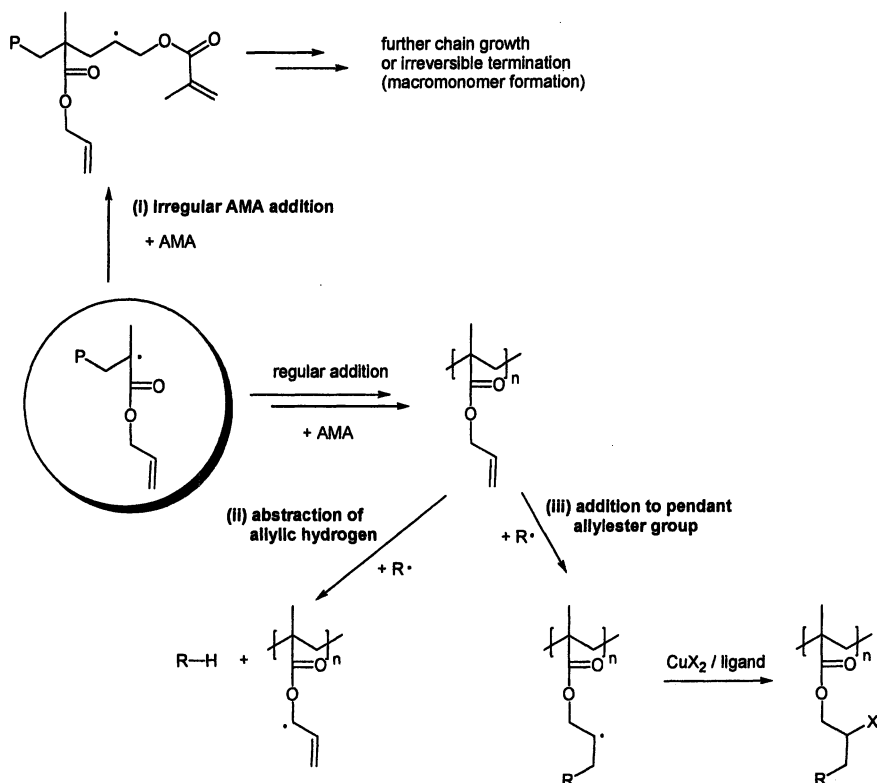
Results and Discussion

Random Copolymers

In contrast to other monomers (e.g., MMA), in the atom transfer radical polymerization and copolymerization of AMA, side reactions have to be taken into consideration. Beside regular chain growth, the following reactions are discussed (cf. Scheme 2):

(i) The allyl group of an AMA monomer is added to the active chain end resulting in a methacrylic side group. (ii) A hydrogen atom of the allyl side group in the copolymer is transferred from the allyl position to the radical chain end leading to chain termination (the allyl radical formed is not reactive enough to continue chain growth). (iii) The radical chain end is added to the allyl ester side group of the polymer resulting in an additional branch; in free radical polymerization, this reaction results in cross-linking, whereas the radical species formed is terminated irreversibly in an ATRP. The importance of these and other side reactions depending on conversion and monomer/initiator ratio are discussed elsewhere (1). Side reactions become less significant if the

AMA/comonomer ratio is decreased. A kinetic investigation of the ATRP of a 20/80 mixture of AMA and styrene using (1-bromoethyl)benzene as the initiator and CuBr/Bpy as the catalyst at 130°C exhibit linear semilogarithmic plots up to ca. 70% overall conversion for both monomers (cf. Figure 1a).



Scheme 2: Proposed side reactions in the atom transfer radical polymerization in the presence of AMA under participation of the allyl ester groups.

The increase of M_n with conversion shows a linear dependence although values are slightly higher than expected at low conversion. This was attributed to the preferential incorporation of AMA during early stages of the polymerization and the higher mass of the AMA repeating unit compared to the St repeating unit. However, reactivity ratios of St and AMA were not determined. The controlled nature of the polymerization process was indicated

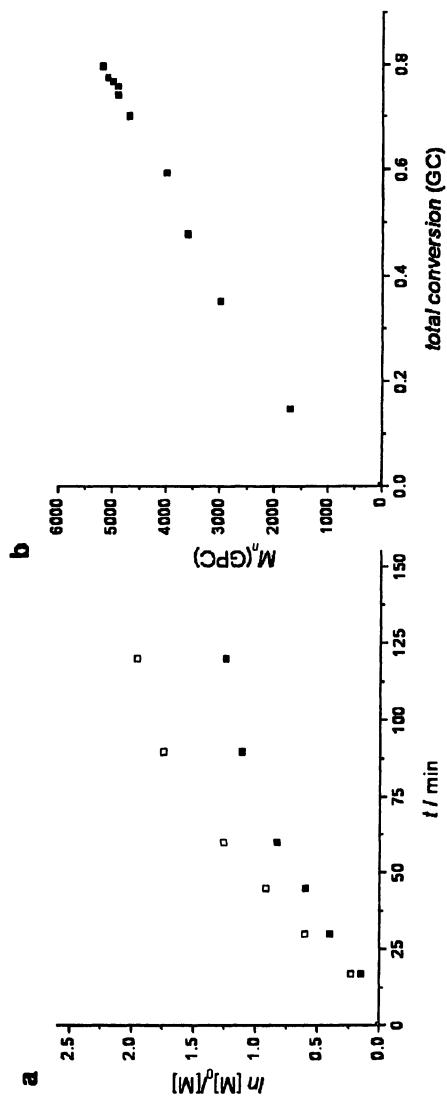


Figure 1: Copolymerization of a 80/20 mixture of styrene (St) and allyl methacrylate (AMA) using the system (1-bromoethyl)benzene, CuBr/2,2'-bipyridine in *n*-butyl acetate at 130 °C. ($[St]_0/[AMA]_0/[I]_0 = 40:10:1$). (a) First order plots (closed boxes represent values for St, open boxes for AMA); (b) molecular weight as a function of total monomer conversion.

by monomodal molecular weight distributions for all experimental points presented in Figure 1 ($M_w/M_n < 1.37$).

P(St-co-AMA) can be cross-linked “on demand” using initiators such as 2,2'-azobis(2-methylpropionitrile) (AIBN) or bis(2,4,6-trimethylbenzoyl)-phenyl-phosphine oxide (Irgacure 819) as reported earlier (1). In further studies, it turned out that in photochemical cross-linking, the extent of cross-linked material can be greatly increased upon addition of a small amount of a low molecular weight cross-linking agent, e.g., diethyleneglycol dimethacrylate (DegDMA):

Results found for P(St-co-AMA) containing 10 mole% of AMA repeating units are presented in Figure 2. It is obvious that at the same concentration of DegDMA (including the absence of DegDMA) an increase on the concentration of the photoinitiator from 1 to 10 wt.% leads to an increase of cross-linked material. However, at the same concentration of photoinitiator, the situation is different below 1 wt.% DegDMA and above this concentration. It must therefore be concluded that a low concentration of photoinitiator is the limiting parameter for the amount of cross-linking reaction.

For P(MMA-co-BMA-co-AMA) the same tendencies during cross-linking were observed (2).

Block Copolymers

Polycondensation processes yielding high performance materials frequently involve reactive monomers with nucleophilic functional groups (e.g., OH or NH_2) and electrophilic functional groups (e.g., $-\text{COOR}$, $-\text{COCl}$, $-\text{NCO}$, $-\text{OCOC}$). Under suitable reaction conditions, amino or hydroxy telechelics are obtained. These telechelics can readily be converted into macroinitiators by amidation or esterification (6) using suitable acid halides such as 2-bromoisobutyryl bromide or α -chlorophenylacetyl chloride. In the present paper, the corresponding macroinitiators were applied for the ATRP of AMA yielding cross-linkable polycondensation products (cf. Scheme 3).

Only a few AMA repeating units at each chain end are expected to be sufficient to achieve a cross-linkable polycondensation product. Therefore, the structures ought not to be termed as “block copolymers” but instead be referred to as chain end functionalized or modified polymers, i.e., the properties of the polycondensation product are not changed significantly.

In our group, recent focus was laid on the preparation of polycarbonate (PC) (4) and polyphenylene oxide (PPO) (5) macroinitiators. Hydroxy telechelic bisphenol A polycarbonate was prepared by melt polycondensation of bisphenol A and diphenyl carbonate using $\text{La}(\text{acac})_3$ as transesterification catalyst (4). Analogously, hydroxy telechelic TMC bisphenol polycarbonate was achieved

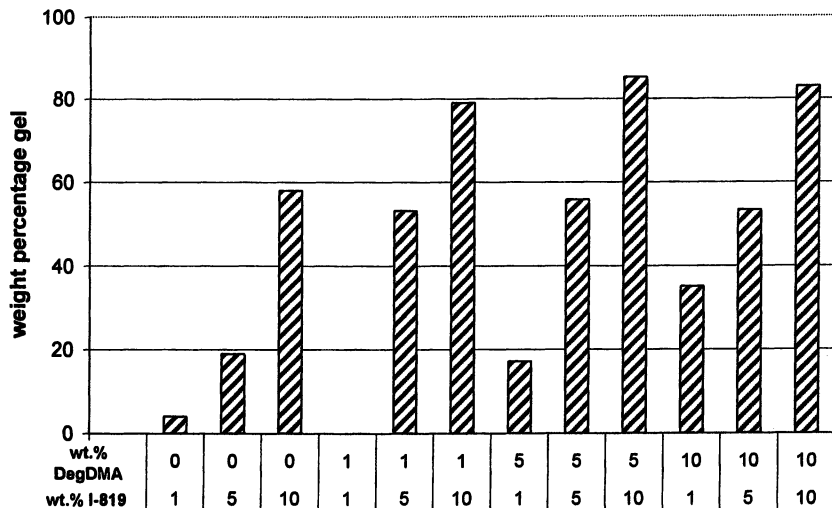
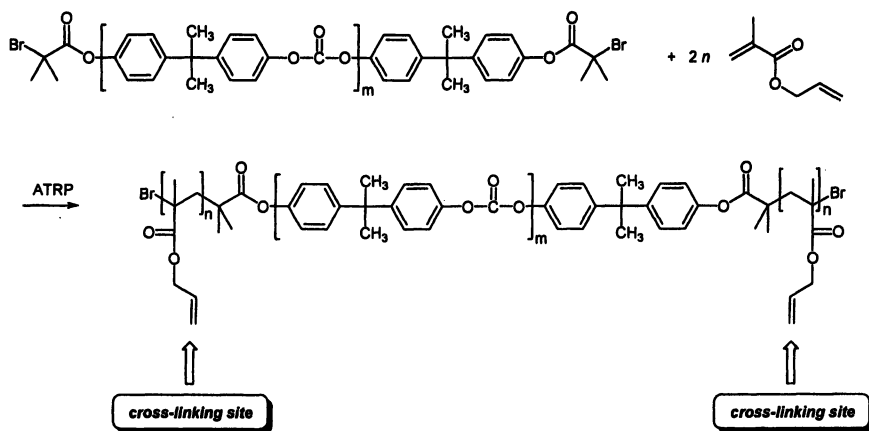


Figure 2: Photochemical cross-linking of *P*(St-co-AMA) (10 mol% AMA repeating units) using variable concentrations of photoinitiator (Irgacure 819) and a low molecular weight cross-linking agent (DegDMA), irradiation time: 3 h; the weight percent of gel is referred to the total mass of the prepolymer photoinitiator and DegDMA.



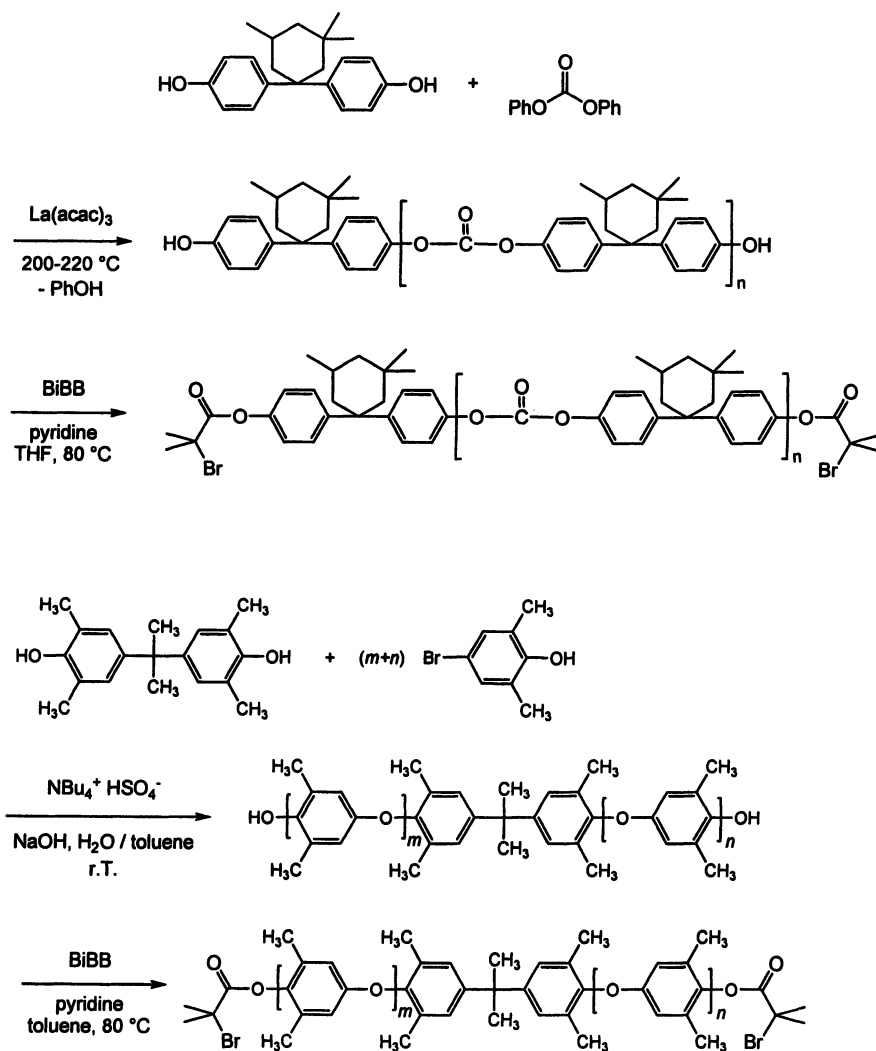
Scheme 3: Concept for the preparation of prepolymers with allyl ester side groups via macroinitiators.

from diphenyl carbonate and TMC bisphenol (3,3,5-trimethylcyclohexyl bisphenol, (cf. Scheme 4, top); TMC bisphenol units cause a significant increase of the glass transition temperature compared to bisphenol A polycarbonate (7,8). The hydroxy telechelic polycarbonates were then converted into bifunctional ATRP macroinitiators by esterification with 2-bromoisobutyryl bromide (BiBB). Bifunctional hydroxy telechelic PPO was prepared by phase transfer catalyzed oxidative coupling of 4-bromo-2,6-dimethylphenol based on a procedure reported by Percec (cf. Scheme 4, bottom) (9,10). According to the literature (5), the PPO was esterified using BiBB to yield a bifunctional macroinitiator.

BPA and TMC-BP Polycarbonate with AMA End Groups

Due to the good solubility of BPA polycarbonate in many organic solvents, we started our investigation of the ATRP of AMA using a BPA-PC macroinitiator. To prevent premature cross-linking, Bpy was employed as the ligand and the reaction was carried out at mild conditions (16 h at 90 °C in anisole). According to ^1H NMR spectroscopy, the macroinitiator employed had an M_n of ca. 3000. Compared to the mass of the macroinitiator, 25 wt.% AMA were used for the polymerization reaction. The presence of AMA repeating units in the product is proven by the ^1H NMR spectrum. The ratio of repeating units was determined by comparison of the integrals of the aromatic protons of the carbonate repeating units (6.5 – 7.6 ppm) and the $-\text{CH}=\text{CH}_2$ proton of the allyl group (5.7 – 6.1 ppm). From these integrals, a molar ratio of 72:28 of carbonate/AMA repeating units was calculated. The average number of AMA repeating units per chain end is thus 2.4. GPC reveals a bimodal molecular weight distribution indicating branching reactions during polymerization (reactant: $M_n = 4400$, $M_w/M_n = 1.60$; product: $M_n = 5400$, $M_w/M_n = 2.13$).

The obtained end group functionalized BPA-PC was cross-linked photochemically. Therefore, polymer and photoinitiator were dissolved in CH_2Cl_2 and - after evaporation of the solvent - the film prepared was irradiated for 9 h at a distance of 10 cm between the UV lamp and the sample. Since BPA polycarbonate repeating units contain aromatic groups and hence show significant UV absorption, Irgacure 819 was used as the photoinitiator analogously to the styrene copolymers. To assure a sufficient generation of radicals, 20 wt.% of initiator were used referring to the polymer mass (for technical application, this amount should be reduced). Furthermore the influence of a low-molecular weight cross-linking agent (DegDMA) on the extent of the cross-linking reaction was investigated. It turned out that the addition of



Scheme 4: Preparation of bifunctional ATRP macroinitiators based on TMC bisphenol polycarbonate (top) and poly(phenylene oxide) (bottom) [acac = acetyl acetate, BiBB = 2-bromoisobutryl bromide].

DegDMA is not necessary to obtain a nearly quantitative degree of cross-linking (degrees of cross-linking higher than 90 % were obtained in all cases), most probably due to the high concentration of photoinitiator. It is remarkable that only 2-3 AMA repeating units are sufficient to obtain nearly quantitative cross-linking. To assure that cross-linking is really attributed to the presence of AMA repeating units (and not by a reaction at the PC aryl units caused by UV radiation) the PC macroinitiator (without AMA units) was treated under the same conditions. Cross-linked product was not formed under these conditions.

Moreover, we compared the thermal properties of the end group functionalized BPA polycarbonate before and after cross-linking. Before cross-linking, the T_g of the polymer is 98 °C. This is remarkably lower than the literature value of BPA-PC (ca. 150 °C) which was attributed to the following: (i) presence of the short PAMA segments (partial miscibility appears possible); (ii) residual amounts of the photoinitiator (plasticizer effect); (iii) most important, the low degree of polymerization of the polycarbonate reduces its T_g . After cross-linking, T_g rises to 148 °C (i.e., literature value) because the molecular weight is now significantly increased. DSC reveals still a sharp glass transition of the cross-linked material (and no broadening) which was attributed to the low cross-linking density with the PC segments working as spacers between the cross-linking sites.

Due to the successful application of the AMA end group concept to bisphenol A polycarbonate, we decided to apply the analogous strategy to TMC bisphenol polycarbonate. The polycarbonate used had a M_n of 4300 (NMR). Again, polymerization was carried out using 25 wt.% AMA (referring to the mass of the macroinitiator) in anisole at 90 °C (catalyst: CuBr/Bpy, $t = 2$ h). The ratio of repeating units in the copolymer obtained is 66:34 (carbonate to AMA, according to ^1H NMR), i.e., 3.0 repeating units of AMA are attached to each chain end on average. The GPC curve of the product is multimodal (reactant: $M_n = 4500$, $M_w/M_n = 1.31$; product: $M_n = 5000$, $M_w/M_n = 1.69$) as a result of branching reactions.

Photochemical cross-linking was carried out analogously to the procedure described before. Two parameters were varied: the amount of DegDMA added (0, 5, and 10 wt.%); in the absence of DegDMA, the concentration of photoinitiator was varied to investigate whether a lower amount of initiator is still sufficient.

Figure 3 reveals the following trends: (i) cross-linking of functionalized TMC-BP polycarbonate is obviously less efficient than the one of functionalized BPC polycarbonate, although the number of AMA repeating units at the chain ends is similar. (ii) To obtain a high amount of cross-linked product, a high concentration of photoinitiator is required. The amount of cross-linked material exceeds 60 % only if 20 wt.% of photoinitiator is added. At the same initiator concentration, the cross-linked product was raised to 74 % by addition of 5 wt.% of DegDMA. A further increase of the DegDMA concentration does not result

in a significant increase of cross-linked material (77 % insoluble product using 10 wt.% DegDMA).

As in the case of BPA polycarbonate, the glass transition temperature of the modified TMC bisphenol polycarbonate increased upon cross-linking, although less pronounced (before cross-linking: 161 °C, afterwards: 172 °C).

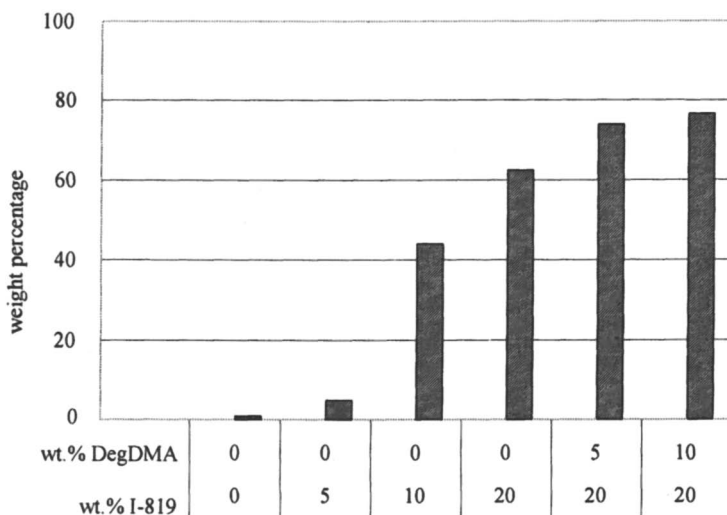


Figure 3: Photochemical cross-linking of end-group modified TMC bisphenol PC using variable amounts of photoinitiator (Irgacure 819) and DegDMA; the weight amounts are referred to the total mass of the prepolymer reactant and DegDMA.

PPO with AMA End Groups

Investigations were carried out using a bifunctional PPO macroinitiator ($M_{n,NMR}=6000$). Reaction conditions of the AMA polymerization were analogous to the conditions described for polycarbonates (CuBr/Bpy, 90 °C, anisole, 25 wt.% of AMA referring to the initiator mass). Gelation was observed after only 50 min (cf. Table 1 and 2, entry 3).

Obviously, the tendency towards cross-linking is increased in the presence of PPO segments. The reasons for that are found in hydrogen abstraction at the methyl group of the dimethylphenylene oxide repeating unit and in radical combination (basically these observations coincide well with results reported for atom transfer radical coupling of polymers containing PPO segments (11)). To prevent premature cross-linking, two variations of the polymerization procedure

were carried out: (i) decrease of the polymerization time (cf. Table 1, entry 4) and (ii) a lower polymerization temperature (Table 1, entry 5).

When the reaction was quenched after 30 min (Tables 1 and 2, entry 4), a soluble product was obtained with a molar phenylene oxide/AMA ratio of 87:13 (NMR), i.e., 3.4 AMA repeating units are located at each chain end. The polymerization is accompanied by branching reactions (a preliminary step to the gelation observed after 50 min) as indicated by the multimodal molecular weight distribution of the product and a significant increase of the M_n in comparison to the macroinitiator used (reactant: $M_n = 7800$, $M_w/M_n = 1.62$; product: $M_n = 16500$, $M_w/M_n = 4.22$). In an alternative experiment, the polymerization temperature was decreased from 90 °C to 70 °C (entry 3) while the reaction was carried out under analogous conditions for 90 min. The composition of the product is similar to the one obtained at 90 °C/30 min: The molar ratio of phenylene oxide to AMA is 89:11 (i.e., 2.7 AMA repeating units at each chain end). However, GPC reveals that cross-linking is less significant in this case than at 90 °C: The weight distribution remains monomodal even though slightly broadened if compared to the macroinitiator (reactant: $M_n = 7800$, $M_w/M_n = 1.62$; product: $M_n = 12500$, $M_w/M_n = 2.11$). The product obtained at 70 °C is more comparable to the modified polycarbonates described before. It was therefore used for further investigation.

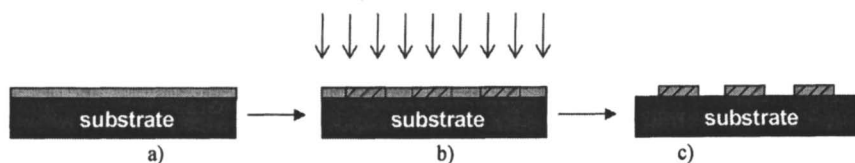
Photochemical cross-linking of end-group modified PPO was carried out on films prepared from a solution of the polymer and of Irgacure 819 (20 wt.% referring to the polymer) in $\text{CH}_2\text{Cl}_2/\text{CHCl}_3$ (1:1 v/v). Irradiation was carried out for 9 h at a distance of 10 cm between the UV lamp and the sample. Even if DegDMA was not added to the sample, the polymer was quantitatively reacted to an insoluble product. In contrast to similar reactions involving the polycarbonates (vide supra), a change in color was observed (reactant: bright yellow, most likely the color of the photoinitiator; product: dark brown). This is an indication for reactions at the aromatic rings. This assumption is supported by DSC measurements: In contrast to the modified polycarbonates, the T_g of the modified PPO did not increase upon cross-linking, but decreases from 199 °C to 180 °C. This is explained by the formation of branched structures and the addition of flexible groups by radical reactions at the PPO repeating units.

In a control experiment, the procedure was carried out using the pure PPO macroinitiator (irradiation of a PPO film using 20 wt.% Irgacure 819 in the absence of AMA repeating units). The reaction was carried out both in the absence and presence of 5 and 10 wt.% DegDMA. The formation of cross-linked product was not observed. However, the color changed into brownish upon irradiation as well. The product obtained was investigated by means of GPC. An increase in molecular weight and polydispersity was detected in all cases, indicating branching reactions caused by radical attacks at the PPO repeating units (reactant macroinitiator: $M_w = 12700$, $M_w/M_n = 1.61$; product obtained after 9 h irradiation without addition of DegDMA: $M_w = 20000$, $M_w/M_n = 2.63$).

The described procedure is not limited to PC or PPO structures. The concept can easily be transferred to a wide variety of polymers, e.g., polyethylene oxide, polypropylene oxide, poly(tetrahydrofuran), polysulfones, polyethersulfones, polyesters, polysiloxanes, polyamides, polyimides, and polyetherketones. Thus, a whole tool box of cross-linkable materials is now accessible. Transfer to new polymer classes is only limited by the availability of appropriate macroinitiators which might be affected by solubility issues. However, in the case of polyethylene oxide (8), poly(tetrahydrofuran) (9), polysulfones (2), and polysiloxanes (10), macroinitiators are readily available according to the literature.

Microstructuring of Polymer Films by means of Photolithography

Microstructuring of polymer layers on solid substrates was achieved by laterally resolved photochemical modification of the layers. The polymer layer functions as a negative resist (Scheme 5).



Scheme 5: Microstructuring of a prepolymer layer by means of photolithography: a) spincoating of the layer on the substrate; b) UV irradiation through a mask; c) resist development.

Irradiation of the layers with UV light through a lithography mask results in the cross-linking of the polymer in the exposed areas. By subsequently placing the substrate in a solvent able to dissolve the non cross-linked polymer (resist development), only the UV exposed polymer pattern is left on the substrate. In order to prevent swelling of the cross-linked material during development, a theta solvent should be used.

Microstructuring experiments were performed with P(St-co-AMA) and P(MMA-co-BMA-co-AMA) layers on silicon and Titanium-Nickel alloy substrates. Cross-linking of both polymers was supported by addition of photoinitiators and cross-linking agents: 20 wt.% Irgacure 819 was added to P(St-co-AMA), 0.2 wt.% DMPAP and 10 wt.% DegDMA were added to P(MMA-co-BMA-co-AMA).

TEM grids with hexagonal holes were positioned on the spincoated polymer layers to act as a shadow mask during the irradiation step. Figure 4 shows the result of the photolithographic patterning of a (MMA-co-BMA-co-

AMA) layer. The hexagonally shaped areas represent the exposed polymer left on the surface after resist development in acetonitrile. The areas in between are bare TiNi substrate. The dimensions of the obtained polymer structures are in good agreement with the pattern on the TEM grid. Similar results were obtained on silicon substrates and with P(St-co-AMA).

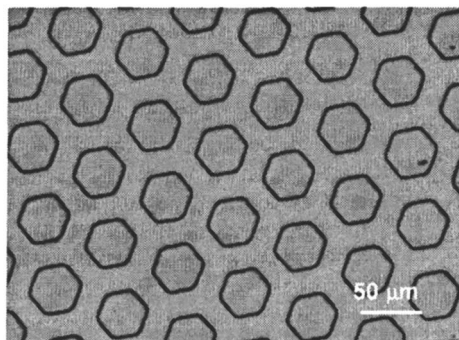


Figure 4: Microstructured P(MMA-co-BMA-co-AMA) polymer layer (molar ratio MMA:BMA:AMA = 62:28:10) on a TiNi substrate. After irradiation for 2 h, the non cross-linked polymer was removed using acetonitrile (24 h at r.T.).

Conclusions

A new approach to cross-linkable polymers by atom transfer radical copolymerization of AMA was reported. Tailored prepolymers containing AMA repeating units were prepared by two concepts: (i) random copolymerization of AMA and a vinyl comonomer (styrene or methacrylates), (ii) ATRP of AMA using a macroinitiator. The latter approach offers the potential for a whole range of prepolymers starting from hydroxy or amino telechelic polycondensation products (e.g., high performance materials). Random copolymers with allyl ester side groups were successfully used for thin film microstructuring. The presented prepolymers therefore represent a novel class of photoresists for photolithography and 3D-lithography.

The results presented in this report complement earlier research on functional well defined polymers prepared via Atom Transfer Radical Polymerization (15-17).

Acknowledgements

The authors would like to thank Dr. G. Schmidt/Ciba Specialty Chemicals for the donation of Irgacure photoinitiators. Financial support of the Center of

Advanced European Studies and Research (caesar) and of the Fonds der Chemischen Industrie is gratefully acknowledged.

References

1. Nagelsdiek, R.; Mennicken, M.; Maier, B.; Keul, H.; Höcker, H. *Macromolecules* **2004**, *37*, 8923-8932.
2. Mennicken, M.; Nagelsdiek, R.; Keul, H.; Höcker, H. *Macromol. Chem. Phys.* **2004**, *205*, 2429-2437.
3. D'Alelio, G. F.; Hoffend, T. R. *J. Polym. Sci., Part A: Polym. Chem.* **1967**, *5*, 323-337.
4. Mennicken, M.; Nagelsdiek, R.; Keul, H.; Höcker, H. *Macromol. Chem. Phys.* **2004**, *205*, 143-153.
5. Nagelsdiek, R.; Keul, H.; Höcker, H. *Polymer Intern.*, **2006**, *55*, 108-117.
6. Gaynor, S. G.; Matyjaszewski K. *Macromolecules* **1997**, *30*, 4241-4245.
7. Freitag D; Westeppe U. *Macromol. Chem., Rapid Commun.* **1991**, *12*, 95-99.
8. Kämpf G.; Freitag D.; Fengler, G. *Kunststoffe* **1992**, *82*, 385.
9. Percec, V.; Wang, J. H. *Polymer Bull.* **1990**, *24*, 493-500.
10. Percec, V.; Shaffer, T.D.; *J. Polym. Sci., Part C* **1986**, *24*, 439.
11. Nagelsdiek, R.; Keul, H.; Höcker, H. *e-Polymers* **2005**, no. 049.
12. Reining, B.; Keul, H.; Höcker, H. *Polymer* **1999**, *40*, 3555-3563.
13. Matyjaszewski, K.; Coessens, V.; Nakagawa, Y.; Xia, J.; Qiu, J.; Gaynor, S.; Coca, S.; Jasieczek, C. In: *Functional Polymers - Modern Synthetic Methods and Novel Structures*; Patil, A. O.; Schulz, D. N.; Novak, B. M., Eds.; ACS Symposium Series 704, Washington 1997; p 16 ff.
14. Huan, K.; Bes, L.; Haddleton, D. M.; Khoshdel, E. *J. Polym. Sci., Part A: Polym. Chem.* **2001**, *39*, 1833-1842.
15. Coca, S.; Matyjaszewski, K. *ACS Polym. Preprints*, **1997**, *38* (1), 691.
16. Nakagawa, Y.; Matyjaszewski, K. *Polymer J.*, **1998**, *30*, 138.
17. Pintauer, T.; Coessens, V.; Matyjaszewski, K. *Progr. Polym. Sci.* **2001**, *26*, 337.

Chapter 13

Controlled Radical Polymerization of 1-Ethoxyethyl (Meth)acrylate: Novel Route for the Synthesis of Poly((meth)acrylic acid) Containing Polymer Structures

Wim Van Camp and Filip E. Du Prez*

Polymer Chemistry Research Group, Department of Organic Chemistry,
Ghent University, Krijgslaan 281 S4 bis, B-9000 Gent, Belgium

*Corresponding author: web: www.filipduprez.com;
email: Filip.DuPrez@UGent.be

The polymerization of 1-ethoxyethyl methacrylate (EEMA) and 1-ethoxyethyl acrylate (EEA) by controlled radical polymerization techniques (ATRP and RAFT) is described, resulting in polymers with a good control of average molar mass (M_n) and narrow molecular weight distribution. These polymers are novel precursors for poly(methacrylic acid) and poly(acrylic acid), respectively. The polyacids can be obtained by a simple heating step in bulk or in solution at temperatures between 80 and 160 °C, which is a significant advantage compared to other existing precursor routes. Using this strategy, a wide variety of poly((meth)acrylic acid) containing polymer structures were prepared in a straightforward way. In the case of the RAFT-procedure, a high-throughput automated synthesizer was used to optimize the reaction conditions.

Introduction

Poly((meth)acrylic acid) polymers are of vast interest for a wide range of applications, because of their pH-responsive nature and hydrophilic characteristics, and for their interaction with metal ions (1,2). For a lot of applications where these poly((meth)acrylic acid) containing copolymers are used, such as emulsifiers, stabilizers, surfactants and wetting agents, it is of great importance that these polymers can be synthesized with good control over the molar mass and polydispersity. To incorporate poly((meth)acrylic acid (P(M)AA) in well-defined copolymer structures, controlled polymerization techniques have to be applied. Traditional polymerization routes toward such polymers include living anionic (3) and group-transfer polymerization (4), both operating using protected analogues of the (meth)acrylic acid monomers.

Recently, controlled radical polymerization routes have been applied for the synthesis of acrylic acid containing polymers (2). Rizzardo *et al.* reported in 1998 the controlled polymerization of acrylic acid (AA) via reversible addition-fragmentation transfer (RAFT) (5). Charleux *et al.* reported the first nitroxide-mediated polymerization (NMP) of AA in 2003 (6). Even though with these two techniques it is possible to directly polymerize AA, their practicability for the synthesis of (block) copolymers with a variety of apolar monomers is strongly limited because polar polymerization conditions are needed. Thus, P(M)AA containing copolymers with a wide range of apolar segments cannot be synthesized in a straightforward manner.

To overcome this incompatibility, protected analogues such as *tert*-butyl (meth)acrylate (7,8,9,10) or benzyl (meth)acrylate (9,10,11) are often used. However, this strategy requires not only a postpolymerization deprotection step (by hydrolysis or debenzilation, respectively) but also subsequent purification to obtain the desired P(M)AA containing copolymer. In addition, quantitative deprotection is not always possible; e.g. (benzyl methacrylate)-rich polymers cannot be debenzylated completely, and catalyst residues limit the utility (11).

To avoid this additional purification step, we report here on the use of 1-ethoxyethyl as the protecting group for (meth)acrylic acid. In this case, deprotection is easily carried out by thermolysis, with the loss of ethyl vinyl ether (boiling point: 33 °C) as a gas, preventing the need of an additional purification step after deprotection.

To illustrate the workability of the use of the 1-ethoxyethyl protecting group, 1-ethoxyethyl acrylate (EEA) and 1-ethoxyethyl methacrylate (EEMA) were polymerized using the ATRP and RAFT polymerization process. Homopolymers of EEA and EEMA as well as a wide variety of PEE(M)A containing (block) copolymers have been synthesized, leading to well-defined P(M)AA (co)polymers after deprotection by a heating step.

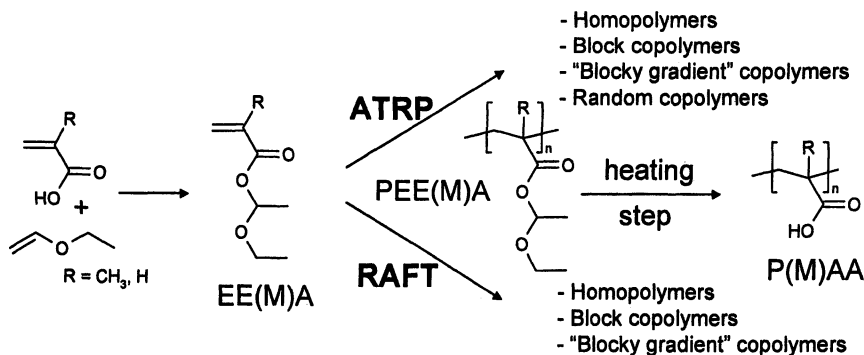


Figure 1. Synthesis of EE(M)A, controlled radical polymerization to PEE(M)A, and subsequent deprotection to P(M)AA by a heating step.

This manuscript aims to highlight the most important results of recently published papers describing this new strategy (12,13), as well as to further illustrate the versatility of this new approach with additional data. An overview of all results is given in Figure 1.

Experimental Part

Materials

1-ethoxyethyl (meth)acrylate (EE(M)A) was synthesized according to a literature procedure (14). *Tert*-butyl acrylate (tBA, Aldrich, 99 %), *n*-butyl acrylate (nBA, Aldrich, 99+%) and the ligand N,N,N',N'',N'''-pentamethyldiethylenetriamine (PMDETA, Aldrich, 99%) were distilled under vacuum prior to use. The initiator, methyl 2-bromopropionate (MBP, Aldrich, 98 %), was used as received. Cu(I)Br (Aldrich, 98%) was purified according to a literature procedure (15). The aluminium oxides (activated neutral and basic Brockmann, Aldrich) and all other reagents were used without further purification. Azobisisobutyronitrile (AIBN, Aldrich) was recrystallized from methanol. 2-Cyano-2-butyl dithiobenzoate (CBDB) was prepared according to a literature procedure for a related compound (16).

Instrumentation

Different size exclusion chromatography (SEC) systems were used. System 1 works in CHCl_3 at 35°C with a $1.5 \text{ mL}\cdot\text{min}^{-1}$ flow rate. The apparatus consists of a manual injector (Rheodyme, $20\mu\text{L}$ loop), an isocratic pump (Waters 1515), 3 linear columns (Waters: HR3, HR4 and HR5 10^3 -, 10^4 - and 10^5 -Å) and a RI detector (Waters 2410), and was calibrated with polystyrene standards. Breeze software (Waters) was used. System 2 is a Shimadzu system equipped with a SCK-10A system controller, a LC-10AD pump, a RID-10A RI detector and a PL gel $5 \mu\text{m}$ Mixed-D column at 50°C utilizing a $\text{CHCl}_3/\text{NET}_3/\text{iPrOH}$ (94/4/2) mixture as eluent (flow rate: $1 \text{ mL}\cdot\text{min}^{-1}$) and calibrated with poly(methyl methacrylate) (PMMA) standards. System 3 is a Waters system with a 1515 pump, a 2414 RI detector and a Waters Styragel HT4 column utilizing *N,N*-dimethylformamide with $5\cdot 10^{-3} \text{ M}$ NH_4PF_6 as eluent at a flow rate of $0.5 \text{ mL}\cdot\text{min}^{-1}$ at 50°C , calibrated with PMMA standards.

RAFT polymerizations were carried out using a Chemspeed AcceleratorTM SLT100 automated synthesizer (13).

Thermogravimetric analysis (TGA) was performed with a PL-TGA (PL-TG 1000, Polymer Laboratories) under N_2 atmosphere (heating rate: $10^\circ\text{C}\cdot\text{min}^{-1}$).

Conversions were determined by ^1H NMR spectroscopy on a Bruker Avance 300 spectrometer, and were measured in CDCl_3 at room temperature.

Polymerization procedures

A typical ATRP (block) copolymerization procedure (e.g. Table I, entry 3) is as follows. The PnBA_{15} macroinitiator was prepared by ATRP of nBA in a similar procedure as described for the homopolymerization of EEA in reference 12 with Cu(I)Br , PMDETA as the ligand and MBP as the initiator, in bulk, with $[\text{nBA}]/[\text{MBP}]/[\text{Cu(I)Br}]/[\text{PMDETA}] = 50/1/1/1$. The monomer EEA was passed through a small column of basic alumina to remove traces of residual acid. The PnBA_{15} macroinitiator (1.0 g; 0.526 mmol;) was dissolved in the monomer EEA (3.79 ml; 0.0263 mol). The mixture was degassed by bubbling with N_2 for 1h. Cu(I)Br (0.0755 g; 0.526 mmol) was added and the flask was immersed in a water bath at 50°C . The polymerization was started by adding ligand PMDETA (0.110 ml; 0.526 mmol). After termination in liquid nitrogen, the block copolymers were dissolved in THF, and passed through a column with neutral alumina to remove copper. The solvent and monomer were removed under high vacuum. In the case of sequential monomer addition, a homopolymerization was started, and a second monomer was added at the chosen time. For random copolymers, the same procedure was followed as for the homopolymers. For the procedure for the RAFT experiments, we refer to reference 13.

Table I. Conditions and Results for the Synthesis of PEE(M)A Containing Polymer Structures by ATRP.

| Macro-initiator strategy | | | | | | | | | |
|---|--|------------------------------------|----------------------|--|--------------------------------|--------------------------------|--|---|------------------|
| Entry | Initiator (In.) | M_n^a In. (g.mol ⁻¹) | PDI ^r In. | [M] ₀ : [In] ₀ : [PMDETA]: [CuBr] ₀ | Temp. (°C) | Time (min) | Conv. (%) | M_n^a (g.mol ⁻¹) | PDI ^r |
| 1 ^{b,c} | PMMA ₇₁ | 8900 | 1.10 | 150:1:0.5:1 | 50 | 120 | 34 | 18600 | 1.19 |
| 2 ^d | PS ₂₁ | 2100 | 1.11 | 50:1:1:1 | 50 | 240 | 71 | 6350 | 1.28 |
| 3 ^d | PnBA ₁₅ | 1900 | 1.14 | 50:1:1:1 | 50 | 240 | 76 | 6600 | 1.18 |
| 4 ^d | PnBA ₁₅ | 1900 | 1.14 | 50:1:1:1 | 60 | 180 | 77 | 6700 | 1.26 |
| 5 ^e | PEEA ₇ | 900 | 1.13 | 50:1:1:1 | 50 | 300 | 42 | 2900 | 1.14 |
| Combination with other controlled polymerization technique: CROP of THF | | | | | | | | | |
| 6 ^d | PTHF ₆₈ | 5200 | 1.21 | 150:1:1:1 | 50 | 150 | 25 | 17400 | 1.12 |
| 7 ^d | PTHF ₄₂ | 3300 | 1.17 | 50:1:1:1 | 50 | 120 | 74 | 11500 | 1.15 |
| Sequential monomer addition | | | | | | | | | |
| Entry | [M] ₁ ₀ : [MBP] ₀ : [PMDETA]: [CuBr] ₀ | Temp. (°C) | Time (min) | DP _n ^h 2 nd block ^g | Total Time (min) | M_n^a (g.mol ⁻¹) | PDI ^r | Final composition ^h | |
| 8 ^f | 20:1:1:1 | 50 | 30 | 20 | 150 | 4600 | 1.12 | PtBA ₁₀ /PtBA ₆ /PEEA ₁₇ | |
| 9 | 20:1:1:1 | 50 | 40 | 20 | 240 | 4800 | 1.18 | PEEA ₁₂ /PEEA ₃ /PtBA ₁₉ | |
| Random copolymerization | | | | | | | | | |
| Entry | [M] ₁ ₀ : [M] ₂ ₀ : [MBP] ₀ : [PMDETA]: [CuBr] ₀ | Temp. (°C) | Time (min) | Conv. (%) | M_n^a (g.mol ⁻¹) | PDI ^r | Final composition ^h | | |
| 10 | 20:20:1:1:1 | 50 | 180 | 88, 87 | 6300 | 1.18 | PEEA ₁₈ /PtBA ₁₇ | | |

^a SEC system 1. ^b polymerization of EEMA. ^c 50 v% of anisole added. ^d polymerization of EEA. ^e polymerization of tBA. ^f 33 v% of ethyl acetate added for the synthesis of the first block. ^g DP_n^h = [M]₁₀: [MBP]₀. ^h theoretical calculations from conversion.

Results and Discussion

ATRP of EE(M)A

Unprotected (meth)acrylic acid ((M)AA) cannot be directly polymerized by Cu(I) mediated ATRP, because (M)AA is able to coordinate with Cu ions and because of protonation of the nitrogen ligands (17,18).

Although the group of Armes was able to polymerize the sodium salt analogue of MAA, an aqueous medium was required, which means that only water soluble (co)polymers can be prepared (19). Moreover, the reported strategy suffered from a poor living character (20).

Generally, as mentioned before in the introduction, the most applied strategy is the use of protected analogues of (meth)acrylic acid. To avoid the required extra purification step after deprotection to the corresponding polyacids, we report here on the use of 1-ethoxyethyl (meth)acrylate as the protected (meth)acrylic acid monomer.

The monomers, 1-ethoxyethyl acrylate (EEA) and 1-ethoxyethyl methacrylate (EEMA), were synthesized by the phosphoric acid-catalyzed addition reaction of (meth)acrylic acid to ethyl vinyl ether (see Scheme 1). This can be done on a large scale in a yield of about 90 %.

In a previous paper, we have already reported on the optimization of the conditions for the homopolymerization of both EEMA and EEA by ATRP and on the deprotection to P(M)AA by a heating step (12). In this chapter, we will focus on the synthesis of different copolymer structures (Figure 1). The EEA strategy was applied to the synthesis of a variety of block, "blocky gradient" and random copolymers with PEE(M)A segments by ATRP to demonstrate the versatility of our approach in the synthesis of more complex polymer architectures.

Block copolymers have been prepared via a macroinitiator strategy on one hand and via sequential monomer addition on the other hand. In addition, random copolymers have been prepared, and ATRP of EEA has been combined with other controlled polymerization techniques.

Macroinitiator Strategy

Block copolymers with PEE(M)A segments have been prepared by ATRP, starting from different macroinitiators. As the polymerization of EE(M)A requires relatively low reaction temperatures (preferably below 60 °C) to avoid deprotection, EE(M)A is usually polymerized as the second block. On one hand, polystyrene (PS) and poly (methyl methacrylate) (PMMA) macroinitiators were used for the synthesis of block copolymers (Table I, entry 1-2). Although these

copolymerizations proceeded in a controlled way, the presence of unreacted macroinitiator in the system could not be avoided (not shown). PS and PMMA are difficult to prepare with 100 % Br end functionality, even at low monomer conversions, due to termination and transfer reactions and also thermal initiation in the case of styrene (21).

On the other hand, also polyacrylates were used as macroinitiators. As an example, EEA was polymerized as the second block, starting from a poly(*n*-butyl acrylate) (PnBA) macroinitiator (Table I, entry 3-4). Polymerizations were carried out with CuBr and PMDETA as the ligand, in bulk. These block copolymerizations were performed with good control over the polymerization reaction, as confirmed by the linear behavior of both the first order kinetic plot and the plot of the M_n as a function of conversion (Figure 2). From SEC, it can be concluded that functionalization of the macroinitiator is close to 100 % (Figure 3, left). Only a small fraction (< 5 %) of unreacted macroinitiator was observed in the system, causing a slight increase of the PDI of the polymer with increasing conversion. This small fraction of unreacted macroinitiator is attributed to radical termination during the start of the synthesis of the macroinitiator, when the ATRP equilibrium is not fully established yet.

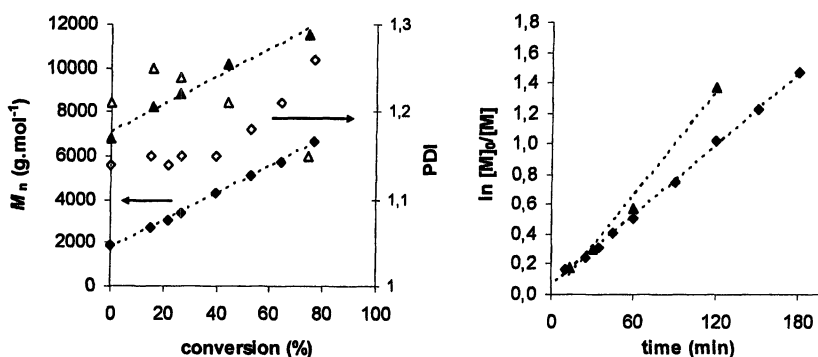


Figure 2. Average molar mass (M_n) and PDI vs. conversion (left) and the first order kinetic plot (right) of a block copolymerization of EEA starting from a PnBA (◆) and PTHF macroinitiator (▲) (Table I, entry 3 and 7).

In addition, block copolymers have also been prepared starting from a PEEA macroinitiator, in the case that low reaction temperatures could be used for the ATRP of the second block. As an example of a block copolymer with PEEA as the first block, a block copolymer with poly(*tert*-butylacrylate) (PtBA) as second segment was synthesized. The SEC traces reveal that this was done in a controlled way (Table I, entry 5; Figure 3, right). Although we demonstrated that block copolymers with PEE(M)A as the first block can be synthesized, the reverse way is often more convenient because of the rather high temperatures

that are needed for the polymerization of some monomers. Even minor deprotection of the PEE(M)A segments could destroy the catalyst system during the synthesis of the second block.

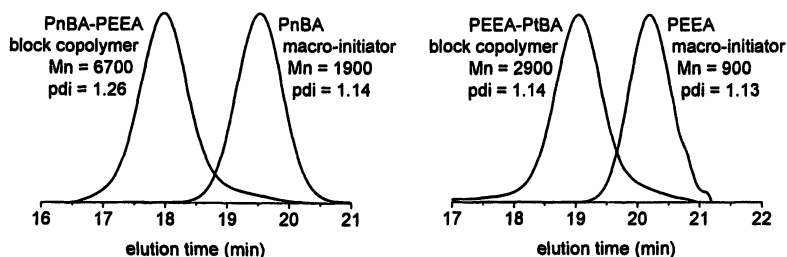


Figure 3. SEC traces of block copolymerizations of EEA and nBA (left; Table I, entry 4) or tBA (right; Table I, entry 5). (SEC System 1).

Further on, the ATRP of EE(M)A was also combined with other controlled polymerization techniques. This is illustrated with the synthesis of a polytetrahydrofuran-PEEA block copolymer, for which the PTHF macroinitiator was synthesized by cationic ring opening polymerization and provided with a Br end group (a 2-bromoisobutyric ester) for ATRP of the EEA block (Table I, entry 6-7). The kinetics are shown in Figure 2, and demonstrate the controlled behavior.

Sequential Monomer Addition

Copolymer structures have also been synthesized by sequential monomer addition of 2 monomers during the polymerization reaction (Table I, entry 8-9). Random copolymerization of EEA and tBA revealed that both monomers show a nearly equal reactivity, resulting in a random copolymer composed of almost equal amounts of EEA and tBA (Table I, entry 10). In this way, the molecular architecture obtained by sequential monomer addition is intermediate to those of block and random copolymers. Thus, the resulting copolymer consists of a first block of tBA or EEA and a random second block of tBA and EEA. Because of this specific composition distribution, the repulsive inter-chain interactions are less strongly changing along the chain in comparison to conventional block copolymers. Therefore these polymers may be of special interest for specific applications such as stabilization of dispersions, micellization applications, etc. (22,23). A copolymer with a structure close to that of a block copolymer can be obtained if a high conversion of the first block is reached upon addition of the second monomer. Well-defined copolymers composed of EEA and tBA have

been synthesized by ATRP with PEEA as the first part (Table I, entry 9), as well as by adding EEA as the second monomer (Table I, entry 8).

Deprotection of PEE(M)A to P(M)AA

We have previously reported on the deprotection of PEEMA homopolymers to PMAA with loss of ethyl vinyl ether (bp: 33 °C) at high temperature (160 °C) by thermogravimetric analysis (TGA) (12). At this temperature, deprotection proceeds fast, but anhydride formation occurs as a side reaction, resulting in partial cross-linking of the formed PMAA. Figure 4 shows that deprotection can also be performed at lower temperatures, during a longer time. By selecting an appropriate temperature program, anhydride formation can be prevented. If necessary, anhydride formation can be undone by stirring the polymer in water (24). Deprotection can be performed in bulk, by spreading out the polymer over a surface, or larger quantities can also be deprotected in solution at lower temperatures (e.g. reflux in THF at 80 °C for 48h).

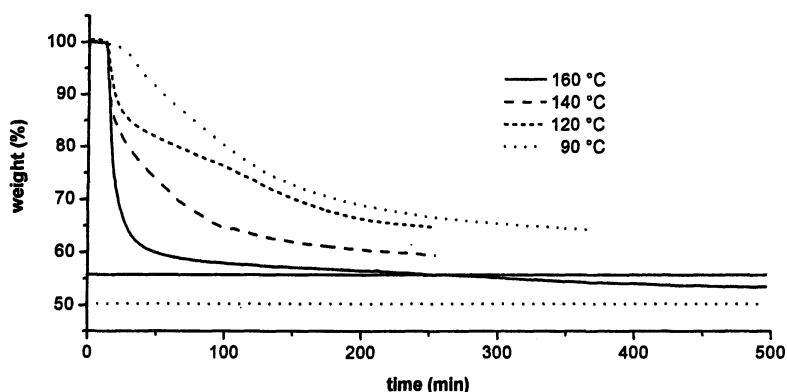


Figure 4. TGA of PEEMA. The horizontal solid line corresponds to 100 % deprotection to PMAA and the dotted one to 100 % anhydride formation.

^1H NMR experiments (Figure 5) confirm that deprotection is quantitative by disappearance of the characteristic PEEMA peaks (3.4-3.9 and 5.6-5.8 ppm in acetone- d_6) and the appearance of a peak at 12.4 ppm (NMR solvent: DMSO- d_6) after the heating process (bulk sample heated for 30 min. at 160°C), which arises from the carboxylic acid functionalities.

Figure 6 shows the results of a thermogravimetric analysis of block copolymer PTHF₆₈-PEEA₃₇ (Table I, entry 6) and the corresponding PTHF₆₈ macroinitiator. Taking the molecular composition into account, the theoretical weight loss is 24.1%. From TGA, an experimental weight loss of 23.0 % (at 180 °C) is obtained, showing a good agreement between the theoretical and

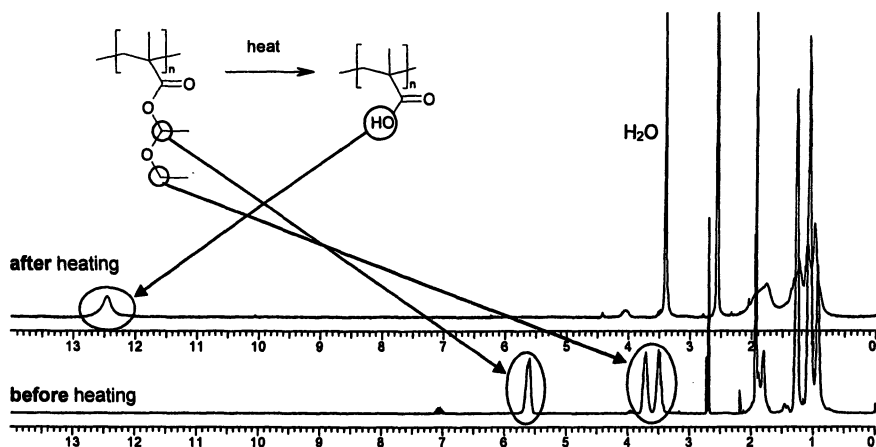


Figure 5. ^1H NMR spectra of a sample of PEEMA before heating (in acetone- d_6) and after heating (in DMSO- d_6).

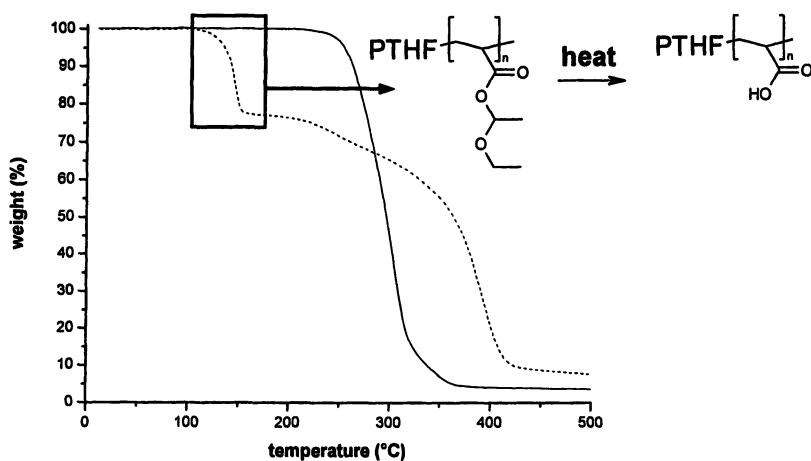


Figure 6. Thermogravimetric analysis (heating rate: $10\text{ }^\circ\text{C}/\text{min}$) of PTHF macroinitiator (—) and PTHF-PEEA block copolymer (---) (Table I, entry 6).

experimental value. Conversion of PTHF-PEEA to PTHF-PAA by heating can be done without degradation of the PTHF-part (Figure 6).

RAFT of EEA

To prove the versatility of our strategy, EEA has also been polymerized by RAFT, another popular controlled radical polymerization technique (13). As the RAFT process is insensitive to traces of acrylic acid, the monomer purification is

less critical. Moreover, partial deprotection of (P)EEA does not influence the RAFT polymerization, allowing higher polymerization temperatures when compared to ATRP. The EEA strategy instead of direct polymerization of AA makes the use of apolar polymerization solvents possible, thus P(M)AA-containing polymers with a wide range of apolar segments can be synthesized in a straightforward manner. All polymerizations were carried out via a high-throughput workflow with 2-cyano-2-butylthiobenzoate (CBDB) as the RAFT-agent and AIBN as the radical initiator in a ratio of 1 to 0.25 (25), in 70 vol% of toluene (Figure 7).

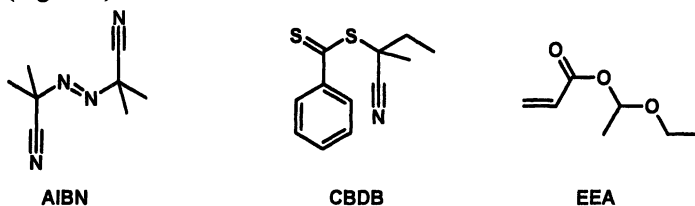


Figure 7. Used reagents for the RAFT (co)polymerizations of EEA.

Homopolymerization

To find the RAFT polymerization conditions providing an optimal control, the homopolymerization of EEA was investigated making use of an automated synthesizer. A temperature screening was carried out, and each experiment was performed twice to demonstrate the reproducibility of the polymerization reactions (Figure 8).

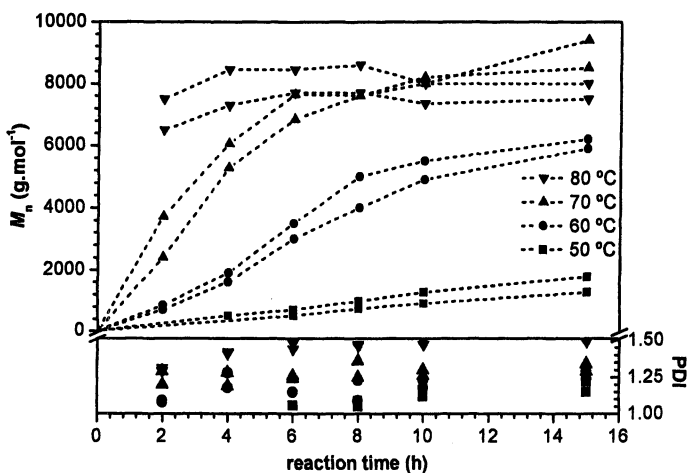


Figure 8. M_n and PDI vs. reaction time for RAFT of EEA. Data of 2 experiments are shown for each polymerization temperature. (SEC system 2). (Adapted with permission from reference 13. Copyright 2005 American Chemical Society).

It was found that the optimal temperature for the RAFT polymerization of EEA is 70 °C, providing an acceptable reaction speed in combination with good control over the molar mass and polydispersity, without significant deprotection. For a detailed analysis of the displayed results, we refer to reference 13.

Copolymerization

Also block copolymerizations with EEA were carried out with the RAFT technique. Various poly(methacrylates) as well as poly(acrylates) were synthesized as the first blocks and EEA was polymerized as the second block with different theoretical degrees of polymerization (25, 50, 75 and 100 for 100% conversion) (13). All polymerizations were carried out by sequential monomer addition. In Figure 9, the SEC traces of the block copolymers with poly(methyl methacrylate) as the first block (25 units) are shown, as well as the increase of the M_n as a function of increasing number of units of EEA of the second block.

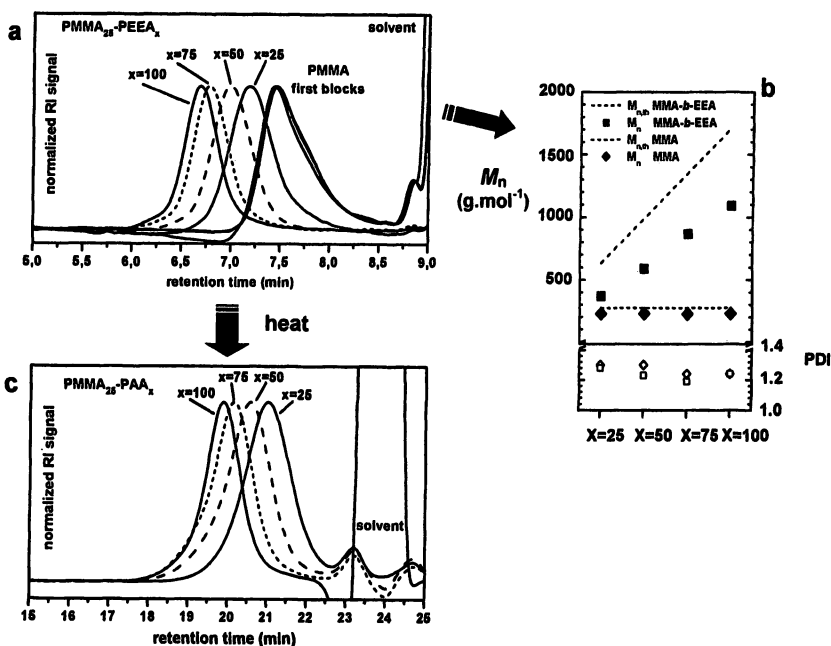


Figure 9. $x = DP_{th}$ of the second block. a) SEC traces of PMMA-PEEA_x block copolymers (SEC system 2); b) Increase of M_n with increasing number of EEA units; c) SEC traces of final PMMA-PAA_x block copolymers (SEC system 3). (Adapted with permission from reference 13. Copyright 2005 American Chemical Society).

The molecular weights obtained for the PMMA first blocks revealed a monomer conversion close to 100 %, as evidenced by the close resemblance with the theoretical M_n (SEC system calibrated with PMMA standards). Polydispersities are low for all polymer structures. After deprotection of the final block copolymer samples by a heating process (at 80 °C in CHCl_3), SEC traces of these PAA- containing block copolymers show a monomodal distribution with low polydispersity for all polymers ($\text{PDI} < 1.2$) (Figure 9), demonstrating absence of chain cleavage or other side reactions due to thermal treatment.

Conclusions

In this chapter we have demonstrated the successful polymerization of 1-ethoxyethyl (meth)acrylate by the ATRP and RAFT polymerization process. PEE(M)A homopolymers and various PEE(M)A containing copolymers were prepared in a controlled way. These polymers can be converted to the corresponding P(M)AA containing polymers by a simple heating step, without the need for an additional purification step. In addition, the EE(M)A strategy was shown to be a facile route for the straightforward synthesis of P(M)AA containing polymers without the need for polar solvents.

Acknowledgement

Research financed by a Ph. D. grant of the Institute for the Promotion of Innovation through Science and Technology in Flanders (IWT-Vlaanderen). Special thanks to S. Bon (Warwick University, UK), and R. Hoogenboom and U. Schubert (Eindhoven University of Technology, the Netherlands) for the collaborations on the ATRP and RAFT experiments, respectively.

References

1. Porasso, R.D.; Benegas, J.C.; Van den Hoop, M.A.G.T. *J. Phys. Chem. B* **1999**, *103*, 2361.
2. for a recent review about (meth)acrylic acid containing polymers see: Mori, H.; Müller, A.H.E. *Prog. Polym. Sci.* **2003**, *28*, 1403.
3. Müller, A.H.E. *Makromol. Chem.* **1981**, *182*, 2863.
4. Doherty, M.A.; Müller, A.H.E. *Makromol. Chem.* **1989**, *190*, 527.
5. Chiefari, J.; Chong, B.Y.K.; Ercole, F.; Krstina, J.; Jeffery, J.; Le, T.P.T.; Mayadunne, R.T.A.; Meijs, G.F.; Moad, C.L.; Moad, G.; Rizzardo, E.; Thang, S.H. *Macromolecules* **1998**, *31*, 5559.

6. Couvreur, L.; Lefay, C.; Belleney, J; Charleux, B.; Guerret, O.; Magnet, S. *Macromolecules* **2003**, *36*, 8260.
7. Davis, K.A.; Charleux, B.; Matyjaszewski, K. *J. Polym. Sci., Part A: Polym. Chem.* **2000**, *38*, 2274.
8. Haddleton, D.M.; Crossman, M.C.; Dana, B.H.; Duncalf, D.J.; Heming, A.M.; Kukulj, D.; Shooter, A.J. *Macromolecules* **1999**, *32*, 2110.
9. Pintauer, T.; Coessens, V.; Matyjaszewski, K. *Progr. Polym. Sci.* **2001**, *26*, 337.
10. Zhang, X.; Xia, J.; Matyjaszewski, K. *Polym. Prepr. (Am. Chem. Soc., Div. Polym. Chem.)* **1999**, *40* (2), 440.
11. Bütün, V.; Vamvakaki, M.; Billingham, N.C.; Armes, S.P. *Polymer* **2000**, *41*, 3173.
12. Van Camp, W.; Du Prez, F. E.; Bon, S. A. F. *Macromolecules* **2004**, *37*, 6673.
13. Hoogenboom, R.; Schubert U.S.; Van Camp, W.; Du Prez, F.E. *Macromolecules* **2005**, *38*, 7653.
14. Guenzet, J.J. *Chem. Abstr.* **1963**, *58*, 3321b; more recently: Nakane, Y.; Ishidoya, M.; Endo, T. *J. Polym. Sci., Part A: Polym. Chem.* **1999**, *37*, 609.
15. Keller, R.; Wycoff, H. *Inorg. Syn.* **1947**, *2*, 1.
16. Bouhadir, G.; Legrand, N.; Quiclet-Sire, B.; Zard, S. Z. *Tetrahedron Lett.* **1999**, *40*, 277.
17. Patten, T.E.; Matyjaszewski, K.; *Adv. Mater.* **1998**, *10*, 901.
18. Zhang, X.; Matyjaszewski, K. *Macromolecules* **1999**, *32*, 7349.
19. Ashford, E.J.; Naldi, V.; O'Dell, R.; Billingham, N.C.; Armes, S.P. *Chem. Commun.* **1999**, 1285.
20. Bories-Azeau X.; Mérian T.; Weaver J.V.M.; Armes S.P. *Macromolecules* **2004**, *37*, 8903.
21. Lutz J.F.; Matyjaszewski K. *J. Polym. Sci., Part A: Polym. Chem.* **2005**, *43*, 897
22. Gray, K.M.; Zhou H.; Nguyen S.T.; Torkelson J.M. *Macromolecules* **2004**, *37*, 5586
23. Kim J.; Gray M.K.; Zhou H.; Nuygen S.T.; Torkelson J.M. *Macromolecules* **2005**, *38*, 1037
24. Lu, S.; Fan, Q.; Liu, S.; Chua, S.; Huang, W. *Macromolecules* **2002**, *35*, 9875.
25. Fijten, M. W. M.; Meier, M. A. R.; Hoogenboom, R.; Schubert, U. S. *J. Polym. Sci., Part A: Polym. Chem.* **2004**, *42*, 5775.

Chapter 14

Novel Organo-Soluble or Water-Soluble Copolymers Containing DNA Nucleobases

Jean-François Lutz, Rainer Nehring, and Sebastian Pfeifer

Research Group Nanotechnology for Life Science, Fraunhofer Institute
for Applied Polymer Research, Geiselbergstrasse 69, 14476 Potsdam,
Germany

Two novel styrene derivatives containing complementary nucleobase moieties were studied: 9-(4-vinylbenzyl)adenine (VBA) and 1-(4-vinylbenzyl)thymine (VBT). Homopolymers of VBA or VBT could be prepared in high yields by simply using conventional radical polymerization. However, the formed polymers could only be dissolved in polar solvents such as DMF, DMSO, NMP or TFE. Copolymers with an enhanced solubility in either apolar solvents or water could be obtained by copolymerizing the nucleobase-monomers with respectively dodecyl methacrylate (DMA) or oligo(ethylene glycol) methacrylate (OEGMA). Moreover, the molecular structure of the copolymers P(VBT-*co*-DMA), P(VBA-*co*-DMA), P(VBT-*co*-OEGMA) and P(VBA-*co*-OEGMA) could be precisely controlled using the atom transfer radical polymerization catalyst system Ethyl 2-chloropropionate/CuCl/BPED. These results confirm that ATRP is a method of choice for preparing self-organizing macromolecules inspired by Nature.

Introduction

Nature is an everlasting source of inspiration for designing innovative synthetic materials.¹ For instance, many advanced concepts used in modern material science such as molecular self-assembly,² hierarchical organization,³ compartmentalization⁴ or hybridation⁵ find their roots in biology. However, such biomimetic approaches can be conceptually rather different. One first strategy consists in imitating the mesoscopic organization of natural materials with fully synthetic molecular building-blocks.^{1, 3, 6} This route has been recently proven to be very efficient for developing high-performance synthetic nanomaterials.¹ Another approach consists in mimicking Nature at the molecular level. Molecules of life such as proteins, lipids, polysaccharides or nucleic acids are fascinating structures, which possess unique capacity of supramolecular organization. Thus, important efforts have been made for transferring these exceptional molecular properties to synthetic structures. Here again, several strategies exist. One popular pathway is molecular conjugation, which consists in linking together molecules of synthetic and natural origin for creating novel generations of hybrid structures.^{7, 8} However, such approach often requires to work at the interface between synthetic chemistry and biochemistry, which frequently restricts experimental conditions and yields. A simpler pathway is the fabrication of artificial structures bearing selected moieties of natural molecules. For example, bases of nucleic acids (or nucleobases), which control the self-recognition of DNA strands, have recently been extensively studied for creating synthetic supramolecular devices.⁹⁻¹¹ Several studies illustrated that, even when used out of their natural context (i.e. in the absence of a phosphate-sugar backbone as naturally found in DNA), nucleobases exhibit interesting supramolecular properties.⁹⁻¹¹

Several pathways have been reported for linking nucleobases to synthetic polymer backbones.¹² In particular, the radical polymerization of vinyl monomers bearing nucleobases has been early investigated.¹³⁻²⁰ The reason for that is that free radical polymerization is a facile synthetic technique, which usually allows straightforward preparation of large polymer quantities. However, it is clear that this polymerization route is not suitable for preparing macromolecules structurally comparable to DNA since radical polymerizations are typically neither stereoselective nor sequence-selective.²¹⁻²³ Nevertheless, new polymers bearing multiple nucleobases repeating units can be prepared using radical polymerization. Such structures have interesting potential for applications in various aspects of nanosciences.²⁴⁻²⁹ Moreover, the recent emergence of controlled radical polymerization techniques such as atom transfer radical polymerization (ATRP),^{30, 31} nitroxide mediated polymerization (NMP)³² or reversible addition-fragmentation transfer polymerization (RAFT)³³ potentially allows the preparation of novel generations of well-defined materials containing nucleobases.³⁴ However, up to now, only a few reports describe the

synthesis of nucleobase-polymers by controlled radical polymerization.^{25, 35-40} Herein, we summarize our recent efforts for preparing polymers containing nucleobases via either conventional radical polymerization or ATRP.^{38, 39}

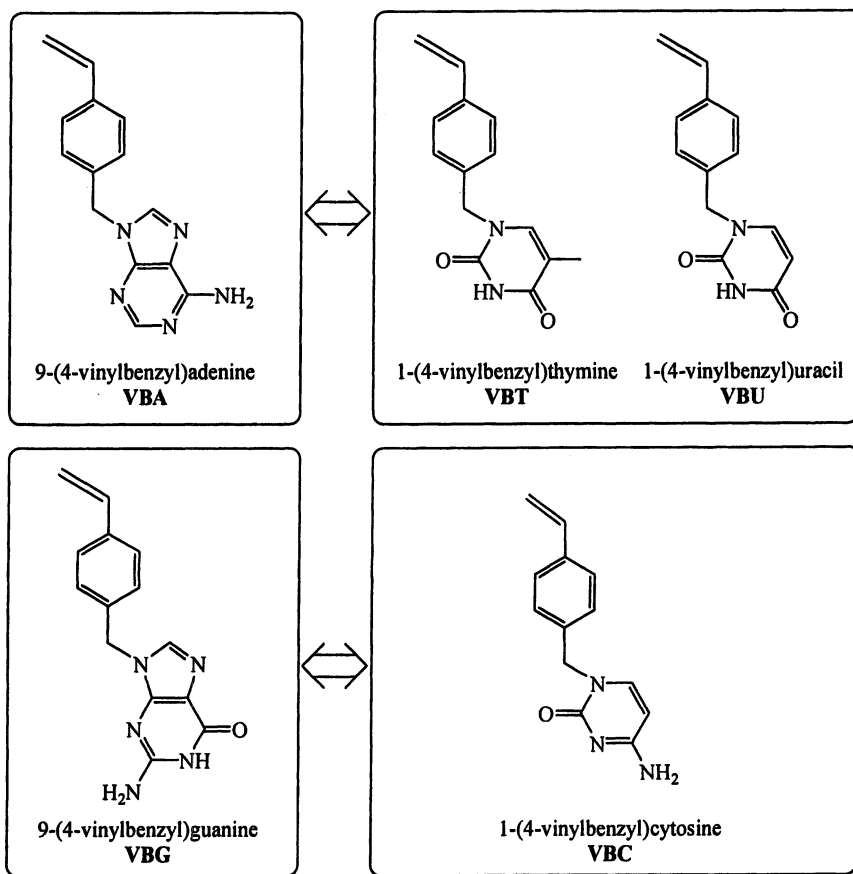


Figure 1. Molecular structures of styrene derivatives bearing either purine (left) or pyrimidine (right) substituents.⁴¹ Arrows represent preferential Watson-Crick base pairing of purine and pyrimidine nucleobases.

In the present work, we studied the radical polymerization of a new class of styrene derivatives bearing nucleobases (Figure 1). The synthesis of these monomers was recently described.⁴¹ Thus, optimized protocols exist for preparing monomers containing either purine (adenine or guanine) or pyrimidine (thymine, uracil or cytosine) nucleobases.⁴¹ At first, we focused only on two model monomers: the purine derivative 9-(4-vinylbenzyl)adenine (VBA) and its

purine counterpart 1-(4-vinylbenzyl)thymine (VBT). This article describes the preparation of homopolymers of VBT and VBA. Moreover, the preparation of copolymers with enhanced solubility in either organic or aqueous media is subsequently described.

Experimental

Chemicals. 1-(4-vinylbenzyl)thymine, 9-(4-vinylbenzyl)adenine, and *N,N'*-bis(pyridin-2-ylmethyl 3-hexoxo-3-oxopropyl)ethane-1,2-diamine were prepared according to procedures reported in the literature.^{41, 42} Ethyl 2-chloropropionate (97%), poly(ethylene glycol) methyl ether methacrylate ($M_n = 475 \text{ g}\cdot\text{mol}^{-1}$), and dodecyl methacrylate (96%) were purchased from Aldrich and used as received. 2,2'-Azobisisobutyronitrile (AIBN) was recrystallized from ethanol, filtered and dried. Copper(I) chloride (Aldrich, 98+%) was washed with glacial acetic acid in order to remove any soluble oxidized species, filtered, washed with ethanol and dried.

General procedure for conventional radical polymerization. In a Schlenk tube were added the styrene derivative (either VBT or VBA), the comonomer (either dodecyl methacrylate or poly(ethylene glycol) methyl ether methacrylate), AIBN and DMF. The tube was closed with a septum and the solution was purged with dry argon for 20 minutes. Subsequently, the mixture was heated at 60°C in an oil bath. After the experiment, the formed polymers were purified by either precipitation or dialysis.

General procedure for atom transfer radical polymerization. Copper chloride, the styrene derivative (either VBT or VBA), the comonomer (either dodecyl methacrylate or poly(ethylene glycol) methyl ether methacrylate) and DMF were added to a flask sealed with a septum. The solution was purged with dry argon for 20 minutes. Then, *N,N'*-bis(pyridin-2-ylmethyl 3-hexoxo-3-oxopropyl)ethane-1,2-diamine was added through the septum with a syringe and the mixture turned homogeneous. Lastly ethyl 2-chloropropionate was added via a syringe. The mixture was heated at 90°C in an oil bath for several hours. The resulting polymers were purified by either precipitation or dialysis.

Characterization. Molecular weights and molecular weight distributions were determined by size exclusion chromatography (SEC) performed in either THF, NMP or DMSO as eluent.³⁸ Monomer conversions were calculated from ¹H NMR spectra in DMSO-*d*₆ by comparing the integrations of vinyl protons of the remaining monomers and the integration of signals of the formed polymers. ¹H NMR Spectra were recorded on a Bruker DPX-400 operating at 400.1 MHz. UV

spectra were recorded on a Cary 5000 UV-VIS-NIR spectrometer from Varian. FT-IR spectra were recorded using a FT-IR spectrometer Equinox55 from Bruker Optical micrographs were made using an Olympus microscope BH-2 with a 50X objective.

Preparation of homopolymers of VBT and VBA

The free radical polymerization of either 9-(4-vinylbenzyl)adenine (VBA) or 1-(4-vinylbenzyl)thymine (VBT) was investigated at 60°C. The main challenge of these homopolymerizations was to select appropriate solvents for allowing homogeneous reaction conditions. Typically, VBT, and VBA exhibit no or very low solubility in organic solvents of low or intermediate polarity such as tetrahydrofuran, toluene, benzene or chloroform. However, they could be easily dissolved in polar solvents such as *N,N*-dimethylformamide (DMF), *N*-methylpyrrolidone (NMP) or dimethylsulfoxide (DMSO). Thus, VBT could be successfully polymerized by radical polymerization in DMF (Table 1). The formed polymer poly(1-(4-vinylbenzyl)thymine) (PVBT) was a solid white powder, which could be redissolved in either DMF, NMP or DMSO.

Table 1. Preparation of Homopolymers by Free Radical Polymerization.^a

| <i>Monomer</i> | <i>solvent</i> | $[M]_0$ (mol/L) | $[M]_0/[AIBN]_0$ | <i>t</i> (h) | <i>conv</i> | M_n | M_w/M_n |
|----------------|----------------|--------------------|------------------|-----------------|-------------|--------|-----------|
| VBT | DMF | 1 | 100/1 | 24 | 0.80 | 24000 | 2.1 |
| VBA | DMSO | 0.6 | 100/1 | 24 | 0.85 | 174500 | 1.7 |

^a Reaction temperature was 60°C in all cases.

The polymerization of VBA in DMF or NMP was found to be heterogeneous since the formed polymer poly(9-(4-vinylbenzyl)adenine) (PVBA) is not soluble in those solvents at 60°C and therefore precipitates during the reaction. However, VBA and PVBA are both soluble in DMSO, thus a successful homogeneous polymerization of VBA was obtained at 60°C in this solvent (Table 1). ¹H NMR spectra confirmed that the prepared polymers possess thymine or adenine repeating-units (i.e. nucleobases are not altered during the free radical polymerization process).³⁸ This first series of experiments confirm that radical polymerization is a method of choice for preparing polymers bearing nucleobases. However, the obtained homopolymers PVBA, and PVBT probably possess a limited potential for applications since they can only be dissolved in polar solvents, which strongly disfavor the molecular recognition of nucleobases. For instance, the only common solvents found for PVBA and its

complementary polymer PVBT were DMSO and 2,2,2-trifluoroethanol (TFE), which prevent the formation of H-bonds. In order to prepare nucleobase-polymers soluble in more interesting media, the copolymerization of either VBT or VBA with comonomers enhancing solubility was studied. Dodecyl methacrylate and oligo(ethylene glycol) methacrylate were chosen as comonomers for promoting solubility respectively in apolar media or water (Figure 2).

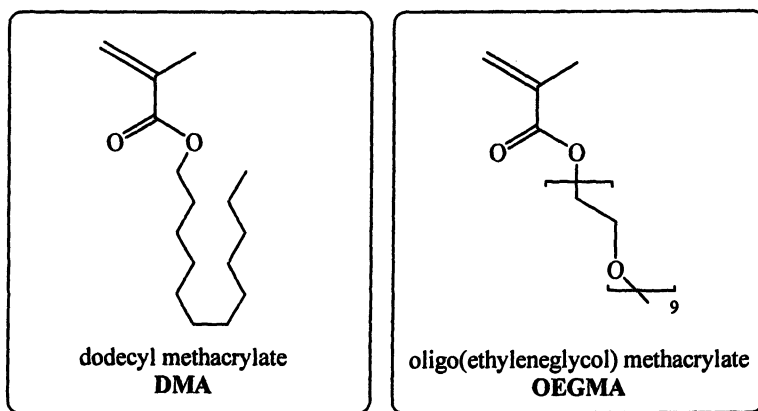


Figure 2. Molecular structure of the comonomers used in this study

Preparation of organo-soluble copolymers

The radical copolymerization of dodecyl methacrylate (DMA) with either VBT or VBA was studied. DMA (Figure 2) was chosen as a comonomer for two main reasons. First, this monomer possesses long alkyl chains, which allow solubility in a large number of organic solvents. Nevertheless, the reactivity ratios of methacrylates and styrene derivatives are usually below unity (for example for styrene and dodecyl methacrylate $r_s = 0.52$ and $r_{DMA} = 0.42$),⁴³ which suggests a tendency towards alternation of the comonomers during copolymerization. Such trend should lead to the formation of polymers with a homogeneous chain-to-chain composition (i.e. no composition drift) and a quite regular distribution of nucleobases along each chain. Table 2 displays the results obtained for the free radical copolymerization of equimolar mixtures of DMA and either VBT or VBA. In all cases the polymerization could be run homogeneously in DMF since all the monomers and the resulting polymers poly(1-(4-vinylbenzyl)thymine-*co*-dodecyl methacrylate) P(VBT-*co*-DMA) and poly(9-(4-vinylbenzyl)adenine *co*-dodecyl methacrylate) P(VBA-*co*-DMA) are soluble in this solvent. However, for the comonomer pair VBA/DMA, a higher

initial dilution was needed as compared to VBT/DMA since VBA is much less soluble in DMF than VBT. Nevertheless, in all cases the nucleobase-polymers could be prepared in high yield. For both P(VBT-*co*-DMA) and P(VBA-*co*-DMA), experimental monomer conversions indicated a nearly equimolar composition of comonomers in the final copolymers, as expected from the reactivity ratios.

Table 2. Preparation of Copolymers by Free Radical Copolymerization.^a

| M_1 | M_2 | $[M_1]_0$ (mol/L) | $M_1/M_2/I$ | t (h) | conv. M_1 | conv. M_2 | M_n | M_w/M_n |
|-------|-------|----------------------|-------------|------------|----------------|----------------|-------|-----------|
| VBT | DMA | 0.85 | 50/50/1 | 20 | 0.85 | 0.81 | 41000 | 2.1 |
| VBA | DMA | 0.30 | 50/50/1 | 20 | 0.72 | 0.64 | 25000 | 1.8 |
| VBT | OEGMA | 0.85 | 50/50/1 | 15 | 0.85 | 0.83 | 32000 | 1.4 |
| VBA | OEGMA | 0.35 | 50/50/1 | 15 | 0.82 | 0.70 | 53000 | 2.0 |

^a All experiments were done at 60°C in DMF. Initiator (I) was AIBN in all cases.

Moreover, as targeted, the resulting polymers P(VBT-*co*-DMA) and P(VBA-*co*-DMA) could be dissolved in a large range of organic solvents. For example, a sample of P(VBT-*co*-DMA) with $M_n \sim 30000$ g/mol could be dissolved in either tetrahydrofuran, chloroform or dioxane. Moreover, in chloroform or dioxane solutions, copolymers P(VBT-*co*-DMA) and P(VBA-*co*-DMA) exhibited interesting self-organization behavior.^{38, 39} In very dilute conditions (i.e. for concentrations around 0.05 mg/mL or lower), both P(VBT-*co*-DMA) and P(VBA-*co*-DMA) could be molecularly dissolved in chloroform. UV-vis spectroscopy measurements indicated that no intermolecular hydrogen bonding occur in this range of concentration for individual copolymer solutions.^{38, 39} However, for mixed solutions of P(VBT-*co*-DMA) and P(VBA-*co*-DMA), intermolecular self-organization due to the formation of A-T base pairs was observed in chloroform for overall concentrations of 0.02 mg/mL or higher.³⁹ Nevertheless, at higher concentrations (e.g. in the range 1-5 mg/mL) micron-sized supramolecular aggregates could be observed for individual or mixed solutions of P(VBT-*co*-DMA) and P(VBA-*co*-DMA).³⁸ Such morphologies were typically obtained after an annealing process, which enhances polymer dispersion. As an example, Figure 3 shows optical micrographs recorded for an individual solution of P(VBT-*co*-DMA) in chloroform. Both ¹H NMR and FTIR studies indicated that the cohesion of the aggregates is due to intermolecular H-bonds (i.e. T-T interactions in the case P(VBT-*co*-DMA) solutions, A-A interactions in the case P(VBT-*co*-DMA) solutions and A-T in the case of polymer mixtures). A detailed morphological study of these supramolecular aggregates is currently in progress.

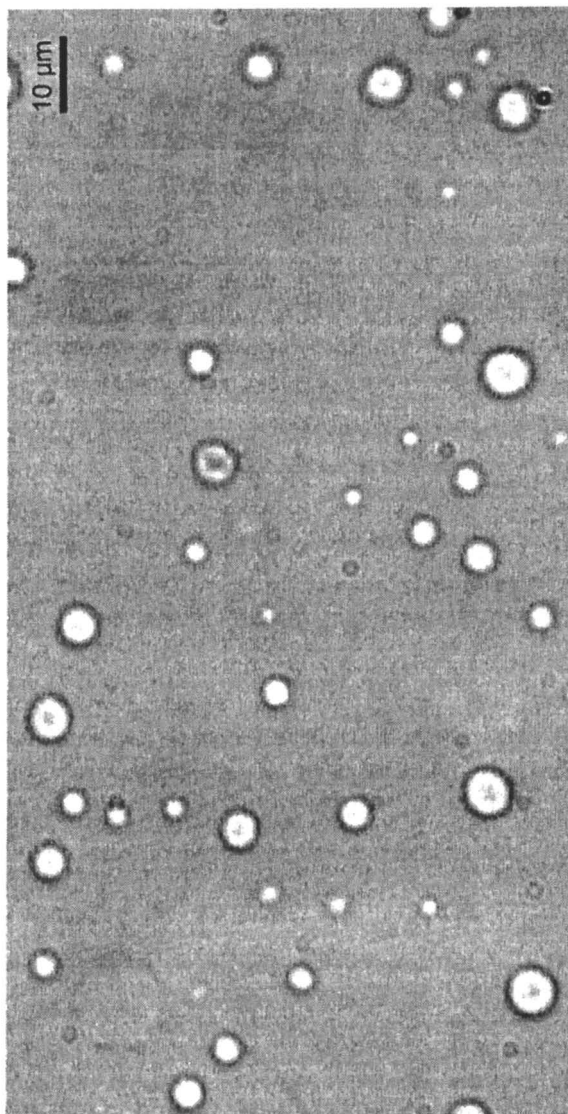


Figure 3. *Optical micrographs measured at room temperature for a solution of P(VBT-co-DMA) in chloroform (3 mg/mL).*

Since the free radical copolymerization of DMA with either VBT or VBA was found to be a straightforward pathway for producing polymers containing nucleobases, the controlled radical copolymerization of VBT/DMA and VBA/DMA was subsequently studied (Table 3). Among the possible methods of CRP, ATRP was selected since this technique was already reported to be efficient for polymerizing nucleobase functional monomers.^{35, 36} However, the outcome of ATRP experiments often strongly depends on the reaction conditions, since the transition metal catalysts used in this technique can interact with other reaction constituents (i.e. solvent or monomers). In that regard, the copolymerization systems studied here are not very appropriate for standard ATRP since the amino-functional monomers VBT and VBA and the solvent DMF can all potentially coordinate the transition metal catalyst and therefore affect its reactivity. However, very recently, it was shown that a new ATRP catalyst system based on copper chloride and the ligand *N,N'*-bis(pyridin-2-ylmethyl 3-hydroxy-3-oxopropyl)ethane-1,2-diamine (BPED) was a very efficient system for controlling the radical polymerization of problematic monomers such as *N,N*-dimethylacrylamide.⁴² The latter is often a problem in ATRP since its polymer probably coordinates the catalysts.⁴⁴ Therefore the catalyst system CuCl/BPED was selected for the present work since BPED probably strongly coordinates with copper and therefore prevents problems due to competitive coordination. Table 3 illustrates that the ATRP catalyst CuCl/BPED allowed the successful preparation of well-defined P(VBT-*co*-DMA) and P(VBA-*co*-DMA). By adjusting the initiator/catalyst ratio, both copolymers could be produced in relatively high yields. Moreover, SEC results confirmed that the prepared copolymers both possess a controlled molecular structure, although measured apparent molecular weights and molecular weight distributions should be cautiously interpreted due to the high structural discrepancies between the analyzed copolymers and the SEC standards. Nevertheless, the present study indicates that ATRP can be successfully used for preparing P(VBT-*co*-DMA) and P(VBA-*co*-DMA). Thus, the macromolecular engineering capabilities of ATRP can be applied to the polymers presented here e.g. blocks copolymers, star copolymers, telechelics or functional surfaces can be prepared.

Preparation of water-soluble copolymers

Oligo(ethylene glycol) methacrylate (OEGMA) was studied as an alternative comonomer in the radical polymerization of either VBT and VBA. The main goal of these copolymerizations was to produce novel structures relevant for applications in biotechnology. Indeed, short poly(ethylene glycol) (PEG) segments are both water-soluble and biocompatible and therefore have been widely used in biomedical applications.^{45, 46} In particular, the use of OEGMA

Table 3. Preparation of Copolymers by ATRP.^a

| M_1 | M_2 | $[M_1]_0$ (mol/L) | $M_1/M_2/ECP/$ $CuCl/BPED$ | t (h) | conv. M_1 | conv M_2 | M_n | M_w/M_n |
|-------|-------|----------------------|-------------------------------|------------|----------------|---------------|-------|-----------|
| VBT | DMA | 0.70 | 50/50/1/1/1 | 24 | 0.60 | 0.55 | 14500 | 1.30 |
| VBT | DMA | 1 | 50/50/1/2/2 | 20 | 0.96 | 0.94 | 17400 | 1.35 |
| VBA | DMA | 0.35 | 50/50/1/2/2 | 66 | 0.57 | 0.53 | 7400 | 1.35 |
| VBT | OEGMA | 0.85 | 50/50/1/1/1 | 24 | 0.31 | 0.26 | 9000 | 1.25 |
| VBT | OEGMA | 0.85 | 50/50/1/2/2 | 48 | 0.74 | 0.63 | 13000 | 1.30 |
| VBT | OEGMA | 0.85 | 25/25/1/2/2 | 24 | 0.75 | 0.64 | 9000 | 1.25 |
| VBT | OEGMA | 0.85 | 12/12/1/2/2 | 24 | 0.73 | 0.60 | 5600 | 1.30 |
| VBA | OEGMA | 0.35 | 25/25/1/2/2 | 72 | 0.61 | 0.52 | 7800 | 1.25 |

^a All experiments were done at 90°C in DMF.

(Figure 2) has been shown to be a straightforward modern alternative for preparing drug-carriers and bioconjugates.⁴⁷⁻⁵⁰

The equimolar free radical copolymerization of OEGMA ($M_n \sim 475$ g/mol) and nucleobases monomers was investigated at 60°C in DMF in the presence of AIBN as a radical initiator (Table 2). These synthetic conditions allowed efficient preparation of the copolymers poly(1-(4-vinylbenzyl)thymine-*co*-oligo(ethylene glycol) methacrylate) P(VBT-*co*-OEGMA) and poly(9-(4-vinylbenzyl)adenine *co*-oligo(ethylene glycol) methacrylate) P(VBA-*co*-OEGMA). Both copolymers were in the rubbery state at room temperature. Moreover, P(VBT-*co*-OEGMA) and P(VBA-*co*-OEGMA) could also be successfully prepared using ATRP. For the same reasons as mentioned in the previous paragraph, the initiator ECP and the catalyst system CuCl/BPED were utilized. In these conditions, copolymers with a relatively narrow molecular weight distribution ($M_w/M_n \sim 1.3$) were obtained in all cases. Moreover, the molecular weight of the copolymers could be controlled by adjusting the initial monomers/initiator ratio. As targeted, P(VBT-*co*-OEGMA) and P(VBA-*co*-OEGMA) could be dissolved in deionized water. However, complete solubilization of the polymers in water was only observed in quite dilute conditions (typically at a concentration of 5 mg/mL or lower). The self-organization of these novel macromolecules in water is currently under investigation. In a protic solvent (H-bond donor) such as water, the main driving force of self-assembly of these macromolecules is not expected to be H-bonding but hydrophobicity.⁵¹ The copolymers backbones contain multiple hydrophobic VBT or VBA units, which should lead to the formation of hydrophobic domains. Such hydrophobic effect can potentially results in the formation of intramolecular or intermolecular H-bonds.⁵¹⁻⁵³

Conclusion

Two styrene derivatives (VBA, VBT) bearing either a purine moiety (adenine) or its complementary pyrimidine moiety (thymine) were investigated. The free radical polymerization of these monomers at 60°C in the presence of the thermal initiator AIBN allowed the preparation of high molecular weight homopolymers containing multiple nucleobases repeating units. However the formed polymers PVBA and PVBT could only be dissolved in polar solvents such as DMF, NMP and DMSO. Polymers with an enhanced solubility in either apolar media (chloroform, tetrahydrofuran) or water could be obtained by copolymerizing VBT or VBA with either dodecyl methacrylate (DMA) or oligo(ethylene oxide) methacrylate (OEGMA). All these copolymers could be obtained in high yields using either conventional radical polymerization or ATRP with the catalyst CuCl/BPED. However, a better control over the macromolecular structure was obtained with ATRP. Moreover, in apolar media, copolymers of P(VBT-*co*-DMA) and P(VBA-*co*-DMA) were found to self-organize via intermolecular H-bonding. The study of the self-assembly of P(VBT-*co*-OEGMA) and P(VBA-*co*-OEGMA) in water is in progress.

Acknowledgments. Fraunhofer society is gratefully acknowledged for financial support. Moreover, the authors thank prof. Andreas Thünemann and Dr. Knut Rurack at the Federal Institute of Materials and testing (Berlin, Germany) for their participation in this work.

References

1. Sanchez, C.; Arribart, H.; Giraud Guille, M. M. *Nature Mat.* **2005**, *4*, 277.
2. Tu, R. S.; Tirrell, M. *Adv. Drug Del. Rev.* **2004**, *56*, 1537.
3. Ikkala, O.; ten Brinke, G. *Chem. commun.* **2004**, 2131.
4. Lutz, J.-F.; Laschewsky, A. *Macromol. Chem. Phys.* **2005**, *206*, 813.
5. Pyun, J.; Matyjaszewski, K. *Chem. Mat.* **2001**, *13*, 3436.
6. Förster, S.; Plantenberg, T. *Angew. Chem. Int. Ed.* **2002**, *41*, 688.
7. Storhoff, J. J.; Mirkin, C. A. *Chem. Rev.* **1999**, *99*, 1849.
8. Klok, H.-A. *J. Polym. Sci. Part A: Polym. Chem.* **2005**, *43*, 1.
9. Shenhar, R.; Rotello, V. M. *Acc. Chem. Res.* **2003**, *36*, 549.
10. Sessler, J. L.; Jayawickramarajah, J. *Chem. Comm.* **2005**, 1939.
11. Sivakova, S.; Rowan, S. J. *Chem. Soc. Rev.* **2005**, *34*, 9.
12. Smith JR, W. T. *Progr. polym. sci.* **1996**, *21*, 209.
13. Kondo, K.; Iwasaki, H.; Ueda, N.; Takemoto, K.; Imoto, M. *Makromol. Chem.* **1968**, *120*, 21.

14. Kondo, K.; Iwasaki, H.; Koichi, N.; Ueda, N.; Takemoto, K.; Imoto, M. *Makromol. Chem.* **1969**, 125, 42.
15. Kondo, K.; Ohbe, Y.; Takemoto, K. *Makromol. Chem.* **1976**, 177, 3461.
16. Akashi, M.; Kita, Y.; Inaki, Y.; Takemoto, K. *Makromol. Chem.* **1977**, 178, 1211.
17. Akashi, M.; Kita, Y.; Inaki, Y.; Takemoto, K. *J. Polym. Sci. Part A: Polym. Chem.* **1979**, 17, 301.
18. Akashi, M.; Takada, H.; Inaki, Y.; Takemoto, K. *J. Polym. Sci. Part A: Polym. Chem.* **1979**, 17, 747.
19. Kondo, K.; Tanioku, S.; Takemoto, K. *Makromol. Chem. Rapid Commun.* **1980**, 1, 303.
20. Inaki, Y.; Sugita, S.-I.; Takahara, T.; Takemoto, K. *J. Polym. Sci. Part A: Polym. Chem.* **1986**, 24, 3201.
21. Matsumoto, A. in *Handbook of Radical Polymerization*; Matyjaszewski, K.; Davis, T. P. Ed; John Wiley & Sons: Hoboken, 2002; Vol. p 691.
22. Lutz, J.-F.; Neugebauer, D.; Matyjaszewski, K. *J. Am. Chem. Soc.* **2003**, 125, 6986.
23. Lutz, J.-F.; Pakula, T.; Matyjaszewski, K. *ACS Symp. Ser.* **2003**, 854, 268.
24. Boal, A. K.; Ilhan, F.; DeRouchey, J. E.; Thurn-Albrecht, T.; Russell, T. P.; Rotello, V. M. *Nature* **2000**, 404, 746.
25. Marsh, A.; Khan, A.; Garcia, M.; Haddleton, D. M. *Chem. Commun.* **2000**, 2083.
26. Dahman, Y.; Puskas, J. E.; Margaritis, A.; Merali, Z.; Cunningham, M. *Macromolecules* **2003**, 36, 2198.
27. Thibault, R. J.; Hotchkiss, P. J.; Gray, M.; Rotello, V. M. *J. Am. Chem. Soc.* **2003**, 125, 11249.
28. Puskas, J. E.; Dahman, Y.; Margaritis, A.; Cunningham, M. *Biomacromolecules* **2004**, 5, 1412.
29. Uzun, O.; Sanyal, A.; Nakade, H.; Thibault, R. J.; Rotello, V. M. *J. Am. Chem. Soc.* **2004**, 126, 14773.
30. Kamigaito, M.; Ando, T.; Sawamoto, M. *Chem. Rev.* **2001**, 101, 3689.
31. Matyjaszewski, K.; Xia, J. *Chem. Rev.* **2001**, 101, 2921.
32. Hawker, C. J.; Bosman, A. W.; Harth, E. *Chem. Rev.* **2001**, 101, 3661.
33. Perrier, S.; Takolpuckdee, P. *J. Polym. Sci. Part A: Polym. Chem.* **2005**, 43, 5347.
34. Matyjaszewski, K. *Prog. Polym. Sci.* **2005**, 30, 858.
35. Marsh, A.; Khan, A.; Haddleton, D. M.; Hannon, M. J. *Macromolecules* **1999**, 32, 8725.
36. Van Hest, J. C. M.; Ayres, L.; Spijker, H.; Vos, M.; Opsteen, J. in *Advances in Controlled/Living Radical Polymerization*; Matyjaszewski, K. Ed; 2003; ACS Symposium Series Vol. 854, p 394.
37. Yang, X.; Xu, P.; Ding, S.; Radosz, M.; Shen, Y. *Polymer Preprints* **2004**, 45, 1061.

38. Lutz, J.-F.; Thünemann, A. F.; Nehring, R. *J. Polym. Sci. Part A: Polym. Chem.* **2005**, *43*, 4805.
39. Lutz, J.-F.; Thünemann, A. F.; Rurack, K. *Macromolecules* **2005**, *38*, 8124.
40. Spijker, H. J.; Dirks, A. J.; Van Hest, J. C. M. *Polymer* **2005**, *46*, 8528.
41. Sedlak, M.; Simunek, P.; Antonietti, M. *J. Heterocyclic Chem.* **2003**, *40*, 671.
42. Ding, S.; Radosz, M.; Shen, Y. *Macromol. Rapid Commun.* **2004**, *25*, 632.
43. Vidovic, E.; Saric, K.; Janovic, Z. *Croat. Chem. Acta* **2002**, *75*, 769.
44. Teodorescu, M.; Matyjaszewski, K. *Macromolecules* **1999**, *32*, 4826.
45. Veronese, F. M. *Biomaterials* **2001**, *22*, 405.
46. Duncan, R. *Nature Rev. Drug Discov.* **2003**, *2*, 347.
47. Jones, M.-C.; Ranger, M.; Leroux, J.-C. *Bioconjugate Chem.* **2003**, *14*, 774.
48. Tao, L.; Mantovani, G.; Lecolley, F.; Haddleton, D. M. *J. Am. Chem. Soc.* **2004**, *126*, 13220.
49. Mantovani, G.; Lecolley, F.; Tao, L.; Haddleton, D. M.; Clerx, J.; Cornelissen, J. J. L. M.; Velonia, K. *J. Am. Chem. Soc.* **2005**, *127*, 2966.
50. Xu, F. J.; Li, Y. L.; Kang, E. T.; Neoh, K. G. *Biomacromolecules* **2005**, *6*, 1759.
51. Baglioni, P.; Berti, D. *Curr. Opin. Colloid Interface Sci.* **2003**, *8*, 55.
52. Nowick, J. S.; Chen, J. S. *J. Am. Chem. Soc.* **1992**, 114.
53. Nowick, J. S.; Chen, J. S.; Noronha, G. *J. Am. Chem. Soc.* **1993**, *115*, 7636.

Chapter 15

Conjugates of Polymers and Sequence-Defined Polypeptides via Controlled Radical Polymerization

Mattijs G. J. Ten Cate and Hans G. Börner*

Max Planck Institute of Colloids and Interfaces, Colloid Department,
MPI KGF Golm, 14424 Potsdam, Germany

*Corresponding author: hans.boerner@mpikg-golm.mpg.de

The assessment of macromolecular conjugates comprising polymers and sequence-defined oligopeptides via either ATRP or RAFT polymerization is described. Therefore, well-defined oligopeptide macroinitiators for the ATRP process, as well as macro chain-transfer agents for the RAFT polymerization were synthesized. These could be obtained by solid-phase supported synthesis approaches, allowing the preparation of ATRP macroinitiators and RAFT agents without the need for a chromatographic purification step. Kinetic investigations were presented, revealing an efficient control of the polymerization processes. However, inherent difficulties were also encountered. Moreover, it has been shown that both the structure and chirality of the peptide segment are not affected by the radical polymerization processes.

Introduction

The combination of both bioorganic and synthetic polymer segments in well-defined architectures has received considerable attention (1-7). Particularly, the tailored incorporation of sequence-defined oligo- or polypeptides into synthetic polymers is interesting for the design of bioactive polymeric materials having the potential to actively interact with biological systems (8-12).

Furthermore, defined structure formation of the peptide segment e.g. the adoption of secondary, tertiary or quaternary structures can be used to induce and guide structure formation processes in synthetic polymers (13). Therefore, specific interactions including molecular recognition of peptide-based receptors-ligand pairs could lead to self-assembled, materials such as nanowires or fibers, useful for biomedical applications. These structures might respond to external stimuli and exhibit potentially auto-correction or self-healing properties due to relative soft but often cooperative interactions in between the building blocks (14). Besides the potential properties of the peptide segment, the inexpensive polymeric block contributes to the solubility and mechanical properties of the resulting materials. This is advantageous compared to exclusively peptidic or protein-based materials (15). In this chapter, the synthetic approaches to obtain conjugates between well-defined oligopeptides and polymers are described. Conjugates synthesized utilizing grafting techniques via the polymerization of oligopeptide functionalized macromonomers will be excluded (16,17).

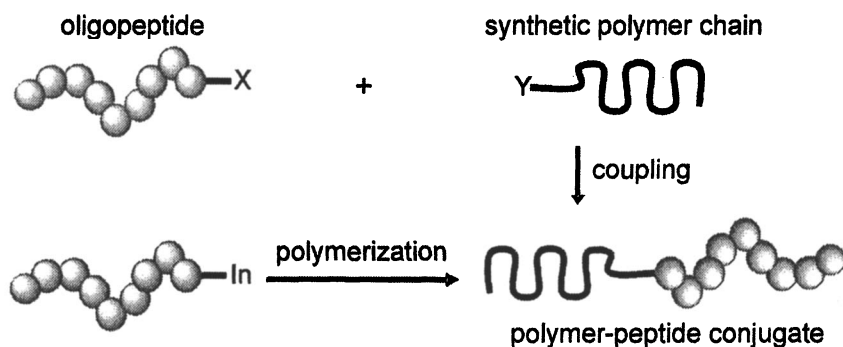


Figure 1. Approaches to integrate sequence controlled polypeptides into synthetic polymer (e.g. $X = NH_2$, $Y = COOH$).

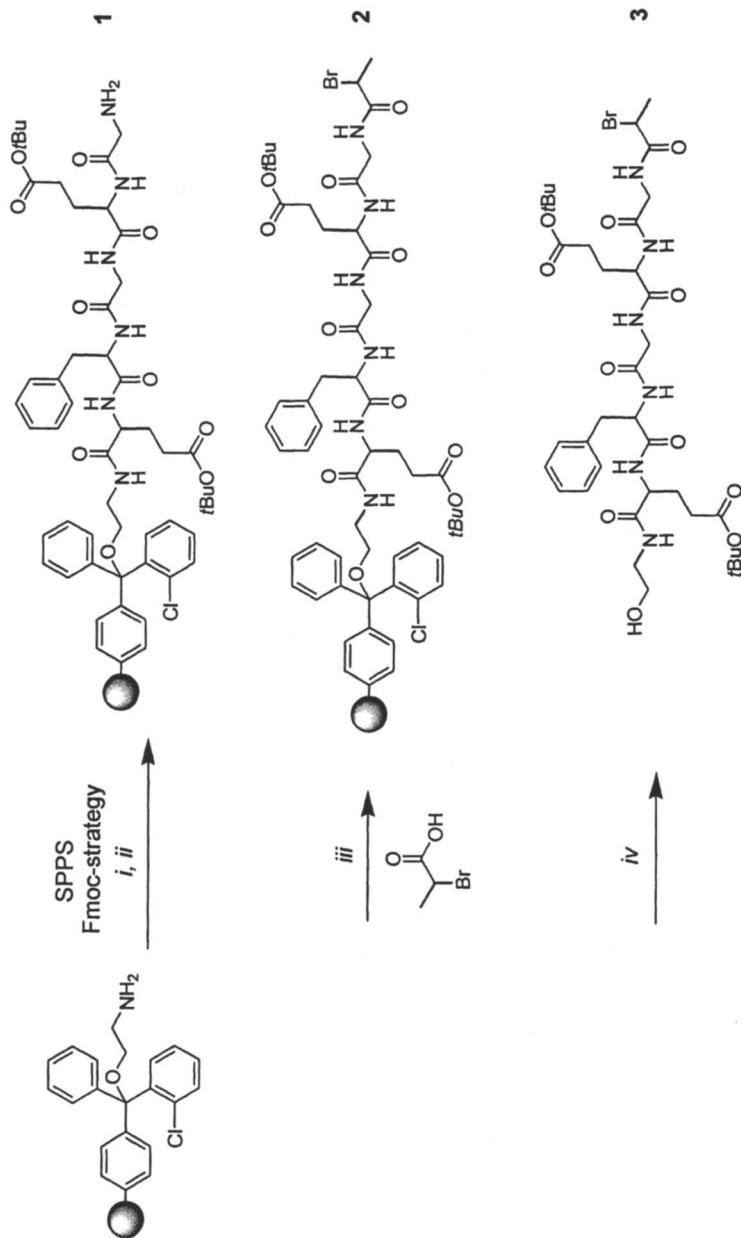
Two synthetic approaches to integrate sequence controlled polypeptides into synthetic polymers are described. These comprise the direct coupling (18-20) of peptides to synthetic polymers and the polymerization from a peptidic macroinitiator (Figure 1). The direct coupling approach becomes progressively more difficult (21) when the molecular weight of the polymer or peptide increases (due to an decrease in chain end-group reactivity) and when complex peptides are coupled (since the establishment of regioselectivity becomes progressively more difficult). By application of the polymerization approach,

these problems can be avoided. Therefore, existing polymerization techniques were adapted to establish generally applicable routes. Controlled radical polymerization (CRP)(22) techniques seem to be most suited for the synthesis of the macromolecular conjugates. Due to the control over molecular weight and molecular weight distribution as well as the high tolerance for diverse functional groups, CRP methods are promising for the production of a variety of well-defined conjugates with broad spectra in composition, topologies and architectures (22). Currently, the application of sequence-defined polypeptides as macroinitiators for various CRP methods have been described (2,23-25), including nitroxide-mediated radical polymerization (NMP (26)), atom transfer radical polymerization (ATRP (27,28)) and reversible addition-fragmentation transfer radical polymerization (RAFT (22,29,30)). The following sections describe recent developments in the use of ATRP and RAFT techniques to obtain well-defined macromolecular conjugates comprising synthetic polymers and sequence-defined oligopeptides.

Atom transfer radical polymerization

ATRP is recognized as a robust polymerization technique, allowing access to a broad range of different polymers (27,31) and polymer architectures (32), while showing tolerance towards diverse functional groups (33). This section describes a two step route involving solid-phase supported synthesis of an oligopeptide macroinitiator and solution-phase controlled radical polymerization. An elegant way towards block copolymers, avoiding purification problems of the product from residual monomer, solvent and catalyst is the controlled solid-phase supported radical polymerization. This is because with this technique impurities can simply be removed by washing. However, compared to solution-phase polymerizations, diffusion limitation of the deactivation step in the ATRP is difficult to overcome (34-36).

A sequence-defined macroinitiator was synthesized by coupling of an ATRP initiator to the amine terminus of a supported oligopeptide (Scheme 1). Since alkyl 2-bromopropionates are standard ATRP initiators for the acrylate polymerization, 2-bromopropionic acid was used for the amidation of the *N*-terminal amine group of the supported oligopeptide. An acid labile 2-chlorotriptyl resin was used for the synthesis of the peptide, allowing the liberation of fully side chain protected oligopeptides from the support under gentle conditions. Therefore, the relatively sensitive ATRP initiator moiety could be introduced before liberation from the resin and critical functionalities (e.g. carboxylates or amines that interfere with the ATRP catalyst) remain reversibly protected. As primary structure of the oligopeptide, Gly-Asp-Gly-Phe-Asp (GDGFD, **1** in Scheme 1) was selected to demonstrate the process of obtaining peptide-polymer



Scheme 1. Solid-phase supported synthesis of the oligopeptide macroinitiator for ATRP
(Conditions: *i*. 2-aminoethanol-2-chlorotriethyl resin, Fmoc-Aa-OH, HBTU, DIPEA, NMP; *ii*. 20% piperidine in NMP; *iii*. DCC, NMP, 12 h; *iv*. 2% trifluoroacetic acid in DCM).

conjugates via ATRP. The Asp residues exhibit bulky tert-butyl ester protecting groups improving solubility and preventing oligopeptide aggregation, while the phenyl ring from the Phe residue can act as a label for quantitative analysis. As a result of the fundamental orientation of this study we renounce the use of a biological active sequence.

The macroinitiator **3** was subsequently used homogeneously in solution for the CRP of *n*-butyl acrylate. As the ATRP catalyst system pentamethyl-diethylenetriamine (PMDETA) complexes of CuBr and CuBr₂ were used. The PMDETA ligand forms a relatively stable and active catalyst, allowing moderate reaction conditions and short reaction times. The solution-ATRP reaction leading to poly(*n*-butyl acrylate)-*block*-polypeptide revealed a process with high level of control, providing molecular weights that increased linearly with reaction time and relatively low polydispersities ($M_w/M_n \approx 1.20$; Figure 2). However, even though the ATRP process involving the oligopeptide **3** resulted in well-defined products, interactions between the copper catalyst and the peptide took place (2). This was indicated by the relatively slow overall polymerization rate compared to the ATRP with non-peptidic initiators and the observed curvature in the first kinetic plot (Figure 2b).

This was, indeed, expected because oligopeptides have the inherent property to act as multi-dentate ligands for metal ions due to their polyamide backbone (37). These interactions were confirmed by additional experiments using various amounts of an oligopeptide with a similar amino acid sequence, but without the ATRP initiator moiety (2). Instead of the peptide macroinitiator, methyl-2-bromopropionate was used to start the ATRP process, while the other reaction conditions were kept constant. A significant decrease of overall polymerization rate was observed with increasing oligopeptide concentration, leading to an inversely proportional relation between overall polymerization rate and peptide concentration. This indicates the occurrence of defined interactions between the catalyst and the peptide, which is most likely due to a ligand exchange reaction with the ATRP metal complex, resulting in partial inhibition of the catalyst. The polyamide backbone and, when relevant, the side chain functionalities of the peptide causes the molecule to function as a multidentate ligand for metal ions (37). A comparable behavior has been reported in the ATRP processes of (meth)acrylamides (38). There, frequently the increase of the amount of catalyst could overcome this problem (38).

Initial attempts to characterize the poly(*n*-butyl acrylate)-*block*-DFGDG conjugate by MALDI-TOF mass spectroscopy failed due to difficult desorption and/or ionization properties of the peptide-polymer conjugate. However, it was possible to analyze the conjugate comprising a GGFGG peptide by MALDI-TOF mass spectrometry (13), indicating the influence of the peptide segment on the polymer properties (Figure 3). The mass spectrum clearly shows the poly(*n*-butyl acrylate)-*block*-polypeptide conjugates. Two homologue series were observed assignable to the same molecular species with either sodium or potassium ion adducts, as indicated by the mass difference of 16 *m/z*.

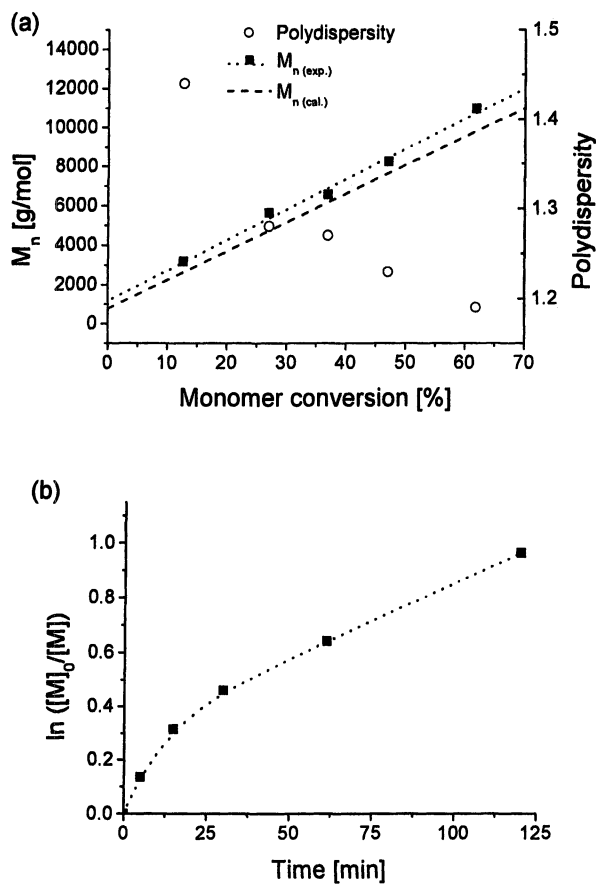


Figure 2. ATRP of nBA initiated by 3 at 60 °C: App. M_n , GPC vs conversion (a) and $\ln([M]_0/[M])$ vs reaction time (b) (cond.: $[nBA]_0/[In]_0/[CuBr]_0/[CuBr_2]_0/[PMDETA]_0 = 114/1/1/0.05/1.05$, DMSO = 60 vol.%).

(Reproduced from reference 2, Copyright 2004 Wiley-VCH)

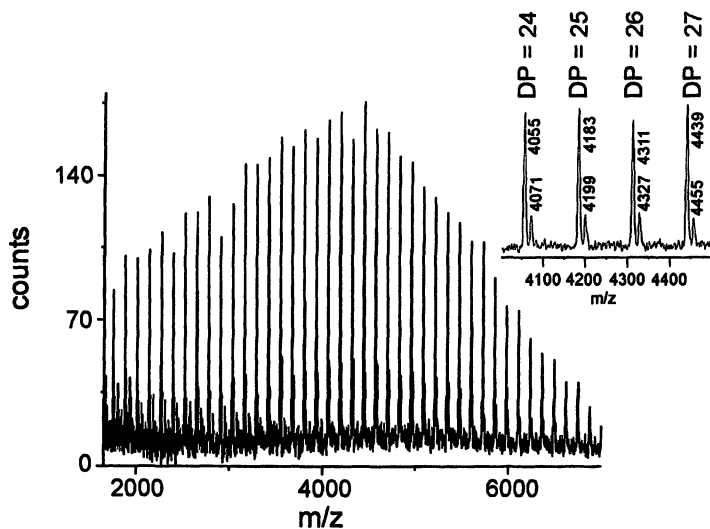


Figure 3. MALDI-TOF mass spectrum showing the sodium and potassium adducts of poly(*n*-butyl acrylate)-block-GGFGG.

Furthermore, in both series, a characteristic mass difference of 128 m/z was found that is consistent with the mass of the *n*BA repeat unit. As end groups, bromine and the GGFGG peptide segment was found with a remainder mass of 0.5 m/z , verifying the chemical structure of the *p**n*BA-peptide conjugate. Neither major side products nor the presence of polymers, lacking the peptide segment could be observed within the error of the MALDI-TOF-MS method. This confirms a clean incorporation of the peptide segment by the ARTP macroinitiator approach.

In conclusion, the two-step synthetic route for the introduction of sequence-defined oligopeptides into synthetic polymers can be utilized for the preparation of oligopeptide-*block*-poly(*n*BA). Well-defined block copolymers with low M_w/M_n and controllable M_n were obtained. Solution-phase ATRP was initiated by an oligopeptide macroinitiator accessible via solid-phase peptide synthesis. Interactions between the catalyst and the oligopeptide, however, were evident and could not be suppressed. Nevertheless, these interactions were not critical in terms of synthesis control of the desired copolymer.

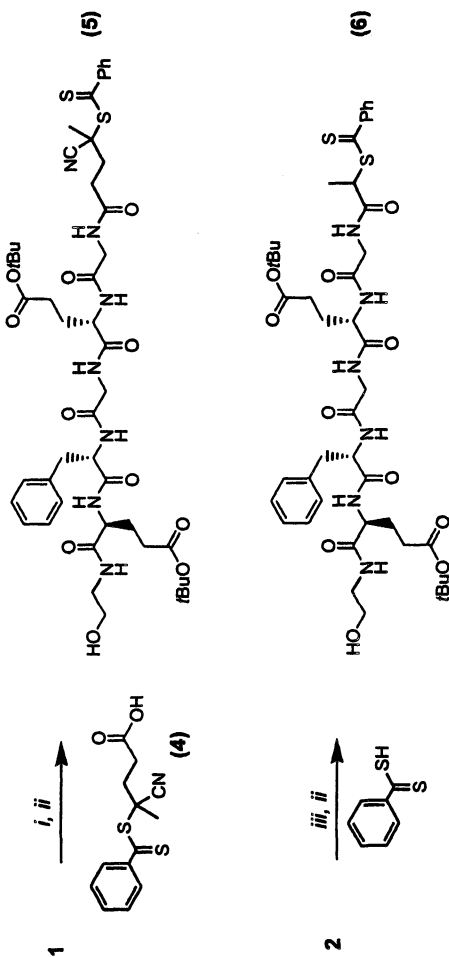
Reversible addition-fragmentation transfer radical polymerization

An inherent difficulty of ATRP involving oligopeptide structures is the interaction between the copper catalyst and the peptide. These interactions cannot be suppressed (2) and likely depend strongly on the length as well as on the amino acid sequence of the oligopeptide. Therefore, the polymerization conditions have to be optimized for each applied oligopeptide, complicating the use of ATRP as a general approach for the synthesis of peptide-polymer conjugates. These ligating properties do not occur within RAFT radical polymerization since this technique does not require a metal catalyst. RAFT radical polymerization has been proven to be a valuable tool to access well-defined polymer-peptide conjugates (25). The RAFT process allows for the controlled polymerization of a large diversity of monomers and is a facile method since the involved components are not air or moisture sensitive. The components can be simply dissolved and deoxygenated prior to the polymerization. Moreover, racemization and thermal degradation is expected to be limited because the polymerizations are performed at moderate reaction temperatures and basic conditions, that might cause racemization, are strictly avoided.

This section describes the straightforward solid-phase supported synthesis (SPPS) approaches to oligopeptide based RAFT agents and their utilization within the solution polymerization of *n*-butyl acrylate. For the SPPS of oligopeptide transfer agents, two different synthetic strategies were evaluated: i. the coupling of a preformed RAFT agent to the *N*-terminus of a peptide and; ii. The transformation of an ATRP macroinitiator into a RAFT functionality (Scheme 2). The GDGFD peptide sequence, utilized in the ATRP section, was used to demonstrate the process, making the results directly comparable to the previously described ATRP study.

Synthesis of the peptide macrotransfer agents

A carboxylic acid functionalized RAFT agent (4 in Scheme 2) was coupled to the *N*-terminus of a resin bound oligopeptide, similar to the established synthesis of oligopeptide ATRP macroinitiators. This approach would allow the regio-selective introduction of the transfer group either at the *N*-terminus or at a specific sequence-position by the modification of an ϵ -amine group of a lysine residue (25). However, besides the oligopeptide chain transfer agent (CTA) 5 the formation of a byproduct was observed. This resulted from the nucleophilic attack of the peptide amine terminus on the dithioester, leading to a thioamide structure. The thioamide was present in significant amounts (~24%), but was not



Scheme 2. Solid-phase supported synthesis of the oligopeptide transfer agents **5** and **6**. (Conditions: i. DCC, NMP, room temperature; ii. 2% trifluoroacetic acid in DCM; iii. dithiobenzoic acid, pyridine, THF, 60 °C).

found to interfere with the CRP process (data not shown) (25). Nevertheless, the method could be applied to the coupling of RAFT agents via hydroxyl moieties, e.g. to side chain functionalities of serine or threonine residues, where the particular side reaction is not expected. This would lead to a hydrolytically labile ester-linkage between the peptide and the polymer that might be interesting for the predefined degradation of peptide-polymer conjugates or for the liberation of peptide segments as bio-functional units in e.g. medical applications.

The second method comprises the functionality switch of an ATRP macroinitiator (2) into an oligopeptide transfer agent (6). With this approach, the formation of a thioamide side product is avoided due to the absence of nucleophilic amines during the introduction of the RAFT chain transfer moiety. The oligopeptide transfer agent 6 was obtained by reaction of the resin bound ATRP initiator 2 with the pyridinium salt of the dithiobenzoic acid (25). The substitution of the bromine of 3 is quantitative and besides the formation of 6 no side reactions occurred. The solid-phase supported synthesis of 6 has shown to be convenient for the synthesis of (oligo)peptide RAFT agents. Moreover, the products are readily purified, while chromatographic purifications that are usually necessary can be avoided.

The RAFT polymerization

The poly(*n*-butyl acrylate)-*block*-polypeptide (7) was synthesized to examine the RAFT radical polymerization of *n*BA (25). The macrotransfer agent 6 was used homogeneously in solution for CRP of *n*-butyl acrylate with AIBN (20 mol%) as radical source.

The polymerization proceeds in a controlled manner, providing well-defined peptide-polymer conjugates with molecular weights that increase linearly with monomer consumption and low polydispersities ($M_w/M_n \approx 1.1$) (Figure 4a). Moreover, the semi-logarithmic plot shows a first order kinetics after a retardation period of about 8 hours (Figure 4b). Though retardation periods are frequently observed within RAFT processes, the causes are still controversially since the mechanism in the early stage of the polymerization remains difficult to access. It has been suggested that retardation within the RAFT process occurs either due to an intermediate radical termination (39-43), or due to a slow fragmentation/reinitiation (39,44). Retardation times should be taken into consideration for controlled polymerizations, especially when low molecular weight compounds are targeted.

A comparable retardation period was observed when only 5 mol% of AIBN was used, excluding the possibility that potential impurities retard the polymerization of *n*BA with 6. The slope of the first order kinetics plot was, expectedly, 4 times smaller (dashed line in Figure 4b); *i.e.* 0.014 for 5% AIBN and 0.056 for 20% AIBN, indicating that the rate of polymerization directly correlates to the amount of formed radicals.

To confirm the incorporation of the oligopeptide segment into the polymer a low molecular weight conjugate of **7** ($M_{n,NMR} = 4.6$ kDa; $DP_{n,NMR} = 29$) was synthesized and precipitated multiple times in MeOH/H₂O. Since this is a good solvent mixture for the oligopeptide segment, the absence of peptides that are not bound to a polymer can be ensured. The formation of the poly(*n*-butyl acrylate)-*block*-polypeptide conjugate was conclusively demonstrated by ¹H NMR spectroscopy, showing the characteristic resonances for the protons of the oligopeptide, the poly(*n*BA) segment, as well as the RAFT moiety (Figure 5a).

Since both the RAFT and peptide end-group functionalities were quantified in a ratio 1:1, formation of the dimerization product, resulting from termination via radical coupling can be excluded within the experimental error of the analytical method. These results are supported by size exclusion chromatography (SEC) showing that **6** has a mono-modal and narrow molecular weight distribution with $M_w/M_n = 1.18$. In addition, the number average molecular weight was determined with $M_{n,app} = 4.1$ kDa, resembling the value calculated based on ¹H NMR end group analysis. Since the RAFT moiety remains quantitatively at the end of the polymer chain of the isolated conjugates, the polymer chain-end can be modified by further block extension or functionality transformation. This may allow access of polymers with advanced architectures.

It is essential to prove that the chirality of the oligopeptide segment is unaffected during the polymerization process, since the structural conformation and, thus, the biological function of peptides, is strongly influenced by the chirality. Circular dichroism (CD) spectroscopy showed conclusively that the chirality of the oligopeptide segment is unaffected during the polymerization process. The similar CD spectra of **6** and **7** (Figure 5b) support the effective incorporation of the peptide segment into the polymer and verify the absence of racemization. These results demonstrate a novel and straightforward synthesis route toward multifunctional RAFT agents that can be utilized within CRP to obtain well-defined peptide-polymer conjugates. Moreover, the method exhibits high potential to be extended to diverse conjugated polymer systems including polypeptides, PNA's and polysaccharides.

Conclusion

It was shown that well-defined conjugates comprising sequence-defined oligopeptides and synthetic polymers can be obtained utilizing ATRP and RAFT radical polymerization. Solution-phase ATRP was initiated by an oligopeptide macroinitiator accessible via solid-phase peptide synthesis. Although interactions between the catalyst and the oligopeptide were evident, they were not critical in terms of synthesis control of the desired copolymer. The use of ATRP introduces the possibility to integrate oligopeptides into a variety of different polymers or

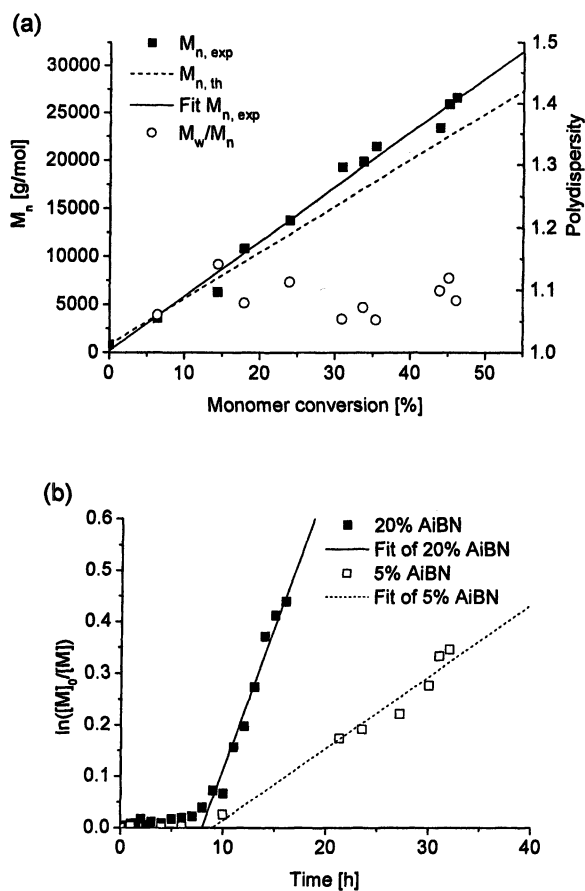


Figure 4. RAFT polymerization of *n*BA controlled by **6** at 60 °C: M_n GPC vs conversion (a) and first-order kinetic plot $\ln([M]_0/[M])$ vs reaction time (b) (Conditions: $[nBA]_0/[6]_0/[AIBN]_0 = 375/1/0.2$, DMF = 60 vol %). (Reproduced from reference 25, Copyright 2005 American Chemical Society.)

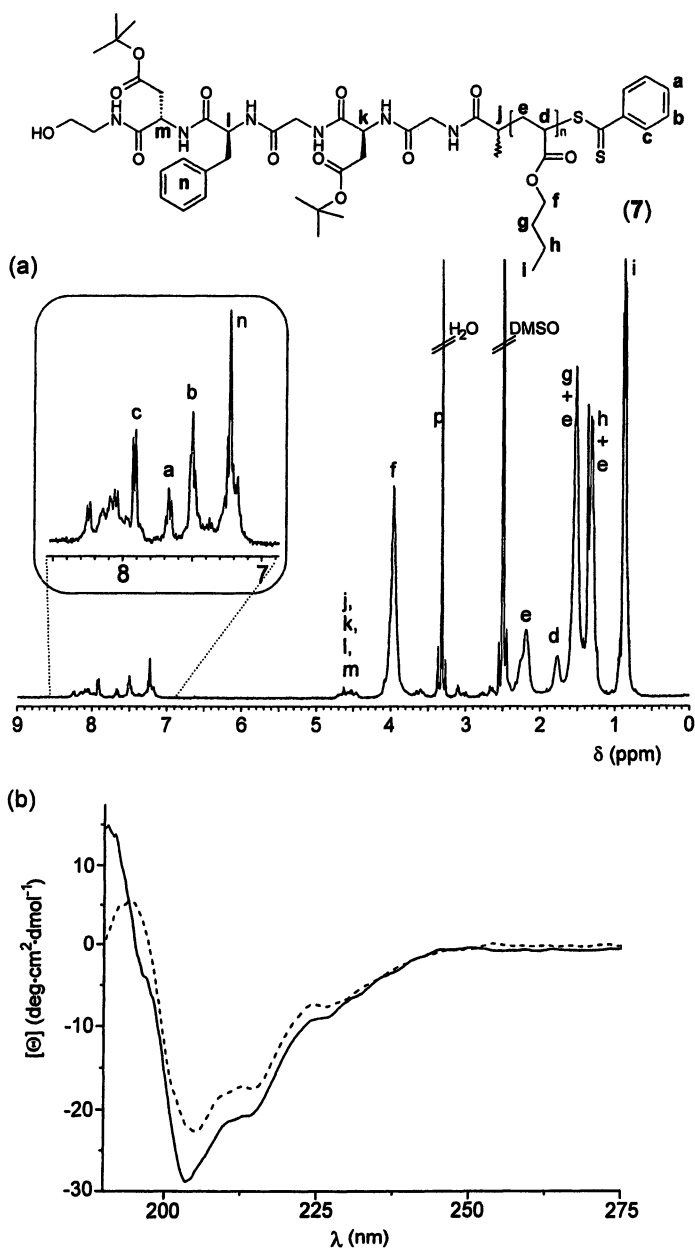


Figure 5. (a) ^1H NMR spectrum (DMSO- d_6) of oligopeptide-poly(*n*-butyl acrylate) conjugate **7** and (b) CD spectrum (MeOH) of oligopeptide transfer agent **6** (dashed line) and oligopeptide-poly(*n*-butyl acrylate) conjugate **7** (solid line). (Reproduced from reference 25, Copyright 2005 American Chemical Society.)

copolymers. However, the interaction between the copper catalyst and the peptide has been found to be an inherent difficulty that could not be suppressed (2). Therefore, the polymerization conditions must be optimized for each applied oligopeptide, complicating the use of ATRP as a general approach for the synthesis of peptide-polymer conjugates.

To avoid these difficulties, the utilization of RAFT radical polymerization was investigated since no metal catalysts are employed in the RAFT polymerization process. Two different strategies were evaluated for the synthesis of oligopeptide transfer agents; namely, the transformation of an ATRP initiator into a RAFT functionality and the coupling of a preformed RAFT agent to a peptide. The functionality change of a resin-bound oligopeptide ATRP macroinitiator into an oligopeptide transfer agent proceeds in a clean manner. The coupling of a carboxylic acid functionalized RAFT agent to the *N*-terminal amine group of a supported oligopeptide was accompanied by the formation of a thioamide side product that could not be significantly suppressed. However, the simplicity of the latter method makes it highly suited for the coupling of RAFT agents to hydroxyl functionalities of resin-bound macromolecules since in this case the formation of a thioamide side product is not expected. The coupling of RAFT agents to hydroxyl functionalities could be of interest for the preparation of transfer agents possessing bioorganic segments such as oligopeptides, oligosaccharides or oligonucleotides.

The RAFT radical polymerization of *n*-butyl acrylate in solution using an oligopeptide transfer agent showed an efficient control of the polymerization processes. Peptide-polymer conjugates exhibited a low molecular weight distribution ($M_w/M_n \approx 1.1$) and controllable molecular weights. A retardation period of about 8 hours was observed prior to the polymerization. The peptide segments were quantitatively incorporated into the polymer and it was shown that both the structure and chirality of the peptide segment were not affected by the polymerization procedures. The RAFT group remains qualitatively at the end of the polymer chain after isolation of the conjugates, allowing further modification of the conjugates by block extensions or functionality transformation. This potentially allows the production of polymers with advanced architectures.

Acknowledgement: E. Krause, H. Rettig, K. Otte, J. Brandt, M. Gräwert, O. Niemeyer and C. Erich are thanked for contributions to this work. Financial support was received from the German Research Foundation through the Emmy Noether Program (BO 1762/2-2) and the Max Planck Society.

References

1. Schlaad, H.; Antonietti, M. *Eur. Phys. J. E* **2003**, *10*, 17-23.
2. Rettig, H.; Krause, E.; Börner, H. G. *Macromol. Rapid Commun.* **2004**, *25*, 1251-1256.

3. Smeenk, J. M.; Lowik, D.; van Hest, J. C. M. *Curr. Org. Chem.* **2005**, *9*, 1115-1125.
4. Vandermeulen, G. W. M.; Klok, H. A. *Macromol. Biosci.* **2004**, *4*, 383-398.
5. Watson, K. J.; Park, S. J.; Im, J. H.; Nguyen, S. T.; Mirkin, C. A. *J. Am. Chem. Soc.* **2001**, *123*, 5592-5593.
6. Muthukrishnan, S.; Zhang, M. F.; Burkhardt, M.; Drechsler, M.; Mori, H.; Muller, A. H. E. *Macromolecules* **2005**, *38*, 7926-7934.
7. Wang, Y.; Armitage, B. A.; Berry, G. C. *Macromolecules* **2005**, *38*, 5846-5848.
8. Tirrell, M.; Kokkoli, E.; Biesalski, M. *Surf. Sci.* **2002**, *500*, 61-83.
9. Langer, R.; Tirrell, D. A. *Nature* **2004**, *428*, 487-492.
10. Di Zio, K.; Tirrell, D. A. *Macromolecules* **2003**, *36*, 1553-1558.
11. Irvine, D. J.; Mayes, A. M.; Griffith, L. G. *Biomacromolecules* **2001**, *2*, 85-94.
12. Yamato, M.; Kwon, O. H.; Hirose, M.; Kikuchi, A.; Okano, T. *J. Biomed. Mater. Res.* **2001**, *55*, 137-140.
13. Eckhardt, D.; Groenewolt, M.; Krausse, E.; Börner, H. G. *Chem. Commun.* **2005**, 2814-2816.
14. Whitesides, G. M.; Mathias, J. P.; Seto, C. T. *Science* **1991**, *254*, 1312-1319.
15. Langer, R.; Tirrell, D. A. *Nature* **2004**, *428*, 487-492.
16. Ayres, L.; Vos, M. R. J.; Adams, P.; Shklyarevskiy, I. O.; van Hest, J. C. M. *Macromolecules* **2003**, *36*, 5967-5973.
17. Godwin, A.; Hartenstein, M.; Muller, A. H. E.; Brocchini, S. *Angew. Chem. Int. Ed.* **2001**, *40*, 594-597.
18. Chapman, A. P. *Adv. Drug Deliv. Rev.* **2002**, *54*, 531-545.
19. Roberts, M. J.; Bentley, M. D.; Harris, J. M. *Adv. Drug Deliv. Rev.* **2002**, *54*, 459-476.
20. Rosler, A.; Klok, H. A.; Hamley, I. W.; Castelletto, V.; Mykhaylyk, O. O. *Biomacromolecules* **2003**, *4*, 859-863.
21. Vandermeulen, G. W. M.; Tziatzios, C.; Klok, H. A. *Macromolecules* **2003**, *36*, 4107-4114.
22. Chiefari, J.; Rizzardo, E. In *Handbook of Radical Polymerization*; Matyjaszewski, K., Davis, T. P., Eds.; Wiley-Interscience: 2002, p 629-690.
23. Becker, M. L.; Liu, J.; Wooley, K. L. *Biomacromolecules* **2005**, *6*, 220-228.
24. Mei, Y.; Beers, K. L.; Byrd, H. C. M.; VanderHart, D. L.; Washburn, N. R. *J. Am. Chem. Soc.* **2004**, *126*, 3472-3476.
25. Ten Cate, M. G. J.; Rettig, H.; Bernhardt, K.; Börner, H. G. *Macromolecules* **2005**, *38*, 10643-10649.
26. Hawker, C. J.; Bosman, A. W.; Harth, E. *Chem. Rev.* **2001**, *101*, 3661-3688.
27. Matyjaszewski, K.; Xia, J. *Chem. Rev.* **2001**, *101*, 2921-2990.
28. Wang, J. S.; Matyjaszewski, K. *J. Am. Chem. Soc.* **1995**, *117*, 5614-5615.

29. Chiefari, J.; Chong, Y. K.; Ercole, F.; Krstina, J.; Jeffery, J.; Le, T. P. T.; Mayadunne, R. T. A.; Meijs, G. F.; Moad, C. L.; Moad, G.; Rizzardo, E.; Thang, S. H. *Macromolecules* **1998**, *31*, 5559-5562.
30. Chong, Y. K.; Le, T. P. T.; Moad, G.; Rizzardo, E.; Thang, S. H. *Macromolecules* **1999**, *32*, 2071-2074.
31. Matyjaszewski, K. *Chem. Eur. J.* **1999**, *5*, 3095-3102.
32. Patten, T. E.; Matyjaszewski, K. *Adv. Mater.* **1998**, *10*, 901-+.
33. Coessens, V.; Pintauer, T.; Matyjaszewski, K. *Prog. Polym. Sci.* **2001**, *26*, 337-377.
34. Pyun, J.; Kowalewski, T.; Matyjaszewski, K. *Macromol. Rapid Commun.* **2003**, *24*, 1043-1059.
35. Angot, S.; Ayres, N.; Bon, S. A. F.; Haddleton, D. M. *Macromolecules* **2001**, *34*, 768-774.
36. Husseman, M.; Malmstrom, E. E.; McNamara, M.; Mate, M.; Mecerreyes, D.; Benoit, D. G.; Hedrick, J. L.; Mansky, P.; Huang, E.; Russell, T. P.; Hawker, C. J. *Macromolecules* **1999**, *32*, 1424-1431.
37. Chen, J. G.; Logman, M.; Weber, S. G. *Electroanalysis* **1999**, *11*, 331-336.
38. Neugebauer, D.; Matyjaszewski, K. *Macromolecules* **2003**, *36*, 2598-2603.
39. Feldermann, A.; Coote, M. L.; Stenzel, M. H.; Davis, T. P.; Barner-Kowollik, C. *J. Am. Chem. Soc.* **2004**, *126*, 15915-15923.
40. Kwak, Y.; Goto, A.; Komatsu, K.; Sugiura, Y.; Fukuda, T. *Macromolecules* **2004**, *37*, 4434-4440.
41. McLeary, J. B.; Calitz, F. M.; McKenzie, J. M.; Tonge, M. P.; Sanderson, R. D.; Klumperman, B. *Macromolecules* **2004**, *37*, 2383-2394.
42. Monteiro, M. J.; de Brouwer, H. *Macromolecules* **2001**, *34*, 349-352.
43. Venkatesh, R.; Staal, B. B. P.; Klumperman, B.; Monteiro, M. J. *Macromolecules* **2004**, *37*, 7906-7917.
44. Barner-Kowollik, C.; Quinn, J. F.; Morsley, D. R.; Davis, T. P. *J. Polym. Sci., Part A: Polym. Chem.* **2001**, *39*, 1353-1365.

Chapter 16

Synthesis and Characterization of Methacrylate-Type Glycopolymers with Branched Architectures

Sharmila Muthukrishnan¹, Hideharu Mori²,
and Axel H. E. Müller^{1,*}

¹Makromolekulare Chemie II, Universität Bayreuth, D-95440 Bayreuth, Germany

²Department of Polymer Science and Engineering, Faculty of Engineering, Yamagata University, 4-3-16, Jonan, Yonezawa 992-8510, Japan

*Corresponding author: Axel.Mueller@uni-bayreuth.de

ABSTRACT: We report the synthesis and characterization of glycopolymers of different topologies via atom transfer radical polymerization (ATRP) of a sugar-carrying methacrylate monomer, 3-*O*-methacryloyl-1,2:5,6-di-*O*-isopropylidene- α -D-glucofuranose (MAIGlc). Hyperbranched glycopolymers were obtained by self-condensing vinyl copolymerization (SCVCP) of the methacrylic AB* inimer, 2-(2-bromoisobutyryloxy)ethyl methacrylate (BIEM) with MAIGlc via ATRP, followed by deprotection of the isopropylidene protecting groups. The branched structures were confirmed by ¹H NMR, elemental analyses, gel permeation chromatography (GPC) and GPC using a viscosity detector (GPC/viscosity) measurements. Then the monomer, MAIGlc and the polyinitiator, poly(2-(2-bromoisobutyryloxy)ethyl methacrylate), (PBIEM) were used to obtain glycocylindrical brushes (“molecular sugar sticks”) with PMAGlc side chains, using the ‘grafting from’ approach via ATRP. The efficiency of the initiating sites of the polyinitiator, PBIEM was determined to be in the range of $0.23 < f < 0.38$ by cleaving the side chains from the backbone. Scanning Force Microscopy (SFM) shows that the morphology of the resulting glycocylindrical brushes is worm-like despite of low grafting efficiency. After deprotection, the water-soluble brushes were investigated using SFM and cryogenic transmission electron microscopy (cryo-TEM) measurements.

The traditional view of carbohydrate polymers as nature's energy source (starch and glycogen) and structural materials has expanded. Glycopolymers, synthetic sugar-containing polymers, are increasingly attracting the chemists due to their role as biomimetic analogues and their potential for commercial applications. There are different polymerization techniques which have enabled the synthesis of glycopolymers featuring a wide range of controlled architectures and functionalities. Methodologies for the synthesis of glycopolymers can be roughly classified into two main categories: (1) polymerization of sugar-bearing monomers and (2) chemical modifications of preformed polymers with sugar-containing reagents. In general, the latter method frequently results in glycopolymers having less regular structures because of incomplete reactions due to steric hindrance. Therefore, it is often better to use polymerizations of sugar-carrying monomers for synthesizing glycopolymers of well-defined architectures.

Synthetic glyco-based polymers are now being used as very important tools to investigate carbohydrate-based interactions (1, 2). Such carbohydrate polymers with biocompatible and biodegradable properties are used in tissue engineering and controlled drug release devices. Many of them are used also as surfactants (3), and biologically active polymers (4). There are various types of synthetic sugar-carrying polymers. Among them, highly branched glycopolymers have adopted nature's multivalent approach to their work (5). The polyvalency inherent in carbohydrate-based polymers, especially in branched polymers, is an important feature, which allows these materials to serve as cell surface mimics to understand and manipulate carbohydrate-protein interactions.

Various polymerization techniques have been developed to synthesize sugar-containing polymers with well-defined structures, which involve cationic polymerization (6), ring-opening polymerization (7), ring-opening metathesis polymerization (8), and free radical polymerization (9). Although a variety of glycopolymers has been synthesized by conventional free radical polymerization of vinyl monomers carrying sugar residues, it was difficult to control molecular weights and architecture. Controlled/"living" radical polymerization, namely atom transfer radical polymerization, (ATRP) has allowed well-defined and controlled synthesis of glycopolymers by a very facile and simple approach (10-14). In this report, the sugar-carrying methacrylate monomer, 3-*O*-methacryloyl-1,2:5,6-di-*O*-isopropylidene- α -D-glucofuranose (MAIGlc) is used for the synthesis of well-defined branched glycopolymers of different topologies via ATRP.

Experimental Section

Materials

CuBr (95%, Aldrich) was purified by stirring overnight in acetic acid. After filtration, it was washed with ethanol, ether, and then dried. N,N,N',N'',N''-Pentamethyldiethylenetriamine (PMDETA, 99%, Aldrich) and ethyl 2-bromoisobutyrate (98%, Aldrich) were distilled and degassed. Bis(triphenylphosphine)nickel (II) bromide ((PPh₃)₂NiBr₂, 99%, Aldrich) was

used as received. 1,1,4,7,10,10-Hexamethyltriethylenetetramine (HMTETA, 97%, Aldrich) was used without further purification. 3-*O*-Methacryloyl-1,2:5,6-di-*O*-isopropylidene-*D*-glucofuranose (MAIGlc) was synthesized by the reaction of 1,2:5,6-di-*O*-isopropylidene-*D*-glucofuranose and methacrylic anhydride in pyridine and purified by vacuum distillation as reported by Klein et al. (3). Synthesis of a methacrylic AB* inimer, 2-(2-bromoisobutyryloxy)ethyl methacrylate (BIEM), was conducted by the reaction of 2-bromo-isobutyryl bromide with 2-hydroxyethyl methacrylate in the presence of pyridine as reported previously (15, 16). The inimer was degassed by three freeze-thaw cycles. The synthesis and characterization of the polyinitiator, poly(2-(2-bromoisobutyryloxy)ethyl methacrylate) (PBIEM), employed for the synthesis of the polymer brushes was described in an earlier publication (17). PBIEM was synthesized from poly(2-hydroxyethyl methacrylate) (PHEMA) obtained via anionic polymerization of trimethylsilyl-protected HEMA. All other reagents were used as received.

General Polymerization Procedure

All polymerizations were carried out in a round bottom flask sealed with a plastic cap. The resulting polymer was dissolved in THF, and was subsequently passed through a silica column, the polymer was precipitated from THF into either methanol or petroleum ether. Then the product was freeze-dried from dioxane and finally dried under vacuum at room temperature.

Deprotection

The transformation of poly(MAIGlc)s of different architectures into water soluble polymers, poly(3-*O*-methacryloyl- α,β -*D*-glucopyranose)s, poly(MAGlc)s was achieved under mild acidic condition (10). The resulting polymer was freeze-dried from water and then dried under vacuum. The deprotected polymers were obtained as white powder in a quantitative yield.

Solvolysis

The solvolysis of the brushes was achieved via base catalyzed transesterification in methanol (18). The molecular weights of the resulting products were analyzed using conventional GPC, GPC/viscosity and GPC with a multi-angle light scattering detector (GPC-MALS) measurements.

Characterization

The linear and branched polymers obtained from MAIGlc were characterized by conventional GPC and GPC with viscosity detector using THF as eluent at a flow rate of 1.0 ml/min at room temperature. A conventional THF-phase GPC system was used to obtain apparent molecular weights. GPC system I; column set: 5 μ m PSS SDV gel, 10², 10³, 10⁴, 10⁵ Å, 30 cm each; detectors: Waters 410 differential refractometer and Waters photodiode array detector operated at 254 nm. Narrow PtBMA, PS and PMMA standards (PSS, Mainz) were used for the calibration of column set I. Molecular weights of the branched polymers

were determined by the universal calibration principle (19) using the viscosity module of the PSS-WinGPC scientific V 6.1 software package. Linear PMMA standards (PSS, Mainz) were used to construct the universal calibration curve. GPC with a multi-angle light scattering detector (GPC-MALS) and a Viscotek viscosity detector H 502B (GPC/viscosity) were used to determine the absolute molecular weights of the glycocylindrical brushes and of side chains cleaved by solvolysis. THF was used as eluent at a flow rate of 1.0 mL/min. column set: 5 μ PSS SDV gel, 10^3 Å, 10^5 Å and 10^6 Å, 30 cm each; detectors: Shodex RI-71 refractive index detector, and Wyatt DAWN DSP-F MALS detector equipped with a 632.8 nm He-Ne laser. The refractive index increment in THF solution of the glycocylindrical brush and cleaved side chains at 25 °C were determined to be $dn/dc = 0.072$ mL/mg and 0.065 mL/mg, respectively using a Chromatix KM-16 laser differential refractometer and PSS DnDc-2010/620 differential refractometer, respectively.

^1H NMR spectra were recorded with a Bruker AC-250 spectrometer. The elemental analyses were performed by Ilse Beetz Mikroanalytisches Laboratorium (Kulmbach) and by using Elementaranalysator Vario EL III (Anorganische Chemie II, University of Bayreuth).

The samples for scanning force microscopy (SFM) measurements were prepared either by dip-coating from dilute solutions of brushes in tetrahydrofuran or dioxane/water or methanol/water mixtures, with concentration of 1mg/L onto freshly cleaved mica surface or by spin casting onto a carbon-coated mica surface. Carbon-coated mica substrates were prepared using the mini-deposition system Balzers MED 010 to deposit carbon of approximately 5 nm thickness by evaporation. The SFM images were taken with a Digital Instruments Dimension 3100 microscope operated in Tapping Mode (free amplitude of the cantilever ≈ 30 nm, set point ratio ≈ 0.98).

For cryogenic transmission electron microscopy (cryo-TEM) studies, a drop of the sample was put on an untreated bare copper transmission electron microscopy (TEM) grid (600 mesh, Science Services, München, Germany), where most of the liquid was removed with blotting paper leaving a thin film stretched over the grid holes. The specimens were instantly shock frozen by rapid immersion into liquid ethane and cooled to approximately 90 K by liquid nitrogen in a temperature-controlled freezing unit (Zeiss Cryobox, Zeiss NTS GmbH, Oberkochen, Germany). The temperature was monitored and kept constant in the chamber during all the sample preparation steps. After freezing the specimens, the remaining ethane was removed using blotting paper. The specimen was inserted into a cryo-transfer holder (CT3500, Gatan, München, Germany) and transferred to a Zeiss EM922 EF-TEM. Examinations were carried out at temperatures around 90 K. The TEM was operated at an acceleration voltage of 200 kV. Zero-loss filtered images ($\Delta E = 0$ eV) were taken under reduced dose conditions ($100 - 1000$ e/nm 2). All images were registered digitally by a bottom mounted CCD camera system (Ultrascan 1000, Gatan) combined and processed with a digital imaging processing system (Gatan Digital Micrograph 3.9 for GMS 1.4).

Results and Discussion

Linear and Branched Glycomethacrylates

The sugar-carrying methacrylate monomer, 3-*O*-methacryloyl-1,2:5,6-di-*O*-isopropylidene- α -D-glucofuranose (MAIGlc) was synthesized as reported by Klein et al. (3). In order to find a suitable catalyst system for the synthesis of highly branched glycopolymers by self-condensing vinyl copolymerization (SCVCP) via ATRP, we initially investigated the influence of the catalyst system (Cu- and Ni-based catalysts) on the homopolymerization of MAIGlc. The homopolymerization of MAIGlc was conducted using three different catalyst systems with ethyl 2-bromoisobutyrate (EBIB), which has a same initiating group as in a methacrylic inimer (BIEM). The homopolymerization proceeded smoothly with CuBr/HMTETA and $(\text{PPh}_3)_2\text{NiBr}_2$ catalyst systems in solution resulting in linear poly(MAIGlc)s having controlled molecular weights and narrow molecular weight distributions as shown in Figure 1.

The synthetic route to highly branched glycopolymers is given in Scheme 1. The curved lines represent polymer chains. A*, B*, and M* are active units, whereas a, b, and m are reacted ones. A is a methacryloyl group, and m stands for MAIGlc units in a linear segment. The influence of the comonomer ratio, $\gamma = [\text{MAIGlc}]_0/[\text{BIEM}]_0$ on SCVCP of BIEM with MAIGlc was investigated with $(\text{PPh}_3)_2\text{NiBr}_2$ in ethyl acetate. The polymerization was conducted at 100 °C at different comonomer ratios, $\gamma = [\text{MAIGlc}]_0/[\text{BIEM}]_0$ between 1 and 25, keeping the comonomer-to-catalyst ratio at a constant value of $\mu = ([\text{MAIGlc}]_0 + [\text{BIEM}]_0)/[(\text{PPh}_3)_2\text{NiBr}_2]_0 = 100$. Under that condition, almost full conversion was reached within 5 h for $\gamma > 10$. The tendency is markedly different from the case of 3-*O*-acryloyl-1,2:5,6-di-*O*-isopropylidene-D-glucofuranose (AIGlc), where ca. 120 h were required to reach full conversion at $\gamma = 10$ (20). This is an indication that the bulky isopropylidene-protected glucofuranoside side group in MAIGlc is not a crucial factor to retard the polymerization rate as in the case of AIGlc. The molecular weights and molecular weight distribution of the copolymers were characterized by GPC/viscosity using universal calibration. The results are given in Table 1. In all samples, the molecular weights determined by GPC-viscosity are higher than the apparent ones obtained by GPC (not shown), indicating highly branched structures. The ratios of $M_{n,\text{GPC-VISCO}}$ to $M_{n,\text{GPC-THF}}$ of the copolymers are 2.35-1.92, suggesting that a suitable amount of AB* inimer, BIEM, in the feed leads to a considerably compact structure, and the difference in the amount has an influence on the molecular weights and compact structure in solution. All samples show relatively low polydispersities.

Mark-Houwink plots and contraction factors (21), $g^2 = [\eta]_{\text{branched}}/[\eta]_{\text{linear}}$, as a function of the molecular weight for representative branched polymers obtained by SCVCP are shown in Figures 2a and 2b. Relationships between solution viscosity and molecular weight have been determined, and the Mark-Houwink constant typically varies between 0.34 and 0.20, depending on the degree of branching. In contrast, the exponent is typically in the region of 0.6-0.8 for linear ho-

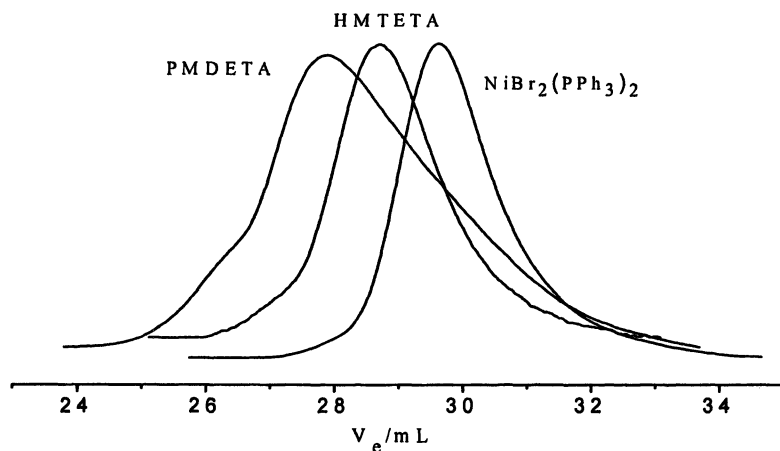
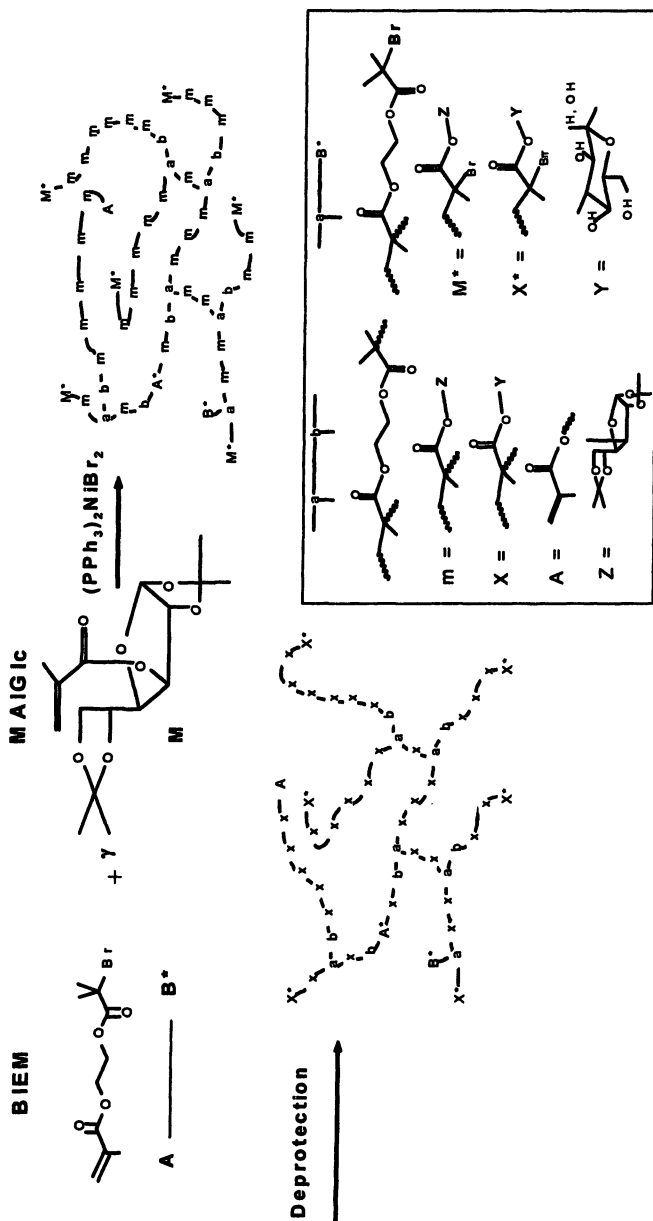


Figure 1. GPC traces of linear poly(MAIGlc)s prepared with various catalyst systems.

Table 1. Self-Condensing Vinyl Copolymerization of BIEM and MAIGlc at Different Comonomer Ratios γ^a

| γ^b | $M_{n, \text{GPC-VISCO}}^c$ (M_w/M_n) | α^d | DB_{NMR}^e | $\text{DB}_{\text{theo}}^f$ | BIEM ratio in polymer | | |
|------------|--|------------|----------------------------|-----------------------------|-----------------------|-----------------------------|----------------------------|
| | | | | | Calcd. ^g | Obsd. (NMR) ^h | Obsd. (EA) ⁱ |
| 1 | 17,500 (2.01) | 0.20 | 0.47 | 0.49 | 0.50 | 0.60 | 0.48 |
| 1.5 | 17,600 (2.12) | 0.22 | 0.42 | 0.47 | 0.40 | 0.40 | 0.36 |
| 2.5 | 18,000 (1.85) | 0.26 | 0.32 | 0.40 | 0.29 | 0.33 | 0.29 |
| 5 | 21,000 (1.55) | 0.30 | 0.24 | 0.24 | 0.17 | 0.19 | 0.18 |
| 10 | 23,300 (1.57) | 0.34 | 0.12 | 0.17 | 0.09 | 0.10 | 0.10 |
| 25 | 29,800 (1.71) | 0.28 | | 0.08 | 0.04 | 0.06 | 0.08 |

^a Copolymerization at 100°C with $(\text{PPh}_3)_2\text{NiBr}_2$ at a constant comonomer-to-catalyst ratio, $\mu = ([\text{MAIGlc}]_0 + [\text{BIEM}]_0) / [\text{catalyst}]_0 = 100$ in the presence of ethyl acetate (50 wt % to MAIGlc); Almost full conversion was reached after 2-5 h; ^b $\gamma = [\text{MAIGlc}]_0 / [\text{BIEM}]_0$; ^c Determined by GPC/viscosity measurement; ^d Mark-Houwink exponent as determined by GPC/viscosity measurement; ^e Degree of Branching as determined by ¹H NMR; ^f Theoretical degree of branching; ^g Calculated from the composition in feed; ^h Determined by ¹H-NMR; ⁱ Determined from elemental analysis using the bromine content.



Scheme 1. General route to branched glycopolymers via self-condensing vinyl copolymerization, followed by deprotection of isopropylidene protecting groups

mopolymers in a good solvent with a random coil conformation. The Mark-Houwink exponent of the mixture of linear poly(MAIGlc)s is 0.51 ± 0.03 . This result suggests that the relatively lower exponent values of the sugar-carrying polymers are mainly due to bulky isopropylidene-protected glucofuranoside side chains, resulting in less favorable interactions with the solvent. As shown in Figure 2a, the intrinsic viscosities of the branched polymers are significantly lower than those of the linear one in the higher molecular weight range ($[M] > 10^4$), suggesting a more compact architecture.

Figure 2b shows that the contraction factors for all the branched polymers decrease with increasing molecular weights. The GPC/viscosity measurements of branched poly(methyl methacrylate) (22), poly(*tert*-butyl acrylate)s (23, 24), poly[2-(diethylamino)ethyl methacrylate] (25), and poly(AIGlc)s (20) obtained by SCVCP with a (meth)acrylic-type inimer showed a similar tendency, suggest

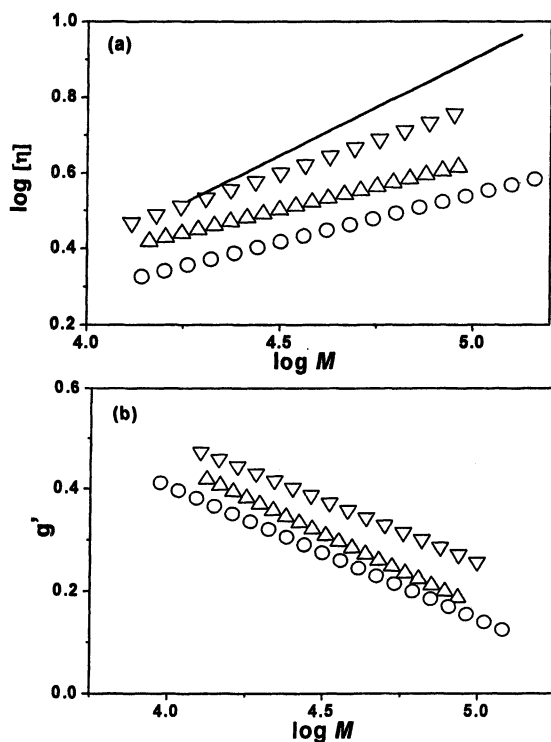


Figure 2. Mark-Houwink plots (a) and contraction factors, $g' = [\eta]_{\text{branched}}/[\eta]_{\text{linear}}$ (b) for the polymers obtained by SCVCP of BIEM and MAIGlc: $\gamma = 1.5$ (∇), 5.0 (\circ), 10 (\times). The intrinsic viscosity of a linear poly(MAIGlc) (\square) is given for comparison.

ing the feasibility of the viscosity improvement by the inimer incorporation, regardless of the nature of inimer and comonomer. In other words, the bulky side groups in MAIGlc and AIGlc have no significant influence on the general tendency of macroscopic quantities in branched polymers, in which intrinsic viscosity and radius of gyration can be controlled by the branched architecture. These observations indicate that the differences in the molecular weights obtained from the GPC/viscosity compared to conventional GPC arises from a systematic decrease in Mark-Houwink exponent, α , and the contraction factor, g' , due to a compact structure resulting from the increased number of branches.

Deprotection of Linear and Branched Poly(MAIGlc)s

The hydrolysis of the isopropylidene groups in the linear and branched poly(MAIGlc)s was performed by treating the samples with formic acid (10, 20). The final product was obtained by freeze-drying from dioxane after deprotected polymer was dialyzed against water. The ^1H NMR spectra of the linear and branched poly(MAGlc)s, are shown in Figure 3. Figure 3a shows that the signals of the isopropylidene protons (1.2-1.4 ppm) completely disappear after the deprotection, and a broad signal attributed to anomeric hydroxyl groups of the sugar moieties (6.4-7.0 ppm) appear. This indicates the quantitative deprotection of the isopropylidene protecting groups. The linear poly(MAGlc)s are white powders completely soluble in water, methanol, and DMSO, but insoluble in THF and acetone. In the case of the branched poly(MAGlc)s, the solubility were dependent upon the comonomer ratios, γ . In the case of $\gamma = 1$, the branched poly(MAGlc)s were partially soluble in water, which is due to the 50% of the non-polar inimer segment. For $\gamma > 1.5$, the polymers were soluble in water, DMSO, and methanol, but insoluble in THF and acetone. Note that the unchanged resonance signal of protons of the ethylene linkage at 4.0-4.6 ppm and the peak at 1.9-2.0 ppm corresponding to methyl protons adjacent to a bromine atom (A* and M* in the polymer chain end and B* in the 2-bromoisobutyryloxy group), respectively. (Figure 3) suggest that the branched structure is intact during the complete deprotection of the isopropylidene groups and the BIEM composition in poly(MAGlc)s is almost same as that before deprotection.

The bromine contents of the representative branched poly(MAGlc)s obtained by elemental analysis were 10.51 %, 2.66 %, and 1.27 % for $\gamma = 1.0$, 5.0 and 10, respectively (Calcd: 15.61 %, 5.2 %, and 2.89 %, respectively), while the values of the same samples before the hydrolysis were 12.75 %, 4.70 %, and 2.70 %. The reasonable bromine content of the hydrolyzed product indicates that most of the terminal bromester groups are kept without any modification during the hydrolysis reaction and can be used for further modifications. The carbon and hydrogen contents of the branched and homo poly(MAGlc)s were also determined using elemental analysis. For instance, the atomic composition of the hydrolyzed homopolymer was C, 43.89; H, 6.8 (Calcd: C, 43.5; H, 5.6)

while the value of the same sample before the hydrolysis was C, 59.05; H, 7.6 (Calcd: C, 54.8; H, 6.7). For the hydrolyzed branched copolymer ($\gamma = 1$), the atomic composition was C, 45.6; H, 6.1 (Calcd: C, 42.96; H, 5.51) while values of the same sample before hydrolysis were C, 52.1; H, 6.6 (Calcd: C, 49.5; H, 6.1). These results indicate that the deprotection of the isopropylidene groups in the branched and linear poly(MAIGlc)s proceeds selectively to yield the desired branched and linear poly(MAIGlc)s.

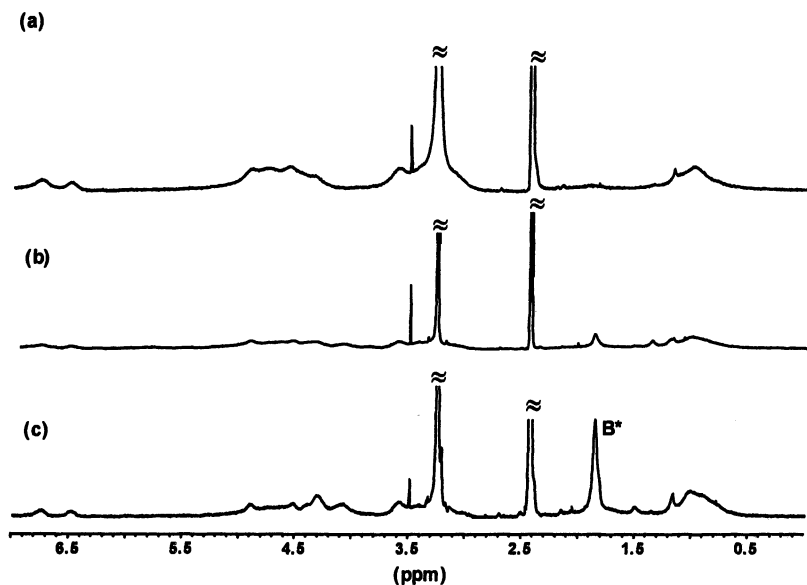


Figure 3. ^1H NMR spectra ($\text{DMSO}-d_6$) of the polymers obtained after deprotection of linear poly(MAIGlc) (a), and branched poly(MAIGlc)s: $\gamma = 10$ (b), $\gamma = 1.0$ (c).

Synthesis of Glycocyindrical Brushes

The synthesis of glycocyindrical brushes (“molecular sugar sticks”) with MAIGlc side chains was obtained by the “grafting from” approach via ATRP initiated from the backbone of the polyinitiator, poly(2-(2-bromoisobutyryloxy)ethyl methacrylate) (PBIEM) as shown in Scheme 2. The polyinitiator was synthesized from the precursor, poly(2-hydroxyethyl methacrylate), (PHEMA) obtained via anionic polymerization. The number-average molecular weight and molecular weight distribution are $M_n = 4.2 \times 10^5$ and $\text{PDI} = 1.08$, respectively, corresponding to the number-average degree of polymerization, $\text{DP}_n = 1,500$ (17, 26).

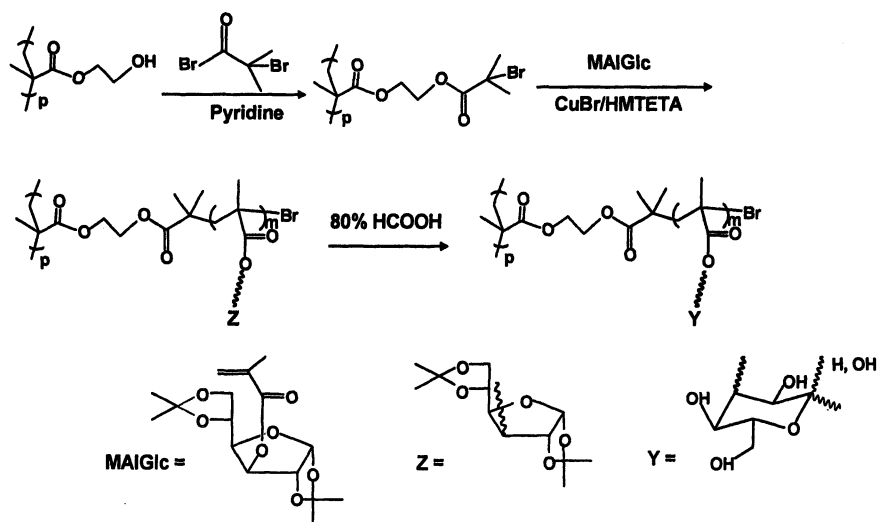
The glycocylindrical brushes were synthesized using CuBr/HMTETA as the catalyst system, MAIGlc as monomer and PBIEM as polyinitiator. As can be seen from Table 2, very low conversions are maintained in all cases in order to obtain well-defined glycocylindrical brushes. Even at such low conversions, the reaction mixture becomes very viscous owing to the very high molecular weights of the resulting brushes. The obtained cylindrical brushes with MAIGlc side chains show monomodal GPC eluograms (Figure 4) and their molecular weight distributions are quite narrow ($PDI < 1.20$), indicating that intermacromolecular coupling reactions are negligible. Hence, without adding Cu (II) salts (27), a high ratio of monomer to initiator and a low conversion are sufficient to suppress undesirable side reactions, and to obtain the desired glycocylindrical brushes.

The true molecular weights of these brushes as well as the radii of gyration, R_g , in THF were determined by GPC-MALS. As can be seen from Table 2, for the same backbone, R_g of the brushes increases with the side chain lengths. The main chain stiffness of the polymer brush increases with increasing side chain length, because the overcrowding of longer side chains forces the otherwise flexible main chain into a more stretched conformation. The molar masses obtained by light scattering are significantly higher than those obtained by GPC. This is due to the compact nature of the brushes.

Figure 5 represents the 1H NMR spectra of linear poly(MAIGlc), polyinitiator and the glycocylindrical brushes. In Figure 5c, there are two typical peaks at 4.21 and 4.37 ppm (a and a'), which represent the methylene protons between two ester groups of the polyinitiator. After the formation of the brush with poly(MAIGlc) side chains, the characteristic peaks at 1.2-1.4 ppm (isopropylidene protons), 3.8-5.0 and 5.7-6.0 ppm are clearly seen in Figure 5b. This indicates the successful formation of glycocylindrical brushes with poly(MAIGlc) side chains.

Solvolysis of the Glycocylindrical brushes

In order to determine the exact side chain length, and thus the initiation site efficiency, the side chains were cleaved from the backbone via base-catalyzed transesterification in methanol (18). 1H NMR spectra of the resulting products revealed that solvolysis with sodium methoxide resulted in side chains consisting of a statistical copolymer of 17 % MMA and 83 % MAIGlc units. In order to calculate the DP of the side chains, the molecular weights of the side chains (see below) were divided by an average molecular weight of the comonomers, $M_0 = 290$ g/mol. Table 3 summarizes the detailed characterization of the side chains cleaved by solvolysis and the corresponding initiation efficiencies, f . The abso-



Scheme 2. General route to the synthesis of glycoylindrical brushes ("Sugar sticks")

Table 2. Synthesis and characterization of glycoylindrical brushes via ATRP^a

| Brush | $[M]_0/[I]_0$ | Time (min) | Conv. ^b (%) | $10^{-4} \times M_{n, GPC}^c$ | PDI ^c | $10^{-4} \times M_{n, MALs}$ | $DP_{n, side\ chain} (calc)^d$ | R_g (nm) |
|-------|---------------|------------|------------------------|-------------------------------|------------------|------------------------------|--------------------------------|------------|
| 1 | 300 | 30 | 5 | 40.8 | 1.19 | 900 | 18 | 41.5 |
| 2 | 200 | 25 | 10 | 58.6 | 1.07 | 1120 | 22 | 59.5 |

^a Solution polymerization in ethylacetate (50 wt% to MAIGlc) at 60 °C at constant $[BIEM]_0 : [CuBr]_0 : [HMTETA]_0 = 1 : 0.5 : 0.5$; ^b Determined by ¹H-NMR; ^c Determined by GPC using THF as eluent with PS standards. ^d Calculated from $M_{n, brush} - M_{n, backbone} / (nM_0)$, where n = degree of polymerization of the backbone and M_0 , monomer molecular weight, respectively.

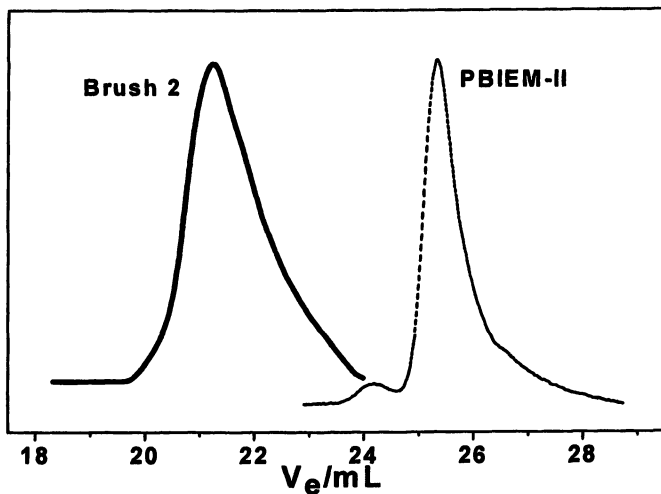


Figure 4. GPC traces of PBIEM ($DP = 1,500$) and the corresponding long glycocylindrical Brush 2 in THF.

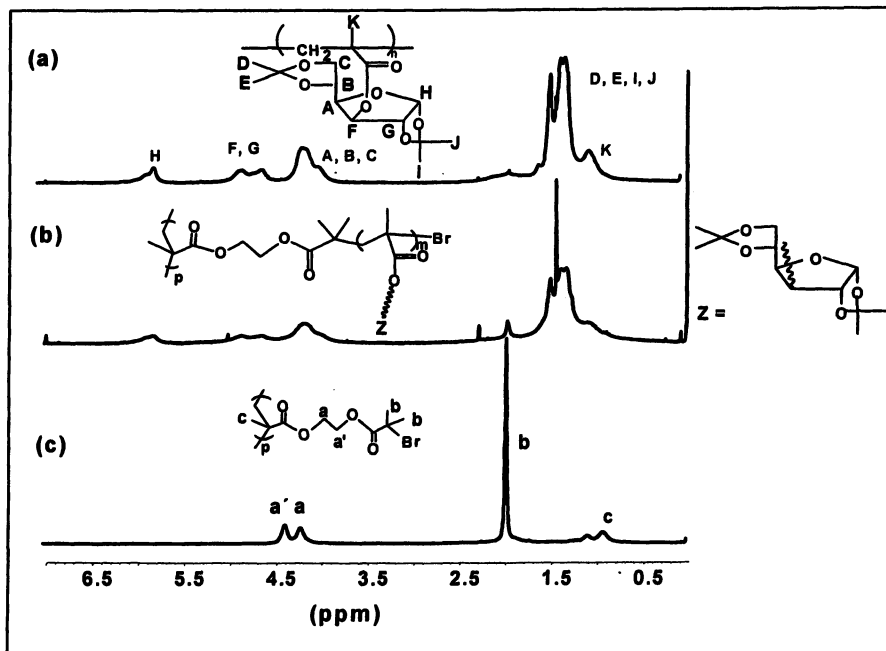


Figure 5. 1H NMR spectra ($CDCl_3$) of (a) linear poly(MAIGlc), (b) cylindrical brush with poly(MAIGlc) side chains, and (c) the polyinitiator (PBIEM).

lute molecular weights of the cleaved side chains were determined by using GPC/viscosity and GPC-MALS measurements which allows the accurate evaluation of the initiation efficiencies. The polydispersity index of the cleaved arms is $M_w/M_n \cong 1.3$ as can be seen from Table 3, which is a typical value for polymer obtained by slow initiation (limiting $M_w/M_n = 1.33$ for $k_p \gg k_i$ in the Gold distribution (28)). Under these conditions all monomer is consumed before complete initiation. The initiating efficiencies of the PMAIGlc brushes investigated are in the range of 23 - 38 %. This value is much smaller than that obtained for the polymerization of styrene using the same polyinitiator, PBIEM (29). Recently, Matyjaszewski et al. (18, 30) have demonstrated that the initiating efficiency is limited to approximately 50 % for the polymerization of MMA using PBIEM and they have also investigated the underlying reasons for the lower initiating efficiency of the brushes than the corresponding linear polymers in detail. In our study, the increased bulkiness of the monomer, MAIGlc, could contribute to the low initiation efficiency of the brushes. In spite of the low grafting efficiency, the bulky sugar moiety of the monomer (MAIGlc), leads to the stronger stretching of the backbone resulting in extended worm-like conformations, as will be discussed below.

Table 3. Characterization of cleaved side chains of PMAIGlc Brushes and of initiation site efficiencies, f^a

| Brush | M_n , GPC-VISCO ^b | M_w/M_n ^b | M_n , GPC-MALS ^c | DP_n ^d | $f^d(\%)$ | DP_{bb}/DP_{sc} |
|-------|--------------------------------|------------------------|-------------------------------|---------------------|-----------|-------------------|
| 1 | 13600 | 1.40 | - | 46.8 | 38.4 | 32 |
| 2 | 27400 | 1.35 | 28100 | 95.6 | 23.0 | 15.6 |

a) $f = DP_{n, calc}/DP_{n, exp}$; ^b Determined by GPC/viscosity measurement; ^c Determined by GPC-MALS measurement; ^d Average of GPC/viscosity and GPC-MALS measurements.

Visualization of the Cylindrical Brushes by SFM and cryo-TEM

The glycocylindrical brushes were then further characterized by SFM. The protected samples were prepared by spin-coating from dilute solutions onto carbon-coated mica. Figure 6 represents the SFM image of the Brush 1, spin-coated from THF onto carbon-coated mica. Carbon-coated mica was chosen in order to avoid problems associated with aggregation and dewetting. Single worm-like macromolecules can be visualized directly. The number-average and weight-average lengths of 20 individual cylinders in Figure 6a are $L_n = 110$ nm and $L_w = 114$ nm, respectively, with a polydispersity $L_w/L_n = 1.04$. The main chain is not completely stretched out but locally coiled which could be due to the low grafting efficiency ($f = 38\%$) of the brush as discussed earlier.

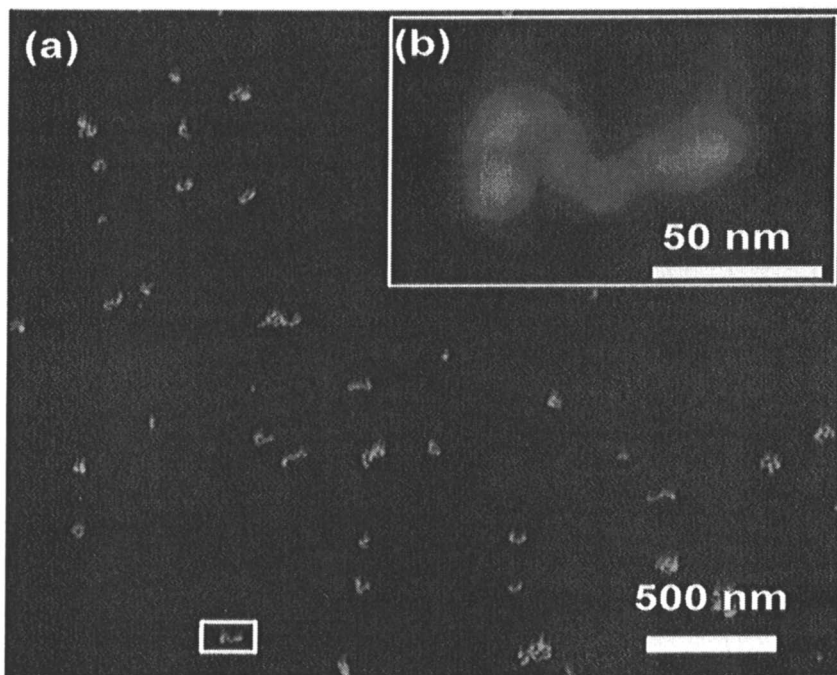


Figure 6. (a) SFM Tapping Mode height image of the Brush 1, spin-coated from dilute solution on carbon-coated mica, (z-range: 20 nm) and (b) 5x magnification of the single cylinder marked by a rectangle in (a).

Deprotection of Glycocylindrical Brushes

The hydrolysis of the isopropylidene groups of the glycocylindrical brushes was performed by treating the samples with formic acid as in the case of linear and hyperbranched glycomethacrylates at room temperature (10, 31). The final product was obtained by dialysis against water and freeze-drying. The brushes are only partially soluble in methanol, but completely soluble in water and water/dioxane (1/1) mixtures. Figure 7 shows the SFM image of the deprotected Brush 1, spin-coated from dioxane-water mixture (volume ratio of 1/1) onto mica. Worm-like macromolecules could be visualized indicating that the structure is preserved during deprotection. The number and weight-average lengths of 40 cylinders are $L_n = 130$ nm and $L_w = 134$ nm, respectively, with a polydispersity, $L_w/L_n = 1.03$. The cylinders appear to be more stretched than those before hydrolysis ($L_n = 110$ nm). The cylinders are still much shorter than the maximum contour length of cylinders in the fully stretched state. The curvature of the brushes is higher than expected. In order to check whether this is due to the interaction of the molecule with the substrate, cryo-TEM measurements in water were performed as discussed in the next section.

The structure of the deprotected glycocylindrical Brush 1 in aqueous solution was characterized using cryo-TEM. This tool allows to directly image the original shape and size of the polymers in solution, since the sample is vitrified before the measurement. The cryo-TEM image of the deprotected Brush 1 (Figure 8), shows worm-like cylinders. The magnification of a single cylinder is also shown as an insert and the length of that single cylinder is found to be 130 nm which agrees very well with the length of the deprotected Brush 1 obtained by SFM measured in the dry state.

Conclusions

We have demonstrated that the $(\text{PPh}_3)_2\text{NiBr}_2$ catalyst system could be successfully employed for the homopolymerization of MAIGlc and SCVCP of BIEM and MAIGlc, which resulted in the synthesis of monodisperse linear poly(MAIGlc)s and randomly branched poly(MAIGlc)s with relatively high molecular weights, respectively. Both the homopolymerization and SCVCP proceeded smoothly within reasonable polymerization time.

The CuBr/HMTETA catalyst system could be successfully employed for the homopolymerization of MAIGlc in "grafting from" a linear polyinitiator, PBIEM, leading to well-defined glycocylindrical brushes or "sugar sticks". Analysis of the side chains detached by basic solvolysis indicated that the grafting efficiency is approximately $0.20 < f < 0.40$. The morphology of the resulting brushes visualized using SFM and cryo-TEM indicates worm-like structure.

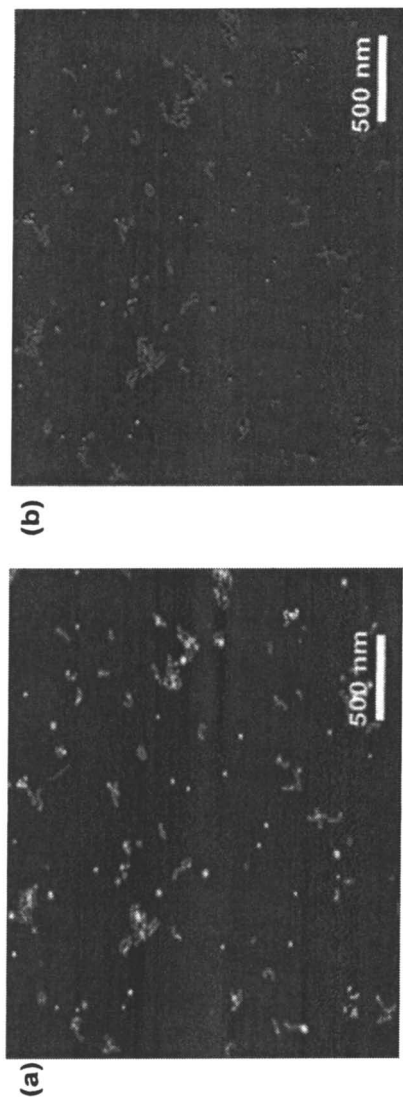
The deprotection of the isopropylidene protecting groups resulted in water-soluble poly(MAIGlc)s of different topologies which can be employed as effective tools for various biological and medicinal applications. This work substantially broadens and extends the scope for generating water-soluble glycopolymers and their precursors by a controlled polymerization technique.

Acknowledgement

This work was supported by the *Deutsche Forschungsgemeinschaft* (grant no. Mu 896/14). The authors would wish to thank Dr. Markus Drechsler for cryo-TEM measurements.

References

1. Lee, Y. C.; Lee, R. T. *Acc. Chem. Res.* **1995**, *28*, (8), 321-327.
2. Bovin, N. V.; Gabius, H. J. *Chem. Soc. Rev.* **1995**, *24*, (6), 413.
3. Klein, J.; Herzog, D.; Hajibegli, A. *Makromol. Chem.* **1985**, *6*, (10), 675-678.
4. Gunay, N. S.; Linhardt, R. J. *Planta Med.* **1999**, *65*, (4), 301-306.
5. Zanini, D.; Roy, R. *J. Org. Chem.* **1998**, *63*, (10), 3486-3491.



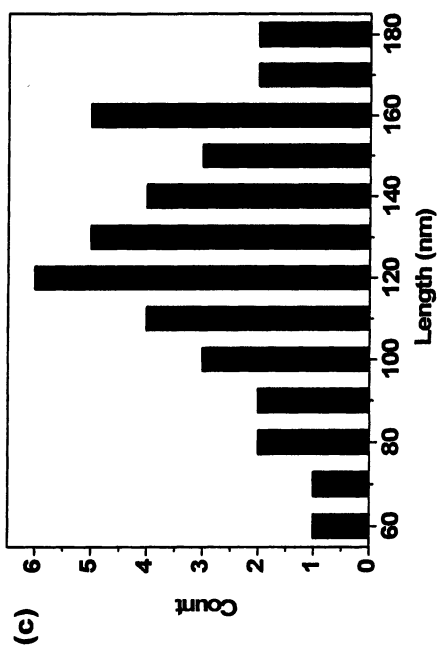


Figure 7. SFM Tapping Mode images of the deprotected Brush 1, spin-coated from dilute water/dioxane (1/1) solution on mica, (a) height image (z-range: 10 nm), (b) phase image (range: 40°), and (c) histogram of the contour length for 40 molecules.

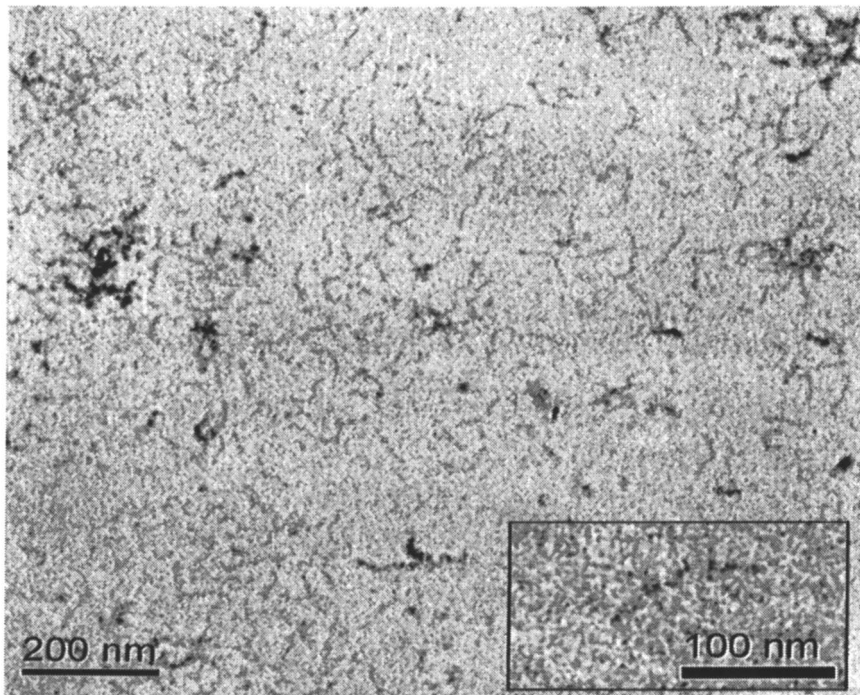


Figure 8. Cryo-TEM image of the deprotected, Brush 1.

6. Yamada, K.; Yamaoka, K.; Minoda, M.; Miyamoto, T. *J. Polym. Sci., Polym. Chem.* **1997**, *35*, (2), 255-261.
7. Aoi, K.; Tsutsumiuchi, K.; Okada, M. *Macromolecules* **1994**, *27*, (3), 875-877.
8. Fraser, C.; Grubbs, R. H. *Macromolecules* **1995**, *28*, (21), 7248-7255.
9. Wulff, G.; Schmid, J.; Venhoff, T. *Macromol. Chem. Phys.* **1996**, *197*, (1), 259-274.
10. Ohno, K.; Tsujii, Y.; Fukuda, T. *J. Polym. Sci., Polym. Chem.* **1998**, *36*, (14), 2473-2481.
11. Narain, R.; Armes, S. P. *Macromolecules* **2003**, *36*, (13), 4675-4678.
12. Narain, R.; Armes, S. P. *Chem. Commun.* **2002**, (23), 2776-2777.
13. Li, Z. C.; Liang, Y. Z.; Chen, G. Q.; Li, F. M. *Macromol. Rapid Commun.* **2000**, *21*, (7), 375-380.
14. Liang, Y. Z.; Li, Z. C.; Chen, G. Q.; Li, F. M. *Polym. Int.* **1999**, *48*, (9), 739-742.
15. Mori, H.; Böker, A.; Krausch, G.; Müller, A. H. E. *Macromolecules* **2001**, *34*, (20), 6871-6882.
16. Matyjaszewski, K.; Gaynor, S. G.; Kulfan, A.; Podwika, M. *Macromolecules* **1997**, *30*, (17), 5192-5194.
17. Zhang, M.; Breiner, T.; Mori, H.; Müller, A. H. E. *Polymer* **2003**, *44*, (5), 1449-1458.
18. Neugebauer, D.; Sumerlin, B. S.; Matyjaszewski, K.; Goodhart, B.; Sheiko, S. S. *Polymer* **2004**, *45*, (24), 8173-8179.
19. Benoît, H.; Grubisic, Z.; Rempp, P.; Decker, D.; Zilliox, J. G. *J. Chem. Phys.* **1966**, *63*, 1507.
20. Muthukrishnan, S.; Jutz, G.; André, X.; Mori, H.; Müller, A. H. E. *Macromolecules* **2005**, *38*, (1), 9-18.
21. Savin, G.; Burchard, W.; Luca, C.; Beldie, C. *Macromolecules* **2004**, *37*, (17), 6565-6575.
22. Simon, P. F. W.; Müller, A. H. E. *Macromolecules* **2001**, *34*, (18), 6206-6213.
23. Mori, H.; Seng, D. C.; Lechner, H.; Zhang, M. F.; Müller, A. H. E. *Macromolecules* **2002**, *35*, (25), 9270-9281.
24. Mori, H.; Müller, A. H. E. *Top. Curr. Chem.* **2003**, *228*, 1-37.
25. Mori, H.; Walther, A.; André, X.; Lanzendörfer, M. G.; Müller, A. H. E. *Macromolecules* **2004**, *37*, (6), 2054-2066.
26. Muthukrishnan, S.; Zhang, M.; Burkhardt, M.; Drechsler, M.; Mori, H.; Müller, A. H. E. *Macromolecules* **2005**, *38*, 7926-7934.
27. Beers, K. L.; Gaynor, S. G.; Matyjaszewski, K.; Sheiko, S. S.; Möller, M. *Macromolecules* **1998**, *31*, (26), 9413-9415.
28. Gold, L. *J. Chem. Phys.* **1958**, *28*, (1), 91.
29. Becker, O.; Cheng, Y. B.; Varley, R. J.; Simon, G. P. *Macromolecules* **2003**, *36*, (5), 1616-1625.
30. Sumerlin, B. S.; Neugebauer, D.; Matyjaszewski, K. *Macromolecules* **2005**, *38*, (3), 702-708.
31. Muthukrishnan, S.; Mori, H.; Müller, A. H. E. *Macromolecules* **2005**, *38*, (8), 3108-3119.

Chapter 17

Acrylate-Based Block Copolymers Prepared by Atom Transfer Radical Polymerization as Matrices for Drug Delivery Applications

Robert E. Richard¹, Marlene Schwarz¹, Shirang Ranade¹,
A. Ken Chan¹, Krzysztof Matyjaszewski², and Brent Sumerlin³

¹Corporate Research and Advanced Technology Development,
Boston Scientific Corporation, Natick, MA 01760

²Department of Chemistry, Carnegie Mellon University, 4400 Fifth Avenue,
Pittsburgh, PA 15213

³Department of Chemistry, Southern Methodist University, P.O. Box
750314, Dallas, TX 75275

Block copolymers, synthesized by atom transfer radical polymerization (ATRP) processes, were evaluated as drug delivery matrices for the controlled release of paclitaxel (PTX) from coronary stents. The polymers were multi-block copolymers consisting of poly(butyl acrylate) or poly(lauryl acrylate) soft blocks and hard blocks composed of poly(methyl methacrylate), poly(isobornyl acrylate) or poly(styrene) homo or copolymers. The block copolymers had variable elastomeric properties which influenced the stent coating integrity when assessed by SEM imaging of over-expanded stents. In vitro PTX release kinetics from coronary stents coated with these copolymers typically showed an early burst followed by sustained release behavior which permitted the elution of the majority of the PTX over a 10 day time period. It was determined that neither the soft or the hard block appeared to affect the release kinetics of PTX at a loading of 25% drug by weight, whereas some effects were observed at 10% drug loading. DSC analysis showed that the PTX was at least partially miscible with the poly(n-butyl acrylate) phase of

these block copolymers. Sterilization stability was evaluated by exposing both the copolymer alone and copolymer/PTX coated stents to e-beam radiation at doses of 25, 50 and 75 kGy. The block copolymers containing segments bearing quaternary carbons within the polymer backbone were found to be less stable to the radiation and showed a decrease in molecular weight as determined by gel permeation chromatography. Whereas, those without quaternary carbons showed no significant change in molecular weight when exposed to the same doses of radiation. There was no significant change in PTX release profile from any of the acrylate-based copolymers after exposure to up to 75 kGy of e-beam radiation, and this was attributed to the inherent radiation stability of the polyacrylate center blocks.

Introduction

Device-based drug delivery often relies on polymeric materials to act as matrices to release therapeutic materials in a controlled fashion. The drug coated coronary artery stent is an excellent example of a device-based drug delivery product which employs a polymer as the depot that releases the drug in a controlled fashion after in vivo implantation (1-2). The clinical success of drug eluting coronary stents has been well documented in the recent literature (3-5). The mechanical requirements of a drug eluting stent coating include elasticity, and toughness to preserve the integrity of the coating. The use of block copolymers for this purpose has been reported previously and is a proven approach to realizing the required mechanical properties (6). In addition, polymer coatings for drug delivery applications need to be compatible with the in vivo environment. This is especially important for the coronary stent application where the polymer coating is exposed to both vascular tissues of the artery as well as flowing blood. Along with biocompatibility, the polymer must also be biostable and not breakdown during the time when drug is being delivered, which could potentially affect the release rate or introduce inflammatory degradants during the lifetime of the implant (7). The exception to this requirement would be when biodegradable polymers are intentionally selected for this application. A number of reports have indicated that biodegradable polymers are well suited for drug eluting stent coatings, where it may be possible to modulate the drug release through the degradation of the polymer (8-10).

Another important consideration for polymeric drug delivery coatings is the ability to modulate the release of the therapeutic to allow for a range of delivery rates to meet the clinical requirements of the intended treatment. One effective

approach to tailoring the release rate of a drug from a polymer is through changes to the polarity of the coating to affect the hydrophilic/hydrophobic balance of the matrix (11). This can allow control of both the ingress of the aqueous environment to dissolve and remove drug as well as the egress of the drug by diffusion through the coating.

Medical devices usually require sterilization by common methods such as radiation, chemicals and heat. It is important to preserve the performance of the device during sterilization since the processes employed have the potential to affect both the polymer matrix as well as the therapeutic agent within the device.

The choice of therapeutic agent for drug eluting stent technology is an important consideration. Paclitaxel, the drug investigated in this study, is a lipophilic natural product which inhibits cellular division with the chemical structure shown in Figure 1. It has been shown in extensive clinical trials to be effective in reducing the incidence of neointimal hyperplasia and restenosis (3). The *in vitro* release profile of paclitaxel from one clinically proven commercial product has been published previously (1).

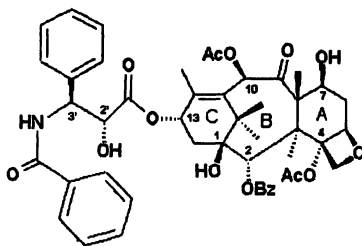


Figure 1. Chemical structure of paclitaxel.

Atom transfer radical polymerization (ATRP) is a versatile technology for preparing block copolymers with well controlled chemical composition and morphology and is applicable to monomers with a wide range of polarity (12-14). This technology has been shown to also allow for the production of a vast range of polymer morphologies with phase separation at the nano-scale. Such morphologies are known to result in materials with unique mechanical properties, providing additional modes for regulating the release of therapeutic agents and for producing surfaces that are compatible with the *in vivo* environment.

The objective of this study was to evaluate a series of elastomeric acrylate-based block copolymers synthesized by ATRP to determine their ability to release paclitaxel (PTX) after coating on to coronary stents. Acrylate-based polymers were chosen due to both their reported biocompatibility as well as their

well know radiation stability (15). These copolymers were composed of immiscible blocks that resulted in unique nano-phase separated materials. In addition, the release rates were evaluated both before and after exposure to doses of electron beam (e-beam) radiation representative of that typically used to sterilize medical devices. The molecular weight distribution of the copolymers following e-beam exposure was measured to determine their stability to ionizing radiation.

Materials and Methods

The compositions of the copolymers used in this study are described in Table I. The difunctional poly(*n*-butyl acrylate) (16) (PBA) and poly(lauryl acrylate) (17) (PLA) macroinitiators were prepared as previously reported. Using the resulting macroinitiators, poly(methyl methacrylate-*block-n*-butyl acrylate-*block*-methyl methacrylate) (P(MMA-BA-MMA)) (18), and poly((styrene-*co*-acrylonitrile)-*block-n*-butyl acrylate-*block*-(styrene-*co*-acrylonitrile)) (P(SAN-BA-SAN)) (19) were prepared. Synthesis of poly(methyl methacrylate-*block*-lauryl acrylate-*block*-methyl methacrylate) (P(MMA-LA-MMA)), poly(isobornyl acrylate-*block*-lauryl acrylate-*block*-isobornyl acrylate) (P(IBA-LA-IBA)), poly(styrene-*block*-lauryl acrylate-*block*-styrene) (P(S-LA-S)), poly(isobornyl acrylate-*block-n*-butyl acrylate-*block*-isobornyl acrylate) (P(IBA-BA-IBA)), poly(styrene-*block-n*-butyl acrylate-*block*-styrene), PBA star macroinitiator and the P(BA-S)₃ star block copolymers has been reported elsewhere (20). The methods used for stent coating, in vitro release of paclitaxel from coronary stents, gel permeation chromatography, differential scanning calorimetry, atomic force and scanning electron microscopy and e-beam sterilization have been reported previously (20)

Results and Discussion

Polymer Synthesis

ATRP is a convenient method to produce multi-block copolymers which have immiscible hard and soft segments. The resulting elastomeric properties are well suited for coatings applied to expandable devices such as coronary stents. The approach taken was to first synthesize macroinitiators consisting of the soft acrylate blocks. These were isolated, purified and then used to initiate polymerization of the hard blocks, again using typical ATRP syntheses. The evolution of the molecular weight for the two P(IBA-BA-IBA) triblock

Table I. Chemical Composition of Block Copolymers Prepared by ATRP

| <i>Polymer Number</i> | <i>Polymer Composition</i> | <i>Block molecular weights kg/mol</i> | <i>Total Mn kg/mol</i> | <i>Mw/Mn</i> | <i>Hard block (wt%)</i> |
|-----------------------|--------------------------------------|---------------------------------------|------------------------|--------------|-------------------------|
| 1 | P(MMA-BA-MMA) | 17.3-48.9-17.3 | 83.5 | 1.07 | 41 |
| 2 | P(MMA-BA-MMA) | 29.3-41.8-29.3 | 100.4 | 1.25 | 58 |
| 3 | P(MMA-BA-MMA) | 23-28-23 | 73.0 | 1.4 | 62 |
| 4 | P(MMA-LA-MMA) | 15-26.5-15 | 56.5 | 1.22 | 53 |
| 5 | P(IBA-BA-IBA) | 21.8-41.8-21.8 | 85.4 | 1.46 | 51 |
| 6 | P(IBA-BA-IBA) | 17.5-55-17.5 | 90.0 | 1.08 | 39 |
| 7 | P(IBA-BA-IBA) | 10.9-55-10.9 | 76.6 | 1.08 | 28 |
| 8 | P(IBA-LA-IBA) | 11.9-26.5-11.9 | 50.3 | 1.19 | 47 |
| 9 | P(STY-LA-STY) | 14.6-24.4-14.6 | 53.6 | 1.26 | 54 |
| 10 | P(SAN-BA-SAN) | 19.8-49-19.8 | 88.6 | 1.40 | 45 |
| 11 | P(STY-BA-STY) | 19.8-55-19.8 | 94.6 | 1.10 | 42 |
| 12 | P(STY-BA-STY) | 10.8-55-10.8 | 76.5 | 1.08 | 28 |
| 13 | P(BA-S) ₃ tri-arm star | (45-6) ₃ | 153 | 1.13 | 12 |
| 14 | P(BA-S) | 28-12 | 40k | 1.15 | 44 |

NOTE: Molecular weights and wt% of the hard blocks were determined by GPC.

copolymers (6 and 7) is illustrated in Figure 2. The GPC chromatograms of the PBA macroinitiator and the resulting block copolymers confirm the increase in molecular weight due to polymerization of the second blocks. Similar results were obtained for the other polymers in Table 1.

Mechanical Integrity of Stent Coatings

After coating coronary stents with each formulation, the mechanical integrity of the acrylate-based coatings were evaluated by scanning electron microscopy (SEM) both before and after stent expansion. Figures 3a-c show SEM images of pre and post-expanded coronary stents coated with two of the P(MMA-PBA-PMMA) block copolymers (1 and 3). These images were representative of other samples as well. It was found that samples with a hard block content greater than 50% by weight typically produced stent coatings that resulted in integrity failure upon expansion of the stents (3c). The drug release testing on all stents was performed on non-expanded stents to avoid drug release effects caused by coating failure.

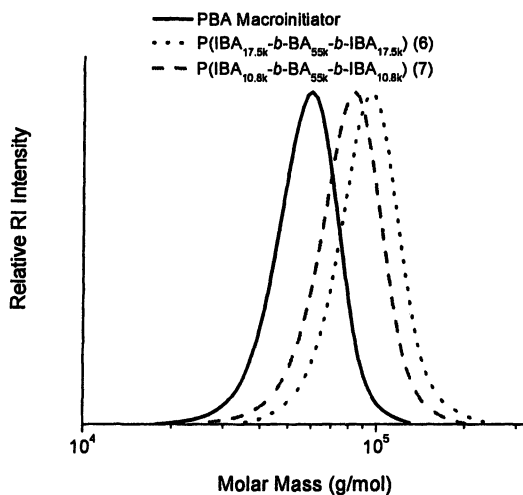


Figure 2. GPC data for PBA macroinitiator and triblock copolymers containing IBA end blocks. (Reproduced from reference 20. Copyright 2005 American Chemical Society)

Differential Scanning Calorimetry (DSC)

DSC analysis confirmed the phase separation of the block copolymers by the presence of two distinct T_g 's for all polymers studied. In addition, it was also used to investigate the miscibility of select polymers with PTX. Table II shows the change in T_g for both blocks as a function of added PTX for triblocks with a PBA mid block and end blocks containing ; polymethyl methacrylate (PMMA) (1), polystyrene (PS) (11) or polyisobornyl acrylate (PIBA) (6). In all cases it was determined that the PBA T_g increased as the PTX content was increased, whereas the T_g of the end blocks showed no significant change. This indicates that the PTX is to some degree miscible with the PBA mid blocks. The T_g of amorphous PTX is reported to be 151 °C (21) and was not detected in any of the samples.

Atomic Force Microscopy (AFM)

The morphology of the polymer coatings both with and without drug was evaluated by AFM. Typical AFM images for triblock copolymers composed of

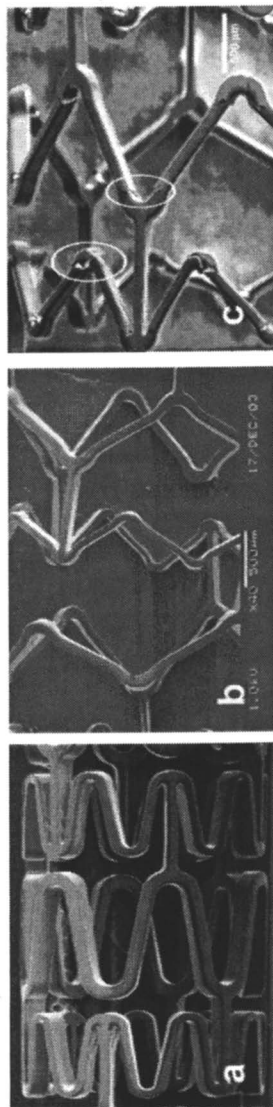


Figure 3. SEM image of expanded coronary stents coated with P(MMA-BA-MMA) block copolymers: (a and b) 41 wt% PMMA (1, Table 1) before and after stent expansion (c) 62 wt% PMMA (3, Table 1) post-expansion. (Reproduced from reference 20.

Copyright 2005 American Chemical Society)

Table II. DSC results for PMMA, PS and PIBA block copolymers (with PBA mid block) containing 0, 10 and 25% PTX by weight

| Sample | Polymer Number | PTX conc. (wt%) | T_g Soft block (°C) | T_g Hard block (°C) |
|---|----------------|-----------------|-----------------------|-----------------------|
| P(MMA _{17.3k} -BA _{48.9k} -MMA _{17.3k}) | 1 | 0 | -43 | 89 |
| | | 10 | -39 | 91 |
| | | 25 | -31 | 89 |
| P(STY _{19.8k} -BA _{55k} -STY _{19.8k}) | 11 | 0 | -41 | 109 |
| | | 10 | -29 | 106 |
| | | 25 | -21 | 105 |
| P(IBA _{17.5k} -BA _{55k} -IBA _{17.5k}) | 6 | 0 | -43 | 105 |
| | | 10 | -33 | 105 |
| | | 25 | -27 | 105 |

a PBA mid block and end blocks containing either (a) PMMA (3), (b) PS (11) or (c) PIBA (6) are shown in Figure 4. The results were obtained from films consisting of polymer alone or with 10 and 25% PTX by weight. The images show the expected micro-phase separated morphology, however it is not well defined due to the non-equilibrium conditions of these films resulting from rapid evaporation of the solvents when producing the coatings. These conditions are representative of the process used to coat coronary stents and would be expected to result in similar morphological structure. Analogous morphologies were observed on coated stents. It was also observed that the triblocks containing either PS or PIBA showed evidence of phase separated PTX particles on the surface, whereas no PTX could be identified in the polymer containing PMMA end blocks.

Paclitaxel Release from Block Copolymers

The PTX release profiles for formulations with PMMA hard blocks with PBA (1-3) or PLA(4) soft blocks containing 25% PTX are shown in Figure 5a. All compositions appear to give the same release rate after the 2 day data point. For these samples, the M_n ranged from approximately 48,300 to approximately 100,000 g/mol and the weight % MMA varied from 41 to 62.

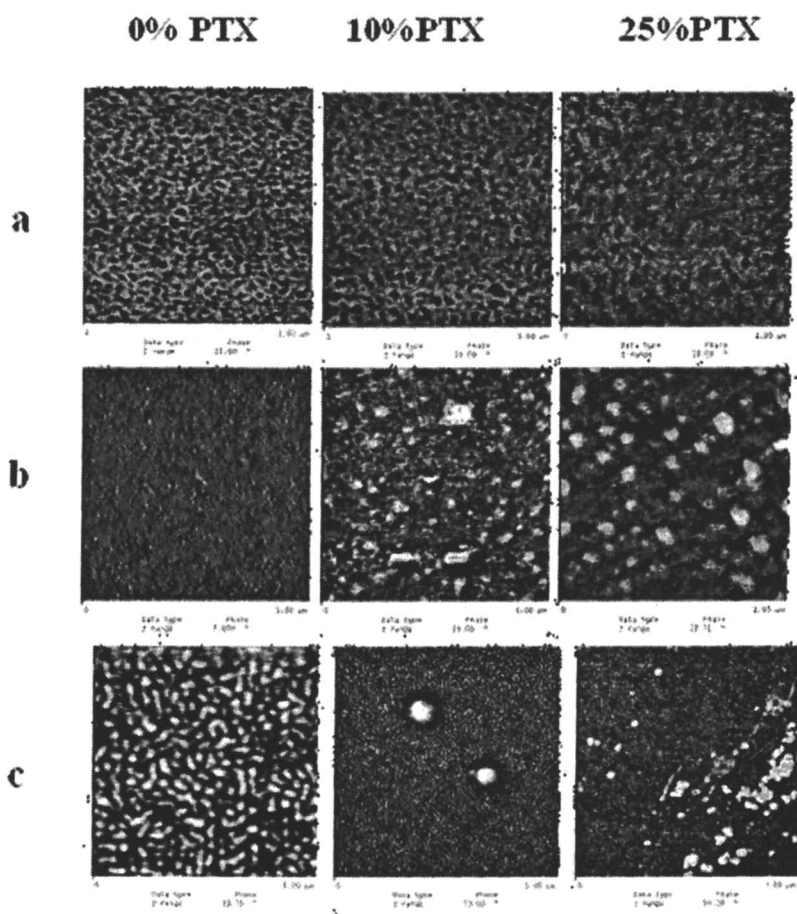


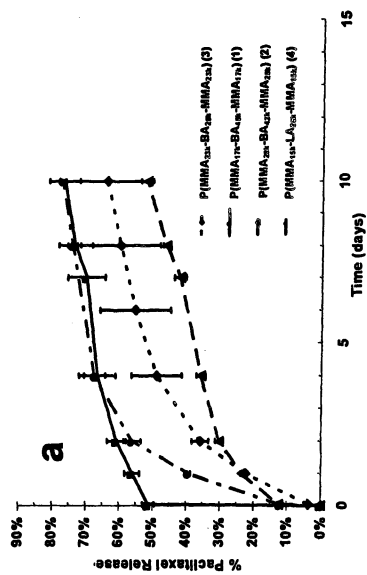
Figure 4. AFM phase images of (a) PMMA, (b) PS and (c) PIBA (3, 11, 6, Table 1) block copolymers (with PBA mid block) containing 0, 10 and 25% PTX by weight. All AFM scans are at 1 micron, except (c) which also contains larger 3 micron scan size to enable visualization of the drug particles. (Reproduced from reference 20. Copyright 2005 American Chemical Society)

The data indicates that at 25% PTX loading, the sustained (post-burst) release rate is independent of % MMA, the nature of the mid-block, and molecular weight. It was observed that one of the P(MMA-BA-MMA) block copolymers released approximately 50% of the PTX within 1 hour, which was substantially different than the other similar polymers tested. This polymer (1) had the lowest %MMA indicating that the initial release of PTX can be affected by changing the hard block for compositions with P(MMA-BA-MMA). Polymers (2) and (3) have similar weight% MMA and corresponding PTX release profiles.

Changing the hard block from PMMA to the less polar PIBA resulted in a more rapid release of PTX at early time points independent of whether the soft block was either PBA (5) or PLA(8) as seen in Figure 5b for coatings containing 25% PTX by weight. Except for the difference in the initial PTX release (1 hour time point); the sustained release rates appear to be similar to each other and also to the PBA or PLA copolymers containing PMMA hard segments. While the morphology of PIBA based triblocks appears similar to PMMA based materials as seen in AFM images, the presence of a separate PTX phase in the PIBA based copolymer may account for the rapid initial release rate.

The PTX release data for the P(BA-S) diblock (14) and P(BA-S)₃ triarm (13) block copolymers at 25% PTX loading are shown in Figure 5c. The diblock and the triarm star copolymers based on PBA and PS show a rapid release of PTX at the early time periods, similar to that observed with the PIBA based polymers. The modification of the styrene hard block with acrylonitrile was investigated to determine if adding a polar feature to an otherwise non-polar block would affect the release of PTX. While the molecular weight and weight percent styrene in the P(SAN-BA-SAN) (10) copolymer is significantly different than either the diblock or the triarm star, the hard block content of the two PS copolymers are on either extreme compared to the P(SAN-BA-SAN). Therefore, the presence of the acrylonitrile group may be providing some specific interaction that helps modulate the PTX release from the copolymer.

Select polymers were evaluated at 10% PTX to determine the effect of drug content. Figure 6 shows typical PTX release data. Reducing the amount of PTX had no effect on the early rapid release of PTX for the PS or the PIBA based copolymers, however the PMMA copolymer showed a marked change in release rate at the lower PTX level. This is consistent with the AFM data for these materials which indicates the presence of PTX particles on the surface of the PS and the PIBA coatings, whereas none can be observed in the PMMA system. The unusual zero order release kinetics for this material are theoretically desirable in the field of controlled drug release because the release rate is constant over time allowing for a consistent dose of therapeutic that is independent of time (22).



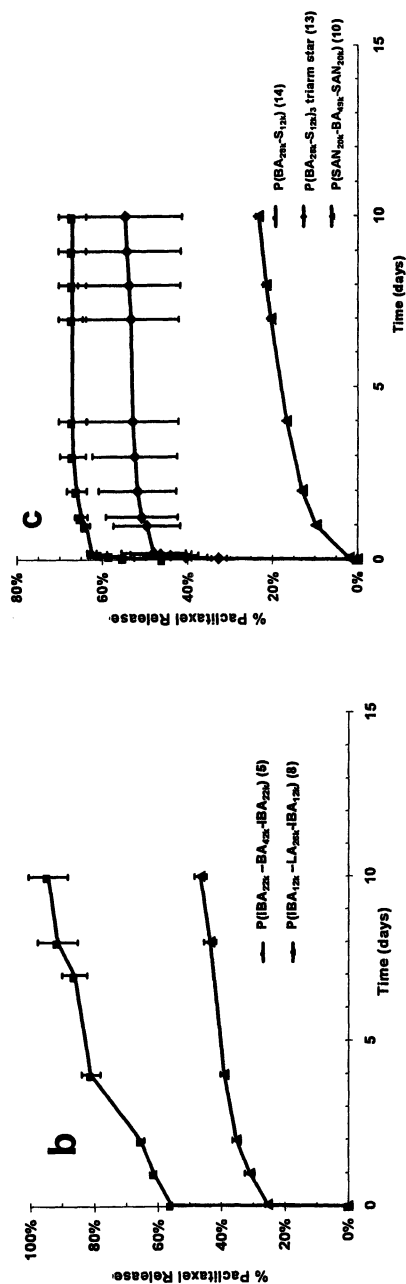


Figure 5. Pacitaxel release from block copolymers containing PBA or PLA soft blocks and MMA (a) or PIBA (b) PS or SAN (c) hard blocks of varying molecular weight and composition) with 25% PTX by weight. (Reproduced from reference 20. Copyright 2005 American Chemical Society)

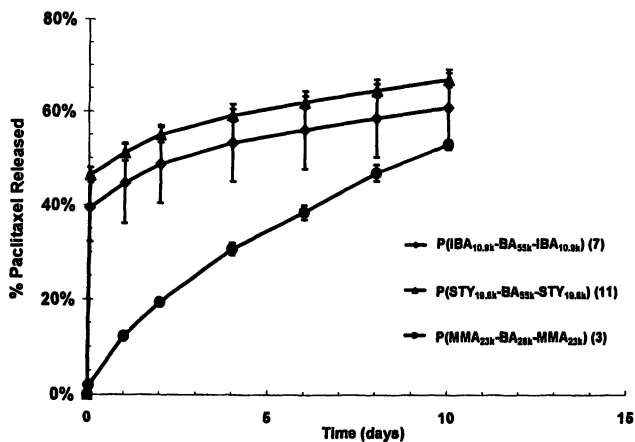


Figure 6. Paclitaxel release from triblock copolymers containing PBA mid-blocks blocks and PS, PIBA or PMMA (3, 7, 11, Table 1) hard blocks containing 10% PTX by weight. (Reproduced from reference 20. Copyright 2005 American Chemical Society)

Radiation Stability of Block Copolymers

The use of radiation for the sterilization of medical devices is quite common due to the fast and simple operations that have been developed within the medical community (23). The exposure of polymers to radiation typically results in either cross-linking or chain scission. This leads to a subsequent increase or decrease in molecular weight depending on which reaction predominates. It is well known that molecular weight can affect the release profile of therapeutics from polymers (24), and it is therefore important to verify the chemical stability of polymers intended for this purpose. It has been established that polymers containing quaternary carbons in the main chain are prone to radiation-induced molecular weight degradation due to the relative stability of tertiary radicals that are produced. These radicals often terminate by a disproportionation reaction leading to chain scission. However, in the absence of quaternary carbons, the predominant reaction is crosslinking (23, 25). The effects of radiation on polyacrylates and polymethacrylates has been previously published. The findings were in agreement with the principles stated above, with acrylates exhibiting predominantly cross-linking and methacrylates chain scission (26).

The polymers studied in this work were subjected to radiation from an electron beam (e-beam) sterilization process at nominal doses of 25 kGy and higher to simulate a typical medical device sterilization cycle. The percent

decrease in number average molecular weight for polymer samples before and after exposure to 25, 50, and 75 kGy e-beam doses are shown in Table III. Copolymers containing either PLA or PBA mid-blocks with PMMA end-blocks decrease in molecular weight due to degradation of the methacrylate segment. This is attributed to the presence of radiation labile quaternary carbons in the PMMA-based hard blocks. The relative decrease in Mn was found to be greater as the amount of methyl methacrylate increased. The polymers containing PIBA or PS and styrene-acrylonitrile (SAN) end segments show little change in molecular weight after exposure to radiation. This confirms that the polymers lacking quaternary main-chain carbons are more stable to the effects of ionizing radiation.

To examine the effects of radiation on the release rate of PTX, various polymer/drug coated stents were subjected to ionizing e-beam radiation and subsequently tested for PTX release. Figure 7 shows the PTX release rates for a P(MMA-BA-MMA) (3) containing 25% by weight PTX after exposure to 0, 25, 50, and 75 kGy doses of e-beam radiation. It was found that the PTX release rates were essentially independent of radiation dose. Even though the PMMA blocks contain quaternary carbons and therefore would be expected to experience some molecular weight reduction upon irradiation, the reduction does not appear to cause a measurable change in the PTX release rate. The greater stability of the P(MMA-BA-MMA) material and the corresponding PTX release rate is attributed to the superior radiation stability of the PBA mid-block and the small size of the less radiation stable PMMA end blocks. Additionally, since DSC data indicated miscibility only with the PBA block of this polymer, it may be that the PTX preferentially resides in this phase. Therefore, changes to the PMMA block would have less influence on the PTX release.

Table III. Effect of Radiation Dose on Mn of Block Copolymer

| Polymer Number | Composition | Wt.% Hard Block | % Decrease in Mn After Radiation Dose | | |
|----------------|---------------|-----------------|---------------------------------------|-------|-------|
| | | | 25 KGy | 50KGy | 75KGy |
| 1 | P(MMA-BA-MMA) | 41 | 00.62 | -2.46 | 5.12 |
| 2 | P(MMA-BA-MMA) | 58 | 12.77 | 23.83 | 43.38 |
| 3 | P(MMA-BA-MMA) | 62 | 7.0 | 13.3 | 21.8 |
| 4 | P(MMA-LA-MMA) | 58 | 3.88 | 5.94 | 11.69 |
| 7 | P(IBA-BA-IBA) | 28 | 1.36 | -0.08 | -0.14 |
| 8 | P(IBA-LA-IBA) | 47 | N/A | N/A | -11.2 |
| 9 | P(STY-LA-STY) | 54 | -0.91 | -1.93 | -2.84 |
| 10 | P(SAN-BA-SAN) | 45 | 0.26 | -0.39 | 3.25 |

NOTE: N/A = Not analyzed, 25 kGy = 1 sterilization dose.

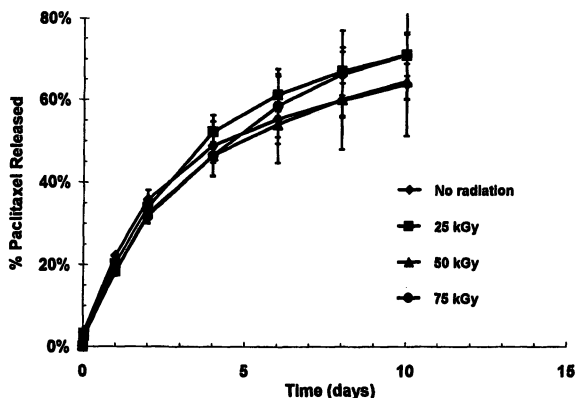


Figure 7. Effect of radiation dose on the release rate of PTX from $P(MMA_{23k}-BA_{28k}-MMA_{23k})$ (3, Table 1) with 25% PTX by weight. (Reproduced from reference 20. Copyright 2005 American Chemical Society)

The effect of a 75 kGy dose of e-beam radiation on the release rate of PTX from polymers contain either PMMA, SAN or IBA hard blocks along with a PLA or PBA soft block was also evaluated. Figures 8a and 8b show that only minor changes to the PTX release profile are observed independent of whether the hard end blocks are composed of radiation stable or labile polymer compositions. This further confirms the observation that radiation sensitivity and chain scission of materials in the end blocks may be of lower significance when the PTX shows no miscibility in this phase.

Conclusions

The release of PTX from acrylate-based block copolymers appears to be independent of the soft mid-block for PBA and PLA based copolymers. However, the nature of the end blocks has a significant impact on the initial PTX release rate for PBA based block copolymers. End blocks composed of highly non-polar monomers release a large amount of PTX (up to 50%) within the first few hours of in vitro release tests. In addition, AFM surface analysis of polymer/PTX films indicate the presence of PTX particles on the surface of block copolymers with non-polar end blocks, which most likely contributes to this phenomenon. Significantly slower and more controlled initial drug release was observed when the end blocks consisted of PMMA or SAN. In the case of

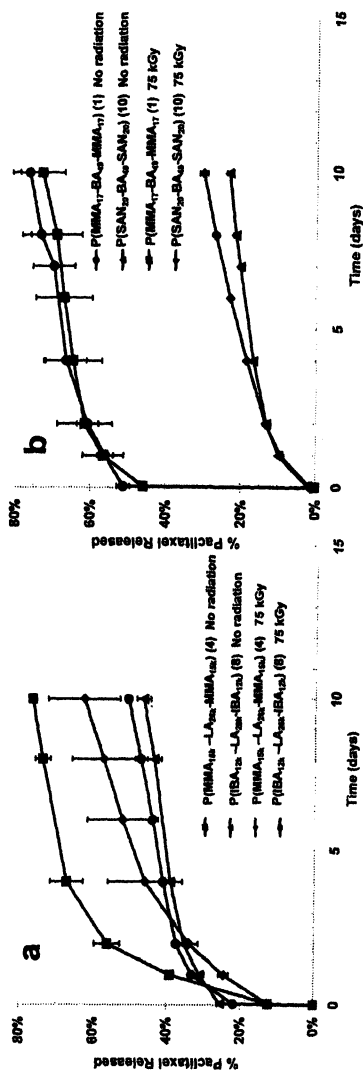


Figure 8. Effect of a 75 kGy radiation dose on the release rate of PTX from triblock copolymers containing PLA (a) or PBA (b) soft blocks and PMMA, PIBA or SAN hard blocks with 25% PTX by weight. (Reproduced from reference 20. Copyright 2005 American Chemical Society)

PMMA end-blocks, no visible PTX was observed by AFM, indicating more miscibility between the components, although no miscibility between PMMA and PTX could be detected by DSC analysis. These observations indicate that polar interactions between the hard-blocks of these copolymers may be affecting the release of PTX from these matrices. The PTX release from the acrylate based block copolymers appears to be unchanged by radiation sterilization for the polymers and doses evaluated in this study.

Acknowledgements

Tatyana Spitsina for GPC measurements and Jinyu Huang for the synthesis of the P(BA-S)₃ triarm star copolymer.

References

1. Ranade, S.; Miller, K.; Richard, R.; Chan, K.; Allen, M.; Helmus, M. J., *Biomed. Mater. Res.*, **2004**, 71A, 625.
2. Richard, R.; Barry, J.; Kamath, K.; Miller, K.; Ranade, S.; Schwarz, M., 31st Annual Meeting of the Controlled Release Society, Honolulu, Hawaii, USA, **2004** June 12-16.
3. Stone, G. W.; Ellis, S. G.; Cox, D. A.; Hermiller, J.; O'Shaughnessy, C.; Mann, J. T.; Turco, M.; Caputo, R.; Bergin, P.; Greenberg, J.; Popma, J. J.; Russell, M. E., *N Engl J Med* **2004**, 350 (3), 221-231.
4. Stone, G. W.; Ellis, S. G.; Cox, D. A.; Hermiller, J.; O'Shaughnessy, C.; Mann, J. T.; Turco, M.; Caputo, R.; Bergin, P.; Greenberg, J.; Popma, J. J.; Russell, M. E., *Circulation* **2004**, 109 (16), 1942-1947.
5. Tanabe, K.; Serruys, P. W.; Grube, E.; Smits, P. C.; Selbach, G.; van der Giessen, W. J.; Staberock, M.; de Feyter, P.; Muller, R.; Regar, E.; Degertekin, M.; Ligthart, J. M. R.; Disco, C.; Backx, B.; Russell, M. E., *Circulation* **2003**, 107 (4), 559-564.
6. Ranade S.; Richard, R.; Helmus, M., *Acta Biomaterialia*, **2005**, 1, 137.
7. Steckel, M.; Richard, R.; Strauman, P.; Barry, J. Society for Biomaterials Philadelphia PA, October 2004.
8. Uhrich, K.; Schmeltzer, R.; Prudencio, A.; Whitake, K. *Polym. Mat. Sci. and Eng* **2005**, 92, 31.
9. Hicks, M.; Pudil, B.; Kanamathareddy, S.; Goodrich, S.; East, A.; Letton, A. *Polym. Mat. Sci. and Eng* **2005**, 92, 26.
10. Zhang, H.; McCarthy, B.; Gopalan, S.; Sizinai, I.; DeFife, K.; Turnell, B.; Darabbeigi, D. *Polym. Mat. Sci. and Eng* **2005**, 92, 25.
11. Schwarz, M.; Ranade, S.; Richard, R. 31st Annual Meeting of the Controlled Release Society, Honolulu, Hawaii, USA, **2004** June 12-16

12. Wang, J.-S.; Matyjaszewski, K. *J. Am. Chem. Soc.* **1995**, *117*, 5614-5615.
13. Matyjaszewski, K.; Xia, J. *Chem. Rev.* **2001**, *101*, 2921-2990.
14. Kamigaito, M.; Ando, T.; Sawamoto, M. *Chem. Rev.* **2001**, *101*, 3689-3745
15. Lendlein, A.; Schmidt, A.; Langer, R. *Proc Natl Acad Sci* **2001**, *98*(3), 842.
16. Beers, K. L.; Woodworth, B.; Matyjaszewski, K. *J. Chem. Educ.* **2001**, *78*, 544-547.
17. Beers, K. L.; Matyjaszewski, K. *J. Macromol. Sci., Pure Appl. Chem.* **2001**, *A38*, 731-739.
18. Shipp, D. A.; Wang, J.-L.; Matyjaszewski, K. *Macromolecules* **1998**, *31*, 8005-8008.
19. Tsarevsky, N. V.; Sarbu, T.; Goebelt, B.; Matyjaszewski, K. *Macromolecules* **2002**, *35*, 6142-6148.
20. Richard, R.; Schwarz, M.; Ranade, S.; Chan, K.; Matyjaszewski, K.; Sumerlin, B., *Biomacromolecules* **2005**, *6*(6), 3410.
21. Liggins, R.T.; Hunter, W.L.; Burt, H. M. *J. Pharm. Sci.* **1997**, *86*, 1458-1463.
22. Langer, R; Peppas, N. *JMS-Rev.Macromol. Chem. Phys.* **1983**, *C23*(1) 61-126.
23. Pruitt, L.A., *Advances in Polymer Science* **2003**, *162*, 63
24. Kim H, Fassih R., *J Pharm Sci.* **1997**, *86*(3), 323.
25. Cardona, F; Hill, D.; Pomery, P.; Whittaker A., *Polym. Int.* **2003**, *52*, 1711.
26. Shultz, A. J. *Polym. Sci.* **1959**, *35*, 369.

Chapter 18

Grafting Chromatographic Stationary Phase Substrates by Atom Transfer Radical Polymerization

Patrick McCarthy¹, Nicolay V. Tsarevsky², Lindsay Bombalski²,
Krzysztof Matyjaszewski², and Christopher Pohl¹

¹Research and Development, Dionex Corporation, 1228 Titan Way,
Building 1, P.O. Box 3603, Sunnyvale, CA 94088

²Department of Chemistry, Carnegie Mellon University, 4400 Fifth Avenue,
Pittsburgh, PA 15213

Chromatographic stationary phases were prepared by “grafting from” and “grafting through” atom transfer radical polymerization (ATRP). Characterization of sacrificial polymer indicated controlled polymerization. Characterization of film thickness, ion exchange capacity and column backpressure indicated that polymerization from surface bound initiator was controlled and comparable to polymerization from sacrificial initiator. Chromatographic performance in standard protein separations suggests that stationary phase selectivity and capacity are affected by both graft chain length and graft chain density.

Controlled radical polymerization (CRP) methods are particularly interesting for commercial product research and development because they allow for preparation of a wide variety of polymers with controlled molecular weight (M_n), molecular weight distribution (PDI) and chain end functionality (1,2). Some CRP methods also make it possible to produce new polymeric materials with segmented, brush and star architectures (3). In general, CRP methods are useful as a tool for identifying product properties which are dependent on M_n and PDI. In some cases applying CRP methods has led to significant advances over current technology (4).

Existing chromatographic stationary phases utilize a variety of base supports and surface modifications. Many commercial products contain porous and nonporous crosslinked polystyrene-divinylbenzene or poly(methyl methacrylate) polymeric stationary phase substrates (5). The surfaces of these substrates are modified to contain analyte interaction sites using polymeric surface modification approaches including bonding, electrostatic assemblies, coatings, encapsulation and/or grafting (6). Development of new chromatographic stationary phases is typically driven by emerging application requirements which are not met by existing materials. Most often, the unmet separation requirement is chromatographic resolution.

Application of CRP methods at every stage of chromatographic stationary phase development has the potential to increase understanding of the relationship between polymeric materials and chromatographic performance. In this manuscript, we describe the application of various ATRP approaches to grafting chromatographic stationary phases. Chromatographic properties of stationary phases produced using ATRP are compared to those of commercially available stationary phases. Sacrificial polymer M_n is compared to stationary phase capacity, backpressure and selectivity. The implications of these data are discussed and the future potential of CRP technology in stationary phase development is considered.

Experimental

Materials. Methacryloyloxyethyltrimethylammonium chloride (TMAEMA) was purchased from Wako and used as received. 2-(N,N-dimethylamino)ethyl methacrylate (DMAEMA) was purified by filtration through a column of basic alumina, Glycidyl methacrylate (GMA) was purified by filtration through a column of MEHQ inhibitor remover resin. The following were purchased from Aldrich and used as received: anhydrous 2-butanone, dioxane, sodium sulphite, sodium carbonate, 2,2'-bipyridyne (bipy), CuBr, CuBr₂, acetone, ethyl-2-bromoisobutyrate (EBiB), 2-bromoisobutyryl bromide (BiBB), hexamethyltriethylenetetramine (HMTETA), hydrochloric acid (HCl), methanol(MeOH), tetrahydrofuran (THF), and triethylamine (TEA). The proprietary chromatographic substrate and substrate with hydrophilic layer modification were obtained from Dionex Corporation.

Grafting from: DMAEMA and TMAEMA.

Surface bound initiator (SBI) beads. To a dry flask were added hydrophilic layer modified beads (60 g) and THF (600 mL). The mixture was stirred under nitrogen in an ice bath for one hour. TEA (12 mL, 0.0861 mol) and BiBB (24 mL, 0.227 mol) were added and the reaction was allowed to stir overnight. Beads were vacuum filtered and washed with THF.

pDMAEMA grafted resin. To a dry flask were added acetone (40 mL), EBiB (0.0225 mL, 0.153 mmol) and SBI beads (30 g). The mixture was stirred while bubbling with nitrogen for two hours. In a separate dry flask were added CuBr (0.0661 g, 0.462 mmol), CuBr₂ (0.0133 g, 0.046 mmol). The flask was evacuated and back-filled with nitrogen. Acetone (15 mL), HMTETA (0.140 mL, 0.515 mmol), and DMAEMA (50 mL, 0.296 mol) (all reagents bubbled with nitrogen for 30 min prior to the experiment) were then added individually to the flask containing copper. The catalyst/monomer solution was transferred to the reaction flask under nitrogen. The sealed reaction mixture was allowed to react in a 35 °C oil bath for 25 hours. The resulting resin was vacuum filtered and washed with 1M NaCl. The ratio of reagents was monomer:initiator:catalyst = 1935:1:3 with 17% of the total copper weight being CuBr₂ deactivator.

pTMAEMA grafted resin. To a dry flask were added SBI beads (2 g) and TMAEMA monomer (4 g, 19.3 mmol). The flask was sealed and evacuated with nitrogen. Degassed MeOH (6 mL) and EBiB (29 µL, 0.193 mmol) were added under nitrogen. The catalyst was assembled in a separate flask by adding bipy (0.0302 g, 0.200 mmol), CuBr (0.0138 g, 0.096 mmol), and CuBr₂ (0.0005 g) evacuating with nitrogen and adding 1.5 mL degassed MeOH. The catalyst solution was transferred to the reaction flask under nitrogen. The sealed flask was allowed to react at 25 °C for 6 h. The resulting resin was vacuum filtered and washed with 1M NaCl. The ratio of reagents was monomer:initiator:catalyst = 100:1:0.5 with 3.6% of the total copper weight being CuBr₂ deactivator.

Grafting though: GMA.

pGMA grafted resin. GMA monomer (60.0 g, 422.1 mmol), anhydrous 2-butanone (60.0 g), and hydrophilic layer modified substrate (30.0 g) were combined in a 250 mL round bottom flask and bubbled with nitrogen for 2 h. In a separate round bottom flask, the copper complex was assembled under nitrogen by combining CuBr (0.75 g, 5.28 mmol), bipy (1.65 g, 10.56 mmol), and anhydrous 2-butanone (2 mL). The catalyst solution was added to the monomer/resin mixture and bubbled with nitrogen for 30 min. Nitrogen purged EBiB (1.03 g, 5.28 mmol) was added. The reaction mixture was sealed, transferred to an oil bath at 50 °C and allowed to react for 4 h. The resulting material was diluted with acetone (250 mL), vacuum filtered, and washed with acetone (250 mL). The resulting pGMA grafted resin was dried at 60 °C in an oven overnight.

Converting pGMA grafts to strong cation exchange grafts. Na_3PO_4 (0.4 g) was dissolved in 20 g de-ionized water and titrated to pH 8 with HCl. Na_2SO_3 (2 g) was added and allowed to dissolve. PGMA-grafted resin (5 g) was added to the mixture and allowed to stir at 60 °C for 4 h. The resulting mixture was diluted with de-ionized water, vacuum filtered, and washed with 1 M NaCl.

HPLC separations. Chromatography was performed on a Dionex Corporation instrument equipped with an AD20 detector, a GP50 pump, an AS50 autosampler and Chromeleon software. Gel permeation chromatography (GPC) was performed on a Waters instrument equipped with a 510 pump, a 2410 refractive index detector and Polymer Standards Services (PSS) Styragel columns (10^5 , 10^3 , and 10^2 Å). GPC conditions included; N,N-dimethylformamide mobile phase, T = 50 °C, and flow rate = 1 mL/min. Molecular weights were determined using PSS software with a calibration based on linear poly(methyl methacrylate) standards (PSS).

Microscopy. Transmission electron microscopy (TEM) measurements were performed on a Zeiss EM109 instrument. Resin samples were stained with 2% phosphotungstic acid (PTA, Ted Pella Inc.), embedded in Spurr low viscosity epoxy resin (Ted Pella Inc.) and cured at 60 °C for 8 hours. Cross-sectioning was carried out on a LKB Nova ultramicrotome with a Diatome diamond knife.

Overview

Major advances in the application of CRP to surface modification have been achieved over the last ten years (7). This progress has led to synthetic approaches for surfaces with not only controlled graft length, PDI and graft density, but also new compositions including multi-block grafts and brush grafts (8). Living polymerization grafting methods (10) have been applied to a variety of substrates including silicon wafers (6,9), chromatographic beads (11), particles (12-14) and monoliths (15).

Several examples of approaches for grafting substrates are illustrated in Figure 1. Grafting is typically carried out by “grafting onto”, “grafting through”, “grafting from”, or “grafting from with sacrificial initiator”. The “grafting onto” approach (Figure 1A) involves covalently bonding preformed polymers to the substrate surface through a reactive end group (16). An advantage to this approach is that a variety of preformed polymer compositions can be generated and characterized prior to reacting with the surface. Typically this approach results in polymer grafts with low graft density due to attached polymers that hinder further polymer attachment (7).

The “grafting through” approach (Figure 1B) involves preparation of a substrate with surface bound monomer (17). A polymerization reaction is carried out in the presence of the substrate. This approach results in *living* polymer grafts with low graft density also due to attached polymers that hinder subsequent polymer attachment.

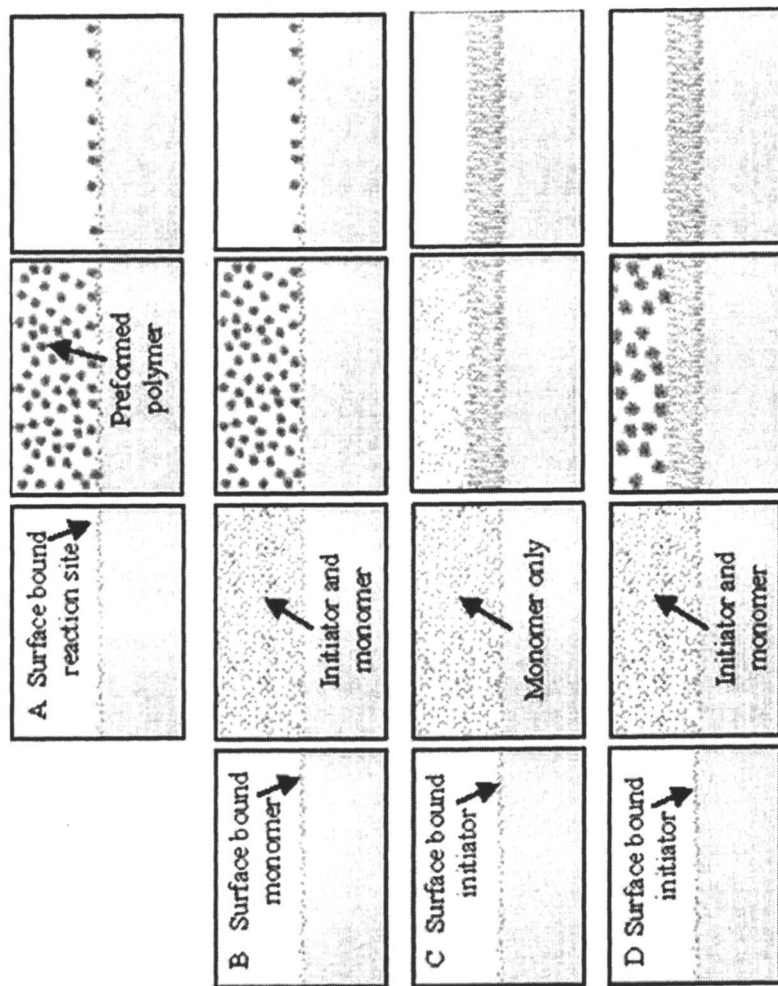


Figure 1. Illustration of approaches. A. Grafting onto. B. Grafting through. C. Grafting from. D. Grafting from with sacrificial initiator.

The “grafting from” approach (Figure 1C) involves polymerization from surface bound initiator. Because polymers are growing from the surface, graft density depends on surface bound initiator density. High surface bound initiator density surfaces can result in very high *living* polymer graft density (9,18,19). Although it is appealing to have polymerization only from the surface, several reports indicate that achieving controlled ATRP from surface bound initiator is challenging (7). Problems in control of “grafting from” systems can be overcome by addition of deactivator prior to initiation (7,11,20,21). Alternatively, the problems in control of “grafting from” systems can be overcome by adding sacrificial initiator (1,7,9). When the amount of sacrificial initiator added is far greater than the amount of surface bound initiator, the monomer:initiator:catalyst ratio can easily be controlled and sufficient deactivator can be present to maintain controlled polymerization.

Characterization of polymers grafted from surfaces is difficult, especially for low surface area substrates (7). It is convenient to characterize sacrificial polymer in “grafting from” with sacrificial initiator systems. Some researchers have achieved systems where polymers grafted from surfaces could be characterized and have found good correlation between sacrificial and surface polymerizations (20). Correlation between sacrificial and graft polymerization is appealing for monitoring and improving lot-to-lot variability in production scale graft reactors.

Particle-particle crosslinking

Figure 2A shows a scanning electron microscope image of the non-porous polystyrene-divinylbenzene beads. The beads are spherical, have narrow polydispersity and average bead diameter is 10 microns. An illustration of a bead grafted with a polymer can be seen in Figure 2B.

A common problem when “grafting from” particles is gelation due to particle-particle crosslinking. Even small amounts of particle-particle crosslinking can impact chromatography column performance. Particle-particle crosslinking can be significantly reduced by the addition of sacrificial initiator. The deactivator generated by coupling in solution controls the polymerization. The presence of sacrificial growing chains increases the probability of particle-sacrificial polymer coupling over particle-particle coupling.

Grafting from

The synthetic approach for the “grafting from” with sacrificial initiator is shown in Figure 3. This approach involved; 1) converting residual –OH groups on the surface of hydrophilic layer modified, 10 μm diameter, nonporous PS-DVB beads to surface bound initiator sites 2) grafting pDMAEMA chains from

the surface bound initiator in the presence of sacrificial initiator. Because initiator was present on the beads and in solution, the polymerization was initiated by the “catalyst last” method.

Fractions I, II, III, and IV were collected 2, 5, 20 and 25 hours after initiating the polymerization. The solution polymer was separated from the bead supports and was characterized by GPC and gravimetry to assess polymerization kinetics, sacrificial polymer M_n and sacrificial polymer PDI. Figure 4A shows that the first order kinetic plot of the polymerization from the sacrificial initiator was linear. Figure 4B shows that the M_n of polymer grown from sacrificial initiator increased linearly with conversion and PDI trended downward with conversion. This data indicates good control and living character of the polymerization from sacrificial initiator. Figure 4C shows a GPC trace of sacrificial polymer present in fraction IV and shows the very small amount of coupled chain even at relatively long reaction time. The illustration in Figure 4D shows relative graft lengths for the four fractions, assuming that polymerization in solution is similar to polymerization from the surface.

Beads without any surface modification (raw resin) and beads with a highly crosslinked hydrophilic layer were embedded in resin and cross-sectioned. The TEM image of the raw resin sample shows that the beads are free of occlusions and the resin surface is smooth (Figure 5A). The TEM image of the hydrophilic layer modified resin shows that the hydrophilic layer is 50 nm thick, it has uniform thickness over long length scales, and covers the entire bead surface (Figure 5B). Beads from fractions I and IV were stained with PTA to enhance the contrast of pDMEAMA grafts. TEM images of samples with beads from fractions I and IV are shown in Figure 5C and Figure 5D, respectively. The pDMAEMA film thicknesses are estimated to be approximately 15 nm and 52 nm for fraction I and IV, respectively. The M_n of pDMAEMA from sacrificial initiator in fractions I and IV was 14,800 g/mol (DP ~ 95) and 61,300 g/mol (DP ~ 390), respectively. Assuming polymerization in solution is similar to polymerization on the surface, there is an increase in film thickness of 1.25 Å per DP unit. High density grafts have been found to be elongated due to high surface density or confinement (9,18). These results are in good agreement with expected sample film thicknesses assuming that surface confinement has elongated the pDMAEMA grafts.

Beads from fractions I, II, III and IV were washed and packed into 2 mm × 50 mm column bodies. Because the pDMAEMA grafts contain tertiary amine functionality, they can be converted back and forth between the base form and salt form by flushing the column with dilute base and dilute acid, respectively. This property allowed us to not only measure the ion exchange capacity of the resin but also the extent of the pH response of the pDMAEMA film by measuring column backpressure.

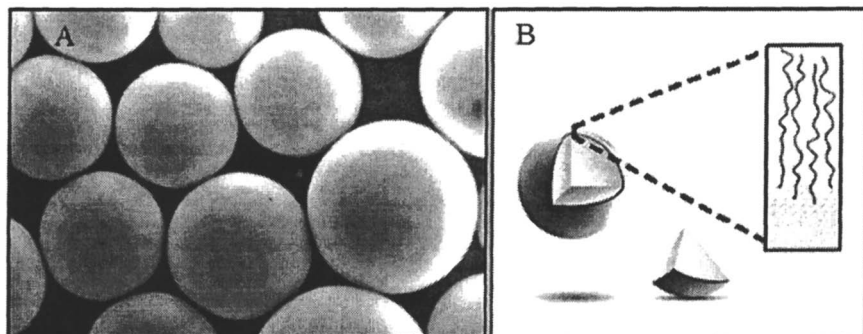


Figure 2. *A. Scanning electron microscopy image of the nonporous, polystyrene-divinylbenzene substrate. B. General illustration of grafted nonporous stationary phase design.*

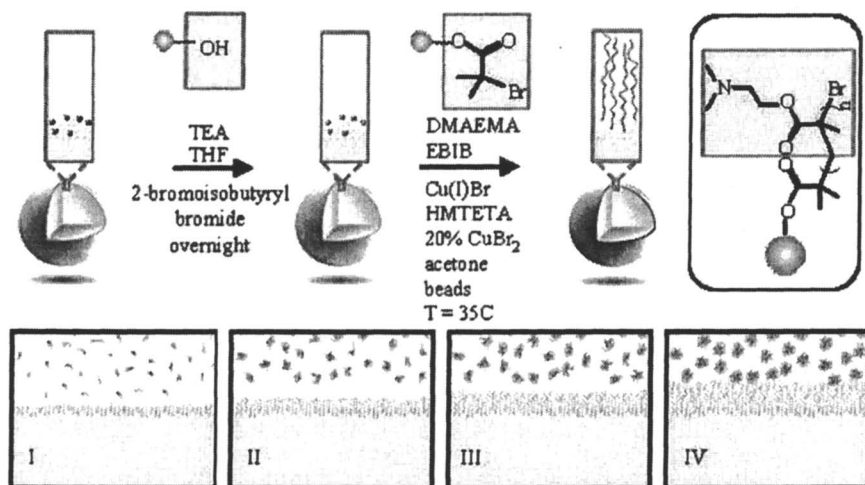


Figure 3. *Schematic of the synthetic approach for preparation of pDMAEMA grafted from a substrate using sacrificial initiator.*

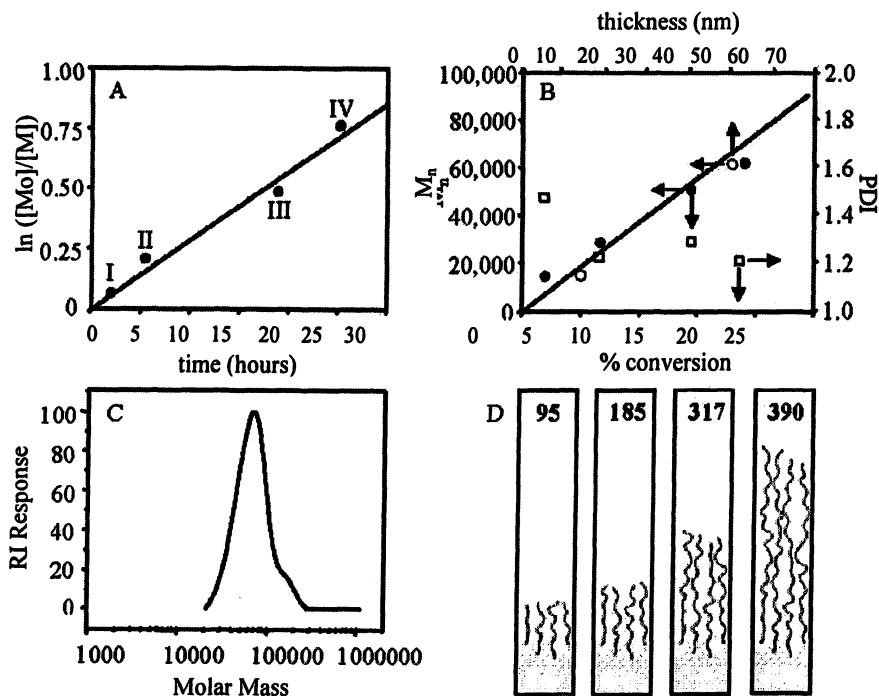


Figure 4. A. First-order kinetic plot for DMEAMA polymerization from sacrificial initiator. Fractions collected were labeled I, II, II, and IV. B. Evolution of M_n with conversion (\bullet), PDI with conversion (\square) and film thickness with conversion (\circ). C. Gel permeation chromatography trace of pDMAEMA from sacrificial initiator in fraction four. D. Illustration of expected relative pDMAEMA grafts length. (Figures 5A and 5B are reproduced from reference 4. Copyright 2005 American Chemical Society.)

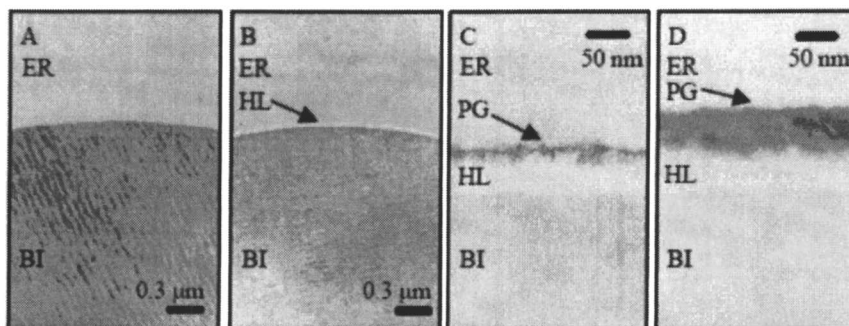


Figure 5. TEM images of cross-sections of beads embedded in resin showing the bead interior (BI), embedding resin (ER), hydrophilic layer (HL), and PTA stained polymer grafts (PG). Panels A, B, C and D show images of raw resin beads, hydrophilic layer coated beads, pDMAEMA grafted beads from fraction (I), and fraction (IV) respectively. (Figures 5A and 5B are reproduced with permission from reference 4. Copyright 2005 by P. McCarthy.)

Resin ion exchange capacity was measured by monitoring nitrate breakthrough (Figure 6A) and expressed as micro equivalents per gram resin ($\mu\text{eq/g}$). The relationship between capacity and sacrificial polymer M_n approaches linearity as seen in Figure 6B (closed circles). Similarly, ion-exchange capacity increased with increasing film thickness (Figure 6B, open circles).

Figure 7A shows column backpressure under typical operating conditions as a function of resin capacity for two separate syntheses and a commercially available WAX column. Column backpressure increased with ion exchange capacity. Columns packed with resin generated with a PMDETA catalyst (Figure 7A, solid circles) had a faster rate of increase in backpressure with capacity compared to columns generated with an HMTETA catalyst system (Figure 7A, open circles). We expect that this is because the HMTETA catalyst system provides better control over polymerization of DMAEMA than the PMDETA catalyst. The highest resin capacity achieved was $295 \mu\text{eq/g}$, which is about three times that of a conventional grafted resin on a nonporous substrate. This data suggests achieving very narrow molecular weight distributions by optimizing ATRP conditions could result in resins with ultra high ion exchange capacities while maintaining acceptable column backpressures.

Figure 7B shows column backpressures as a function of column capacity for resin generated by the PMDETA catalyst system. Backpressures were measured while pumping 15 mM ammonium hydroxide (Figure 7B, open triangles) and 4 mM nitric acid (Figure 7B, closed circles) through the column at a constant flow rate of 0.25 mL/min. As expected, the column backpressure was greater with acidic eluent than basic eluent. This is due to the protonation and chain expansion of pDMAEMA grafts at low pH. Also, as resin capacity increases so does the difference in backpressure or extent of pH response.

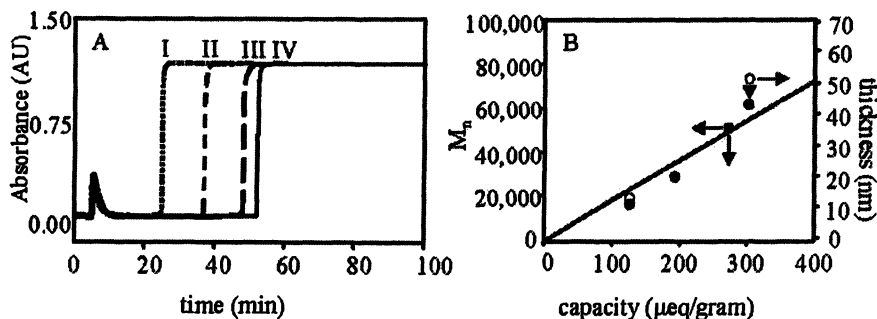


Figure 6. A. Breakthrough traces for 2 mm by 50 mm columns packed with resin from fractions I, II, III, and IV. Columns were flushed at 0.25 mL/min with 15mM ammonium hydroxide (1 hr), DI water (5 min) and 4 mM nitric acid (100 min). Nitrate breakthrough was monitored at 230 nm. B. Correlation of resin capacity and sacrificial polymer M_n (●) and resin capacity and film thickness (○). (Figure 6B is reproduced with permission from reference 4. Copyright 2005 by P. McCarthy.)

Figure 8 shows a low magnification TEM image of a stained cross-section of pDMAEMA beads from fraction IV. This image shows uniform pDMAEMA film thickness over the entire bead.

Chromatographic resolution of ovalbumin phosphorylation variants was competitive with the ProPac[®] WAX-10 column, a commercially available weak anion exchange column designed for protein separations (4). Because pDMEAMA begins to deprotonate as the eluent pH is increased above pH 7.5, the phase has limited utility as an anion exchanger above pH 8.0. Therefore, for separation of double stranded DNA (dsDNA), we generated a pTMAEMA stationary phase by “grafting from” in the presence of sacrificial initiator. The synthetic approach was similar to the approach illustrated in Figure 4. Since pTMAEMA contains a quaternary amine site, it retains its charge even at high pH.

A 2 mm × 50 mm column was packed with pTMAEMA grafted beads and compared to the DNAPac[®] PA100 column for separation of a 1 kilo base pair (kbp) dsDNA ladder. Elution of linear dsDNA is expected to be in order of ladder number (Figure 9). Hence, the peaks beginning at ~ 24 minutes represent dsDNA containing 2, 3, 4, 5, 6, 7, 8, 9, 10, 11, and 12 kbp. The resolution of dsDNA fragments larger than 1000 base pairs by the pTMAEMA prototype is remarkably better than the current leading commercially available column (23). Because the pTMAEMA phase was generated from a similar synthetic approach, we expect that it has similar graft density and long range film homogeneity. We speculate that the increased resolving power of the pTMAEMA column over the DNAPac PA100 is at least partly due to long length scale film homogeneity.

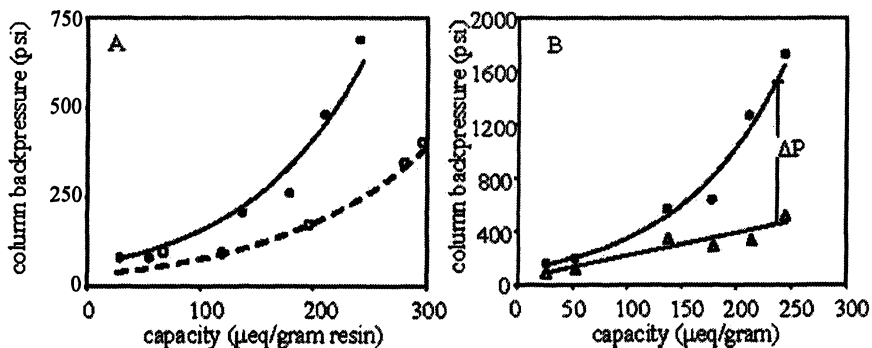


Figure 7. Backpressure was measured while pumping 20 mM HEPES + 10 mM NaCl, pH 7.5 at 0.25 mL/min. A. Relationship between column backpressure and resin capacity for pDMAEMA grafted resin using a PMDETA catalyst system (●) and an HMTETA catalyst system (○). B. Comparison of column backpressure with 4 mM nitric acid eluent (●) and 15 mM ammonium hydroxide eluent (Δ) at 0.25 mL/min for columns with increasing capacity.

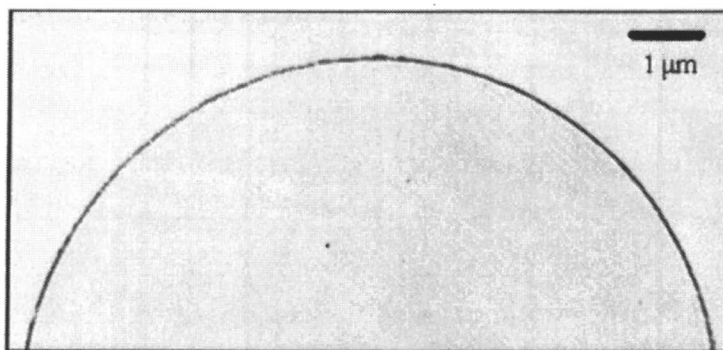


Figure 8. TEM image of the cross-section of a sample containing PTA stained pDMAEMA grafted beads from fraction IV.

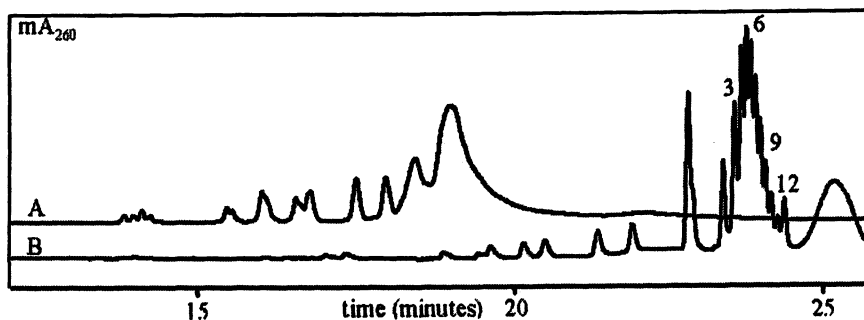


Figure 9. Separation of a dsDNA 1 kbp ladder on DNAPac PA100 (trace A) and pTMAEMA prototype (trace B). Samples were eluted at 0.3 mL/min with a gradient of 175 - 550 mM NaCl at pH 8.5 and 50 °C.

Grafting through

The synthetic approach for preparation of stationary phases by “grafting through” ATRP is shown in Figure 10. This approach involved polymerization of GMA in the presence of hydrophilic layer modified beads with surface bound monomer. Several separate “grafting through” syntheses were carried out using monomer-to-initiator (M/I) ratios equal to 20, 40, 60, 80, 100, and 200. The epoxy side chains were reacted with Na₂SO₃ resulting in strong cation exchange (SCX) pendant groups.

Beads from the six syntheses were packed into 4 mm by 250 mm column bodies and tested for chromatographic performance in the separation of ribonuclease A (peak 1), cytochrome c (peak 2) and lysozyme (peak 3) (Figure 11). The increase in protein retention time with M/I ratio was non-linear. Ribonuclease A and cytochrome c were almost baseline resolved in the column generated from M/I = 20. As M/I ratio increased, resolution of ribonuclease A from cytochrome c decreased. Ribonuclease A and cytochrome c co-elute above M/I = 80.

Substrates generated by “grafting through” have been found to have lower chain density than their grafting from counterparts (8). Because the ratio of solution monomer to surface monomer is very high, we expect that polymer begins to attach to the surface at high conversion and hinder subsequent polymer attachment as in “grafting onto”. We expect that larger attached polymers hinder attachment of subsequent polymers more than smaller attached polymers. If these assumptions are true then “grafting through” reactions with increasing M/I ratio should produce stationary phases with decreasing graft density. This effect may partly account for the nonlinear relationship between protein retention time and M/I ratio.

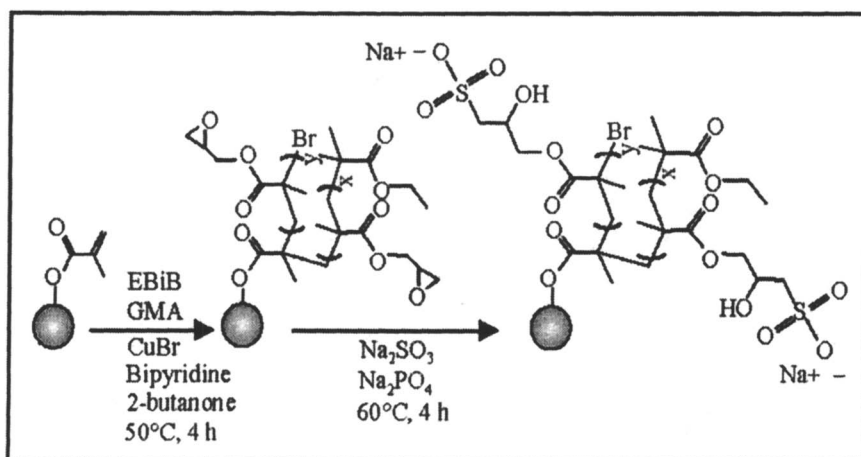


Figure 10. Schematic of the preparation of a "grafted through" pGMA beads and conversion to an SCX stationary phase.

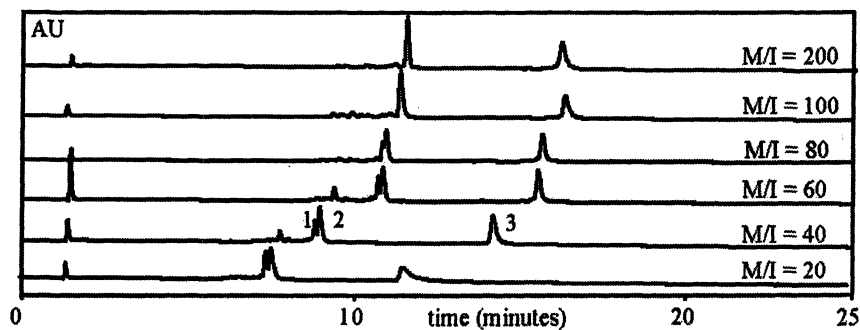


Figure 11. Separation of standard proteins. The samples were eluted from the column at 1.0 mL/min with a gradient of 40 - 180 mM NaCl in 20 mM MES buffered to pH 5.7.

Comparing “grafting through” and “grafting from”

To compare the “grafting through” and “grafting from” approaches, a pGMA “grafted from” phase was made and converted to a SCX phase as described earlier. Column performance was also evaluated as described earlier. The run time ratio of cytochrome c and lysozyme was different for the two phases. This indicates differences in selectivity. The “grafted from” column (Figure 12B) also had significantly lower lysozyme peak efficiency (peak 3) than the “grafted through” column (Figure 12A). We speculate that high chain density causes poor mass transport.

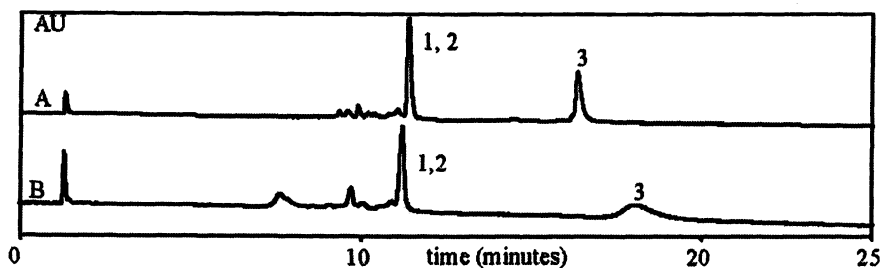


Figure 12. Separation of ribonuclease A (peak 1), cytochrome c (peak 2) and lysozyme (peak 3). A. “grafting through” $M/I = 100$. B. “grafting from” with sacrificial initiator $M/I = 100$.

The chromatographic data suggests that column performance can be affected by changes in graft chain length and graft chain density. Because these two variables are likely to be inter-related, chromatographic data on a library of surfaces with varying graft lengths and graft densities would be useful in understanding their relationships. Although there is not a convenient way to control graft density in “grafting through”, surfaces with varying graft density have been achieved in “grafting from” by adding “dummy” initiator during the initiator-surface bonding reactions (24). Future experiments will be pursued toward these ends.

Conclusions

A variety of stationary phases were prepared and studied in this report. Advantages and disadvantages were identified for both “grafting from” and “grafting through” approaches. For instance: the “grafting from” approach allowed for preparation of phases with very high ion exchange capacity and low backpressure; sacrificial initiator M_n could be used to monitor stationary phase

ion exchange capacity during polymerization; surfaces generated had long range film homogeneity; and columns packed had exceptional resolving power for very large dsDNA. For protein separation applications, however, “grafting from” materials exhibited poor peak efficiency. The “grafting through” approach allowed us to identify a relationship between graft length and graft density on stationary phase selectivity and peak efficiency for protein separation applications. “Grafting through”, however, cannot easily generate surfaces with controlled graft density. In general, this report demonstrates that ATRP is an excellent tool for studying the relationships between M_n (and PDI) and commercial product properties, and has potential for not only improving current commercial products but generating new technological platforms for the next generation.

Acknowledgements

We would like to thank David Shimmin (Nanocraft, Mountain View) for microscopy, James Thayer for methods development contributions and Jennifer Kindred for proofreading assistance.

References

1. Matyjaszewski, K., Davis, T. P., Eds. *Handbook of Radical Polymerization*; Wiley: Hoboken, 2002.
2. Wang, J.S., Matyjaszewski, K., *J. Am. Chem. Soc.*, **1995**, *117*, 5614.
3. Matyjaszewski, K., Xia, J., *J. Chem. Rev.*, **2001**, *101*, 2921
4. McCarthy, P., Bombalski, L., Tsarevsky, N. V. T., Thayer, J. R., Shimmin, D., Matyjaszewski, K., Avdalovic, A., Pohl, C., *Polymer Preprints*, **2005**, *46*, 177-178.
5. Leonard, M., *J. Chromatogr. B*, **1997**, *699*, 3-27.
6. Pohl, C., *LC/GC Europe*, **2003**, *3*, 1-4.
7. Pyun, J., Kowalewski, T., Matyjaszewski, K., *Macromol. Rapid Comm.*, **2003**, *24*, 1043-1059.
8. Advincula, R. Brittain, W. J., Caster, K., Ruhe, J., *Polymer Brushes*; Wiley: Weinheim, 2004.
9. Matyjaszewski, K., Miller, P.J., Shukla, N., Immaraporn, B., Gelman, A., Luokala, B.B., Siclovan, T.M., Kickelbick, G., Vallent, T., Hoffmann, H., Pakula, T., *Macromolecules*, **1999**, *32*, 8716.
10. a. Brittain, W., *Surface Science*, **2004**, *570*, 1-12. b. M. Zhao, B., Brittain, W.J., *Prog. Polym. Sci.*, **2000**, *25*, 677.
11. Huang, X., Wirth, M. J., *Analytical Chemistry*, **1997**, *69*, 4577.
12. Zheng, G., Stover, H.D.H., *Macromolecules*, **2002**, *35*, 6828.
13. Pyun, J., Matyjaszewski, K., *Chem. Mater.*, **2001**, *13*, 3436-3448.

14. Perruchot, C., Khan, M.A., Kamitsi, A., Armes, S.P., von Werne, T., Patten, T., *Langmuir*, **2001**, *17*, 4479-4481.
15. Meyer, U., Svec, F., Frechet, J.M.J., Hawker, C.J., Irgum, K., *Macromolecules*, **2000**, *33*, 7769.
16. Edmondson, S., Huck, W. T. S., *J. Mater. Chem.*, **2004**, *14*, 730-734.
17. Neugebauer, D., Zhang, Y., Pakula, T., Sheiko, S., Matyjaszewski, K., *Macromolecules*, **2003**, *36*, 6746.
18. Ejaz, M., Yamamoto, S., Ohno, K., Fukuda, T., *Macromolecules*, **1998**, *2*, 89.
19. Husseman, M., Malmstrom, E.E., McNamara, M., Mate, M., Mecerreyes, O., Benoit, D.G., Hedrick, J.L., Mansky, P., Huang, E., Russell, T.P., Hawker, C.J., *Macromolecules*, **1999**, *32*, 1424.
20. Kim, J. B., Baker, M. L., Bruening, G. L., *J. Am. Chem. Soc.*, **2000**, *122*, 7616.
21. Tsarevsky, N. V., Pintauer, T., Matyjaszewski, K., *Macromolecules*, **2004**, *37*, 9768.
22. Weitzhandler, M., Farnan, D., Rohrer, J., Avdalovic, N., *Proteomics*, **2001**, *1*, 179.
23. Thayer, J., McCormick, R., Avdalovic, N., *Methods in Enzymology*, **1996**, *271*, 147.
24. Jones, D. M., Brown, A. A., Huck, W. T. S., *Langmuir*, **2002**, *18*, 1265.

Chapter 19

Synthesis of Inorganic–Polymer Nanocomposites by Atom Transfer Radical Polymerization Using Initiators or Polymerizable Groups Attached to Transition Metals via Bidentate Ligands

Guido Kickelbick, Dieter Holzinger, Dieter Rutzinger,
and Sorin Ivanovici

Institute of Materials Chemistry, Vienna University of Technology,
Getreidemarkt 9, A1060 Vienna, Austria

Metal alkoxides were functionalized by bidentate ligands based on β -diketones or acetoacetoxy-derivatives. The resulting complexes either carried initiator or polymerizable groups for ATRP. In addition these compounds were used as precursors for the sol-gel process. Depending on the functional group attached to the metal and the further processing of the derived compounds core-shell nanoparticles or crosslinked materials were obtained. Atom transfer radical polymerization proved that it is a valuable tool for the controlled formation of inorganic-organic hybrid materials.

Introduction

Inorganic-organic nanocomposites have currently attracted much scientific interest due to the combination of two moieties in one material and their resulting properties.(1, 2) The properties of the resulting nanocomposites are often distinguished by physical size effects and the large surface to volume ratio of the inorganic building blocks. In many cases free radical polymerizations were used for the preparation of these materials, such as cluster-reinforced polymers or nanoparticle embedded systems.(3, 4) The major advantage of radical polymerization compared to other techniques is its robustness against various reaction conditions (temperature, purity, solvents). One of the drawbacks is the lack of structural control of the synthesized polymers. The development of controlled living polymerization techniques, which allow a good control over composition and morphology of organic polymers, opened new ways for a tailored preparation of inorganic-organic nanocomposites.(5) In particular the functionalization of inorganic surfaces by well-defined organic polymers applying *grafting from* or *grafting to* techniques established as a important domain of ATRP.(6-8)

Various inorganic building blocks can be used for the incorporation into polymers (Fig. 1). Different types of materials are produced depending on the function (polymerizable or initiating groups) and the number of functionalities (linear, crosslinked or star shaped polymers) attached to the inorganic compounds. Probably the most prominent representative of these building blocks are polyhedral oligomeric silsesquioxanes (POSS) or spherosilicates which both have a rigid inorganic silicon-based cube as the major structural element in common, which can be functionalized by organic groups forming for example macroinitiators or monomers for ATRP.(9-12) Depending on their number of polymerizable groups the inorganic building blocks resulted in crosslinked polymers or polymer chains containing pending inorganic molecules. If these systems were used as initiators either end-functionalized or star polymers were obtained. The organic functionalization of the inorganic components occurred either in situ during the preparation of the building blocks, for example in the case of POSS-based compounds, or via a post-functionalization. In most cases the chemical connection between organic group and the inorganic segment was formed using silane coupling agents of the general formula $R_{4-n}SiX_n$ ($n = 1-3$, $X = Cl$ or OR) yielding to strong covalent bonds that connect the functional organic group to the inorganic core. Similar interactions can also be applied for silica or silsesquioxane nanoparticles.(13-15) Contrary, in the case of metal oxides often other interaction mechanisms have to be used, for example coordinative interactions, due to the lack of reactivity of surface $M-OH$ groups, which are necessary for a covalent attachment of silane coupling agents. In previous studies we showed that carboxylate surface-functionalization of metal oxo clusters can

be used to attach initiator or polymerizable groups to the surface of these inorganic species.(16-18) In all mentioned studies it was not intended that the inorganic part of the molecule undergoes further reactions but forms a rigid and stable building block. A possible incorporation of reactive inorganic groups would, however, open the way for the preparation of a second crosslinked network, for example applying the sol-gel process. Compounds containing both an organic group that allows ATRP polymerization and an inorganic group for the formation of a metal oxide network are particularly interesting because two totally different polymerization methods can be applied under dissimilar conditions providing an additional parameter to control the structure of the resulting nanocomposites. In the present study we show how β -diketones and acetoacetoxy-derivatives containing polymerizable or initiator groups can be used to coordinatively bind early transition metal alkoxides that can be used as precursors for sol-gel reactions and thus the formation of metal oxide/polymer nanocomposites.

Results and Discussions

β -Diketones (Scheme 1) are well-known for their coordination chemistry of transition metals. These ligands are also often used to limit reactivity of metal alkoxides in the sol-gel process by blocking free coordination sites. In addition, usually the coordination of these ligands survives the conditions of the sol-gel process and thus they allow an organic modification of metal oxides prepared by this method. Preparation of bidentate ligand coordinated metal alkoxides can occur, for example, by simple ligand exchange reactions.(19, 20) If a stable linkage between the sol-gel precursor and the organic polymer should be formed either polymerizable or initiating groups have to be attached to the diketones. For such functionalization reactions the central position between the two carbonyl groups is preferred because it can be easily deprotonated and reacted with nucleophiles. Applying this approach we introduced various organic groups that can act as initiators.(19) A selection of prepared ligands is shown in Scheme 2. The modification of acetylacetonone with polymerizable groups at the same position was much more difficult due to polymerization induced during the reaction with polymerizable group containing synthons. Only small yields of the desired products were obtained and therefore we applied the acetylacetoxy-based systems as described below for a functionalization with polymerizable groups.

Coordination via alkoxide exchange was proven for $\text{Ti}(\text{O}^i\text{Pr})_4$, $\text{Zr}(\text{O}^n\text{Bu})_4$, $\text{Ta}(\text{OEt})_5$, $\text{Y}(\text{OPr})_3$, and $\text{VO}(\text{OEt})_3$. The resulting bidentate ligand functionalized precursors were used in a microemulsion-based sol-gel approach for the preparation of surface-functionalized nanoparticles. FT-IR analysis of the particles revealed a surface-functionalization with the organic groups. The materials were used as multifunctional initiators in ATRP reactions for the

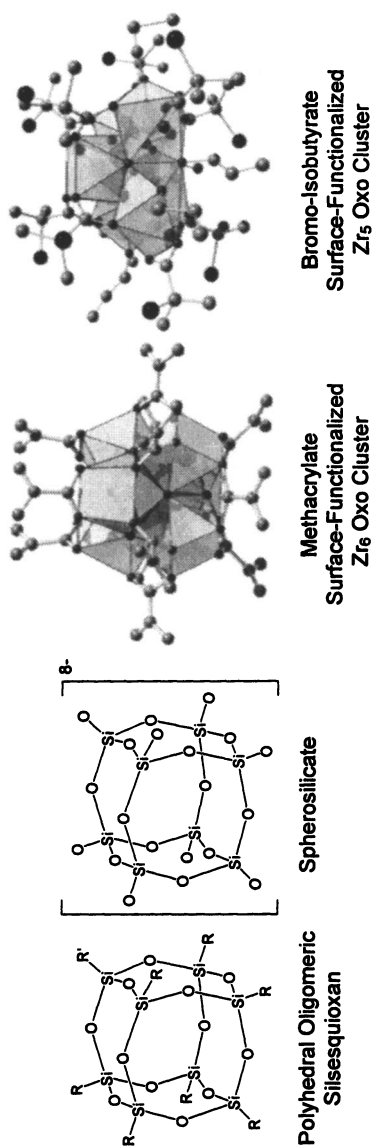
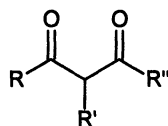


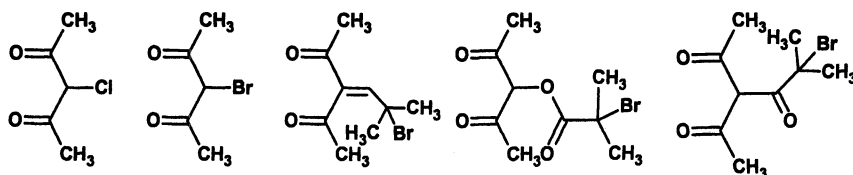
Figure 1. Well-defined molecular inorganic building blocks for the preparation of nanocomposites.

Scheme 1

 β -Diketones

R''= OR: Acetoacetoxy-Derivatives

Scheme 2



grafting of polystyrene and poly(methyl methacrylate) from the amorphous metal oxide core (19). The diameter of the polymer shell was easily controlled by the kinetics of ATRP. The polymers were cleaved from the surface of the particles and it was shown that a good control over molecular weight and molecular weight distribution can be achieved.

An alternative type of ligand that can be used to connect metal alkoxides to (meth)acrylates are acetoacetoxy derivatives (Scheme 1). In these compounds the functional group is introduced via the ester functionality. A prominent type of these compounds is 2-(methacryloyloxy)ethyl acetoacetate (HAAEMA). These ligands can be used for the preparation of metal containing polymers or to crosslink an organic polymer via a metal or metal oxide species.(21-23) We studied this type of β -keto ester and its modification with various Ti alkoxides ($\text{Ti}(\text{O}^i\text{Pr})_4$ and $\text{Ti}(\text{OEt})_4$). HAAEMA was coordinated to the metal alkoxide via the above mentioned alkoxide exchange reaction. The resulting product is a mixture of monosubstituted dimers in equilibrium with disubstituted monomers. This was proven via NMR and single crystal X-ray structure analysis. A separation of the two different complexes is not possible due to fast exchange reactions. We investigated this mixture in homo- and copolymerizations with MMA. Polymerizations were performed under commonly applied ATRP reaction conditions using $\text{CuBr}/\text{PMDETA}$ as catalyst, 2-ethylbromoisobutyrate as initiator in solvents such as dichlorobenzene or toluene or in bulk. The temperature of the reactions was 85°C and the reaction time was varied between 4 and 8 hours. The metal containing polymers were not soluble in common solvents, most likely because crosslinking through the metal alkoxides occurred (Scheme 3). Due to fast gelation during polymerization even in presence of a

solvent we decided to copolymerize the preformed substituted Ti complexes with MMA in 1:1, 1:5 and 1:10 ratios. As model systems we prepared non-metal containing copolymers of HAAEMA and MMA in the same ratios for reasons of comparison. In Figure 2 SEC-plots of the unmodified poly(HAAEMAcO₂MMA) in the various ratios are presented. A monomodal molecular weight distribution was observed and it could be shown that both of the monomers were successfully incorporated in the backbone by NMR. However, the molecular weight distribution increased with increasing content of MMA (Table 1). One potential reason for this observation is the different reactivity of the two monomers.

Polymerization of metal-containing monomers resulted in metal-alkoxide crosslinked polymers. This can be based on two facts, on the one hand already disubstituted monomers were used on the other hand ligand exchange reactions can increase the crosslinking density. Therefore the final polymers could not be analyzed by SEC. Instead ¹³C MAS NMR and FT-IR were used to investigate the resulting polymers. A representative FT-IR spectrum of poly[Ti(OⁱPr)₃AAEMAcO₂MMA] is shown in Figure 3. The band at 1724 cm⁻¹ corresponds to the C=O stretching of the ester groups of the methacrylate moieties. The intensity is high corresponding to a higher content of MMA in the copolymer chains. The most important observation is that the linkage between the β-keto ester group and the Ti atom is maintained after the polymerization. This is proven by the presence of the specific bands of the chelating ligand at 1619.81 cm⁻¹ (C=C) and 1529.38 cm⁻¹ (C-O). The C-O bands of the alkoxide moieties are present at 1145.8 cm⁻¹ while the CH₂ groups give a signal at 750.35 cm⁻¹.

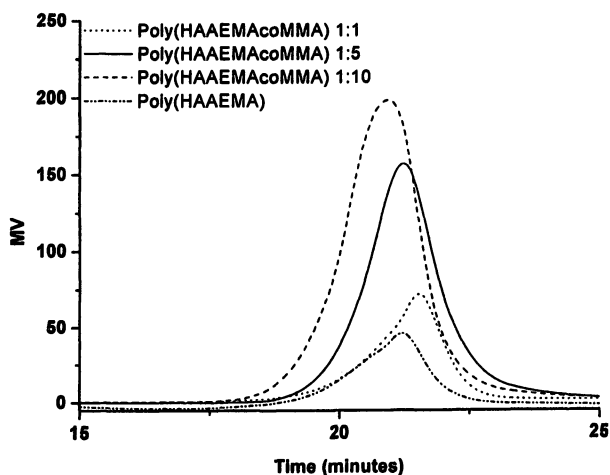


Figure 2. SEC-plot of poly(HAAEMAcO₂MMA) copolymers in 1:1, 1:5 and 1:10 monomer ratios.

Scheme 3

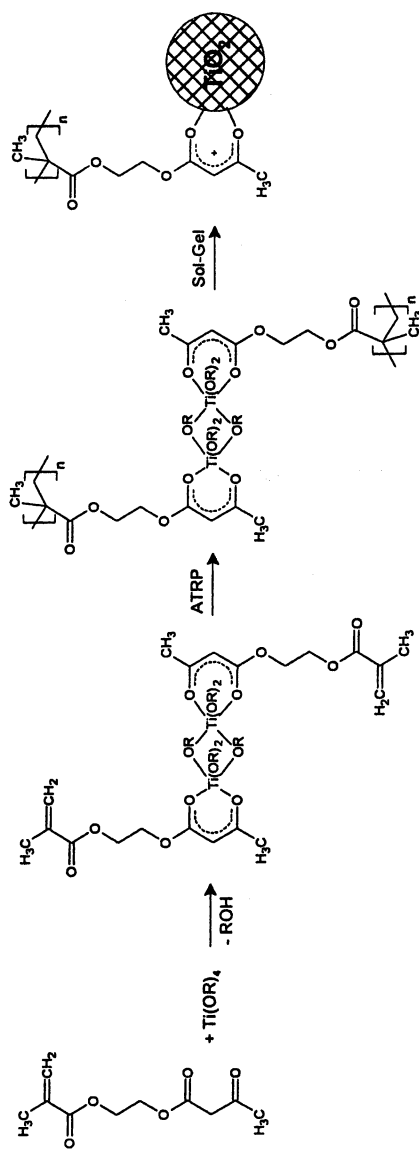


Table 1. SEC data for ATRP [CuBr/PMDETA, 2-ethylbromoisobutyrate initiator, in toluene at 85°C]

| <i>Polymer</i> | <i>Ratio between monomers</i> | <i>M_n</i> | <i>PDI</i> | <i>DP_{theor}</i> | <i>DP_{obs SEC}</i> |
|---------------------------------|---------------------------------------|----------------------|------------|---------------------------|-----------------------------|
| Poly(HAAEMA) | - | 37040 | 1.23 | 200 | 175 |
| Poly(HAAEMAcO ₂ MMA) | 1:1 | 28120 | 1.39 | 100 | 90 |
| Poly(HAAEMAcO ₂ MMA) | 1:5 | 27920 | 1.82 | 200 | 195 |
| Poly(HAAEMAcO ₂ MMA) | 1:10 | 43250 | 1.89 | 400 | 360 |

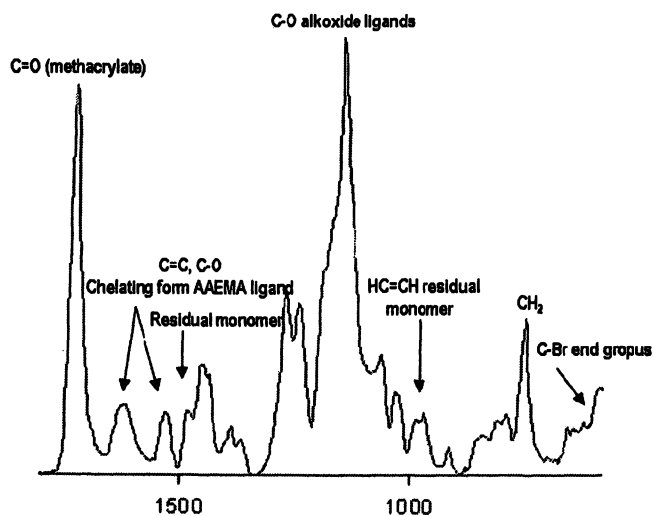


Figure 3. FT-IR spectrum of poly[Ti(OⁱPr)₃AAEMAcO₂MMA] (1:5 ratio metal complex/MMA)

^{13}C MAS NMR analysis revealed that in the cases of the metal-containing monomers the polymerization is not complete even after very long reaction times. This observation is supported by the detection of the bands corresponding to residual unreacted monomers at 1498 cm^{-1} and at 968 cm^{-1} ($\text{HC}=\text{CH}$) in the FT-IR spectrum. Most likely residual monomer is still present because ligand exchange reactions lead to a decreased mobility of the polymerizable groups that hinder further chain growth. This was not observed in polymerizations of pure HAAEMA homo- and copolymers where a complete conversion of the double bonds was obtained. With regard to the formation of inorganic-organic nanocomposites the most important feature is that the linkage between the inorganic part and the organic polymer is still maintained after polymerization. The resulting hybrid polymers allowed for the preparation of such materials via hydrolysis and condensation of the metal alkoxides in sol-gel reactions.

Conclusions

Metal alkoxides that can be used as precursors in the sol-gel process can easily be modified with functional bidentate ligands such as β -diketones or acetylacetoxy-derivatives. Depending on the functionalization the resulting metal complexes are precursors that contain either initiating or polymerizable groups for ATRP. β -Diketone derivatives were successfully used in the preparation of surface-functionalized amorphous metal oxide nanoparticles which were used as multifunctional initiators for ATRP. These systems allowed a grafting from functionalization from the surface and a good control over the polymer layer diameter.

2-(Methacryloyloxy)ethyl acetoacetate was homopolymerized and copolymerized with MMA by ATRP. This monomer was also used to attach methacrylate groups to titanium alkoxides by alkoxide exchange reactions resulting in a mixture of mono and disubstituted titanium alkoxide complexes. These systems were successfully applied in ATRP reactions leading to crosslinked nanocomposites in which the titanium atoms were coordinatively connected to the organic polymer.

Acknowledgments

We gratefully acknowledge the financial support by the Fonds zur Förderung der wissenschaftlichen Forschung Austria.

References

1. Kickelbick, G. *Progr. Polym. Sci.* **2002**, *28*, 83-114.
2. Sanchez, C.; Julian, B.; Belleville, P.; Popall, M. *J. Mater. Chem.* **2005**, *15*, 3559-3592.
3. Caseri, W., Nanocomposites of polymers and inorganic particles. In *Encyclopedia of Nanoscience and Nanotechnology*, Nalwa, H.S., Ed. American Scientific Publishers: Stevenson Ranch, CA, USA, 2004; Vol. 6, pp 235-247.
4. Schubert, U. *Chem. Mater.* **2001**, *13*, 3487-3494.
5. Pyun, J.; Matyjaszewski, K. *Chem. Mater.* **2001**, *13*, 3436-3448.
6. Kruk, M.; Dufour, B.; Celer, E.B.; Kowalewski, T.; Jaroniec, M.; Matyjaszewski, K. *J. Phys. Chem. B* **2005**, *109*, 9216-9225.
7. Matyjaszewski, K.; Miller, P.J.; Shukla, N.; Immaraporn, B.; Gelman, A.; Luokala, B.B.; Siclován, T.M.; Kickelbick, G.; Vallant, T.; Hoffmann, H.; Pakula, T. *Macromolecules* **1999**, *32*, 8716-8724.
8. Saleh, N.; Phenrat, T.; Sirk, K.; Dufour, B.; Ok, J.; Sarbu, T.; Matyjaszewski, K.; Tilton, R.D.; Lowry, G.V. *Nano Lett.* **2005**, *5*, 2489-2494.
9. Costa, R.O.R.; Vasconcelos, W.L.; Tamaki, R.; Laine, R.M. *Macromolecules* **2001**, *34*, 5398-5407.
10. Holzinger, D.; Kickelbick, G. *J. Polym. Sci., Part A: Polym. Chem.* **2002**, *40*, 3858-3872.
11. Ohno, K.; Sugiyama, S.; Koh, K.; Tsujii, Y.; Fukuda, T.; Yamahiro, M.; Oikawa, H.; Yamamoto, Y.; Ootake, N.; Watanabe, K. *Macromolecules* **2004**, *37*, 8517-8522.
12. Pyun, J.; Xia, J.; Matyjaszewski, K. *ACS Symp. Ser.* **2003**, *838*(*Synthesis and Properties of Silicones and Silicone-Modified Materials*), 273-284.
13. Liu, P.; Tian, J.; Liu, W.; Xue, Q. *Polym. Int.* **2004**, *53*, 127-130.
14. Pyun, J.; Matyjaszewski, K.; Kowalewski, T.; Savin, D.; Patterson, G.; Kickelbick, G.; Hüsing, N. *J. Am. Chem. Soc.* **2001**, *123*, 9445-9446.
15. Savin, D.A.; Pyun, J.; Patterson, G.D.; Kowalewski, T.; Matyjaszewski, K. *J. Polym. Sci., Part B: Polym. Phys.* **2002**, *40*, 2667-2676.
16. Kickelbick, G.; Holzinger, D.; Brick, C.; Trimmel, G.; Moons, E. *Chem. Mater.* **2002**, *14*, 4382-4389.
17. Kickelbick, G.; Schubert, U. *Chem. Ber.* **1997**, *130*, 473-477.
18. Kickelbick, G.; Schubert, U. *Monatsh. Chem.* **2001**, *132*, 13-30.
19. Holzinger, D.; Kickelbick, G. *Chem. Mater.* **2003**, *15*, 4944-4948.
20. Zhang, J.; Luo, S.; Gui, L. *J. Mater. Sci.* **1997**, *32*, 1469-1472.
21. Gbureck, U.; Probst, J.; Thull, R. *J. Sol-Gel Sci. Techn.* **2003**, *27*, 157-162.
22. Grosse-Sommer, A.; In, M.; Prud'homme, R.K. *J. Polym. Sci., Part A: Polym. Chem.* **1996**, *34*, 1447-1453.
23. Miele-Pajot, N.; Hubert-Pfalzgraf, L.G.; Papiernik, R.; Vaissermann, J.; Collier, R. *J. Mater. Chem.* **1999**, *9*, 3027-3033.

Chapter 20

Surface Modification of Inorganic Nanotubes by Atom Transfer Radical Polymerization

Yuan Gao and Deyue Yan

College of Chemistry and Chemical Engineering, Shanghai Jiao Tong
University, Shanghai, Peoples Republic of China

In situ ATRP “grafting from” approach was successfully applied to the surfaces of multi-walled carbon nanotubes (MWNT) and titanate nanotubes (TNT). Novel hybrid core-shell nanomaterials with nanotubes as the core and polymer as the shell were fabricated. The resulting nanotubes-based polymer brushes were characterized and confirmed with FTIR, ^1H NMR, TEM and TGA.

Introduction

In the recent decade, nanotubes have been a symbol of the new and fast developing research area of nanotechnology. The first report on carbon nanotubes in 1991 by S.Iijima (1) and inorganic (WS_2) nanotube by R.Tenne in 1992 (2), have been followed by abundant experimental and theoretical researches on hollow cylindrical structures such as 1992- WS_2 (2); 1993- MoS_2 (3); 1995-BN (4), SiO_2 (5); 1998- TiO_2 (6), VO_x (7), NiCl_2 (8); 2000- NbSe_2 (9), Au (10), Co and Fe (11); 2001- CdS (12), CdSe (13), ZnS (14), NiS (15), $\text{Cu}_{5.5}\text{FeS}_{6.5}$ (16), Al_2O_3 (17), In_2O_3 and Ga_2O_3 (18), GaN (19); 2002- ZrS_2 and HfS_2 (20), NbS_2 and TaS_2 (21), (Er, Tm, Yb, Lu) oxide (22), ZnO (23), BaTiO_3 and PbTiO_3 (24), Cu and Ni (25), Te (26), ReS_2 (27), silicon nanotubes (28), etc. Owing to their great diversity, carbon and non-carbon inorganic nanotubes can exhibit a wide range of different properties. Thus they can be useful in many potential applications, for example, new materials for the development of novel

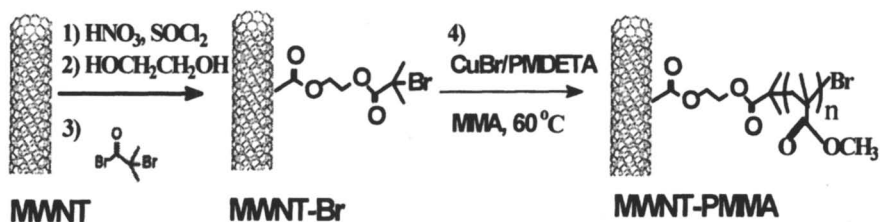
single-molecular transistors, scanning probe microscope tips, molecular computing elements, electron-field-emitting flat-panel displays, gas and electrochemical storage, molecular-filtration membranes, artificial muscles, and sensors, etc.

Because of van der Waals interaction between nanotubes, nanotubes are held together as bundles and ropes, leading to very low solubility in water and most organic solvents (29). The insolubility of nanotubes in most solvents limits their wide applications such as the preparation of blends with conventional polymers, molecular electronics, and the production of homogeneously dispersed conducting layers in electroluminescent devices. Noncovalent or covalent surface functionalization can improve their solubility. The advantage of noncovalent attachment is that the nanotube structure and its electronic properties are not altered. But the surfactants and polymers that can be used for this method are limited. Covalent surface functionalization can be realized by either surface initiated polymerization or direct addition of polymers to the surface of nanotubes. High functionalization density is necessary for high solubility because the attached organic molecules are very small compared with the tube length. Though direct addition approaches lead to soluble materials, it is difficult to control the functionalization density.

Here, we describe a “grafting from” approach to the “growth” of polymers from the surface of nanotubes by first covalently attaching initiators and then polymerize a wide range of monomers based nanotube macroinitiators. Atom transfer radical polymerization (ATRP) is the method used most to graft polymer chains of controlled molecular weight from colloidal particles, flat or concave surfaces such as silicon wafers, gold particles, and polymer backbones (30-34). In this contribution, we summarize our works concerning functionalized multi-walled carbon nanotubes (MWNTs) via ATRP. Moreover, we present a new inorganic/organic hybrid – surface functionalized titanate nanotubes (TNTs).

Functionalized MWNTs via ATRP

Carbon nanotubes are the most promising candidate in designing novel ultrahigh strength polymer composites (35, 36). Up to now, various compounds and strategies have been used to functionalize MWNTs in order to improve the solubility and processing properties of these promising tubular nanomaterials (37, 38). However, functionalized MWNTs with well-controlled thickness are difficult to fabricate. In situ surface initiating ATRP can provide us with a remarkable route to tailor the structure and properties of the modified MWNTs and to construct novel MWNTs-based hybrid nanomaterials. Preliminary work on PMMA-grafted MWNTs in our lab has been reported in other communication (39). The general strategy of grafting from the MWNTs via ATRP is described in Scheme 1.



Scheme 1

The thickness of the polymer layer in the functionalized MWNTs can be controlled by the feed ratio of MMA to MWNT-Br (R_{wt}) (Table 1). The MWNT-PMMA shows a relatively good solubility in weakly polar solvents such as THF and CHCl_3 , and a poor solubility in strong polar solvents such as DMF and DMSO as shown in Figure 1. The different solubility gives direct evidence for the conclusion that the PMMA is covalently grafted onto the MWNT-PMMA samples.

Table 1. The Reaction Conditions and Some Results

| | R_{wt}^a | r^b | temp/ $^\circ\text{C}$ | time/h | $f_{wt}/\% ^c$ | d/nm^d |
|-----|------------|--------|------------------------|--------|----------------|-----------------|
| CP1 | 1:1 | 5:1:1 | 60 | 20.0 | 31.9 | 3.8 |
| CP2 | 2:1 | 10:1:1 | 60 | 20.0 | 50.0 | 5.3 |
| CP3 | 5:1 | 25:1:1 | 60 | 25.0 | 70.0 | 8.0 |
| CP4 | 10:1 | 50:1:1 | 60 | 30.0 | 82.0 | 14.0 |

^a R_{wt} = monomer: MWNT-Br (wt:wt)

^b r = monomer: CuBr: N,N,N',N'',N'''-pentmethyl-diethylenetriamine (PMDTA) (mol:mol:mol)

^c f_{wt} : the loss weight fraction of polymer calculated from TGA

^d d : the average thickness of grafted polymer layers measured from TEM images

The structure of the resultant SWNT-PMMA was detected with TEM. Figure 2 shows the images of a part of crude MWNT which diameters are not completely identical with one another. The polymer layers of modified MWNT with various thicknesses displayed in Figure 3A-D are somewhat shallower and more transparent color. The average thickness of the wrapped polymer layers are about 3.8, 5.3, 8, and 14 nm, respectively. It is found that the thickness of the polymer layer increases with an increase in the feed ratio R_{wt} . Therefore, the thickness of polymer layer can be controlled by the in situ ATRP.

The chemical structure of MWNT-PMMA was characterized by ^1H NMR as displayed in Figure 4. The inherent shifts (3.59 ppm ($-\text{OCOCH}_3$), 1.78 ppm ($\text{C}-\text{CH}_2-\text{C}$) and 0.75-0.92 ($-\text{CH}_3$)) are attributed to PMMA. This result demonstrates the presence of grafted PMMA.

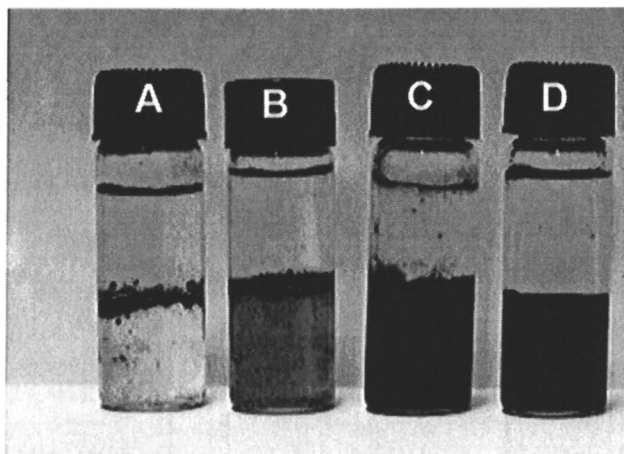


Figure 1. A photo of the samples placed in solvents (the upper solvent of A, B, C, D is water, and the lower solvent is CHCl_3). A: MWNT-COOH, B: MWNT-OH, C: MWNT-Br, D: CP3 in CHCl_3 . The content of the sample is around 1.25 mg of sample per 1 mL of solvent.

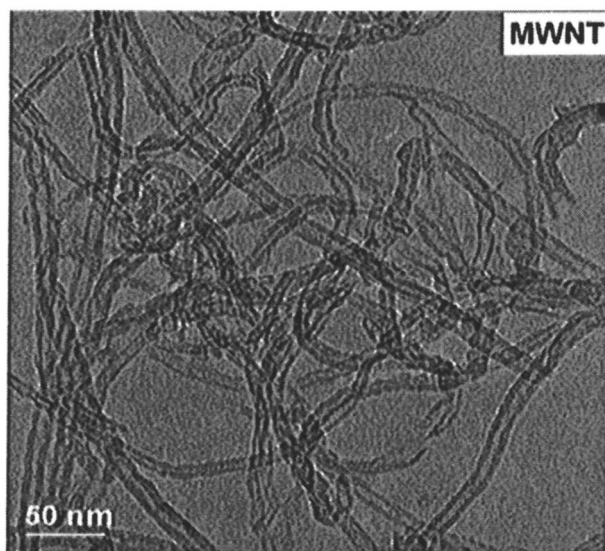


Figure 2. TEM images of crude MWNT.

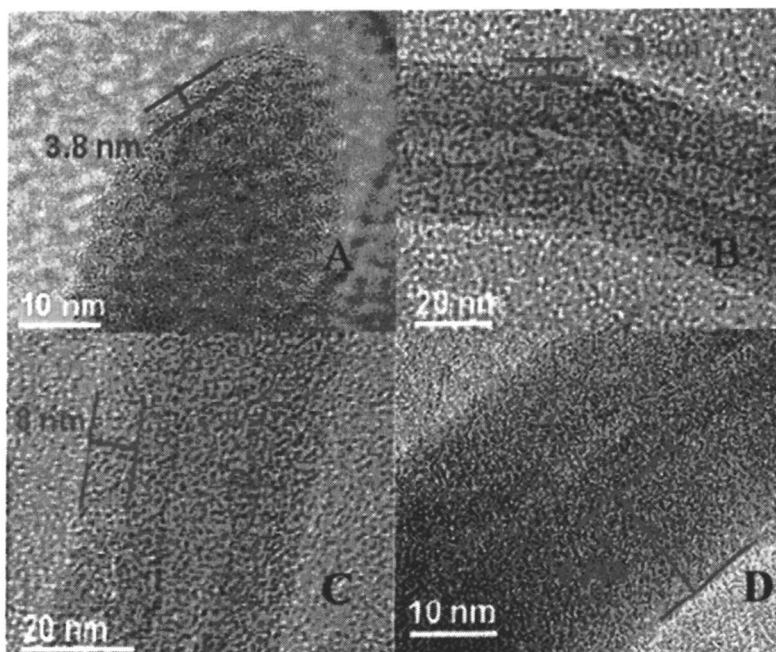


Figure 3. TEM images of CP1 (A), CP2 (B), CP3 (C) and CP4 (D).

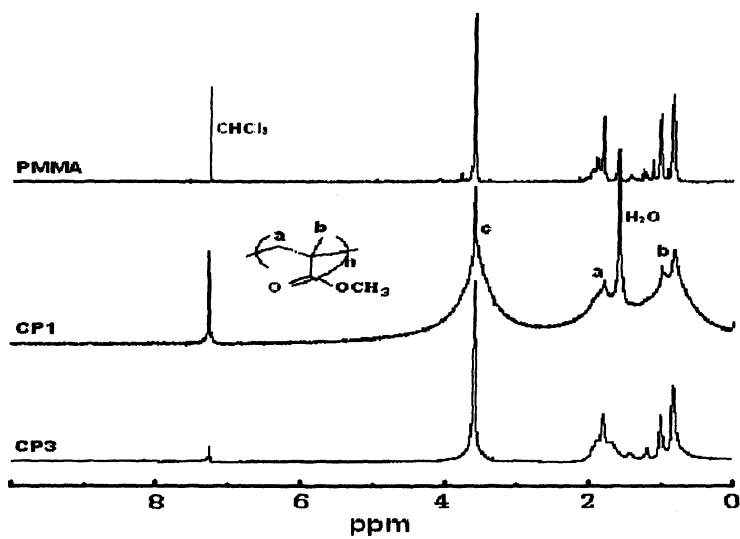


Figure 4. ^1H NMR of PMMA (CDCl_3), CP1 (CDCl_3) and CP3 (CDCl_3).

Furthermore, the result from TGA well accords with that the outcome of TEM. As shown in Figure 5, the sample of the crude MWNT is steady without significant weight loss below 600 °C. The rapid weight decrease in the region (200-380°C) may readily be attributed to the decomposition of PMMA polymers grafted on MWNTs. The weight loss fraction of the polymer layers for the MWNT-PMMA ranges from 31.9% to 82.0% and increases with increasing Rwt, indicating that the amount of the polymer in the functionalized MWNT can be controlled.

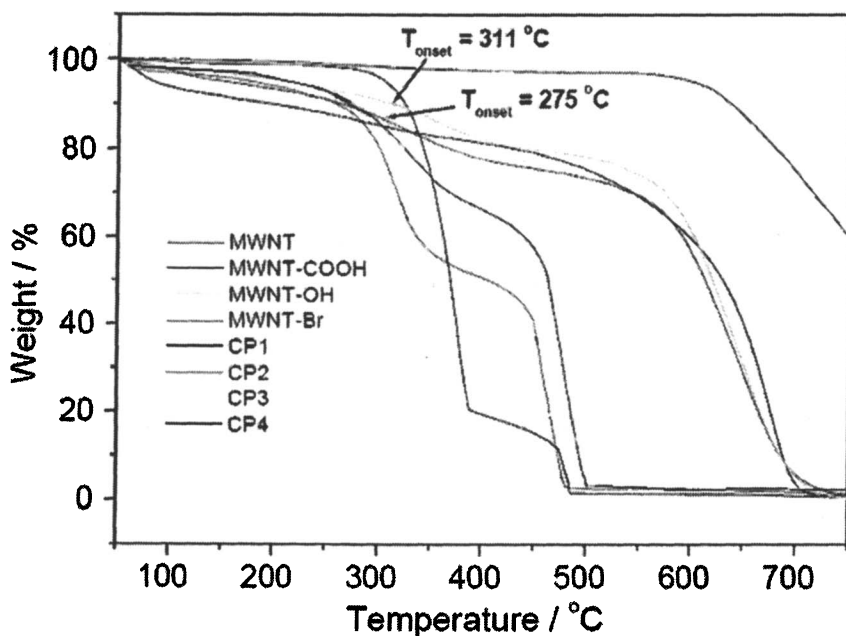


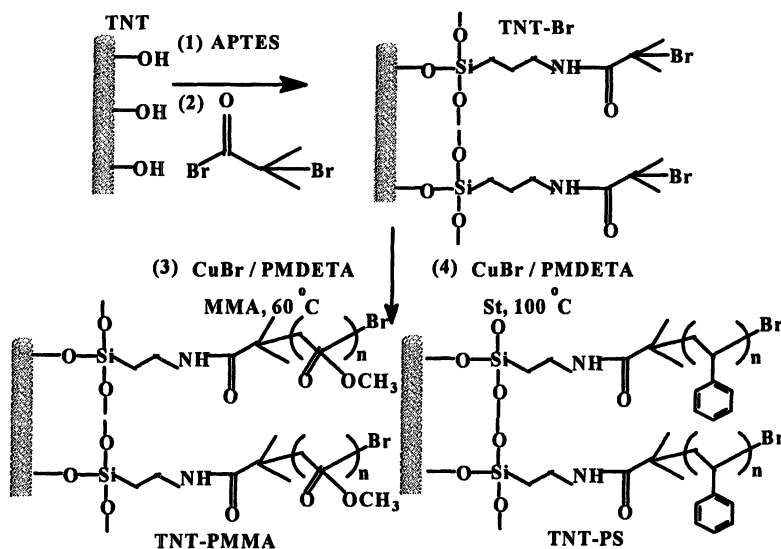
Figure 5. TGA curves of the crude MWNT and functionalized MWNT.

Through all the aforementioned experiments demonstrate that PMMA-grafted MWNTs have been successfully fabricated by ATRP, we still puzzle whether or not this strategy for growth of polymer layers on MWNTs can be extended to other ATRP-active monomers. Thus we further go deep into fabrications of various polymer grafted MWNTs such as styrene (40), temperature-sensitive (41), amphiphilic polymer brushes (42), polyelectrolyte-functionalized MWNTs (43) and multihydroxyl hyperbranched polymers modified MWNTs etc.

Functionalized TNTs via ATRP

Titanates are well known as dielectric, piezoelectric, ferroelectric, and low absorption of infrared radiation functional ceramic materials (44-47). Recently, it has been proposed that one-dimensional nanostructural forms of titanates (nanotube, nanofiber, nanorod) have great potential for advanced applications as catalyst supports, semiconductors, materials for solar-energy conversion, gas sensors, electrochemical capacitors, and lithium-ion-battery materials (48,49). For example, long titanate fibers one-dimensional nanoscale composite exhibited desirable photocatalytic properties for potential applications in the elimination of organic pollutants and can be separated readily from the liquid after use (50). On the other hand, their high surface area and tubular morphology have initiated heterogeneous catalytic studies in which the titanate nanotubes served as carrier of Au (51) and Pt (52) nanoparticles. Covalent surface modification of titanate nanomaterials is of great interest in view of its importance in medical implants, catalysis and photocatalysis, polymer fillers, and so on. Herein, we investigate ATRP "grafting from" approach to functionalize titanate nanotubes (TNTs). To the best of our knowledge, this is the first report of grafting polymers from titanate nanotubes. The work presented here may break a new path for exploring and preparing novel nanotubes-based nanomaterials and molecular devices with special structures and properties.

The general strategy for grafting polymers from TNT via ATRP is described in Scheme 2. Here we focus PMMA and PS grafted TNTs.



Scheme 2

According to the formation of titanate nanotubes, a lot of the Ti-OH or Ti-O bands exist on the surface of the nanotubes. When appropriate silanes are added into the nanotube toluene solvent, silanes can hydrolyze and then are absorbed onto the surface because of the trace water existing on the surfaces of nanotubes via physical adsorption. Thus the surfaces of nanotubes are covered with the hydrophobic group. The initiator-functionalized TNTs well disperse into organic solvents such as DMF and CHCl_3 , but it flocculates like white fiber bundles suspended in solvent in less than one week. After the silanization, the characteristic Si-O-Si and Si-O-C asymmetric stretching vibration absorption bands can be respectively observed at 1150 and 1051 cm^{-1} in FTIR (Figure 6). The initiator linkage from the TNTs was confirmed from the new amide bands at 1531, 1641, 1210 cm^{-1} .

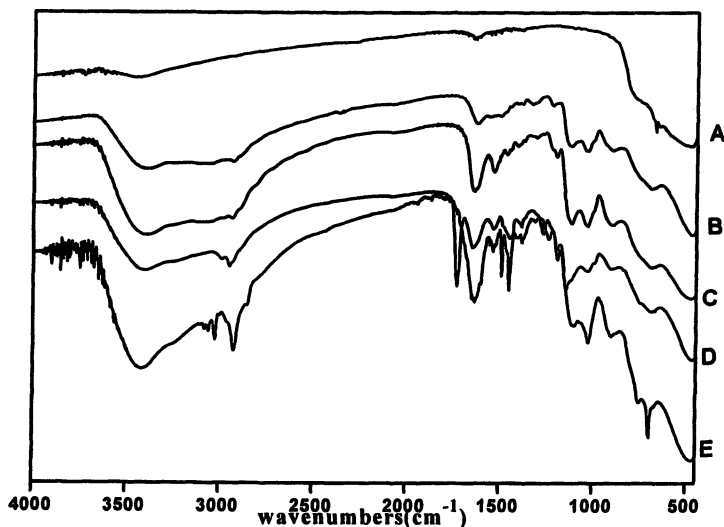


Figure 6. FTIR spectra of TNT (A), TNT-NH₂ (B), TNT-Br (C) and TNT-PMMA (D).

Moreover, XPS was used to confirm the initiator monolayer. The initiator characteristic peaks of Br 3d were found around 104.3eV. Binding energy of Ti2p_{3/2} shifts from 458.24 to 457.9eV (Figure 7). These changes may ascribe to a decrease in the positive charge on Ti atoms in the initial state because of the formation of mixed Ti-O-Si bonds at the interface. For these reasons we conclude that the initiators were covalently grafted to the TNT. Thermal gravimetric analysis (TGA) (Figure 8) gives about 2.25 initiator functions/1000 titanium atoms.

We noted that the surface modified nanotube can exist in the toluene solvent with no precipitation for several weeks. This phenomenon can further

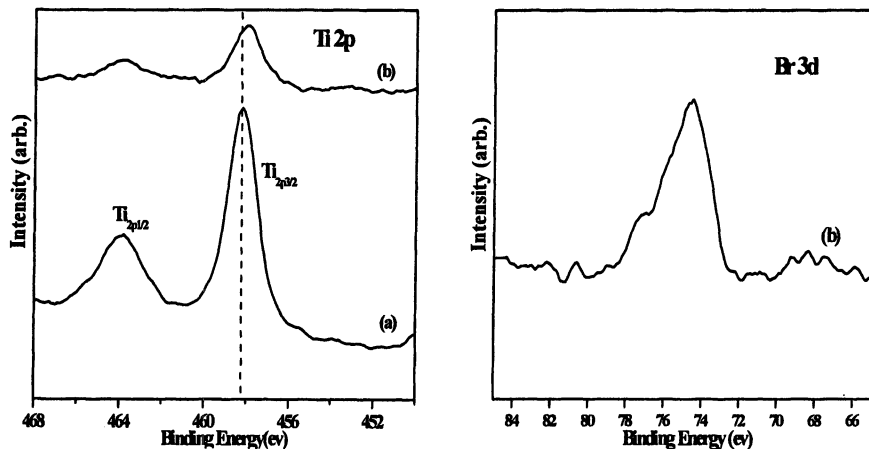


Figure 7. X-ray photoelectron spectra of the Ti 2p and Br 3d of the TNT (a), and TNT-Br (b).

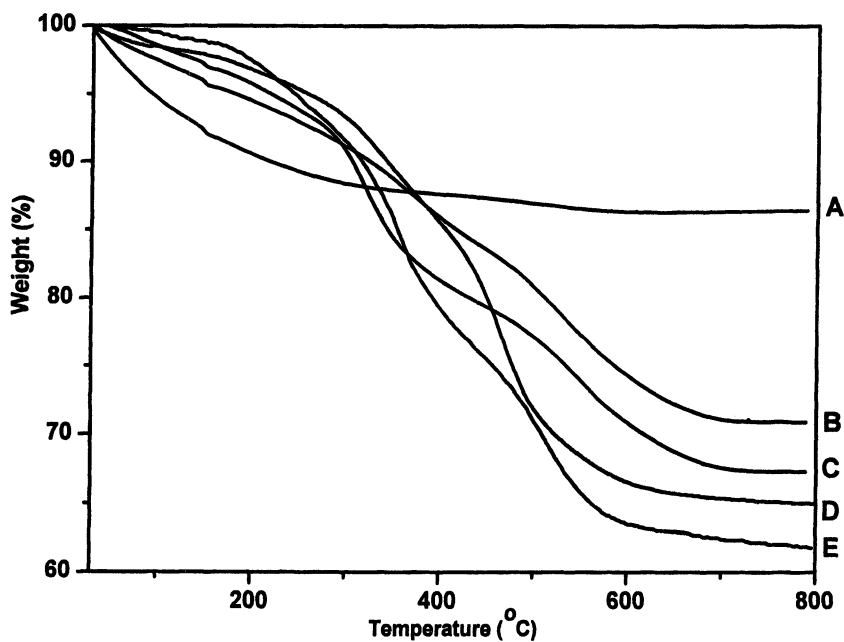


Figure 8. TGA curves of the crude TNT (A), TNT- NH_2 (B), TNT-Br (C), TNT-PMMA (D), TNT-PS (E).

confirm that the nanotubes are indeed surface-modified by polymer, because the surfaces of original nanotubes are hydrophilic and they are completely insoluble in toluene even after sonication.

The chemical structures of TNT-PMMA and TNT-PS were characterized by FTIR as displayed in Figure 6. The FTIR spectrum of polymer functionalized TNTs showed characteristic vibration bands for PMMA (in KBr: νCH_3 at 2922, $\nu\text{C}=\text{O}$ at 1725, $\nu\text{C-H}$ at 1440 cm^{-1} ; Figure 6D) and PS (in KBr: aromatic ν C-Hs at 3025, C-H ν at 2922, 1662, 1028, and 694 cm^{-1} ; Figure 6E).

Furthermore, ^1H NMR spectra (Figure 9) of polymer functionalized TNTs in CDCl_3 exhibit the signals of PMMA (δ (-OCOCH₃) at 3.59 ppm, δ (C-CH₂-C) at 1.78 ppm and δ (-CH₃) at 0.75-0.92) and PS (δ aromatic at 7.40-6.30, δ (-CH₂, -CH) at 1.74-1.25 ppm). However, considerable line broadening was observed as a result of the present of paramagnetic substances in the TNTs.

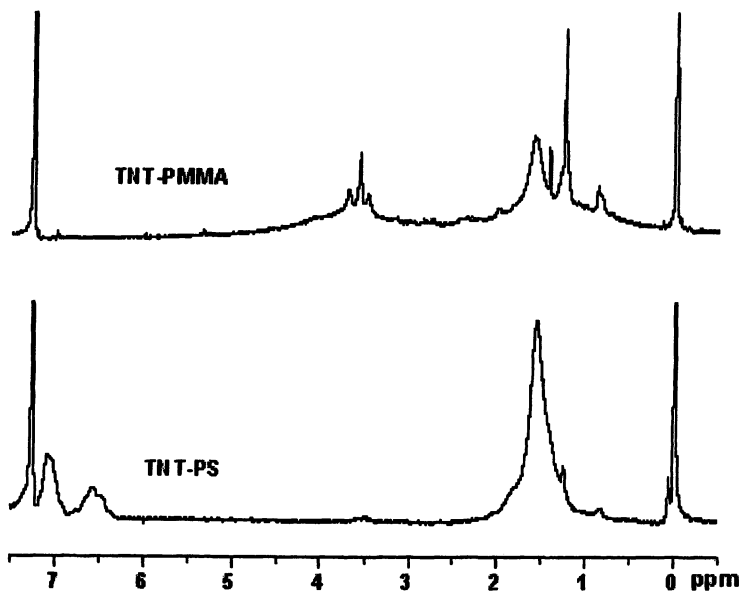


Figure 9. ^1H NMR of TNT-PMMA (CDCl_3) and TNT-PS (CDCl_3).

The amount of PMMA and PS covalently attached to TNTs determined by TGA is about 30% as shown in Figure 8. TGA analysis shows that the major decompositions happened in the temperature range of 225-400°C corresponding to grafted PMMA and PS, while no weigh loss occurred at temperature above 500°C, which indicates titanate completely transferred into titanium dioxide. TEM was used to investigate the size and distribution of the TNTs before and after chemical modification. Figure 10A and B show a few nanotubes with a

tubular structure and an outer diameter of about 10 nm. It is notable that the inner and outer diameters along their length are almost uniform, essentially straight edged, and open-ended in our observation. Figure 10C and D displays the images of modified TNTs with polymer layers which exhibit somewhat shallower and more transparent color. The average thickness of the wrapped polymer layers are about 3 and 3.5 nm (measured from 8 to 10 tubes).

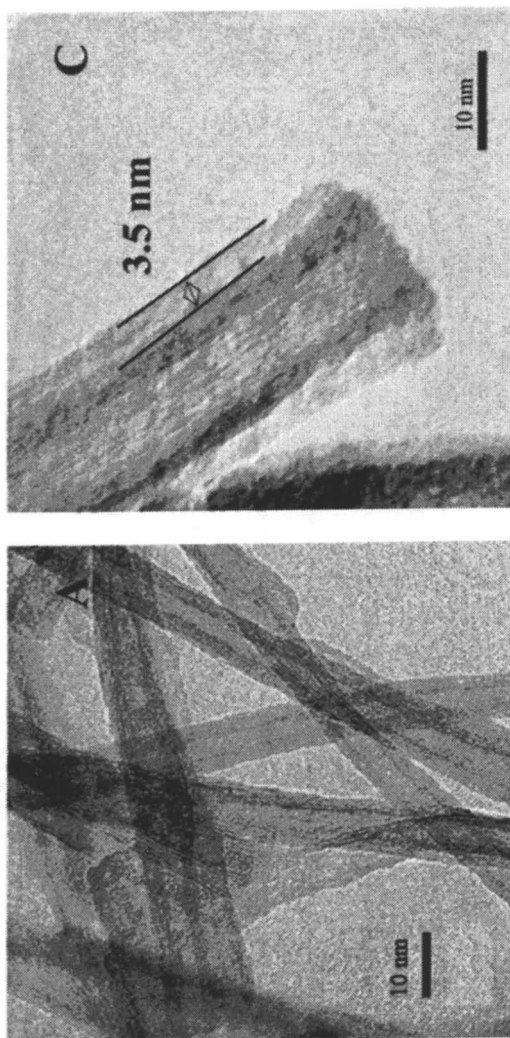
In conclusion, the "grafting from" approach has been successfully employed to grow PMMA and PS from functionalized titanate nanotubes by ATRP. Dense polymer brushes were formed around titanate nanotubes cores as demonstrated by TEM. The controllable radical polymerization with other monomers, kinetics of the polymerization and the solution properties of polymer grafted titanate nanotubes are under investigation.

Experimental

Materials: Methyl methacrylate (MMA) and hydroxyethyl methacrylate (HEMA) were purchased from Aldrich; the inhibitor was removed by passing a column of alumina and distilling in vacuum. CuBr was obtained from Aldrich and purified according to the published procedures (53). 2-bromo-2-methylpropionyl bromide (α -bromoisobutyryl bromide), ethyl 2-bromoisobutyrate, N, N, N', N'', N'''-pentmethyldiethylenetriamine (PMDETA) were purchased from Acros and without purification. Tetrahydrofuran (THF), N, N, N'-dimethylformamide (DMF), dimethyl sulfoxide (DMSO), acetone, methanol, ethanol, chloroform (CHCl₃) and other organic reagents or solvents were obtained from domestic market; they were previously distilled and kept in the presence of 4Å molecular sieve to eliminate any traces of water before use.

Polymerization Procedures: The general procedure of the polymerization was as follows: the macro-initiator, the ligand, solvent and the monomer were added to a flask with stirring; three cycles of vacuum-nitrogen are applied in order to remove oxygen; after the mixture was stirred at 25°C for one hour, the catalyst was added. Then the flask was immersed in an oil bath at the required temperature. After a given time, the flask was opened and a certain amount of tetrahydrofuran (THF) was added into the reaction system to dissolve the resulting polymer.

Measurements: FTIR spectra were obtained on a PE Paragon 1000 spectrometer with a disc of KBr. ¹H NMR measurements were carried out on a Varian Mercury Plus 400 MHz spectrometer. The molecular weight was measured on PE Series 200 GPC with PMMA as standards using THF as eluent at the flow rate of 1 mL/min. TGA were carried out on a PE TGA-7 instrument with a heating rate of 20 °C/min in the nitrogen flow (20 mL/min). TEM analysis were conducted on a JEOL JEL2010 electron microscope at 200 kV, and the samples for TEM measurements were prepared by placing one drop of sample on copper grids coated with carbon. The photo of the samples placed in solvent was taken with a digital camera (Sony, DSC-S70).



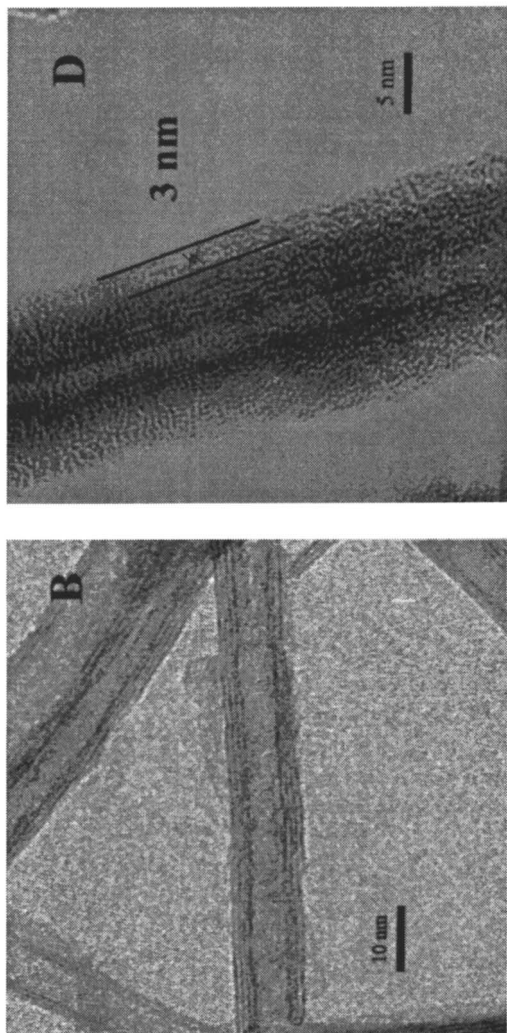


Figure 10. TEM images of crude TNT (A) and (B), TNT-PMMA (C), TNT-PS (D).

Conclusion

Taking advantage of the merits of living/controlled ATRP, a very powerful tool for building of polymeric brushes, in situ polymerization realized on the surfaces of inorganic nanotubes such as MWNTs and TNTs. Significantly, the approach may open an avenue for exploring and preparing novel nanotube-based nanomaterials and molecular devices with tailormade structures and properties.

References

1. Iijima, S. *Nature* **1991**, *354*, 56-58.
2. Tenne, R.; Margulis, L.; Genut, M.; Hodes, G. *Nature* **1992**, *360*, 444-446.
3. Feldman, Y.; Wasserman, E.; Srolovitz, D.J.; Tenne, R. *Science* **1995**, *267*, 222-225.
4. Chopra, N. G.; Luyken, R. G.; Cherrey, K.; Crespi, V. H.; Cohen, M. L.; G. Louie, S.; Zettl, A. *Science* **1995**, *269*, 966-967.
5. Nakamura, H.; Matsui, Y. *J. Am. Chem. Soc.* **1995**, *117*, 2651-2652.
6. Hoyer, P. *Langmuir* **1996**, *12*, 1411-1413.
7. Spahr, M. E.; Bitterli, P.; Nesper, R.; Muller, M.; Krumeich, F.; Nissen, H. *U. Angew. Chem. Int. Ed.* **1998**, *37*, 1263-1265.
8. Hacothen, Y. R.; Grunbanum, E.; Tenne, R.; Sloan, J.; Hutchison, J. L. *Nature* **1998**, *395*, 336-337.
9. Galvan, D. H.; Kim, J. H.; Maple, M.B.; Avalos-Berja, M.; Adem, E. *Fullerene Sci. Technol.* **2000**, *8*, 143-151.
10. Hulteen, J.C.; Jirage, K. C.; Martin, C. R. *J. Am. Chem. Soc.* **1998**, *120*, 6603-6604.
11. Tourillon, G.; Pontonnier, L.; Levy, J. P.; Langlais, V. *Electrochem. Solid-State Lett.* **2000**, *3*, 20-23.
12. Rao, C. N. R.; Govindaraj, A. G.; Deepak, F. L.; Gunari, N. A.; Nath, M. *Appl. Phys. Lett.* **2001**, *78*, 1853-1855.
13. Govindaraj, A.; Deepak, F. L.; Gunari, N. A.; Rao, C. N. R. *Isr. J. Chem.* **2001**, *41*, 23-30.
14. Dlozik, L.; Engelhardt, R.; Ernst, K.; Fiechter, S.; Seiber, I.; Konenkamp, R. *Appl. Phys. Lett.* **2001**, *78*, 3687-3689.
15. Jiang, X.; Xie, Y.; Zhu, L.; He, W.; Qian, Y. *Adv. Mater.* **2001**, *13*, 1278-1281.
16. Peng, Y.; Meng, A.; Zhong, C.; Lu, J.; Xu, L.; Zhang, S.; Qian, Y. *New J. Chem.* **2001**, *25*, 1359-1361.
17. Pu, L.; Bao, X.; Zou, J.; Feng, D. *Angew. Chem. Int. Ed.* **2001**, *40*, 1490-1493.
18. Cheng, B.; Samulski, E. T. *J. Mater. Chem.* **2001**, *11*, 2901-2902.
19. Li, J. Y.; Chen, X. L.; Qiao, Z. Y.; Cao, Y.G.; Li, H. *J. Mater. Sci. Lett.* **2001**, *20*, 1987-1988.
20. Nath, M.; Rao, C. N. *Angew. Chem. Int. Ed.* **2002**, *41*, 3451-3454.

21. Nath, M.; Rao, C. N. *J. Am. Chem. Soc.* **2001**, *123*, 4841-4842.
22. Yada, M. A.; Mihara, M.; Mouri, S.; Kuroki, M.; Kijima, T. *Adv. Mater.* **2002**, *14*, 309-313.
23. Wu, J. J.; Kiu, S.; Wu, C.; Chen, K.; Chen, L. *Appl. Phys. Lett.* **2002**, *81*, 1312-1314.
24. Hernandez, B. A.; Chang, K. S.; Fisher, E. R.; Dorhout, P. K. *Chem. Mater.* **2002**, *14*, 480-482.
25. Han, C. C.; Bai, M. Y.; Lee, J. T. *Chem. Mater.* **2001**, *13*, 4260-4268.
26. Mayers, B.; Xia, Y. *Adv. Mater.* **2002**, *14*, 279-282.
27. Brorson, M.; Hansen, T. W.; Jacobsen, J. H. *J. Am. Chem. Soc.* **2002**, *124*, 11582-11583.
28. Sha, J.; Niu, J.; Ma, X.; Xu, J.; Zhang, X.; Yang, Q.; Yang, D. *Adv. Mater.* **2002**, *14*, 1219-1221.
29. Ausman, K. D.; Piner, R.; Lourie, O.; Ruoff, R. S. *J. Phys. Chem. B* **2000**, *104*, 8911-8915
30. Matyjaszewski, K.; Xia, J. *Chem. Rev.* **2001**, *101*, 2921-2990.
31. Matyjaszewski, K.; Miller, P. J.; Shukla, N.; Immaraporn, B.; Gelman, A.; Luokala, B. B.; Siclovan, T. M.; Kickelbick, G.; Vallant, T.; Hoffmann, H.; Pakula, T. *Macromolecules* **1999**, *32*, 8716-8724.
32. Pyun, J.; Matyjaszewski, K.; Kowalewski, T.; Savin, D.; Patterson, G.; Kickelbick, G.; Huesing, N. *J. Am. Chem. Soc.* **2001**, *123*, 9445-9446.
33. Pyun, J.; Kowalewski, T.; Matyjaszewski, K. *Macro. Rap. Commun.* **2003**, *24*, 1043-1059.
34. Kruk, M.; Dufour, B.; Celer, E. B.; Kowalewski, T.; Jaroniec, M.; Matyjaszewski, K. *J. Phys. Chem. B* **2005**, *109*, 9216-9225.
35. Ajayan, P. M. *Chem. Rev.* **1999**, *99*, 1787-1799.
36. Frankland, S. J. V.; Caglar, A.; Brenner, D. W.; Griebel, M. *J. Phys. Chem. B* **2002**, *106*, 3046-3048.
37. Banerjee, S.; Kahn, M. G. C.; Wong, S. S. *Chem-Eur. J.* **2003**, *9*, 1898-1908.
38. Niyogi, S.; Hamon, M.A.; Hu, H.; Zhao, B.; Bhowmik, P.; Sen, R.; Itkis, M.E.; Haddon, R.C. *Acc. Chem. Res.* **2002**, *35*, 1105-1113.
39. Kong, H.; Gao, C.; Yan, D. *J. Am. Chem. Soc.* **2004**, *126*, 412-413.
40. Kong, H.; Gao, C.; Yan, D. *Macromolecules* **2004**, *37*, 4022-4030.
41. Kong, H.; Li, W. W.; Gao, C.; Yan, D.; Jin, Y.Z.; Walton, D. R. M.; KROTO, H.W. *Macromolecules* **2004**, *37*, 6683-6686.
42. Kong, H.; Gao, C.; Yan, D. *J. Mater. Chem.* **2004**, *14*, 1401-1405.
43. Kong, H.; Luo, P.; Gao, C.; Yan, D. *Polymer* **2005**, *8*, 2472-2485.
44. Hennings, D.; Klee, M.; Waser, R. *Adv. Mater.* **1991**, *3*, 334-340.
45. Newnham, R. E. *MRS Bull.* **1997**, *22*, 20-33.
46. Rusina, O.; Eremenko, A.; Frank, G.; Strunk, H. P.; Kisch, H. *Angew. Chem. Int. Ed.* **2001**, *40*, 3993-3995.
47. Urban, J. J.; Yun, W. S.; Gu, Q.; Park, H. *J. Am. Chem. Soc.* **2002**, *124*, 1186-1187.
48. Tokudome, H.; Miyauchi, M. *Chem. Commun.* **2004**, 958-959.

49. Wu, J. J.; Yu, C. C., *J. Phys. Chem. B* **2004**, *108*, 3377-3379.
50. Zhu, H. Y.; Gao, X. P.; Lan, Y.; Song, D. Y.; Xi, Y. X.; Zhao, J. C. *J. Am. Chem. Soc.* **2004**, *126*, 8380-8381.
51. Idakiev, V.; Yuan, Z. Y.; Tabakova, T.; Su, B. L. *Appl. Catal. A* **2005**, *281*, 149-155.
52. Liu, Z. L.; Guo, B.; Hong, L.; Jiang, H. X. *J. Photochem. Photobiol. A* **2005**, *72*, 81-88.
53. Cheng, G.; Böker, A.; Zhang, M.; Krausch, G.; Müller, A. H. E. *Macromolecules* **2001**, *34*, 6883-6888.

Chapter 21

Advances in Nanostructured Carbons from Block Copolymers Prepared by Controlled Radical Polymerization Techniques

**Tomasz Kowalewski¹, Chuanbing Tang¹, Michal Kruk^{1,2},
Bruno Dufour¹, and Krzysztof Matyjaszewski¹**

¹Department of Chemistry, Carnegie Mellon University, 4400 Fifth Avenue, Pittsburgh, PA 15213

²Current address: Department of Chemistry, College of Staten Island, City University of New York, 2800 Victory Boulevard, Staten Island, NY 10314

This chapter summarizes recent progress toward the preparation of nanostructured carbons from well-defined polyacrylonitrile (PAN) copolymers synthesized by controlled/living radical polymerization, particularly atom transfer radical polymerization (ATRP). Nanoscale PAN domains are formed via self-assembly driven by phase separation between PAN and a sacrificial block. PAN domains are then converted into carbon nanostructures by pyrolysis. This approach allows us to prepare thin film and bulk nanostructured carbon with different morphologies and considerable porosities. Control of the long range order in these materials was achieved through a directional casting technique, i.e., zone casting. Routes were developed to prepare highly porous silica and carbon via supramolecular templating using a water soluble PAN block copolymer and by grafting PAN from the surface of the porous silica template.

Controlled/living radical polymerizations (CRPs)¹⁻³ based on a fast dynamic equilibrium between dormant and active radical species, are particularly suitable for assuring the relatively simple synthesis of numerous classes of well-defined block copolymers with predetermined molecular weights, narrow molecular weight distributions, and precisely controlled architectures. Herein we describe some recent advances in the application of these techniques to the synthesis of nanostructured carbons based on polyacrylonitrile (PAN) and its copolymers. Interest in nanostructured carbons is driven by their unique chemical, mechanical and electrical properties and their potential applications as gas storage media, catalyst supports, as well as components of nanocomposites, proximal probes, and field effect transistors.^{4,5}

PAN represents a particularly interesting case of a segment in phase-separated block copolymers. Due to the *intramolecular* dipole repulsion from the nitrile groups, PAN macromolecules have a tendency to adopt a stiff, rod-like, irregular helical structure.⁶⁻⁸ In addition, the *intermolecular* dipole attraction packs the helices into laterally ordered domains or “paracrystals”,⁹⁻¹² despite the lack of tacticity that is typically a prerequisite for polymer crystallizability. Much of the interest in PAN and its random copolymers is related to the possibility of their conversion into carbonaceous materials, which found a major application in the manufacturing of high-performance carbon fibers.

Recently, we utilized well-established CRP techniques,¹³⁻¹⁵ including atom transfer radical polymerization (ATRP),^{16,17} nitroxide-mediated polymerization (NMP)¹⁸ and reversible addition-fragmentation chain transfer (RAFT),¹⁹ to prepare PAN diblock copolymers. The principles we developed in the synthesis of these PAN diblock copolymers have directed us to prepare other well-defined PAN copolymers with more complex architectures. We have then demonstrated that well-defined PAN block copolymers can be easily fabricated in the form of films, and therefore our route provides an excellent way to prepare nanostructured carbons for the use in thin-film-based devices.^{13,20-22}

This chapter will describe progress in the development of novel nanostructured materials based on these PAN copolymer systems, ranging from simple diblock copolymers to organic/inorganic hybrids. Well-defined character of copolymers that constitute these materials or serve as their precursors facilitates good control over their nanostructure and morphology. Further opportunities for control of these structures are arising from recent developments in the area of processing techniques, exemplified here by the directional casting technique known as zone casting.

Nanostructured Carbons from Polyacrylonitrile Block Copolymers

One of the recent examples of novel nanostructured materials derived from block copolymers prepared by ATRP are carbons obtained by pyrolysis of block

copolymers containing PAN and a sacrificial block (e.g., poly(*n*-butyl acrylate, PBA) (Scheme 1).^{13,20} Through self-assembly driven by phase separation between PAN and the sacrificial block, the PAN domains act as nanoscale precursors for the final carbon nanostructure. Upon simple thermal treatment (pyrolysis), PAN domains are converted into nanostructured carbon, whereas the sacrificial phase decomposes and burns away. Preservation of the original morphology of PAN domains is facilitated by thermal stabilization in the oxidative atmosphere, which is then followed by carbonization under inert gas flow at higher temperature. Based on differential scanning calorimetry, the thermal stabilization is completed before the onset of significant thermal decomposition of PBA, which promotes the preservation of nanostructures during thermal transformation.

PAN copolymers used in our studies formed a range of "classical" morphologies (Figure 1) such as spherical, cylindrical and lamellar. Following thermal stabilization, these block copolymers were then converted by pyrolysis into carbon spheres, filaments, lamellae and more complex structures.

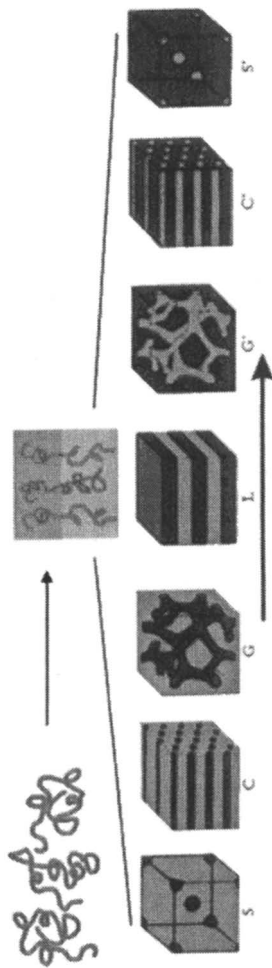
Nanostructured Carbons from Block-Copolymer-Derived Precursors Containing a Thermally Stable Sacrificial Phase

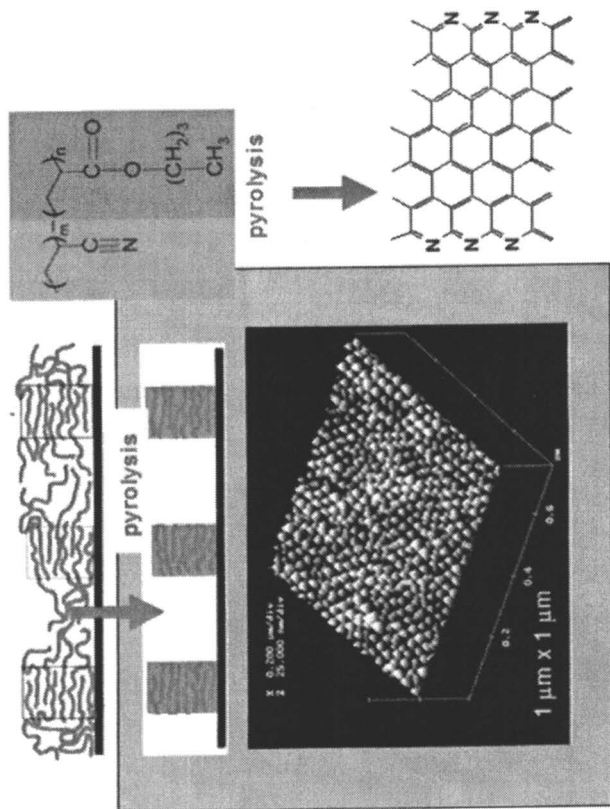
In order to achieve high porosities, we have designed a new system in which domains of sacrificial blocks of the copolymer are reinforced with inorganic material (see Scheme 2). At first, our approach seems to resemble the synthesis of mesoporous carbon through the inverse replication of mesoporous silica templates.²³⁻²⁵ This established synthetic route usually involves: (i) the preparation of the mesoporous silica template (often using self-assembled organic molecules to template the mesopores; these organics are subsequently burned out or extracted), (ii) infiltration of the pores of the template with carbon precursors (organic compounds), (iii) carbonization of the precursors, and (iv) then removal of the silica template. In our case, steps (i) and (ii) are combined into a single step. It should be noted that another group followed a similar pathway in their attempt to carbonize the poly(ethylene oxide)-poly(propylene oxide)-poly(ethylene oxide) copolymer surfactant after it has self-assembled with silica into an ordered copolymer-silica composite.²⁶

In the new template system we developed, the sacrificial block of the PAN copolymer is water soluble and the copolymer micelles are used as supramolecular templates for formation of nanostructured silica.²⁷ Subsequently, the siliceous phase can act as a scaffold that supports the evolving carbon phase during pyrolysis. This scaffold is subsequently etched away, leaving behind the nanoporous carbon (Scheme 2).

The synthesis of well-defined poly(ethylene oxide)-*b*-polyacrylonitrile (PEO-*b*-PAN) block copolymers was accomplished using ATRP. The PEO-*b*-

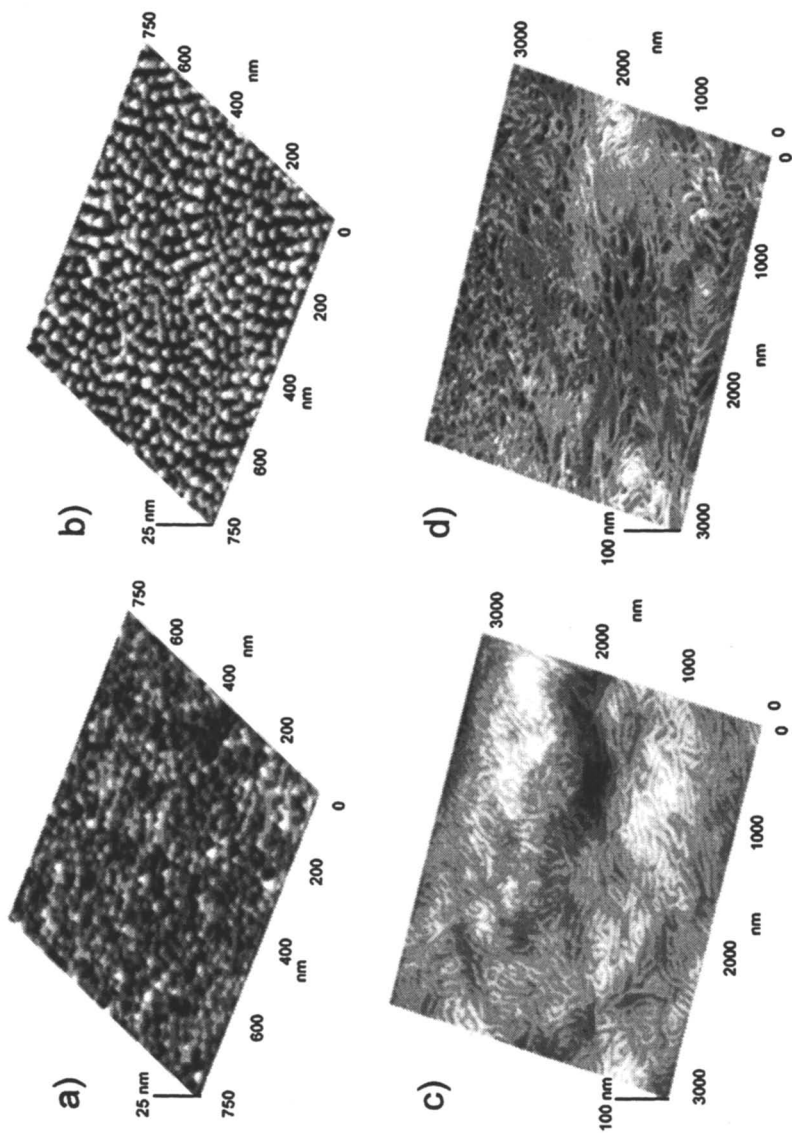
block copolymers consisting of immiscible segments... self-assemble into a variety of nanostructures dictated by the relative content of both blocks





**Partially graphitic carbon nanostructures formed by PYROLYSIS
of nanostructured polyacrylonitrile block copolymer precursors**

Scheme 1. Nanostructured carbon by pyrolysis of self-assembled polyacrylonitrile block copolymer precursors.
(The phase diagram reproduced from Bates, F. S.; Fredrickson, G. *Physics Today*, 1999, 52, 32-38)



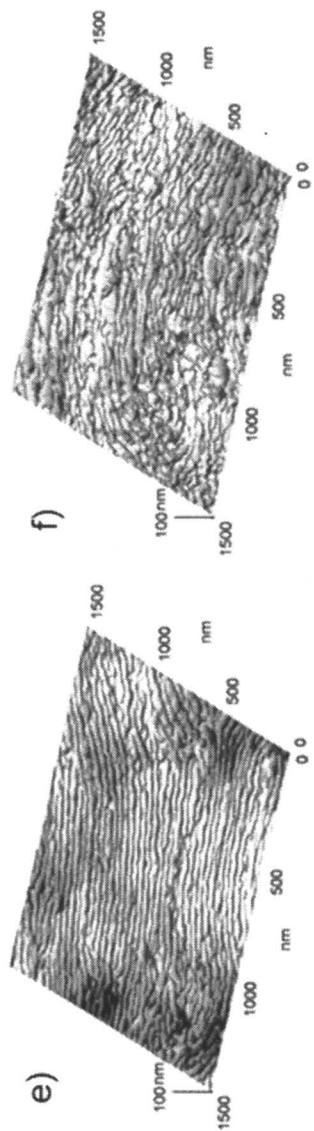


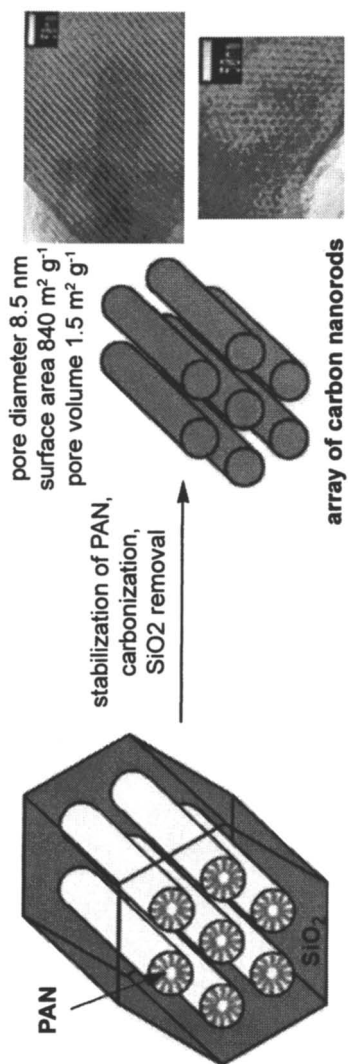
Figure 1 Atomic force microscopy (AFM) height images of PAN block copolymer films: a) spherical (after thermal stabilization); b) cylindrical; c) lamellar. AFM height images of corresponding carbon films after pyrolysis: b) dots; d) filaments; f) sheets. (Reproduced from Reference 13. Copyright 2002 the American Chemical Society and Reference 20. Copyright 2003 with permission from Springer-Verlag GmbH.)

PAN copolymers were used as templates for mesoporous silicas and as precursors for mesoporous carbons. The diblock copolymers were designed to feature: (i) hydrophilic poly(ethylene oxide) (PEO) blocks, which can favorably interact with silica species, and (ii) hydrophobic polyacrylonitrile (PAN) blocks that are suitable for templating the mesoporosity in silica nanostructures, and can be converted into carbon through a suitable thermal treatment. The development of methods for the controlled polymerization of PAN via ATRP provided a convenient and robust avenue for the synthesis of well-defined PAN containing precursors. As a first step, we demonstrated that these new PEO-*b*-PAN copolymers can indeed be used to synthesize silicas with short-range-ordered uniform mesopores. More importantly, the synthesis of mesoporous carbons from silica/PEO-*b*-PAN composites was also successful, although the latter exhibited broader pore size distributions (PSDs) and lower degree of structural ordering.²⁷

Analysis of nitrogen adsorption isotherms revealed that the obtained carbons exhibited high specific surface area (typically 750-1000 m² g⁻¹), large pore volumes (up to 2.8 cm³ g⁻¹) and pore diameters ranging from about 4 to 25 nm. In contrast with most mesoporous carbons reported to date, they exhibited very low microporosity (micropores are pores of diameter below 2 nm). The polymeric precursors, carbons, and silica scaffolds were extensively characterized size exclusion chromatography, NMR, nitrogen adsorption, TGA, transmission electron microscopy (TEM) and powder X-ray diffraction.

TEM images presented in Scheme 2 show that although carbon appears to be templated with good fidelity after the nanostructured silica, the system lacks long range order. We have demonstrated however, that significantly more ordered carbons can be obtained using the inverse replication approach,^{23,24} relying on the controlled polymerization of acrylonitrile within the cavities of ordered mesoporous silicas,²⁸ whose surface was modified with bromoisobutyrate-containing organosilyl groups and trimethylsilyl (TMS) groups to yield bromine-containing ATRP initiating sites. These initiating sites were then successfully used to graft PAN from the silica surface (see Scheme 3). The mesoporous silica scaffolds were synthesized using a well known approach that utilizes PEO-PPO-PEO and poly(ethylene oxide)-poly(butylene oxide)-poly(ethylene oxide) PEO-PBO-PEO copolymers as templates.^{29,30}

The obtained carbons had high specific surface area (750-1000 m² g⁻¹) and large pore volumes (1.1-2.4 cm³ g⁻¹). Analysis of pore size distributions revealed that while exhibiting high adsorption capacity, they were characterized by very low microporosity, in contrast with most mesoporous carbons reported to date. The pore size analysis revealed that the primary source of very high adsorption capacity were mesopores. Very high porosities make these materials attractive candidates for supercapacitor applications, and perhaps for electron acceptor scaffolds for photovoltaic cells. Importantly, silica/carbon nanocomposites, which represent the penultimate step in these approaches for the synthesis of mesoporous carbons, are quite interesting by themselves. They may be especially



Scheme 3. Synthesis of ordered mesoporous carbon using silica template and carbon precursor formed via surface-initiated controlled radical polymerization. (Adapted from Reference 28. Copyright 2005 the American Chemical Society).

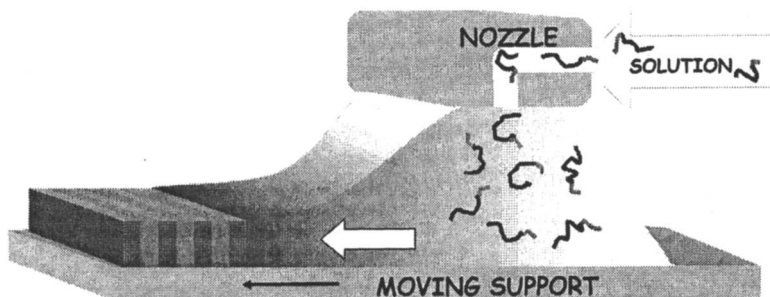
suitable as field emission materials, with silica providing the rigid framework enhancing the overall structural stability of carbon.

Long-Range Ordered Nanostructured Carbons

One of the most vigorously pursued goals in the field of block copolymers is achievement of long-range ordered, periodic nanostructures. Such long-range order is of particular interest in the fabrication of nanostructured materials for magnetic data storage^{31,32} or for lithography.^{33,34} Typical approaches to this task involve the use of external stimuli, such as electric field,³⁵ shear (e.g., roll casting),³⁶ or employ such phenomena as eutectic solidification,³⁷ orientation during solvent evaporation,³⁸ graphoepitaxy,^{39,40} and alignment on lithographically patterned substrates.^{41,42} Recently, we have achieved this goal using the directional casting technique,²² also referred to as "zone-casting" (Scheme 4), which had been originally developed to facilitate the oriented growth of molecular crystals.⁴³ We have demonstrated that zone casting is applicable to PAN-*b*-PBA block copolymers yielding uniform thin films with long-range ordered copolymer domains. Such ordered PAN-*b*-PBA films were then converted into anisotropic nanostructured carbons.

In the zone-casting process, the block copolymer solution is supplied through a nozzle onto a substrate withdrawn at controlled speed, facilitating control of nanostructure formation through precise control of the advancement of solidification front. Zone casting experiments with PAN-*b*-PBA copolymers were carried out using copolymers prepared by nitroxide-mediated polymerizations as described earlier.¹⁴ The block copolymer had a number-average molecular weight of 37500 g/mol (the structural formula (BA)₂₄₀(AN)₁₂₄) and polydispersity index of 1.22. Thin and ultra-thin copolymer films were prepared by drop-casting or zone-casting N,N-dimethylformamide (DMF) solutions onto pre-cleaned silicon wafers covered with the layer of native oxide. Due to the high boiling point of DMF, in order to achieve a desirable evaporation rate, the temperatures of the copolymer solution and of the substrate had to be maintained at 90 °C. The film thickness was controlled in the range from 100 nm to 1 μm by adjusting the solution concentration under a constant solution supply rate and a constant rate of movement of the substrate.

The surface morphology of thin films of PBA-*b*-PAN block copolymers was visualized with tapping mode atomic force microscopy (TMAFM). Figure 3 (left image) shows a typical meandering surface morphology of thin films prepared by



Scheme 4. Illustration of zone casting of a solution of block copolymers. (Reproduced from Reference 22. Copyright 2005 the American Chemical Society)

a traditional drop-casting technique. PAN and PBA domains were well contrasted in so-called phase images, which primarily reflect the differences in mechanical energy dissipation between different regions of the surface. As expected, more lossy PBA phase exhibited stronger phase shifts (darker regions in phase images). In height images (not shown), elongated, meandering, rigid PAN domains appeared as protrusions surrounded by the soft PBA matrix. Although the domains of the copolymer exhibited a short- or middle-range ordering (up to a few hundred nanometers), long-range ordering was not observed in any area of many drop-cast films, which were studied by AFM.

In contrast, films prepared by zone casting exhibited prominent long-range ordering, with long axes of striped structures oriented perpendicular to the casting (substrate withdrawal) direction. An example of such long-range ordered film is shown in Figure 2 (middle image). This long-range ordering was preserved over the whole casting substrates (3 cm × 5 cm). The observed domain orientation suggests that it was governed by the attempt to align along the solvent evaporation front (phase separation zone), rather than by the solvent flow towards the front.

Thermal stabilization and carbonization were carried out on the above zone-cast copolymer films by heating the copolymer films to 280 °C under air, followed by heating to 800 °C under nitrogen. As shown in Figure 2 (right image), long-range ordered lamellar morphology of block copolymers was preserved after thermal stabilization and carbonization. Moreover, the spacing between the elongated parallel carbon domains remained nearly unchanged in comparison with the block copolymer precursor.

In contrast, carbon films prepared from samples prepared by drop-casting did not show any evidence of long-range ordering, and meandering PAN domains were converted into entangled carbon nanofilaments.

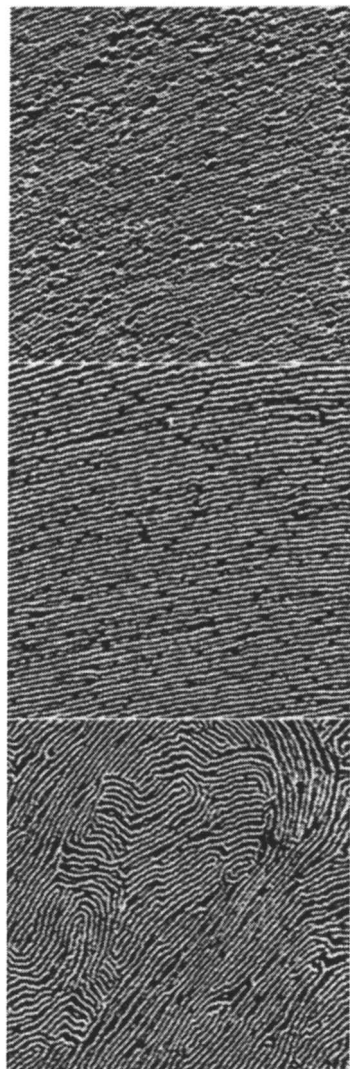


Figure 2. Tapping mode AFM phase images (size: $3\ \mu\text{m} \times 3\ \mu\text{m}$) of thin films of PBA-*b*-PAN block copolymers prepared by drop-casting (left), zone-casting (middle) and of nanostructured carbons prepared by subsequent pyrolysis of zone-cast films (right). (Reproduced from Reference 22. Copyright 2005 the American Chemical Society)

Ordered anisotropic films prepared using this approach represent a good model system for the elucidation of electrical transport properties in nanostructured carbons. They also show promise as field emission electrodes. The applicability of zone-casting to the control the nanoscale morphology of other block copolymer systems is currently under investigation.

Conclusions

In conclusion, we have developed a novel and promising route toward the synthesis of nanostructured carbons from phase-separated PAN block copolymers. Anisotropic nanostructured carbons were prepared via pyrolysis of PAN block copolymers with long-range order. The nanostructure orientation and long-range ordering of block copolymers over the whole substrate was achieved using a directional casting method referred to as zone casting. Nanoporous carbons with high porosity were prepared from water-soluble PAN block copolymers with the aid of silica scaffold formed in situ in the process of copolymer-silica self-organization. Ordered mesoporous carbons were synthesized by grafting PAN from the surface of ordered silica templates.

Acknowledgement

The National Science Foundation (T.K. DMR-0304508 and 0210247, K.M. DMR-0090409) and the CRP Consortium at Carnegie Mellon are acknowledged for funding.

References

1. Matyjaszewski, K., Ed. *Controlled radical polymerization*, ACS Symp. Ser.; American Chemistry Society: Washington, D.C., 1998; Vol. 685.
2. Matyjaszewski, K., Ed. *Controlled/living radical polymerization. Progress in ATRP, NMP, and RAFT*, ACS Symp. Ser.; American Chemistry Society: San Francisco, 2000; Vol. 768.
3. Matyjaszewski, K., Ed. *Advances in Controlled/living radical polymerization*, ACS Symp. Ser.; American Chemistry Society: Washington, D.C., 2003; Vol. 854.
4. Burchell, T. D. *Carbon materials for advanced technologies*; Pergamon: Amsterdam, Oxford, 1999.
5. Dresselhaus, M. S.; Dresselhaus, G.; Avouris, P. *Carbon Nanotubes Synthesis, Structure, Properties, and Applications*; Springer: Berlin, 2001.
6. Frushour, B. G. *Polym. Bull.* **1981**, *4*, 305-314.

7. Gupta, A.; Harrison, I. R. *Carbon* **1996**, *34*, 1427-1445.
8. Olive, G. H.; Olive, S. *Adv. Polym. Sci.* **1979**, *32*, 123-187.
9. Kaji, H.; Schmidt-Rohr, K. *Macromolecules* **2000**, *33*, 5169-5180.
10. Kaji, H.; Schmidt-Rohr, K. *Macromolecules* **2001**, *34*, 7368-7381.
11. Kaji, H.; Schmidt-Rohr, K. *Macromolecules* **2001**, *34*, 7382-7391.
12. Kaji, H.; Miura, N.; Schmidt-Rohr, K. *Macromolecules* **2003**, *36*, 6100-6113.
13. Kowalewski, T.; Tsarevsky, N. V.; Matyjaszewski, K. *J. Am. Chem. Soc.* **2002**, *124*, 10632-10633.
14. Tang, C.; Kowalewski, T.; Matyjaszewski, K. *Macromolecules* **2003**, *36*, 1465-1473.
15. Tang, C.; Kowalewski, T.; Matyjaszewski, K. *Macromolecules* **2003**, *36*, 8587-8589.
16. Wang, J. S.; Matyjaszewski, K. *J. Am. Chem. Soc.* **1995**, *117*, 5614-5615.
17. Matyjaszewski, K.; Xia, J. H. *Chem. Rev.* **2001**, *101*, 2921-2990.
18. Hawker, C. J.; Bosman, A. W.; Harth, E. *Chem. Rev.* **2001**, *101*, 3661-3688.
19. Chiefari, J.; Chong, Y. K.; Ercole, F.; Krstina, J.; Jeffery, J.; Le, T. P.; Mayadunne, R. T. A.; Meijs, G. F.; Moad, C. L.; Moad, G.; Rizzardo, E.; Thang, S. H. *Macromolecules* **1998**, *31*, 5559-5562.
20. Kowalewski, T.; McCullough, R. D.; Matyjaszewski, K. *Eur. Phys. J. E* **2003**, *10*, 5-16.
21. Tang, C.; Qi, K.; Wooley, K.; Matyjaszewski, K.; Kowalewski, T. *Angew. Chem. Int. Ed.* **2004**, *43*, 2783-2787.
22. Tang, C.; Tracz, A.; Kruk, M.; Zhang, R.; Smilgies, D.-M.; Matyjaszewski, K.; Kowalewski, T. *J. Am. Chem. Soc.* **2005**, *127*, 6918-6919.
23. Ryoo, R.; Joo, S. H.; Jun, S. *J. Phys. Chem. B* **1999**, *103*, 7743-7746.
24. Lee, J.; Yoon, S.; Hyeon, T.; Oh, S. M.; Kim, K. B. *Chem. Commun.* **1999**, 2177-2178.
25. Knox, J.; Kaur, B.; Millward, G. R. *J. Chromatogr.* **1986**, *352*, 3-25.
26. Kim, J.; Lee, J.; Hyeon, T. *Carbon* **2004**, *42*, 2711-2719.
27. Kruk, M.; Dufour, B.; Celer, E. B.; Kowalewski, T.; Jaroniec, M.; Matyjaszewski, K. *Chem. Mater.*, submitted.
28. Kruk, M.; Dufour, B.; Celer, E. B.; Kowalewski, T.; Jaroniec, M.; Matyjaszewski, K. *J. Phys. Chem. B* **2005**, *109*, 9216-9225.
29. Zhao, D.; Feng, J.; Huo, Q.; Melosh, N.; Frederickson, G. H.; Chmelka, B. F.; Stucky, G. D. *Science* **1998**, *279*, 548-552.
30. Yu, C.; Yu, Y.; Zhao, D. *Chemical Communications (Cambridge)* **2000**, 575-576.
31. Park, M.; Harrison, C.; Chaikin, P. M.; Register, R. A.; Adamson, D. H. *Science* **1997**, *276*, 1401-1404.

32. Ross, C. *Annu. Rev. Mater. Res.* **2001**, *31*, 203-235.
33. Hamley, I. W. *The Physics of Block Copolymers*; Oxford University Press: Oxford, U.K., 1998.
34. Hadjichristidis, N.; Pispas, S.; Floudas, G. *Block Copolymers: Synthetic Strategies, Physical Properties, and Applications*; John Wiley & Sons, Inc.: Hoboken, 2003.
35. Morkved, T. L.; Lu, M.; Urbas, A. M.; Ehrichs, E. E.; Jaeger, H. M.; Mansky, P.; Russell, T. P. *Science* **1996**, *273*, 931-933.
36. Albalak, R. J.; Thomas, E. L. *J. Polym. Sci. Part B: Polym. Phys.* **1994**, *32*, 341-350.
37. De Rosa, C.; Park, C.; Thomas, E. L.; Lotz, B. *Nature* **2000**, *405*, 433-437.
38. Kimura, M.; Misner, M. J.; Xu, T.; Kim, S. H.; Russell, T. P. *Langmuir* **2003**, *19*, 9910-9913.
39. Segalman, R. A.; Yokoyama, H.; Kramer, E. J. *Adv. Mater.* **2001**, *13*, 1152-1155.
40. Cheng, J. Y.; Ross, C. A.; Chan, V. Z. H.; Thomas, E. L.; Lammertink, R. G. H.; Vancso, G. J. *Adv. Mater.* **2001**, *13*, 1174-1178.
41. Kim, S. O.; Solak, H. H.; Stoykovich, M. P.; Ferrier, N. J.; de Pablo, J. J.; Nealey, P. F. *Nature* **2003**, *424*, 411-414.
42. Stoykovich, M. P.; Muller, M.; Kim, S. O.; Solak, H. H.; Edwards, E. W.; de Pablo, J. J.; Nealey, P. F. *Science* **2005**, *308*, 1442-1446.
43. Tracz, A.; Jeszka, J. K.; Waston, M. D.; Pisula, W.; Mullen, K.; Pakula, T. *J. Am. Chem. Soc.* **2003**, *125*, 1682-1683.

Chapter 22

An Overview of the Emulsion Stable Free Radical Nanoprecipitation Polymerization Process

Andrea R. Szkurhan and Michael K. Georges*

Department of Chemical and Physical Sciences, University of Toronto at Mississauga, 3359 Mississauga Road North, Mississauga, Ontario L5L 1C6, Canada

A brief overview of living-radical aqueous polymerization is provided with an emphasis on recent work that has been performed in our laboratory in this area. Featured in this discussion is a unique nanoprecipitation technology that has been developed to allow emulsion polymerizations of both styrene and *n*-butyl acrylate monomers under stable free radical polymerization (SFRP) conditions.

Introduction

The discovery of living-radical polymerization has allowed for the production of polymers with controlled microstructures by free radical polymerization techniques. Currently three such processes exist: stable free radical polymerization (SFRP) (1), atom transfer radical polymerization (ATRP) (2), and reversible addition fragmentation chain transfer (RAFT) (3) polymerization. These processes have allowed for the synthesis of narrow molecular weight

distribution homopolymers and block copolymers; and polymers with complex architectures including star, graft- and comb-type polymers all by free radical techniques. Previously, such polymers could only be produced by anionic polymerization techniques that require rigorous purification procedures due in large part to the high reactivity of the living anionic chain end to hydroxyl containing molecules. Since free radicals do not exhibit this sensitivity there has been extensive research conducted in the application of living-radical polymerization to aqueous based systems (4), such as suspension, dispersion, miniemulsion and emulsion polymerization. These systems offer many advantages over homogeneous systems since they lend themselves to large-scale materials production and are environmentally safe primarily because the dispersing medium is water.

Performing a living-radical polymerization in a heterogeneous system adds further complexity to an already complex process since the species, including the living-radical support (nitroxide, metal complex, RAFT agent), may partition between the aqueous and organic phases. Most of the earlier attempts to produce a conventional emulsion using living-radical techniques were fraught with problems(5). These systems produced emulsions with poor colloidal stability as seen by the formation of large particles, or phase separation of the latex into an upper foamy oily layer and a lower aqueous layer. When colloidal stability was achieved in these systems, it was often at the expense of the system's livingness and resulted in polymers with poor molecular weight control or broad molecular weight distributions.

Although living-radical emulsion polymerization processes have been met with much difficulty, there has been a lot of progress in the application of living-radical polymerizations to miniemulsion systems (6). Mechanistically, miniemulsion systems are much simpler than emulsion systems since they contain preformed small stabilized droplets. Nucleation and further polymerization of these droplets allows for the formation of polymer particles. The downfall of miniemulsion systems is that the addition of a small molecule hydrophobe is required to impart stability of the small monomer droplets, and is often regarded as an impurity in the final latex particle. Furthermore, the use of a high shear device is required for the formation of the small droplets, adding difficult to very large scale synthesis. Nevertheless, colloidally stable latexes can be achieved using living-radical techniques under these conditions.

Unlike a miniemulsion system where the monomer is divided into nano-sized droplets, the majority of the monomer in an emulsion exists in large monomer droplets that are typically 1-10 μm in diameter. Only a small portion of the monomer will be contained in monomer-swollen micelles, or dissolved in the aqueous phase. The function of the monomer droplets is to act as reservoirs and provide monomer to the growing particles in the first phase of emulsion polymerization. While highly unstable, the monomer droplets become depleted as the polymerization proceeds and shrink until they are completely gone at 40%

conversion (7). In a living-radical emulsion polymerization, the monomer droplets may not disappear as readily, if at all. In the case of the SFRP process, the polymerization is performed at elevated temperatures ($>125^{\circ}\text{C}$); temperatures above which styrene is known to autopolymerize (8). Autoinitiation and subsequent polymerization in the monomer droplets would cause them to lose their ability to act as effective reservoirs since there would no longer be a driving force for the monomer to leave the droplets once polymer is present inside them. Thus, these large unstable droplets can remain indefinitely in the reaction mixture contributing to phase separation or the formation of large polymer particles depending upon the conditions of the polymerization.

Alternatively, or in combination with the aforementioned autoinitiation issue, the difference in the rate of chain growth in conventional and living-radical polymerizations may also contribute to the failure of living-radical emulsion polymerizations. In a conventional radical polymerization chain growth is fast and within seconds very high molecular weight chains are formed, which, in the case of an emulsion polymerization, help to stabilize the polymer particles. Chain growth is much slower in a living-radical polymerization system. The polymer chains continuously increase in molecular weight throughout the polymerization but at the beginning of the process the chains are not large enough to effectively stabilize the polymer particles. This lack of stabilization causes the particles to stabilize themselves by reducing their total free interfacial surface energy by increasing in size through particle coalescence and Ostwald ripening (9). The fact that living-radical systems will have a large number of oligomeric chains growing simultaneously in the early stages of polymerization completely changes the classical particle formation mechanisms.

Despite the difficulties that have been encountered in trying to perform living-radical polymerizations under *ab initio* emulsion conditions, there has been some success accomplished in the use of specialized emulsion systems that contain preformed stable particles. Such systems include that of seeded emulsion polymerizations (5a, 10), which use particles from a conventionally prepared latex as seeds. A living-radical support is transported into the seed particles, which are then swelled with additional monomer. Polymerization of these particles produces a colloiddally stable latex product. Although a living-polymer population is produced, there is also the presence of the conventional polymer population from the seed. Another system that has shown promise uses polymeric surfactants as emulsion stabilizers in which particles are created using amphiphilic block copolymers (11). These block copolymers, which were synthesized using RAFT polymerization techniques, contain both a hydrophilic and hydrophobic segment making them surface active, resulting in the ability for them to self-assemble into a micellar structure. Emulsion polymerizations are performed using these micelles as particle precursors under starved-feed conditions, in which the formation of monomer droplets is avoided. Propagation takes place in the interior of the micelles and proceeds to a point where the

chains are too hydrophobic to desorb from the micelle, signifying the conversion of the micelle into a particle. Propagation continues to produce stable emulsion latexes containing polymers that increase in molecular weight with time and conversion with narrow molecular weight distributions.

Another emulsion system has been developed that uses a water soluble alkoxyamine as an initiating species to perform an SFRP emulsion (12). Emulsion polymerization with the alkoxyamine initiator was completed in a two step process. In the first step a seed latex was created by the living polymerization of *n*-butyl acrylate under very dilute emulsion polymerization conditions (0.7% monomer loading). Under these conditions, the formation of monomer droplets was severely limited and the majority of the monomer existed either dissolved in the aqueous phase or in micelles, so as to favour micellar nucleation over droplet nucleation. The dilute emulsion polymerization produced seed particles with an average particle diameter between 150 – 200 nm depending on the amount of surfactant used. In the second step, a batch polymerization was performed using the seed latex from the first step. High conversion polymers were produced under controlled conditions, showing an increase in molecular weight and conversion with time. More importantly, the latexes produced using this two step process were colloidally stable, and produced particles with a final average particle size of ~600 nm.

This two-step emulsion work using an alkoxyamine unimer was followed up with a report on a batch process (13) using the same alkoxyamine unimer, only in this work, it was used to form a SG1-terminated poly(acrylic acid) macroinitiator prior to emulsion polymerization. An emulsion polymerization of styrene or *n*-butyl acrylate was then conducted under batch conditions (20% monomer loading) in which the SG1-terminated macroinitiator was dissolved in the aqueous phase without any added surfactant. This system produced a colloidally stable latex, giving particles with an average diameter of 90 nm. Although colloidal stability was achieved in this system, the polymers produced showed broad molecular weight distributions that would increase throughout the course of the polymerization (final PDIs between 2.0 and 3.0). This broad molecular weight distribution was attributed to the accumulation of dead chains throughout the course of the reaction.

In this paper we present a technique that allows for the production of colloidally stable latexes by an SFRP emulsion process. A nanoprecipitation process is used to create particles containing a preformed TEMPO-terminated oligomer that serves as a macroinitiator and a particle stabilizer. The particles are then swollen with monomer and subsequent polymerization produces a living polymer under emulsion conditions in which excellent chain growth is demonstrated. Importantly, no high shear device is required to form small particles and the use of a high molecular weight conventionally formed polymer that would contaminate the living polymer product is avoided.

Experimental

Materials and Equipment. The inhibitor was removed from styrene (Aldrich) by passing it through a 4-*tert*-butylcatechol inhibitor removal column (Aldrich). Inhibitor was removed from *n*-butyl acrylate (Aldrich) by passing it through a 4-methoxyphenol inhibitor removal column (Aldrich). Benzoyl peroxide (BPO) (Aldrich) was purified by recrystallization from methanol. Sodium dodecylbenzene sulfonate (SDBS) (Aldrich), poly(vinyl alcohol) (PVA), 87-89% hydrolyzed, average M_w 31,000-50,000 g/mol, (Aldrich) and TEMPO (Chemipan, Russia) were used as received. The acyclic nitroxide, 2,2,5-trimethyl-4-phenyl-3-azahexane-3-nitroxide, was synthesized according to a reported procedure (14). For starved-feed experiments, monomer was added to the reactor using a Harvard PHD 4400 syringe pump equipped with a 9 mL stainless steel syringe (diameter = 9.525 mm) that was connected to the reactor using stainless steel HPLC tubing as a needle (1/16th outer diameter, 0.40 inner diameter, void length of tubing: 69.5 cm).

Characterizations. Polymer molecular weights and polydispersity indices (PDIs) were estimated by gel permeation chromatography (GPC) using a Waters 2690 Separations Module with Ultrastayragel columns HR1, HR3 and HR4E, and a Waters model 410 differential refractometer (RI). Polystyrene standards were used for calibration. THF was used as the eluent at a flow rate of 0.5 mL min⁻¹. GPC was performed on samples taken directly from the reaction mixture without any prior precipitation that may remove low molecular weight chains. Excess monomer was removed by evaporation with a stream of air prior to GPC analysis. Percentage conversions were determined gravimetrically. Particle sizes were determined by dynamic light scattering using a Nicomp model 370 submicron particle sizer.

General procedure for TEMPO-terminated oligomer synthesis. A polystyrene oligomer was prepared by dissolving TEMPO (1.7 g; 10.9 mmol) in styrene (100 mL; 0.87 mol) in a 3-necked round bottom flask equipped with an argon inlet, condenser, and thermometer. The resulting solution was bubbled with argon gas for 20 minutes. BPO (2.0 g; 8.3 mmol) was added and the reaction temperature was maintained at 135 °C for 4 h. The solution was cooled to room temperature, diluted with dichloromethane (100 mL) and precipitated into methanol (1000 mL). The resulting polymer was filtered, washed with methanol and air dried. By GPC: $M_n = 3,300 \text{ g mol}^{-1}$, PDI = 1.13.

General procedure for nanoprecipitation emulsion polymerizations. An emulsion was prepared by dissolving the TEMPO-terminated polystyrene oligomer (1 g) in acetone (50 mL), and adding this solution drop-wise to a

stirred solution of PVA (1 g) in distilled water (100 mL). The acetone was removed from the emulsion by rotary evaporation at 35 °C. Since water and acetone form an azeotrope, some water also evaporated during this process. The solution was made up to 100 mL by the addition of distilled water. Styrene (10 mL) was added and the reaction mixture was stirred covered for 1.5 h to allow the particles to swell with monomer. The mixture was then placed in a modified Parr bomb reactor equipped with a pressure gauge, 4-bladed propeller mixer, thermocouple, argon inlet and sampling tube. The reaction mixture was stirred while being purged by pressurizing the reactor to 6.9 bar with argon gas for 1 min and then depressurizing the reactor. This process was repeated ten times. The reactor was placed under a 6.9 bar atmosphere of argon and heated for typically 6-8 h at 135 °C. Samples were taken throughout the course of the reaction for GPC and conversion analysis.

General procedure for block copolymer synthesis. To an emulsion latex prepared by the nanoprecipitation procedure (70 mL) was added a second monomer (7 mL). The reaction mixture was stirred covered for 1.5 h to allow the particles to swell. The mixture was then placed in a modified Parr bomb reactor equipped with a pressure gauge, 4-bladed propeller mixer, thermocouple, argon inlet and sampling tube. The reaction mixture was stirred while being purged by pressurizing the reactor to 6.9 bar with argon gas for 1 min and then depressurizing the reactor. This process was repeated ten times. The reactor was placed under a 6.9 bar atmosphere of argon and heated for typically 6-8 h at 135 °C. Samples were taken throughout the course of the reaction for GPC and conversion analysis.

Results and Discussion

The combination of the failures resulting from our *ab initio* emulsion work (15), along with the more promising results of these published emulsion experiments in which stabilized particles were used made us change the focus of our emulsion work. Earlier work in the area of SFRP miniemulsion polymerization (16) showed that the use of the co-stabilizer, hexadecane, could be eliminated by using a low conversion TEMPO-terminated polystyrene oligomer to make the miniemulsion particles. In this process the function of the TEMPO-terminated oligomer was two-fold: it acted to stabilize the miniemulsion particles, thereby eliminating the need for a co-stabilizer, which is often viewed as an impurity in the final latex product, and the TEMPO-terminated oligomer also functioned as an initiator. We were interested applying this idea of using the stabilizing ability of oligomeric polymer chains to stabilize particles created in an SFRP emulsion process (17).

Initial experiments were conducted in which an emulsion was prepared by adding a low conversion TEMPO-terminated polystyrene oligomer to an aqueous solution of sodium dodecylbenzenesulfonate (SDBS) (1% by weight relative to water). The resulting emulsion was stirred mechanically and then polymerized by heating at 135 °C. The product that resulted was not a colloiddally stable latex, but instead a suspension of polymer beads 1-2 mm in diameter (18). From the results of this experiment, it was thought that the shear from stirring was not great enough to overcome the viscosity of the bulk oligomeric solution to break it into nano-sized particles, thus producing large beads and preventing the formation of small particles. By isolating the TEMPO-terminated oligomer by precipitation and then dissolving it in acetone and adding this solution drop-wise to a stirred solution of aqueous SDBS (1% by weight relative to water) addressed the viscosity issue. It was envisioned that upon addition to the aqueous surfactant solution, the oligomeric chains would precipitate on the molecular level (as in the case of homogenous nucleation) and stabilize themselves through the adsorption of the dissolved surfactant. Unfortunately, precipitation of this solution into an aqueous solution of SDBS was unsuccessful. Upon addition of the oligomer solution, large particles, that settled once the stirring was stopped, continually resulted. A polymerization was conducted using the filtrate of one of these precipitation experiments, which proceeded to give a living polymer. More importantly, the resulting latex had an average particle size of 2 μm . While still too large to give a stable latex, these were the smallest particle sizes that we had obtained up to that point. Attempts at achieving smaller particles by adding the oligomer as a more dilute solution in acetone failed to allow for the formation of smaller particles.

A major improvement to this precipitation approach to making particles was the replacement of the anionic surfactant SDBS with the nonionic surfactant, poly(vinyl alcohol) (PVA). When a solution of the TEMPO-terminated polystyrene oligomer in acetone was added drop-wise to a solution of PVA in water (1% by weight with respect to water) a stable emulsion resulted in which no large particles were present. Following acetone removal, polymerization under starved-feed conditions gave a colloiddally stable latex; however, the molecular weight distributions of the polymer products formed in the early stages of the polymerization were distinctly bimodal (Figure 1).

Allowing the precipitated particles to swell with monomer over a 12 h period prior to polymerization instead of adding the monomer under starved-feed conditions led to a colloiddally stable latex with a narrow, unimodal particle size distribution that had an average particle size of 460 nm. Particles larger than 1 μm , so prominent in all previous attempts to prepare stable latexes, were completely absent. In an effort to eliminate the lengthy process involved in making these particles, acetone evaporation was performed using a rotary evaporator instead of air evaporation and the particle swell time was decreased to 1.5 h. These changes appeared to have no adverse effects on the outcome of

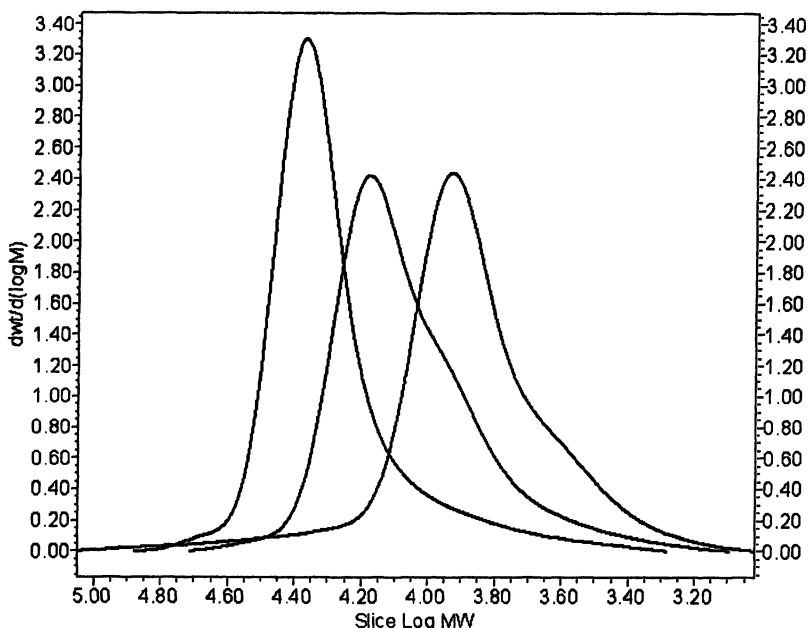


Figure 1: GPC MWD Plot for the SFRP Starved-Feed Emulsion Polymerization of Styrene Using a Nanoprecipitation Process with PVA as the Surfactant. The above curves (from right to left) correspond to the 2 h ($M_n = 6400$; $PD = 1.40$), 4 h ($M_n = 9900$; $PD = 1.30$) and 6 h ($M_n = 17000$; $PDI = 1.26$) samples of the polymerization.

the polymerization. The polymers produced were living, showing an incremental increase in molecular weight with both time and conversion (Figures 2 and 3), and gave an emulsion that was colloidally stable with an average particle diameter of 420 nm. Two factors that may be contributing to the colloidal stability of the latex obtained are the choice of surfactant and the rapid nucleation of all particles, which is known to increase particle stability. PVA is a better stabilizer for larger particles than SDBS and because of the way the particles are created in our process nucleation of all particles is effectively completed before polymerization begins.

Initial experiments conducted with the microprecipitation procedure were performed using 10% monomer loading; however, no adverse effects on the polymer's livingness, the colloidal stability of the latex, or the resulting particle size were observed when the monomer loading was increased to 20% (19).

This nanoprecipitation emulsion process is rather robust and has been extended to allow for the polymerization of acrylates. For this work, a 1.5 K oligomer was synthesized using 2,2,5-trimethyl-4-phenyl-3-azahexane-3-nitroxide, which has been reported to work well in the polymerization of

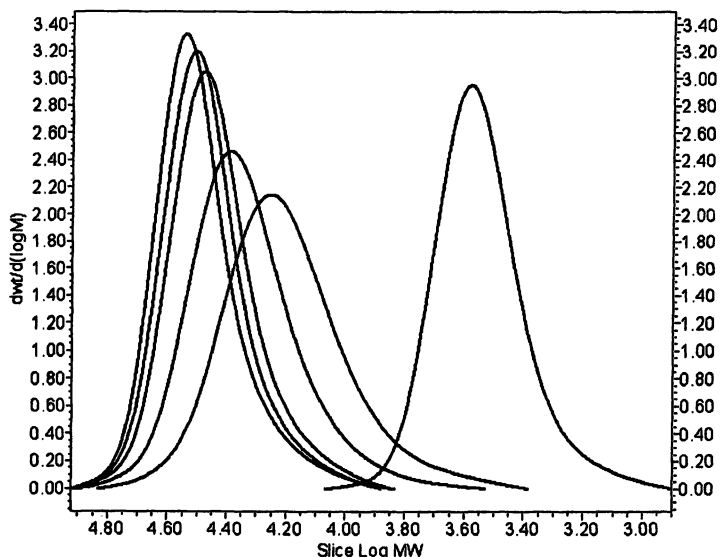


Figure 2: GPC MWD Plot for the SFRP Styrene Emulsion Polymerization Using the Nanoprecipitation Process with Monomer Particle Swelling. The above curves (from right to left) correspond to the prepolymer ($M_n = 3\,300$), 1 h ($M_n = 14\,100$; $PD = 1.26$), 2 h ($M_n = 19\,900$; $PD = 1.19$), 4 h ($M_n = 26\,000$; $PD = 1.13$), 6 h ($M_n = 28\,100$; $PD = 1.12$) and 8 h ($M_n = 29\,500$; $PD = 1.12$) samples of polymerization.

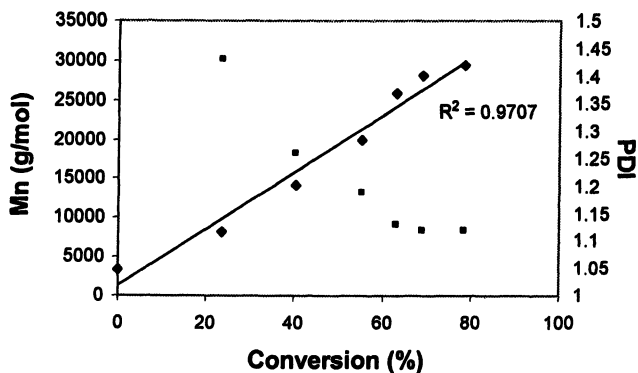


Figure 3: Number Average Molecular Weight vs Conversion Plot for the Styrene Emulsion Polymerization Using a Nanoprecipitation Process with PVA and Monomer Particle Swelling.

acrylates under SFRP conditions (14). Using the same procedures as in our styrene polymerizations, the nitroxide-terminated oligomer was dissolved in acetone and added drop-wise to a 1% by weight solution of PVA in water to create particles. The particles were then swelled with *n*-butyl acrylate and polymerized at 135 °C to give a stable emulsion latex with a polymer that showed a very nice increase in molecular weight with time and conversion and narrow molecular weight distributions (Figures 4 and 5).

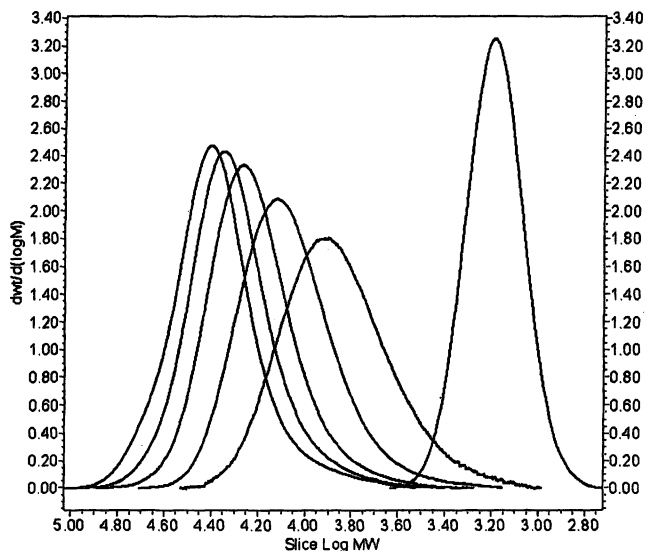


Figure 4: GPC MWD Plot for the SFRP *n*-Butyl Acrylate Emulsion Polymerization Using a Nanoprecipitation Process. The above curves (from right to left) correspond to the macroinitiator ($M_n = 1\,500$; $PD = 1.08$), 0.5 h ($M_n = 6\,200$; $PD = 1.32$), 1 h ($M_n = 10\,800$; $PD = 1.22$), 2 h ($M_n = 15\,300$; $PD = 1.19$), 4 h ($M_n = 18\,600$; $PD = 1.21$), and 6 h ($M_n = 22\,100$; $PD = 1.20$) samples of polymerization.

In addition to the synthesis of homopolymers, the nanoprecipitation emulsion process has been extended to make specialty polymers. Various block copolymers have been synthesized using the SFRP nanoprecipitation emulsion process. Block copolymers were prepared by taking a latex prepared using nanoprecipitation emulsion (without the removal of residual monomer) and adding a second monomer to it. The reaction mixture was allowed to stir for 2 h to allow the latex particles to swell and then heated again at 135 °C. By GPC analysis, a distinct shift in the molecular weight distribution to a higher molecular weight was experienced (Figure 6). A list of some of the block

copolymers that have been synthesized using nanoprecipitation emulsion is outlined in Table I.

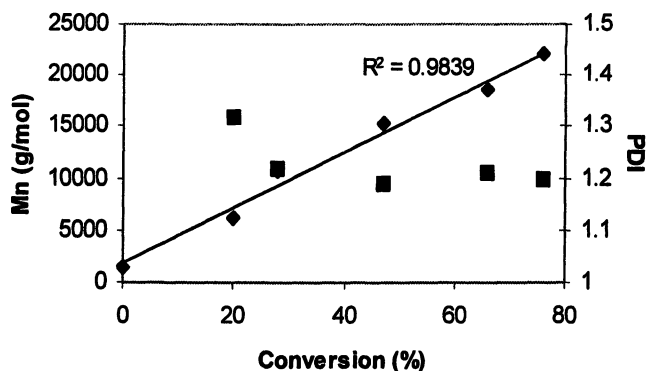


Figure 5: Number Average Molecular Weight vs Conversion Plot for the *n*-Butyl Acrylate Emulsion Polymerization Using a Nanoprecipitation Process.

Table I: Block Copolymer Synthesis Using Nanoprecipitation Emulsion Polymerization

| Polymer – A block | Final Mn | Polymer – B block | Final Mn |
|--------------------------|----------|-----------------------------------|----------|
| <i>n</i> -butyl acrylate | 19 000 | styrene | 31 900 |
| <i>n</i> -butyl acrylate | 24 100 | acetoxystyrene | 41 100 |
| <i>n</i> -butyl acrylate | 22 100 | styrene/ <i>t</i> -butyl acrylate | 44 600 |
| Styrene | 3 500 | acetoxystyrene | 20 400 |

More recently, we have been able to extend this technique to allow emulsion polymerization by both ATRP (20) and RAFT (21) polymerization techniques to take place using nanoprecipitation emulsion polymerization. Emulsion polymerization by both ATRP and RAFT polymerization systems using the nanoprecipitation process has required certain modifications to the overall process, since these systems do differ from that of SFRP.

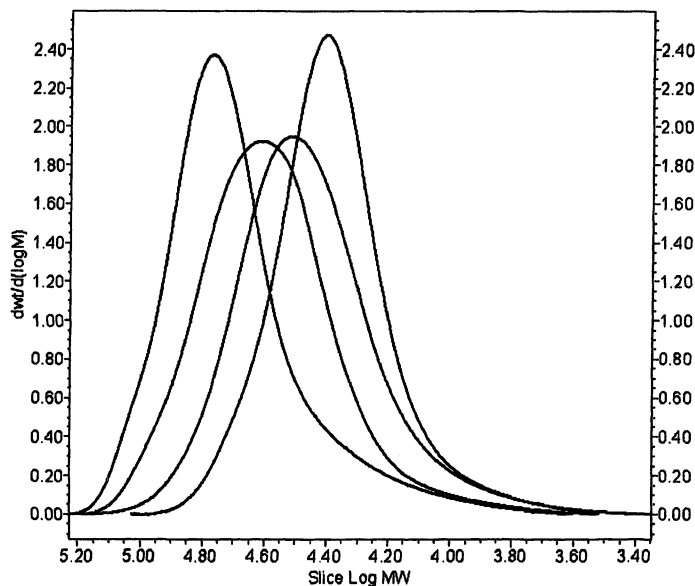


Figure 6: GPC MWD Plot for the SFRP Block Copolymer Synthesis Using a Nanoprecipitation Emulsion Process. The curve farthest to the right corresponds to the poly(*n*-butyl acrylate) starting block ($M_n = 22\ 100$; $PD = 1.20$), the remaining three curves (from right to left) correspond to the poly(*n*-butyl acrylate-*b*-poly(*t*-butyl acrylate-*r*-styrene) block copolymer: 1 h ($M_n = 29\ 200$; $PD = 1.26$), 3 h ($M_n = 34\ 900$; $PD = 1.28$), and 6 h ($M_n = 44\ 600$; $PD = 1.32$) samples of polymerization.

In conclusion, successful emulsion polymerizations using the SFRP process can be performed by using monomer-swollen preformed particles stabilized with a TEMPO-terminated polystyrene oligomer. One of the advantages of this system is the ease with which the particles can be prepared. There is no need for a high shear device as in the case of a miniemulsion polymerization and the product does not contain conventionally formed polymer, as was the case for the earlier seeded emulsion polymerizations. This process can be used to make both homopolymers and block copolymers using a SFRP emulsion process. Further, this process is robust, and has been extended to allow for emulsion polymerization to proceed using both ATRP and RAFT polymerization processes.

References and Notes

1. Solomon, D. H.; Rizzardo, E.; Cacioli, P. European Patent 135280, 1985. (b) Rizzardo, E. *Chem. Aust.*, **1987**, *54*, 32. (c) Georges, M. K.; Veregin, R. P. N.; Kazmaier, P. M.; Hamer, G. K. *Macromolecules*, **1993**, *26*, 2987. (d) Georges, M. K.; Veregin, R. P. N.; Kazmaier, P. M.; Hamer, G. K. *Trends Polym. Sci.*, **1994**, *2*, 66.
2. Wang, J. S.; Matyjaszewski, K. *J. Am. Chem. Soc.*, **1995**, *117*, 5614.
3. Chiefari, J.; Chong, Y. K.; Ercole, F.; Krstina, J.; Jeffery, J.; Le, T. P. T.; Mayadunne, R. T. A.; Meijs, G. F.; Moad, C. L.; Moad, G.; Rizzardo, E.; Thang, S. H. *Macromolecules*, **1998**, *31*, 5559.
4. (a) Qiu, J.; Charleux, B.; Matyjaszewski, K. *Prog. Polym. Sci.*, **2001**, *26*, 2083. (b) Cunningham, M. F. *Prog. Polym. Sci.*, **2002**, *27*, 1039.
5. (a) Bon, S. A. F.; Bosveld, M.; Klumperman, B.; German, A. L. *Macromolecules*, **1997**, *30*, 324. (b) Marestin, C.; Noël, C.; Guyot, A.; Claverie, J. *Macromolecules*, **1998**, *31*, 4041. (c) Uzulina, I.; Kanagasabapathy, S.; Claverie, J. *Macromol. Symp.*, **2000**, *150*, 33. (d) Monteiro, M. J.; Hodgson, M.; De Brouwer, H. *J. Polym. Sci. Part A: Polym. Chem.*, **2000**, *38*, 3864. (e) Cao, J.; He, J.; Li, C.; Yang, Y. *Polym. J.*, **2001**, *33*, 75.
6. (a) Prodpran, T.; Dimonie, V. L.; Sudol, E. D.; El-Aasser, M. S. *Polym. Mater. Sci. Eng.*, **1999**, *80*, 534. (b) MacLeod, P. J.; Keoshkerian, B.; Odell, P. G.; Georges, M. K. *Polym. Mater. Sci. Eng.*, **1999**, *80*, 539. (c) Lansalot, M.; Farcet, C.; Charleux, B.; Vairon, J. P.; Pirri, R.; Tordo, P. *ACS Symp. Series*, **2000**, 138-151. (d) Farcet, C.; Lansalot, M.; Charleux, B.; Pirri, R.; Vairon, J. P. *Macromolecules*, **2000**, *33*, 8559. (e) Pan, G.; Sudol, E. D.; Dimonie, V. L.; El-Aasser, M. S. *Macromolecules*, **2002**, *35*, 6915. (f) Cunningham, M. F.; Xie, M.; McAuley, K. B.; Keoshkerian, B.; Georges, M. K. *Macromolecules*, **2002**, *35*, 59.
7. Lovell, P. A.; El-Aasser, M. S. *Emulsion Polymerization and Emulsion Polymers*; John Wiley and Sons: New York, 1997; Chapter 2, pp. 42-43.
8. Mayo, F. R. *J. Am. Chem. Soc.*, **1968**, *90*, 1289; Chong, Y. K.; Rizzardo, E.; Solomon, D. H. *J. Am. Chem. Soc.*, **1983**, *105*, 7761.
9. Taylor, P. *Adv. Colloid Interface Sci.*, **1998**, *75*, 107.
10. Prescott, S. W.; Ballard, M. J.; Rizzardo, E.; Gilbert, R. G. *Macromolecules*, **2002**, *35*, 5417.

11. (a) Ferguson, C. J.; Hughes, R. J.; Pham, B. T. T.; Hawket, B. S.; Gilbert, R. G.; Serelis, A. K.; Such, C. H. *Macromolecules*, **2002**, *35*, 9243. (b) Ferguson, C. J.; Hughes, R. J.; Nguyen, D.; Pham, B. T. T.; Gilbert, R. G.; Serelis, A. K.; Such, C. H.; Hawket, B. S. *Macromolecules*, **2005**, *38*, 2191.
12. Nicolas, J.; Charleux, B.; Guerret, O.; Magnet, S. P. *Angew. Chem. Int. Ed.*, **2004**, *43(45)*, 6186.
13. Delaitre, G.; Nicolas, J.; Lefay, C.; Save, M.; Charleux, B. *Chem. Comm.* **2005**, *5*, 614.
14. Benoit, D.; Chaplinski, V.; Brauslau, R.; Hawker, C. J. *J. Am. Chem. Soc.*, **1999**, *121*, 3904.
15. We have performed hundreds of *ab initio* emulsion experiments that have resulted in emulsion failure. A more detailed discussion of these failures are found in reference 14.
16. Keoshkerian, B.; MacLeod, P. J.; Georges, M. K. *Macromolecules*, **2001**, *34*, 3594.
17. Szkurhan, A. R.; Georges, M. K. *Macromolecules*, **2004**, *37*, 4776.
18. Szkurhan, A. R.; Georges, M. K. Manuscript submitted for publication.
19. We are currently investigating the maximum monomer loading possible with this system, while still maintaining colloidal stability.
20. Chan Seng, D.; Georges, M. K. Manuscript submitted for publication.
21. Szkurhan, A. R.; Kasahara, T.; Georges, M. K. Manuscript submitted for publication.

Chapter 23

Crowded Phosphonylated Alkoxyamines with Low Dissociation Temperatures: A Milestone in Nitroxide-Mediated Polymerization

Florence Chauvin¹, Jean-Luc Couturier², Pierre-Emmanuel Dufils¹,
Pierre Gérard³, Didier Gimes^{1,*}, Olivier Guerret³,
Yohann Guillaneuf¹, Sylvain R. A. Marque^{1,*}, Denis Bertin^{1,*},
and Paul Tordo^{1,*}

¹UMR 6517 “Chimie, Biologie et Radicaux Libres” CNRS et Universités
d’Aix-Marseille 1, 2 et 3, Faculté des Sciences de Saint Jérôme, Av.
Escadrille Normandie-Niemen, Case 542, 13397 Marseille Cedex 20, France

²Centre de Recherche de Rhônes Alpes, Arkema, Rue Henri Moissan,
B.P. 63, 69493 Pierre Bénite, France

³Groupement de Recherche de Lacq, Arkema, B.P. 34, 64170 Lacq, France

*Corresponding authors: paul.tordo@univ-provence.fr; denis.bertin@univ-provence.fr; sylvain.marque@up.univ-mrs.fr; and gimes@srepir1.univ-mrs.fr

During the last decade, Nitroxide Mediated Polymerization emerged as a promising technique to prepare controlled/living polymers *via* free radical polymerization. However, its scope remained limited because of the restricted number of nitroxides and alkoxyamines exhibiting the required characteristics to exert an efficient control on radical polymerization of various monomers. The combination of tertiary alkyl radicals [(Me₂CY)’, Y = COOH, COOR, CN] with the *N-tert-butyl-N-(1-diethylphosphono-2,2-dimethylpropyl)* nitroxide, called SG1, led to an original series of alkoxyamines SG1-C(Y)Me₂, some of them being isolated as stable solids easy to handle and to store.

In solution, these alkoxyamines dissociate at room temperature, they exert an efficient control on the radical polymerization of various monomers and open up many new possibilities for the controlled synthesis of complex macromolecular architectures.

Introduction

The synthesis of precision-engineered polymers is an important aspect of polymer science since there is a growing demand for functionalized, well-defined materials to use as building blocks in many applications.⁽¹⁾ Until recently, efficient control on the structure and architecture of vinyl polymers could only be obtained through anionic or cationic polymerization techniques.^(2,3) However, not only these techniques are unsuitable for the polymerization of a wide range of functionalized vinylic monomers but they also require stringent reaction conditions such as the use of ultrapure reagents and the total exclusion of water and oxygen.⁽²⁾ Radical polymerization is widely used in the industry and in research laboratories for synthesizing a variety of polymeric materials and it may be considered as a mature technology with millions of tons of vinyl based homo- and co-polymers produced annually.⁽⁴⁾ However, for the preparation of well-defined macromolecules, free radical procedures have severe limitations, which are related to the propensity of the propagating free radical chain to undergo a variety of different termination reactions. Due to these uncontrolled termination reactions, the materials obtained are polydisperse and the control over macromolecular weight and architecture is very limited.⁽⁴⁾

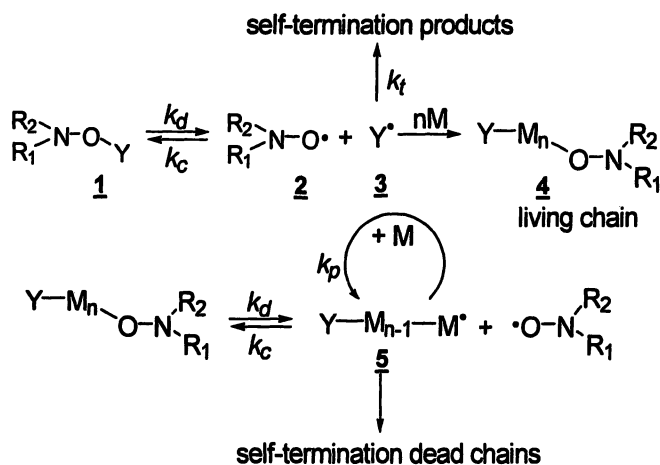
The widespread adoption of free radical polymerization is due to its synthetic ease, its versatility and compatibility with a wide variety of functional groups, and its tolerance to water and protic media. These advantages have motivated the efforts of synthetic polymer chemists to discover original free-radical polymerization procedures possessing the characteristics of a living process, and this field has witnessed explosive growth in recent years.

Three main procedures have emerged: Atom Transfer Radical Polymerization (ATRP), Reversible Addition Fragmentation/Transfer (RAFT) and Nitroxide Mediated radical Polymerization (NMP).⁽⁴⁾ Although each procedure has its advantages and disadvantages, NMP is potentially the simplest, since in most cases it requires only adding an appropriate alkoxyamine to the polymerization system.

NMP is based on the Persistent Radical Effect⁽⁵⁾ (PRE) and its principle is shown in Scheme 1. Nitroxide **2** and the propagating radical **3** are produced by

the reversible dissociation of alkoxyamine **1**. In the absence of a monomer M, the transient radicals **3** disappear by self-termination, whereas the stable nitroxide **2** does not self-terminate but disappears only by cross-reaction. Hence, every self-termination event of **3** causes a build-up of excess **2**, and this build-up continues as time proceeds. The permanently increasing concentration of **2** accelerates the cross-reaction at the expense of the self-termination, which becomes slower and slower with time. In the presence of a monomer M, the self-termination of polymeric radicals **5** is almost quenched by the excess of **2**. Hence, a majority of dormant living chains **4** can grow until the monomer is depleted, resulting in a polymer with large living character and small polydispersity index.⁽⁴⁻⁶⁾ However, this result will hold only under favorable kinetic circumstances. A complete kinetic modelling of NMP has been carried out, and the kinetic conditions required for a successful process have been established.⁽⁴⁻⁶⁾ These studies and various experimental results⁽⁷⁾ have pointed out the pivotal importance of the equilibrium constant $K = k_d/k_c$ for a successful NMP process.

Scheme 1

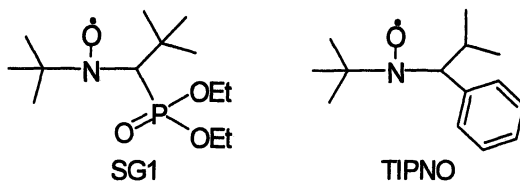


2,2,6,6-Tetramethyl-1-piperidinyloxy radical (TEMPO) was the first nitroxide to be used for NMP,⁽⁸⁾ however, its use remains limited to styrenic monomers. To overcome the TEMPO limitations, other types of nitroxides were designed,⁽⁹⁾ and the most significant breakthrough was the use of acyclic nitroxides in which one of the α -carbons bears a hydrogen atom, in contrast to the two quaternary α -carbons present in TEMPO and all the other nitroxides designed for NMP.⁽¹⁰⁾

We ⁽¹¹⁾ first introduced the [*N-tert*-butyl-*N*-(1-diethylphosphono-2,2-dimethylpropyl) nitroxide, called SG1] and the [*N-tert*-butyl-*N*-(1-phenyl-2-

methylethyl)nitroxide, called TIPNO(12)] (scheme 2), and we showed that they are better than TEMPO at controlling the polymerization of styrene.

Scheme 2



Later, Hawker and co-workers developed the use of TIPNO(13) and TIPNO – based alkoxyamines(14) and reported the successful controlled polymerization of various monomers. However, neither TIPNO nor its alkoxyamines allowed the controlled polymerization of methyl methacrylate (MMA), which represents a major challenge for NMP.(9-14) We(15) have developed the use of SG1 for NMP and we have recently discovered that crowded SG1 – based alkoxyamines, represent a new fascinating class of control agents for NMP. Some of these alkoxyamines are obtained as solids easy to handle and store and in solution their homolysis already occur at room temperature. Herein, we present the properties of these molecules and some of their applications for NMP and organic synthesis.

Experimental Section

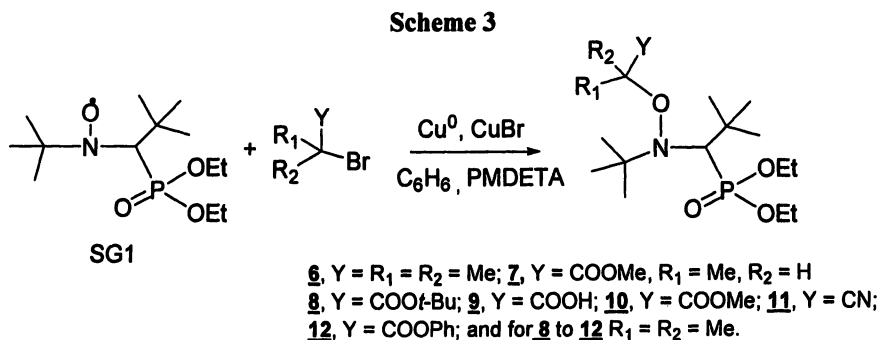
Solvents for synthesis, copper bromide, copper metal, triethylamine, 4-dimethylamino pyridine (DMAP), N,N,N',N',N''-pentamethyldiethylenetriamine (PMDETA) and 2-bromo-2-methyl propionic acid bromide, 2-bromo-2-methyl propionic acid were purchased from Aldrich and used as received. *tert*-Butylbenzene was purchased from Aldrich and purified by a conventional procedure.(16) Nitroxyl radical SG1 was kindly provided by ARKEMA. 2-Bromo-2-methyl propionic acid phenyl ester was prepared as described in the literature.(17) Alkoxyamines **6**, **7**, **9**, **10**, and **12** were prepared as described in reference (18), **8** as described in reference (19) and **11** as described in reference (20). For polymerization processes, monomer conversion was determined by ¹H NMR. Number average molecular weight (M_n) and polydispersity indexes (PDI) were determined by GPC (Waters 515 HPLC) using 3 “styragel” columns (HR 3, 4 and 5), UV/visible (Waters 486) and RI (Waters 2414) detectors. Measurements were performed in THF at room temperature with a 1 mL/min

flow and calibration based on polystyrene standards and Mark-Houwink parameters of analyzed polymers.

Results and Discussion

Synthesis of phosphonylated alkoxyamines **6-12**.

Alkoxyamines **7-12** were easily prepared from SG1 and the corresponding activated bromides (Scheme 3), in the presence of Cu(I) and a small amount of Cu(0).(21) Alkoxyamine **6** was prepared by reacting two equivalents of SG1 with one equivalent of *t*-BuBr Grignard reagent.(22) The yields after purification were in the range 30 to 70 % and all these alkoxyamines were isolated as solids (melting point values are listed in Table 1).



C-O Bond homolysis in phosphonylated alkoxyamines **6-12**.

The experimental rate constants k_d were measured using either the plateau of the increasing ESR nitroxide signal(23) or the decay of the ^{31}P NMR signal,(24) in the presence of TEMPO as an alkyl radical scavenger. For each alkoxyamine three runs were carried out in *tert*-butylbenzene as solvent. The average k_d values and the activation energies are reported in Table 1. The activation energies E_a were estimated using $A = 2.4 \cdot 10^{14} \text{ s}^{-1}$.(23,25,26) The estimated E_a values given in Table 1 correspond to E_a averaged over the investigated temperature range. Individual values differed by less than 2 kJ mol^{-1} from the average value presented in Table 1.

The activation energies for the dissociation of the C-O bond in alkoxyamines **8-12** are small and in solution the cleavage of these molecules

occurs at or close to room temperature. As expected due to steric congestion(23,25) the dissociation rate constants for **8-12** are much higher than that for **7** ($k_d[10]/k_d[7] \approx 266$), however, within the series **8**, **9**, **10** and **12**, the rate constant k_d does not increase monotonously with the size of the COOR group (R = *t*-Bu, H, Me, Ph). Thus, for **10** (R = Me), k_d is about three times higher than for **8** (R = *t*-Bu), and the highest k_d was observed for R = Ph.(27).

Table I. Rate constants at 120 °C and activation energies for the dissociation of the C-O bond for alkoxyamines **6-12.**

| Alkoxyamine | E_a (kJ·mol ⁻¹) ^a | k_d (120) (s ⁻¹) ^b | $t_{1/2}$ (30 °C) | T_c (°C) ^c | M_p (°C) |
|-----------------------|--|---|-------------------|-------------------------|------------|
| 6 | 139.7 | $6.5 \cdot 10^{-5}$ | 120 y | 95 | 58 |
| 7 ^d | 127.2/131 | $3.0 \cdot 10^{-3}/10^{-3}$ | 280 d / 3 y | 75 | 59 |
| 8 | 112.3 | 0.28 | 18 h | - | 45 |
| 9 | 111.7 | 0.34 | 15 h | 35 | 123 |
| 10 | 108.9 | 0.80 | 5 h | -(^e) | 57 |
| 11 | 107.3 | 1.31 | 2.5 h | -(^e) | 40 |
| 12 | 104.8 | 2.8 | 56 min. | -(^e) | 75 |

^a Average values estimated using a mean frequency factor A of $2.4 \cdot 10^{14} \text{ s}^{-1}$ as suggested in previous papers.(23, 25, 26)

^b Homolysis rate constant at 120 °C, in *t*-BuPh.

^c Temperature of cleavage estimated by ESR monitoring of the SG1 signal, as described in reference (15).

^d The two diastereoisomers exhibit different k_a .(23,24)

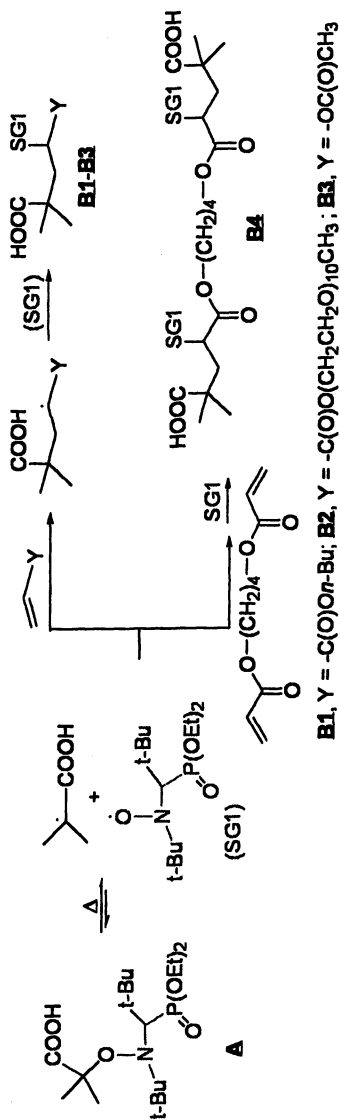
^e Close to room temperature.

Intermolecular radical addition of **9** onto alkenes to prepare new functional mono- and polyalkoxyamines.

Alkoxyamines have recently been used to carry out environmentally benign radical reactions.(28-30) The intermolecular radical addition of a starting alkoxyamine, **A**, onto an olefin is expected to yield a product alkoxyamine, **B**, (Scheme 4).

In order to circumvent the polymerization, the cleavage temperatures of the starting and product alkoxyamines have to be tuned carefully. Owing to their low cleavage temperatures our original series of crowded phosphonylated alkoxyamines were expected to lead to clean intermolecular radical addition onto various olefins. Preliminary results obtained during the addition of **9** onto *n*-

Scheme 4



butyl acrylate, poly(ethylene glycol)methyl ether acrylate, vinyl acetate and 1,4-butanediol diacrylate are described hereafter. For **B1** and **B2**, the reactions were performed in deoxygenated *t*-butanol solutions (1 M) at 80 °C for 6 hours with 1 equivalent of olefins. For **B3**, the reaction was conducted with a four-fold excess of vinyl acetate at 60 °C for 36 h.

B4 was prepared by reacting **9** (1.9 eq) with 1,4-butanediol diacrylate (1 eq), in refluxing ethanol (78 °C) for 20 h. When these reactions were monitored by ³¹P NMR, the decay of the signal of **9** was accompanied by the growth of a major peak, attributable to one diastereoisomer of the targeted compound. After work up, **B1**, **B2**, **B3** and **B4** were isolated in good to excellent yields (65 %, 80 %, 60 % and 94 % respectively).

Applications of **9** to NMP.

Polymerization of styrene.

Living polystyrenes with Mn up to 30 000 g mol⁻¹ and narrow polydispersity indexes can be easily obtained from bulk polymerizations of styrene conducted at 120-130 °C, and initiated with SG1 – based alkoxyamines, like **7** or SG1-CH(Me)Ph.^(12,15) However, when we tried to obtain controlled living polystyrenes with Mn close to 100 000 g mol⁻¹, we found that the Mn plateaued at 60000 g mol⁻¹,⁽¹⁵⁾ the isolated polystyrenes exhibiting a poor livingness and polydispersity indexes close to 1.7. These results can be accounted for by the contribution of the autopolymerization of styrene, which at 120-130 °C is expected to generate a significant amount of initiating radicals as the reaction time increases. Therefore, we reconsidered the bulk NMP of styrene at lower temperatures.

When **7** was used as initiator at 90 °C, a complete lack of control was observed (Fig. 1), although we showed that a majority (90 %) of polymer chains were living. At 90 °C, even if the PRE is working, the *k_d* value (1.2 10⁻⁵ s⁻¹) for **7** is too small to allow a linear evolution of molecular weight with conversion and a final polydispersity index close to one. However, when **9** (*k_d* = 2.0 10⁻² s⁻¹) was used as initiator, a linear evolution of Mn with conversion was observed (Fig. 1). After 31 h, at 57 % conversion, the isolated polystyrene exhibited a Mn of 9 850 (targeted Mn = 20 000 g mol⁻¹) and a polydispersity index of 1.

When a Mn of 100 000 g mol⁻¹ was targeted using **9** as initiator, at 79 % conversion (110 h), the Mn value was 73 500 g mol⁻¹ and the polydispersity index 1.15. To estimate the number of polystyrene chains end-capped with SG1, a sample of polystyrene in *t*-butyl benzene was heated at 120 °C, in the presence of an excess of dioxygen to scavenge the polymer radicals. The amount of

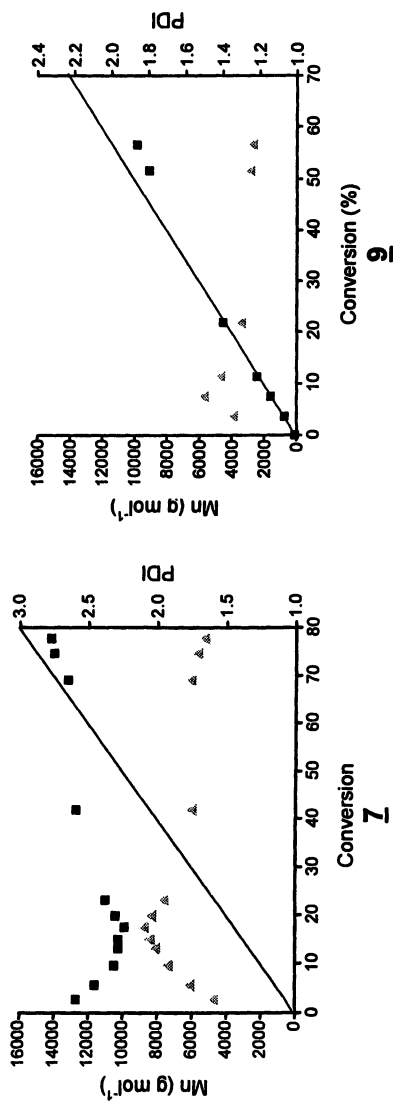


*Figure 1. Bulk polymerization of styrene at 90 °C, in the presence of **7** and **9** (■ : Mn, ▲ : PDI, straight line: theoretical Mn).*

released SG1 was monitored by Electron Paramagnetic Resonance, and indicated at least 95 % of living chains.(31,32)

The above results clearly show that during NMP initiated with alkoxyamines having a too low k_d , the control of the polymer chains cannot be obtained, although the PRE is operating and accounts for the formation of a substantial amount of living chains.

Polymerization of n-butyl acrylate.

In the experimental conditions used with styrene (bulk, 120°C), NMP of acrylic monomers are more difficult to control even if the involved macroalkoxyamines exhibit an appropriate K value ($K = 10^{-10}$ mol L⁻¹).⁽⁴⁾ Very fast polymerization rates were observed (ca. 90 % conversion in 1h), however, the control is poor leading to a polydispersity index higher than 2.0.⁽¹³⁾ In the case of *n*-butyl acrylate polymerization, a complete loss of control can occur, the reaction reaching an explosive regime.^(33,1) The different behaviour of acrylic monomers and styrene towards NMP can be accounted for by the large difference in their propagation rate constants ($k_p = 1.8 \cdot 10^3$ L mol⁻¹ s⁻¹ for styrene⁽³⁴⁾ and $k_p = 8.7 \cdot 10^4$ L mol⁻¹ s⁻¹ at 120°C for *n*-butyl acrylate⁽³⁵⁾) and its consequence on the contribution of the PRE. When the rate of polymerization is much higher than the dissociation rate of the initiating alkoxyamine, the PRE regime cannot be established and the control of the polymerization is poor although partial livingness could be observed.^(36,37) Different authors^(13, 38,39) have shown that a retarding initial addition of nitroxide can restore a good control during a small scale NMP of *n*-butyl acrylate, initiated with **7**. However, we observed that the optimum amount of additional free nitroxide is strongly dependent on the process (size of the reactor, temperature regulation, stirring ...) and it turned out that on a large scale this polymerization process could be very hazardous.

To circumvent the problem, we looked for an alkoxyamine with the appropriate k_d to force the existence of the PRE, even in the presence of a monomer with a large k_p . A kinetic modelling performed with the Predici software⁽⁴⁰⁾ showed that the polymerization should be controlled, as long as $k_p/k_d \leq 2 \cdot 10^6$ L mol⁻¹. Therefore, the polymerization of *n*-butyl acrylate initiated with any of the alkoxyamines **8** to **12** should be controlled. Indeed, the results of the bulk polymerization (at 120 °C) of *n*-butyl acrylate initiated with **9** were similar to those obtained when the polymerization was initiated with **7** in the presence of an additional amount of SG1 (2.5 %). A linear evolution of the

1. Grimaldi, S.; Finet, J.-P.; Le Moigne, F.; Zeghdaoui, A.; Tordo, P.; Benoit, D.; Fontanille, M.; Gnanou, Y. *Macromolecules* **2000**, *33*, 1141-1147.

molecular weight M_n with conversion was observed, the polydispersity index was close to 1.3 at complete conversion, and the living character of the final polymer allowed us to prepare a well-defined living poly-(*n*-butylacrylate)-*b*-polystyrene, PBA-*b*-PS-SG1, copolymer. Successful NMP initiated with **9** were also obtained for other alkyl acrylates ($R = C_{18-22}$, 2-ethylhexyl), and it should be mentioned that no thermal overheating was observed during these polymerizations(41).

Polymerization of Methyl Methacrylate (MMA).

Among the nitroxides designed for NMP, none was reported to control the radical polymerization of methacrylic esters. In the presence of nitroxide, the methacrylate monomer conversion was very low (less than 20 %) and no significant livingness was observed. The model alkoxyamines corresponding to the macroalkoxyamines which must be involved in NMP of MMA have been prepared for various nitroxide moieties.(7,10,15,23,42) For TEMPO- and SG1-based alkoxyamines (TEMPO-C(Me)₂CO₂Me and **10** respectively) k_d and k_c have been determined. According to the results of Fischer,(36) at 120 °C, the k_d and k_c values for TEMPO-C(Me)₂CO₂Me fit the kinetic conditions for the existence of a living and controlled MMA polymerization. However, Fischer(43) has shown that the thermal decomposition of TEMPO-C(Me)₂CO₂Me yields substantial amounts of alkenes and TEMPO-H, through non radical decay and radical cross-disproportionations. These reactions strongly alter the polymerization of MMA in the presence of TEMPO, and account for the low conversion and lack of control. Although these side reactions were shown to be negligible for **10**, at 120 °C its k_d (0.8 s⁻¹) and k_c ($\approx 1.2 \cdot 10^6$ L mol⁻¹ s⁻¹) values are far from fitting the kinetic conditions required for the existence of a living and controlled MMA polymerization. However, owing to their exceptionally low temperatures of dissociation, alkoxyamines **8-12** can be used over a large temperature range, and at a low temperature ($T \leq 60$ °C) their k_d and k_c values approach the kinetic conditions required for at least the existence of a partially living and controlled MMA polymerization.

Therefore, we carried out the bulk polymerization of MMA at 45 °C in the presence of **9** and 0.1 eq. of SG1. After 4 h, the monomer conversion was 66 % with a molecular weight of 27000 g.mol⁻¹ and a PDI of 1.6. In a second experiment the polymerization was quenched after 30 min, at 15 % conversion, and the polymer was purified by precipitation. Using the purified PMMA as macroinitiator and styrene (0.1 mole) as monomer, a block copolymerization was then carried out. After 3 hours at 120 °C, a “copolymer” characterized by a M_n close to 94 000 g mol⁻¹ and a polydispersity index close to 2.0 was obtained. Although size exclusion chromatography showed the presence of residual

PMMA homopolymer, this result indicates that the PMMA used as macroinitiator contained living chains (close to 20 %).

Although these preliminary results are encouraging, at 45 °C the rate constant of initiation with **9** ($k_d = 10^{-4} \text{ s}^{-1}$) and the rate constant for the scavenging of MMA polymer radicals with SG1 ($k_c = 2.5 \cdot 10^4 \text{ L mol}^{-1} \text{ s}^{-1}$)(44) are too small to obtain a completely controlled and living MMA polymerization. To improve the control, work is in progress to adjust the k_d and k_c values of the initiating and macro – alkoxyamines involved in the process.

Use of **9** for building complex macromolecular architectures.

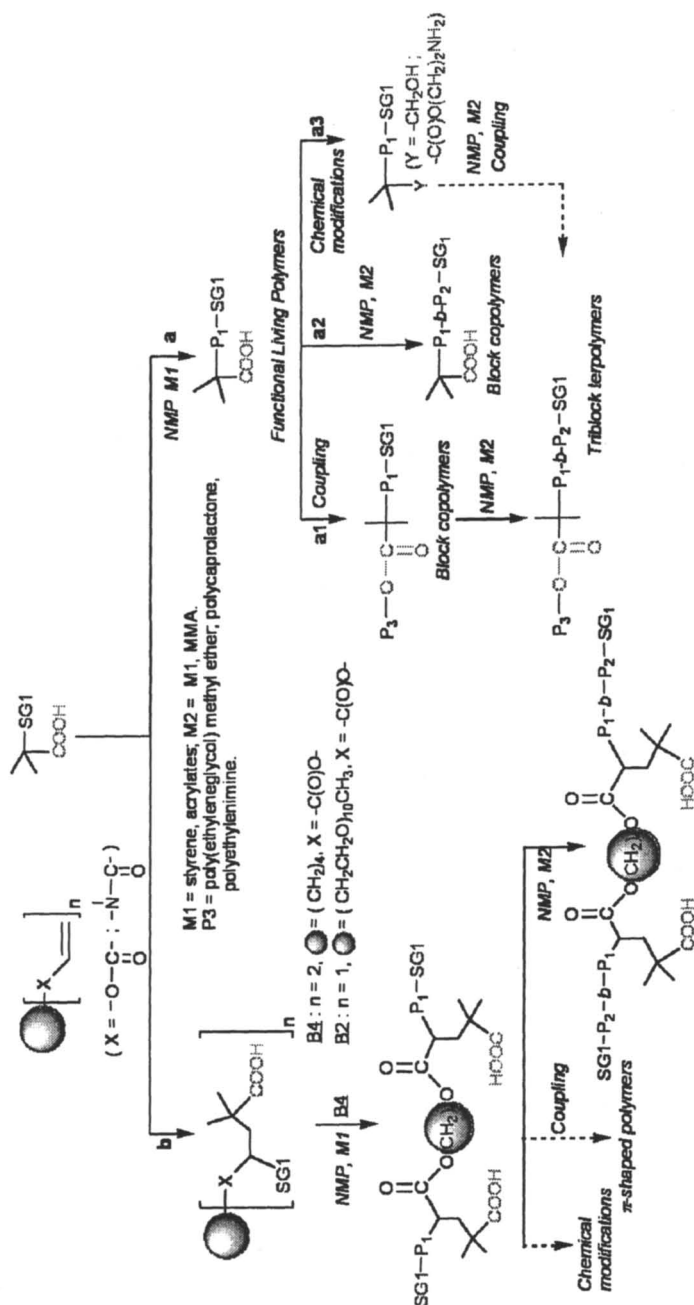
Engineering advanced materials displaying new or improved properties is a constant aim of many academic and industrial laboratories. A common feature of many of these materials is their well-defined nature: the number of functional groups, molecular weight, polydispersity index and absence or presence of branching are precisely controlled.(45) We have performed various experiments (scheme 5) which show that the use of alkoxyamine **9** can significantly expand the access to such precisely controlled macromolecular architectures.

In the presence of **9**, the NMP of various styrenics and acrylates yielded controlled living functional polymers HO(O)CCMe₂-P₁-SG1 (scheme 5, route a) with P₁= polystyrene, polyalkyacrylates. Well defined block copolymers such as PS-*b*-PBA and PBA-*b*-PS were prepared from these α,ω -functional living polymers (route a2). Hence, polymer chemists could once again focus their attention on such block copolymers, that could be used as “baroplastics”,(46) provided they are easy to synthesize.(47)

From HO(O)CCMe₂-P₁-SG1, whose α -carboxylic acid group can be transformed into other chemical groups, we prepared HOCH₂CM₂-PS-SG1 and H₂N(CH₂)₂O(O)CCMe₂-PS-SG1 (route a3). From HO(O)CCMe₂-P₁-SG1 polymers, coupling reactions involving the α -carboxylic acid group can lead to living block copolymers (route a1). Following route a1, we prepared the block PEO-*b*-PS-SG1, PCL-*b*-PS-SG1 and graft PEI-*g*-PS-SG1 copolymers. Owing to the living nature of the amphiphilic PEO-*b*-PS-SG1 copolymer, the Hydrophilic/Lipophilic Balance (HLB) can be easily tuned, either by adding a third block or by increasing the size of the polystyrene block. Thus, starting with an M_n of 12 000 g mol⁻¹ for the polystyrene block, we controlled the increase of M_n to 33 000 g mol⁻¹.

As described in a previous section, various functional mono- and poly-alkoxyamines can be prepared by the intermolecular radical addition of **9** onto alkenes (route b). The coupling of poly(ethylene glycol) methyl ether with **B2**

Scheme 5



introduced a second PEO chain to form a (PEO)₂-SG1 2-miktoarm living homopolymer, from which an amphiphilic 3-miktoarm star copolymer, (PEO)₂-*b*-PS-SG1, was easily obtained.

The polymerization of *n*-butyl acrylate, carried out with **B4** as initiator, led to PBA polymer chains with both ends capped with SG1. Then, a block copolymerization was carried out with MMA, leading to a γ functional triblock copolymer. As shown on Scheme 5, these (co)polymers could be used as intermediates to prepare various complex architectures like π -shaped (co, ter)polymers ((AB)(AB) or (ABC)(ABC)).

The above examples clearly show, that the outstanding properties of **9** and its derivatives or analogs open up new possibilities for the controlled synthesis of complex macromolecular architectures.

Acknowledgments

The financial support of Arkema, CNRS and University of Provence is greatly acknowledged.

References

1. *Handbook of Radical Polymerization*, (Eds.: K. Matyjaszewski, T. P. Davis), Wiley-Interscience, 2002.
2. Hsieh, H. L.; Quirk, R. P. *Anionic Polymerization*, Marcel Dekker, New York, 1996.
3. Matyjaszewski, K. *Cationic Polymerization*, Marcel Dekker, New York, 1996.
4. *Advances in Controlled/Living Radical Polymerization*, (Eds.: K. Matyjaszewski) ACS Symposium Series, American Chemical Society, Boston, 2003, vol. 854.
5. Fischer, H. *Chem. Rev.* 2001, 101, 3581-3610.
6. Fischer, H.; Souaille, M. *Chimia* 2001, 55, 109-113.
7. Ananchenko, G. S.; Souaille, M.; Fischer, H.; Le Mercier, C.; Tordo, P. *J. Polym. Sci.: Part A: Polym. Chem.* 2002, 40, 3264-3283.
8. Georges, M. K.; Veregin, R. P. N.; Kazmaier, P. M.; Hamer, G. K. *Macromolecules* 1993, 26, 2987-2988.
9. Knoop, C.; Studer, A. *J. Am. Chem. Soc.* 2003, 125, 16327-16333.
10. Benoit, D.; Grimaldi, S.; Finet, J.-P.; Tordo, P.; Fontanille, M.; Gnanou, Y. *ACS Symposium Series* 1998, 685, 225-.
11. Finet, J.-P. Lemoigne, F.; Gnanou, Y.; Nicol, P.; Grimaldi, S.; Plechot, N.; Tordo, P. Patent n° EP0832902

12. Le Mercier, C.; Lutz, J.-F.; Marque, S.; Le Moigne, F.; Tordo, P.; Lacroix-Desmazes, P.; Boutevin, B.; Couturier, J.-L.; Guerret, O.; Martschke, R.; Sobek, J.; Fischer, H. *ACS Symposium Series* **2000**, *768*, 108-122.
13. Benoit, D.; Chaplinski, V.; Braslau, R.; Hawker, C. J. *J. Am. Chem. Soc.* **1999**, *121*, 3904-3920.
14. Harth, E.; van Horn, B.; Hawker, C. J. *J. Chem. Soc., Chem. Commun.* **2001**, 823-824.
15. Le Mercier, C.; Acerbis, S.; Bertin, D.; Chauvin, F.; Gignes, D.; Guerret, O.; Lansalot, M.; Marque, S.; Le Moigne, F.; Fischer, H.; Tordo, P. *Macromol. Symp.* **2002**, *182*, 225-247.
16. Armarego, W. L. F.; Chai, C. C. L. *In Purification of Laboratory Chemicals, 5th Ed.*, Butterworth Heinemann: Amsterdam, **2003**.
17. Moriwake, T. *J. Org. Chem.* **1966**, *31*, 983-985.
18. Bertin, D.; Gignes, D.; Le Mercier, C.; Marque, S. R. A.; Tordo, P. *J. Org. Chem.* **2004**, *69*, 4925-4930.
19. Ananchenko, G. S.; Marque, S.; Gignes, D.; Bertin, D.; Tordo, P. *Org. Biomol. Chem.* **2004**, *2*, 709-714.
20. Beaudoin, E.; Bertin, D.; Gignes, D.; Marque, S. R. A.; Siri, D.; Tordo, P.; *Eur. J. Org. Chem.* **2006**, in press
21. Matyjaszewski, K.; Woodworth, B. E.; Zhang, X.; Gaynor, S.; Metzner, Z. *Macromolecules* **1998**, *31*, 5955-5957.
22. Nagashima, T.; Curran, D. P. *Synlett* **1996**, 330-332.
23. Marque, S.; Le Mercier, C.; Tordo, P.; Fischer, H. *Macromolecules* **2000**, *33*, 4403-4410.
24. Bertin, D.; Gignes, D.; Marque, S.; Tordo, P. *e-Polymers* **2003**, paper 2.
25. Marque, S.; Fischer, H.; Baier, E.; Studer, A. *J. Org. Chem.* **2001**, *66*, 1146-1156.
26. Marque, S.; Sobek, J.; Fischer, H.; Kramer, A.; Nesvadba, P.; Wunderlich, W. *Macromolecules* **2003**, *36*, 3440-3442.
27. Bertin, D.; Gignes, D.; Marque, S.; Maurin, R.; Tordo, P. *J. Polym. Sci. Part A: Polym. Chem.* **2004**, *42*, 3504-3515.
28. Leroi, C.; Bertin, D.; Dufils, P.-E.; Gignes, D.; Marque, S.; Tordo, P.; Couturier, J.-L.; Guerret, O.; Ciufolini, M. A. *Org. Lett.* **2003**, *26*, 4943-4945.
29. Allen, A. D.; Fenwick, M. H.; Henry-Riyad, H.; Tidwell, T. T. *J. Org. Chem.* **2001**, *66*, 5759-5765.
30. Wetter, C.; Jantos, K.; Woithe, K.; Studer, A. *Org. Lett.* **2003**, *5*, 2899-2902.
31. Bertin, D.; Chauvin, F.; Marque, S.; Tordo, P. *Macromolecules* **2002**, *35*, 3790-3791.
32. Guerret, O.; Couturier, J.-L.; Chauvin, F.; El-Bouazzy, H.; Bertin, D.; Gignes, D.; Marque, S.; Fischer, A.; Tordo, P. *ACS Symposium Series* **2003**, *854*, 412-423.

33. Benoit, D.; Grimaldi, S.; Robin, S.; Finet, J.-P.; Tordo, P.; Gnanou, Y. *J. Am. Chem. Soc.* **2000**, *122*, 5929-5939.
34. Buback, M.; Gilbert, R. G.; Hutchinson, R. A.; Klumpermann, B.; Kuchta, F. D.; Manders, B. G.; O'Driscoll, K. F.; Russel, G. T.; Schweer, J. *Macromol. Chem. Phys.* **1995**, *196*, 3267-3280.
35. Asua, J. M.; Beuermann, S.; Buback, M.; Castignolles, P.; Charleux, B.; Gilbert, B. G.; Hutchinson, R. A.; Leiza, J. R.; Nikitin, A.; Vairon, J. P.; Van Herk, A. M. *Macromol. Chem. Phys.* **2004**, *205*, 2151.
36. Souaille, M.; Fischer, H. *Macromolecules* **2000**, *33*, 7378-7394.
37. Souaille, M.; Fischer, H. *Macromolecules* **2002**, *35*, 248-261.
38. Chauvin, F.; Alb, A. M.; Bertin, D.; Tordo, P.; Reed, W. F. *Macromol. Chem. Phys.* **2002**, 2029-2041.
39. Lacroix-Desmazes, P.; Lutz, J.F.; Chauvin, F.; Severac, R.; Boutevin *Macromolecules* **2001**, *34*, 8866-8871
40. Wulkow, M. PREDICI Software, CiT GmbH.
41. Gigmes, D.; Marque, S.; Guerret, O.; Couturier, J.-L.; Chauvin, F.; Dufils, P.-E.; Bertin, D.; Tordo, P. Patent n° FR2843394, **2004**, WO 2004014926.
42. Ananchenko, G. S.; Marque, S.; Gigmes, D.; Bertin, D.; Tordo, P. *Org. Biomol. Chem.* **2004**, *2*, 709-714.
43. Ananchenko, G. S.; Fischer, H. *J. Polym. Sci.: Part A: Polym. Chem.* **2001**, *39*, 3604-3621.
44. Fischer, H. private communication.
45. Fréchet, J. M. J. *Science* **1994**, *263*, 1710-1715.
46. Gonzales-Leon, J. A.; Acar, M. H.; Ryu, S. W.; Ruzette, A. V.; Mayes, A. *Nature* **2003**, *426*, 424-428.
47. Borman, S. *Chemical & Engineering News* **2003**, *81*, 6.

Chapter 24

Reactive Block Copolymers as Versatile Compatibilizers

Leticia Flores-Santos¹, Alfonso González-Montiel¹,
and Enrique Saldívar-Guerra²

¹CID, Centro de Investigación y Desarrollo Tecnológico, S. A. de C.V.,
Av. de los Sauces No 87 Mz 6, Parque Industrial Lerma, Lerma,
Edo. Mexico, CP 52000, México

²Centro de Investigación en Química Aplicada, Blvd. Enrique Reyna 140,
Saltillo, Coahuila 25100, México

A series of block copolymers synthesized via CRP containing epoxy functional groups are used as compatibilizers for a variety of polymer blends. The CRP technique allows fine tuning of the architecture, molecular weight of reactive and non reactive block, the amount of functional groups and the composition of the non reactive block in order to obtain an optimal compatibility between two non miscible polymers. A selection based on the performance of these copolymers as compatibilizers in polycarbonate and polyethylene terephthalate blends will be addressed and a correlation of the average particle size observed in optical or transmission electron microscopy with the intrinsic variables of the compatibilizer (M_n , composition, etc.) is also discussed.

The blending of polymers provides a powerful route for obtaining materials with improved property/cost performance. Since most blended polymers are immiscible, compatibilization is required to obtain maximum synergy. This strategy is usually more cost effective and less time-consuming than the development of new monomers and/or new polymerization routes, as the basis for entirely new polymeric materials. An additional advantage of polymer blends is that a wide range of material properties is within reach by merely changing the blend composition (1).

Compatibilization of polymer blends can be achieved using specialized additives which are typically macromolecular species exhibiting interfacial activity in heterogeneous polymer blends (2, 3). Usually the compatibilizers are copolymers with a block or graft structure with one constitutive block/graft miscible with one blend component and a second block/backbone miscible with the other blend component. Other option for compatibilization is the addition of a reactive polymer, miscible with one blend component and reactive towards functional groups attached to the second blend component, which results in the *in-situ* formation of block or grafted copolymers. This technique has certain advantages over the addition of pre-made block or grafted copolymers. Usually reactive polymers can be generated by free radical copolymerization or by melt grafting of reactive groups onto a polymer backbone. Furthermore, reactive polymers only generate block or grafted copolymers at the site where they are needed, i.e. at the interface of an immiscible polymer blend.

By the early 1970's compatibilizers based on maleated polypropylene were available for the manufacture of polyolefin based composite materials. The maleic anhydride domain of these compatibilizers can react with nucleophilic groups in polyamides, polyesters and polycarbonates, and with amino silanes (4). The maleic anhydride graft occurs naturally on the ends of the polypropylene chain, obtaining a non-random structure. Attempts to apply the analogous solution to styrenic systems of blends have been without success, mainly because the architecture of the compatibilizers is random, there are no separate domains, and therefore, there is no domain that is compatible with the polystyrenic phase of the blends. As a result, the required improvement in the physical properties of the blends is not achieved, and, indeed, sometimes there is even a degradation of physical properties compared to the same alloy without the proposed compatibilizer (5, 6, 7).

Block Copolymers as Compatibilizers

In order to obtain well defined block copolymers to be used as compatibilizers, several approaches can be taken; one of them is the use of living polymerization processes (8). In living polymerization processes, termination reactions are suppressed or significantly reduced, allowing the formation of

block copolymers. It is possible to produce block copolymers by anionic polymerization. However due to the sensitivity of the process to impurities such as water and its intolerance of many functional groups, the process presents limitations. A more promising technique for producing block copolymers with a large variety of monomers is that based on living or quasi-living free radical polymerization (9). This can be achieved by adding to an otherwise standard free radical polymerization recipe, a chemical agent that significantly reduces the extent of irreversible termination or chain transfer reactions, providing a living or quasi-living character to the polymerization, which is also called "controlled polymerization" or "controlled free radical polymerization" (CRP) (10). There are several chemical routes for CRP polymerizations but most of them are limited in an industrial practice because they require chemical agents that are not readily commercially available in the market. Among these techniques, one that is particularly useful, and for which the required chemical agents are available in the market, is a quasi-living free radical polymerization controlled by nitroxides (nitroxide mediated radical polymerization, NMP), and derivatives thereof (like alkoxyamines (11)), which act as stable free radicals capping polymeric growing radicals and uncapping them in a fast and reversible way, allowing for short periods of propagation through monomer-addition steps (12-29).

Compatibilizers Design

Compatibilizers presented in this work were designed as block copolymers with functional groups for *in-situ* compatibilization. In this way a variety of monomers can be incorporated, obtaining a controlled microstructure and composition. These diblocks (shown in figure 1) have one block miscible with one component of the polymer blend, and another block that contains functional molecules like anhydride, epoxy or acid, which can react with a variety of polymers .

CRP allows control over the molecular weight of both blocks and over the degree of functionality in the second block. The advantages of this strategy are that functionality is obtained where it is needed and that molecules can be designed to have a variable degree of functionality to match different applications. These advantages are supposed to render compatibilizers superior to other molecules containing functional groups that are random copolymers or are produced via reactive extrusion.

The functional copolymers obtained via CRP can be used as compatibilizers for several polymer systems, examples are: polystyrene, high impact polystyrene and polystyrene compatible polymers (polyphenylene oxide) with glass fiber and polar fillers. They can also compatibilize blends of styrene, high impact polystyrene or styrenic copolymers (ABS, SAN, St-co-MMA, etc.) with polycarbonates and polyamides to name a few.

and total are experimentally determined whereas M_n of the second block is calculated as the difference between M_n of the diblock minus M_n of the first block.

Compatibilizers Synthesis.

The synthesis of the compatibilizers proceeded in two steps. First a reactive block copolymer was synthesized using either NMP regulators in a bulk-batch process at temperatures between 120-150°C. The monomers ratio and the controlling agent concentration were determined by the amount of epoxy groups desired in each diblock, and the desired molecular weight. In the case of 4-hydroxy TEMPO, BPO was used as an initiator at a constant ratio ([4-hydroxy TEMPO]/[BPO]=1.3:1. The resulting polymer of the first block was dissolved in the monomers used for the second block. The second block was synthesized in the same bulk-batch process at the same temperature range to reach a final conversion according to the desired molecular weight of the diblock. The general structure of the reactive copolymer is depicted in Figure 1. The copolymer is composed of a reactive block with epoxy functionality and a block that is typically a homopolymer.

Blending conditions.

PET and PC were dried overnight in a vacuum oven at 65 °C and 100°C respectively, prior to processing them. PET/PSt-*co*-MMA blends were prepared by direct melt blending of the compatibilizer and the polymers in a HAAKE mixer at 150°C and 60rpm. PC/compatibilizers and PC/PSt blends were also prepared by direct melt blending in a HAAKE mixer at 270°C and 60 rpm.

Microscopy.

Specimens for microscopy were prepared by trimming samples with a razor blade to form blocks of approximately 5 x 5 x 2 mm. These blocks were further trimmed to the shape of a truncated pyramid. An RMC MT-X ultramicrotome was used to obtain thin sections (50 nm thick) from these blocks. Sections were analyzed in an OLYMPUS M50 optical microscope in the case of large size particles or with a JEOL TEM microscope operating at 120 kV. Phase contrast between the different components of the blend was achieved by staining with Ruthenium oxide to distinguish the styrenic phase.

Results and Discussion

In this work, two polymer blends will be discussed: PET/PSt-*co*-MMA and PC/PSt. The compatibilizers are diblock copolymers with one functional block, capable of reacting with PET or PC and a second block miscible with St-MMA or PSt. Table 1 depicts the variety of compatibilizers with different molecular weights at the first and the second block and also with different amounts of epoxy groups used as compatibilizers. For both blends, the resulting average particle size of the dispersed phase is discussed in terms of the compatibilizers structure.

Table I. Compatibilizers of the general structure presented in figure 1. Functional groups refers to the number of epoxy molecules in block one.

| <i>Compatibilizer ID</i> | <i>First Block Mn</i> | <i>First Block PDI</i> | <i>Epoxy Groups</i> | <i>Diblock Mn</i> | <i>Diblock PDI</i> |
|--------------------------|-----------------------|------------------------|---------------------|-------------------|--------------------|
| 1 | 7826 | 1.13 | 11 | 16782 | 1.20 |
| 2 | 15269 | 1.10 | 2 | 50648 | 1.50 |
| 3 | 15965 | 1.13 | 10 | 25329 | 1.21 |
| 4 | 20212 | 1.12 | 21 | 92618 | 1.54 |
| 5 | 23156 | 1.17 | 24 | 91460 | 1.41 |
| 6 | 24144 | 1.14 | 28 | 67697 | 1.55 |
| 7 | 27526 | 1.19 | 34 | 49768 | 1.50 |
| 9 | 27682 | 1.10 | 9 | 93273 | 1.54 |

PET/PSt-*co*-MMA blends.

Blends were prepared (according to the experimental procedure) in a 80/20/3 weight ratio of amorphous PET, St-MMA and compatibilizer. Figure 2 shows photomicrographs of the resulting blends. It is possible to observe that the non compatibilized blend has particles whose mean diameter is of 1630nm, while using different compatibilizers, particle sizes can be reduced to 1010nm and down to 347 nm depending on the compatibilizers structure.

Since the structure and composition of the compatibilizers can be controlled, relations between the compatibilizers properties and their performance, seen through particle size in this case, can be found. In the group of graphs shown in Figure 3, the effect of the molecular weight of the functional block and the nonfunctional block, and the number of functional molecules on the particle-size can be analyzed. In Figure 3A, it can be observed that there is no apparent relationship between the molecular weight of the functional block

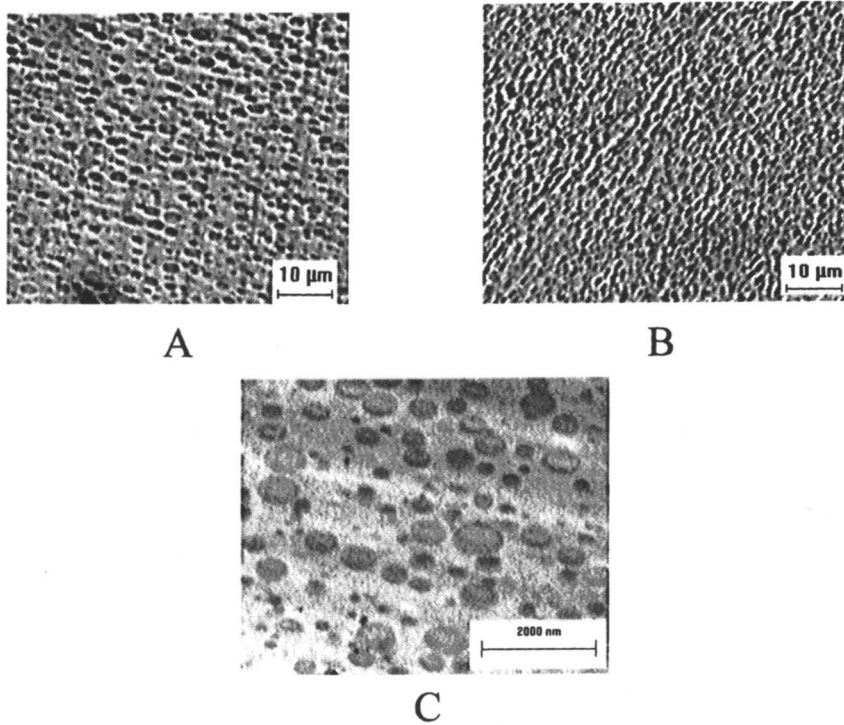


Figure 2. Three examples of PET/St-co-MMA blends. *A.* Optical microscopy photograph of the non compatibilized blend showing particles with a mean diameter of 1630nm; *B.* Optical microscopy photograph of a compatibilized blend showing particles with a mean diameter of 1010nm; *C.* TEM photograph of a compatibilized blend showing particles with a mean diameter=347nm.

and the particle size of PSt-co-MMA. Figure 3B shows that two of the three best blends have a low molecular weight of the nonfunctional block while one has a relatively high molecular weight, so a low molecular weight in this particular block might help to obtain smaller particle sizes. Finally, the number of functional groups in the compatibilizer is the key to obtaining small particles. Figure 3C shows that the three best compatibilizers have an average number of epoxy groups per chain of about ten. This number of epoxy groups seems to be the ideal number for the specified blend.

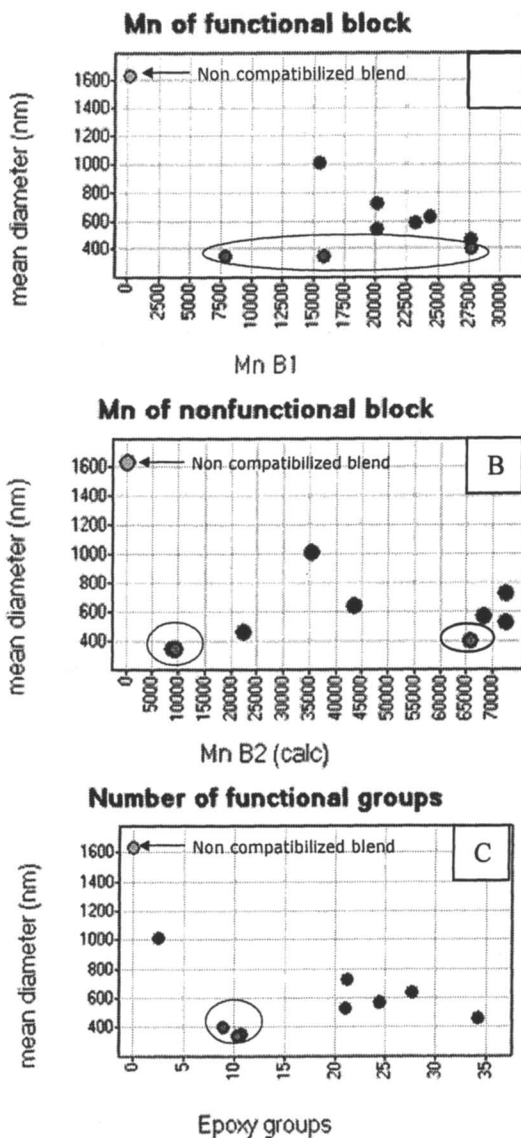


Figure 3. Graphs showing the influence of the number average molecular weight of the functional block (A), the number average molecular weight of the nonfunctional block (B) and the number of functional groups (C) on the mean diameter of PSSt-co-MMA particles observed in optical microscopy or TEM of PET/PSSt-co-MMA blends. The best three blends (the ones with smaller particle size) are grouped in an oval.

It is generally recognized that in ternary blends of two homopolymers (A and B) with a copolymer A-B the molecular weight of the copolymer blocks should be higher than the molecular weights of the corresponding homopolymers, so as to maximize segmental repulsion between the individual blocks compared with the parent homopolymers (1). It has also been reported that the emulsifying effect of a block copolymer in such blends increases as the molecular weight of the copolymer increases up to a certain point where the tendency seems to reverse. This is understood by considering the possibility of micelle formation as the copolymer molecular weight increases leading to a three state equilibrium among copolymer chains adsorbed at the interface, chains homogeneously mixed in the bulk phases and copolymers at micelles within the bulk phases (31).

However, the results in Figure 3B point out that two of the best dispersions are achieved when the molecular weight of the nonfunctional block is in the low range. These observations can be explained if we consider the case where the blocks of the copolymer are chemically different from but miscible with the corresponding homopolymers. In this particular case exothermic interactions may develop and provide additional driving force for the block to be anchored into the parent miscible homopolymer. Then strong interface adhesion can be promoted independently of the relative molecular weight of the block/homopolymer pairs (1,32). Therefore, it seems that for the PSt-co-MMA/PET system a low molecular weight in the polystyrene block (nonfunctional block) of the compatibilizer helps to localize the copolymer at the interface. Similar observations have been reported in a ternary A/B/C-D system where the homopolymer pair of PPO and Phenoxy have been compatibilized with a PS-*b*-PMMA copolymer (33). In that particular case the molecular weight of the PMMA block needed to be twice as short as the Phenoxy homopolymer to localize the copolymer at the interface.

In a second set of blends, the influence of the amount of compatibilizer in the blend is studied, using one of the compatibilizers detected as optimum in the 80/20/3 (PET/PSt-*co*-MMA/compatibilizer) blends. In this second set, a fixed ratio of PET/St-*co*-MMA of 80/20 was used and different amounts of the compatibilizer, from 0.5 to 5 were evaluated.

Figure 4 shows the results of varying the amount of the compatibilizer. It is apparent from this figure that by increasing the amount of compatibilizer a smaller average diameter of PSt-*co*-MMA in the blends is obtained. For this blend, the use of 5 wt% of compatibilizer leads to a broad distribution of particle sizes, having very small particles together with large ones, therefore, these results point out that it is better to use 3 wt% of the compatibilizer to obtain a more homogeneous distribution of particle sizes (see Figure 2C).

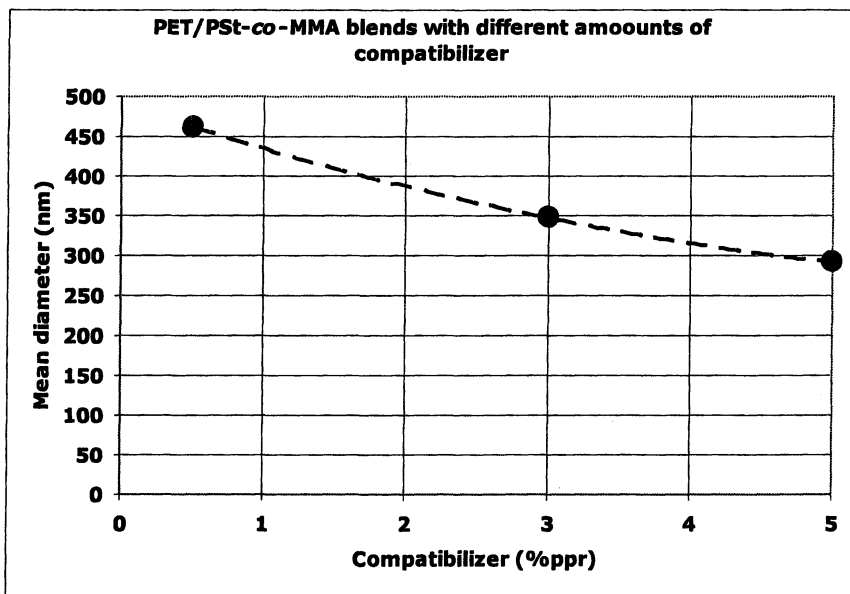


Figure 4. Influence of the amount of compatibilizer in the particle size of PSt-co-MMA in PET/ PSt-co-MMA blends.

Polycarbonate/Polystyrene blends.

In contrast with the approach taken with PET/pSt-co-MMA, in this case the dispersion of the compatibilizer in polycarbonate was studied first. Polycarbonate and compatibilizers were mixed in a 70/30 weight ratio and the samples were analyzed using optical or transmission electron microscopy.

Figure 5 shows optical microscopy photographs and TEM photographs of three blends. These images show how particle sizes vary from 19 micrometers down to 136 nm, depending on the structure and composition of the compatibilizer. All of the compatibilizers are diblock copolymers containing epoxy as the functional group in the reactive block. But the presence of blocks and adequate reactive groups (epoxy) does not guarantee a good interaction between the compatibilizers and polycarbonate. Since composition and molecular weight of the compatibilizers can be controlled and modified, the relationship between the compatibilizer and its dispersion in polycarbonate can be studied.

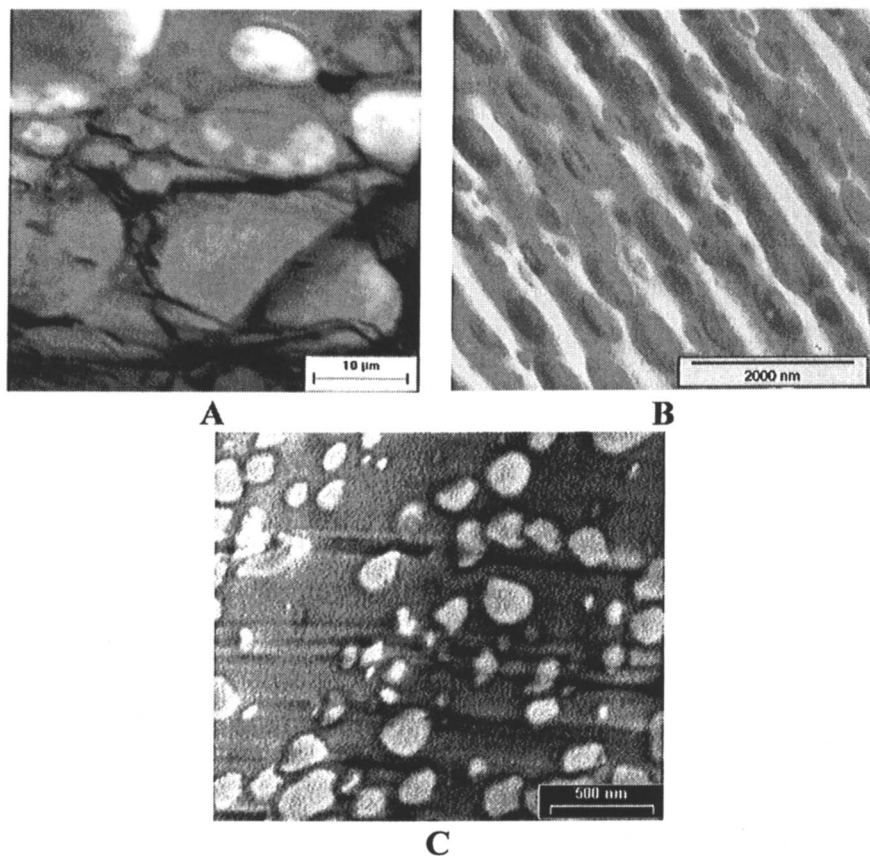


Figure 5. Three examples of PC/compatibilizers blends. *A.* Optical microscopy photograph showing particles with a mean diameter of 19 μm; *B.* TEM photograph showing particles with a mean diameter of 528 nm; *C.* TEM photograph showing particles with a mean diameter = 136 nm.

If we analyze Figures 6A and 6B, which show the effect of the molecular weight of the reactive and non reactive block, we observe that the compatibilizer with the worst performance is the one that combines a low molecular weight in both blocks. Analyzing the effect of the number of functional groups of the compatibilizer on its dispersion (Figure 6D), we observe that an increase in the amount of epoxy groups favors the dispersion of the compatibilizer in polycarbonate.

Two of the compatibilizers showing the best dispersions in PC were evaluated in PC-PSt blends at different PC/PSt ratios and maintaining constant the amount of compatibilizer: 60/40/1.5, 75/25/1.5 and 90/10/1.5.

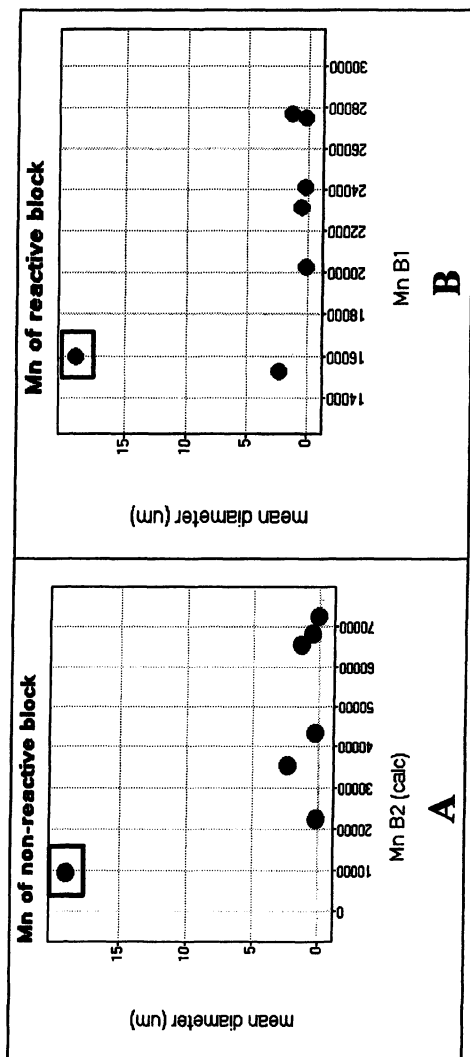
In the case of the uncompatibilized 60/40 blend, we observe a phase morphology in the co-continuity region, but when compatibilizer B is added, we get a good dispersion, obtaining an average particle size of 2.5 micrometers (see figure 7). Decreasing the amount of polystyrene in the blends, diminishes the polystyrene particle size, so, in the case of the 90/10 blend, the uncompatibilized blend shows an average particle size of 0.43, while the compatibilized blend allows us to obtain an average particle size of 330 nanometers. Overall the presence of both compatibilizers seems to reduce the interfacial tension of the system and help the dispersion of PSt domains.

Conclusions

Reactive block copolymers can be effectively synthesized by CRP (controlled radical polymerization) technologies. The reactive block copolymers act as compatibilizers for PET/PSt-co-MMA and PC/PSt polymer blends. Since CRP allows a control of the molecular weight of both blocks in the copolymer and of the amount of functional groups in the compatibilizers, the influence of these variables on the dispersion of the components of the blend could be analyzed and optimum compatibilizers were found. The technology is very cost effective and will lead to commercial compatibilizers based on the novel block copolymers

References

1. Koning, C.; Van Duin, M.; Pangoulle, C.; Jérôme, R. *Prog. Polym. Sci.* **1998**, *23*, 707-757.
2. Utracki, L.A. *Polymer Blends Handbook*; Kluwer Academic Publishers, **2002**, 295-414.



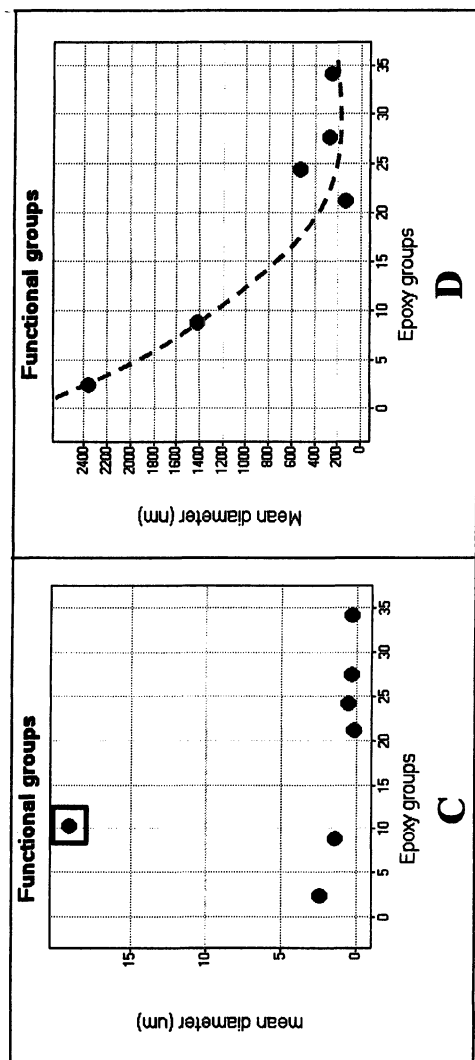


Figure 6. Graphs showing the influence of the number averagemolecular weight of the non-reactive block (A), the number averaged molecular weight of the reactive block (B) and the number of functional groups (C, D) on the mean diameter of particles observed in optical microscopy or TEM of PC/compatibilizer blends. Figure D is an amplification of figure C, eliminating the result obtained with the worst blend. The worst blend (having the largest average particle size) is shown in a square.

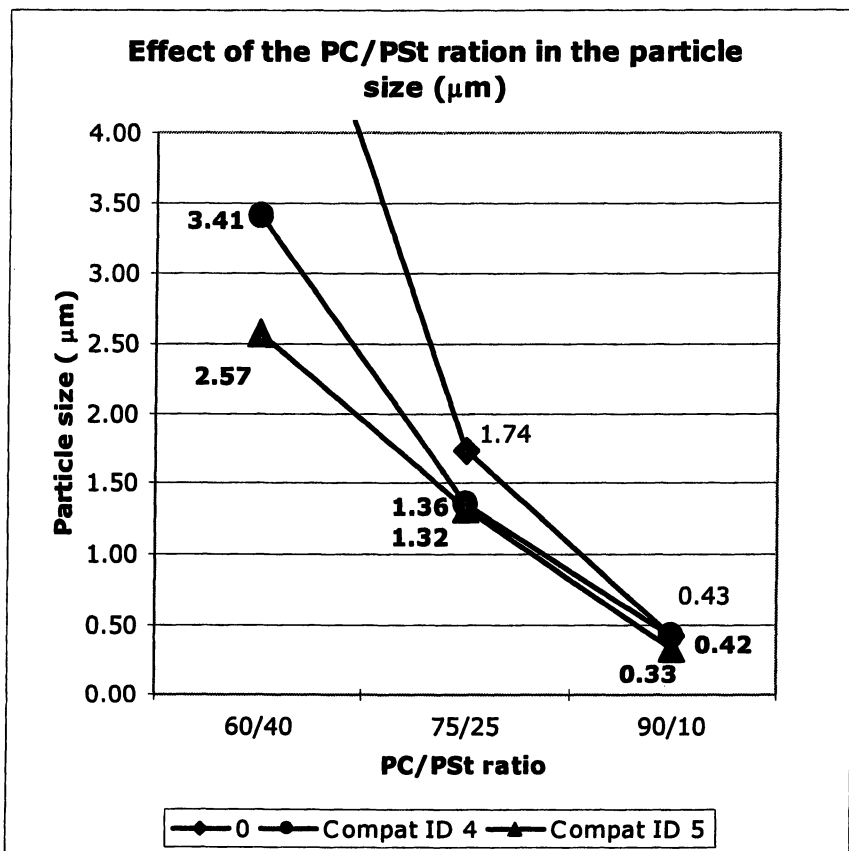


Figure 7. PSt average particle size (shown beside each point) depending on the PC/PSt ratio, using two different compatibilizers A and B, selected from the binary blends of PC and compatibilizers.

3. Paul, D.R.; Bucknall, C.B. *Polymer Blends*; John Wiley and Sons, Inc., 2000, 539-579
4. Ide, F.; Hasegawa, A. *J. Appl. Polym. Sci.* **1974**, *18*, 4, 963-974.
5. Dong P. C.; Ho J. H.; Sung L. M. *Polymer* **1996**, *37*, 14, 3055-3063.
6. Chang, F.-C.; Hwu, Y.-C. *Polym. Eng. Sci.* **1991**, *31*, 1509-1519.
7. Jannasch, P.; Wesslén, B., *J. Appl. Polym. Sci.* **1995**, *58*, 4, 753-770.
8. Davis, K.A.; Matyjaszewski, M. *Adv. Polym. Sci.* **2002**, *159*, 1-169.
9. Coessens, V.; Pintauer, T.; Matyjaszewski, K., *Progr. Polym. Sci.* **2001**, *26*, 337-377.

10. *Controlled Radical Polymerization*. Matyjaszewski, K., Editor; American Chemical Society, Washington, DC. 1997. Chapter 1.
11. Nesvadba, P.; Kramer, A.; Steinmann, A.; Stauffer, W. U.S. Patent 6,455,706B2, 2002.
12. Georges, M.K.; Veregin, R.P.N.; Kazmaier, P.M.; Hamer, G.K. U.S. Patent 5,401,804, 1995.
13. Lai, J.T.-Y.; Masler, W.F.; Nicholas, P.P.; Pourahmady, N.; Puts, R.D.; Tahiliani, S. EP 0869137 B1, 1998.
14. Goerges, M. K.; Inoue, H. T.; Hamer, G. K.; Kazmaier, P. M.; Veregin, R. P. N. U.S. Patent 6,258,911 B1, 2001.
15. Nesvadba, P.; Kramer, A.; Steinmann, A.; Stauffer, W. U.S. Patent 6,262,206 B1, 2001.
16. Georges, M. K.; Veregin, R. P. N.; Kazmaier, P. M.; Hamer, G. K. *Macromolecules* **1993**, *26*, 2987-2988.
17. Listigovers, N. A. ; Georges, M. K.; Odell, P. G.; Keoshkerian, B. *Macromolecules* **1996**, *29*, 8992-8993;
18. Fukuda, T.; Terauchi, T.; Goto, A.; Ohno, K.; Tsujii, Y; Miyamoto, T.; Kobatake, S., Yamada, B. *Macromolecules* **1996**, *29*, 6393-6398.
19. Devonport, W.; Michalak, L.; Malmström, E.; Mate, M.; Kurdi, B.; Hawker, C. J.; Barclay, G. C. and Sinta, R. *Macromolecules* **1997**, *30*, 1929-1934.
20. Georges, M. K.; Hamer, G. K.; Listigovers, N. A. *Macromolecules* **1998**, *31*, 25, 9087-9089.
21. Fischer, H. *J. Polym. Sci. A: Polym. Chem.* **1999**, *37*, 1885-1901.
22. Benoit, D.; Chaplinski, V.; Braslau, R.; Hawker, C.J. *J. Am. Chem. Soc.* **1999**, *121*, 16, 3904-3920.
23. Souaille, M.; Fischer, H. *Macromolecules*, **2000**, *33*, 7378-7394.
24. Souaille, M.; Fischer, H. *Macromolecules*, **2001**, *34*, 2830-2838.
25. Souaille, M.; Fischer, H. *Macromolecules*, **2002**, *35*, 248-261.
26. Fukuda, T.; Goto, A.; Tsujii, Y. in *Handbook of Radical Polymerization*, Ed. by K. Matyjaszewski and T. P. Davis, Wiley Interscience, Hoboken, 2002, Chapter XX.
27. Le Mercier, C.; Acerbis, S.B.; Bertin, D.; Chauvin, F.; Gigmes, D.; Guerret, O.; Lansalot, M.; Marque, S.; Le Moigne, F.; Fischer, H.; Tordo, P. *Macromol. Symp.* **2002**, *182*, 225-247.
28. Goto, A.; Fukuda, T. *Prog. Polym. Sci.*, **2004**, *29*, 329 -385.
29. Grimaldi, S.; Lemoigne, F.; Finet, J.-P.; Tordo, P.; Nicol, P.; Plechot, P.; Gnanou, Y., US Patent US6255448B1.
30. Nesvadba, P.; Kramer, A., United Kingdom GB Patent 2,335,190 A, 1999.
31. Retsos H., Margiolaki, I.; Messaritaki, A.; Anastasiadis, S. H. *Macromolecules* **2001**, *34*, 5295-5305.
32. Tucker, P. S.; Barlow, J. W.; Paul, D. R. *Macromolecules* **1988**, *21*, 2794.
33. Kim, H. C.; Nam, K. H.; Jo, W. H. *Polymer* **1993**, *34*, 4043.

Chapter 25

Living Radical Polymerizations Mediated by Metallo-Radical and Organo-Transition Metal Complexes

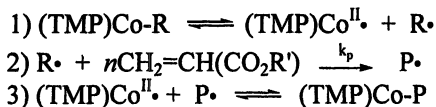
Bradford B. Wayland, Xuefeng Fu, Chi-How Peng, Zhi Lu,
and Michael Fryd

Department of Chemistry, University of Pennsylvania,
Philadelphia, PA 19104-6323

Abstract

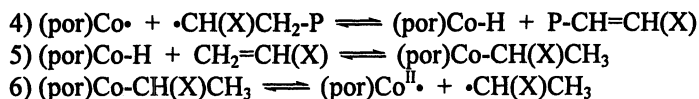
Cobalt porphyrin derivatives are observed to participate in the control of living radical polymerization (LRP) by two distinctly different mechanisms. Cobalt (II) porphyrin (Co(II)) metallo-radicals mediate a LRP by reacting with polymeric radical (P•) to produce a quasi-equilibrium with an organometallic complex (Co-P) which gives living character through the persistent radical effect. Diamagnetic organo-cobalt complexes in combination with an additional radical source such as AIBN produces an alternate form of LRP. The rates of polymerization by the organo-cobalt mediated route are relatively fast and approach that of regular radical polymerization because the radical concentration is determined by the organic radical source. The cobalt (II) metallo-radical concentration is vanishingly small in the organo-cobalt mediated process which removes the need for ligands that use large steric requirements to suppress cobalt (II) catalyzed chain transfer. Radical polymerizations of alkyl acrylates, acrylic acid and vinyl acetate mediated by the organo-cobalt porphyrin route are used in illustrating the principal mechanistic features of this process.

Cobalt(II) tetramesityl porphyrin ((TMP)Co^{II}•) is a prototype persistent metal-centered radical that mediates the living radical polymerization of acrylates by forming a dormant organometallic complex ((TMP)Co-P) with the acrylate polymer radical (P•) (eq 1-3).^{1,2} The (TMP)Co^{II}• mediated polymerization is a metal-centered



radical example of a broader class of LRP processes often categorized under the name of stable free radical polymerization (SFRP).³ All SFRP processes use a stable “persistent” radical to control the propagating polymer radical (P•) concentration through a quasi-equilibrium with a dormant complex (P-X). The best known subcategory of SFRP is nitroxide radical polymerization (NRP)⁴ mediated by stable organo nitroxide radicals (R₂NO•).

Applications of the cobalt(II) metallo-radical mediated LRP are limited by both a small rate of polymerization that results from the required low radical concentrations for SFRP, and termination of polymer radical chain growth by cobalt (II) β-H abstraction with subsequent catalytic chain transfer (eq 4-6).⁵

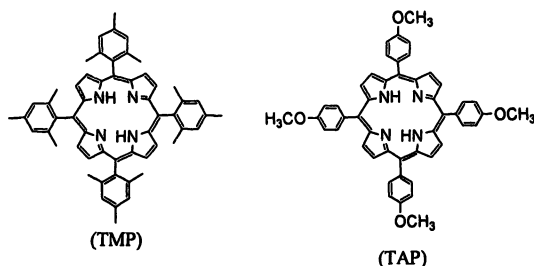


The large steric requirements of the TMP ligand suppress the chain transfer by (TMP)Co^{II} from acrylate polymer radicals which permits formation of high molecular weight acrylate polymers with low polydispersity.^{1,2}

In addition to the cobalt (II) mediated SFRP, cobalt porphyrins manifest an entirely separate category of controlled/living radical polymerization that is mediated by diamagnetic organo-cobalt (III) complexes. This organo-cobalt controlled process utilizes radical sources like alkyl azo compounds to provide a slow continuous influx of new radicals. The cobalt porphyrin system thus has the capability to mediate living radical polymerization by several different mechanistic pathways which is a feature shared with organo-complexes of tellurium,⁶ stibine,⁷ germanium,⁸ and titanium.⁹

Prototype transition metal mediators for LRP

Cobalt complexes of tetra mesityl porphyrin (TMP) and tetra anisyl porphyrin (TAP) are examples of large and small steric requirement complexes for applications in organic solvent media. Phenyl sulfonated porphyrin derivatives such as tetra (3, 5-disulfonato mesityl) porphyrin provide analogous species for application in aqueous media.¹⁰



LRP of acrylates mediated by (TMP)Co^{II}

Solutions of methyl acrylate (2.5M), (TMP)Co^{II} (1.2×10^{-3} M), and V-70 ($((\text{CH}_3)_2(\text{OCH}_3)\text{C}(\text{CH}_2)\text{C}(\text{CH}_3)(\text{CN})_2\text{N}_2)$) ($0.7\text{--}2.0 \times 10^{-3}$ M) in benzene were heated to 333K and the conversion to polymer was followed by ¹H NMR (Figure 1). The induction time periods prior to observing polymerization, decrease with increasing concentration of V-70 and correspond to the time required to inject sufficient radicals to convert effectively all of the (TMP)Co^{II} into diamagnetic organometallic complexes, (TMP)Co-R. Production of a modest excess of total organic radicals compared to the initial concentration of (TMP)Co^{II} results in large increases in the rate of polymerization without loss of control (Figure 1). The acrylate polymers formed when using this procedure showed a linear increase in number average molecular weight (M_n) with conversion, low polydispersity (~ 1.06) and molecular weights close to the theoretical values corresponding to one polymer chain per cobalt porphyrin (Figure 2).

The methyl acrylate (MA) polymerizations using V-70 ($t_{1/2}(333\text{ K}) = 11$ min.) as a radical source that shown in Figure 1 illustrate both the cobalt (II) metallo-radical mediated (Figure 1A) and the organo-cobalt mediated processes (Figure 1 (B, C)). When the ratio of total moles of radicals injected into solution from the radical source to the initial moles of (TMP)Co^{II} is less than unity the polymerization process is mediated by the excess of (TMP)Co^{II} through a SFRP process. The polymerization is very slow because the radical is maintained at a low concentration by a quasi-equilibrium between (TMP)Co^{II} and the organo-Co(TMP) species (Figure 1A). The living character of this SFRP is a manifestation of the persistent radical effect.¹¹

Radical polymerization of MA for the condition where the total moles of radicals from V-70 exceeds the initial moles of (TMP)Co^{II} is illustrated in Figure 1 (B, C). The process has an induction period where only a small fraction of the polymer forms followed by a period of rapid polymerization that begins when the moles of radicals that enter solution from V-70 exceed the initial moles of (TMP)Co^{II}. At that point all the (TMP)Co^{II} has been converted to (TMP)Co-P and the excess radicals change the polymerization process from a Co^{II} mediated SFRP to an organo-cobalt mediated polymerization. The most important feature is that during this period of fast polymerization the process

remains controlled and produces low polydispersity polymers where M_n increases linearly with monomer conversion. (Figure 1, 2).¹²

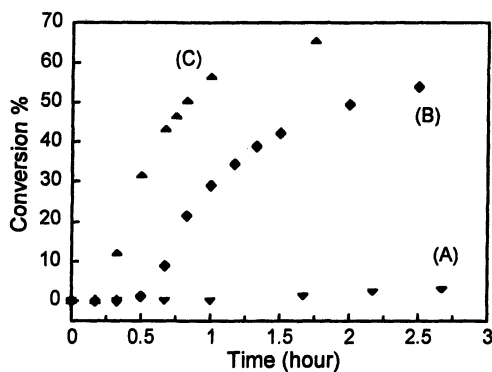


Figure 1. Monomer conversion as a function of time in the radical polymerization of methyl acrylate in benzene at 333K with $[MA]_i = 2.5M$ and $[(TMP)Co^{II}\cdot]_i = 1.2 \times 10^{-3}M$. The quantity of V-70 radical initiator added was varied to produce different ratios of the total $\cdot C(CN)(CH_3)(CH_2C(CH_3)_2(OCH_3))$ radicals injected into solution to that of total cobalt porphyrin ($R_{\cdot T}/Co^{II}\cdot T$). (A) ($R_{\cdot T}/Co^{II}\cdot T$) = 0.70, conversion = 47%, reaction time = 62 hours, $M_n = 9.9 \times 10^4$, $M_w/M_n = 1.11$, theoretical $M_n = 1.2 \times 10^5$; (B) ($R_{\cdot T}/Co^{II}\cdot T$) = 1.2, conversion = 54%, reaction time = 150min, $M_n = 9.5 \times 10^4$, $M_w/M_n = 1.04$, theoretical $M_n = 9.7 \times 10^4$; (C) ($R_{\cdot T}/Co^{II}\cdot T$) = 2.0, conversion = 69%, reaction time = 105min, $M_n = 1.2 \times 10^5$, $M_w/M_n = 1.06$, theoretical $M_n = 1.2 \times 10^5$.

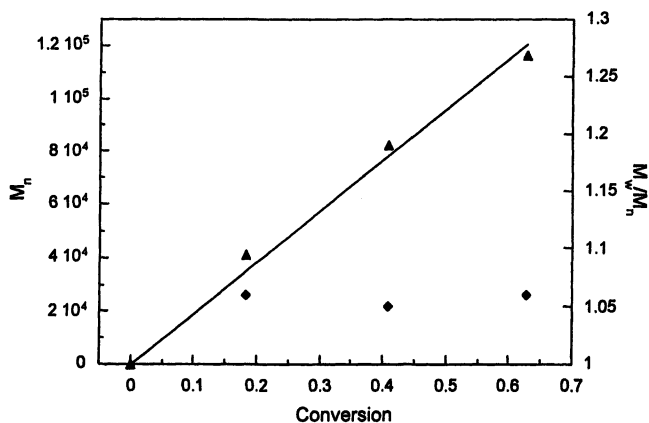


Figure 2. Change in the number average molecular weight M_n (▲) and polydispersity (M_w/M_n) (◆) with methyl acrylate conversion to PMA initiated by V-70 when $[MA]_i = 2.5 M$, $[(TMP)Co^{II}\cdot]_i = 1.2 \times 10^{-3}M$, and $[V-70]_i = 1.0 \times 10^{-3}M$; ($R_{\cdot T}/Co^{II}\cdot T$) = 1.2 at 333K in benzene.

First order rate plots for the polymerization of methyl acrylate initiated by a series of concentrations of AIBN in the presence of cobalt (II) and organo-cobalt porphyrin complexes are illustrated in Figure 3 A-D. AIBN has a half life time of ~ 18.5 hours at 333K in benzene and the much slower entry of radicals into solution compared to V-70 ($t_{1/2}$ (333K) ~ 11 min) permits attaining a near constant steady state radical concentration for kinetic studies. Subsequent to an induction period, the polymerization of MA follows first order rate behavior where the slope of $\ln(M_0/M_t)$ versus time is proportional to $[AIBN]^{1/2}$. The observed induction periods result from formation of an organo-cobalt complex and correspond to the time required to produce slightly more than one radical from AIBN per cobalt (II) in solution. Conversion of the metallo radical $((TMP)Co^{II})$ to the organometallic complex $((TMP)Co-CH(CH_3)CO_2CH_3)$ is directly observed by following changes in the 1H NMR during the induction period (Figure 3). The pyrrole hydrogens of $(TMP)Co-CH(CO_2CH_3)CH_3$ and $(TMP)Co-PMA$ are diastereotopic and observed as an AB pattern in the 1H NMR because of the chiral centers in the organo ligand bonded to cobalt (Figure4 (2-4)).

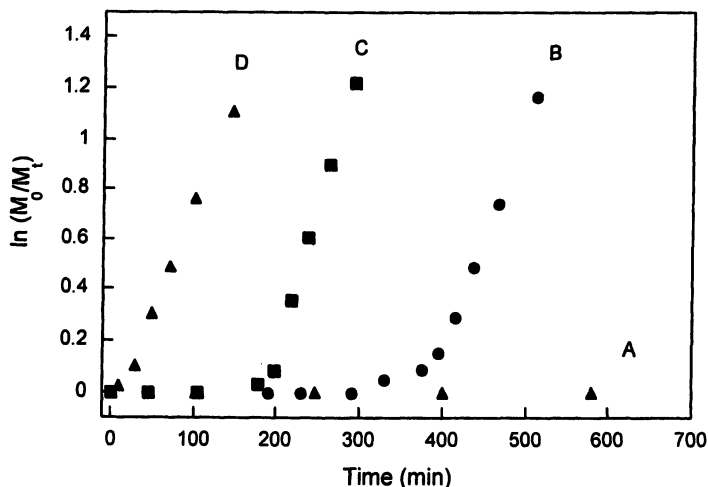


Figure 3. First order rate plots of methyl acrylate ($[MA]_i = 2.5 M$) polymerization in benzene at 333 K. **A)** $AIBN = 1 \times 10^{-3} M$ and $[(TMP)Co^{II}]_i = 1.0 \times 10^{-3} M$; **B)** $AIBN = 4.8 \times 10^{-3} M$ and $[(TMP)Co^{II}]_i = 1.0 \times 10^{-3} M$; **C)** $AIBN = 9.5 \times 10^{-3} M$ and $[(TMP)Co^{II}]_i = 1.0 \times 10^{-3} M$; **D)** $AIBN = 4.1 \times 10^{-3} M$; $[(TMP)Co-CH(CH_3)CO_2CH_3]_i = 1.0 \times 10^{-3} M$.

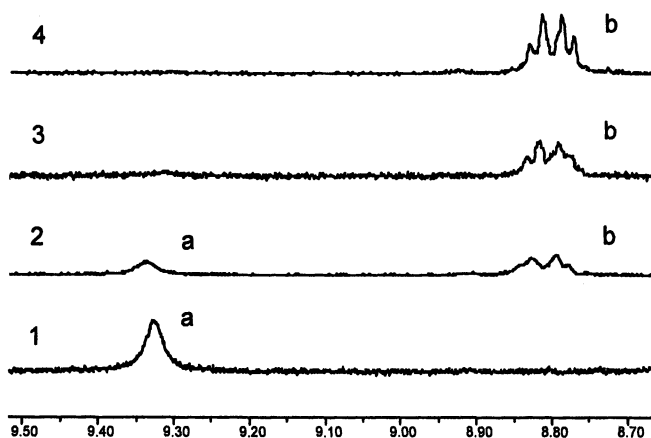
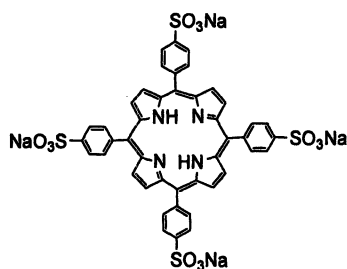


Figure 4. Porphyrin ^1H NMR(300 MHz) spectra in C_6D_6 illustrate that the formation of an organo-cobalt complex during the induction period for the organo-Co(TMP) mediated LRP of MA. a) $(\text{TMP})\text{Co}^{\text{II}}$ *m*-phenyl H, b) $(\text{TMP})\text{Co}-\text{CH}(\text{CH}_3)\text{CO}_2\text{CH}_3$ pyrrole AB pattern. 1) $(\text{TMP})\text{Co}^{\text{II}}$; 2) $(\text{TMP})\text{Co}^{\text{II}}$ and $(\text{TMP})\text{Co}-\text{CH}(\text{CH}_3)\text{CO}_2\text{CH}_3$; 3) 90% $(\text{TMP})\text{Co}-\text{P}$, 1-3% polymer formed; and 4) $(\text{TMP})\text{Co}-\text{P}$, rapid polymer propagation starts.

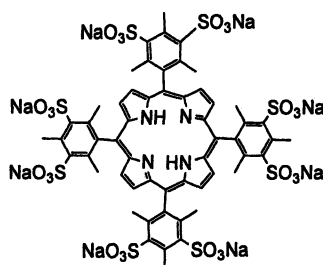
The induction period disappears when the polymerization is carried out in the presence of a preformed organo-cobalt complex (Figure 4D). Acrylate homo polymers and block copolymers formed in this type of process are found to have relatively small polydispersities resulting from rapid exchange of radicals between active and dormant forms, and manifest a near linear increase in molecular weight with conversion associated with a living radical polymerization process.

LRP of Acrylic acid in water mediated by cobalt (II) and organo-cobalt porphyrins

Sulfonated porphyrins provide a series of water soluble cobalt(II) metallo-radical and organo cobalt complexes for mediating LRP in aqueous media.¹⁰



TSPP



TMPS

Table 1. Representative acrylate homopolymers and diblock copolymers synthesized using organo-cobalt mediated radical polymerization

| Homo- ^(a) polymers | M_n | PDI | Diblock ^(b) Copolymers | M_n | PDI |
|----------------------------------|-------------------|------|--------------------------------------|-------------------|------|
| PMA | 5.1×10^4 | 1.09 | PMA-b-PBA | 1.7×10^5 | 1.07 |
| PMA | 8.6×10^5 | 1.17 | PMA-b-PBA | 1.5×10^6 | 1.29 |
| PMA | 3.4×10^4 | 1.04 | PMA-b-PtBA | 8.7×10^4 | 1.10 |
| PAA | 2.4×10^5 | 1.18 | | | |

Monomeric units include: MA-methyl acrylate, BA-butyl acrylate, tBA-t-butyl acrylate, AA-acrylic acid. b) The block copolymers are derived from the homopolymers in the left column.

Radical polymerization of acrylic acid in water mediated by (TMPS)Co-organo species is illustrated in Figures 5, 6. The large rate for the process compared to the SFRP pathway is shown in Figure 5, and the relatively low polydispersity and linear growth in molecular weight with conversion are depicted in Figures 6. Representative acrylate polymers produced by the organo-cobalt porphyrin mediated polymerizations are listed in Table 1.

Cobalt porphyrin mediated LRP of vinyl acetate

Living radical polymerization mediated by cobalt (II) metalloradicals and diamagnetic organo-cobalt complexes have been extended to vinyl esters. Radical polymerization of vinyl acetate mediated by (TMP)Co^{II} and (TMP)Co-CH(CH₃)OC(O)CH₃ are illustrated in Figure 7 and Table 1.

Studies of the Organo-Cobalt Mediated Living Radical Polymerization

The organo-cobalt/azo-radical source process occurs at rates comparable to polymerizations where the radical concentration is entirely determined by the concentration of the organic radical source (AIBN, V-70). The slow continual influx of organic radicals into solution from an organic radical source such as AIBN keeps the metallo-radicals ((por)Co^{II}) sequestered in organometallic complexes and circumvents the limitations of both low rate of polymerization and β -H abstraction from the polymer radical that are associated with the metallo-radical ((por)Co^{II}). The large observed rate increases compared to the SFRP pathway are illustrated in Figures 1, 5 and 7. In the organo-cobalt mediated process the concentration of radicals is determined by the rate of radical formation from the organic radical source (AIBN, V-70) and the rate of radical termination ($[R\cdot] = (k_i[I]/2k_t)^{1/2}$), but in SFRP the concentration of radicals is defined by the equilibrium between the cobalt (II) and organometallic complexes ($[R\cdot] = K_d[(por)Co-R]/[(por)Co^{II}\cdot]$).

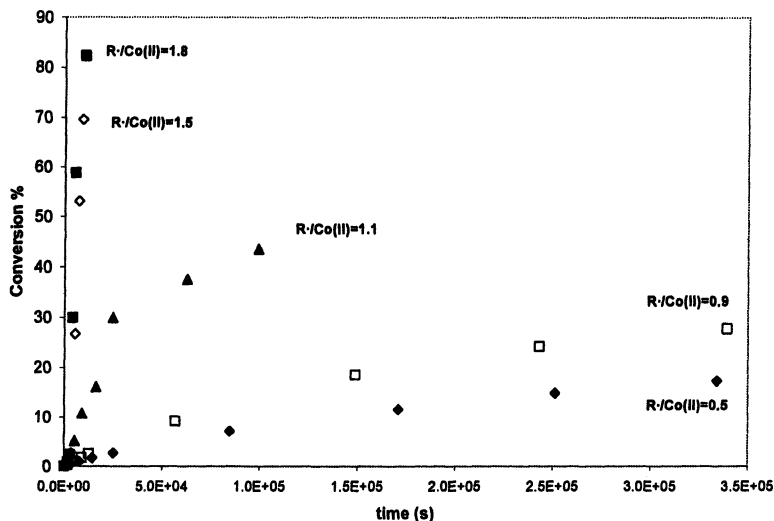


Figure 5 Monomer conversion as a function of time in the radical polymerization of acrylic acid in D_2O initiated by V-70 at 333K with $[AA]_i = 2.5 M$ and $[(TMPS)Co^{II}]_i = 1.0 \times 10^{-3} M$. $[R_{\bullet T}]/[Co^{II}_{\bullet T}] = 1.8, 1.5, 1.1, 0.9$ and 0.5 .

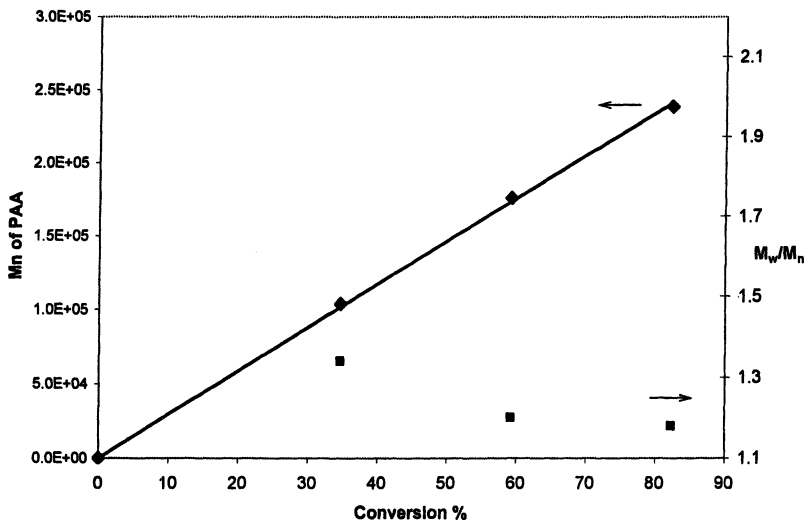


Figure 6. Change in the number average molecular weight and polydispersity as a function of acrylic acid (AA) conversion to poly acrylic acid (PAA) initiated by V-70 when $[AA]_i = 2.5 M$, $[(TMPS)Co^{II}]_i \sim 7 \times 10^{-4} M$, and $(R_{\bullet T}/Co^{II}_{\bullet T}) = 1.8$ at 333K in water.

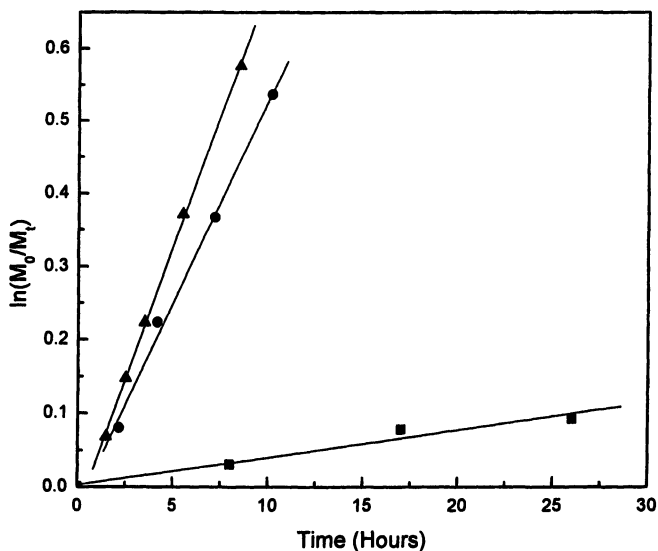


Figure 7. First order rate plot for polymerization of vinyl acetate ($[Vac]_i = 2.5 M$) ($[(TMP)Co-CH(CH_3)OC(O)CH_3]_i = 1.0 \times 10^{-3} M$) in benzene. ■ $[AIBN]_i = 0$, ● $[AIBN]_i = 1.9 \times 10^{-2} M$, ▲ $[AIBN]_i = 3.8 \times 10^{-2} M$.

Table 2 Polyvinyl acetate (PVAc) prepared in C_6D_6 at $60^\circ C$

| Monomer | Polymer | Reaction Time | M_n | M_w/M_n | Conv% |
|------------------|------------|---------------|---------|-----------|-------|
| Vac ^a | PVAc | 26 h | 17,000 | 1.1 | 9 |
| Vac ^b | PVAc | 2 h | 142,000 | 1.3 | 17 |
| Vac ^c | PMA-b-PVAc | 6 h | 64,000 | 1.13 | 15 |

a: 2.5M Vac C_6D_6 , $[(TMP)Co-CH(CH_3)OC(O)CH_3]_i = 1 \times 10^{-3} M$

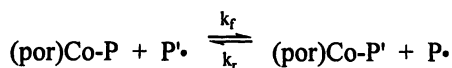
b: bulk, $[AIBN]_i = 4.7 \times 10^{-3} M$, $[(TMP)Co-CH(CH_3)OC(O)CH_3]_i = 1 \times 10^{-3} M$

c: 2.5M C_6D_6 solutions of Vac, $[AIBN]_i = 3 \times 10^{-3} M$, $[(TMP)Co-PMA]_i = 1 \times 10^{-3} M$, $M_n(PMA) = 4.2 \times 10^4$

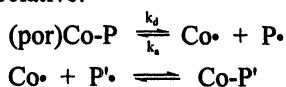
The interchange of radicals between the small number of propagating radical (P \cdot) in solution and the large pool of latent radicals in the dormant complex is the primary means for controlling the polydispersity. The exchange of radicals between the active (P \cdot) and dormant form ((por)Co-P) can be accomplished by both associative and dissociative pathways (Scheme I).

Scheme I: Radical interchange mechanisms

A) Associative:



B) Dissociative:



The dissociative and associative radical interchange mechanisms are radical analogs (S_{H1}, S_{H2}) of the more familiar nucleophilic substitution reactions (S_{N1}, S_{N2}). The net result of exchange of radicals (P \cdot) in solution with latent radicals (P) in the dormant complex ((por)Co-P) is the same irrespective of whether the process is dissociative or associative. The S_{H1} and S_{H2} processes are kinetically different in that the S_{H1} is first order in the [(por)Co-R] and zero order in the P \cdot , while an S_{H2} pathway is first order in both (por)Co-P and P \cdot . In the general case both S_{H1} and S_{H2} processes simultaneously occur and the rate of radical exchange is a sum of the rates from the two pathways.

The rate constant for unimolecular homolytic dissociation of (TMP)Co-CH(CH₃)CO₂CH₃ at 333K is $\sim 5 \times 10^{-2} \text{ s}^{-1}$ is sufficiently fast to account for the low polydispersity observed for the poly methyl acrylate (Figure 1, 2). However, the rate constant for (TMP)Co-CH(CH₃)OC(O)CH₃ bond homolysis at 333 K of $\sim 4 \times 10^{-5} \text{ s}^{-1}$ is too small to control the polymerization by a dissociative pathway. Therefore, the radical interchange in the organo-cobalt mediated polymerization of vinyl acetate must occur by an associative pathway. Associative reactions are generally much faster than dissociative and thus unless the associative pathway is blocked the fastest radical exchange should occur by an associative route through a three centered transition state (P \cdot ...Co...P). Availability of a readily accessible site for the incoming radical in a position trans to the leaving radical provides a facile exchange pathway for the sixteen electron organo-cobalt complexes. There is no evidence at this time that a finite concentration of the possible 17-electron dialkyl complex (P'-Co-P) occurs in the cobalt porphyrin system.

The effective absence of cobalt (II) metallo-radicals during the organo-cobalt mediated process reduces the requirements for having sterically demanding complexes as an approach to suppress β -H abstraction from the growing oligomer/polymer radicals. This important feature of the process is

illustrated by studies of cobalt complexes with tetra (p-methoxy phenyl) porphyrin ((TAP)Co), which has much smaller steric demands than the tetramesityl porphyrin complex ((TMP)Co). When (TAP)Co^{II} is used as a mediator for SFRP of acrylates initiated by (TAP)Co-CH(CH₃)CO₂CH₃, the resulting polymers have polydispersities in the range of 1.8-2.2 and grow only to a maximum degree of polymerization of ~200 before catalytic chain transfer occurs through β-H abstraction⁵ (Figure 8A). Under the organo-cobalt mediated conditions of continual injection of radicals the cobalt (II) concentration is maintained at a sufficiently small concentration such that β-H abstraction is effectively quenched. The homo polymers and block copolymers grow much larger and have relatively small polydispersities in the process mediated by organo-Co(TAP) compared to the SFRP pathway (Figure 8 B).

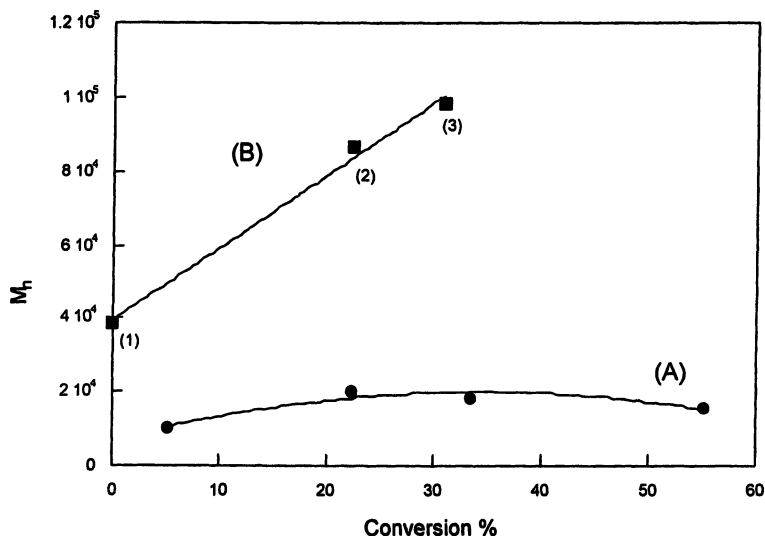


Figure 8. Changes in number average molecular weight with conversion of MA to PMA ($[MA]_i = 2.5 \text{ M}$; 333K). **A)** SFRP mediated by (TAP)Co^{II}; $[(TAP)Co^{II}]_i = 1.2 \times 10^{-3} \text{ M}$, $[V-70]_i = 0.9 \times 10^{-3} \text{ M}$; $([R_{\bullet T}]/[Co^{II}_{\bullet T}]) = 0.9$; **B)** RIP-DT mediated by (TAP)Co-R; $[(TAP)Co-PtBA]_i = 1.2 \times 10^{-3} \text{ M}$, $[V-70]_i = 0.1 \times 10^{-3} \text{ M}$; PDI(%conv., Mn): 1) 1.09(14.4, 3.86×10^4), 2) 1.10(22.3, 8.67×10^4), 3) 1.15 (30.8, 9.84×10^4).

Direct comparisons of the polymerization rates in the presence and absence of the organo-cobalt porphyrin mediator indicate that there is a small retardation in the rate associated with the presence of the organo-cobalt complex (Figure 9). Similar rate decreases have also been observed for radical polymerizations controlled by RAFT reagents.^{13, 14} Reduction in the rate of polymerization results from decreasing the effective radical concentration ($[P\bullet]$), ($R_p = k_p[P\bullet][M]$). The

rate of radicals entering solution from AIBN is the same in the presence and absence of (por)Co-P and thus the decrease in effective P \cdot concentration must result from an increase in the rate of radical termination. The two most probable reasons for this behavior are chain length effects on the termination rate and additional termination pathways that occur through the organometallic complex like that illustrated in eq 7.

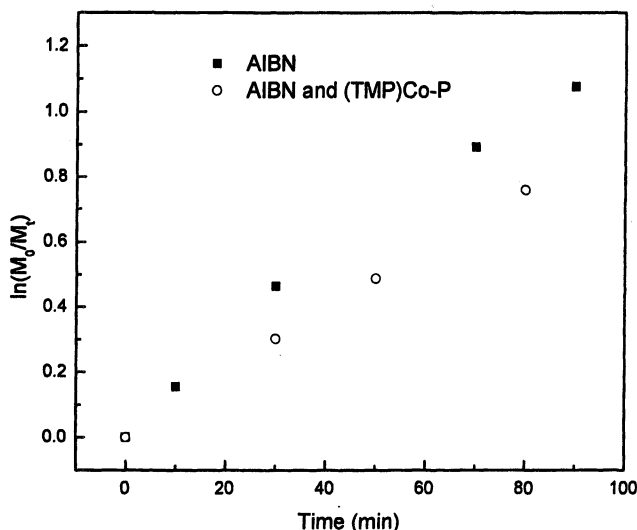


Figure 9. Monomer conversion as a function of time in the radical polymerization of methyl acrylate ($[MA]_i = 2.5 \text{ M}$) in benzene at 333 K with $[AIBN] = 5 \times 10^{-3}$. ■ $[(TMP)Co] = 0$; ○ $[(TMP)Co-R] = 1.2 \times 10^{-3} \text{ M}$.

Mechanisms for living character in radical polymerization

The living character for both stable free radical polymerization (SFRP) and atom transfer radical polymerization (ATRP)^{3, 15-17} is derived from the persistent radical effect. Presence of a stable chemical species (X) that exclusively binds reversibly with the propagating radical (P \cdot) to form a dormant complex (P-X) provides an inherent kinetic effect that suppresses irreversible bimolecular radical termination by coupling and disproportionation. This kinetic phenomenon was first recognized for stable radicals in SFRP processes and became known as the persistent radical effect.¹¹ The kinetic effect is more general and pertains to any stable species that reversibly binds with the propagating radical which includes ATRP processes.^{3, 15-17} Understanding of the origin of living character is less well developed for controlled radical polymerizations that utilize radicals from an external source such as AIBN in

conjunction with a diamagnetic organo-X mediator such as organo-metal, organo-metalloid, and RAFT agents.^{13, 14} In these cases, radicals from an external source like AIBN are injected into solution and subsequently produce an active propagating radical ($P\cdot$) that exchanges with the dormant complex ($P-X$). Radical interchange of freely diffusing propagating radicals with latent radicals in the dormant complex provides a mechanism to obtain relatively small polydispersity, but does not account for the observed living character. One factor that contributes to living character is to use the minimum number of radicals from the external radical source compared to the radicals stored in a latent form in the dormant complex. The ratio of latent radicals in $P-X$ to the total radicals injected by the external radical source is set as large as possible to obtain the desired molecular weight and monomer conversion. In order to obtain approximately one living polymer chain per mediator molecule ($P-X$) the stored latent polymer chains must grow faster than the radicals newly formed from the radical source like AIBN. Large decrease in the radical termination constant (k_t) as the polymer degree of polymerization increase favors selective growth of the larger polymer radical which produces living character.

Characteristics of organo-cobalt / azo radical LRP

Low-polydispersity homopolymers and block copolymers of acrylates and vinyl acetate are produced at relatively fast rates when an azo radical source generates organic radicals and organo-cobalt complexes guide the polymerization. Polymerizations that occur through the organo-cobalt mediated pathway circumvent the steric constraints needed to repress β -H abstraction and chain transfer by cobalt (II) which simplifies and expands the potential catalyst materials. The large observed increase in the rate of monomer conversion compared to the cobalt (II) SFRP is an expected consequence of the increase in total radical concentration, but the near linear growth in the observed polymer length with conversion indicates that the polymerization is well controlled. The growth in chain length approaches the theoretical value for one growing polymer chain per (por)Co-P unit. The vast majority of monomers are observed to be incorporated into growing polymer radicals from (por)Co-P rather than the new chains formed by propagation of radicals from the radical source. The preferential growth of the polymer radicals ($P\cdot$) is partly a consequence of the decline in termination rate constant as the size of the polymer radical increases.

Coordinate and electronic unsaturation of the five coordinate sixteen-electron organo-cobalt porphyrin complexes provide a highly favorable situation for fast associative radical interchange. Expansion of the scope of organo-metal controlled LRP processes to encompass a wide range of metal centers is a fertile area for continuing catalyst development. New classes of organo-metal mediators can be anticipated to emerge from among the many examples of coordinately unsaturated sixteen and seventeen electron organo-metal complexes of both early and late transition metals.

Acknowledgement

This research was supported by grant NSF-CHE-0501198.

References

1. Wayland, B. B.; Poszmik, G.; Mukerjee, S. L.; Fryd, M. *J. Am. Chem. Soc.* **1994**, *116*, 7943.
2. Wayland, B. B.; Basicckes, L.; Mukerjee, S.; Wei, M. L.; Fryd, M. *Macromolecules* **1997**, *30*, 8109.
3. Matyjaszewski, K.; Xia, J. H. *Chem. Rev.* **2001**, *101*, 2921.
4. Hawker, C. J.; Bosman, A. W.; Harth, E. *Chem. Rev.* **2001**, *101*, 3661.
5. Gridnev, A. A.; Ittel, S. D. *Chem. Rev.* **2001**, *101*(12), 3611-3659.
6. Goto, A.; Kwak, Y.; Fukuda, T.; Yamago, S.; Iida, K.; Nakajima, M.; Yoshida, J. *J. Am. Chem. Soc.* **2003**, *125*, 8720.
7. Yamago, S.; Ray, B.; Iida, K.; Yoshida, J.; Tada, T.; Yoshizawa, K.; Kwak, Y.; Goto, A.; Fukuda, T. *J. Am. Chem. Soc.* **2004**, *126*(43), 13908.
8. Goto, A.; Zushi, H.; Kwak, Y.; Fukuda, T. *Polym. Prepr.* **2005**, *46*(2), 245.
9. Asandei, A. D.; Moran, I. W. *J. Am. Chem. Soc.* **2004**, *126*, 15932.
10. Lu, Z.; Li, Y.; Wayland, B. B. *Polym. Prepr.* **2004**, *45*(1), 1053.
11. Fischer, H. *Chem. Rev.* **2001**, *101*, 3581.
12. Lu, Z.; Fryd, M.; Wayland, B. B. *Macromolecules* **2004**, *37*, 2686.
13. Chiefari, J.; Chong, Y. K.; Ercole, F.; Krstina, J.; Jeffery, J.; Le, T. P. T.; Mayadunne, R. T. A.; Meijs, G. F.; Moad, C. L.; Moad, G.; Rizzardo, E.; Thang, S. H. *Macromolecules* **1998**, *31*, 5559.
14. Goto, A.; Sato, K.; Tsujii, Y.; Fukuda, T.; Moad, G.; Rizzardo, E.; Thang, S. H. *Macromolecules* **2001**, *34*, 402.
15. Kamigaito, M.; Ando, T.; Sawamoto, M. *Chem. Rev.* **2001**, *101*, 3689.
16. Matyjaszewski, K.; Editor *Advances in Controlled/Living Radical Polymerization. ACS Symp. Ser.*, 2003; 854, 2003.
17. Gaynor, S. G.; Wang, J. S.; Matyjaszewski, K. *Macromolecules* **1995**, *28*, 8051.

Chapter 26

Cobalt-Mediated Radical Polymerization of Vinyl Acetate: A New Tool for Macromolecular Engineering

Antoine Debuigne¹, Christophe Detrembleur¹, Rayna Bryaskova¹,
Jean-Raphaël Caille², and Robert Jérôme^{1,*}

¹Center for Education and Research on Macromolecules (CERM),
University of Liège, Sart-Tilman, B6, 4000 Liège, Belgium

²Solvay Research and Technology, Rue de Ransbeek 310, B-1120 Brussels,
Belgium

Cobalt(II)acetylacetonate is an effective mediator for the radical polymerization of vinyl acetate in bulk, suspension and miniemulsion, even when high molar mass is targeted. The mechanism, which basically relies on the reversible combination of the growing poly(vinyl acetate) (PVAc) chains with the cobalt complex, has been analyzed by UV-visible and NMR spectroscopies. The influence of both the temperature and the concentration of the initiator and the cobalt complex has also been investigated. With the macromolecular engineering of PVAc and poly(vinyl alcohol) (PVOH) in mind, a series of end-functional chains and PVAc (PVOH) containing block copolymers have been successfully synthesized.

In spite of remarkable progress in living/controlled radical polymerization for the last decades, it is quite a problem to have the radical polymerization of vinyl acetate under control, particularly when high molecular weight and high monomer conversion are targeted (1-10). The origin of the problem has to be found in the high reactivity of the growing poly(vinyl acetate) radicals, which are not stabilized by the acetate substituent and engage themselves in transfer reactions to the monomer and to the polymer, and in irreversible termination reactions, as well.

Recently, attention has been paid to cobalt complexes as potential mediators for the radical polymerization of VAc. In the presence of cobalt complexes, polymeric radicals can follow two different routes. Either dehydrocobaltation takes place and "catalytic chain transfer polymerization" is the actual mechanism (CCT) (11-13), or a cobalt-carbon bond is reversibly formed, in which the monomer can be inserted and a "cobalt mediated radical polymerization" (CMRP) is effective (14). The issue of the competition between these two processes depends on the structure of the cobalt complex and, above all, on the monomer. For example, methacrylic monomers with an abstractable hydrogen are prone to catalytic chain transfer (CCT) (13), whereas acrylic monomers are preferentially polymerized in a controlled manner, as originally reported by Wayland *et al.* in the presence of cobalt porphyrin (14-16).

Similarly to acrylates, vinyl acetate is a non-active CCT monomer, more prone to combine with the cobalt complex than to transfer. This propensity was a strong incentive to investigate the possible extension of the CMRP of acrylates to VAc. Recently, we reported on the unmatched control of the bulk radical polymerization of vinyl acetate in the presence of $\text{Co}(\text{acac})_2$ (17). Since then, Matyjaszewski *et al.* observed that the radical copolymerization of VAc and *n*-butylacrylate was also controlled by this cobalt complex (18).

This paper aims at discussing recent results on the mechanism of the CMRP of vinyl acetate and on the extension of the bulk polymerization to polymerization in aqueous dispersed media, such as suspension and miniemulsion. The potential of this system in the macromolecular engineering of PVAc and easily derivatized poly(vinylalcohol) (PVOH) is also emphasized.

Experimental Section

Materials and characterization. All monomers were dried over calcium hydride, degassed by several freeze-thawing cycles before being distilled under reduced pressure and stored under argon. Cobalt(II) acetylacetonate ($\text{Co}(\text{acac})_2$, >98% Merck), 2,2'-azo-bis(4-methoxy-2,4-dimethyl valeronitrile) (V-70) (Wako) were used as received. Size exclusion chromatography (SEC) was carried out in THF (flow rate : 1 mL min^{-1}) at 40 °C with a Waters 600 liquid chromatograph equipped with a 410 refractive index detector and styragel HR

columns (four columns HP PL gel $5\mu\text{m}$ 10^5\AA , 10^4\AA , 10^3\AA , 10^2\AA). Polystyrene standards were used for calibration. ^1H NMR spectra were recorded with a Bruker AM 400 Spectrometer (400 MHz) in CDCl_3 . UV-visible spectra were recorded with a Perkin-Elmer P14 spectrophotometer equipped with a thermostat and a magnetic stirrer. An ultrasonic probe B. Braun labosonic 2000 ($l=127\text{ mm}$, $\varnothing = 4\text{ mm}$, 200Hz) was used for the ultrasonication.

General procedure for the bulk polymerization of VAc. Bulk polymerization of vinyl acetate was initiated by V-70 at 30°C in the presence of $\text{Co}(\text{acac})_2$ under argon. The purple mixture was stirred and heated at 30°C . No polymerization occurred for few hours. During this induction period, the colour changed from purple to dark brown-green, followed by a substantial increase in the solution viscosity. The monomer conversion was determined gravimetrically after evaporation of the unreacted monomer.

Block copolymerization of VAc and styrene by CMRP. PVAc end-capped by a cobalt complex ($M_{n, \text{SEC}}=7000\text{g/mol}$, $M_w/M_n=1.18$, 0.29g, $0.41\times 10^{-4}\text{ mol}$) was added into a glass tube, that was capped by a three-way stopcock and purged by three vacuum-argon cycles before addition of degassed styrene (1.5 ml, $131\times 10^{-4}\text{ mol}$). The mixture was heated at 30°C under stirring. After 24h, the reaction was stopped and the product was precipitated in heptane, filtered and dried in vacuo at 50°C . The unreacted PVAc macroinitiator was extracted from the PVAc-b-PS copolymer, with methanol in a Soxhlet extractor for 15h.

Synthesis of PVOH-b-PS copolymers by methanolysis of the ester groups of PVAc-b-PS. A solution of the PVAc-b-PS copolymer (200 mg) in THF (10ml) was added into a solution of potassium hydroxide (500 mg) in methanol (150ml, p.a). After 48h at room temperature under stirring, the PVOH-b-PS copolymer was collected by filtration and dried in vacuo at 50°C .

Results and Discussion

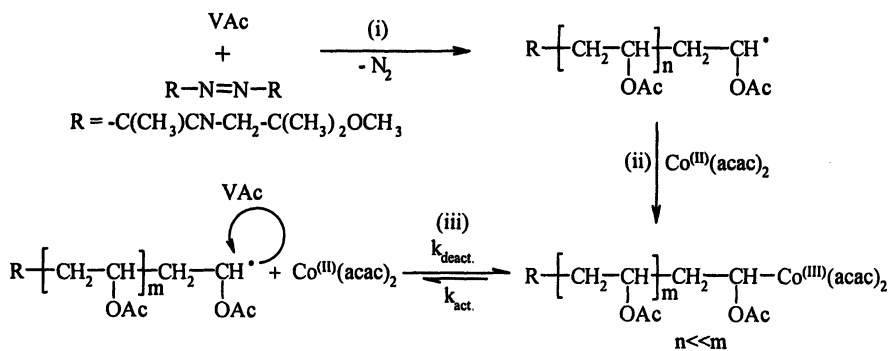
Bulk Polymerization of VAc in the Presence of $\text{Co}(\text{acac})_2$

Whenever the bulk radical polymerization of vinyl acetate is initiated by V-70 at 30°C in the presence of $\text{Co}(\text{acac})_2$, a control is observed although after an induction period of several hours (12h, when $[\text{VAc}]/[\text{Co}(\text{acac})_2][\text{V-70}]=542/1/6.5$) (17). Under these conditions, all the criteria of control are fulfilled, i.e., linear dependence of molar mass on conversion, narrow molar

mass distribution (~ 1.2), linear time dependence of $\ln([M]_0/[M])$, and successful chain extension experiments.

Mechanism

Because the cobalt(II) complex is a well-known trap for radicals, the radical polymerization of vinyl acetate is inhibited as long as the complex persists in the reaction medium. By analogy with the mechanism for the cobalt porphyrin mediated acrylate polymerization (14-16), a three-step mechanism based on the persistent radical effect has been proposed as shown in Scheme 1, i.e., (i) initiation of the vinyl acetate polymerization by the azoinitiator V-70, (ii) trapping of the carbon centered radicals by the persistent metallo-radical cobalt(II) complex, (iii) equilibrium between dormant and active species by cleavage of the Co-C bond, which is the basic mechanism of control.



Scheme 1. Mechanism of the cobalt mediated radical polymerization of vinyl acetate.

This ideal three-step mechanism might however be perturbed by a series of side reactions, including bimolecular radical termination, hydrogen transfer to monomer or polymer responsible for chain branching and broadening of the PVAc molar mass distribution, hydrogen abstraction by the cobalt species with formation of an unsaturated end-group as observed in the catalytic chain transfer polymerization (11, 12), and head-to-head addition of the monomer which forms a more stable primary alkyl cobalt(III) complex reluctant to propagation. Nevertheless, all these side reactions are minimized as assessed by the criteria of control for the vinyl acetate polymerization.

According to the general mechanism shown in scheme 1, the two first steps lead to the formation of dormant species that consists of a few vinyl acetate units

end-capped by the persistent cobalt(II) complex. During this incubation period, the reaction medium changes from dark purple, characteristic of the $\text{Co}(\text{acac})_2$ complex, to dark green-brown, in line with a change in the oxidation state of the cobalt from two to three and formation of dormant species. Because starting reagents and final products have quite a different colour, the induction period has been probed by UV-visible spectroscopy in the 400-800 nm range (Figure 1). The UV-visible spectrum changes extensively for the twelve first hours, and a new compound is detected at 650 nm, which more likely corresponds to the dormant species. Indeed, beyond this period of time, the spectrum remains unchanged, consistent with the complete formation of the dormant species. These observations are in very good agreement with the kinetic data and the 12h induction period observed (17). As soon as the cobalt complex is completely consumed, an equilibrium takes place between active and dormant species, as result of the reversible cleavage of the cobalt-carbon bond, which allows monomer to be inserted (Scheme 1, step iii). The UV-visible spectroscopy is thus an appropriate tool to determine the length of the induction period.

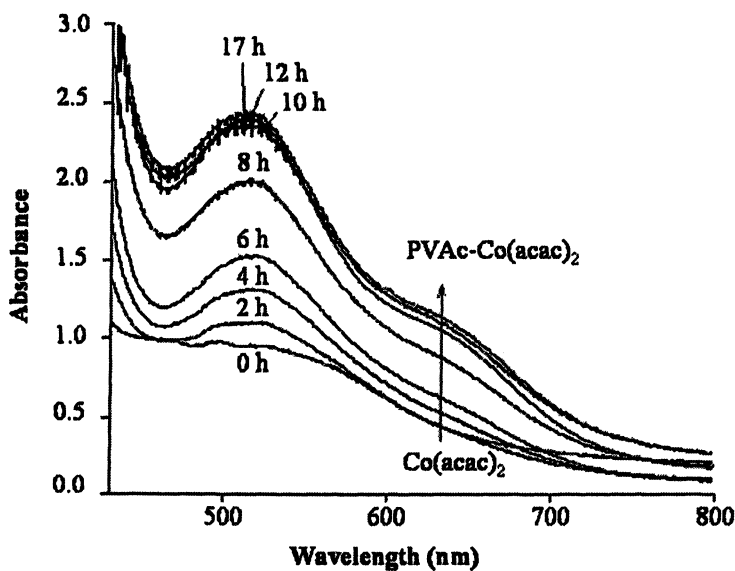


Figure 1. Time dependence of the UV-visible spectrum for the controlled bulk radical polymerization of VAc initiated by V-70 at 30°C in the presence of $\text{Co}(\text{acac})_2$. ($[\text{VAc}]/[\text{Co}(\text{acac})_2]/[\text{V-70}] : 542/1/6.5$).

Moreover, the ^1H NMR spectrum of PVAc (Figure 2) synthesized by cobalt mediated polymerization and recovered after repeated precipitation in water (M_n ,

$M_{SEC} = 18800 \text{ g/mol}$, $M_w/M_n = 1.14$), confirms that the VAc polymerization is actually initiated by radicals released by the thermolysis of V-70 (Scheme 1). Indeed, the molar mass of poly(vinyl acetate), calculated from the intensity ratio of peaks characteristic of the initiator residue ($-\text{OCH}_3$ of V-70 (e)) and the methyne protons of the main chain ($-\text{CH}-\text{OCOCH}_3$ (e)), respectively, ($M_{n, NMR} = 18100 \text{ g/mol}$), is in good agreement with $M_{n, SEC}$. The very small peak at 3.21 ppm is due to the methoxy groups of residual V70 which can not be totally eliminated by repeated precipitations.

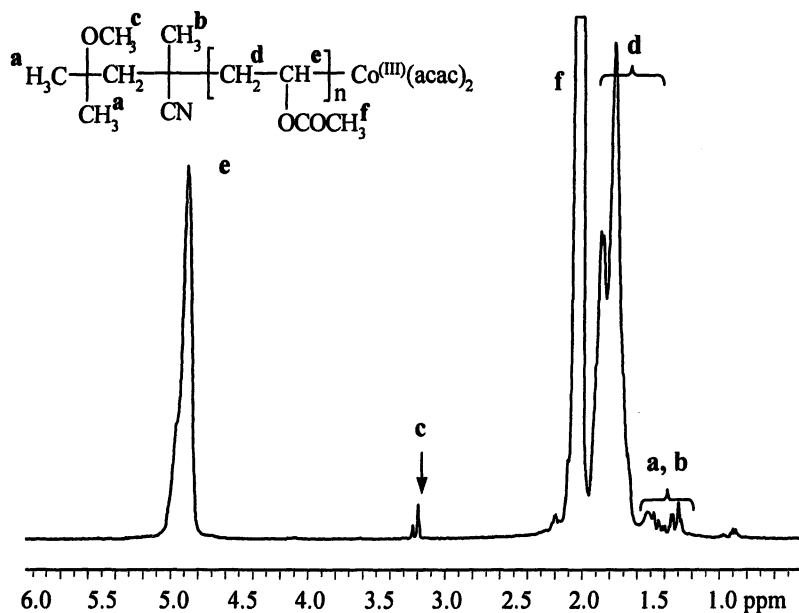


Figure 2. ^1H NMR (400MHz) spectrum of poly(vinyl acetate) initiated in the bulk by V-70 in the presence of $\text{Co}(\text{acac})_2$. ($M_{n, NMR} = 18100 \text{ g/mol}$, $M_w/M_n = 1.14$).

Concentration of the Initiator and the Cobalt Complex

The experimental dependence of the PVAc molar mass on the $[\text{VAc}]_0/[\text{Co}(\text{acac})_2]_0$ ratio and the monomer conversion, is strong evidence that the cobalt complex is the control agent (17). As shown in Table I, the molar mass is predictable and increases with the $[\text{VAc}]_0/[\text{Co}(\text{acac})_2]_0$ ratio, and the polydispersity is low, even at high $[\text{monomer}]/[\text{cobalt}]$ ratios (Table I).

Although the polymerization of VAc was originally carried out with a [V-70]/[Co(acac)₂] ratio of 6.5, the polymerization control is maintained when this ratio is decreased by a factor of two (Table II). Indeed, the polydispersity remains low, and the experimental molar mass of PVAc increases again regularly with the monomer conversion in close agreement with the theoretical dependence based on the [VAc]₀/[Co(acac)₂]₀ ratio (Table II). For the polymerization to occur, the number of radicals formed in the medium should exceed the number of cobalt atoms. Matyjaszewski et al. reported in a recent publication that this system is effective even when this molar ratio is 1/1. (18)

Table I. Bulk radical polymerization of vinyl acetate at 30°C for different VAc/Co(acac)₂ molar ratios and constant V70/Co(acac)₂ molar ratio (6.5)

| Entry | [VAc]/ [Co(acac) ₂] | Time (h) | Conv (%) | <i>M_{n, exp}</i> (g/mol) | <i>M_{n, theor.}</i> ^a (g/mol) | <i>M_w/M_n</i> |
|-------|------------------------------------|-------------|-------------|--------------------------------------|--|------------------------------------|
| 1 | 542 | 24 | 64 | 25 400 | 30 100 | 1.21 |
| 2 | 813 | 22 | 70 | 51 400 | 49 000 | 1.23 |
| 3 | 1626 | 14 | 56 | 70 500 | 78 400 | 1.22 |
| 4 | 2168 | 14 | 60 | 99 000 | 112 000 | 1.33 |

^a*M_{n, theor.}* = ([VAc]₀/[Co(acac)₂]₀) × 86.09 × conv. Data listed are from ref. 17.

Table II. Bulk radical polymerization of vinyl acetate at 30°C for different VAc/Co(acac)₂ molar ratios and constant V70/Co(acac)₂ molar ratio (3.25)

| Entry | [VAc]/ [Co(acac) ₂] | Time (h) | Conv (%) | <i>M_{n, exp}</i> (g/mol) | <i>M_{n, theor.}</i> ^a (g/mol) | <i>M_w/M_n</i> |
|-------|------------------------------------|-------------|-------------|--------------------------------------|--|------------------------------------|
| 1 | 136 | 51 | 6 | 1 200 | 700 | 1.20 |
| | | 71 | 34 | 5 800 | 4 000 | 1.17 |
| | | 143 | 64 | 11 100 | 7 500 | 1.20 |
| 2 | 271 | 40 | 27 | 8 500 | 6 300 | 1.14 |
| | | 49 | 46 | 13 000 | 10 700 | 1.15 |
| | | 72 | 62 | 16 700 | 14 500 | 1.24 |
| 3 | 542 | 20 | 11 | 7 300 | 5 100 | 1.23 |
| | | 25 | 36 | 19 300 | 16 800 | 1.20 |
| | | 44 | 70 | 30 000 | 32 700 | 1.40 |

^a*M_{n, theor.}* = ([VAc]₀/[Co(acac)₂]₀) × 86.09 × conv.

According to the mechanism, the inhibition period in the VAc polymerization is the time required for the radicals released by V-70 to react

with the cobalt(II) complex and to form dormant species. Therefore, it is not surprising that the induction period is longer (19h instead of 12 h) when the $[V70]_0/[Co(acac)_2]_0$ ratio is decreased and less radicals are made available at constant $Co(acac)_2$ concentration. However, the slope of the $\ln([M]_0/[M])$ versus time plot (Figure 3) and thus the polymerization rate appear to be independent of the V-70/ $Co(acac)_2$ molar ratio.

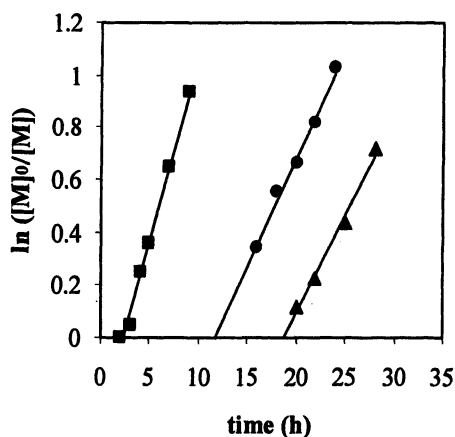


Figure 3. Plot of $\ln([M]_0/[M])$ versus time for the bulk radical polymerization of VAc, with different $[V-70]/[Co(acac)_2]$ molar ratios, at different temperatures. $[VAc]/[Co(acac)_2] = 542$. (▲) $[V-70]/[Co(acac)_2] = 3.25$, at 30°C (●) $[V-70]/[Co(acac)_2] = 6.5$, at 30°C (data from ref. 17) (■) $[V-70]/[Co(acac)_2] = 3.25$, at 50°C.

Influence of Temperature

Finally, when the bulk radical polymerization of VAc is conducted in the presence of $Co(acac)_2$ at 50°C instead of 30°C, the molar mass increases with the monomer conversion although a significant deviation from the ideal behavior is observed beyond 50% conversion and the polydispersity is much higher (Table III).

This deleterious effect results from the shift of the equilibrium towards the active species, which makes irreversible termination more probable, but is also due to the transfer reactions to the monomer and the polymer whose contribution increases with the temperature. Moreover, the increase in temperature has a favourable kinetic effect, as assessed by a much shorter

inhibition period (2h instead of 19h) and a higher polymerization rate (Figure 3, comparison of ■ and ▲). So, temperature has a direct effect on the balance between polymerization rate and polymerization control.

Table III. Bulk radical polymerization of vinyl acetate initiated by V-70 in the presence of Co(acac)₂ at 50°C.

| <i>Time</i> (h) | <i>Conv</i> (%) | <i>M_{n, exp}</i> (g/mol) | <i>M_{n, theor.}^a</i> (g/mol) | <i>M_w/M_n</i> |
|--------------------|--------------------|--------------------------------------|---|------------------------------------|
| 4 | 22 | 12 200 | 10 300 | 1.23 |
| 7 | 48 | 22 900 | 22 300 | 1.37 |
| 9 | 61 | 23 500 | 28 400 | 1.63 |

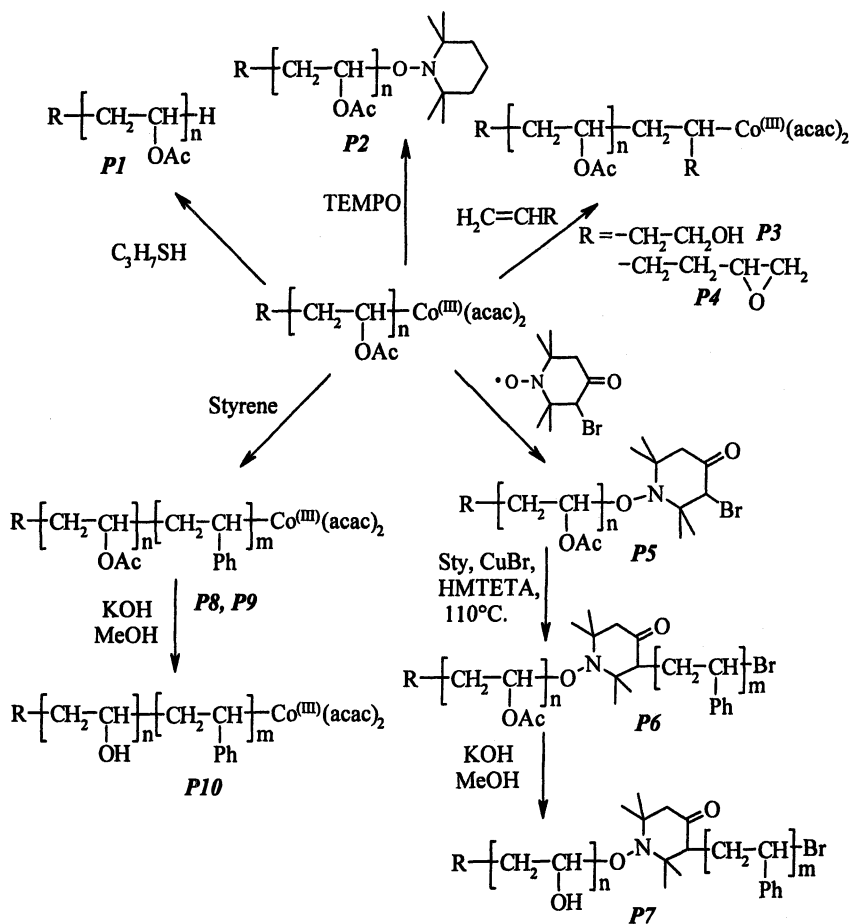
$$\frac{[\text{VAc}]}{[\text{Co}(\text{acac})_2]} = 542, \quad \frac{[\text{V70}]}{[\text{Co}(\text{acac})_2]} = 3.25. \quad {}^a M_{n, \text{theor.}} = \frac{[\text{VAc}]_0}{[\text{Co}(\text{acac})_2]_0} \times 86.09 \times \text{conv.}$$

Macromolecular Engineering Based on CMRP

Controlled radical polymerization extensively contributes to impart well-defined molecular characteristics (length, chain-end, composition and architecture) to a large range of polymers. However, only few studies dealt with the design of PVAc (19-25), which is an incentive to contemplate the potential of CMRP to prepare well-defined PVAc containing block copolymers and end-functional PVAc chains, as well (Scheme 2).

It was previously shown that the cobalt complex at the end of the PVAc chains is replaced by either a hydrogen atom or TEMPO upon addition of either propanethiol or TEMPO to the VAc polymerization medium (P1 and P2; Scheme 2) (26). Furthermore, the addition of these radical scavengers to the polymerization medium is a very efficient strategy for making PVAc free of metal contaminants. Having in mind the end-functionalization of PVAc, non-polymerizable olefins, such as 3-butene-1-ol and 1,2-epoxy-5-hexene, were also added to the polymerization medium, so end-capping the PVAc chains with an hydroxyl and an epoxy group, respectively (P3 and P4; Scheme 2) (26).

Finally, well-defined PVAc and PVOH containing block copolymers have been prepared by a three-step approach (Scheme 2): (i) synthesis of PVAc chains end-capped by the cobalt complex, (ii) displacement of this complex by an α -bromoketone (or an α -bromoester) containing nitroxide (P5), (iii) polymerization of the second monomer by ATRP (27). PVAc-*b*-PS copolymers (P6) of a low polydispersity have been accordingly synthesized and converted into PVOH-*b*-PS amphiphilic copolymers (P7) by methanolysis of the poly(vinyl acetate) block. Poly(vinyl acetate)-*b*-poly(ethylacrylate) (PVAc-*b*-PEA) and poly(vinyl acetate)-*b*-poly(methylmethacrylate) (PVAc-*b*-PMMA) have also been prepared according to the same strategy.



Scheme 2. Synthesis of end-functional PVAc and PVAc and PVOH containing block copolymers. **P1** (7.2K), $I_p = 1.15$; **P2** (12.0K), $I_p = 1.15$; **P3** (10.5K), $I_p = 1.30$; **P4** (10.5K), $I_p = 1.20$; **P5** (6.9K), $I_p = 1.15$; **P6** (PVAc(6.9K)-b-PS(16600)), $I_p = 1.30$; **P7** (PVOH(3.5K)-b-PS(16.6)); **P8** (PVAc(7.0K)-b-PS(20K)), $I_p = 1.68$; **P9** (PVAc(12.0K)-b-PS(10K)), $I_p = 1.56$; **P10** (PVOH(3.6K)-b-PS(13K)). Synthesis of the **P1-P7** was detailed in references 26 and 27.

Finally, the styrene polymerization has been directly initiated by a PVAc-Co macroinitiator with formation of PVAc-*b*-PS diblocks. The efficiency of this two-step strategy has been assessed by the disappearance of the elution peak of the PVAc macroinitiator (Figure 4). Nevertheless, the styrene conversion is low (<50%), the polydispersity of the copolymer is rather high ($1.5 \leq M_w/M_n \leq 2.0$), and the control of the PS block is limited. Quantitative hydrolysis of the PVAc block into PVOH leads to amphiphilic PVOH(3.6K)-*b*-PS(20K) (P10) diblock copolymer, which forms vesicles and bigger aggregates in water. The outer diameter of these vesicles is in the 50nm range, compared to 100-300nm for the aggregates. A variety of PVOH-*b*-PS copolymers have been prepared by this approach, in order to investigate their self-organization in water.

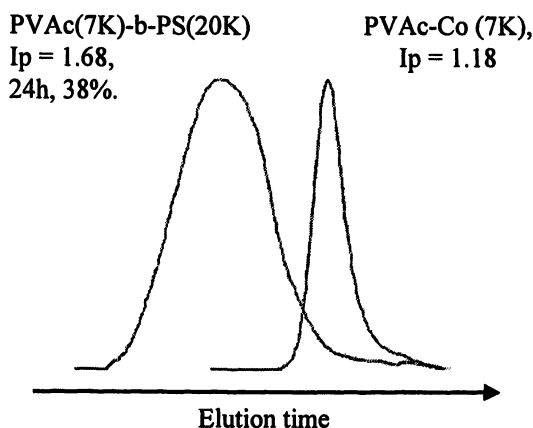


Figure 4. Size exclusion chromatograms for the PVAc(7K)-*b*-PS(20K) diblock (P8, Scheme 2) and the PVAc macroinitiator.

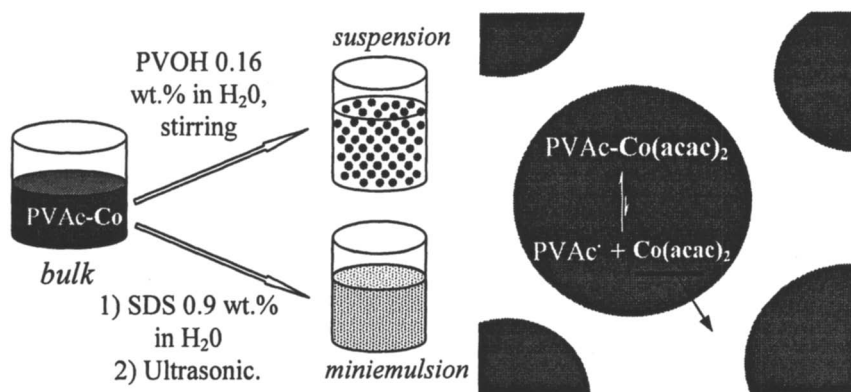
The cobalt mediated radical polymerization of vinyl acetate is clearly a valuable strategy for the macromolecular engineering of PVAc and PVOH and more complex macromolecules that contain them.

CMRP of Vinyl Acetate in Aqueous Media

The implementation of radical polymerization in aqueous media rather than in bulk or in solution is highly desirable in industry and explains why living/controlled radical polymerizations have been investigated in suspension, emulsion and miniemulsion (28-30), including vinyl acetate (31,32). Therefore,

CMRP of vinyl acetate has been carried out in suspension and miniemulsion (Scheme 3).

Vinyl acetate has been first conducted in suspension in water as follows : (i) bulk synthesis of PVAc end-capped by a cobalt complex with a low monomer conversion, (ii) dispersion of this polymerization medium (mixture of PVAc-Co and non converted VAc) in the aqueous solution of a surfactant, (iii) initiation of the cobalt mediated radical polymerization of VAc by the PVAc-Co macroinitiator in the organic droplets at 30°C (Scheme 3) (33). Under these conditions, the suspension polymerization is controlled consistent with a reasonably low polydispersity and the PVAc molar mass in agreement with the [VAc]/[PVAc-Co] ratio and monomer conversion (Table IV, entry 1). Typically, the collected beads of PVAc are in the millimeter range.



Scheme 3. Cobalt mediated radical polymerization in suspension and miniemulsion.

Compared to the PVAc particles prepared in suspension, smaller particles are formed in miniemulsion (below 200nm). Because this finer dispersion is prepared under ultrasonication a local overheating results in a high monomer conversion within 6 minutes, and a stable latex is formed (particle size ~ 100nm) (34). Again, the molar mass of PVAc depends on the [VAc]/[PVAc-Co] ratio and the polydispersity remains acceptable (Table IV, entry 2).

Compared to bulk polymerization, the $M_{n, \text{theor.}}/M_{n, \text{exp}}$ ratio deviates from unity in case of suspension and the polymerization rate is higher. This observation suggests that the hydrosoluble $\text{Co}(\text{acac})_2$ leaves the organic droplets in which the equilibrium is shifted towards the active species. These effects are more pronounced in miniemulsion because the probability for the cobalt complex to exit the organic particles is higher as result of a larger surface area.

Table IV. Cobalt mediated radical polymerization of vinyl acetate in suspension and miniemulsion.

| Entry | Bulk prepolymer. ^a | | | Dispersion polymerization | | | | | |
|----------------|-------------------------------|---------|----------|---------------------------|----------|----------------------|-----------------------------|-------------|-------------------------------|
| | $[VAc]/[Co]$ | t (h) | Conv (%) | t (min) | Conv (%) | $M_{n, exp}$ (g/mol) | $M_{n, th.}^d / M_{n, exp}$ | M_w / M_n | Size ^e (μm) |
| 1 ^b | | | | 30 | 37 | 26000 | 0.67 | 1.20 | |
| | 542 | 22 | 1 | 120 | 65 | 44000 | 0.69 | 1.20 | |
| | | | | 240 | 95 | 60500 | 0.73 | 1.35 | ~1000 |
| | | | | 25 | 36 | 49000 | 0.69 | 1.35 | |
| | 1084 | 14 | 9 | 40 | 48 | 66000 | 0.68 | 1.30 | |
| 2 ^c | | | | 70 | 75 | 100000 | 0.70 | 1.40 | ~1000 |
| | 433 | 26 | 17 | 6 | 71 | 46500 | 0.57 | 1.50 | 0.100 |
| | 542 | 23 | 11 | 6 | 79 | 71000 | 0.52 | 1.39 | 0.097 |
| | | | | 6 | 89 | 139200 | 0.60 | 1.66 | 0.095 |
| | 1084 | 22 | 13 | 6 | 89 | 139200 | 0.60 | 1.66 | 0.095 |

^a Bulk prepolymerization at 30°C with $[V-70]/[Co(acac)_2] = 3.25$.

^b Suspension. Addition of the pre-polymerized medium to a PVOH-co-PVAc aqueous solution (0.16 wt. %), $v_{VAc}/v_{H_2O} = 0.83$.

^c Miniemulsion. Addition of the pre-polymerized medium to a SDS aqueous solution (0.9 wt. %), $v_{VAc}/v_{H_2O} = 0.26$, followed by emulsification under ultrasonication for 6 min at 0°C.

^d $M_{n, theor.} = ([VAc]_0/[Co(acac)_2]_0) \times 86.09 \times conv$

^e The size of the beads (suspension) and the particles (miniemulsion) was measured with an optical microscope and by dynamic light scattering, respectively. Data listed are from references 33 and 34.

Conclusion

The commercially available cobalt(II)acetylacetonate complex is an effective mediator for the bulk radical polymerization of vinyl acetate at 30°C. The mechanism has been investigated by UV, NMR analysis of the chain-ends and analysis of the effect of several experimental parameters. This cobalt mediated radical polymerization has been successfully conducted in aqueous dispersed media, such as suspension and miniemulsion. Finally, the CMRP of vinyl acetate is an easy way to design end-functional PVAc and PVOH and block copolymers containing them. Clearly CMRP has a great potential in the macromolecular engineering of materials based on PVAc and PVOH.

Acknowledgements. The authors gratefully acknowledge Solvay for financial support and fellowship to A.D. They are grateful to Dr. A. Momtaz and Dr. V. Bodart for fruitful discussions. They also thank Wako for the gift of V-70. They are thankful to Prof. B. Charleux (University of Paris VI, France) and N. Willet (CERM) for their assistance in the miniemulsion process and characterization of latex particles, respectively. They are indebted to the "Belgian Science Policy" for financial support in the frame of the "Interuniversity Attraction Poles Programme (PAI V/03) - Supramolecular Chemistry and Supramolecular Catalysis". C. Detrembleur is "Chercheur Qualifié" by the "Fonds National de la Recherche Scientifique" (F.N.R.S.), Belgium.

References

1. Wakioka, M.; Baek, K.-Y.; Ando, T.; Kamigaito, M.; Sawamoto M. *Macromolecules* **2002**, *35*, 330-333.
2. Iovu, M. C.; Matyjaszewski, K. *Macromolecules* **2003**, *36*, 9346-9354.
3. Charmot, D.; Corpart, P.; Adam, H.; Zard, S.Z.; Biadatti, T.; Bouhadir, G. *Macromol. Symp.* **2000**, *150*, 23-32.
4. Destarac, M.; Charmot, D.; Franck, X.; Zard, S. Z. *Macromol. Rapid. Commun.* **2000**, *21*, 1035-1039.
5. Rizzardo, E.; Chiefari, J.; Mayadunne, R. T. A.; Moad, G.; Thang, S. H. *ACS Symp. Ser.* **2000**, *768*, 278-296.
6. Rizzardo E.; Chiefari, J.; Mayadunne, R.; Moad, G.; Thang, S. *Macromol. Symp.* **2001**, *174*, 209-212.
7. Destarac, M.; Taton, D.; Zard S.Z.; Saleh, T.; Six, Y. *ACS Symposium Series* **2003**, *854*, 536-550.
8. Stenzel, M. H.; Cummins, L.; Roberts, G. E.; Davis, T. P.; Vana, P.; Barner-Kowollik, C. *Macromol. Chem. Phys.* **2003**, *204*, 1160-1168.
9. Favier, A.; Barner-Kowollik, C.; Davis, T. P.; Stenzel, M. H. *Macromol. Chem. Phys.* **2004**, *205*, 925-936.
10. Coote, M. L.; Radom, L. *Macromolecules* **2004**, *37*, 590-596.
11. Gridnev, A. *J. Polym. Sci., Part. A : Polym. Chem.* **2000**, *38*, 1753-1766.
12. Gridnev, A.A.; Ittel, S.D. *Chem. Rev.* **2001**, *101*, 3611-3660.
13. Davis, T.P.; Kukulj, D.; Haddleton, D.M.; Maloney D.R. *Trends. Polym. Sci.* **1995**, *3(11)*, 365-373.
14. Wayland, B.B.; Poszmik, G.; Mukerjee, S.L.; Fryd, M. *J. Am. Chem. Soc.* **1994**, *116*, 7943-7944.
15. Wayland, B.B.; Basicke, L.; Mukerjee, S.; Wei, M.; Fryd, M. *Macromolecules* **1997**, *30*, 8109-8112.
16. Lu, Z.; Fryd, M.; Wayland, B.B. *Macromolecules* **2004**, *37*, 2686-2687.

17. Debuigne, A.; Caille, J.-R.; Jerome, R. *Angew. Chem., Int. Ed.* **2005**, *44*, 1101-1104.
18. Kaneyoshi, H.; Matyjaszewski, K. *Macromolecules* **2005**, *38*, 8163-8169.
19. Corpart, P.; Charmot, D.; Biadatti, T.; Zard, S.; Michelet, D., (Rhodia) WO9858974 **1998**.
20. Destarac, M.; Pees, B.; Boutevin, B. *Macromol. Chem. Phys.* **2000**, *201*, 1189-1199
21. Paik, H.-J.; Teodorescu, M.; Xia, J.; Matyjaszewski, K. *Macromolecules* **1999**, *32*, 7023-7031.
22. Qin, S.-H.; Qiu, K.Y. *Polymer* **2001**, *42*, 3033-3042.
23. Nuyken, O.; Wieland, P. C.; Heischkel, Y.; Raether, B. *Polym. Prepr. (Amer. Chem. Soc., Div. Polym. Chem.)* **2002**, *43(2)*, 84-85.
24. Ando, T.; Kamigaito, M.; Sawamoto, M. *Polym. Prepr. (Amer. Chem. Soc., Div. Polym. Chem.)* **2002**, *43(2)*, 179-180.
25. Gignes, D.; Bertin, D.; Marque, S.; Guerret, O.; Tordo, P. *Tet. Lett.* **2003**, *44*, 1227-1229.
26. Debuigne, A.; Caille, J.-R.; Jerome, R. *Macromolecules* **2005**, *38*, 5452-5458.
27. Debuigne, A.; Caille, J.-R.; Willet, N.; Jérôme, R. *Macromolecules* **2005**, *38(23)*, 9488-9496.
28. Qiu, J.; Charleux, B.; Matyjaszewski, K. *Prog. Polym. Sci.* **2001**, *26*, 2083-2134.
29. Cunningham, M. F. *Prog. Polym. Sci.* **2002**, *27*, 1039-1067.
30. Prescott, S.W.; Ballard, M. J.; Rizzardo, E.; Gilbert, G. *Aust. J. Chem.* **2002**, *55*, 415-424.
31. Simms, R.W.; Davis, T.P.; Cunningham, M.F. *Macromol. Rapid Commun.* **2005**, *26(8)*, 592-596.
32. Russum, J.P.; Barbre, N.D.; Jones, C.W.; Schork, F.J. *J. Polym. Sci. Part A: Polym. Chem.* **2005**, *43*, 2188-2193.
33. Debuigne, A.; Caille, J.-R.; Detrembleur, C.; Jerome, R. *Angew. Chem., Int. Ed.* **2005**, *44*, 3439-3442.
34. Detrembleur, C.; Debuigne, A.; Bryaskova, R.; Charleux, B.; Jérôme, R. *Macromol. Rapid. Commun.* **2006**, *27*, 37-41.

Chapter 27

Borane-Mediated Control Radical Polymerization: Synthesis of Chain End Functionalized Fluoropolymers

T. C. Chung, H. Hong, Z. C. Zhang, and Z. M. Wang

**Department of Materials Science and Engineering, The Pennsylvania State
University, University Park, PA 16802**

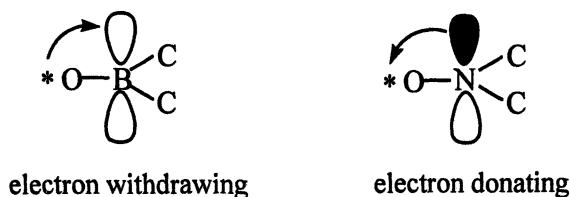
This paper summarizes our experimental results in a new family of borane-based control radical initiators and their unique application in the synthesis of fluoropolymers containing one or more terminal functional groups. The chemistry is advantaged by its simplicity of borane initiator and mild reaction condition, and applicable to a broad range of fluoromonomers, including VDF, f-acrylic, etc. Two type borane initiators, including cycloborane and functional borane, will be discussed to illustrate the functionalization scheme. The control radical polymerization is characterized by predictable molecular weight, narrow molecular weight distribution, formation of diblock copolymer, and tolerance to many functional groups that usually cause chain transfer reactions in regular free radical polymerization. In turn, the chain end functionalized fluoropolymers exhibit very high surface activities in the polymer/inorganic composites. For example, the polymer can exfoliate clay interlayer structure in PVDF/clay nanocomposite, and maintaining the disorder state even after further mixing with neat (unfunctionalized) polymer.

Fluoropolymers, such as poly(tetrafluoroethylene) (PTFE), poly(vinylidene fluoride) (PVDF), poly(vinylidene-co-hexafluoropropene) (VDF/HFP elastomer), etc., exhibit an unique combination of properties, including thermal stability, chemical inertness (acid and oxidation resistance), low water and solvent absorptivities, self-extinguishing, excellent weatherability, very interesting surface properties, and becoming important electric and electronic properties. They are commonly used in many high-end applications, such as aerospace, automotive, textile finishing, and microelectronics (1). However, fluoropolymers also have some drawbacks, including limited processibility, poor adhesion to substrates, limited crosslinking chemistry, and inertness to chemical modification, which limit their applications when interactive and reactive properties are paramount. Functionalization of fluoropolymers, having specific functional groups, have been a constant research interest in the past decades. Most of research approaches have been focusing on copolymerization of fluorinated monomers with functional comonomers to form functional fluorocopolymers containing pendent functional groups (2-6). Few reports discussed the preparation of fluoropolymers containing terminal functional groups (7-10). Recently, Saint-Loup et al. (11) prepared telechelic VDF/HFP elastomers containing two opposing hydroxy terminal groups by using hydrogen peroxide as an initiator. However, many side reactions occur in this polymerization, and the final product contains not only hydroxy terminal groups but also carboxylic acid terminal groups, as well as some unsaturated terminal groups.

Living radical polymerization provides a very useful method to prepare a wide range of polymers with well-defined molecular structures; i.e. narrow molecular weight distribution, control molecular weight, and desirable polymer chain ends. Early attempts to realize living radical polymerization involved the concept of reversible termination of the growing polymer chains by iniferters (12,13), such as N,N-diethyldithiocarbamate derivatives, with some success. The first living radical polymerization was observed in reactions involving a stable nitroxyl radical, such as TEMPO (14, 15), which does not react with monomers but forms a reversible end-capped propagating chain end. Usually, the reactions have to be carried out at an elevated temperature (>100 °C) to obtain a sufficient concentration of propagating radicals for monomer insertion. Subsequently, several research groups have replaced the stable nitroxyl radical with transition metal species or reversible chain transfer agents as the capping agents to mediate living free radical systems. These polymerization reactions follow the mechanisms of atom transfer radical polymerization (ATRP) (16,17) or reversible addition-fragmentation chain transfer (RAFT) (18), respectively. Overall, these systems have a central theme-reversible termination via equilibrium between the active and dormant chain ends at an elevated temperature.

In our group, we have been studying a new free radical initiation system based on the oxidation adducts of organoborane and oxygen, which contains boroxyl radical - a mirror-image of the stable nitroxyl radicals - as shown in

Scheme 1. Our early interest in the borane/oxygen radical initiator stemmed from the desire to develop a new effective route in the functionalization of polyolefins (19-22) (i.e. PE, PP) and block/graft copolymers (23-26), which has been a long-standing scientific challenge area with great potential for industrial applications.



Scheme 1

The unexpected good control in the incorporation of borane groups to polyolefin by metallocene catalysis and the subsequent radical chain extension by the incorporated borane groups prompted us to examine this free radical polymerization mechanism in greater details. Several relatively stable borane-based radical initiators were discovered, which exhibited living radical polymerization characteristics, with a linear relationship between polymer molecular weight and monomer conversion (27) and producing block copolymers by sequential monomer addition (28). This stable radical initiator system was recently extended to the polymerization of fluorinated monomers, which can effectively occur in bulk and solution conditions. Some interesting ferroelectric fluoro-terpolymers (29), showing large electromechanical response, have been prepared with high molecular weight and controlled polymer structure with narrow molecular weight and composition distributions. In this paper, we will focus on the application of this stable borane initiator technology to prepare fluoropolymers having one or two terminal functional groups, which includes the published results in fluorinated acrylate (30, 31) and new observation in VDF-based polymers.

Experimental

Synthesis of 8-boraindane Initiator

Under Ar atmosphere at 0° C, 21.6 g (0.2 mol) of 1,3,7-octatriene in 50 ml of THF solution was added dropwise with 200 ml (1.0 M) of borane THF complex in THF solution. After the addition was complete, stirring continued for 1 hour at 0° C. Then the mixture was refluxed for 1 hour before THF was removed completely under vacuum at room temperature. The attained white

solid was heated to 210°C for 3 hours then 9.6 g of 9-bora-indane (yield: 41%) was distilled from the mixture at about 50 °C to 60 °C (0.3 mmHg). The spectra data were as follows: ¹H-NMR (25° C in CDCl₃) δ .08~1.6 ppm (m); ¹¹B-NMR (25°C in CDCl₃) δ 91.14 ppm (s); ¹³C-NMR (25°C in CDCl₃) δ 21.9 ppm (b, CH₂-B), δ 25.6 ppm (s, CH₂), δ 26.3 ppm (s, CH₂), δ 27.4 ppm (b, CH₂-B), δ 28.4 ppm (s, CH₂), δ 31.6 ppm (s, CH₂), δ 34.4 ppm (s, CH₂), δ 42.4 ppm (b, CH-B).

Synthesis of [(C₂H₅O)₃SiCH₂CH₂]₃B Functional Initiator

In a 500 ml flame-dried flask equipped with a magnetic stir bar, 250 ml of dry THF and 35 g (180 mmol) of vinyltriethoxysilane was injected under argon. After cooling the solution to 0° C, 60 ml of BH₃ in THF (1.0 M) was added. The mixture was stirred at 0° C for 4 hours and then was warmed to ambient temperature for 1 hour to assure complete hydroboration reaction. After solvent-removal, the product was subjected to vacuum distillation at 170° C to obtain 23.4 g of tri-(triethoxyethylsilyl)borane product. ¹H NMR spectrum indicates the hydroboration reaction involving mainly anti-markovnikov addition (>90%). The spectra data were as follows: ¹¹B-NMR (25°C in CDCl₃) δ 81.52 ppm (s); ¹H-NMR (25° C in CDCl₃) δ 0.52-0.58 ppm (b, CH₂-Si), δ 1.14 ppm (s, CH₃), δ 1.44 ppm (b, CH-B). δ 3.72 ppm (s, CH₂-O).

Synthesis of Telechelic Poly(trifluoroethyl acrylate) with Two Terminal OH Groups Using 8-Bora-indane/O₂ initiator

In a 150 ml flask, 40 ml of THF, 6 ml (50 mmol) of 2',2',2'-trifluoroethyl acrylate (TFEA) monomer, and 70 mg (0.6 mmol) of 8-bora-indane were introduced under argon. After injecting 5 ml of O₂, the solution was mixed for about 5 minutes. The solution was then kept at room temperature for various times before exposing the solution to air that stops the reaction. The solution was then poured into 200 ml of well stirred methanol to quench the polymerization and precipitate PTFEA polymer. To assure complete oxidation of all borane moieties, the isolated polymer was then re-dissolved in 20 ml THF before adding 0.2 ml (6N) NaOH solution, followed by dropwise 0.4 ml, 33% H₂O₂ at 0° C. The resulting mixture was stirred for 1 hour to complete the oxidation. After cooling to room temperature, the solution was poured into 200 ml of well stirred methanol. The precipitated telechelic poly(trifluoroethyl acrylate) was collected, washed, and dried in vacuum at 60° for 2 days, then was characterized by Gel Permeation Chromatography (GPC) and ¹H and ¹³C NMR-DEPT measurements.

Synthesis of poly(methyl methacrylate-*b*-trifluoroethyl acrylate) diblock copolymer Using 8-Bora-indane/O₂ initiator

In a flame-dried 50 ml flask, 5.0 ml (50 mmol) of MMA and 70 mg (0.6 mmol) of 8-bora-indane were mixed under argon. To this mixture 5.0 ml of O₂ (0.2 mmol) was injected, following by vigorous shaking to assure complete mixing. The system was then kept at room temperature for 20 min, followed by removal of all the volatiles by vacuum distillation. About 5.0 ml of 2',2',2'-trifluoroethyl acrylate (TFEA) was subsequently injected into the system. The mixture was shaken vigorously to dissolve the solid as soon as possible. After complete dissolution, the solution was kept at room temperature for 1 hour before adding 10 ml of acetone to reduce the viscosity and then opening the system to air to oxidize all the borane moieties. The solution was then poured into 200 ml of well stirred methanol. The precipitated telechelic diblock polymer was collected, washed, and dried in vacuum at 60°C for 2 days. The resulting telechelic poly(methyl methacrylate-*b*-trifluoroethyl acrylate) diblock copolymer was characterized by GPC and ¹H and ¹³C NMR-DEPT measurements.

Synthesis of PVDF Polymers with A Terminal (C₂H₅O)₃Si Group

In a typical reaction, 2.9 g of [(C₂H₅O)₃SiCH₂CH₂]₃B (5 mmol) was dissolved in 100 ml of CH₂Cl₂ in a dry box, the reactor was then connected to a vacuum line, and 25.6 g of VDF (400 mmol) was condensed into a autoclave reactor under vacuum by liquid nitrogen. VDF has a vapor pressure of ~ 40 atm at 25 °C. About 2.5 mmol O₂ was charged into the reactor to oxidize borane moiety and initiate the polymerization that was carried out at ambient temperature for 4 hours. After releasing the pressure, the mixture was transferred into a flask containing 100 ml of hexane. After stirring for 30 min, the polymer powder was filtered, washed, and then dried under vacuum at 60°C for 6 hours. About 21 g of polymer was obtained with yield of 82 %. The resulting polymer was characterized by intrinsic viscosity (M_v) and ¹H NMR measurements.

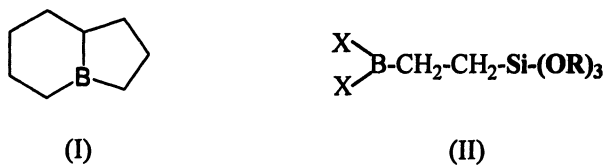
Preparation of PVDF/Clay Nanocomposite.

In a typical example, a PVDF-*t*-Si polymer (T_m = 170° C, M_v = 30,000 g/mol) was mixed with Na⁺-mmt clay. Static melt intercalation was employed by heating the mixture at 190° C for 3 hr under nitrogen condition. The resulting PVDF-*t*-Si/Na⁺-mmt nanocomposite shows a featureless XRD pattern, indicating the formation of an exfoliated clay structure. The resulting binary PVDF-*t*-Si/Na⁺-mmt exfoliated nanocomposite was further melting mixing (50/50 weight

ratio) with commercial neat PVDF ($M_n = 70,000$ and $M_w = 180,000$ g/mol). The resulting ternary PVDF/ PVDF-*t*-Si/Na⁺-mmt nanocomposite also shows a featureless XRD pattern.

Results and Discussion

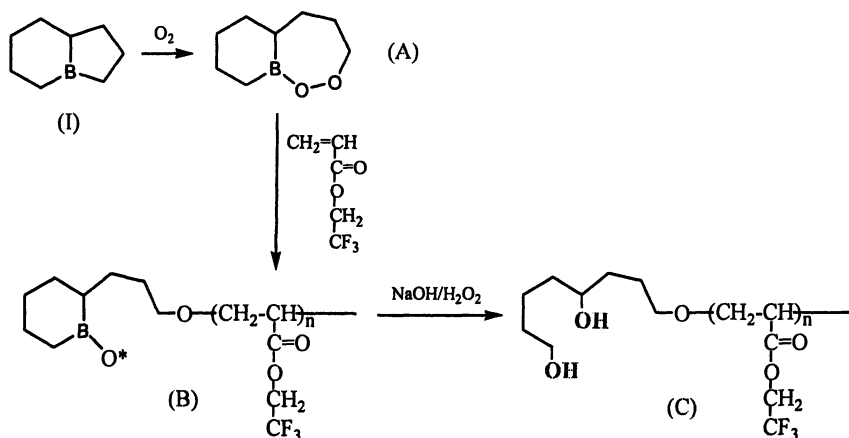
In this paper, we discuss two borane initiators, including cycloborane (I) and silane containing borane (II) shown in Scheme 2, which can introduce one or more functional groups in the beginning of perfluorinated polymers, such as poly(vinylidene fluoride) (PVDF) and fluorinated acrylic polymers.



Scheme 2

Chain end functionalized acrylic fluoropolymers (30, 31)

Equation 1 illustrates the preparation of chain end functionalized acrylic fluoropolymer by using the 8-boraindane initiator (I). The cyclic B-C bond in 5-member ring of 8-boraindane (I) may be preferly oxidized under a controlled oxidation condition to form a peroxide compound (C-O-O-BR₂) (A) that initiates control radical polymerization of 2,2,2-trifluoroethylacrylate (TFEA) monomers at ambient temperature. The C-O-O-BR₂ species is decomposed to an alkoxy radical (C-O*) and a borinate radical (*O-BR₂) in the presence of fluoromonomers. The alkoxy radical is active in initiating the polymerization of TFEA. On the other hand, the borinate radical is too stable to initiate polymerization due to the back-donating of electrons to the empty p-orbital of boron. However, this "stable" borinate radical may form a reversible bond with the radical at the growing chain end to form dormant species and prolong the lifetime of the propagating radical. In the whole polymerization process, the mono-oxidized bicycloborane residue remains bonded to the beginning of the polymer chain (B), despite the continuous growth of the polymer chain. After terminating the control radical polymerization, the two unreacted cyclic B-C bonds in the borane residue can be completely interconverted to functional groups, such as two OH groups by NaOH/H₂O₂ reagent. The resulting poly(2,2,2-trifluoroethylacrylate) (C) contains two OH groups located at the beginning of polymer chain.



Equation 1

Table 1 summarizes several comparative polymerization runs in the preparation of telechelic PTFEA polymers. The polymer molecular weight is linearly increased with the monomer conversion, and polymers maintain relatively narrow molecular weight distribution throughout the polymerization process, implying a "stable" propagation without significant termination and chain transfer reactions. This chemistry is applicable to many acrylate and methacrylate monomers, including fluorinated and unfluorinated ones and their mixtures (30, 31). Apparently, a constant number of active sites are formed after the oxidation reaction, which maintained reactivity throughout the polymerization process (30). This controlled radical polymerization was also evidenced by end group analysis and diblock copolymers, such as poly(methyl methacrylate-*b*-trifluoroethyl acrylate), by sequential monomer addition (discussed later).

Table 1. A summary of TFEA polymerization^a by 8-bora-indane/O₂ in THF

| Run | Time (hr) | Conversion (%) | Mn ^b (g/mole) | Mw ^b (g/mole) | PDI (Mw/Mn) |
|-----|--------------|-------------------|-----------------------------|-----------------------------|----------------|
| 1 | 2.0 | 12 | 7,000 | 14,000 | 2.0 |
| 2 | 4.0 | 19 | 12,000 | 23,500 | 2.0 |
| 3 | 6.0 | 40 | 25,000 | 49,000 | 1.9 |
| 4 | 8.0 | 52 | 30,500 | 52,500 | 1.7 |
| 5 | 10 | 60 | 33,000 | 56,000 | 1.6 |

a. Reaction temperature: 25° C.

b. Molecular weight determined by GPC.

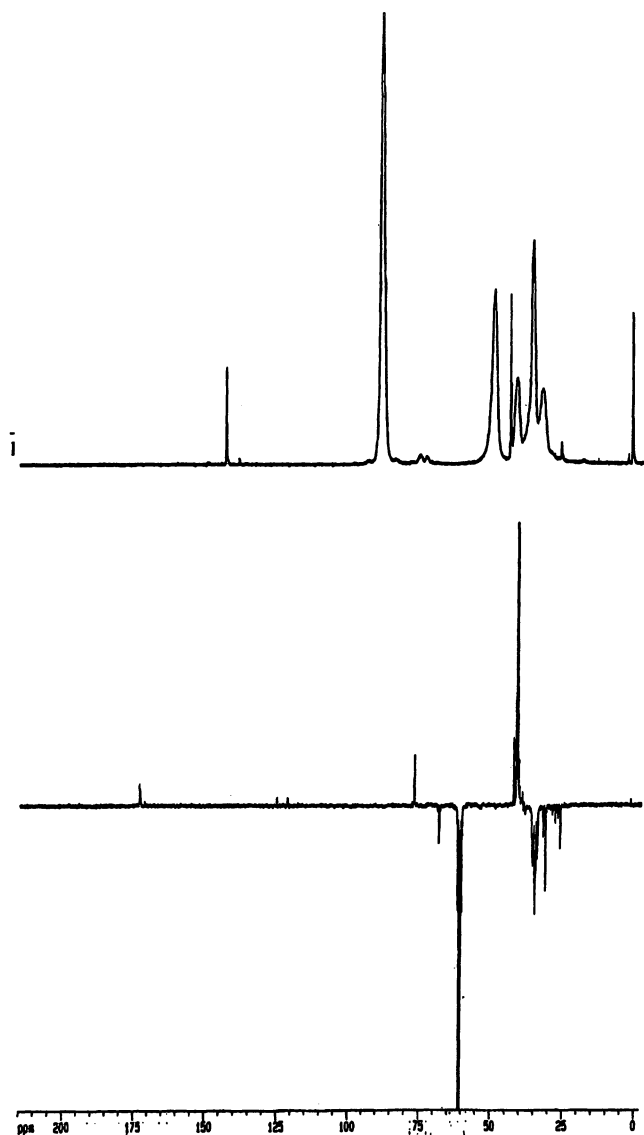


Figure 1. (top) ^1H and (bottom) ^{13}C NMR-DEPT 135 spectra of PTFEA prepared by 8-bora-indane/ O_2 in benzene at 0°C . (Reproduced with permission from *Macromolecules* 2004, 37, 6260-6263. Copyright 2004 American Chemical Society.)

Figure 1 shows ^1H and ^{13}C NMR-DEPT 135 spectra of the resulting telechelic poly(trifluoroethyl acrylate) having two terminal OH groups (run 1 in Table 1). In ^1H NMR spectrum, there are two weak peaks at 3.7-4.0 ppm, indicating the existence of two type OH groups, and some expected chemical shifts between 1.7-2.8 ppm for CH_2 and CH groups and a strong peak at 4.6 ppm for O-CH_2 group in the PTFEA chain. To provide direct evidence for the existence of both primary and secondary OH groups, the telechelic polymer was also examined by ^{13}C NMR (DEPT-135). In addition to three expected chemical shifts at 25.4-35.6 (negative), 41.1 (positive), and 60.1 (negative) ppm, corresponding to the CH_2 , CH , and O-CH_2 groups, respectively, in the PTFEA backbone, there are two distinctive chemical shifts - one negative peak at 68.2 ppm, corresponding to the primary $\text{CH}_2\text{-OH}$ group, and one positive peak at 77.6 ppm, corresponding to the secondary CH-OH group. For quantitative end group analysis, both OH groups in the telechelic PTFEA polymer were completely converted to the corresponding silane derivative by reacting with $\text{Cl-Si}(\text{CH}_3)_3$ reagent. A new chemical shift at 0.15 ppm corresponding to $\text{-O-Si}(\text{CH}_3)_3$ is clearly observed with a reasonable intensity for qualitative analysis. The peak intensity ratio between two peaks (4.6 and 0.15 ppm) and the representing protons indicate about two OH groups per PTFEA chain.

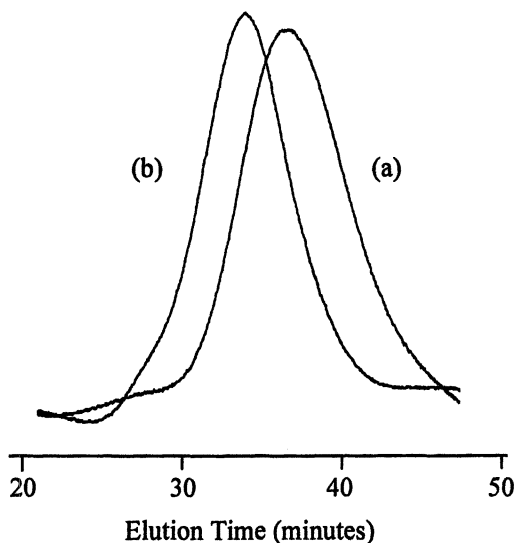


Figure 2. GPC curve comparison between (a) PMMA and (b) PMMA-*b*-PTFEA diblock Copolymer Prepared by Using 8-Bora-indane/ O_2 initiator. (Reproduced with permission from *Macromolecules* 2004, 37, 6260-6263. Copyright 2004 American Chemical Society.)

It is also possible to extend the functional borane-mediated control radical polymerization to block copolymers by means of sequential monomer addition. After completing the polymerization of a first monomer to form a first polymer "block", a second monomer is introduced into the reaction mass to polymerize the second monomer to form a second polymer "block". After terminating the living polymerization, the partially oxidized borane residue located at the beginning of polymer chain can be completely interconverted to two reactive functional groups. Figure 2 compares GPC curves of a telechelic poly(methyl methacrylate-*b*-trifluoroethylacrylate) diblock copolymer (graph b) and the corresponding poly(methyl methacrylate) homopolymer (graph a). The molecular weight almost doubles from the homopolymer ($M_n = 12,400$ and $M_w = 24,000$ g/mol) to the diblock copolymer ($M_n = 32,800$ and $M_w = 58,000$ g/mol) without a broadening in the molecular weight distribution.

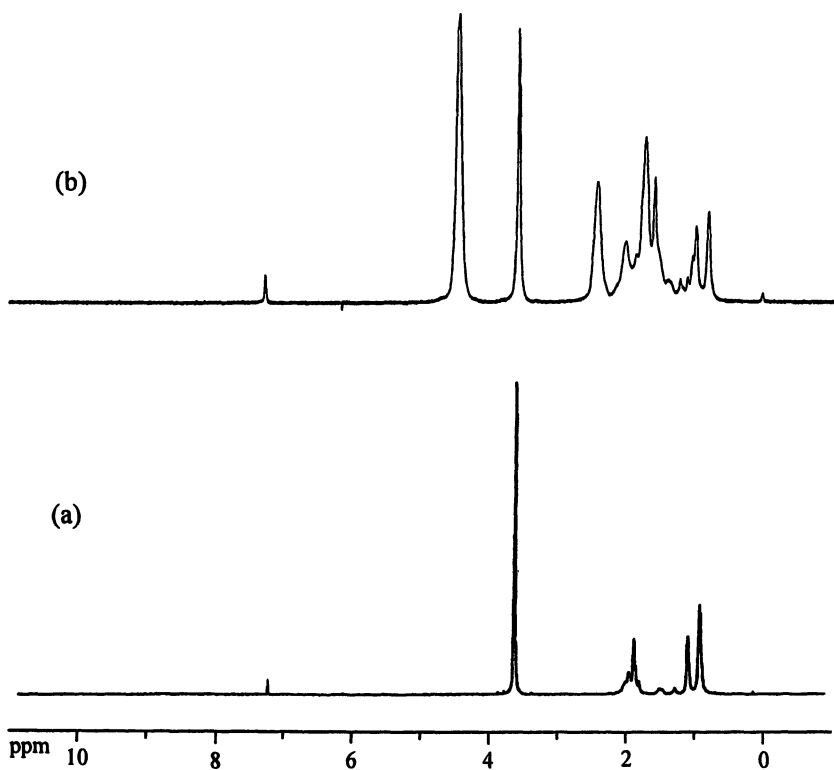
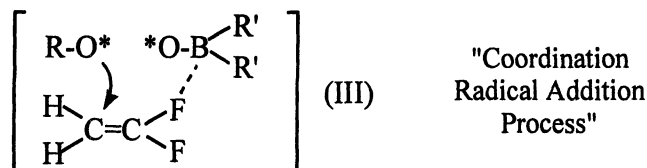


Figure 3. ^1H NMR spectra between (a) PMMA and (b) PMMA-*b*-PTFEA diblock Copolymer Prepared by 8-Bora-indane/ O_2 initiator. (Reproduced with permission from *Macromolecules* 2004, 37, 6260-6263. Copyright 2004 American Chemical Society.)

Figure 3 compares the same two polymers, poly(methyl methacrylate-*b*-trifluoroethylacrylate) diblock copolymer (top) and the corresponding poly(methyl methacrylate) homopolymer (bottom). The incorporation of second polymer block is clearly evidenced with strong new peaks for PTFEA. Basically, the copolymer composition is controlled by the monomer feed ratio and reaction time. The combined experimental results strongly indicate 8-boraindane as a clear and effective control radical initiator for both fluoro- and non-fluoro acrylic monomers. This bicyclic initiator provides the route to prepare not only well-defined homo- and block copolymers but also telechelic polymers having two OH groups at the same polymer chain end.

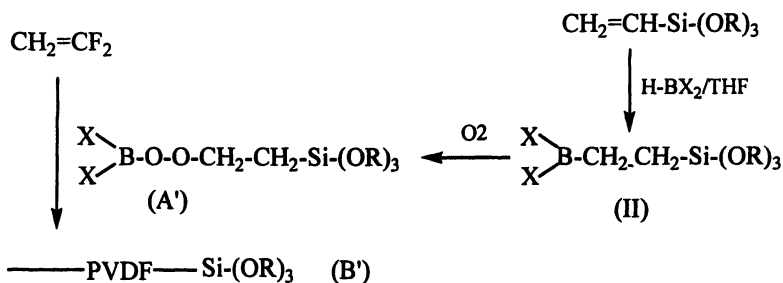
Chain end functionalized PVDF

The borane based radical initiators are also active in polymerization of olefinic fluoro monomers (32), such as VDF (vinylidene fluoride), TrFE (trifluoroethylene), HFP (hexafluoropropene), and their mixtures, at ambient temperature. During the propagating reaction, a coordination intermediate (III) may be formed due to the B-F acid-base complex between the active site and the incoming monomer, as illustrated in Scheme 3. Such an interaction may enhance the reactivity of fluoromonomer and minimize side reactions, and therefore produce functional fluoro-copolymers with the controlled molecular structures. As the alkoxy radical initiates the polymerization, the "dormant" borinate radical may form a reversible bond with the radical at the growing chain end to prolong the lifetime of the propagating radical and reduce chain transfer reactions.



Scheme 3

By using functional borane initiators, containing some specific functional groups that are stable during the borane oxidation and polymerization process, it's possible to prepare olefinic fluoropolymers containing terminal functional group(s). Equation 2 illustrates an example, in which the preparation of silane terminated poly(vinylidene fluoride) [PVDF-*t*-Si(OR)₃] by using a silane containing borane initiator.



Equation 2

The functional borane initiator (II), containing a silane group, was quantitatively prepared by simple hydroboration reaction of vinylsilane (commercially available) with a borane compound containing at least one B-H group at ambient temperature. The subsequent mono-oxidation reaction of functional borane initiator (II) with a controlled quantity of oxygen is spontaneously occurred at room temperature to form the corresponding peroxyborane (A') for initiating polymerization. This oxidation reaction can be carried out in situ during the controlled radical polymerization with the presence of monomers. The resulting fluoropolymers (B') have a terminal silane group at the beginning of the polymer chain. Table 2 summarizes the experimental conditions and results of VDF polymerization reactions initiated by $[(\text{C}_2\text{H}_5\text{O})_3\text{SiCH}_2\text{CH}_2]_3\text{B}/\text{O}_2$ system, which results in PVDF-*t*-Si(OC₂H₅)₃ (silane-terminated PVDF) polymers. The monomer conversion under a constant reaction time (4 hours) is basically controlled by the active sites governed by borane and oxygen concentrations.

Table 2. Summary of PVDF Polymers Containing A Terminal Silane Group Prepared by $[(\text{C}_2\text{H}_5\text{O})_3\text{SiCH}_2\text{CH}_2]_3\text{B}/\text{O}_2$ Initiator

| Run | B (mmol) | O ₂ (mmol) | VDF (mmol) | Yield (%) |
|-----|-------------|--------------------------|---------------|--------------|
| 4 | 5.0 | 1.0 | 400 | 32 |
| 5 | 5.0 | 2.5 | 400 | 82 |
| 6 | 5.0 | 5.0 | 400 | 73 |
| 7 | 10.0 | 5.0 | 400 | 86 |

Figure 4 shows ¹H NMR spectrum of a PVDF-*t*-Si(OC₂H₅)₃ polymer (*M_v* = 10,600 g/mole), with two insets of the expanded regions exhibiting chain end and side chain structures. Two major chemical shifts at $\delta = 2.3$ ppm (weak) and $\delta = 2.9$ ppm (strong) correspond to CH₂ units with head-to-head and head-to-tail monomer sequence in the PVDF backbone, respectively. In the expanded

regions, there are two dominate chemical shifts at 1.15 ppm (CH_3) and 3.75 ppm (OCH_2), almost identical with those in $[(\text{C}_2\text{H}_5\text{O})_3\text{SiCH}_2\text{CH}_2]_3\text{B}$ initiator, which represent the existence of terminal $(\text{C}_2\text{H}_5\text{O})_3\text{Si}$ silane group in PVDF polymer chain end. In addition, the peak intensity ratio between chain end and main chain indicates about one silane per polymer chain, using polymer molecular weight estimated from intrinsic viscosity and Mark-Houwink equation. Recently, some solubility studies by immobilizing PVDF- $t\text{-Si}(\text{OC}_2\text{H}_5)_3$ polymer chains onto a silicate substrate also indicate that most of polymer chains contain silane group. It's interesting to note that the weak chemical shift at 6.3 ppm (CF_2H) is associated with the conventional intra-chain transfer process (33).

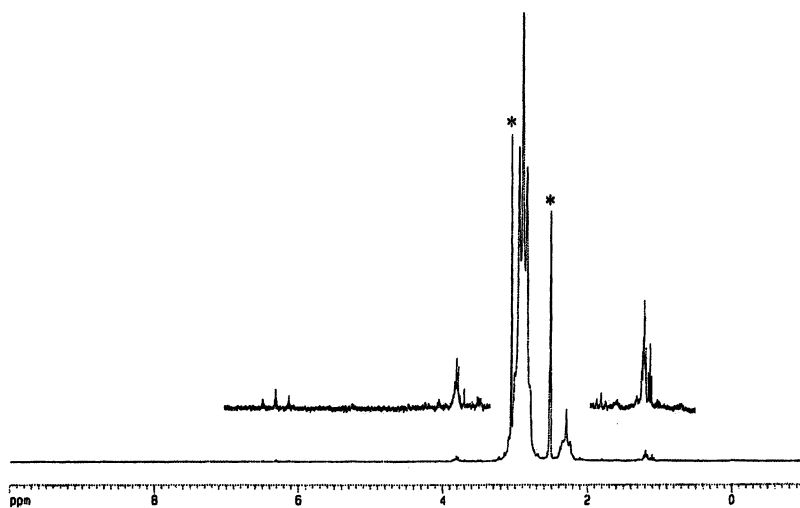
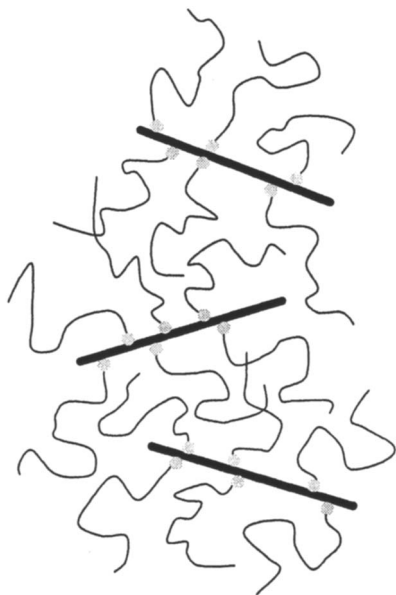


Figure 4. ^1H NMR spectrum of PVDF- $t\text{-Si}(\text{OC}_2\text{H}_5)_3$ polymer ($M_v = 10,600$ g/mole), with two insets of the expanded regions.

One major advantage of the fluoropolymer having terminal functional group(s) in one end of polymer chain is that they exhibit very high surface activity on the silicate clay surfaces to exfoliate clay interlayer structure, even using the pristine clay material (without treatment with organic surfactants or acids). Figure 5 illustrates the interaction pattern between chain end fluoropolymer and the clay interlayer surfaces (34). The terminal functional group can anchor fluoropolymer chain to the clay surfaces between interlayers by chemical bond (such as Si-O-Si or Si-O-C bond). On the other hand, the rest unperturbed high molecular weight hydrophobic and oleophobic fluoropolymer

chain, disliking the hydrophilic clay surfaces, exfoliates the clay layer structure and maintains this disorder clay structure even after further mixing with neat (unfunctionalized) polymer that is compatible with the backbone of the chain end functionalized fluoropolymer.



- Residue after the reaction between clay surface and fluoropolymer terminal functional group, such as $\text{Si}(\text{R})_n(\text{OH})_{3-n}$, $\text{Si}(\text{R})_n(\text{OR})_{3-n}$, OH, NH_2 , COOH, anhydride, ammonium, imidazolium, sulfonium, phosphonium.

Figure 5. Illustration of an exfoliated fluoropolymer/clay nanocomposite using chain end functionalized fluoropolymer as the interfacial agent.

Figure 6 shows X-ray diffraction study of a typical example. A PVDF-*t*-Si polymer containing a terminal $\text{C}_2\text{H}_5\text{OSi}(\text{CH}_3)_2$ group ($T_m = 170^\circ\text{C}$, $M_v = 30,000$ g/mol) was mixed with Na^+ -mmt clay, which has an ion-exchange capacity of ca. 90 mequiv/100g (WM). Static melt intercalation was employed by firstly mixing and grinding PVDF-*t*-Si dried powder and Na^+ -mmt with 90/10 weight ratio in a mortar and pestle at ambient temperature. The XRD pattern (shown in Figure 6,a) of this simple mixture shows a (001) peak at $2\theta \sim 7$, corresponding to Na^+ -mmt interlayer structure with a d-spacing of 1.45 nm. The mixed powder was then heated at 190°C for 3 hr under nitrogen condition. The resulting PVDF-*t*-Si/ Na^+ -mmt nanocomposite shows a featureless XRD pattern (shown in Figure 6,b), indicating the formation of an exfoliated clay structure. The resulting binary PVDF-*t*-Si/ Na^+ -mmt exfoliated nanocomposite was further melting mixing (50/50 weight ratio) with commercial neat PVDF ($M_n = 70,000$ and $M_w = 180,000$ g/mol). Firstly the PVDF-*t*-Si / Na^+ -mmt exfoliated nanocomposite and neat PVDF with 50/50 weight ratio were ground

together in a mortar and pestle at ambient temperature. The mixed powder was then heated at 200° C for 3 hr under nitrogen condition. The resulting ternary PVDF/ PVDF-t-Si/Na⁺-mmt nanocomposite also shows a featureless XRD pattern (shown in Figure 6,c), indicating that the stable exfoliated structure in the binary PVDF-t-Si/Na⁺-mmt exfoliated nanocomposite is clearly maintained after further mixing with PVDF that is compatible with the backbone of PVDF-t-Si.

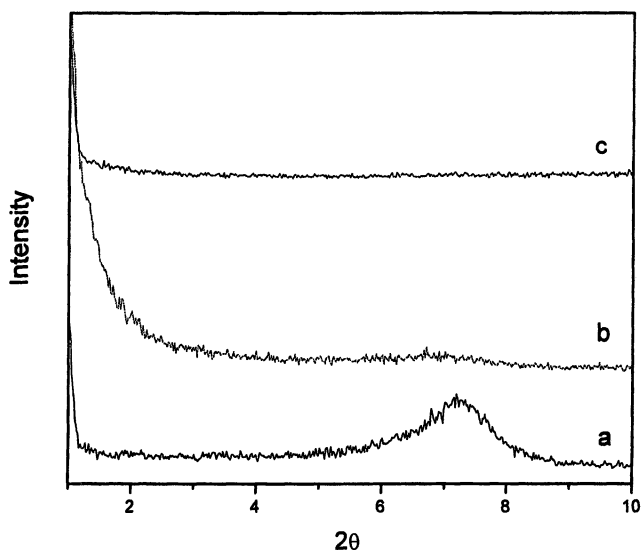


Figure 6. X-ray diffraction patterns of (a) physical mixture of PVDF-t-Si and Na⁺-mmt (90/10 wt%), (b) the same mixture after static melt-intercalation, and (c) the 50/50 mixture by weight of exfoliated PVDF-t-Si/ Na⁺-mmt structure (from b) and neat PVDF.

Conclusion

We have developed two type borane-based control radical initiators, including cycloborane and functional borane, for preparing fluoropolymers containing one or more terminal functional groups. The chemistry is advantaged by its simplicity of borane initiator and mild reaction condition, and applicable to both olefinic and acrylic fluoromonomers. The control radical polymerization is characterized by predictable molecular weight, narrow molecular weight

distribution, formation of chain end functional polymer and diblock copolymer, and tolerance to many functional groups that usually cause chain transfer reactions in regular free radical polymerization. The chain end functionalized fluoropolymers, with a terminal polar group and hydrophobic polymer chain, exhibit very high surface activities in the polymer/clay composites, which show an exfoliated clay nanocomposite structure.

Acknowledgements

The authors would like to thank the Office of Naval Research and Daikin Corporation for the financial support.

References

1. Scheirs, J. "Modern Fluoropolymers" J. Wiley and Sons, Australia, 1997.
2. Yamabe, M. Y. *Makromol. Chem., Macromol. Symp.* **1992**, *64*, 11.
3. Takakura, T. "CTFE-Vinyl Ethers copolymers In Modern Fluoropolymers"; Scheirs, J., Ed.; Wiley: New York, 1997; Chapter 29, p 557.
4. Boutevin, B.; Ameduri, B. *Macromol. Symp.* **1994**, *82*, 1.
5. Kostov, G. K.; Matsuda, O.; Machi, S.; Tabata, Y. *J. Polym. Sci. Part A, Polym. Chem.* **1979**, *17*, 3991.
6. Kostov, G.; Ameduri, B.; Boutevin, B. *J. of Fluorine Chem.* **2002**, *114*, 171.
7. Rice, D. E.; Sandberg, C. L. *U. S. Patent* 3,461,155.
8. Maxwell Robinson, I.; Kochi, J. K. *Macromolecules* **1983**, *16*, 526.
9. Oka, M.; Tatemoto, M. *Comtemp. Topics in Polym. Sci.* **1984**, *4*, 763.
10. Tatemoto, M.; Nakagawa, T. *U. S. Patent* 4,158,678.
11. Saint-Loup, R.; Manseri, A.; Ameduri, B.; Lenret, B.; Vignane, P. *Macromolecules* **2002**, *35*, 1542.
12. Otsu, T.; Yoshida, M. *Makromol. Chem., Rapid Commun.* **1982**, *3*, 127.
13. Otsu, T.; Kuriyama, A. *J. Macromol. Sci., Chem.* **1984**, *A21*, 921.
14. Georges, M. K.; Veregin, P. R. N.; Kazmaier, P. M.; Hamer, G. K. *Macromolecules* **1993**, *26*, 2987.
15. Hawker, G. J. *J. Am. Chem. Soc.* **1994**, *116*, 11185.
16. Wang, J. S.; Matyjaszewski, K. *J. Am. Chem. Soc.* **1995**, *117*, 5614.
17. Kato, M.; Kamigaito, M.; Sawamoto, M.; Higashimura, T. *Macromolecules* **1995**, *28*, 1721.
18. Chiefari, J.; Chong, Y. K.; Ercole, F.; Krstina, J.; Jeffery, J.; Le, T.; Mayadunne, R.; Meijs, G. F.; Moad, C. L.; Moad, G.; Rizzardo, E.; Thang, S. H. *Macromolecules* **1998**, *31*, 5559.

19. Chung, T. C. *U. S. Patents* 4,734,472 and 4,751,276.
20. Chung, T. C. *Macromolecules* **1988**, 21, 865.
21. Chung, T. C.; Jiang, G. J. *Macromolecules* **1992**, 25, 4816.
22. Chung, T. C. "Functionalization of Polyolefins" Academic Press, London, 2002.
23. Chung, T. C.; Jiang, G. J.; Rhubright, D. *Macromolecules* **1993**, 26, 3467.
24. Chung, T. C.; Rhubright, D.; Jiang, G. J. *U. S. Patent* 5,286,800.
25. Chung, T. C.; Lu, H. L.; Janvikul, W. *Polymer* **1997**, 38, 1495.
26. Xu, G.; Chung, T. C. *J. Am. Chem. Soc.* **1999**, 121, 6763.
27. Chung, T. C.; Lu, H. L.; Janvikul, W. *J. Am. Chem. Soc.* **1996**, 118, 705.
28. Chung, T. C. *Progress in Polymer Science* **2002**, 27, 39.
29. Chung, T. C.; Petchsuk, A. *Macromolecules* **2002**, 35, 7678.
30. Hong, H.; Chung, T. C. *Macromolecules* **2004**, 37, 6260.
31. Chung, T. C.; Hong, H.; Oka, M.; Kubo, K. *U. S. Patent* 6,911,509.
32. Chung, T. C.; Petchsuk, A. *U. S. Patent* 6,355,749.
33. Pianca, M.; Barchiesi, E.; Esposto, G.; Radice, S. *J Fluorine Chem.* **1999**, 95, 71.
34. Wang, Z. M.; Nakajima, H.; Manias, E.; Chung, T. C. *Macromolecules* **2003**, 36, 8919.

Chapter 28

An Ab Initio Guide to Structure–Reactivity Trends in Reversible Addition Fragmentation Chain Transfer Polymerization

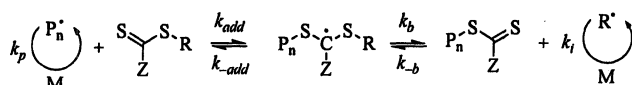
Elizabeth H. Krenske, Ekaterina I. Izgorodina,
and Michelle L. Coote*

ARC Centre of Excellence in Free Radical Chemistry and Biotechnology,
Research School of Chemistry, Australian National University,
Canberra ACT 0200, Australia

The effects of substituents on the addition–fragmentation reaction, $P_n \cdot + S=C(Z)SR \rightarrow P_n SC \cdot (Z)SR \rightarrow P_n SC(Z)=S + R \cdot$, of the reversible addition fragmentation chain transfer (RAFT) process have been studied via high-level ab initio calculations. A number of simple isodesmic quantities are introduced in order to rank the stabilities of the RAFT agents and the RAFT-adduct radicals, together with the efficiency of addition–fragmentation and of the overall chain transfer process. The stabilities of the RAFT agents and RAFT-adduct radicals are mainly affected by the Z group, while the chain transfer efficiency depends mainly on the R group. The rankings can be used as a first-reference guide for selecting an R and Z group for a given polymerization.

Introduction

The reversible addition fragmentation chain transfer (RAFT) process is an important new method for controlling molecular weight and architecture in free-radical polymerization (1). RAFT can be used to generate complex macromolecular architectures such as comb, star and block copolymers, for use in bioengineering and nanotechnology applications (2). Control is achieved by protecting the majority of the growing polymer chains from bimolecular termination processes, through their reversible trapping into a dormant thiocarbonyl compound (known as the polyRAFT agent), as follows:



A delicate balance of the rates of these various reactions is required, so as to ensure that the dormant species is orders of magnitude greater in concentration than the active species but that the exchange between the two forms is rapid. The reactivity of the RAFT agent must thus be tailored to the reactivity and stability of the polymeric propagating radical; information on the mechanism, kinetics and thermodynamics of these individual steps can greatly assist in the design and selection of optimal RAFT agents.

Although many experimental groups have examined the effects of substituents on the RAFT process (2, 3), these experimental studies have necessarily focussed on measurable quantities such as the polydispersity of the resulting polymer or the apparent chain transfer constant (4) – parameters that are a complicated function of several individual rate coefficients. Hence, although experimental studies have provided extremely useful quantitative information on the performance of specific RAFT agents, and provided a number of important qualitative insights, the tasks of interpreting the more subtle structure-reactivity trends and predicting the behavior of as-yet-untested RAFT agents are not straightforward. Computational quantum chemistry offers an attractive complementary approach to studying the effects of substituents on this complicated process. Using high-level *ab initio* molecular orbital calculations, it is possible to obtain the rate and equilibrium constants for each individual reaction and the stabilization energies of the individual species *directly*, without recourse to kinetic model-based assumptions. Moreover, the calculations yield additional mechanistic information (such as the geometries of the reactants, products and transition structures, and the charge and spin density distributions within these species) that can assist in the interpretation of results. Computational chemistry also offers the possibility of considering a much wider range of substituents, including RAFT agents that have not as yet been synthesized.

Recently, we have used high-level *ab initio* calculations to study the kinetics and thermodynamics of the addition–fragmentation reaction in the RAFT process (5). Based on these results we have been able to design a new class of

multi-purpose RAFT agent that has subsequently been demonstrated to control free-radical polymerization (6). Others have used lower-level semi-empirical or density functional theory calculations to study the overall chain transfer reaction, and have shown that the results have practical value in choosing appropriate leaving groups (3b, 7). However, although there is now a reasonable qualitative understanding of structure-reactivity trends in the RAFT process, the current data is not in a generally useful form. In particular, results from the low-level and high-level computational studies are not directly comparable, and a number of the more important RAFT agent substituents (especially belonging to the xanthate and dithiocarbamate sub-classes) are not represented. The aim of the present work is to provide a more comprehensive account of the effects of substituents on the RAFT process, and build a practical database of reagent stabilities that should assist in the design and selection of optimal RAFT agents for controlling the various classes of monomers.

In the present work we study the effects of the R, R' and Z substituents on the addition-fragmentation reaction, $R\cdot + S=C(Z)SR \rightarrow R'SC\cdot(Z)SR \rightarrow R'SC(Z)=S + R\cdot$, for a wide range of practical R, R' and Z-substituents. The substituents considered embrace the various classes of compounds currently in use as RAFT agents (including dithioesters, xanthates, dithiocarbamates, and trithiocarbonates) with leaving groups that represent a wide range of monomeric radicals and their tertiary methyl-substituted derivatives. We also study the effects of R, R' and Z on the stabilization energies of the various radical and thiocarbonyl species, via a series of isodesmic reactions.

Computational Procedures

Standard ab initio molecular orbital theory and density functional theory calculations have been performed using the GAUSSIAN 03 (8) and Molpro 2000.6 (9) software. Calculations were performed at a high level of theory that was chosen on the basis of recent assessment studies covering both the specific case of addition-fragmentation (10) and a range of related radical reactions (11). Geometries were optimized at the B3-LYP/6-31G(d) level of theory, and zero-point vibrational energy corrections were calculated using B3-LYP/6-31G(d) frequencies, and scaled by the appropriate scale factors (12). Improved energies were then calculated using the G3(MP2)-RAD level of theory, a high-level composite procedure designed to reproduce coupled cluster energies [CCSD(T)] with a large triple zeta basis set via additivity corrections (13). For the reactions of the largest xanthate ($Z = OCH(CF_3)PO(OMe)_2$), G3(MP2)-RAD calculations were approximated using an ONIOM-based approach as follows (10). The "core", corresponding to $Z = OCH_2CF_3$, was studied at G3(MP2)-RAD, and then corrected for the substituent effect of the full system, as calculated at the RMP2/6-311+G(3df,2p) level. We have recently shown that this approach is capable of reproducing the G3(MP2)-RAD calculations of the full system to within 1 kcal mol⁻¹ at a fraction of the computational cost (10).

Although direct comparison with experimental data for addition-fragmentation reactions is problematic, studies of related systems indicate that the computational approach is capable of achieving chemical accuracy. For instance, Scaiano and Ingold (14) have reported an experimental equilibrium constant (based on laser flash photolysis studies) of $1.2 \times 10^6 \text{ L mol}^{-1}$ for the addition of *tert*-butyl radicals to di-*tert*-butyl thioetone at 25°C, whereas we have calculated a value of $7.9 \times 10^5 \text{ L mol}^{-1}$ using this ab initio approach (15). Likewise, our calculated propagation rate coefficients for the radical polymerization of vinyl chloride and acrylonitrile are within a factor of 2 of the experimental values (16).

Results and Discussion

The key to controlling free-radical polymerization via the RAFT process is to choose RAFT agent substituents (R and Z) and reaction conditions such that the equilibrium between the propagating radical and dormant thiocarbonyl species is rapidly established during the early stages of the process, and that this dormant species is orders of magnitude greater in concentration than the propagating species, and that the exchange between the two forms is rapid. These requirements entail that (a) the RAFT agent is sufficiently reactive relative to the propagation step, but not so reactive that the propagating radical becomes irreversibly trapped as the RAFT-adduct radical; and (b) the initial leaving group (R•) fragments from the RAFT-adduct radical in preference to the propagating species, but is still capable of reinitiating polymerization. To assist in RAFT agent design, we present here a database of substituent effects on (a) the addition-fragmentation equilibrium and (b) the chain transfer reaction.

For a complete treatment of substituent effects, one must consider the combined effects of R and Z on each individual addition-fragmentation reaction, from both kinetic and thermodynamic viewpoints. However, given the broad range of R and Z combinations possible, such a study would be very cumbersome, and it would be difficult to identify chemical trends and to predict the behavior of as-yet untested combinations of substituents. Instead, we define some simple thermodynamic measures for the isolated effects of the R and Z substituents on the addition-fragmentation and chain transfer reactions, and on the stabilities of the component species.

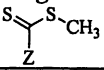
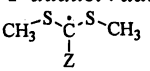
- We define the fragmentation efficiency (ΔH_{frag}) for a specific Z-group as the enthalpy (0 K) of the following isodesmic reaction: $\text{CH}_3\text{SC}(\text{Z})\text{SCH}_3 + \text{S}=\text{C}(\text{H})\text{SCH}_3 \rightarrow \text{CH}_3\text{SC}(\text{H})\text{SCH}_3 + \text{S}=\text{C}(\text{Z})\text{SCH}_3$. This measures the susceptibility of the RAFT-adduct radical to β -scission (i.e., the reaction $\text{CH}_3\text{SC}(\text{Z})\text{SCH}_3 \rightarrow \text{S}=\text{C}(\text{Z})\text{SCH}_3 + \text{CH}_3\cdot$), relative to the reference case where Z = H; the more exothermic the reaction, the more susceptible the radical is to β -scission.

- We define the chain transfer efficiency for a specific R-group as the enthalpy (0 K) of the overall chain transfer reaction $\text{CH}_3^\bullet + \text{S}=\text{C}(\text{CH}_3)\text{SR} \rightarrow \text{R}^\bullet + \text{S}=\text{C}(\text{CH}_3)\text{SCH}_3$. This measures the leaving group ability of R^\bullet relative to the reference CH_3^\bullet radical; the more exothermic the reaction, the better the leaving group. A related approach based on bond dissociation energies has recently been used by Matyjaszewski and Poli (7b) to study chain transfer in RAFT.
- We measure the stabilities of the RAFT-adduct radicals and leaving group radicals as their radical stabilization energies (RSE), in the usual manner (5e, 17). That is, the RSE of a radical R^\bullet is measured as the enthalpy (0 K) of the isodesmic reaction $\text{R}^\bullet + \text{CH}_4 \rightarrow \text{R}-\text{H} + \text{CH}_3^\bullet$.
- We measure the stabilities of the RAFT-agents using analogous isodesmic reactions. When the interest is in the effect of Z, stability is estimated by the enthalpy change for the reaction $\text{S}=\text{C}(\text{Z})\text{SCH}_3 + \text{CH}_3-\text{H} \rightarrow \text{S}=\text{C}(\text{H})\text{SCH}_3 + \text{CH}_3-\text{Z}$. When the interest is in the effect of R, the relevant reaction is $\text{S}=\text{C}(\text{CH}_3)\text{SR} + \text{CH}_3-\text{SH} \rightarrow \text{S}=\text{C}(\text{CH}_3)\text{SCH}_3 + \text{R}-\text{SH}$.

Analyzing the chain transfer efficiency in these simple terms allows the effects of R and Z to be conveniently separated and ordered. Below, we describe these effects, and demonstrate how the rankings of R and Z can be used to select a RAFT agent to control a given monomer. Occasionally, special situations arise in which subtle stereoelectronic effects transpire to override the general trends. We will also give some examples of this below. Despite these exceptions, the tables of data serve as a useful starting point from which one can identify a range of candidate RAFT agents for detailed testing.

Choice of Z group. In the overall chain transfer reaction $\text{P}_n^\bullet + \text{S}=\text{C}(\text{Z})\text{SR} \rightarrow \text{P}_n\text{SC}(\text{Z})=\text{S} + \text{R}^\bullet$, the group Z is contained within a thiocarbonyl compound on both sides of the equation. On this basis, one might expect Z to contribute minimally to chain transfer efficiency. However, such an assumption is inadequate, as one must also take into account the intermediate RAFT-adduct radical $\text{P}_n\text{SC}^\bullet(\text{Z})\text{SR}$. For efficient chain transfer, it is necessary to use a Z group that promotes both the addition of P_n^\bullet to the RAFT agent (step 1), and the fragmentation of R^\bullet (or P_n^\bullet in the case of the polymeric equilibrium) from the RAFT-adduct radical (step 2). There are two possible scenarios. If the propagating radical P_n^\bullet is relatively unstable (i.e. reactive), step 1 poses little problem. The main concern in this case is to promote step 2 so that the propagating radical does not become irreversibly trapped as the RAFT-adduct radical. In contrast, if the propagating radical is relatively stable (unreactive), then step 2 is favoured and the priority is instead to promote step 1. In the first of these two scenarios, a Z group must be chosen that either destabilizes the RAFT-adduct radical or stabilizes the thiocarbonyl product. In the second scenario, the Z group must destabilize the RAFT agent or stabilize the RAFT-adduct radical.

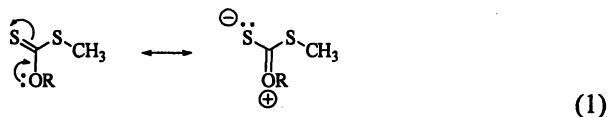
Table I. Effect of Z group on stabilities and fragmentation enthalpies.^a

| Z | Stability of RAFT Agent  | RSE of RAFT-adduct radical  | ΔH_{frag} |
|---|--|--|-------------------|
| CN | -5.9 | 99.2 | 48.8 |
| Ph | 41.3 | 96.3 | 21.0 |
| CF ₃ | -17.1 | 62.6 | 17.8 |
| H | 0.0 | 61.1 | 0.0 |
| Cl | 29.9 | 63.9 | -1.3 |
| imidazole- <i>N</i> | 44.8 | 74.5 | -1.5 |
| CH ₂ Ph | 39.2 | 65.0 | -1.9 |
| SCH ₂ CH ₃ | 59.4 | 81.5 | -4.4 |
| pyrrole- <i>N</i> | 54.5 | 76.0 | -5.4 |
| CH ₃ | 35.1 | 59.9 | -10.0 |
| SCH ₃ | 59.3 | 76.5 | -11.1 |
| F | 43.5 | 46.9 | -24.0 |
| OCH(CF ₃)P(O)(OCH ₃) ₂ | 80.0 | 61.3 | -29.3 |
| OCH ₂ CF ₃ | 80.2 | 63.7 | -35.4 |
| OC(CH ₃) ₃ | 81.0 | 59.0 | -37.1 |
| OCH(CH ₃)P(O)(OCH ₃) ₂ | 89.3 | 65.2 | -37.9 |
| NH ₂ | 92.8 | 73.5 | -38.5 |
| OCH(CH ₃) ₂ | 90.7 | 63.2 | -40.8 |
| OCH ₂ CH ₃ | 86.8 | 59.0 | -44.3 |
| OCH ₃ | 85.9 | 58.5 | -45.0 |
| N(CH ₃) ₂ | 94.2 | 76.9 | -46.9 |
| N(CH ₂ CH ₃) ₂ | 105.6 | 95.5 | -50.2 |

^aRSEs and enthalpies (0 K, kJ mol⁻¹) were calculated at the G3(MP2)-RAD level of theory using B3-LYP/6-31G(d) optimized geometries and include scaled B3-LYP/6-31G(d) zero-point energy corrections.

In Table I are shown the effects of Z on the stabilities of RAFT agents and RAFT-adduct radicals (for R = R' = CH₃). The Z groups are listed in order of increasing fragmentation efficiency of the RAFT-adduct radicals. Considering first the RAFT agents, it can be seen that the Z groups fall into three main classes. The first class comprises those Z groups that strongly stabilize RAFT agents. Alkoxy and amino groups fall into this class, and typically give stabilities in excess of 80 kJ mol⁻¹. The high stability of RAFT agents with Z = OR or NR₂ arises from lone-pair donation onto the C=S bond, as shown in eq 1. At the other end of the spectrum are the σ -withdrawing Z groups CN and CF₃, which destabilize the RAFT agents relative to Z = H. The remaining Z groups

fall into an intermediate range. Thus, typical dithioesters, such as those with $Z = \text{CH}_3$, Ph, or CH_2Ph , have stabilities of approximately 40 kJ mol^{-1} . The fluorinated RAFT agent $\text{S}=\text{C}(\text{F})\text{SCH}_3$ also comes within this range, at 43.5 kJ mol^{-1} . In this case, the effects of lone-pair donation and σ -withdrawal counteract each other.

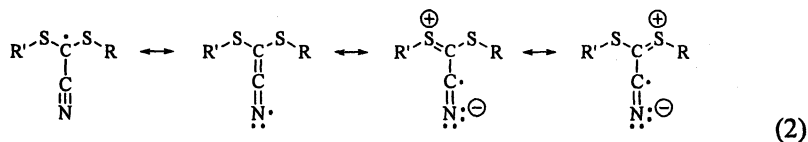


Within these three classes, the positions of certain RAFT agents are worthy of note. One example is the trithiocarbonate RAFT agents. Although the SR group is potentially a good lone-pair donor, it is not as effective as oxygen or nitrogen, and the trithiocarbonates' stabilities fall short of the xanthates and dithiocarbamates by approximately $20\text{--}35 \text{ kJ mol}^{-1}$. A second noteworthy case is the dithiocarbamates that have $Z = \text{pyrrole}$ or imidazole. These agents have stabilities much lower than those of typical dithiocarbamates. Such an observation supports the principle upon which these agents were designed (18), namely that the donor ability of Z should be restricted if the nitrogen lone pair is delocalized over the aromatic ring. As a third example, note can be made of the special xanthate agents having $Z = \text{OCH}_2\text{CF}_3$, $\text{OCH}(\text{CH}_3)\text{P}(\text{O})(\text{OCH}_3)_2$, or $\text{OCH}(\text{CF}_3)\text{P}(\text{O})(\text{OCH}_3)_2$. These agents were designed (3d) on the basis that the σ - and π -withdrawing characteristics of the trifluoromethyl and phosphonate substituents would reduce the lone pair donor ability of Z . It appears, however, that the destabilizing characteristics of such α -substituents are minor, because these agents' stabilities fall only slightly below those of the corresponding regular xanthates.

Considering next the RAFT-adduct radicals, it must first be pointed out that the stability of these radicals is generally high, regardless of the Z group – the RSEs for these radicals are typically in excess of 60 kJ mol^{-1} . Stability arises because lone-pair donation by the two SR groups provides an effective means for delocalization of the unpaired electron. Nevertheless, the Z groups can be divided into several distinct categories based on whether Z enhances or diminishes this stabilizing feature.

In one category lie the π -acceptor Z groups CN, Ph, pyrrole, and imidazole. These give highly stable RAFT-adduct radicals. In isolation these substituents are typically strong radical stabilizers because the unpaired electron is able to be delocalized into their vacant π^* orbitals (5e). In combination with the lone pair donor SR groups, the stabilizing effect of small π -acceptor groups such as CN is enhanced by captodative interactions as shown in eq 2. For larger aromatic π -acceptor groups such as Ph, the captodative effect can be outweighed by steric effects, as a compromise must be reached between the optimum geometry of a benzylic radical (planar carbon centre) and that of a simple alkylthio-substituted

radical (puckered). Nonetheless, they remain strong radical stabilizers, and give rise to relatively long-lived intermediate radicals (19).



In another category lie the lone-pair donor Z groups, NR₂, OR, SR, Cl and F. Their effects on the stability of the RAFT-adduct radical are not straightforward. To start with, the stabilization associated with the presence of a single SCH₃ group on a carbon-centered radical (i.e., CH₃S-CH₂•) is 40.7 kJ mol⁻¹, but if a second SCH₃ group is present (i.e., CH₃SC•(H)SCH₃) the RSE is only 61.1 kJ mol⁻¹ (5e). The diminished capacity for extra stabilization by the second SCH₃ group arises because the interaction between carbon and the lone pair of the first sulfur atom places the unpaired electron into a higher-energy molecular orbital, reducing the ability of the second sulfur atom to interact with it. The capacity for stabilization by a third lone pair donor substituent (i.e., Z) is similarly reduced unless Z is a stronger lone-pair donor than SCH₃. Moreover, the stabilizing effect of these lone pair groups is countered to varying extents by σ-withdrawal. Thus, the Z groups NH₂, N(CH₃)₂, N(CH₂CH₃)₂, SCH₃, and SCH₂CH₃ provide nett stabilization to the RAFT-adduct radical (RSE's > 70 kJ mol⁻¹), but the alkoxy groups OCH₃, OCH₂CH₃, OCH(CH₃)₂, and O(CH₃)₃ provide no additional stabilization relative to Z = CH₃. In the latter radicals, the σ-withdrawing character of Z outweighs the lone-pair donor ability. The importance of σ-withdrawal in the RAFT-adduct radicals is further demonstrated by the similarity between the RSEs of the NR₂ and SR₂ groups, despite the stronger lone-pair donor character of the former (17). In the RAFT agents, also, the relative stabilities of the alkoxy-, amino-, and alkylthio-substituted agents reveal similar trends in σ-withdrawing character, but in these species the lone-pair donor character of Z is more important.

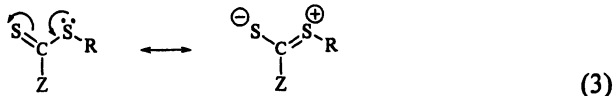
By considering all of these trends, a Z group can be chosen to suit the reactivity of a desired propagating radical. For example, in the polymerization of vinyl acetate (VA), the propagating radical is relatively unstable. Therefore, the fragmentation of the propagating radical from the RAFT-adduct radical is a major concern, and the traditional solution has been to employ Z groups that stabilize the thiocarbonyl product of fragmentation. Thus, xanthates and dithiocarbamates are the agents of choice for VA polymerization (2, 3d, 20). This solution comes at a cost, however. Because the lone-pair donor OR and NR₂ groups render a thiocarbonyl species less reactive, xanthates and dithiocarbamates are not as useful for more stable propagating radicals – for instance when preparing copolymers of VA with more stable monomers. We have recently noted (6a) that a better solution would be to promote fragmentation by destabilizing the RAFT-adduct radical, rather than stabilizing the RAFT agent. From Table I, it is clear that a fluorine Z-group is capable of

achieving this. Thus, when $Z = \text{F}$, the strong σ -withdrawing character destabilizes both the RAFT-adduct radical and the RAFT agent, relative to a xanthate or dithiocarbamate. The net result is that fragmentation is only $\sim 13\text{--}26 \text{ kJ mol}^{-1}$ less thermodynamically favourable than that for the xanthates and dithiocarbamates, yet the addition of a propagating radical to the $\text{S}=\text{C}$ bond is not inhibited. The compounds $\text{S}=\text{C}(\text{F})\text{SR}$ are currently under testing as dual-purpose RAFT agents for controlling both stable and unstable monomers.

Choice of R group. It is only in exceptional cases that the effect of R on the overall chain transfer efficiency depends on the intermediate RAFT-adduct radical. Thus, for an analysis of the effects of R, one can consider two species: the RAFT agent $\text{S}=\text{C}(\text{Z})\text{SR}$ and the leaving-group radical $\text{R}\cdot$. In Table II are shown the effects of typical R groups on the stabilities of RAFT agents and the corresponding leaving-group radicals $\text{R}\cdot$. The R groups are ranked in order of increasing efficiency of the chain transfer reaction $\text{S}=\text{C}(\text{CH}_3)\text{SR} + \text{CH}_3\cdot \rightarrow \text{S}=\text{C}(\text{CH}_3)\text{SCH}_3 + \text{R}\cdot$. Considering the relative magnitudes of the RAFT agent stabilities and of the $\text{R}\cdot$ RSEs, one may conclude that the major influence on chain transfer enthalpy is the stability of $\text{R}\cdot$. In a practical RAFT agent, the release of $\text{R}\cdot$ from the RAFT-adduct radical $\text{P}_n\text{SC}(\text{Z})\text{SR}$ should be competitive with the release of $\text{P}_n\cdot$, and the radical whose release is favoured is normally the one whose stability is greater.

The leaving-group radicals listed in Table II are subject to the typical stabilizing influences that affect carbon-centered radicals. For example, the $\text{R}\cdot$ radicals $\cdot\text{C}(\text{CH}_3)_2\text{CN}$ and $\cdot\text{C}(\text{CH}_3)_2\text{Ph}$ are relatively stable due to delocalization of the unpaired electron onto the π -acceptor substituent. Hyperconjugative stabilization also comes into play, as evidenced by the trend toward increased stability as the number of CH_3 groups attached to the radical centre is increased.

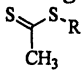
In the RAFT agents, the electronic and steric properties of R influence stability in the opposite sense. R groups containing electron-withdrawing substituents destabilize RAFT agents, by restricting the capacity for the electron delocalization shown in eq 3. Increasing methylation causes destabilization by inducing nonbonded interactions over the rigid $\text{S}=\text{C}(\text{Z})\text{--SR}$ framework.



Since, in the overall chain transfer process, the RAFT agent is consumed and the radical $\text{R}\cdot$ is produced, the steric and electronic effects of R are exerted in two complementary ways. This result agrees well with the recent interesting work of Matyjaszewski and Poli (7b), who used density functional calculations to show that chain transfer is favoured by bulky R groups and is subject to polar effects. One might thus conclude that in order to promote chain transfer, an R group should be chosen such that the RSE of $\text{R}\cdot$ is greater than the RSE of $\text{P}_n\cdot$. However, the need to promote the release of $\text{R}\cdot$ must be balanced against the need for $\text{R}\cdot$ to initiate further polymerization. If $\text{R}\cdot$ is too stable, then the re-

initiation step $R\cdot + M \rightarrow R-M\cdot$ will be inhibited. It is therefore not easy to predict how well a given R group will perform on the basis of its chain transfer exothermicity alone.

Table II. Effect of R group on stabilities and chain transfer enthalpies.^a

| <i>R</i> | Stability of RAFT Agent  | RSE of $R\cdot$ | ΔH_{CT} |
|---|---|-----------------|-----------------|
| CH(CH ₃) ₂ | -1.2 | 24.0 | 2.0 |
| CH ₂ CH ₃ | -0.8 | 14.1 | 1.8 |
| CH ₃ | 0.0 | 0.0 | 0.0 |
| CH ₂ OCOCH ₃ | -11.8 | 17.9 | -4.8 |
| CH ₂ CONH ₂ | -0.8 | 21.2 | -6.5 |
| CH(CH ₃)OCOCH ₃ | -15.9 | 24.4 | -8.6 |
| C(CH ₃) ₃ | -14.1 | 29.7 | -10.1 |
| CH(CH ₃)Cl | -7.1 | 27.0 | -14.3 |
| CH(CH ₃)CONH ₂ | 2.9 | 41.1 | -14.3 |
| CH ₂ Cl | -7.3 | 21.1 | -15.9 |
| CH ₂ COOCH ₃ | -5.1 | 21.5 | -20.0 |
| C(CH ₃) ₂ OCOCH ₃ | -29.6 | 18.0 | -22.0 |
| CH ₂ COOH | -5.5 | 21.2 | -22.3 |
| C(CH ₃) ₂ Cl | -16.3 | 31.1 | -24.3 |
| CH(CH ₃)COOCH ₃ | -7.5 | 41.3 | -29.4 |
| CH(CH ₃)COOH | -8.4 | 41.3 | -33.2 |
| C(CH ₃) ₂ COOCH ₃ | -8.3 | 54.9 | -35.9 |
| C(CH ₃) ₂ CONH ₂ | -18.7 | 54.7 | -36.9 |
| CH ₂ CN | -5.5 | 31.9 | -41.4 |
| CH ₂ Ph | 0.4 | 58.9 | -41.7 |
| C(CH ₃) ₂ COOH | -11.3 | 56.1 | -41.8 |
| CH(CH ₃)Ph | -0.8 | 68.0 | -42.2 |
| CH(CH ₃)CN | -4.6 | 47.3 | -42.6 |
| C(CH ₃) ₂ CN | -15.8 | 59.0 | -56.6 |
| C(CH ₃) ₂ Ph | -14.9 | 70.3 | -57.5 |

^aRSEs and enthalpies (0 K, kJ mol⁻¹) were calculated at the G3(MP2)-RAD level of theory using B3-LYP/6-31G(d) optimized geometries and include scaled B3-LYP/6-31G(d) zero-point energy corrections.

A practical example of this difficulty is provided by the polymerization of methyl methacrylate (MMA). It has been found experimentally (*3b*) that, when using dithiobenzoate RAFT agents having different R groups ($Z = \text{Ph}$) in MMA polymerization, control is good when R is C(CH₃)₂Ph or C(CH₃)₂CN, but not when R is CH₂Ph, C(CH₃)₃, CH(CH₃)Ph, C(CH₃)₂CONH(alkyl), or

$C(CH_3)_2COO(\text{alkyl})$. The poor performance of the $C(CH_3)_3$ group could be readily understood on the sole basis of an unfavourable ΔH_{CT} relative to the model propagating radical $\bullet C(CH_3)_2COOCH_3$. The remaining findings, however, cannot. It must be recognized that the use of the monomer radical as a model for the propagating radical is at best a rough approximation, since penultimate unit effects can be significant. In the case of the initial “unimeric” propagating radical, the penultimate unit will be the initiator-derived end-group (typically $C(CH_3)_2CN$). Once this substituent is incorporated, the calculated ΔH_{CT} value for the propagating radical decreases substantially (to $-50.5 \text{ kJ mol}^{-1}$). For this corrected species, only the $C(CH_3)_2Ph$ or $C(CH_3)_2CN$ radicals in Table II have favorable ΔH_{CT} values, which is then in accord with the experimental observations.

Incorporating penultimate unit effects is an important but computationally laborious task that needs to be considered for a proper analysis of a given polymerization. However, with the simple monomer radicals at hand, Table II provides a method for allowing unsuitable R groups to be disregarded without investing in a rigorous theoretical or experimental study. Groups for which the chain transfer enthalpy is much more or much less exothermic than that of the monomeric radical are unlikely to be worthy of pursuit, and the best R group candidates would be those for which ΔH_{CT} is only slightly more or slightly less exothermic than that for M^\bullet .

Exceptions to the trends. Tables I and II can be used as a first-reference guide for selecting an R and Z group for a given polymerization. The use of these tables should, however, be made with due regard to their implicit assumptions. Firstly, the rankings are based on the assumption that the thermodynamics of chain transfer are a predictor of the kinetics. This simplification was drawn from the earlier finding (21) that radical additions to $C=S$ bonds typically have very low activation barriers – that is, that ΔH^\ddagger_β is equivalent to ΔH_β . A second approximation implicit in the rankings is that any effects of the R group on the stability of the RAFT-adduct radical can be ignored. Furthermore, the possibility of synergistic interactions between the R, Z, and P_n groups has also been ignored.

An important situation in which thermodynamics are not a good predictor of kinetics is the fragmentation step of the xanthate-mediated polymerization of vinyl acetate. As depicted in Figure 1, the activation barrier for fragmentation of the radical $CH_3SC\bullet(OCH_3)SCH_2OCOCH_3$ is nearly 23 kJ mol^{-1} lower than that of the radical $CH_3SC\bullet(O^tBu)SCH_2OCOCH_3$ (5b). The barrier lowering cannot be due to steric effects alone, however, as the barriers for the corresponding methyl-substituted radicals $CH_3SC\bullet(OCH_3)SCH_3$ and $CH_3SC\bullet(O^tBu)SCH_3$ are almost identical to that for the $Z = ^tBuO$ and $R = VA$ case. Instead, the difference stems from a hydrogen-bonding interaction in the transition state for the $Z = CH_3O$ and $R = VA$ adduct. A close contact between the carbonyl oxygen and one of the OCH_3 protons takes place in the transition state for the $Z = CH_3O$

and R = VA adduct, but is absent in the Z = ^tBuO and R = VA analogue. This feature corresponds to a rate enhancement of three orders of magnitude, and could only be identified by conformational screening of the transition states and direct calculation of the fragmentation rates.

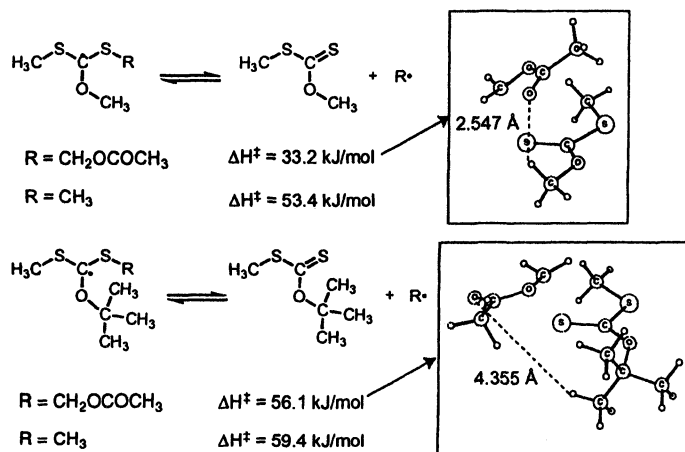


Figure 1. Acceleration of fragmentation in a xanthate-derived RAFT-adduct radical due to hydrogen-bonding in the transition state.

More generally, isodesmic quantities provide no information on the absolute thermodynamics (let alone kinetics) of the individual addition-fragmentation steps and this can be very important for the understanding of the overall process. In particular, when radical addition to the RAFT agent is highly exothermic (typically, if $K > 10^6 \text{ L mol}^{-1}$), the intermediate RAFT-adduct radical can function as a radical sink and contribute to the overall control mechanism (22). This in turn can lead to rate retardation or even, in the extreme case, inhibition of the polymerization process. The kinetics and thermodynamics for a range of individual addition-fragmentation reactions have been reported elsewhere (5, 19). For most common combinations of R and Z substitutions, addition of R• to the RAFT agent $\text{S}=\text{C}(\text{Z})\text{SCH}_3$ is indeed exothermic, as can be inferred from the fact that the enthalpy of the reference reaction $\bullet\text{CH}_3 + \text{S}=\text{C}(\text{H})\text{SCH}_3 \rightarrow \text{CH}_3\text{SC}(\text{H})\text{SCH}_3$ is $-74.2 \text{ kJ mol}^{-1}$ (5e). Despite this, in most cases the exothermicity is not sufficiently large to impair the overall polymerization kinetics except when RAFT-agent is substituted with strongly stabilizing Z-groups such as phenyl (19) and/or when the propagating radical is a poor radical leaving group, as in vinyl acetate polymerization. In these cases, the overall polymerization kinetics can only be understood through a detailed examination of the kinetics and thermodynamics of the individual addition-fragmentation reactions. Nonetheless, the isodesmic quantities in Tables I and II can allow one to anticipate when rate retardation is likely to be important: namely, when Z-

groups having high values of ΔH_{frag} (Table I) are combined with leaving groups or propagating radicals that have high values of ΔH_{CT} (Table II).

The possibility of synergistic interactions between substituents is another important consideration. In particular, attention has been drawn to the importance of homoanomeric interactions in certain RAFT-adduct radicals (5e). In the simple RAFT-adduct radical $\text{CH}_3\text{SC}\cdot(\text{CH}_3)\text{SCH}_3$, the preferred geometry allows maximum orbital overlap between the unpaired electron and the sulfur lone pairs. However, when the R-group of the RAFT-adduct radical is substituted with a strong π -acceptor group, it reduces the lone-pair donor ability of its attached sulfur atom and instead the unpaired electron is delocalized into the antibonding orbital of the S–R bond. This stabilizes the radical overall but weakens the S–R bond and promotes fragmentation of $\text{R}\cdot$, often in opposition to considerations of steric and radical stabilization effects. Thus for example, $\cdot\text{C}(\text{CH}_3)_2\text{CN}$ is a considerably better leaving group than $\cdot\text{C}(\text{CH}_3)_2\text{Ph}$, despite their near identical RSEs and steric bulk, because the CN substituent is a much stronger π -acceptor and is thus subject to stronger homoanomeric interaction (5e). As a further complicating factor, we have noted that the homoanomeric effect is further modulated by Z; for example, a fluorine substituent has been shown to inhibit the homoanomeric effect and alter leaving group abilities (6b). Hence, it is possible for all three groups R, P_n , and Z to interact within a RAFT-adduct radical, leading to complicated structure-reactivity trends.

Conclusions

Ab initio calculations can assist in the rationalization of substituent effects in the chain transfer reaction of RAFT polymerization. Broadly speaking, Z groups can be categorized according to whether they are suited to relatively unstable propagating radicals ($Z = \text{OR}, \text{NR}_2$) or to relatively stable propagaing radicals ($Z = \text{alkyl, aryl, SR, aromatic amines}$). The ordering of the R groups shows that the stability of $\text{R}\cdot$ is most important; one must choose an R group that is a sufficiently good leaving group compared with $\text{P}_n\cdot$ but that is still capable of re-initiating polymerization. Although some more complicated situations arise in which the predictions of these rankings break down due to more subtle stereoelectronic effects, the rankings are useful for selecting a range of candidate RAFT agents that are appropriate for detailed theoretical or experimental testing.

Acknowledgement. Financial support from the Australian Research Council, useful discussions with Dr David Henry and Professor Leo Radom, and a generous allocation of computing time on the National Facility of the Australian Partnership for Advanced Computing are gratefully acknowledged.

References

- (a) Le, T. P. T.; Moad, G.; Rizzardo, E.; Thang, S. H. PCT Int. Appl. WO 9801478 A1 980115 1998; *Chem. Abstr.* **1998** *128*, 115390. (b) Charmot, D.; Corpart, P.; Michelet, D. Zard, S. Z., Biadatti, T. PCT Int. Appl. WO 9858974, 1998; *Chem. Abstr.* **1999**, *130*, 82018.
- See for example: Moad, G.; Rizzardo, E.; Thang, S. H. *Aust. J. Chem.* **2005**, *58*, 379, and references cited therein.
- See for example: (a) Chiefari, J.; Mayadunne, R. T. A.; Moad, C. L.; Moad, G.; Rizzardo, E.; Postma, A.; Skidmore, M. A.; Thang, S. H. *Macromolecules* **2003**, *36*, 2273. (b) Chong, (B.) Y. K.; Krstina, J.; Le, T. P. T.; Moad, G.; Postma, A.; Rizzardo, E.; Thang, S. H. *Macromolecules* **2003**, *36*, 2256. (c) Stenzel, M. H.; Cummins, L.; Roberts, G. E.; Davis, T. P.; Vana, P.; Barner-Kowollik, C. *Macromol. Chem. Phys.* **2003**, *204*, 1160. (d) Destarac, M.; Taton, D.; Zard, S. Z.; Saleh, T.; Six, I. *ACS Symp. Ser.* **2003**, *854*, 536. (e) Adamy, M.; van Herk, A. M.; Destarac, M.; Monteiro, M. J. *Macromolecules* **2003**, *36*, 2293. (f) Destarac, M.; Bzducha, W.; Taton, D.; Gauthier-Gillaizeau, I.; Zard, S. Z. *Macromol. Rapid Commun.* **2002**, *23*, 1049.
- $C_{tr} = k_{tr}/k_p$ where $k_{tr} = k_{add}(k_p/(k_p + k_{-add}))$. This formula assumes that the quasi-steady-state assumption holds, the adduct does not undergo side-reactions, and the fragmentation step is irreversible. In real systems the relationship between the observed transfer coefficient and the individual rate coefficients would be more complex.
- (a) Coote, M. L.; Radom, L. *J. Am. Chem. Soc.* **2003**, *125*, 1490. (b) Coote, M. L.; Radom, L. *Macromolecules* **2004**, *37*, 590. (c) Coote, M. L. *Macromolecules* **2004**, *37*, 5023. (d) Coote, M. L. *J. Phys. Chem. A* **2005**, *109*, 1230. (e) Coote, M. L.; Henry, D. J. *Macromolecules* **2005**, *38*, 1415.
- (a) Coote, M. L.; Henry, D. J. *Macromolecules* **2005**, *38*, 5774. (b) Theis, A.; Stenzel, M. H.; Davis, T. P.; Coote, M. L.; Barner-Kowollik, C. *Aust. J. Chem.* **2005**, *58*, 437.
- (a) Farmer, S. C.; Patten, T. E. *J. Polym. Sci. A Polym. Chem.* **2002**, *A40*, 555; (b) Matyjaszewski, K.; Poli, R. *Macromolecules* **2005**, *38*, 8093.
- Frisch, M. J.; Trucks, G. W.; Schlegel, H. B.; Scuseria, G. E.; Robb, M. A.; Cheeseman, J. R.; Montgomery Jr., J. A.; Vreven, T.; Kudin, K. N.; Burant, J. C.; Millam, J. M.; Iyengar, S. S.; Tomasi, J.; Barone, V.; Mennucci, B.; Cossi, M.; Scalmani, G.; Rega, N.; Petersson, G. A.; Nakatsuji, H.; Hada, M.; Ehara, M.; Toyota, K.; Fukuda, R.; Hasegawa, J.; Ishida, M.; Nakajima, T.; Honda, Y.; Kitao, O.; Nakai, H.; Klene, M.; Li, X.; Knox, J. E.; Hratchian, H. P.; Cross, J. B.; Adamo, C.; Jaramillo, J.; Gomperts, R.; Stratmann, R. E.; Yazyev, O.; Austin, A. J.; Cammi, R.; Pomelli, C.; Ochterski, J. W.; Ayala, P. Y.; Morokuma, K.; Voth, G. A.; Salvador, P.; Dannenberg, J. J.; Zakrzewski, V. G.; Dapprich, S.; Daniels, A. D.; Strain, M. C.; Farkas, O.; Malick, D. K.; Rabuck, A. D.; Raghavachari, K.;

- Foresman, J. B.; Ortiz, J. V.; Cui, Q.; Baboul, A. G.; Clifford, S.; Cioslowski, J.; Stefanov, B. B.; Liu, G.; Liashenko, A.; Piskorz, P.; Komaromi, I.; Martin, R. L.; Fox, D. J.; Keith, T.; Al-Laham, M. A.; Peng, C. Y.; Nanayakkara, A.; Challacombe, M.; Gill, P. M. W.; Johnson, B.; Chen, W.; Wong, M. W.; Gonzalez, C.; Pople, J. A. *Gaussian 03, B.03*; Gaussian, Inc.: Pittsburgh PA, 2003.
9. Werner, H.-J.; Knowles, P. J.; Amos, R. D.; Bernhardsson, A.; Berning, A.; Celani, P.; Cooper, D. L.; Deegan, M. J. O.; Dobbyn, A. J.; Eckert, F.; Hampel, C.; Hetzer, G.; Korona, T.; Lindh, R.; Lloyd, A. W.; McNicholas, S. J.; Manby, F. R.; Meyer, W.; Mura, M. E.; Nicklass, A.; Palmieri, P.; Pitzer, R.; Rauhut, G.; Schütz, M.; Stoll, H.; Stone, A. J.; Tarroni, R.; Thorsteinsson, T. MOLPRO 2000.6; University of Birmingham: Birmingham, 1999.
 10. Izgorodina, E. I.; Coote, M. L. *J. Phys. Chem. A* **2006**, in press.
 11. (a) Henry, D. J.; Parkinson, C. J.; Mayer, P. M.; Radom, L. *J. Phys. Chem. A* **2001**, *105*, 6750. (b) Henry, D. J.; Parkinson, C. J.; Radom, L. *J. Phys. Chem. A* **2002**, *106*, 7927. (c) Coote, M. L.; Wood, G. P. F.; Radom, L. *J. Phys. Chem. A* **2002**, *106*, 12124. (d) Gómez-Balderas, R.; Coote, M. L.; Henry, D. J.; Radom, L. *J. Phys. Chem. A* **2004**, *108*, 2874. (e) Izgorodina, E. I.; Coote, M. L.; Radom, L. *J. Phys. Chem. A* **2005**, *109*, 7558.
 12. Scott, A. P.; Radom, L. *J. Phys. Chem.* **1996**, *100*, 16502.
 13. D. J. Henry; M. B. Sullivan; L. Radom. *J. Chem. Phys.* **2003**, *118*, 4849.
 14. J. C. Scaiano; K. U. Ingold. *J. Am. Chem. Soc.* **1976**, *98*, 4727.
 15. Ah Toy, A.; Chaffey-Millar, H.; Davis, T. P.; Stenzel, M. H.; Izgorodina, E. I.; Coote, M. L.; Barner-Kowollik, C. *Chem Commun* **2006**, in press.
 16. Izgorodina, E. I.; Coote, M. L. *Chem. Phys.* **2006**, ASAP Article.
 17. The use of RSEs to compare the stabilities of two radicals R• and R'• is only meaningful if there is negligible discrepancy between the R–H and R'–H bond strengths. For carbon-centered radicals this is generally the case, but there are a few minor exceptions. For example, in Table I the apparent increase in stability of the RAFT-adduct radicals as Z is varied from NH₂ to N(CH₂CH₃)₂ probably reflects the increased steric destabilization of the alkane CH₃SCH(Z)SCH₃ as the size of the Z-group increases.
 18. Mayadunne, R. T. A.; Rizzardo, E.; Chiefari, J.; Chong, Y. K.; Moad, G.; Thang, S. H. *Macromolecules* **1999**, *32*, 6977.
 19. Feldermann, A.; Coote, M. L.; Stenzel, M. H.; Davis, T. P.; Barner-Kowollik, C. *J. Am. Chem. Soc.* **2004**, *126*, 15915.
 20. (a) Rizzardo, E.; Chiefari, J.; Mayadunne, R. T. A.; Moad, G.; Thang, S. H. *ACS Symp. Ser.* **2000**, *786*, 278. (b) Destarac, M.; Charlot, D.; Franck, X.; Zard, S. Z. *Macromol. Rapid Commun.* **2000**, *21*, 1035.
 21. Henry, D. J.; Coote, M. L., Gómez-Balderas, R.; Radom, L. *J. Am. Chem. Soc.* **2004**, *126*, 1732.
 22. Vana, P.; Davis, T. P.; Barner-Kowollik, C. *Macromol. Theory Simul.* **2002**, *11*, 823.

Chapter 29

Tailoring Molecular Weight Distribution and Structure with Difunctional Reversible Addition Fragmentation Chain Transfer Agent. A Model Study

Geoffrey Johnston-Hall and Michael J. Monteiro*

Australian Institute of Bioengineering and Nanotechnology, School of Molecular and Microbial Sciences, The University of Queensland, Brisbane QLD 4072, Australia

The work in this paper describes a theoretically methodology to synthesize a polymer with any desired molecular weight distribution. It was found through simulations that a single highly reactive difunctional RAFT agent could be used for this purpose, while maintaining chain end functionality with negligible dead polymer. The method is based on varying the initiator concentration to ratios well above those used for monofunctional RAFT-mediated polymerizations. The resulting polymer is a mixture of monofunctional (PX, where X is the RAFT moiety and P denotes a polymeric chain) and difunctional (XPX) dormant species, in which the relative ratio of each is governed by the amount of initiator decomposed. Importantly, the amount of dead polymer is extremely low and fulfils the criterion as suggested by Szwarc (Nature 1956) that to meet 'living' requirements non-functional polymeric species formed by side reactions in the process should be undetectable by analytical techniques. In addition, this novel methodology allows the synthesis of AB, ABA and statistical multiblock copolymers with predetermined ratios to be produced in a one pot reaction.

Introduction

Controlled synthesis of the molecular weight distribution of linear polymers using controlled/living radical polymerization (LRP) has opened an exciting realm of applications, ranging from molecular computers¹⁻³ to miniature medical devices capable of entering individual cells to carry out a variety of functions⁴. The advantage of LRP is that linear polymers can be synthesized in which all chains are of approximately the same chain length, and can with a judicious choice of initiator and living agent produce a polymer with desired functionality on either chain-end. In contrast, conventional free-radical polymerization produces polymer chains of a broad distribution controlled through radical-radical termination events, and with little control of chain-end functionality. However, polymers synthesized by conventional free-radical polymerization are still the most widely used in most commercial applications. There are only few examples of the use of polymers synthesized by LRP as superior substitutes for conventional free-radically synthesized polymers. It would be useful to have one agent to produce any desired molecular weight distribution polymers in a simple one step (one pot) synthesis.

In the case of reversible addition-fragmentation chain transfer (RAFT) polymerization, it has been shown that polymers with controlled distributions can be synthesized using a variety of RAFT agents.⁵⁻¹⁰ The polydispersity (PDI) is controlled by selecting the appropriate activating Z group and leaving R group on the RAFT agent,^{11, 12} and in particular its chain transfer constant ($C_{tr} = k_{tr}/k_p$, for the reaction of polymeric radicals towards the S=C(Z)S- moiety). The greater the activating power of the Z group the narrower the molecular weight distribution (MWD). Therefore, to obtain a desired MWD, one must choose from a variety of RAFT agent. It has been shown through modeling and experiment that using a RAFT agent with a low C_{tr} constant (Xanthates¹³) can produce any PDI ranging from 1 to 2 through a monomer feed technique.^{7, 14} The control relies on maintaining a low and constant monomer concentration in the reaction vessel, but is experimentally not viable as extremely long reaction times are required to produce near uniform polymer chains.

In this work, we demonstrate through a comprehensive kinetic model that a highly reactive difunctional RAFT agent¹⁵ can be used to produce a wider range of molecular weight distributions than previously demonstrated and at faster rates. The approach we take is to vary the ratio of radical initiator to RAFT agent concentration. At first sight this is counter intuitive, as it has been found for monofunctional RAFT agents that ratios of initiator to RAFT greater than 1:10 results in a substantial amount of dead polymer. However, the use of difunctional RAFT agents allows the production of polymer with a mixture of difunctional and monofunctional polymer chains, and importantly even though as the initiator concentration increases and greater radical-radical termination events occurs the yield of dead polymer remains negligible. This procedure also provides a

unique opportunity to chain extend these polymers to form AB, ABA and multiblock copolymers in the same reaction mixture.

Kinetic Modelling

Simulations were performed on an IBM compatible 1.6GHz, 512MB RAM Pentium 4 using MATLAB 7.1. The model was developed based on the method of moments^{16, 17} and based on degenerative chain transfer similar to simulations carried out for RAFT block copolymerizations.⁸ The mechanism is given in Scheme 1, and the model is applicable to RAFT by assuming no other side reactions (e.g. intermediate radical termination¹⁸, impurities¹⁹, etc), and the exclusion of other events such as poor leaving group effects.

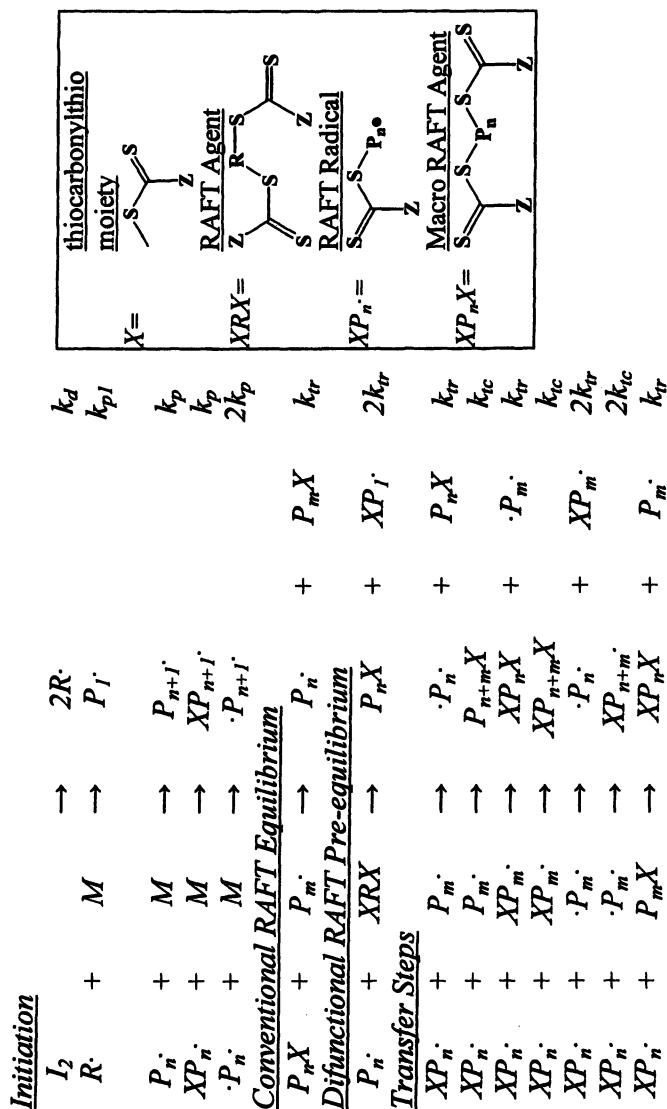
Table I. Kinetic parameters used to model the di-functional RAFT-mediated polymerization of styrene (STY) and methyl acrylate (MA).

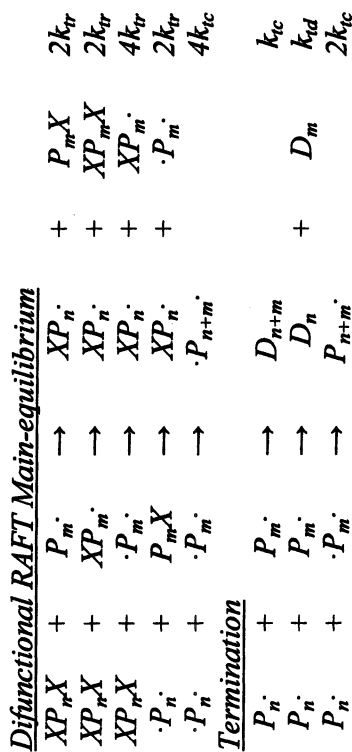
| | k_p ($L \text{ mol}^{-1} \text{ s}^{-1}$) | k_d (s^{-1}) | $[XRX]_0$ (mol L^{-1}) | $[M]_0$ (mol L^{-1}) |
|--------------------|--|------------------------------|--------------------------------------|------------------------------------|
| STY ^(a) | 341 ²⁰ | 9.443×10^{-6} | 0.005 | 5.5 |
| MA ^(b) | 2200 ²¹ | 4.964×10^{-7} | 0.0035 | 5.5 |

(a) 60°C, (b) 40°C, Other parameters used are termination by combination $k_t = 1 \times 10^8 \text{ L mol}^{-1} \text{ s}^{-1}$, initiator efficiency $f = 0.6$, and $C_{tr} = 1000$

Results and Discussion

The kinetic simulations are based on the homopolymerizations of styrene (60°C) and methyl acrylate (40°C) in the presence of a difunctional RAFT agent. These monomers were chosen to represent commercially important polymerizations and the very different rates of polymerization of each monomer. It allows the elucidation of the important kinetic parameters that control the MWD. The simulations consider the S=C(Z)S- moiety to be highly reactive (i.e. $C_{tr} = 1000$). In addition, the model was simplified such that no side reactions participate in the mechanism either to influence the rate of polymerization or the MWD. The parameters used in the simulations are given in Table 1. In contrast to monofunctional RAFT agents there are many other species found for a difunctional RAFT-mediated polymerization (Scheme 1). These include (where X is equivalent to S=C(Z)S): dead polymer (D_n), dormant mono-functional dormant species (P_nX), active propagating radicals ($P_n\bullet$), difunctional dormant species (XP_nX), di-radicals ($\bullet P_n\bullet$), and polymeric species that have a radical at one end and a RAFT moiety at the other ($XP_n\bullet$). This produces a rich mixture of different species. The aim of this work is to determine the conditions to allow





Scheme 1. The mechanism for the difunctional RAFT-mediated polymerization, which was used in the simulations.

control of the concentrations of each species and consequently the MWD of the overall polymer. We have denoted D, PX, P, XPX, ·P, and XP as the sum of all chains from $n = 1 \rightarrow \infty$.

Kinetic Modelling of Styrene at 60°C

The first set of kinetic simulations were carried out to examine the effect of increasing initiator (I) concentration on both the rate of polymerization and the MWD (Figure 1). In all the simulations the RAFT agent concentration was kept constant. The ratio of RAFT agent to initiator concentration was varied from 20:1 to 1:1. In Figure 1A it can be seen that as the ratio of initiator was increased (from curve a to e) the rate also increased as expected. The number-average molecular weight (M_n) increased linearly with conversion at 1:20 (i.e. the lowest initiator concentration, Figure 1B, curve a) in line with equation 1. As the concentration of I was increased, deviation away from curve a was observed, and was due to the increase in the relative concentration of XP to XPX (seen more clearly in Figure 2). The evolution of the PDI with conversion is given in Figure 1C. It was found at the lowest [I] (1:20), the PDI was close to 1 at ~30% conversion. At the highest initiator concentration the PDI increased from close to 1.1 to 2 at high conversion (80%). Interestingly, it can be seen that the PDI can be controlled between 1 and 2 by simply varying the ratio of RAFT to initiator. More importantly, by using a difunctional RAFT agent the amount of dead polymer was very small (Figure 1D). Only at equal concentrations of RAFT to initiator (1:1) was the amount of dead polymer, D, similar to that found for a monofunctional RAFT agent at a ratio of 1:10 (initiator to RAFT). At lower initiator concentrations, the percentage of dead polymer was well below any analytical detection (curves a to c). It is also interesting to note that at the lower initiator concentrations, in which control and functionality on both chain end-groups is retained, the conversion reached after 120 h was less than 40% due to the very low k_p .

In the case of a mono-functional RAFT agent, increasing the initiator concentration to increase the rate of polymerization would result in significant dead polymer and significant loss of chain end functionality. For example, using mono-functional xanthates (Ctr ~ 1)²² to produce PSTY with PDI of 2 and negligible dead polymer under the same experimental conditions requires the same time (120 h) to reach 40% conversion.

The use of our method (difunctional RAFT agent) allowed a PDI approaching 2 to be reached more rapidly on the polymerization time-scale with negligible dead polymer, an advance for commercially slow monomers.

$$M_n = \frac{[M]_0 x}{([RAFT]_0 - [RAFT]_x) + \alpha f([I]_0 - [I]_x)} \times M_w \quad (1)$$

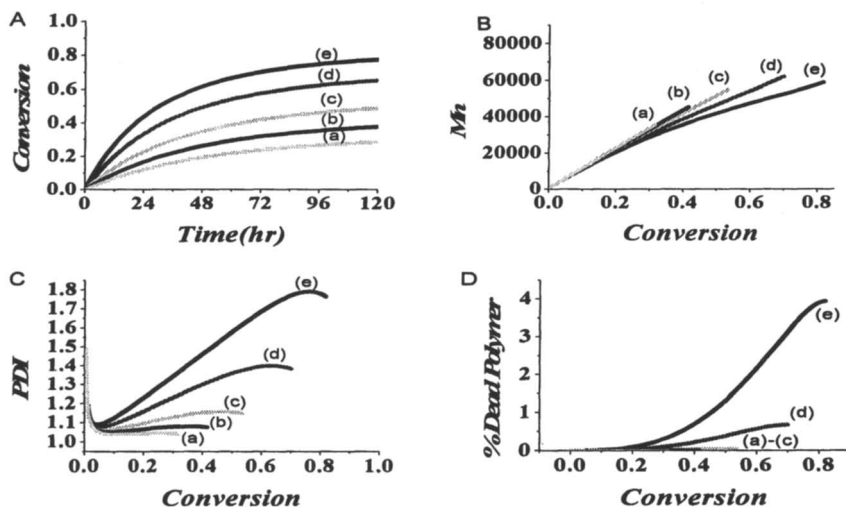


Figure 1. Simulations used to examine the effect of initiator concentration on the reaction rate and MWD 's of styrene at $[M]_0:[XRX]_0 = 5.5/0.005$: (A) conversion vs time, (B) M_n vs conversion, (C) PDI vs conversion and (D) dead polymer versus conversion. The $[I]_0:[XRX]_0$ ratios for curves (a) 1:20, (b) 1:10, (c) 1:5, (d) 1:2, and (e) 1:1.

Figure 2 shows the effect of varying the ratio of RAFT to initiator on the concentrations of individual species (shown in Scheme 1) as a function of conversion. The zeroth moment was used to quantify the sum of the molar concentrations of polymeric species P^\bullet , $\bullet P^\bullet$, XP^\bullet , PX , XPX and D vs conversion for the series of styrene experiments given in Figure 2. The sum of propagating radicals ($[P^\bullet]$ and $[XP^\bullet]$) are in the concentration range 10^{-7} to 10^{-9} mol L^{-1} , which is in the same range as conventional free-radical polymerization. The concentration of the polymeric di-radical $[\bullet P^\bullet]$ is negligible and is approximately 6 orders of magnitude lower than $[P^\bullet]$ at 10^{-13} to 10^{-15} mol L^{-1} . The unusual dormant radical species (XP^\bullet) undergo radical-radical coupling to form the difunctional dormant (XPX) species. This later species is dominant compared to all other polymeric species in the system. The concentration of dead polymer, $[D]$, is in the range of 10^{-8} to 10^{-5} mol L^{-1} , and was based on termination by combination. Obviously, should termination be through disproportionation then the concentration of dead polymer will increase but by no more than an order of magnitude. In addition, transfer to monomer will only have a small effect especially at these M_n 's and reaction temperatures.

The evolution of the MWD at a molar ratio of 1:2 (initiator to RAFT, curve d in Figure 1) at conversions of 5, 40 and 70% is given in Figure 3. The MWD of the species (PX and XPX) is determined using a Gaussian distribution that

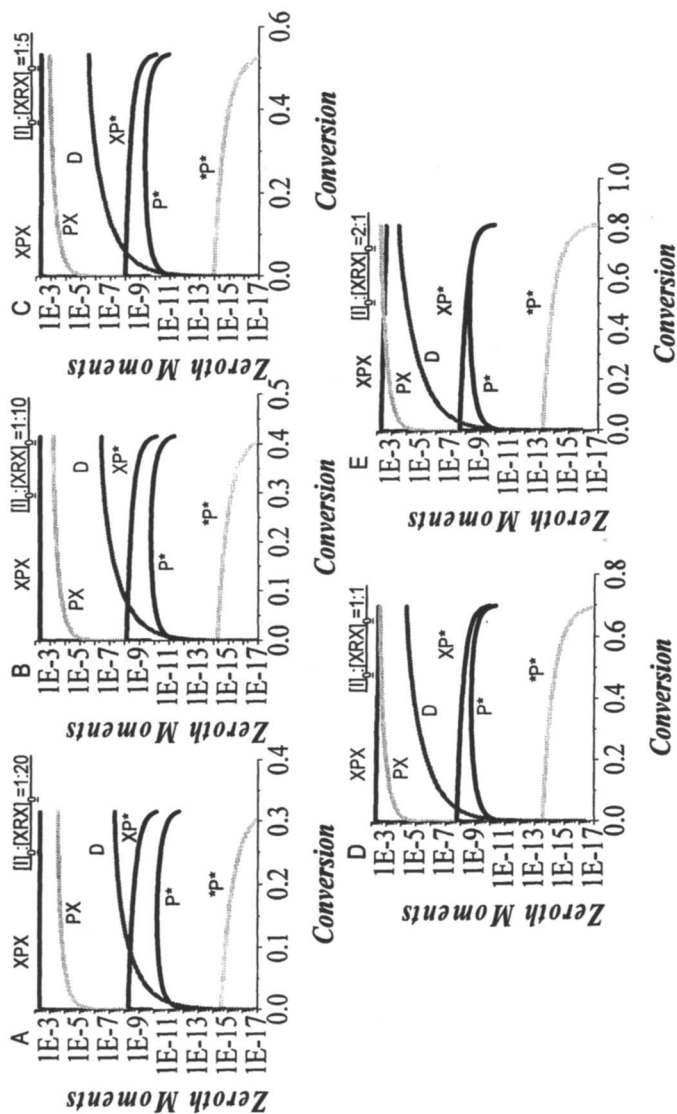


Figure 2. Simulations used to examine the effect of increasing initiator concentrations on the molar concentrations (zeroth moments) of the polymeric species for styrene at $[I]_0:[XRX]_0$ ratios of (A) 1:20, (B) 1:10, (C) 1:5, (D) 1:2, and (E) 1:1. $[M]_0:[XRX]_0 = 5.5/0.005$.

applies both the M_n and PDI of each species from the simulations, and represents the full distribution as the amount of dead polymer is negligible (less than 1% at 75% conversion). The Gaussian distribution function was chosen as the system is neither truly 'living' (where a Poisson distribution would apply²³) nor governed by conventional free-radical polymerization (where a Schultz-Flory distribution would apply²⁴). Therefore, the Gaussian distribution is a good approximation, and for the purpose of this paper shows the effect of the relative ratios of PX and XPX on the overall MWD.²⁵

Figure 3A shows the MWD at 5% conversion. The amount of PX was approximately two orders of magnitude lower than XPX, and the distribution close to a Poisson with a PDI value below 1.1. An increase in conversion to 40% shows the evolution of PX and XPX to concentrations of $2 \times 10^{-3} \text{ mol L}^{-1}$ and $4 \times 10^{-3} \text{ mol L}^{-1}$, respectively. A further increase in conversion to 70% resulted in a growth of PX ($2.9 \times 10^{-3} \text{ mol L}^{-1}$) compared to XPX ($3.5 \times 10^{-3} \text{ mol L}^{-1}$). The distribution broadened with conversion due to the greater amount of chains formed through initiation. This also resulted in a greater amount of PX dormant species. The relative ratio of PX to XPX can be determined using equation 5 below. The validity of this equation is based on the criterion that there is negligible dead polymer, which is satisfied under our reaction conditions.

Equation 5 is derived by the mass balance of equation 2, and incorporating this into equation 3 (which provides the ratio of PX to XPX). The amount of PX is equal to the formation of radical that propagate to form polymer and is given by equation 4. Substituting equations 2 and 4 into 3 gives equation 5, allowing prediction of the relative proportions of [PX] and [XPX] for difunctional RAFT agents with a high transfer constants ($C_{tr} > 100$), and is proportional to the amount of initiator decomposed in the reaction.

$$[XPX] = [XRX]_0 - \frac{1}{2}[PX] \quad (2)$$

$$\frac{[PX]}{[PX] + [XPX]} = \frac{[PX]}{[XRX]_0 + \frac{1}{2}[PX]} \quad (3)$$

$$[PX] = 2f([I]_0 - [I]) \quad (4)$$

$$\frac{[PX]}{[PX] + [XPX]} = \left(\frac{1}{2} + \frac{[XRX]_0}{2f([I]_0 - [I])} \right)^{-1} \quad (5)$$

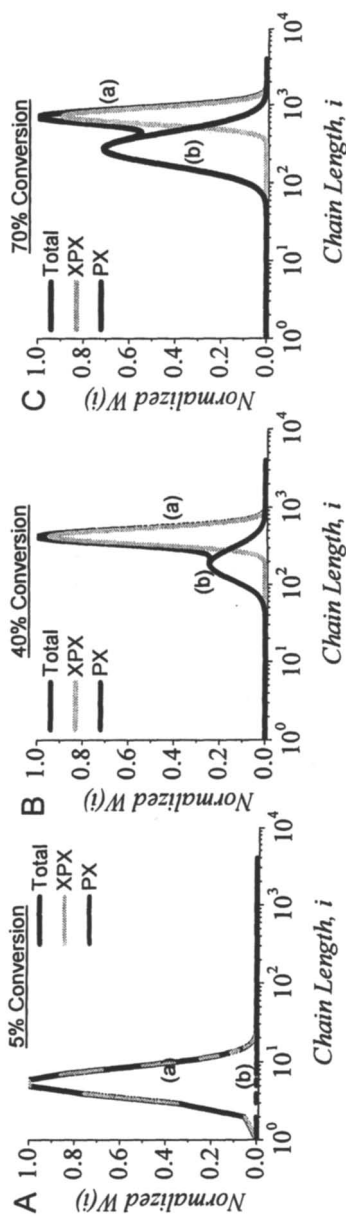


Figure 3. Simulations of the MWDs (using a Gaussian distribution function) determined at different conversions (A) 5%, (B) 40%, and (C) 70% for the reaction of styrene with an $[I]_0:[XRX]_0$ ratio of 1:2. Distributions of the dormant species curves (a) XP_rX and (b) P_rX are also shown.

Equation 5 allows prediction of the relative proportions of diblock AB and triblock ABA copolymers to be produced in a one pot reaction using a second stage copolymerization. This may be commercially important as the mechanical properties of the resultant polymer will be controlled by the ratio of AB to ABA and chemical composition of these blocks in the system.

Chain Extension of PSTY after 120 h with STY

The evolution of M_n , PDI and % dead polymer with conversion for the chain extension of PSTY is given in Figure 4. The starting PSTY blocks cover a range of M_n and PDI values (data from Figure 1, curves a to e at 120 h), and are extended with STY at two initiator concentrations (i.e. ratios of initiator to dormant polymer of 1:1 (denoted as 1) and 1:10 (denoted as 2)). The M_n increased with conversion under both initiator concentrations for the 5 different starting blocks.

Interestingly, in the 1:1 case all the M_n profiles converge to a similar end value (~80% conversion) close to 70 K. Similarly, the PDI (Figure 4B) showed a linear increase with conversion until 70% conversion. This shows that at high initiator concentrations the M_n was relatively constant but the PDI increased linearly with conversion from its starting value. The only disadvantage for starting blocks with a high proportion of PX to XPX (curves d and e in Figure 1) was that in the chain extension at high initiator concentrations the amount of dead polymer was above acceptable limits (>10%). In the case where the initiator concentration was low (1:10), the M_n increased linearly with conversion, the PDI was close to the original starting block and the amount of dead polymer was negligible (see for example curves 2a and 2b). This shows that the original starting block distribution can be simply increased to any desired M_n while maintaining the starting PDI. In other words, the MWD can be translated to a higher molecular weight with out compromising the distribution. These results show the versatility of using a difunctional RAFT agent. It is now theoretically possible to dial up the desired M_n and PDI (within limits), and show that the highly reactive difunctional RAFT agent is the most versatile agent to produce a desired distribution.

Kinetic Modelling of Methyl Acrylate at 40°C

In comparison to the styrene polymerizations in the presence of a difunctional RAFT agent, methyl acrylate at 40°C has a k_p that is approximately

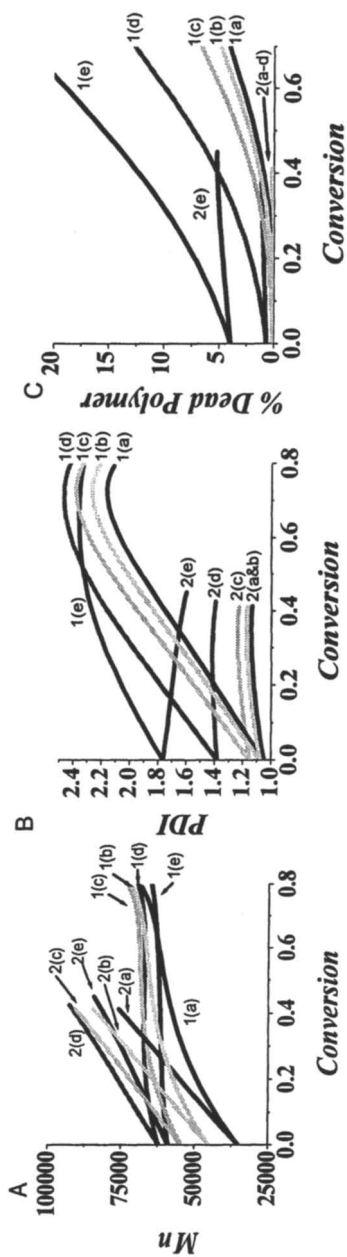


Figure 4. Simulations used to examine the effect of initiator concentration on MWD's for chain extended polystyrene using high and low $[I]_0:[XP_nX]_0$ ratios (1) 1:1 and (2) 1:10: (A) M_n , (B) PDI and (C) dead polymer, versus conversion. Polymeric RAFT agent as taken from Figure 1 after 120 hours for which $[I]_0:[XRX]_0$ ratios of (a) 1:20, (b) 1:10, (c) 1:5, (d) 1:2, and (e) 1:1 were implemented) and chain extended.

three orders of magnitude greater than that for styrene at 60°C. Therefore, the influence of initiator concentration will have a much smaller effect on controlling the MWD (c.f. equation 5). Figure 5A shows the conversion vs time profiles for MA at increasing initiator concentrations (curve a represents the lowest concentration and curve e the highest concentration). As expected the increased initiator concentration resulted in an increased rate of polymerization. The result of this on the MWD are shown in Figures 5B and 5C, in which the M_n for all initiator concentrations demonstrate ideal 'living' behaviour; a linear increase in M_n with conversion and PDIs well below 1.1. Figure 5D showed that the relative ratio of PX to XPX was very small (below 0.025), and was the same as that calculated from equation 5.

Figure 6 shows the zeroth moment of all the polymeric species during the polymerization of MA with the difunctional RAFT agent. As discussed above XPX and PX are the major species, the amount of dead polymer is extremely low, ranging from 10^{-9} to 10^{-11} mol L⁻¹, and the radical concentrations (P', XP' and 'P') are similar to conventional free-radical polymerization. Although the amount of dead polymer is extremely low and well below any analytical detection, the existence of dead polymer suggests that 'true' living conditions will never be met for a RAFT systems. However, for metal catalysed or nitroxide mediated polymerizations using a difunctional agent, 'true' living conditions in which zero dead polymer is formed only occurs if radical-radical termination is by combination.

Multiblock Copolymers

The difunctional RAFT technique offers a novel methodology to make tailored multiblock and statistical AB and ABA block copolymer structures. The dormant polymeric species (XPX), where P can be built from one or more types of monomer units, can be coupled together to form statistical multiblock copolymers in the presence of initiator. The reaction mechanism is given in Figure 7A and would consist of, for example, XP1X + XP2X (where P1 and P2 are different polymers) and initiator in solvent and heated to the desired temperature. The resulting products would be a statistical distribution of multiblock copolymers. Figure 7B shows the simulations using this approach, starting with a monodisperse difunctional polystyrene macroRAFT agent (XPX). The molecular weight distribution increased but at the same time broadens, a similar result found from condensation polymerizations. Radical termination and leaving group effect are the critical parameters in controlling these distributions. The commercial advantage is that these reactions are facile and their MWDs can be changed by simply changing the initiator concentration and temperature.

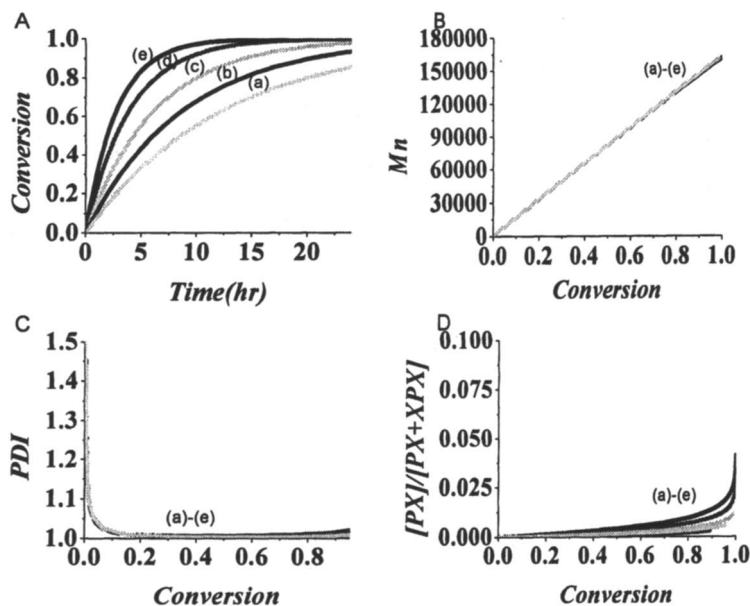


Figure 5. Simulations used to examine the effect of increasing initiator concentrations on the MWD of methyl acrylate: (A) conversion vs time, (B) M_n vs conversion, (C) PDI vs conversion, and (D) fraction of PX in the polymer. Ratios of $[I]_0$ to $[XRX]_0$ varied from (a) 1:20, (b) 1:10, (c) 1:5, (d) 1:2, and (e) 1:1. (For other parameters see Table 1.)

Conclusion

The use of a single highly reactive difunctional RAFT agent was shown by simulations to control the molecular weight to any M_n and PDI (between 1 and 2). The method relied on varying the initiator concentration to form the dormant species PX and XPX. Control is governed by the rate of polymerization and the amount of initiator decomposed. An important result was that the amount of dead polymer formed was well below any analytical detection limits. This is what Szwarc²⁶ suggested that to meet 'living' requirements non functional polymeric species formed by side reactions in the process should be un-detectable by analytical techniques.. It was also discovered that predetermined ratios of AB and ABA block copolymers could be formed in situ using this polymerization technique. In addition, statistical multiblocks would be formed through the addition of initiator to dormant polymeric species (XP1X and XP2X).

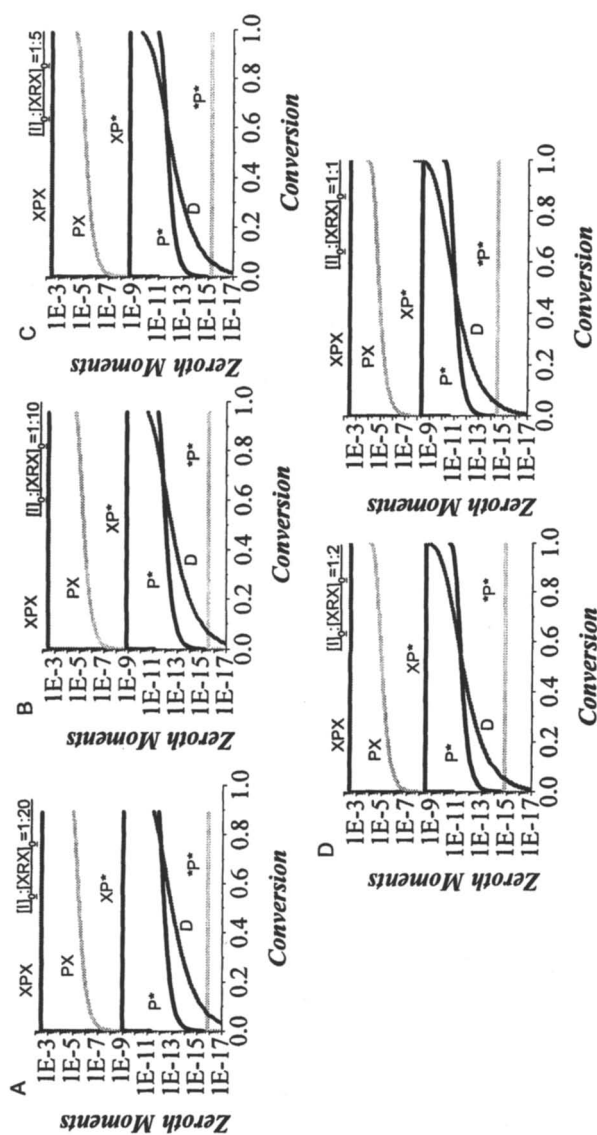
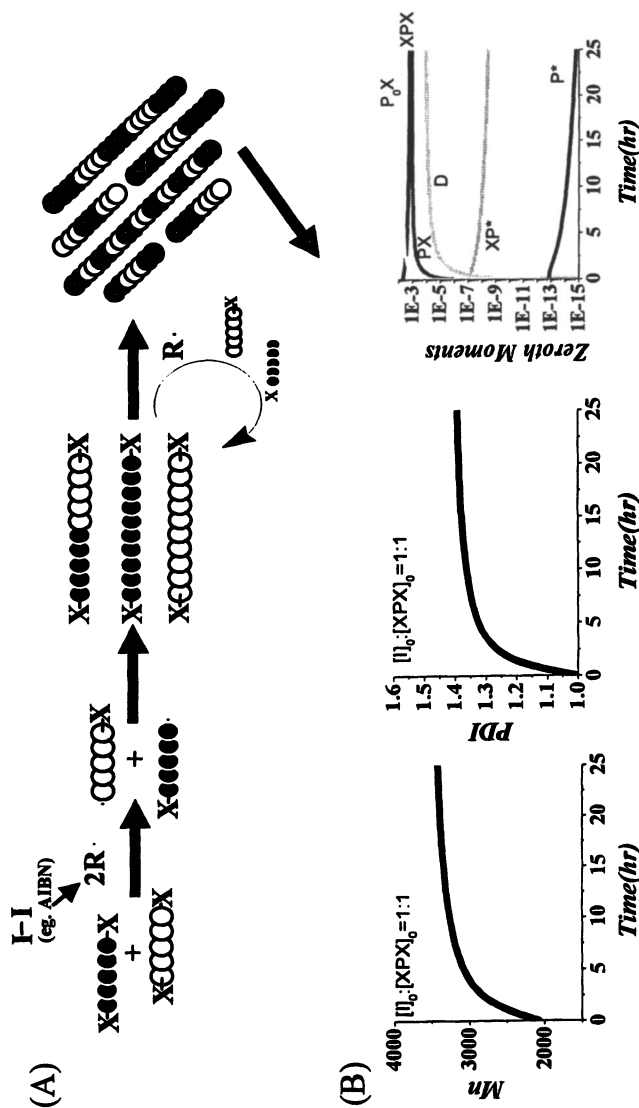


Figure 6. Simulations used to examine the effect of increasing initiator concentration on the molar concentrations (zeroth moments) of polymeric species in the polymerization of methyl acrylate at $[I]_0:[XRX]_0$ ratios of (A) 1:20, (B) 1:10, (C) 1:5, (D) 1:2, and (E) 1:1. $[M]_0:[XRX]_0 = 5.5/0.0035$.



References

1. Xia, Y.; Rogers, J. A.; Paul, K. E.; Whitesides, G. M. *Chem. Rev.* 1999, *99*, 1823-1848.
2. Barrett, C. R. *Mater. Res. Soc. Bull.* 1993, *3*
3. Service, R. F. *Science* 1996, *273*, 1834.
4. Liu, J.; Zhang, Q.; Remsen, E. E.; Wooley, K. L. *Biomacromolecules* 2001, *2*, 362-368.
5. Le, T. P.; Moad, G.; Rizzardo, E.; Thang, S. H., 1998; Vol. PCT Int. Appl. WO 98/01478 (Chem Abs, (1998) 128: 115390).
6. Moad, G.; Chiefari, J.; Chong, B. Y. K.; Krstina, J.; Mayadunne, R. T. A.; Postma, A.; Rizzardo, E.; Thang, S. H. *Polymer International* 2000, *49*, 993-1001.
7. Monteiro, M. J. *J. Polym. Sci., Part A: Polym. Chem.* 2005, *43*, 3189-3204.
8. Monteiro, M. J. *J. Polym. Sci., Part A: Polym. Chem.* 2005, *43*, 5643-5651.
9. Perrier, S.; Takolpuckdee, P. *J. Polym. Sci., Part A: Polym. Chem.* 2005, *43*, 5347-5393.
10. Moad, G.; Rizzardo, E.; Thang, S. H. *Aust J Chem* 2005, *58*, 379-410.
11. Chiefari, J.; Mayadunne, R. T. A.; Moad, C. L.; Moad, G.; Rizzardo, E.; Postma, A.; Skidmore, M. A.; Thang, S. H. *Macromolecules* 2003, *36*, 2273-2283
12. Chong, B. Y. K.; Krstina, J.; Le, T. P. T.; Moad, G.; Postma, A.; Rizzardo, E.; Thang, S. H. *Macromolecules* 2003, *36*, 2256-2272.
13. Charlot, D.; Corpart, P.; Michelet, D.; Zard, S.; Biadatti, T. Patent. In: *Rhodia Chemie*; 1998.
14. Smulders, W.; Monteiro, M. J. *Macromolecules* 2004, *37*, 4474.
15. Patton, D. L.; Mullings, M.; Fulghum, T.; Advincula, R. C. *Macromolecules* 2005, *38*, 8597-8602.
16. Bamford, C. H.; Tompa, H. *Transactions of the Faraday Society* 1954, *50*, 1097.
17. Wang, A. R.; Zhu, S. *J. Polym. Sci., Part A: Polym. Chem.* 2003, *41*, 1553-1566.
18. Monteiro, M. J.; De Brouwer, H. *Macromolecules* 2001, *34*, 349.
19. Plummer, R.; Goh, Y.-K.; Whittaker, A. K.; Monteiro, M. J. *Macromolecules* 2005, *38*, 5352-5355.
20. Buback, M.; Gilbert, R. G.; Hutchinson, R. A.; Klumpermann, B.; Kutcha, F.-D.; Manders, B. G.; O'Driscoll, K.; Russell, G. T.; Schweer, J. *Macromol Chem. Phys.* 1995, *196*, 3267.
21. Schoonbrood, H. A. S.; van den Reijen, B.; de Kock, J. B.; Manders, B. G.; van Herk, A. M.; German, A. L. *Macromol. Rapid Comm.* 1995, *16*(2), 119-124.
22. Adamy, M.; van Herk, A. M.; Destarac, M.; Monteiro, M. J. *Macromolecules* 2003, *36*, 2293-2301.
23. Flory, P. J. *Principles of Polymer Chemistry*; Cornell University Press: Ithaca, 1953.
24. Russell, G. T. *Aust. J. Chem.* 2002, *55*, 399-414.
25. O'Shaughnessy, B.; Vavylonis, D. *Macromol. Theory Simul.* 2003, *12*, 401-412.
26. Szwarc. *Nature* 1956, *178*, 1168-1169.

Chapter 30

Progress in RAFT/MADIX Polymerization: Synthesis, Use, and Recovery of Chain Transfer Agents

Sébastien Perrier¹, Pittaya Takolpuckdee², Steven Brown¹,
Thomas M. Legge¹, Debashish Roy¹, Murray R. Wood¹,
Steven P. Rannard³, and David J. Duncalf³

¹Department of Colour and Polymer Chemistry, The University of Leeds,
Leeds LS2 9JT, United Kingdom

²Chemistry Program, Faculty of Science and Technology, Valayalongkorn
Rajabhat University, Phatumtani 13180, Thailand

³Unilever Research and Development, Port Sunlight Laboratories,
Quarry Road East, Bebington, Wirral L63 3JW, United Kingdom

We report the synthesis of novel chain transfer agents for RAFT/MADIX polymerization, and their use to mediate the polymerization of a variety of monomers, in order to produce a range of functional materials. After polymerization, the chain transfer agent is recovered in a one pot reaction, which also permits to introduce functional groups at the chain-end of the polymers.

Introduction

Since the first reports in the early 1990's, living radical polymerization techniques such as ATRP,¹ NMP² and RAFT/MADIX^{3,4} have received a strong interest from both academic and industrial laboratories. RAFT and MADIX are both based on a radically induced degenerative chain transfer reaction between a thiocarbonyl-thio containing compound and a propagating radical, following the principle of degenerative chain transfer first reported by Zard's group in the late 80's.⁵ The process offers all advantages of living polymerization techniques (e.g. production of complex polymeric architectures) without suffering from traditional downfalls attached to such techniques (low temperatures, ultra-pure reactants, etc.). Moreover, the versatility of RAFT/MADIX towards functional groups permits the synthesis of a wide range of functional macromolecules.⁶ For the last few years, our group has focused on the design of alternative techniques for the synthesis of polymerization mediators (chain transfer agents, CTA's), and their use in polymerization reactions. We report here our latest results, and provide simple techniques of CTA synthesis, and their use to produce specific functional materials. The last section of this chapter covers a straight forward technique to replace the thiocarbonyl-thio moiety present at the chain-end of the polymer by a functional group, whilst recycling the chain transfer agent.

Experimental Section

Materials. All solvents, monomers, and other chemicals were purchased from Aldrich at the highest purity available and used as

received unless otherwise stated. All monomers were filtered before utilization through a basic alumina (Brockmann I) column, to eliminate the radical inhibitor. Tetrahydrofuran (THF, Riedel-deHaën, HPLC grade) was dried over molecular sieves 4 Å. 2,2-Azobisisobutyronitrile (AIBN, 99%, Fisher) was recrystallized twice from ethanol. Diethyl ether, ethyl acetate and n-hexane were purchased from Riedel-deHaën (AR grade). Magnesium turnings (AnalaR) was purchased from BDH. Cellulose supported S-methoxycarbonyl- α -phenylmethyl dithiobenzoate⁷ and silica / Merrifield supported S-methoxycarbonyl- α -phenylmethyl dithiobenzoate^{8,9} were synthesised as previously reported. Air and moisture sensitive compounds were manipulated using standard Schlenk techniques under a nitrogen atmosphere.

General synthesis method of trithiocarbonates / xanthates using 1,1'-thiocarbonyl diimidazole – Typical synthesis of 2-ethylsulfanylthiocarbonyl-sulfanylpropionic acid ethyl ester (ETSPE, 14, Figure 2). Dry toluene (60 mL) was added to a stoppered three-necked flask. 1,1'-Thiocarbonyl diimidazole (TCDI) ((95%) 3.60 g, 19.2 mmol) and potassium hydroxide (0.05 g, 0.86 mmol) was added, in one portion, under nitrogen. To the solution was added ethyl 2-mercaptopropionate ((95%) 2.63 mL, 2.71 g, 19.2 mmol) drop wise. The reaction mixture was heated to 60 °C and refluxed for 7 h. After this time, the mixture was allowed to cool to room temperature and left to stand, under nitrogen, overnight. Ethanethiol ((99%) 1.34 mL, 1.49 g, 19.2 mmol) was added drop wise, under nitrogen, to the stirred solution. The reaction mixture was heated to 60 °C, refluxed for 6 h, then left to cool to room temperature overnight. The solution was filtered, concentrated under vacuum and subjected to flash chromatography (silica, 5% ethyl acetate in hexane as eluent). The desired fraction was concentrated under vacuum and subjected to Kugelrohr distillation, affording the product as a bright yellow oil. (62 %). ¹H-NMR (400MHz, CDCl₃) δ 1.26-1.30 (3H, t, J= 7.2 Hz, SCH₂CH₃), 1.34-1.38 (3H, t, J= 4.2 Hz, OCH₂CH₃), 1.57-1.61

(3H, d, $J = 7.7$ Hz, SCHCH₃), 3.34-3.40 (2H, q, $J = 6.5$ Hz, SCH₂CH₃), 4.17-4.23 (2H, q, $J = 3.8$ Hz, OCH₂CH₃), 4.78-4.83 (1H, q, $J = 7.4$ Hz, SCHCH₃) ¹³C-NMR (100MHz) δ 221.9, 171.1, 61.9, 48.0, 31.5, 31.1, 17.0, 14.3, TOF-MS (ES⁺) $m/z = 239.023$ (MH⁺)

General polymerization and end-group modification method.

To an ampoule was added methyl methacrylate (6.10g, 60.9 mmol), bromophenyl acetic acid dithiobenzoate (0.035g, 0.122 mmol) and AIBN (0.002g, 0.012 mmol). The solution was degassed with N₂ for 10 mins then heated to 60°C for 8 h. The solution was cooled and the polymer precipitated by dropwise addition of the solution into cold hexane to yield 34% of poly(methyl methacrylate) and characterized by size exclusion chromatography (Mn = 13 500, PDI = 1.18). The isolated polymer was added to an ampoule (0.256g, 0.019 mmol) with AIBN (0.063g, 0.380 mmol) and toluene (5 mL). The solution was degassed with N₂ for 10 mins then heated to 80°C for 2.5 h. The solution was cooled and the poly(methyl methacrylate) precipitated by dropwise addition of the solution into cold hexane. The polymer was filtered off and characterized by size exclusion chromatography (Mn = 13 400, PDI = 1.17).

Results and Discussions

Synthesis of chain transfer agents.

Synthesis of functional chain transfer agents. Living radical polymerization techniques offer the potential to introduce specific functionalities within polymeric architectures.¹⁰ For instance, by using tailor-made chain transfer agents, one can introduce chain-end functionalities into polymeric chains. We and others have shown that derivatives of a methyl phenylacetate radical (R¹, Figure 1) are attractive leaving / re-initiating (R) group

for chain transfer agents.¹¹ Indeed, their potential for fragmentation from the thiocarbonyl-thio moiety is promoted by the stabilization of the resulting radical by the phenyl group on the α -C of the radical, whilst its ability to reinitiate polymerization is enhanced by the low steric hindrance of the secondary radical. Furthermore, the presence of a carboxylic moiety allows the introduction of a variety of functionalities. We have synthesized a series of dithiobenzoates and trithiocarbonates showing a range of functional groups via esterification of a molecule bearing the relevant functionality with 2-chloro-2-phenylacetyl chloride or α -bromophenyl acetic acid, including (Figure 1) methyl ester (1 and 2), carboxylic acid (3 and 4) and its sodium salt (5 and 6), amide (7), hydroxyl (8) and also multifunctional CTA's (e.g. 9).

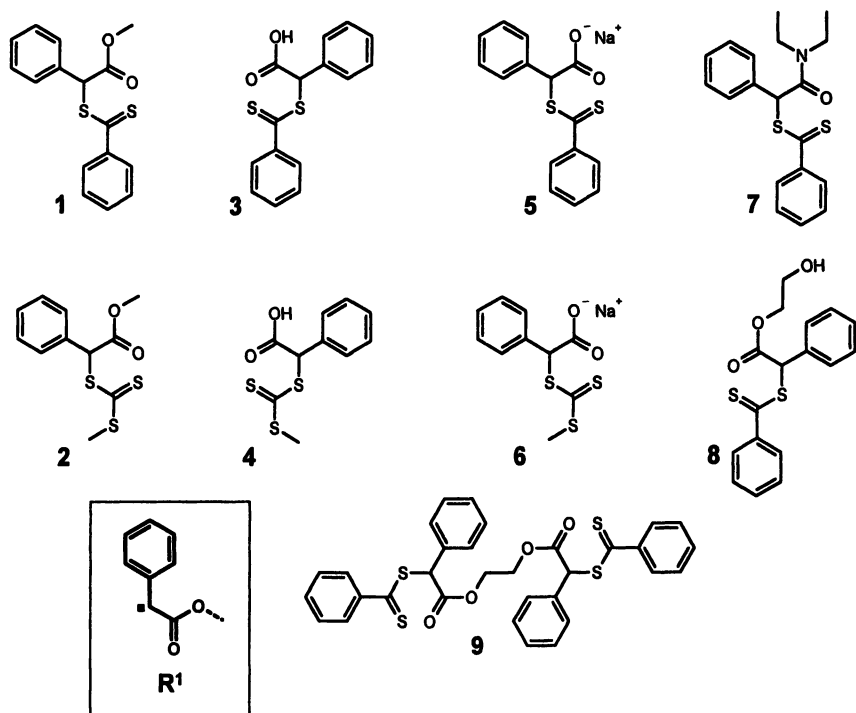


Figure 1. Functional CTA's produced from 2-chloro-2-phenylacetyl chloride or α -bromophenyl acetic acid and derivatives.

Synthesis of trithiocarbonates via one pot reaction from 1,1'-thiocarbonyl diimidazole. The syntheses of trithiocarbonates and xanthates following traditional routes have significant drawbacks for laboratories that are unfamiliar with compounds of considerable safety concerns (e.g. high flammability, risks of explosion, water sensitivity, and so on) and have contributed to the limited spread of RAFT and MADIX in academic and industrial laboratories worldwide. There have been many reports of alternative synthetic routes for the production of CTA's, but very few of them concerns trithiocarbonate derivatives.⁶ We have developed a synthetic method based on the use of 1,1'-thiocarbonyl diimidazole (TCDI, 10) to produce in a one-pot reaction a range of trithiocarbonates and xanthates. Such syntheses present clear advantages in terms of yield, reaction time and simplicity (Figure 2).

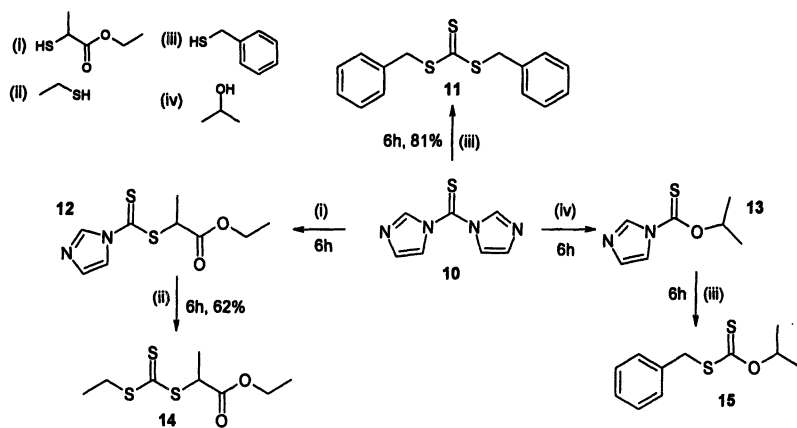


Figure 2. Synthetic schemes for the production of trithiocarbonates and xanthates using 1,1'-thiocarbonyl diimidazole (10).

With two equivalents of a primary thiol reacted onto TCDI, the symmetrically disubstituted product (11) is readily obtained. Furthermore, when TCDI is reacted with a secondary thiol or secondary alcohol, only the intermediate *S/O*-ester of imidazole-*N*-thionocarboxylic acid is produced (12 and 13). 12 and 13 may be further reacted with a primary thiol, to give a trithiocarbonate (14) or a xanthate (15).

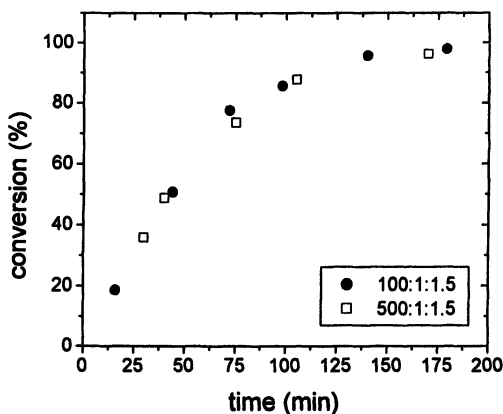


Figure 3. Conversion vs. time for the polymerization of methyl acrylate mediated by 2-ethylsulfanylthiocarbonylsulfanyl-propionic acid ethyl ester (ETSPE) at various Monomer:CTA ratios.

Trithiocarbonates have the added advantages by comparison to other CTA's (e.g. dithiobenzoates) in that they induce very little, or no, retardation in RAFT polymerization.⁶ Indeed, polymerizations mediated by 2-ethylsulfanylthiocarbonylsulfanyl-propionic acid ethyl ester (ETSPE) show similar kinetics, despite increasing the monomer concentration by a factor 5 (Figure 3 and 4).

RAFT/MADIX polymerization process. In addition to allowing the introduction of specific functionalities into polymeric architectures, RAFT/MADIX polymerization benefits from a straight forward process. Indeed, the polymerization relies on the simple introduction of a small amount of chain transfer agent into a classical free radical system (monomer + initiator). The transfer of the CTA between growing radical chains, present at very low concentration, and dormant polymer chains, present at higher concentration (three or four orders of magnitude), will regulate the growth of the molecular weight, and limit the termination

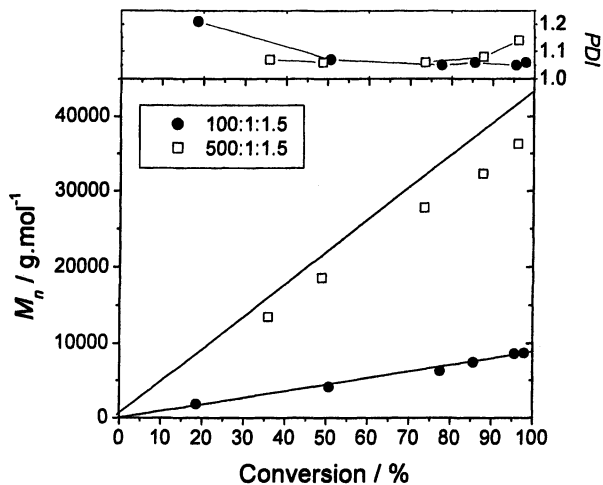


Figure 4. Molecular weight and PDI evolution with conversion for the polymerization of methyl acrylate mediated by 2-ethylsulfanylthiocarbonylsulfanyl-propionic acid ethyl ester (ETSPE) at various Monomer:CTA ratios.

reactions. In the system, the concentration of radical initiator is a key parameter. Free radicals are required at the start of the polymerization in order to trigger the degenerative chain transfer reactions which control the polymerization. However, these radicals also generate 'dead' polymeric chains, which affect the level of control over molecular weight distribution. Therefore, an increase in the concentration of free radical initiator leads to faster polymerizations, but increases the probability of irreversible terminations between growing chains, resulting in a worse control over molecular weight distribution.⁶

In order to promote faster polymerizations whilst keeping good control over the molecular weight distribution, we investigated microwave-assisted RAFT polymerizations. Microwave-assisted polymerizations have been shown to perform faster, and to higher yields, than equivalent reactions performed under more traditional heating conditions, and this effect is generally attributed to a temperature effect. Bulk RAFT polymerization of methyl acrylate,

methyl methacrylate and styrene was attempted in the presence of 2-ethylsulfanylthiocarbonylsulfanyl-propionic acid ethyl ester (ETSPE) as the chain transfer agent. We observed for methyl acrylate and methyl methacrylate that the kinetics of polymerization were greatly enhanced, whilst keeping an excellent control over the molecular weight ($PDI < 1.10$) (Figure 5 and 6). On the other hand, the polymerization of styrene did not show any increase in rate. Similar polymerization kinetics were reported for the free radical polymerization of these monomers,¹²⁻¹⁴ but previous studies have shown no noticeable effect of microwave heating on other LRP techniques.¹⁵

Synthesis of functional polymeric architectures. The versatility of the RAFT process towards functional groups permits the synthesis of a range of functional materials and indeed polymeric architectures. The use of methyl phenylacetate derivatives as leaving groups does not only permit to introduce functional end-groups, but also to synthesize more complex architectures, as illustrated below.

Telechelic polymers and ABA triblock copolymers. The use of compound (9) as chain transfer agent to mediate the polymerization of methacrylate or acrylate derivatives lead to the production of telechelic homopolymers with a dithiobenzoate functionality. The resulting telechelic polymers can be further reacted with free radical initiators (see below) to produce α,ω -functional homopolymers. Polymerization of methyl methacrylate and butyl methacrylate yielded telechelic homopolymers with well controlled molecular weights. Polymerization of butyl acrylate, on the other hand, led to polymers showing multimodal molecular weight distribution. We explained these observations by the initial fragmentation of the R group occurring at different rates on each side due to one side overcoming single polymer unit inhibition significantly earlier than the other. Such a situation may exist to a lesser extent for methacrylate derivatives, due to the faster fragmentation of methacrylate polymer units.¹⁶

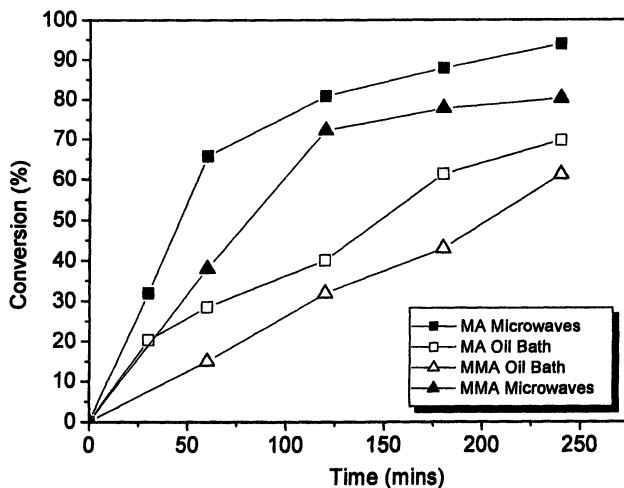


Figure 5. Conversion vs. time for the microwave-assisted polymerization of methyl acrylate and methyl methacrylate mediated by ETSPE using a ratio Monomer:ETSPE:AIBN = 500:1:0.25.

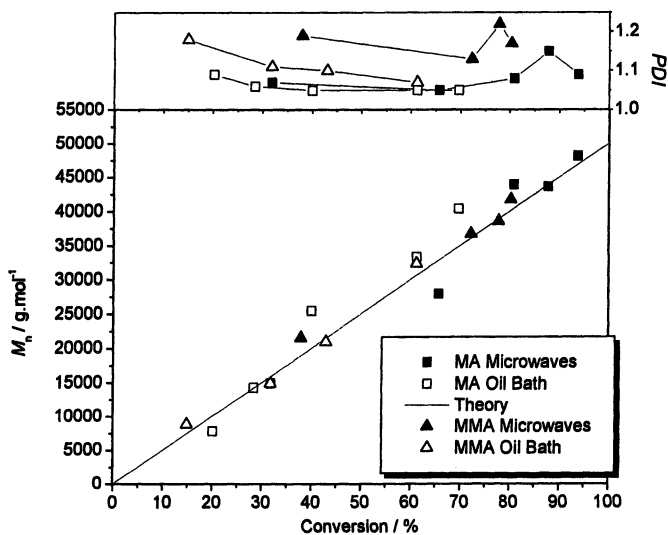


Figure 6. Molecular weight and PDI evolution with conversion of the microwave-assisted polymerization of methyl acrylate and methyl methacrylate mediated by ETSPE using a ratio Monomer:ETSPE:AIBN = 500:1:0.25.

Table 1. (Co)polymers synthesized via RAFT in toluene at 60 °C

| <i>M</i> | <i>CTA:I:M:S</i> ^a | <i>time</i> / <i>min</i> | <i>conv</i> ^b /% | <i>M_n</i> | <i>M_{n,theo}</i> | <i>PDf</i> ^c |
|------------------|-------------------------------|-----------------------------|--------------------------------|----------------------|---------------------------|-------------------------|
| BMA [†] | 1:0.2:500:100 | 810 | 82.5 | 37,900 ^c | 59,500 | 1.18 |
| BMA [†] | 1:0.4: 500:100 | 810 | 83.4 | 48,400 ^c | 59,300 | 1.23 |
| MMA [†] | 1:0.4:500:100 | 810 | 88.8 | 30,000 ^c | 44,500 | 1.26 |
| BA [†] | 1:0.4:500:100 | 2868 | 79.8 | 51,200 ^c | 51,200 | 1.70 |
| BA [‡] | 1:0.4:800:1200 | 1030 | 96 | 53,300 ^d | 95,800 | 1.36 |
| BA [‡] | 1:0.4:800:1200 | 175 | 40 | 15,700 ^d | 39,800 | 1.20 |
| BA [‡] | 1:0.25:800:1200 | 860 | 18 | 21,700 ^d | 19,800 | 1.55 |
| BA [‡] | 1:0.25:800:1200 | 3000 | 80 | 73,900 ^d | 82,000 | 1.73 |
| BMA [‡] | 1:0.25:800:1200 | 4180 | 91 | 90,700 ^d | 100,700 | 1.24 |

[†] CTA = 9, Figure 2; [‡] CTA = PMMA

^a CTA = chain transfer agent, I = initiator, M = monomer, S = solvent; ^b determined by gravimetric analysis; ^c determined by SEC using poly(methyl methacrylate) as standards; ^d determined by ¹H NMR by comparing the integrations of known proton signals from each block, and standardized using the molecular weight of the original macroCTA (determined by SEC).

BMA = *n*-butyl methacrylate, MMA = methyl methacrylate, BA = *n*-butyl acrylate.

Block extension of the poly(methyl methacrylate) with butyl methacrylate and butyl acrylate led to the formation of ABA triblock copolymers. Whilst the use of the methacrylate derivatives yielded block copolymers of well controlled molecular weights for conversions above 90%, the block extension using butyl acrylate showed the presence of a second peak at high molecular weights for conversion above 40%. Inspection of the molecular weight distribution data suggested that cross-terminations by combination may explain the presence of these high molecular weight peaks.

Cellulose supported RAFT polymerization. The treatment of cellulose fiber (cotton fabric and paper substrate) with 2-chloro-2-phenylacetyl chloride followed by reaction with a dithiobenzoate salt leads to the formation of cellulose supported chain transfer agents (Cellulose-CTA), attached to the cellulose via the R group (R-supported CTA's). We use these R-supported CTA's to mediate

the polymerization of styrene and dimethylaminoethyl methacrylate (DMAEMA). The use of free chain transfer agent in solution was found to improve the graft ratio, and limit the production of free polymeric chains in solution.

Table 2. Graft polymerizationa of styrene (Sty) and dimethyl aminoethylmethacrylate (DMAEMA) mediated by a cellulose-CTA in a molar ratio Monomer/Cellulose-CTA/AIBN = 100/1/0.1^a

| <i>Monomer</i> | <i>Monomer concentration</i> | <i>Time / h</i> | <i>Graft ratio / wt %</i> | <i>Monomer conversion%</i> |
|----------------|------------------------------|-----------------|---------------------------|----------------------------|
| Sty | 0.5M | 8 | 14 | 7 |
| | 0.5M | 16 | 16 | 11 |
| | 0.5M | 24 | 195 | 17 |
| DMAEMA | 0.5M | 4 | 1 | 13 |
| | 0.5M | 20 | 7 | 60 |
| | 0.5M | 48 | 11 | 75 |
| | 2M | 4 | 8 | 29 |
| | 2M | 20 | 12 | 78 |
| | 2M | 48 | 25 | 94 |
| | 2M ^b | 20 ^b | 20 ^b | 66 ^b |

^a Solvent = toluene; Temperature =60 °C. See reference⁷ for experimentals; ^b Undertaken in the presence of free CTA (MCPDB) in a ratio cellulose-CTA/free CTA = 1/1

Recovery of chain transfer agents. A key feature of living radical polymerization systems is the presence of a functional group at the polymeric chain-end (e.g. halogen, alkoxyamine, thiocarbonyl-thio group for ATRP, NMP and RAFT, respectively), which is responsible for the living character of the polymerization. There has been a variety of studies aiming to modify this end group for ATRP,^{17,18} NMP^{19,20} and RAFT.⁶ In the case of RAFT polymerization, we found that the in-situ addition of a radical to the reactive C=S bond of the thiocarbonyl-thio polymer end-group leads to the formation of an intermediate radical, which can then either fragment back to the original attacking radical or towards the polymeric chain radical. In the presence of an excess of free radicals, the equilibrium is displaced toward the formation of the

polymeric chain radical, which can then recombine irreversibly with one of the free radicals present in excess in solution, thus forming a dead polymeric chain. The process was shown to work in a variety of conditions and is easy to undertake (Figure 7).²¹

Besides the color removal, the system also allows the production of end-functional polymers and the recovery of the chain transfer agent (up to three polymerization cycles were undertaken using the same recovered CTA each time).

The recovery of the CTA might however be a problem for large scale production. Whilst in a typical laboratory set-up on the multi-gram scale, the polymer chemist would precipitate the polymer after radical modification and recover the CTA from the solution, larger productions require an alternative technique of recovery. A potential solution is the use of a solid-supported CTA, covalently linked to a solid support via its Z group. Such Z-supported CTA can be easily isolated after radical cleavage by simple filtration from the polymer product. The process also allows removal of all side products, including dead polymeric chains (irreversibly terminated), and non-reacted monomer by a filtration after polymerization. This additional feature makes this process unique, as it is the only radical polymerization system able to provide chains that are 100% living (All non-living chains, i.e. not terminated by the thiocarbonyl-thio moiety, are washed off after polymerization – on the other hand, 100% of the polymeric chains recovered have kept their end-group functionality, and are therefore able to re-initiate polymerization).^{8,9} A direct outcome of such system is the possibility to produce ‘pure’ block copolymers via radical polymerization. Indeed, homopolymers impurities arising from termination reactions are separated from the ‘living’ (controlled) chains by filtration. After filtration, the isolated living chains, attached to the support, can be chain extended to produce block copolymers (Figure 8).

In this system, the concentration in dead polymeric chains (non-attached to the solid support) is noticeably higher than that observed in the case of homogenous RAFT polymerization. We

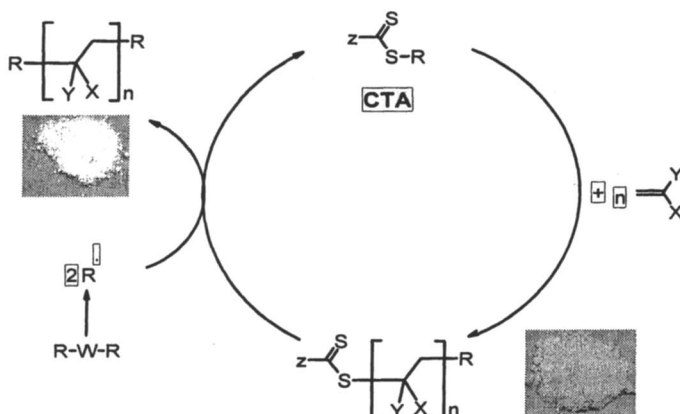


Figure 7. Schematic of the RAFT/MADIX polymerization and CTA recovery cycle. (Reproduced from reference 8. Copyright 2005 American Chemical Society.)

attributed this effect to the presence of two competing polymerization reactions in the system. Free radical polymerization occurs in solution, leading to the formation of uncontrolled, high molecular weight polymers that remain free in solution. On the other hand, RAFT polymerization occurs in presence of the solid support, and leads to attached living polymeric chains. Following these observations, and in order to improve the control over attached polymeric chains and reduce the amount of dead chains left in solution, we introduced a free chain transfer agent into the system (ratio free CTA : Z-supported CTA = 1:1). After cleavage, the molecular weight for both attached and free polymeric chains is greatly reduced by comparison to a system without free chain transfer agent, as the polymerization is slowed down by the presence of a free CTA in solution. Moreover, the molecular weight of the attached chains is close to that expected and the PDI's remain below 1.2 for both types of chains. Furthermore, quantification of the ratio of attached: free polymeric chains revealed that the proportion of free chains has decreased.

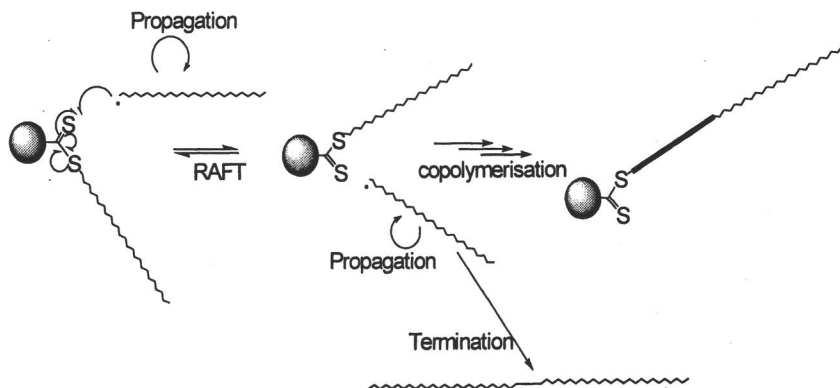


Figure 8. Schematic of the (co)polymerization process using Z-supported RAFT polymerization.

Conclusion

RAFT/MADIX polymerization is one of the most versatile living radical polymerization techniques to date. We have demonstrated the use of simple synthetic schemes in order to produce effective chain transfer agents able to control polymerization, the use of these chain transfer agents to synthesize complex functional polymeric architectures (block copolymers and graft copolymers), the optimization of the polymerization processes to increase the polymerization rate whilst keeping good control over the products, and the recovery of the chain transfer agent for further use. We believe the simplicity of this synthetic cycle makes it possible for non-specialists scientists to produce complex functional polymeric architectures which, to date, were only available to the well-trained polymer chemists.

Acknowledgement

We acknowledge the support of Unilever, ICI, EPSRC, the Royal Thai Government, the Green Chemistry Centre for Industrial Collaboration and Yorkshire Forward, the University of Leeds and the Department of Colour and Polymer Chemistry for funding.

References

1. Matyjaszewski, K.; Xia, J. H. *Chem. Rev.* **2001**, *101*, 2921.
2. Hawker, C. J.; Bosman, A. W.; Harth, E. *Chem. Rev.* **2001**, *101*, 3661.
3. Chiefari, J.; Chong, Y. K.; Ercole, F.; Krstina, J.; Jeffery, J.; Le, T. P. T.; Mayadunne, R. T. A.; Meijs, G. F.; Moad, C. L.; Moad, G.; Rizzardo, E.; Thang, S. H. *Macromolecules* **1998**, *31*, 5559.
4. D. Charmot, P. Corpart, H. Adam, S. Z. Zard, T. Biadatti, G. Bouhadir, *Macromol. Symp.* **2000**, *150*, 23.
5. Delduc, P., Tailhan, C., Zard, S. Z. *J. Chem. Soc.-Chem. Commun.* **1988**, 308.
6. Perrier, S., Takolpuckdee, P. *J. Polym. Sci. Pol. Chem.* **2005**, *43*, 5347.
7. Roy, D.; Guthrie, J. T.; Perrier, S.; *Macromolecules* **2005**, *38*, 10363
8. Perrier, S; Takolpuckdee, P; Mars, CA *Macromolecules* **2005**, *38*, 6770.
9. Takolpuckdee, P; Mars, CA; Perrier, S *Org. Lett.* **2005**, *7* (16), 3449.
10. Matyjaszewski, K.; Editor *Controlled/Living Radical Polymerization. Progress in ATRP, NMP, and RAFT. (Proceedings of a Symposium on Controlled Radical Polymerization held on 22-24 August 1999, in New Orleans.) [In: ACS Symp. Ser., 2000; 768]*, **2000**.
11. Perrier, S., Takolpuckdee, P., Westwood, J., Lewis, D.M. *Macromolecules* **2004**, *37*, 2709; Mayadunne, R. T. A.; Rizzardo, E.; Chiefari, J.; Krstina, J.; Moad, G.; Postma, A.; Thang, S. H. *Macromolecules* **2000**; *33*, 243; Lebreton, P.; Ameduri, B.; Boutevin, B.; Corpart, J. M. *Macromol. Chem. Phys.* **2002**, *203*, 522.
12. F.Y.C. Boey, H.L. Chia and J. Jacob, *J. Appl. Polym. Sci.* **1997**, *63*, 787.
13. V. Karmore and G. Madras, *Polym. Int.*, **2001**, *50*, 1324.

14. F.Y.C. Boey, H.L. Chia and J. Jacob, *J. Polym. Sci., Part A: Polym. Chem.* **2000**, *34*, 2087.
15. Schubert, U.S., Zhang, H. *Macromol. Rap. Commun.*, **2004**, *25*, 1225; Leenen, M., Wiesbrock, F., Hoogenboom, R., Schubert, U. S. *e-Polymers* **2005**.
16. Moad, G.; Chiefari, J.; Chong, Y. K.; Krstina, J.; Mayadunne, R. T. A.; Postma, A.; Rizzardo, E.; Thang, S. H. *Polym. Int.* **2000**, *49*, 993.
17. Bon S.A.F., Steward A.G., Haddleton D.M. *J. Polym. Sci. Pol. Chem* **2000**, *38*, 2678.
18. Snijder A., Klumperman B., Van der Linde R.J. *Polym. Sci. Pol. Chem* **2002**, *40*, 2350.
19. Harth E., Hawker C.J., Fan W., Waymouth, R.M. *Macromolecules* **2001**, *34*, 3856.
20. Beyou, E., Chaumont, P., Chauvin, F., Devaux, C., Zydowicz, N. *Macromolecules* **1998**, *31*, 6828.
21. Perrier, S.; Takolpuckdee, P.; Mars, C. A. *Macromolecules* **2005**, *38*, 2033.

Chapter 31

Pulsed-Laser Initiated Reversible Addition Fragmentation Chain Transfer Polymerization

M. Buback, T. Junkers, and P. Vana

Institut für Physikalische Chemie, Georg-August-Universität Göttingen,
D-37077 Göttingen, Germany

The almost instantaneous production of radicals via laser pulse initiation during RAFT polymerization in conjunction with measuring the subsequent decay of the intermediate RAFT radical concentration by μs time-resolved ESR spectroscopy allows for deducing addition and fragmentation rate coefficients of the RAFT process. By tracing monomer concentration via μs time-resolved NIR spectroscopy after an initiating laser pulse during RAFT polymerization, the rate coefficient of termination between propagating radicals and its chain-length dependence may be assessed. Results obtained by the novel SP-PLP-ESR-RAFT and SP-PLP-NIR-RAFT techniques are presented for butyl acrylate polymerization.

Introduction

Reversible addition-fragmentation chain transfer (RAFT) polymerization (1) has become one of the major controlled/living radical processes for generating materials with narrow molecular weight distribution and with complex microstructure (1-3). In contrast to other prominent controlled polymerization techniques, such as atom transfer radical polymerization (ATRP) (4) or nitroxide-mediated radical polymerization (NMP) (5), a permanent supply of initiating radicals is required for RAFT polymerization to proceed. When producing primary radicals by thermal decomposition of initiators, such as peroxides or azo compounds, elevated temperatures are required. In order to perform RAFT polymerizations under ambient temperature conditions, continuous gamma- (6,7), plasma- (8) and UV-irradiation (photoinitiation) (9,10) were applied. Due to the intense UV/VIS absorbance of dithio compounds, decomposition of mediating RAFT agents was observed in case of photoinitiation (9,10), which thus requires judicious adjustment of excitation wavelength to the UV/VIS absorbance of the RAFT agent, in order to prevent a significant loss of mediating compounds during polymerization.

A key advantage of photoinitiation by laser pulses relates to the possibility of externally triggering the amount of photoinitiator-derived primary radicals, which are produced at a precisely known instant in time. This feature enables detailed kinetic analysis of individual reactions steps. Laser pulsing may, e.g., be performed by using an excimer laser with a pulse width of a few tens of nanoseconds. In the pulsed-laser-polymerization size-exclusion-chromatography (PLP-SEC) method (11), a sequence of evenly spaced laser pulses is used for accurately measuring propagation rate coefficients, k_p . In SP-PLP experiments, photoinitiation by a laser single pulse (SP) is carried out in conjunction with μs time-resolved measurement of either monomer concentration, via near-infrared spectroscopy (SP-PLP-NIR) (12,13), or of propagating radical concentration via ESR-spectroscopy (SP-PLP-ESR) (14,15). The quality of measuring termination rate coefficients, k_t , in conventional radical polymerization has enormously been improved by using such SP-PLP techniques. It appears hence to be a matter of priority to apply pulsed-laser techniques also to the in-depth study of RAFT polymerization kinetics.

The present article addresses three topics: (a) controlled RAFT polymerization under pulsed-laser initiation, (b) the measurement of the RAFT addition and fragmentation rate coefficients by combining a laser single pulse experiment with ESR spectroscopy, and (c) the determination of chain-length dependent k_t values by SP-PLP-NIR in RAFT polymerization systems, where radical chain length is controlled.

The SP-PLP-ESR experiments were carried out at ambient pressure, whereas most of the SP-PLP-NIR experiments were run under high pressure, typically at 1000 bar, to improve signal to noise. There is no reason to assume that high pressure changes the RAFT mechanism and a recent study into styrene RAFT polymerization demonstrated that molecular weight control is even slightly improved toward high pressure (16).

Experimental

Materials. Butyl acrylate (BA, 99 %, Fluka) was freed from the inhibitor by passing over a column of activated basic alumina. α -Methyl-4-(methyl-mercapto)- α -morpholino-propiofenone (MMMP, 98 %, Aldrich), which was employed as the photoinitiator, 2,2,6,6-tetramethylpiperidine-1-oxyl (TEMPO, 99%, Aldrich), and toluene (99.5 %, Fluka) were used as received. The RAFT agent S-S'-bis(methyl-2-propionate)-trithiocarbonate (BMPT, see Figure 1) was synthesized according to the protocol described elsewhere (13). Solutions of BA, toluene, and BMPT were deoxygenized by three freeze-pump-thaw cycles. The photoinitiator was added under an argon atmosphere.

SP-PLP-NIR measurements. The mixtures for laser-induced polymerization were introduced into an internal cell, consisting of two CaF₂ windows and a cylindrical teflon tube. The internal cell was fitted into a high-pressure optical cell of transmission type (17). Polymerizations are induced at 60 °C and pressures of 5 or 1000 bar by XeF excimer laser pulses (at 351 nm) each of 2 to 3 mJ. Monomer conversion was monitored after each laser pulse via μ s time-resolved NIR spectroscopy at around 6170 cm⁻¹, that is, in the first-overtone range of C–H modes in α -position to a C–C double bond. After applying a series of laser pulses, the high-pressure cell was inserted into the optical compartment of an IFS 88 FT–NIR spectrometer to determine overall monomer conversion by measuring the full C–H first-overtone NIR spectrum.

SP-PLP-ESR measurements. ESR experiments were performed on a Bruker Elexsys[®] E 500 series *cw*-ESR spectrometer. The mixture of monomer, photoinitiator, and RAFT agent in toluene solution was filled into a quartz tube of 5 mm outer and 4 mm inner diameter and was irradiated inside a grid cavity using a Lambda Physik COMPex 102 excimer laser on the XeF line at 351 nm with a laser output energy of about 50 mJ per pulse. The ESR spectrometer and the excimer laser were triggered by a Scientific Instruments 9314 pulse generator. Radical concentration vs. time profiles were deduced from ESR intensities measured with μ s time resolution at the magnetic field that is associated with the peak maximum of the ESR spectrum of the radical species under investigation. Radical concentrations were obtained by a two-fold calibration procedure: First, the double integral of the ESR spectrum was calibrated against a TEMPO solution in BA/toluene mixtures at conditions close to the ones of the actual polymerizations. Secondly, the peak signal intensity at fixed magnetic field was calibrated against the double integral of the full ESR spectrum (15).

UV/VIS spectroscopy. UV/VIS spectra were recorded from 220 to 440 nm on a Bruins Omega 10 double-beam spectrometer.

Simulations. Simulations were carried out using PREDICI[®], version 6.4.1.

SEC analyses. Molecular weight distributions were determined via size-exclusion chromatography (SEC), using a Waters 712 WISP autosampler, a Waters 515 HPLC pump, PSS-SDV columns with nominal pore sizes of 10⁵, 10³ and 10² Å, a Waters 2410 refractive index detector, and THF at 35 °C as the eluent. Molecular weight distributions were evaluated according to the principle of universal calibration using reported Mark-Houwink parameters (18).

RAFT polymerization under PLP conditions

So far, kinetic investigations into RAFT polymerization systems were limited to reaction conditions with continuous initiation. In such experiments, individual RAFT-specific rate coefficients can be obtained under the assumption of a steady state and by combining several independent experiments (19). Alternatively, kinetic coefficients of the RAFT process may be estimated by quantum-chemical calculations (20), which at present are restricted to small molecules, or by modeling the overall rate of polymerization (20,21), whereby kinetic information is deduced from the decrease in polymerization rate upon increasing RAFT agent concentration. The rate coefficients resulting from the latter method are highly dependent on the model used for describing rate retardation. RAFT experiments under instationary conditions after laser single pulse excitation should be suitable for deducing RAFT addition and fragmentation rate coefficients under less stringent assumptions. Moreover, chain-length dependent k_t may be obtained from SP-PLP experiments carried out on RAFT polymerization systems.

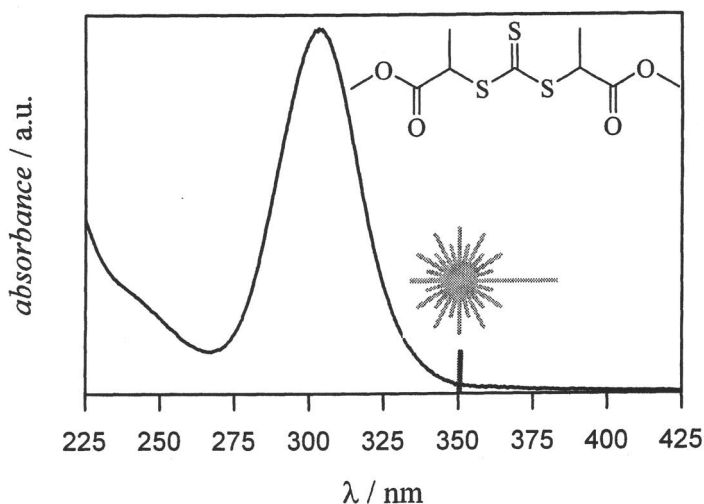


Figure 1. Chemical structure and UV spectrum of BMPT ($c_{\text{BMPT}} = 1 \cdot 10^{-4} \text{ mol} \cdot \text{L}^{-1}$ in heptane). The laser wavelength of 351 nm is indicated by the grey symbol.

To employ pulsed-laser initiation without affecting any features of the RAFT polymerization, the RAFT agent has to be stable under intense laser irradiation. Common RAFT agents are colored and exhibit significant UV/VIS absorbance, which may lead to decomposition. Photoinitiation of RAFT polymerizations should hence be carried out at relatively long wavelengths, e.g., at the 351 nm XeF excimer laser line, using RAFT agents with poor absorption cross

section in this region. Figure 1 depicts the UV spectrum of BMPT, which has a pale yellow color as is typical for RAFT agents of the trithiocarbonate type. The absorbance at 351 nm is relatively low. Thus, BMPT and the associated macroRAFT species, which are assumed to have similarly low absorptivity, should only be weakly affected by laser pulsing at 351 nm.

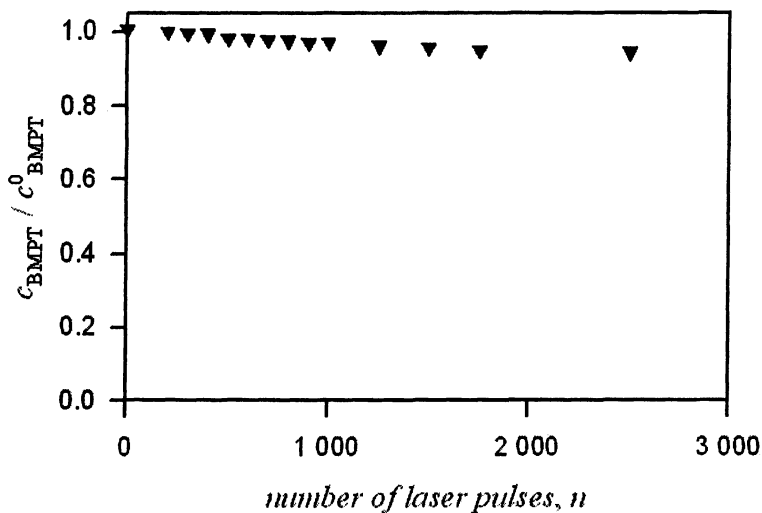


Figure 2. Relative BMPT concentration, determined by half-band integration of the UV spectrum (see Figure 1) between 303 and 400 nm, vs. the number of applied laser pulses (~ 2.5 mJ/pulse, 351 nm). The dark time between two successive laser pulses was 10 s.

Figure 2 illustrates the change in BMPT concentration in *n*-heptane solution under pulsed-laser irradiation at 351 nm. Applying 2500 laser pulses results in a decay in BMPT concentration by about 6%. Since 100 laser pulses are sufficient for 50% of monomer conversion in BA bulk polymerization at 60 °C and 1000 bar, the amount of BMPT (and of derived macroRAFT species) may be assumed to stay approximately constant during XeF excimer laser-induced BMPT-mediated BA polymerization up to moderately high conversion.

It can be seen from Figure 3 and Figure 4 that BMPT is capable of effectively controlling polymer molecular weight in the laser-induced BA polymerization. Figure 3 depicts the evolution of the molecular weight distribution (MWD) of poly(BA) upon increasing the degree of monomer conversion in BMPT-mediated BA bulk homopolymerization at 60 °C and 1000 bar. With rising monomer conversion, which change is easily effected by applying laser pulses at will, the MWD curves are shifted toward higher molecular weights.

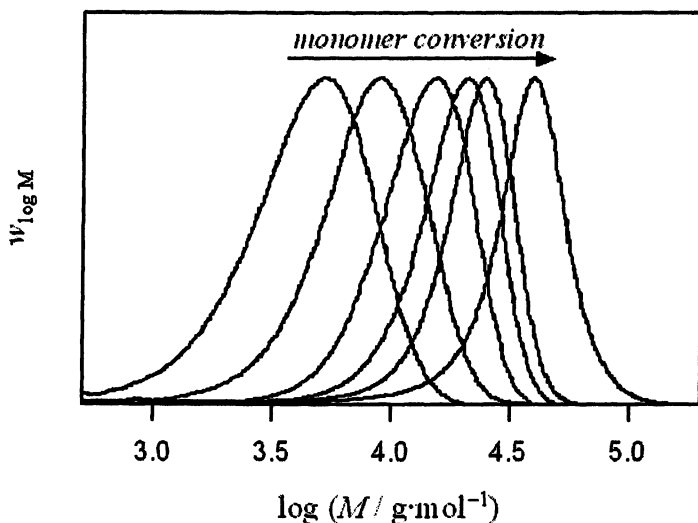


Figure 3. Molecular weight distributions from SEC of poly(BA) samples produced by pulsed-laser initiated RAFT polymerizations at 60 °C and 1000 bar with BMPT ($2.1 \cdot 10^{-2} \text{ mol} \cdot \text{L}^{-1}$) acting as the RAFT agent.

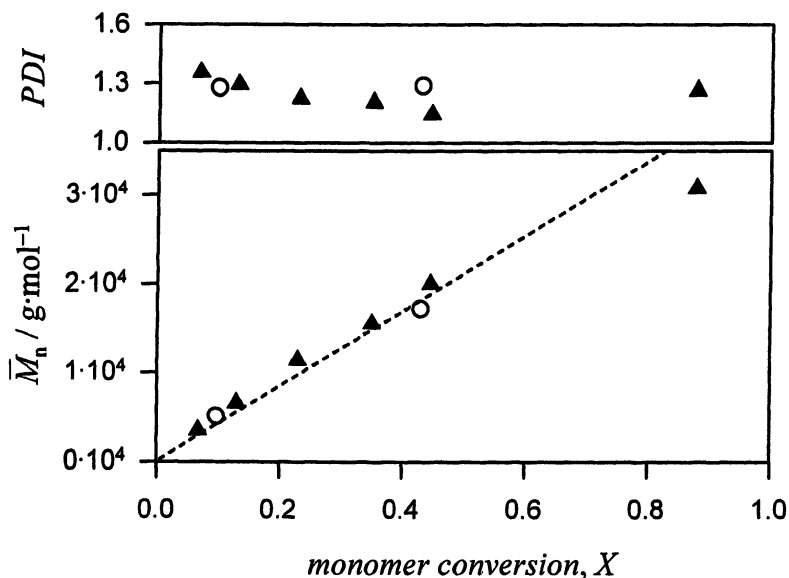
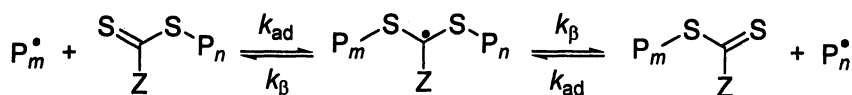


Figure 4. Number average molecular weight, \bar{M}_n , and polydispersity index, PDI, plotted vs. monomer conversion in bulk polymerization of BA, mediated by $2.1 \cdot 10^{-2} \text{ mol} \cdot \text{L}^{-1}$ BMPT at 60°C and 1000 bar (triangles) or 5 bar (circles). The dashed line represents the theoretical values of \bar{M}_n .

Figure 4 shows the number average molecular weights, \bar{M}_n , and the polydispersity indices, *PDI*, of polymer produced in BA RAFT polymerizations. The triangles refer to 1000 bar and 60 °C, and the circles to 5 bar and 60 °C. The experimental \bar{M}_n data are in excellent agreement with the theoretical values (represented by the dashed line). Only for the sample taken at the highest experimental monomer conversion of around 90 %, the measured \bar{M}_n is slightly below the theoretical value. The associated *PDI* value, which is below 1.5, demonstrates that polymerization is controlled even at such a high degree of monomer conversion.

Determination of RAFT addition and fragmentation rate coefficients via SP-PLP-ESR

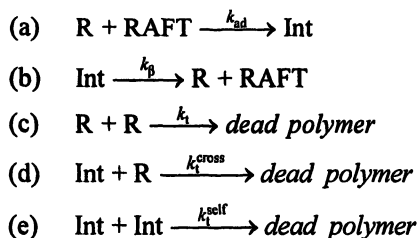
Precisely knowing the addition and fragmentation rate coefficients, k_{ad} and k_{β} , respectively, of the RAFT equilibrium (see Scheme 1) is mandatory for establishing structure-rate correlations for the stabilizing Z- and the leaving R-groups and thus for the design of RAFT agents. The degenerative nature of the overall transfer reaction, which is associated with the concentrations of propagating radicals and RAFT species staying constant, poses a problem for directly accessing k_{ad} and k_{β} . Depending on the specific assumptions used for the analysis of experiments performed under continuous thermal initiation, the numbers reported for k_{β} differ by several orders of magnitude (22,23). This unfavorable situation indicates the urgent need for new experimental methods.



Scheme 1. RAFT main equilibrium

We designed a method for the simultaneous determination of k_{ad} and k_{β} from a single experiment (24). After laser-induced production of photoinitiator-derived radicals during a RAFT polymerization, the formation and decay of the intermediate RAFT radical (central component in Scheme 1) is monitored via μs time-resolved ESR spectroscopy (see Figure 5). The build-up of intermediate radical concentration, c_{int} , reflects the addition of radicals to RAFT species. The actual (narrowly distributed) size of the RAFT species depends on initial RAFT agent concentration and on overall monomer conversion. The decay kinetics of the intermediate species is determined by both the fragmentation rate of the intermediate RAFT radical and by irreversible termination reactions of any radical species. The individual rate coefficients indicated in Scheme 1 may be determined by fitting intermediate radical concentration vs. time profiles to a rather

simple kinetic scheme (Scheme 2), which exclusively considers propagating radicals, R, RAFT species, RAFT, and intermediate RAFT radicals, Int:



Scheme 2. Reaction steps and associated rate coefficients contributing to time-dependent intermediate radical concentration in SP-PLP-ESR-RAFT experiments.

The reaction steps (a), (b), and (c) are sufficient for modeling the observed change in c_{Int} . More detailed estimates can be made by using the extended scheme which includes cross-termination (d) and/or self-termination (e) of Int. The chain length of the participating species needs not to be considered in modeling time-resolved c_{Int} , as radical size is not or not significantly changing during the course of one single-pulse experiment (13). Figure 5 demonstrates that the simple kinetic model given in Scheme 2 (without steps (d) and (e)) provides an adequate fit of c_{Int} vs. time plots measured by ESR spectroscopy during BMPT-mediated BA polymerizations (24). Including cross-termination yields fits of similar quality as the ones shown in Figure 5. The same observation is made in case of including step (e), i.e., self-termination, which was not considered in the present study, as this reaction would lead to the formation of six-arm stars which is unlikely to occur because of steric reasons.

The k_{ad} and k_{p} values deduced from modeling BMPT-mediated BA polymerization at -30°C are listed in Table 1. This relatively low temperature has been chosen for validation of the new method, as mid-chain radicals generated by transfer reactions are occurring in the BA polymerizations at elevated temperatures. The presence of such radicals adds complexity to the data evaluation.

Table 1. Addition and fragmentation rate coefficients in BMPT-mediated BA polymerization at -30°C ;
 $c_{\text{RAFT}}^0 = 4.1 \cdot 10^{-3} \text{ mol} \cdot \text{L}^{-1}$, $k_{\text{t}} = 2.2 \cdot 10^7 \text{ L} \cdot \text{mol}^{-1} \cdot \text{s}^{-1}$, and $k_{\text{t,cross}} = k_{\text{t}}/2$

| <i>kinetic model includes:</i> | $k_{\text{ad}} / \text{L} \cdot \text{mol}^{-1} \cdot \text{s}^{-1}$ | $k_{\text{p}} / \text{s}^{-1}$ |
|--------------------------------|--|--------------------------------|
| no termination of intermediate | $2.0 \cdot 10^5$ | $2.1 \cdot 10^2$ |
| cross termination | $2.0 \cdot 10^5$ | $0.8 \cdot 10^2$ |

Whether or not reactions between an intermediate and a propagating radical (cross-termination) take place (see Table 1), has no effect on k_{ad} , which agrees well with previously reported values for this system (25), and influences k_{β} by less than one order of magnitude. A possibly reversible termination of the intermediates yields k_{β} values that lie in between those obtained by these limiting models. This is a largely reduced uncertainty in k_{β} compared to the difference by several orders of magnitude between k_{β} values of cumyl dithiobenzoate-mediated polymerizations, which have been derived by modeling rate of polymerization data on the basis of different model assumptions (20).

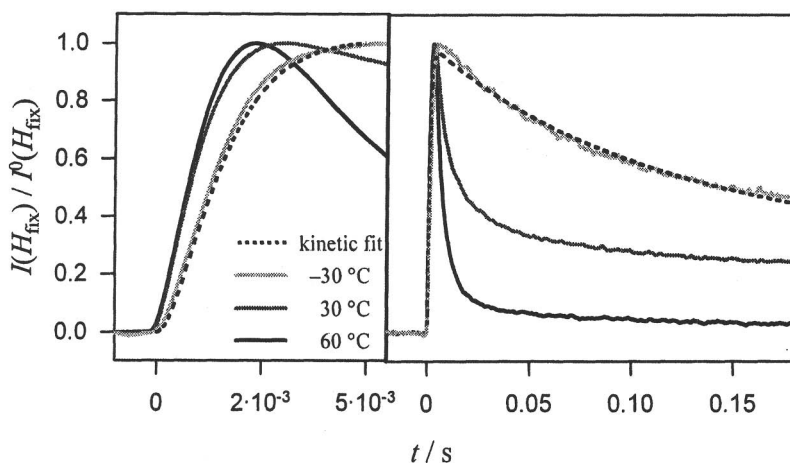


Figure 5. Time evolution, after applying a single laser pulse at $t = 0$, of the normalized ESR signal at the field position that corresponds to the peak maximum of the full spectrum (see Figure 6) in BMPT-mediated BA polymerizations ($c_{BMPT} = 4.1 \cdot 10^{-3} \text{ mol} \cdot \text{L}^{-1}$, $c_{BA} = 2.0 \text{ mol} \cdot \text{L}^{-1}$, in toluene). (Reproduced from ref. 24. Copyright 2006 Wiley-Interscience)

As a single-pulse technique, the novel method may be applied at any time and thus at any monomer conversion during RAFT polymerization. Thus, at least in principle, chain-length dependent rate parameters may be deduced and the situations of pre- and main RAFT equilibrium may be examined separately. Figure 6a depicts the full ESR spectrum of BMPT-derived intermediate radicals, which is obtained under quasi-stationary reaction conditions at a laser repetition rate of 20 Hz. Closer inspection of the spectrum indicates that there is an overlap of two singlet lines of different band width. The contributions of the two species change during polymerization. The SP-PLP-ESR-RAFT experiments in Figure 5 have been carried out at conditions corresponding to the ones depicted in Figure 6a. The intermediate radical in BMPT-mediated RAFT polymerization has no proton in the immediate vicinity of the radical site. Thus, no hyperfine splitting of the ESR spec-

trum is expected. The observation of two overlapping singlet components may be due to the fact that the intermediate RAFT radical occurs under both pre- and main equilibrium conditions. This hypothesis is in line with the observation of the sharper peak becoming weaker upon continuing laser irradiation.

As illustrated in Figure 6b, a third radical species evolves after application of about 700 laser pulses. This component is assigned to the four-line spectrum of the secondary propagating radical in BA polymerization. The variation in the ratio of intermediate radical to propagating radical concentration with progressive polymerization corresponds to a change in the equilibrium constant, K , by about one order of magnitude. This observation suggests that k_{ad} and k_{β} may be different for the pre- and main equilibrium regions and, additionally, may be chain-length dependent.

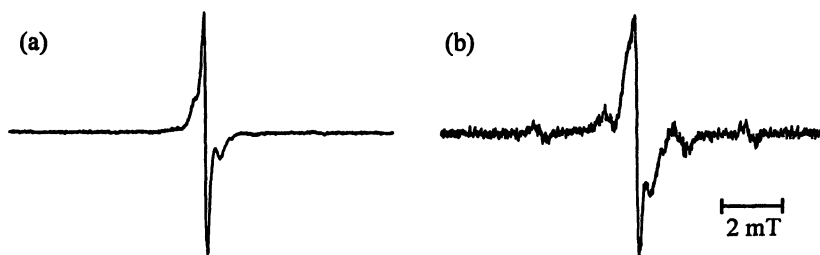


Figure 6. ESR spectra recorded during a quasi-stationary BMPT-mediated ($c_{BMPT} = 4 \cdot 10^{-3} \text{ mol} \cdot \text{L}^{-1}$) BA polymerization ($c_{BA} = 2 \text{ mol} \cdot \text{L}^{-1}$) in solution of toluene at $-30 \text{ }^{\circ}\text{C}$, using a laser pulse repetition rate of 20 Hz, after applying approximately (a) 300, and (b) 700 laser pulses.

Estimating k_{β} from fits of the measured c_{int} vs. time curves to the model presented above, is restricted to systems where self-termination of intermediate radicals is not significant. In case that such self-termination is included into the kinetic modeling, the resulting k_{β} values decrease with increasing extent of self-termination. Assuming the intermediate radicals to be stable, i.e., $k_{\beta} = 0$, the experimentally observed decay of the intermediate radical concentration can exclusively be assigned to self-termination. The underlying situation is however unreasonable in that no propagating radicals occur in such a system. In order to resolve the degree of self-termination, it appears desirable to additionally determine the concentration of propagating radicals, which may be achieved by measuring the change in intensity of the ESR components at either low or high magnetic field (see Figure 6b), or via SP-PLP experiments, in which the propagating radical concentration is also measured with high time resolution. Knowing the time evolution of both intermediate and propagating radical concentration enables a comprehensive kinetic analysis of RAFT kinetics. From the measured time evolution of propagating radical concentration, the chain-length dependence of k_t may unambiguously be determined, once the RAFT rate coefficients, k_{ad} and k_{β} , are known.

Chain-length dependent termination rate coefficients deduced from SP-PLP-NIR-RAFT experiments

In SP-PLP-NIR experiments (12), monomer conversion induced by a laser single pulse is detected by μs time-resolved NIR spectroscopy, e.g., in the first-overtone region of C–H modes at the C–C double bond. In conventional SP-PLP-NIR, the kinetic analysis for the termination rate coefficient, k_t , from measured conversion vs. time traces is difficult, because of the steadily increasing chain length with time, t , after applying the laser pulse. As changes of chain length affect k_t , the analysis of monomer conversion vs. time traces has to be carried out by implementing models for the chain-length dependence of k_t . As an alternative, it appears highly attractive to perform SP-PLP-NIR experiments on systems where the molecular weight is controlled by a RAFT agent (13,25). To elucidate whether such an SP-PLP-NIR-RAFT experiment is feasible, PREDICI simulations have been carried out for butyl acrylate polymerization. In these simulations, the RAFT main equilibrium, the cross-termination of the intermediate radical, and the chain-length dependence of k_t (according to $k_t(i,j) = k_t^0 \cdot (i \cdot j)^{-\alpha/2}$, where i and j are the chain lengths of two terminating radicals and k_t^0 is the termination rate of radicals of chain length unity), were considered. The rate coefficients of butyl acrylate polymerization were taken from ref. (25).

The transformation of the laser pulse-induced primary radicals species into radicals of the size that is characteristic for the polymerizing RAFT system, is visualized in Figure 7. The simulated (SEC-weighted) distribution of propagating radicals is given for an equilibrium constant $K = k_{\text{ad}}/k_{\text{p}} = 1000 \text{ L} \cdot \text{mol}^{-1}$ for the early time interval of up to 1 ms after applying the laser pulse. Figure 7a refers to the situation directly after the generation of the primary radicals. These radicals are propagating as well as rapidly transforming into radicals of the par-

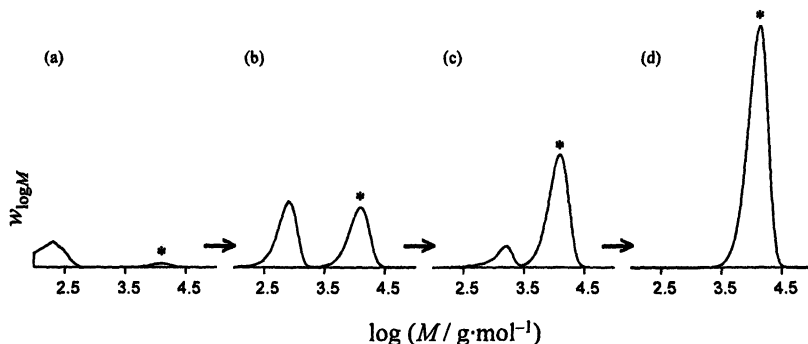


Figure 7. Simulated transformation of laser-induced small radicals into macroradicals of uniform size (indicated by *), which is controlled by the RAFT kinetics. The time interval covered from (a) to (d) refers to the initial period of up to 1 ms after firing the laser pulse. (Reproduced from ref. 25. Copyright 2005 American Chemical Society)

ticular size (indicated by the asterisk), which is characteristic of the RAFT system and is given by the initial RAFT agent concentration and by the actual degree of monomer conversion. Figure 7b and c show transitional situations. In Figure 7d, which corresponds to about 1 ms delay after firing the laser, the radicals have nearly quantitatively been transformed into radicals exhibiting the RAFT-specific narrow chain-length distribution.

The simulated variation in polydispersity of both propagating and RAFT intermediate radicals with time, that is, with increasing number of evenly separated laser pulses, is shown in Figure 8. The chosen dark time of 50 s between successive laser pulses allows for an almost complete decay of radical concentration after each pulse. The narrow time span, during which primary radicals are produced and transformed into radicals of the characteristic size, is reflected by the intense sharp peaks occurring upon application of each individual laser pulse. The negative amplitude appearing up to the third pulse is an artifact associated with PREDICI simulations for small-size species. The distribution in size of propagating radicals and of the polyRAFT species becomes narrower toward larger numbers of applied laser pulses and thus toward increasing monomer conversion. This simulation result is in full agreement with the experimental observations made on RAFT polymerizations under PLP-conditions (see Figure 4).

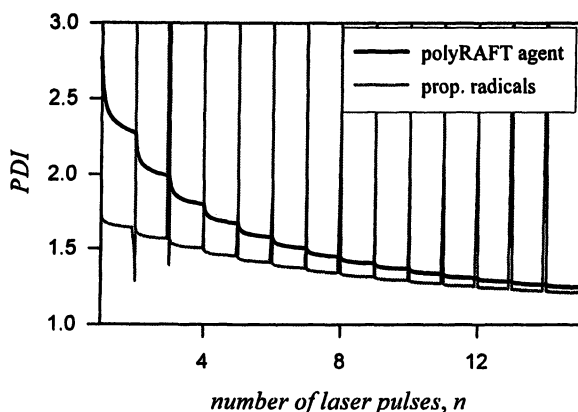


Figure 8. Simulated time evolution of polydispersity index of polyRAFT agent and of the propagating radicals in single-pulse initiated RAFT polymerization. The time is scaled to the number of initiating laser pulses with the dark time between two successive laser pulses being 50 s.

Influence of the stability of RAFT intermediate radicals

As the RAFT equilibrium constant K may not exactly be known for a system that is subjected to SP-PLP-NIR-RAFT studies, the effect of variations in K , and

thus in the stability of the RAFT intermediate radical, on the data analysis has been estimated via simulations. The influences of cross-termination between an intermediate radical and a propagating radical as well as of decreasing fragmentation rates of the intermediate radicals were assessed. k_t data was obtained from simulations of SP-PLP-NIR-RAFT experiments described above, followed by fitting the resulting monomer conversion vs. time traces to the integrated rate law, Eq.(1), for an ideal SP-PLP experiment, in which k_t is assumed to be chain-length independent.

$$\frac{c_M(t)}{c_M^0} = (2 \cdot k_t \cdot c_R^0 \cdot t + 1)^{-k_p/2k_t} \quad (1)$$

Although a chain-length dependence of k_t was included into the simulations, the fitting to Eq.(1) worked almost perfectly, since the radicals of uniform chain length (see Figure 7d) are trapped in the RAFT equilibrium and do not exhibit significant chain growth during one SP-PLP experiment. The chain-length dependence of k_t was implemented by $k_t^0 = 10^8 \text{ L}\cdot\text{mol}^{-1}\cdot\text{s}^{-1}$ and $\alpha = 0.16$ as input parameters. Plotting k_t data (obtained from the simulated SP-PLP-NIR-RAFT experiments) vs. chain length (deduced from monomer conversion), allowed for the evaluation of k_t^0 and α values, according to the power-law expression $k_t(i) = k_t^0 \cdot i^{-\alpha}$ for termination of two radicals of (almost) identical size i .

The impact on simulated k_t^0 and α values of variations in k_p and of cross-termination occurring to different extents is illustrated in Figure 9. In the absence of cross-termination (left graph of Figure 9), the power-law exponent $\alpha = 0.16$, obtained by fitting the calculated signals to Eq.(1), is not significantly affected by changing K by several orders of magnitude. In contrast, the absolute level of k_t , characterized by k_t^0 , is decreasing with increasing stability of the intermediate, and drops by one order of magnitude when going from $K = 1$ to $1000 \text{ L}\cdot\text{mol}^{-1}$. Simulations using K values above $1000 \text{ L}\cdot\text{mol}^{-1}$ did not yield typical SP-PLP traces and could hence not be evaluated. This finding suggests that when monomer conversion vs. time traces after single laser pulse initiation are found exhibiting typical SP-PLP characteristics, the equilibrium constant does not exceed $1000 \text{ L}\cdot\text{mol}^{-1}$.

For studying the impact of cross-termination, a fixed, relatively high value of $K = 1000 \text{ L}\cdot\text{mol}^{-1}$ was chosen, as the associated higher concentration of intermediate radicals make the cross-termination reaction more likely. It should be stressed that the impact of cross-termination is much weaker in case K is lower. As can be seen from the right graph of Figure 9, an increasing level of cross termination slightly lowers the α value obtained by SP-PLP-NIR-RAFT in comparison to the input value. A variation in $k_{t,\text{cross}}/k_t$ from 0.001 to 1 reduces α only by about 25 %. An equilibrium constant of $K = 1000 \text{ L}\cdot\text{mol}^{-1}$ together with $k_{t,\text{cross}}/k_t$ being close to unity, refers to a very strongly retarded system, as has been observed in cumyl dithiobenzoate-mediated methyl acrylate polymerization (21). Consequently, in weakly or non-retarding systems, no problems for

the determination of α are foreseen. With respect to using the SP-PLP-NIR-RAFT technique for k_t determinations on systems where both the equilibrium constant K and the extent of cross-termination are not precisely known, it can be concluded that absolute k_t may be uncertain by about one order of magnitude, whereas reliable estimate of the power-law exponent α appear to be within reach.

Determination of chain-length dependent termination rate coefficients

The preceding simulations indicate that the SP-PLP-NIR-RAFT technique is suitable for determining chain-length dependent k_t for situations where K is below $1000 \text{ L}\cdot\text{mol}^{-1}$. As has been shown above, BMPT is not only capable of effectively controlling the molecular weight in butyl acrylate polymerization, but also exhibits RAFT rate coefficients which fulfill the requirements for adequate SP-PLP-NIR-RAFT experiments even at $-30 \text{ }^\circ\text{C}$. The situation should further improve toward increasing temperature (26), making BMPT a suitable RAFT agent for SP-PLP-NIR-RAFT experiments on butyl acrylate. We performed such single pulse experiments at 1000 bar and $60 \text{ }^\circ\text{C}$ for three BMPT concentrations and carried out a few experiments at 5 bar and $60 \text{ }^\circ\text{C}$ for the medium RAFT agent concentration. The experiments were run up to reaction times, thus, monomer conversions, which allowed for mapping out the chain-length dependence of k_t for the regime from $i = 1$ to about 250. The correlation between monomer conversion and chain length in this RAFT system has already been presented in Figure 4. To account for the occurrence of mid-chain radicals (27), which have a strong impact on effective k_p in BA polymerization above ambient temperature, a virtual conversion dependence of k_p has been considered. The procedure, which rests on an empirical reaction order in monomer concentration for BA polymerization rate (28), is described elsewhere (25). Although this virtual change in k_p has not a very pronounced impact on the k_t values, it needs to be implemented in order to achieve good overlap of k_t data deduced from experiments at different RAFT agent concentrations. It should be noted that k_t values for a specific chain length are accessible from SP-PLP-NIR-RAFT measurements at different degrees of monomer conversion and suitably chosen RAFT agent concentration.

Shown in Figure 10 is the variation of k_t with chain length as obtained via SP-PLP-NIR-RAFT experiments on BMPT-mediated BA bulk polymerization. The k_t values for 1000 bar were extrapolated to 5 bar via the reported activation volume, $\Delta V^\ddagger(k_t) = 16 \text{ cm}^3\cdot\text{mol}^{-1}$ (29). k_t is decreasing upon increasing i , which effect is particularly pronounced at low chain lengths up to about $i = 20$. A stronger variation of k_t with chain length is consistent with the composite model introduced by Smith et al. (30), which assumes a higher value of α at lower

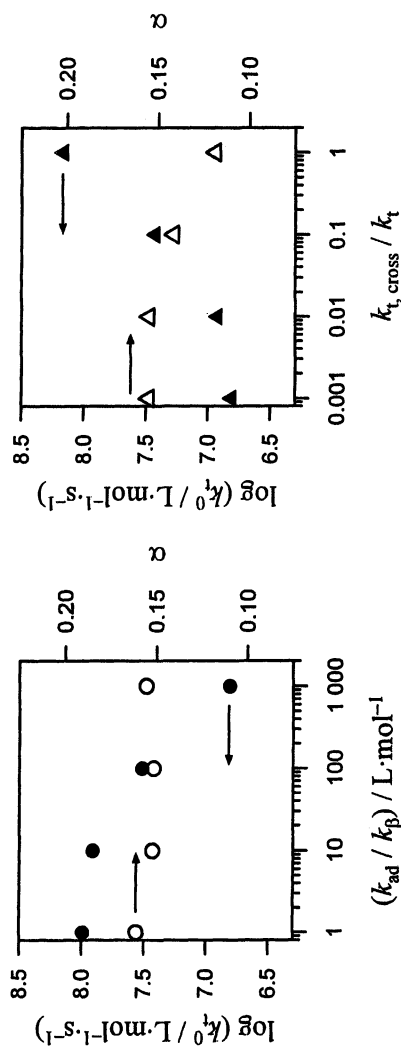


Figure 9. Simulated k_t^0 (full symbols) and α (open symbols) as function of the RAFT equilibrium constant, $K = k_{ad} / k_{\beta}$, assuming absence of cross-termination (left graph), and as function of the ratio of rate coefficients of cross-termination to termination of propagating radicals, $k_{t, \text{cross}} / k_t$, for $K = 1000 \text{ L}\cdot\text{mol}^{-1}$ (right graph). The data is obtained from simulated SP-PLP-NIR traces. (left graph reproduced from reference 25. Copyright 2005 American Chemical Society)

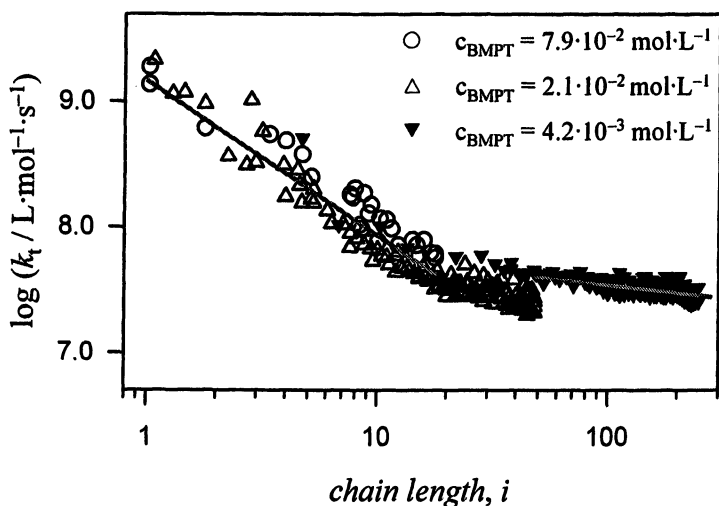


Figure 10. Termination rate coefficients, k_t , obtained by SP-PLP-NIR-RAFT at 60 °C and pressures of 5 and 1000 bar using three BMPT concentrations. 1000 bar data was extrapolated to 5 bar via literature values of the activation volume for k_t . The lines represent best fits according to the power-law model. (Reproduced from ref. 25. Copyright 2005 American Chemical Society)

chain length and vice versa. Adopting such composite model behavior results in an α_1 value for the short chains that slightly exceeds unity, and an $\alpha_2 = 0.22$ value for chain lengths above $i = 50$. These numbers are in close agreement with previous experimental data on the termination rate in BA polymerization by de Kock (31) and with recently reported data from stationary RAFT polymerization (25). The k_t^0 value obtained from extrapolation of the short chain-length regime, which slightly exceeds $10^9 \text{ L}\cdot\text{mol}^{-1}\cdot\text{s}^{-1}$, is in excellent agreement with values found for the diffusion-controlled termination step of two small radicals (32). The value of α_2 can be understood on the basis of segmental diffusion within coiled macroradicals and is close to 0.16, the theoretical values for $k_t(i)$ in dilute athermal solutions (33). The strong dependence in the low chain length regime, represented by α_1 being close to or even exceeding unity, may be assigned to the shielding of the radical functionality during collisions of small non-entangled radicals (13). This hypothesis is supported by findings from stationary RAFT polymerization methods (25,34,35), which indicate an increasing α_1 value with increasing size of the acrylate ester side chain. The enhanced flexibility of longer side groups may allow for a more effective shielding of the radical site. This explanation is also in agreement with the observation of α_1 values being significantly lower for methacrylate monomers, where α_1 is close to 0.5 (14,36).

Conclusions and Outlook

Pulsed-laser experiments on RAFT-mediated polymerizations, carried out in conjunction with μs time-resolved ESR or NIR spectroscopy, provide access to RAFT-specific rate coefficients (k_{ad} , k_{p}) and enable accurate determinations of the chain-length dependence of the conventional termination rate coefficient, k_t , respectively. It appears to be a matter of priority to extend the novel SP-PLP-ESR-RAFT and SP-PLP-NIR-RAFT methods to investigations into other types of monomers, in particular to methacrylates, where mid-chain radicals will not disturb kinetic analyses over a wider range of temperature. Moreover, SP-PLP-ESR-RAFT should be carried out within extended monomer conversion ranges in order to determine RAFT-specific rate coefficients for both the pre- and the main equilibrium periods separately and to check for a chain-length dependence of these coefficients. To overcome difficulties in estimating average M_n values from monomer conversion data, these studies should be accompanied by experiments in which macroRAFT agents are used as mediating compounds. The simultaneous determination of the decay of both RAFT intermediate and propagating radical concentration is of particular interest. The resulting data will allow for detailed analysis of contributions of cross- and self-termination reactions of the RAFT intermediate radical. Moreover, measuring the decay of the propagating radical concentration with time in pulsed-laser initiated RAFT polymerization offers the possibility of determining chain-length dependent k_t values without knowing k_p .

Acknowledgments. Support by the *Deutsche Forschungsgemeinschaft* within the Graduate School GK 782 program and by the *Fonds der Chemischen Industrie* is gratefully acknowledged.

References

1. Moad, G.; Rizzardo, E.; Thang, S. H. *Aust. J. Chem.* **2005**, *58*, 379.
2. Barner-Kowollik, C.; Davis, T. P.; Heuts, J. P. A.; Stenzel, M. H.; Vana, P.; Whittaker, M. J. *Polym. Sci., Part A: Polym. Chem.* **2003**, *41*, 365.
3. Perrier, S.; Takolpuckdee, P. *J. Polym. Sci., Part A: Polym. Chem.* **2005**, *43*, 5347.
4. Matyjaszewski, K.; Xia, J. *Chem. Rev.* **2001**, *101*, 2921.
5. Hawker, C. J.; Bosman, A. W.; Harth, E. *Chem. Rev.* **2001**, *101*, 3661.
6. Barner, L.; Quinn, J. F.; Barner-Kowollik, C.; Vana, P.; Davis, T. P. *Eur. Polym. J.* **2003**, *39*, 449.
7. Hua, D. B.; Bai, R. K.; Lu, W. Q.; Pan, C. Y. *J. Polym. Sci., Part A: Polym. Chem.* **2004**, *42*, 5670.
8. Chen, G. J.; Zhu, X. L.; Zhu, J.; Cheng, Z. P. *Macromol. Rapid Commun.* **2004**, *25*, 818.
9. Quinn, J. F.; Barner, L.; Barner-Kowollik, C.; Rizzardo, E.; Davis, T. P. *Macromolecules* **2002**, *35*, 7620.

10. Lu, L. C.; Yang, N. F.; Cai, Y. L. *Chem. Commun.* **2005**, *42*, 5287.
11. Olaj, O. F.; Bitai, I.; Hinkelmann, F. *Makromol. Chem.* **1987**, *188*, 1689.
12. Buback, M.; Hippler, H.; Schweer, J.; Vögele, H. P. *Makromol. Chem., Rapid Commun.* **1986**, *7*, 261.
13. Buback, M.; Junkers, T.; Vana, P. *Macromol. Rapid Commun.* **2005**, *26*, 796.
14. Buback, M.; Egorov, M.; Junkers, T.; Panchenko, E. *Macromol. Rapid Commun.* **2004**, *25*, 1004.
15. Buback, M.; Egorov, M.; Junkers, T.; Panchenko, E. *Macromol. Chem. Phys.* **2005**, *206*, 333.
16. Arita, T.; Buback, M.; Janssen, O.; Vana, P. *Macromol. Rapid Commun.* **2004**, *25*, 1376.
17. Buback, M.; Hinton, C., in *High-pressure Techniques in Chemistry and Physics - A practical approach*, Holzapfel, B. W.; Isaacs, N.S, eds., Oxford University Press: Oxford, 1997.
18. Penzel, E.; Goetz, N. *Angew. Makromol. Chem.* **1990**, *178*, 191.
19. Kwak, Y.; Goto, A.; Tsujii, Y.; Murata, Y.; Komatsu, K.; Fukuda, T. *Macromolecules* **2002**, *35*, 3026.
20. Feldermann, A.; Coote, M. L.; Stenzel, M. H.; Davis, T. P.; Barner-Kowollik, C. *J. Am. Chem. Soc.* **2004**, *126*, 15915.
21. Drache, M.; Schmidt-Naake, G.; Buback, M.; Vana, P. *Polymer* **2005**, *46*, 8483.
22. Wang, A. R.; Zhu, S.; Kwak, Y.; Goto, A.; Fukuda, T.; Monteiro, M. S. *J. Polym. Sci., Part A: Polym. Chem.* **2003**, *41*, 2833.
23. Barner-Kowollik, C.; Coote, M. L.; Davis, T. P.; Radom, L.; Vana, P. *J. Polym. Sci., Part A: Polym. Chem.* **2003**, *41*, 2828.
24. Buback, M.; Hesse, P.; Junkers, T.; Vana, P. *Macromol. Rapid Commun.* **2006**, *27*, 182.
25. Junkers, T.; Theis, A.; Buback, M.; Davis, T. P.; Stenzel, M.; Vana, P.; Barner-Kowollik, C. *Macromolecules* **2005**, *38*, 9497.
26. Arita, T.; Buback, M.; Vana, P. *Macromolecules* **2005**, *38*, 7935.
27. Plessis, C.; Arzamendi, G.; Alberdi, J. M.; van Herk, A. M.; Leiza, J. R.; Asua, J. M. *Macromol. Rapid Commun.* **2003**, *24*, 173; Willemse, R. X. E.; van Herk, A. M.; Panchenko, E.; Junkers, T.; Buback, M. *Macromolecules* **2005**, *38*, 5098.
28. Nikitin, A. N.; Hutchinson, R. A. *Macromolecules* **2005**, *38*, 1581.
29. Beuermann, S.; Buback, M. *Prog. Polym. Sci.* **2002**, *27*, 191.
30. Smith, G. B.; Russell, G. T.; Heuts, J. P. A. *Macromol. Theory Simul.* **2003**, *12*, 299.
31. de Kock, J. B. L.; van Herk, A. M.; German, A. L. *J. Macromol. Sci., Polym. Rev.* **2001**, *C41*, 199.
32. Fischer, H.; Paul, H. *Acc. Chem. Res.* **1987**, *20*, 200.
33. Friedman, B.; O'Shaughnessy, B. *Macromolecules* **1993**, *26*, 5726.
34. Theis, A.; Feldermann, A.; Charton, N.; Stenzel, M. H.; Davis, T. P.; Barner-Kowollik, C. *Macromolecules*, **2005**, *38*, 2595.
35. Theis, A.; Feldermann, A.; Charton, N.; Davis, T. P.; Stenzel, M. H.; Barner-Kowollik, C. *Polymer* **2005**, *46*, 6797.
36. Johnston-Hall, G.; Theis, A.; Monteiro, M. J.; Davis, T.P.; Stenzel, M. H.; Barner-Kowollik, C. *Macromol. Chem. Phys.* **2005**, *206*, 2047.

Chapter 32

Tailor-Made Copolymers via Reversible Addition Fragmentation Chain Transfer the Fast Way

Richard Hoogenboom, Martin W. M. Fijten, Renzo M. Paulus,
and Ulrich S. Schubert*

Laboratory of Macromolecular Chemistry and Nanoscience, Eindhoven
University of Technology and Dutch Polymer Institute (DPI), P.O. Box 513,
5600 MB Eindhoven, The Netherlands

*Corresponding author: email: u.s.schubert@tue.nl; Internet:
www.schubert-group.com

The utilization of automated parallel synthesis robots for the preparation of libraries of poly(methyl methacrylate-*N,N'*-dimethylaminoethyl methacrylate) [pMMA-DMAEMA] statistical and block copolymers *via* the RAFT polymerization process is described in this chapter. The synthesized pMMA-*stat*-DMAEMA and pMMA-*b*-DMAEMA copolymers were characterized utilizing both gel permeation chromatography and ¹H-NMR spectroscopy. Both the resulting polymer compositions and the control over the RAFT copolymerizations in the parallel synthesis robots are discussed on the basis of these characterization data.

Introduction

During the last decades, many investigations have been performed to develop and improve living/controlled polymerization techniques based on e.g., anionic,¹ cationic,^{2,3} metathesis⁴ and radical polymerization mechanisms.⁵⁻⁸ The main advantage of such living/controlled polymerization techniques is that all polymer chains are initiated at the same time and that all living/controlled polymer chains grow with the same rate. In the absence of termination and irreversible chain-transfer reactions, the resulting polymers will all have a similar length and thus a narrow molecular weight distribution will be obtained. Moreover, the living/controlled character allows the formation of well-defined random, gradient and block copolymers with a large variety of different architectures like graft, comb or star-shaped structures.

A versatile class of polymerization techniques are the controlled radical polymerizations,⁵ which are less sensitive to impurities and functional groups than ionic and metathesis polymerization processes. In fact, the controlled radical polymerizations are only sensitive towards oxygen and can be performed in aqueous solutions. The most successful controlled radical polymerization techniques are atom transfer radical polymerizations (ATRP),⁵ nitroxide mediated polymerizations (NMP)⁷ and reversible addition fragmentation chain-transfer (RAFT) polymerizations.⁸ The control over the radical polymerizations rely on an equilibrium between dormant and reactive chain ends, whereby the concentration of active radical chain ends should be sufficiently low to prevent the occurrence of radical termination reactions and thus to retain the control over the polymerization. This equilibrium can be influenced by a wide range of parameters, such as monomer, initiator, controlling agent, solvent, reaction temperature and ratios of the reactants. As a result, the optimization of such controlled polymerization techniques can be very time-consuming.

In large contrast to the rapid developments in the polymerization reactions (e.g. ATRP, RAFT and NMP), the used experimental techniques have not radically changed over the past decades. Still, most of the polymerizations are performed in standard glass round-bottom flasks or slenk tubes that are heated by an oil bath as depicted in Figure 1, left. In contrast to organic and pharmaceutical research, the application of automated parallel synthesis robots (Figure 1, right)⁹ in polymer chemistry is only flourishing in the last several years.^{10,11} The advantages of using such synthesis robots are, first of all, the increased throughput and speed of the research and, secondly, the high reproducibility and comparability of the performed reactions.¹² Therefore, such automated parallel approaches seem to be very promising for the optimization of controlled radical polymerization processes. Moreover, synthesis robots might be applied for the synthesis of systematical libraries of copolymers to identify possible structure-property relationships.

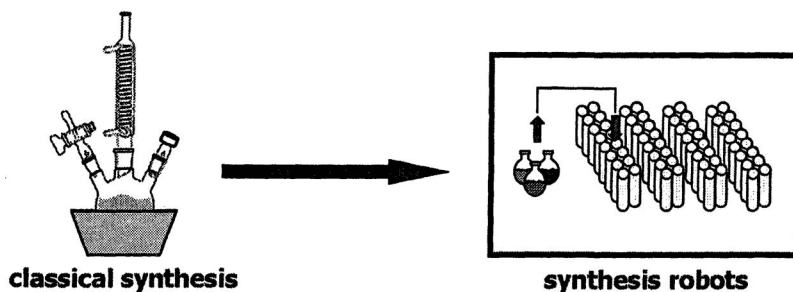
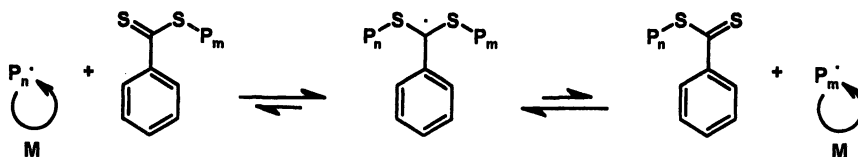


Figure 1. Comparison of traditional polymerization methods and high-throughput experimentation.

In this contribution, we have investigated the reversible addition-fragmentation chain transfer (RAFT) polymerization process utilizing high-throughput experimentation techniques. The control over the radical polymerization during the RAFT process is achieved by establishing an equilibrium between a dormant polymeric RAFT transfer-agent and the free polymeric radicals as depicted in Scheme 1.



Scheme 1. Schematic representation of the RAFT polymerization mechanism.

Previously, we have demonstrated the applicability and reproducibility of the RAFT polymerization of methyl methacrylate (MMA) using 2-cyano-2-butyl dithiobenzoate (CBDB) as RAFT agent and 2,2'-azobisisobutyronitrile (AIBN) as initiator in toluene. During these studies, it was elucidated that a RAFT to initiator ratio of 0.25 and a polymerization temperature of 70 °C were the optimal polymerization conditions, with regard to both control over the polymerization and polymerization rate, for the RAFT polymerization of methyl acrylate, *tert*-butyl acrylate, benzyl acrylate, ethylhexyl acrylate, *n*-butyl methacrylate, benzyl methacrylate, *N,N*'-dimethylaminoethyl methacrylate (DMAEMA) and MMA.^{13,14}

Here, we report our investigations on the synthesis of random and block copolymers of MMA and DMAEMA *via* the RAFT process utilizing the automated parallel synthesis robots. These copolymers are of interest because of

their amphiphilic character resulting from the combination of hydrophilic pDMAEMA and hydrophobic pMMA. Moreover, the pDMAEMA segment introduces both pH and temperature sensitivity into the copolymers: The pDMAEMA can be protonated and it exhibits a lower critical solution temperature.¹⁵ In addition, amphiphilic pMMA-*b*-DMAEMA block copolymers with a small pMMA content were shown to self-assemble into micellar structures in aqueous solutions.^{16,17} The synthesis of pMMA-*b*-DMAEMA copolymers has been previously reported using both group transfer¹⁸ and anionic polymerization methods.^{19,20} In addition, pMMA-*stat*-DMAEMA copolymers were synthesized by a Pd(II) catalyzed polymerization process.²¹ However, the RAFT polymerization process has not been applied for the synthesis of pMMA-DMAEMA copolymers to the best of our knowledge. During these studies we have synthesized libraries of both random and block copolymers of MMA and DMAEMA utilizing the automated parallel synthesis robots. The monomer compositions were systematically varied in the synthesized copolymers as schematically depicted in Figure 2. The block copolymer library is composed of copolymers with a first block of 25, 50, 75 or 100 MMA units and a second block of 25, 50, 75 or 100 DMAEMA units resulting in 16 different block copolymers. In addition, 16 random copolymers with similar monomer compositions were synthesized.

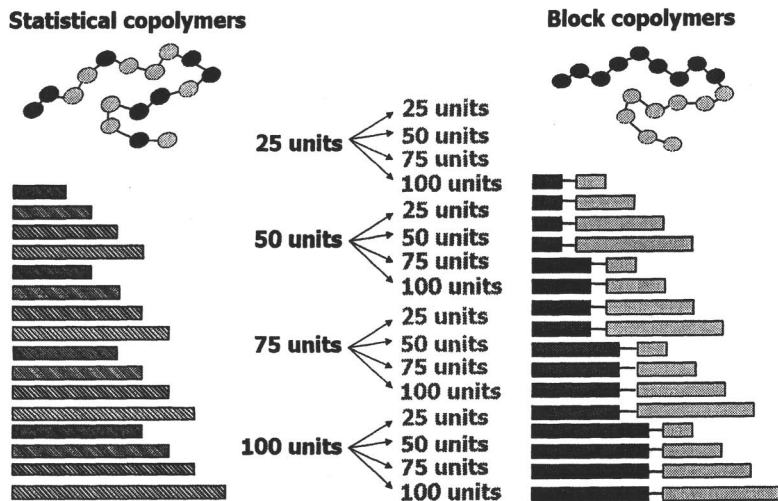


Figure 2. Schematic representation of the synthesis of a library of block and statistical copolymers.

Experimental part

Materials and instrumentation

Methyl methacrylate (MMA, Aldrich) and *N,N'*-dimethyl aminoethyl methacrylate (DMAEMA, Aldrich) were purified by passing over a basic aluminum oxide filtration column. 2,2'-Azobisisobutyronitrile (AIBN, Aldrich) was recrystallized from methanol. 2-Cyano-2-butyl dithiobenzoate (CBDB) was prepared as described in literature for a related compound.²² Analytical grade solvents were purchased from Biosolve Ltd. All solutions were deoxygenated by purging with argon for 30 minutes prior to use.

GPC was measured on a Shimadzu system equipped with a SCK-10A system controller, a LC-10AD pump, a RID-10A refractive index detector and a PL gel 5 μm Mixed-D column at 50 °C utilizing a chloroform : triethylamine : isopropanol (94 : 4 : 2) mixture as eluent at a flow rate of 1 $\text{mL}\cdot\text{min}^{-1}$. Molecular weights were calculated against a pMMA calibration. ¹H-NMR spectra were recorded in CDCl_3 on a Varian Mercury 400 spectrometer.

Statistical copolymerizations

The statistical copolymerizations were performed in a computer controlled Chemspeed ASW2000 synthesis robot equipped with an array of 16 parallel 13 mL reactors. The double jacketed reactors were connected to a Huber Unistat Tango (heating range: -40 °C to 145 °C) and were equipped with a cold-finger reflux condenser that could be cooled or heated from -5 °C till 50 °C. A double inert atmosphere was maintained by applying a 1.1 bar flow over the reactors and a 1.5 bar argon flow through the hood of the robotic system. After programming the reaction steps and preparing the stock solutions, the complete polymerization process can be performed in an unattended automated fashion.

To obtain an inert atmosphere, the hood of the ASW2000 synthesizer was flushed for at least 45 minutes with argon before starting the polymerization procedure. An inert atmosphere was created inside the reaction vessels by performing two cycles of heating (120 °C) under vacuum (15 min at ~ 25 mbar) followed by argon flushing (1 min). Subsequently, the reactors were filled with different amounts of MMA, DMAEMA and stock solutions containing AIBN or CBDB in toluene resulting in 4.2 mL polymerization mixtures. The total monomer concentration was kept constant at 2.21 M and the RAFT to initiator ratio was 0.25. The polymerizations were performed at 70 °C for 10 hours. During the polymerizations, the temperature of the cold-finger reflux condensers was set to -5 °C. The final polymerization mixtures were transferred into 8 mL sample vials and dried under vacuum. The resulting polymers were analyzed using ¹H-NMR spectroscopy and GPC.

Block copolymerizations

The block copolymerizations were performed in an automated Chemspeed Accelerator SLT100 synthesis robot. The reactors and peripherals of this robot system are similar to the previously described ASW2000.

The block copolymerizations were performed similar to the random copolymerizations utilizing an array of 16 parallel 13 mL reactors with a double jacket for heating. After creating an inert atmosphere in the hood and the reaction vessels, the first monomer (MMA), stock solutions of AIBN and CBDB in toluene and additional toluene were dispensed into the reactors resulting in 1.5 mL polymerization mixtures with a monomer/RAFT/initiator ratio of [25, 50, 75 or 100]/1/0.25 and a monomer concentration of 2.21 M. Four separate polymerizations were performed for each monomer to RAFT ratio. After three hours polymerization time, GPC samples were taken from the polymerizations with [MMA]:[RAFT] = 25. Subsequently, different amounts of the second monomer (DMAEMA) was added to these polymerization mixtures resulting in a theoretical amount for full conversion of 25, 50, 75 or 100 units DMAEMA and the polymerizations were continued for 3, 6, 9 or 12 hours, respectively. All other block copolymerizations were performed in a similar manner, whereby the polymerization time was 3 hours per 25 monomer units. The samples of the first block, before addition of the second monomer, and the final polymers were used for GPC analysis. Moreover, the final polymers were also analyzed by ¹H-NMR spectroscopy.

Results & Discussion

Nowadays, the synthesis of well-defined macromolecules is one of the major topics in polymer science. More specifically, well-defined amphiphilic block copolymers are of major interest for their phase separation²³⁻²⁵ and solution aggregation²⁶⁻²⁹ behavior. In this study, we have chosen to use pDMAEMA as hydrophilic part in the copolymers. The incorporation of pDMAEMA into the copolymers might open the way towards 'smart' switchable materials, because pDMAEMA can be protonated resulting in different properties at different pH's.¹⁵ Moreover, pDMAEMA has a lower critical solution temperature (LCST),¹⁵ which could be explored for the preparation of thermosensitive materials. RAFT polymerizations of the libraries of random and block copolymers of MMA and DMAEMA were performed using commercially available automated synthesis robots.⁹ The polymerizations were performed in toluene at 70 °C with a RAFT to initiator ratio of 0.25 as it was elucidated to be the optimum between control over the polymerization and polymerization speed.^{13,14}

Synthesis of pMMA-*stat*-DMAEMA statistical copolymers

A library of statistical copolymers consisting of MMA and DMAEMA was synthesized utilizing a high-throughput experimentation approach. 16 different copolymers were synthesized in one parallel synthesis run, whereby both the monomer composition as well as the polymer length were varied as schematically depicted in Figure 2, left. Four series of copolymers were synthesized consisting of 25, 50, 75 or 100 MMA units. Each of these series contained polymers with 25, 50, 75 and 100 DMAEMA units. As a result the total copolymer library consisted of 16 different copolymers. The polymerization times were varied according to the total number of monomer units, whereby 3 hours polymerization time was used per 25 monomer units present. As a result, the shortest copolymer (pMMA₂₅-*stat*-DMAEMA₂₅) was synthesized in 6 hours and the longest copolymer (pMMA₁₀₀-*stat*-DMAEMA₁₀₀) in 24 hours. After the required polymerization time, the polymerization mixtures were transferred from the reactors to sample vials. The molecular weight (distribution) of these resulting polymers was determined by GPC. The obtained molecular weights of all the synthesized pMMA-*stat*-DMAEMA copolymers are plotted against the theoretical molecular weight in Figure 3. From this Figure it can be concluded that the molecular weight of the copolymers is close to the theoretical molecular weights (dotted lines). The obtained molecular weights for the copolymers with 25 MMA units (1-4) are lower than theoretical. This is most likely caused by incomplete conversion as it was also reported for the homopolymerizations.¹⁴

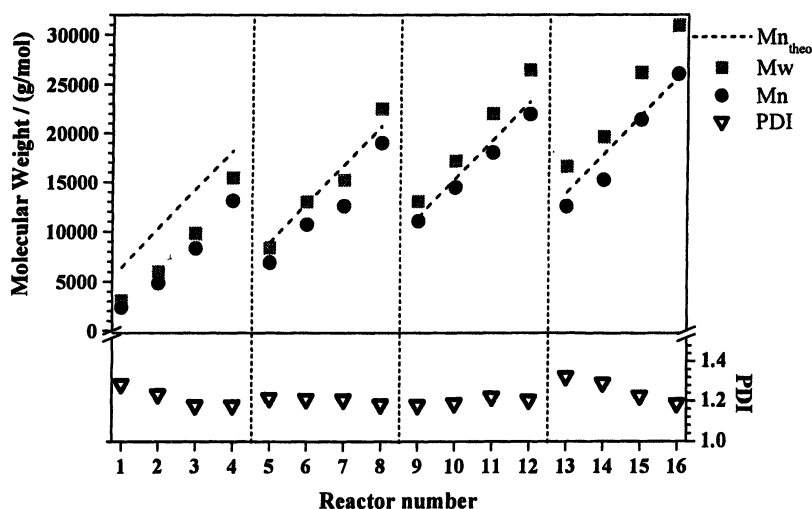
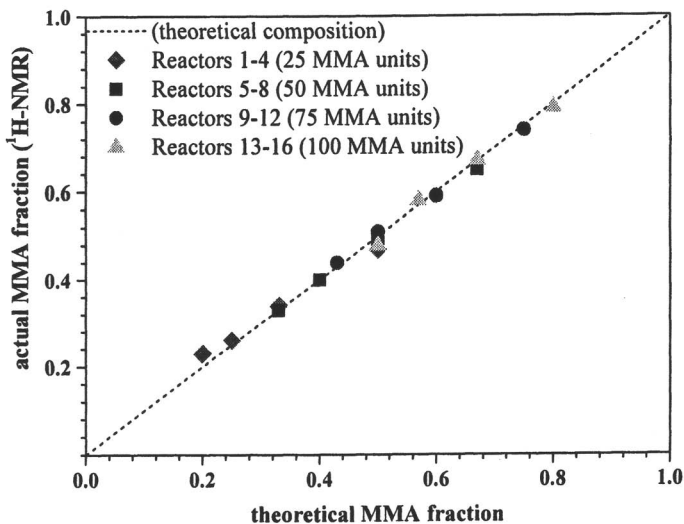


Figure 3. Molecular weight (distribution) from GPC, for the library of statistical copolymers that was synthesized in an automated synthesizer. Reactors 1-4, 5-8, 9-12 and 13-16 contain 25, 50, 75 or 100 MMA units with 25, 50, 75 and 100 DMAEMA units respectively. Eluent: CHCl₃:NEt₃:¹PrOH (94:4:2).

In addition, the molecular weight distributions of the polymers were below 1.30. Both the molecular weights and the low molecular weight distributions demonstrate that the copolymers were made in a controlled manner. Therefore, it can be concluded that the RAFT polymerization process is well suitable for the preparation of pMMA-*stat*-DMAEMA copolymers. The monomer composition of the final copolymers was determined utilizing $^1\text{H-NMR}$ spectroscopy. The resulting mole fraction of MMA in the copolymers is plotted against the theoretical mole fraction in Figure 4.



*Figure 4. Relationship between the theoretical and actual MMA fraction in the synthesized pMMA-*stat*-DMAEMA copolymer.*

This graph clearly demonstrates that all the synthesized pMMA-*stat*-DMAEMA copolymers have the desired MMA fraction. During this study, the objective was the preparation of well-defined copolymers and thus only the final polymers were analyzed. Therefore, no conclusions about the reactivity ratios of the RAFT copolymerization of MMA and DMAEMA can be drawn at this moment. Nevertheless, the copolymerization parameters under free radical conditions ($r_{\text{MMA}} = 0.74$; $r_{\text{DMAEMA}} = 1.30$)³⁰ and by a Pd(II) catalyzed polymerization process ($r_{\text{MMA}} = 1.07$; $r_{\text{DMAEMA}} = 1.13$)²¹ were reported previously. Therefore, it can be assumed that the synthesized copolymers have a nearly random monomer distribution through the polymer chains. The structural characterization data (GPC and $^1\text{H-NMR}$ spectroscopy) of the library of pMMA-*stat*-DMAEMA copolymers are summarized in Table I. Although the actual monomer composition of the copolymers resembles the theoretical monomer composition, the number of incorporated monomer units is generally lower than the theoretical values revealing incomplete conversion.

Table I. Structural characterization of the pMMA-*stat*-DMAEMA copolymers.

| Theoretical Molar Ratio | | ¹ H-NMR (in CDCl ₃) | | GPC | |
|-------------------------|--------|--|--------|----------------|------|
| MMA | DMAEMA | MMA | DMAEMA | M _n | PDI |
| 25 | 25 | 9 | 10 | 2400 | 1.29 |
| 25 | 50 | 12 | 23 | 4800 | 1.23 |
| 25 | 75 | 15 | 43 | 8300 | 1.18 |
| 25 | 100 | 21 | 70 | 13100 | 1.18 |
| 50 | 25 | 37 | 20 | 6900 | 1.22 |
| 50 | 50 | 41 | 42 | 10700 | 1.21 |
| 50 | 75 | 37 | 56 | 12600 | 1.21 |
| 50 | 100 | 45 | 92 | 19000 | 1.18 |
| 75 | 25 | 72 | 25 | 11000 | 1.18 |
| 75 | 50 | 69 | 48 | 14400 | 1.19 |
| 75 | 75 | 71 | 69 | 18000 | 1.22 |
| 75 | 100 | 73 | 93 | 21900 | 1.20 |
| 100 | 25 | 89 | 23 | 12500 | 1.32 |
| 100 | 50 | 85 | 42 | 15200 | 1.29 |
| 100 | 75 | 100 | 72 | 21400 | 1.22 |
| 100 | 100 | 97 | 104 | 26000 | 1.19 |

Synthesis and characterization of pMMA-*b*-DMAEMA block copolymers

Besides the synthesis of the library of statistical copolymers, pMMA-*b*-DMAEMA block copolymers with compositions comparable to the statistical copolymers were prepared *via* the RAFT polymerization process in an automated parallel manner. The first blocks of MMA were synthesized in parallel, whereby 3 hours polymerization time was used per 25 monomer units. After the required polymerization times, aliquots were taken from the polymerization mixtures to analyze the first block. Subsequently, the second monomer was added and the polymerization was continued. The resulting block copolymers were analyzed by GPC and ¹H-NMR spectroscopy. Figure 5 depicts the GPC traces of the pMMA₂₅ (left) and pMMA₅₀ (right) first blocks together with the corresponding block copolymers demonstrating their successful synthesis. The resulting molecular weights of both the first blocks and the final block copolymers are represented in Figure 6. The molecular weight of the first

blocks is close to the theoretical molecular weights (dotted lines), whereby the longer MMA blocks show a larger deviation. This is probably due to insufficient polymerization times as it was previously found for pMMA homopolymerizations as well.¹⁴

Moreover, the molecular weight distributions are reasonably narrow ($PDI \leq 1.30$) indicating that the polymerizations proceeded in a controlled manner. After the polymerization of the second blocks, the molecular weights increased and the PDI values decreased (mostly below 1.20), which further demonstrated the controlled character of the RAFT block copolymerizations. The theoretical molecular weights were also not reached for the block copolymers suggesting incomplete conversion and thus insufficient polymerization times. Nevertheless, the successful automated parallel synthesis of this library of block copolymers clearly demonstrates the applicability of the RAFT process for the preparation of pMMA-*b*-DMAEMA block copolymers.

Table II. Structural characterization of the pMMA-*b*-DMAEMA copolymers.

| Reactor | ¹ H-NMR in CDCl ₃ (theoretical) | | GPC 1 st block | | GPC diblock | |
|---------|--|----------|---------------------------|------|----------------|------|
| | MMA | DMAEMA | M _n | PDI | M _n | PDI |
| 1 | 19 (25) | 14 (25) | 1800 | 1.32 | 4200 | 1.25 |
| 2 | 21 (25) | 39 (50) | 1800 | 1.33 | 8200 | 1.20 |
| 3 | 21 (25) | 66 (75) | 2200 | 1.3 | 12400 | 1.15 |
| 4 | 25 (25) | 95 (100) | 1900 | 1.34 | 17400 | 1.11 |
| 5 | 39 (50) | 11 (25) | 3600 | 1.28 | 5600 | 1.22 |
| 6 | 43 (50) | 33 (50) | 3900 | 1.26 | 9600 | 1.16 |
| 7 | 46 (50) | 61 (75) | 4000 | 1.28 | 14100 | 1.15 |
| 8 | 43 (50) | 83 (100) | 3900 | 1.25 | 17400 | 1.14 |
| 9 | 64 (75) | 10 (25) | 5100 | 1.26 | 8000 | 1.10 |
| 10 | 68 (75) | 29 (50) | 6200 | 1.21 | 11400 | 1.16 |
| 11 | 65 (75) | 50 (75) | 6200 | 1.21 | 14300 | 1.16 |
| 12 | 68 (75) | 74 (100) | 6600 | 1.20 | 18400 | 1.16 |
| 13 | 74 (100) | 6 (25) | 6900 | 1.22 | 8300 | 1.18 |
| 14 | 86 (100) | 22 (50) | 7800 | 1.23 | 12100 | 1.18 |
| 15 | 85 (100) | 43 (75) | 8200 | 1.22 | 15300 | 1.18 |
| 16 | 83 (100) | 61 (100) | 8700 | 1.17 | 18000 | 1.20 |

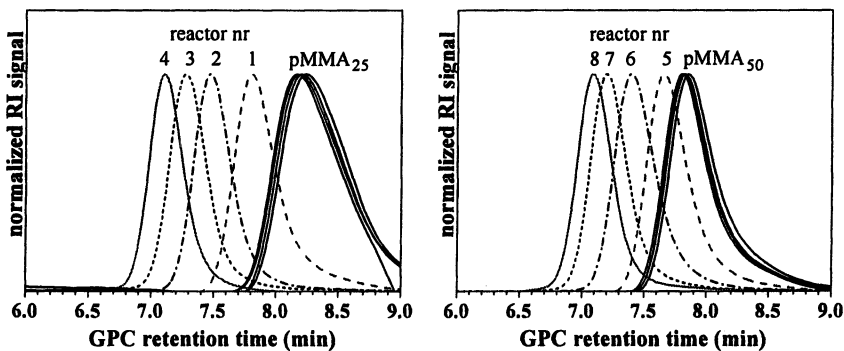


Figure 5. GPC traces of the first blocks and the resulting pMMA-*b*-DMAEMA block copolymers 1-4 (left) and 5-8 (right), which 25 (1-4) or 50 MMA units with 25, 50, 75 or 100 DMAEMA, respectively.

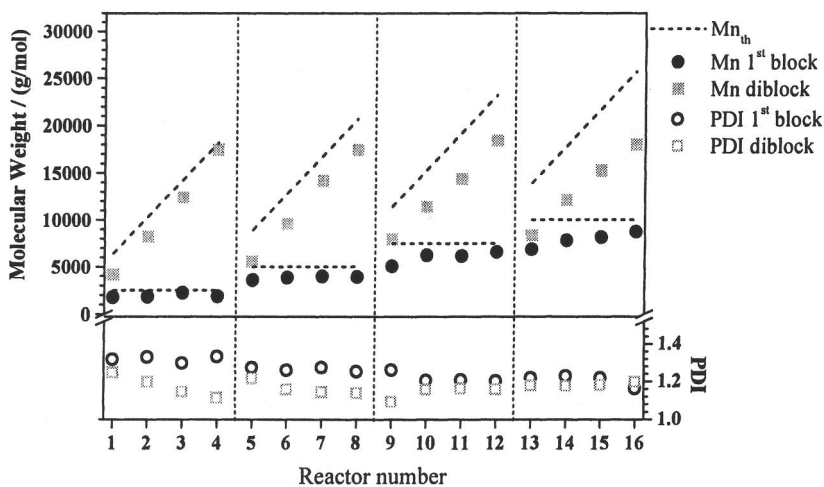


Figure 6. Molecular weight (distribution) obtained by GPC for the library of block copolymers that was synthesized in an automated synthesizer. Reactors 1-4, 5-8, 9-12 and 13-16 contain 25, 50, 75 or 100 MMA units with 25, 50, 75 and 100 DMAEMA units respectively. Eluent: $\text{CHCl}_3:\text{NEt}_3: {}^i\text{PrOH}$ (94:4:2).

In addition to the GPC characterization, the final block copolymers were also investigated by $^1\text{H-NMR}$ spectroscopy. Both the GPC data as well as the degree of polymerization obtained by $^1\text{H-NMR}$ spectroscopy are summarized in Table II. The degree of polymerization from the $^1\text{H-NMR}$ spectra is also lower than the theoretical amount of monomer units, which confirms the observation of lower molecular weights by GPC. The amount of MMA units (from $^1\text{H-NMR}$ spectroscopy) in each of the four reactors that should have the same number of MMA units is very comparable indicating the good reproducibility of the automated parallel polymerizations. Moreover, the amount of DMAEMA units and the molecular weights are increasing within each set of four polymerizations (1-4, 5-8, 9-12 and 13-16).

Conclusions and outlook

In conclusion, we have demonstrated the successful application of high-throughput synthesis equipment for the RAFT polymerization process. More specifically, we have synthesized libraries of pMMA-*stat*-DMAEMA and pMMA-*b*-DMAEMA copolymers. These libraries were characterized by GPC and $^1\text{H-NMR}$ spectroscopy demonstrating that the polymers were prepared *via* a controlled polymerization mechanism. However, the obtained polymerization degrees were lower than the theoretical number of monomer units, which is probably due to insufficient polymerization times.

Future work will focus on further characterization of the synthesized libraries of copolymers, whereby special attention will be given to the comparison of statistical and block copolymers with similar compositions.

Acknowledgments

The authors thank the *Dutch Scientific Organization* (NWO), the *Dutch Polymer Institute* (DPI) and the *Fonds der Chemischen Industrie* for financial support. Chemspeed Technologies is acknowledged for the fruitful collaboration.

References

1. Hadjichristidis, N.; Pitsikalis, M.; Pispas, S.; Iatrou, H. *Chem. Rev.* **2001**, *101*, 3747-3792.
2. Webster, O. W. *Science* **1991**, *496*, 887-893.
3. Goethals, E. J.; Dubreuil, M.; Wang, Y.; De Witte, I.; Christova, D.; Verbrugge, S.; Yanul, N.; Tanghe, L.; Mynarczuk, G.; Du Prez, F. *Macromol. Symp.* **2000**, *153*, 209-216.

4. Grubbs, R. H.; Khosravi, E. *Mater. Sci. Technol.* **1999**, *20*, 65-104.
5. Davis, K. A.; Matyjaszewski, K. *Adv. Polym. Sci.* **2002**, *159*, 1-169.
6. Matyjaszewski, K.; Xia, J. *Chem. Rev.* **2001**, *101*, 2921-2990.
7. Hawker, C. J.; Bosman, A. W.; Harth, E. *Chem. Rev.* **2001**, *101*, 3661-3688.
8. Perrier, S.; Takolpuckdee, P. *J. Polym. Sci., Part A: Polym. Chem.* **2005**, *43*, 5347-5393.
9. Hoogenboom, R.; Schubert, U. S. *Rev. Sci. Instrum.* **2005**, *76*, 062202/1-062202/7.
10. Hoogenboom, R.; Meier, M. A. R.; Schubert, U. S. *Macromol. Rapid Commun.* **2003**, *24*, 15-32.
11. Meier, M. A. R.; Hoogenboom, R.; Schubert, U. S. *Macromol. Rapid Commun.* **2004**, *25*, 21-33.
12. Hoogenboom, R.; Schubert, U. S. *J. Polym. Sci., Part A: Polym. Chem.* **2003**, *41*, 2425-2434.
13. Fijten, M. W. M.; Meier, M. A. R.; Hoogenboom, R.; Schubert, U. S. *J. Polym. Sci., Part A: Polym. Chem.* **2004**, *42*, 5775.
14. Fijten, M. W. M.; Paulus, R. M.; Schubert, U. S. *J. Polym. Sci., Part A: Polym. Chem.*, **2005**, *43*, 3831-3839.
15. Yuk, S. H.; Cho, S. H.; Lee, S. H. *Macromolecules* **1997**, *30*, 6856-6859.
16. Baines, F. L.; Armes, S. P.; Billingham, N. C.; Tuzar, Z. *Macromolecules* **1996**, *29*, 8151-8159.
17. Antoun, S.; Gohy, J.-F.; Jerome, R. *Polymer* **2001**, *42*, 3641-3648.
18. Baines, F. L.; Billingham, N. C.; Armes, S. P. *Macromolecules* **1996**, *29*, 3416-3420.
19. Antoun, S.; Teyssie, P.; Jerome, R. *Macromolecules* **1997**, *30*, 1556-1561.
20. Zhao, Q.; Ni, P. *Polymer* **2005**, *46*, 3141-3148.
21. Pang, X. A.; Sun, H. M.; Shen, Q. *Polymer* **2004**, *45*, 4029-4035.
22. Bouhadir, G.; Legrand, N.; Quiclet-Sire, B.; Zard, S. Z. *Tetrahedron Lett.* **1999**, *40*, 277.
23. Thomas, E. L.; Anderson, D. M.; Henkee, C. S.; Hoffman, D. *Nature* **1988**, *334*, 598.
24. Bates, F. S.; Fredrickson, G. H. *Annu. Rev. Phys. Chem.* **1990**, *41*, 525.
25. Lohmeijer, B. G. G.; Wouters, D.; Yin, Z.; Schubert, U. S. *Chem. Commun.* **2004**, 2886.
26. Discher, D. E.; Eisenberg, A. *Science* **2002**, *297*, 967.
27. Jain, S.; Bates, F. S. *Science* **2003**, *300*, 460.
28. Pochan, D. J.; Chen, Z.; Cui, H.; Hales, K.; Qi, K.; Wooley, K. L. *Science* **2004**, *306*, 94.
29. Zhibo, L.; Kesselman, E.; Talmon, Y.; Hillmyer, M. A.; Lodge, T. P. *Science* **2004**, *306*, 98.
30. Camail, M.; Essaoudi, H.; Margailan, A.; Vernet, J. L. *Eur. Polym. J.* **1995**, *31*, 1119-1125.

Chapter 33

Obtaining Chain Length Dependent Termination Rate Coefficients via Thermally Initiated Reversible Addition Fragmentation Chain Transfer Experiments

Current Status and Future Challenges

Alexander Theis, Martina H. Stenzel, Thomas P. Davis,
and Christopher Barner-Kowollik*

Centre for Advanced Macromolecular Design, School of Chemical Engineering and Industrial Chemistry, The University of New South Wales, Sydney, New South Wales 2052, Australia

*Corresponding author: camd@unsw.edu.au

The reversible addition fragmentation chain transfer (RAFT) process can be utilized in conjunction with rate of polymerization measurements to accurately map the chain length dependence of the termination rate coefficient. This novel approach was originally applied to styrene polymerization and has been termed the RAFT chain length dependent termination (RAFT-CLD-T) method. The RAFT-CLD-T technique is discussed in the context of the prerequisite analysis parameters as well as the choice of RAFT agent. In the present contribution we critically compare the data obtained via RAFT-CLD-T thus far for the monomers styrene (Sty), methyl methacrylate (MMA), methyl acrylate (MA), butyl acrylate (BA), dodecyl acrylate (DA), and vinyl acetate (VAc). For monomers with relatively low reactivity propagating radicals (MMA), a strong chain length dependence of k_t in the small chain length regime was observed, indicated by a relatively high α value (in the frequently used expression $k_t^{i,i} = k_t^0 \cdot \bar{r}^\alpha$). With increasing chain length, the α value is continuously decreasing, caused by a slow transition from translational diffusion to segmental diffusion as predicted by the composite model of chain length dependent termination. For monomers with higher reactivity propagating radicals (MA, VAc), a linear dependence of k_t with chain length was observed ($\alpha = 0.36$ for MA and 0.09 for VAc). Within the acrylate class, an interesting influence of the side chain was found. In the small chain length regime, α is in-

creasing with increasing length of the side chain from 0.36 in case of MA to 1.2 in DA, which may be attributed to an increased shielding of the polymeric radical. At longer chain lengths, the α value of MA is significantly higher than those for BA and DA, where α is strongly decreasing with increasing chain length. This may indicate a different flexibility and coil structure of MA compared to BA and DA. In general, the acrylates display significantly higher α values in the long chain region than MMA and VAc, which we assign to the presence of mid-chain radicals. The data obtained via three dimensional simultaneous mapping of the chain length and conversion dependence of k_t (3D-RAFT-CLD-T) for MA and VAc are also highlighted.

Introduction

Obtaining reliable termination rate coefficients, k_t , in free radical polymerization has been an on-going research theme over the last decades and to date a variety of methods have been developed to probe this parameter as both a function of the monomer to polymer conversion and the chain length of the propagating radicals. The complexities involved in obtaining reliable termination rate coefficient data as well as a critical evaluation of the most prominent methods for their determination have recently been reviewed (1, 2). A relatively simple experimental approach to map out the termination rate coefficient as a function of the chain lengths of the terminating radicals via the RAFT polymerization process was recently devised by our group (3). We termed this approach the RAFT chain length dependent termination (RAFT-CLD-T) technique. Under ideal circumstances, the RAFT methodology allows for a direct correlation of the macromolecular chain length, i , with the monomer to polymer conversion without – in the case of chain length independent rate coefficients – affecting the propagating radical concentration. With a relatively simple set of kinetic equations, time dependent rate of polymerization data recorded during a RAFT polymerization can be analyzed to yield the termination rate coefficient as a function of the chain lengths of the terminating radicals, when the rate coefficient for initiator decomposition and its efficiencies (k_d and f) as well as the propagation rate coefficient, k_p , are known (3). Initially, the methodology was applied to map out chain length dependent termination rate coefficients in styrene polymerizations (3, 4). Subsequently, we demonstrated that the RAFT-CLD-T method could also be adapted to methyl acrylate (MA) (5), butyl acrylate (BA) (6), and dodecyl acrylate (DA) (7) polymerization as well as methyl methacrylate (MMA) (8) and vinyl acetate (VAc) (9). In the present contribution we will initially outline the mathematical approaches taken to analyze the obtained rate data and spell out the prerequisite parameters that are required for a successful analysis. Subsequently, we will discuss the chain length dependencies obtained for the above mentioned monomer systems and engage in a comparative analysis of these dependencies in the context of the currently discussed models for chain length de-

pendent termination. We will further put the results obtained via the RAFT-CLD-T method in the context of results obtained with other methods for measuring chain length dependent k_t .

Data Evaluation Procedure

The underpinning key idea of RAFT-CLD-T is simple: In an ideal RAFT process where the RAFT agent does not induce rate retardation and/or inhibition effects and the evolution of the number average molecular weight follows those that are theoretically predicted, the change in termination rate as a function of the macro radical chain length is directly reflected in the rate of polymerization, $R_p(t)$. Thus, one can deduce $k_t(t)$ via a rearrangement of the rate of polymerization equation under the consideration of non-steady state kinetics as given by eq 1 (7).

$$\langle k_t \rangle(t) = \frac{2 \cdot f \cdot k_d \cdot [I]_0 \cdot e^{-k_d t} - \frac{d}{dt} \left(\frac{R_p(t)}{k_p^* \cdot \left([M]_0 - \int_0^t R_p(t) dt \right)^\omega} \right)}{2 \cdot \left(\frac{R_p(t)}{k_p^* \cdot \left([M]_0 - \int_0^t R_p(t) dt \right)^\omega} \right)^2} \quad (1)$$

Since the time axis is directly correlated with the molecular weight, the resulting $k_t(t)$ values are easily transformed into k_t^{ii} where f is the initiator efficiency, k_d is the rate coefficient for the thermally decaying initiator, $[M]_0$ is the initial monomer concentration, k_p^* is the propagation rate coefficient, and ω is the monomer reaction order. Eq 1 represents the most general form of the RAFT-CLD-T equation as it does not require steady state conditions and allows for non-idealities, e.g. caused by chain transfer reactions in the polymerization process. Chain transfer to polymer is often encountered when using monomers with highly reactive radicals (such as acrylates) and leads to higher monomer reaction orders (as expressed in ω values larger than unity) and an effectively reduced propagation rate coefficient, k_p^* . In many of the monomer systems studied via the RAFT-CLD-T method, so called hybrid behavior (10) of the polymerization is observed, implying that the evolution of the molecular weight with conversion does not start at a chain length of unity (11). Thus, the molecular weight axis must be constructed by experimentally determining the M_n vs. conversion evolution. In addition, such an observation requires that high RAFT agent concentrations are applied, if the low chain length regime is to be covered. On the other hand, some

monomers require that conversions be kept relatively low in order to avoid an overlap of the chain length dependence of k_t with its conversion dependence. With monomers displaying strong Trommsdorff effects such as MA (5) and MMA (8), low RAFT agent concentrations need to be applied to cover the high chain length regime at relatively low conversion (3). As a consequence – the chain length dependence of k_t is preferentially constructed in a stepwise fashion (5–8). However, the inherent polydispersity of the polymer samples leads to an averaging of k_t values. Thus – strictly speaking – the reported $k_t(i)$ data are averages of the (very narrow) distribution of chain lengths present at each point in time. Recently, the RAFT-CLD-T methodology has also been shown to be applicable to map conversion and chain length dependencies up to high conversions (12). The special factors requiring consideration when mapping $k_t(X, i)$ surfaces will be addressed in a dedicated section below.

Prerequisite Parameters

Inspection of eq 1 indicates that a range of parameters have to be known in order to compute reliable values for $\langle k_t \rangle(t)$. Each parameter influences the outcome of the calculation procedure in a specific fashion. As a drawback for all kinetic experiments using thermally decomposing initiators, the *initiator efficiency*, f , is a crucial parameter as it affects the absolute value of $\langle k_t \rangle(t)$ in a linear fashion as well as the shape of the $\langle k_t \rangle(t)$ curve, since f is a function of conversion, i.e. $f(X)$. While the absolute value of f is of less concern when determining chain length dependent k_t , its conversion dependence is a crucial parameter. For some monomers $f(X)$ has been determined experimentally and found to decrease in a close to linear fashion (13). Consequently, similar assumptions have been assumed to hold for other monomers, too. The problem of knowing $f(X)$ can partly be avoided by restricting X to low values in the RAFT-CLD-T experiments. The *rate coefficient of initiator decomposition*, k_d , can be measured with relative ease and high accuracy via UV/VIS photospectrometry in the case of the initiator 2,2'-azobisbutyronitrile (ABIN) (14), which has been employed in all RAFT-CLD-T experiments. Typically, the k_d determination is carried out in a solvent which is equivalent to the monomer except for the vinyl functionality (i.e. methyl acrylate is mimicked by methyl propionate). The *initial monomer and initiator as well as RAFT reagent concentrations* can be accessed with high accuracy by measuring the density of the polymerization mixture at the reaction temperature. The *propagation rate coefficient*, k_p , that is required for an evaluation of eq 1 can be obtained with good accuracy (for true chain end propagation) via the IUPAC recommended pulsed laser polymerization – size exclusion chromatography (PLP-SEC) method (15). An outstanding problem regarding accurate values for the propagation rate coefficient is the determination of its chain length dependence. This issue is addressed in more detail in the section 'Future Challenges' of this chapter. The *monomer reaction order* should be determined for monomers which display highly reactive radicals and are prone to transfer reactions to the polymer backbone and formation of mid-chain radicals. The presence of such mid-chain radicals that display a lower reactivity towards

monomer addition leads to monomer reaction orders of greater than unity. The monomer reaction order can be determined by measuring the rate of polymerization, $R_p(t)$ for varying monomer concentrations up to high conversions and plotting $(\log R_p(t) - (\log [I]_0)^{0.5})$ vs $\log [M]$ (7). The slope of the resulting graph is the monomer reaction order. It is advisable to restrict the fitting procedure of the plot to the initial part of the $(\log R_p(t) - (\log [I]_0)^{0.5})$ plot for each concentration, because at higher conversion deviations from the linear behavior can occur. Typical monomer reaction orders for acrylates are in the range of 1.5 for $T = 60\text{ }^\circ\text{C}$ to 1.75 for $T = 80\text{ }^\circ\text{C}$ (7, 12). It must be kept in mind that once a monomer reaction order higher than unity is employed, one must recalculate the corresponding propagation rate coefficient, k_p , and use an adapted coefficient, k_p^* .

Choice of RAFT Agent

For the success of the RAFT-CLD-T method, the choice of RAFT agent is critical. Foremost, it must be ensured that the RAFT agent does not induce any rate retardation and/or inhibition effects into the polymerization processes, as those will inevitably lead to an overestimation of the chain length dependent termination rate coefficients. While there is on-going uncertainty about the factors that contribute to rate retardation and inhibition being observed in RAFT mediated polymerization, there is general agreement on how RAFT agents should be ideally designed to induce no adverse effects. In particular, the Z- or stabilizing group of the RAFT agent should sufficiently destabilize the intermediate radical (such as $Z = \text{benzyl}$ or alkylthioxy) to avoid a built up of its concentration (and possible side reactions resulting as a consequence, such as intermediate radical termination). Of course, the intermediate radical stability is not alone dictated by the Z-group, but to a large extent also by the reactivity of the propagating radical. Thus, a RAFT agent which may be suitable for a less reactive species such as the MMA propagating radical may not be suitable for the investigation of acrylates. In the case of vinyl acetate – arguably yielding the radical with the highest reactivity among the investigated monomers – the RAFT agent has to be a xanthate (i.e. a MADIX agent) in order to reduce the reactivity of the C=S double bond and decrease the intermediate radical stability. Further, the choice of the R-group is highly important; ideally, one should select it such that it mimics the electronic characteristics of the propagating radical as has been realized in our studies on acrylates by using methoxy carbonyl ethyl phenyldithioacetate (MCEPDA) (5). Choosing the RAFT end group such will effectively eliminate the pre-equilibrium sequence from the RAFT processes. If such a choice is not available – sometimes caused by synthetic limitations – it is important to establish whether a potential slow re-initiation of the R-group causes a distortion of k_t derived at small chain lengths (9).

The individual reaction conditions and reagent concentrations used for the RAFT-CLD-T method for the various monomers will not be reiterated in the present comparative analysis as they can be found in the referenced literature.

Results and Discussion

Mapping $k_t^{i,i}$ for Several Monomer Families

One of the key advantages of the RAFT-CLD-T method is its low operational cost, its relative ease of use and wide applicability to a range of monomers families, while at the same time providing a relatively high accuracy (6). Consequently, after pioneering the RAFT-CLD-T method in 2002 with styrene as monomer (3), a range of monomers have been investigated, including a homologous series of acrylates. With extending the method to further monomers, general improvements have been implemented: (i) The molecular weight axis is constructed via experimental data rather than the expected theoretical molecular weights according to the initial RAFT agent concentration. (ii) The RAFT agent leaving group is selected with respect to a reinitiation rate which is comparable to the first propagation step in the corresponding conventional polymerization. With regard to the reported data for styrene it must be noted that due to possible hybrid behavior and high initiator concentrations some deviations from the theoretical expected molecular weight cannot be excluded. Further, there exists the possibility that a cumyl leaving group may not be ideally suited as it cannot be ruled out that at 80 °C the overall re-initiation efficiency is low, e.g. due to a possible back reaction and the combination of cumyl fragments (16). Thus, although the analysis of the original RAFT-CLD-T styrene data in the long chain regime returns α values that are in good agreement with previously reported data ($\alpha \approx 0.15$) and the long chain evaluation procedure has been verified in simulations (3), these data should be reconfirmed via more refined measurements.

Figure 1 shows an overview of the obtained chain length dependencies for various monomers at 80 °C. Each subfigure contains a structural image of the RAFT agent that was employed in the measurement and the (independently determined) value of ω that was used in the evaluation procedure. In order to compare more quantitatively the various chain length dependencies, the commonly used function $k_t^{i,i} = k_t^0 \cdot i^{-\alpha}$ was employed to deduce α values for the quasi-linear sections of the chain length dependencies (1). Inspection of Figure 1 allows for the deduction of some interesting trends: It can immediately be seen that acrylates display significantly higher α values in the long chain region (starting from approximately $i > 10$) than MMA and – interestingly – vinyl acetate. Typically α values for the acrylates range from 0.36 for MA to 0.22 for BA and 0.28 for DA. In the small chain length regime, α is increasing with increasing chain length of the side chain from 0.36 in case of MA to 1.2 in dodecyl acrylate, which may be attributed to an increased shielding of the radical towards other polymeric radical chains during the first few propagation steps. At longer chain lengths, the α value of MA is significantly higher than the ones observed for BA and DA, indicating a significantly different flexibility and coil structure of MA compared to BA and DA. The relatively high average α values in acrylate systems

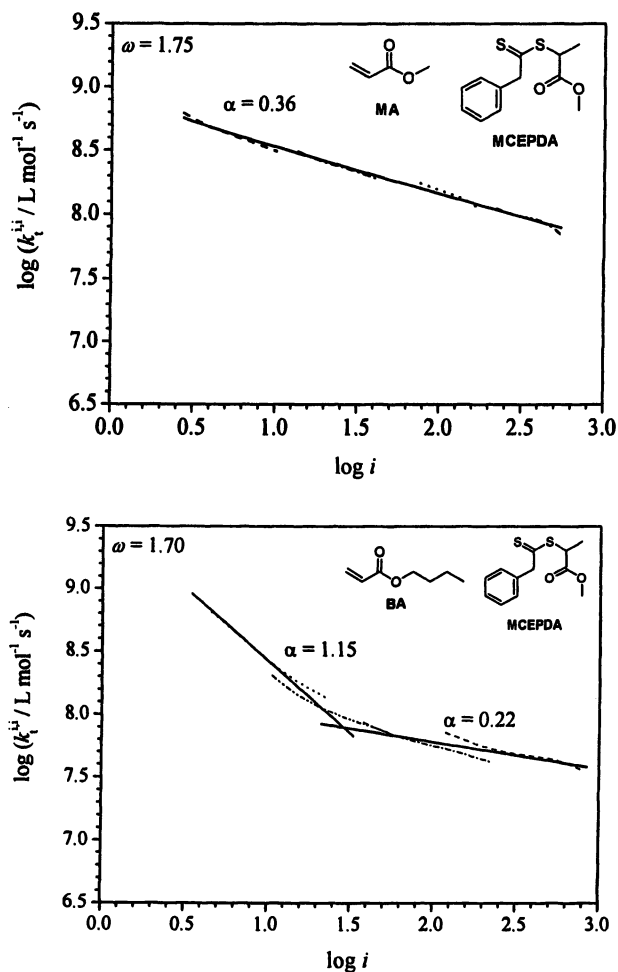


Figure 1. Chain length dependence of the termination rate coefficient of two macroradicals of nearly similar size, $k_t^{i,i}$, for methyl acrylate (MA), butyl acrylate (BA), dodecyl acrylate (DA), methyl methacrylate (MMA) and vinyl acetate (VAc) at 80 °C. The employed RAFT/MADX agent is depicted within each subfigure alongside the monomer reaction order used in the data evaluation procedure according to eq. (1).

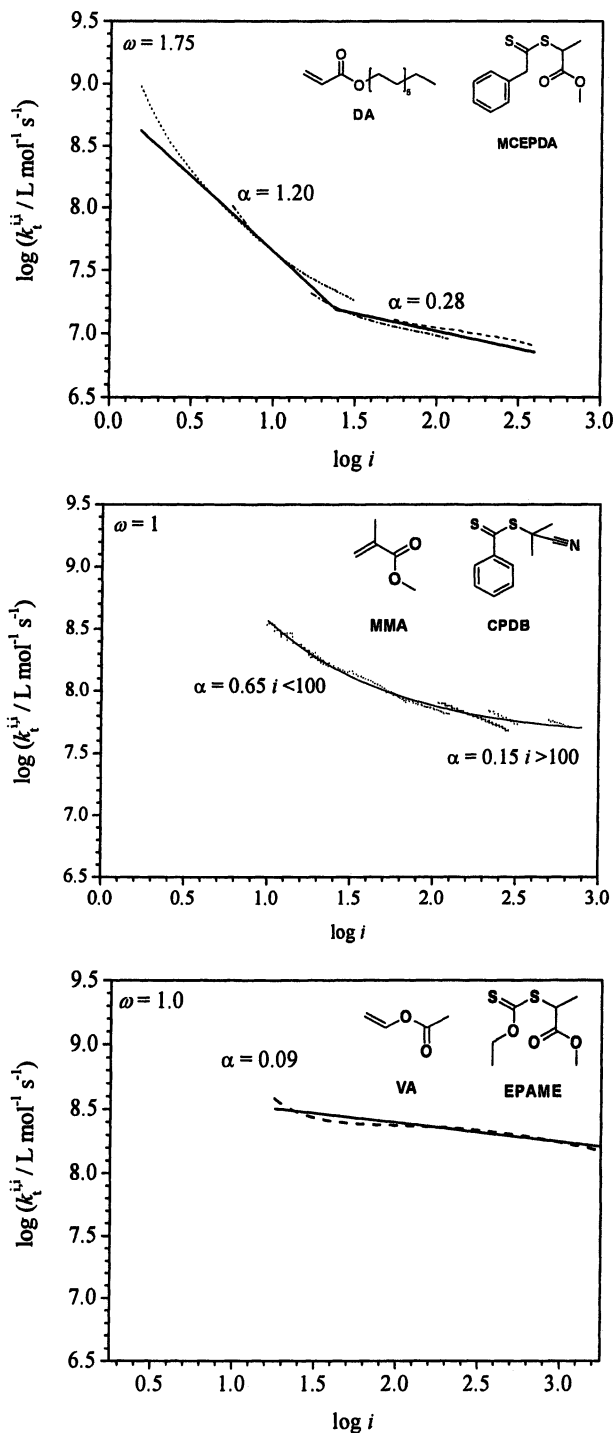


Figure 1. Continued.

are in good agreement with earlier findings via SP-PLP ($\alpha(\text{MA}) = 0.32$ (17) and $\alpha(\text{DA}) = 0.4$ (18)). In addition, our results are in excellent agreement with previous data obtained by pulsed laser polymerization by de Kock (19, 20) for MA and BA, where a short chain α values ($i = 6-10$) of 0.41 for MA and 0.80-0.85 for BA as well as long chain values ($i = 50-100$) of 0.35-0.36 for MA and 0.17-0.19 for BA were found. However, it should be noted that these former results display increased α values above 1 for medium chain lengths of $i = 15-30$, which may be a result of transfer reactions, which have not been considered in the study of de Kock. It was recently noted in a study comparing SP-PLP-RAFT with the RAFT-CLD-T method that small chain length regimes may be more accurately mapped out via the SP-PLP-RAFT method in the case of acrylates. It would thus constitute a worthwhile effort to study MA via SP-PLP-RAFT at small chain lengths.

The overall higher level of α in acrylate systems may be tentatively attributed to an increased presence of mid-chain radicals in acrylate polymerizations generated via intramolecular chain transfer reactions (21). Friedman and O'Shaughnessy have demonstrated that such a concept is indeed compatible with larger α values (22). It comes thus at no surprise that the long chain values obtained for monomers with less reactive propagating radicals are significantly lower than those observed for acrylates, with α for MMA reading 0.15, in excellent agreement with the theoretical predictions made for systems where no mid chain radicals are present. Nevertheless, the short chain regime also displays for these monomers larger α values (in the vicinity of those observed for acrylates), indicating centre of mass diffusion to be the dominating process.

It is worthwhile to consider vinyl acetate separately from the other monomers. To our knowledge, the RAFT-CLD-T method was the first method employed to deduce chain length dependent termination rate coefficients for this monomer. The VAc propagating radicals are highly reactive and thus it would a priori not be unreasonable to assume that backbiting reactions (similar to those observed in acrylate systems) occur to a significant extent. Somewhat surprisingly, this is not the case for VAc which shows a far decreased tendency to undergo both inter- as well as intramolecular chain transfer reactions (23). This notion is underpinned by measurements of the monomer reaction order for VAc, which lead to an ω of 1.17 (at 80 °C) (9) far lower than the ω values observed for the homologous series of acrylates ($\omega \approx 1.70$ at 80 °C). Under such circumstances, it can thus be expected that the chain length dependence of k_t is more in line with those determined for MMA and styrene. Inspection of the comparative Figure 1 largely confirms this notion: Analysis of k_t in the long chain regime (the short chain regime is inaccessible due to hybrid behavior in the RAFT process and overlapping rate retardation effects) returns α values close to 0.09 (9).

Mapping $k_t(X, i)$: Constructing a Three Dimensional Image of the Termination Process

The data reported in Figure 1 are limited to low conversions to avoid an overlap of the chain length dependence of k_t with its conversion dependence. Initially, data evaluation in all RAFT-CLD-T experiments was restricted to conversion regimes where k_t does not vary with conversion. Such a restriction had to be implemented because the primary database of the RAFT-CLD-T method (i.e. time dependent rates of polymerization, R_p) is sensitive to both changes in k_t caused by either chain length or conversion dependence. Thus, data obtained in high conversions regimes – although collected – were discarded. However, through a three dimensional analysis of the termination rate coefficient data as a function of *both* chain length and conversion, one can obtain a detailed picture of k_t as function of these variables. Such a plotting technique allows for the extraction of the chain length dependence of k_t at a constant conversion as well as the conversion dependence at a constant chain length. To our knowledge there exists no other technique which yields these dependencies with the relatively limited experimental difficulty. Typical (X, i, k_t) surfaces derived by measuring k_t up to high conversions and chain lengths for MA and VAc at 80 °C can be found in refs. (9) and (12). A simple way to extract the chain length dependence at constant conversion is to prepare slash graphs at a fixed conversion and analyze the obtained $k_t(i)$ functionality to give α . It is thus possible to deduce $\alpha(X)$. In line with earlier findings via the SP-PLP technique (18) the α value of MA increases significantly when going from 10% conversion ($\alpha = 0.36$) to 80% conversion ($\alpha = 0.80$), which is a consequence of an increasing Trommsdorff effect with increasing chain lengths. A similar trend is observed in the case of VAc, albeit at an overall lower level of α ($\alpha(10\%) = 0.09$ and $\alpha(80\%) = 0.55$). Figure 2 depicts the evolution of α as a function of monomer to polymer conversion in MA and VAc free radical polymerization studied via the RAFT-CLD-T method (at 80 °C and 1 bar) (9, 12) along side values for MA obtained at 1000 bar and 40 °C obtained via classical SP-PLP experiments (18).

Inspection of the Figure demonstrates the different levels of α for MA and VAc over a wide conversion range. At low conversions, there is some discrepancy between the data obtained via SP-PLP and those measured via RAFT-CLD-T (conversions below 20%). However, when comparing SP-PLP and RAFT-CLD-T data it has to be kept in mind that the chain length regimes covered to obtain a single α value are vastly different: While SP-PLP covers several thousands of chain lengths with one single laser pulse and an (average) α value is deduced, RAFT-CLD-T uses a more restricted chain length regime. Further, the reaction conditions – especially the pressure – is different. When applying higher pressure, the initial plateau section with no changes of k_t with monomer to polymer conversion may be less pronounced and allow for changes of α with conversion as observed with SP-PLP. It will be a matter of priority to investigate the underlying physical causes of the low conversion discrepancy in the case of MA. Nevertheless, it is interesting that the RAFT-CLD-T(except the two initial

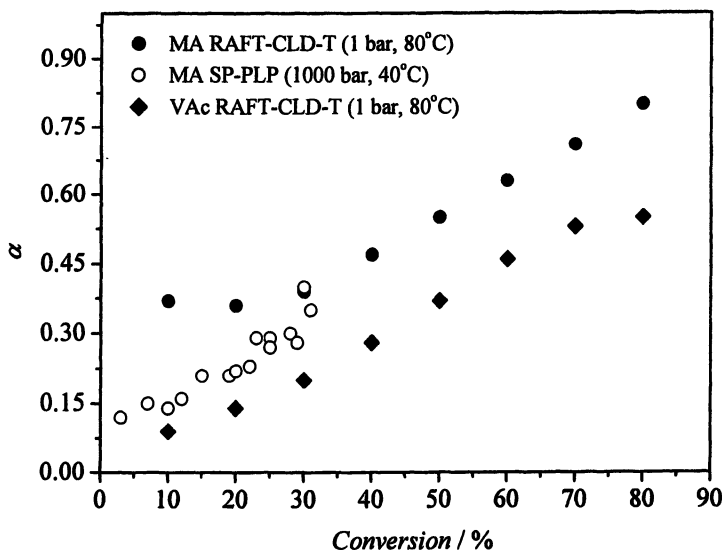


Figure 2. Evolution of α as a function of monomer to polymer conversion for the MA and VAc system studied via RAFT-CLD-T and for MA studied via classical SP-PLP experiments. The SP-PLP data are from ref. (18) The reaction conditions are given in the figure.

data points) and the SP-PLP data provide a uniform picture of the (linear) conversion dependent evolution of α . Whether this remarkable agreement is a true reflection of physical reality in this system or is largely coincidental remains to be established. Yet, it is undoubtedly so that living free radical techniques such as RAFT-CLD-T and RAFT-SP-PLP are potentially more accurate in probing the chain length dependence of k_t than model dependent approaches such as classical SP-PLP.

Future Challenges

In terms of future challenges that need to be addressed for further increased accuracy of the RAFT-CLD-T method one main aspect is the size of the propagation rate coefficient: At present – especially when discussing the obtained chain length dependencies in a comparative fashion – some caution has to be exercised regarding the very low chain length regime ($i < 8$). There is some evidence in the literature that the propagation rate coefficient is also beset with a chain length dependence (24). For some of the monomer systems studied via the RAFT-CLD-T technique such as the acrylates and vinyl acetate, there are very limited literature data available on the potential extend of chain length dependent k_p . Thus, in order to obtain a more accurate assessment of the very low chain length regime it is a priority to measure k_p^i . Such a chain length dependence can – also retrospectively – be easily incorporated into the current data. Interestingly, the provision of k_p^i data will not only benefit the RAFT-CLD-T method, but also

derivatives of it such as SP-PLP-RAFT (25) and also in fact any other method requiring the exact knowledge of k_p^i . To illustrate the effect chain length dependent termination can potentially have on the observed k_t^i , Figure 3 shows the effect of variable k_p^i on the outcome of RAFT-CLD-T methodology calculated by eq 1. The chain length dependence of k_p was varied according to eq 2 suggested earlier (26). Eq. 2 is an empirical relation that nevertheless captures the essence of CLD k_p and varying the parameters C_1 and $i_{0.5}$ gives access to different shapes of k_p^i dependencies.

$$k_p^i = k_p^\infty \left\{ 1 + C_1 \exp\left(\frac{-\ln 2}{i_{0.5}}(i-1)\right) \right\} \quad (2)$$

Since the experimental data on direct measurements of k_p^i are strongly divergent, it is reasonable to estimate the magnitude of C_1 from measured data of long chain k_p values compared to the corresponding small radical addition reactions determined by Fischer *et al.* (27). Such a comparison shows that the differences of k_p with chain length are merely caused by the frequency factor with only minor variations in the activation energy (24). However, in contrast to what is stated in ref. (24), the frequency factors for the small radical additions of styrene and MA should be adjusted for secondary radicals, which typically are close to $\log(A / \text{L mol}^{-1} \text{s}^{-1}) = 8$ (27). Employing a frequency factor of $10^8 \text{ L mol}^{-1} \text{s}^{-1}$ results in C_1 values of 3.3 for styrene, 10.7 for MMA and 9.8 for MA. In addition, the C_1 value for MA is in excellent agreement with the value of $C_1 = 9.7$, which was obtained by nitroxide trapping experiments of this monomer by Moad *et al.* (28). The same authors further suggest an $i_{0.5}$ value, which governs the magnitude of the decrease of k_p^i , of 0.27, however also extremely high values of $i_{0.5} = 1.12$ are under discussion (29). We note from ref. (26) that if $i_{0.5} = 1$, for every increase of i by 1, k_p^i decreases by a factor of 2. In the present analysis, we use a value for $C_1 = 10$ and test the cases of $i_{0.5} = 1, 0.5$ and 0.25 . For demonstration of the effects, a chain length independent k_t value of $\log(k_t) = 7.5$ was selected.

Inspection of Figure 3 clearly shows that the low chain length regime is very sensitive to changes in k_p^i . This is due to the fact that the propagation rate coefficient is directly proportional to the rate of polymerization, whereas the termination rate coefficient affects the rate only by the square root. Consequently, k_p in eq 1 squared. Since chain length effects in the activation energy in both, the propagation and termination steps can be expected to be minor (and the frequency factor from collision theory is highly dominated by the smaller molecule) the effect of the chain length dependence of k_t itself should – although not squared – be at least in the same range. It is thus reasonable that k_t in the small chain length is regime in our experiments is increasing with decreasing chain length, although a chain length dependent k_p^i was not considered. However, consideration of a chain length dependent k_p^i in conjunction with data from the RAFT-CLD-T method would lead to extremely high short chain α and $k_t^{1,1}$

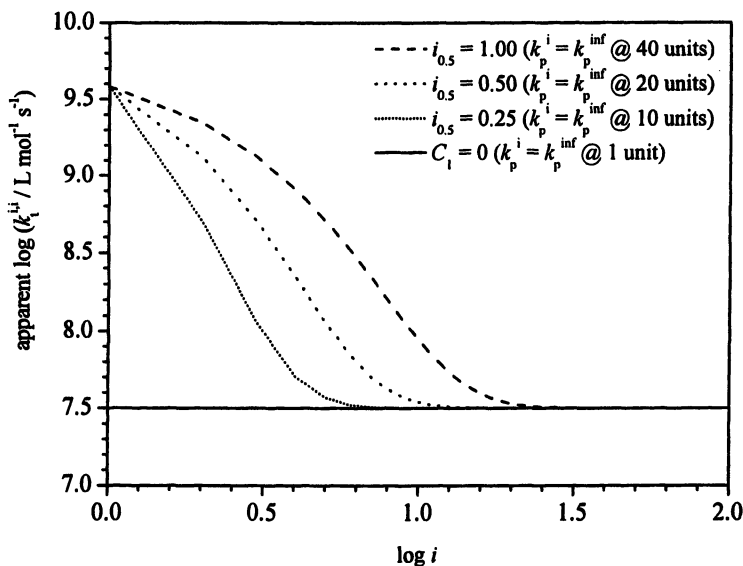


Figure 3. Effect of chain length dependent propagation (simulated via eq 2) on the observed chain length dependence of k_t , obtained via RAFT-CLD-T. The graph maps varying values of $i_{0.5}$ (see text).

values. While such values can not be excluded a priori, it seems more realistic to assume that k_p^i decays to its infinity value within the first 10 addition steps or possibly even faster. Additionally, it must be kept in mind that the above analysis is based on an estimated C_1 value deduced from model reactions, and propagation rate coefficients are extrapolated from different temperature ranges, where side reactions such as transfer to polymer in case of the acrylates may not occur. This may affect both, the absolute value of the k_t data obtained by RAFT-CLD-T method and of the value of C_1 . Assuming the employed parameters are reasonable, the present analysis highlights that obtaining reliable k_p^i values for acrylates (as well as other monomers) is important to increase the accuracy for k_t^{ii} for approximately $i < 15$.

Although the chain length dependence of k_t has been mapped out via RAFT-CLD-T for a range of monomers, some interesting candidates remain to be addressed. Most prominently among those are the so-called sterically hindered 1,1-disubstituted monomers such as dicyclohexyl itaconate (DCHI). Due to their rod-like chain structure an unusual chain length dependence of the termination rate coefficient may be expected. However, finding an appropriate RAFT agent for these monomers is challenging since the addition of such hindered macro-radicals to C=S double bonds may be slow and rate retardation effects are commonly observed (30). A novel class of so-called F-RAFT agents (31) may hold some promise for these monomers, since such agents may display extremely low intermediate radical stabilities while they may retain a high C=S double bond reactivity (32).

The RAFT-CLD-T methodology holds potential to address one of the most important outstanding problems with regard to chain length dependent termination, i.e. the measurement of the termination rate coefficient of radicals of dissimilar size. At present, most techniques (whether RAFT based or conventional) return k_t^{ij} values, whereas probing short-long termination over a range of chain lengths in polymerizing systems has not yet been addressed in detail. RAFT-CLD-T offers a unique opportunity to measure the rate of polymerization in the presence of an initial RAFT agent and a macroRAFT agent of chain length j . Thus, k_t^{ij} may potentially be extracted by deconvoluting the resulting $\langle k_t \rangle(t)$ with those obtained under conditions where termination is observed between macro-radicals of identical (or similar) size. Investigations using RAFT-CLD-T to map out k_t^{ij} are currently underway in our laboratories.

Acknowledgments. C.B.-K. and M.H.S. thank the *Australian Research Council* for financial support in the form of a *Discovery Grant*. TPD acknowledges receipt of a *Federation Fellowship*. The authors would like to thank Dr. Leonie Barner and Mr. Istvan Jacenyik for their excellent management of CAMD.

References

1. Barner-Kowollik, C.; Buback, M.; Egorov, M.; Fukuda, T.; Goto, A.; Olaj, O. F.; Russell, G. T.; Vana, P.; Yamada, B.; Zetterlund, P. B. *Prog. Polym. Sci.* **2005**, *30*, 605-643.
2. Buback, M.; Egorov, M.; Kaminsky, V.; Olaj, O. F.; Russell, G. T.; Vana, P.; Zifferer, G. *Macromol. Chem. Phys.* **2002**, *203*, 2570-2582.
3. Vana, P.; Davis, T. P.; Barner-Kowollik, C. *Macromol. Rapid Commun.* **2002**, *23*, 952-956.
4. Feldermann, A.; Stenzel, M. H.; Davis, T. P.; Vana, P.; Barner-Kowollik, C. *Macromolecules* **2004**, *37*, 2404-2410.
5. Theis, A.; Feldermann, A.; Charton, N.; Stenzel, M. H.; Davis, T. P.; Barner-Kowollik, C. *Macromolecules* **2005**, *38*, 2595-2605.
6. Junkers, T.; Theis, A.; Buback, M.; Davis, T. P.; Stenzel, M. H.; Vana, P.; Barner-Kowollik, C. *Macromolecules*, **2005**, *38*, 9497-9508.
7. Theis, A.; Feldermann, A.; Charton, N.; Davis, T. P.; Stenzel, M. H.; Barner-Kowollik, C. *Polymer* **2005**, *46*, 6797-6809.
8. Johnston-Hall, G.; Theis, A.; Monteiro, M.; Davis, T. P.; Stenzel, M. H.; Barner-Kowollik, C. *Macromol. Chem. Phys.* **2005**, *206*, 2047-53.
9. Theis, A.; Davis, T. P.; Stenzel, M. H.; Barner-Kowollik, C. *Polymer* **2006**, in press.
10. Barner-Kowollik, C.; Quinn, J. F.; Nguyen, T. L. U.; Heuts, J. P. A.; Davis, T. P. *Macromolecules* **2001**, *34*, 7849-7857.
11. It is important to note that only an addition rate coefficient of infinity for the addition of propagating radicals, k_p , to the initial RAFT agent would lead to the molecular weight evolution starting with chain length one. In practice,

- all RAFT polymerization display some degree of hybrid behaviour, but in several cases the ratio of k_p to k_p is so favourable that very limited hybrid behaviour is observed. For a detailed description of these effects and the consequences for RAFT-SP-PLP see ref.(5).
12. Theis, A.; Davis, T. P.; Stenzel, M. H.; Barner-Kowollik, C. *Macromolecules* **2005**, *38*, 10323-10327.
 13. Buback, M.; Huckstein, B.; Kuchta, F.-D.; Russell, G. T.; Schmidt, E. *Macromol. Chem. Phys.* **1994**, *195*, 2117-2140.
 14. Charton, N.; Feldermann, A.; Theis, A.; Davis, T. P.; Stenzel, M. H.; Barner-Kowollik, C. *J. Polym. Sci. Polym. Chem.* **2004**, *42*, 5170-5179.
 15. Beuermann, S.; Buback, M.; Davis, T. P.; Gilbert, R. G.; Hutchison, R. A.; Olaj, O. F.; Russell, G. T.; Heuts, J. P. A.; van Herk, A. M. *Macromol. Chem. Phys.* **1997**, *198*, 1545-1560.
 16. McLeary, J. B.; Calitz, F. M.; McKenzie, J. M.; Tonge, M. P.; Sanderson, R. D.; Klumperman, B. *Macromolecules*, **2005**, *38*, 3151-3161.
 17. Buback, M.; Busch, M.; Kowollik, C. *Macromol. Theory Simul.* **2000**, *9*, 442-542.
 18. Buback, M.; Egorov, M.; Feldermann, A. *Macromolecules*, **2004**, *37*, 1768-1776.
 19. de Kock, J. B. L.; van Herk, A. M.; German, A. L. *J. Macromol. Sci., Polym. Rev.* **2001**, *C41*, 199-252.
 20. de Kock, J. B. L. *PhD Thesis*, 1999, Technische Universiteit Eindhoven, ISBN 90-386-2701-7.
 21. Willemse, R. X. E.; van Herk, A. M.; Panchenko, E.; Junkers, T.; Buback, M. *Macromolecules* **2005**, *38*, 5098-5103.
 22. (a) Friedman, B.; O'Shaughnessy, B. *Macromolecules* **1993**, *26*, 5726; (b) Karatekin, E.; O'Shaughnessy, B.; Turro, N. J. *Macromol. Symp.* **2002**, *182*, 81.
 23. Britton, D.; Heatley, F.; Lovell, P.A. *Macromolecules* **1998**, *31*, 2828-2837.
 24. Heuts, J. P. A.; Russell, G. T. *Europ. Polym. J.* **2006**, *42*, 3-20.
 25. Buback, M.; Junkers, T.; Vana, P. *Macromol. Rapid Commun.* **2005**, *26*, 796-802.
 26. Smith, G. B.; Russell, G. T.; Yin, M.; Heuts, J. P. A. *Europ. Polym. J.* **2005**, *41*, 225-230.
 27. Fischer, H.; Radom, L. *Angew. Chem. Int. Ed.* **2001**, *40*, 1340-1371.
 28. Moad, G.; Rizzardo, E.; Solomon, D. H.; Beckwith, A. L. *J. Polym. Bull.* **1992**, *29*, 647-652.
 29. Willemse, R. X. E.; Staal, B. B. P.; van Herk, A. M.; Pierik, S. C. J.; Klumperman, B. *Macromolecules* **2003**, *36*, 9797-9803.
 30. Szablan, Z.; Ah Toy, A.; Davis, T. P.; Hao, X.; Stenzel, M. H. Barner-Kowollik, C. *J. Polym. Sci. Polym. Chem.* **2004**, *42*, 2432-2443.
 31. Theis, A.; Stenzel, M. H.; Davis, T. P.; Coote, M. L.; Barner-Kowollik, C. *Aust. J. Chem.* **2005**, *58*, 437-441.
 32. Coote, M. L.; Henry, D. J. *Macromolecules* **2005**, *38*, 5774-5779.

Chapter 34

Reversible Addition Fragmentation Chain Transfer-Mediated Copolymerizations: The Challenge of Random Copolymer Blocks

Bert Klumperman^{1,2}, James B. McLeary²,
Eric T. A. van den Dungen², Willem-Jan Soer¹,
and Jelena S. Božović¹

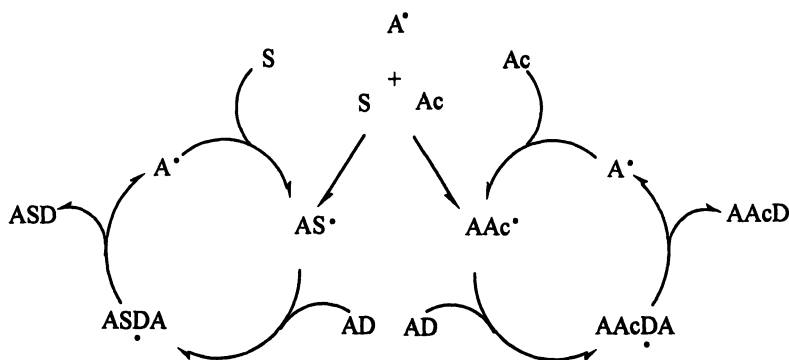
¹Laboratory of Polymer Chemistry, Eindhoven University of Technology,
P.O. Box 513, 5600 MB Eindhoven, The Netherlands

²UNESCO-Associated Center for Macromolecules and Materials,
University of Stellenbosch, Private Bag X1, 7602 Matieland, South Africa

The synthesis of random copolymer blocks as part of a block copolymer is potentially one of the unique features of living radical polymerization. However, in this contribution it is shown that subtle variations, such as the choice of a different initiating radical are sufficient to induce variations in copolymer composition at the early stages of the chain growth. The very first few monomer additions in a RAFT-mediated styrene – acrylonitrile copolymerization are studied using *in situ* ¹H NMR spectroscopy. Initialization behavior is observed in a similar fashion as seen in a RAFT-mediated homopolymerization. In a RAFT-mediated alternating styrene – maleic anhydride copolymerization, the effect of the nature of the leaving group of the RAFT-agent is clearly demonstrated by careful analysis of the resulting (low molar mass) copolymers.

Introduction

The invention of various living radical polymerization (LRP) techniques induced great excitement about the possibilities of synthesizing polymeric materials with advanced architectures, and precisely controlled chain length^{1,2,3}. In comparison to the well-known living anionic polymerization the choice of monomers is much wider, and in terms of polymerization conditions, LRP also offers great advantages. Among the most versatile LRP techniques is Reversible Addition-Fragmentation Chain Transfer (RAFT) mediated polymerization¹. However, this technique is sometimes hampered with inhibition-like phenomena^{2,3} as well as with retardation phenomena⁴. For RAFT-mediated homopolymerization it was earlier shown that the original RAFT-agent is converted into its single monomer adduct in a highly selective reaction, which is schematically depicted in Scheme 1.^{5,6} This selective reaction was termed initialization, and appears to be dependent on monomer type and type of RAFT-agent. This then also raises the question about the effect of initialization on RAFT-mediated copolymerization.



Scheme 1. A schematic representation of the initialization process in which primary radicals ($A\cdot$) react with styrene (S), and this adduct in turn reacts with the RAFT-agent (AD) to form the intermediate radical ($ASD(\cdot)A$). Upon fragmentation, the single monomer adduct (ASD) is formed and a leaving group-based radical ($A\cdot$) that can again react with monomer to form ($AS\cdot$), etc. A similar process is shown for acrylonitrile (Ac)

In earlier work on Atom Transfer Radical Copolymerization it was already shown that the early stages of the chain growth can deviate from the long chain limit.^{7,8,9} From modeling studies it was clearly shown that this effect is most likely due to selectivity of the primary radical for addition to the one or the other comonomer in combination with differences in the equilibrium between active and dormant chains for the two different terminal monomer units.

Initialization in RAFT-mediated homopolymerization In order to understand copolymerization results, a brief summary of recent discoveries on initialization of RAFT-mediated homopolymerizations will be presented. The investigations into initialization were aimed at unraveling the origin of reported inhibition effects during RAFT-mediated polymerization. Quickly it turned out that this initial period was not a true inhibition period. It is a period in which one monomer unit is inserted in the RAFT-agent between the leaving group and the sulphur atom. In some cases, such as the dithiobenzoate mediated polymerization of methyl acrylate, some chain growth starts to take place before the complete consumption of the RAFT-agent⁵. However, in the dithiobenzoate mediated polymerization of styrene, the decrease in RAFT-agent concentration is pseudo-zero order in RAFT-agent concentration^{6,10}.

From these results it was concluded that the rate-determining step during initialization is the addition of the leaving group radical to monomer. In Figure

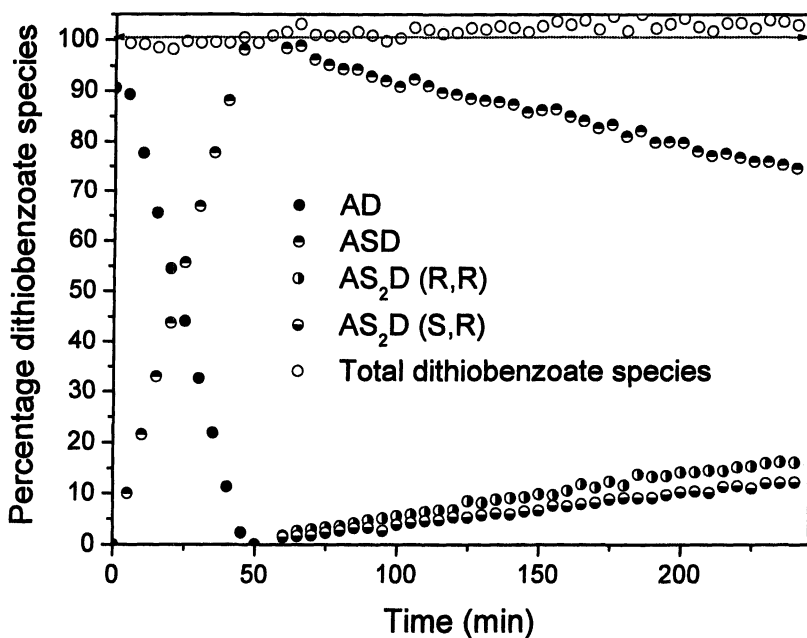


Figure 1. Relative concentrations of methyl protons of dithiobenzoate species versus time in the in situ free radical polymerization of styrene at 70 °C. Cyanoisopropyl dithiobenzoate was used to mediate the polymerization in the presence of AIBN as an initiator. $3.56 \cdot 10^{-3}$ mol C_6D_6 , $6.75 \cdot 10^{-5}$ mol AIBN, $2.40 \cdot 10^{-3}$ mol styrene, $4.84 \cdot 10^{-4}$ mol cyanoisopropyl dithiobenzoate. AD is the original RAFT-agent, and AS_iD is the RAFT agent with i styrene units inserted. (Reproduced from reference 9. Copyright 2004 American Chemical Society.)

1, a typical example is shown of a cyanoisopropyl dithiobenzoate mediated styrene polymerization. In this polymerization, the initiator-derived primary radicals (cyanoisopropyl radicals, derived from AIBN as initiator) are identical to the leaving group radicals⁶. This makes the interpretation of the NMR spectra somewhat less complicated compared to the system of dissimilar radicals. However, the main conclusions appear to be independent of this variation.

Experimental

Chemicals Styrene (STY, 99.9%) (Protea Chemicals) was washed with a 0.3 M potassium hydroxide (KOH, 85%) (ACE) solution followed by vacuum distillation to remove the inhibitor and polymer. Acrylonitrile (AN, Aldrich, 99+%) was purified by filtration through a column filled with inhibitor remover for removing hydroquinone and monomethyl ether hydroquinone (Aldrich). Maleic anhydride (MAh, Aldrich, 99%, briquettes) was used as supplied. Solvents: Toluene (Hi-DryTM, anhydrous solvent, Romil Ltd), Methyl Ethyl Ketone (MEK, Merck, 99%), Tetrahydrofuran (THF, Aldrich, AR) were used without further purification. Azo-initiators: Azo bis(isobutyronitrile) (AIBN, Riedel De Haen) was recrystallized from AR grade methanol and found to be ~99% pure by ¹H NMR spectroscopy; 1,1'-azobis(1-cyclohexanecarbonitrile) (ACHN, Wako, >98%) was used as received. Deuterated solvent (C₆D₆ 99.6%, 0.1% TMS Sigma-Aldrich) and formic acid (96%, Sigma-Aldrich) were used as received.

Synthesis of transfer agents The synthesis of bis(thiobenzoyl) disulfide was carried out following the method of Thang *et al.*,¹ with the modifications of de Brouwer *et al.*² The synthesis of cyanoisopropyl dithiobenzoate (CiPDB) was carried out according to the method of Le *et al.*³ and purified by liquid chromatography on a silica column using a 9:9:2 vol. ratio of pentane: heptane: diethyl ether. The product was dried under vacuum to provide the compound with a ¹H NMR purity estimated at ~ 98%.

Sample preparation for styrene-*co*-acrylonitrile reactions A stock solution was prepared by mixing 0.99 g deuterated benzene, 40 mg AIBN (2.41×10^{-4} mol), 0.67 g STY (6.43×10^{-3} mol), 0.34 g AN (6.43×10^{-3} mol), and 0.29 g CiPDB (1.34×10^{-3} mol). The NMR tube was filled to an appropriate level with the stock solution. The tube was flushed with ultra-high purity nitrogen for 10 minutes. At this point a sealed glass insert containing the integration referencestandard (formic acid) was inserted and the tubes were sealed. The use of the reference standard was solely for integration purposes.

Synthesis of poly(styrene-*alt*-maleic anhydride), SMAh A typical copolymerization of styrene (STY) and maleic anhydride (MAh) was carried out

as follows: 0.132 g of the RAFT-agent, (CIPDB, 5.97×10^{-4} mol) and 14.2 mg of the azo-initiator, (ACHN, 5.82×10^{-5} mol) were accurately weighed, and transferred into a 15-mL, three-necked, round-bottom flask equipped with a magnetic stirrer. 6.02 g of MEK was added as a solvent[‡], followed by the addition of monomers: 0.744 g MAH (7.59×10^{-3} mol) and 0.889 g STY (8.55×10^{-3} mol). After the reaction mixture was bubbled with argon for 45 min, an initial sample was removed for gas chromatography (GC) analysis and the flask was immersed in a thermostated oil bath kept at 70 °C, as the reaction temperature. The reaction was carried out under an argon atmosphere. After 12 hrs the reaction was stopped by exposing it to air, and conversion of styrene was 62%, determined by GC analysis. The final reaction mixture was precipitated in an excess of n-heptane (5-fold volumetric excess with respect to the total polymer solution) and then dried under vacuum at 30 °C overnight. 100 mg of dried polymer was dissolved in 10 mL of THF and used for SEC analysis, to determine a molar mass ($M_{n,SEC}$) and a polydispersity index (PDI): $M_{n,SEC} = 1927$ g/mol and PDI = 1.12. MALDI analysis was also performed using a similar solution of polymer in THF (1mg/mL).

Analysis

Determination of monomer conversion by GC Monomer, STY conversion was determined by a gas chromatography (GC). Hewlett-Packard (HP-5890) GC, equipped with an AT-Wax capillary column (30 m \times 0.53 mm \times 10 μ m) was used, employing the GC gradient (see Table 1). Toluene was employed as an internal standard.

$M_{n,SEC}$ and PDI were measured by size exclusion chromatography (SEC), at ambient temperature using a Waters GPC equipped with Waters model 510 pump and a model 410 differential refractometer. Tetrahydrofuran, THF (Biosolve, stabilised with BHT) with 5 wt% of acetic acid¹¹ was used as the eluent at a flow rate of 1.0 mL/min. A set of two mixed bed columns (Mixed-C, Polymer Laboratories, 30 cm, 40 °C) was used. Calibration was carried out using narrow molar mass distribution polystyrene (PSTY) standards ranging from 600 to 7×10^6 g/mol. The masses were calculated using the PSTY calibration curve. Samples were filtered over a 13 mm \times 0.2 μ m PTFE filter, PP housing, Alltech. Data acquisition and processing were performed using WATERS Millennium32 (v3.2 or 4.0) software.

[‡] Toluene was added (5 wt% related to MEK) as the internal standard, for the GC analysis.

Table 1. GC temperature gradient

| Temperature (°C) | 40 | 110 | 220 |
|-------------------|----|-----|-----|
| Time (min) | 5 | 0 | 2 |
| Rate (°C / min) | 10 | 25 | |

Matrix Assisted Laser Desorption/ Ionization – Time Of Flight – Mass Spectrometry (MALDI-ToF-MS) MALDI-ToF-MS analysis was carried out on a Voyager DE-STR from Applied Biosystems. The matrix trans-2-[3-(4-tert-butylphenyl)-2-methyl-2-propenylidene]malononitrile (DCTB) was synthesized according to literature procedures.¹² Potassium trifluoroacetate (PTFA, Aldrich, >99%) was added as cationization agent. The matrix was dissolved in THF at a concentration of 40 mg/mL. The PTFA salt was added to THF at typical concentrations of 1 mg/mL. Polymer was dissolved in THF at approximately 1mg/mL. In a typical MALDI-ToF-MS analysis the matrix, salt and polymer solution were premixed in a ratio of 10:1:5. The premixed solutions were handspotted on the target well and left to dry. Spectra were recorded in both the linear mode and reflector mode. Additionally, the obtained data were analyzed using in-house developed software.

¹H Nuclear Magnetic Resonance (¹H NMR) analysis NMR spectra were recorded on a 600 MHz Varian ^{Unity}Inova spectrometer. A 5 mm inverse detection PFG probe was used for the experiments and the probe temperature was calibrated using an ethylene glycol sample in the manner suggested by the manufacturer using the method of Van Geet.⁴ ¹H spectra were acquired with a 3 μs (40°) pulse width and a 4 sec acquisition time. For the ¹H kinetic experiments, samples were inserted into the magnet at 25 °C and the magnet fully shimmed on the sample. A spectrum was collected at 25 °C to serve as a reference. The sample was then removed from the magnet and the cavity of the magnet was raised to the required temperature. Once the magnet cavity had stabilized at the required temperature, the sample was re-inserted (time zero) and allowed to equilibrate for approximately 5 minutes. Additional shimming was then carried out to fully optimize the system and the first spectra were recorded less than 10 min after the sample was inserted into the magnet. Peak assignment was carried out via model compounds and first principles, and automated integration was carried out using ACD Labs 8.0 ¹H processor® using manual peak selection and reintegration to account for overlapping peaks.

Results and Discussion

The *in situ* ^1H NMR experiment was conducted in a fashion similar to our previous homopolymerization experiments^{6,10}. However, the resulting NMR spectra are considerably more complex due to the presence of two different monomers. As an example, Figures 2a – 2d show an expansion of the NMR spectra at 5, 30, 60 minutes and 180 minutes. The signals in this part of the NMR spectra are assigned to the ortho protons of the phenyl group of the dithiobenzoate. At time $t = 5$, the spectrum is largely that of the original cyanoisopropyl dithiobenzoate. Time $t = 30$ minutes coincides with the end of the initialization period. At this point, the original RAFT-agent is fully converted into a small number of specific monomeric or oligomeric polymer chains. After that, polymerization starts and at $t = 60$ minutes it is clear that a number of different species are beginning to form, and at time $t = 180$ minutes the reaction is stopped and the presence of numerous dithiobenzoate species is clear. From the differences among the spectra it is obvious that large differences exist in terms of monomer units neighbouring the thiocarbonyl thio moiety.

Detailed investigation, and comparison with the styrene homopolymerization study leads to the observation that addition of the primary radicals to both monomers occurs in the system to produce two mono-adducts, one derived from styrene and one from acrylonitrile. Figure 2a shows that the two forming mono-adducts are formed in unequal amounts. In Figure 3, the decrease in the styrene and acrylonitrile signals are depicted. It is clear that the initial consumption rates of acrylonitrile and styrene monomer are larger than the rates of consumption after initialization is completed, *i.e.* after 30 minutes. The consumption of monomer prior to initialization is driven by the addition of cyanoisopropyl radicals to the respective monomer units. It is also clear that the predominant mono-adduct that is formed is derived from styrene and this was confirmed by comparison of chemical shifts of species to the homopolymerization studies. One more remarkable point in Figure 3, especially after initialization, is that the styrene concentration decreases linearly with time, whereas that of acrylonitrile seems to fluctuate to some extent. This fluctuation seems to diminish somewhat towards larger reaction times. It is therefore likely that the fluctuation in acrylonitrile consumption rate is caused by chain length dependence of the propagation and chain transfer reactions. In Figure 4, the concentration profiles of the four most prominent adducts are shown. It is apparent that the ratio of the mono-styrene adduct to the mono-acrylonitrile adduct is reasonably constant during the initialization period. This is a fairly logical consequence of the selectivity of the cyanoisopropyl radical towards styrene and acrylonitrile. At approximately 30 minutes both single monomer adducts reach a maximum. The chain extension of the mono-acrylonitrile adduct with a styrene unit commences already from time zero, but there is a significant increase in the rate of this reaction at $t = 30$ minutes. Conversely, the addition of

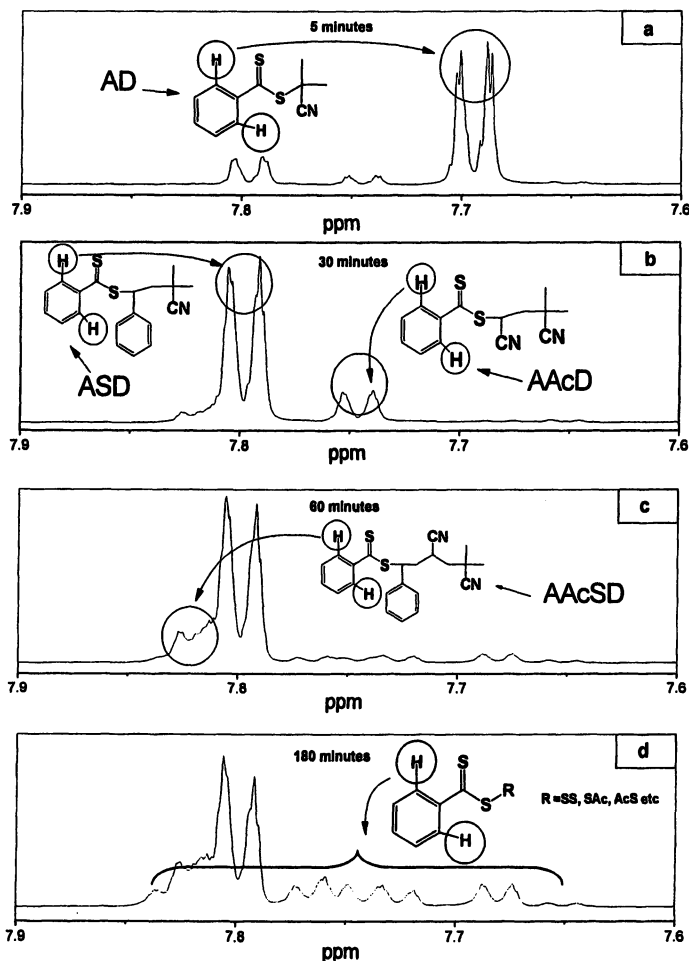


Figure 2a-2d. Expansion of the ^1H NMR spectra taken during the STY/AN ymerization after 5, 30, 60 and 180 minutes reaction time.

an acrylonitrile unit to the mono-styrene adduct does not take place to any measurable extent before the completion of initialization. It is tempting to draw further conclusions with respect to the origin of this difference. One might argue that the large selectivity of the formation of the single monomer adduct is stronger for the styrene adduct than for the acrylonitrile adduct.

However, this would be a premature conclusion, since there are two ways to arrive at the dimer adduct. The one way is the reactivation of a single monomer adduct, and the subsequent formation of a dimer adduct. The other way is the addition of two monomers to the initiating cyanoisopropyl radical before

addition to the RAFT-agent. Subsequent release of the leaving group from the intermediate radical leads to the formation of the dimer adduct. A similar question applies for example to the dithiobenzoate mediated polymerization of methyl acrylate. Without additional information it is impossible to distinguish between the two scenarios. This will definitely be subject of future investigations.

At $t = 60$ minutes the initial acrylonitrile mono-adduct has been consumed, predominantly by the addition of a styrene monomer unit. At this point the rate of acrylonitrile consumption in the reaction changes, as seen in Figure 3. Although a number of species are not presented in Figure 4 it becomes clear that the nature of the propagating radical and its addition rate coefficients to the respective monomers as well as related intermediate radicals have a significant effect on the rate of consumption of the respective monomers with strong changes in rates of monomer consumption possible early in RAFT mediated copolymerization.

The oligomers with a terminal acrylonitrile unit present a shorter lifetime than those with a terminal styrene unit (the role played by the intermediate radical species in affecting the propagating radical concentrations cannot be discounted, meaning that a simplistic comparison of propagation rates could lead to misleading conclusions), this has significant implications to the distribution of the monomer units within the polymeric chains and longer chain polymers would need to be investigated to confirm whether this effect is only observed at short chain lengths. The effect of selectivity of the primary radical is also clearly seen when the copolymerization of STY and maleic anhydride (MAh) is studied. This copolymerization has a large tendency towards alternation. Previous work where pulsed laser polymerization (PLP) was applied to the STY/MAh copolymerization has unambiguously shown that the penultimate unit model is the suitable model to describe this copolymerization¹³.

Furthermore, on the basis of the reactivity ratios it can easily be estimated that over the majority of the comonomer feed range, the terminal unit in a growing polymer chain is STY for more than 90%. Recent results from Kajiwara and co-workers¹⁴ at first glance seem to be in contradiction with this observation. They carried out RAFT-mediated copolymerization of STY and MAh, and determined the nature of the intermediate radical by ESR spectroscopy. It was convincingly shown that the intermediate radical carries a MAh terminal unit at both sides. However, this finding is not necessarily in contradiction with the large fraction of STY terminal chain ends reported in conventional copolymerization. The nature of the propagating radical in the reaction may be predominantly styrenic while the intermediate radical is strongly MAh on both sides. This would be the case if addition of a MAh chain end radical to a macro-RAFT agent is of larger or comparable rate as its addition to a STY monomer, and simultaneously the fragmentation rate to form a MAh terminal chain end radical is smaller than that to form a STY terminal chain end radical.

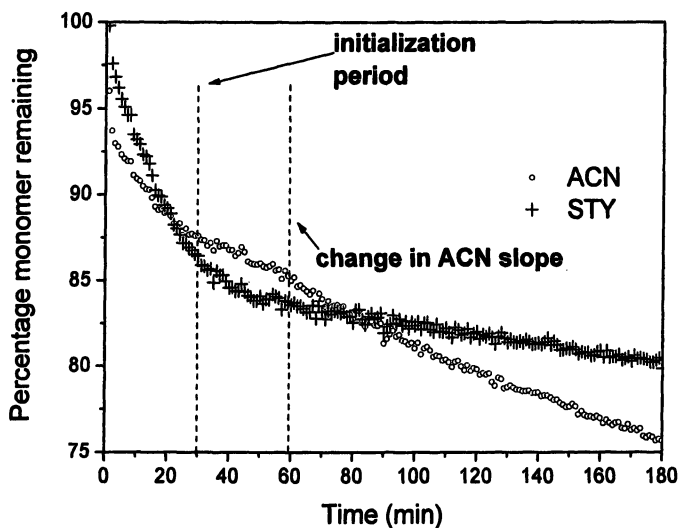


Figure 3. Concentration versus time profiles for STY (+) and for AN (o) during the copolymerization of STY and AN.

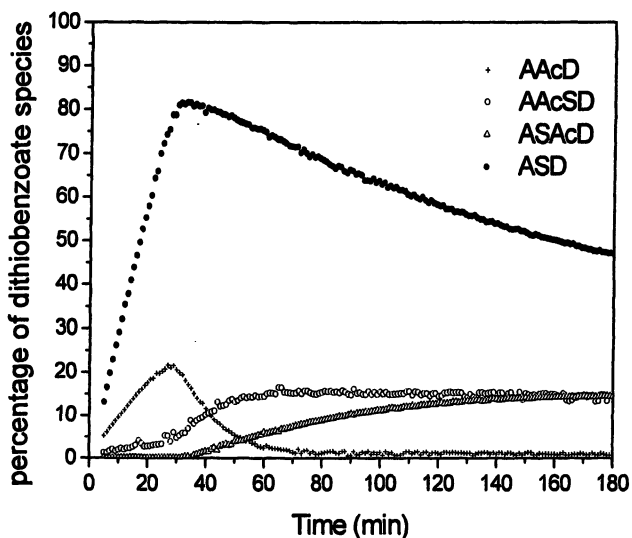


Figure 4. Concentration versus time profiles during the copolymerization of STY and AN for single monomer adducts (AAcD and ASD), and dimer adducts (AAcSD and ASAcD), where A and D are the cyanoisopropyl and dithiobenzoate moieties, respectively.

Figure 5 shows the MALDI-ToF mass spectrum of a STY – MAh copolymer. The copolymer was synthesized via cyanoisopropyl dithiobenzoate mediated copolymerization. With the help of an in-house developed software tool¹⁵ we analyzed the mass spectrum and obtained a copolymer fingerprint as shown in Figure 6.

It is easily recognized that the number of STY units in the copolymer is typically one larger than the number of MAh units. If it is taken into account that the polymerization is a virtually ideal alternating copolymerization, the $n_{\text{STY}} = n_{\text{MAh}} + 1$ signature of this fingerprint can only originate from the very first one or

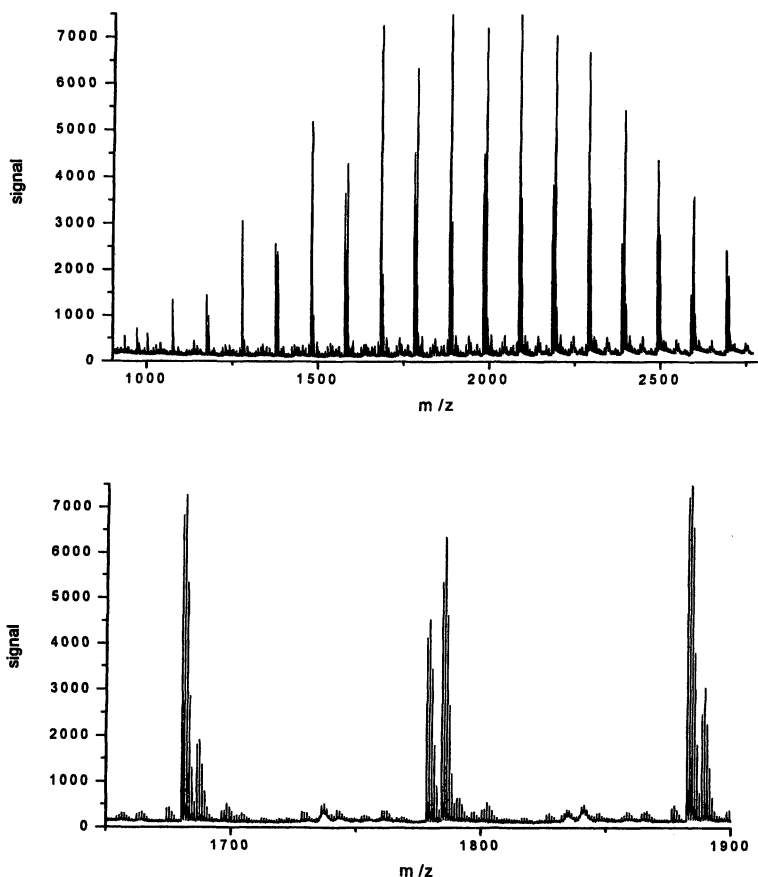


Figure 5. MALDI-ToF Mass spectrum of an alternating STY-MAh copolymer, and an expansion thereof. The polymer was synthesized in a cyanoisopropyl dithiobenzoate mediated polymerization.

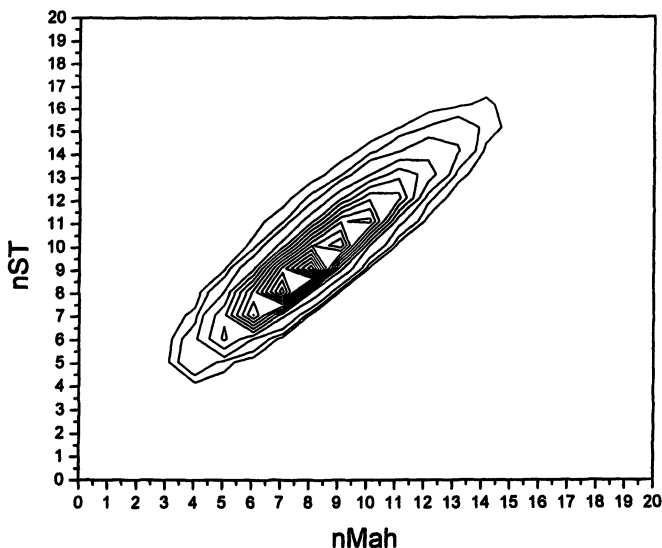


Figure 6. Copolymer fingerprint of the STY – MAh copolymer shown in Figure 5.

two monomer addition steps. Moreover, if the polymerization is mediated by a cumyl dithiobenzoate it is immediately recognized that the fingerprint show a maximum at $n_{\text{STY}} = n_{\text{MAh}}$ (result not shown). Again, this points at the importance of the first monomer additions. After a few monomer additions, the effect of the cyanoisopropyl or cumyl chain end is no longer a factor in determining the reactivity of the growing chain end.

Conclusions

Initialization occurs in RAFT-mediated copolymerization just like it does in RAFT-mediated homopolymerizations. This was convincingly shown using *in situ* ^1H NMR spectroscopy during the RAFT-mediated copolymerization of STY and AN. From the same experiment, indications are obtained that the selectivity of the initial additions of the leaving group radical to both comonomers plays an important role in the early stages of RAFT-mediated polymerization. This is similar to the initiator effect in Atom Transfer Radical Copolymerization as was seen before. Further evidence for this effect of the initiating radical was obtained from the RAFT-mediated copolymerization of STY and MAh.

References

1. Matyjaszewski, K. *Controlled Radical Polymerization*; ACS Symp. Ser. 685, ACS, Washington, D.C., 1998
2. Matyjaszewski, K. *Controlled/Living Radical Polymerization, Progress in ATRP, NMP, and RAFT*; ACS Symp. Ser. 768, ACS, Washington, D.C., 2000
3. Matyjaszewski, K. *Advances in Controlled/Living Radical Polymerization*; ACS Symp. Ser. 854, ACS, Washington, D.C., 2003
4. Chiefari, J.; Chong, Y. K. B.; Ercole, F.; Krstina, J.; Jeffery, J.; Le, T. P. T.; Mayadunne, R. T. A.; Meijs, G. F.; Moad, C. L.; Moad, G.; Rizzardo, E.; Thang, S. H. *Macromolecules* 1998, **31**, 5559-5562
5. Monteiro, M. J.; de Brouwer, H. *Macromolecules* 2000, **34**, 349-352.
6. Vana, P.; Davis, T. P.; Barner-Kowollik, C. *Macromol. Theory Simul.* 2002, **11**, 823-835.
7. Perrier, S.; Barner-Kowollik, C.; Quinn, J. F.; Vana, P.; Davis, T. P. *Macromolecules* 2002, **35**, 8300-8306.
8. McLeary, J. B.; McKenzie, J. M.; Tonge, M. P.; Sanderson, R. D.; Klumperman, B. *Chem. Comm.* 2004, 1950-1951.
9. McLeary, J. B.; Calitz, F. M.; McKenzie, J. M.; Tonge, M. P.; Sanderson, R. D.; Klumperman, B. *Macromolecules* 2004, **37**, 2383-2394
10. Klumperman, B.; Chambard, G.; Brinkhuis, R.H.G. in *Advances in Controlled/Living Radical Polymerization*; ACS Symp. Ser. 854, ACS, Washington, D.C., 2003, 180-192.
11. Ziegler, M.J.; Matyjaszewski, K. *Macromolecules* 2001, **34**, 415-424.
12. Matyjaszewski, K. *Macromolecules* 2002, **35**, 6773-6781.
13. McLeary, J. B.; Calitz, F. M.; McKenzie, J. M.; Tonge, M. P.; Sanderson, R. D.; Klumperman, B. *Macromolecules* 2005, **38**, 3151-3161
14. Tacx, J.C.J.F.; Meijerink, N.L.J.; Suen, K. *Polymer* 1996, **37**, 4307-4310.
15. Ulmer, L.; Mattay, J.; Torres-Garcia, H. G.; Luftmann, H. *Eur. J. Mass Spectrom.* 2000, **6**, 49-52.
16. Sanayei, R.A.; O'Driscoll, K.; Klumperman, B. *Macromolecules* 1994, **27**, 5577-5582.
17. Du, F.-S.; Zhu, M.-Q.; Guo, H.-Q.; Li, Z.-C.; Li, F.-M.; Kamachi, M.; Kajiwara, A. *Macromolecules* 2002, **35**, 6739-6741
18. Willemse, R. X. E.; Staal, B. B. P.; Donkers, E. H. D.; van Herk, A. M. *Macromolecules* 2004, **37**, 5717-5723.

Chapter 35

RAFT Copolymerization and Its Application to the Synthesis of Novel Dispersants– Intercalants–Exfoliants for Polymer–Clay Nanocomposites

Some Interesting Results from RAFT (Co)polymerization

Graeme Moad^{1,2}, Guoxin Li^{1,2}, Rudolf Pfaendner^{1,3},
Almar Postma^{1,2}, Ezio Rizzardo^{1,2}, San Thang¹,
and Hendrik Wermter^{1,3}

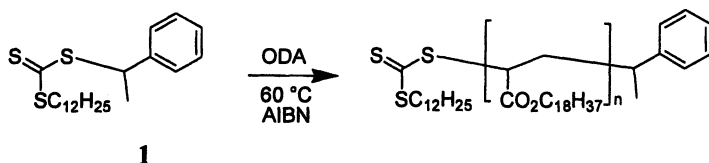
¹CRC for Polymers and ²CSIRO Molecular and Health Technologies,
Bag 10 Clayton South, Victoria, Australia

³Ciba Specialty Chemicals Inc., Lampertheim, Germany

This paper will discuss aspects of (co)polymerization of acrylates with reversible addition-fragmentation chain transfer (RAFT). An explanation for bimodal molecular weight distributions observed when making high molecular weight acrylic polymers with narrow molecular weight distributions ($\bar{M}_w/\bar{M}_n \leq 1.1$) at high conversion involves copolymerization of the macromonomer formed by backbiting- β -scission. Evidence for this mechanism is provided. RAFT copolymerization is illustrated by the synthesis of novel copolymer intercalants/ exfoliants/dispersants for unmodified layered silicates (sodium montmorillonite) in polypropylene (PP) nanocomposites. Block and gradient copolymers were prepared based on a long chain acrylate (e.g. octadecyl acrylate, ODA) and various polar comonomers (e.g. acrylic acid, dimethylaminoethyl acrylate, maleic anhydride, methacrylic acid, *N*-vinyl pyrrolidone).

Polymerization with reversible addition fragmentation chain transfer (RAFT polymerization) with thiocarbonylthio compounds (dithioesters, trithiocarbonates, xanthates, dithiocarbamates) as RAFT agents was first described in 1998 (1) and has emerged as one of the most versatile processes for conferring living characteristics on a radical polymerization (2). The overall process involves insertion of monomer units into the C-S bond of an organic thiocarbonylthio compound as shown in the following Scheme. This means that end groups are retained and the polymer product is also a RAFT agent. This, in part, accounts for the living characteristics of RAFT polymerization.

Scheme 1



The differences between and similarities of a conventional radical polymerization and one carried out in the presence of an effective RAFT agent can be summarized as follows:

- Both processes are chain reactions with chains being continuously initiated and terminated. A source of initiating radicals is required.
- In RAFT there is a similar number of kinetic chains to conventional but a much greater number of polymer chains (moles polymer chains \sim moles RAFT agent).
- In RAFT: Degree of polymerization \sim [monomer consumed]/[RAFT agent].
- In RAFT most chain ends are living (dormant). Fast activation/deactivation processes cause rapid equilibration between living chains.
- In RAFT all chains grow simultaneously, molecular weight distributions are narrow.
- Both processes are compatible with a wide range of unprotected functionalities (these include: poly(ethylene glycol), carboxylic acid, phosphonic acid, anhydride, tertiary amine, pyridine, quaternary amine, amide).
- Copolymers synthesized by RAFT show remarkable homogeneity in both composition and molecular weight when compared to copolymers made by conventional copolymerization.

RAFT polymerization of acrylates

The origin of humps. Many papers have appeared on RAFT polymerizations of acrylates (5,10-12). Bimodal or multimodal molecular weight distributions are sometimes observed in RAFT polymerization of acrylate esters (10,13) and certain other monomers. In some cases, (e.g. styrene polymerization (10) *N,N*-dimethyl acrylamide polymerization (14)) this has been rationalized in terms of by-products by radical-radical termination involving the propagating species.

The evolution of the molecular weight distribution as a function of conversion for a RAFT polymerization with trithiocarbonate **3** is shown in Figure 1 (15). A high molecular weight shoulder with peak molecular weight approximately twice that of the main peak is clearly evident for conversions >60%. The size of the shoulder is such that it cannot be wholly explained as a by-product from combination of propagating radicals. Moreover, it is clear from the UV-visible spectrum that the shoulder contains a trithiocarbonate chromophore. The product from radical-radical termination by combination would not contain a trithiocarbonate group thus it should not appear in a GPC trace when UV detection at 305 nm is employed.

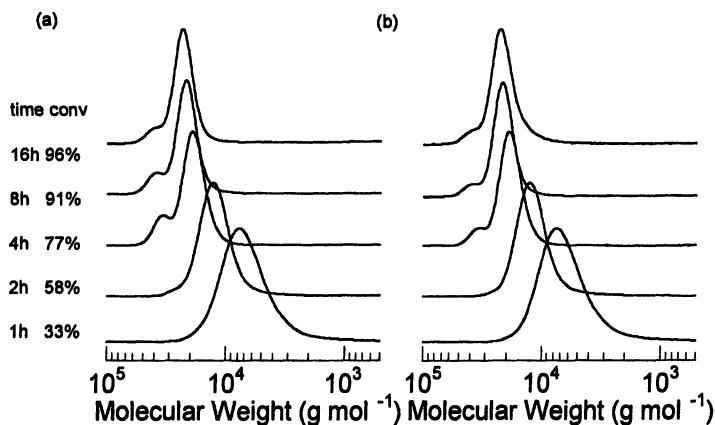


Figure 1. Normalized GPC traces at various reaction times/conversions for RAFT polymerization of *n*-butyl acrylate with trithiocarbonate **3** (a) UV detection at 220 nm and (b) UV detection at 305 nm.

The RAFT agent **3** has two chromophores, the trithiocarbonate of the 'ZC(=S)S' group with absorption at ~305 nm and a phthalimido group on the 'R' group with absorption at ~220 nm and a much weaker absorption at ~292 nm. While polymer of the main peak has R:Z in the expected ~ 1:1 ratio, the high molecular weight shoulder has these groups in ~ 2:1 ratio (Figure 2). In a previous paper, we proposed that this shoulder might arise by copolymerization

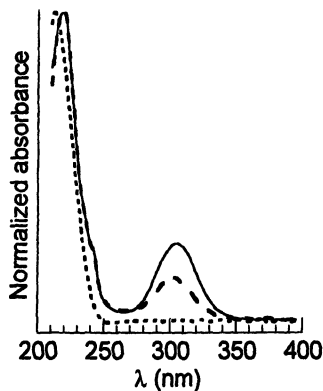


Figure 2. Normalized UV spectra of poly(*n*-butyl acrylate) with trithiocarbonate **3** (4hr, 77% conv) in tetrahydrofuran (extracted from GPC data). The main peak (—) and the high molecular weight shoulder (---) are compared to a conventional poly(*n*-butyl acrylate) (····). Trithiocarbonate absorption maximum at 305 nm, phthalimide absorption maximum at 220 nm, poly(*n*-butyl acrylate) maximum at 200 nm.

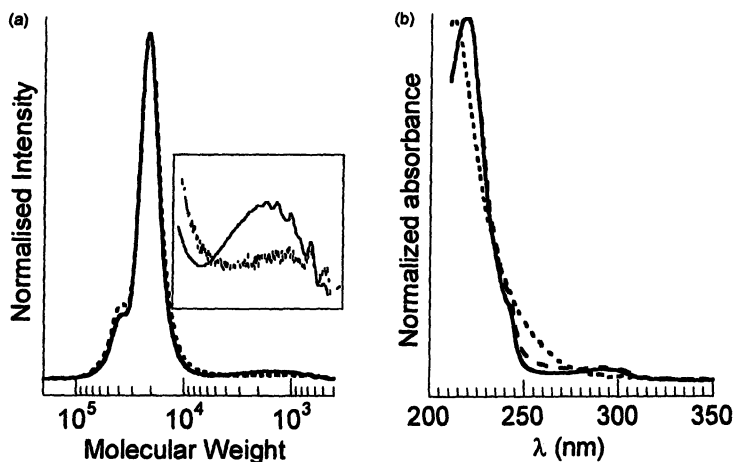
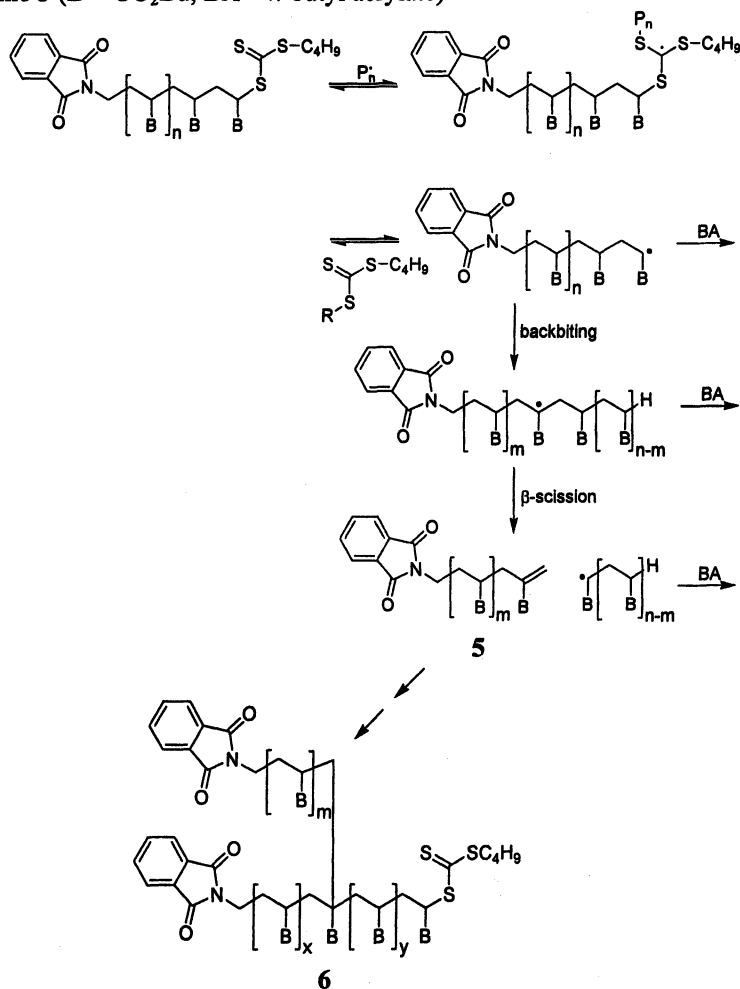


Figure 3. (a) Normalized GPC traces with UV detection at 292 nm (····) and RI detection (—) for poly(*n*-butyl acrylate) with trithiocarbonate **3** (4hr, 77% conv) after thermolysis at 220 °C under nitrogen (inset is a 10× vertical expansion) and (b) normalized UV traces in tetrahydrofuran solvent (extracted from GPC data) for: the main peak (—) and the high molecular weight shoulder (---) and the oligomer fraction (····).

of the macromonomer **5** which is formed by backbiting- β -scission as shown in Scheme 3. The present data are entirely consistent with this hypothesis and with the shoulder being due to polymer with structure **6**.

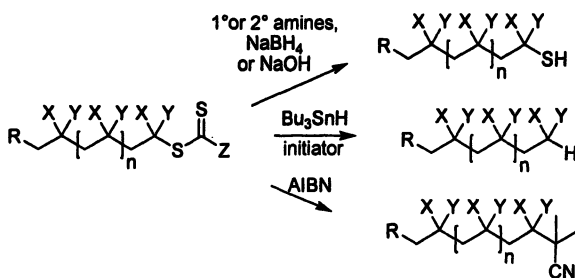
Scheme 3 (B = CO₂Bu, BA = *n*-butyl acrylate)



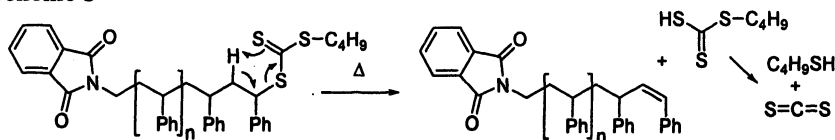
RAFT end-group removal. Some of the possibilities for removal of the thiocarbonylthio end group from RAFT-synthesized polymers are shown in Scheme 4 (2). They include hydrolysis or aminolysis (1,7) and radical-induced

reduction (7,16) or group exchange (11,17). We have recently shown that thermolysis is a convenient way of cleanly removing a trithiocarbonate group from the end or within a polymer chain (7,18). In the case of polystyrene the mechanism is believed to involve an elimination reaction which occurs selectively as shown in Scheme 5 (18). The thermolysis of xanthate terminated polymers has also been reported (19). For the case of both *S*-polystyrene and *S*-poly(*t*-butyl acrylate) *O*-isobutyl xanthate, the mechanism involves selective elimination to provide 2-butene and a polymer with a thiol end group.

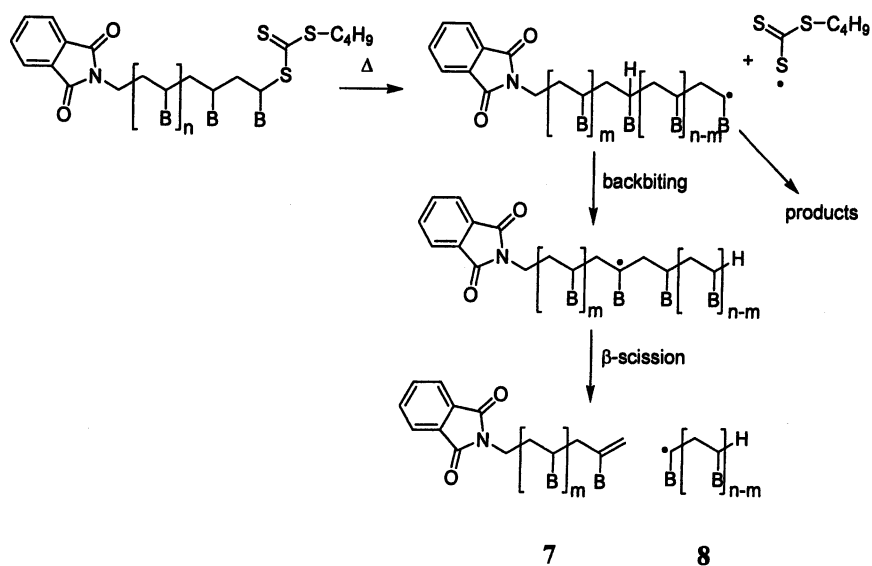
Scheme 4



Scheme 5



In contrast, with poly(*n*-butyl acrylate) (PBA) end group loss is thought to involve initial C-S bond homolysis followed by backbiting- β -scission as shown in Scheme 6 (18). Examination of the product post-thermolysis by GPC with UV detection shows that the trithiocarbonate group is gone and that the high molecular weight shoulder contains twice the number of phthalimido groups as the main peak (main peak has structure 7 while the shoulder is derived from 6). The oligomer fraction (derived from 8) contains few phthalimido residues so appears of reduced intensity in the trace with UV vs RI detection (Figure 3). This suggests that fragmentation following consecutive backbiting events occurs specifically to give a low molecular weight radical and a high molecular weight macromonomer. Such specificity is also observed when backbiting- β -scission occurs during polymerization as has been attributed to steric factors.

Scheme 6 (B=CO₂Bu)

RAFT copolymerization

One of the major advantages of radical polymerization over most other forms of polymerization is that statistical copolymers can be prepared from a very wide range of monomer types that can contain various unprotected functionality. RAFT polymerization retains these advantages.

Although, there are reports on differences in reactivity ratios in living (20-25) vs conventional radical copolymerization, most reports suggest that reactivity ratios are identical in living and conventional radical polymerization. In comparing observed reactivity ratios in living vs conventional polymerization systems it is important to take into account the effect of molecular weight on copolymer composition (24-27). In a conventional polymerization the molecular weight is typically high even at low conversion. In a living polymerization molecular weights are low at low conversion and increase with conversion. When molecular weights are very low, the initiator process influences the overall copolymer composition. The effects of specificity in the initiation and termination process on copolymer composition are known.

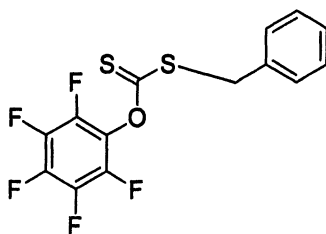
Copolymers produced by living polymerization processes differ from those produced by conventional polymerization in one important aspect. Living polymerization processes produce gradient or tapered copolymers. Disparity in reactivity ratios causes the composition of the monomer feed to drift with conversion. As a consequence, in conventional radical copolymerization the copolymer macromolecules formed at the beginning of the experiment will be different from those formed at higher monomer conversion; the high conversion product is a polymer blend. In a living polymerization process compositional drift is captured within each chain. The copolymer will have a blocky character and the degree of blockiness will depend on the disparity of the reactivity ratios.

If reactivity ratios are particularly disparate then it is possible to form a block copolymer from a batch polymerization. Thus the copolymerization of MAH with styrene by NMP (28) or RAFT (29,30) with excess styrene provides P(MAH-*alt*-styrene)-block-PS. There is a similar outcome in other copolymerizations which show a strong alternating tendency such as styrene with maleimides or acrylonitrile (AN) (2). The copolymerization of *t*-butyl acrylate (tBA) with vinyl acetate (VAc) by RAFT provides P(tBA-*stat*-VAc)-block-VAc (2,31).

A related issue is that differences in the activation and deactivation processes for the propagating species with different monomers at the chain ends may also affect copolymer composition, particularly when conversion is very low or very high or the rates of activation are very disparate. RAFT polymerization of MMA with benzyl dithiobenzoate provides very poor control (13) yet copolymerizations of styrene with MMA succeed while there is styrene in the monomer feed.

Exfoliants/Intercalants/Dispersants for Polymer-Clay Nanocomposites

A series of copolymers all based on long chain acrylates or methacrylates but of differing composition, molecular weight and architecture (homopolymers, statistical copolymers, block copolymers and gradient copolymers) were prepared using RAFT agents 1, 3 or 9. All allowed the preparation of high conversion poly(octadecyl acrylate) (PODA) with a narrow molecular weight distribution ($\overline{M}_w / \overline{M}_n$ generally < 1.3). Typical polymerization procedures have been given elsewhere (32).



9

Octadecyl acrylate (ODA) was chosen because of the known compatibility of ODA and ODMA based polymers with hydrocarbons including PP. Copolymers based on dodecyl acrylate (DA) were also effective. However, copolymers based on lower acrylates (BA) were poorer dispersants. ODA copolymers, being solids (mp ~ 60 °C), were easier to handle and were more readily purified than DA copolymers. There are previous reports of the preparation of ODA or octadecyl methacrylate (ODMA) copolymers using ATRP (33-37) or RAFT (38) though not of the compositions considered here. The RAFT process has an advantage in allowing very high monomer conversions to be readily achieved. This was important both from an economic point of view because of the proposed industrial application and because the polymers were difficult to separate from unreacted ODA. Functional (clayophilic) comonomers used included acrylic acid (AA), methacrylic acid (MAA), glycidyl methacrylate (GMA), 2-(dimethylamino)ethyl acrylate (DMAEA), *N*-vinylpyrrolidone (NVP) and maleic anhydride (MAH), ω -methyl[poly(ethylene glycol)] acrylate (PEGMA), 2-(2-methoxyethoxy)ethyl acrylate (DEGMA) A summary of the polymers prepared is provided in Table 1 (block copolymers) and Table 2 (gradient copolymers). The DMAEA copolymers were used directly or were quaternized with HCl, methyl iodide or *n*-butyl bromide. Copolymerization reactivity ratios which would enable prediction of composition of ODA gradient copolymers have yet not been determined and only limited data is available in the literature (39-42).

Table 1. Properties of block copolymers synthesized by RAFT Polymerization

| Block Polymer/RAFT Agent ^a | DP1 ^b | DP2 ^b | \bar{M}_n ^c | \bar{M}_w ^d | \bar{M}_w / \bar{M}_n ^d |
|--|------------------|------------------|--------------------------|--------------------------|--------------------------------------|
| 10 PODA/3 | 14.8 | - | 5200 | 5200 | 1.08 |
| 11 PODA- <i>b</i> -PDMAEA/3 | 14.8 | 3.7 | 5600 | 5400 | 1.09 |
| 12 PODA- <i>b</i> -PDMAEA | 13.3 | 1.7 | 4900 | 5900 | 1.08 |
| 13 PODA- <i>b</i> -PDMAEA/3 | 41.7 | 8.5 | 14800 | 15600 | 1.21 |
| 14 PODA- <i>b</i> -PNVP/9 | 21.6 | 2.9 | 7700 | ^f | ^f |
| 15 PODA- <i>b</i> -(PMMA- <i>co</i> -MAH) | 15.9 | 2.5/1.8 | 6000 | 5800 | 1.14 |
| 16 PODA- <i>b</i> -(PMA- <i>co</i> -MAA) ^e | 51.0 | 2.7/2.7 | 17400 | 13500 | 1.21 |
| 17 PODA- <i>b</i> -(PMAH- <i>co</i> -AA) ^e | 50.9 | 5.7/1.7 | 17500 | 12500 | 1.28 |

^a P(monomer A)-*b*-P(monomer B), for monomer abbreviations see text. PODA 1st block prepared to >95% monomer conversion with RAFT agent 1 and AIBN initiator at 60 °C in toluene (43). 2nd block prepared with addition of further monomer and AIBN initiator at 60 °C unless indicated otherwise. Monomer conversions were >95% after 60 h.

^b Average degree of polymerization from NMR analysis (DP1 = PODA block; DP2 = polar block).

^c \bar{M}_n from NMR based on end group determination.

^d \bar{M}_n and \bar{M}_w / \bar{M}_n from GPC (tetrahydrofuran 1 mL min⁻¹, 22 °C) in polystyrene equivalents. Molecular weight distributions were monomial in all cases.

^e Polymerization at 70 °C.

^f Polymer not compatible with tetrahydrofuran GPC.

The use of gradient copolymers (Table 2) as dispersants provided nanocomposites with slightly better tensile properties than statistical copolymers of similar molecular weight and composition prepared by conventional radical polymerization. This difference is attributed to greater uniformity of composition. An additional factor is that RAFT-synthesized copolymers had a narrow molecular weight distribution. Those prepared by conventional copolymerization (depending on the comonomer) had a very broad molecular weight distribution. Attempts were made to control molecular weight and dispersity using conventional chain transfer agents (thiols) but this proved problematical with certain comonomers (MAH). In the case of PODA-*co*-MAH, molecular weight control in conventional polymerization was achieved through the use of high initiator concentrations. Interestingly the block copolymers dispersants (Table 1) did not offer an advantage over gradient copolymers of nominally similar overall composition. While a polar comonomer was important, the identity of this comonomer appeared secondary and ~2 units/chain appeared sufficient. The optimal level of additive was 20-50 wt% of clay. Use of larger amounts gave improved dispersion in some cases but also caused a reduction in tensile properties as did use of the additive alone. The additives are effective as plasticizers for PP.

Table 2. Properties of gradient copolymers synthesized by RAFT polymerization

| Copolymer/RAFT Agent ^a | DP1 ^b | DP2 ^b | \overline{M}_n ^c | \overline{M}_w ^d | $\overline{M}_w / \overline{M}_n$ ^d |
|---|------------------|------------------|-------------------------------|-------------------------------|--|
| 18 PODA- <i>co</i> -DMAEA | 12.5 | 1.4 | 4600 | 5800 | 1.07 |
| 19 PODA- <i>co</i> -DMAEA/3 | 12.3 | 3.1 | 4700 | 5600 | 1.08 |
| 20 PODA- <i>co</i> -DMAEA | 19.3 | 3.8 | 6000 | 6300 | 1.06 |
| 21 PODA- <i>co</i> -DMAEA/3 | 30.0 | 7.0 | 11000 | 13700 | 1.20 |
| 22 PODA- <i>co</i> -DMAEA | 96.7 | 10.8 | 33500 | 34900 | 1.14 |
| 23 PODA- <i>co</i> -MAH ^e | 44.0 | 13.6 | 15000 | 6300 | 1.29 |
| 24 PODA- <i>co</i> -MAH ^f | 38.5 | 9.0 | 13800 | 10400 | 1.28 |
| 25 PODA- <i>co</i> -MAH ^e | 50 | 7.0 | 17300 | 7200 | 1.27 |
| 26 PODA- <i>co</i> -MAH ^e | 45.5 | 2.3 | 15400 | 8000 | 1.32 |
| 27 PODA- <i>co</i> -NVP/3 | 53.1 | 14.2 | 19250 | 16200 | 1.23 |
| 28 PODA- <i>co</i> -NVP ^g | 45.9 | 6.1 | 16000 | 14400 | 1.25 |
| 29 PODA- <i>co</i> -NVP | 41.7 | 6.0 | 17100 | 14600 | 1.16 |
| 30 PODA- <i>co</i> -MMA- <i>co</i> -MAH | 11.0 | 2.0/2.0 | 4300 | 5300 | 1.13 |
| 31 PODA- <i>co</i> -MAH- <i>co</i> -AA | 57.6 | 4.2/6.5 | 20000 | 12800 | 1.18 |
| 32 PODA- <i>co</i> -MA- <i>co</i> -MAA | 57.6 | 6.3/6.3 | 20200 | 14900 | 1.21 |
| 33 PODA- <i>co</i> -MAA | 59.3 | 6.0 | 20100 | 14500 | 1.21 |
| 34 PODA- <i>co</i> -MAA | 51.9 | 11.3 | 18200 | 13900 | 1.21 |
| 35 PDA- <i>co</i> -MAH ^e | 69.0 | 21.0 | 18900 | 4000 | 1.62 |
| 36 PODA- <i>co</i> -MEP ^e | 43.6 | 1.53 | 14900 | 8400 | 1.41 |
| 37 PODA- <i>co</i> -PEGMEA/3 | 26.1 | 6.6 | 11500 | 8800 | 1.16 |
| 38 PODA- <i>co</i> -DEGEEA | 12.5 | 1.4 | 4700 | 5900 | 1.06 |
| 39 PODA- <i>co</i> -GMA | 54.8 | 15.1 | 20300 | 15600 | 1.29 |
| 40 PODA- <i>co</i> -AN/9 | 41.7 | 21.0 | 7000 | h | h |

^a P(monomer A-*co*-monomer B), for abbreviations see text. Copolymers prepared by batch polymerization to >95% monomer conversion with RAFT agent 1 and AIBN initiator (10:1 mole ratio) at 60 °C in toluene unless indicated otherwise. Monomer conversions were >95% after 60 h

^b Average no of monomer units per copolymer chain from NMR analysis (DP1 = ODA or DA; DP2 = polar comonomer).

^c \overline{M}_n from NMR based on end group determination.

^d \overline{M}_n and $\overline{M}_w / \overline{M}_n$ from GPC (tetrahydrofuran 1 mL min⁻¹, 22 °C) in polystyrene equivalents.

^e Polymerization in tetrahydrofuran solvent at 60 °C.

^f Polymerization in toluene:2-butanone (1:1) solvent at 80 °C.

^g Polymerization at 80 °C.

^h Polymer insoluble in tetrahydrofuran.

Polypropylene (PP) nanocomposites were prepared by melt mixing unmodified sodium montmorillonite (Cloisite Na⁺), dispersant and PP to form a masterbatch containing up to 70% of the clay which was then processed with further PP to form a 5 wt% clay composite. The melt mixing steps were carried out with a twin screw extruder. The nanocomposite samples were then injection molded into standard dumbbells. The experimental protocol has been described elsewhere (32,44).

The visual appearance of nanocomposites containing 5 wt-% Cloisite Na⁺ and 1% acrylic copolymer is similar to those of 'benchmark' systems prepared with an organoclay (Cloisite 20A) with 7-15 wt-% PP-*graft*-MAH as compatibilizer. The state of clay dispersion for the nanocomposites was assessed by wide angle X-ray scattering and by scanning (SEM) and transmission electron microscopy (TEM). There was excellent dispersion and partial exfoliation as indicated by Figure 4 (SEM) and Figure 5 (TEM).

The nanocomposites based on unmodified clay (5 wt% Cloisite Na⁺) and our dispersants (1 wt %) showed similar improvements in modulus, of 20-30%, and were significantly more ductile than the reference nanocomposite based on Cloisite 20A) with PP-*graft*-MAH (Table 3). Our copolymer additives have the effect of simultaneously improving both the modulus and the elongation at break of the Cloisite Na⁺ composite. The improvement in properties for the Cloisite Na⁺ based nanocomposites is in line with the extent of exfoliation as observed by microscopy. Improvements in thermal and thermooxidative stability follow the same trend. Differences in crystallinity may in part account for the greater ductility and slightly lower modulus of the systems based on Cloisite Na⁺ vs reference organoclay based systems.

Table 3. Summary of Tensile Properties for Polypropylene Samples

| Material | Elongation at break | | Elastic modulus | |
|------------------------------|---------------------|-----------|-----------------|---------|
| | actual% | rel. PP % | actual (MPa) | rel. PP |
| PP | (~1000) | 100 | 1500 | 1 |
| Cloisite Na ^a | 20-40 | 2-4 | ~1700 | 1.2 |
| + copolymer ^b | 300 | 30 | 2000 | 1.3 |
| Cloisite 20A+PB ^c | 40 | 4 | 2200 | 1.4 |

^a 5 wt-% Cloisite Na.

^b 5 wt-% Cloisite Na and 1 wt-% poly(ODA-*grad*-MAH) (23).

^c Reference nanocomposite – 5 wt-% Cloisite 20A and 7.5 wt-% PP-*graft*-MAH (Polybond 3200).

Thermogravimetric analysis (TGA) analysis (Figure 6) showed that the thermooxidative stability of nanocomposites prepared with 5 wt-% unmodified clay and 1 wt-% copolymer is substantially improved (~ 40 °C) with respect to PP or PP with the clay alone. The enhancement of thermooxidative stability of these materials is not as great as that of a reference organoclay-based nanocomposite prepared with 5 wt-% Cloisite 20A and 7.5 wt-% PP-graft-MAH (Table 3). It is of interest that addition of 7.5 wt-% PP-graft-MAH by itself (no clay) provides an improvement in thermooxidative stability.

The thermal stability under nitrogen was also improved over PP for the nanocomposite samples with copolymer additives. The addition of Cloisite Na by itself has no substantial effect on the stability of PP. The reference nanocomposite based on Cloisite 20A had comparatively poor thermal stability with a more sudden weight loss profile (Figure 6).

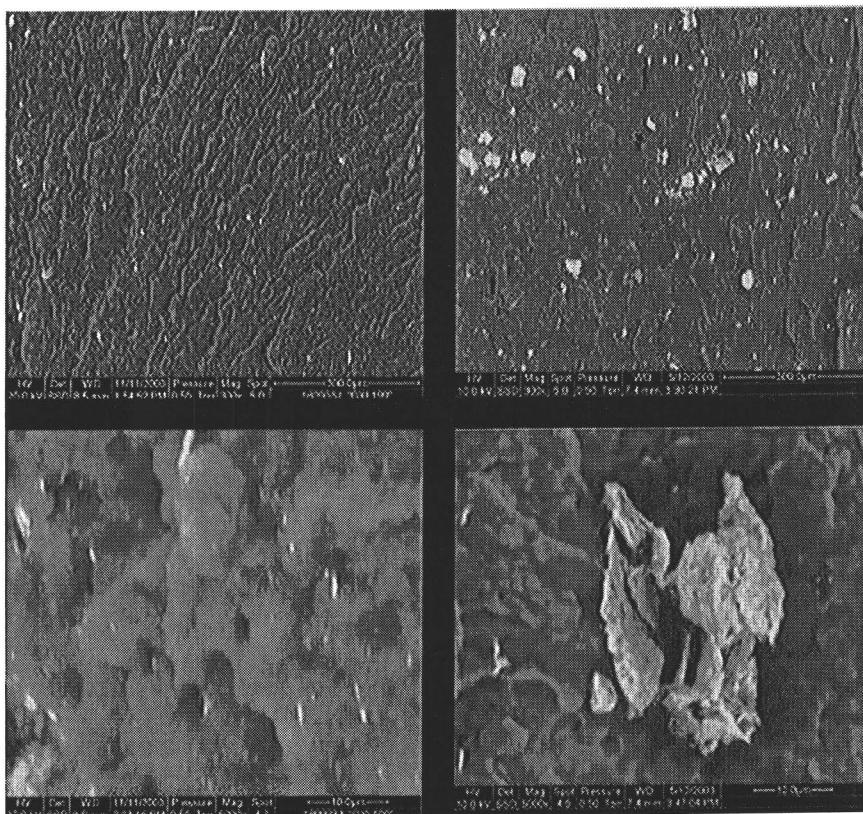


Figure 4. Low (upper) and high (lower) magnification ESEM images of cryofracture surface for PP composites with 5 wt% Cloisite Na+ alone (right) and with 1 wt% poly(ODA-grad-MAH) (23) additive (left).



Figure 5. TEM image of cryofracture surface for PP composite with 5 wt% Cloisite Na⁺ and 1% poly(ODA-grad-MAH) (23) additive (reproduced with permission from reference (32). Copyright 2006 Wiley-VCH).

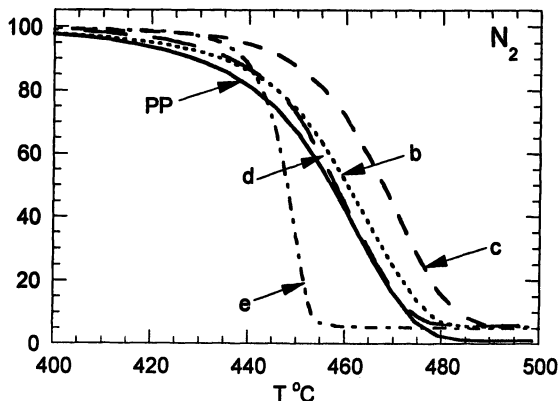
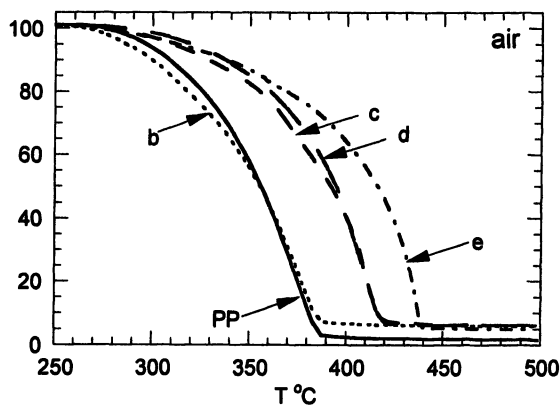


Figure 6. TGA mass loss curves for heating rate 10 °C min⁻¹ in air and under nitrogen for (a) polypropylene (PP, Moplen HP400N processed with 0.2 wt-% B225 stabilizer) (—); (b) PP with 5 wt-% Cloisite Na⁺ (·····); (c) PP with 5 wt-% Cloisite Na⁺ and 1 wt-% poly(ODA-grad-MAH) (23) (----); (d) PP with 7.5 wt-% PP-graft-MAH (— · —); (e) PP with 5 wt-% Cloisite 20A and 7.5 wt-% PP-graft-MAH (— — —).

The mechanism of stabilization by nanoparticulate fillers has been attributed in part (45) to the formation of a barrier which impedes both ingress of oxygen and evolution of volatiles. Consistent with this hypothesis we see an improvement in thermal stability according to the extent of exfoliation of the clay.

It was also found that higher processing temperatures could be used both for producing the nanocomposite and in injection molding with no adverse affect on PP properties. While nanocomposites were typically produced with extrusion temperatures of 200 °C and a throughput of 10 kg h⁻¹, several experiments showed that processing temperatures of 260 °C and throughput of 20 kg h⁻¹ could be used without detriment to the MFI, tensile properties, color or state of clay dispersion and without formation of odorous by-products.

Conclusions

High molecular weight acrylic polymers with $\overline{M}_w/\overline{M}_n \leq 1.1$ prepared with high monomer conversion often show a bimodal molecular weight distribution. We propose that this arises through copolymerization of the macromonomer formed by backbiting- β -scission. Evidence is obtained using GPC with UV detection and a RAFT agent that contains chromophores in both 'ZC(=S)' and 'R' substituents. RAFT copolymerization has been used to synthesize a series of novel copolymer intercalants/exfoliants/dispersants for unmodified layered silicates (sodium montmorillonite) in PP.

Gradient copolymers based on a long chain acrylate (*e.g.* ODA) and various polar comonomers (*e.g.* AA, DMAEA, MAH, PEGMA, NVP) proved most effective. PP-clay nanocomposites can be prepared by direct melt mixing using unmodified montmorillonite clays and a copolymer additive added at a level of only 1 wt-% with respect to PP for 5 wt-% clay. The additives provide substantially improved clay dispersion and cause partial exfoliation. The nanocomposites have improved elastic modulus with respect to PP and are more ductile than conventional nanocomposites that are based on organoclays with PP-graft-MAH as additive. Also notable are better thermal and thermooxidative stability as compared to PP and "clay alone" composites.

Acknowledgement. We are grateful to DuPont Performance Coatings, the CRC for Polymers and Ciba Specialty Chemicals for their support of various aspects of this work. AP thanks the CRC for Polymers for a PhD scholarship in conjunction with CSIRO Molecular and Heath Technologies and the University of New South Wales.

References

1. Chiefari, J.; Chong, Y. K.; Ercole, F.; Krstina, J.; Jeffery, J.; Le, T. P. T.; Mayadunne, R. T. A.; Meijs, G. F.; Moad, C. L.; Moad, G.; Rizzardo, E.; Thang, S. H. *Macromolecules* **1998**, *31*, 5559-5562.
2. Moad, G.; Rizzardo, E.; Thang, S. H. *Aust. J. Chem.* **2005**, *58*, 379-410.
3. Le, T. P.; Moad, G.; Rizzardo, E.; Thang, S. H. Int. Patent Appl. WO 9801478 (1998)
4. Mayadunne, R. A.; Moad, G.; Rizzardo, E. *Tetrahedron Lett.* **2002**, *43*, 6811-6814.
5. Mayadunne, R. T. A.; Rizzardo, E.; Chiefari, J.; Krstina, J.; Moad, G.; Postma, A.; Thang, S. H. *Macromolecules* **2000**, *33*, 243-245.
6. Lai, J. T.; Filla, D.; Shea, R. *Macromolecules* **2002**, *35*, 6754-6756.
7. Moad, G.; Chong, Y. K.; Rizzardo, E.; Postma, A.; Thang, S. H. *Polymer* **2005**, *46*, 8458-8468.
8. Thang, S. H.; Chong, Y. K.; Mayadunne, R. T. A.; Moad, G.; Rizzardo, E. *Tetrahedron Lett.* **1999**, *40*, 2435-2438.
9. Bouhadir, G.; Legrand, N.; Quiclet-Sire, B.; Zard, S. Z. *Tetrahedron Lett.* **1999**, *40*, 277-280.
10. Moad, G.; Mayadunne, R. T. A.; Rizzardo, E.; Skidmore, M.; Thang, S. *ACS Symp. Ser.* **2003**, *854*, 520-535.
11. Chiefari, J.; Mayadunne, R. T. A.; Moad, C. L.; Moad, G.; Rizzardo, E.; Postma, A.; Skidmore, M. A.; Thang, S. H. *Macromolecules* **2003**, *36*, 2273-2283.
12. Feldermann, A.; Toy, A. A.; Davis, T. P.; Stenzel, M. H.; Bamer-Kowollik, C. *Polymer* **2005**, *46*, 8448-8457.
13. Chong, Y. K.; Krstina, J.; Le, T. P. T.; Moad, G.; Postma, A.; Rizzardo, E.; Thang, S. H. *Macromolecules* **2003**, *36*, 2256-2272.
14. Donovan, M. S.; Lowe, A. B.; Sumerlin, B. S.; McCormick, C. L. *Macromolecules* **2002**, *35*, 4123-4132.
15. Postma, A.; Davis, T. P.; Li, G.; Moad, G.; O'Shea, M. *Macromolecules* **2006**, to be submitted.
16. Destarac, M.; Kalai, C.; Petit, L.; Wilczewska, A.; Mignani, G.; Zard, S. Z. *Polym. Prepr. (Am. Chem. Soc., Div. Polym. Chem.)* **2005**, *46(2)*, 372-373.
17. Perrier, S.; Takolpuckdee, P.; Mars, C. A. *Macromolecules* **2005**, *38*, 2033-2036.
18. Postma, A.; Davis, T. P.; Moad, G.; O'Shea, M. *Macromolecules* **2005**, *38*, 5371-5374.
19. Destarac, M.; Kalai, C.; Wilczewska, A.; Mignani, G.; Zard, S. Z. *Polym. Prepr. (Am. Chem. Soc., Div. Polym. Chem.)* **2005**, *46(2)*, 213-214.
20. Haddleton, D. M.; Crossman, M. C.; Hunt, K. H.; Topping, C.; Waterson, C.; Suddaby, K. G. *Macromolecules* **1997**, *30*, 3992-3998.

21. Lad, J.; Harrisson, S.; Haddleton, D. M. *ACS Symp. Ser.* **2003**, *854*, 148-160.
22. Lad, J.; Harrisson, S.; Mantovani, G.; Haddleton, D. M. *Dalton Trans.* **2003**, 4175-4180.
23. Davis, K. A.; Matyjaszewski, K. *Adv. Polym. Sci.* **2002**, *159*, 2-166.
24. Klumperman, B.; Chambard, G.; Brinkhuls, R. H. G. *ACS Symp. Ser.* **2003**, *854*, 180-192.
25. Feldermann, A.; Toy, A. A.; Phan, H.; Stenzel, M. H.; Davis, T. P.; Barner-Kowollik, C. *Polymer* **2004**, 3997-4007.
26. Galbraith, M. N.; Moad, G.; Solomon, D. H.; Spurling, T. H. *Macromolecules* **1987**, *20*, 675-679.
27. Spurling, T. H.; Deady, M.; Krstina, J.; Moad, G. *Makromol. Chem., Macromol. Symp.* **1991**, *51*, 127-146.
28. Benoit, D.; Hawker, C. J.; Huang, E. E.; Lin, Z. Q.; Russell, T. P. *Macromolecules* **2000**, *33*, 1505-1507.
29. De Brouwer, H.; Schellekens, M. A. J.; Klumperman, B.; Monteiro, M. J.; German, A. L. *J. Polym. Sci. Part A Polym. Chem* **2000**, *38*, 3596-3603.
30. Du, F. S.; Zhu, M. Q.; Guo, H. Q.; Li, Z. C.; Li, F. M.; Kamachi, M.; Kajiwara, A. *Macromolecules* **2002**, *35*, 6739-6741.
31. Moad, G.; Mayadunne, R. T. A.; Rizzardo, E.; Skidmore, M.; Thang, S. *Macromol. Symp.* **2003**, *192*, 1-12.
32. Moad, G.; Dean, K.; Edmond, L.; Kukaleva, N.; Li, G.; Mayadunne, R. T. A.; Pfaendner, R.; Schneider, A.; Simon, G.; Wermter, H. *Macromol. Symp.* **2006**, in press.
33. Street, G.; Illsley, D.; Holder, S. J. *J. Polym. Sci. Part A Polym. Chem* **2005**, *43*, 1129-1143.
34. Jakubowski, W.; Lutz, J. F.; Slomkowski, S.; Matyjaszewski, K. *J. Polym. Sci. Part A Polym. Chem* **2005**, *43*, 1498-1510.
35. Zhu, X. L.; Gu, Y. R.; Chen, G. J.; Cheng, Z. P.; Lu, J. M. *J. Appl. Polym. Sci.* **2004**, *93*, 1539-1545.
36. Qin, S. H.; Saget, J.; Pyun, J. R.; Jia, S. J.; Kowalewski, T.; Matyjaszewski, K. *Macromolecules* **2003**, *36*, 8969-8977.
37. Qin, S. H.; Matyjaszewski, K.; Xu, H.; Sheiko, S. S. *Macromolecules* **2003**, *36*, 605-612.
38. Zhu, J.; Zhu, X. L.; Cheng, Z. P.; Lu, J. M.; Liu, F. *J. Macromol. Sci. Chem.* **2003**, *A40*, 963-975.
39. Tamikado, T.; Iwakura, Y. *J. Polym. Sci.* **1959**, *36*, 529-532.
40. O'Leary, K.; Paul, D. R. *Polymer* **2004**, *45*, 6575-6585.
41. Jordan, E. F., Jr.; Bennett, R.; Shuman, A. C.; Wrigley, A. N. *J. Polym. Sci. Polym. Chem. Ed.* **1970**, *8*, 3113-3121.
42. Zhuang, D. Q.; Shi, L. P.; Yu, Y. H.; Zhang, Y. X. *Chinese J. Chem.* **2000**, 626-634.

43. Moad, G.; Li, G.; Rizzardo, E.; San H Thang; Pfaendner, R.; Wermter, H. *Polym. Prepr. (Am. Chem. Soc. Div. Polym. Chem.)* **2005**, *46* (2), 376-377.
44. Moad, G.; Dean, K.; Edmond, L.; Kukaleva, N.; Li, G.; Mayadunne, R. T. A.; Pfaendner, R.; Schneider, A.; Simon, G.; Wermter, H. *Macromol. Mater. Eng.* **2006**, *291*, 37-52.
45. Zanetti, M.; Camino, G.; Reichert, P.; Mulhaupt, R. *Macromol. Rapid Commun.* **2001**, *22*, 176-180.

Chapter 36

Controlled Synthesis of Amino Acid-Based Polymers by Reversible Addition Fragmentation Chain Transfer Polymerization

Hideharu Mori, Kazuhiko Sutoh, Hideyuki Iwaya, Atsushi Nagai,
and Takeshi Endo

Department of Polymer Science and Engineering, Faculty of Engineering,
Yamagata University, 4-3-16, Jonan, Yonezawa 992-8510, Japan

We here report controlled synthesis of polyacrylamides having amino acid moieties by reversible addition-fragmentation chain transfer (RAFT) polymerization. Three acrylamides, *N*-acryloyl-L-phenylalanine methyl ester (A-Phe-OMe), *N*-acryloyl-L-phenylalanine (A-Phe-OH), and *N*-acryloyl-L-proline methyl ester (A-Pro-OMe), were selected as amino acid-containing monomers. The RAFT polymerization of these monomers using suitable chain transfer agents allowed the synthesis of well-defined amino acid-based polymers with pre-determined molecular weights, narrow molecular weight distributions, and characteristic stimuli-responsive properties. Poly(A-Phe-OH) was a weak polyelectrolyte, in which the degree of ionization of carboxylic acids can be easily controlled by the pH value. Poly(A-Pro-OMe) and the random copolymers exhibited a characteristic Lower Critical Solution Temperature (LCST = 15-45 °C) in aqueous solution.

Introduction

Amino acids are the constitutional components of peptides and proteins, which are able to produce highly ordered hierarchical structures scaling from a few nanometers to several microns. Due to their unique structures and properties, recently much interest has been devoted to develop a variety of amino acid-based polymers (1-4). The desirable requirement is to create synthetic methods to control the sequence and composition of amino acids, chain chirality, conformation, amphiphilicity, and chain length. It is also important to produce amino acid-based polymers possessing narrow chain length distributions and controlled molecular weights. However, there is still a large gap between the performance and architectures of most synthetic polymers and biologically produced polymers. An attractive approach is integration of peptide segments via controlled radical polymerization of peptidic macromonomers (5). Another direction is to produce peptide-polymer hybrids by combining solid-phase synthesis and controlled radical polymerization (6,7).

We here report controlled synthesis of polyacrylamides having amino acid moieties in the side chains by reversible addition-fragmentation chain transfer (RAFT) polymerization. Three acrylamides, *N*-acryloyl-L-phenylalanine methyl ester (A-Phe-OMe), *N*-acryloyl-L-phenylalanine (A-Phe-OH), and *N*-acryloyl-L-proline methyl ester (A-Pro-OMe), were selected as amino acid-containing monomers, as shown in Figure 1. So-called "intelligent" or "smart" materials that can sense signals and produce a definite dynamic response in the form of a change in shape, size, or structure, is another central to developments in various scientific fields (8,9). The poly(A-Phe-OH) obtained in this study was a weak polyelectrolyte, whereas poly(A-Pro-OMe) exhibited a thermo-responsive property. Our attention was focused on amino-acid based polymers with not only well-defined architectures but also characteristic stimuli-responsive properties.

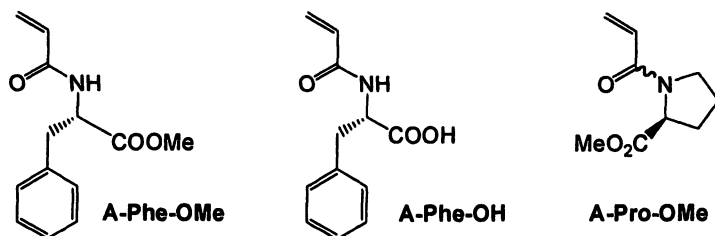


Figure 1. Amino acid-containing monomers.

Experimental

The syntheses of chain transfer agents (Figure 2), benzyl 1-pyrrolocarbodithioate (CTA 1) (10,11) and benzyl dithiobenzoate (CTA 2) (12,13), were carried out according to the procedures reported in the literatures. The monomers, A-Phe-OMe (14), A-Phe-OH (15), and A-Pro-OMe (16), were prepared by the reactions of acryloyl chloride with the corresponding amino acids according to methods reported previously.

For a typical polymerization, the monomer, CTA, AIBN, and solvent were placed in a dry glass ampule equipped with a magnetic stirring bar, and then the solution was degassed by three freeze-evacuate-thaw cycles. The ampule was flame-sealed off under vacuum, and it was agitated at 60 °C for desired time.

^1H and ^{13}C NMR spectra were recorded with a JEOL EX-270 and a Varian INOVA-500. Number-average molecular weight (M_n) and molecular weight distribution (M_w/M_n) were estimated by size-exclusion chromatography (SEC) using a Tosoh HPLC HLC-8220 system equipped with refractive index and ultraviolet detectors at 40 °C. The system was operated at a flow rate of 0.6 mL/min using *N,N*-dimethylformamide (DMF) containing 10 mM LiBr as an eluent. Polystyrene standards were employed for calibration. Specific rotations ($[\alpha]_D$) were measured on a JASCO DIP-1000 digital polarimeter equipped with a sodium lamp as a light source. Circular dichroism (CD) spectra were measured on a JASCO J-720 spectropolarimeter.

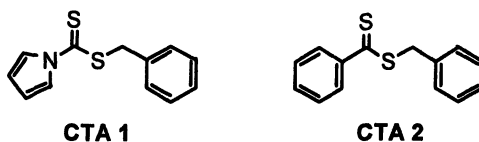


Figure 2. Chain transfer agents used in this study.

Results and Discussion

RAFT Polymerization of A-Phe-OMe

We recently demonstrated the first successful controlled radical polymerization of a monosubstituted acrylamide having an amino acid moiety, *N*-acryloyl-L-phenylalanine methyl ester (A-Phe-OMe), via RAFT process (17). The polymerizations of A-Phe-OMe were conducted using CTA 1 or CTA 2 under various conditions. When A-Phe-OMe was polymerized using CTA 1

with AIBN as an initiator at $[A\text{-Phe-OMe}]_0/[CTA\ 1]_0/[AIBN]_0 = 100/2/1$ in 1,4-dioxane (0.5 g/mL), almost full conversion (93%, as determined by $^1\text{H NMR}$) was obtained at 60 °C after 24 h. The characteristic pale yellow color maintained throughout the polymerization without significant change in the viscosity. The resulting polymer showed sharp symmetrical unimodal SEC peak ($M_w/M_n = 1.23$) without shoulders and tailings. The number-average molecular weight of the poly(A-Phe-OMe), measured by a GPC in DMF with 10 mM LiBr, was $M_n = 7800$, which is roughly comparable to the theoretical value ($M_n = 11000$) calculated from molar ratio of monomer/CTA and the monomer conversion. The polymerization with AIBN in the presence of CTA 2 at 60 °C produced the polymer with a relatively narrow molecular weight distribution ($M_w/M_n = 1.20$), while achieving only 45% conversion even after 24 h. This is an indication that the polymerization with CTA 2 is much slower than that with CTA 1.

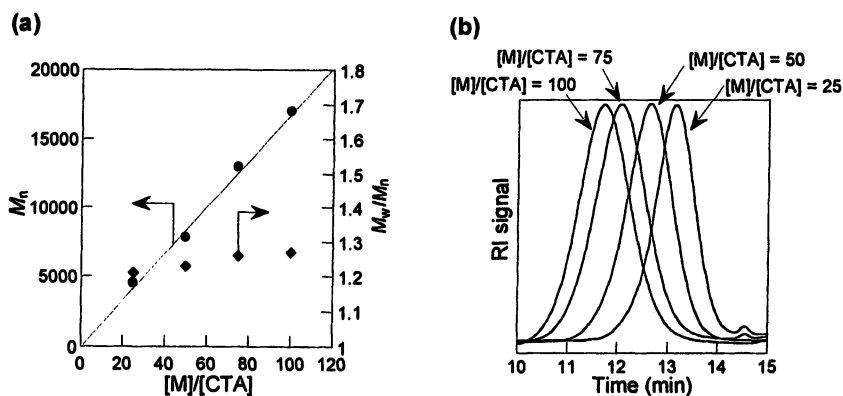


Figure 3. (a) Dependence of M_n and M_w/M_n on $[M]_0:[CTA]_0$ ratio for the polymerization of A-Phe-OMe with AIBN in the presence of CTA 1 in 1,4-dioxane (0.5 g/mL) at 60 °C. $[CTA\ 1]_0/[AIBN]_0 = 2/1$. (b) SEC traces of the corresponding poly(A-Phe-OMe)s. Reproduced with permission from *Macromolecules* 2005, 38, 9055-9065. Copyright 2005 Am. Chem. Soc.

The polymerization of A-Phe-OMe was conducted with AIBN in the presence of CTA 1 in 1,4-dioxane at 60 °C for 24 h at different $[A\text{-Phe-OMe}]_0:[CTA\ 1]_0$ ratios between 25 and 100, while the AIBN:CTA 1 molar ratio was held constant at 1:2. Under the conditions, the conversions were quantitative ($> 90\%$, as determined by $^1\text{H NMR}$) in all cases. Figure 3a shows the relation of the molecular weight and polydispersity with the $[M]_0:[CTA]_0$ ratio. A linear increase of the number-average molecular weight with the ratio is observed clearly, and the molecular weight distributions remain narrow (M_w/M_n

= 1.21-1.26), indicating a feasibility to control the molecular weights. The SEC traces are unimodal, as can be seen in Figure 3b.

In all cases, the experimental molecular weights determined by GPC were slightly lower than calculated ones. These discrepancies may result from the difference in hydrodynamic volume between poly(A-Phe-OMe) and the linear polystyrene standards used for GPC calibration. In order to clarify the point, GPC with a multi-angle light scattering detector (GPC-MALS) was applied for the determination of the absolute molecular weights of representative samples. The polymers obtained at $[A\text{-Phe-OMe}]_0:[CTA]_0$ ratios = 75 and 100 had $M_w = 23400$ and $M_w/M_n = 1.20$ ($M_{n,\text{GPC-MALS}} = 19400$, as determined by GPC-MALS), compared to $M_{n,\text{calcd}} = 16000$ and $M_{n,\text{GPC}} = 13000$ ($M_w/M_n = 1.26$), and $M_w = 30000$ and $M_w/M_n = 1.19$ ($M_{n,\text{GPC-MALS}} = 25200$, as determined by GPC-MALS), compared to $M_{n,\text{calcd}} = 20000$ and $M_{n,\text{GPC}} = 17000$ ($M_w/M_n = 1.25$), respectively. There was no significant difference between $M_{n,\text{GPC-MALS}}$ and $M_{n,\text{calcd}}$, suggesting that the number of living polymer chains is comparable to that of CTA.

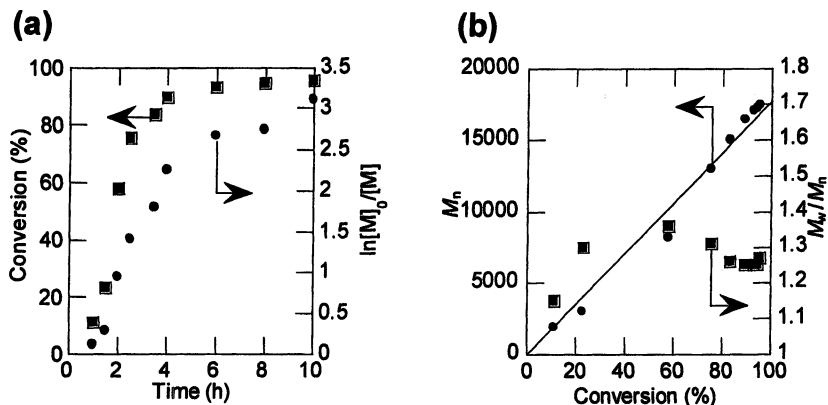


Figure 4. (a) Time-conversion (squares) and the first-order kinetic (circles) plots for the polymerization of A-Phe-OMe with AIBN in the presence of CTA 1 in 1,4-dioxane (0.5 g/mL) at 60°C and (b) M_n (circles) and M_w/M_n (squares) as a function of conversion. $[A\text{-Phe-OMe}]_0/[CTA]_0/[AIBN]_0 = 200/2/1$.

Reproduced with permission from *Macromolecules* 2005, 38, 9055-9065.

Copyright 2005 Am. Chem. Soc.

The time-conversion and the pseudo-first-order kinetic plots are shown in Figure 4a. An induction period of less than 2 h is seen in the pseudo-first-order kinetic plot. An induction period and the S-shaped time-conversion plots are often observed in RAFT polymerization of various monosubstituted and disubstituted acrylamides (18-21). Figure 4b shows the evolution of M_n and M_w/M_n with conversion during the polymerization of A-Phe-OMe. The linearity

of the M_n versus conversion plot is seen, indicating that the polymerization proceeded in a controlled fashion without nondegenerative chain transfer. Symmetrical unimodal SEC peaks were observed for the polymers ($M_w/M_n = 1.15-1.36$) obtained even at higher conversion ($> 90\%$). The controlled character of the polymerization was also confirmed by the successful chain extension by the second addition of the monomer.

We also examined the effect of Lewis acid on RAFT polymerization of A-Phe-OMe. Poly(A-Phe-OMe) with controlled molecular weight, low polydispersity, and enhanced isotacticity ($m = 49-68\%$) was prepared by RAFT polymerization in the presence of catalytic amounts of Lewis acid, $Y(OTf)_3$, as shown in Table I.

Table I. RAFT Polymerization of *N*-Acryloyl-L-phenylalanine Methyl Ester (A-Phe-OMe) with AIBN/CTA 1 in the presence of Lewis acids ^{a)}

Reproduced with permission from *Macromolecules* 2005, 38, 9055-9065.

Copyright 2005 Am. Chem. Soc.

| Lewis acid | [Lewis acid] / [M] | conv. ^{b)} % | M_n ^{c)} (theory) | M_n ^{d)} (SEC) | M_w/M_n ^{d)} (SEC) | tacticity m/r ^{e)} |
|-------------|--------------------|-----------------------|------------------------------|---------------------------|-------------------------------|-------------------------------|
| - | - | 93 | 22000 | 17000 | 1.25 | 49/51 |
| $Y(OTf)_3$ | 0.05 | 93 | 22000 | 14000 | 1.35 | 62/38 |
| $Y(OTf)_3$ | 0.1 | 98 | 23500 | 18500 | 1.53 | 67/33 |
| $Y(OTf)_3$ | 0.2 | 98 | 23500 | 18000 | 1.55 | 68/32 |
| $Yb(OTf)_3$ | 0.05 | 95 | 23000 | 21000 | 1.63 | 65/35 |
| $Sc(OTf)_3$ | 0.05 | 84 | 20000 | 17000 | 1.55 | 61/39 |

^{a)} Polymerization was conducted in 1,4-dioxane at 60 °C for 6 h. $[CTA\ 1]_0/[AIBN]_0 = 2$, $[M]_0/[CTA\ 1]_0 = 100$, monomer conc. = 0.5 g/mL ($[M] = 1.38$ mol/L). ^{b)} Calculated by ¹H NMR in $CDCl_3$. ^{c)} The theoretical molecular weight ($M_{n,theory}$) = (MW of M) × conv. × $[M]_0/[CTA]_0 +$ (MW of CTA). ^{d)} Measured by size-exclusion chromatography (SEC) using polystyrene standards in *N,N*-dimethylformamide (DMF, 10 mM LiBr).

^{e)} Determined by ¹H NMR in dimethyl sulfoxide-*d*₆ (DMSO-*d*₆) at 170 °C.

RAFT Polymerization of A-Phe-OH

Controlled polymerization of amino acid-based monomer with carboxylic acid moiety is promising for producing tailored functional polymers for various

applications, because the carboxylic acid groups in polymers can be interacted with various metal ions, nonionic proton-accepting polymers, their derivatives, and cationic polyelectrolytes. Polymers containing carboxylic acid groups can be also regarded as weak polyelectrolytes, in which the degree of ionization is governed by the pH and ionic strength of aqueous solution. Their chemical structure and three-dimensional architectures of block and complex polymers containing carboxylic groups may be tuned for a wide range of applications covering different aspects, such as stabilization of colloids, induced micelle formation, and components of intelligent materials (22).

Controlled synthesis of polyacrylamide having amino acid moieties in the side chains is a challenging subject, as most of the traditional living polymerization systems are not tolerant of the functional groups. Recent development in controlled radical polymerization methods has provided a useful methodology to synthesize functional polymers containing carboxylic acids, such as poly[(meth)acrylic acid]s, without protecting chemistry (22). On the basis of the considerations, we attempted direct RAFT polymerization of *N*-acryloyl-L-phenylalanine (A-Phe-OH), in which the carboxylic acid is intact without protecting group.

The unprotected monomer, A-Phe-OH, was directly polymerized with AIBN/CTA under various conditions and the results are summarized in Table II. For SEC measurements, the resulting polymers were modified by methylation of the carboxylic acid groups using trimethylsilyldiazomethane (23). The polymerization of A-Phe-OH with AIBN in the presence of CTA 1 in 1,4-dioxane (0.25 g/mL) at 60 °C produced the polymer quantitatively after 24 h. The characteristic pale yellow color remained throughout the polymerization without significant change in the viscosity. Unimodal SEC trace with no evidence of high molecular weight species was obtained, while the molecular weight distribution was relatively broad. The polymerization with CTA 2 was relatively slow. Better control of the polymerization was attained using CTA 1 in MeOH at lower temperature. When the polymerization of A-Phe-OH was conducted at $[A-Phe-OH]_0/[CTA\ 1]_0/[AIBN]_0 = 100/2/1$, the poly(A-Phe-OH) having controlled molecular weight and low polydispersity ($M_w/M_n = 1.25$, Figure 5) was obtained in MeOH at 45 °C. The resulting polymer was soluble in DMF, EtOH, MeOH, and basic aqueous solution (pH > 11), while insoluble in water under acidic and neutral environments. Note that phenylalanine is most hydrophobic amino acid and pKa value of poly(A-Phe-OH) is considered to be higher than that of phenylalanine. It was found that well-defined amino acid-based polyacrylamide having pH-responsive property can be achieved via RAFT polymerization by using suitable CTA and polymerization conditions.

Table II. RAFT Polymerization of *N*-Acryloyl-L-phenylalanine (A-Phe-OH) with AIBN/CTA Under Different Conditions^{a)}

| CTA | solvent | temp (°C) | conv ^{b)} (%) | M_n | | M_w/M_n ^{d)} |
|-------|---------|--------------|---------------------------|---------------------|--------------------|-------------------------|
| | | | | calcd ^{c)} | obsd ^{d)} | |
| CTA 1 | Dioxane | 60 | 97 | 11500 | 10500 | 1.42 |
| CTA 1 | Dioxane | 45 | 84 | 10000 | 7100 | 1.45 |
| CTA 2 | Dioxane | 60 | 42 | 5100 | 3500 | 1.31 |
| CTA1 | MeOH | 60 | 94 | 11200 | 12800 | 1.30 |
| CTA1 | MeOH | 45 | 76 | 9100 | 6500 | 1.25 |

^{a)} $[CTA]_0/[AIBN]_0 = 2$, $[M]_0/[CTA]_0 = 50$, monomer conc. = 0.25 g/mL. ^{b)} Calculated by ¹H NMR. ^{c)} (MW of A-Phe-OMe) \times [A-Phe-OH]₀/[CTA]₀ \times conv. + (MW of CTA). ^{d)} Methylated samples were measured by SEC using PSt standards in DMF (0.01M LiBr).

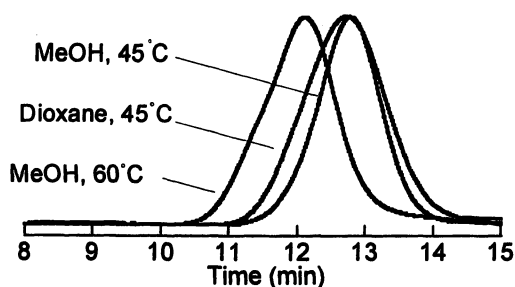


Figure 5. SEC traces of the methylated poly(A-Phe-OH)s obtained by RAFT polymerization of A-Phe-OH under different conditions. See Table II for detailed polymerization conditions.

RAFT Polymerization of A-Pro-OMe

During recent years, there has been increasing attention paid to artificial and model proteins having stimuli-responsive properties, in which these repeating sequences hold and/or self-assemble into more highly ordered structures when the temperature is raised in water (8,24). Polymers susceptible to reversible thermoprecipitation from aqueous solution have been also used as simple analogs to the solubility and denaturing of proteins and biopolymers (25). We focused on controlled synthesis of amino acid-based polymers derived from L-

proline (13), which have characteristic thermoresponsive property in aqueous medium (26,27). For the precise manipulation of the thermosensitive property, it is important to produce polymers possessing narrow chain length distributions. Reversibility and transition sharpness of typical stimuli-responsive systems can be achieved by utilizing polymers with well-defined primary structures, attainable via controlled/living polymerization (28,29).

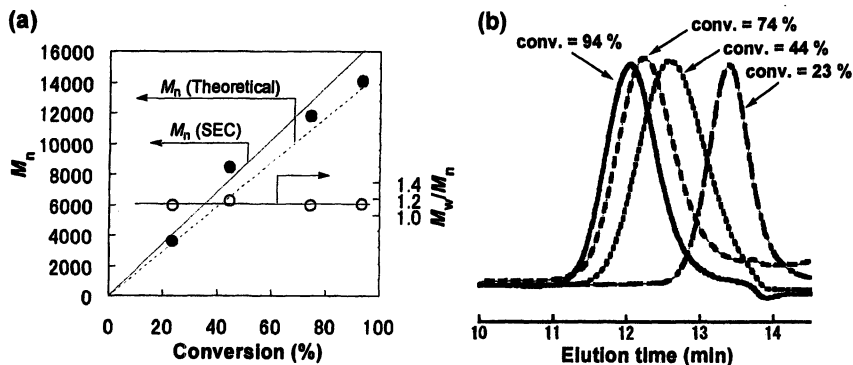


Figure 6. (a) M_n and M_w/M_n as a function of conversion, and (b) evolution of SEC traces with conversion. $[A\text{-Pro-Ome}] = 1.0\text{ M}$. $[A\text{-Pro-Ome}]_0/[CTA\ 2]_0 = 112.4$, $[CTA\ 2]_0/[AIBN]_0 = 2/1$, $60\text{ }^\circ\text{C}$. Reproduced with permission from *Chemical Communications* 2005, 4872-4874. Copyright 2005 Royal Society of Chemistry.

Controlled radical polymerization of an acrylamide containing L-proline moiety, *N*-acryloyl-L-proline methyl ester (A-Pro-OMe), was attained via RAFT process (13). In this case, benzyl dithiobenzoate (CTA 2) was efficient as the chain transfer agent for the preparation of poly(A-Pro-OMe)s with controlled molecular weights and low polydispersities. When A-Pro-OMe was polymerized at $[CTA\ 2]_0/[AIBN]_0 = 2/1$ in chlorobenzene at $60\text{ }^\circ\text{C}$, the characteristic pale red solution kept constant during the polymerization. The number-average molecular weight of the polymer, measured by a GPC in DMF with 10 mM LiBr, was $M_n = 5500$, which is comparable to the theoretical value ($M_n = 7000$) calculated from the molar ratio of monomer/CTA and the monomer conversion.

Controlled character of the RAFT polymerization of A-Pro-OMe was investigated in terms of the time-dependent change in the molecular weights and polydispersity of the resulting polymers. When the polymerization was conducted in chlorobenzene at $60\text{ }^\circ\text{C}$ at a constant chain transfer agent/initiator

molar ratio, $[CTA\ 2]_0/[AIBN]_0 = 2/1$, more than 90% conversion was reached within 5 h. Figure 6 shows the evolution of M_n and M_w/M_n with conversion for A-Pro-OMe during the polymerization. The linearity of the M_n versus conversion plot was observed, and the resulting polymers showed sharp symmetrical unimodal SEC peaks ($M_w/M_n = 1.12-1.18$). The feasibility to control molecular weight based on the molar ratio of monomer/CTA was also observed, indicating good control of the polymerization. The synthesis of the poly(A-Pro-OMe) with improved stereoregularity was attempted by the addition of Lewis acids, as shown in Table III. The specific rotations and circular dichroism (CD) spectra of the resulting polymers were compared, in order to clarify the effect of the tacticity (Figure 7). The poly(A-Pro-OMe) was soluble in water at low temperature, which undergoes a clear phase transition upon heating at LCST around 15-20 °C, depending on the tacticity. Unfortunately, it was difficult to evaluate directly the tacticity of poly(A-Pro-OMe) by NMR measurements.

Table III. RAFT Polymerization of *N*-Acryloyl-L-proline Methyl Ester (A-Pro-OMe) with AIBN/CTA 2 in the presence of Lewis acids ^a

| Lewis acid | M_n (M_w/M_n) ^b | $[\alpha]_D^{26}$ ^c (°C) | T_{d5} ^d (°C) | LCST ^e (°C) |
|----------------------|----------------------------------|--|-------------------------------|---------------------------|
| - | 12300 (1.22) | - 145.2 | 335 | 17 |
| Y(OTf) ₃ | 10000 (1.44) | - 168.0 | 330 | 19 |
| Yb(OTf) ₃ | 16000 (1.30) | - 173.6 | 322 | 21 |
| Sc(OTf) ₃ | 3200 (1.87) | - 156.0 | 296 | 16 |

^a Condition; A-Pro-OMe (0.27 g, 1.5 mmol), AIBN (0.67 mol%), CTA 2 (1.3 mol%), Lewis acids (13 mol%), chlorobenzene (1.0 M), 60 °C, 20 h. ^b Measured by SEC using PSt standards in DMF (0.01M LiBr). ^c Measured by a polarimeter at 26 °C ($c = 0.1$ g/dL, CHCl₃). ^d Measured by TG/DTA. ^e Estimated by UV/vis spectra.

In LCST-type phase separation, the occurrence and position of a phase transition temperature are known to depend on the distribution of hydrophilic and hydrophobic groups within the polymers (30). With this in mind, we attempted to manipulate LCST of the amino acid-based polymers by the copolymerization of A-Pro-OMe with *N,N*-dimethylacrylamide (DMA), by which appropriate hydrophilic/hydrophobic balance can be achieved.

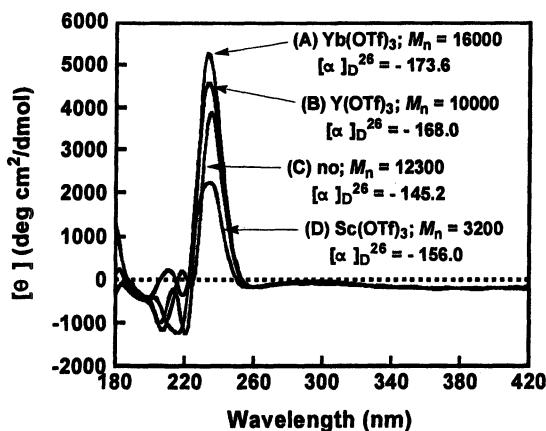


Figure 7. CD spectra ($c = 0.1$ g/dL, CHCl_3) of poly(A-Pro-OMe)s prepared by RAFT polymerization in the absence and presence of Lewis acid.

The copolymerization via RAFT process was conducted at different A-Pro-OMe:DMA molar ratio in the feed at $([\text{A-Pro-OMe}] + [\text{DMA}]) / [\text{CTA 2}] = 50$ and $[\text{CTA 2}] / [\text{AIBN}] = 2$. Depending on the comonomer ratio (A-Pro-OMe:DMA = 95:5, 90:10, 80:20, 70:30, 50:50), the copolymers with number-average molecular weights between 8300 and 5100 and the A-Pro-OMe content between 92 and 48% were obtained with high conversion (yield > 87%) at 60 °C after 20 h. The compositions of the copolymers determined by ^1H NMR are in good agreement with the calculated values from the conversion and the feed ratio of both monomers, irrespective of the comonomer ratio in the feed. The polydispersity indices (M_w/M_n) for all samples ranged between 1.22 and 1.28.

Figure 8a shows the dependence of the solution turbidity of the copolymers having different DMA contents on the temperature. The transmittance decreased sharply in all aqueous solutions at a specific temperature on heating, indicative of a sharp phase transition (LCST type). The mole fraction of A-Pro-OMe, x , was found to determine the temperature of the phase separation, varying from 15 °C at $x = 1.0$ to 44 °C at $x = 0.67$ for a 1.0 mg/mL aqueous solution. The phase separation occurred with a similar sharpness in all cases, irrespective of the ratio of DMA to A-Pro-OMe. The LCST increased linearly with increasing DMA content, whereas the LCST phenomenon disappeared when hydrophilic DMA contains more than 50% in the copolymers. It was demonstrated that the copolymerizations via RAFT afforded the amino acid-based polymers having well-defined structure, and the transition temperature can be manipulated in the range of 15–45 °C by the hydrophilic comonomer composition.

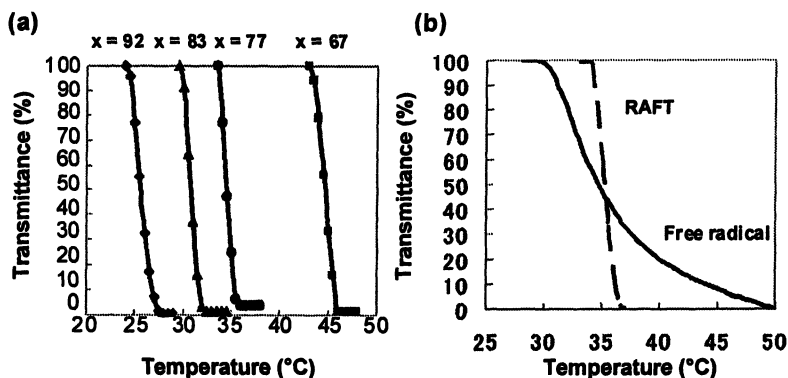


Figure 8. (a) Temperature dependence of the solution turbidity of the copolymers ($x = A\text{-Pro-OMe}$, $y = \text{DMA}$) and (b) comparison of the copolymers obtained by RAFT and conventional free radical polymerization. Reproduced with permission from *Chemical Communications* 2005, 4872-4874. Copyright 2005 Royal Society of Chemistry.

In the case of the copolymer containing 23% of DMA unit, the aqueous solution transformed into an opaque liquid when warmed to above 33 °C, as monitored by the transmittance at 500 nm. The transmittance decreased sharply during 33.5-36.5 °C, indicating that the phase separation was highly sensitive. When the white turbid solution was cooled, it returned to the homogeneous state. Note that this phase separation was not only extremely sensitive but also reversible on heating and cooling without hysteresis. Figure 8b compares the temperature-dependent solution turbidity of the copolymers obtained by RAFT ($M_n = 6200$, $M_w/M_n = 1.25$, $x = A\text{-Pro-OMe} = 0.77$, $y = \text{DMA} = 0.23$) and conventional free radical polymerization ($M_n = 242000$, $M_w/M_n = 2.25$, $x = 0.68$, $y = 0.32$) under the similar condition. The transition curve of the copolymer obtained by free radical polymerization becomes broad, and the transition width is approximately 20 °C (30-50 °C) on heating. The significant difference in the transition behaviors between the copolymers suggests that reversibility and transition sharpness of the thermoresponsive system can be achieved by utilizing the amino acid-based copolymers having well-defined primary structures.

Conclusions

This work presented that the RAFT polymerization of acrylamides having amino acid moieties allows the synthesis of well-defined amino acid-based polymers with pre-determined molecular weight, narrow molecular weight distribution, and characteristic stimuli-responsive properties. This procedure may be extended to the synthesis of well-defined polymers derived from various

amino acids and controlled architectures, such as graft, star, and block copolymers. Since specific intra- and intermolecular interactions via hydrogen-bonding and ionic complexation may be manipulated by the nature of the amino acid moieties, the self-organization of the well-defined polymers can provide a viable route to the production of tailored amino acid-based materials with unique intelligent properties for various applications, such as controlled release, biochemical sensing, biocompatible materials, and optical resolution.

Acknowledgments. This work has been supported by a Grant-in-Aid for Scientific Research from the Ministry of Education, Culture, Sports, Science, and Technology, Japan (17550112).

References

1. Sanda, F.; Endo, T. *Macromolecular Chemistry and Physics* **1999**, *200*, 2651-2661.
2. Deming, T. J. *Nature (London)* **1997**, *390*, 386-389.
3. Deming, T. J. *Journal of Polymer Science: Part A: Polymer Chemistry* **2000**, *38*, 3011-3018.
4. Nagai, A.; Sato, D.; Ishikawa, J.; Ochiai, B.; Kudo, H.; Endo, T. *Macromolecules* **2004**, *37*, 2332-2334.
5. Ayres, L.; Koch, K.; Adams, P. J. H. M.; van Hest, J. C. M., *Macromolecules* **2005**, *38*, 1699-1794.
6. Ying, M.; Kathryn, L.; Beers, H. C.; Michelle, B.; David, L. V.; Newell, R. W. *Journal of the American Chemical Society* **2004**, *126*, 3472-3476.
7. Becker, M. L.; Liu, J. Q.; Wooley, K. L. *Chemical Communications (Cambridge)* **2003**, 180-181.
8. Petka, W. A.; Hardin, J. L.; McGrath, K. P.; Wirtz, D.; Tirrell, D. A. *Science (Washington, D. C.)* **1998**, *281*, 389-392.
9. Osada, Y.; Gong, J.-P. *Advanced Materials (Weinheim, Germany)* **1998**, *10*, 827-837.
10. Chiefari, J.; Mayadunne, R. T. A.; Moad, C. L.; Moad, G.; Rizzardo, E.; Postma, A.; Skidmore, M. A.; Thang, S. H. *Macromolecules* **2003**, *36*, 2273-2283.
11. Mori, H.; Nakano, S.; Endo, T. *Macromolecules* **2005**, *38*, 8192-8201.
12. Chong, Y. K.; Krstina, J.; Le, T. P. T.; Moad, G.; Postma, A.; Rizzardo, E.; Thang, S. H. *Macromolecules* **2003**, *36*, 2256 - 2272.
13. Mori, H.; Iwaya, H.; Nagai, A.; Endo, T. *Chemical Communications (Cambridge)* **2005**, 4872-4874.
14. Sanda, F.; Abe, T.; Endo, T. *Journal of Polymer Science: Part A: Polymer Chemistry* **1997**, *35*, 2619-2629.

15. Bueno, M. P.; Cativiela, C. A.; Mayoral, J. A.; Avenoza, A. *Journal of Organic Chemistry* **1991**, *56*, 6551-6555.
16. Sanda, F.; Kamatani, J.; Handa, H.; Endo, T. *Macromolecules* **1999**, *32*, 2490-2494.
17. Mori, H.; Sutoh, K.; Endo, T. *Macromolecules* **2005**, *38*, 9055-9065.
18. Donovan, S. M.; Lowe, B. A.; Sumerlin, S. B.; McCormick, L. C. *Macromolecules* **2002**, *35*, 4123-4132.
19. Schilli, C.; Lanzendörfer, M. G.; Müller, A. H. E. *Macromolecules* **2002**, *35*, 6819-6827.
20. Ray, B.; Isobe, Y.; Matsumoto, K.; Habaue, S.; Okamoto, Y.; Kamigaito, M.; Sawamoto, M. *Macromolecules* **2004**, *37*, 1702-1710.
21. Favier, A.; Charreyre, M. T.; Chaumont, P.; Pichot, C. *Macromolecules* **2002**, *35*, 8271-8280.
22. Mori, H.; Müller, A. H. E. *Progress in Polymer Science* **2003**, *28*, 1403-1439.
23. Couvreur, L.; Lefay, C.; Belleney, J.; Charleux, B.; Guerret, O.; Magnet, S. *Macromolecules* **2003**, *36*, 8260-8267.
24. Urry, W. D. *Angew. Chem. Int. Ed.* **1993**, *32*, 819-941.
25. Kauzmann, W. *Nature* **1987**, *325*, 763-764.
26. Yoshida, M.; Safran, A.; Omichi, H.; Katakai, R. *Macromolecules* **1996**, *29*, 2321-2323.
27. Yoshida, M.; Asano, M.; Omichi, H.; Kamimura, W.; Kumakura, M.; Katakai, R. *Macromolecules* **1997**, *30*, 2795-2796.
28. Sugihara, S.; Hashimoto, K.; Okabe, S.; Shibayama, M.; Kanaoka, S.; Aoshima, S. *Macromolecules* **2004**, *37*, 336-343.
29. Sugihara, S.; Kanaoka, S.; Aoshima, S. *Macromolecules* **2004**, *37*, 1711-1719.
30. Baltes, T.; Garret-Flaudy, F.; Freitag, R. *Journal of Polymer Science: Part A: Polymer Chemistry* **1999**, *37*, 2977-2989.

Chapter 37

Applications of Telechelic Reversible Addition Fragmentation Chain Transfer Polymers

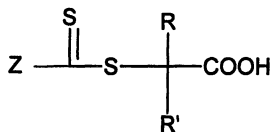
John Lai*, Dave Egan, Raymond Hsu, Carole Lepilleur,
Alex Lubnin, Anthony Pajerski, and Ronald Shea

Noveon Inc., A Subsidiary of Lubrizol Corporation, 9911 Brecksville Road,
Brecksville, OH 44141

*Corresponding author: john.lai@noveon.com

Telechelic di(mono)hydroxyl and di(mono)carboxyl-RAFT agents were synthesized and transformed to other functional blocks. The block-containing macro-RAFT agents underwent radical polymerization to prepare different block copolymers. These block copolymers, as well as the functional RAFT agents found applications in toughening epoxy resins, associative-thickening, *ab initio* emulsion and surfactant free emulsion polymerization, polyurethane synthesis, cross-linked polyacrylic acid synthesis and alkoxy-silane moisture-cure resins synthesis.

We reported the synthesis of mono- and di-carboxyl-terminated RAFT agents including trithiocarbonates (1) **1**, dithiocarbamates (2) **2** and xanthates (3) **3**.

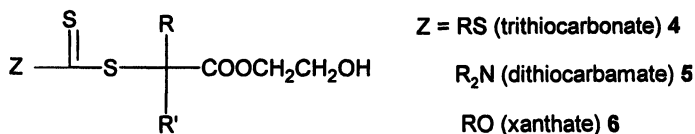


Z = RS (trithiocarbonate) **1**

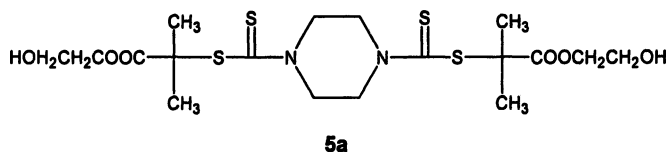
R₂N (dithiocarbamate) **2**

RO (xanthate) **3**

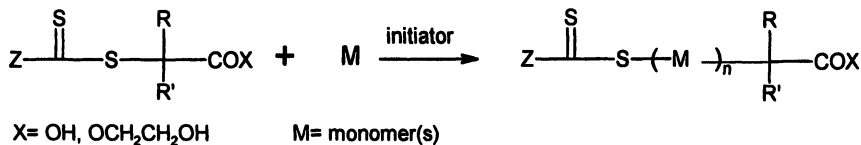
The carboxyl group can be transformed to the hydroxyl group by esterification with excess ethylene glycol (10).



One of the hydroxyl-terminated RAFT agents **5a** is a highly purified white solid.

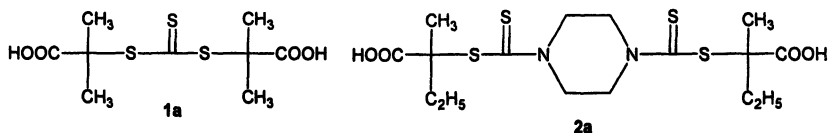


Telechelic polymers are of great interest (3) because of their ability to perform many useful operations, including a. chain extension of short chains to long ones by means of bifunctional linking groups, b. formation of networks by use of multifunctional linking agents and c. formation of (poly)block copolymers by combination of telechelics with different backbones. As depicted in Scheme 1, telechelic di- (Z is difunctional) and mono-carboxyl- and hydroxyl-terminated polymers have been made from these functionalized RAFT agents.



Scheme 1. Polymerization with functionalized RAFT agents

Due to the difference in their chain-transfer constants, RAFT agents with different Z groups behave differently. For simple alkyl Z derivatives (4,5,6, R=alkyl), trithiocarbonate has greater chain-transfer constant and is in general more efficient in making block copolymers through sequential polymerization than dithiocarbamate and xanthate (4). However, with the presence of the terminal functional groups, dithiocarbamate and xanthate 2,3,5 and 6 can also make block copolymers in a different manner. They can do so by introducing the first block through condensation with the carboxyl or hydroxyl groups, followed by radical polymerization to attach the second block of vinyl polymer. Alternatively, polymerization first followed by condensation reactions on the functional group can give rise to block polymers. Scheme 2 illustrates block copolymer formation from the carboxyl-terminated RAFT agent. This is a very versatile process since there are many hydroxyl-terminated species that are

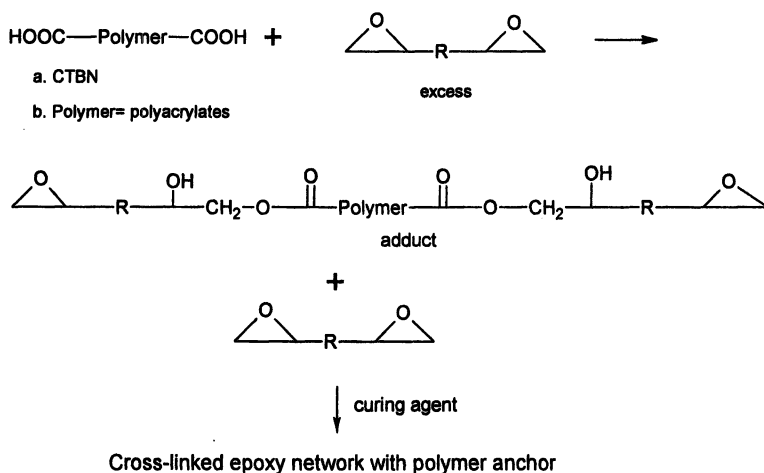


There are other differences among these RAFT agents. Trithiocarbonates and the polymers made from them are usually yellow in color. They are less stable toward water and amines (6) and are not suitable for aqueous polymerizations (7). Dithiocarbamates, on the other hand, are usually white solids and the polymers made from them are very light-colored and stable. Emulsion or dispersion polymers are totally white and are usually free from sulfur odor. Examples of the possible condensations with functionalized RAFT agents and polymers include reaction of the carboxyl group with epoxide, or esterification of the carboxyl group with alcohol. The hydroxyl group can react with isocyanate, or condense with a carboxyl group to form an ester. This article describes some of the processes and their use in different applications, including toughener for epoxy resins (8), associative thickener for latex paint (9), thermoplastic polyurethane and water-borne polyurethane dispersion (10), *ab initio* emulsion and surfactant-free emulsion polymers, cross-linked polyacrylic acid and moisture-cure coating. It provides a general scheme for their utilities, but by no means is a detailed study.

Toughener For Epoxy Resins

Epoxy resin is often brittle and needs to be toughened for many applications. One of the most common commercial tougheners for epoxy resin is carboxyl-terminated poly(butadiene/acrylonitrile)(CTBN) (11). CTBN is made through recombination of a propagating poly(butadiene/acrylonitrile) radical initiated by a carboxyl-terminated initiator such as 4,4'-azobis(4-cyanovaleric acid) (ACVA). CTBN is usually a very viscous liquid with rather low molecular weight ($M_n \sim 3\text{--}4\text{K}$). The expensive initiator takes up more than 10% of the toughener's weight. The functionality of CTBN is usually in the 1.8-1.9 range. The presence of double bonds also makes them susceptible to oxidation. There has been effort (12) to use carboxyl-terminated polyacrylates as epoxy tougheners. Although showing some effectiveness, these polyacrylates still need high dosage of ACVA and mercaptan chain-transfer agent.

Scheme 4 represents the technique typically used to toughen an epoxy resin with a carboxyl-terminated polymer. Initially an epoxy adduct is prepared by employing an excess of epoxy to carboxyl equivalents. Ultimately a curing agent is used to achieve a cross-linked epoxy network.

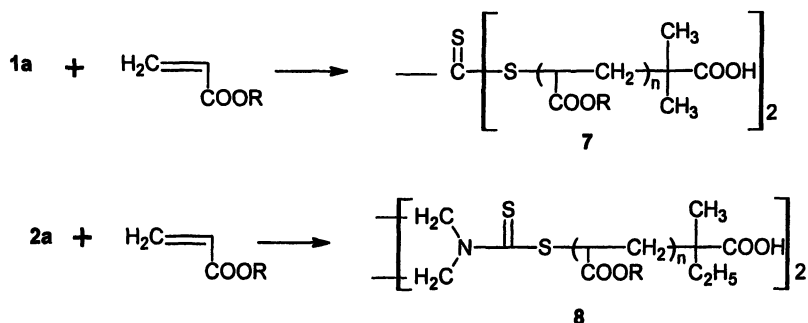


Scheme 4. Toughening epoxy resins with carboxyl-terminated polymers

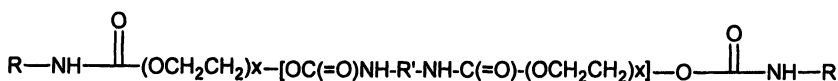
Telechelic di-carboxyl-terminated polyacrylates are prepared from **1a** and **2a** with bisphenol A diglycidyl ether as solvent. MALDI mass spectra (2,3) and HPLC with evaporative light-scattering detector (13) show that the functionalities are essentially completely transferred to the polymer chain ends. After being cross-linked with curing agent, the polyacrylate with Mn 10-20K phase-separates from the epoxy resin and shows good properties as toughener. Since the initiator is only used in a few mole% in relation to **1a** or **2a** during radical polymerization, there is no drop-off in toughening effectiveness if ACVA is replaced with a non-carboxyl initiator such as AIBN. Scheme 5 illustrates telechelic dicarboxyl-terminated polyacrylates **7** and **8** synthesized with bisphenol A diglycidylether as solvent in 40% solid. The condensation between the epoxy and the carboxyl groups is performed *in situ*. The adduct then is ready to be cured with a curing agent.

Associative Thickener for Latex Paint

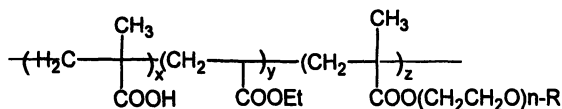
Rheological modifiers are extremely important additives in industrial and architectural coating systems (14). Different thickeners are added to latex paints to enhance their rheological properties. Traditional non-associative thickener such as hydroxyethyl cellulose works primarily by thickening the aqueous phase. Use of non-associative thickener alone is usually not sufficient due to the problems of roller spatter, poor leveling, water sensitivity and storage stability, etc. A second associative thickeners such as hydrophobically-modified ethoxylated urethanes (HEUR) or hydrophobically-modified alkali-swella-



Scheme 5. synthesis of telechelic dicarboxyl acrylates



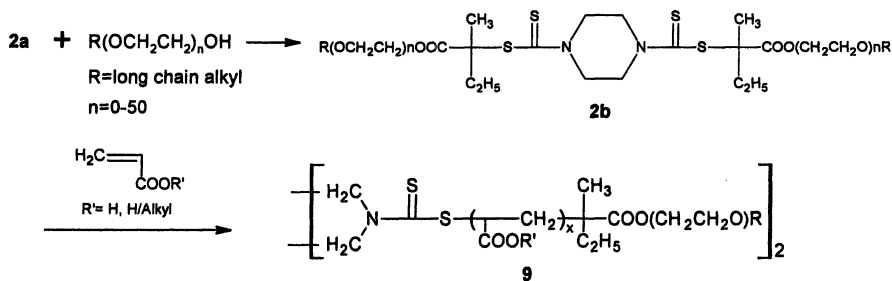
HEUR R= long chain alkyl



HASE R= long chain alkyl

emulsions (HASE) is also needed (15) to provide the correct rheology for the paint systems. The interaction of the hydrophobic part of the thickener molecule with components of the paint such as the polymer binder molecule, pigment and extenders overcomes the aforementioned problems.

We believe that a water-soluble (dispersible) telechelic polyacrylate with α , ω long chain alkyl groups may combine the better features of both HEUR and HASE by providing the associative-thickening performance from the end-hydrophobes, with a polymer structure similar to that of the latex and lower cost to produce. The dicarboxyl-terminated dithiocarbamate **2a** reacted with a long-chain alkyl alcohol such as 1-hexadecanol or various Brij® PEG ether alcohols to provide the ester **2b** with long chain alkyl at both ends. Subsequent polymerization with (meth)acrylates containing acid functions, followed by neutralization yields water soluble, or dispersible polyacrylates with telechelic hydrophobic groups.



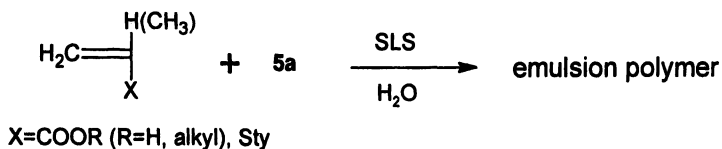
Scheme 6. Synthesis of associative thickener

The dicarboxyl-terminated trithiocarbonate **1a** yields similar ABA hydrophobe-hydrophile-hydrophobe block copolymers in the same manner. Limited evaluation of these block copolymers for low and high shear viscosities demonstrate that they do show associative thickening properties by providing thixotropic behaviors.

Emulsion Polymer

a. *Ab Initio* Emulsion Polymer

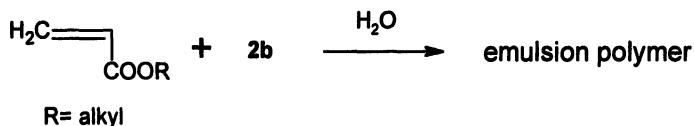
Among different types of controlled radical polymerizations in an aq. emulsion, RAFT hold the best promise (16) to overcome challenges such as colloidal stability, molecular weight control and rate retardation. There have been many efforts reported in the literature, including using fluoro-containing xanthates (17), miniemulsions (18), seeded polymerization (18), water-soluble initiator (19) and other special method (18). We would like to report some successful results with dihydroxyl-terminated dithiocarbamate **5a** as the RAFT agent to control emulsion polymerization. We believe that the emulsion polymerization works because the growing oligomeric radicals and the final polymers made from **5a** can stay in the micelles from the help of the two hydrophilic terminal-hydroxyl groups. The molecular weight control and the polydispersity are essentially the same as in solution polymerization. Monomers conversions are very high, as in solution polymerization, with no retardation observed. *Ab Initio* emulsion polymerization, where monomers, **5a**, surfactant and initiator are simply mixed with water and polymerized at elevated temperature, works well with different monomer combinations such as alkyl acrylate / styrene / (acrylic acid) and alkyl acrylate/alkyl methacrylate/acrylic acid to obtain fairly clean latex with little coagulum. Using polymer seeds can also give extremely clean emulsion with **5a** (20). High molecular weight polymers ($M_n \sim 100K$) with narrow polydispersity ($Pd < 1.8$) can be obtained with high monomer/**5a** weight ratio ($\sim 200/1$).



Scheme 7. *Ab Initio* emulsion polymerization with 5a

b. Surfactant-free Emulsion Polymer

Dithiocarbamate, such as **2b** with telechelic long PEG groups, can polymerize hydrophobic monomer like butyl acrylate in water to yield the emulsion polymer without additional surfactant in a controlled manner.



Scheme 8. Surfactant-free emulsion polymerization with 2b

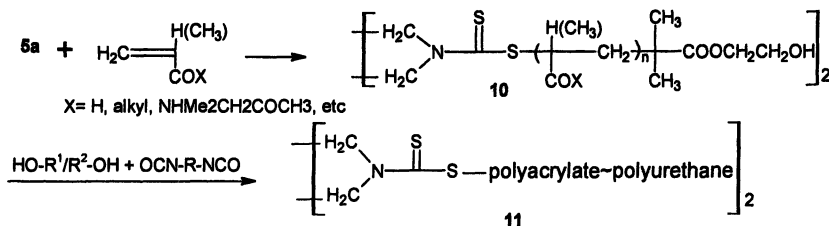
Polyurethane-polyacrylate Block Copolymers

Waterborne polyurethane dispersions (PUD) have been used widely in the coatings industry, and continue to show healthy growth in their consumption (21). Recently there has been active development of polyurethane/polyacrylate hybrid dispersions (22) where PUD and polyacrylates latex are blended together, or acrylate monomers are polymerized in the presence of PUD. The hybrids aim not only at reducing cost, also increasing the performance and lowering the amount of volatile organic chemicals (VOC) by reducing or even eliminating the commonly used solvent NMP (N-methyl-2-pyrrolidone).

Telechelic dihydroxyl and monohydroxyl-terminated RAFT agents and polymers offer the opportunity to make true polyurethane-polyacrylate block copolymers. The benefits besides those aforementioned for the hybrids, they will not have any compatibility issues associated with the two different polymers. Different monomers can be incorporated in the polyacrylates for additional properties, e.g. acrylonitrile for solvent resistance, diacetone acrylamide for self-crosslinking, and (meth)acrylic acid and/or side-chain PEG methacrylates for self-dispersing into water.

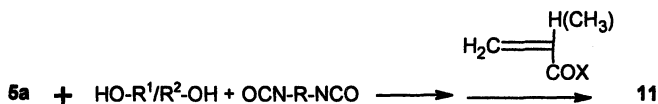
Telechelic dihydroxy-polyacrylates with different combination of monomers such as alkyl (meth)acrylate, (meth)acrylic acid, diacetone acrylamide, acrylonitrile are easily prepared from **5a**. They are converted to PUD by using the polyacrylate diol **10** as the only polyol or as one of two or

more polyols according to the following scheme. Optionally, a dispersing diol such as dimethylol propionic acid can be used if no dispersing groups are include in the polyacrylate diol. The copolymer **11** can be end-capped with isocyanates and further chain-extended in the water with hydrazine or a diamine as commonly practiced.



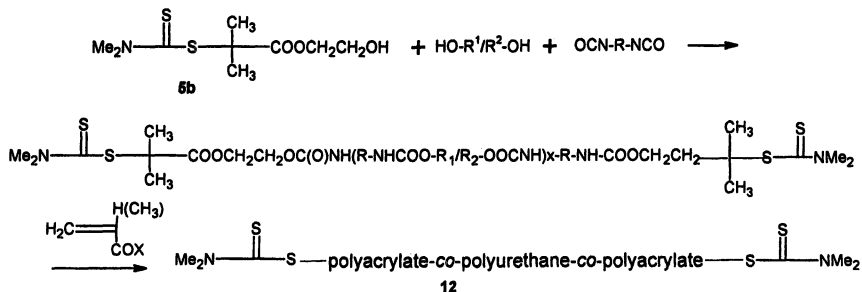
Scheme 9. Synthesis of acrylate/urethane copolymer

Similarly the copolymer **11** can also be synthesized from **5a**, or its combination with other polyols by reacting with the diisocyanate first to preform the polyurethane-RAFT agent, before polymerization with acrylate monomers.



Scheme 10. Alternative synthesis of acrylate/urethane copolymer

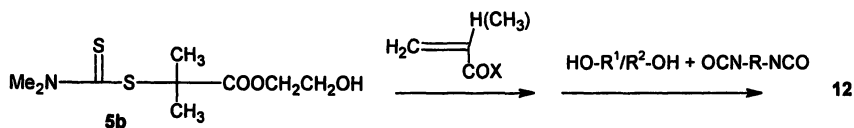
Polyacrylates can be the side blocks if a mono-hydroxyl dithiocarbamate such as **5b** is used as the end-caps of a polyurethane RAFT-prepolymer, followed by the controlled radical polymerization to obtain the copolymer, according to the following scheme:



Scheme 11. Synthesis of poly(acrylate-co-urethane-co-acrylate) **12**

An interesting possibility exists with the RAFT end capped polyurethane prepolymers for waterborne polyurethane: due to the absence of reactive isocyanate groups one can employ unusual neutralizing agent such as ammonia, dimethyl ethanol amine or sodium hydroxide, etc. to ionize acid dispersing groups in the prepolymer prior to dispersing the prepolymer into water. Moreover, the absence of reactive isocyanate groups in the prepolymer broadens the process window for dispersing the polyurethane "prepolymer" allowing one to use higher processing temperatures as well as long process times in handling and dispersing the prepolymer. Highly reactive aromatic isocyanates which are typically difficult to work with in preparing waterborne polyurethanes are easily handled using the above scheme 11. Additional molecular weight build can be obtained from the dispersed RAFT capped prepolymer by incorporating acrylic monomers with reactive functionality such as epoxy, ketone, hydroxyl, amide, nitrile, etc.

The copolymer 12 can similarly be made from monohydroxyl-terminated polyacrylate, then continue with the polyurethane synthesis by reacting with diisocyanate and optional other polyols, according to scheme 12:



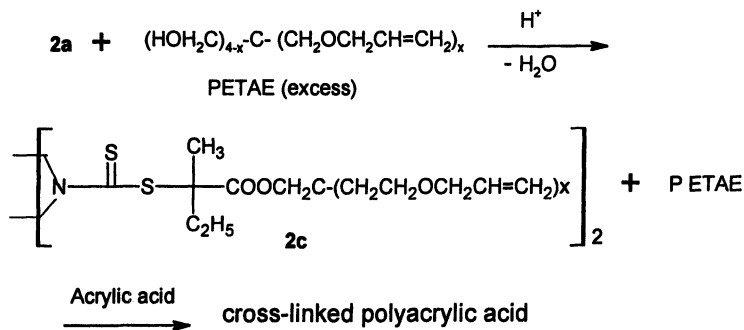
Scheme 12. Alternative synthesis of copolymer 12

Thermoplastic polyurethane-polyacrylate block copolymers are also made from 5a or 5b in solution, e.g. with THF as solvent or in bulk at elevated temperature.

Cross-linked Polyacrylic Acid Thickener

Cross-linked polyacrylic acid, or carbomer is used widely commercially as thickener in coating and personal care products (23). It is produced by radical polymerization of acrylic acid in the presence of crosslinkers such as polyallyl polyether or an acrylate such as trimethylolpropane triacrylate. The isolated polymer is dispersed in water and then neutralized with a base such as sodium hydroxide to give a thick gel through volume expansion of the cross-linked polyacrylic acid. The viscosity of a 0.5% aq. solution of neutralized polymer can reach 40K mPa sec. with good clarity. Functional RAFT agent is used to make carbomers in controlled radical polymerization with the benefits of better process control and higher solids in the polymerization. When dicarboxyl-terminated dithiocarbamate 2a is esterified with excess pentaerythritol triallyl ether (PETAE), followed by polymerization with acrylic acid in an inert organic solvent, the cross-linked polymer can be isolated as white powders after

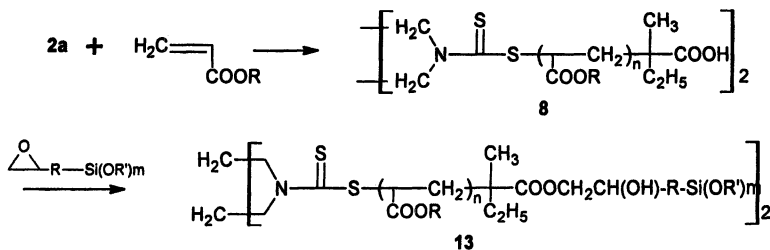
removing the solvent. Dilute neutralized aq. mucilage of the polymer forms smooth colorless gel with viscosity and clarity comparable to the commercial products. Interestingly, replacing **2a** with mono-carboxyl dithiocarbamate RAFT agent does not give similar thickening performance, probably the result of too much reduction of cross-linked structures.



Scheme 13. RAFT synthesis of cross-linked polyacrylic acid

Telechelic Alkoxysilyl-terminated Polymers

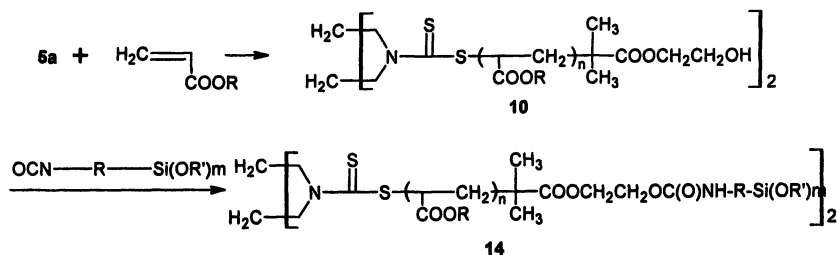
Alkoxysilyl groups have been incorporated into polymers, either at side chains or at chain ends. They can be cross linked from reaction with moisture or water to find applications in adhesives (24), sealants / caulks (25) and organic-inorganic sol-gels (26). The introduction of many functional alkoxysilanes such as glycidyl alkyl alkoxysilane or isocyanatoalkyl alkoxysilane makes the attachment to the polymer chains viable processes. Report of the commercialization of telechelic di-trimethoxysilyl-terminated polyacrylates as sealant was recently published (25). Telechelic carboxyl-terminated polymer made from carboxyl-terminated RAFT agent such as **2a** is reacted with epoxy-terminated alkoxysilane such as glycidoxypropyltrimethoxysilane to form telechelic trimethoxysilyl-terminated polymer **13**.



Scheme 14. Synthesis of alkoxysilyl-terminated polyacrylate 13

Similarly trimethoxysilyl-terminated polymer **13** can be made through hydroxyl-terminated polymer from hydroxyl-terminated RAFT agent such as **5a**, by

reacting with isocyanate-terminated alkoxyisilane such as γ -isocyanatopropyltrimethoxysilane. These trimethoxysilyl-terminated polymers can be cured by adding small amount of water to form elastomeric materials.



Scheme 15. Synthesis of alkoxyisilyl-terminated polyacrylate 14

Conclusion

There are many opportunities for telechelic RAFT polymers in industrial applications. The RAFT agents and macromers reported here are very robust in controlling the radical polymerization, making them practical in large-scale production. With the choice of trithiocarbonate, xanthate and dithiocarbamate types of RAFT agents and the functionalities that are available, many different structures and architectures can now be constructed via RAFT polymerization.

Acknowledgement

The authors wish to thank the Lubrizol Corp. for the permission to publish this paper, Dr. Shy-chang Huang for GPC data, Dr. George Benedikt and Dr. Bob Lattimer for obtaining H^1 -NMR and Mass spectra, respectively, and Miss Debby Filla, Sue Lenhard and Randy Collins for their laboratory work.

Experimental Section

All monomers and chemicals are purchased from Aldrich or Acros, and were used without or removing polymerization inhibitors or purification. Vazo® 67 initiator was acquired from DuPont Specialty Chemicals, Wilmington, Delaware. Epon® 828 was a free sample from Resolution Performance Products, a subsidiary of Hexion Specialty Chemicals, Houston, Texas.

Toughening epoxy resin with telechelic di-carboxyl-terminated polyacrylates 7 and 8: 2.82 g trithiocarbonate **1a**, 80g butyl acrylate, 80g ethyl acrylate, 240g bisphenol A diglycidyl ether (Epon® 828), 0.05g AIBN were mixed and purged with nitrogen for 15 minutes before gradually heating up to 80°C for 8 hours to give polyacrylate **7** of Mn=17K and polydispersity 1.07. 0.04g triphenylphosphine was then added and the mixture was heated to 95-100°C for 2 hour. IR and titration of the acid confirmed that the conversion was complete. Similarly, polybutyl acrylate **8** of Mn=17.6K and Pd = 1.89 was prepared from 1.3g **5a** and 40g butyl acrylate in 60g Epon® 828. The polymerization was initiated by 0.15g of ACVA. After 8 hrs at 80°C, 0.2g triphenyl phosphine was added to the reaction mixture and heating was continued at 100°C for 1.5 hrs. In curing of the epoxy resin, the adduct was further diluted with Epon®828 to make the concentration 15% (e.g. 37.5g was diluted to 115g). Different curing agents were added at different levels, and were cured at different temperatures according to the recommendations from the suppliers. Commercial CTBN toughener Epon® 58006 was used at the same level as the control.

Associative thickener polyacrylate 9: a. synthesis of RAFT ester 2b: 50g dicarboxyl dithiocarbamate **2a**, 269.6g Brij® 58 (C₁₆H₃₃(OCH₂CH₂)₂₀OH) and 8.7g toluenesulfonic acid were heated to 110°C under 60 mmHg vacuum to distill off the water that was formed. After 2 hrs, the reaction was cooled down and 600ml toluene was added. The solution was washed 3 times with 100ml 20% NaOH, dried over magnesium sulfate and was concentrated on a rotary evaporator. The product turned into a yellow solid on standing and was used directly in the polymerization. **b. synthesis of polymer 9 in water:** 6.65g **2b** as described, 15g acrylic acid, 53g ethyl acrylate 100g deionized water were mixed with 0.03g ammonium persulfate and were purged with nitrogen for 15 minutes before heating to 70°C for 5 hrs. 0.03g ammonium persulfate was added again and the polymerization continued at 80°C for 2 more hrs. After cooling down to ambient temperature, 200g water was added followed by 36g 25% sodium hydroxide in portions. The clear aq. solution is 19.0% solid with pH 8.3. No residual ethyl acrylate was detected (<20ppm) from GC analysis. The same polymer can be made in a hydrolytic solvent such as t-butanol, then solvent exchanged into water by co-distilling off water-t-butanol azeotrope. The similar polyacrylate with telechelic polyethylene glycol mono-long chain alkyl tails made from dicarboxyl trithiocarbonate **1a** was described in the patent application (**9**).

Ab Initio emulsion polymerization with 5a: a. poly(ethyl acrylate-co-styrene). 0.2g **5a**, 30g ethyl acrylate, 15g styrene, 2.5g sodium lauryl sulfate, 0.02g ammonium persulfate and 85g water were purged with nitrogen for 15 minutes, then mixed for 30 more minutes before heating to 75°C for 4 hours. White latex with very little coagulum was obtained. From GPC, Mn= 91Kg/mole and PDI= 1.75. ave. particle size: 110nm

b. poly(butyl acrylate-co-styrene-co-acrylic acid). 0.2g **5a**, 30g butyl acrylate, 15g styrene, 1g acrylic acid, 2.5g sodium lauryl sulfate 0.02g ammonium persulfate and 85g water were mixed and neutralized with 1.5g sodium carbonate to about pH 8. After purging with nitrogen and emulsified by mixing, the polymerization was brought to 75°C for 4 hours to obtain fairly clean white latex. Mn= 82K and PDI= 1.73. ave. particle size: 122nm. The polymerization was also run at pH 5.4 to give similar result.

c. poly(ethyl acrylate-co-methyl methacrylate-co-acrylic acid). 0.2g **5a**, 28g ethyl acrylate, 17g methyl methacrylate, 1g acrylic acid, 2g sodium lauryl sulfate, 0.02g ammonium persulfate and 85g water were neutralized with 0.65g 50% sodium hydroxide to pH 8.0, then polymerized at 65°C for 3 hours to get white latex. Mn= 96K and PDI= 1.70. ave. particle size: 270nm

Surfactant-free emulsion polymerization of butyl acrylate: 11.64g **2b**, 50g butyl acrylate, 0.03g 2,2'-azobis(2-methylproprionamidine) dihydrochloride and 50g water were purged with nitrogen for 15 minutes before polymerized at 65°C for 6.5 hours. A white paste was obtained and the dispersion remained stable for over 12 months. Mn= 12.6K, PDI= 1.46.

Synthesis of acrylate-urethane copolymer 11 dispersion from polyacrylate diol 10. A polyethyl acrylate diol, **10** (X= OEt), Mn 2635, hydroxyl number= 43.5 was prepared from 58g **5a**, 524.3g ethyl acrylate, 0.33g Vazo® 67 and 580 ml. The polymerization was run at 65°C for 4.5 hours. The liquid was used after solvent was stripped. 280g **10** (R= Et), 20.8g dimethylolpropanoic acid, 80g N-methylpyrrolidone and 117g isophorone diisocyanate were mixed in a 4-neck flask at 60°C, then raised to 85°C for 30 minutes. 0.1g stannous octoate was added and the temperature was held at 85°C for another 1.5 hour when the theoretical %NCO was reached. A polyurethane dispersion was prepared by neutralizing the prepolymer with 16.4g triethylamine at about 70°C, and dispersing the neutralized prepolymer in water while maintaining the water/dispersion temperature below 28°C. The dispersed prepolymer was extended with hydrazine to give a 40.4% solids polyurethane dispersion with low sediment, with a viscosity of 170 cps @25°C and pH of 7.5.

For a self-cross linking **11**, a poly(ethylacrylate-co-diacetone acrylamide) diol **10** was made from 139.3g **5a**, 560g ethyl acrylate, 140g diacetone acrylamide, 840ml MEK and 0.8g Vazo® 67 at 80°C for 7 hrs. 120g of the **10** (X= OEt/NHMe₂CH₂COCH₃), OH#= 39.7. 120g tetramethyleneoxide polyol (OH#= 38.6), 18.2g dimethylolpropionic acid, 67g N-methylpyrrolidone, 117g 4,4'-methylene bis(cyclohexyl) diisocyanate and 0.1g stannous octoate were reacted in the same manner as before. It was then neutralized with 14.4g triethylamine and then dispersed in water and chain-extended with hydrazine to give a 43.6% solids polyurethane dispersion with low sediment, a viscosity of 105 cps @25°C at a pH of 9.3. To this dispersion adipic acid dihydrazide was added to render it self-crosslinking.

Synthesis of acrylate-urethane copolymer 11 by making the polyurethane first. 20.7g **5a**, 28.3g 1,4-butanediol, 27.0g dimethylbutanoic acid, 46g methyl methacrylate, 184g butyl acrylate and 153.9g isophorone diisocyanate were mixed in a reaction flask under nitrogen and heated to 85°C for 30 minutes before adding 0.1g stannous octoate and heated for another 1.5 hrs when theoretical %NCO was reached by titrating a small sample. The prepolymer was neutralized with 20.2g triethylamine at 69°C and then dispersed in water using high speed stirring while maintaining the water/dispersion temperature below 28°C. While stirring the dispersed prepolymer was extended with hydrazine. Copolymer with the (meth)acrylates was carried out by adding 0.3g of a 1% Fe(EDTA) solution and 3g 3.5% t-butyl hydroperoxide solution, heating to 35°C and then adding 5g of a 2% erythorbic acid solution neutralized with triethylamine. The resulting copolymer dispersion has a solids content of 34.5% with low level of sediment, a viscosity of 50 cps @25°C at pH 7.5.

Synthesis of acrylate-urethane copolymer 12 with monohydroxyl RAFT agent 5b. 119.3g PPG 2025 polyol (a dihydroxyl-terminated polypropylene glycol, OH# = 56), 17.8g dimethylbutanoic acid, 64.3g methyl methacrylate, 192.8g butyl acrylate and 4,4'-diphenyl-methylene diisocyanate (MDI) were mixed and heated at 45-50°C for 30 minutes under nitrogen, then at 70-75°C for 1.5 hrs. 30.2g **5b** was then added to cap the remaining isocyanate group. The temperature was held at 70-75°C for another hour until most of the NCO group was depleted as indicated by titration. A polyurethane dispersion was prepared by neutralizing the above prepolymer with 12.7g triethylamine at 68-70°C (typically not feasible with aromatic isocyanate based prepolymers containing active NCO groups) and then dispersed in water with high speed stirring while maintaining the water/dispersion temperature. 7g of diacetone acrylamide in 7g water was then added to the dispersion. Polymerization of the (meth)acrylates was effected by adding 0.3g of a 1% Fe(EDTA) and 2.5g of a 2% erythorbic acid neutralized with triethylamine, and heating to 38-40°C, then adding 1.4g of a 3.5% t-butyl hydroperoxide solution. The resulting polymeric dispersion has a solids content of 31.3% with low level of sediment, a viscosity of 30 cps @25°C at a pH of 7.6. Adipic acid dihydrazide can be added to effect self-cross linking.

Cross-linked polyacrylic acid. 5.7g **2a** and 13.3g pentaerythritol triallyl ether were mixed in a 25ml 3-neck flask equipped with a short-stem distillation column, a magnetic stirrer and a thermometer. 0.4g methanesulfonic acid was then added. The reaction was heated to 100°C under 60mmHg vacuum to distill off the water that was formed. After 3 hours the vacuum was increased to 10mmHg and held there for 3 more hours to afford yellow-colored liquid. 0.4g of the liquid, 50g of acrylic acid, 131.76g ethyl acetate and 112.2g cyclohexane were mixed in a 500ml 3-neck flask equipped with a mechanical stirrer, a thermometer and a reflux condenser. 0.078g di-(2-ethylhexyl)

peroxydicarbonate was added and the polymerization was effected at 45°C for 8 hrs under nitrogen. Solvent was removed in a rotary evaporator and the white powders were dried in a forced air oven at 50°C for 5 hrs. A 0.5% aq. solution of the powder was neutralized with sodium hydroxide to give a viscous gel with viscosity 31,100 cps and clarity of 95.6% transmittance.

Synthesis of trimethoxysilyl-terminated polyacrylate 13 from 8. 80.4g of 8 (R=Bu, Mn= 11514) and 3.3g 2-trimethoxysilylethyl glycidyl ether were heated at 105°C with 0.07g triphenylphosphine for 3 hours, when the carboxyl group was totally reacted as indicated by IR and titration., The yellow-colored oil turned elastomeric overnight when stirred with small amount of water.

Synthesis of trimethoxysilyl-terminated polyacrylate 14 from 10. 5g of 5a and 50g butylacrylate were mixed with 0.1g Vazo® 67 and 50ml methyl ethyl ketone, and was purged with nitrogen for 15 minutes. The temperature was then raised to 80°C for 3 hours before 0.1 g more Vazo® 67 was added and the polymerization continued under nitrogen for 5 more hours. Solvent was removed on a rotary evaporator to afford 54.5g yellow-colored oil. Mn: 4737, PDI: 1.51. 27.3g of the oil and 1.9g 3-isocyanatopropyl trimethoxysilane were mixed and heated to 120°C with 2 drops of dibutyltin dilaurate for 3 hrs under nitrogen. IR indicated that all the isocyanate groups were reacted. The viscous oil was mixed with small amount of water and turned elastomeric in 10 hrs at 60°C.

References

1. a. Lai, J. T., Filla, D and Shea, R. *Macromolecules*, **2002**, 35, 6754. b. Lai, J. T. *US Pat.* 6,596,899, Jul. 22, 2003.
2. a. Lai, J. T. and Shea, R. *Polymer Preprints*, **2005**, 46(2), 193. b. Lai, J. T. *U.S. Pat. Appl.* 10/278335, 2002.
3. Goethals, E. J. in *Telechelic Polymers: Synthesis and Application*, CRC press, Inc., 1989, Chap. 1.
4. a. Mayadunne, R. T. A., Rizzardo, E., et. al., *Macromolecules*, **1999**, 32,6977.
b. Perrier, S. and Takolpuckdee, P., *J. Polym. Sci; Part A: Polym. Chem.*, **2005**, 43, 5347 and ref. cited therein.
5. a. Matyjaszewski, M and Xia J. *Chem. Rev.*, **2001**, 101, 2921.
b. Huddleton, D. M., et. al. *Polymer Preprints*, **2005**, 46(2), 468.
6. Mayadunne, R. T. A., Rizzardo, E. et. al, *Macromolecules*, **2000**, 33, 243.
7. a. Thomas, D., Converine, A., Hester, R., Lowe A. and McCorick, C. *Macromolecules*, **2004**, 37, 1735. b. Convertine, A. J, Lokitz, B. S., Lowe, A. B., Scales, C. W., Myrick, L. J. and McCormick, C. L. *Macromol. Rapid Comm.* **2005**, 26, 791.
8. Lai, J. T., Lepilleur, C. A., Weber, C. D., Egan, D. R. and Filla, D. S., *U.S. Pat.* 6894116, May 17, 2005.
9. Lai, J. T. and Hsu, R., *U. S. Pat. Appl.* 11/206393, 2004.

10. Lai, J. T., Pajerski, A. D. and Shea, R., *US. Pat. Appl.* 10/913972, **2004**.
11. Chen, D., Pascault J. P., Bertsch R. J., Drake R. S. and Siebert, A. R. *J. Appl. Polym. Sci.* **1994**, 51, 1959 and ref. cited therein.
12. a. Ratna, D. and Banthia, A. K., *Polym. Int.* **2000**, 49, 281. b. Ratna, D., Banthia, A. K. and Deb P. C., *J. Appl. Polym. Sci.* **2000**, 78, 716. c. Ratna, D., Banthia, A. K. and Deb P. C. *J. Appl. Polym. Sci.* **2001**, 80, 1792.
13. Lima, V., Jiang, s., Brokken-zijp, J., schoenmakers, P. J., Klumperman B. and Ven Der Linde, R. J. *Polym. Sci: Part A: Polym. Chem.* **2005**, 43,939.
14. Sauer, F., *Paint and Coating Industry*, **June 2004**, 72.
15. Glass, J. E., *J. Coating Tech.*, **2001**, 73, 79.
16. Prescott, S. W., Ballard, M. J., Rizzardo, E, Gilbert, R. G. *Aust. J. Chem.* **2002**, 55, 415.
17. Monteiro, M., Adamy, M., Leeuwen, B., Van Herk, A., Desarac, M. *Macromolecules*, **2005**, 38, 1538.
18. Moad, G., Rizzardo E., and Thang, S. H. *Aust. J. Chem.* **2005**, 58, 379 and ref. cited therein.
19. Freal-Saison, S., Magnet s., Save M., Charleux B. *Polymer Preprints*, **2005**, 46(2), 128.
20. Lubnin, A., Lenard, S. and Lai, J. T. *Waterborne and High Solids Symposium*, Brussels, Belgium, **Mar. 7-8, 2006**.
21. *Coatings World*, **June 2001**, 49.
22. a. Galgoci, E. C., et. al., *J. Coating Tech.* **2005**, 28. b. Manock, H. L., *Pigments and Resin Technology*, **2000**, 29(3), 143.
23. a. Amjad, Z., Hemker, W. J., Maiden, C. A., Rouse, W. M. and Sauer, C. E. *Cosmetics & Toiletries*, **1992**, 107, 81. b. Hsu, C. C. *U. S. Patent* 4,923,940, **May 8, 1990**.
24. a. Witucki, G. L., *J. Coating Technology*, **1993**, 65(822), 57. b. Huang, M., Lehmann, P., Waldman, B. and Osterholtz, F. *Adhesives Age*, **Apr. 2002**, 33. c. Plueddemann, E. P., *Progress in Organic Coatings*, **1983**, 11,297.
25. Telechelic di(trimethoxysilyl)polyacrylates prepared by ATRP was recently commercialized by Kaneka Corp. for sealant and caulk applications: Nakagawa, Y. *Polymeric Materials: Science & Engineering*, **2004**, 90, 183. Kaneka also markets telechelic di(trimethoxysilyl)polyisobutylene for similar applications under Epion® trade name.
26. Messori, M., et. al. *Paint & Coatings Industry*, **Oct. 2005**, 76 and ref. cited therein.

Chapter 38

Various Strategies for the Chemical Transformation of Xanthate-Functional Chain Termini in MADIX Copolymers

Mathias Destarac^{1,*}, Chakib Kalai², Agnieszka Wilczewska^{1,2},
Laurence Petit¹, Eric Van Gramberen¹, and Samir Z. Zard^{2,*}

¹Rhodia Recherches et Technologies, Centre de Recherches et Technologies d'Aubervilliers, 52 Rue de la Haie Coq, 93308 Aubervilliers Cedex, France

²Laboratoire de Synthèse Organique, Ecole Polytechnique, 91128 Palaiseau Cedex, France

Although the MADIX process is undoubtedly one of the most promising controlled free radical polymerization technique for an industrial development, one of its potential drawback may lie in the fact that the xanthate terminal group, if not deactivated, is likely to be degraded during the lifetime of the polymer or under some specific application conditions. Several appropriate treatments were developed by our group in order to prevent an uncontrolled degradation over time which may eventually generate low molecular weight malodorous, potentially toxic sulfur-based by-products. For instance, the radical reduction of xanthate terminal groups of PDMS and MADIX polymers was efficiently conducted with peroxide and percarbonate initiators in secondary alcohols, e.g. isopropanol. The thermally-induced elimination of xanthate terminal groups of MADIX polymer chains was also successfully accomplished using five different secondary xanthates. This allowed the generation of terminal thiol groups for PDMS and MADIX polymers.

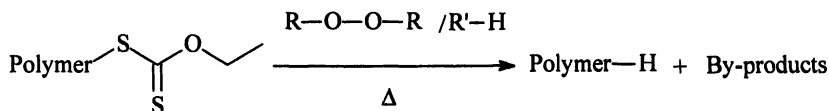
Introduction

Macromolecular Design via the Interchange of Xanthates (MADIX)(1,2) has attracted a great deal of attention over the last few years because of its ability to produce polymers with well-controlled macromolecular properties from numerous monomer types under mild pressure and temperature conditions. This controlled free radical polymerization (CRP) technique, based on a reversible addition-fragmentation transfer of xanthates $R-S(C=S)OZ$ during polymerization, is undoubtedly one of the most promising approaches to transform complex polymer architectures into an industrial reality. Amongst its main advantages, it is highly tolerant to functional groups, water is a solvent of choice for MADIX polymerization in homogeneous or dispersed media, and the rate of polymerization is nearly insensitive to the initial xanthate concentration. However, one potential drawback of MADIX lies in the fact that the xanthate terminal group, if not deactivated, is likely to be degraded during the lifetime of the polymer or under some specific application conditions. Our group aimed at developing several appropriate treatments in order to prevent an uncontrolled degradation over time which may eventually generate low molecular weight malodorous, potentially toxic sulfur-based by-products (3-6).

Numerous methods for the chemical modification of a xanthate group are reported in the literature. For instance, several procedures for the cleavage of a xanthate group into the corresponding thiol are known. Aminolysis using amines (7) and ammonia (8), and reduction with $LiAlH_4$ (9) were successfully implemented on xanthate derivatives. As part of our continuing work in this area, we have explored practical ways of usefully modifying the xanthate group on polymer structures. Two methods have been explored involving, on the one hand, the complete reductive removal of the xanthate motif (3) and, on the other, its conversion into the corresponding thiol using the Chugaev fragmentation (4).

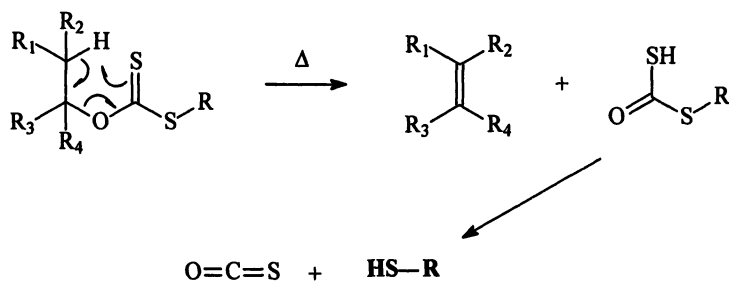
The first approach hinges on an earlier work by Zard and collaborators (10), who found that exposure of a xanthate $RS(C=S)OZ$ to stoichiometric amounts of peroxide in refluxing 2-propanol resulted in the complete replacement of the xanthate group by a hydrogen atom to give the corresponding alkane $R-H$. This method is ecologically superior to the traditionally employed Raney Nickel (11) and Bu_3SnH (12), in the sense that it avoids the use of toxic heavy metal residues which are difficult to remove. We have now found that the terminal xanthate group present in poly(dimethylsiloxane) (PDMS) and poly(acrylic acid) (PAA) prepared by the MADIX technique can be efficiently removed by a combination of peroxide and secondary alcohol as summarized in Scheme 1.

The second modification is based on a thermolysis process known as the Chugaev reaction (13). It consists in the thermal cleavage of a xanthate of



Scheme 1. Peroxide-induced radical reduction of MADIX polymers.

general structure $\text{R}_1\text{R}_2\text{HC}-\text{CR}_3\text{R}_4-\text{O}-(\text{C}=\text{S})-\text{SR}$ to give olefin $\text{R}_1\text{R}_2=\text{R}_3\text{R}_4$, carbon oxysulfide (COS), and thiol RSH (Scheme 2). Interestingly, this unimolecular elimination reaction generates volatile by-products, which may be fully removed from the reaction mixture by evaporation, simply by heating the polymer.



Scheme 2. The Chugaev reaction.

In the present study, we show that the xanthate terminal group can be eliminated simply by heating solutions of MADIX polymers, without the need for additional reagents. This economical and convenient technique was applied to xanthate-terminated polystyrene and poly(*t*-butyl acrylate) (P(*t*-BuA)), as well as to MADIX derived PDMS and related triblock copolymers with *t*-BuA.

Experimental

Radical Reduction. *O*-Ethyl-*S*-(1-ethoxycarbonyl)ethyl xanthate X_1 was synthesized according to general procedures reported elsewhere (14).

Synthesis of a *O*-ethyl xanthate-capped silicone oil (C). Step 1: 1.9 mL (2.4 equivalents) of 2-bromopropionyl bromide were added dropwise at room temperature to a solution made of 10 g of silicone oil A (1 equivalent) and 2.6 g (4 equivalents) of pyridine in 200 mL ether. After one night at room temperature,

50 mL of water were added. The aqueous phase was then extracted twice with 100 mL of ethyl acetate. The organic layers were combined, then washed successively with an aqueous NaOH solution (1M), a 10 % aqueous HCl solution, water, brine, and then dried over magnesium sulfate. The solvents were evaporated and the crude product purified by column chromatography on a silica gel (heptane 9/ether 1) to give 11 g of the functional silicone oil **B**. ^1H NMR (CDCl_3) δ 0 (m, Si- CH_3), 0.55 (m, 4H), 1.7 (m, 4H), 1.83 (d, 6H), 4.12 (m, 4H), 4.37 (q, 2H). **Step 2:** 5 g of brominated silicone oil **B** were added to a solution of 2.22 g of potassium O-ethyl xanthate (4 equivalents) in 150 mL of acetonitrile. The reaction was left for 4 h at room temperature. The solvent was then evaporated, diethyl ether was added, and the mixture filtered. After the evaporation of the solvent, 5.2 g of silicone **C** were recovered.

Radical reduction of xanthate-terminated PDMS C. One equivalent of the silicone **C** was dissolved in 2-octanol (50 wt.%) and the mixture was heated to reflux. One equivalent of di-*t*-butyl peroxide was added over a period of 30 min. 1 h after the end of the addition, the reaction mixture was cooled and the solvent evaporated under vacuum together with the sulfur-containing by-products. The ^1H NMR spectrum of the reaction product shows no residual characteristic signal of the xanthate groups. Thus, the quartets at δ 4.60 and δ 4.40 corresponding respectively to the two methylene hydrogens of the starting xanthate ($\text{RO}(\text{C}=\text{O})\text{CH}(\text{Me})\text{S}(\text{C}=\text{S})\text{OCH}_2\text{-CH}_3$) and the methine hydrogen ($\text{RO}(\text{C}=\text{O})\text{CH}(\text{Me})\text{S}(\text{C}=\text{S})\text{OCH}_2\text{-CH}_3$) disappear completely. The latter is replaced by a quartet at δ 2.35 corresponding to the methylene hydrogens in the product **D** ($\text{RO}(\text{C}=\text{O})\text{CH}_2\text{Me}$).

Dethiocarboxylation. Synthesis of Xanthate Derivatives. The following experimental procedure was repeated for all the xanthate salts of the series. **Sodium O-(1-methylpropyl) xanthate (1).** One mole of 2-butanol was added dropwise, at 0 °C, to a suspension of 1.1 equivalent of NaH in 1 L of THF. Evolution of hydrogen was observed, which subsided after about 1 h. At this time, 4 equivalents of CS_2 were added and the reaction mixture was left overnight at room temperature. Then most of the THF was evaporated and 1 L of petroleum ether was added to wash and aid the filtration of the solid obtained. The solid was finally dried under vacuum. ^1H NMR (CDCl_3) δ 5.45 (sext., 1H), 1.84 and 1.62 (m, 2H), 1.32 (d, 2H), 0.93 (t, 3H). **Sodium O-(1,2-dimethylpropyl) xanthate (2)** ^1H NMR (CDCl_3) δ 5.7 (quint., 1H), 2.16 (d, 1H), 1.42 (d, 3H), 1.19 (d, 3H), 1.18 (d, 3H). **Sodium O-cyclohexyl xanthate (3)** ^1H NMR (CDCl_3) δ 5.01 (m, 1H), 0.5-1.5 (m, 10H). **Sodium O-(2-methylcyclohexyl) xanthate (4)** ^1H NMR (CDCl_3) δ 5.27 (m, 1H), 2.3 (m, 1H), 1.8 (m, 5H), 1.35 (m, 4H), 1.1 (m, 1H), 1.0 (d, 3H). **Sodium O-(1-phenylethyl) xanthate (5)** ^1H NMR (CDCl_3) δ 7.62 (d, 2H), 7.5 (t, 2H), 7.4 (t, 1H), 6.93 (q, 1H), 1.72 (d, 3H).

Secondary xanthate-capped poly(dimethyl siloxane) C₁'. 1 g of brominated silicone oil **B** was added to a solution of 0.5 g of xanthate salt **1** (4 equivalents) in 10 ml of acetonitrile. The reaction mixture was left overnight at room temperature. The solvent was then evaporated, diethyl ether was added, and a filtration was performed to eliminate the excess of xanthate salt and the sodium salt formed. The ¹H NMR analysis of the silicone C₁' demonstrated that the bromine was completely displaced by the xanthate salt. ¹H NMR (CDCl₃) δ 5.56 (sext, 2H), 4.32 (quad, 2H), 4.06 (t, 4H), 1.6-1.8 (m, 8H), 1.51 (d, 6H), 1.30 (m, 6H), 0.90 (t, 6H), 0.52 (m, 4H), 0.1 (m, Si-CH₃).

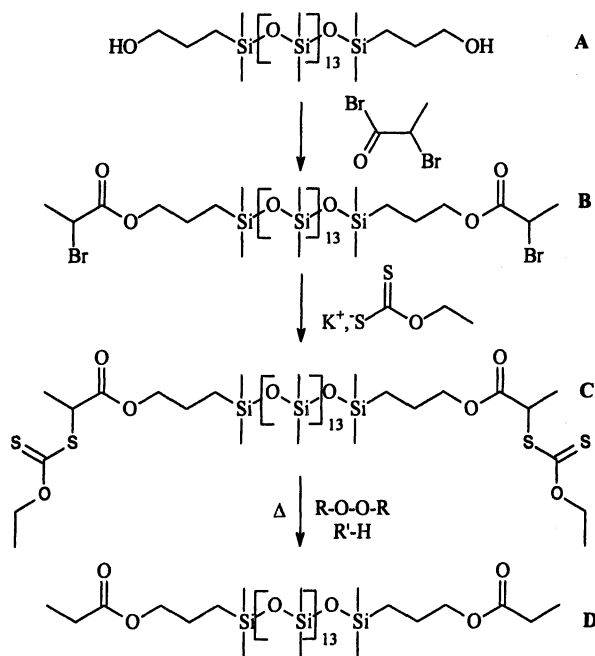
Dethiocarboxylation of xanthate-capped PDMS C₁'. 0.2 g of the silicone C₁' were dissolved in 1 mL of *o*-dichlorobenzene. The mixture was heated under reflux for 2 h. The solvent was then evaporated under vacuum at 100°C together with the elimination products. The silicone D' was recovered in quantitative yield. ¹H NMR (CDCl₃) δ 4.09 (td, 4H), 3.50 (m, 2H), 1.72 (m, 4H), 1.5 (d, 6H), 0.55 (m, 4H), 0.1 (m, Si-CH₃).

Results and Discussion

Radical reduction

An *O*-ethyl xanthate-terminated PDMS was synthesized according to the first two steps described in Scheme 3. Two reduction reactions were carried out either with dilauryl peroxide (DLP) at 80 °C in isopropanol, or with di-*t*-butyl peroxide (DTBP) in 2-octanol at 175°C. The peroxide to xanthate molar ratio for DTBP and DLP was equal to 1 and 1.4, respectively. In the case of reduction in 2-propanol, the DLP was added portionwise over several hours, whereas in 2-octanol, DTBP was added all at once to the refluxing solution. In both cases, the reduction was quantitative as shown by the total disappearance of the xanthate characteristic signals (-OCH₂CH₃) in the ¹H NMR spectra as detailed above. Furthermore, the ¹H NMR spectra of the treated polymers exhibited a quartet at 2.35 ppm which was assigned to the newly formed -O(C=O)CH₂CH₃ terminal group. The reduction by DLP in 2-propanol generated lauric acid and *S*-undecyl-*O*-ethyl xanthate co-products, which could not be eliminated by evaporation because of their low volatility. Therefore, precipitation of the polymer in a selective solvent or column chromatography was necessary to remove these unwanted products from the PDMS. Unlike DLP, DTBP yielded low molecular weight co-products which could be totally separated from the reduced polymer by evaporation under vacuum at 80-100 °C.

A reduction study was performed on a PAA synthesized in the presence of the xanthate X₁. The reaction was carried out at 75 °C in ethanol (AA / ethanol=



Scheme 3. Process for the preparation of xanthate-terminated PDMS and subsequent desulfuration by a radical reduction by means of a peroxide/secondary alcohol combination.

1/ 2.5 weight ratio) over four hours, with 2,2'-azodi(2-methylbutyronitrile) as the initiator. The initial monomer and xanthate conditions were calculated to obtain a PAA with M_n equal to 950 g/mole. A M_n value of 2100 g/mol ($M_w/M_n=1.40$) was estimated by size exclusion chromatography (water/acetonitrile=80/20) calibrated with poly(ethylene oxide) standards. This value was in good agreement with a previous report from our group (15). The aforementioned efficiency of DLP at moderate temperatures for xanthate-terminated PDMS led us to consider this initiator for the reduction of PAA- X_1 . In order to maintain an acceptable flux of radicals during the reaction, the reductions were performed at 80 °C ($t_{1/2}\sim 1$ h) in 2-propanol. The intense absorption of the thiocarbonylthio group chromophore of PAA- X_1 at 290 nm was used to follow the evolution of the reaction over time. Prior to the study, we checked that PAA is totally transparent to UV light at this wavelength. Also, by choosing the concentration of the initial PAA- X_1 sample (RI detection) as a reference for calculation, the corrected area below the UV trace at time t (taking into account the differences

of concentrations between the sample at time t and the reference) allowed determination of the reaction conversion with a good accuracy. The PAA solution in ethanol was diluted in 2-propanol in such a manner that 2-propanol / PAA- X_1 = 100 (mol. %). At 80 °C, 20 % mol. of DLP relative to PAA- X_1 were added to the reaction mixture. Then, constant portions of DLP (the same amount as that for t_0) were added every two hours. The overall amount of DLP corresponded to one equivalent relative to PAA- X_1 . After 10 hrs of reaction, the conversion reached over 99 %. The evolution of the reaction is illustrated in Figure 1. It is worth mentioning that the reduction of PAA- X_1 had no effect on the molecular weight and polydispersity index of the polymer ($M_n=2000$ g/mol, $M_w/M_n=1.48$).

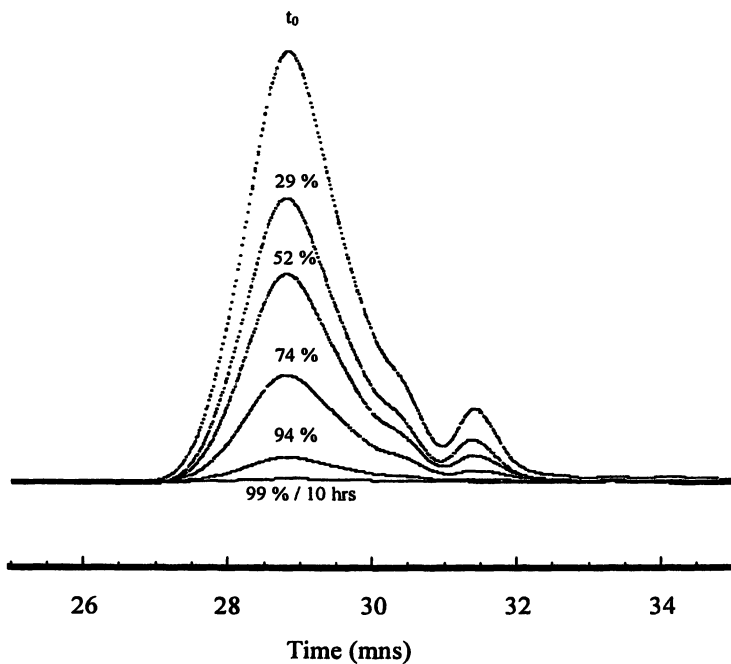


Figure 1. SEC traces (UV detector at $\lambda=290$ nm) of a PAA- X_1 reacted with DLP added portionwise at 80°C in 2-propanol. Samples taken at $t = 0, 2, 4, 6, 8$ and 10 h. The conversion of the reduction reaction is given for each sample.

In order to be able to operate at a lower reaction temperature, di-*t*-butylcyclohexyl percarbonate (DTBCP) was selected as a radical source at 60 °C ($t_{1/2} \sim 1$ h). A similar procedure to that for DLP was followed. At 60 °C, 20 % mol. of DTBCP relative to PAA- X_1 was added to the reaction mixture, and constant portions of initiator were added every two hours. The overall amount of DTBCP corresponded to a DTBCP / PAA- X_1 molar ratio equal to 1.4. After 24 h of reaction, the conversion reached over 99 %. The total reduction of the

xanthate chain end of PAA is illustrated in Figure 2. The same experiment was performed by initially adding 2 % mol. of DTBCP relative to PAA- X_1 , and constant portions of initiator were added every two hours. The overall amount of DTBCP corresponded to a DTBCP / PAA- X_1 molar ratio equal to 0.2. After 50 h of reaction, the conversion reached a value of 33 %, which shows that the rate of reduction is governed by the cumulated concentration of radicals generated by DTBCP over time. 2-Propanol acts only as a hydrogen atom donor, and the radical created by transfer to 2-propanol does not participate in the reduction process but gets oxidized to acetone by electron transfer to the peroxide or to the percarbonate.

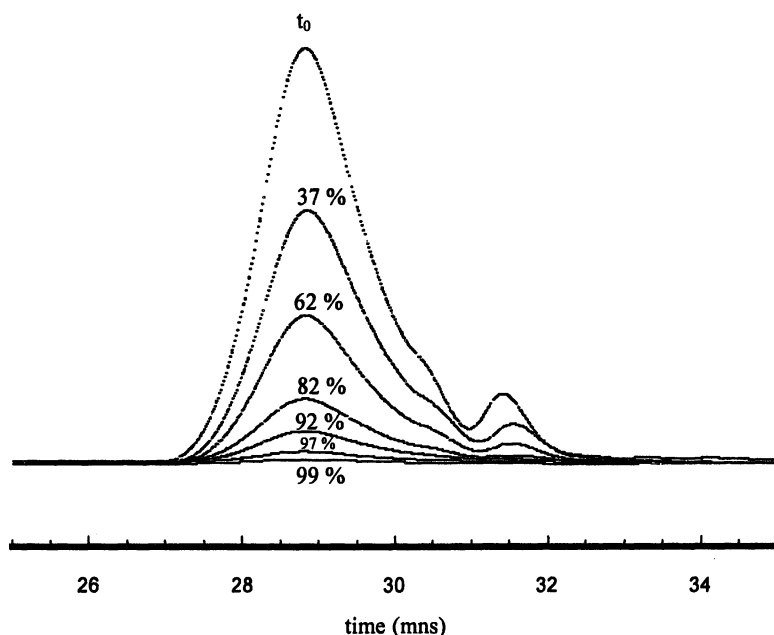


Figure 2. SEC traces (UV detector at $\lambda=290$ nm) of a PAA- X_1 reacted with DTBCP added portionwise at 60°C in 2-propanol. Samples taken at $t = 0, 2, 4, 6, 8, 10$ and 20 h. The conversion of the reduction reaction is given for each sample.

The PAA, which was totally reduced by the excess of DTBCP (Figure 2), was purified by neutralizing the polymer in alcohol with a 20 wt. % NH_4OH solution. The polymer precipitated during neutralization, and was washed with ethanol and THF. ^{13}C NMR analysis of the starting PAA- X_1 and the purified final product are shown in Figure 3. Five main signals characterize the xanthate fragments in PAA- X_1 (cf. Figure 3 for details). After reduction, it is clearly apparent on Figure 3b that the four signals (b, c, d and e) assigned to the *O*-ethyl xanthate chain end have totally disappeared.

The radical reduction of xanthate terminal groups of PDMS and MADIX polymers was efficiently conducted with peroxide and percarbonate initiators in secondary alcohols. This technique advantageously leads to sulfur-free polymers, unlike most of the known alternative techniques for the transformation of xanthates and, importantly, without the need for heavy metal based or otherwise expensive reagents.

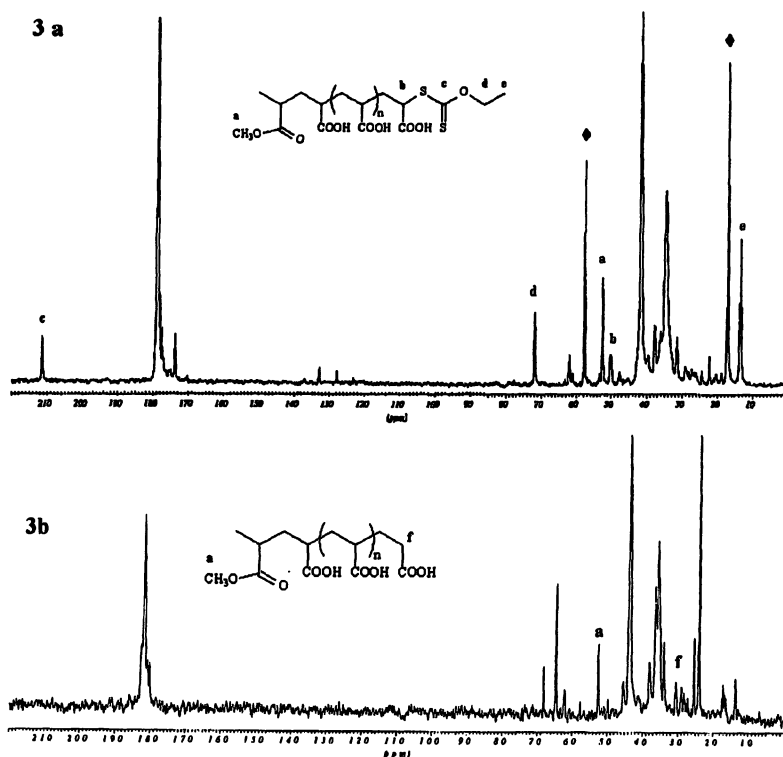
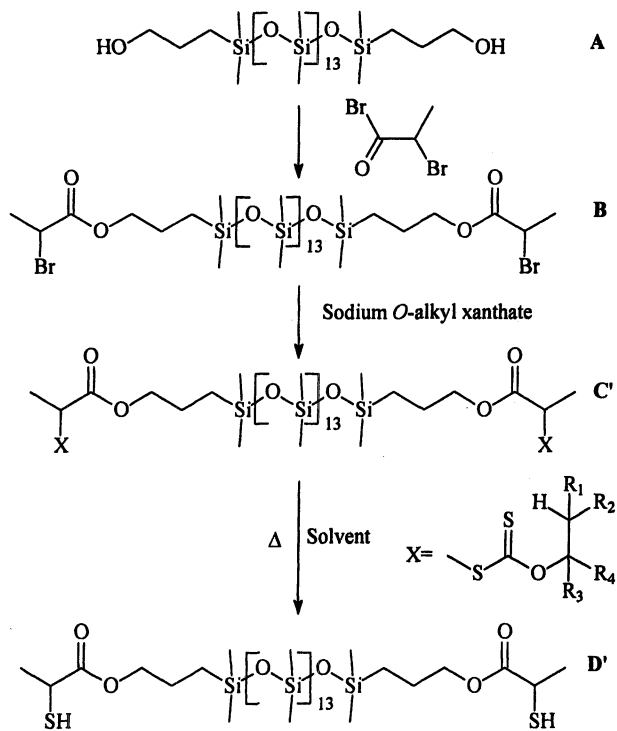


Figure 3. ^{13}C NMR spectra (D_2O) of (a) PAA- X_1 (b) PAA-H reduction product.

Dethiocarboxylation

In the case of the widely studied *O*-ethyl xanthates, the Chugaev reaction only occurs at very high temperatures, because of the primary nature of the C-O bond. In order to perform such reactions at acceptable temperatures, secondary xanthate structures were considered. Secondary xanthate salts 1-5 were synthesized and used to modify a low MW α,ω -functional PDMS according to the first two steps described in Scheme 4. Dethiocarboxylation of the PDMS

chain ends was expected to yield a α,ω -SH-terminated PDMS, an alkene and carbon oxysulfide.



Scheme 4. Process for preparation of a secondary xanthate-terminated PDMS and subsequent thermally-induced dethiocarboxylation.

The experiments were performed in solvents purposely chosen according to their boiling points, depending on the desired reaction temperature. Toluene, chlorobenzene, cyclohexanol and *o*-dichlorobenzene were used for reactions occurring at 100, 130, 160 and 180 °C, respectively. The results of the Chugaev reactions carried out with different xanthate terminal groups at various temperatures over one hour are collected in Table 1. The reaction was monitored by ¹H NMR, through the disappearance of the characteristic signal of the hydrogen geminal to the oxygen atom in the xanthate (-OCH(R₃)(R₄)). At 130 or 160 °C, no reaction was observed after two hours for silicone C₁' (C₁' = silicone B – see Scheme 4– reacted with xanthate salt 1) bearing *O*-1-methylpropyl xanthate groups. By heating C₁' at 180 °C in *o*-dichlorobenzene for one hour, the elimination of the xanthate group was successful, as evidenced by the total disappearance of the characteristic signal for (-OCH(CH₃)(CH₂CH₃)) at 5.56 ppm. Concomitantly, a new peak appeared at 3.5 ppm, which was assigned to the

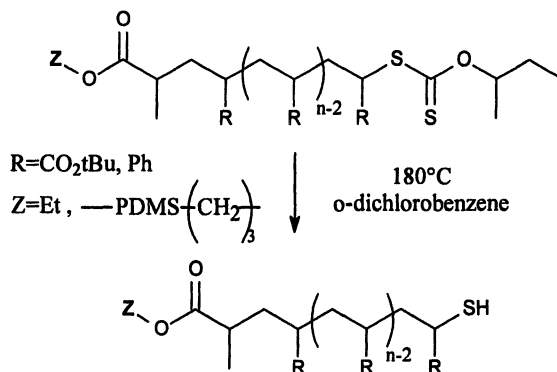
–CH(CH₃)SH terminal group. The structure of the xanthate derivatives C₂'–C₅' were selected for their potential reactivity at temperatures below 180 °C. Indeed, at 160 °C in cyclohexanol, more than 90 % of the xanthate was eliminated from starting silicones C₂' and C₃' (cf. Table 1). The conversion did not exceed 40 % for C₄'. We believe that heating the reaction mixture for prolonged times at 160 °C will help increase the overall yield of xanthate deactivation for the whole series of silicones C₂'–C₄'. Advantageously, silicone C₅' bearing *O*-(1-phenylethyl) xanthates was fully converted at 130 °C, whereas no reaction occurred at 100 °C after two hours. However, the latter kind of xanthate may be an inappropriate MADIX agent for controlled polymerization, because of a possible irreversible β-scission of the C–O bond.

Table 1. Dethiocarboxylation Reactions on PDMS Bearing Different Xanthate Terminal Groups, at Various Temperatures

| T (°C) | 100 | 130 | 160 | 180 |
|------------------|-------------|---------------------|------------------------------------|---------------------|
| X | | | | |
| C ₁ ' | | No reaction | No reaction | 100 % RSH formation |
| C ₂ ' | No reaction | No reaction | RSH > 90 % | |
| C ₃ ' | | | RSH > 90 % | |
| C ₄ ' | | | 40 % RSH 60 % starting material | |
| C ₅ ' | No reaction | 100 % RSH formation | | |

We took advantage of the results collected in this preliminary study to establish the relevant conditions for a complete elimination of xanthate ends from MADIX polymers. Three polymers were synthesized and evaluated under the Chugaev reaction conditions (Scheme 5): (i) P(*t*-BuA)-PDMS-P(*t*-BuA) triblock copolymers from silicone C₁' precursor (ii) PSt and P(*t*-BuA) capped with *O*-(1-methylpropyl)-*S*-(1-ethoxycarbonyl)ethyl xanthate. The polymerization of *t*-BuA was carried out with silicone C₁', using azobisisobutyronitrile (AIBN) as the initiator in cyclohexane under reflux. The initial monomer and xanthate concentrations were calculated in order to obtain ABA triblock copolymers with P(*t*-BuA) A blocks of DP_n equal to 10. At the end of the polymerization, the cyclohexane was evaporated under vacuum and the

polymer was dissolved in *o*-dichlorobenzene. The polymer solution was heated under reflux for one hour. The solvent was separated together with the reaction residues from the polymer by heating at 100 °C under vacuum. The ^1H NMR analysis of the purified polymer reported in Figure 4 shows no residual characteristic signal of the *O*-1-methylpropyl terminal group ($-\text{OCH}(\text{CH}_3)\text{CH}_2\text{CH}_3$ at 5.55 ppm).



*Scheme 5. Chugaev reaction of PSt, P(*t*-BuA) and P(*t*-BuA)-PMDS-P(*t*-BuA) MADIX polymers.*

A similar study was performed with P(St) and P(*t*-BuA) polymers which were synthesized in the presence of *O*-(1-methylpropyl)-*S*-(1-ethoxycarbonyl)ethyl xanthate, with a 10-fold excess of monomer relative to xanthate. AIBN was used in both cases to initiate polymerization. PSt was synthesized in toluene at 60 °C, and *t*-BuA was polymerized in refluxing ethanol. After drying and transfer of the polymers into *o*-dichlorobenzene, the complete elimination of the xanthate terminal group was observed by ^1H NMR after one hour at 180 °C for both PSt and P(*t*-BuA) polymers.

Thermally-induced elimination of xanthate terminal groups of polymer chains was efficiently conducted with five different secondary xanthates. This allowed the generation of thiol groups at the end of PDMS and MADIX polymer chains; it can thus be seen either as a convenient way to strongly increase the chemical stability of the chain ends, since the C–S bond in the resulting thiols are difficult to break and malodorous substances will not likely be generated, or as an entry into the extremely rich chemistry of thiols. It is worth pointing out that this technique is unique to xanthates (i. e. MADIX generated polymers) and cannot be transposed to other thiocarbonyl derivatives such as dithioesters or trithiocarbonates usually listed under the RAFT acronym, even though the mechanism of the polymerization is basically the same.

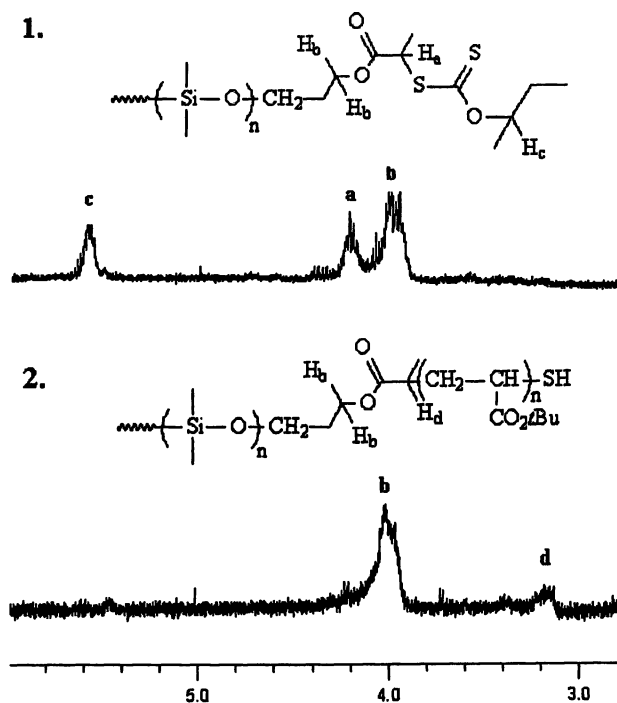


Figure 4. 1H NMR spectra ($CDCl_3$) of (1) α,ω -(O-(1-methylpropyl) xanthate)-capped PDMS C_1' and (2) C_1' -based P(t-BuA)-PDMS-P(t-BuA) triblock copolymer after thermal elimination of the xanthate terminal groups.

Conclusions

Radical reduction and dethiocarboxylation of xanthate groups at MADIX polymer ends were successfully implemented and led to their complete transformation into hydrogen and thiol end groups, respectively. These chemical treatments strongly reduce the risk of possible undesired chemical ageing during the lifetime of the MADIX (co)polymer.

Acknowledgement. The authors are grateful to Rhodia for permission to publish this work.

References

1. Corpart, P.; Charmot, D.; Biadatti, T.; Zard, S.Z.; Michelet, D. WO 9858974, Rhodia Chimie.
2. Destarac, M.; Taton, D.; Zard, S. Z.; Saleh, T.; Six, Y. *ACS Symposium Series*, **2003**, *854*, 536-550.
3. (a) Wilczewska, A-Z.; Destarac, M.; Zard, S.Z.; Kalai, C.; Mignani, G.; Adam, H. WO 2002090397, Rhodia Chimie. (b) Destarac, M.; Kalai, C.; Petit, L.; Wilczewska, A.; Mignani, G.; Zard, S.Z. *Polym. Prepr. (Am. Chem. Soc., Div. Polym. Chem.)* **2005**, *46(2)*, 372-373.
4. (a) Wilczewska, A-Z.; Destarac, M.; Zard, S.Z.; Kalai, C.; Mignani, G.; Adam, H. WO 2002090424, Rhodia Chimie. (b) Destarac, M.; Kalai, C.; Wilczewska, A.; Mignani, G.; Zard, S.Z. *Polym. Prepr. (Am. Chem. Soc., Div. Polym. Chem.)* **2005**, *46(2)*, 213-214.
5. Adam, H.; Liu, W-L. WO 2003070780, Rhodia Chimie.
6. Zard, S.Z.; Quiclet-Sire, B., Jost, P. WO 2005040233, Rhodia Chimie.
7. Chan, M-F.; Garst, M.E. *J. Chem. Soc. Chem. Commun* **1991**, *7*, 540-541.
8. Chen, B-C.; Bednarz, M.S.; Kocy, O.R.; Sundeen, J.E. *Tetrahedron Asym.* **1998**, *9(10)*, 1641-1644.
9. Mulvey, D.M.; Jones, H. *J.Heterocyclic Chem.* **1978**, *15*, 233-235.
10. Liard, A.; Quiclet-Sire, B.; Zard, S.Z. *Tetrahedron Lett.* **1996**, *37*, 5877-5880.
11. Barton, D.H.R.; George, M.V.; Tomoeda, M. *J. Chem. Soc.* **1962**, 1967.
12. Udding, J.H.; Giesselink, J.P.M.; Hiemstra, H.; Speckamp, W.N. *J. Org. Chem.* **1994**, *59(22)*, 6671.
13. Nace, H. R. *Org. React.* **1962**, *12*, 57.
14. Destarac, M.; Brochon, C.; Catala, J-M.; Wilczewska, A.; Zard, S.Z. *Macromol. Chem. Phys.*, **2002**, *203*, 2281-2289.
15. Taton, D.; Wilczewska, A.-Z.; Destarac, M. *Macromol. Rapid Commun.* **2001**, *22*, 1497-1503.

Chapter 39

Direct Synthetic Strategies to Hydrophilic Starlike Polymers by MADIX

Daniel Taton^{1,2,*}, Jean-François Baussard¹, Ludovic Dupayage¹,
Yves Gnanou¹, Mathias Destarac^{2,*}, Catherine Mignaud²,
and Claire Pitois²

¹Laboratoire de Chimie des Polymères Organiques, ENSCPB, 16 Avenue
Pey Berland, 33 607 Pessac Cedex, France

²Rhodia Recherches et Technologies, Centre de Recherches et Technologies
d'Aubervilliers, 52 Rue de la Haie Coq, 93308 Aubervilliers Cedex, France

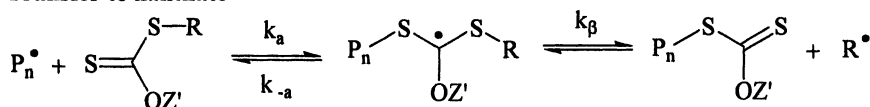
Three direct synthetic routes to branched polymers based on poly(acrylic acid) (PAA) are proposed. Three-arm PAA stars were obtained by the “core-first” approach using trifunctional *O*-alkyl xanthates as reversible chain transfer agents for MADIX solution polymerization of acrylic acid (AA). Chain extension of PAA star precursors with acrylamide afforded double hydrophilic star-block copolymers. Star-like structures consisting of a microgel core were also prepared by the “arm-first” approach using linear chains derived by MADIX and *N,N'*-methylene-bis(acrylamide) (MBA) as the linking agent. Finally, polymeric nanogels were synthesized by radical solution radical crosslinking copolymerization of AA and MBA in the presence of a *O*-ethyl xanthate as a MADIX agent. Up to 15% mol. of MBA could be incorporated without macrogel formation. Core-shell star structures were obtained by chain extension from the xanthate chain-ends present in these polymeric precursors.

Introduction

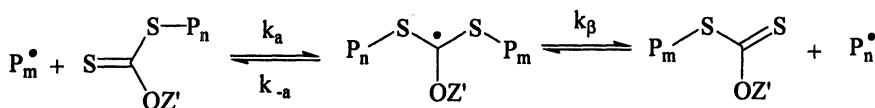
The radical addition by xanthate group transfer (1) has been applied by Rhodia to develop a new controlled radical polymerization system that was coined MADIX for Macromolecular Design *via* Interchange of Xanthates (2,3). In the meantime and, independently, the CSIRO discovered the reversible addition-fragmentation chain transfer polymerization (the RAFT process) (4). From a mechanistic viewpoint (see Scheme 1), both RAFT and MADIX processes are identical and only differ by the chemical nature of the chain transfer agent (CTA), that is a thiocarbonylthio compound of general structure Z-C(=S)-S-R (2-4). RAFT terminology prevails for CTAs in general, including dithioesters, dithiocarbamates, trithiocarbonates and xanthates whereas MADIX refers to xanthates exclusively, where Z = OZ'.

Among advantages of RAFT/MADIX processes, one can mention the possibility to directly polymerize hydrophilic monomers in aqueous media (5), making these methodologies environmentally friendly with a high potential of transfer into industrially viable processes. Earlier studies have demonstrated that controlled polymerizations of hydrophilic monomers (e.g. acrylic acid, N-vinylpyrrolidone, etc.) can be performed in solution by MADIX so as to obtain pH-responsive or temperature-sensitive polymers (6,7). Here we describe three facile synthetic routes to star-like structures based on poly(acrylic acid), including three-arm stars, star-like polymers comprising a microgel as the core and polymeric nanogels. In the last decade, there has been an increasing number of reports on the preparation of star polymers by CRP (8). Synthesis of star-like polymers by RAFT/MADIX using either the core-first or the arm-first approach—named in this context the R-group and the Z-group approach, respectively—has also been addressed (9). To our knowledge, however, no report on the direct

Transfer to xanthate



Chain-to-chain transfer



Scheme 1. Transfer events in the MADIX process

synthesis of hydrophilic stars has been reported. Due to its versatility, MADIX might offer various possibilities for the synthesis of branched (co)polymers.

Experimental

Acrylic acid, ethanol, dimethylformamide (DMF) (Aldrich) were purified using standard procedures. 4,4'-azobis(4-cyanopentanoic acid) (ACP) was recrystallized from methanol. N,N'-methylene-bis(acrylamide) was used as received. The xanthate **3** was synthesized as described previously (1-3). **Synthesis of trifunctional xanthates.** The tris-bromo intermediate was synthesized according to ref. 10. The sodium salt of *O*-1,1,1-trifluoroethyl xanthic acid was formed in situ from 1,1,1-trifluoroethanol and CS₂ in the presence of NaOH following a similar procedure to that described in ref. 3. The xanthic acid salt was added in excess (3.3 eq) to the tris-bromo derivative in acetonitrile. The MADIX agent **2** was recovered as yellow oil by column chromatography over SiO₂ (toluene then ethanol). The trifunctional xanthate **1** was prepared following a similar procedure except that the commercially available xanthic acid salt C₂H₅OC(=S)S⁻K⁺ was used. **Polymerizations.** All polymerizations were performed in batch under homogeneous conditions at 70 °C under a slight flow of nitrogen in a two-neck flask equipped with a magnetic stirrer and a reflux condenser. Typical polymerization experiments can be found in ref. 6 and 11. **Characterization.** NMR spectra were obtained using a Bruker AC400 NMR spectrometer. Molar masses were determined using aqueous size exclusion chromatography (ASEC) apparatus fitted with three Shodex columns (10⁴ Å, 1500 Å, 250 Å) and equipped with a Varian refractive index detector (flow rate = 1 mL/min) using a mixture of acetonitrile/water (4/1 %vol.) with 0.1 mol.L⁻¹ NaNO₃. Calibration was performed using linear poly(ethylene oxide) standards (Tosoh).

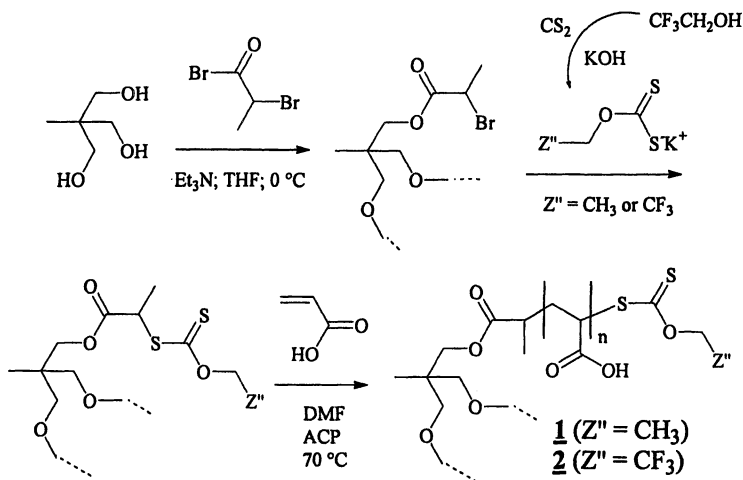
Results & Discussion

Three-arm star polymers by the core-first method.

Trifunctional MADIX agents consisting of similar homolytic leaving and activating groups as those of monofunctional xanthates that proved effective for controlling free-radical polymerizations of AA and Am (δ) were first designed. These compounds were obtained in a two step-sequence (Scheme 2). First, trimethylolpropane was treated with an excess of 2-bromopropionyl bromide in the presence of Et₃N and the obtained tris-(bromopropionate) was subsequently

subjected to nucleophilic substitution of its secondary bromines using the potassium salt of two *O*-alkyl xanthic acids in acetonitrile. The *O*-ethyl xanthic acid potassium salt (with $Z'' = \text{CH}_3$) is commercially available while the xanthic salt containing the trifluoro group ($Z'' = \text{CF}_3$) can be readily synthesized from trifluoroethanol and carbon disulfide (CS_2) under basic conditions (see Scheme 1 and Experimental). Characterization by NMR of the tris-xanthates confirmed their high purity. As an illustration, the ^{13}C NMR spectrum of the xanthate **1** with the assigned peaks is shown in Figure 1, where one can detect the presence of all the expected peaks, in particular that due to the $\text{C}=\text{S}$ double bond around 220 ppm. The use of these two CTAs in MADIX polymerization implies an outward growth of arms from the core following a divergent ("core-first") approach, the homolytic propionate-type leaving groups generated after the fragmentation step being part of the core of the stars.

AA was polymerized in solution either in dimethylformamide or ethanol or in acetone - the latter solvent was used for very low molar mass targeted - at 70 °C in the presence of **1** or **2**, using ACP as the radical source (10% mol. relative to the CTA). The polymerization was stopped at different reaction times to follow the kinetics. Polymers were recovered by precipitation in an excess of acetonitrile, filtered, freeze-dried from water solutions and analyzed by size exclusion chromatography in the aqueous eluent (ASEC). The polymerization of AA using the trifunctional MADIX agent containing trifluoromethyl groups (**2**) was investigated in DMF so as to get a homogeneous solution. The control of the polymerization was evidenced by the increase of M_n with monomer conversion whereas polydispersities (PDIs) were in the range 1.2-1.3 (Figure 2).



Scheme 2. Synthesis of hydrophilic core-first stars by MADIX

Synthesis of core-first stars is often complicated by irreversible terminations between stars, especially for poorly reactive radicals such as polystyryl ones (8,9). A method to predict and quantify reactions occurring during multi-arm polymer synthesis was recently proposed by Barner-Kowollik and coll. (9n). With more reactive radicals, however, like those deriving from poly(acrylic acid) (PAA), the probability for stars to get coupled can be minimized, as attested by no visible side population in the high molar mass region of SEC traces. This supports the advantage of polymerizing highly reactive monomers divergently *via* this core-first methodology. A ^{13}C NMR spectrum in D_2O of a low molar mass polymer synthesized in acetone and that was freeze-dried for NMR analysis revealed the presence of the peak of the $\text{C}=\text{S}$ double bond at 220 ppm, in addition to the peaks due to the AA units as well as those of the core of the star. This indicated that the xanthate chain-ends were not subjected to hydrolysis, at least during the timescale of the polymerization. The presence of MADIX agent **1** that would not have been consumed over the course of the polymerization can be ruled out just because **1** is insoluble in D_2O .

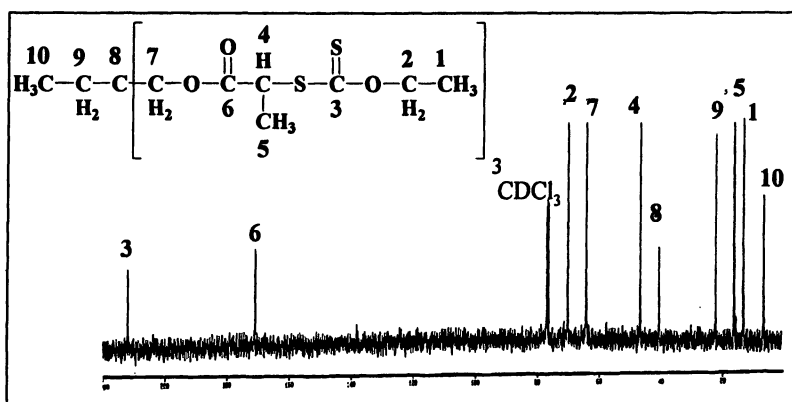


Figure 1. ^{13}C NMR spectrum (50 MHz, CDCl_3) of trifunctional MADIX agent **1**

Figure 2 also shows the symmetrical and monomodal ASEC trace of a three-arm PAA star obtained by direct polymerization of AA, using the *O*-ethyl version of the trifunctional xanthate (**1**). Such a PAA precursor could be subsequently used as a trifunctional macro-CTA for the direct polymerization of acrylamide (Am) by MADIX in water, using ACP as the radical source. The shift toward the higher molar masses unambiguously confirmed the possible reactivation of the xanthates chain ends with efficient chain extension, affording in this case a double hydrophilic star-block copolymer with neutral PAm blocks outside and pH-responsive PAA blocks inside.

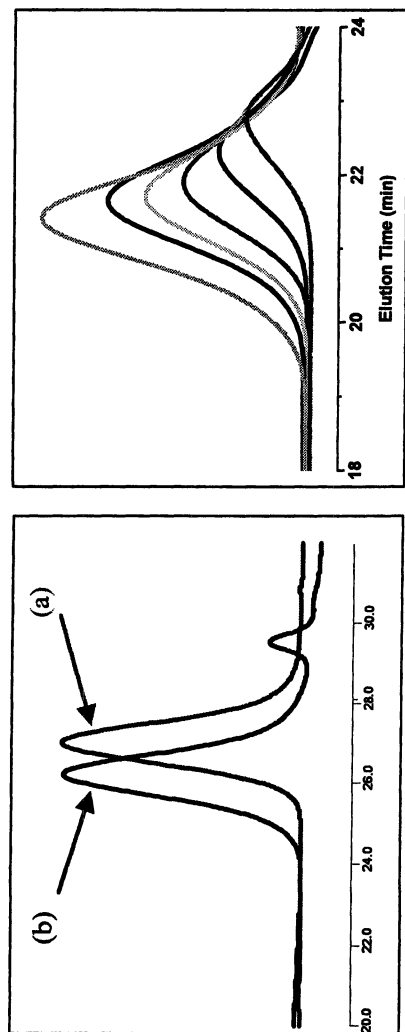


Figure 2. ASEC of stars based on PAA. Left side: (a) synthesis of a star precursor (PAA)₃ in ethanol using **1** as a CTA: AA/1/ACP = 50/1/0.1 ($M_n = 6,500$; PDI = 1.26) and (b) the corresponding star-block copolymer (PAA)₃-b-(PAm)₃ after chain extension with acrylamide in water ($M_n = 13,700$; PDI = 1.30). Right side: ASEC traces of MADIX polymerization in DMF at 70 °C of AA: AA/2/ACP = 210/1/0.1. From right to left: $M_n = 10,500$ and PDI = 1.25 ($t = 30$ min.; conv. = 8%); $M_n = 16,000$ and PDI = 1.24 ($t = 60$ min.; conv. = 18%); $M_n = 20,100$ and PDI = 1.27 ($t = 90$ min.; conv. = 33%); $M_n = 22,200$ and PDI = 1.31 ($t = 120$ min.; conv. = 48%); $M_n = 23,100$ and PDI = 1.34 ($t = 150$ min.; conv. = 62%); $M_n = 26,500$ and PDI = 1.40 ($t = 180$ min.; conv. = 76%).

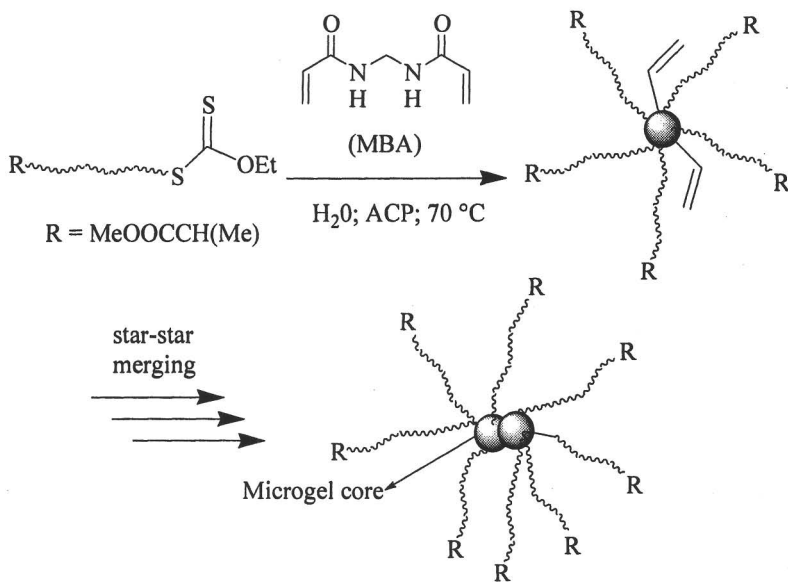
Arm-first star polymers by the “nodulus” method

Addition of a divinyllic monomer as a crosslinking agent onto re-activable linear chains is an arm-first synthetic route to star polymers of high molar masses that was developed in the context of anionic polymerizations in the late 60's (12). This method was recently applied to CRP methodologies, including atom transfer radical polymerisation (ATRP) (13), nitroxide-mediated polymerization (NMP) (14), but only a few studies have been reported by RAFT/MADIX (15). In particular, no report has described the direct synthesis of hydrophilic arm-first stars by RAFT/MADIX. Key parameters having a dramatic influence on the number of chains attached to the core not only include the feed molar ratio (r) between the crosslinker and the linear precursor ($r = [\text{crosslinker}]_0/[\text{P}_n\text{-X}]_0$), but also the nature of the linking agent, the size (M_n) of the precursor, the overall concentration of the reaction mixture and solvent nature. In contrast to stars synthesized by the core-first methodology, however, one cannot expect to obtain stars carrying a precise number of arms, but at best to minimize the fluctuation of their functionality. Among advantages of this “nodulus” approach, one can mention i) its potential application to any linear precursor preformed by MADIX and ii) the possibility to synthesize star-like polymers in a one-pot process without necessarily isolating the linear precursor.

Dormant linear chains of PAA were first synthesized by MADIX using a xanthate (**3**) of structure $\text{C}_2\text{H}_5\text{O-C(=S)S-CH}(\text{CH}_3)\text{COOCH}_3$, following a procedure published elsewhere (7). These linear precursors were subsequently reacted with N,N' -methylene-bis(acrylamide) (MBA) as the crosslinking agent, using deionized water as a solvent at 70 °C, in the presence of ACP as a radical source (Scheme 3). Increasing the feed molar ratio (r) of MBA with respect to a well-defined PAA linear precursor of $5000 \text{ g}\cdot\text{mol}^{-1}$ at a polymer concentration of 10% in weight led to a shift of the SEC traces to the higher molar mass region (Figure 3).

This supports the formation of star-like polymers comprising a microgel core stabilized by hydrophilic arms consistently with Scheme 3. The suitable range for star formation at this polymer concentration was in between 5 and 15, which is consistent with values generally obtained following other techniques such as ATRP (13), NMP (14) or RAFT (15). Above a value of $r = 15$, gel formation generally occurred and below $r = 5$, poor yield of star formation was observed. Another potential problem associated with this approach is the presence of noticeable amounts of parent linear chains left over and that contaminated the star polymers.

This method was applied to various types of hydrophilic precursors, including homopolymers, statistical copolymers and block copolymers as well, as summarized in Table I. In all these experiments, xanthate **3** was employed to synthesize linear precursors and, the r ratio was varied from 5 to 15, value above which gel formation was observed. Successful star synthesis could thus be



Scheme 3. Synthesis of hydrophilic arm-first stars by MADIX

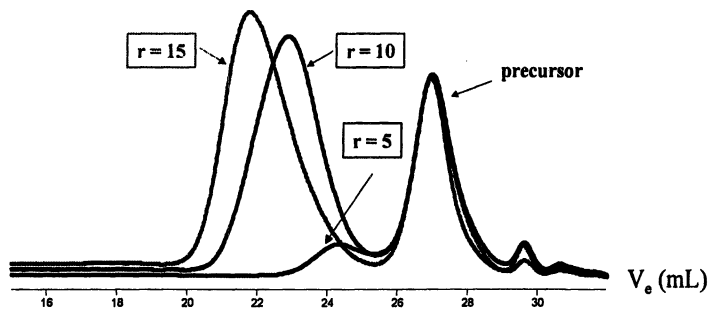


Figure 3. Refractometric response of ASEC before and after chain extension in H_2O at 70°C of a xanthate-terminated PAA precursor ($M_n = 5,200$; $\text{PDI} = 1.23$): $r = 10$: $M_n = 174,000$; $\text{PDI} = 1.54$. $r = 15$: $M_n = 258,000$; $\text{PDI} = 1.73$.

achieved starting from a polyacrylamide (PAm) precursor, which, to the best of our knowledge, represents the first example of a star based on PAm obtained by CRP. In addition, statistical copolymers of AA and Am could be coupled *via* MBA to form stars consisting of statistical copolymeric branches. Finally, DHBC obtained by MADIX could also be chain extended with MBA to produce, in this case, double hydrophilic star-block copolymers. A clear shift to the higher molar masses region was systematically observed by SEC in an aqueous eluent, though these values are likely underestimated since obtained from a calibration with PEO standards. A simple calculation indicates that the number of arms for these star polymers is in the range 20 to 50, depending on the r value, though the actual functionality is likely much higher.

Partial conversion of the linear precursors to star molecules is explained by an increasing steric crowding around the core as the coupling reactions proceed. One easy way to improve the yield of star polymer formation was to add MBA with a monovinyllic comonomer onto the preformed polymer. By doing so, the size of the core can be increased thus decreasing the steric hindrance around the core. Figure 4 shows the SEC monitoring using a PAA precursor of $15000 \text{ g}\cdot\text{mol}^{-1}$ prepared by MADIX that was subjected to a chain extension using a MBA/AA mixture at different MBA contents: as the amount of the crosslinker increases, there was less and less precursor left over. The response of the SEC traces was provided, in this case, from a UV detector operating at 290 nm, which is characteristic of the absorption of the xanthate end groups only. All UV traces superimposed with traces obtained using a refractometric detector, which strongly supported that the vast majority of the chains were living.

Polymeric nanogels by MADIX radical crosslinking copolymerization

“Microgels” sometimes called “polymeric nanogels” are soluble intramolecularly crosslinked polymer chains in the submicron size range that can also be viewed as “hyperbranched polymers”. A method generally employed for synthesizing microgels is the radical crosslinking copolymerization (RCC) of a vinyllic monomer with a crosslinker using one of the three following processes: highly diluted solution, emulsion and precipitation/dispersion polymerizations (16). Intramolecular crosslinking predominates at the early stages of a regular RCC, generating highly heterogeneous microgels whose branching points are irregularly distributed. Recently, Sherrington and coll. carried out solution RCC at relatively high monomer concentrations and succeeded to avoid macrogelation by employing mercaptans as “conventional” CTA (17). Recent attempts at preventing macrogelation and generating polymeric nanogels of better structural homogeneity include the use of NMP (18) and ATRP (19). In a recent addition, advantage of xanthates was taken to obtain hydrophilic and other branched copolymers by MADIX (11). Contemporarily, Perrier and coll. reported the

Table I. Synthesis of arm-first star polymers by the “nodulus” method from different MADIX-derived linear precursors using MBA as the crosslinker.^a

| Entry | Precursor (M_n , PDI) | r^b | $M_n^{STAR^c}$ ($g \cdot mol^{-1}$) | PDI ^c | Conv. ^d (%) |
|-------|---|-------|--|------------------|---------------------------|
| 1 | PAA (7,300; 1.30) ^e | 5 | nd | nd | < 25 |
| 2 | PAA (7,300; 1.30) ^e | 10 | 174,000 | 1.54 | 66 |
| 3 | PAA (7,300; 1.30) ^e | 15 | 258,000 | 1.73 | 67 |
| 4 | PAm (1,100; 1.30) ^f | 7 | 95,000 | 3.4 | 60 |
| 5 | P(AA-co-Am) (11,500; 1.45) ^g | 5 | 150,000 | 1.25 | 40 |
| 6 | P(AA-co-Am) (11,500; 1.45) ^h | 10 | 231,000 | 1.37 | 27 |
| 7 | P(AA-co-Am) (11,500; 1.45) ^h | 15 | 274,000 | 1.40 | 37 |
| 8 | PAA-b-PAm (21,000; 1.72) ^h | 15 | 438,000 | 1.27 | 37 |

^a Polymerizations in deionized water at 70 °C. Linear polymers were synthesized using **3**.

^b $r = [MBA]/[xanthate\text{-ended\ precursor}]$. ^c Number average molar masses determined by SEC in the aqueous eluent from calibration with linear PEO standards. ^d Conversions determined by SEC from the relative integration of the star and the parent linear polymer.

^e PAA: poly(acrylic acid). ^f PAm: polyacrylamide. ^g Statistical copolymer of Am and AA; theoretical molar mass: $M_n = 11000 \text{ g} \cdot \text{mol}^{-1}$. ^h Block copolymer based on AA and Am units theoretical molar mass: $M_n = 35000 \text{ g} \cdot \text{mol}^{-1}$.

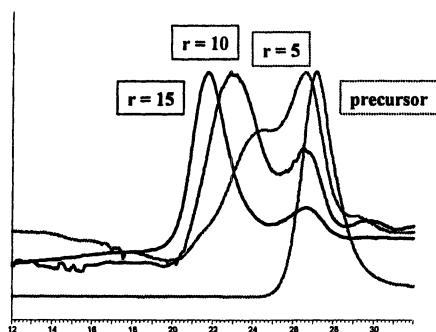
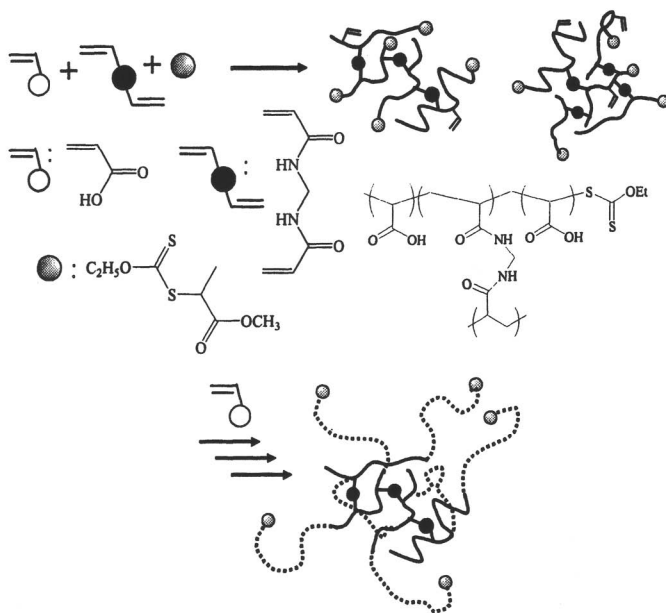


Figure 4. UV response at 290 nm of ASEC before and after chain extension in H_2O at 70 °C of a xanthate-terminated PAA precursor ($M_n = 15,000$; PDI = 1.46): $r = 5$: $M_n = 21,300$; PDI = 3.8; $r = 10$: $M_n = 287,000$; PDI = 2.4; $r = 15$: $M_n = 383,000$; PDI = 2.3.

synthesis of hydrophobic “hyperbranched” copolymers of polymethacrylate by RAFT (20). To synthesize hydrophilic PAA-based nanogels, xanthate **3** was, again, chosen to mediate the direct and one-pot RCC of AA at 70 °C in ethanol, using MBA as the crosslinker and ACP as the radical source. Different MBA/AA/**3** ratios were investigated to determine both the effect of MBA and the MADIX agent during these xanthate-mediated RCCs. The sketch of the branched copolymers formed under such conditions is displayed in Scheme 4.



*Scheme 4. RCC in ethanol of AA and MBA in the presence of **3** and ACP.*

Monomers' and xanthate conversions were determined by gas chromatography (GC), HPLC and ^1H NMR spectroscopy. Under the conditions mentioned above, near quantitative yields were obtained after 4 hours at 70 °C, 0.004-0.015% for MBA (by GC), 0.13-2.67% for AA (by HPLC) and 0.11-0.15% for **3** (by GC) being the residual amounts respectively found. ^1H NMR spectroscopy proved useful as an *in-situ* real time monitoring method of monomers' and xanthate consumption in deuterated ethanol. The ^1H NMR spectra (D_2O , 400 MHz) of the PAA samples confirmed the presence of the branching MBA moieties. Integration of the peaks attributable to the three reagents allowed us to conclude that MBA, AA and X_A exhibited quasi-identical reactivities in these conditions and were incorporated at approximately the same

rate in the copolymeric chains. It was also checked by ^1H NMR that no residual double bond was left in the final polymer.

Table II summarizes the evolution of molar masses and PDIs during xanthate-assisted RCC of AA/MBA/**3** mixtures. Characterization by ASEC shows an increase of M_w and PDI values with the MBA content for a same concentration of the xanthate. For low xanthate concentration (entries 1 to 3 of Table 2), gel formation occurred above a 5% molar content of the crosslinker and the higher the MBA, the higher the molar masses and the higher the polydispersities as well, although the latter values were kept lower ($\text{PDI} < 2$ in general), as compared to values reported by others for hydrophobic systems (17-20). The same trend was observed at higher xanthate concentrations (entries 4-7 and 8-12 of Table 2) but, in this case, higher amounts of crosslinker could be added without any gel formation. While it is highly recommended to perform "regular" RCC under highly dilute conditions ($< 5\%$ weight) and discontinue polymerization before completion in order to obtain polymeric nanogels, the use of MADIX agent **3** permitted high monomer conversion -if not quantitative-, higher solid content as well as a much higher content in crosslinker without occurrence of gelation. For instance, for the highest concentration of the xanthate that is 6.5 molar, up to 15 % mol of MBA could be added still maintaining soluble compounds in ethanol. Thus, both the crosslinker and the xanthate concentrations have a dramatic effect on the build-up of molar masses of the branched copolymers: i) the higher the concentration of MBA, the larger the molar masses and polydispersities for a given concentration in xanthate (Figure 5a) and, ii) the lower the concentration in xanthate, the larger the molar masses for a fixed [MBA] (Figure 5b).

One major advantage of this synthetic access to polymeric nanogels is the possibility to carry out chain extensions from the dormant chains deriving from the xanthate (see Scheme 4). In this way, star-like structures composed of a polymeric nanogel-based core are obtained in a divergent fashion. As a proof of concept, Figure 6 shows the shift to the higher molar masses observed in the SEC traces, after a direct chain extension with AA, from a parent copolymer of initial composition $\text{MBA/AA/3} = 89/4.5/6.5$ (entry 9, Table 2). In the latter case, the parent polymeric nanogel served as a macromolecular multifunctional CTA for the MADIX polymerisation of AA in pure water, using ACP as the radical source. Near quantitative yields were obtained after 7 hours of polymerization with no visible formation of macrogel, confirming the very low probability of intermolecular couplings, as discussed above for the synthesis of core-first stars from trifunctional xanthates. This is related to the high reactivity of AA in free-radical polymerization, which implies a higher k_p^2/k_t ratio as compared to styrene, for instance (11).

Table II. Xanthate-mediated RCC of AA and MBA at 70 °C.^a

| Entry | AA (mol) | MBA (mol) | <u>3</u> (mol) | M_n^b (g.mol ⁻¹) | M_w^b (g.mol ⁻¹) | PDI |
|-------|-------------|--------------|-------------------|-----------------------------------|-----------------------------------|-------------------|
| 1 | 98 | 0 | 2 | 2500 | 2800 | 1.15 |
| 2 | 93 | 5 | 2 | 5700 | 24400 | 4.27 |
| 3 | 88 | 10 | 2 | gel | gel | gel |
| 4 | 95.4 | 0 | 4.6 | 2300 | 2600 | 1.16 |
| 5 | 90.5 | 4.9 | 4.6 | 4900 | 7600 | 1.53 |
| 6 | 85.5 | 9.9 | 4.6 | 5100 | 10200 | 1.99 |
| 7 | 80.6 | 14.8 | 4.6 | gel | gel | gel |
| 8 | 93.5 | 0 | 6.5 | 1500 | 1800 | 1.19 |
| 9 | 89.0 | 4.5 | 6.5 | 4700 | 5900 | 1.25 |
| 10 | 83.7 | 9.8 | 6.5 | 5300 | 9000 | 1.71 |
| 11 | 78.8 | 14.7 | 6.5 | 2300 ^c | 3480 ^c | 1.51 ^c |
| 12 | 73.8 | 19.7 | 6.5 | gel | gel | gel |

^a Copolymerisations in ethanol using ACP (10% mol. relative to X_A); conversions of monomers higher than 98%. ^b ASEC calibrated with poly(ethylene oxide) standards. ^c A gel fraction was obtained; ASEC performed with the soluble part.

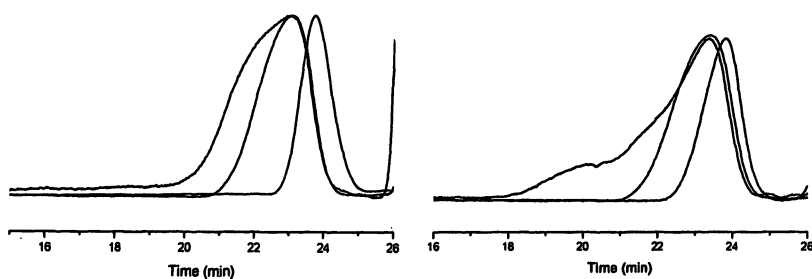


Figure 5. Left side: crosslinker effect on SEC traces of branched copolymers obtained by RCC of AA/MBA/3 (entry 1 to 3, Table 1). Right side: xanthate effect on the SEC traces of branched copolymers obtained by RCC of AA/MBA/3 (entries 2, 5 and 9, Table 1).

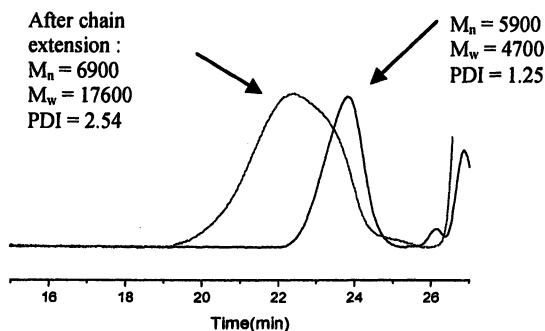


Figure 6. SEC traces of a parent copolymer (entry 9 of Table 1) and of star-like copolymer obtained after chain extension by MADIX polymerisation of AA.

Conclusion

Easy synthetic accesses to hydrophilic multiarm stars based on poly(acrylic acid) are possible by MADIX, using both core-first or arm-first methods. For instance, well-defined three-arm stars can be directly synthesized in solution from trifunctional xanthates, minimizing side reactions such as star-star couplings owing to the very high reactivity of acrylic acid in free-radical polymerization. Fidelity of the xanthate chain ends is demonstrated by their reactivation in chain extension experiments of the three-arm stars with acrylamide, thus affording novel double hydrophilic star-block copolymers. Alternatively, water-soluble arm-first star (co)polymers can also be readily synthesized by adding a bis(acrylamide) comonomer playing the role of a crosslinking agent, which resulted in the formation of a microgel at the core of these stars after couplings of preformed linear chains. This “nodulus” method can be applied to various hydrophilic precursors, including not only homopolymers composed of acrylamide or acrylic acid but also statistical and block copolymers of these two monomers. Finally, The one-pot batch solution radical crosslinking copolymerization of acrylic acid in the presence of the same bisacrylamide mentioned above and a *O*-ethyl-xanthate allows the preparation soluble branched polymers referred to as microgels or polymeric nanogels. The molar masses and polydispersities of these polymeric nanogels can be varied as a function of the concentrations of the starting reagents. Even in the presence of a rather high proportion of crosslinker (up to 15% mol.), no macrogelation is observed provided that enough xanthate is utilized. Chain extension from these nanogels affords multiarm star polymers and a practical pathway to this kind of

architectures. Investigation is in progress to determine how evenly are distributed the branching points within these branched copolymers, xanthate-mediated RCC being expected to afford more uniform polymeric nanogels than those obtained under regular RCC conditions.

Acknowledgment. The authors are grateful to Rhodia for permission to publish this work.

References

1. (a) Delduc, P.; Tailhan, C.; Zard, S. Z. *J. Chem. Soc., Chem. Comm.* **1988**, 308; (b) Zard, S. Z. *Angew. Chem. Int. Ed. Engl.* **1997**, *37*, 672.
2. (a) WO. 9858974 (1998), Rhodia Chimie, invs.: Corpart, P.; Charmot, D.; Biadatti, T.; Zard, S. Z.; Michelet, D. [*Chem. Abstr.* **1999**, *130*, 82018].
3. (a) Destarac, M.; Taton, D.; Zard, S. Z.; Saleh, T.; Six, in *Advances in Living/Controlled Radical Polymerization*; Matyjaszewski, K., Ed.; *ACS Symposium Series 854*; American Chemical Society: Washington, DC, **2003**, 536. (b) Destarac, M.; Bzducha, W.; Taton, D.; Gauthier-Gillaizeau, I.; Zard, S. Z. *Macromol. Rapid Commun.* **2002**, *23*, 1049.
4. (a) Moad, G.; Chiefari, J.; Chong, B. Y. K.; Krstina, J.; Mayadunne, R. T. A.; Postma, A.; Rizzardo, E.; Thang, S. H. *Polym. Int.* **2000**, *49*, 993. (b) Rizzardo, E.; Chiefari, J.; Mayadunne, R. T. A.; Moad, G.; Thang, S. H. *ACS Symposium Series 768 Ed. K. Matyjaszewski* **2000**, *20*, 282. (c) Moad, G.; Rizzardo, E.; Thang, S. H. *Aust. J. Chem.* **2005**, *58*, 379.
5. (a) Lowe, A. B.; McCormick, C. L. *Aust. J. Chem.* **2002**, *55*, 367. McCormick, C. L.; Lowe, A. B. *Acc. Chem. Res.* **2004**, *37*, 312.
6. Taton, D.; Wilczewska, A.-Z.; Destarac, M. *Macromol. Rapid Commun.*, **2001**, *22*, 1497.
7. Devasia, R.; Gnanou, Y.; Borsali, R.; Lecommandoux, S.; Mougin, N. *Polym. Prepr. ACS* **2005**, *46(2)*, 448.
8. (a) Angot, S.; Murthy, K.S.; Taton, D.; Gnanou, Y. *Macromolecules* **2000**, *33*, 7261 and references therein. (b) Gnanou, Y.; Taton, D. *Handbook of Radical Polymerization* Ed K. Matyjaszewski & T. Davis, Wiley Interscience, New York **2002**, *14*, 775.
9. (a) Stenzel-Rozenbaum, M. H.; Davis, T. P.; Chen, V.; Fane, A. G. *J. Polym. Sci.: Part A Polym. Chem.* **2001**, *39*, 2777. (b) Quinn, J. F.; Chaplin, R.; Davis, T. P. *J. Polym. Sci.: Part A Polym. Chem.* **2002**, *40*, 2956. (c) Stenzel, M. H.; Davis, T. *J. Polym. Sci.: Part A Polym. Chem.* **2002**, *40*, 4498. (d) Rizzardo, E.; Thang, S. H. *Macromolecules*, **2003**, *36*, 2256. (e) Chiefari, J.; Mayadunne, R. T. A.; Moad, C. L.; Moad, G.; Rizzardo, E.; Postma, A.; Skidmore M. A.; Thang, S. H. *Macromolecules*, **2003**, *36*,

2273. (f) Mayadunne, R. T. A.; Jeffery, J.; Moad, G.; Rizzardo, E. *Macromolecules* **2003**, *36*, 1505. (g) Duréault, A.; Taton, D.; Destarac, M.; Leising, F.; Gnanou, Y. *Macromolecules* **2004**, *37*, 5513. (h) Darcos, V.; Duréault, A.; Taton, D.; Gnanou, Y.; Marchand, P.; Caminade, A.-M.; Majoral, J.-P.; Destarac, M.; Leising, F. *Chem. Commun.* **2004**, 2110. (i) Jesberger, M.; Barner, L.; Stenzel, M. H.; Malmström, E.; Davis, T. P.; Barner-Kowollik, C. *J. Pol. Sci. Part A: Chem.*, **2003**, *41*, 3847. (j) Chen, M.; Ghiggino, K. P.; Thang, S. H.; Wilson, G. J. *Angew. Chem. Int. Ed.* **2005**, *44*, 4368. (k) Zheng, Q.; Pan, C.-Y. *Macromolecules* **2005**, *38*, 6841. (l) Bernard, J.; Favier, A.; Zhang, L.; Nilasaroya, A.; Davis, T. P.; Barner-Kowollik, C.; Stenzel, M. H. *Macromolecules* **2005**, *38*, 5475. (m) Stenzel, M. H.; Davis, T. P.; Barner-Kowollik, C. *Chem. Commun.* **2004**, 1546. (n) Chaffey-Millar, H.; Busch, M.; Davis, T. P.; Stenzel, M. H. Barner-Kowollik, C. *Macromol. Theory Simul.* **2005**, *14*, 143.
10. Mühlebach, A.; Rime, F.; *Intern. Pat. Appl.*, **2000**, Ciba PCT/WO0043344.
11. Destarac, M.; Bavouzet, B.; Taton, D. *Rhodia WO* 2004 014535.
12. (a) Worsfold, D. J.; Zilliox, J. G.; Rempp, P. *Can. J. Chem.* **1969**, *47*, 3379. (b) Eschwey, H.; Hallensleben, M. L.; Burchard, W. *Makromol. Chem.* **1973**, *173*, 235.
13. (a) Xia, J.; Zhang, X.; Matyjaszewski, K. *Macromolecules* **1999**, *32*, 4482. (b) Zhang, X.; Xia, J.; Matyjaszewski, K. *Macromolecules* **2000**, *33*, 2340. (c) Baek, K.-Y.; Kamagaito, M.; Sawamoto, M. *Macromolecules* **2001**, *34*, 215. (d) Baek, K.-Y.; Kamigaito, M.; Sawamoto, M. *J. Polym. Sci.: Part A: Polym. Chem.* **2002**, *40*, 2245.
14. (a) Abrol, S.; Kambouris, P. A.; Looney, M. G.; Solomon, D. H. *Macromol. Rapid. Comm.* **1997**, *18*, 755. (b) Bosman, A. W.; Heumann, A.; Klaerner, G.; Benoit, D.; Fréchet, J. M. J.; Hawker, C. J. *J. Am. Chem. Soc.* **2001**, *123*, 6462.
15. (a) Lord, H. T.; Quinn, J. F.; Angus, S. D.; Whittaker, M. R.; Stenzel, M. H.; Davis, T. P. *J. Mater. Chem.* **2003**, *13*, 2819. (b) Moad, G.; Mayadunne, R. T. A.; Rizzardo, E.; Skidmore, M.; Thang, S. H. *Macromol. Symp.* **2003**, *192*, 1.
16. (a) Funke, W.; Okay, O.; Müller-Joos B. *Adv. Polym. Sci.* **1998**, *136*, 139. (b) Ulanski, P.; Rosiak, J. M. *Encyclopedia of Nanoscience and Nanotechnology* **2004**, Vol. X, 1.
17. (a) O'Brien, N.; McKee, A.; Sherrington, D. C.; Slark, A. T.; Titterton, A. *Polymer*, **2000**, *41*, 6027. (b) Costello, P. A.; Martin, I. K.; Slark, A. T.; Sherrington, D. C.; Titterton, A. *Polymer*, **2002**, *43*, 245. (c) Isaure, F.; Cormack, P. A. G.; Sherrington, D. C. *Macromolecules* **2004**, *37*, 2096. (d) Graham, S.; Cormack, P. A. G.; Sherrington, D. C. *Macromolecules* **2005**, *38*, 86.

18. (a) Abrol, S.; Caulfield, M. J.; Qiao, G. G.; Solomon, D. H. *Polymer*, **2001**, *42*, 5987. (b) Ide, N.; Fukuda, T. *Macromolecules* **1997**, *30*, 4268. (c) Ide, N.; Fukuda, T. *Macromolecules* **1999**, *32*, 95. (d) Zetterlund, P. B.; Alalm, M. D.; Minami, H.; Okubo, M. *Macromolecular Rapid Communications*, **2005**, *26*, 955.
19. (a) Isaure, F.; Cormack, P. A. G.; Graham, S.; Sherrington, D. C.; Armes, S. P.; Büttin, V. *Chem Commun.* **2004**, 1138. (b) Li, Y.; Armes, S. P. *Macromolecules* **2005**, *38*, 8155.
20. Liu, B.; Kazlauciunas, A.; Guthrie, J. T.; Perrier, S. *Macromolecules* **2005**, *38*, 2131.

Chapter 40

Germanium- and Tin-Catalyzed Living Radical Polymerizations of Styrene

Atsushi Goto, Hirokazu Zushi, Yungwan Kwak,
and Takeshi Fukuda*

Institute for Chemical Research, Kyoto University, Uji, Kyoto 611-0011,
Japan

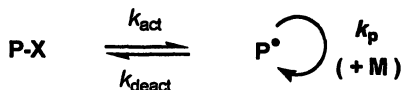
Ge and Sn (non-transition-metal) catalyzed living radical polymerizations were developed. Low-polydispersity ($M_w/M_n \sim 1.1-1.2$) polystyrenes with predicted molecular weights were obtained with a fairly high conversion in a fairly short time. The significant rate retardation observed for the GeI_4 system with relatively large concentrations of GeI_4 was kinetically proved to be mainly due to the cross-termination between P^\bullet with GeI_3^\bullet . Attractive features of the Ge and Sn catalysts include their *high reactivity* hence small amounts being required under a *mild condition* (at 60-80 °C) and *high solubility* in organic media without ligands. Ge catalysts may also be attractive for their *low toxicity*.

Living radical polymerization (LRP) has attracted much attention as a robust and versatile synthetic route for well-defined polymers (1). The basic concept of LRP is the reversible activation of the dormant species P-X to the propagating radical P[•] (Scheme 1a) (1,2). A number of activation-deactivation cycles are requisite for good control of chain length distribution. Examples of the capping agent X include nitroxides, halogens, dithioesters, telluride, and stibine (1). Halogens have been used mainly in two systems: namely, in iodide-mediated polymerization (3), P-X (X = I) is activated by P[•] (degenerative chain transfer; Scheme 1b), and in atom transfer radical polymerization (ATRP) (4), P-X is activated by a transition metal complex (Scheme 1c, where A is an activator, and XA is a deactivator).

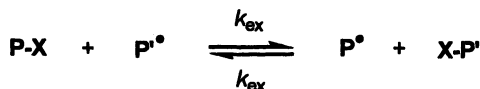
Percec et al. used Na₂S₂O₄ and its analogues as non-transition-metal catalysts (5). These catalysts worked as an *irreversible* activator, which only once activated alkyl halides forming no effective deactivator. We have attempted to use Ge and Sn compounds as non-transition-metal catalysts. Ge (III) or Sn (III) radical is known to abstract halogen from alkyl halide to give an alkyl radical and a Ge (IV) or Sn (IV) halide (6). This reaction and the subsequent reduction of the alkyl radical with a hydride are widely utilized for the transformation of alkyl halide to alkyl hydride in organic chemistry. If the formation of the alkyl radical can be made reversible (Scheme 2) by use of an appropriate Ge or Sn compound, it may lead to development of a new class of LRP.

In this work, we used four Ge and Sn compounds as non-transition-metal catalysts in the polymerization of styrene and examined their molecular weight and molecular weight distribution controllability. Results will be presented below along with some kinetic features of those systems.

(a) Reversible Activation



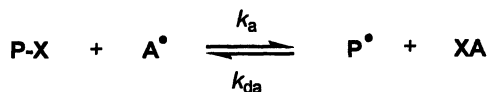
(b) Degenerative Chain Transfer



(c) Atom Transfer



Scheme 1. Reversible Activation Processes.



$X = I$ and $A = GeI_3, GeI, SnI_3,$ and SnI in this work

Scheme 2. Reversible activation catalyzed by Ge and Sn.

Experimental

Materials: Styrene (99%, Nacalai Tesque, Japan), benzoyl peroxide (BPO; 75% (25% water), Nacalai), and azobis(isobutyronitrile) (AIBN; 98%, Wako Pure Chemical, Japan) were purified by distillation or recrystallization from methanol. 1-Phenylethyl iodide (PE-I) was prepared, as described elsewhere (7). GeI_4 (99.999%, Alfa Aesar) was purified by recrystallization from carbon tetrachloride (8). GeI_2 (99.99%, Aldrich), SnI_4 (99.999%, Aldrich), and SnI_2 (95%, Aldrich) were used as received.

Gel Permeation Chromatography (GPC): The GPC analysis was made on a Shodex GPC-101 liquid chromatograph (Tokyo, Japan) equipped with two Shodex KF-804L polystyrene (PSt) mixed gel columns (300 × 8.0 mm; bead size = 7 μm; pore size = 20–200 Å). Tetrahydrofuran (THF) was used as eluent with a flow rate of 0.8 mL/min (40 °C). Sample detection and quantification were made with a Shodex differential refractometer RI-101 calibrated with known concentrations of PSts in THF. The column system was calibrated with standard PSts.

Polymerization: A mixture of styrene (3 mL), PE-I, GeI_4 (or GeI_2 , SnI_4 , and SnI_2), and BPO (or AIBN) in a Schlenk flask was heated at 80 °C (or 60 °C) under argon atmosphere. After a prescribed time t , an aliquot (0.1 mL) of the solution was taken out by a syringe, quenched to room temperature, diluted by THF to a known concentration, and analyzed by GPC. For kinetic analysis, a polystyrene-iodide (PSt-I; see below) was used instead of PE-I

Preparation of Polystyrene iodide (PSt-I): A mixture of styrene (3 mL), PE-I (80 mM), GeI_4 (5 mM), and BPO (20 mM) in a Schlenk flask was heated at 80 °C for 4 h. After purification by reprecipitation from methanol, a PSt-I with $M_n = 2000$ and $M_w/M_n = 1.20$ was isolated, where M_n and M_w are the number- and weight-average molecular weights, respectively.

Results and Discussion

Molecular Weight and Molecular Weight Distribution: We first examined the polymerization of styrene at 80 °C, using PE-I as a low-mass alkyl halide initiator, GeI₄ as a Ge (IV) halide (deactivator), and BPO as a conventional radical initiator. In this polymerization, the propagating radical P[•], originally supplied by the radical initiator BPO, is supposed to react with GeI₄, in situ producing the activator GeI₃[•] (and the polymer dormant species P-I). This protocol was used in copper-catalyzed ATRP and termed simultaneous reverse and normal initiation (SR&NI) ATRP (9). If this radical GeI₃[•] effectively eliminates I from PE-I (or P-I) to produce PE[•] (or P[•]), a useful chain of activation and deactivation will be completed.

Table 1. Polymerization of Styrene with PE-I in the Presence of Ge and Sn Iodides.

| entry | XA | $[PEI]_0/[I^a]_0$ / $[XA]_0$ (mM) | T (°C) | t (h) | con v (%) | M_n ($M_{n,theo}$) ^b | PDI |
|-------|------------------|---|-----------|----------|-----------------|-------------------------------------|------|
| 1 | GeI ₄ | 80/20/5 | 80 | 4 | 26 | 2500 (2600) | 1.19 |
| | | | | 7 | 37 | 3500 (3700) | 1.16 |
| | | | | 21 | 47 | 4300 (4700) | 1.16 |
| 2 | | 80/20/2 | 80 | 4 | 30 | 3300 (3000) | 1.17 |
| | | | | 7 | 47 | 4600 (4700) | 1.16 |
| 3 | | 80/40/2 | 80 | 4 | 51 | 5200 (5100) | 1.27 |
| | | | | 7 | 85 | 8200 (8500) | 1.24 |
| 4 | | 25/10/5 | 80 | 21 | 40 | 11400 (13300) | 1.29 |
| 5 | GeI ₂ | 80/20/5 | 80 | 4 | 27 | 2700 (2700) | 1.21 |
| | | | | 21 | 62 | 5700 (6200) | 1.15 |
| 6 | | 80/40/10 | 80 | 4 | 32 | 2800 (3200) | 1.17 |
| | | | | 25 | 85 | 6800 (8500) | 1.16 |
| 7 | SnI ₄ | 80/20/5 | 60 | 6 | 16 | 1700 (1600) | 1.15 |
| | | | | 21 | 36 | 3600 (3600) | 1.13 |
| 8 | | 8/4/1 | 60 | 21 | 24 | 22000 (24000) | 1.18 |
| 9 | | 8/4/4 | 60 | 21 | 16 | 15000 (16000) | 1.13 |
| 10 | SnI ₂ | 80/20/5 | 60 | 6 | 17 | 2000 (1700) | 1.26 |
| | | | | 21 | 50 | 4800 (5000) | 1.23 |
| 11 | none | 80/20/0 | 80 | 4 | 41 | 4200 (4100) | 1.55 |
| | | | | 21 | 90 | 7800 (9000) | 1.35 |

^a BPO for entries 1-6 and 11 and AIBN for entries 7-10. ^b Theoretical M_n calculated with $[M]$, $[PE-I]$, and conversion.

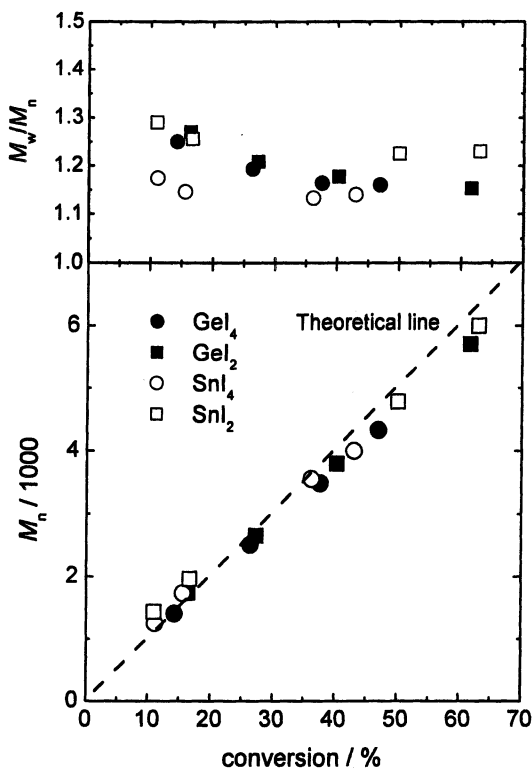


Figure 1. Plot of M_n and M_w/M_n vs conversion for the Ge and Sn catalyzed polymerizations of St for entries 1, 5, 7, and 10 in Table 1.

Table 1 (entries 1-4) and Figure 1 (filled circle) show the results. As shown in Figure 1, M_n linearly increased with conversion and agreed with the theoretical value $M_{n,theo}$. The polydispersity index (PDI) M_w/M_n reached a low value of about 1.2 from an early stage of polymerization, indicating a high frequency of activation-deactivation cycles. The small amount of GeI₄ required to control the polydispersity suggests a high reactivity of this catalysis. For example, the addition of 2 mM of GeI₄ to the system with 80 mM of PE-I and 20 mM of BPO (entry 2) produces, after 4 h of polymerization at 80 °C, a polymer with $M_n = 3000$ and $M_w/M_n = 1.17$ with a 30 % conversion, which contrasts to the polymerization without GeI₄ (but with other conditions set the same) giving $M_n = 4200$, $M_w/M_n = 1.55$, and a conversion of 41% (entry 11). The reasonable control of polydispersity in the latter system (entry 11) is due to the degenerative

chain transfer mechanism, i.e., the chain transfer reaction of the propagating radical to PE-I or P-I. (Scheme 1b) (10). The catalytic activation by GeI_3^\bullet should play a main role in the activation process in the GeI_4 system, with a small contribution of degenerative chain transfer.

The results obtained with SnI_4 deactivator (entries 7-9) suggest that the Sn system is somewhat better than the GeI_4 system in polydispersity controllability, even though exact comparison of the two systems is difficult because of the differences in temperature and (conventional) initiator. Both GeI_2 and SnI_2 deactivators (entries 5, 6, and 10) also have a clear controllability of polydispersity, but the results obtained with them are not as good as those with GeI_4 and SnI_4 .

Ge and Sn halides are Lewis acids. SnCl_4 , which is a strong Lewis acid, can abstract a halogen anion from an alkyl halide to give the alkyl carbocation and is widely used for living cationic polymerizations (11). On the other hand, Ge and Sn iodides (used in this work) are relatively weak Lewis acids. The tacticities of the produced polymers confirmed that the polymerizations in this work proceeded in a radical mechanism.

Kinetics: In the presence of Ge and Sn iodides, the polymerization rate R_p was somewhat smaller than in their absence (Table 1). This is because Ge and Sn radicals (A^\bullet : Scheme 2) undergo irreversible cross-termination with P^\bullet (rate constant k_t') and irreversible self-termination between A^\bullet (rate constant k_t''). This mechanism is analogous to the one for the rate retardation in reversible addition-fragmentation chain transfer (RAFT) polymerization (12,13).

In the activation-deactivation quasi-equilibrium (Scheme 2) and the stationary-state of radical concentrations ($d[P^\bullet]/dt = d[A^\bullet]/dt = 0$), R_p is theoretically given by (13)

$$R_p = R_{p,0} \left(1 + 2 \left(\frac{k_t'}{k_t K} \right) \frac{[XA]}{[P-X]} + \left(\frac{k_t''}{k_t K^2} \right) \frac{[XA]^2}{[P-X]^2} \right)^{-1/2} \quad (1)$$

where XA is a deactivator (Scheme 2), $R_{p,0}$ is the R_p without XA, K is the activation-deactivation equilibrium constant ($K = k_a/k_{da}$), and k_t is the self-termination rate constant of P^\bullet . This means that R_p decreases with the ratio $[XA]/[P-X]$.

We examined the R_p for the GeI_4 system. Figure 2 shows the first order plot of the monomer concentration $[M]$ with various amounts of GeI_4 (0-5 mM) and fixed amounts of PSt-I ($M_n = 2000$; $M_w/M_n = 1.20$; 20 mM) and BPO (5 mM) at 80 °C. PSt-I was used instead of PE-I to minimize the possible effect of chain length dependence of k_t on R_p . In Figure 2, R_p (hence $[P^\bullet]$) was stationary in the studied range of time in all cases and decreased with $[XA]_0/[P-X]_0$, as expected.

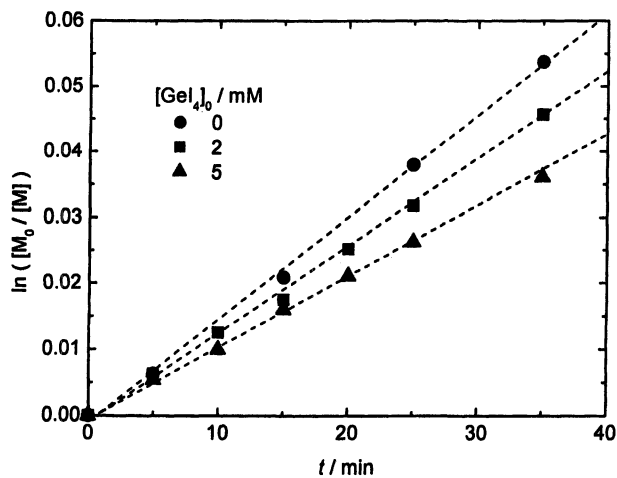


Figure 2. Plot of $\ln([M]_0/[M])$ vs t for the St/PSt-I/BPO/(Gel₄) system (80 °C): $[PSt-I]_0 = 20$ mM; $[BPO]_0 = 10$ mM; $[Gel_4]_0$ as indicated in the figure.

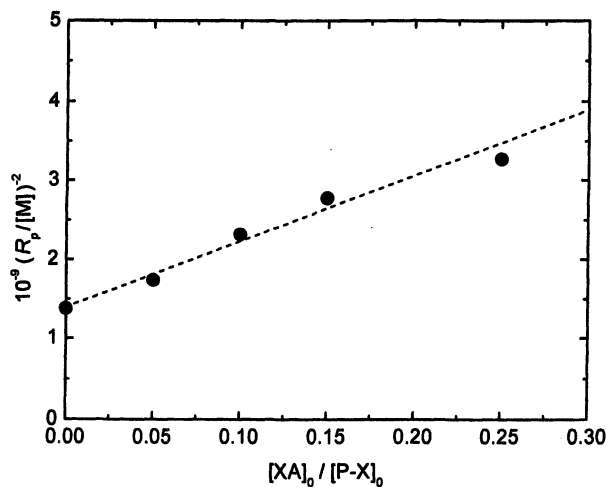


Figure 3. Plot of $(R_p/[M])^2$ vs $[XA]_0/[P-X]_0$ for the St/PSt-I/BPO/(Gel₄) system (80 °C): for experimental conditions, see the caption in Figure 2.

Now in the present experiments, it holds that $[XA]_0/[P-X]_0 \leq 1/4$, hence $[XA]_0/[P-X]_0 \gg ([XA]_0/[P-X]_0)^2 \sim 0$. Since k_t' and k_t'' should be of the same order of magnitude, the $A^\bullet-A^\bullet$ homo-termination (the k_t'' term in eq 1) should be minor (in the present experimental condition) compared with the $P^\bullet-A^\bullet$ cross-termination (the k_t' term). Setting the k_t'' term zero and $[XA]/[P-X] = [XA]_0/[P-X]_0$ in eq 1, we have

$$R_p^{-2} = R_{p,0}^{-2} \left(1 + 2 \left(\frac{k_t'}{k_t K} \right) \frac{[XA]_0}{[P-X]_0} \right) \quad (2)$$

Figure 3 shows the plot of R_p^{-2} vs $[XA]_0/[P-X]_0$. The plot represents a straight line, confirming the validity of eq 2. From this plot, we have $k_t'/(k_t K) = 3$. Thus, for the GeI_4 system, when $[XA]_0/[P-X]_0$ is relatively small, as in entries 1-4 in Table 1 ($[XA]_0/[P-X]_0 \sim 0.1$), cross-termination is the main cause for the retardation. The cross-termination results in a loss of GeI_4 , but it is a minor one at an early stage of polymerization. Moreover, the cross-termination products $PSt-GeI_3$ (by recombination) and $HGeI_3$ (by disproportionation) are Ge (IV) iodides and would still work as XA, contributing to polydispersity control.

Conclusions

Ge and Sn (non-transition-metal) catalyzed LRP were developed. Low-polydispersity ($M_w/M_n \sim 1.1-1.2$) polystyrenes with predicted molecular weights were obtained. The significant rate retardation observed for the GeI_4 system with relatively large concentrations of GeI_4 was due to the cross-termination between P^\bullet with GeI_3^\bullet . Attractive features of the Ge and Sn catalysts include their *high reactivity* hence small amounts being required under a *mild condition* (at 60-80 °C) and *high solubility* in organic media without ligands. Ge catalysts may also be attractive for their *low toxicity*.

References

1. (a) *Handbook of Radical Polymerization*; Matyjaszewski, K., Davis, T. P., Eds.; Wiley-Interscience: New York, 2002. (b) Matyjaszewski, K. Ed. *ACS Symp. Ser.* 1998, 685, 2000, 768 & 2003, 854.
2. For reviews on kinetics: (a) Fischer, H. *Chem. Rev.* 2001, 101, 3581. (b) Goto, A.; Fukuda, T. *Prog. Polym. Sci.* 2004, 29, 329. (c) Fukuda, T. *J. Polym. Sci.: Part A: Polym. Chem.* 2004, 42, 4743.

3. (a) Yutani, Y.; Tatemoto, M. *Eur. Pat. Appl.* 048937OA1, 1991. (b) Kato, M.; Kamigaito, M.; Sawamoto, M.; Higashimura, T. *Polym. Prepr., Jpn.* **1994**, *43*, 255. (c) Matyjaszewski, K.; Gaynor, S.; Wang, J.-S. *Macromolecules* **1995**, *28*, 2093.
4. For reviews: (a) Matyjaszewski, K.; Xia, J. H. *Chem. Rev.* **2001**, *101*, 2921. (b) Kamigaito, M.; Ando, T.; Sawamoto, M. *Chem. Rev.* **2001**, *101*, 3689.
5. (a) Percec, V.; Popov, A. V.; Ramirez-Castillo, E.; Coelho, J. F. J.; Hinojosa-Falcon, L. A. *J. Polym. Sci.: Part A: Polym. Chem.* **2004**, *42*, 6267. (b) Percec, V.; Popov, A. V.; Ramirez-Castillo, E.; Coelho, J. F. J.; *J. Polym. Sci.: Part A: Polym. Chem.* **2005**, *43*, 773.
6. For reviews: (a) Studer, A.; Amrein, S. *Synthesis (Stuttgart)* **2002**, 835. (b) Newcomb, M. *Adv. Organomet. Chem.* **1999**, *44*, 67.
7. Matyjaszewski, K.; Gaynor, S.; Wang, J.-S. *Macromolecules* **1995**, *28*, 2093.
8. Laubengayer, A. W.; Brandt, P. L. *J. Am. Chem. Soc.* **1932**, *54*, 621.
9. Gromada, J.; Matyjaszewski, K. *Macromolecules* **2001**, *34*, 7664.
10. Goto, A.; Ohno, K.; Fukuda, T. *Macromolecules* **1998**, *31*, 2809.
11. Fore reviews: (a) Sawamoto, M. *Prog. Polym. Sci.* **1991**, *16*, 111. (b) Puskas, J. E.; Kaszas, G. *Prog. Polym. Sci.* **2000**, *25*, 403.
12. (a) de Brouwer, H.; Schellekens, M. A. J.; Klumperman, B.; Monteiro, M. J.; German, A. L. *J. Polym. Sci., Part A: Polym. Chem.* **2000**, *38*, 3596. (b) Kwak, Y.; Goto, A.; Tsujii, Y.; Murata, Y.; Komatsu, K.; Fukuda, T. *Macromolecules* **2002**, *35*, 3026. (c) Calitz, F. M.; McLeary, J. B.; Mckenzie, J. M.; Tonge, M. P.; Klumperman, B.; Sanderson, R. D. *Macromolecules* **2003**, *36*, 9687. (d) Wang, A. R.; Zhu, S.; Kwak, Y.; Goto, A.; Fukuda, T.; Monteiro, M. J. *J. Polym. Sci., Part A: Polym. Chem.* **2003**, *41*, 2833. (e) Arita, T.; Beuermann, S.; Buback, M.; Vana, P. *Macromol. Mater. Eng.* **2005**, *290*, 283.
13. Kwak, Y.; Goto, A.; Fukuda, T. *Macromolecules* **2004**, *37*, 1219.

Chapter 41

Living Radical *Ab Initio* Emulsion Polymerization of *n*-Butyl Acrylate by Reverse Iodine Transfer Polymerization

J. Tonnar, P. Lacroix-Desmazes*, and B. Boutevin

Laboratoire de Chimie Macromoléculaire, UMR 5076 CNRS-ENSCM, Ecole Nationale Supérieure de Chimie de Montpellier, 8 Rue de l'Ecole Normale, 34296 Montpellier Cedex 5, France

The use of elemental iodine I_2 in living radical polymerization, called reverse iodine transfer polymerization (RITP), represents a new straightforward way to prepare smart macromolecular architectures. Herein, *ab initio* emulsion polymerization of *n*-butyl acrylate in the presence of molecular iodine has been successfully performed. The polymerization was initiated by 4,4'-azobis(4-cyanopentanoic acid) with dodecyl sulfate sodium salt as surfactant, yielding a stable and uncolored latex. The molecular weight of the polymer chains could be modulated by the concentration of iodine. Lastly, a block copolymer poly(butyl acrylate)-*b*-poly(styrene-*co*-butyl acrylate) was synthesized by seeded emulsion polymerization, proving the living characteristics of the polymerization. A simplified mechanism of RITP of *n*-butyl acrylate in emulsion has been proposed.

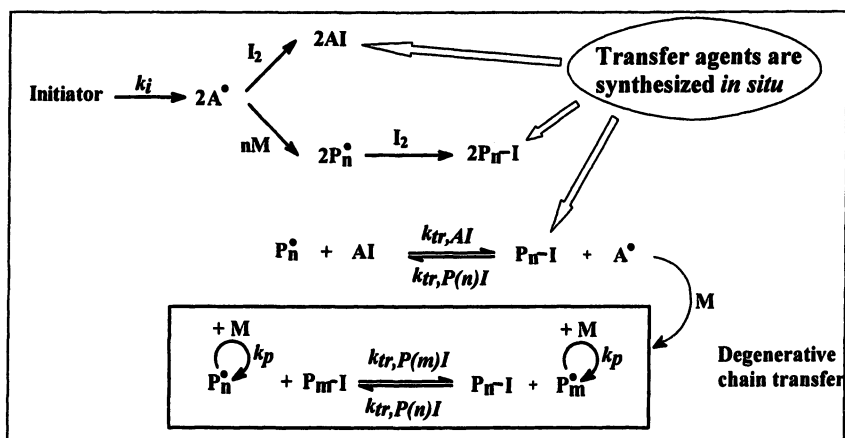
Introduction

Living free-radical polymerization (LFRP) affords the possibility to prepare polymers with well-defined architectures such as block copolymers, gradient copolymers, and star copolymers to name a few (1,2). Several radical polymerization methods have been developed so far to achieve this goal, among which nitroxide-mediated polymerization (NMP), atom transfer radical polymerization (ATRP), iodine transfer polymerization (ITP), and reversible addition-fragmentation chain transfer polymerization (RAFT/MADIX) are the most popular (3).

However, most studies on living radical polymerization dealt with solution polymerization and the successful implementation of LFRP in dispersed media, especially in aqueous medium which is largely used in industry, remains a challenge (4,5). Some attempts were reported in aqueous suspension, miniemulsion or emulsion polymerization by NMP, ATRP, ITP, RAFT, and MADIX, but only a few systems were effective in *ab initio* emulsion polymerization (4,6,7). Considering ITP with iodo-alkyl transfer agents (8,9), promising results were obtained in *ab initio* emulsion polymerization of styrene (10), miniemulsion polymerization of styrene (10-12), seeded emulsion polymerization of *n*-butyl acrylate (12), and microemulsion copolymerization of vinylidene fluoride with hexafluoropropylene (13).

Recently, a new living radical polymerization technique based on the use of elemental iodine I_2 , called reverse iodine transfer polymerization (RITP), was proposed by us (14,15), and patented (16-18). The basic mechanism of RITP is shown in Scheme 1. The radicals coming from the initiator can react with iodine or propagate before reacting with iodine to give iodinated compounds. Propagating radicals can also reversibly react with the previously formed A-I adduct to give dormant chains. Then, the core equilibrium of degenerative chain transfer between active and dormant chains takes place. The fundamental difference with ITP is that the transfer agents are now synthesized *in situ* during the process. From this scheme, one can conclude that one molecule of iodine will control two polymer chains. So, in this process, the molecular weight of the polymer is controlled by the ratio between the mass of monomer and twice the number of moles of iodine: $M_{n,targeted} = (\text{mass of monomer}) / (2 \times n_{I_2,initial}) + M_{A-I}$. The validity of RITP was first checked in the case of solution polymerization. For instance, in the case of the solution polymerization of methyl acrylate in benzene initiated by AIBN at 65°C in the presence of iodine (15), the experimental molecular weight determined by SEC was in very good agreement with the theoretical value: $M_{n,SEC} = 10\,900 \text{ g}\cdot\text{mol}^{-1}$ and $PDI = 1.91$ ($M_{n,theoretical} = 10\,500 \text{ g}\cdot\text{mol}^{-1}$). The molecular weight distribution is not narrow, which is consistent with the low degenerative chain transfer constant $C_{ex} = 2.2$ (minimal $PDI = 1 + 1/C_{ex} = 1.46$ in an ideal case) (19). Furthermore, proton NMR and MALDI-TOF

analyses confirmed that the polymer chains were initiated by AIBN and end-capped by an iodine atom. Therefore, RITP is a very simple and powerful method to control the molecular weight and the structure of the polymers. Last but not least, RITP is very cheap compared to other living radical polymerization methods (estimation for 1 mole of polymer, based on common catalogue prices): 15€ for RITP, 400€-2800€ for ATRP with CuCl/2bipy or CuBr/2HMTETA, 1000€ for NMP with TEMPO, and 760€ for RAFT with S-(thiobenzoyl)thioglycolic acid which is the only commercial (but very inefficient) RAFT agent so far. Herein, some results on the *ab initio* emulsion polymerization of *n*-butyl acrylate by reverse iodine transfer polymerization (RITP) are reported.



Scheme 1. Simplified mechanism of reverse iodine transfer polymerization (RITP) in solution (A^\bullet : radical from the initiator; I_2 : molecular iodine; M : monomer unit; n : mean number degree of polymerization).

Experimental

Materials

n-Butyl acrylate (BuA, Aldrich, 99%) was purified by vacuum distillation before use. Iodine (I_2 , Aldrich, 99.8%), 4,4'-azobis(4-cyanopentanoic acid) (ACPA, Fluka, 98%), dodecyl sulfate sodium salt (SDS, Aldrich, 98%), and

sodium hydroxide (NaOH, Carlo Erba, 97%) were used as received. Water was de-ionized by passing through columns packed with ion exchange resins.

General procedure for emulsion polymerization of BuA

Typically, 120 g of water were placed in a 250 mL glass reactor and thoroughly purged with argon for 30 minutes. Then, the reactor was thermostated at 85°C under stirring at 250 rpm. A solution of SDS (58.5 mg) in water (10 g) was added in the reactor under argon flow, followed by a solution of I₂ (192 mg) in BuA (15.05 g). Lastly, a solution of ACPA (336.6 mg) neutralized with aqueous sodium hydroxide (NaOH, 96 mg; water, 20 g) was added, and the polymerization proceeded under argon atmosphere for 8 hours. Monomer conversion was determined by gravimetric analysis.

Characterizations

Size Exclusion Chromatography (SEC) was performed on dried samples dissolved in tetrahydrofuran, with a Spectra Physics Instruments SP8810 pump equipped with a Shodex RIse-61 refractometer detector, a Milton Roy Ultra-Violet spectrometer detector, and two 300 mm columns thermostated at 30°C (columns mixed-C PL-gel 5µm from Polymer Laboratories : 2×10^2 - 2×10^6 g.mol⁻¹ molecular weight range). Tetrahydrofuran was used as eluent at a flow rate of 1.0 mL.min⁻¹. Calibration was performed with polystyrene standards from Polymer Laboratories and Mark Houwink coefficients for polystyrene ($K=11.4 \times 10^{-5}$ dL.g⁻¹, $\alpha=0.716$) (20) and poly(*n*-BuA) ($K=12.2 \times 10^{-5}$ dL.g⁻¹, $\alpha=0.700$) (20) were used for the calculations (except for the block copolymerization in Table III, runs 1-2).

Particle size of the latex particles was determined with a Nanotracs 250 particle analyzer (Microtracs Inc.). The measurements of *pH* were performed with a Consort P500 apparatus from Bioblock Scientific.

Results and Discussion

RITP in emulsion

This work has focused on *ab initio* emulsion polymerization because this is the most often used process in industry. The monomer is butyl acrylate, the

control agent is iodine, the initiator is 4,4'-azobis(4-cyanopentanoic acid) ($pK_a \approx 5.1$) ($t_{1/2} = 65$ min at $T = 85$ °C) (21), the temperature of the polymerization was kept constant at $T = 85$ °C, and sodium dodecyl sulfate was used as the surfactant (critical micelle concentration, $CMC = 2.6$ g.L⁻¹). The main parameters which have been investigated are the concentration of surfactant and the concentration of iodine. Lastly, the living properties of the latex have been checked by performing a block copolymerization.

Effect of the concentration of surfactant

For the series shown in Table I, the targeted molecular weight is kept constant at 10000 g.mol⁻¹ and an excess of initiator over iodine of 1.6 has been used. The concentration of the surfactant was varied and it was equal or lower than its critical micelle concentration. In all cases, a high monomer conversion was obtained without flocculation, and the latex was uncolored, indicating that iodine has been consumed. The final pH of the latex was always around the pK_a of the initiator which acts as a buffer. In contrast to results of RITP in solution, the molecular weight of the latex is much higher than the targeted molecular weight. This issue will be discussed later. More importantly, the deviation between the experimental molecular weight and the targeted molecular weight increases when the concentration of surfactant increases. Moreover, as shown in Figure 1a, the molecular weight distribution significantly broadens and a slight bimodality appears when the concentration of surfactant increases. As expected, the particle size decreases when the surfactant concentration increases (Figure 1b). In the absence of SDS, much larger particles are produced but the latex is still stable: the formation of stable particles without SDS indicates that ionizable chain-ends from the ACPA initiator do participate in the electrostatic stabilization of the latex. In conclusion to this part, it appears that the best results in terms of molecular weight, molecular weight distribution, particle size and particle size distribution are obtained at low SDS concentration, where homogeneous nucleation is favored compared to micellar nucleation. The reasons for the better results at low SDS concentration are still unclear.

Effect of the concentration of iodine

For the series shown in Table II, the excess of initiator over iodine was kept constant at 1.6 and the surfactant was used at low concentration, much below its critical micelle concentration. The concentration of iodine was varied in order to target molecular weights of about 5000, 10000, and 20000 g.mol⁻¹. In addition, in each case, a reference experiment in the absence of iodine has been

Table I. Effect of the concentration of surfactant^a

| Run | [SDS]/CMC | Time (h) | Conv. (%) ^b | pH | $M_{n,exp}$ (g.mol ⁻¹) | PDI | d_p (nm) |
|-----|-----------|----------|------------------------|-----|------------------------------------|------|------------|
| 1 | 0 | 15 | 83 | 5.1 | 22000 | 1.88 | 443 |
| 2 | 0.1 | 8 | 95 | 5.1 | 28200 | 2.21 | 119 |
| 3 | 0.15 | 7.7 | 90 | 5.2 | 21200 | 1.97 | 87 |
| 4 | 0.25 | 17 | 90 | 4.8 | 45500 | 4.32 | 59 |
| 5 | 1.0 | 7 | 96 | 4.9 | 37400 | 5.18 | 44 |

^aPolymerization of BuA in *ab initio* emulsion polymerization at $T=85^\circ\text{C}$ in the presence of ACPA as initiator: targeted molecular weight $M_n=10\,000\text{ g.mol}^{-1}$, $[\text{ACPA}]/[\text{I}_2]=1.6$.

^bConversion determined by gravimetry.

performed. Again, one can observe that the experimental molecular weight of the latex is always higher than the targeted molecular weight. Nevertheless, these results clearly show that the molecular weight of the polymer increases when the concentration of iodine decreases. Furthermore, even if tailing at low molecular weight is observed, the chromatograms show that the whole molecular weight distribution is shifted toward higher values when the quantity of iodine is decreased (Figure 2). Thus, this set of experiments indicates that the molecular weight of the poly(BuA) latex is efficiently tuned by varying the concentration of iodine.

By focusing on a RITP experiment and its reference counterpart in the absence of iodine (Table II, runs 2a and 2b), a first observation is that the final pH is more acidic in the RITP experiment than in the reference experiment. This low pH might be the result of the formation of hydriodic acid HI as discussed later in this paper. As previously noticed, the value around $\text{pH}=5$ corresponds to the pK_a of the initiator which acts as a buffer.

Another remarkable effect of iodine is that the molecular weight distribution is much narrower and monomodal in RITP than for the reference experiment (Figure 3a). In the case of emulsion polymerization of butyl acrylate, chain transfer to polymer usually occurs and leads to the formation of microgel (22). Thus, multimodality and broadening at high molecular weight in the reference experiment could be ascribed to chain transfer to polymer. Interestingly, because RITP modulates the molecular weight of the polymer chains, multiple intermolecular chain branching is minimized. Therefore, RITP prevents the polymer chains from forming poly(BuA) microgel.

Besides, RITP leads to much smaller particles than the reference experiment (Figure 3b). This is an indirect proof of the production *in situ* of surface active

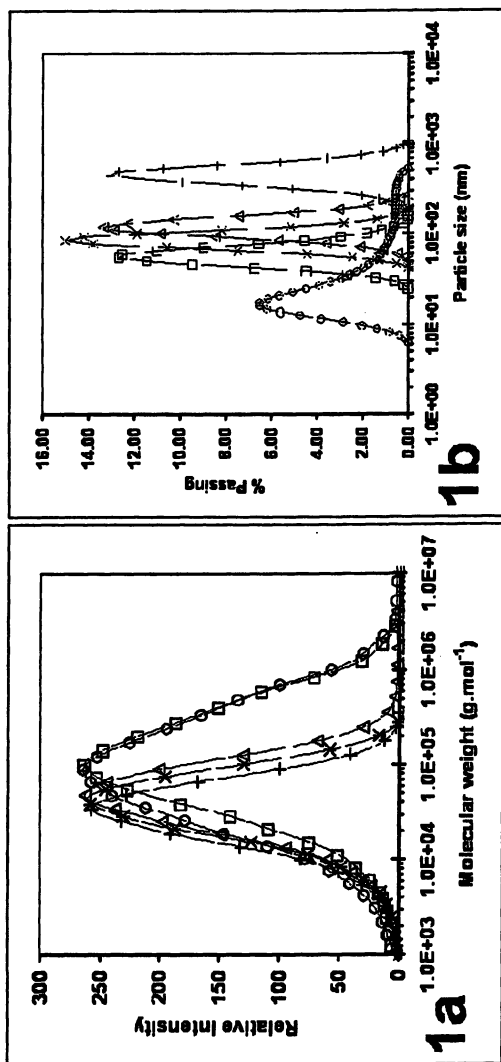


Figure 1. Molecular weight distributions (figure 1a) and particle size distributions (figure 1b) of poly(BuA) samples prepared by RITP in emulsion at different emulsifier concentrations : (+) no SDS ; (Δ) [SDS]=0.1 xCMC ; (\ast) [SDS]=0.15 xCMC ; (\square) [SDS]=0.25 xCMC ; (\circ) [SDS]=1 xCMC.

Table II. Effect of the concentration of iodine^a

| Run | $[I_2]/[BuA]$ | $M_{n,targeted}$ ($g \cdot mol^{-1}$) | Time (h) | Conv. (%) | pH | $M_{n,exp}$ ($g \cdot mol^{-1}$) | PDI | d_p (nm) |
|-----|------------------------|--|-------------|--------------|-----|---------------------------------------|------|---------------|
| 1a | 12.9×10^{-3} | 5200 | 15 | 53 | 4.7 | 12000 | 1.69 | 79 |
| 1b | No iodine ^b | - | 5.25 | 99 | 7.1 | 47400 | 8.90 | 124 |
| 2a | 6.5×10^{-3} | 10100 | 7.7 | 90 | 5.2 | 21200 | 1.97 | 87 |
| 2b | No iodine ^b | - | 6.5 | 96 | 7.1 | 48600 | 7.74 | 134 |
| 3a | 3.3×10^{-3} | 19500 | 7 | 93 | 5.6 | 47000 | 2.78 | 69 |
| 3b | No iodine ^b | - | 5.5 | 94 | 7.1 | 40300 | 6.80 | 128 |

^aPolymerization of BuA in *ab initio* emulsion polymerization at $T=85^\circ\text{C}$ in the presence of ACPA as initiator : $[ACPA]/[I_2]=1.6$, $[SDS]=0.15 \times \text{CMC}$.

^bConducted without iodine but with the same concentration of initiator as in the corresponding RITP experiment.

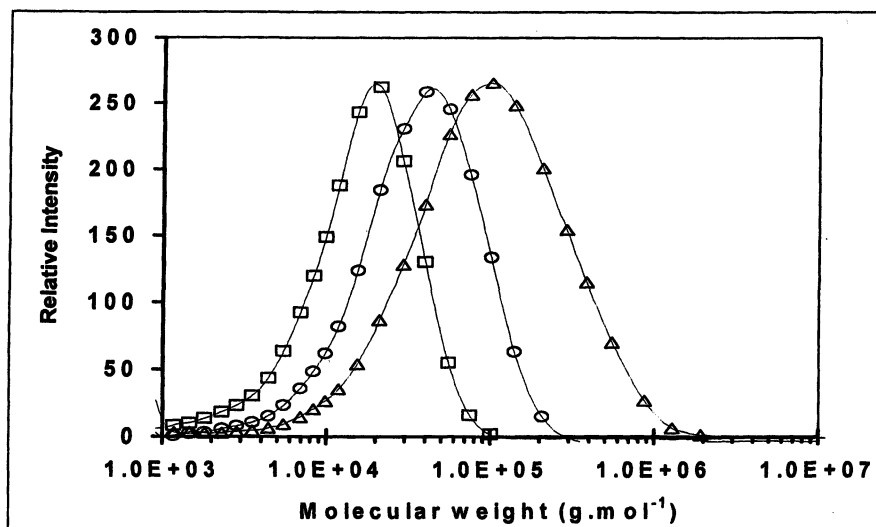


Figure 2. Molecular weight distributions of poly(BuA) samples prepared by RITP in emulsion. Targeted molecular weight : (□) 5 200 $g \cdot mol^{-1}$, (○) 10 100 $g \cdot mol^{-1}$, (△) 19 500 $g \cdot mol^{-1}$.

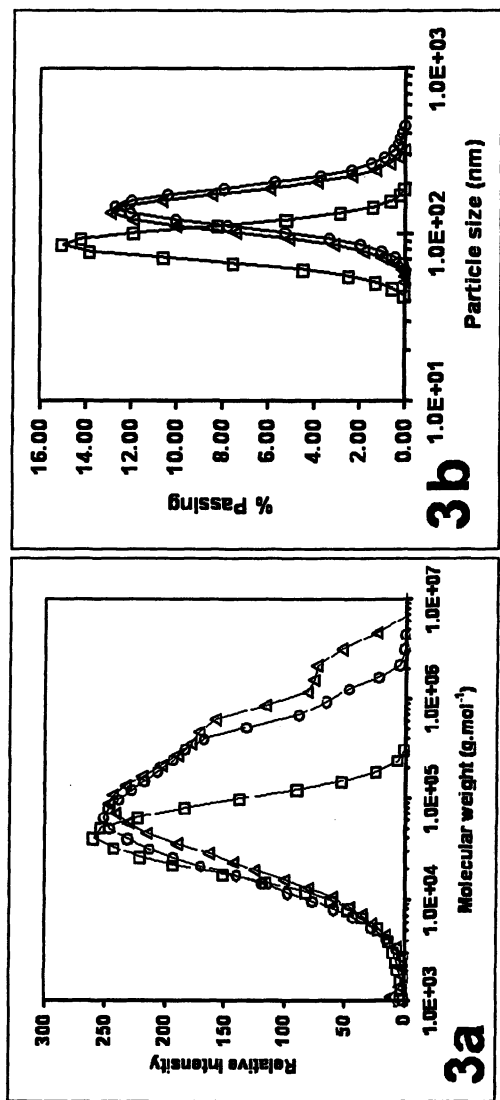


Figure 3. Molecular weight distributions and particle size distributions of poly(BuA) samples prepared by RITP in emulsion at $T=85^{\circ}\text{C}$: (□) RITP experiment, $M_{n,\text{targeted}}=10100\text{ g mol}^{-1}$; (○) RITP experiment with the same concentration of iodine but in the presence of an excess of NaI; (Δ) Reference experiment without iodine but with the same concentration of initiator.

species. Indeed, the polymer chains contain a hydrophilic head (carboxylic acid) and a hydrophobic tail. The smaller particle size in the case of RITP indicates that the concentration of the oligomeric surfactants builds up during the RITP process and that these oligomers take part in the nucleation step. So, from this comparison, one can conclude that RITP creates *in situ* ionizable surfactants that contribute to the electrostatic stabilization of the latex.

Kinetics of RITP in emulsion

Kinetically, iodine is known to be a powerful terminator. So, one can typically divide the process into two periods. A first inhibition period where the radicals essentially react with iodine to form the iodinated transfer agents (A-I and A-M_n-I oligomers), and a second period where the polymerization takes place (15). Figure 4 shows the evolution of monomer conversion versus time for a RITP experiment in emulsion. As in solution polymerization, an inhibition period is clearly observed, and then the monomer conversion increases up to high conversion. This inhibition period is in qualitative agreement with the expected mechanism of RITP: indeed, it means that the rate of the reaction between radicals (A[•] or A-M_n[•] oligoradicals) and iodine is higher than the rate of propagation. So, the presence of the inhibition period confirms the favored reaction of radicals with iodine.

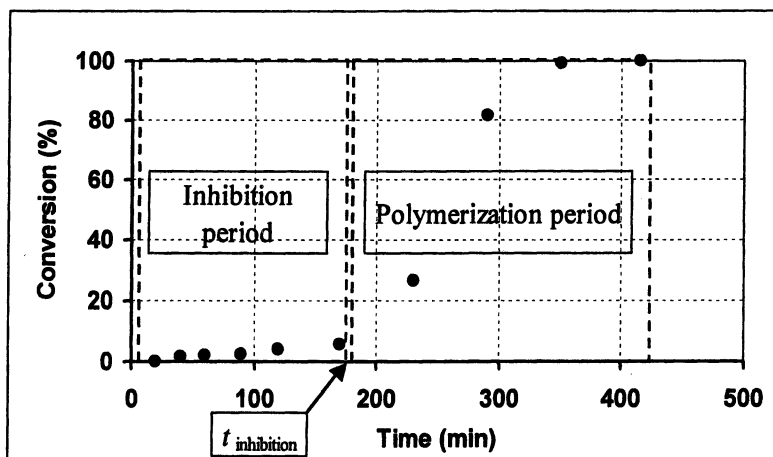


Figure 4. Evolution of monomer conversion versus time for RITP of BuA in emulsion at $T=85^{\circ}\text{C}$ ($[\text{ACPA}]/[\text{I}_2]=1.7$, $[\text{SDS}]=0.15\times\text{CMC}$, $M_{n,\text{targeted}}=10\ 100\ \text{g}\cdot\text{mol}^{-1}$).

For the same experiment, the evolution of molecular weight versus monomer conversion shows a linear trend and the polydispersity index remains in an acceptable range for iodine transfer polymerization of butyl acrylate (Figure 5a). The size exclusion chromatograms at low, medium and high monomer conversion clearly show that the whole molecular weight distribution shifts toward higher molecular weights when the monomer conversion increases (Figure 5b). Therefore, this kinetic survey indicates that the evolution of the molecular weight and molecular weight distribution is compatible with a living process dominated by degenerative chain transfer.

Block copolymerization in emulsion

In order to check the living properties of the poly(BuA) chains, a latex prepared by RITP was used as a seed for block copolymerization (Table III). Styrene was chosen as the second monomer and it was added to the seed latex in a batch process. 86% monomer conversion was reached in the second stage of polymerization. The increase of the particle size is consistent with a constant number of particles (Figure 6a). It means that there is no re-nucleation which is a necessary condition for block copolymerization.

The experimental molecular weight for the copolymer is 55100 g.mol⁻¹. It is close to the theoretical value of 58600 g.mol⁻¹. Furthermore, the chromatograms show that the molecular weight distribution shifts toward higher molecular weights, indicating that the polymer chains are reactivated, and the UV signal is similar to the refractive index signal, giving evidence for the formation of a diblock copolymer rather than the formation of two homopolymers (Figure 6b). So, all these results indicate that the preparation of the block copolymer was successful and it confirms the high potential of RITP to tailor polymers directly in dispersed aqueous media.

Table III. Block copolymerization in emulsion^a

| <i>Run</i> | <i>Type</i> | <i>Time</i> (<i>h</i>) | <i>Conv.</i> (%) | <i>pH</i> | <i>M_{n,exp}</i> (g.mol ⁻¹) | <i>PDI</i> | <i>d_p</i> (nm) |
|------------|--|-----------------------------|---------------------|-----------|--|------------|------------------------------|
| 1 | Seed latex Poly(BuA) | 8 | 95 | 5.1 | 26700 | 2.18 | 119 |
| 2 | Block copolymerization Poly(BuA)- <i>b</i> - poly(styrene- <i>co</i> -BuA) | 15 | 86 | 5.0 | 55100 | 1.68 | 167 |

^aSeed: [ACPA]/[I₂]=1.6, [SDS]=0.10×CMC, targeted *M_n*= 10 000 g.mol⁻¹; Second monomer: styrene; Monomer_{Feed}/Monomer_{Seed}=1.3 w/w.

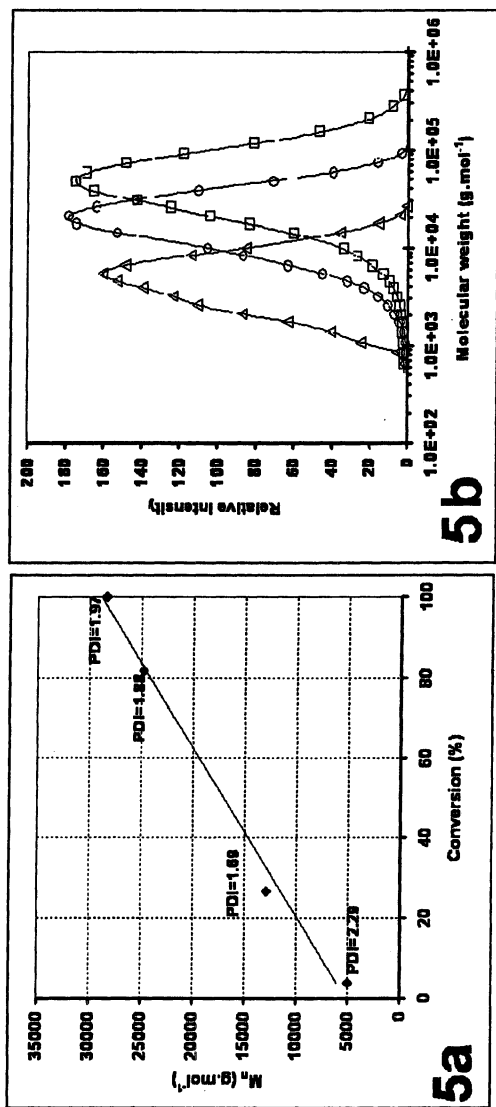


Figure 5. RITP of BuA in emulsion at $T=85^\circ\text{C}$ ($[\text{ACPA}]/[\text{I}_2]=1.7$, $[\text{SDS}]=0.15\times\text{CMC}$, targeted $M_n=10$ $100\text{ g}\cdot\text{mol}^{-1}$): (a) Evolution of M_n and PDI versus monomer conversion; (b) Evolution of the molecular weight distribution with monomer conversion: (Δ) conversion=6%, (\circ) conversion=27%, (\square) conversion=99%.

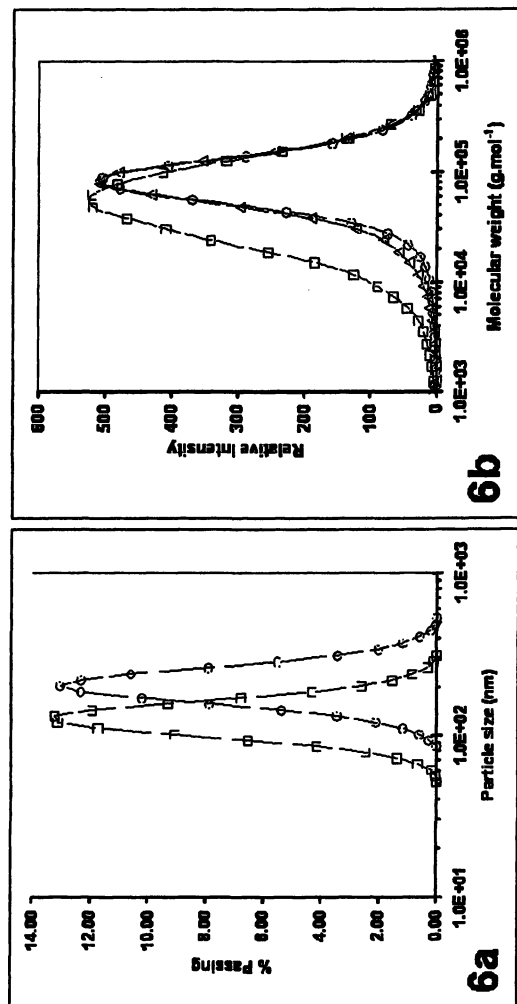
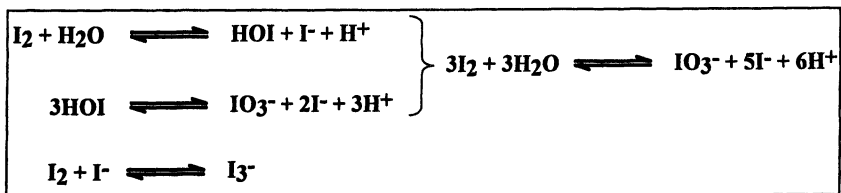


Figure 6. Characterizations of the seed poly(BuA) latex prepared by RITP and of the block copolymer latex prepared by seeded emulsion polymerization of styrene. (a) Overlay of particle size distributions : (□) seed latex, (○) copolymer latex; (b) Molecular weight distributions: (□) refractive index detector (seed latex), (○) UV detector at 254nm (copolymer latex), (△) refractive index detector (copolymer latex).

Features of RITP in emulsion

Results presented above show some discrepancies between experimental and theoretical molecular weights for RITP in emulsion. One important feature in emulsion polymerization is the partitioning of the different species between the different phases. In the present case, one important reaction to consider is the hydrolytic disproportionation of iodine in the aqueous phase (23,24) ($[I_2]_{aq} = 1.32 \times 10^{-3} \text{ mol.L}^{-1}$) (25). Many equilibria are actually taking place and they are leading to the formation of hypoiodous acid (HOI), iodide (I^-), iodate (IO_3^-), and triiodide (I_3^-). It also forms protons and thus it tends to lower the pH , as observed in Table II. Such side reactions of iodo compounds in water do occur and they complicate the mechanism of RITP in emulsion. In order to illustrate this point, the effect of iodide ions on RITP in emulsion has been investigated. The addition of an excess of sodium iodide versus iodine conducts to the formation of triiodide. It has a dramatic effect on the polymerization: the addition of excess iodide ions leads to the loss of control of the RITP in emulsion (Figure 3). The iodine is consumed in a competitive reaction to form triiodide and therefore iodine is no longer available to control the polymerization. This set of experiments clearly shows that the formation of triiodide competes with the RITP mechanism.



Scheme 2. Hydrolytic disproportionation of iodine and some other related reactions.

Based on our knowledge, a simplified mechanism of RITP in emulsion can be tentatively proposed. In the water phase, the ionizable radicals A^\bullet coming from the initiator can react with iodine to form $A-I$ or propagate before reacting with iodine to give surface active transfer agents $A-M_n-I$. The propagating radicals $A-M_n^\bullet$ can also reversibly react with the previously formed $A-I$ adduct to give surface active dormant chains $A-M_n-I$. In the same time, side reactions with water such as hydrolytic disproportionation of I_2 consume a part of the iodine ($n_{I_2, effective} < n_{I_2, initial}$). During the inhibition period, the concentration of the surface active transfer agents builds up. Then, the nucleation step occurs and the

core equilibrium between active and dormant chains takes place inside the latex particles. From this description, one can conclude that the side reactions of iodo compounds with water account for the upward deviation of the molecular weight from the ratio between the mass of monomer and twice the initial number of moles of iodine in the reaction medium. By analyzing the evolution of pH for a targeted M_n of 10 000 g.mol⁻¹, preliminary attempts to quantify the loss of iodine through side reactions ($\alpha = n_{I_2, effective} / n_{I_2, initial}$) lead to a reasonable agreement between the experimental value $M_{n, SEC}$ and the corrected targeted value $M_{n, targeted(corrected)} = (mass\ of\ monomer) / (2\alpha \times n_{I_2, initial}) + M_{A-I}$.

Conclusions

A new living radical polymerization method named RITP has been invented. It is an easy-to-make method which does not require the synthesis nor storage of control agents. Furthermore, RITP can be performed in dispersed aqueous media (such as in *ab initio* emulsion polymerization). Work is in progress in our laboratory about side reactions in water in order to get a better control of the molecular weight of polymers prepared by RITP in emulsion. Based on our knowledge, RITP is a robust and economical method which is expected to boost the development of living/controlled radical polymerization at an industrial scale.

Acknowledgments

Chantal RUFIER is acknowledged for her early contribution to this topic during her training period in our laboratory. Vincent Bodart and Christophe Fringant (SOLVAY) are acknowledged for their constant interest in the RITP process.

References

1. Matyjaszewski, K. *ACS Symposium Series* **2003**, *854*, 2-9.
2. Lacroix-Desmazes, P.; Ameduri, B.; Boutevin, B. *Collection of Czechoslovak Chemical Communications* **2002**, *67*, 1383-1415.
3. Goto, A.; Fukuda, T. *Progress in Polymer Science* **2004**, *29*, 329-385.
4. Cunningham, M. F. *Progress in Polymer Science* **2002**, *27*, 1039-1067.
5. Qiu, J.; Charleux, B.; Matyjaszewski, K. *Polimery (Warsaw, Poland)* **2001**, *46*, 663-672.

6. Monteiro, M. J.; Adamy, M. M.; Leeuwen, B. J.; van Herk, A. M.; Destarac, M. *Macromolecules* **2005**, *38*, 1538-1541.
7. Qiu, J.; Charleux, B.; Matyjaszewski, K. *Progress in Polymer Science* **2001**, *26*, 2083-2134.
8. Matyjaszewski, K.; Gaynor, S.; Wang, J.-S. *Macromolecules* **1995**, *28*, 2093-2095.
9. Gaynor, S. G.; Wang, J.-S.; Matyjaszewski, K. *Macromolecules* **1995**, *28*, 8051-8056.
10. Lansalot, M.; Farcet, C.; Charleux, B.; Vairon, J.-P.; Pirri, R. *Macromolecules* **1999**, *32*, 7354-7360.
11. Butte, A.; Storti, G.; Morbidelli, M. *Macromolecules* **2000**, *33*, 3485-3487.
12. Farcet, C.; Lansalot, M.; Pirri, R.; Vairon, J. P.; Charleux, B. *Macromolecular Rapid Communications* **2000**, *21*, 921-926.
13. Apostolo, M.; Arcella, V.; Storti, G.; Morbidelli, M. *Macromolecules* **2002**, *35*, 6154-6166.
14. Lacroix-Desmazes, P.; Severac, R.; Otazaghine, B.; Boutevin, B. *Polymer Preprints (American Chemical Society, Division of Polymer Chemistry)* **2003**, *44*, 683-684.
15. Lacroix-Desmazes, P.; Severac, R.; Boutevin, B. *Macromolecules* **2005**, *38*, 6299-6309.
16. Lacroix-Desmazes, P.; Severac, R.; Boutevin, B.; Bodart, V.; Kurowsky, V. F.R. Patent 2,839,724, 2003.
17. Boutevin, B.; Otazaghine, B.; Lacroix-Desmazes, P.; Dubreuil, M.; Bodart, V. F.R. Patent 2,839,725, 2003.
18. Lacroix-Desmazes, P.; Severac, R.; Boutevin, B.; Bodart, V.; Kurowski, V. W.O. Patent 094,356, 2004.
19. Mueller, A. H. E.; Zhuang, R.; Yan, D.; Litvinenko, G. *Macromolecules* **1995**, *28*, 4326-4333.
20. Beuermann, S.; Paquet, D. A., Jr.; McMinn, J. H.; Hutchinson, R. A. *Macromolecules* **1996**, *29*, 4206-4215.
21. Lewis, F. M.; Matheson, M. S. *Journal of the American Chemical Society* **1949**, *71*, 747-748.
22. Plessis, C.; Arzamendi, G.; Leiza, J. R.; Schoonbrood, H. A. S.; Charmot, D.; Asua, J. M. *Macromolecules* **2000**, *33*, 5041-5047.
23. Murray, H. D. *Journal of the Chemical Society, Abstracts* **1925**, *127*, 882-885.
24. Nagy, K.; Koertvelyesi, T.; Nagypal, I. *Journal of Solution Chemistry* **2003**, *32*, 385-393.
25. Bower, J. G.; Scott, R. L. *Journal of the American Chemical Society* **1953**, *75*, 3583-3585.

Author Index

- Acar, Metin H., 97
Ando, Tsuyoshi, 14
Asandei, Alexandru D., 125
Barner-Kowollik, Christopher, 486
Baussard, Jean-François, 578
Becer, C. Remzi, 97
Bertin, Denis, 326
Bombalski, Lindsay, 252
Börner, Hans G., 198
Boutevin, B., 604
Božović, Jelena S., 501
Brooks, Samuel J., 56
Brown, Steven, 438
Bryaskova, Rayna, 372
Buback, M., 455
Caille, Jean-Raphaël, 372
Chan, A. Ken, 234
Chauvin, Florence, 326
Chen, Yanhui, 125
Chung, T. C., 387
Coote, Michelle L., 406
Couturier, Jean-Luc, 326
Davis, Thomas P., 486
Debuigne, Antoine, 372
Delaude, Lionel, 40
Delfosse, Sébastien, 40
Demonceau, Albert, 40
Destarac, Mathias, 564, 578
Detrembleur, Christophe, 372
Ding, Shijie, 71
Du Prez, Filip E., 171
Dufils, Pierre-Emmanuel, 326
Dufour, Bruno, 295
Duncalf, David J., 438
Dupayage, Ludovic, 578
Egan, Dave, 547
Endo, Takeshi, 533
Faucher, Santiago, 85
Fijten, Martin W. M., 473
Flores-Santos, Leticia, 342
Fryd, Michael, 358
Fu, Xuefeng, 358
Fukuda, Takeshi, 595
Gao, Haifeng, 140
Gao, Yuan, 279
Georges, Michael K., 312
Gérard, Pierre, 326
Gigmes, Didier, 326
Gnanou, Yves, 578
Golas, Patricia, 140
González-Montiel, Alfonso, 342
Goto, Atsushi, 595
Guerret, Olivier, 326
Guillaneuf, Yohann, 326
Holzinger, Dieter, 269
Hong, H., 387
Hoogenboom, Richard, 473
Hsu, Raymond, 547
İnceoğlu, Sebnem, 97
Ivanovici, Sorin, 269
Iwaya, Hideyuki, 533
Izgorodina, Ekaterina I., 406
Jérôme, Robert, 372
Johnston-Hall, Geoffrey, 421
Junkers, T., 455
Kajiwara, Atsushi, 111
Kalai, Chakib, 564
Kamigaito, Masami, 14, 26
Keul, Helmut, 153
Kickelbick, Guido, 269

- Klumperman, Bert, 501
Koumura, Kazuhiko, 26
Kowalewski, Tomasz, 295
Krenske, Elizabeth H., 406
Kruk, Michal, 295
Kwak, Yungwan, 595
Lacroix-Desmazes, P., 604
Lai, John, 547
Lee, Robert Y., 140
Legge, Thomas M., 438
Lepilleur, Carole, 547
Li, Guoxin, 514
Louche, Guillaume, 140
Lu, Zhi, 358
Lubnin, Alex, 547
Lutz, Jean-François, 185
Marque, Sylvain R. A., 326
Matyjaszewski, Krzysztof, 2, 56, 140, 234, 252, 295
McCarthy, Patrick, 252
McLeary, James B., 501
Mela, Petra, 153
Mennicken, Martina, 153
Mignaud, Catherine, 578
Moad, Graeme, 514
Möller, Martin, 153
Monteiro, Michael J., 421
Moran, Isaac W., 125
Mori, Hideharu, 214, 533
Müller, Axel H. E., 214
Muthukrishnan, Sharmila, 214
Nagai, Atsushi, 533
Nagelsdiek, René, 153
Nehring, Rainer, 185
Noels, Alfred F., 40
Okamoto, Yoshio, 26
Ondur, H. Alper, 97
Pajerski, Anthony, 547
Paulus, Renzo M., 473
Peng, Chi-How, 358
Perrier, Sébastien, 438
Petit, Laurence, 564
Pfaendner, Rudolf, 514
Pfeifer, Sebastian, 185
Pitois, Claire, 578
Pohl, Christopher, 252
Postma, Almar, 514
Radosz, Maciej, 71
Ranade, Shrirang, 234
Rannard, Steven P., 438
Richard, Robert E., 234
Richel, Aurore, 40
Rizzardo, Ezio, 514
Roy, Debashish, 438
Rutzinger, Dieter, 269
Saha, Gobinda, 125
Saldivar-Guerra, Enrique, 342
Satoh, Kotaro, 26
Sawamoto, Mitsuo, 14
Schubert, Ulrich S., 473
Schwarz, Marlene, 234
Shea, Ronald, 547
Shen, Youqing, 71
Shibata, Takuya, 26
Soer, Willem-Jan, 501
Stenzel, Martina H., 486
Sugiyama, Yuya, 26
Sumerlin, Brent S., 140, 234
Sutoh, Kazuhiko, 533
Szkurhan, Andrea R., 312
Takolpuckdee, Pittaya, 438
Tang, Chuanbing, 295
Tang, Wei, 56
Taton, Daniel, 578
Ten Cate, Mattijs G. J., 198
Thang, San, 514
Theis, Alexander, 486
Tonnar, J., 604
Tordo, Paul, 326

- Tsarevsky, Nicolay V., 56, 140, 252
Van Camp, Wim, 171
van den Dungen, Eric T.A., 501
Van Gramberen, Eric, 564
Vana, P., 455
Wan, Decheng, 26
Wang, Z. M., 387
Watanabe, Yasuhiro, 14
Wayland, Bradford B., 358
Wermter, Hendrik, 514
Wilczewska, Agnieszka, 564
Wood, Murray R., 438
Yan, Deyue, 279
Yoshitani, Toshihide, 14
Zard, Samir Z., 564
Zhang, Z. C., 387
Zhu, Shiping, 85
Zushi, Hirokazu, 595

Subject Index

A

Ab initio calculations

- addition-fragmentation reaction in reversible addition-fragmentation chain transfer (RAFT) process, 407–408
- computational procedures, 408–409
- See also* Reversible addition-fragmentation chain transfer (RAFT)

Ab initio emulsion polymer

- telechelic reversible addition-fragmentation chain transfer (RAFT) polymers as, 553–554, 559–560

See also Reverse iodine transfer polymerization (RITP)

Acidic monomers, atom transfer radical polymerization (ATRP) systems, 64–65

Acrylamides

- iron-catalyzed systems with metal triflates for, 30–32
- See also* Amino acid-based polymers

Acrylate-based block copolymers

- atomic force microscopy (AFM), 239, 241, 242*f*
- chemical composition of, by ATRP, 238*t*
- differential scanning calorimetry (DSC), 239
- DSC results for poly(methyl methacrylate) (PMMA), polystyrene (PS) and poly(isobutyl acrylate) (PIBA) block copolymers containing paclitaxel (PTX), 241*t*

effect of radiation dose on Mn of, 247*t*

effect of radiation dose on PTX release rate, 248*f*, 249*f*

gel permeation chromatography (GPC) for PBA macroinitiator and triblock copolymers, 239*f*

materials and methods, 237

matrices for drug delivery, 235–236

mechanical integrity of stent coatings, 238

PTX and stent technology, 236

PTX release from, 241, 243, 244*f*, 245*f*, 246*f*

polymer synthesis, 237–238

radiation stability, 246–248

scanning electron microscopy (SEM) of coronary stents coated with P(MMA-BA-MMA), 240*f*

Acrylate polymerization

- characteristics of organo-cobalt/azo radical living radical, 370
- nanoprecipitation emulsion, 319, 321

reversible addition-fragmentation chain transfer (RAFT), 517–520

Acrylic acid (AA)

change in Mn and polydispersity as function of AA conversion to poly(AA), 365*f*

controlled radical polymerization, 172

living radical polymerization (LRP) in water mediated by cobalt(II) and organo-cobalt porphyrins, 363–364

monomer conversion vs. time in radical polymerization of, 365*f*

Acrylonitrile (AN). *See* Reversible addition-fragmentation chain transfer (RAFT) copolymerizations

N-Acryloyl-L-phenylalanine (A-Phe-OH)

chemical structure, 534*f*

controlled polymerization by reversible addition-fragmentation chain transfer (RAFT), 538–539

experimental, 535

size exclusion chromatography (SEC) traces of methylated, 540*f*
varying polymerization conditions, 539, 540*t*

See also Amino acid-based polymers

N-Acryloyl-L-phenylalanine methyl ester (A-Phe-OMe)

chemical structure, 534*f*

controlled polymerization by reversible addition-fragmentation chain transfer (RAFT), 535–538

dependence of Mn and polydispersity with monomer to chain transfer agent ratio, 536*f*

effect of Lewis acids, 538*t*

experimental, 535

size exclusion chromatography (SEC) traces, 536*f*

time-conversion and pseudo-first-order kinetic plots, 537–538

See also Amino acid-based polymers

N-Acryloyl-L-proline methyl ester (A-Pro-OMe)

chemical structure, 534*f*

circular dichroism (CD) spectra of poly(A-Pro-OMe) with and without Lewis acid, 543*f*

controlled polymerization by reversible addition-fragmentation chain transfer (RAFT), 540–544

copolymer comparison by RAFT and conventional free radical polymerization, 544*f*

copolymerization with *N,N*-dimethylacrylamide (DMA), 542–544

effect of Lewis acids, 542*t*, 543*f*

evolution of size exclusion chromatography (SEC) traces, 541*f*

Mn and polydispersity vs. conversion, 541*f*

temperature dependence of solution turbidity of copolymers, 544*f*

See also Amino acid-based polymers

Activators generated by electron transfer (AGET), atom transfer radical polymerization (ATRP), 6

Activators re-generated by electron transfer (ARGET), atom transfer radical polymerization (ATRP), 6

Activity, copper-based catalysts, 60–63

Addition-fragmentation process

effect of Z group on stabilities and fragmentation enthalpies, 411*t*

fragmentation efficiency, 409

See also Reversible addition-fragmentation chain transfer (RAFT)

Alkoxyamines

applications in nitroxide mediated polymerization (NMP), 333–337

C–O bond homolysis in phosphonylated, 330–331

experimental, 329–330

intermolecular radical addition of, onto alkenes for new functional mono- and polyalkoxyamines, 331–333

polymerization of methyl methacrylate (MMA), 336–337

polymerization of *n*-butyl acrylate, 335–336

- polymerization of styrene, 333, 334*f*, 335
- rate constants and activation energies for dissociation of C–O bond for, 331*t*
- synthesis of phosphorylated, 330
- use for building complex macromolecular architectures, 337–339
- See also* Nitroxide-mediated polymerization (NMP)
- Alkoxysilyl-terminated polymers, telechelic reversible addition-fragmentation chain transfer (RAFT) polymers, 557–558, 562
- Alkylated linear amine ligands
- atom transfer radical polymerization (ATRP), 99
- common amine ligands for use in Cu-based ATRP, 99, 100*t*
- ethylene linkage of amines, 99
- experimental, 100–102
- ¹H NMR spectra of 1,1,4,7,7-pentaethyldiethylene triamine (PEDETA), 103*f*
- instrumentation, 101
- kinetic plots of methyl methacrylate (MMA) and styrene polymerizations using PEDETA as ligand, 105*f*
- ligand synthesis, 102–103
- MMA polymerization by ATRP using, 106*t*
- Mn vs. conversion plots of MMA and styrene polymerizations using PEDETA as ligand, 105*f*
- solubility of, and metal complex in organic media, 99
- structures of, 104*t*
- styrene polymerization by ATRP using, 107*t*
- synthesis, 101
- typical ATRP polymerization procedure, 102
- Alkyne-terminal polymers
- monomer unit functionalization, 146, 148–150
- polymer-small molecule click reactions, 142–145
- synthesis, 142
- See also* Click functionalization of well-defined copolymers
- Allyl ester side groups
- cross-linking potential, 154–155
- See also* Pendant allyl ester groups on polymers
- Allyl methacrylate (AMA)
- atom transfer radical polymerization (ATRP) using bifunctional ATRP macroinitiators, 157*t*
- copolymerization of 80:20 styrene:AMA, 160*f*
- poly(phenylene oxide) (PPO) with AMA end groups, 166–168
- polymerization results, 158*t*
- proposed side reactions in ATRP, 159–160
- radical copolymerization, 154–155
- random copolymers, 158–161
- synthesis of poly(MMA-*co*-GMA-*co*-AMA), 156
- synthesis of poly(styrene-*co*-AMA), 156
- See also* Pendant allyl ester groups on polymers
- Amine ligands. *See* Alkylated linear amine ligands
- Amino acid-based polymers
- acrylamide *N*-acryloyl-L-phenylalanine (A-Phe-OH), 535
- acrylamide *N*-acryloyl-L-phenylalanine methyl ester (A-Phe-OMe), 535
- acrylamide *N*-acryloyl-L-proline methyl ester (A-Pro-OMe), 535
- benzyl 1-pyrrolocarbodithioate (CTA 1) and benzyl dithiobenzoate (CTA 2) for chain transfer agents, 535

- chemical structures of monomers, 534*f*
- controlled synthesis of polyacrylamides by reversible addition-fragmentation chain transfer (RAFT) polymerization, 534
- copolymerization of A-Pro-OMe with *N,N*-dimethylacrylamide (DMA), 542–544
- experimental, 535
- "intelligent" or "smart" materials, 534
- RAFT polymerization of A-Phe-OH, 538–539, 540*f*
- RAFT polymerization of A-Phe-OMe, 535–538
- RAFT polymerization of A-Pro-OMe, 540–544
- time conversion and pseudo-first-order kinetic plots for A-Phe-OMe, 537–538
- Aqueous media**
- atom transfer radical polymerization (ATRP) systems, 63–64
- organic reactions and polymerizations, 15
- Architectures**
- ability to control molecular, 40
- atom transfer radical polymerization (ATRP), 57
- prepolymers for crosslinking, 154
- reversible addition-fragmentation chain transfer (RAFT) polymerization, 446, 448–449
- use of alkoxyamines for building complex macromolecular, 337–339
- See also* Glycopolymers, methacrylate-type
- Arm-first star polymers**
- nodulus method, 584–586, 587*t*
- See also* Star-like polymers by macromolecular design via interchange of xanthates (MADIX)
- Associative thickener for latex paint, telechelic RAFT polymers as**, 551–553, 559
- Atom transfer radical addition (ATRA), modeling end groups by**, 112
- Atom transfer radical polymerization (ATRP)**
- acidic and coordinating monomers, 64–65
- activators generated by electron transfer (AGET), 6
- activators re-generated by electron transfer (ARGET), 6
- catalyst activity, 85–86
- catalysts activity in ring-opening metathesis, 41
- controlled/living radical polymerization, 27
- equilibrium and components, 57–59
- 1-ethoxyethyl acrylate (EEA) and 1-ethoxyethyl methacrylate (EEMA), 176–179
- evaluation of catalyst performance, 57–60
- exchange process, 5*f*
- functionalized multi-walled carbon nanotubes (MWNT), 280–284
- functionalized titanate nanotubes (TNT), 285–289
- MALDI-ToF mass spectrometry of poly(*N*-butyl acrylate)-*b*-GGFGG peptide, 202, 204
- measurement of equilibrium constants and rate constants, 59–60
- mechanisms for living character, 369–370
- methyl methacrylate (MMA) using different ligands, 106*t*
- MMA with magnetic nanoparticles supported catalyst, 76–77

- molecular architecture of polymers, 57, 72
- Mw and Tg of polyacrylates, 119*t*
- poly(EE(M)A) containing polymer structures by, 175*t*
- poly(*N*-butyl acrylate)-*b*-polypeptide, 200–204, 202, 203*f*
- proposed side reactions, 159
- range of monomers, 6
- recovery of chain transfer agents, 449
- SciFinder Scholar search, 3*f*
- sequence-defined macroinitiator, 200, 201
- simultaneous reverse and normal initiation (SR&NI), 6
- styrene using different ligands, 107*t*
- 4-vinylpyridine (4VP), 67
- See also* Acrylate-based block copolymers; Alkylated linear amine ligands; Batch supported atom transfer radical polymerization (ATRP); Catalyst activity; Click functionalization of well-defined copolymers; Conjugates of polymers and sequence-defined polypeptides; Continuous supported atom transfer radical polymerization (ATRP); Copper-based ATRP catalysts; Electron spin resonance (ESR) study of (meth)acrylate radicals; Glycopolymers, methacrylate-type; Magnetic nanoparticle supported catalyst; Pendant allyl ester groups on polymers
- Azide-terminal polymers**
- monomer unit functionalization, 146, 148–150
- polymer-polymer click reactions, 145–146
- polymer-small molecule click reactions, 142–145
- synthesis, 142
- See also* Click functionalization of well-defined copolymers
- 3-Azidopropyl methacrylate (AzPMA), atom transfer radical polymerization (ATRP), 148–150**
- B**
- Backbiting- β -scission mechanism, 519**
- Batch supported atom transfer radical polymerization (ATRP)**
- catalyst activity retention, 94–95
- catalyst recycling and regeneration, 87
- comparing catalysts in continuous and batch ATRP, 92
- copper losses with catalyst recycling in, 88
- effect of silica-gel loading, 93–94
- experimental, 87
- loss and regeneration of catalyst activity, 88–89
- mechanism, 95, 96*f*
- monomer conversion, polymer molecular weights and distributions for three, 90*f*
- split filter test, 92–93
- See also* Atom transfer radical polymerization (ATRP); Catalyst activity; Continuous supported atom transfer radical polymerization (ATRP)
- Bidentate ligands. *See* Inorganic-organic nanocomposites**
- Bioconjugates, controlled radical polymerization (CRP), 9**
- S,S'-Bis(methyl-2-propionate)-trithiocarbonate (BMPT)**
- change in concentration under pulsed-laser irradiation, 459
- chemical structure, 458*f*
- laser-induced butyl acrylate (BA) polymerization, 459–461

- reversible addition-fragmentation chain transfer (RAFT) agent, 457
- UV spectrum, 458*f*
- See also* Pulsed-laser initiated reversible addition-fragmentation chain transfer (RAFT) polymerization
- Bisphenol A (BPA) polycarbonate, allyl methacrylate (AMA) end groups, 163, 165–166
- Blends, compatibilization of polymer, 343
- Block copolymerization
- magnetic nanoparticle supported catalyst, 82
 - poly(ethylene glycol) (PEG) macroinitiator and PEG-*b*-PMMA, 81*f*
 - reverse iodine transfer polymerization (RITP) in emulsion, 614, 616*f*
- Block copolymers
- equations predicting proportions of AB and ABA, 429, 431
 - gel permeation chromatography (GPC) for, synthesis using nanoprecipitation emulsion, 323*f*
 - multiblock copolymers by difunctional reversible addition-fragmentation chain transfer (RAFT), 433, 436*f*
 - nanoprecipitation emulsion procedure, 317, 321–322
 - polycondensation processes, 161, 163
 - reversible addition-fragmentation chain transfer (RAFT) polymerization, 446, 448, 548–550
 - synthesis by nanoprecipitation emulsion polymerization, 322*t*
 - telechelic RAFT polyurethane-polyacrylate, 554–556, 560–561
- See also* Acrylate-based block copolymers; Nanoprecipitation emulsion polymerization; Nanostructured carbons; Polyacrylonitrile (PAN) block copolymers; Reactive block copolymers; Tailor-made copolymers
- Bond homolysis, C–O, in phosphonylated alkoxyamines, 330–331
- Borane-mediated control radical polymerization
- borane initiators, 392
 - chain end functionalized acrylic fluoropolymers, 392–397
 - chain end functionalized PVDF, 397–401
 - ¹³C NMR spectra of poly(trifluoroethyl acrylate) (PTFEA), 394*f*
 - coordination radical addition process, 397
 - experimental, 389–392
 - gel permeation chromatography (GPC) comparison of poly(methyl methacrylate) (PMMA) and PMMA-*b*-PTFEA, 395*f*
 - ¹H NMR spectra of PMMA and PMMA-*b*-PTFEA, 396*f*
 - ¹H NMR spectrum of poly(vinylidene fluoride) (PVDF)-*t*-Si(OC₂H₅)₃, 399*f*
 - interaction pattern between chain end fluoropolymer and clay interlayer surfaces, 399–400
 - preparation of PVDF/clay nanocomposite, 391–392
- PVDF polymers with terminal silane group, 398*t*
- synthesis of 8-boraindane initiator, 389–390

- synthesis of
 $[(C_2H_5O)_3SiCH_2CH_2]_3B$
 functional initiator, 390
 synthesis of poly(MMA-*b*-TFEA),
 391
 synthesis of PVDF polymers with
 terminal $(C_2H_5O)_3Si$ group, 391
 synthesis of telechelic
 poly(trifluoroethyl acrylate)
 with two terminal OH groups,
 390
 TFEA polymerization by 8-bora-
 indane/O₂, 393*t*
 X-ray diffraction study of PVDF-*t*-
 Si polymer, 400–401
 Branched architectures. *See*
 Glycopolymers, methacrylate-type
 1-Bromoethyl)benzene, initiator for
 styrene polymerization, 42*t*, 46*t*,
 48*t*, 51*t*
 1,4-Butanediol diglycidyl ether
 (BDGE)
 radical ring opening (RRO)
 initiation, 130, 132, 134
 See also Ti-catalyzed living radical
 polymerization (LRP)
 Butyl acrylate (BA)
 block copolymer synthesis, 237–
 238
 chain length dependence of
 termination rate coefficient, 491,
 492*f*, 494
 laser-induced BA polymerization,
 459–461
 M_n vs. conversion for
 nanoprecipitation emulsion
 polymerization, 322*f*
 paclitaxel release from block
 copolymers with, 241, 243,
 244*f*, 245*f*, 246*f*
 reversible addition-fragmentation
 chain transfer (RAFT)
 polymerization, 517–520
 telechelic polymers and ABA
 triblock copolymers, 446, 448
 See also Acrylate-based block
 copolymers; Nanoprecipitation
 emulsion polymerization;
 Pulsed-laser initiated reversible
 addition-fragmentation chain
 transfer (RAFT) polymerization;
 Reverse iodine transfer
 polymerization (RITP)
t-Butyl acrylate (tBA), electron spin
 resonance (ESR) study of radicals,
 114–120
 Butyl methacrylate (BMA)
 telechelic polymers and ABA
 triblock copolymers, 446, 448
 See also Pendant allyl ester groups
 on polymers
- C**
- Carbohydrate polymers. *See*
 Glycopolymers, methacrylate-type
 Carbon nanotubes. *See* Inorganic
 nanotubes
 Catalyst activity
 batch supported atom transfer
 radical polymerization (ATRP)
 with catalyst recycling and
 regeneration, 87
 continuous supported ATRP with
 catalyst regeneration, 87–88
 copper-based catalysts, 60–63
 copper losses with catalyst
 recycling in batch ATRPs, 88
 copper lost with supernatant
 solution as function of settling
 time and catalyst washes, 89*t*
 CuBr/1,1,4,7,10,10-
 hexamethyltriethylenetetramine
 (HMTETA) on silica gel, 86
 effect of silica gel loading, 93–94
 experimental, 86–88
 kinetic data for filtered solutions
 away from supported catalyst,
 93*t*

- loss and regeneration of, in batch supported ATRP, 88–89
- loss and regeneration of, in continuous ATRP, 89–92
- measured copper losses and, 94–95
- mechanism of ATRP using CuBr/HMTETA, 95, 96*f*
- monomer conversion, polymer molecular weights and distribution for three batch supported ATRPs, 90*f*
- monomer conversion, polymer molecular weights and distribution of continuous reactor product stream, 92*f*
- performance comparison of catalysts in continuous and batch reactors, 92
- recyclability, 95
- regeneration, 95
- solid supported catalysts, 85–86
- split filter test, 92–93
- Catalyst immobilization, efficiency for catalyst separation, 72–73
- Catalyst recycling
- batch supported atom transfer radical polymerization (ATRP), 87
 - catalyst removal, 20–21
 - copper losses with, in batch ATRPs, 88
 - magnetic nanoparticle supported catalyst, 79–80
- Catalyst regeneration
- batch supported atom transfer radical polymerization (ATRP), 87
 - continuous supported ATRP, 87–88
 - magnetic nanoparticle supported catalyst, 79–80
- Catalyst removal
- catalyst recycling, 20–21
 - phase transfer catalysis, 19–20
- Catalyst selection. *See* Copper-based ATRP catalysts
- Catalytic chain transfer (CCT), SciFinder Scholar search, 3*f*, 4
- Cellulose support, reversible addition-fragmentation chain transfer (RAFT) polymerization, 448–449
- Chain extension, polystyrene with styrene, 431, 432*f*
- Chain length dependent termination. *See* Reversible addition-fragmentation chain transfer chain length dependent termination (RAFT-CLD-T)
- Chain transfer
- effect of R group on stabilities and chain transfer enthalpies, 415*t*
 - efficiency, 410
 - See also* Reversible addition-fragmentation chain transfer (RAFT)
- Chain transfer agents (CTAs)
- cellulose supported reversible addition-fragmentation chain transfer (RAFT) polymerization, 448–449
 - copolymers via RAFT, 448*t*
 - 2-ethylsulfanylthiocarbonyl-sulfanylpropionic acid ethyl ester (ETSPE) synthesis, 440–441
 - experimental, 439–441
 - general polymerization and end-group modification method, 441
 - general synthesis method of trithiocarbonates/xanthates, 440–441
 - graft polymerization of styrene and dimethylaminoethyl methacrylate (DMAEMA) by cellulose CTA, 449*t*
 - microwave-assisted RAFT polymerization, 445–446, 447*f*
 - molecular weight and PDI evolution for methyl acrylate (MA) polymerization by ETSPE, 445*f*

- monomer conversion vs. time for MA polymerization by ETSPE, 444*f*
- production of trithiocarbonates and xanthates using 1,1'-thiocarbonyl diimidazole, 443*f*
- RAFT/MADIX polymerization, 439
- RAFT/MADIX polymerization process using Z, 444–446
- recovery, 449–451
- schematic of copolymerization process using Z-supported RAFT polymerization, 452*f*
- schematic of RAFT/MADIX polymerization and CTA recovery cycle, 451*f*
- synthesis of functional CTAs, 441–442
- synthesis of functional polymeric architectures, 446, 448–449
- synthesis of trithiocarbonates via one pot reaction, 443–444
- telechelic polymers and ABA triblock copolymers, 446, 448
- Chemical transformation of xanthate-functional terminal groups
- Chugaev reaction, 565, 566, 574–575
- ¹³C NMR spectra of xanthate-terminated poly(acrylic acid) (PAA-X₁) and PAA-H reduction product, 572*f*
- dethiocarboxylation reaction, 567–568
- dethiocarboxylation reactions on poly(dimethylsiloxane) (PDMS) bearing different xanthate terminal groups, 574*t*
- di-*t*-butylcyclohexyl percarbonate (DTBCP) as radical source, 570–571
- dithiocarboxylation, 572–576
- experimental, 566–568
- ¹H NMR spectra of xanthate-capped PDMS and copolymer after thermal elimination, 576*f*
- peroxide-induced radical reduction of MADIX polymers, 565–566
- preparation of secondary xanthate-terminated PDMS and subsequent thermally induced dethiocarboxylation, 573*f*
- preparation of xanthate-terminated PDMS and subsequent desulfuration, 569
- radical reduction, 568–572
- radical reduction reaction, 566–567
- SEC (size exclusion chromatography) traces of PAA-X₁ reacted with dilauryl peroxide (DLP), 570*f*
- SEC traces of PAA-X₁ reacted with DTBCP, 571*f*
- thermally induced elimination of xanthate terminal groups, 575–576
- See also* Macromolecular design via interchange of xanthates (MADIX)
- Chromatographic stationary phases
- application of controlled radical polymerization (CRP) methods, 253
- approaches to grafting, 255–257
- breakthrough traces, 261, 262*f*
- comparing column backpressure with increasing capacity, 263*f*
- comparing "grafting through" and "grafting from", 266
- experimental, 253–255
- grafting from 2-(*N,N*-dimethylamino)ethyl methacrylate (DMAEMA) and methacryloyloxyethyltrimethylammonium chloride (TMAEMA), 254
- "grafting from" approach, 258, 261–262

- "grafting through" approach, 264
 grafting through glycidyl methacrylate (GMA), 254–255
 illustration of grafted nonporous stationary phase design, 259f
 illustration of grafting approaches, 256f
 molecular weight and dispersity of pDMAEMA, 260f
 particle-particle crosslinking, 257
 pDMAEMA graft lengths, 260f
 polymerization kinetics for pDMAEMA from sacrificial initiator, 260f
 preparation of "grafted through" pGMA beads, 265f
 preparation of pDMAEMA grafted from substrate using sacrificial initiator, 259f
 relationship between column backpressure and resin capacity for pDMAEMA grafted resin, 261, 263f
 scanning electron microscopy (SEM) of nonporous polystyrene-divinylbenzene substrate, 259f
 separation of dsDNA on DNAPac PA100 and pTMAEMA prototype, 264f
 separation of ribonuclease, cytochrome c, and lysozyme, 266f
 separation of standard proteins, 265f
 TEM (transmission electron microscopy) images of cross-sections of beads embedded in resin, 258, 261f
 TEM of cross section of sample containing stained pDMAEMA, 262, 263f
- Chugaev reaction**
 dethiocarboxylation, 572–576
 fragmentation, 565
- macromolecular design via interchange of xanthates (MADIX) polymers, 574–576
 scheme, 566
See also Chemical transformation of xanthate-functional terminal groups
- Clay.** *See* Polymer-clay nanocomposites
- Click chemistry**
 end group functionalization, 142–146
 post-polymerization modification, 141
See also Click functionalization of well-defined copolymers
- Click functionalization of well-defined copolymers**
 atom transfer reaction
 polymerization (ATRP), 142
 conversion vs. time for reaction of propargyl alcohol (PgOH) with poly(3-azidopropyl methacrylate) (polyAzPMA), 150f
 end group functionalization, 142–146
 fraction of dihydroxy-, monohydroxy-, and nonhydroxy-PS as function of reaction time, 145f
 gradient polymer elution chromatography (GPEC), 143–144
 methods for ATRP synthesis of azide- and alkyne-terminal polymers, 142
 methods for introducing pendant azido or alkyne functionality, 148
 monomer unit functionalization, 146, 148–150
 polymer-polymer click reactions, 145–146

- polymer-small molecule click reactions, 142–145
- post-polymerization modification, 141
- strategy for end-functionalized polymers, 141
- synthesis of AzPMA and subsequent reaction, 148, 149
- synthesis of α -acetylene- ω -azido-terminated PS and diazido-terminated PS and subsequent coupling, 146, 147
- synthesis of difunctional PS via ATRP and subsequent reaction, 143
- terminal functionality capable of derivatization by click chemistry, 144–145
- Cobalt mediated radical polymerization (CMRP)
- block copolymerization of vinyl acetate (VAc) and styrene by, 374
- bulk polymerization of VAc in presence of $\text{Co}(\text{acac})_2$, 374–380
- bulk radical polymerization of VAc, 378*t*
- CMRP of VAc in aqueous media, 382–383, 384*t*
- concentration of initiator and cobalt complex, 377–379
- experimental, 373–374
- general procedure for bulk polymerization of VAc, 374
- ^1H NMR spectrum of P(VAc), 377*f*
- influence of temperature, 379–380
- macromolecular engineering based on, 380–382
- mechanism, 375–377
- plot of $\ln([M]_0/[M])$ vs. time for bulk radical polymerization of VAc, 379*f*
- size exclusion chromatography (SEC) for PVAc and PVAc macroinitiator, 382*f*
- suspension and miniemulsion, 383
- synthesis of end-functional PVAc and PVAc and PVOH containing block copolymers, 381
- synthesis of PVOH-*b*-PS copolymers, 374
- time dependence of UV-visible spectrum for controlled bulk polymerization of VAc, 376*f*
- Cobalt porphyrin derivatives
- acrylic acid (AA) by organo-cobalt porphyrin mediated polymerization, 365*f*
- applications of cobalt(II) metallo-radical mediated living radical polymerization (LRP), 359
- characteristics of organo-cobalt/azo radical LRP, 370
- cobalt complexes of tetra mesityl porphyrin (TMP) and tetra anisyl porphyrin (TAP), 359, 360
- comparing polymerization rates in presence and absence of organo-cobalt porphyrin mediator, 368–369
- first order rate plots for methyl acrylate (MA) polymerization, 362*f*
- living radical polymerization of acrylates, 359
- LRP of acrylates mediated by (TMP)Co-R, 360–363
- LRP of acrylic acid in water by cobalt(II) and organo-cobalt porphyrins, 363–364
- LRP of vinyl acetate, 364, 366*f*
- MA polymerization, 360–363
- mechanisms for living character in radical polymerization, 369–370
- Mn changes with conversion of MA to PMA, 368*f*

- porphyrin ^1H NMR spectra of organo-cobalt complex during induction period, 363*f*
- prototype transition metal mediators for LRP, 359, 360
- radical interchange mechanisms, 367
- stable free radical polymerization (SFRP), 359
- steric demands, 367–368
- studies of organo-cobalt mediated LRP, 364, 367–369
- unimolecular homolytic dissociation, 367
- C–O bond homolysis, phosphonylated alkoxyamines, 330–331
- Compatibilizers
- block copolymers as, 343–344
 - design, 344
 - polymer blends, 343
 - See also* Reactive block copolymers
- Complexation agents, controlled radical polymerization (CRP), 7
- Composites. *See* Polymer-clay nanocomposites
- Conditional stability constant, dependence on pH, 64–65
- Conjugated monomers, status quo of living and stereospecific radical polymerization, 36*t*
- Conjugates of polymers and sequence-defined polypeptides
- atom transfer radical polymerization (ATRP), 200–204
 - circular dichroism (CD) spectrum of oligopeptide transfer agent and oligopeptide-poly(*N*-butyl acrylate) conjugate, 210*f*
 - ^1H NMR spectrum of oligopeptide-poly(*N*-butyl acrylate) conjugate, 210*f*
 - MALDI-ToF mass spectrometry of poly(*N*-butyl acrylate)-*b*-GGFGG peptide, 202, 204
 - poly(*N*-butyl acrylate)-*b*-polypeptide, 202, 203*f*
 - RAFT (reversible addition-fragmentation transfer) radical polymerization, 205–208
 - RAFT polymerization of nBA and first-order kinetic plot vs. reaction time, 209*f*
 - solid-phase supported synthesis (SPPS), 201
 - SPPS approaches to RAFT agents, 205, 206
 - synthesis of peptide macrotransfer agents, 205–207
 - synthetic approaches, 199–200
- Continuous supported atom transfer radical polymerization (ATRP)
- catalyst activity retention, 94–95
 - catalyst performance comparison in continuous and batch, 92
 - catalyst regeneration, 87–88
 - experimental, 87–88
 - loss and regeneration of catalyst activity, 89–92
 - mechanism, 95, 96*f*
 - monomer conversion, polymer molecular weight and molecular weight distribution of continuous reactor product stream, 92*f*
 - See also* Atom transfer radical polymerization (ATRP); Batch supported atom transfer radical polymerization (ATRP); Catalyst activity
- Controlled radical polymerization (CRP)
- acrylic acid containing polymers, 172
 - approach to steady state, 4
 - aqueous media, 15
 - compatibilizers design, 344

- complexation agents, 7
 cost-performance balance, 8
 developing area, 3
 1-ethoxyethyl (meth)acrylate, 173*f*
 exchange between active and dormant radicals, 5
 exchange process, 5–6
 formation of dynamic equilibrium, 4
 hybrids and bioconjugates, 9
 imperfections, 8
 Lewis acids, 7
 macromolecular design via interchange of xanthates (MADIX), 27, 565
 mechanisms, 8
 olefins and non-conjugated vinyl monomers, 7–8
 outlook, 7–9
 persistent radical effect (PRE), 5–6
 SciFinder Scholar search, 3–4
 status quo of monomers, 36*t*
 structure-property relationship, 8
 structure-reactivity correlation, 8
 well-defined block copolymers, 296
See also Borane-mediated control radical polymerization; 1-Ethoxyethyl (meth)acrylate (EE(M)A)
- Coordinating monomers, atom transfer radical polymerization (ATRP) systems, 64–65
- Copolymerizations
 reversible addition-fragmentation chain transfer (RAFT), 522
See also Polymer-clay nanocomposites; Reversible addition-fragmentation chain transfer (RAFT) copolymerizations
- Copolymers
N-acryloyl-L-proline methyl ester and *N,N*-dimethylacrylamide (DMA), 542–544
 microstructuring of polymer films by photolithography, 168–169
See also Tailor-made copolymers
- Copper(II) bromide, improving initiator efficiency, 77, 79
- Copper-based atom transfer radical polymerization (ATRP) catalysts
 acidic and coordinating monomers, 64–65
 aqueous ATRP systems, 63–64
 atom transfer representation, 58*f*
 ATRP of 4-vinylpyridine (4VP), 67
 ATRP equilibrium and its components, 57–59
 catalyst activity, 60–63
 deactivation rate constant and stability of polymeric dormant state, 66–67
 dependence of conditional stability constant of, on pH of medium, 65*f*
 disproportionation of catalyst, 63–64
 evaluating catalyst performance, 57–60
 halogenophilicity of Cu^{II}Ln complex, 66
 ligand selection, 60–65
 map for selection of, in aqueous media, 64*f*
 measurement of ATRP equilibrium constants and rate constants, 59–60
 nitrogen-containing ligands forming, 61*f*
 role of halide ligand, 66–67
 structural features and redox potentials of ligands of, 62*f*
- Core-first approach
 three-arm star polymers, 580–582
See also Star-like polymers by macromolecular design via interchange of xanthates (MADIX)

- Cost-performance balance, controlled radical polymerization (CRP), 8
- Crosslinked polyacrylic acid thickener, telechelic RAFT polymers as, 556–557, 561–562
- Crosslinking
particle-particle, of stationary phase preparation, 257, 259*f*
See also Star-like polymers by macromolecular design via interchange of xanthates (MADIX)
- Cross-linking materials
microstructuring of polymer films by photolithography, 168–169
photochemical, of end-group modified TMC bisphenol polycarbonate (PC), 166
prepolymer concept, 154
See also Pendant allyl ester groups on polymers
- Cyclic voltammetry
Grubbs complexes, 53*t*
phosphines vs. *N*-heterocyclic carbene ligands in atom transfer radical polymerization (ATRP), 52–54
ruthenium complexes, 52*t*
vs. ATRP, 52–53
- D**
- Deactivation rate constant, copper-based catalyst, 66–67
- Degenerative transfer (DT)
exchange process, 5*f*
RAFT and MADIX processes, 6–7, 439
SciFinder Scholar search, 3*f*, 4
See also Chain transfer agents (CTAs)
- Density functional theory, addition-fragmentation process, 408–409
- Deoxyribonucleic acid (DNA) nucleobases. *See* Styrene derivatives bearing nucleobases
- Deprotection
glycocylindrical brushes, 227–229
linear and branched glycopolymers, 222–223
poly(1-ethoxyethyl (meth)acrylate) to poly((meth)acrylic acid) (P(M)AA), 173*f*, 179–180
- Dethiocarboxylation
xanthate-terminated
poly(dimethylsiloxane) (PDMS), 567–568, 572–576
See also Chemical transformation of xanthate-functional terminal groups
- Difunctional reversible addition-fragmentation chain transfer (RAFT)
chain extension of polystyrene after 120 h with styrene, 431, 432*f*
comprehensive kinetic model, 422–423
effect of increasing initiator concentrations on molar concentrations for styrene, 427, 428*f*
effect of increasing initiator concentrations on molar concentrations of methyl acrylate (MA) polymerization, 435*f*
effect of increasing initiator concentrations on molecular weight distribution (MWD) of MA, 434*f*
effect of initiator concentration on reaction rate and MWD of styrene, 427*f*
evolution of MWD by conversion for reaction of styrene, 427, 429, 430*f*

- homopolymerizations of styrene and MA in kinetic simulations, 423, 426
- kinetic modeling, 423
- kinetic modeling of MA, 431, 433
- kinetic modeling of styrene, 426–431
- kinetic parameters modeling, styrene and MA, 423*t*
- mechanism of, polymerization, 424, 425
- multiblock copolymers, 433, 436*f*
- predicting proportions of diblock AB and triblock ABA copolymers, 429, 431
- See also* Reversible addition-fragmentation chain transfer (RAFT)
- N,N*-Dimethylacrylamide (DMA)
- copolymerization of *N*-acryloyl-L-proline methyl ester (A-Pro-OMe), 542–544
- iron-catalyzed polymerization, 30–31
- 2-(*N,N*-Dimethylamino)ethyl methacrylate (DMAEMA)
- "grafting from" approach, 254, 259*f*, 261–262
- graft polymerization of, and dimethylaminoethyl methacrylate (DMAEMA) by cellulose chain transfer agent, 449*t*
- See also* Chromatographic stationary phases; Tailor-made copolymers
- Dispersants
- gradient copolymers, 524, 525*t*
- See* Polymer-clay nanocomposites
- Disproportionation of catalyst, atom transfer radical polymerization (ATRP) systems, 63–64
- Dithiocarbamates, reversible addition-fragmentation chain transfer (RAFT) agents, 547–548
- Dodecyl acrylate (DA), chain length dependence of termination rate coefficient, 491, 493*f*
- Dodecyl methacrylate (DMA)
- copolymerization with 1-(4-vinylbenzyl)thymine (VBT) or 9-(4-vinylbenzyl)adenine (VBA), 190–193
- molecular structure, 190*f*
- optical micrographs of P(VBT-*co*-DMA) solution at room temperature, 192*f*
- preparation of copolymers by atom transfer radical polymerization (ATRP), 194*t*
- preparation of copolymers by free radical copolymerization, 191*t*
- See also* Styrene derivatives bearing nucleobases
- Drop casting, thin films of poly(butyl acrylate)-*b*-polyacrylonitrile (PBA-*b*-PAN), 306, 307*f*
- Drug delivery. *See* Acrylate-based block copolymers
- Dynamic equilibrium, formation in controlled radical polymerization methods, 4
- ## E
- Electron spin resonance (ESR) study of (meth)acrylate radicals
- t*-butyl acrylate (tBA), 114–120
- chain length dependent change of angle between C β -H and π -orbital, 121*f*
- chain lengths of propagating methacrylate radicals, 113
- energy diagram of rotation around C α -C β bond of propagating radical of methacrylate, 121*f*
- ESR spectra for pentameric model radical and polymerization of tBA, 118*f*

- ESR spectra of tetrameric model radical, 116*f*
- ESR spectra of trimeric model radical, 115*f*
- experimental, 122–123
- gel permeation chromatography (GPC) elution diagram of purified dimer, trimer, and tetramer of tBA, 114*f*
- generation of propagating radicals and oligomeric model radicals, 112
- 1,5-hydrogen shift of propagating radical of tBA, 117*f*
- methyl methacrylate (MMA), 120–122
- mid-chain radical formation, 113
- Mw and Tg for polytBA by ATRP and thermal radical polymerization, 119*t*
- observed ESR spectrum of propagating radical of MMA in radical polymerizations, 120*f*
- propagating radicals, 112
- Emulsion polymerization**
- block copolymerization, 614, 616*f*
- kinetics of reverse iodine transfer polymerization (RITP) in emulsion, 613–614, 615*f*
- reverse iodine transfer polymerization in emulsion, 607–608
- See also* Reverse iodine transfer polymerization (RITP)
- Emulsion polymer, telechelic reversible addition-fragmentation chain transfer (RAFT) polymers as,** 553–554, 559–560
- Emulsion polymerization**
- chain growth rate, 314
- living radical, 313–314
- micelles as particle precursors, 314–315
- miniemulsion systems, 313
- seeded, 314
- two-step process using alkoxyamine unimer, 315
- water soluble alkoxyamine as initiating species, 315
- See also* Nanoprecipitation emulsion polymerization
- End-functionalized polymers**
- click chemistry, 141
- functionalization of end groups, 142–146
- polymer–polymer click reactions, 145–146
- polymer–small molecule click reactions, 142–145
- See also* Click functionalization of well-defined copolymers
- Epoxide radical ring opening (RRO)**
- Ti-catalyzed living radical polymerization of styrene, 129–130
- See also* Ti-catalyzed living radical polymerization (LRP)
- Epoxy resins, telechelic RAFT polymers as tougheners,** 550–551, 559
- Equilibrium**
- atom transfer radical polymerization (ATRP), 57–59
- measurement of ATRP, constants and rate constants, 59–60
- 1-Ethoxyethyl (meth)acrylate (EE(M)A)**
- atom transfer radical polymerization (ATRP) of EE(M)A, 176–179
- average molar mass and polydispersity index (PDI) vs. conversion, 177*f*
- conditions and results for synthesis of PEE(M)A containing polymer structures, 175*t*
- controlled radical polymerization to PEE(M)A, 173*f*
- copolymerization, 182–183

- deprotection of PEE(M)A to poly((meth)acrylic acid) (P(M)AA), 173*f*, 179–180
- experimental, 173–174
- first order kinetic plot of block copolymerization of EEA, 177*f*
- ¹H NMR confirming deprotection, 179, 180*f*
- homopolymerization, 181–182
- instrumentation, 174
- macroinitiator strategy, 176–178
- Mn and PDI vs. reaction time for RAFT of EEA, 181*f*
- Mn increase with increasing EEA units, 182*f*
- monomer synthesis, 173, 176
- polymerization procedures, 174
- protecting group for (meth)acrylic acid, 172
- reversible addition-fragmentation transfer (RAFT) of EEA, 180–183
- SEC traces of block copolymerizations of EEA and *n*-butyl acrylate (nBA) or *t*-butyl acrylate (tBA), 178*f*
- SEC traces of final PMMA-PAA block copolymers, 182*f*
- SEC traces of PMMA-PEEA block copolymers, 182*f*
- sequential monomer addition, 178–179
- size exclusion chromatography (SEC) method, 174
- synthesis of EE(M)A, 173*f*
- thermogravimetric analysis (TGA) of PEEMA, 179*f*
- thermogravimetric analysis of PTHF macroinitiator and PTHF-PEEA block copolymer, 180*f*
- used reagents for RAFT (co)polymerization of EEA, 181*f*
- 2-Ethylsulfanylthiocarbonylsulfanylpropionic acid ethyl ester (ETSPE) methyl acrylate (MA) polymerization by, 444*f*, 445*f*
- synthesis, 440–441
- See also* Chain transfer agents (CTAs)
- Exchange process, controlled radical polymerization (CRP) methods, 5–6
- Exfoliants. *See* Polymer-clay nanocomposites
- ## F
- Fluoroalcohols
- iodine-transfer radical polymerization for vinyl acetate, 32–33
- N*-vinylpyrrolidone polymerization by RAFT/MADIX, 34–36
- ruthenium-catalyzed systems for methyl methacrylate, 28–30
- Fluoropolymers
- advantage of terminal functional groups, 399–400
- applications, 388
- borane initiators for polymerization, 388–389, 392
- chain end functionalized acrylic, 392–397
- chain end functionalized poly(vinylidene fluoride) (PVDF), 397–401
- ¹³C NMR spectra of poly(trifluoroethyl acrylate) (PTFEA), 394*f*
- gel permeation chromatography (GPC) of poly(methyl methacrylate) (PMMA) and PMMA-*b*-PTFEA, 395*f*
- ¹H NMR spectra of PMMA and PMMA-*b*-PTFEA, 396*f*
- interaction between chain end, and clay interlayer surfaces, 399–400

- preparation of PVDF/clay composite, 391–392
 properties, 388
 PVDF polymers with terminal silane group, 398*t*
 synthesis of P(MMA-*b*-TFEA) block copolymer, 391
 synthesis of PVDF with terminal (C₂H₅O)₃Si group, 391
 synthesis of telechelic PTFEA with terminal OH groups, 390
 TFEA polymerization by 8-boraindane/O₂, 393*t*
 X-ray diffraction of PVDF-*t*-Si polymer, 400–401
See also Borane-mediated control radical polymerization
- Fragmentation.** *See* Addition-fragmentation process; Reversible addition-fragmentation chain transfer (RAFT)
- Free radical polymerization**
N-vinyl pyrrolidone (NVP) in fluoroalcohols, 35*t*
 Free radicals. *See* Electron spin resonance (ESR) study of (meth)acrylate radicals
- Functionalization.** *See* Borane-mediated control radical polymerization; Click functionalization of well-defined copolymers; Fluoropolymers
- G**
- Germanium iodides**
 reversible activation catalyzed by Ge and Sn, 597
 styrene polymerization with 1-phenylethyl iodide (PE-I) in presence of, 598*t*
See also Living radical polymerization (LRP)
- Glycidyl methacrylate (GMA)**
 "grafting through" approach, 254–255, 266
See also Chromatographic stationary phases
- Glycocylindrical brushes**
 cryogenic transmission electron microscopy (cryo-TEM), 217, 232*f*
 deprotection of, 227–229
 solvolysis, 224, 227
 synthesis, 223–224, 225
 visualization by SFM and cryo-TEM, 227, 228*f*
See also Glycopolymers, methacrylate-type
- Glycopolymers, methacrylate-type applications, 215**
 ATRP of 3-*O*-methacryloyl-1,2:5,6-di-*O*-isopropylidene- α -D-glycofuranose (MAIGlc), 215, 218
 2-(2-bromoisobutyryloxy)ethyl methacrylate (BIEM) comonomer with MAIGlc, 218, 219*t*
 characterization methods, 216–217
 characterization of cleaved side chains of PMAIGlc brushes, 227*t*
 cryogenic transmission electron microscopy (cryo-TEM) image of deprotected brush, 232*f*
 cryo-TEM method, 217
 cylindrical brushes visualization, 227, 228*f*
 deprotection of glycocylindrical brushes, 227–229
 deprotection of linear and branched poly(MAIGlc)s, 222–223
 deprotection process, 216
 experimental, 215–217
 gel permeation chromatography (GPC) of linear poly(MAIGlc)s, 219*f*

general polymerization procedure, 216

general route to branched glycopolymers via self-condensing vinyl copolymerization (SCVCP) and deprotection, 220

GPC traces of PBIEM and glycocylindrical brush, 226*f*

¹H NMR spectra of linear and branched polymers after deprotection, 223*f*

¹H NMR spectra of linear poly(MAIGlc), cylindrical brush, and polyinitiator PBIEM, 226*f*

linear and branched glycomethacrylates, 218, 221–222

Mark–Houwink plots and contraction factors for polymers by SCVCP of BIEM and MAIGlc, 218, 221*f*

methodologies for synthesis, 215

scanning force microscopy (SFM) of cylindrical brush, 228*f*

SCVCP of BIEM and MAIGlc at different comonomer ratios, 219*t*

SFM of deprotected cylindrical brush, 230*f*, 231*f*

solvolysis method, 216

solvolysis of glycocylindrical brushes, 224, 227

synthesis and characterization of glycocylindrical brushes via ATRP, 225*t*

synthesis of glycocylindrical brushes, 223–224

synthesis route to glycocylindrical brushes, 225

Gradient copolymers, dispersants, 524, 525*t*

Gradient polymer elution chromatography (GPEC),

dibromo-, diazido-, and dihydroxy-terminated polystyrene, 143–144

Grafting approaches. *See* Chromatographic stationary phases

Grubbs ruthenium-carbene complex, olefin metathesis, 41–42

H

Halide ligand

deactivation rate constant, 66–67

halogenophilicity, 66

role of, 66–67

stability of polymeric dormant state, 66–67

Halogenophilicity, copper-based catalyst, 66

N-Heterocyclic carbenes (NHC). *See* Ruthenium *N*-heterocyclic carbene (NHC) complexes

Homogeneous atom transfer radical polymerization (ATRP). *See* Alkylated linear amine ligands

Hybrids, controlled radical polymerization (CRP), 9

1,5-Hydrogen shift

mechanism of chain transfer reaction, 118–119

propagating radical of *t*-butyl acrylate, 117*f*

transfer reaction mechanism, 113

I

Immobilization of catalysts, efficiency for catalyst separation, 72–73

Imperfections, controlled radical polymerization (CRP), 8

Initiation rate, achieving steady state, 4

Initiator effect, Ti-catalyzed styrene polymerizations, 132*f*, 133*f*

Initiator efficiency, Cu(II)Br₂ for improving, 77, 79

Inorganic nanotubes

amounts of poly(methyl methacrylate) (PMMA) and polystyrene (PS) covalently attached to titanate nanotubes (TNTs), 287*f*, 288

developing research area, 279–280

experimental, 289

Fourier transform infrared (FTIR) of TNT, TNT-NH₂, TNT-Br, and TNT-PMMA, 286*f*

FTIR confirming chemical structures of TNT-PMMA and TNT-PS, 288

functionalized multi-walled carbon nanotubes (MWNTs) via atom transfer radical polymerization (ATRP), 280–284

functionalized titanate nanotubes (TNTs) via ATRP, 285–289

general strategy for grafting

polymers from TNT via ATRP, 285

general strategy of grafting from MWNTs, 280, 281

¹H NMR of PMMA and MWNT-PMMA samples, 281, 283*f*

initiator-functionalized TNTs, 286

photo of samples in solvents, 282*f*

reaction conditions, 281*t*

size and distribution of TNTs

before and after modification, 288–289

TEM (transmission electron microscopy) images of crude MWNT, 282*f*

TEM images of crude TNT, TNT-PMMA, and TNT-PS, 290*f*, 291*f*

TEM images of modified MWNT samples, 283*f*

TGA (thermogravimetric analysis)

curves of crude and functionalized MWNT, 284

TGA of crude TNT, TNT-NH₂, TNT-Br, TNT-PMMA, and TNT-PS, 286, 287*f*

X-ray photoelectron spectra (XPS) of Ti 2p and Br 3d of TNT and TNT-Br, 286, 287*f*

Inorganic-organic nanocomposites

acetoacetoxy derivatives

connecting metal alkoxides to (meth)acrylates, 273

advantage of radical polymerization, 270

atom transfer radical polymerization (ATRP), 271

bidentate ligands functionalizing metal alkoxides, 271, 273

coordination via alkoxide exchange, 271, 273

copolymers of 2-(methacryloyloxy)ethyl acetoacetate (HAAEMA) and methyl methacrylate (MMA), 273–274

β-diketones ligands in coordination chemistry, 271, 273

Fourier transform infrared (FTIR) spectrum, 276*f*, 277

incorporation of inorganic building blocks into polymers, 270–271

polymerization of metal-containing monomers, 274, 276*f*, 277

size exclusion chromatography (SEC) of poly(HAAEMA-co-MMA), 274*f*, 276*t*

well-defined molecular inorganic building blocks for, 272*f*

Intercalants. *See* Polymer-clay nanocomposites

Iodine-transfer radical polymerization features of reverse iodine transfer polymerization (RITP) in emulsion, 617–618

hydrolytic disproportionation of iodine and related reactions, 617

- vinyl acetate in fluoroalcohols, 32–33
See also Reverse iodine transfer polymerization (RITP)
 Iron-catalyzed systems, metal triflates for acrylamides, 30–32
 Isobornyl acrylate (IBA)
 block copolymer synthesis, 237–238
See also Acrylate-based block copolymers
 Isodesmic reactions, reversible addition-fragmentation chain transfer (RAFT), 410

K

- Kinetic models. *See* Difunctional reversible addition-fragmentation chain transfer (RAFT)
 Kinetics
 atom transfer radical polymerization (ATRP) of methyl methacrylate (MMA) and styrene using 1,1,4,7,7-pentaethyldiethylene triamine (PEDETA) as ligand, 103, 105*f*
 batch supported ATRP of MMA varying silica gel loading, 93–94
 polymerization of styrene using Ge and Sn iodides, 600–602
 reverse iodine transfer polymerization (RITP) in emulsion, 613–614, 615*f*

L

- Latex paint, telechelic RAFT polymers as associative thickener for, 551–553, 559
 Lauryl acrylate (LA)
 block copolymer synthesis, 237–238

- See also* Acrylate-based block copolymers
 Lewis acid-mediated polymerization
 iron-catalyzed living radical polymerization, 30
 stereospecific, 27
 Lewis acids, controlled radical polymerization (CRP), 7
 Ligand effects, Ti-catalyzed styrene polymerizations, 132*f*, 133*f*, 134, 135*f*
 Ligands. *See* Alkylated linear amine ligands; Ti-catalyzed living radical polymerization (LRP)
 Ligand selection
 acidic and coordinating monomers, 64–65
 catalyst activity, 60–63
 disproportionation of catalyst, 63–64
 map for catalyst selection, 64*f*
 nitrogen-containing ligands for Cu-based ATRP catalysts, 61*f*
 redox potentials of copper complexes, 62*f*
 role of halide ligand, 66–67
 structural features of copper complexes, 62*f*
 Living radical polymerization (LRP)
 acrylic acid in water by cobalt(II) and organo-cobalt porphyrins, 363–364
 aqueous media, 15
 characteristics of organo-cobalt/azo radical LRP, 370
 controlling molecular weight and polydispersity, 126
 experimental for styrene, 597
 gel permeation chromatography (GPC) method, 597
 kinetics of Ge and Sn iodides for LRP of styrene, 600–602
 mechanisms for living character, 369–370
 metal-catalyzed, 15

- molecular weight and molecular weight distributions, 598–600
 preparation of polystyrene iodide (PSt-I), 597
 prototype transmission metal mediators for, 359, 360
 reversible activation catalyzed by Ge and Sn, 597
 reversible activation processes, 596
 SciFinder Scholar search, 3*f*
 status quo of monomers, 36*t*
 studies of organo-cobalt mediated, 364, 367–369
 styrene polymerization procedure, 597
 thermosensitive Ru(II) catalyst, 16
See also Cobalt porphyrin derivatives; Nanoprecipitation emulsion polymerization; Reverse iodine transfer polymerization (RITP); Stereospecific living radical polymerization; Thermosensitive Ru(II) complexes; Ti-catalyzed living radical polymerization (LRP)
- Long-range order, nanostructured carbons, 305–308
- M**
- Macromolecular architectures, use of alkoxyamines for building complex, 337–339
- Macromolecular design via interchange of xanthates (MADIX) controlled/living radical polymerization, 27, 565
 degenerative transfer process, 6–7, 439
- N*-vinylpyrrolidone (NVP) polymerization in fluoroalcohols, 34–36
- peroxide-induced radical reduction of MADIX polymers, 565–566
 polymerization process, 444–446
 recovery of chain transfer agents, 449–451
 transfer events in MADIX process, 579
See also Chain transfer agents (CTAs); Chemical transformation of xanthate-functional terminal groups; Star-like polymers by macromolecular design via interchange of xanthates (MADIX); Xanthates
- Macromolecular engineering, cobalt-mediated radical polymerization, 380–382
- Magnetic nanoparticle supported catalyst
 atom transfer radical polymerization (ATRP), 72
 ATRP of methyl methacrylate (MMA), 76–77
 block copolymerization, 82
 catalyst immobilization on solids, 72–73
 catalyst recycling and regeneration, 79–80
 characterization methods, 75–76
 experimental, 73–76
 gel permeation chromatography (GPC) of poly(ethylene glycol) (PEG)-*b*-PMMA and PEG macroinitiator (ini-PEG), 81*f*
 grafting *N,N,N'',N'''*-tetraethyldiethylenetriamine (TEDETA) ligand onto Fe₃O₄ magnetic nanoparticles (MNP-tEDETA), 73–74, 76
 improving initiator efficiency, 77–79
 MMA polymerization by fresh, recycled, and regenerated, 80*f*

- PMMA molecular weight and polydispersity as function of conversion using fresh, re-used and regenerated catalysts, 81*f*
- PMMA molecular weights and distribution as function of MMA conversion, 78*f*
- polymerization of CuBr/MNP-TEDETA catalyst, 74–75
- preparation of ini-PEG, 74
- recycle of CuBr/MNP-TEDETA catalyst, 75
- regeneration of CuBr/MNP-TEDETA catalyst, 75
- Maleic anhydride (MAh). *See* Reversible addition-fragmentation chain transfer (RAFT) copolymerizations
- Mechanisms
- backbiting- β -scission of reversible addition-fragmentation chain transfer (RAFT), 519
 - controlled radical polymerization (CRP), 8
 - difunctional RAFT polymerization, 424, 425
 - 1,5-hydrogen shift transfer reaction, 113
 - living character in radical polymerization, 369–370
 - reverse iodine transfer polymerization (RITP), 605–606
 - stabilization by nanoparticulate fillers, 529
 - Ti-catalyzed living radical polymerization of styrene, 129
- Metal alkoxides. *See* Inorganic-organic nanocomposites
- Metal-catalyzed living radical polymerization, controlled/living radical polymerization, 27
- Metal-catalyzed polymerization, living radical, 15
- Metal triflates, iron-catalyzed systems with, for acrylamides, 30–32
- Metathesis, styrene undergoing, and radical polymerization, 47–48
- (Meth)acrylate radicals. *See* Electron spin resonance (ESR) study of (meth)acrylate radicals
- Methacrylate-type glycopolymers. *See* Glycopolymers, methacrylate-type
- 3-*O*-Methacryloyl-1,2:5,6-di-*O*-isopropylidene- α -D-glucopyranose (MAIGlc)
- deprotection of linear and branched poly(MAIGlc)s, 222–223
 - gel permeation chromatography of linear poly(MAIGlc), 219*f*
 - linear and branched glycomethacrylates, 218, 221–222
 - synthesis of glycocylindrical brushes, 223–224
 - See also* Glycopolymers, methacrylate-type
- Methacryloyloxyethyltrimethylammonium chloride (TMAEMA)
- "grafting from" approach, 254, 262
 - See also* Chromatographic stationary phases
- Methyl acrylate (MA)
- chain length dependence of termination rate coefficient, 491, 492*f*, 494
 - change in Mn and polydispersity with conversion to PMA, 361*f*
 - changes in Mn with conversion of MA to PMA, 368*f*
 - cobalt(II) metallo-radical mediated and organo-cobalt mediated processes, 360–363
 - first order rate plots of MA polymerization, 362*f*
 - kinetic modeling, 431, 433
 - kinetic parameters modeling difunctional reversible addition-fragmentation chain transfer (RAFT) polymerization, 423*t*

- kinetic simulations for
 homopolymerization, 423, 426
- microwave-assisted
 polymerization, 445–446, 447*f*
- monomer conversion vs. time in
 radical polymerization, 361*f*,
 369*f*
- organo-cobalt mediated living
 radical polymerization (LRP),
 364, 367–369
- polymerization mediated by 2-
 ethylsulfanylthiocarbonylsulfan-
 ylpropionic acid ethyl ester
 (ETSPE), 444*f*, 445*f*
- porphyrin ¹H NMR spectra of
 organo-cobalt complex during
 induction for LRP, 363*f*
- simulations of effect of increasing
 initiator concentrations on molar
 concentration of polymeric
 species, 435*f*
- simulations of effect of increasing
 initiator concentrations on
 MWD, 434*f*
- See also* Cobalt porphyrin
 derivatives
- Methyl methacrylate (MMA)**
- atom transfer radical
 polymerization (ATRP) using
 different amine ligands, 106*t*
- ATRP with magnetic nanoparticles,
 76–77
- batch ATRP varying silica gel
 loading, 93–94
- block copolymer synthesis, 237–
 238
- chain length dependence of
 termination rate coefficient, 491,
 493*f*
- chain length dependent change of
 angle between C β -H and π -
 orbital, 121*f*
- effects of silica-gel loading on
 kinetics of batch supported
 ATRP of, 94*f*
- electron spin resonance (ESR)
 study of propagating radicals,
 120–122
- energy diagram of rotation around
 C α -C β bond of propagating
 radical of methacrylate, 121*f*
- ethyl 2-bromo-2-methylpropionate
 initiation and ruthenium
 complex catalysis, 41*t*, 45*t*, 48*t*,
 50*t*
- kinetic plots of ATRP of, and
 styrene using 1,1,4,7,7-
 pentaethyldiethylene triamine
 (PEDETA) as ligand, 105*f*
- microwave-assisted
 polymerization, 445–446, 447*f*
- Mn vs. conversion plots of MMA
 and styrene polymerization
 using PEDETA as ligand, 105*f*
- polymerization by magnetic
 nanoparticles supported catalyst
 and CuBr₂, 78*f*
- polymerization protocol using
 ruthenium complexes, 42
- polymerization with
 Ru(Cp*)Cl(PEG-phosphine) in
 toluene, 17
- reversible addition-fragmentation
 chain transfer (RAFT), 415–416
- ruthenium-catalyzed systems in
 fluoroalcohols, 28–30
- suspension polymerization with
 Ru(II) catalyst in water, 18–19
- synthesis of poly(MMA-*co*-BMA-
co-AMA), 156
- See also* Acrylate-based block
 copolymers; Magnetic
 nanoparticle supported catalyst;
 Pendant allyl ester groups on
 polymers; Poly(methyl
 methacrylate) (PMMA);
 Reactive block copolymers;
 Ruthenium *N*-heterocyclic
 carbene (NHC) complexes;
 Tailor-made copolymers

- Microgels, macromolecular design via interchange of xanthates (MADIX) radical crosslinking copolymerizations, 586, 588–589**
- Microstructuring**
 photolithography of polymer films, 168–169
 procedure, 156
See also Pendant allyl ester groups on polymers
- Microwave-assisted polymerization, reversible addition-fragmentation chain transfer (RAFT), 445–446, 447f**
- Miniemulsion systems, living radical polymerization, 313**
- Modeling. *See* Difunctional reversible addition-fragmentation chain transfer (RAFT)**
- Molecular architecture**
 ability to control, 40
 atom transfer radical polymerization (ATRP), 57, 72
- Molecular sugar sticks. *See* Glycopolymers, methacrylate-type; Sugar sticks**
- Molecular weight distribution (MWD) evolution of, as function of conversion for reversible addition-fragmentation chain transfer (RAFT) polymerization, 517–518**
 living radical polymerization of styrene, 598–600
 poly(butyl acrylate) by reverse iodine transfer polymerization, 610f, 611f, 612f
See also Difunctional reversible addition-fragmentation chain transfer (RAFT)
- Molecular weights**
 living radical polymerization of styrene, 598–600
 simultaneous control of, and stereochemistry, 26–28
- Monomers, status quo of living and stereospecific radical polymerization, 36t**
- Multi-walled carbon nanotubes (MWNT)**
 functionalization by atom transfer radical polymerization (ATRP), 280–284
 general strategy for grafting, 280, 281
See also Inorganic nanotubes
- N**
- Nanocomposites**
 poly(propylene) (PP), 526–527, 528f
 preparation of poly(vinylidene fluoride) (PVDF)/clay, 391–392
See also Borane-mediated control radical polymerization; Inorganic-organic nanocomposites; Polymer-clay nanocomposites
- Nanoprecipitation emulsion polymerization**
 acrylate polymerizations, 319, 321
 block copolymers using stable free radical polymerization (SFRP), 321–322
 block copolymer synthesis using, 322t
 characterization methods, 316
 colloiddally stable latexes by SFRP emulsion, 315
 experimental, 316–317
 extension to atom transfer radical polymerization (ATRP) and reversible addition-fragmentation transfer (RAFT) techniques, 322
 extension to specialty polymers, 321–322

- gel permeation chromatography (GPC) MWD plot for SFRP starved-feed styrene emulsion polymerization, 319*f*
- general procedure for 2,2,6,6-tetramethyl-1-piperidinyloxy radical (TEMPO)-terminated oligomer synthesis, 316
- general procedure for block copolymer synthesis, 317
- GPC MWD plot for SFRP block copolymer synthesis using, 323*f*
- GPC MWD plot for SFRP *N*-butyl acrylate emulsion polymerization, 321*f*
- GPC MWD plot for SFRP styrene emulsion polymerization, 320*f*
- Mn vs. conversion for *N*-butyl acrylate emulsion polymerization, 322*f*
- Mn vs. conversion for styrene emulsion polymerization, 320*f*
- monomer-swollen preformed particles, 318–319, 323
- replacing anionic surfactant with nonionic surfactant poly(vinyl alcohol) (PVA), 318
- TEMPO-terminated oligomer, 317–318
- Nanostructured carbons**
- analysis, 303
- atomic force microscopy (AFM) height images of polyacrylonitrile (PAN) block copolymer films, 300*f*, 301*f*
- atom transfer radical polymerization (ATRP) of block copolymer poly(ethylene oxide)-*b*-polyacrylonitrile (PEO-*b*-PAN), 297, 303
- block-copolymer-derived precursors with thermally stable sacrificial phase, 297, 303–305
- drop-casting technique, 306, 307*f*
- long-range ordered, 305–308
- pore analysis, 303, 305
- pyrolysis of polyacrylonitrile (PAN) block copolymers, 296–297, 298, 299
- surface morphology of block copolymer poly(butyl acrylate)-*b*-PAN (PBA-*b*-PAN), 305–306
- synthesis of nanoporous silicas and carbons from self-assembled silica/poly(ethylene oxide)-*b*-PAN composites, 302
- synthesis of ordered mesoporous carbon using silica template and carbon precursor, 303–305
- tapping mode AFM phase images of thin films of PBA-*b*-PAN by drop- and zone-casting, 307*f*
- thermal stabilization and carbonization, 306
- transmission electron microscopy (TEM), 303, 304
- zone-casting process, 305, 306
- Nanotubes. *See* Inorganic nanotubes
- N*-heterocyclic carbenes (NHCs)
- ruthenium-benzylidene complexes bearing Schiff base and NHC ligands, 49–51
- structure, 43
- vs. phosphines, 43–44
- See also* Ruthenium *N*-heterocyclic carbene (NHC) complexes
- Nitrogen-containing ligands, copper-based ATRP catalysts, 61*f*
- Nitroxide-mediated polymerization (NMP)
- applications of alkoxyamines, 333–337
- controlled/living radical polymerization, 27
- persistent radical effect (PRE), 327–328
- polymerization of methyl methacrylate (MMA) with alkoxyamines, 336–337

polymerization of *N*-butyl acrylate with alkoxyamines, 335–336

polymerization of styrene with alkoxyamines, 333, 334*f*, 335

precision-engineered polymers, 327

recovery of chain transfer agents, 449

[*N*-*tert*-butyl-*N*-(1-diethylphosphono-2,2-dimethylpropyl) nitroxide (SG1), 328–329

[*N*-*tert*-butyl-*N*-(1-phenethyl-2-methylethyl)nitroxide (TIPNO), 328–329

2,2,6,6-tetramethyl-1-piperidinyloxy radical (TEMPO), 328

use of alkoxyamines for building complex macromolecular architectures, 337–339

See also Alkoxyamines

Nodulus method

arm–first star polymers by, 584–586, 587*t*

See also Star–like polymers by macromolecular design via interchange of xanthates (MADIX)

Non-conjugated vinyl monomers, controlled radical polymerization (CRP), 7–8

N-*tert*-butyl-*N*-(1-diethylphosphono-2,2-dimethylpropyl)nitroxide (SG1), nitroxide mediated polymerization (NMP), 328–329

N-*tert*-butyl-*N*-(1-phenyl-2-methylethyl)nitroxide (TIPNO), nitroxide mediated polymerization (NMP), 328–329

Nucleobases. *See* Styrene derivatives bearing nucleobases

O

Octadecyl (meth)acrylate (OD(M)A)

block copolymers by reversible addition-fragmentation chain transfer (RAFT), 524*t*

gradient copolymers by RAFT, 524, 525*t*

See Polymer-clay nanocomposites

Olefin metathesis, Grubbs ruthenium-carbene complex, 41–42

Olefins, controlled radical polymerization (CRP), 7–8

Oligo(ethylene glycol) methacrylate (OEGMA)

copolymerization with 1-(4-vinylbenzyl)thymine (VBT) and 9-(4-vinylbenzyl)adenine (VBA), 193–194

molecular structure, 190*f*

preparation of copolymers by atom transfer radical polymerization (ATRP), 194*t*

preparation of copolymers by free radical polymerization, 191*t*

See also Styrene derivatives bearing nucleobases

Oligomeric model radicals, generation, 112

Order, long-range, nanostructured carbons, 305–308

Organic reactions, aqueous media, 15

Organo-cobalt porphyrins. *See* Cobalt porphyrin derivatives

Organo-soluble copolymers. *See* Styrene derivatives bearing nucleobases

P

Paclitaxel (PTX)

atomic force microscopy phase images of block copolymers containing, 242 *f*

- chemical structure, 236*f*
- release from acrylate-based copolymer coating, 236–237
- release from block copolymers, 241, 243, 244*f*, 245*f*, 246*f*
- stent technology, 236
- See also* Acrylate-based block copolymers
- Particle-particle crosslinking
 - stationary phase preparation, 257, 259*f*
 - See also* Chromatographic stationary phases
- Particle size distributions
 - poly(butyl acrylate) by reverse iodine transfer polymerization, 609, 610*f*, 612*f*
 - See also* Reverse iodine transfer polymerization (RITP)
- Pendant allyl ester groups on polymers
 - architectures for prepolymers
 - cross-linked via radical process, 154
 - atom transfer radical polymerization (ATRP) of allyl methacrylate (AMA) using bifunctional macroinitiators, 157*t*
 - bisphenol-A (BPA) and TMC-bisphenol polycarbonate (TMC-BP PC) with AMA end groups, 163, 165–166
 - block copolymers, 161, 163
 - concept for preparing prepolymers with allyl ester side groups, 162
 - copolymer and end-group functionalized polymer syntheses, 156–158
 - copolymerization of 80/20 styrene and AMA, 160*f*
 - experimental, 155–158
 - microstructuring polymer films by photolithography, 168–169
 - photochemical cross-linking of end-group modified TMC-BP PC, 166*f*
 - photochemical cross-linking of P(Sty-*co*-AMA), 162*f*
 - polymerization reactions results, 158*t*
 - PPO with AMA end groups, 166–168
 - preparation of bifunctional ATRP macroinitiators based on TMC-BP PC and poly(phenylene oxide) (PPO), 164
 - prepolymer concept, 154
 - procedures, 155–156
 - proposed side reactions in ATRP in presence of AMA, 159
 - random copolymers, 158–161
 - 1,1,4,4,7,7-Pentaethyldiethylene triamine (PEDETA)
 - ¹H NMR spectrum of PEDETA, 103*f*
 - structure, 104*t*
 - synthesis, 101, 102–103
 - See also* Alkylated linear amine ligands
- Peroxide-induced radical reaction
 - macromolecular design via interchange of xanthates (MADIX), 565, 566
 - See also* Chemical transformation of xanthate-functional terminal groups
- Persistent radical effect (PRE)
 - equations describing, 60
 - exchange process, 5–6
- Phase transfer catalysis
 - catalyst removal, 19–20
 - liquid-liquid biphasic polymerization, 72
 - thermally dictated, 15
 - thermally regulation, 18–19
- Phosphines
 - N*-heterocyclic carbenes (NHC) vs., 43–44

- See also* Ruthenium *N*-heterocyclic carbene (NHC) complexes
- Phosphonylated alkoxyamines. *See* Alkoxyamines
- Photochemical cross-linking, end-group modified TMC bisphenol polycarbonate (PC), 166*f*
- Photolithography, microstructuring of polymer films, 168–169
- Poly(acrylate-*co*-urethane), telechelic RAFT polymers, 554–555, 560–561
- Poly(acrylic acid) (PAA)
aqueous size exclusion chromatography (ASEC) of stars based on, 583*f*
arm-first star polymers by "nodulus" method, 584–586, 587*t*
polymeric nanogels by MADIX radical crosslinking copolymerizations, 586, 588–589
reduction study on PAA synthesized in presence of xanthate, 569–571
three-arm star polymers by core-first method, 580–582
See also Chemical transformation of xanthate-functional terminal groups; Star-like polymers by macromolecular design via interchange of xanthates (MADIX)
- Polyacrylic acid thickener, crosslinked, telechelic RAFT polymers as, 556–557, 561–562
- Polyacrylonitrile (PAN) block copolymers
morphologies, 300*f*, 301*f*
nanostructured carbons from, 296–297
poly(ethylene oxide)-*b*-PAN, 297, 302, 303
pyrolysis of self-assembled, 298, 299
See also Nanostructured carbons
- Poly(2-(2-bromoisobutyryloxy)ethyl methacrylate) (PBIEM). *See* Glycopolymers, methacrylate-type
- Poly(*t*-butyl acrylate), Chugaev reaction, 574, 575
- Polycarbonate (PC)
end-group functionalization, 156–157
See also Reactive block copolymers
- Poly(2-(*N,N*-Dimethylamino)ethyl methacrylate) (pDMAEMA)
"grafting from" approach, 254, 259*f*, 261–262
See also Chromatographic stationary phases; Tailor-made copolymers
- Poly(dimethylsiloxane) (PDMS)
Chugaev reaction, 574–576
dethiocarboxylation of xanthate-terminated PDMS, 567–568, 572–576
radical reduction of xanthate-terminated PDMS, 566–567, 568–569
See also Chemical transformation of xanthate-functional terminal groups
- Polydispersity, reversible addition-fragmentation chain transfer (RAFT), 422
- Poly(ethylene oxide) (PEO)
phase-transfer catalysis, 15
synthesis of well-defined PEO-*b*-polyacrylonitrile block copolymers, 297, 303
- Poly(ethylene terephthalate) (PET)
blends. *See* Reactive block copolymers
- Poly(isobornyl acrylate)

- atomic force microscopy phase images of block copolymers containing paclitaxel, 242*f*
- block copolymer synthesis, 237–238
- differential scanning calorimetry of block copolymers, 239, 241*t*
- paclitaxel release from block copolymers with, 241, 243, 244*f*, 245*f*, 246*f*
- See also* Acrylate-based block copolymers
- Poly(lauryl acrylate)
- block copolymer synthesis, 237–238
- See also* Acrylate-based block copolymers
- Polymer blends, compatibilization, 343
- Polymer-clay nanocomposites
- backbiting and β -scission actions, 519
- differences and similarities of conventional radical polymerization and reversible addition-fragmentation chain transfer (RAFT), 515
- exfoliants/intercalants/dispersants for, 523–529
- gradient copolymers as dispersants, 524, 525*t*
- mechanism of stabilization by nanoparticulate fillers, 529
- mechanisms for polymerization of *n*-butyl acrylate (nBA), 519
- normalized gel permeation chromatography (GPC) traces at various reaction times/conversions for RAFT of nBA, 517*f*
- normalized GPC traces of poly(nBA) with trithiocarbonate with ultraviolet (UV) detection and refractive index (RI) detection, 518*f*
- normalized UV spectra of poly(nBA) with trithiocarbonate, 518*f*
- octadecyl acrylate (ODA) and octadecyl methacrylate (ODMA), 523
- origin of humps in molecular weight distributions, 517–519
- polypropylene (PP)
- nanocomposites, 526–527
- properties of block copolymers by RAFT, 524*t*
- RAFT copolymerization, 522
- RAFT end-group removal, 519–520, 521
- RAFT polymerization of acrylates, 517–520
- tensile properties for PP samples, 526*t*
- thermogravimetric analysis (TGA) analyses for PP and PP-clay nanocomposites, 528*f*
- transmission electron microscopy (TEM) image of cryofracture surface of PP, 528*f*
- trithiocarbonate RAFT agents, 516
- visual appearance of nanocomposites, 526, 527*f*
- Polymer films, microstructuring by photolithography, 168–169
- Polymeric nanogels, macromolecular design via interchange of xanthates (MADIX) radical crosslinking copolymerizations, 586, 588–589
- Polymeric surfactants, emulsion stabilizers, 314
- Polymerization, aqueous media, 15
- Poly((meth)acrylic acid). *See* 1-Ethoxyethyl (meth)acrylate (EE(M)A)
- Poly(methacryloyloxyethyltrimethylammonium chloride) (pTMAEMA). *See* Chromatographic stationary phases
- Poly(methyl methacrylate) (PMMA)

- atomic force microscopy phase images of block copolymers containing paclitaxel, 242*f*
- block copolymers with *N,N'*-dimethylaminoethyl methacrylate (DMAEMA), 481–484
- block copolymer synthesis, 237–238
- block extension of, with butyl methacrylate and butyl acrylate, 446, 448
- differential scanning calorimetry of block copolymers, 239, 241*t*
- grafting, from multi-walled carbon nanotubes (MWNT), 280, 281
- grafting, from titanate nanotubes (TNTs), 285
- molecular weight and polydispersity using fresh, reused, and regenerated catalyst, 81*f*
- molecular weights and polydispersity of, using magnetic nanoparticle supported catalyst, 78*f*, 79*f*
- paclitaxel release from block copolymers with, 241, 243, 244*f*, 245*f*, 246*f*
- poly(ethylene glycol) (PEG) macroinitiator and PEG-*b*-PMMA, 81*f*
- scanning electron microscopy (SEM) of stents coated with block copolymer, 240*f*
- statistical copolymers with DMAEMA, 479–480, 481*t*
- See also* Acrylate-based block copolymers; Inorganic nanotubes; Methyl methacrylate (MMA); Reactive block copolymers; Tailor-made copolymers
- Polypeptides**
- integrating sequence controlled, into synthetic polymer, 199–200
- See also* Conjugates of polymers and sequence-defined polypeptides
- Poly(phenylene oxide) (PPO)**
- end-group functionalization, 156–157
- PPO with allyl methacrylate (AMA) end groups, 166–168
- preparation of bifunctional ATRP macroinitiators, 164
- Poly(propylene) (PP) nanocomposites**, 526–527, 528*f*
- Polystyrene (PS)**
- atomic force microscopy phase images of block copolymers containing paclitaxel, 242*f*
- block copolymer synthesis, 237–238
- chain extension of, with styrene, 431, 432*f*
- Chugaev reaction, 574, 575
- differential scanning calorimetry of block copolymers, 239, 241*t*
- gradient polymer elution chromatography (GPEC) of dibromo-, diazido-, and dihydroxy-terminated PS, 143–144
- grafting, from titanate nanotubes (TNTs), 285
- multiblock copolymers by difunctional RAFT, 433, 436*f*
- paclitaxel release from block copolymers with, 241, 243, 244*f*, 245*f*, 246*f*
- polymer-small molecule click reactions, 142–145
- synthesis of difunctional PS via ATRP and subsequent reaction, 143
- See also* Acrylate-based block copolymers; Click functionalization of well-defined

- copolymers; Inorganic nanotubes; Reactive block copolymers; Styrene
- Poly(styrene-*co*-acrylonitrile) [P(SAN)]
 paclitaxel release from block copolymers with, 241, 243, 244*f*, 245*f*
See also Acrylate-based block copolymers
- Poly(trifluoroethyl acrylate) (PTFEA)
 borane-mediated control radical polymerization, 392–397
¹³C NMR spectra, 394*f*
 gel permeation chromatography of poly(methyl methacrylate) (PMMA) and PMMA-*b*-PTFEA, 395*f*
¹H NMR spectra of PMMA and PMMA-*b*-PTFEA, 396*f*
 polymerization by 8-bora-indane/O₂, 393*t*
 synthesis of poly(methyl methacrylate-*b*-TFEA) copolymer, 391
 synthesis of telechelic, with terminal OH groups, 390
See also Fluoropolymers
- Polyurethane-polyacrylate block copolymers, telechelic RAFT polymers as, 554–556, 560–561
- Poly(vinyl alcohol) (PVOH)
 nonionic surfactant in emulsion polymerization, 318, 319*f*
 synthesis of block copolymers, 380, 381
 synthesis of PVOH-*b*-polystyrene copolymers, 374
- Poly(vinylidene fluoride) (PVDF)
 chain end functionalized PVDF, 397–401
 preparation of PVDF/clay nanocomposite, 391–392
 synthesis of, with terminal silane group, 391
- See also* Borane-mediated control radical polymerization; Fluoropolymers
- Pore analysis
 nanostructured carbons, 303, 305
 ordered mesoporous carbon, 304
- Post-polymerization modification
 click chemistry, 141
 coupling reactions between two polymers, 145–146
See also Click functionalization of well-defined copolymers
- Prepolymer concept
 cross-linked materials, 154
 preparation, 162
- Propagating radicals
 chain lengths of methacrylates, 113
 electron spin resonance (ESR) spectroscopy, 112
 generation, 112
 1,5-hydrogen shift of, of *t*-butyl acrylate (tBA), 117*f*
See also Electron spin resonance (ESR) study of (meth)acrylate radicals
- Propagation, emulsion polymerization, 314–315
- Propagation rate, achieving steady state, 4
- Pulsed-laser initiated reversible addition-fragmentation chain transfer (RAFT) polymerization
 addition and fragmentation rate coefficients in S,S'-bis(methyl-2-propionate)-trithiocarbonate (BMPT)-mediated butyl acrylate (BA) polymerization, 462*t*
 advantage of photoinitiation by laser pulses, 456
 chain-length dependent termination rate coefficients from single-pulsed pulsed-laser polymerization near-infrared spectroscopy-RAFT (SP-PLP-NIR-RAFT), 465–470

- chemical structure and UV spectrum of BMPT, 458*f*
determination of chain-length dependent termination rate coefficients, 468–470
electron spin resonance (ESR) spectra during quasi-stationary BMPT-mediated BA polymerization, 464*f*
evolution of molecular weight distribution (MWD) of poly(BA), 459, 460*f*, 461
experimental, 457
future outlook, 471
influence of stability of RAFT intermediate radicals, 466–468
kinetic model, 462, 463*f*
measurements of SP-PLP-ESR, 457
measurements of SP-PLP-NIR, 457
Mn and polydispersity (PDI) in bulk polymerization of BA, 460*f*, 461
RAFT addition and fragmentation rate coefficients via SP-PLP-ESR, 461–464
RAFT polymerization under PLP conditions, 458–461
reaction steps and rate coefficients of time-dependent intermediate radical concentration, 462
relative BMPT concentration vs. number of applied laser pulses, 459*f*
self-termination in kinetic modeling, 464
simulated time evolution of polydispersity index (PDI) of polyRAFT agent and propagating radicals, 466*f*
simulated transformation of laser-induced small radicals into macroradicals, 465*f*
simulations, 457
single-pulsing technique, 463–464
size exclusion chromatography (SEC) analyses, 457
termination rate coefficients by SP-PLP-NIR-RAFT, 470*f*
See also Reversible addition-fragmentation chain transfer (RAFT)
Pyrolysis. *See* Nanostructured carbons
- ## R
- Radical crosslinking copolymerization (RCC)
polymeric nanogels by macromolecular design via interchange of xanthates (MADIX), 586, 588–589
size exclusion chromatography (SEC) traces of branched copolymers by, 590*f*, 591*f*
xanthate-mediated RCC of acrylic acid and crosslinker, 590*t*
- Radical polymerization
comparing conventional, with one using reversible addition-fragmentation chain transfer (RAFT) agent, 515
controlling tacticity, 27
See also Stereospecific living radical polymerization
- Radical reduction
xanthate-terminated poly(dimethylsiloxane) (PDMS), 566–567, 568–572
See also Chemical transformation of xanthate-functional terminal groups
- Radical ring opening (RRO). *See* Ti-catalyzed living radical polymerization (LRP)
- Radicals. *See* Electron spin resonance (ESR) study of (meth)acrylate radicals

- Radical stabilization energies,
reversible addition-fragmentation
chain transfer (RAFT), 410
- Random copolymers. *See* Pendant
allyl ester groups on polymers;
Reversible addition-fragmentation
chain transfer (RAFT)
copolymerizations
- Rate constants, atom transfer radical
polymerization (ATRP) catalysts,
59–60
- Reactive block copolymers
block copolymers as
compatibilizers, 343–344
compatibilizers synthesis, 346
effect of polycarbonate/polystyrene
(PC/PSt) in particle size, 356*f*
experimental, 345–346
influence of amount of
compatibilizer on particle size of
PSt-*co*-MMA in poly(ethylene
terephthalate) PET/PSt-*co*-
MMA blends, 351*f*
influence of Mn of functional
block, Mn of nonfunctional
block, and number of functional
groups on mean diameter of
PST-*co*-MMA, 349*f*
influence of Mn of non-reactive
block, Mn of reactive block, and
number of functional groups on
mean diameter of particles in
PC/compatibilizer blends, 354*f*,
355*f*
optical microscopy method, 346
optical microscopy of PET/St-*co*-
MMA blends, 348*f*
optical microscopy of
PC/compatibilizer blends, 352*f*
PET/PSt-*co*-MMA blends, 347–
350
polycarbonate/polystyrene blends,
351, 353
schematic representation of diblock
copolymers, 345*f*
- Recovery, chain transfer agents, 449–
451, 452*f*
- Recyclability
Cu-based catalyst for atom transfer
radical polymerization, 95
See also Catalyst activity; Catalyst
recycling; Catalyst regeneration
- Recycling, magnetic nanoparticle
supported catalyst, 79–80.
- Redox potentials, copper-based ATRP
catalysts, 62*f*
- Reduction, radical. *See* Chemical
transformation of xanthate-
functional terminal groups
- Regeneration
magnetic nanoparticle supported
catalyst, 79–80
See also Catalyst regeneration
- Reverse iodine transfer polymerization
(RITP)
block copolymerization in
emulsion, 614, 616*f*
characterization methods, 607
characterizations of seed poly(*n*-
butyl acrylate) [poly(BuA)]
latex by RITP and block
copolymer latex by seeded
emulsion polymerization of
styrene, 614, 616*f*
effect of concentration of iodide,
608–609, 611*t*, 613
effect of concentration of
surfactant, 608, 609*t*
evolution of monomer conversion
vs. time for, 613*f*
experimental, 606–607
features of RITP in emulsion, 617–
618
general procedure for emulsion
polymerization of BuA, 607
hydrolytic disproportionation of
iodine and related reactions,
617
kinetics of RITP in emulsion, 613–
614

- living radical polymerization
 technique, 605–606
 mechanism, 605–606
 molecular weight distributions
 (MWD) and particle size
 distributions of poly(BuA) by,
 610*f*
 MWD of poly(BuA) by RITP in
 emulsion, 611*f*
 MWD and particle size
 distributions of poly(BuA), 612*f*
 RIPT in emulsion, 607–608
 RITP of BuA in emulsion, 615*f*
 Reversible activation processes, living
 radical polymerization (LRP), 596
 Reversible addition-fragmentation
 chain transfer (RAFT)
ab initio calculations studying
 kinetics and thermodynamics,
 407–408
 acceleration of fragmentation and
 hydrogen bonding, 417*f*
 chain transfer efficiency, 410
 choice of R group, 414–416
 choice of Z group, 410–414
 comparing conventional radical
 polymerization with one using
 RAFT agent, 515
 computational procedures, 408–409
 controlled/living radical
 polymerization, 27, 407
 controlling polydispersity, 422
 copolymerization, 522
 degenerative transfer process, 6–7,
 439
 effect of R group on stabilities and
 chain transfer enthalpies, 415*t*
 effect of Z group on stabilities and
 fragmentation enthalpies, 411*t*
 effects of R, R', and Z substituents,
 408
 1-ethoxyethyl acrylate (EEA), 180–
 183
 exceptions to trends, 416–418
 fragmentation efficiency, 409
 homopolymerization of EEA, 181–
 182
 isodesmic reactions, 410
 methyl methacrylate (MMA), 415–
 416
N-vinylpyrrolidone (NVP)
 polymerization in
 fluoroalcohols, 34–36
 oligopeptide based RAFT agents
 and use in polymerization of *N*-
 butyl acrylate, 205–208
 poly(MMA)–poly(acrylic acid)
 block copolymers, 182–183
 poly(MMA)–poly(EEA) block
 copolymers, 182–183
 polymerization of acrylates, 517–
 520
 polymerization process, 444–
 446
 polymerization with RAFT agents,
 548–550
 radical stabilization energies, 410
 RAFT main equilibrium, 461
 recovery of chain transfer agents,
 449–451, 452*f*
 SciFinder Scholar search, 3*f*, 4
 solid-phase supported synthesis of
 oligopeptide transfer agents,
 205, 206
 trithiocarbonate RAFT agents,
 516
 vinyl acetate (VAc), 413–414
See also Amino acid-based
 polymers; Chain transfer agents
 (CTAs); Conjugates of polymers
 and sequence-defined
 polypeptides; Difunctional
 reversible addition-
 fragmentation chain transfer
 (RAFT); Pulsed-laser initiated
 reversible addition-
 fragmentation chain transfer
 (RAFT) polymerization; Tailor-
 made copolymers; Telechelic
 polymers

Reversible addition-fragmentation chain transfer (RAFT) copolymerizations analysis, 505–508
 concentration vs. time profiles for single monomer adducts and dimer adducts, 510f
 concentration vs. time profiles for styrene (STY) and acrylonitrile (AN) during copolymerization, 510f
 consumption rates of STY and AN, 508, 510f
 copolymer fingerprint of STY-maleic anhydride (MAh), 512f
 copolymerization of styrene and MAh, 509, 512
 expansion of ^1H NMR spectra during styrene/acrylonitrile (STY/AN) copolymerization, 508f
 experimental, 504–505
 gas chromatography (GC) for monomer conversion determination, 505–506
 GC temperature gradient, 506f
 ^1H nuclear magnetic resonance (NMR) analysis, 506–508
 in situ ^1H NMR experiment, 507
 MALDI-ToF-MS (matrix assisted laser desorption/ionization-time of flight-mass spectrometry), 506
 MALDI-ToF-MS of alternating STY-MAh, 511f
 $M_{n,SEC}$ and polydispersity index (PDI), 505–506
 sample preparation for styrene-co-acrylonitrile reactions, 504
 synthesis of poly(styrene-*alt*-maleic anhydride) (SMAh), 504
 synthesis of transfer agents, 504
See also Polymer-clay nanocomposites

Reversible addition-fragmentation chain transfer chain length dependent termination (RAFT-CLD-T)
 butyl acrylate (BA), 487, 491, 492f
 chain length dependencies for various monomers, 491, 492f, 493f, 494f
 choice of RAFT agent, 490
 constructing three dimensional image of termination process, 495–496
 data evaluation procedure, 488–489
 dodecyl acrylate (DA), 487, 491, 493f
 effect of chain length dependent propagation on observed chain length dependence of k_t , 498f
 evolution of α as function of monomer to polymer conversion for methyl acrylate (MA) and vinyl acetate (VAc) system, 496f
 future challenges, 496–499
 initial monomer and initiator concentrations, 489
 initiator efficiency, f , 489
 key idea, 488
 mapping k_t for several monomer families, 491, 494–495
 mapping termination process, 495–496
 methyl acrylate (MA), 487, 491, 492f
 methyl methacrylate (MMA), 487, 491, 493f
 monomer reaction order, 489
 obtaining reliable termination rate coefficients, 487
 prerequisite parameters, 489–490
 propagation rate coefficient, k_p , 489
 RAFT reagent concentration, 489
 rate coefficient of initiator decomposition, 489
 technique term, 487
 vinyl acetate (VAc), 487, 491, 494f

- Ruthenium-benzylidene complexes bearing *N*-heterocyclic carbene (NHC) ligands, 48–49
- bearing Schiff base and NHC ligands, 49–51
- Ruthenium-catalyzed systems
- methyl methacrylate in fluoroalcohols, 28–30
- thermosensitive poly(ethylene glycol) (PEG), 15
- See also* Thermosensitive Ru(II) complexes
- Ruthenium *N*-heterocyclic carbene (NHC) complexes
- 18-electron complexes, 40
- cyclic voltammetry data for Grubbs complexes, 53*t*
- cyclic voltammetry data for Ru complexes, 52*t*
- Fischer-type Ru-alkylidene complex bearing Schiff base and NHC ligands, 51
- Grubbs Ru-carbene complex for olefin metathesis, 41–42
- metathesis and radical polymerization of styrene, 47–48
- NHCs as phosphine-substitutes for late transition metal catalysts, 42
- NHCs vs. phosphines, 43–44
- phosphines vs. NHC ligands in ATRP cyclic voltammetry investigations, 42–45
- polymerization of methyl methacrylate (MMA) initiated by ethyl 2-bromo-2-methylpropionate and catalyzed by, 41*t*
- polymerization of MMA initiated by ethyl 2-bromo-2-methylpropionate and catalyzed by, 44, 45*t*, 48*t*, 50*t*
- polymerization of styrene initiated by (1-bromoethyl)benzene and catalyzed by, 42*t*, 44, 46*t*, 48*t*, 51*t*
- polymerization protocol, 42
- Ru-benzylidene complexes bearing NHC ligands, 48–49
- Ru-benzylidene complexes bearing Schiff base and NHC ligands, 49–51
- Ru-*p*-cymene complexes bearing NHC ligand, 44–48
- Ru-triphenylphosphine complex bearing Schiff base and NHC ligands, 51
- structure of NHC, 43
- structures, 41
- synthesis and reactivity, 43
- Ruthenium-*p*-cymene complexes, *N*-heterocyclic carbene (NHC) ligand, 44–48
- ## S
- Schiff base, ruthenium-benzylidene complexes bearing, and NHC ligand, 49–51
- SciFinder Scholar search, controlled radical polymerization systems, 3*f*, 4
- Self-condensing vinyl copolymerization (SCVCP)
- general route to branched glycopolymers, 220
- See also* Glycopolymers, methacrylate-type
- Self-termination, kinetic modeling of reversible addition-fragmentation chain transfer (RAFT), 464
- Sequence-defined polypeptides. *See* Conjugates of polymers and sequence-defined polypeptides
- Side reactions, atom transfer radical polymerization (ATRP), 159
- Silica gel supporting catalysts, 76

- See also* Catalyst activity
- Simulations. *See* Difunctional reversible addition-fragmentation chain transfer (RAFT)
- Simultaneous reverse and normal initiation (SR&NI), atom transfer radical polymerization, 6
- Sn iodides
 reversible activation catalyzed by Ge and Sn, 597
 styrene polymerization with 1-phenylethyl iodide (PE-I) in presence of, 598*t*
See also Living radical polymerization (LRP)
- Solvent-mediated polymerization, stereospecific, 27
- Split filter test
 batch and continuous atom transfer radical polymerization (ATRP), 92–93
See also Catalyst activity
- Stability
 effect of R group on, and chain transfer enthalpies, 415*t*
 effect of Z group on, and fragmentation enthalpies, 411*t*
 radicals and agents of reversible addition-fragmentation chain transfer (RAFT), 410
 reversible addition-fragmentation chain transfer (RAFT) intermediate radicals, 466–468
- Stability of polymeric dormant state, copper-based catalyst, 66–67
- Stable free radical polymerization (SFRP)
 exchange process, 5*f*
 mechanisms for living character, 369–370
 SciFinder Scholar search, 3*f*
See also Nanoprecipitation emulsion polymerization
- Star-like polymers by macromolecular design via interchange of xanthates (MADIX)
 aqueous size exclusion chromatography (ASEC) of stars based on poly(acrylic acid) (PAA), 583*f*
 arm-first star polymers by "nodulus" method, 584–586
 characterization methods, 580
¹³C NMR spectrum of trifunctional MADIX agent, 582*f*
 core-first method for three-arm star polymers, 580–582
 crosslinker effect on size exclusion chromatography (SEC) traces of branched copolymers, 590*f*
 experimental, 580
 polymeric nanogels by MADIX radical crosslinking copolymerization, 586, 588–589
 polymerization method, 580
 polymerizing hydrophilic monomers, 579–580
 radical crosslinking copolymerization (RCC) of vinylic monomer with crosslinker, 586, 588
 refractometric response of ASEC before and after chain extension of xanthate-terminated PAA precursor, 585*f*
 SEC traces of parent copolymer and star-like copolymer after chain extension, 591*f*
 synthesis of arm-first polymers by "nodulus" method from different MADIX-derived precursors, 587*t*
 synthesis of hydrophilic arm-first stars by MADIX, 585
 synthesis of hydrophilic core-first stars, 581
 synthesis of trifunctional xanthates, 580

- transfer events in MADIX process, 579
- UV response of ASEC before and after chain extension of xanthate-terminated PAA precursor, 587*f*
- xanthate effect on SEC traces of branched copolymers, 590*f*
- xanthate-mediated RCC of AA and *N,N'*-methylene-bis(acrylamide) (MBA), 590*t*
- See also* Macromolecular design via interchange of xanthates (MADIX)
- Status quo, living and stereospecific radical polymerization, 36*t*
- Steady state, convention vs. controlled radical polymerization processes, 4
- Stent technology
- mechanical integrity of coatings, 238
 - paclitaxel, 236
 - scanning electron microscopy (SEM) of stents coated with block copolymer, 240*f*
- Stereochemistry, simultaneous control of molecular weights and, 26–28
- Stereospecific living radical polymerization
- N,N*-dimethylacrylamide (DMAM) polymerization, 30, 31*f*
 - free radical polymerization of NVP in fluoroalcohols, 35*t*
 - ¹H NMR spectra for poly(VAc) and poly(vinyl alcohol), 33, 34*f*
 - ¹H NMR spectra of poly(DMAM), 31*f*
- iodine-transfer radical polymerization in fluoroalcohols for vinyl acetate, 32–33
- iron-catalyzed, with Lewis acid, 30
- iron-catalyzed systems with metal triflates for acrylamides, 30–32
- macromolecular design via interchange of xanthates (MADIX), 27
- MMA polymerizations with Ru complexes in fluoroalcohols, 29*f*
- RAFT/MADIX polymerization in fluoroalcohols for *N*-vinylpyrrolidone (NVP), 34–36
- Ru-catalyzed living radical polymerization in fluoroalcohols, 28
- ruthenium-catalyzed systems in fluoroalcohols for methyl methacrylate (MMA), 28–30
- simultaneous control of molecular weight and stereochemistry, 26–28
- status quo of monomers, 36*t*
- xanthate-mediated polymerization of NVP, 35*f*
- Structural features, copper-based ATRP catalysts, 62*f*
- Structure-property relationships, controlled radical polymerization (CRP), 8
- Styrene
- atom transfer radical polymerization (ATRP) using different amine ligands, 107*t*
 - block copolymer synthesis, 237–238
 - (1-bromoethyl)benzene initiation and ruthenium complex catalysis, 42*t*, 46*t*, 48*t*, 51*t*
 - chain extension of polystyrene (PS) with, 431, 432*f*
 - copolymerization of 80:20 styrene:allyl methacrylate (AMA), 160*f*
 - gel permeation chromatography (GPC) MWD plot for, using nanoprecipitation process, 319*f*, 320*f*
 - graft polymerization of, and dimethylaminoethyl

- methacrylate (DMAEMA) by cellulose chain transfer agent, 449*t*
- kinetic modeling, 426–431
- kinetic parameters modeling
- difunctional reversible addition-fragmentation chain transfer (RAFT) polymerization, 423*t*
- kinetic plots of ATRP of MMA and, using 1,1,4,7,7-pentaethyldiethylene triamine (PEDETA) as ligand, 105*f*
- kinetic simulations for homopolymerization, 423, 426
- metathesis and radical polymerization, 47–48
- Mn vs. conversion of, using nanoprecipitation emulsion polymerization, 320*f*
- Mn vs. conversion plots of MMA and, polymerization using PEDETA as ligand, 105*f*
- polymerization protocol using ruthenium complexes, 42
- polymerizations catalyzed by Ti complexes, 131*t*
- polymerization with 1-phenylethyl iodide (PE-I) in presence of Ge and Sn iodides, 598*t*
- simulations of effect of increasing initiator on molar concentrations of polymeric species, 428*f*
- simulations of effect of initiator concentration on reaction rate and MWD of, 427*f*
- simulations of MWDs at different conversion, 427, 429, 430*f*
- synthesis of poly(*St-co-AMA*), 156
- Ti-catalyzed living radical polymerization by epoxide radical ring opening (RRO), 129–130
- See also* Acrylate-based block copolymers; Nanoprecipitation emulsion polymerization;
- Pendant allyl ester groups on polymers; Polystyrene (PS); Reverse iodine transfer polymerization (RITP); Reversible addition-fragmentation chain transfer (RAFT) copolymerizations; Ruthenium *N*-heterocyclic carbene (NHC) complexes; Ti-catalyzed living radical polymerization (LRP)
- Styrene derivatives bearing nucleobases
- characterization methods, 188–189
 - comonomers dodecyl methacrylate (DMA) and oligo(ethyleneglycol) methacrylate (OEGMA), 190*f*
 - experimental, 188–189
 - general procedure for atom transfer radical polymerization (ATRP), 188
 - general procedure for conventional radical polymerization, 188
 - homopolymers by free radical polymerization, 189*t*
 - model monomers 9-(4-vinylbenzyl)adenine (VBA) and 1-(4-vinylbenzyl)thymine (VBT), 187–188
 - optical micrographs at room temperature of P(VBT-*co*-DMA) solution, 192*f*
 - pathways linking nucleobases to synthetic polymer backbones, 186–187
 - preparation of copolymers by ATRP, 194*t*
 - preparation of copolymers by free radical copolymerization, 191*t*
 - preparation of homopolymers of VBT and VBA, 189–190
 - preparation of organo-soluble copolymers, 190–193

preparation of water-soluble copolymers, 193–194
 radical polymerization, 187–188
 structures of, with purine or pyrimidine substituents, 187*f*
 Substituent effects. *See* Reversible addition-fragmentation chain transfer (RAFT)
 Sugar-carrying methacrylate monomer. *See* Glycopolymers, methacrylate-type
 Sugar sticks
 glycocylindrical brushes, 223–224
 solvolysis of glycocylindrical brushes, 224, 227
 synthetic route to glycocylindrical brushes, 225
See also Glycopolymers, methacrylate-type
 Supported catalyst
 activity, 87–88
See also Catalyst activity
 Surface morphology
 poly(butyl acrylate)-*b*-polyacrylonitrile (PBA-*b*-PAN) block copolymers, 305–306
 polyacrylonitrile copolymers, 297, 300*f*, 301*f*
 Surfactant-free emulsion polymer, telechelic RAFT polymers as, 554, 560
 Surfactants. *See* Reverse iodine transfer polymerization (RITP)
 Suspension polymerization
 methyl methacrylate (MMA) with Ru(II) catalyst in water, 18–19
 procedure, 18*f*, 23
 Synthetic polymers, integrating sequence controlled polypeptides, 199–200

T

Tacticity
 radical polymerization controlling, 27

See also Stereospecific living radical polymerization
 Tailor-made copolymers
 block and random copolymers of methyl methacrylate (MMA) and *N,N'*-dimethylaminoethyl methacrylate (DMAEMA), 475–476
 block copolymerization procedure, 478
 comparison of traditional polymerization methods and high-throughput experimentation, 474, 475*f*
 controlled radical polymerization techniques, 474
 experimental, 477–478
 future work, 484
 gel permeation chromatography (GPC) of first blocks and resulting pMMA-*b*-DMAEMA, 483*f*
 high throughput experimentation by reversible addition-fragmentation chain transfer (RAFT), 475
 materials and instrumentation, 477
 molecular weight and polydispersity index for library of block copolymers, 483*f*
 molecular weight and polydispersity index for library of statistical copolymers, 479*f*
 pDMAEMA as hydrophilic part, 478
 schematic of synthesis of library of block and statistical copolymers, 476*f*
 statistical copolymerization procedure, 477
 structural characterization of pMMA-*b*-DMAEMA copolymers, 482*t*

- structural characterization of
pMMA-*stat*-DMAEMA
copolymers, 481*t*
- synthesis of pMMA-*b*-DMAEMA
block copolymers, 481–484
- synthesis of pMMA-*stat*-
DMAEMA statistical
copolymers, 479–480
- theoretical vs. actual MMA fraction
in pMMA-*stat*-DMAEMA
copolymer, 480*f*
- Telechelic alkoxysilyl-terminated
polymers, reversible addition-
fragmentation chain transfer, 557–
558, 562
- Telechelic fluoropolymers
synthesis, 390
See also Fluoropolymers
- Telechelic polymers
ab initio emulsion polymer, 553,
554
- associative thickener for latex
paint, 551–553
- atom transfer radical
polymerization (ATRP)
synthesis with α -halo ester, 549
- block copolymer formation from
carboxyl-terminated reversible
addition-fragmentation chain
transfer (RAFT) agent, 548–
549
- constructing ABA block
copolymers, 549–550
- cross-linked polyacrylic acid
thickener, 556–557
- emulsion polymer, 553–554
- experimental, 558–562
- issues of RAFT polymers, 549
- polymerization with functionalized
RAFT agents, 548
- polyurethane-polyacrylate block
copolymer, 554–556
- RAFT polymerization, 446, 448
- surfactant-free emulsion polymer,
554
- synthesis of acrylate/urethane
copolymer, 555
- synthesis of mono- and di-
terminated RAFT agents, 547–
548
- synthesis of poly(acrylate-*co*-
urethane-*co*-acrylate), 555–556
- synthesis of telechelic dicarboxyl
acrylates, 551, 552
- telechelic alkoxysilyl-terminated
polymers, 557–558
- toughener for epoxy resins, 550–
551, 559
- Temperature effects
competing side reactions, 136
- influence on polymerization of
vinyl acetate, 379–380
- polydispersity in living radical
polymerization, 136–137
- Ti-catalyzed styrene
polymerizations, 133*f*, 135, 136*f*
- Terminal functionalization
click chemistry, 144–145
See also Chemical transformation
of xanthate-functional terminal
groups; Click functionalization
of well-defined copolymers
- Termination process
constructing three dimensional
image of, 495–496
See also Reversible addition-
fragmentation chain transfer
chain length dependent
termination (RAFT-CLD-T)
- Termination rate, achieving steady
state, 4
- Termination rate coefficients
determination of chain-length
dependent, 468, 470
See also Pulsed-laser initiated
reversible addition-
fragmentation chain transfer
(RAFT) polymerization
- Tetraethyldiethylenetriamine
(TEDETA)

- grafting ligand onto magnetic nanoparticles, 73–74, 76
See also Magnetic nanoparticle supported catalyst
- 2,2,6,6-Tetramethyl-1-piperidinyloxy radical (TEMPO)
 nitroxide mediated polymerization (NMP), 328–329
 TEMPO-terminated oligomers in nanoprecipitation emulsion polymerization, 316, 317–318
- Thermal polymerization, M_w and T_g of polyacrylates, 119*f*
- Thermosensitive poly(ethylene glycol), ruthenium catalysis, 15
- Thermosensitive Ru(II) complexes
 methyl methacrylate (MMA)
 polymerization with Ru(Cp)Cl(polyethylene glycol (PEG)-phosphine), 17
 catalyst recycling, 20–21
 catalyst removal from products, 19–20
 experimental, 21–24
 living radical polymerization with, 16
 polymer characterization, 23–24
 procedure for MMA suspension polymerization, 18*f*
 solution polymerization, 23
 suspension polymerization, 23
 suspension polymerization in water, 18–19
 synthesis of end-chlorinated PEG, 22
 synthesis of PEG methyl ether 4-iodophenyl ether, 22
 synthesis of PEG-phosphine, 22
 synthesis of sodium 4-iodophenoxide, 22
 thermally regulated phase transfer catalysis, 18–19
- Thickener for latex paint,
 associative, telechelic reversible
 addition-fragmentation chain transfer (RAFT) polymers as, 551–553, 559
- Three-arm polymers
 core-first method, 580–582
See also Star-like polymers by macromolecular design via interchange of xanthates (MADIX)
- Ti-catalyzed living radical polymerization (LRP)
 1,4-butanediol diglycidyl ether (BDGE) diepoxide as initiator, 130
 competing side reactions, 136
 controlling molecular weight and polydispersity, 126
 conversion dependence of M_n and M_w/M_n for, of styrene, 130–136
 effect of ligand, epoxide/Ti(III) ratio, and temperature, 133*f*
 effect of ligand structure in RCp_2TiCl_2 -catalyzed LRP of styrene, 134, 135*f*
 effect of temperature and Ti(IV)/Zn ratio, 135, 136*f*
 epoxide radical ring opening (RRO) initiation of styrene, 126, 129
 experimental, 128–129
 ligand and initiator effect in styrene polymerizations, 132*f*
 polydispersity and temperature, 136–137
 polymerization procedure, 128–129
 proposed mechanism of, of styrene, 129
 RRO of epoxides, 126
 steric effect of Ind ligands in Ind_2TiCl_2 , 134–135
 structures of L_nTiX_m precursors, 127
 styrene polymerizations, 131*f*
 Ti complex for initiation and reversible termination steps, 127

Tin iodides

reversible activation catalyzed by Ge and Sn, 597

styrene polymerization with 1-phenylethyl iodide (PE-I) in presence of, 598*t*

See also Living radical polymerization (LRP)

Titanate nanotubes (TNTs)

functionalized, by atom transfer radical polymerization, 285–289

general strategy for grafting, 285

See also Inorganic nanotubes

TMC-bisphenol polycarbonate (TMC-BP PC)

allyl methacrylate (AMA) end groups, 163, 165–166

preparation of bifunctional ATRP macroinitiators, 164

Tougheners for epoxy resins,

telechelic RAFT polymers as, 550–551, 559

Transfer reaction, 1,5-hydrogen shift mechanism, 113

Triblock copolymers, reversible addition-fragmentation chain transfer, 446, 448

Trithiocarbonates

end-group removal, 519–520
general synthesis method, 440–441

reversible addition-fragmentation chain transfer (RAFT) agents, 516

synthesis of RAFT agents, 547–548

U

Unconjugated monomers, living and stereospecific radical polymerization, 36*t*

V

Vinyl acetate (VAc)

block copolymerization of VAc and styrene, 374

bulk polymerization in presence of Co(acac)₂, 374–380

bulk radical polymerization, 378*t*

chain length dependence of termination rate coefficient, 491, 494*f*

characteristics of organo-cobalt/azo radical living radical polymerization, 370

cobalt porphyrin mediated living radical polymerization, 364, 366*t*

concentration in initiator and cobalt complex, 377–379

first order rate plot for polymerization, 366*f*

¹H NMR spectra of poly(VAc) and poly(vinyl alcohol), 33, 34*f*

influence of temperature on polymerization, 379–380

iodine-transfer radical polymerization in fluoroalcohols, 32–33

mechanism for cobalt-mediated radical polymerization, 375–377

propagating radical of reversible addition-fragmentation chain transfer, 413–414

See also Cobalt mediated radical polymerization (CMRP); Cobalt porphyrin derivatives

9-(4-Vinylbenzyl)adenine (VBA) homopolymer preparation, 189–190

molecular structure, 187*f*

organo-soluble copolymers with comonomer dodecyl

methacrylate (DMA), 190–193

water-soluble copolymers with comonomer

- oligo(ethyleneglycol) methacrylate (OEGMA), 193–194
See also Styrene derivatives bearing nucleobases
- 1-(4-Vinylbenzyl)thymine (VBT) homopolymer preparation, 189–190
 molecular structure, 187*f*
 organo-soluble copolymers with comonomer dodecyl methacrylate (DMA), 190–193
 water-soluble copolymers with comonomer
 oligo(ethyleneglycol) methacrylate (OEGMA), 193–194
See also Styrene derivatives bearing nucleobases
- Vinyl monomer polymerization. *See* Ruthenium *N*-heterocyclic carbene (NHC) complexes
- 4-Vinylpyridine (4VP), atom transfer radical polymerization, 67
- N*-Vinyl pyrrolidone (NVP)
 free radical polymerization in fluoroalcohols, 35*t*
 RAFT/MADIX polymerization in fluoroalcohols, 34–36

W

- Water, organic reactions and polymerizations, 15

- Water-soluble copolymers. *See* Styrene derivatives bearing nucleobases
- Well-defined copolymers. *See* Click functionalization of well-defined copolymers

X

- Xanthates
 general synthesis method, 440–441
 molecular design via interchange of, (MADIX), 27
 polymerization of *N*-vinyl pyrrolidone (NVP), 35*f*
 synthesis of RAFT agents, 547–548
See also Chemical transformation of xanthate-functional terminal groups; Macromolecular design via interchange of xanthates (MADIX); Star-like polymers by macromolecular design via interchange of xanthates (MADIX)

Z

- Zone casting
 illustration of, of block copolymer solution, 306
 long-range ordering, 306
 polyacrylonitrile-*b*-poly(butyl acrylate) (PAN-*b*-PBA) block copolymers, 305
 thin films of PBA-*b*-PAN, 307*f*